

## PREFACE

In the last century, we witnessed an array of exciting events in the growth of the radiation chemistry field. Radiation chemistry contributed not only to chemistry but also to physics, materials processing, biology, and medicine. This wide impact is due to the unique capability of radiation chemical techniques to selectively generate free radicals and ions, with precise and measurable yields. Their formation is independent of the optical absorption of the precursor species. The recent panoply of projects investigating the chemical aspects of radiation biology, solvation and electron transfer reactions, free radical chemistry of fullerenes, oxidative degradation of pollutants in water and studies on the catalytic mechanisms in zeolites have shown how radiation chemical techniques can be an important tool for chemists and biologists.

The recent advent of laser and laser-driven electron accelerators, providing pulses of high energy electrons in picoseconds or less, and powerful lasers producing photoionization in the sub-picosecond regime, made possible the study of ultrafast phenomena. Chemical processes can now be studied in picoseconds or less. A chemist can now study fast reactions using both lasers and electron pulses. With the synergy provided by these two techniques, the understanding of fundamental processes in radical and ionic chemistry has been greatly advanced.

Despite the growth of the possible applications of radiation chemistry, the limited knowledge of radiation chemical techniques and the large facilities necessary to employ these techniques have limited its use. However, new accelerator facilities, with faster time resolution and greater ease of use, will lead to both a quantum jump in research capabilities and research opportunities in radiation chemistry. In the present book, we endeavor to provide an overall view of the different aspects of the subject in its present status. We also want to show chemists in general and chemical kineticists, photochemists, physical-organic chemists and spectroscopists in particular the opportunities in utilizing radiation chemical techniques to study their chemical problems

Because of the diverse nature of the field, the chapters of this book are authored by several experts in their particular areas of research. The introductory chapter highlights the accomplishments of radiation chemistry during the last century and set out some possible future developments. This is followed by chapters on techniques in ultra-fast radiation chemistry techniques, on techniques using heavy ions, the observation of chemistry using spin and the chemistry evolving from the use of muons. These provide an experimental foundation for the science. After discussion of the techniques, fundamental radiation-chemical

processes in different systems including gases, high temperature aqueous systems (even more relevant now than in the recent past because of the resurgence of interest in nuclear power prompted by energy shortages), inorganic systems, organic systems and organic halides. These sections are followed by applications of radiation chemistry to the understanding of the fundamental chemistry of different systems including fullerenes, quinones, substituted benzenes and ending with the study of hetero-atom-centered free radicals – a field that was developed using radiation chemistry. Radiation chemistry has provided important tools in understanding processes in solids, including catalysis in zeolites, nanoclusters and colloids.

The biological effects of radiation, both positive and negative, have been important, and this is reflected by chapters on the effects of radiation on porphyrins, carbohydrates, nucleobases, proteins and DNA. These are followed by the use of radiation chemistry in the development of anti-cancer drugs, in the treatment of water pollution, polymers and in food pasteurization and sterilization.

As we stand just inside the portico of the third millennium, the obvious question that comes to mind is where does radiation chemistry go from here? Will it become just a part of photochemistry or will it disappear? We are optimistic. It is our firm belief that, as Peter Wardman put it; ' Radiation chemistry is alive and well and living in all areas of molecular science where free radicals reside' . It provides one of the simplest pathways to produce well-defined radicals. We sincerely hope that this book will act as a guide for young scientists entering or contemplating this field of research and for professionals who need information on radiation science or who may need to make use of these techniques to unravel their scientific problems.

More than 3 years have passed since our conception of this book. We regret that it is less comprehensive than what was initially planned – but we understand that the goal should be further than our reach. As Editors, we enjoyed the job of putting through the chapters, which is a less strenuous task than that of the authors whom we would like to profusely thank (especially those who have met their deadline and had to wait for so long!). We wish to thank Andrew Dempster, Derek Coleman and Cecilia Hughes at Elsevier Science who have helped us in the planning and execution of the project. One of us (BSMR) would like to thank Sujata Shinde for her assistance in the editing of the book. Finally, we would like to thank our wives for sacrificing the time (and the space for manuscripts) that rightfully belonged to them.

Charles D. Jonah and B. S. Madhava Rao

**List of Authors**

- Klaus-Dieter Asmus**--Radiation Laboratory and the Department of Chemistry and Biochemistry, University of Notre Dame, Notre Dame, IN 46556 USA (*asmus.1@nd.edu*)
- Jacqueline Belloni**--Laboratoire de Chimie Physique, UMR 8000 Université Paris-Sud-CNRS, Bât. 349, Centre Universitaire, F-91405 Orsay cedex, France (*Jacqueline.Belloni@lcp.u-psud.fr*)
- John Bentley**--Radiation Laboratory, University of Notre Dame, Notre Dame, IN 46556 USA (*John.J.Bentley.1@nd.edu*)
- George V. Buxton**--The School of Chemistry, University of Leeds, Leeds LS2 9JT, UK (*george.buxton@breathemail.net*)
- Ronald Cooper**--Radiation Chemistry Group, School of Chemistry, University of Melbourne, Parkville 3010, Victoria, Australia (*r.cooper@chemistry.unimelb.edu.au*)
- Dirk M. Guldi**--Radiation Laboratory, University of Notre Dame, Notre Dame, IN 46556 USA (*guldi.1@nd.edu*)
- Chantal Houée-Levin**-- Laboratoire de Chimie Physique, UMR 8000 Université Paris-Sud-CNRS, Bât. 350, Centre Universitaire, F-91405 Orsay cedex, France (*chantal.houee@lcp.u-psud.fr*)
- Mats Jonsson**--Department of Chemistry, Nuclear Chemistry, Royal Institute of Technology, SE -100 44 Stockholm, Sweden (*matsj@nuchem.kth.se*)
- Yosuke Katsumura**--Nuclear Engineering Research Laboratory, School of Engineering, The University of Tokyo, 2-22 Shirakata Shirane, Tokai-mura, Ibaraki 319-1106 Japan (*katsu@q.t.u-tokyo.ac.jp*)
- Hisaaki Kudoh**--Takasaki Radiation Chemistry Research Establishment, Japan Atomic Energy Research Institute, 1233 Watanuki, Takasaki, Gunma 370-1292 Japan
- Dan Meisel**--Radiation Laboratory and the Department of Chemistry and Biochemistry, University of Notre Dame, Notre Dame, IN 46556 USA (*Dani@nd.edu*)
- Stephen P. Mezyk**--Department of Chemistry, University of North Carolina at Wilmington, Wilmington, NC, 28403, USA (*mezyks@uncwil.edu*)

- Jai P. Mittal**-- Radiation Chemistry & Chemical Dynamics Division, Bhabha Atomic Research Centre, Trombay, Mumbai 400 085, India  
(*mittaljp@magnum.barc.ernet.in*)
- Hari Mohan**--Radiation Chemistry and Chemical Dynamics Division, Bhabha Atomic Research Centre, Trombay, Mumbai 400 085, India  
(*harim@apsara.barc.ernet.in*)
- Yuri N. Molin**--Institute of Chemical Kinetics and Combustion, 630090 Novosibirsk, Russia (*molin@ns.kinetics.nsc.ru*)
- Mehren Mostafavi**-- Laboratoire de Chimie Physique, UMR 8000 Université Paris-Sud-CNRS, Bât. 349, Centre Universitaire, F-91405 Orsay cedex, France (*mehran.mostafavi@lcp.u-psud.fr*)
- Tulsi Mukherjee**--Radiation Chemistry and Chemical Dynamics Division, Bhabha Atomic Research Centre, Trombay, Mumbai 400 085, India  
(*mukherji@magnum.barc.ernet.in*)
- P. Neta**--Physical and Chemical Properties Division, National Institute of Standards and Technology, Gaithersburg, MD 20899, USA  
(*pedi@mailserver.nist.gov*)
- Peter O'Neill**--Medical Research Council, Radiation & Genome Stability Unit, Harwell, Didcot, Oxfordshire, OX11 ORD, UK (*p.oneill@har.mrc.ac.uk*)
- Emil Roduner**--Institut für Physikalische Chemie, Universität Stuttgart Pfaffenwaldring 55, D-70569 Stuttgart, Germany (*e.roduner@ipc.uni-stuttgart.de*)
- Kyoichi Saito**--Department of Materials Technology, Chiba University, Inage, Chiba 263-8522, Japan and "Form and Function", PRESTO, Japan Science and Technology Corporation, Japan (*marukyo@xtal.tf.chiba-u.ac.jp*)
- Myran C. Sauer, Jr.**--Chemistry Division, Argonne National Laboratory, Argonne, IL 60439, USA.
- Heinz-Peter Schuchmann**--Max-Planck-Institut für Strahlenchemie, P. O. Box 101365, Stiftstrasse 34-36, D-45470 Mülheim an der Ruhr, Germany  
(*schuchmann@mpi-muelheim.mpg.de*)
- Ilya A. Shkrob**--Chemistry Division, Argonne National Laboratory, Argonne, IL 60439, USA.

**Cécile Sicard-Roselli**-- Laboratoire de Chimie Physique, UMR 8000 Université Paris-Sud-CNRS, Bât. 350, Centre Universitaire, F-91405 Orsay cedex, France (*cecile.roselli@lcp.u-psud.fr*)

**Takanobu Sugo**--Takasaki Radiation Chemistry Research Establishment, Japan Atomic Energy Research Institute, Takasaki, Gunma 370-1292, Japan (*sugo@taka.jaeri.go.jp*)

**Irwin A. Taub**--U.S. Army Soldier and Biological Chemical Command, Natick, MA, 01760-5018, USA. (*Irwin.Taub@Natick.army.mil*)

**Alexander D. Trifunac**--Chemistry Division, Argonne National Laboratory, Argonne, IL 60439, USA.

**Clemens von Sonntag**--Max-Planck-Institut für Strahlenchemie, P. O. Box 101365, Stiftstrasse 34-36, D-45470 Mülheim an der Ruhr, Germany (*clemens@vonsonntag.de*)

**Peter Wardman**--Gray Cancer Institute, P.O. Box 100,Mount Vernon Hospital, Northwood, Middlesex HA6 2JR, UK(*wardman@graylab.ac.uk*)

**David W. Werst**--Abbott Laboratories, 100 Abbott Park Road,Abbott Park, IL 60064-6076 (*werstdw@hpd.abbott.com*)

**James F. Wishart**--Chemistry Department, Brookhaven National Laboratory, Upton, NY 11973 USA (*Wishart@bnl.gov*)

## **Radiation Chemistry: from the Early Days to the Next Millennium**

**John Bentley and Dan Meisel**

Radiation Laboratory, and the Department of Chemistry and Biochemistry,  
University of Notre Dame, Notre Dame, Indiana 46556

### **Introduction**

Soon after the discovery of radium at the end of the eighteenth century, the effect of the radiation emanating from the radioactive isotope on chemical substances became evident. Ramsay's observation that  $H_2$  and  $O_2$  are generated upon the irradiation of water is often quoted as the beginning of the field of radiation chemistry (1). In the nearly a century that followed the field has matured to engulf a broad range of materials from simple molecules to complex composites. Today, the effects of radiation are utilized in numerous technologies, from food preservation to initiation of polymerization, from power generation to arms production and from radiotherapy to sterilization. Yet, studies are still conducted on the fundamental aspects of the effects of radiation in diverse exotic media from supercritical fluids to wet soils. It seems, therefore, appropriate to reflect on the evolution of radiation chemistry in the nearly century that has passed, to highlight some of its lasting contributions and point to future directions that may emerge. This contribution is, however, neither comprehensive nor objective. Several volumes including this one will provide both timely accounting and comprehensive details of the field (2-4). Rather, this is our own perception of the field as we see it now. We first scan a few major achievements of radiation chemistry, address open questions, and then suggest future directions. In particular we attempt to indicate contributions from radiation chemistry to the broader area of physical chemistry and other areas of general contemporary interest in chemistry.

### **Theory**

Theory has played an essential role in the development of radiation chemistry, especially in its early days when experiment was unable to probe the early events that set the stage for the observable chemical reactions. Three themes that were established early on were scattering processes, electronic structure determinations, and track simulations. Work done in the 1950s through 1970s depended greatly on formal development, both because the basic possibilities needed to be identified and because the available computational tools could not tackle the complexity of the problems. The decades that followed

provided such an explosive development in computer power and techniques that essentially all aspects of radiation chemistry are today susceptible to modelling with reasonable expectation for meaningful answers. Indeed, with the ongoing integration of quantum mechanics with molecular dynamics techniques, the three themes mentioned above will eventually lose their separate identities. However, those days are still to come.

One area that has seen tremendous development in the past two decades is electronic structure computation, and radiation chemistry has benefited along with most areas of chemistry. The questions one poses with such calculations are what are the molecular and electronic structures of the radicals and other transient species? What are the observable properties of these species? What reactions can they undergo (i.e., what are the potential energy surfaces that connect reactants to products)? The experimental properties that are amenable to predictive computations with electronic structure methods include molecular geometries and the corresponding electronic structures, relative energies of molecules (including enthalpies and free energies), spectroscopic quantities such as hyperfine coupling constants, vibrational frequencies or electronic transition energies, ionization potentials, electron affinities, heats of reactions, free energies and activation energies, solvation energies, and more. Some of these properties are readily calculable with widely available programs; others require effort and ingenuity to obtain a satisfactory answer. Species brought to light by radiation chemistry have always presented a challenge to electronic structure theory: open-shell radicals are more difficult to describe correctly than stable, closed-shell molecules (5), and the solvated electron or the three-electron bond (e.g., in  $(R_2S)_2^+$ ) are even harder to describe.

Early work focused principally on molecular and electronic structures and properties of free radicals. Of considerable interest were the calculations of hyperfine coupling constants of organic free radicals, because a considerable body of ESR work was becoming available (6,7) and because the computational methodology (semiempirical and small-basis, single-configuration *ab initio* methods) permitted such questions to be addressed directly (8). A fair body of work was also addressed to the question of the nature of the hydrated electron. Calculations of the structures and energies of anions of small clusters of water were the most frequently attempted efforts (9). For small radicals (four or fewer atoms) for which gas-phase experiments were possible, ambitious configuration interaction calculations often gave satisfactory agreement with observed results.

Since then, galloping improvements in computer power, combined with the development of new algorithms, have enabled us to address many problems with quantitative accuracy. Gradient techniques permit the determination of equilibrium structures, vibrational frequencies and transition state properties;

Perturbation and coupled cluster theories (e.g., MP2 or CCSD) provide correlation corrections. Density functional theory (DFT) appears to offer the best of all worlds, correlation-quality results at single-determinant prices. However, there is always a limit somewhere. The choice today seems to be between correlated methods with large basis sets, such as CCSDT, which systematically approach the "correct" answer at appreciable cost, and DFT, with its relatively economical efficiency, but which cannot be systematically improved (5).

With the widespread availability of electronic structure programs such as GAUSSIAN (10), GAMESS (11), or CADPAC (12), computational studies that used to be in the realm of the specialized theoreticians are now performed by graduate students. This, of course, is a two-edged sword: Much can be learned from the calculations, but one must also be aware of their limitations. Computations of interest to radiation chemists will frequently feature radicals in condensed media. Radicals and other energetic intermediates are more likely to possess low-lying excited states, which tend to make the single-configuration Hartree-Fock wavefunction inappropriate (5). In this case, calculated molecular structures, energies, and properties that are based on these methods may be inaccurate. This includes the popular MP2 perturbation theory. These problems are greatly reduced with DFT calculations, but DFT has its own modes of weakness. For instance, present DFT methods cannot describe the dissociation of symmetric radical species such as  $\text{H}_2^+$ ,  $\text{He}_2^+$ ,  $\text{F}_2^-$ ,  $(\text{H}_2\text{O})_2^+$  and related systems with 3-electron bonds (13-15).

Hyperfine coupling constants (hfcc) are a property on which much computational (as well as experimental) effort has been spent. Early success with semiempirical methods, such as INDO (16), in reproducing hfccs from ESR was accompanied by inconsistency of results. It was discovered that fortuitous cancellation of errors was behind the apparent agreement (17). As technical capabilities improved, it became clear that accurate computation of hfccs is a subtle problem, requiring both a basis set with flexibility near the magnetic nuclei and a substantial amount of electron correlation. At the present time, calculation of hfccs is essentially a resolved question: The effort needed in *ab initio* calculations to achieve accurate results is known (18), and recent work with DFT theory seems to indicate that hfccs calculated by DFT methods are in quite satisfactory agreement with experiment (19). Even molecules that have been considered "pathological" can be correctly described with a systematic theoretical approach (20).

The development of time-resolved resonance Raman spectroscopy as a tool for examining transients was paralleled by an interest in computing vibrational frequencies (21,22). In some ways this is an easier problem than



computing hfccs. For closed-shell molecules, a single-configuration wavefunction may be able to predict frequencies that agree with experiment ( $\pm 50 \text{ cm}^{-1}$ ) to within a scaling factor (23). Those radicals that are adequately described by single-configuration wavefunctions will have comparably satisfactory frequencies. If the underlying description of the radical is inadequate, some of the computed frequencies are liable to be greatly different from experiment ( $>100 \text{ cm}^{-1}$ ) (24). This situation can be rectified by systematic improvement of the level of theory, usually beyond MP2, and again, some versions of DFT have been found to predict frequencies quite well (23).

Electron affinities (EA), ionization potentials (IP) and heats of reaction arise from differences in energies computed for the species involved in the transitions. EAs and IPs usually require a difference between the energy of a closed-shell, singlet state and that of a doublet state. At lower computational levels of theory, these calculated energies are not of the same quality, even if calculated in exactly the same way. Chipman's detailed discussion of the electron affinity of the hydroxyl radical (25) shows how the qualitatively incorrect single-configuration result (negative EA) is systematically improved by the addition of configurations to the wavefunction. Energies of reaction, on the other hand, may converge more rapidly than the EAs or IPs, because systematic errors in the energies tend to cancel between the reactants and products. However, quantitative results for reactions involving radicals still demand competent basis sets and a degree of electron correlation beyond the MP2 level (26). Results of almost the same quality have been obtained with DFT at a fraction of the cost (27).

Many of the available computations on radicals are strictly applicable only to the gas phase; they do not account for any medium effects on the molecules being studied. However, in many cases, medium effects cannot be ignored. The solvated electron, for instance, is *all* medium effect. The principal frameworks for incorporating the molecular environment into quantum chemistry either place the molecule of interest within a small cluster of substrate molecules and compute the entire cluster quantum mechanically, or describe the central molecule quantum mechanically but add to the Hamiltonian a potential that provides a semiclassical description of the effects of the environment. The 1975 study by Newton (28) of the hydrated and ammoniated electron is the classic example of merging these two frameworks: Hartree–Fock wavefunctions were used to describe the solvated electron together with all the electrons of the first solvent shell, while more distant solvent molecules were represented by a dielectric continuum. The intervening quarter century has seen considerable refinement in both quantum chemical techniques and dielectric continuum methods relative to Newton's seminal work, but many of his basic conclusions

have been sustained with the passage of time. Recent work along these lines has resulted in the development of quantitative theoretical electrochemistry (29), and the improved ability to model hydrated electrons in reactive environments (30). Extension of these approaches to heterogeneous media is under active development.

Theoretical description of the early events in condensed phase radiolysis has been a primary domain of radiation chemistry since the early development of prescribed diffusion models of spurs by Mozumder and Magee (31), and Schwarz (32). These deterministic models were found to be inappropriate for the distributions and reaction processes of energetic species, and the simulation of track processes is now generally done by stochastic techniques. The problem is multiplex: The ionizing radiation deposits energy in the medium at a rate and over a range that varies with its energy, then the activated molecules diffuse from their creation sites and react with other substrates or each other. The energy deposition phase requires scattering cross sections or oscillator strengths as input parameters, which are frequently not available and so must be calculated or estimated (33). The chemical evolution sequence of the calculation depends upon an appropriate spatial distribution of reaction species from the energy deposition sequence. Simulations of electron tracks seem to be well in hand, with an increasing emphasis on incorporating details of the molecular environment into the calculations (34). Extension to high LET particle tracks with their much denser distributions of reactive species can be expected in the near future, as can applications to heterogeneous media and interfacial processes.

## **Instrumentation**

Whereas much of the underlying mechanisms for the effects of radiation on materials were outlined using steady state radiation sources, the advent of pulse radiolysis on the heels of flash photolysis opened a window into direct observation of the intermediates. One of the early discoveries utilizing pulse radiolysis was the spectrophotometric detection of the hydrated electron by Boag and Hart (35,36). Since then thousands of rate constants, absorption spectra, one-electron redox potentials and radical yields have been collected using the pulse radiolysis technique. The Radiation Chemistry Data Center at the University of Notre Dame accumulates this information and posts it (at [www.rcdc.nd.edu/](http://www.rcdc.nd.edu/)) for the scientific community to use. They cover the reactions of the primary radicals of water and many organic radicals and inorganic intermediates.

To collect this volume of data, linear accelerators with nanosecond time resolution were, and still are now, routinely used around the world. Faster, picosecond linac machines were built first in Toronto and then at Argonne National Laboratory. Picosecond accelerators for pulse radiolysis have been in use for nearly three decades at Argonne, at the Osaka University Radiation Laboratory, and the University of Tokyo Nuclear Engineering Research

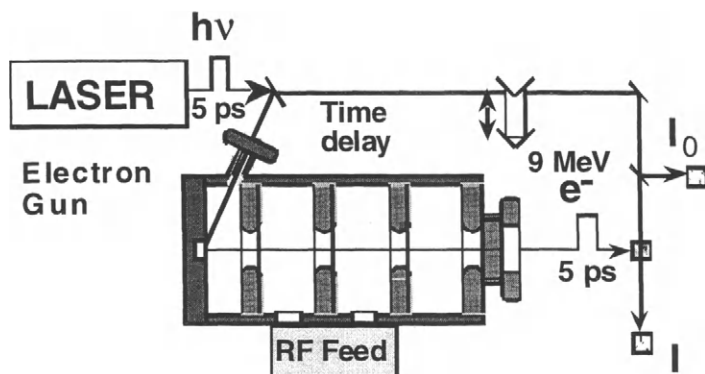


Figure 1: Schematic representation of the Laser-Electron Accelerator Facility at Brookhaven National Laboratory. The laser beam is split to generate both the electron pulse and the probe light (scheme courtesy of Dr. J. Wishart, Brookhaven National Laboratory).

Laboratory in Japan. These machines operate with electron pulses of several tens of ps and led to the observation of scavenging of the precursor to the hydrated electron. Using sub-ps laser techniques this species, in fact a variety of precursors, were later discovered upon photo-ionization (37,38). These early events are presently a matter of discussion in the literature and faster time resolution will be required in order to directly observe and identify the radiolytic precursors to the hydrated electron.

To exploit the capabilities of fast lasers, a new picosecond Laser-Electron Accelerator Facility (LEAF) has been recently developed at Brookhaven National Laboratory. In this facility, schematically shown in Figure 1, laser light impinging on a photocathode inside a resonant cavity gun merely 30 cm in length produces the electron pulse. The emitted electrons are accelerated to energies of 9.2 MeV within that gun by a 15 MW pulse of RF power from a 2.9 GHz klystron. The laser pulse is synchronized with the RF power to produce the electron pulse near the peak field gradient (about 1 MeV/cm). Thus the pulse length and intensity are a function of the laser pulse properties, and electron

pulse lengths as short as 5 ps are attainable. This machine is described in detail elsewhere in this book. Similar machines are presently under construction at several other laboratories around the world. In addition to the obvious advantages of the shorter electron pulses that such machines provide, the close synchronization between the laser and electron pulses is a major advantage. To observe the chemical events that occur at the fast time domain, a pulsed probe laser is required and therefore, timing of the probe with the electron pulse is of major importance. Since the same laser can be used to generate the white probe light, jitter between the two pulses can be minimized. Other designs of even faster linac facilities, based on laser technologies are currently under consideration at other laboratories.

Accelerators for heavy ions abound but low currents and limitations imposed by short penetration depth hamper their use in radiation chemical pulse radiolysis applications. Nonetheless, a high LET pulse radiolysis facility, based at the Heavy Ion Medical Accelerator in Chiba, Japan, has been recently used to determine yields of radicals in the radiolysis of water. Beams of 24 MeV  $\text{He}^{2+}$  and 6 MeV  $\text{H}^+$  with pulses of 5 or 10  $\mu\text{s}$  were used and because of the short penetration ( $\sim 400 \mu\text{m}$  in water) a tightly focused narrow laser beam was required for the spectrophotometric detection. The common observation of reduced primary radicals yields upon increasing the LET was observed with these  $\mu\text{s}$  time-resolution machines as well (39-41). The advent of synchrotron radiation, now in its third generation with a fourth on the horizon, led to an explosion of information primarily, however, from various X-ray diffraction, scattering, absorption and emission spectroscopies. Even though many of them can provide very short ps-regime pulses of ionizing radiation, time domain experiments on synchrotrons today are limited to structural determinations. It is quite conceivable that future machines will provide high enough dose rates to allow detection of chemical intermediates initiated by the passage of the radiation. Laser flash photolysis, in conjunction with pulse radiolysis to generate radicals can be used to probe the photochemistry and photophysics of radicals (42). This may lead to rather unusual photochemistry and unexpected photophysics in the radical doublet manifold (43). Perhaps not surprisingly, the quartet manifold in simple radicals has never been convincingly reported. Most probably, the presence of the quartet state will be observed only with ultra-fast sub-picosecond laser techniques.

Most of the techniques used in the analysis of intermediates are utilized today in pulse radiolysis as well. These include spectrophotometric, emission, near-IR, conductivity, resonance-enhanced Raman, and ESR techniques. Early attempts to observe surface-enhanced Raman scattering (SERS) from adsorbed radicals were inconclusive (44) but they led to the realization that the sensitivity

of SERS may rival that of absorption spectrophotometry (45). Indeed recent experiments using confocal microscopy have shown SERS from single dye molecules adsorbed on single colloidal silver and gold particles (46,47). Whereas no experiment has yet demonstrated such capabilities on irradiated samples, we fully expect implementation of single molecule spectroscopies in

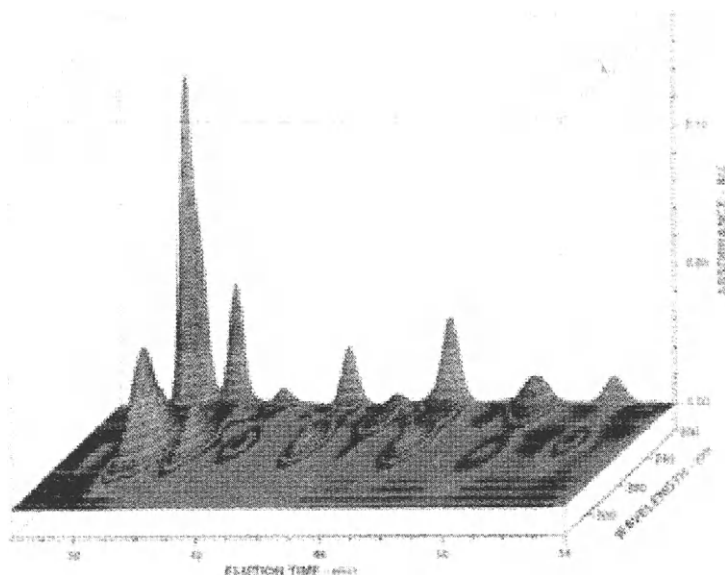


Figure 2: Three-D chromatograph of pentane containing 1 mM  $I_2$  following 200 krad irradiation. X-axis is time of elution; Z-axis is wavelength. Main peaks by order of appearance from left to right are: Partially resolved 2- and 3-Iodopene, 1- Iodopene, 1-Iodobutane, 1-Iodopropane, ethyliodide and methyl iodide. Reproduced by permission from J. Phys. Chem. 104, 1348 (2000).

radiation chemistry, especially on large biomolecules, in the foreseeable future. Combined with microbeams that were developed in the last decade and single-cell microdosimetry they will contribute significantly to radiation biology

(48,49). On the practical side, such an approach may help resolve the low-dose threshold issue that has been debated for many years in the radiobiology community. However, such capabilities will reach beyond the obvious applications to the nano-size regime. Because of the very short penetration depth of high-LET radiation, the availability of microscopic detection techniques should allow time-domain studies with heavy-ion irradiation.

Product analysis of irradiated samples attains the ppb level and separation of geometrical isomers is routinely performed. Using gel permeation chromatography the product distribution of  $\gamma$ -irradiated n-alkanes has been recently mapped (50). As can be seen in Figure 2, unprecedented resolution of the various isomers can now be achieved with modern chromatographic techniques. Capillary electrophoresis is presently used to determine the product distribution of various cresols and yields as low as 0.1 molecules/100 eV are routinely measured (51).

## Homogeneous Systems

*Aqueous Solutions:* For obvious reasons a concerted effort has been invested since the emergence of the field in understanding the radiation chemistry of aqueous solutions. Among the primary radicals of water radiolysis the hydrated electron is the most intriguing species. Precursors to  $e_{aq}^-$  were identified mostly using ultrafast laser photo-ionization techniques (37,38,52). The long-standing dogma that the time dependence of the concentration of primary radicals can be transformed into yield dependence on concentrations has indeed been confirmed (53). A report of considerable practical consequences is the observation that all of the molecular hydrogen, including the so-called residual, unscavengeable  $G(H_2)$ , can in fact be reduced to nil by scavengers of the precursor to the hydrated electron and not by those of  $e_{aq}^-$  (54). Since the production of combustible  $H_2$  is of prime concern in many technological applications of radiation, it seems clear that the scavenging capacity for the precursor (as well as  $e_{aq}^-$ ) need to be considered when choosing a candidate that will minimize  $G(H_2)$ . Furthermore, comparison of the effect of these scavengers on  $G(H_2)$  upon irradiation with various LET particles, and attempts to simulate the yield as a function of concentration (time), lead to the conclusion that a significant component of that yield arises from a second-order dissociative recombination of the non-hydrated electron (probably not the p-like state) with water holes, perhaps  $H_2O^+$ . If confirmed, this observation may require a significant reevaluation of the sequence of events that lead to the primary radicals in water radiolysis. Since essentially no information is available on the

precursor of OH radicals this may open up a new direction for studies of the oxidative pathway in water radiolysis (55).

*Other solvents:* Hydrocarbons were intensively studied in the last couple of decades. The debate around the lifetime and trapping ability of the high mobility holes seems to have been settled (56-58). Apparently fast electron transfer equilibrium between at least two conformers in cyclohexane, and perhaps other hydrocarbons, could account for most of the kinetic observations from both spectrophotometric and dc-conductivity observations (59). However, the rather nondescript spectra of the intermediates in these solvents hampers further elucidation of the primary processes in hydrocarbons.

More exotic solvents became targets of research as their use in technological applications could realistically be envisioned. Supercritical (SC) and near-supercritical fluids (SCFs) are now a subject of investigation by several groups as the use of supercritical CO<sub>2</sub> in environmentally acceptable chemical processing is often sought. Nonetheless, the use of SCFs as a medium for radiolysis is still in its infancy, inasmuch as the first demonstration of pulse radiolysis in SCF was made in 1995, and the current output is still very limited. The reasons for performing radiolysis in SCFs are the same as those for carrying out other experiments in SCFs: The considerable range of accessible densities and the possibility of selective solvation of solutes may lead to substantial enhancement or suppression of reaction rates relative to those in subcritical media. However, the detailed reaction schemes that have been assembled for radiolysis of subcritical solvents are almost totally lacking for SCFs, and thus interpretation of the results is not straightforward.

The initial studies of Chateaufeuf and Brennecke (60,61) examined benzhydrol in SC fluoroform. Radiolysis led to the (C<sub>6</sub>H<sub>5</sub>)<sub>2</sub>CH<sup>+</sup> cation, which decayed by addition to cosolvents. Jonah and coworkers, using SC ethane (62), made the first observation of an electron transfer reaction in a SCF, the reaction of biphenyl anion with pyrene. The apparently anomalous pressure dependence of the reaction was thought to indicate a pressure-dependent solvent reorganization energy. The same group then turned its attention to SC CO<sub>2</sub> (63,64), trying to characterize the reactive transients from the radiolysis of the medium itself. Among the transients, radical-ion clusters of CO<sub>2</sub> were identified but other transient remained to be determined. Ferry and Fox (65) describe the radiolysis of SC water, in which competition between OH addition and oxidation of halophenols was observed. Percival *et al.* observed muonium in SC water (66), with apparently large effects on the muonium formation rate. They hypothesized that muonium may probe the way density and hydrogen-bonding structure affect the rate of proton transfer. Finally, Holroyd's group (67) has studied the attachment of electrons to CO<sub>2</sub> in SC ethane, and conclude that the

negative volume of reaction of ethane indicates clustering around the anion. The tentative nature of the conclusions drawn by all of these reports highlights the need to establish the fundamental properties of radiolytic effects of SCFs.

A major contribution from radiation chemistry to general physical chemistry was the experimental confirmation of the Marcus theory for electron transfer by Miller and Closs (68-71). The advantage of the radiolytic approach over the analogous laser flash photolysis technique, in this context, is the ability to generate only the reduced radical on one donor-acceptor molecule. Thus a charge-shift reaction could be studied rather than an electron-hole recombination that is commonly generated photolytically. Nonetheless, the implications of the theory, which gain credence from the experimental verification, are far reaching especially in photoinduced electron transfer. Rational design of supramolecules in efforts to control charge separation and charge recombination is now possible based on the principles outlined by Miller & Closs (71). It is commonly utilized with a high degree of confidence in studies of natural and artificial photosynthesis and in energy conversion schemes. It is now taken for granted that for efficient photo-induced charge separation one would like to work near the maximum rate in the "normal" region of the Marcus curve for electron-transfer. However, for the highly energetic, but energy wasting, back reaction one strives to operate in the "inverted" region. Furthermore, it also provided a rationale for the rate of hole and triplet energy transfer. As the activity in photoinduced electron transfer intensifies, pulse radiolysis is often used to resolve issues that cannot be explained by photolysis alone. Such was the case in the identification of the intermediates in the most commonly used photoelectrochemical cell based on the  $\text{Ru}(\text{bpy})_3^{2+}$  photosensitizer (72).

Numerous solutes, from inorganic complexes to DNA components were investigated in much detail using radiation chemical approaches. One can safely assume that as mechanisms of the reactions of the primary radicals with simple solutes are unravelled a shift to increasingly complex molecules and molecular assemblies will take place. Currently, the mechanism of oxidation of even the simplest of amino acids is still under intense scrutiny (73,74). Nonetheless, studies of radiation damage in DNA are constantly proceeding from frozen, matrix isolated environments to liquid solutions at ambient temperatures. The question of the rate and distance of electron transfer along the DNA chains is still under debate (75). Recent measurements of single-step hole transport in synthetic DNA indicate that it is fast enough to compete with strand breakage thus allowing hole hopping for large distances along the DNA chain. On the other hand, it is too slow to compete with charge recombination within the ion-pair of the photochemical cage (76). This direction of charge transport in DNA will continue to be a mainstream direction in radiation biochemistry. The



emphasis on kinetics in radiolysis notwithstanding, a wealth of thermodynamic information can be collected using pulse radiolysis, for example from the establishment of electron-transfer equilibria. Wardman's compilation of one-electron redox potentials, all collected by pulse radiolysis, includes hundreds of redox couples (77).

### **Organized Assemblies and Heterogeneous Systems**

Along with the rest of the chemistry community, attention of radiation chemistry in recent years is shifting from single molecules in condensed phases to ensembles of molecules and materials. Several objectives are driving these studies, in addition to the inherent interest in the effects of radiation on the assembly. The effects of the assembly on solutes' behavior, in particular kinetic parameters, is quite often a primary motivation. Furthermore, as already mentioned above for supercritical fluids, one often learns quite detailed information on the medium itself from these studies. Initial studies of radiolysis in organized assemblies focused on micellar solutions (78,79). The interaction of the solute with the surface potential of the micelle can significantly affect the kinetics of reactions at the micellar surface. More interestingly, the dimensionality of the reaction can significantly alter the dynamics of a process. Indeed Henglein and Proske showed that cations, e.g.,  $\text{Ag}_2^+$ , can be confined to the interfacial surface of an anionic micelle and their kinetics then are distinct from those in three dimensional space (80). Other parameters of the micellar-organized assembly that influence radiolytically produced intermediates include modification of the pH at the vicinity of the micellar interface and hydrophobic interactions of the micellar core with less-soluble solutes.

The effects of ionizing radiation on solid dispersions in liquids have been studied from the early days of radiation chemistry (81). However, with the discovery of quantum size effects, with the growing interest in interfacial processes in energy conversion, and with the widespread activities surrounding nano-materials much effort has been directed into the use of radiation chemistry in the study of these materials. The unusual properties of the solids at the borderline between molecular and bulk dimensions lead indeed to many interesting discoveries. In that regard, the ability of pulse radiolysis to selectively prepare a system with one kind of radicals, reducing or oxidizing, is very instrumental in these investigations. The seminal series of papers by Henglein and coworkers introduced the concept of "microelectrode", where a small metallic particle may accumulate a large number of electrons on a single particle (82,83). This led to a rational application of metallic colloids as multi-electron redox catalysts. The addition of a single electron, e.g., from  $e_{\text{aq}}^-$ , to a

small semiconductor nanoparticle, leading to essentially complete bleaching of the absorption by the particle near the band edge of the particle, has far reaching implications (84). It means that these particles should have very large non-linear optical effects following photoinduced charge injection into the particles, as indeed was verified by optical excitation. Very large surface potential effects on the kinetics, as well as the thermodynamics, of charge injection from reducing radicals into oxide particles were observed and fully interpreted using electrochemical theories for electron transfer across the solid/electrolyte interface (85,86). Using spectrophotometric pulse radiolysis, in combination with conductivity techniques it was recognized that addition of electrons to oxide particles leads to the phenomenon of charge compensation (87), which was later observed in electrochemical experiments as well (88).

The few examples listed above demonstrate the tremendous impact that radiation chemistry had on the understanding of microheterogeneous systems and the advancement of nanostructured materials. In addition many studies have focused on the fate of radiation absorbed by one phase on the other (79,89,90). Can the energy pass onto the interface? Does it produce radicals, and what are their properties when adsorbed on the surface? Silica particles and zeolites are common matrixes where these studies were done since they may generate a variety of radical that are difficult to trap in other media, especially radical cations in the zeolite framework (91). Experiments at the solid/liquid interface are scarcer. Nonetheless, for silica in water we have shown recently that, contrary to holes, essentially all of the electrons that are generated by absorption of the radiation in the nanoparticles do appear in water as  $e_{aq}^-$  (92,93). However, it is not clear at the moment whether this is a general observation or material-specific. One may expect that in different materials trapping processes will have different efficiencies, and therefore, different escape probabilities from one phase to the other. However, no systematic study has yet been performed on this issue. Because of its significant practical implications, especially in nuclear waste management and power generation applications, this question will have to be addressed in the imminent future.

Radiolysis was found to be a useful tool in the synthesis of nanoparticles. Henglein and coworkers and Belloni and coworkers prepared many metallic (and pre-metallic) particles of a large variety of compositions over the last two decades. Both groups were able to show size dependence of the redox potential of the metallic ion/metallic atom (or cluster) couples from single atoms to relatively large clusters (94-97). Commonly the synthesis involves radiolytic reduction of metal ions in aqueous solutions but radiolytic production of silver particles was recently achieved in supercritical fluids as well (98). The particles produced by radiolytic reduction of the ions can be designed to assume a variety

of morphologies, from core-shell structures to alloys. The size and size distribution of the particles can be judiciously controlled and methodologies for narrowing size distribution of seed metallic particles were developed (99). This high quality of particles in turn allowed Hodak et al. to determine the cooling processes in the ultrafast time regime following fs laser excitation (100). Furthermore, exploiting dissociative electron transfer processes (e.g., release of halide ions from alkyl halides (101,102) or sulfide from thiols (103-105) upon reaction with  $e_{aq}^-$ ) one can initiate growth of semiconductor materials (e.g., of AgX or CdS respectively) using radiolytic techniques. Thus, the instantaneous initiation of growth processes afforded by radiolytic techniques offers opportunities to study the growth processes of semiconductor materials essentially from the stage of the single molecule to the bulk size materials. In analogy with the redox potential of metallic clusters, the stability constant of the molecule obtained from the two component ions depends on the size of the cluster. A single CdS molecule is highly soluble and its dissociation is essentially complete in water even though the solubility product of this material is only  $3.6 \times 10^{-29} \text{ M}^2$ .

## Applications

The impact of radiation chemistry on technology reaches beyond the direct use of radiation in the technology. Obvious technologies where radiation is directly involved include power generation, arms production, nuclear waste (106-108), initiation of polymerization, cross-linking(109), medical sterilization, food irradiation (110) and environmental clean-up (111). Many of the radiolytic processing applications that are already in use are summarized in Woods and Pikaev's recent volume (112). Irradiation of solid wet interfaces is proposed as an economically viable radio-catalytic approach for polluted-soil decontamination (113). Radiation chemical studies of the radiation-induced processes in nuclear waste were crucial in developing predictive models that describe gas generation in nuclear waste (114,115). Often considered beyond the scope of radiation chemistry, radiotherapy relies extensively on models for the underlying radiolytic processes in living tissues. As the models are refined they can be expected to provide increasing accuracy in targeting the irradiated areas. Electron-beam nano-lithography is emerging as the ultimate technology in its superior resolution (116-118). Combined with clever nanoparticle deposition techniques it will find utility in molecular computing in the foreseeable future (119-121).

The fundamental nature of the studies described above find applications in many other technologies. To cite a few examples, the growth of silver seeds

upon reduction of silver ions led Belloni and coworkers to develop a model for silver development in photographic processes (97,122). Ultimately this insight into silver photography led the same group to develop methodologies to significantly enhance the sensitivity of the process using “current-doubling” in formate doped silver halides matrixes (123). As already mentioned, the pioneering studies of Henglein and coworkers on multi-electron redox catalysis is now implemented in many energy conversion schemes.

## Conclusions

A clear trend that emerges in the continuing research in radiation chemistry is the contribution of radiation chemical techniques to other fields in physical chemistry. Furthermore, these contributions continuously tilt towards systems of increasing complexity. In the evolution of radiation chemistry the development of faster instruments for pulse radiolysis will continue be pursued. The application of such machines will lead to a clearer picture of the earliest events that follow the absorption of the energy in the medium, including characterization of the precursors to the longer-lived primary species. In parallel development of more finely resolved imaging technologies will give us the means to probe radiation effects in specific locations and in progressively smaller quantities at increasing spacial resolution. With the development of theory and its increased reliability the need for experimental verification of theoretical predictions will decrease. On the other hand, the interest in the effects of radiation on assemblies of supramolecules, material at the nano-scale regime, surfaces and interfaces will replace the emphasis on the single molecule.

**Acknowledgement:** This work is supported by the US Department of Energy, Office of Basic Energy Sciences. This is contribution NDRL No. 4272 from The Notre Dame Radiation Laboratory.

## References

- (1) Ramsay, W. J. *Chem. Soc.* 1907, 91, 931.
- (2) Tabata, Y.; Ito, Y.; Tagawa, S. In: *CRC Handbook of Radiation Chemistry*; CRC Press, Boca Raton, 1991.
- (3) Spinks, J. W.; Woods, R. J. In: *An Introduction to Radiation Chemistry*; 3rd ed.; J. Wiley & Sons: New York, 1990.
- (4) Farhataziz; Rodgers, M. A. J. In: *Radiation Chemistry: Principles and Applications*; VCH Publishers, New York, 1987.
- (5) Bally, T.; Borden, W. T., In: *Reviews of Computational Chemistry*; Lipkowitz, K and Boyd, D., Eds., Wiley-VCH, New York, 1999; Vol. 13, pp 1-97.
- (6) Fessenden, R. W.; Schuler, R. H. *J. Chem. Phys.* 1963, 39, 2147.

- (7) Shkrob, I. A.; Trifunac, A. D. *Radiat. Phys. Chem.* 1997, 50, 227-224.
- (8) Dewar, M. J. S. In: *The Molecular Orbital Theory of Organic Chemistry*; McGraw-Hill, New York, 1969.
- (9) Schwartz, M. E.; Naleway, C. A. *J. Phys. Chem.* 1972, 76, 3905-3908.
- (10) Frisch, M. J., et al. *GAUSSIAN 98*, Gaussian, Inc., Pittsburgh, PA, 1998.
- (11) Schmidt, M. W., et al. *GAMESS*, described in: *J. Comput. Chem.* 1993, 14, 1347-1363.
- (12) Amos, R. D., et al. *CADPAC*, Cambridge University, Cambridge, U.K., 1995.
- (13) Bally, T.; Sastry, G. N. *J. Phys. Chem. A* 1997, 101, 7923-7925.
- (14) Braida, B.; Hiberty, P. C.; Savin, A. *J. Phys. Chem. A* 1998, 102, 7872-7877.
- (15) Sodupe, M.; Bertran, J.; Rodríguez-Santiago, L.; Baerends, E. J. *J. Phys. Chem. A* 1999, 103, 166-170.
- (16) Pople, J. A.; Beveridge, D. L.; Dobosh, P. A. *J. Am. Chem. Soc.* 1968, 90, 4201-4209.
- (17) Chipman, D. M. *J. Chem. Phys.* 1983, 78, 3112-3132.
- (18) Perera, S. A.; Salemi, L. M.; Bartlett, R. J. *J. Chem. Phys.* 1997, 106, 4061.
- (19) Batra, R.; Giese, B.; Spichty, M.; Gescheidt, G.; Houk, K. N. *J. Phys. Chem.* 1996, 100, 18371.
- (20) Carmichael, I. *J. Phys. Chem.* 1991, 95, 108-111.
- (21) Schuler, R. H.; Tripathi, G. N. R.; Prebenda, M. F.; Chipman, D. M. In *J. Phys. Chem.*, 1983; Vol. 87, pp 5357-5361.
- (22) Tripathi, G. N. R.; Chipman, D. M.; Schuler, R. H.; Armstrong, D. A. *J. Phys. Chem.* 1995, 99, 5264-5268.
- (23) Scott, A. P.; Radom, L. *J. Phys. Chem.* 1996, 100, 16502-16513.
- (24) Chipman, D. M. *J. Phys. Chem. A* 1999, 103, 11181-11187.
- (25) Chipman, D. M. *J. Chem. Phys.* 1986, 84, 1677-1682.
- (26) Chuang, Y.-Y.; Coitiño, E. L.; Truhlar, D. G. *J. Phys. Chem. A* 2000, 104, 446-450.
- (27) Wong, M. W.; Radom, L. *J. Phys. Chem. A* 1998, 102, 2237-2245.
- (28) Newton, M. D. *J. Phys. Chem.* 1975, 79, 2795-2808.
- (29) Winget, P.; Weber, E. J.; Cramer, C. J.; Truhlar, D. G. *Phys. Chem. Chem. Phys.* 2000, 2, 1231-1239.
- (30) Sobolewski, A. L.; Domcke, W. *Chem. Phys. Lett.* 2000, 321, 479-484.
- (31) Mozumder, A.; Magee, J. L. *Radiat. Res.* 1966, 28, 215-231.
- (32) Schwarz, H. A. *J. Phys. Chem.* 1969, 73, 1928-1937.
- (33) Pimblott, S. M.; LaVerne, J. A.; Mozumder, A. *J. Phys. Chem.* 1996, 100, 8595-8606.
- (34) Pimblott, S. M.; LaVerne, J. A. *Radiat. Res.* 1998, 150, 159-169.
- (35) Hart, E. J.; Boag, J. W. *J. Am. Chem. Soc.* 1962, 84, 4090.
- (36) Boag, J. W.; Hart, E. J. *Nature* 1963, 197, 45.
- (37) Gauduel, Y.; Gelabert, H. *Adv. Chem. Ser.* 1998, 254, 331.
- (38) Yokoyama, K.; Silva, C.; Son, D.-H.; Walhout, P. K.; Barbara, P. F. *J. Phys. Chem. A* 1998, 102, 6957.
- (39) Chitose, N.; Katsumura, Y.; Zuo, Z.; Domae, M.; Ishigure, K.; Murakami, T. *J. Chem. Soc., Faraday Trans.* 1997, 93, 3939-3944.
- (40) Chitose, N.; Katsumura, Y.; Domae, M.; Zuo, Z.; Murakami, T. *Radiat. Phys. Chem.* 1999, 54, 385-391.
- (41) Chitose, N.; Katsumura, Y.; Domae, M.; Zuo, Z.; Murakami, T.; LaVerne, J. A. *J. Phys. Chem. A* 1999, 103, 4769-4774.
- (42) Bromberg, A.; Schmidt, K. H.; Meisel, D. *J. Am. Chem. Soc.* 1984, 106, 3056.

- (43) Meisel, D.; Das, P. K.; Hug, G. L.; Bhattacharyya, K.; Fessenden, R. W. *J. Am. Chem. Soc.* 1986, 108, 4706.
- (44) Lee, P. C.; Schmidt, K.; Gordon, S.; Meisel, D. *Chem. Phys. Lett.* 1981, 80, 242-247.
- (45) Lee, P. C.; Meisel, D. *J. Phys. Chem. A* 1982, 86, 3391-3395.
- (46) Kneipp, K.; Wang, Y.; Kneipp, H.; Perelman, L. T.; Itzkan, I.; Dasari, R. R.; Feld, M. *S. Phys. Rev. Lett.* 1997, 78, 1667-1670.
- (47) Nie, S.; Emory, S. R. *Science* 1997, 275, 1102-1106.
- (48) Folkard, M.; Prise, K. M.; Vojnovic, B.; Bowey, A. G.; Pullar, C.; Schettino, G.; Michael, B. D., In: *Microdosimetry: An Interdisciplinary Approach*; Goodhead, D. T., O'Neill, P., Menzel, H. G., Eds.; The Royal Society of Chemistry, Cambridge, 1997; pp 323-326.
- (49) Folkard, M.; Vojnovic, B.; Prise, K. M.; Bowey, A. G.; Locke, R. J.; Schettino, G.; Michael, B. D. *Int. J. Radiat. Biol.* 1997, 72, 375-385.
- (50) Wojnarovits, L.; Schuler, R. H. *J. Phys. Chem. A* 2000, 104, 1346-1358.
- (51) Schuler, R. H.
- (52) Shi, X.; Long, F. H.; Lu, H.; Eisenthal, K. B. *J. Phys. Chem.* 1996, 100, 11903-11906.
- (53) Pimblott, S. M.; LaVerne, J. A.; Bartels, D. M.; Jonah, C. D. *J. Phys. Chem.* 1996, 100, 9412-9415.
- (54) Pastina, B.; LaVerne, J. A.; Pimblott, S. M. *J. Phys. Chem. A* 1999, 103, 5841-5846.
- (55) LaVerne, J. A.; Pimblott, S. M. *J. Phys. Chem. A* 2000, Web release of Oct. 19,.
- (56) Beck, G.; Thomas, J. K. *J. Phys. Chem.* 1972, 76, 3856-3863.
- (57) Warman, J. M. In: *The Dynamics of Electrons and Ions in Non-Polar Liquids*; Report IRI 134-81-23, Delft, The Netherlands, 1981.
- (58) Warman, J. M., In: *The Study of Fast Processes and Transient Species by Electron Pulse Radiolysis*; Baxendale, J. H., Busi, F., Eds.; Reidel, Dordrecht, Holland, 1982; pp 433-533.
- (59) Sauer, M. C., Jr.; Shkrob, I. A.; Yan, J.; Schmidt, K.; Trifunac, A. D. *J. Phys. Chem.* 1996, 100, 11325-11335.
- (60) Zhang, J.; Connery, K. A.; Strebing, R. B.; Brennecke, J. F.; Chateaufneuf, J. E. *Rev. Sci. Instrum.* 1995, 66, 3555-3559.
- (61) Zhang, J. W.; Connery, K. A.; Brennecke, J. F.; et al., *J. Phys. Chem.* 1996, 100, 12394-12402.
- (62) Takahashi, K.; Jonah, C. D. *Chem. Phys. Lett.* 1997, 264, 297-302.
- (63) Dimitrijevic, N. M.; Bartels, D. M.; Jonah, C. D.; et al., *Chem. Phys. Lett.* 1999, 309, 61-68.
- (64) Dimitrijevic, N. M.; Takahashi, K.; Bartels, D. M.; et al., *J. Phys. Chem. A* 2000, 104, 568-576.
- (65) Ferry, J. L.; Fox, M. A. *J. Phys. Chem. A* 1998, 102, 3705-3710.
- (66) Percival, P. W.; Brodovitch, J. C.; Ghandi, K.; et al., *Phys. Chem. Chem. Phys.* 1999, 1, 4999-5004.
- (67) Nishikawa, M.; Itoh, K.; Holroyd, R. A. *J. Phys. Chem. A* 1999, 103, 550-556.
- (68) Calcaterra, L. T.; Closs, G. L.; Miller, J. R. *J. Am. Chem. Soc.* 1983, 105, 670.
- (69) Closs, G. L.; Calcaterra, L. T.; Green, N. J.; Penfield, K. W.; Miller, J. R. *J. Phys. Chem.* 1986, 90, 3673-3683.
- (70) Miller, J. R.; Calcaterra, L. T.; Closs, G. L. *J. Am. Chem. Soc.* 1984, 106, 3047.
- (71) Closs, G. L.; Miller, J. R. *Science* 1988, 240, 440.
- (72) Das, S.; Kamat, P. V. *J. Phys. Chem. B* 1998, 102, 8954-8957.

- (73) Bonifacic, M.; Armstrong, D. A.; Carmichael, I.; Asmus, K.-D. *J. Phys. Chem. B* 2000, 104, 643-649.
- (74) Bonifacic, M.; Stefanic, I.; Hug, G. L.; Armstrong, D. A.; Asmus, K.-D. *J. Am. Chem. Soc.* 1998, 120, 9930-9940.
- (75) Barbara, P. F.; Meyer, T. J.; Ratner, M. A. *J. Phys. Chem.* 1996, 100, 13148-13168.
- (76) Lewis, F. D.; Liu, X.; Liu, J.; Miller, S. E.; Hayes, R. T.; Wasielewski, M. R. *Nature* 2000, 406, 51 - 53.
- (77) Wardman, P. *J. Phys. Chem. Ref. Data* 1989, 18, 1637-1755.
- (78) Wheeler, J.; Thomas, J. K. In: *Inorganic Reactions in Organized Media*; ACS Symp. Ser. 1982, 177, 97-111.
- (79) Thomas, J. K. *The Chemistry of Excitation at Interfaces*; ACS monograph 181., 1984.
- (80) Henglein, A.; Proske, T. *Ber. Bunsenges. Phys. Chem.* 1978, 82, 471-476.
- (81) Allen, A. O., In: *The Radiation Chemistry of Water and Aqueous Solutions*; Van Nostrand Co., Princeton, 1961; pp 113-116.
- (82) Henglein, A.; Lilie, J. *J. Am. Chem. Soc.* 1981, 103, 1059-1066.
- (83) Henglein, A. *J. Phys. Chem.* 1993, 97, 5457-5471.
- (84) Henglein, A.; Kumar, A.; Janata, E.; Weller, H. *Chem. Phys. Lett.* 1986, 132, 133-136.
- (85) Mulvaney, P.; Swayambunathan, V.; Grieser, F.; Meisel, D. *J. Phys. Chem.* 1988, 92, 6732.
- (86) Mulvaney, P.; Grieser, F.; Meisel, D., In: *Kinetics and Catalysis in Microheterogeneous Systems*; Graetzel, M., Kalyanasundaram, K., Eds.; Marcel Dekker, New York, 1991; pp 303-373.
- (87) Borgarello, E.; Pelizzetti, E.; Mulac, W. A.; Meisel, D. *J. Chem. Soc., Faraday Trans. 1* 1985, 81, 143-159.
- (88) Lyon, L. A.; Hupp, J. T. *J. Phys. Chem.* 1995, 99, 15718-15720.
- (89) Zhang, G.; Mao, Y.; Thomas, J. K. *J. Phys. Chem. B* 1997, 101, 7100-7113.
- (90) Thomas, J. K. *Chem. Rev.* 1993, 93, 301.
- (91) Werst, D. W.; Trifunac, A. D. *Acc. Chem. Res.* 1998, 31, 651-657.
- (92) Dimitrijevic, N. M.; Henglein, A.; Meisel, D. *J. Phys. Chem. B*, 1999, 103, 7073-7076.
- (93) Schatz, T.; Cook, A. R.; Meisel, D. *J. Phys. Chem.* 1998, 102, 7225-7230.
- (94) Henglein, A.; Tausch-Treml, R. *J. Colloid Interface Sci.* 1981, 80, 84-93.
- (95) Henglein, A. *Ber. Bunsenges. Phys. Chem.* 1990, 94, 600-603.
- (96) Mostafavi, M.; Marignier, J. L.; Amblard, J.; Belloni, J. *Radiat. Phys. Chem.* 1989, 34, 605-617.
- (97) Mostafavi, M.; Marignier, J. L.; Amblard, J.; Belloni, J. *Z. Phys. D, At., Mol. Clusters* 1989, 12, 31-35.
- (98) Jonah, C. D.; et al., Private communication 2000.
- (99) Henglein, A.; Meisel, D. *Langmuir* 1998, 14, 7392-7396.
- (100) Hodak, J. H.; Henglein, A.; Hartland, G. V. *Pure Appl. Chem.* 2000, 72, 189-197.
- (101) Schmidt, K. H.; Patel, R.; Meisel, D. *J. Am. Chem. Soc.* 1988, 110, 4882-4884.
- (102) Hayes, D.; Schmidt, K. H.; Meisel, D. *J. Phys. Chem.* 1989, 93, 6100-6109.
- (103) Hayes, D.; Micic, O. I.; Nenadovic, M. T.; Swayambunathan, V.; Meisel, D. *J. Phys. Chem.* 1989, 93, 4603-4608.
- (104) Swayambunathan, V.; Hayes, D.; Schmidt, K. H.; Liao, Y. X.; Meisel, D. *J. Am. Chem. Soc.* 1990, 112, 3831-3837.
- (105) Hayes, D.; Meisel, D.; Micic, O. *Colloids Surf.* 1991, 55, 121-136.

- (106) Bradley, D. J. In: Behind the Nuclear Curtain: Radioactive Waste Management in the Former Soviet Union; Battelle Press, Columbus, Richland, 1997.
- (107) Crowley, K. D. *Physics Today* 1997, 50, 32-39.
- (108) McCrombie, C. *Physics Today* 1997, 50, 56-62.
- (109) Wilson, J. E. In: Radiation Chemistry of Monomers, Polymers, and Plastics; Marcel Dekker, New York, N.Y., 1974.
- (110) Taub, I. A. *J. Chem. Educ.* 1981, 58, 162-167.
- (111) Cooper, W. J.; O'Shea, K.; Curry, R. D. In: Environmental Applications of Ionizing Radiation; Wiley & Sons, New York, 1999.
- (112) Woods, R. J.; Pikaev, A. K. In: Applied Radiation Chemistry : Radiation Processing; Wiley & Sons, New York, 1993.
- (113) Zacheis, G. A.; Gray, K. A.; Kamat, P. V. *J. Phys. Chem. B* 103, 1999, 2142-2150.
- (114) Meisel, D.; Camaioni, D.; Orlando, T., In: First Accomplishments of the EMSP; Eller, G. and Heinman, W., Ed.; ACS Symposium Series, Accepted for Publication, 2000.
- (115) Orlando, T. M.; Meisel, D., In: First Accomplishments of the EMSP; Eller, G. and Heinman, W., Ed.; ACS Symposium Series, Accepted for Publication, 2000.
- (116) Jensen, T. R.; Duval, M. L.; Kelly, K. L.; Lazarides, A. A.; Schatz, G. C.; Van Duyne, R. P. *J. Phys. Chem. B* 1999, 103, 9846-9853.
- (117) Hulteen, J. C.; Treichel, D. A.; Smith, M. T.; Duval, M. L.; Jensen, T. R.; Van Duyne, R. P. *J. Phys. Chem. B* 1999, 103, 3854-3863.
- (118) Jensen, T. R.; Schatz, G. C.; Van Duyne, R. P. *J. Phys. Chem. B* 1999, 103, 2394-2401.
- (119) Collier, C. P.; Wong, E. W.; Belohradski'i, M.; Raymo, F. M.; Stoddart, J. F.; Kuekes, P. J.; Williams, R. S.; Heath, J. R. *Science* 1999, 285, 391-394.
- (120) Henrichs, S. E.; Sample, J. L.; Shiang, J. J.; Heath, J. R.; Collier, C. P.; Saykally, R. J. *J. Phys. Chem. B* 1999, 103, 3524-3528.
- (121) Markovich, G.; Collier, C. P.; Henrichs, S. E.; Remacle, F.; Levine, R. D.; Heath, J. R. *Acc. Chem. Res.* 1999, 32, 415-423.
- (122) Belloni, J.; Mostafavi, M.; Marignier, J. L.; Amblard, J. J. *Imaging Sci.* 1991, 35, 68-74.
- (123) Belloni, J.; Treguer, M.; Remita, H.; Keyzer, R. D. *Nature* 1999, 402, 865 - 867.



## Accelerators for Ultrafast Phenomena

James F. Wishart

Chemistry Department, Brookhaven National Laboratory,  
Upton, NY 11973, U. S. A.

### 1. INTRODUCTION

The purpose of this chapter is to describe the technology that enables the investigation of radiation chemical phenomena at picosecond and femtosecond timescales. Several research groups have used femtosecond laser photoionization techniques to examine electron solvation dynamics and other processes relevant to early radiation chemistry events [1,2]. This chapter will focus on ultrafast studies using ionizing radiation, primarily electron beams, as the excitation source.

In this context, it is useful to reiterate the inherent time resolution limitations of techniques that combine charged particle excitation with optical detection. Energetic charged particles travel through a medium at velocity  $\beta c$ , where  $c$  is the velocity of light in vacuum, and  $\beta = 0.98$  and  $0.9988$  for 2 and 10 MeV electrons, respectively. Light travels through a medium at velocity  $c/n$ , where  $n$  is the refractive index ( $n = 1.33$  for water at 600 nm, for example). In the time it takes 600 nm photons to travel unit distance through water, 10 MeV electrons will travel  $\beta n = 1.33$ , meaning that the photons will fall 1.1 ps behind for every millimeter of sample depth, if the pulses were pure impulse functions.

Empirical measurements with near-Gaussian optical and electron pulses at 800 nm with 8.5 MeV electrons indicate that the FWHM response function broadening increases by 700 fs for every millimeter of travel through water [3]. Therefore, time resolution is ultimately limited by sample depth, the choice of which is affected by considerations such as detection sensitivity, signal strength and the ability of the sample to tolerate signal averaging. Because of this limitation, ultrafast in the context of accelerators refers to timescales from a few hundred femtoseconds to tens of picoseconds.

## 2. ACCELERATION METHODS FOR ULTRAFAST STUDIES

### 2.1. Picosecond thermionic prebunching injectors

Particle accelerators of every size and type consist of two major components: a particle source (sometimes called an injector) and an acceleration stage. The job of the injector is to generate a particle beam with the desired position-momentum relationship for acceptance into the acceleration section. Ultrafast accelerators require an injection system which deposits the entire electron bunch in a single RF period. The method employed to accomplish this in the first generation of picosecond accelerators was the sub-harmonic prebuncher (Figure 1). The electron pulse is generated by gating the thermionic cathode of an electrostatic electron gun on and off within a few nanoseconds. After a short drift space the electrons enter a series of RF cavities tuned to a sub-harmonic (typically a few hundred MHz) of the main accelerator frequency (typically 1-3 GHz). The timing of cathode gating is controlled to insert the electron bunch into only one prebuncher period. The RF field in the prebuncher reduces the temporal spread of the electron pulse until it can be injected, with the proper phase adjustment, into a single period of the main accelerator RF frequency. A linear accelerator (linac) section then accelerates the electron bunch to energies of 20 – 30 MeV. Picosecond accelerators using this type of injector for pulse radiolysis have been in use for many years at Argonne National Laboratory in Illinois, and in Japan at the Osaka University Radiation Laboratory and the University of Tokyo Nuclear Engineering Research Laboratory (NERL) at Tokai-mura.

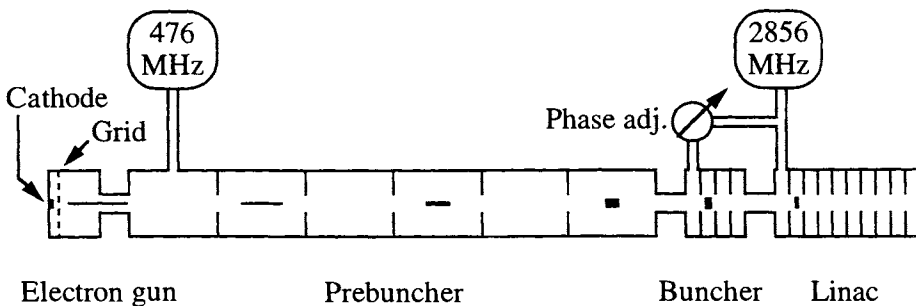


Figure 1. Schematic representation of an S-band thermionic injection system for a picosecond linear accelerator.

## 2.2. RF photocathode electron guns

Another type of injector developed in recent years for ultrafast accelerators is the radio-frequency photocathode electron gun (Figure 2). RF photocathode electron guns consist of one or more conducting resonant cavities, which are filled with several megawatts of microwave power to create transient electric field gradients of 80 to 100 MV/m. The first cavity, or cell, of the electron gun is typically only 50-60% as long as the microwave wavelength, with a disk of photocathode material mounted in the back plate of the gun. When the field gradient is optimal at the photocathode surface a pulse of laser light is used to generate photoelectrons. The high field gradient accelerates the photoelectrons to MeV energies in a distance of several centimeters. A 1.5 cell photocathode electron gun can accelerate several nanocoulombs of electrons to ~4 MeV using 8 megawatts of RF power. A 3.5 cell gun, such as the one driving the Laser-Electron Accelerator Facility at Brookhaven National Laboratory, uses 15 MW to accelerate electrons to 9 MeV in a distance of 30 cm. Beam energies of 4 – 9 MeV are sufficient for most pulse radiolysis applications, however, additional acceleration stages may be used. RF photocathode guns can generate electron bunches with very clean phase space correlations between their position and momentum distributions. This attribute is very desirable for applications where beam manipulation is important, such as pulsewidth compression. This type of accelerator is becoming very common as an injector for free electron laser systems, another application where beam quality is essential.

The key to the RF photocathode gun technology is the existence of laser systems that can be synchronized to the microwave frequency to high precision (i.e., one degree of RF phase, or 1 ps at 2.856 GHz) and stability. Several commercial titanium sapphire (Ti:Sapphire) and Nd:YAG oscillators are available which actively regulate their cavity length to match their frequency to that of an external reference with the required precision and stability. The choice of laser system is governed by the required excitation energy (determined by the work function of the cathode), laser pulse duration (dependent on several factors) and laser pulse energy (determined by cathode quantum efficiency and the required per-pulse charge). Picosecond Nd:YAG systems are economical and may be used in some applications where their fixed pulse width is acceptable, however, femtosecond Ti:Sapphire systems are the prevailing choice because their high bandwidth permits adjustment of the laser pulse width to suit

the application and they provide probe and pump beams with femtosecond resolution.

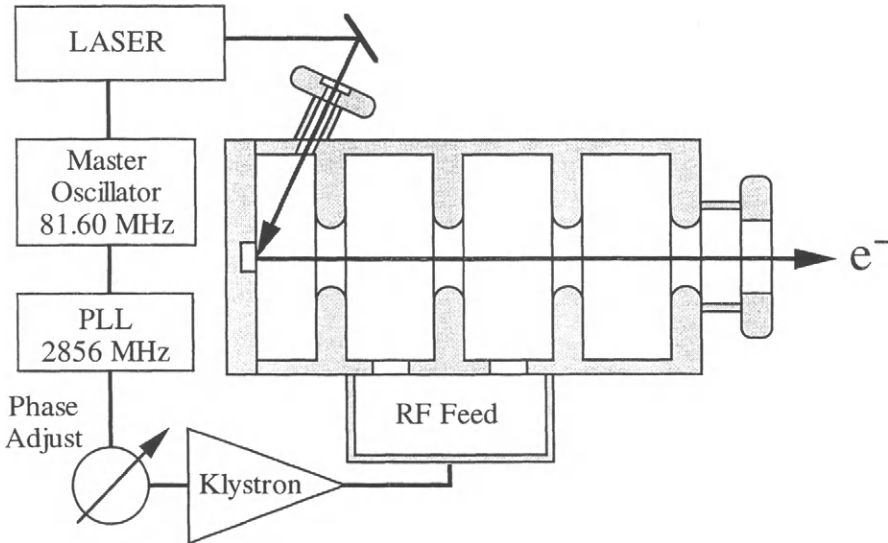


Figure 2. Schematic representation of an S-band RF Photocathode electron gun injector system. In actuality, the accelerator is about 30 cm long.

Photocathode selection is a trade-off between efficiency and ease of maintenance [4,5]. Metal photocathodes such as copper or magnesium are durable but have low quantum efficiency ( $\phi \sim 10^{-3} - 10^{-4}$ ). Semiconductor cathodes such as cesium telluride ( $\text{Cs}_2\text{Te}$ ) or lanthanum hexaboride ( $\text{LaB}_6$ ) have higher efficiencies, however their useful lifetimes are short before reconditioning is needed. All of these materials require excitation in the ultraviolet region; typically 266 nm is used because it is the fourth harmonic of Nd:YAG and the third harmonic of the Ti:Sapphire optimum gain region. Measurements on several operating accelerators indicate that approximately 20 microjoules of 266 nm light will excite 1 nanocoulomb of electrons from a clean magnesium cathode. Amplified, 10 Hz laser systems can easily produce pulses in excess of 1 mJ at 266 nm, therefore available laser energy is not the limiting factor for charge extraction even with low-efficiency metal photocathodes.

However, the high peak power at higher pulse energies can make it more difficult to maintain good mode quality as the laser beam propagates.

The duration and timing of the laser pulse incident on the photocathode is very important for the control of pulse characteristics at the radiolysis target. Due to the charges on the electrons within the bunch, the intuitive assumption that the shortest laser pulse will produce the shortest electron pulse is incorrect. Space-charge effects, caused by the mutual repulsion of each electron with every other electron in the bunch, force the bunch to expand in all directions as it propagates to the target. Longitudinal expansion (along the direction of transport) broadens the pulse duration, requiring compensation in the beam transport system as discussed below. Expansion in the transverse directions (perpendicular to transport) requires periodic focusing which affects the total travel distance, and hence, the distribution of arrival times on target. Space-charge effects can disrupt the strong position-momentum correlation of the electron bunch and limit the ability of the transport system to compress the pulse. Typically, the optimal laser pulse width on the photocathode surface is 2 – 10 ps depending on the system and application.

Another important consideration for selection of laser pulse characteristics is the effect of RF field saturation at the cathode surface. A 3 mm radius, uniformly thin disk of electrons generates an electrostatic field of 2 MV/m per nanocoulomb at its surface. As mentioned above, peak field gradients for RF photocathode guns are 80 – 100 MV/m, (however optimum beam characteristics for compression are obtained if the electrons are launched at ~85% of peak). For the cathode radius selected as an example here, extracted charges on the order of 10 nC and above can significantly affect the field gradient at the cathode surface, particularly if cathode illumination is not uniform. Field saturation places the ultimate limitation on the amount of charge that can be extracted in a single pulse. The most effective means of overcoming this limitation is to lower the charge density by using the largest practical cathode diameter and spreading the laser pulse width as much as possible. The adjustable pulse width afforded by the high bandwidth of a Ti:Sapphire laser system is especially useful in this regard. It should be mentioned for the sake of clarity that field saturation is a separate phenomenon from beam loading, where the electron bunch extracts enough energy from the cavity to reduce the microwave power and therefore reduces the field gradient in the accelerating structure. Due to the high power density in RF photocathode guns, beam loading is a secondary consideration.

As mentioned above, a 3.5-cell RF photocathode gun is in operation as the accelerator for the Brookhaven National Laboratory Laser-Electron Accelerator Facility. Recently, 1.6-cell RF photocathode guns have replaced thermionic cathode systems as injectors for 30 MeV linear accelerators at Osaka University and the Nuclear Engineering Research Laboratory in Tokai-mura, Japan [6]. Another RF photocathode gun accelerator is under construction at the ELYSE facility at the Université de Paris-Sud at Orsay, France. A magnesium cathode is in use at LEAF, copper is used at NERL, while the Orsay accelerator will use  $\text{Cs}_2\text{Te}$ .

### 3. BEAM TRANSPORT AND PULSE COMPRESSION TECHNIQUES

Ultimate control of the electron beam pulse width of an ultrafast accelerator system rests with the beam transport system. Space charge effects spread the electron bunch in the longitudinal and transverse directions. Transverse spreading is typically controlled by pairs of quadrupole magnets spaced along the beam line. The primary consideration for transverse focusing is to prevent loss of the beam against the sides of the beam pipe while avoiding compressing the beam into a tight waist until it reaches the target, in order to avoid scrambling the position-momentum correlation which permits strong temporal compression.

Longitudinal compression of the electron bunch is used to reduce the pulse width at the target to the shortest value possible. Compression schemes rely on having a correlation between particle velocity and position within the bunch. Such correlations obtain naturally from photocathode injectors; they can be induced in thermionic-generated beams by modulation of the phase and power of accelerating sections. Dipole bending magnets can then be used to make particles of various energies travel paths of different lengths to arrive at the target at the same time.

An example of a chicane-type compressor is given in Figure 3. On the left of the figure, a diagram shows the phase-space distribution of the electron bunch before traverse of the chicane. The velocity of each particle ( $v_z$ ) is plotted as a function of particle position ( $z$ ) along the axis of propagation. The leading edge of the bunch is at the lower right (a), meaning that the slower electrons are leading. The bending magnets in the chicane cause the lower energy electrons

to take the longest path so that they are delayed to coincide with the faster electrons at the exit to the chicane, as indicated in the phase-space diagram on the right. In actual cases the compression would be slightly less than complete at the exit of the chicane in order to allow for evolution of the packet until it hits the target.

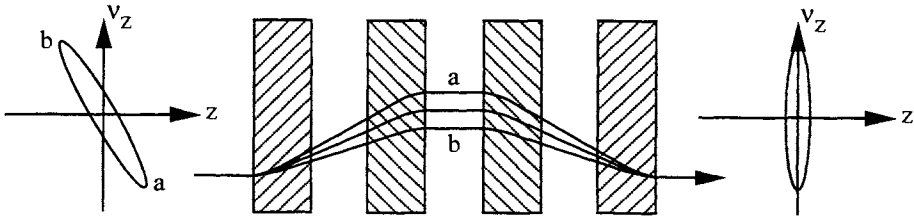


Figure 3. Pulse compression using a chicane configuration.

To compress a pulse with the opposite (fast-to-slow) velocity skew, an alpha magnet can be used (Figure 4). In an alpha magnet, the field is varied along the axis  $x$  which bisects the input and output vectors. The highest energy particles take the longest path.

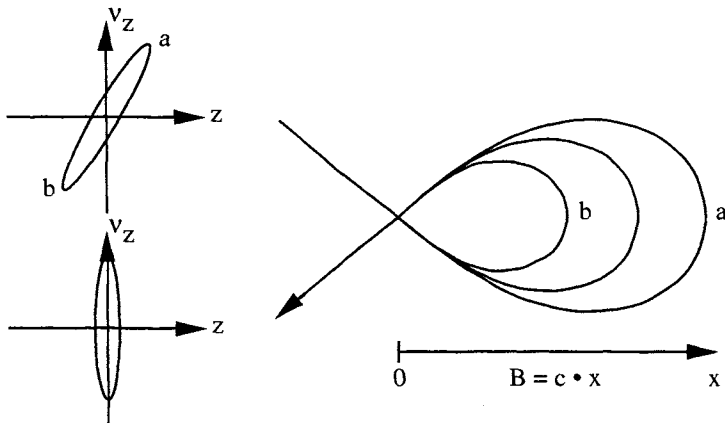


Figure 4. Schematic representation of particle paths through an alpha magnet.

Both the chicane and alpha magnet compression schemes are achromatic, that is to say that the exit path is the same for all particle energies. Non-achromatic

compression can be obtained from a pair of  $45^\circ$  bending dipoles separated by a quadrupole pair. Scientists at NERL have managed to compress 1 nC of electrons down to 900 fs FWHM using such a scheme [7].

#### 4. PULSE WIDTH DETERMINATION

Measurement of the pulse width of an ultrafast electron beam can be accomplished by several means. One of the first methods used with success was generation of Cerenkov light, followed by detection using a streak camera [7,8]. Cerenkov light is generated when a charged particle passes through a medium with a velocity greater than the speed of light in that medium. The particle generates an electromagnetic plane wave that propagates at angle  $\theta_c$  with respect to the particle's trajectory, where  $\beta$  and  $n$  are defined as in Section 1:

$$\cos \theta_c = 1/\beta n \quad (1)$$

According to Equation 1, Cerenkov light will be generated if the product  $\beta n \geq 1$ . For electrons with energies of 20 and 30 MeV, for example,  $\beta = 0.99969$  and  $0.99986$ , respectively. At these electron energies, media with very low refractive indices, such as gases, can be used to generate narrow, forward-directed beams of Cerenkov light ( $\beta n \sim 1$ , therefore  $\theta_c \sim 0$ ). This can be accomplished with a cell containing 1 atmosphere of xenon gas ( $n = 1.00078$ ) for 20 MeV electrons [8] or in plain air ( $n = 1.00029$ ) if the beam energy is 30 MeV [7]. Because the media in these cases are selected so that  $\beta n \sim 1$ , the electron beam and the Cerenkov light it generates remain coincident in time over cell depths of several centimeters. The Cerenkov light is then transported via a mirror and optical relay to the input slit of a streak camera for temporal analysis.

For beam energies less than 20 MeV a gas Cerenkov cell would have to be pressurized to meet the criterion of  $\beta n \sim 1$ . Instead, it is more practical to use a thin fused silica plate as a Cerenkov radiator. The optical collection system should be aligned with the Cerenkov cone angle ( $\theta_c \sim 47^\circ$ ) and the plate should be normal to the detection axis, at an angle to the electron beam, to minimize internal reflection problems.

Transition radiation (TR) is generated when an energetic charged particle passes across an interface between regions of substantially different dielectric



constants [9]. TR emission occurs over a wide range of wavelengths depending on the particle energy and TR radiator material. Typically, an aluminum plate or foil is used to generate the TR, which has specular optical characteristics and is emitted backward (upstream) and forward (downstream) as the beam crosses the front and back surfaces of the aluminum foil. If the foil surface is oriented at an angle of  $45^\circ$  with respect to the beam, the backward TR will be emitted at an angle of  $90^\circ$  to the beam. At the BNL LEAF facility, polished Al plates that can be inserted into the beam at  $45^\circ$  angles are used as optical TR beam profile monitors. The TR beam images are collected by ordinary video cameras.

Transition radiation is considerably weaker than Cerenkov radiation, however since it is a surface phenomenon it avoids problems with radiator thickness and reflections inherent to Cerenkov-generating silica plates. Optical TR can be measured using a streak camera. An optical TR system has been used to time-resolve the energy spread of an electron macropulse in a free-electron laser facility [10]. Interferometry of coherent, far-infrared TR has been used to measure picosecond electron pulse widths and detect satellite pulses at the UCLA Saturnus photoinjector, using charges on the order of 100 pC [11].

Another method for pulse length determination uses the electromagnetic fields produced by the electron bunch itself to measure the longitudinal length of the bunch, and therefore derive the pulse width. A pulse of a given width has a characteristic microwave power spectrum as shown in Figure 5.

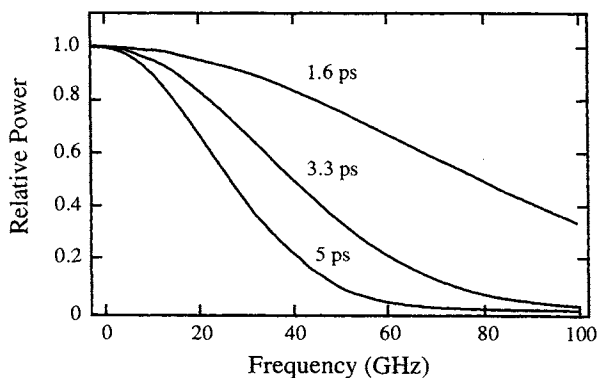


Figure 5. Power spectra of electron bunches of various widths. Data from Reference 12.

Comparison of microwave power at two frequencies, for example 20 and 40 GHz, permits the determination of the pulse width. This method has been demonstrated by measuring the power induced in a pair of 25- and 36-GHz cavities attached to the beam line as pick-ups [12], and also by measurement of the power spectrum using a sweep oscillator [13]. This method is extremely attractive because it does not intercept the beam; it can therefore be used in real time to monitor pulse width during experiments.

Other non-destructive pulse length diagnostic techniques which have been proposed are based on diffraction radiation, which is generated when a beam passes through an aperture [14], and on coherent Smith-Purcell radiation, which is induced by passing the beam over a conductive grating with a period comparable to the bunch length [15].

It is also possible to determine the pulse width by measurement of a prompt optical signal induced in the radiolysis sample, as described in the next section.

## 5. EXPERIMENTAL DETECTION METHODS

Ultrafast accelerator systems present some challenges in the design of experimental detection systems which can take full advantage of their time resolution. Digitizer-based transient absorption systems are not fast enough to measure transients on the order of a few picoseconds. Several years ago, methods were developed to use a narrow beam of Cerenkov radiation (generated in gas as described above) as a stroboscopic optical probe with variable delay controlled by a translation stage [16]. This development opened a new time regime for kinetic studies, which led to many important findings on reactions within spurs. While the technique has proven very powerful, there are certain limitations. Since the detection system is single beam, separate  $I_0$  and  $I_{\text{sample}}$  shots are required, making shot-to-shot reproducibility very important for accurate absorbance measurements. The intensity of the probe Cerenkov beam falls off at longer wavelengths, and the signal from Cerenkov light generated within the sample itself can amount to 10 – 20% of the probe beam intensity, requiring careful correction.

With the advent of laser-pulsed photocathode accelerators, a new approach to pulse-probe detection is possible. Spare output from the laser system used to generate the photoelectrons can be used to create a probe beam synchronized to the electron pulse with resolution on the order of 100 fs. Optical parametric

amplification can be used to generate probe wavelengths from the visible to the near-infrared. Near-infrared wavelengths are important for optical studies of the electron in non-polar solvents. A laser probe beam will have much lower divergence and higher intensity than a Cerenkov probe; both features serve to reduce interference from Cerenkov light generated from irradiation of the sample itself. Figure 6 shows the layout of the dual-beam pulse-probe laser detection system installed at LEAF [17].

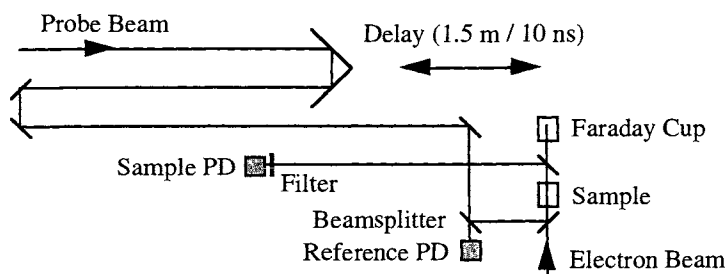


Figure 6. Schematic representation of the LEAF pulse-probe detection system.

Placement of the sample photodiode at a distance from the sample allows Cerenkov light from the sample to diverge, reducing its effect on the absorbance measurement. Absorbance measurements can be normalized using the Faraday cup readings to correct for fluctuations in beam intensity.

Pulse-probe transient absorbance data on the rise time of prompt species such as the aqueous electron can be used to measure the instrument response of the system and deduce the electron pulse width. Figure 7 shows the rise time of aqueous electron absorbance measured with the LEAF system at 800 nm in a 5 mm pathlength cell. Differentiation of the absorbance rise results in a Gaussian response function of 7.8 ps FWHM. Correcting for pathlength, the electron pulsewidth is 7.0 ps in this example.

The pulse-probe technique can be extended to multiwavelength detection by using the ultrafast laser pulse to generate a white-light continuum probe, which can be dispersed with a spectrograph across a diode array or CCD detector after traversing the sample. Due to lower probe intensity, Cerenkov emission from the sample would be expected to be more of a complication in this case, but the correction methods developed for stroboscopic Cerenkov detection would also work here.

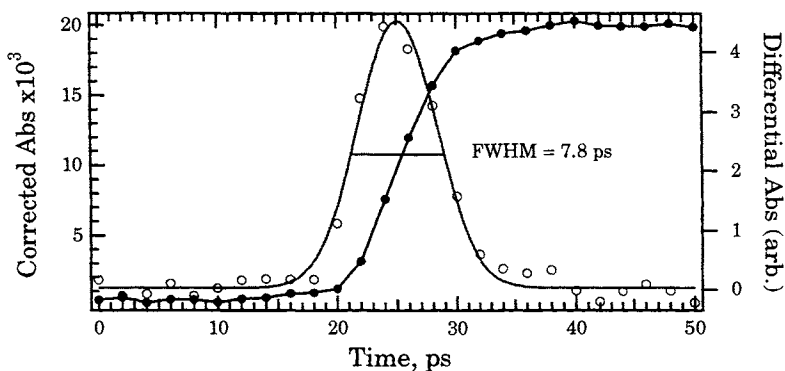


Figure 7. Pulse-probe transient absorption measurement of the rise time of  $e_{aq}^-$  measured at 800 nm in a pathlength of 5 mm.

Formation of excited states of hydrocarbons via geminate recombination has been studied by detection of emission on the picosecond time scale using a streak camera [18]. Single-shot streak cameras with resolution on the order of 200 fs are now available.

One final example of ultrafast kinetics performed at radiolysis facilities is the study of excited states of radical ions. An accelerator pulse can be used to generate radical species, which can then be excited by a pump laser beam and probed with femtosecond resolution by another laser pulse with variable optical delay. This application does not depend on precise correlation of the electron and laser pulses and can be done at almost all radiolysis facilities. The availability of femtosecond lasers in photocathode facilities places all the necessary components to hand. Effective pump-probe measurements will require significant concentrations of radical ions. This can be accomplished by frequency-quadrupling a 5-9 nanosecond Nd:YAG pulse to irradiate the photocathode, thereby creating a macropulse containing several tens of nanocoulombs which will produce a high concentration of radicals for the pump-probe experiment.

## 6. CONCLUSION

Picosecond accelerators for ultrafast radiolysis studies are undergoing a period of renewal as the RF photocathode electron gun technology becomes

widely adopted. New accelerator facilities will make ultrafast radiolysis accessible for larger numbers of researchers. The pace of technological development in detection systems for these facilities is bound to increase as techniques are transferred from laser systems to accelerator facilities.

## ACKNOWLEDGMENT

This work was carried out at Brookhaven National Laboratory under contract DE-AC02-98CH10886 with the U.S. Department of Energy and supported by its Division of Chemical Sciences, Office of Basic Energy Sciences.

## REFERENCES

Wherever possible, reference has been made to articles in published journals. In some cases the information is only available via conference proceedings. Electronic copies of these proceedings are available on the world wide web.

1. Y. Gauduel, H. Gelabert, Ultrafast electron transfer and short-lived prereactive steps in solutions, in "Photochemistry and Radiation Chemistry: Complementary Methods for the Study of Electron Transfer" J. F. Wishart, and D. G. Nocera, , Eds.; Adv. Chem. Ser. 254, Ch. 6, American Chemical Society, Washington, DC, (1998), p.331.
2. K. Yokoyama, C. Silva, D.-H. Son, P.K. Walhout and P.F. Barbara, Detailed Investigation of the Femtosecond Pump-Probe Spectroscopy of the Hydrated Electron, *J. Phys. Chem. A*, 102 (1998), 6957.
3. J. F. Wishart, A. R. Cook, unpublished results.
4. S. H. Kong, J. Kinross-Wright, D. C. Nguyen, R. L. Sheffield, Photocathodes for Free Electron Lasers, *Nucl. Inst. Meth. Phys. Res. A* 358 (1995) 272.
5. P. Michelato, Photocathodes for RF Photoinjectors, *Nucl. Inst. Meth. Phys. Res. A* 393 (1997) 455.
6. M. Uesaka, K. Kinoshita, T. Watanabe, T. Ueda, K. Yoshii, H. Harano, K. Nakajima, A. Ogata, F. Sakai, H. Kotaki, M. Kando, H. Dewa, S. Kondo, Y. Shibata, K. Ishi, M. Ikezawa, Femtosecond electron beam generation and measurement for laser synchrotron radiation, *Nucl. Inst. Meth. Phys. Res. A* 410 (1998) 424.

7. M. Uesaka, T. Ueda, T. Kozawa, T. Kobayashi, Precise measurement of a subpicosecond electron single bunch by the femtosecond streak camera, *Nucl. Inst. Meth. Phys. Res. A* 406 (1998) 371.
8. G. S. Mavrogenes, C. Jonah, K. H. Schmidt, S. Gordon, G. R. Tripp, L. W. Coleman, Optimization of isolated electron pulses in the picosecond range from a linear accelerator using a streak camera-TV diagnostic system, *Rev. Sci. Instrum.* 47 (1976) 187.
9. A. H. Lumpkin, R. B. Feldman, D. W. Feldman, S. A. Apgar, B. E. Carlsten, R. B. Fiorito, D. W. Rule, Optical-transition radiation measurements for the Los Alamos and Boeing free-electron laser experiments, *Nucl. Inst. Meth. Phys. Res. A* 285 (1989) 343.
10. W. A. Gillespie, A. M. MacLeod, P. F. Martin, A. F. G. van der Meer, P. W. van Amersfoort, Time-resolved electron spectrun diagnostics for a free-electron laser, *Rev. Sci. Instrum.* 67 (1996) 641.
11. A. Murokh, J. B. Rosenzweig, M. Hogan, H. Suk, G. Travish, U. Happek, Bunch length measurement of picosecond electron beams from a photoinjector using coherent transition radiation, *Nucl. Inst. Meth. Phys. Res. A* 410 (1998) 452.
12. E. Babenko, R. K. Jobe, D. McCormick, J. T. Seeman, Length monitor for 1 mm SLC bunches, SLAC-PUB-6203, Proceedings of the 1993 Particle Accelerator Conference (PAC 93).
13. H. H. Braun, C. Martinez, Non-intercepting bunch length monitor for picosecond electron bunches, Proceedings of the 1998 European Particle Accelerator Conference (EPAC 98) page 1559.
14. W. D. Kimura, R. B. Fiorito, D. W. Rule, Development of diffraction radiation diagnostics for noninvasive beam size, divergence, and emittance measurements, Proceedings of the 1999 Particle Accelerator Conference (PAC 99) page 487.
15. M. C. Lampel, Coherent Smith-Purcell radiation as a pulse length diagnostic, *Nucl. Inst. Meth. Phys. Res. A* 385 (1997) 19. D. C. Nguyen, Electron bunch length diagnostic with coherent Smith-Purcell radiation, Proceedings of the 1998 European Particle Accelerator Conference (EPAC 98) page 1990.
16. M. J. Bronskill, J. W. Hunt, A pulse-radiolysis system for the observation of short-lived transients, *J. Phys. Chem.*, 72 (1968) 3762. M. J. Bronskill, W. B. Taylor, R. K. Wolff, J. W. Hunt, Design and performance of a pulse radiolysis system capable of picosecond time resolution, *Rev. Sci. Instrum.*,

- 41 (1970) 333. C. D. Jonah, A wide-time range pulse radiolysis system of picosecond time resolution, *Rev. Sci. Instrum.*, 46 (1975) 62.
17. A. R. Cook, S. V. Lyman, J. F. Wishart, J. R. Miller, manuscript in preparation.
18. M. C. Sauer, Jr., C. D. Jonah, B. C. Le Motais, A. C. Chernovitz, Sources of excited cyclohexane in the radiolysis of cyclohexane, *J. Phys. Chem.* 92 (1988) 4099.

## **Ion-beam radiation chemistry**

**H. Kudoh<sup>a</sup> and Y. Katsumura<sup>b</sup>**

<sup>a</sup> Takasaki Radiation Chemistry Research Establishment, Japan Atomic Energy Research Institute, 1233 Watanuki, Takasaki, Gunma 370-1292 JAPAN

<sup>b</sup> Nuclear Engineering Research Laboratory, School of Engineering, The University of Tokyo, 2-22 Shirakata Shirane, Tokai, Ibaraki 319-1106 JAPAN

### **1. INTRODUCTION**

One of new aspects of radiation chemistry at present and in the near future will be the use of “new” radiation sources. In addition to rather “conventional” or “traditional” radiation sources such as  $\gamma$ -rays and electron beams (EB), development in accelerator science and electronics has brought various kinds of new radiation such as ion beam, meson beam, positron beam ( $e^+$ ), SR (synchrotron radiation), etc. Fundamentals of radiation chemistry on “new” radiation have been studied extensively, and in some cases application is already at industrial stage, though much is still left to be elucidated for both fundamental and application aspects.

Amongst them, ion beam is most extensively studied and widely used at present. Radiation sciences such as physics and biology related to ion beam are also expanding. The character and potential advantages of ion beam compared to “conventional” radiation would be; (1) Large and localized energy deposition in materials with high spatial resolution. (2) The materiality of the beam that can implant atoms into the target, which can endow the product with novel function. (3) Wide variety of secondarily produced radiation that enables sophisticated analysis of material bulk and surface. (4) Transmutability of material including nuclear reaction. The physical or chemical scheme, of course, depends on mass and energy of ions and characteristics of target materials. For radiation chemistry, phenomena related to (1) and (2) may be of primary interest among the above aspects.

The peculiarity related to large and localized energy deposition is sometimes called as Linear Energy Transfer (LET) effects. LET effects on radiation



chemistry have been studied extensively, and at present a lot of literature is available. Similar to other fields, for detailed information one can contact database services such as Chemical Abstract or INIS etc. University of Notre Dame provides web-site at <http://allen.rad.nd.edu/>. This chapter introduces a brief background on LET, some of the research activities and some technical aspects of ion beam radiation chemistry.

## 2. ENERGY DEPOSITION PROCESSES

An ion beam loses energy through interaction with target material. The energy deposition or energy loss in depth direction per unit thickness  $-dE/dx$ , where  $E$  is energy and  $x$  is depth, is defined as stopping power. The scheme of energy losses includes (1) excitation and transmutation of a nucleus, (2) radiative energy loss such as bremsstrahlung and Cerenkov radiation, (3) electronic energy loss, and (4) nuclear energy loss. The energy losses through (1) and (2) become appreciable in very high energy region only, therefore they may be out of the scope of this chapter. Stopping power related to radiation chemistry or materials science can be described in terms of electronic stopping power and nuclear one. The former is related to inelastic "collision", that is, ionization and excitation of target materials, and the latter is responsible for elastic collision, that is, displacement of atoms from the original sites. Electronic energy loss is predominant over nuclear for high energy ion, and the nuclear predominates over the electronic when ions become very slow. As mentioned later, electronic stopping power is much higher than nuclear for energy used in studies in radiation chemistry.

LET is, strictly speaking, different from stopping power. LET excludes contribution of energetic (for example, higher than 200 eV) secondary electrons, whereas stopping power considers every contribution. However, they are very close to each other in most cases of radiation chemistry, therefore many studies deal with them without distinction.

The energy deposition from ion to materials is spatially non-homogeneous. The non-homogeneity is a complex function of depth, time, and fluence. It can be considered in two aspects: non-homogeneity in depth (longitudinal, along an ion's path) and in radial (lateral or radial, around an ion's path) directions. Figure 2-1 schematically illustrates the non-homogeneous energy deposition happening stochastically [1, 2]. Compared to low LET radiation, an ion beam is less scattered and deposits energy to material at a high density per thickness. As well, in the center region around an ion's path, the density of energy deposition is high compared to the periphery.

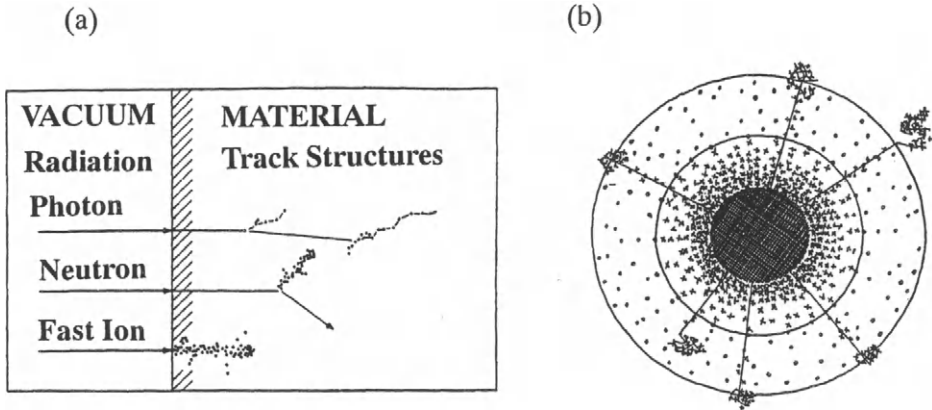


Figure 2-1. Non-homogeneous energy deposition in longitudinal or depth direction (a)[1, reprinted with permission, © 1995 International Atomic Energy Agency], and in lateral or radial direction (b)[2, reprinted with permission, © 1987 John Wiley & Sons]. For detail see the refs.

Non-homogeneity of energy deposition in depth originates from the fact that stopping power is a function of energy that varies with depth in the material. Stopping power can be generally described as shown in Figure 2-2a. The electronic stopping power,  $S$  takes the maximum at velocity of approximate  $v_B Z_2^{2/3}$ , where  $v_B$  is Bohr velocity  $2.19 \times 10^8$  cm/s, and  $Z_2$  is atomic number of target material, respectively. When the ions' velocity  $v$  is well below  $v_B Z_2^{2/3}$ ,  $S$  is proportional to  $v$ , and well above  $v_B Z_2^{2/3}$ ,  $S$  is roughly proportional to  $v^{-2} \log(v^2)$ . If one redraws the figure as a function of depth for high energy ions, the depth-profile of the stopping power should be as Figure 2-2b, which is sometimes called as Bragg curve. Because of high stopping power near the range, radiation effect is assumed to be peculiar compared to one under ordinary stopping power such as by electron beam. The value of electronic stopping power for high velocity ions can be obtained by Bethe's formula [3] :

$$S = 4 \pi Z_1^2 e^4 / (m_e v^2) N Z_2 \log_e(2m_e v^2/I), \quad (1)$$

where  $e$  is charge of an electron,  $m_e$  is static mass of an electron,  $Z_1$  is atomic number of incident ion,  $Z_2$  is atomic number of target material,  $N$  is the number density of electrons,  $v$  is velocity of ion,  $I$  is mean excitation potential of target, respectively. The data on mean ionization potential for elements are compiled, for example by Seltzer and Burger [4] or ICRU report [5]. Roughly it can be described as  $I$  (eV) =  $10Z_1$ . Corrections arising from chemical bonds are also found there. In the case of compounds, Bragg's additivity rule [6] is applicable

as far as electronic states are not influenced heavily. However, one should keep in mind again that Bethe's formula is applicable in limited case only, where ion's velocity is sufficiently high. On the other hand, electronic stopping power for slow ions was formulated by LSS [7] or Firsov [8] to be proportional to ions' velocity. In this case as well, one should keep in mind that the applicability of the formulae has strong limitation.

Nuclear stopping power,  $S_n$  for fast ions is similarly obtained as follows;

$$S_n = 2\pi Z_1^2 Z_2^2 e^4 / (M_2 v^2) N \log_e \{ 4M_1 M_2 E / [(M_1 + M_2)^2 E_d] \}, \quad (2)$$

where  $M_1$  is mass number of incident ion,  $M_2$  is mass number of target,  $E$  is energy of incident ion, and  $E_d$  is the displacement energy of target materials, respectively. As one can see by taking a ratio, nuclear stopping power is lower than the electronic by a factor of  $10^{-3}$ . For slow ions the nuclear stopping power is formulated by Lindhard et al [9].

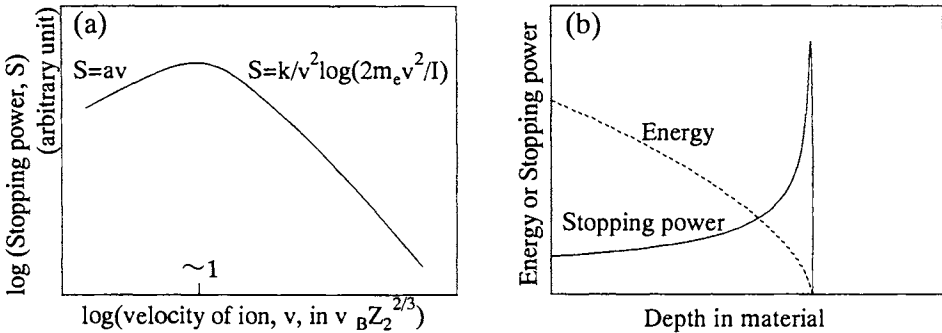


Figure 2-2. Schematic illustration of stopping power as a function of velocity of ion (a) or depth in material (b). Scale is in arbitrary unit.

Compiled data of stopping power and range are available by, for example, Northcliffe and Schilling [10], Ziegler et al [11], or Hubert et al [12]. Comparative studies have been also carried out [13]. Data for protons and alpha particles were published in the ICRU report [14]. Computational methods to evaluate stopping power have been also established. For example, TRIM (TRansport of Ions in Matter) code is one of the most commonly used software. For detail of the code, one should see Ziegler et al [11] or the web home page at the address of <http://www.research.ibm.com/ionbeams/hom.htm>. However, it should be noted that TRIM may not always be correct. Comparisons between energy deposition depth-profile by TRIM code and experimentally observed phenomena have been performed [15, 16]. TRIM recently has been updated to

“SRIM” (Stopping and Range of Ions in Matter). As another example, ELOSS code was established at Japan Atomic Energy Research Institute (JAERI), and the detail is published by Hata and Baba [17].

As an example, Figure 2-3 shows stopping power and range of proton,  $\alpha$ -particle and electron in polyethylene. Data were taken from ICRU reports [5, 14], where the total stopping power is the sum of electronic and nuclear for proton and  $\alpha$ -particle, or collision and radiative for electron respectively, and range is continuous slowing down approximation (CSDA) range. It is easily understood that ion beam gives higher stopping power and shorter range than electron and that nuclear stopping power is much lower than electronic one.

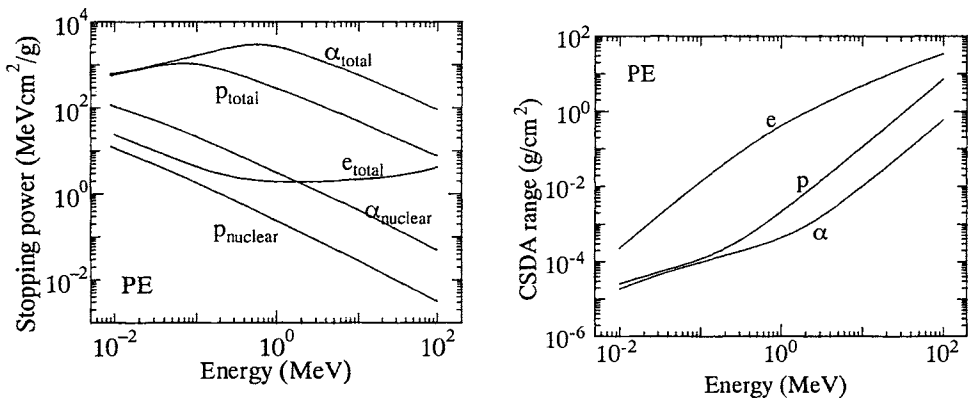


Figure 2-3. Stopping power (left) and continuous slowing down approximation (CSDA) range (right) of proton (p),  $\alpha$ -particle ( $\alpha$ ) and electron (e) in polyethylene. Data were taken from [14] for proton and  $\alpha$ -particle, and [5] for electron, respectively.

One may be interested in charge state of the ion. As suggested by Bohr[18], a high energy ion behaves as full-strip, and picks up electrons as it is slowed down, and eventually it becomes neutral. Charge distribution has also been compiled [19]. Velocity-dependent effective charge  $Z_{eff}$  has been well studied. Berkas’s formula [20], as given below, is often used. Some works use more complex and sophisticated formula.

$$Z_{eff} = Z_1 \{1 - \exp[-0.95v/(v_B Z_1^{2/3})]\} \quad (3)$$

Non-homogeneity of energy deposition in radial direction is of importance when elementary processes are concerned or fluence is low. Upon beam incident to material, energy deposition would cause track structure. Substructure is presumed: “(physical) core” at which an electronic ionization and excitation can

be created, and “penumbra” where the knock-on electron reaches [2]. The size of the core  $r_c$  is given as,

$$r_c = v/\Omega_p, \text{ where } \Omega_p \text{ is the plasma oscillation frequency } (4\pi N e^2/m_e)^{1/2}, \quad (4)$$

where  $N$ ,  $e$ ,  $m_e$  have the same definitions as previously and  $\Omega_p$  is in gaussian units. The size of penumbra  $r_p$  is determined by the maximum energy of secondary electron,  $2m_e v^2 (1 - v^2/c^2)^{-1}$ , where  $c$  is velocity of light. A table of  $r_c$  and  $r_p$  as a function of specific energy is available in [2]. It is expected that the energy density within the core is constant and that the density within the penumbra is a decreasing function of radial distance from the path,  $r$ . Average initial densities within core,  $\rho_c$  and penumbra,  $\rho_p$  at a fixed LET are also given as follows;

$$\rho_c = \text{LET}/2 (\pi r_c^2)^{-1} + \text{LET}/2 [2 \pi r_c^2 \log_e(e^{1/2} r_p/r_c)]^{-1} \quad (r \leq r_c), \quad (5)$$

$$\rho_p = \text{LET}/2 [2 \pi r^2 \log_e(e^{1/2} r_p/r_c)]^{-1} \quad (r_c \leq r \leq r_p). \quad (6)$$

In radiation chemistry, “chemical core” would be of importance [2]. The chemical core is in the medium size of core and penumbra, and effectively attributable to radiation chemical events depending on the competition of chemical reactions. The dose distribution around the path and related topics are extensively studied in radiation chemistry and radiation biology [21]. Experimental approaches to measure the radial dose distribution are also in progress [22], and it was found that the radial dose distribution follows  $r^{-2}$  law in the inner region of a critical distance and obeys  $r^{-3}$  law outside of the region. The energy deposition is initially non-homogeneous and will form intermediate species such as cation, electron, anion, excited states, etc. in spatially non-homogeneous way. The intermediates diffuse and the system approaches homogeneity as time elapses. The substructures as core and penumbra would be also diffused with increasing fluence. The macroscopically averaged dose could be evaluated as product of fluence and stopping power. However, if a substructure is presumed, microscopic dose could be high around the ions’ paths. This idea evoked a concept of micro-dosimetry. If the dose within the substructures as core and penumbra is sufficiently high, some radiation-induced events may be caused to a detectable level even if the macroscopically averaged dose is still very low. With increasing fluence, the tracks will overlap with each other, and diffuse the local unevenness in dose. Figure 2-4 schematically represents the distribution and the average of dose. After bombardment of fluence  $F$ , the total energy deposition (macroscopically averaged dose) is FS,

where  $S$  is stopping power, and the effectively affected area would be  $1 - \exp(-sF)$ , where  $s$  is cross section of substructure such as core and penumbra. Therefore the microscopically averaged dose within the substructure would be  $FS / [1 - \exp(-sF)]$ . As the curves in Figure 2-4b demonstrate, the microscopic averaged dose is almost constant and higher than the macroscopic average for low fluence, but it goes close to the macroscopic average with increasing fluence.

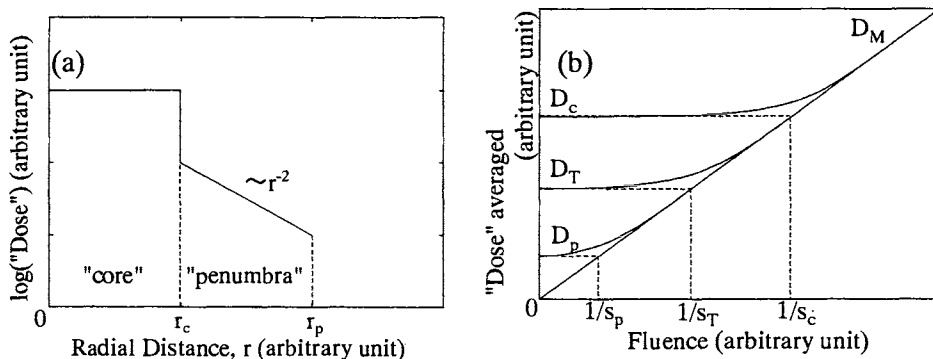


Figure 2-4. Distribution of "dose" around the ions' path (a) and averaged "dose" within track entities and whole cross section (b).  $D_M$  is macroscopically averaged dose at a fixed depth,  $D_M = FS$  where  $F$  is fluence and  $S$  is stopping power,  $D_p$  is averaged dose for penumbra,  $D_c$  for core,  $D_T$  for intermediate-sized track, such as chemical core, respectively. The  $s_c$ ,  $s_T$  and  $s_p$ , mean the cross section for core, track and penumbra respectively. Scale is in arbitrary unit.

### 3. EXPERIMENTAL TECHNIQUES

#### 3.1. Irradiation Sources and Facilities

Historically, fast or thermal neutrons from a nuclear reactor, fission fragment,  $\alpha$ -particles through nuclear reaction of neutron and  $^{10}\text{B}$ , natural  $\alpha$ -emitters such as Po and Cm, etc., have been employed as the irradiation sources for the study of LET effects in radiation chemistry. Nowadays, in addition to traditional sources, various kinds of ion accelerators are at an industrial stage, and a large number of facilities are ready for making studies using ion beam. The selection of the system depends on the object and characteristics of the target, that is, acceleration energy, current etc. For high-energy ion beam (typically higher than several MeV/u), cyclotrons or synchrotrons are used, and tandem, Van de Graff, or single-ended accelerators for medium energy. Ion implanters are used for low energy (typically less than a few hundred keV) and high fluence. In case of need, simultaneous dual or triple beam irradiations, or sequential irradiations are

are adopted to simulate specific radiation environment or to educe potential characteristics. Some examples of published ion beam facilities in the field of radiation chemistry are given below. Ion beam accelerators of High fluence Irradiation facility at the University of Tokyo (HIT) has two ion accelerators of Van de Graff and Tandetron, and beam lines for pulsing system and beam sweeper [23]. Takasaki Ion Accelerators for Advanced Radiation Application (TIARA) at Japan Atomic Energy Research Institute (JAERI) have an AVF cyclotron, a Tandem accelerator, a single-ended accelerator and an ion implanter. The detailed specifications of the facilities were published [24-28]. Various irradiation procedures are available, including uniform irradiation on wide area, vertical irradiation, irradiation under air, pulse irradiation, simultaneous dual or triple beam irradiation, etc. The irradiation facility at Oak Ridge National Laboratory (ORNL) has three Van de Graff accelerators, and multiple beam irradiation is available [29]. Heavy Ion Medical Accelerators in Chiba (HIMAC), at the National Institute of Radiological Sciences, Japan provides beam for scientific research as well [30]. It has LINAC as injector and synchrotron as the main storage ring [31].

### 3.2. Irradiation procedures, chambers or vessels

Elaborate irradiation procedures, vessels and analyzing techniques are also requisite for specific irradiation and measurements.

(1) For solid systems: Irradiations are carried out mostly under vacuum for beam transportation. Focused beam may cause undesirable temperature rise on irradiated specimen, or abrupt deterioration of vacuum. One can use defocused beam, by using a scatterer if necessary, but the uniformity could be sometimes dubious; therefore it is not always recommended. To avoid beam heating and abrupt gas evolution, beam scanning is often adopted for uniform irradiation on

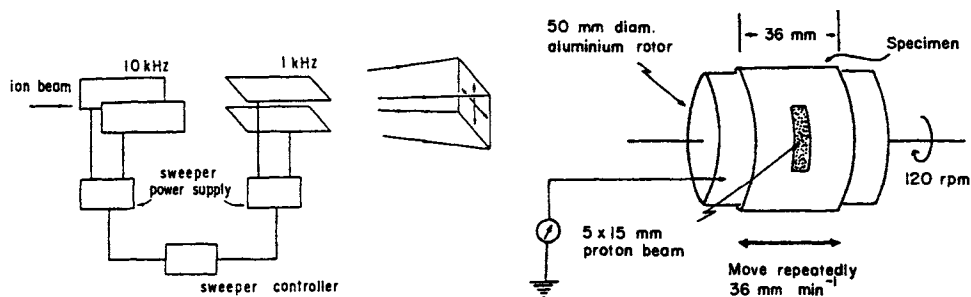


Figure 3-1. Beam scanning (left)[23, reprinted with permission, © 1989 Elsevier] and sample scanning (right)[34, reprinted with permission, © 1989 Elsevier].

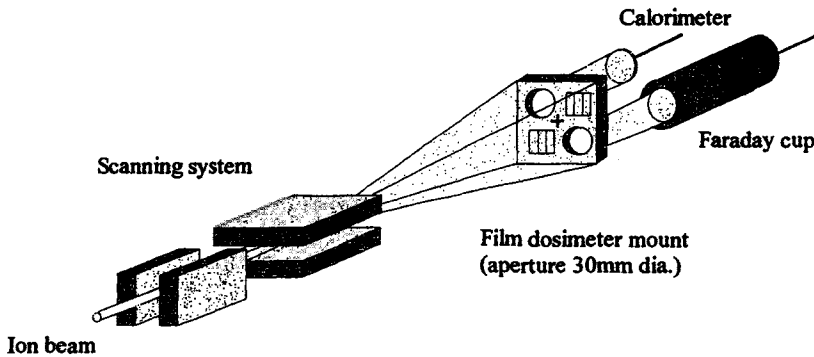


Figure 3-2. Example of fluence measurements method [36, reprinted with permission, © 1998 Elsevier].

materials with substantial dimensions [32, 33]. The scanning frequencies should be selected so that the beam does not draw a Lissajous figure. By using a rotating turret on which samples lie, several samples can be irradiated in a batch without breaking vacuum. Sample scanning by using a rotor is also adopted for uniform irradiation [34]. Figure 3-1 shows examples of beam and sample scanning. For biological systems, irradiation should be carried out sometimes under air [13], after energy loss by beam window (typically made of Ti) and air layer was evaluated. Beam current is monitored during irradiation, or before and after irradiation. Recently, a sophisticated procedure to measure fluence was developed as shown in Figure 3-2, by using calorimeter and Faraday cup simultaneously [36]. Ion beam pulse radiolysis system for solid target has also been established [37].

(2) For liquid systems: Time resolved-spectroscopy experiments have been carried out. Stable product analysis such as titration, electrolytic measurements and fundamental absorbance has been carried out also to determine the yield. Figure 3-3 shows a typical example of a beam targeting system [38], and an irradiation cell for pulse-radiolysis for absorbance measurement [39]. The ion beam is injected through a beam-window made of thin film of, for example, Ni, Ti, mica or Mylar (polyethylene terephthalate, PET) with the solutions stirred or bubbled. Ti-window is most recommended for less energy loss, high mechanical strength and resistance to heat and radiation. Charge is collected through a wire inserted into the cell. Temperature can be controlled if a thermister is attached to the cell. Fluorescence, photon-counting is advantageous over absorbance in achieving a significant signal, and the technique has been established as shown in Figure 3-4 with examples [40]. Usually, the emission intensity at a certain



wavelength is normalized to the peak of the time profile, but recently, a sophisticated procedure aligning two photo-multipliers vertically circumvents the uncertainty of the intensity [41].

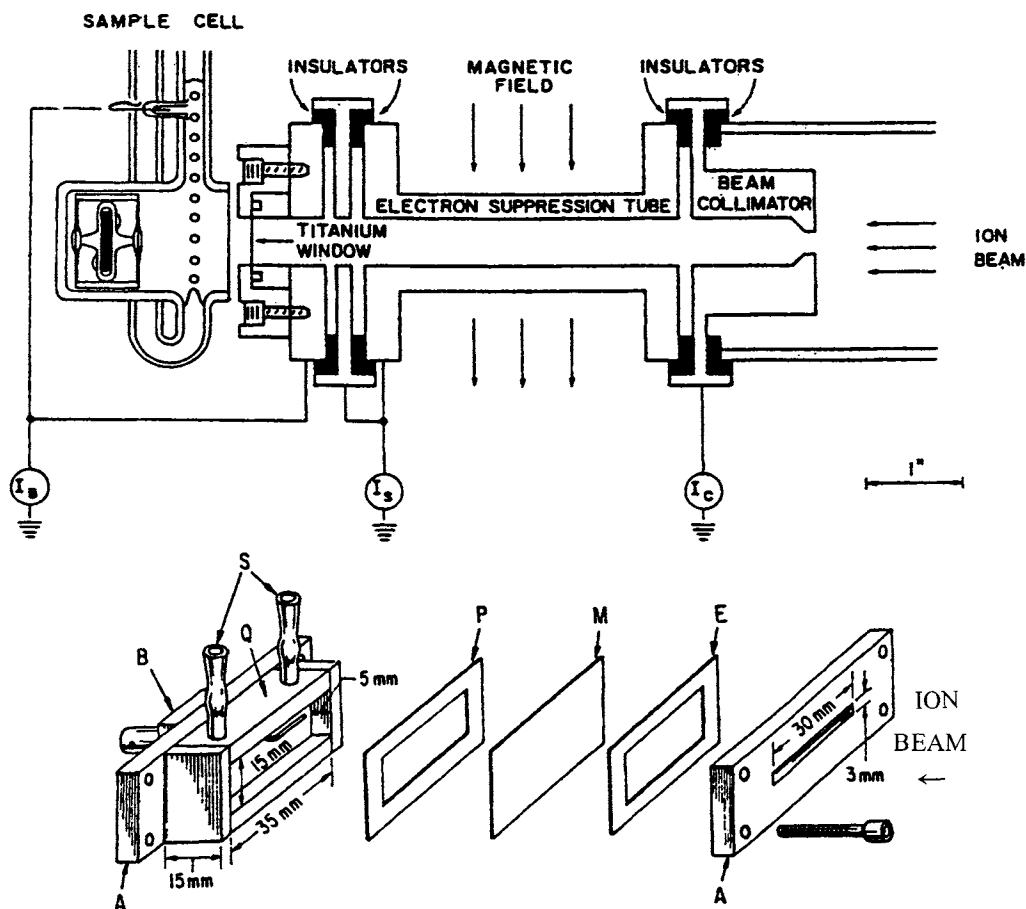


Figure 3-3. Typical targeting system (top)[38, reprinted with permission, © 1987 American Chemical Society] and irradiation cell for pulse radiolysis system (bottom)[39, reprinted with permission, © 1977 Radiation Research Society] (Q: quartz cell body; B: BNC connector, P: paraffin gasket; M: mica window; E: electrical tape gasket, A: aluminum frame; S: standard taper joint).

(3) For gas systems: The pressure inside the vessel should be well controlled and kept low. An example of a gas-containing vessel is given in Figure 3-5a [22]. Apertures serve as a differentially evacuating system and sample gas is admitted into the chamber through an automatically controlled leak valve. The pressure is

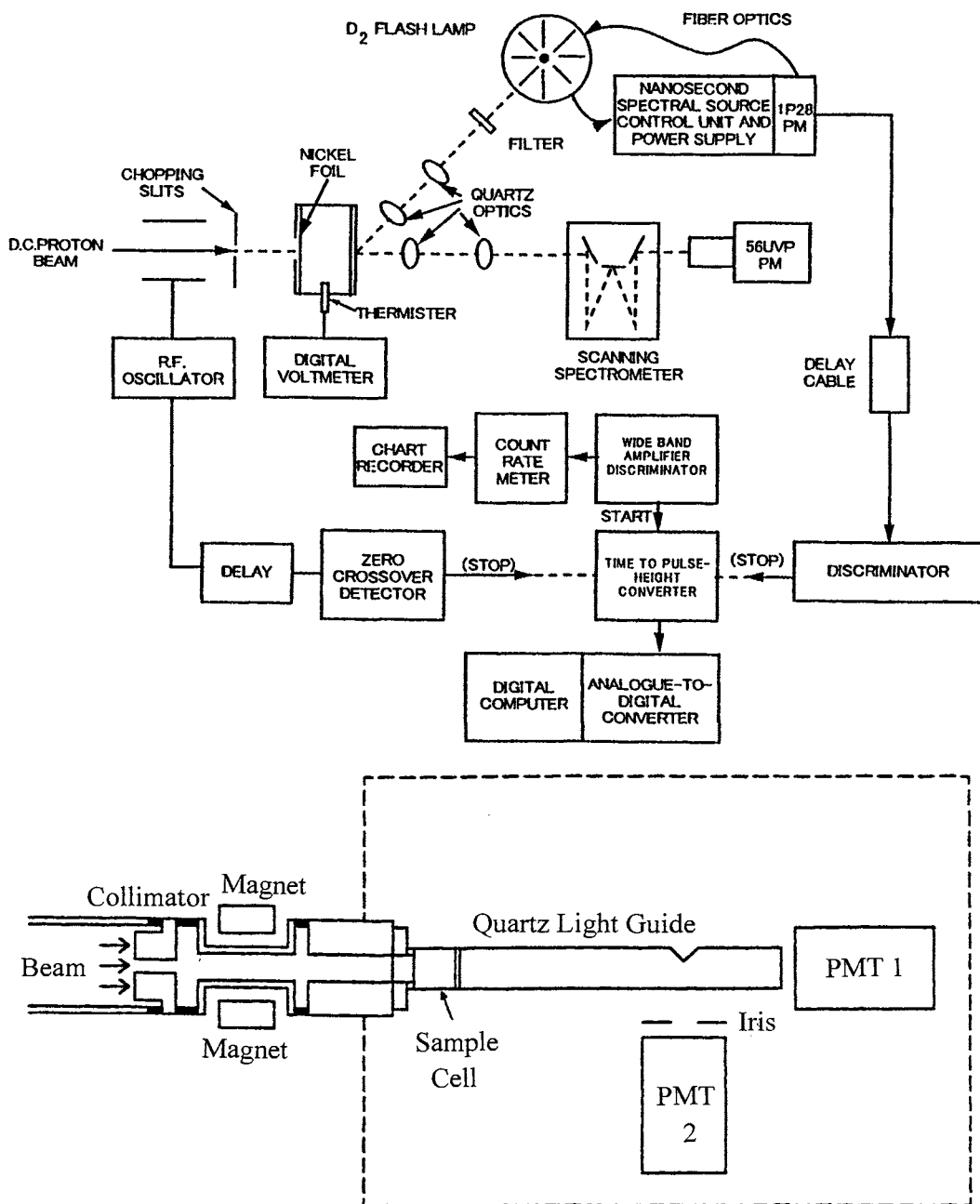


Figure 3-4. Examples of photon-counting system. Top: typical block diagram [40, reprinted with permission, © 1979 Institute of Electrical and Electronic Engineers]. Bottom: a sophisticated cell system to measure the absolute intensity [41, reprinted with permission, © 1996 American Chemical Society] (PMT: photo-multiplier).

measured with a manometer. Spatial non-homogeneity of energy deposition is analyzed by placing a wall-less ionization chamber, as described in Figure 3-5b, in the vessel.

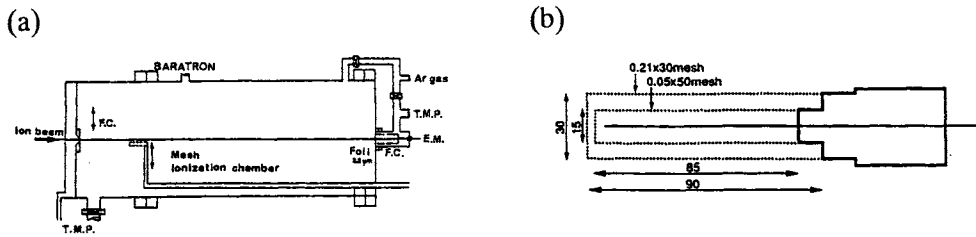


Figure 3-5. A cylindrical chamber for gas target (a) (F.C.: Faraday cup; T.M.P.: turbo-molecular pump; E.M.: electrometer), and wall-less mesh ionization chamber (b) (unit in mm) [22, reprinted with permission, © 1997 Elsevier].

### 3.3. Stable Detection or Analyzing Technique

(1) Product analysis: Time resolved measurements such as pulse radiolysis system were described in the previous section. For product analysis, most of ordinary analyzing procedures in traditional radiation chemistry can be applied, such as changes in molecular weight, gel fraction, infrared or ultra-violet spectroscopy. In the case of ion beam, elaboration to characterize surface or very thin layers has been tried. For example, development of spin coated thin film is used for monitoring gel fraction [42]. Another characteristic may be depth dependent phenomena. Depth-profile of optical absorption is performed as

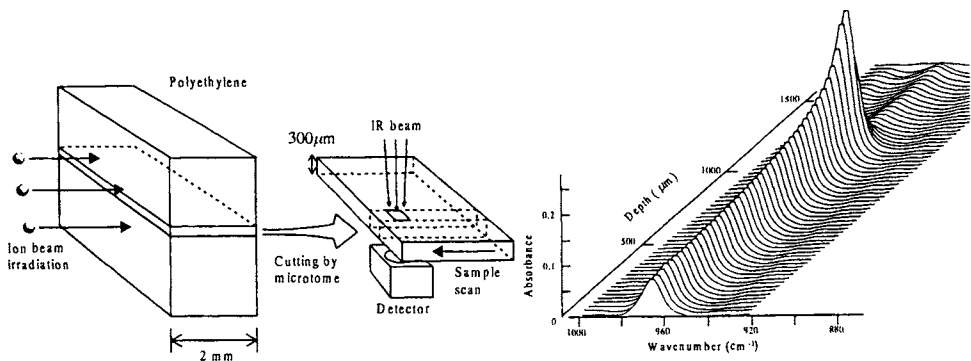


Figure 3-6. Depth-profiling and example of data for infrared absorbance [16, reprinted with permission, © 1997 Japan Atomic Energy Research Institute].

shown in Figure 3-6 [16]. A stepping motor facilitates mapping, and depth-profile of infrared absorbance similar to Bragg curve is obtained. Irradiation on stacked thin layers has also been well carried out to monitor depth-dependence of radiation chemical events. The spatial resolution depends on the thickness of a layer.

(2) Practical, material mechanical properties: Most of the traditional testing methods have been applied similarly to ordinary cases. Electronic properties are well monitored through change in resistivity at surface or in bulk. Optical property is often described through transmittance of light at a certain wavelength. Mechanical property tests, such as tensile and flexural tests, are widely accepted in monitoring the radiation deterioration of materials. Nano-indentation, a typical method in characterization of surface of inorganic materials, has been successfully applied for ion-irradiated organic systems [43].

## 4. WATER AND AQUEOUS SOLUTIONS

### 4.1. Historical Review

In order to understand the development of ion beam radiation chemistry in aqueous solutions, it is worthwhile to review its history. Before the World War II, the effects depending on the type of radiation had been measured in the radiolysis of aqueous solutions; the  $H_2$  gas evolution in  $\alpha$  radiolysis is much larger than that in low LET radiolysis. During the World War II this was successfully explained by the concept of the smaller radical yields ( $e_{aq}^-$ , H and OH) and larger molecular yields ( $H_2$  and  $H_2O_2$ ) in high LET radiolysis, leading to the idea of the spur and track structure [44, 45]. At that time  $\alpha$ -emitters such as Po were solely used for ion beam irradiation. In 1950s cyclotrons and Van de Graaff accelerators were introduced for the ion beam radiolysis of aqueous solutions and organic liquids at Brookhaven (BNL) and Argonne National Laboratory (ANL) in USA. In aqueous solutions, two types of subjects, G-value determination of the Fricke dosimeter and neutral solutions, had been carried out using continuous wave (CW) beam. G-values of the products in neutral aqueous solutions irradiated with ion beams determined at BNL are shown in Table 4-1 [46]. It is clear that the radical yields are decreasing while molecular yields are increasing with an increase in LET value of ion beams. Since the  $G_{H_2}$  is much larger than the  $G_{OH}$  in high LET radiolysis, it is quite understandable that  $H_2$  gas can be accumulated. On the contrary, in the case of low LET radiolysis, the steady state concentration of  $H_2$  is very low and controlled by the higher value of  $G_{OH}$  as compared with the  $G_{H_2}$ .

Table 4-1. Dependence of the yields of radiolysis products from neutral water on LET [46].

LET / eVnm <sup>-1</sup>	G						
	-H <sub>2</sub> O	e <sub>aq</sub> <sup>-</sup>	OH	H	H <sub>2</sub>	H <sub>2</sub> O <sub>2</sub>	HO <sub>2</sub>
0.23	4.08	2.68	2.72	0.55	0.45	0.68	0.008
12.3	3.46	1.48	1.78	0.62	0.68	0.84	
61.0	3.01	0.72	0.91	0.42	0.96	1.00	0.050
108.0	2.84	0.42	0.54	0.27	1.11	1.08	0.070

To get highly reproducible results, it was found that the average ion beam current had to be limited to nA. In addition, the strong stirring of the liquid is also necessary to avoid the accumulation of the decomposition products at the surface of the irradiation window (see experimental section) [47]. Another important concept is a differential (segmental or thin-target) yield [47]. Normally an ion beam is injected through the thin window and it loses the whole energy in the medium. The observable yield of the products of interest is the sum of those produced by the irradiation with different energy of the beam slowing down along the path and, thus, it becomes the average yield. As a first step to derive the G-value at certain energy or LET value, the differential yield, the precise measurement of the total yield as a function of wide range of energy of the particles should be done. The polynomial fitting is applied to the result of  $G_0E_0$  plot, where  $G_0$  stands for the average G-value obtained using the beam energy of  $E_0$ . Then, the differential  $G_i$  value can be obtained by the differentiating the fitting curve as  $G_i = d(G_0E_0)/dE_0$ . This procedure would be easily understood in a series of figures as later shown in Figure 4-1. It is noted that the kinetic diffusion model [48] was introduced around 1960 in order to explain the change of the yield depending on the LET.

In the late 1970s pulse radiolysis technique was introduced in ion beam radiation chemistry of aqueous solutions. A sophisticated system using 3 MeV protons in a pulse of 1 ns was constructed at Harwell and the first direct observation of highly time resolved track reactions of hydrated electron was reported [49]. At the same time, the yields of the transient products including hydrated electron at various positions along the penetration range were measured with a few tens microseconds pulsed deuteron and helium ions from a cyclotron at ANL [39]. The yields were converted to the data as a function of energy, namely LET. Recently, a microsecond pulse radiolysis system with 6 MeV <sup>1</sup>H<sup>+</sup> and 24 MeV <sup>4</sup>He<sup>2+</sup> beams was constructed at HIMAC (Heavy Ion Medical Accelerator in Chiba) [30], where the yield of the transient as a function of scavenger capacity of OH was determined. In addition, methyl viologen (MV<sup>2+</sup>) solution was proposed as a useful dosimeter for both ion beam pulse and steady state radiolysis [50]. Swift heavy ions higher than GeV were also employed for the pulse radiolysis study at GANIL (Grand Accélérateur National

d'Ions Lourds, Caen/France) and the formation of  $e_{aq}^-$  and  $O_2^{\bullet-}$  were detected [51].

#### 4.2. The Fricke Solution

The most intensively investigated subject in aqueous solutions is the Fricke dosimeter; 10 or 1 mM  $Fe^{2+}$  in 0.4 M  $H_2SO_4$  because of the clear reaction mechanism and its popularity in radiation chemistry. The dosimeter can be used under aerated and deaerated conditions and their yields of  $Fe^{3+}$  can be expressed by the following equations [44].

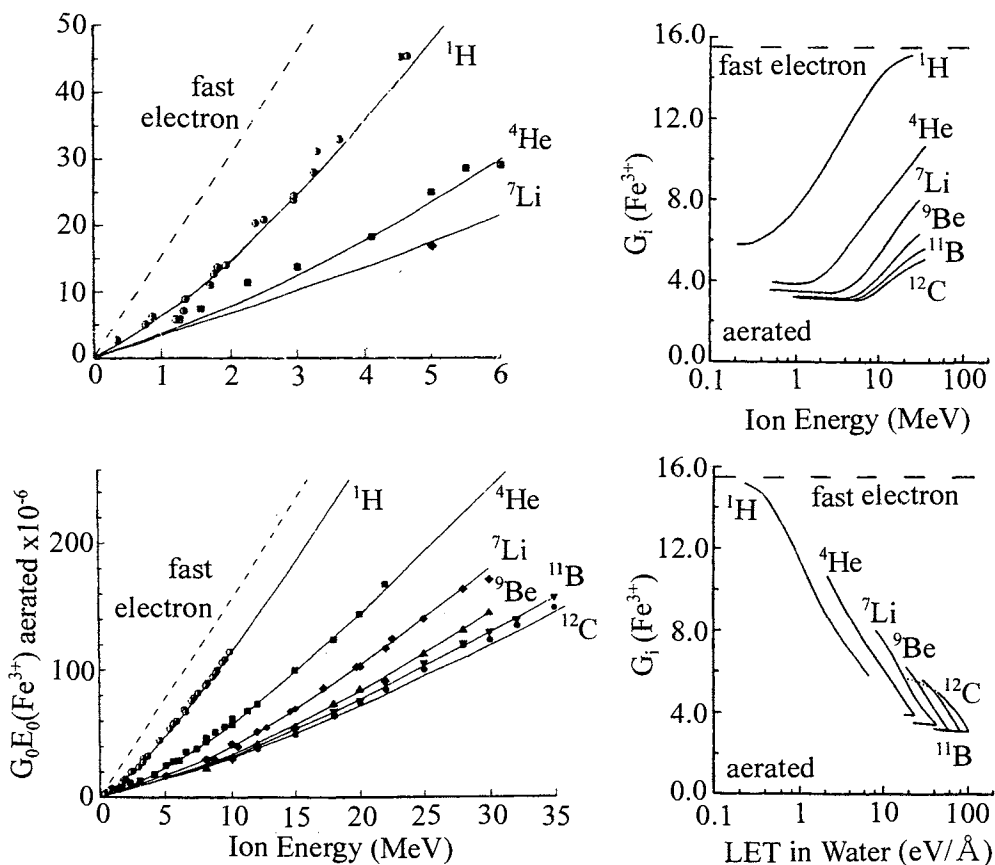


Figure 4-1. Ferric ions produced (left) and differential yields (right) in aerated solution as a function of initial ion energy and LET [54, reprinted with permission, © 1987 American Chemical Society].

$$G(\text{Fe}^{3+})_A = 3(G_{e^-_{\text{aq}}} + G_{\text{H}}) + G_{\text{OH}} + 2G_{\text{H}_2\text{O}_2} \quad (7)$$

$$G(\text{Fe}^{3+})_D = (G_{e^-_{\text{aq}}} + G_{\text{H}}) + G_{\text{OH}} + 2G_{\text{H}_2\text{O}_2} \quad (8)$$

where A and D indicate the aerated and deaerated solution, respectively, and the yield of the water decomposition products are described as  $G_{\text{H}}$ ,  $G_{\text{OH}}$  etc. Once one obtains the experimental data, the values of  $(G_{e^-_{\text{aq}}} + G_{\text{H}})$  and  $(G_{\text{OH}} + 2G_{\text{H}_2\text{O}_2})$  can be derived separately. The value of  $(G_{\text{OH}} + 2G_{\text{H}_2\text{O}_2})$  is equivalent to the  $G$ -value for the consumption of water,  $G(-\text{H}_2\text{O})$ , when the formation of  $\text{HO}_2\cdot$  can be neglected.

The Fricke solution has been the most popular subject of ion beam radiation chemistry in aqueous solutions, and proton, helium ions, heavier ions including particle energy higher than GeV [52] and even uranium ions have been employed [53]. Some typical results are shown in Figure 4-1 [54]. The radical yields increase and the water decomposition decreases with increasing the LET of the particles. At a glance, it is clear that the value is strongly dependent on both LET and the kind of particles.

Another problem that was addressed is to explain how  $\text{HO}_2\cdot$  is formed and why its yield is increasing with increase of the LET. Recently, the proposed mechanisms were compared and discussed [55].

### 4.3. Neutral Solutions

From practical viewpoints of problems induced by ion beam irradiation such as radiation biology and medicine, and water chemistry of coolant in the nuclear power plants, understanding of the radiation effects in neutral solution is inevitably important. In low LET radiolysis, in order to determine the water decomposition products, product analysis after the irradiation in the presence of scavenger is normally employed. However, in high LET radiolysis, the yield is strongly dependent on the scavenging capacity,  $k[\text{S}]$ , due to the spur reactions along the track. Here,  $k$  and  $[\text{S}]$  are rate constant of the scavenging reaction and the concentration of the scavenger, respectively. Most of the reported evaluation of the water decomposition work has been carried out at the scavenging capacity around  $10^6 \text{ s}^{-1}$ , similar to the low LET radiolysis conditions. Some typical data are summarized, as already shown in Table 4-1. It is noted that the primary yields of water decomposition products can be defined and have been measured in low LET radiolysis. However, it is known that the primary yields in high LET radiolysis are hardly measured because track reactions occur continuously for longer time. The values can be only defined and measured at a certain value of  $k[\text{S}]$ . Recently, the measurements of the scavenging yield as a function of  $k[\text{S}]$  have been reported in glycylglycine [56] and formic acid [57] solutions because

this is an equivalent data of time resolved behavior [58]. It was clearly pointed out that the stability of the product after the scavenging reaction plays an important role [50]. Much data is still needed in neutral solutions as compared with the accumulation for the Fricke solution.

Relevant to water radiolysis in nuclear reactor, G-values of the water decomposition by fast neutrons have been determined by using a fast reactor at elevated temperatures [59]. Since fast neutron radiolysis is equivalent to proton radiolysis because of the recoil proton formation through the elastic collision of fast neutrons with H<sub>2</sub>O molecules [60], an alternative approach as a model experiment is the ion beam radiolysis with different LET particles from accelerators at elevated temperatures [61].

#### 4.4. Comparison with Simulation

The radiolysis of aqueous solutions has a clearer picture compared to other liquids. The characterization of ion induced phenomena in aqueous solutions has been a subject for theoretical approaches because the prediction is necessary from the calculation, for example, DNA damages in biological system. In place of the kinetic diffusion model, Monte Carlo methods have been also applied to ion beam radiolysis and recent status was reported [62].

## 5. ORGANIC LIQUIDS

### 5.1. Aromatic Hydrocarbons

In 1950s cyclotrons were introduced for radiation chemical studies and protons, deuterons and He<sup>2+</sup> ions became available as well as particles from Po-210 and <sup>10</sup>B(n, α)<sup>7</sup>Li. In the ion beam radiolysis of aliphatic hydrocarbons, it was observed that G(H<sub>2</sub>) does not change significantly [63]. On the contrary, in high LET radiolysis of benzene, a clear increase of the G(H<sub>2</sub>) was observed. Formation of acetylene was also observed and the ratio of G(H<sub>2</sub>)/G(C<sub>2</sub>H<sub>2</sub>) was determined independent of ions as 1.8-2.0 [64, 65]. At that time, from a practical point of view, much attention had been paid to the thermal stability and radiation resistance of aromatic compounds such as biphenyl and terphenyl as the candidates of the organic coolants for nuclear reactors. Intensive work was made not only with γ-rays but also fast neutrons and α particles [66]. In benzene radiolysis, experimental results clearly showed the higher G(H<sub>2</sub>) with decreasing energy of ion beams and it was speculated the importance of the charge exchange cycle at the end of the range for this increase [67].

Precise and systematic measurements were made with <sup>1</sup>H, <sup>4</sup>He, <sup>7</sup>Li, <sup>9</sup>Be, <sup>11</sup>B and <sup>12</sup>C, as shown in Figure 5-1. The G(H<sub>2</sub>) is strongly dependent on the particle type and energy, and reaches up to 0.7 in <sup>12</sup>C radiolysis, which is much larger



than the value of 0.038 in  $\gamma$ -radiolysis. The origin of the large  $H_2$  evolution is evaluated to be coming from higher order effects: interactions between excited states and ions in the core part of the track, but not from charge exchange processes [68].

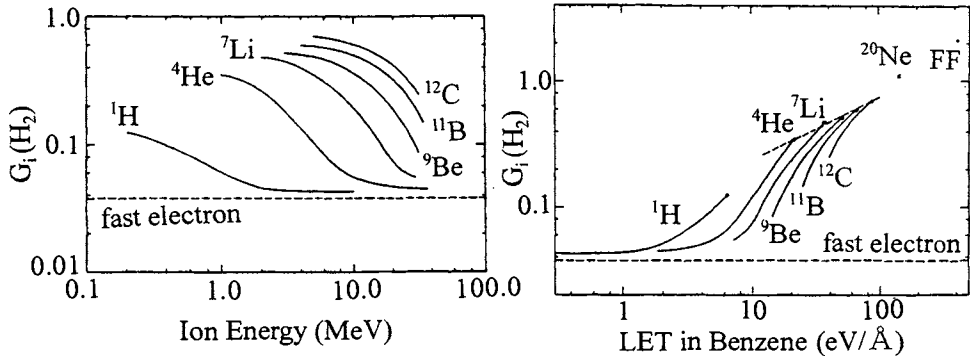


Figure 5-1. Variation of the differential molecular hydrogen yield  $G_i(H_2)$  with ion energy (left) and LET (right) for the various ions [68, reprinted with permission, © 1984 American Chemical Society].

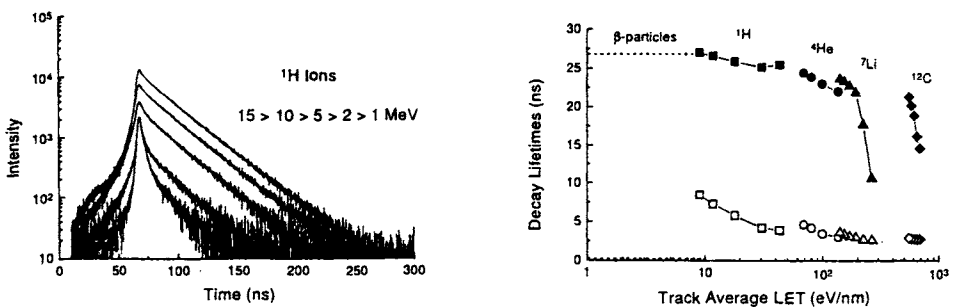


Figure 5-2. Fluorescence intensity from neat liquid benzene irradiated with 1-15 MeV protons as a function of time (left), and lifetimes for the dual exponential deconvolution (right) [41, reprinted with permission, © 1996 American Chemical Society]. Solid symbols are for the slow component and open symbols are for the fast component.

Emission measurement from the excited states is also a powerful method to investigate the ion beam radiation chemistry because a very sensitive time resolved photon-counting technique can be applied. In 1970s, temporal behavior of the emission from benzene excited states in 40 mM benzene in cyclohexane irradiated with pulsed proton and  $^4\text{He}$  ion particles was measured and compared with UV pulse irradiation. It was found that immediately after the irradiation there is a short decay ( $< 10$  ns) followed by a longer decay corresponding to the life-time of the benzene excited states (26-28 ns). The fraction of the shorter decay component increases with increasing LET of the particle. This was explained by a quenching mechanism that radical species formed in the track core attack and quench the benzene excited states, which would take place only shorter period less than 10 ns after irradiation [69].

While the photon-counting method is powerful, the conventional one hardly compares the absolute emission intensities induced with different particles. This weak point was overcome by using the start and stop pulses from original emission and benzene excited states and excimers in the irradiation with  $\gamma$ -ray from  $^{90}\text{Sr}$ ,  $^1\text{H}$ ,  $^4\text{He}$ ,  $^7\text{Li}$  and  $^{12}\text{C}$  particles were precisely inspected and compared from not only temporal behaviors but also emission yields. The emissions were expressed by using two exponential decay components: fast and slow, as shown in Figure 5-2. In the Figure, it is clear that the total yield is changing with increasing LET not in a simple manner [41]. Other emission studies were reported and a clear difference on magnetic field effect was also detected [70, 71].

## 5.2. Aliphatic hydrocarbons

As no large difference of  $G(\text{H}_2)$  between low LET and ion beam radiolysis was observed [12], as mentioned before, much interest has been paid to aromatic hydrocarbons. In 1990s, precise analysis was reported on the radiolytic products induced by irradiation of cyclopentane [73], cyclohexane [74] and cyclooctane [75] with low LET and heavy ion beams ( $^1\text{H}$ ,  $^4\text{He}$ ,  $^{12}\text{C}$  and  $^{16}\text{O}$ ). The combination of gas chromatography and mass spectroscopic analysis enabled to detect the  $\mu\text{M}$  level products after the irradiation with 250Gy to avoid the secondary reaction of the products. Scavenging methods by using  $\text{I}_2$  as a radical scavenger were also used. Before the introduction of the results, the basic idea will be briefly presented.

During the irradiation of liquids, both ionization and excitation occur and its distribution is strongly affected by the LET value of radiation employed. In liquid alkanes, geminate ion recombination reaction takes place in the time range of one to ten ps [76], leading to the formation of the excited states. The excited states of alkanes have lifetimes of around 1ns and decay to give mainly  $\text{H}_2$  and alkene products [77]. In ion beam radiolysis of liquid alkanes, at ns after

the energy deposition, radicals, H atoms, H<sub>2</sub> molecules and alkenes would be formed locally and densely, reflecting the initial spatial distribution of the energy deposition. Therefore, the variation of the final products in high LET radiolysis is expected to be strongly influenced by the intra-track reactions of the transient species. For the first approximation, the initial yields of the products would be the same irrespective to the type of radiation employed. Here, it is noted that the alkene products are formed not only through the dissociation of the excited states but also the disproportionation reaction of radicals and, thus, reliable evaluation of the formation ratio of dimer to alkene in the disproportionation reaction is essential for the product analysis. When I<sub>2</sub> is added to the system, radical species are scavenged and the time scale is defined as the inverse of the scavenging capacity, (k[S])<sup>-1</sup>. The rate constants of I<sub>2</sub> reaction with various alkyl radicals have been determined to be around 10<sup>10</sup> M<sup>-1</sup>s<sup>-1</sup> [78]. At very low concentration such as 0.1mM I<sub>2</sub>, the time of the scavenging reaction is μs and only radicals remained after the intra-track reactions would be scavenged. With increasing concentration of I<sub>2</sub>, scavenging reaction competes more effectively with the intra-track reactions. From the relations between scavenged yield and I<sub>2</sub> concentration, one can compare and discuss the degree of the intra track reactions in the radiolysis with different ion beams.

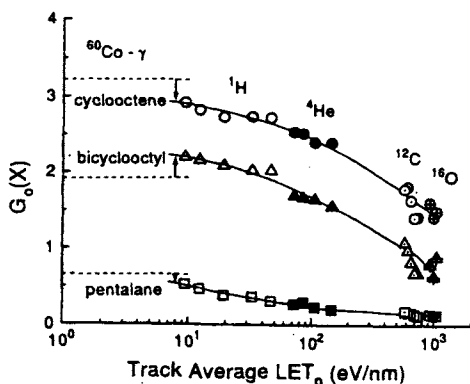


Figure 5-3. Integral  $G_0$  values for the production of cyclooctene, bicyclooctyl and pentalane in neat cyclooctane as a function of track average LET<sub>0</sub> [75].

(reprinted with permission, © 1995 American Chemical Society)

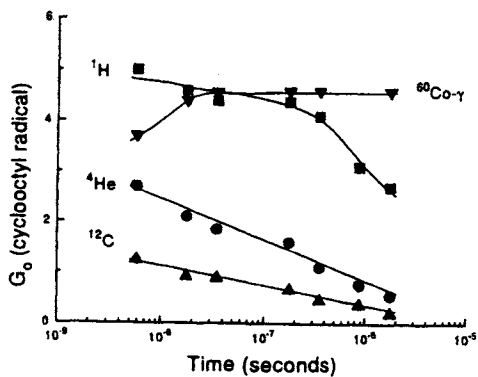


Figure 5-4. Temporal dependences of the integral  $G_0$  values for the production of cyclooctyl radicals in the track of the various particles [75].

The radiolysis of cyclooctane with different kinds of radiation was reported. In Figure 5-3, variation of the integral yields of cyclooctene, bicyclooctyl and pentalane as a function of the integrated  $LET_0$  is shown. The pentalane is assumed to be coming from the dissociation of the excited states [79]. The initial yield of the products is decreasing with LET and strongly dependent on the LET value, which seems contrary to the assumption that initial yields are independent of LET. From the  $I_2$  scavenging experiment the concentration change of the cyclooctyl radical as a function of time was evaluated (Figure 5-4). While almost 70% of the cyclooctyl radicals survive until a few microseconds in  $\gamma$ -radiolysis, the yields in carbon and oxygen radiolysis are about an order of magnitude lower. The concentration of the cyclooctyl radical in the track core in radiolysis with carbon ions was evaluated as an order of 1M and the importance of the mixing of geminate ion pairs in high LET radiolysis was also pointed out [75]. Ion beam radiolysis of ketone compounds were reported elsewhere [80].

## 6. POLYMERIC SYSTEMS

Polymeric systems have been one of principal fields in radiation chemistry since its inception. Its importance will remain unchanged when new radiation becomes widely available. Ion-beam-induced radiation chemistry in polymeric systems has been studied extensively. Below examples are given. The most comprehensive conference covering this field may be "IRaP" (Ionizing Radiation and Polymers) conference; the proceedings of this biennial meeting are available as a special volume of Nuclear Instruments and Methods in Physics Research part B (as of 1999) [81, 82]. This section describes two aspects of ion beam radiation chemistry in polymers: one is fundamental-oriented and the other is application-oriented.

### 6.1. Fundamental-oriented research activities

#### (1) Time Resolved Spectroscopy

Time resolved spectroscopy has developed assignments of intermediate species in radiation chemistry as revealed in the other sections. However, because solid polymers are less transparent, the works obtained so far seem to be limited mainly to polymer solution systems or liquid model-compounds. The lifetime of intermediates depends on LET; the fluorescence lifetime of n-dodecane is shorter for higher LET radiation [83], which was studied as liquid model compounds for polyethylene. The observation is attributed to scavenging upon encountering of intermediates. Light emission from excimers of solid polystyrene has constant lifetime irrespective to LET [84], whereas polystyrene

solution in cyclohexane showed shorter lifetime for high LET. By investigating effect of polymer concentration, the difference in LET dependence is attributed to mobility of intermediates. Ion beam pulse radiolysis on polysilane films is also in progress [37].

## (2) Product Analysis

The final products on polymeric systems are cross-linking between chains, scission of chain and double bond formation, stable radical formation, gas evolution, etc. The dependence of these radiation chemical yields on stopping power or other suitable parameters to describe beam is of interest. The probability of cross-linking for polystyrene [41], polyethylene [85] and polysilanes [86] increases with LET. On the other hand, the probability of scission for polymethylmethacrylate [87] decreases with increasing LET. These observations are attributed to, at least to a certain degree, increased probability of interaction between intermediates. Conversion from scission type to cross-linking type is confirmed for polysulfone [34, 85] and polysilanes [88]. Temperature-rise during irradiation is anticipated in the former case because polysulfone undergoes gel formation by  $\gamma$  rays at elevated temperature [89]. However, the pure LET effect is observed in the latter case as temperature effect is discriminated by using polymers that undergoes scission on  $\gamma$  irradiation at elevated temperature [90]. Double bonds formed in polyethylene showed similar depth profile as energy deposition by TRIM for fast ion but deviated for slow ion, and the yield of double bonds is constant for low LET ions and  $\gamma$  rays, but less for high LET [16]. TRIM code should be appropriate for fast ions but may still need some modification for slow ions. Radiation-induced coloration in UV region of cellulose tri-acetate become less sensitive compared to low LET radiation [91] while aromatic polymers such as polyethylene terephthalate and poly-ether-ether-ketone showed the opposite tendency [92]. The constant yield to a certain LET and change in yield at higher LET has evoked the idea of threshold LET, at which intra-track interaction of intermediates can occur along the ions' path [91]. Yield of stable radicals in alanine goes down with increasing LET [93]. Evolution of gaseous products as  $H_2$  and hydrocarbons from polymer is slightly enhanced by high LET [94].

Track radius, corresponding to chemical core in the previous section, is discussed from fluence-dependence of radical saturation [95], convergence of molecular weight distribution [88], and decay of optical density [96], under the assumption that inter-track overlapping would affect these phenomena. The track radius thus evaluated ranges from a few to several dozen nanometers, and increase with increasing LET.

However, the general tendency seems that, in despite of large difference in stopping power, the yield is influenced less profoundly. Furthermore, the

stopping power can not be the universal parameter though it is still “good” one, that is, even at a fixed stopping power, the velocity of ions can severely affect the irradiation effects [41, 97]. The similar example was already found for liquid hydrocarbons as seen in the previous section [68]. These findings have evoked the concept of “radiation-quality” effect, as a natural extension of LET effect.

## 6.2. Application-oriented research activities

### (1) Ion-beam induced modification of polymeric materials

This would be the most fascinating aspect of ion beam irradiation. Remarkable successes have been achieved, and examples are given below.

(a) Mechanical property: Mechanical hardness of polymers can be harder even than steel by ion beam irradiation. Abrasion resistance is also greatly improved [98]. The performance is a function of stopping power of incident ions and fluence. Melting behavior of poly (ether-ether-ketone) is improved [99]. These improvements are due to heavy cross-linking. Excellent performance against abrasion demonstrates that application of treated polymer for artificial prosthesis is promising [100].

(b) Optical property: Reflective index of transparent polymer, such as polymethylmethacrylate [101] and polycarbonate [102] was increased by ion bombardment and can be controlled. Changes in chemical bonds including conjugate or double bonds would be responsible. This technology can be applied for optical wave-guide etc.

(c) Surface modification: On ion irradiation, contact angle of silicone or polystyrene onto liquid drop decreases showing adaptability of the surface to the solvent is improved [103]. Various surface analyses were examined, and introduction of polar or hydrophilic groups to the surface was found to be effective. Adaptability to water, for instance, shows promise for usage as artificial blood vessel [104].

(d) Synthesis of particle track membrane: The surrounding area around ions' tracks becomes sensitive to chemicals such as alkali solutions. Pores are derived on etching [105], and the number density and size of the pores can be successfully controlled. Porous membrane thus synthesized is promising, for example, as environmentally intelligent materials [105], material [106] or gas separator [107], particle detector [108] etc. Successful results have been obtained mainly for polycarbonate [109] and polyimide [110].

(e) Electrical property: Insulating polymers become electrically conductive upon ion irradiation [111]. This is due to partly carbonization of the surface, and partly implantation of conductive impurities. Formation of novel junction in conductive polymers can be possible and would be useful as well.

(f) Superfine surface patterning: Application of ion beam is gaining much

attention in microelectronics including lithography as well. High density excitation by ion beam irradiation has possibility to pattern the surface more precisely than thermal ablation. Proton beam can tailor resist materials at a higher sensitivity per particle than electron [112].

## (2) Ion-beam induced deterioration of polymeric materials

Radiation resistance of polymer materials is of critical importance when the materials are applied in radiation environments. To  $\gamma$  rays or electron beams, the radiation resistance is well studied, especially by JAERI [113] and CERN [114]. Polymeric materials will be applied for space or a fusion reactor as constructing or insulating materials. The materials are subjects to “in-conventional” radiation such as protons, heavy ions, and neutrons having high LET to materials. With this fact, radiation resistance to high LET radiation would be different from that to low LET radiation. However, the underlying radiation chemical effects that cause deterioration are cross-linking and/or main chain scission, therefore microscopic and macroscopic effects have a close correlation with each other.

Change in mechanical properties is less dependent on LET for aliphatic polymers when the irradiation effect is described as a function of dose [115], where the dose is macroscopically averaged in a sense of the previous section. For aromatic polymers on the other hand, difference in degradation behavior in tensile tests was observed; ion beam caused less deterioration compared to electron beam [85]. Therefore appearance of LET effects depends severely on characteristic of the target polymers, and “aromaticity” is pointed out, because energy dissipation due to phenyl ring may be effective. This interpretation seems to be still controversial, because aromatic polyimide showed no LET dependence in tensile test [116]. Deterioration of optical thermal properties of polymer based temperature-controlling films for artificial satellites were examined by using particle accelerators on the ground and the radiation resistance was demonstrated [117].

Neutron irradiation of materials itself is a well-established field. To study the susceptibility of materials around nuclear plants, articles are well found in journals related to nuclear materials. Irradiation in a nuclear reactor is carried out, however with some exception, the beam provided is combination of  $\gamma$  rays and neutron beams. Therefore one should be prudent in evaluating dose. Neutron loses its energy through nuclear collision because of electric neutrality. For organic materials, neutrons can make light mass nucleus recoiled, such as hydrogen. Based on this speculation, neutron irradiation on polymer materials can be simulated by proton irradiation. For example, proton beam (30 MeV) irradiation on glass fiber reinforced epoxy was carried out and it was found that deterioration behavior was identical between proton 30 MeV and  $\gamma$  rays [118]. It

agrees with a finding that neutron irradiation on composites showed the identical deterioration as far as the reinforcing glass does not contain boron that generates  $\alpha$  particles and dosimetry was carried out properly [119].

### Acknowledgement

Y. K. has been supported partly by a project of JSPS-RFTF 98P00901 and a Grand-in-Aid for Scientific Research (B-10480115) of the Ministry of Education, Science, Sports and Culture, Japanese Government.

### REFERENCES

- [1] H. G. Paretzke, D. T. Goodhead, I. G. Kaplan and M. Terrissol, "Track structure quantities" in "Atomic and Molecular data for radiotherapy and radiation research", chapter 9, IAEA-TECDOC-799 IAEA (1995)
- [2] J. L. Magee and A. Chatterjee, "Track reactions of radiation chemistry", in G. R. Freeman (eds.), "Kinetics of non-homogeneous processes", Chapter 4, John Wiley & Sons, New York, 1987
- [3] H. A. Bethe, *Ann. Phys.* 5 (1930) 325
- [4] S. M. Seltzer and M. J. Berger, *Int. J. Appl. Isot.*, 33 (1982) 1189
- [5] ICRU Report 37, "Stopping powers for electrons and positrons", Bethesda, Maryland, 1984
- [6] U. Fano, *Ann. Rev. Nucl. Sci.*, 13 (1963) 1
- [7] J. Lindhard, *Dan. Vid. Selsk. Mat.-Fys. Medd.* 28, No. 8 (1954); J. Lindhard and M. Scharff, *Phys. Rev.*, 124 (1961) 128; J. Lindhard, M. Scharff and H. E. Schiott, *Dan. Vid. Selsk. Mat.-Fys. Medd.*, 33, No. 14 (1963)
- [8] O. B. Firsov, *Zh. Eksp. Teor. Fiz.* 36 (1959) 1517
- [9] J. Lindhard, V. Nielsen and M. Scharff, *Dan. Vid. Selsk. Mat.-Fys. Medd.*, 36, No. 10 (1968)
- [10] L. C. Northcliffe and R. F. Schilling, *Nuclear Data Tables*, A7 (1970) 233
- [11] J. F. Ziegler, J. P. Biersack and U. Littmark, "The stopping and range of ions in solids", Pergamon Press, New York, 1985
- [12] F. Hubert, R. Bimbot and H. Gauvin, *Atomic Data and Nuclear Data Tables*, 46 (1990) 1
- [13] S. K. Sharma, Shyam Kumar, J. S. Yadav and A. P. Sharma, *Appl. Radiat. Isot.*, 46 (1995) 39; G. S. Randhawa and H. S. Virk, *Radiat. Meas.*, 26 (1996) 541
- [14] ICRU Report 49, "Stopping power and ranges for protons and alpha particles", Bethesda, Maryland, 1993
- [15] D. Fink, L. T. Chadderton, F. Hosoi, H. Omichi and A. Schmoldt, *Radiation Effects and Defects in Solids*, 133 (1995) 121
- [16] M. Sugimoto, H. Kudoh, T. Sasuga, T. Seguchi, Y. Hama, K. Hamanaka and H.



- Matsumoto, JAERI-Conf 97-003 (1997) 269
- [17] K. Hata and H. Baba, JAERI-M 88-184 (1988)
- [18] N. Bohr, Dan. Vid. Selsk. Mat.-Fys. Medd., 18, No. 8 (1948)
- [19] A. B. Wittkower and H. D. Betz, Atomic Data, 5 (1973) 113; K. Shima and T. Mikumo, Atomic Data and Nuclear Data Tables, 34 (1986) 357
- [20] W. H. Barkas, "Nuclear research emulsion", vol. 1, Chapter 9, Academic Press, New York, 1963
- [21] M. P. R. Waligorski, R. N. Hamm and R. Katz, Radiat. Meas., 11 (1986) 309
- [22] K. Furukawa, S. Ohno, H. Namba, M. Taguchi and R. Watanabe, Radiat. Phys. Chem., 49 (1997) 641
- [23] N. Kouchi, S. Tagawa, H. Kobayashi and Y. Tabata, Radiat. Phys. Chem., 34 (1989) 453
- [24] K. Arakawa, Y. Nakamura, W. Yokota, M. Fukuda, T. Nara, T. Agematsu, S. Okumura, I. Ishibori, T. Kamiya, R. Tanaka, T. Tachikawa, K. Hoshika, M. Tachibana, Y. Kumata, Y. Hayashi, K. Ishii, M. Sano, K. Iso, T. Torii, K. Suzuki, J. Sagawa and T. Tonooka, JAERI-M 93-047 (1993) 1
- [25] S. Tajima, I. Takada, K. Mizuhashi, Y. Saito, S. Uno, K. Okoshi, Y. Ishii, M. Ishii, K. Yotsumoto and R. Tanaka, JAERI-M 93-047 (1993) 57
- [26] S. Tajima, I. Takada, K. Mizuhashi, S. Uno, K. Okoshi, Y. Saitoh, Y. Ishii, T. Kamiya, T. Suda and T. Sasuga, JAERI-Review 94-005 (1994) 216
- [27] K. Yotsumoto, S. Tajima, I. Takada, K. Mizuhashi, T. Kamiya, Y. Saitoh, S. Uno and K. Ohgoshi, JAERI-M 93-047 (1993) 66
- [28] H. Watanabe, S. Tanaka, K. Nishimura, I. Takada, Y. Nakamura, K. Mizuhashi, N. Ohnuma, N. Akiyama and M. Murayama, JAERI-Review 94-005 (1994) 211
- [29] M. B. Lewis and E. H. Lee, Nucl. Instr. and Meth. in Phys. Res., B 61 (1991) 457
- [30] N. Chitose, Y. Katsumura, Z. Zuo, M. Domae and K. Ishigure, J. Chem. Soc., Faraday Trans., 93 (1997) 3939
- [31] T. Murakami, H. Tsujii, Y. Furusawa, K. Ando, T. Kanai, S. Yamada and K. Kawachi, J. Nucl. Mater., 248 (1997) 360
- [32] T. Sasuga, H. Kudoh and T. Seguchi, JAERI-M 93-047 (1993) 117
- [33] M. Asano, M. Yoshida, M. Tamada, H. Omichi and R. Katakai, JAERI-M 93-047 (1993) 109
- [34] T. Sasuga, S. Kawanishi, T. Seguchi and I. Kohno, Polymer, 30 (1989) 2054
- [35] M. Kikuchi, A. Tanaka, Y. Kobayashi, R. Nozawa and H. Watanabe, JAERI-M 93-047 (1993) 159
- [36] T. Kojima, H. Sunaga, H. Takizawa, H. Tachibana and R. Tanaka, Radiat. Phys. Chem., 53 (1998) 115
- [37] H. Shibata, S. Seki, S. Tagawa, Y. Yoshida and K. Ishigure, Nucl. Instr. and Meth. in Phys. Res., B 105 (1995) 42
- [38] J. A. LaVerne and R. H. Schuler, J. Phys. Chem., 91 (1987) 6560

- [39] M. C. Sauer, Jr., K. H. Schmidt, E. J. Hart, C. A. Naleway and C. D. Jonah, *Radiat. Res.*, 70 (1977) 91
- [40] J. H. Miller and M. L. West, *IEEE Trans. on Nucl. Sci.*, NS-26 (1979) 1766
- [41] J. A. LaVerne, *J. Phys. Chem.*, 100 (1996) 18757
- [42] Y. Aoki, N. Kouchi, H. Shibata, S. Tagawa and Y. Tabata, *Nucl. Instr. and Meth. in Phys. Res.*, B 33 (1988) 799
- [43] E. H. Lee, W. C. Oliver and L. K. Mansur, *J. Mater. Res.*, 8 (1993) 377
- [44] A. O. Allen, *Radiation Chemistry of Water and Aqueous Solutions*, Van Nostrand Reinhold, Princeton, New Jersey, 1961
- [45] I. G. Draganic and Z. D. Draganic, chapter 1, *Historical Survey of the Radiation Chemistry of Water*, *The Radiation Chemistry of Water*, Academic Press, New York, 1971
- [46] A. Appleby and H. Schwarz, *J. Phys. Chem.*, 73 (1969) 1937
- [47] R. H. Schuler and A. O. Allen, *J. Am. Chem. Soc.*, 79 (1957) 1565
- [48] A. Kupperman and G. Belford, *J. Chem. Phys.*, 36 (1962) 1412; A. Kupperman and G. Belford, *J. Chem. Phys.*, 36 (1962) 1427
- [49] W. G. Burns, R. May, G. V. Buxton and G. S. Tough, *Faraday Discuss. Chem. Soc.*, 63 (1977) 47
- [50] N. Chitose, Y. Katsumura, M. Domae, Z. Zuo, T. Murakami and J. A. LaVerne, *J. Phys. Chem. A*, 103 (1999) 4769
- [51] G. Baldacchino, D. Le Parc, B. Hickel, M. Gardes-Albert, Z. Abedinzadeh, D. Jore, S. Deycard, S. Bouffard, V. Mouton and E. Balanzat, *Radiat. Res.*, 149 (1998) 128
- [52] E. A. Christman, and A. Appleby, *Radiat. Res.*, 85 (1981) 443, and references cited herein.
- [53] J. A. LaVerne and R. H. Schuler, *J. Phys. Chem.*, 100 (1996) 16034
- [54] J. A. LaVerne and R. H. Schuler, *J. Phys. Chem.*, 91 (1987) 5770
- [55] C. Ferradini and J.-P. Jay-Gerin, *Radiat. Phys. Chem.*, 51 (1998) 263
- [56] J. A. LaVerne and H. Yoshida, *J. Phys. Chem.*, 97 (1993) 10720
- [57] J. A. LaVerne, *Radiat. Res.*, 118 (1989) 201
- [58] S. M. Pimblott and J. A. LaVerne, *J. Phys. Chem.*, 96 (1992) 746
- [59] G. R. Sunaryo, Y. Katsumura, D. Hiroishi and K. Ishigure, *Radiat. Phys. Chem.*, 45 (1995) 131
- [60] W. G. Burns and P. B. Moore, *Radiation Effects*, 30 (1976) 233
- [61] A. J. Elliot, M. P. Chenier, D. C. Quellete and V. T. Kosolowsky, *J. Phys. Chem.*, 100 (1996) 9014
- [62] H. Nikjoo, S. Uehara, W. E. Wilson, M. Hoshi and D. T. Goodhead, *Int. J. Radiat. Biol.*, 73 (1998) 355
- [63] R. H. Schuler and A. O. Allen, *J. Am. Chem. Soc.*, 77 (1955) 507
- [64] T. Gaeumann and R. H. Schuler, *J. Phys. Chem.*, 65 (1961) 703
- [65] W. G. Burns, *Trans. Faraday Soc.*, 58 (1962) 961

- [66] A. W. Boyd, *J. Nucl. Mater.*, 9 (1963) 1
- [67] R. H. Schuler, *Trans. Faraday Soc.*, 61 (1965) 100
- [68] J. A. LaVerne and R. H. Schuler, *J. Phys. Chem.*, 88 (1984) 1200
- [69] M. L. West and J. H. Miller, *J. Phys. Chem.*, 83 (1979) 1205 and references cited herein.
- [70] Y. Ito, T. Azuma, Y. Katsumura, Y. Aoki, Y. Tabata and K. Kimura, *Radiat. Phys. Chem.*, 29 (1987) 31
- [71] J. A. LaVerne and B. Brocklehurst, *J. Phys. Chem.*, 100 (1996) 1682
- [72] R. H. Schuler, *J. Phys. Chem.*, 63 (1959) 925
- [73] L. Wojnarovits and J. A. LaVerne, *J. Phys. Chem.*, 99 (1995) 11292
- [74] J. A. LaVerne, R. H. Schuler and G. Foldiak, *J. Phys. Chem.*, 96 (1992) 2588
- [75] J. A. LaVerne and L. Wojnarovits, *J. Phys. Chem.*, 99 (1995) 9862 and references cited herein.
- [76] B. J. Brocklehurst, *J. Chem. Soc. Faraday Trans.*, 88 (1992) 167 and 2823
- [77] P. Ausloos, S. G. Lias and R. E. Rebbert, *J. Phys. Chem.*, 85 (1981) 2322
- [78] J. A. LaVerne and L. Wojnarovits, *J. Phys. Chem.*, 98 (1994) 12635
- [79] L. Wojnarovits and J. A. LaVerne, *J. Phys. Chem.*, 98 (1994) 8014 and references cited herein.
- [80] M. Matsui and M. Imamura, *Bull. Chem. Soc. Jpn.*, 48 (1975) 2346 and references cited herein.
- [81] *Nucl. Instr. and Meth. in Phys. Res.*, B 105 (1995)
- [82] *Nucl. Instr. and Meth. in Phys. Res.*, B 130 (1997)
- [83] S. Tagawa, *Advances in Polymer Science*, 105 (1993) 99
- [84] Y. Yoshida, S. Seki, Y. Mizutani, S. Tagawa, Y. Aoki, M. Taguchi and H. Namba, *JAERI-Review 98-016* (1998) 96
- [85] T. Sasuga, H. Kudoh and T. Seguchi, *Polymer*, 40 (1999) 5095
- [86] S. Seki, H. Shibata, H. Ban, K. Ishigure and S. Tagawa, *Radiat. Phys. Chem.*, 48 (1996) 539
- [87] W. Schnabel and S. Klauwenzner, *Radiat. Phys. Chem.*, 37(1991) 131
- [88] S. Seki, K. Kanzaki, Y. Kunimi, S. Tagawa, Y. Yoshida, H. Kudoh, M. Sugimoto, T. Sasuga, T. Seguchi and H. Shibata, *Radiat. Phys. Chem.*, 50 (1997) 423
- [89] R. W. Garrett, R. W., D. J. T. Hill, T. T. Le, K. A. Milne, J. H. O'Donnell, S. M. C. Perera and P. J. Pomery, *ACS Symposium Series 475, "Radiation Effects on Polymers"* R. L. Clough and W. S. Shalaby (eds.) (1991) 146
- [90] S. Seki, K. Kanzaki, Y. Yoshida, S. Tagawa, H. Shibata, K. Asai and K. Ishigure, *Jpn. J. Appl. Phys.*, 36 (1997) 5361
- [91] H. Kudoh, T. Sasuga, T. Seguchi and Y. Katsumura, *Polymer*, 37 (1996) 2903
- [92] N. Kasai, T. Arakawa and T. Seguchi, *JAERI-Conf 97-003* (1997) 277
- [93] H. Koizumi, T. Ichikawa, H. Yoshida, H. Namba, M. Taguchi and T. Kojima, *Nucl. Instr. and Meth. in Phys. Res.*, B 117 (1996) 431

- [94] M. B. Lewis and E. H. Lee, *J. Nucl. Mater.*, 203 (1993) 224
- [95] H. Koizumi, T. Ichikawa, H. Yoshida, H. Shibata, S. Tagawa and Y. Yoshida, *Nucl. Instr. and Meth. in Phys. Res., B* 117 (1996) 269
- [96] M. Taguchi, Y. Matsumoto, H. Namba, Y. Aoki and H. Hiratsuka, *Nucl. Instr. and Meth. in Phys. Res., B* 134 (1998) 427
- [97] S. Seki, Y. Kunimi, K. Maeda, Y. Yoshida, S. Tagawa, H. Kudoh, M. Sugimoto, Y. Morita and T. Seguchi, proceedings of the 41st symposium on radiation chemistry, Japan, October 1998, Kobe, Japan
- [98] E. H. Lee, "Ion beam modification of polyimide" in M. K. Ghosh and K. L. Mittal (eds.), "Polyimide-fundamentals and applications", Marcel Dekker, Inc. New York, 1996; E. H. Lee, G. R. Rao and L. K. Mansur, *Trends in Polymer Science*, 4 (1996) 229, and references therein.
- [99] S. Shukushima, N. Nishikawa, Y. Matsumoto and Y. Hibino, *Nucl. Instr. and Meth. in Phys. Res., B* 80/81, 1119 (1993)
- [100] J. Rieu, A. Pichat, L. M. Rabbe, A. Ranbert, C. Chabrol and M. Robelet, *Biomaterials*, 12 (1991) 139
- [101] J. P. Biersack and R. Kallweit, *Nucl. Instr. and Meth. in Phys. Res., B* 46 (1990) 309
- [102] C. Darraud, B. Bennamane, C. Gagnadre, J. L. Decossas and J. C. Vareille, *Polymer*, 35 (1994) 2447
- [103] Y. Suzuki, M. Kusakabe and M. Iwaki, *Nucl. Instr. and Meth. in Phys. Res., B* 91 (1994) 584
- [104] M. Iwaki, A. Nakao, M. Kaibara, H. Sasabe, S. Kaneko, H. Nakajima, Y. Suzuki, M. Kusakabe and T. Fujihana, *Nucl. Instr. and in Phys. Res., B* 106 (1995) 618
- [105] H. Omichi, M. Yoshida, M. Asano, N. Nagaoka, H. Kubota, R. Katakai, R. Spohr, N. Reber, A. Wolf, G. M. Alder, V. Ang and C. L. Bashford, *Nucl. Instr. and Meth. in Phys. Res., B* 131(1997) 350
- [106] N. Nagaoka, M. Yoshida, M. Asano, P. Apel, H. Kubota and R. Katakai, *Pharm. Sci.*, 2 (1996) 265
- [107] X. L. Xu, J. Y. Dolveck, G. Boiteux, M. Escoubes, M. Monchanin, J. P. Dupin and J. Davenas, *J. Appl. Polym. Sci.*, 55 (1995) 99
- [108] K. Ogura, T. Hattori, M. Hirata, M. Asano, M. Yoshida, M. Tamada, H. Omichi, N. Nagaoka, H. Kubota and R. Katakai, *Radiat. Meas.*, 25 (1995) 159
- [109] M. Yoshida, M. Asano, A. Safranj, H. Omichi, R. Spohr, J. Vetter and R. Katakai, *Macromolecules*, 29 (1996) 8987
- [110] A. I. Vilenskii, V. A. Oleinikov, I. V. Kuptsova, N. G. Markov, B. V. Mchedlishvili and G. M. Gusinskii, *High Energ. Chem.*, 28 (1994) 285; A. I. Vilenskii, N. G. Markov, V. A. Oleinikov, I. V. Kuptsova, V. V. Kushin, D. L. Zagorskii, E. P. Dontsova, B. V. Mchedlishvili, N. A. Nesterov and S. V. Plotnikov, *High Energ. Chem.*, 28 (1994) 359; A. I. Vilenskii, N. G. Markov, V. A. Oleinikov, D. L. Zagorskii and B. V. Mchedlishvili, *High Energ. Chem.*, 28 (1994) 449

- [111] T. V. Congedo and K. F. Schoch, Jr., *J. Polym. Sci. part B, Polymer Physics*, 32 (1994) 2715
- [112] R. G. Brauldt and L. J. Miller, *Polym. Eng. Sci.*, 20 (1980) 1064
- [113] T. Seguchi, T. Sasuga, K. Yoshida, H. Yagyu and Y. Yamamoto, EIM 82-114 (1982) (in Japanese); T. Seguchi and Y. Morita, "Radiation resistance of plastics and elastomers", in *Polymer Handbook*, VI-583, John Wiley and Sons, New York (1999)
- [114] H. Schoenbacher and M. Tavlet, "Compilation of radiation damage test data-part 1" (2nd edition), CERN 89-12; M. Tavlet, A. Fontaine and H. Schoenbacher, "Compilation of radiation damage test data-part 2" (2nd edition), CERN 98-01
- [115] H. Kudoh, T. Sasuga, T. Seguchi and Y. Katsumura, *Polymer Comm.*, 37 (1996) 3737
- [116] D. J. T. Hill and J. Hopewell, *Radiat. Phys. Chem.*, 48 (1996) 533
- [117] H. Kudoh, M. Sugimoto, N. Kasai, T. Seguchi, M. Tagashira and K. Imagawa, to be published; H. Kudoh, M. Sugimoto, T. Seguchi, M. Tagasghira, M. Nakai and K. Imagawa, DEI 97-152 (1997) (in Japanese); NASDA GDM 98-003 (1998)
- [118] H. Kudoh, T. Sasuga, T. Seguchi and Y. Katsumura, *Polymer*, 37 (1996) 4663
- [119] K. Humer, H. W. Weber, E. K. Tschegg, S. Egusa, R. C. Birtcher and H. Gerstenberg, *J. Nucl. Mater.*, 212-215 (1994) 849

JAERI-M, JAERI-Review, JAERI-Conf report is irregularly issued by staff of Japan Atomic Energy Research Institute (JAERI). Inquiries about availability of the reports should be addressed to, Research Information Division, Department of Intellectual Resources, JAERI, Tokai-mura, Naka-gun, Ibaraki-ken, 319-1195 Japan.

## **Radiation chemistry under magnetic fields. Spin coherence effects**

**Yu.N.Molin**

Institute of Chemical Kinetics and Combustion, 630090 Novosibirsk, Russia

### **1. INTRODUCTION**

Investigations of magnetic field effects in radiation-chemical reactions belong to a new research area [1-3] called, for short, "spin chemistry". For the last 15 years, both the magnetic field effects in radiolysis [4-7] and the related highly sensitive methods such as optically/fluorescent detected ESR (OD/FD ESR) [7-10] have been a subject of extensive reviews.

The phenomena studied in spin chemistry (magnetic field effects, magnetic isotopic effect, spin polarization of electrons and nuclei, effects of resonance microwave pumping, etc.) are based on the peculiarities of reactions of spin-correlated radical or radical ion pairs in condensed media. These pairs arise from dissociation (ionization) of molecules under heat, light or ionizing radiation, preserving spin multiplicity of their precursors.

Magnetic field effects in reactions of spin-correlated pairs are related to singlet-triplet transitions in these pairs which perform switching between the singlet and triplet channels of the reaction. These transitions usually take the form of dynamic oscillations (beats) between the singlet and triplet states of a pair whose frequencies depend on both the strength of external magnetic field and the ESR parameters of the radicals, such as  $g$ -factors and hyperfine coupling constants. In terms of quantum mechanics, the dynamic character of transitions reflects the fact that the spin-correlated pairs are formed in the so-called coherent states since neither singlet nor triplet initial states are the stationary states of a pair. Spin coherence in pairs is conserved until destroyed by spin-relaxation processes.

In a radiation track, the geminate radical ion pairs originate in singlet state in which the partner spins are antiparallel and the total electron spin  $S$  is zero. Description of the pair spin evolution in an arbitrary magnetic field is a fairly complex problem. Common, however, is the fact that the expression for the

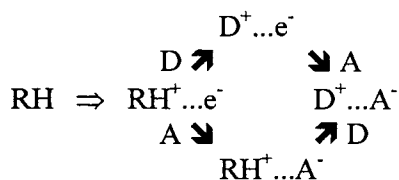
probability  $P_s(t)$  of finding the singlet-born pair at time  $t$  in the singlet state involves the oscillating terms  $\cos(\omega_1 - \omega_k)t$ , where  $\omega_1$ ,  $\omega_k$  are the energies (in frequency units) of the stationary spin states of the pair.

The presence of oscillating terms leads to two peculiarities of the reactions of singlet-correlated pairs related to their coherent origin: (i) The singlet product yield, determined by the probability  $P_s(t)$  at the instant of pair recombination, oscillates with time. This phenomenon (quantum beats) can be observed in time-resolved experiments. (ii) In the region of intersection of levels ( $\omega_1 - \omega_k = 0$ ), some singlet-pair subassemblies stop evolving into the triplet state. Thus, the probability of singlet product formation increases. Since the position of levels depends on magnetic field, this effect is detected as narrow resonances on the magnetic field dependence of singlet product yield in stationary experiments (so-called MARY spectra).

The feasibility of observing these effects and thus, of extracting the useful information is determined by the proper choice of charge acceptors with suitable ESR spectra. These acceptors play the role of molecular probes in studying the primary processes in a radiation track. This review is limited to the manifestations of spin coherence in the recombination of radical ion in irradiated hydrocarbon solutions. Although certain aspects of these studies are available in the literature [6,7,11], some prospects of their application for studying track processes have become evident only recently.

## 2. SINGLET-CORRELATED RADICAL ION PAIRS IN IRRADIATED ALKANES

The formation of singlet-correlated radical ion pairs in alkane (RH) solutions containing acceptors of electrons (A) and holes (D) can be represented by the scheme below



Both the primary pair  $RH^+ \dots e^-$  and the secondary pairs  $D^+ \dots e^-$ ,  $RH^+ \dots A^-$  and  $D^+ \dots A^-$  can undergo singlet-triplet evolution and yield an excited product whose multiplicity corresponds to the spin pair multiplicity upon recombination. From the prospects of recording the spin coherence effects, such pairs exhibit the

following favorable properties:

- 1) The probability of their recombination is close to unity, because in hydrocarbons, for most pairs, the initial distances between the partners are well within the Onsager radius.
- 2) The time of the diffusive approach of radical ions in the pairs  $D^+ \dots A^-$  and  $RH^+ \dots A^-$  is large enough and can exceed the typical time of singlet-triplet evolution. In organic radical ions, the latter is usually determined by the constants of hyperfine interactions (hfi) and varies from nanoseconds to tens of nanoseconds.
- 3) The singlet-triplet evolution is not complicated by the exchange interaction between pair radicals, because the initial distances in pairs are large enough and the act of recombination (electron transfer) needs no contact of reagents in nonpolar solutions.
- 4) The singlet and triplet pairs give different recombination products, i.e., either singlet or triplet excited molecules. Therefore, the singlet-triplet evolution is readily detected by highly sensitive luminescence methods, i.e., either stationary or time-resolved. In the latter case, the photon counting technique is usually used.

### 3. STATIONARY EFFECTS, MARY-SPECTROSCOPY

Figure 1 (bottom) schematically depicts a typical dependence of radioluminescence intensity under stationary conditions on the external magnetic field (magnetically affected reaction yield curve, or MARY spectrum)

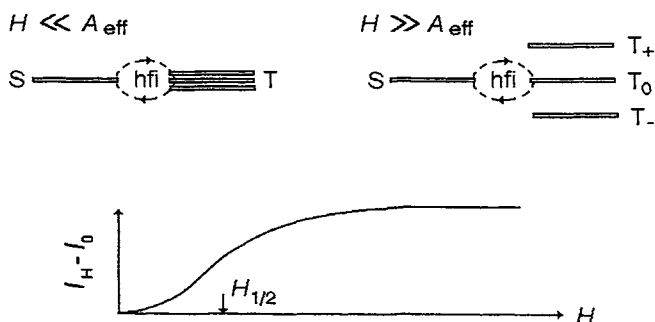


Figure 1. Typical magnetic field effect curve (bottom) and the energy level diagram showing the S/T transitions for a radical pair in zero and high magnetic fields (top).



for alkane solutions with small additions of luminescing acceptors of electrons and holes. Such curves are often observed experimentally. They correspond to the case when spin coherence is rapidly destroyed, e.g., by the processes of phase relaxation. The increase in fluorescence intensity with magnetic field is related, in this case, to the Zeeman splitting of the triplet term of the pair (Figure 1, top). In weak magnetic field, the hfi induces transitions to all the three triplet states whereas in high magnetic field - to the  $T_0$  state only. Therefore, magnetic field decreases the probability of leaving the singlet state, and thus, increases the fluorescence intensity. Such curves are not very informative and allow one just to find the effective hfi constant  $A_{\text{eff}}$  in radical ions which determines the half saturation field  $H_{1/2}$  on the curve.

When the spin coherence of the pair is not destroyed, narrow lines corresponding to the points of intersection (degeneracy) of hyperfine pair levels can appear on the curve of the stationary magnetic field effect. Figure 2 shows a fragment of the spin level diagram of a radical ion pair (*p*-terphenyl- $d_{14}$ )<sup>+</sup>/(C<sub>6</sub>F<sub>6</sub>)<sup>-</sup> in which the radical cation has negligible hfi while coupling constant with six equivalent F<sup>19</sup> is equal to 135 G in the radical anion. The figure points to the level degeneracy in zero field and the intersection of levels in the field equal to  $3A$  where  $A$  is a hfi constant. The figure presents also the experimental curve [12] of magnetic field effect for the radical ion pair. The curve is recorded as the first derivative, which allows one to clearly distinguish the narrow lines in zero field and in the  $3A$  field (marked by the arrow).

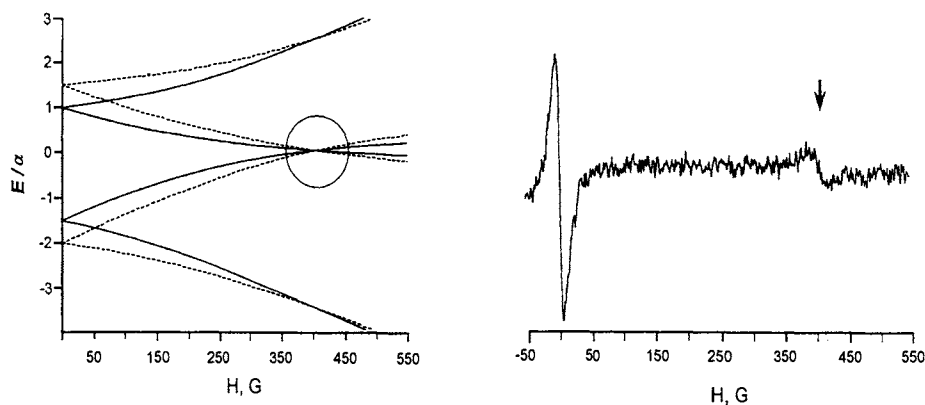


Figure 2. A fragment of energy levels diagram (left) and MARY spectrum (first derivative) for (*p*-terphenyl- $d_{14}$ )<sup>+</sup>/(C<sub>6</sub>F<sub>6</sub>)<sup>-</sup> radical ion pair (right) [12]. Solid and dotted lines in the diagram correspond to different nuclear configurations.

Degeneracy in zero field is common for any pairs with hyperfine couplings and results in the strongest line [13,14]. The position of intersection points in nonzero fields depends on the particular set of hfi parameters [15]. For instance, for an even number  $n \geq 4$  of equivalent nuclei with spin 1/2 the first intersection occurs always in the field  $H = 3A$ . The corresponding resonances have been observed in many systems [12]. The next weaker line was observed for tetramethylethylene radical cation [12] and for hexafluorobenzene and perfluorocyclobutane radical anions [16, 17] in experiments on photoionization. It is predicted [18] that resonances can also occur in the fields substantially exceeding the hyperfine ones if there is a difference in radical  $g$ -factors. The narrow MARY spectra have so far been recorded only in systems with known ESR spectra in order to demonstrate the phenomenon itself. However, actually, the method can be used to obtain parameters of ESR spectra and identify the unknown short-lived pairs.

A particular property of the line in zero magnetic field is that its width is determined by the decay rate of the coherent pair state. This decay can be due to either spin relaxation or chemical transformation of pair partners. If the rate of spin relaxation in zero field is not large, as is expected for organic radical ions, the analysis of the lines allows direct determination of the rate of the chemical decay of pair partners.

Such an approach has recently been applied for determining the decay time of radical cations (holes) forming under  $\beta$ - and X-rays in viscous branched hydrocarbon, squalane, [19] and in the series of linear alkanes [20]. To this end, the MARY spectra of the  $(RH)^+/(C_6F_6)^-$  pairs were recorded where RH is the alkane molecule. The line in the  $3A$  field was used to control the fact that the magnetic field effect results from recombination of just this pair. The lines in zero field were found to have a substantially greater width as compared with the  $(p\text{-terphenyl})^+/(C_6F_6)^-$  pair. This difference was assigned to the fast decay of alkane holes. The time of hole decay estimated from the difference in widths increases with the length of hydrocarbon from nanoseconds to tens of nanoseconds (Table 1). These estimates provide the lower limit for the time of alkane cations decay. They neglect a possible contribution of spin relaxation as well as geminate recombination to the width of the MARY line.

The broadening of the MARY lines was also analyzed to study the degenerate electron exchange in the irradiated alkane solutions involving *cis*-decalin radical cation [21] and hexafluorobenzene radical anion [20, 21]. It was found that for *cis*-decalin radical cation, the rate of charge transfer was determined by the number of diffusion collisions, while for hexafluorobenzene radical anion, it was lower and reached the diffusion-controlled limit only at high viscosity.

Table 1

Summary of some of the characteristics of radical ions in irradiated alkane solutions

Alkane	$K_{\text{exch}}^a$	$\Delta H_{\text{total}}^b$	$\Delta H_h^c$	$\tau_h^d$
C <sub>5</sub> H <sub>12</sub>	$5 \times 10^9$	62	53	1
C <sub>6</sub> H <sub>14</sub>	$4.5 \times 10^9$	40	35	2
C <sub>8</sub> H <sub>18</sub>	$4.5 \times 10^9$	25	14	5
C <sub>10</sub> H <sub>22</sub>	$3 \times 10^9$	15	10	7
C <sub>12</sub> H <sub>26</sub>	$2 \times 10^9$	12	5	13
C <sub>16</sub> H <sub>34</sub>	$2 \times 10^9$	7	2	33

<sup>a</sup>Rate constant of the ion-molecular charge exchange reaction of hexafluorobenzene radical anion,  $M^{-1}c^{-1}$ .

<sup>b</sup>MARY line width at zero field, extrapolated to zero concentration of hexafluorobenzene, G.

<sup>c</sup>Contribution to the line width, attributed to the hole decay, G.

<sup>d</sup>Lifetime of the solvent hole estimated assuming exponential recombination kinetics, ns.

The exponential model of geminate recombination of pairs is often used as a first approximation when analyzing the MARY line shape. The recent theoretical analysis [22] shows that taking into account the non-exponential character of geminate recombination kinetics gives a number of characteristic features. First, the contours of the lines can substantially differ from the Lorentzian contour, which has been confirmed by experiments. Second, the geminate recombination with its slowly decaying diffusion asymptote does not make an additive contribution to the line width measured between the points of the maximum slope. Moreover, the change in the line shape causes quite different relationships between the time of coherence decay and the line broadening as compared with the Lorentzian contour. As a result, the lifetime can be 2-3 times underestimated when calculated in the framework of the exponential model.

#### 4. TIME-RESOLVED EFFECTS, QUANTUM BEATS

As has already been mentioned, the spin-correlated pair can oscillate between the singlet and triplet states. The origin of these oscillations is illustrated by the vector diagram for the case when a pair is located in strong magnetic field (Figure 3). The pair born in the singlet state can convert into the  $T_0$  state and vice versa if the Larmor precession frequencies of two spins are different. The difference in the frequencies can be due to a difference in both  $g$ -factors and

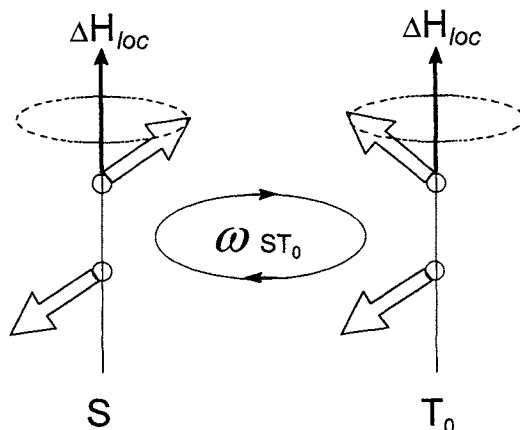


Figure 3. Vector diagram, explaining the appearance of  $S$ - $T_0$  oscillations in a radical pair in high external magnetic field. Oscillations arise if spins precess at different Larmor frequencies due to the difference  $\Delta H_{loc}$  of local magnetic fields.

local hyperfine fields. The frequency of oscillations in this case obeys the formula

$$\omega_{ST} = \left| \beta_e \hbar^{-1} H_0 (g_1 - g_2) + \sum a_{1i} m_{1i} - \sum a_{2k} m_{2k} \right| \quad (1)$$

where  $a_{1i}$  and  $a_{2k}$  are the hfi constants in radicals 1 and 2,  $m_{1i}$  and  $m_{2k}$  are the projections of corresponding nuclear spins onto external magnetic field  $H_0$ . As follows from the formula, the frequency of oscillations is determined by the difference in the ESR line positions (in frequency units) of pair partners.

As compared with high field, in zero and weak ( $H_0 < a\hbar/g\beta_e$ ) magnetic fields singlet term is mixed up with all three triplet sublevels. This complicates the problem of describing quantum oscillations which, in the general case, can be solved only numerically. However, for equivalent nuclei in one of the radicals, there is a compact analytical expression for zero magnetic field.

Since different nuclear configurations correspond to different frequencies, experiment often shows a smoothed curve instead of oscillations. The pattern of beats has, however, a simple form and is readily observed for two cases. If hyperfine interactions are negligibly small, the oscillations come with a single frequency (Figure 4) determined by the difference in  $g$ -factors and the external magnetic field [23]. The oscillations are seen to occur at the background of the fast decay of recombination luminescence. Therefore, the oscillating component is more convenient to analyze by studying the ratio of two curves taken in high

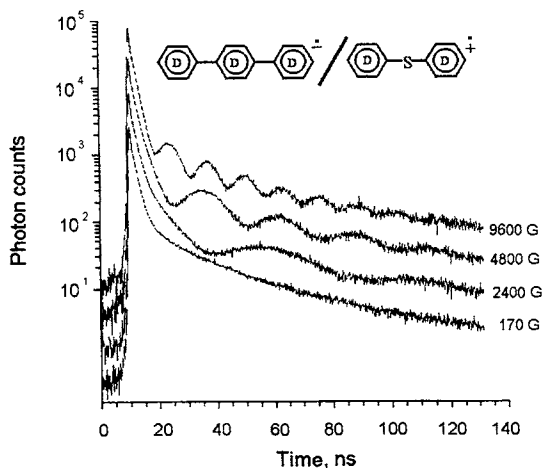


Figure 4. The decay of recombination fluorescence for solution of  $10^{-3}$  M *p*-terphenyl- $d_{14}$  and  $3 \times 10^{-2}$  M diphenylsulfide- $d_{10}$  in iso-octane in various magnetic fields [23]. For convenience, the curves are shifted relative to each other. The oscillating component comes from the recombination of the singlet-born pairs (diphenylsulfide- $d_{10}$ )<sup>+</sup>/(*p*-terphenyl- $d_{14}$ )<sup>-</sup>.

and weak (or zero) magnetic fields. In the other simple case, where all magnetic nuclei are equivalent and  $\Delta g = 0$ , the oscillations occur with multiple frequencies and their superposition gives sharp peaks on the curve of the time-resolved magnetic field effect [24]. Although in this case the oscillations are observed in both high and zero fields, the division of two curves is also a useful experimental method.

Formally, a pattern of quantum beats can be characterized by the parameters such as the set of oscillation frequencies, oscillation decay time, the phase shift of oscillations, and, finally, their amplitude. Each parameter contains useful information about the processes in radiation spurs. The oscillation frequencies correspond to the splittings in the ESR spectrum of radical ions. The decay of oscillations contains information about spin relaxation times. The phase shift reflects the time delay of pair formation from its precursor. Finally, the amplitude of oscillating component is determined by the fraction of spin correlated pairs.

#### 4.1. The fraction of singlet spin-correlated pairs

The fraction of singlet-correlated pairs is a very important characteristic of primary radiation chemical events. The scale of magnetic field effect as well as the product composition are the functions of this quantity.

In irradiated solutions this fraction is substantially below unity because of the complex structure of the radiation track. While isolated pairs are believed to be singlet correlated, for a double pair, the fraction might be as low as 1/2 due to cross recombination. For multi-pair spurs, the spin correlation might be completely lost.

There are several approaches [4, 25] that try to determine the fraction of spin-correlated radical ion pairs in radiolysis. The transient emission and absorption [25] suffer, however, from the lack of exact data on the extinction coefficients and luminescence quantum yields of intermediate products. The magnetic field effect technique [4] is more straightforward. However, it requires a detailed knowledge of spin evolution in zero field which is a problem in most cases.

When applying the quantum beats technique, it is essential that only the singlet-correlated pairs contribute to the oscillating component of spin evolution. Therefore, for systems with a single oscillation frequency, the singlet state population  $P_s(t)$  is determined by

$$P_s(t) = \theta \cos^2(\omega_{ST} t/2) + 0.25(1 - \theta), \quad (2)$$

where  $\theta$  is the fraction of singlet born spin-correlated pairs. The second term in this formula takes into account the time-independent contribution of uncorrelated pairs.

To determine the fraction of singlet-correlated pairs in alkanes irradiated by X-rays and fast electrons, the quantum beats in recombination of the (diphenylsulphide- $d_{10}$ )<sup>+</sup>/(*p*-terphenyl- $d_{14}$ )<sup>-</sup> radical ion pairs have been studied [26, 27]. As expected, the X-rays show a much weaker oscillating component (Figure 5) which corresponds to a higher track density for the secondary X-ray

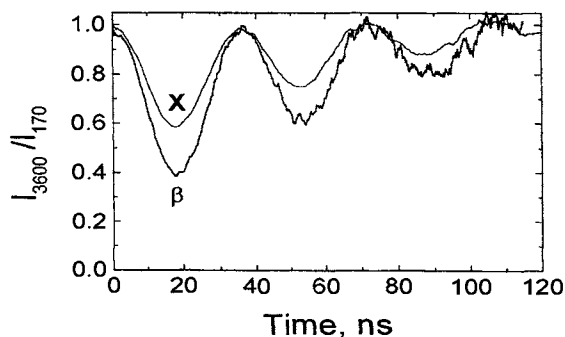


Figure 5. The ratio  $I_{3600}/I_{170}$  of fluorescence intensities at 3600 G and 170 G for solution of 0.12 M diphenylsulphide- $d_{10}$  and  $10^{-3}$  M *p*-terphenyl- $d_{14}$  in *cis*-decalin irradiated by X-rays and fast electrons [27].

Table 2.

The fraction  $f_s$  of the singlet channel of recombination  $f_s = \theta + 0.25(1 - \theta)$ 

Solvent	Method		
	Magnetic field effect [4]	Transient emission and absorption [25]	Quantum oscillations [26,28]
Hexane		0.5	0.65
Isooctane		0.5	0.66
Cyclohexane	0.65	0.5	0.60
<i>trans</i> -Decalin			0.52
<i>cis</i> -Decalin			0.52
Squalane	0.65		0.40 (RT) 0.60 (90°C)

electrons. The fraction of spin correlated pairs can be determined either from the oscillation amplitude extrapolated to zero time or by computer simulation of the entire oscillation curve. Two methods gave consistent results.

The results for different alkanes irradiated by fast electrons are compared in Table 2 with those obtained by other techniques. To this end, the fraction of singlet recombination  $f_s$  is given in the Table for all cases. This value contains an extra singlet contribution from uncorrelated pairs.

The quantum oscillation results correlate well with the published data. It is seen also that the fraction does not vary much among alkanes. The only exception is a very viscous solvent, squalane, in which the quantum beats give a substantially lower  $f_s$ -value as compared to other techniques. It was found, however [28], that for squalane the oscillation amplitude increases up to the ordinary value with increasing temperature. Obviously, the quantum beats technique has some limitations at high viscosity. The reason is not clear yet. On the other hand, at low viscosity the method seems to be quite reliable and universal.

#### 4.2. Phase shift and hole capture rate

Since the formation of the secondary  $D^+ \dots A^-$  pairs occurs with some delay, this can cause a phase shift in quantum oscillations. The spread of phase shifts also leads to a decrease in oscillation amplitude. The delay results mainly from the finite time of the solvent hole trapping by an acceptor molecule D. Due to high electron mobility, its capture by acceptor A is much faster. Under these conditions, the phase shift  $\varphi$  is related to the concentration [D] of the hole acceptor via a simple relationship

$$\omega \cot \varphi = k [D] + k_{dec} \quad (3)$$

if the ESR spectra of all radical ions are narrow singlets and the hole capture by the acceptor is followed by a change in the  $g$ -factor. In this case,  $\omega = \Delta g \beta_e H_0 / \hbar$  is the difference in the Larmor frequencies of  $\text{RH}^+$  and  $\text{D}^+$ ;  $k$  is the bimolecular reaction rate constant of solvent hole trapping by acceptor D; and  $k_{\text{dec}}$  is the monomolecular rate constant of hole decay in any reactions other than trapping by D. In this case, one can extract the hole capture and the decay rate constants from the slope and intercept of the concentration dependence.

The phase shifts of quantum oscillations were observed recently [29,30] in various alkanes for the radical pair (diphenylsulphide- $d_{10}$ ) $^+/(p$ -terphenyl- $d_{14})^-$ , in which the beats are driven by the difference in  $g$ -factors. The hyperfine couplings in this pair are insignificant owing to the use of deuterated acceptor molecules. It is also assumed that in the  $\text{S}^+$  radical cations the effective hfi are also small due to fast electron exchange with solvent molecules.

Figure 6 exemplifies the experimental curves of oscillations for two different concentrations of diphenylsulphide- $d_{10}$  in isooctane. It is seen that as the concentration decreases, the phase shift appears and the oscillation amplitude decreases. It was shown that, in accordance with the theoretical model,  $\cot \varphi$  increases linearly with the concentration of hole acceptor. The rate constant of isooctane cation capture by diphenylsulphide molecules was determined from the slope to be  $(3.5 \pm 1) \times 10^{10} \text{ M}^{-1} \text{ s}^{-1}$ .

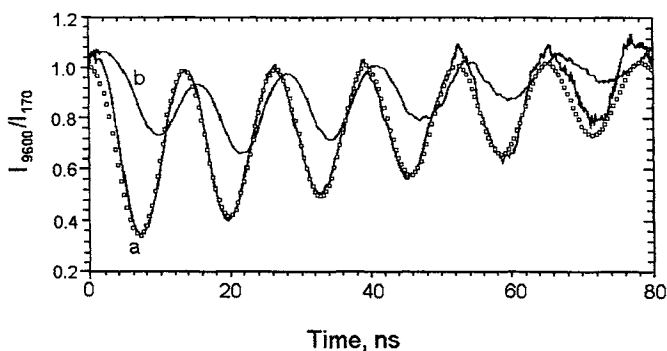


Figure 6. The ratio between the fluorescence decay curves in high (9600 G) and weak (170 G) magnetic fields for recombination of (diphenylsulphide- $d_{10}$ ) $^+/(p$ -terphenyl- $d_{14})^-$  pairs in isooctane [29]. The concentration of  $p$ -terphenyl- $d_{14}$  is  $10^{-3} \text{ M}$ . It is seen that as the concentration of the hole acceptor, diphenylsulphide- $d_{10}$ , decreases from 0.12 M (curve a) to 0.012 M (curve b), the phase shift in oscillations appears and the oscillation amplitude decreases. Circles: the theoretical fit to curve (a).



The phase shifts of quantum beats have been studied in other alkanes as well [30]. As expected, in linear alkanes the rate constants of hole trapping by acceptors, determined from the shifts, were close to the diffusion-controlled ones. In cyclic alkanes (cyclohexane, *cis*-decalin, and *trans*-decalin), the hole mobility is known to considerably exceed the mobility of molecular ions [31]. In these solvents the observed phase shifts had an intermediate value between that expected for the highly mobile holes and that assumed for molecular ions. Both types of ions are likely to take part in the formation of diphenylsulphide radical cation in cyclic alkanes.

The quantum beats method has been also applied for studying viscous squalane solutions [19], where highly mobile holes were found [32] in pulse radiolysis experiments. The rate constant of hole capture was determined from the slope to be  $6.1 \times 10^9 \text{ M}^{-1} \text{ s}^{-1}$ , which confirms conclusion on the high mobility of holes in squalane. The rate constant of squalane hole decay was estimated from the intercept to be  $(8.3 \pm 2) \times 10^7 \text{ s}^{-1}$ , which is also in fair agreement with experiments on pulse radiolysis [32].

### 4.3. ESR spectrum parameters

In most quantum beats experiments, the radical pairs were generated whose ESR spectra were either known or could be obtained independently, e.g., using the OD ESR method. These experiments [23,24] show a fair agreement between the observed beat frequencies and the splittings in the ESR spectra of a pair. Figure 7 shows the recent results of the study of quantum beats in the systems

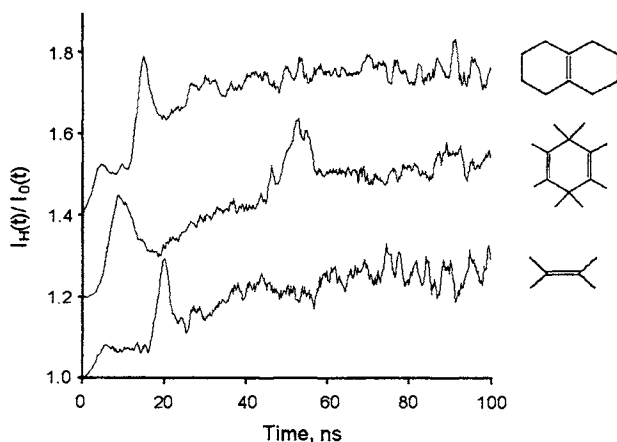


Figure 7. The ratio of fluorescence decay curves in high and zero magnetic fields for solutions of hole acceptors with equivalent protons [33].

with equivalent protons [33]. As hole acceptors, different hydrocarbons were chosen, whose radical cations have an even number of equivalent protons with the known hfi constants. The counterion in geminate pairs was the *p*-terphenyl- $d_{14}$  radical anion whose hfi constants are small and do not contribute much to the spin evolution of the pair. Cyclohexane was used as a solvent. In this hydrocarbon, the mobility of solvent holes substantially exceeds that for molecular ions which provides the fast capture of holes by added acceptors even at their low concentrations.

The theoretical analysis shows that the most characteristic feature of the  $I_H(t)/I_0(t)$  ratio for systems with an even number of equivalent protons is the existence of strong narrow peaks. The strongest peak arises at time  $\tau = 2\pi/a$  determined only by the hfi constant  $a$  independently of the number of equivalent protons. The appearance of this peak is related to the coincidence of the positions of maximum and minimum of singlet state population in high and zero fields, respectively. The width of this peak as well as the position and intensity of the weaker ones are determined by the number of equivalent protons.

Two narrow peaks are clearly observed on all experimental curves, and some systems showed also the third and fourth peaks. The position of the strongest second peak corresponds to the published hfi constants. The form of the curves indicates that spin relaxation has substantial effect on spin evolution. The curves have a smoothly rising background and the amplitudes of peaks decay with time.

Recently, the quantum beats technique was used to determine the unknown hfi constants of several short-lived radical anions [34]. Radical ion pairs were generated in the decane  $10^{-3}$  M solutions of 1,2,3,4- tetraphenylcyclopentadiene and its silicon and germanium analogs (A).

When low acceptor concentrations are used, the main contribution to the pattern of beats is made by the (decane) $^+/A^-$  pairs. It was shown that the beats are due to the hyperfine couplings with either the protons of CH<sub>2</sub>, SiH<sub>2</sub>, and

Table 3.

HFI constants for 1,2,3,4- tetraphenylcyclopentadiene radical anion and its analogs $^-$  obtained from OD ESR spectra and from quantum beats

Molecular fragment responsible for hfi	Atom	A, G OD ESR	A, G Quantum beats
CH <sub>2</sub>	H(2)	24.6	25.0
SiH <sub>2</sub>	H(2)	17.0	15.6
GeH <sub>2</sub>	H(2)	15.4	15.0
GeCl <sub>2</sub>	Cl(2)	7.0	7.0
GeCH <sub>3</sub> Cl	Cl	12.4	11.4

GeH<sub>2</sub> moieties or chlorine atoms in the GeCl<sub>2</sub> and GeClMe moieties of radical anions. The hfi constants derived from quantum beats simulation are collected in Table 3. They were supported later by independent OD ESR experiments in viscous squalane solvent at low temperatures [35].

## 5. CONCLUSION

An in-depth study of spin coherence effects provides information that is related to the information available from magnetic resonance studies. The frequencies of quantum beats and the positions of lines in MARY-spectra are determined by the same parameters as the ESR spectrum structure. Actually, the methods discussed can be considered as a variant of ESR-spectroscopy of spin-correlated radical ion pairs without mw-pumping. The main advantage of these methods as well as the OD ESR technique is their extremely high sensitivity. Recording luminescence, it is possible to study the spin-correlated pairs at stationary concentrations down to 100 particles per sample. Therefore, the weak radioactive sources can be used for radical ion pairs generation. Compared with the OD ESR technique, the given methods have, however, an essential advantage. They can be used to study the spin-correlated pairs with shorter lifetimes. In OD ESR, this time is limited by the time of electron spin flip around microwave magnetic field of spectrometer (up to several Gauss), whereas in the case of quantum beats or MARY spectroscopy, this limit depends on hyperfine fields (usually, tens of Gauss) or the difference in radical g-factors. Therefore, the lifetime threshold changes from tens of nanoseconds to nanoseconds.

An obvious limitation on the methods discussed in this review is the need for a choice of radical ion pairs with suitable ESR spectra. Actually, this limitation is due to the insufficient time resolution (quantum beats) or sensitivity (MARY-spectra) of available equipment. Improving these characteristics, one can obtain the spectral information about the systems with a more complex set of hyperfine interactions. Therefore, the further development of observation technique is an urgent task.

Development of the methods and their application in radiation chemistry will be substantially determined by extending the range of systems and problems that are now only outlined but not exhausted. Undoubtedly, both of the methods will be applied for obtaining spectroscopic information about radical ions not studied in liquid solutions by means of the ESR method due to their short lifetimes. They can include alkane radical cations, radical anions of halide-

containing compounds, radical ions of element-organic compounds, etc. The phase shifts measurements can be used for obtaining rate constants of very fast reactions, especially those of highly mobile solvent holes and quasifree electrons. Because of its universality, the method of quantum beats can be widely used to determine the fraction of spin-correlated pairs and to study the influence of various factors on the fraction of geminate recombination in the tracks of ionizing particles. At present, the number of theoretical papers on this subject substantially exceeds the body of reliable experimental data. The methods offer interesting future possibilities for determining relaxation times, which is certain to provide additional information about the interaction of paramagnetic particles in radiation tracks.

Although the effects of spin coherence have been mainly studied using radiation-chemical processes as an example, published are the first works on the MARY spectra of radical ion pairs produced in solutions by photoionization. Probably, there are no principle obstacles to the application of the method of quantum beats to these systems. Interpretation of results is expected to be more simple, in this case, because of the use of monochromatic sources of ionization and the absence of cross recombination effects typical of the ionization track. Another manifestation of spin coherence, observed experimentally but omitted in this review, is the beats induced by resonance microwave pumping [36-38]. The range of applications of this phenomenon for studying spin-correlated radical ion pairs has yet to be outlined.

## REFERENCES

1. K.M. Salikhov, Yu.N. Molin, R.Z. Sagdeev and A.L. Buchachenko, *Spin Polarization and Magnetic Effects in Radical Reactions*, Elsevier, Amsterdam, 1984.
2. U.E. Steiner and T. Ulrich, *Chem. Rev.* 89 (1989) 51.
3. S. Nagakura, H. Hayashi and T. Azumi (eds.), *Dynamic Spin Chemistry*, Kodansha, Tokyo, 1998.
4. B. Brocklehurst, *Intern. Rev. Chem.* 4 (1985) 279.
5. B. Brocklehurst, *Radiat. Phys. Chem.* 50 (1997) 213.
6. A.V. Veselov, O.A. Anisimov and Yu.N. Molin, in *Pulse Radiolysis*; Y. Tabata (ed.), CRC Press, Boca Raton, FL, 1991; p.27.
7. O.A. Anisimov, in *Radical Ionic Systems*, A. Lund and M. Shiotani (eds.), Kluwer Academic Publishers, Dordrecht, 1991; p. 285.
8. Yu.N. Molin, O.A. Anisimov, V.I. Melekhov and S.N. Smirnov, *Discuss. Faraday Soc.* No 78 (1984) 289.
9. A.D. Trifunac and D.W. Werst, in *Radical Ionic Systems*, A. Lund and M. Shiotani (eds.), Kluwer Academic Publishers, Dordrecht, 1991; p. 195.

10. A.D. Trifunac, D.M. Bartels and D.W. Werst, in *Pulse Radiolysis*; Y. Tabata (ed.), CRC Press, Boca Raton, FL, 1991; p. 53.
11. Yu.N. Molin, *Bull. Korean Chem. Soc.* 20 (1999) 7.
12. D.V. Stass, B.M. Tadjikov and Yu.N. Molin, *Chem. Phys. Lett.* 235 (1995) 511.
13. D.V. Stass, N.N. Lukzen, B.M. Tadjikov and Yu.N. Molin, *Chem. Phys. Lett.* 233 (1995) 444.
14. C.R. Timmel, U.Till, B.Brocklehurst, K.A. McLauchlan and P.J. Hore, *Molec. Phys.* 95 (1998) 71.
15. S.A. Sukhenko, P.A. Purtov and K.M. Salikhov, *Sov. J. Chem. Phys.* 2 (1985) 29.
16. V.O. Saik, A.E. Ostafin and S. Lipsky, *J. Chem. Phys.* 103 (1995) 7347.
17. V.M. Grigoryants, S.D. McGrane and S. Lipsky, *J. Chem. Phys.* 109 (1998) 7354.
18. B. Brocklehurst, *Molec. Phys.* 9 (1999) 283.
19. O.M. Usov, D.V. Stass, B.M. Tadjikov and Yu.N. Molin, *J. Phys. Chem.* A101 (1997) 7711.
20. F.B. Sviridenko, D.V. Stass and Yu.N. Molin, *Chem. Phys. Lett.* 297 (1998) 343.
21. D.V. Stass, N.N. Lukzen, B.M. Tadjikov, V.M. Grigoryants and Yu.N. Molin, *Chem. Phys. Lett.* 243 (1995) 533.
22. Yu.V. Toropov, F.B. Sviridenko, D.V. Stass, A.B. Doktorov and Yu.N. Molin, *Chem. Phys.* (presented for publication)
23. A.V. Veselov, V.I. Melekhov, O.A. Anisimov and Yu.N. Molin, *Chem. Phys. Lett.* 136 (1987) 263.
24. O.A. Anisimov, V.L. Bizyaev, N.N. Lukzen, V.M. Grigoryants and Yu.N. Molin, *Chem. Phys. Lett.* 101 (1983) 131.
25. M.C. Sauer, Jr. and C.D. Jonah, *Radiat. Phys. Chem.* 44 (1994) 281.
26. O.M. Usov, V.M. Grigoryants, B.M. Tadjikov and Yu.N. Molin, *Radiat. Phys. Chem.* 49 (1997) 237.
27. S.V. Anishchik, O.M. Usov, O.A. Anisimov and Yu.N. Molin, *Radiat. Phys. Chem.* 51 (1998) 31.
28. S.Yu. Milikisyants, unpublished.
29. V.M. Grigoryants, B.M. Tadjikov, O.M. Usov and Yu.N. Molin, *Chem. Phys. Lett.* 246 (1995) 392.
30. O.M. Usov, Thesis, 1997, Novosibirsk
31. J.M. Warman, in *The Study of Fast Processes and Transient Species by Pulse Radiolysis*; J.H. Baxendale and F. Busi (eds.), Reidel, Boston, MA, 1981; p 433.
32. I.A. Shkrob, M.C. Sauer, Jr. and A.D. Trifunac, *J. Phys. Chem.* 100 (1996) 5993.
33. V.A. Bagryansky, O.M. Usov, V.I. Borovkov and Yu.N. Molin, *Dokl. AN* 364 (1999) 488 (in Russian).
34. V.A. Bagryansky, V.I. Borovkov, Yu.N. Molin, M.P. Egorov and O.M. Nefedov, *Chem. Phys. Lett.* 295 (1998) 230.
35. V.A. Bagryansky, Yu.N. Molin, M.P. Egorov and O.M. Nefedov, *Mendeleev Commun.* (1998) 236.
36. V.O. Saik, O.A. Anisimov, A.V. Koptuyug and Yu.N. Molin, *Chem. Phys. Lett.* 165 (1990) 142.
37. I.A. Shkrob and A.D. Trifunac, *J. Chem. Phys.* 103 (1995) 551.
38. S.V. Anishchik, V.I. Borovkov, V.I. Ivannikov, I.V. Shebolaev, Yu.D. Chernousov, N.N. Lukzen, O.A. Anisimov and Yu.N. Molin, *Chem. Phys.* 242 (1999) 319.

## Muonium chemistry

Emil Roduner

Institute of Physical Chemistry, University of Stuttgart,  
Pfaffenwaldring 55, D-70569 Stuttgart

### 1 INTRODUCTION

Irradiation of matter with  $\gamma$ -rays, x-rays, or with high energy charged particles leads to a sequence of ionization events along their track during which most of the excess energy is dissipated. The ionization electrons themselves are normally highly energetic, and each of them is capable of initiating its own ionizations and excitations of the medium. By far the most of the defects or transient radicals and ions left behind in a thermalization track arise from these secondary electrons ( $\delta$ -rays), and the direct effect of the primary particle is detectable separately only in solids but not in liquids or in gases. The study of the nature of these defects and their interactions with themselves and with the environment along a macroscopic portion of the track is called radiation chemistry. It is essentially all chemistry of energetic electrons, and differences between the primary particles arise only as a consequence of the different linear energy transfer (LET), the energy deposition per unit length of a track, which varies with mass, charge and energy of the primary particle, leading to much higher densities of defects in the tracks of heavy particles.

In contrast to conventional radiation chemistry where only the integral effect along the tracks is measured there are a number of nuclear probe techniques where the high energy particle is suitably used as a "spy" able to probe selectively and sensitively the local environment of its implantation on a microscopic scale. They take advantage of the properties of radioactive recoil atoms from nuclear reactions, or of unstable nuclei or elementary particles from accelerators. Popular examples are recoil tritium [1], indium, used in particular by the perturbed angular correlation technique, the positive muon [2-5], and the positron [6]. They cover a wide range of masses and chemical properties, and the common aspects of all are that they probe the end of their ionization tracks with high sensitivities, due to their radioactive decays which permit the detection of single events with some signature of the chemical environment. The time scales

of the radiation-induced processes which can be probed with optimum sensitivity corresponds roughly to the lifetimes of these probes, which vary by many orders of magnitude from less than one nanosecond for the positron to a few microseconds for positive muons to years for tritium.

Here we shall focus on the positive muon ( $\mu^+$ ) as a probe in chemistry, and we shall introduce some basic aspects which range from typical radiation chemical effects to spectroscopic observations and to applications in investigations of kinetics and dynamics. With a single positive charge and a mass one-ninth of the proton mass, the muon mimics a light proton in matter, even though physicists tend to classify it as a heavy positron with a mass 207 times the electron mass. Like the proton, the muon can form a bound state with an electron. This one-electron atom has the same Bohr radius and ionization potential, to within 0.5%, as the hydrogen atom. It is called muonium ( $\mu^+e^-$ , chemical symbol: Mu), and in a chemical sense it is simply a light hydrogen isotope. The muon is a spin-1/2 particle with a magnetic moment 3.18 times that of the proton, and it is obtained at the ports of suitable accelerators with a spin polarization close to 100%. This makes it an ideal magnetic probe. The signature of its chemical nature is based on its magnetic properties, and the experimental techniques are closely related to magnetic resonance [4]. Muons are implanted in the sample of interest with their spins either perpendicular or parallel to an applied external magnetic field. The experimental observable is the direct analog of a Free Induction Decay (FID) in magnetic resonance, but the method of detection, rather than monitoring a magnetic induction, relies on a single particle counting technique originally developed to confirm parity violation in muon decay. The parameters of interest in time resolved experiments in transverse fields are the muon precession frequencies, their associated amplitudes, relaxation rates and initial phases; in longitudinal fields they are the relaxation rates as a function of field, and corresponding initial amplitudes. In plots of the time-integrated muon polarization this reveals resonances due to relaxation maxima at specific fields where there are avoided crossings of magnetic energy levels. Details of the experimental techniques have been described elsewhere [2-5] and shall not be reviewed here.

Because of its low mass the quantum nature of the muon is much more pronounced than that of the proton. This is reflected in higher zero-point energies in spatially confined (bound) states, and in increased tunneling probabilities through potential barriers. The unprecedented mass ratio of a factor of nine between the muon and the proton, or between Mu and H, leads to very pronounced isotope effects. It is often these which are of particular interest to probe dynamics, and they are extremely sensitive probes of potential energy surfaces. On the other hand, if the muon is attached to a molecule by a stable

chemical bond it can act as a neutral spectator, a spin label that does not significantly influence the process of interest via its mass. In this way it can be used to measure chemical reactions or reorientation dynamics that may be difficult to access by conventional methods.

## 2 THE MUON, AN END-OF-TRACK PROBE

### 2.1 Muonated species

Radiation chemical processes near the end of its thermalization track determine the environment in which the muon is found on an experimental time scale corresponding to its lifetime,  $\tau_\mu = 2.2 \mu\text{s}$ . In experiments in transverse fields we distinguish between different components according to their signal amplitudes which are converted to fractional muon polarizations  $P_i$ , with  $\sum P_i = 1.0$ , if the full initial polarization in the beam is accounted for.

- *Muons in diamagnetic environments* (D) precess at the Larmor frequency of 0.01355 MHz/G. The muon lifetime does not permit the observation of an equivalent FID signal for a duration sufficiently long to resolve chemical shifts or nuclear spin-spin couplings. We can therefore in general only speculate about the exact nature of this component. In liquid water it may represent  $\text{MuOH}$ ,  $\text{MuOH}_2^+$ , or  $\text{MuH}$ , and the fraction observed is  $P_D = 0.62$  [7]. Metals, or liquid carbon tetrachloride give  $P_D = 1.0$ , and  $\text{CCl}_4$  was therefore frequently used to calibrate absolute polarizations.
- In gases, solid insulators, water, and in other chemically inert environments a fraction  $P_{\text{Mu}}$  of muon polarization represents *muonium*. It is easily distinguished from  $P_D$  by its characteristic precession frequency of 1.394 MHz/G in fields below ca. 20 G. The frequency is higher by two orders of magnitude than for diamagnetic environments because it is mainly the electron in the coupled  $\mu^+e^-$  system that determines the Larmor frequency.
- In the presence of unsaturated organic molecules Mu can add to double or triple bonds and form *free radicals* (R) in which the muon is chemically bound as a polarized spin label, as in:



- and is correspondingly represented by a fractional polarization  $P_R$ . Only in exceptional cases are muonated radicals detected in the sample simultaneously with muonium: in  $\text{C}_{60}$  and  $\text{C}_{70}$  a fraction of Mu is trapped in a metastable state inside the fullerene cage, only those Mu atoms which are formed outside the cage can add and form  $\text{MuC}_{60}$  or  $\text{MuC}_{70}$  radical states [8].



- The sum of the observed polarizations,  $P_D + P_{Mu} + P_R$ , often does not add up to the original polarization in the muon beam. The amplitudes of high frequency precession signals need to be corrected for losses due to insufficient experimental time resolution, and effects due to sample size and density and muons stopping in the cell walls can be accounted for [9]. Even then, there is usually a *lost fraction of polarization*  $P_L = 1 - P_D - P_{Mu} - P_R$ . In water,  $P_L$  was found to amount to 0.18, and it was shown to originate from depolarizing encounters due to spin exchange of muonium with hydrated electrons from the track on a time scale of about 1 ns after the muon stop [10,11]. The same mechanism can partly depolarize radicals. Alternatively, polarization may be lost due to incoherent transfer from a precursor state, for example when a radical is formed slowly from a Mu precursor. If the chemical lifetime of the precursor is sufficiently long that there is significant spin evolution the muons arrive in the radical with different phases. The polarization transfer depends on the difference of precession frequencies in reactant and product, and thus on the external magnetic field [12]. To avoid such losses, the Mu lifetime should be  $\tau_{Mu} \ll \omega_0^{-1} = 36$  ps, where  $\omega_0 = 2\pi \times 4463$  MHz is the Mu hyperfine splitting constant.
- Because of the lost fraction  $P_L$ , the fractional polarizations  $P_i$  represent lower limits of the fractional chemical yields. While it is often non-trivial to account quantitatively for  $P_L$  it can be said that in most cases  $P_D$  is not affected, but the fractions of paramagnetic species,  $P_{Mu}$  and  $P_R$ , may be smaller than they would be in the absence of depolarizing effects.

## 2.2 Intercepting end-of-track processes

According to Bethe the stopping power of particles of energy  $E$ , mass  $M$ , charge  $Z$  and velocity  $v$  is proportional to  $2Z/mv^2 = ZM/mE$ , where  $m$  is the electron mass [13,14]. Thus, when  $v$  of the incident particle is large compared with the orbital velocities of electrons bound to an atom, which is where the Bethe theory holds, particles of the same charge and velocity have the same linear energy transfer, and for particles of the same energy the LET scales with  $M$ . For electrons in water, this relation holds down to energies of the order of 50 eV, while the corresponding limit of validity is around 10 keV for muons and around 100 keV for protons. The LET for electrons, positive muons and protons adopt maxima at these energies, as depicted in Figure 1 according to calculations by Mozumder [13]. At energies below these limits there is a marked drop-off in the LET, until for positive particles but not for electrons charge exchange takes over as an energy loss mechanism. Thus, at energies around 100 eV, and after two cross-overs again around 10 eV, the LET is predicted to be highest for

electrons and lowest for the particle of intermediate mass ( $\mu^+$ ). From the plot in Figure 1 we may conclude that an electron (and also a positron [13] but not the neutral positronium atom) spends its last 100 eV over a distance of ca. 1.5 nm, which means that it comes to rest inside or very close to its last spur, containing on the order of 5 radical pairs in water (mainly  $e^-_{aq}$ ,  $H_2O^+$ ,  $\cdot OH$ )[14]. In the same energy range, the LET is lower than that of the electron by about one order of magnitude for the proton, and even lower for the muon. This means that the proton and in particular the muon come to rest in water at a distance of at least 10-50 nm downstream of the last radical species arising mostly from charge exchange events. Experimentally, this very end of a track is not well known, and even theoretical calculations are rare, and the models are difficult to test experimentally.

Recent theoretical work has suggested that, in contrast to charged particles, neutralized particles slow down by optical phonon scattering, which has the consequence that the mean displacement of Ps, following its last neutralization event, is larger by four orders of magnitude than that of Mu with the same energy [15]. Thus, in the absence of experimental results, the situation may be depicted schematically as shown in Figure 2: the thermalized and solvated positron comes to rest in the last spur within reach of radiolytic ions, whereas the neutral Ps atom

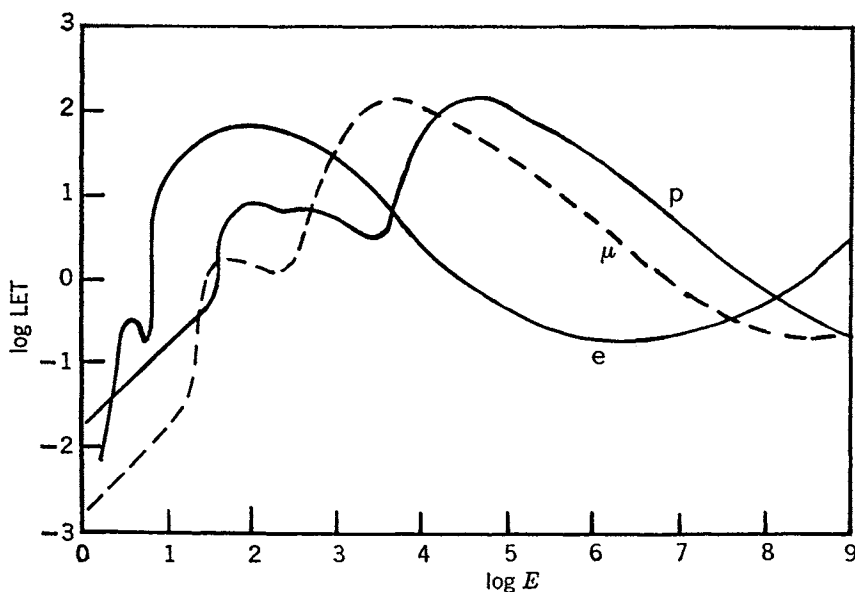


Figure 1. Stopping power of water for electrons, positive muons and protons according to Mozumder [13] (Copyright John Wiley & Sons Limited. Reproduced with permission). The LET is given in eV/nm, the energy  $E$  in eV.

which is born at high energies has left the last spur far behind. In addition to this prompt Ps there will be a second fraction of Ps which forms slightly delayed by combination of the positron with one of the spur electrons. In contrast, the muon and the Mu atom are both thought to come to rest very close to the end of the ion track, so that they will both be able to interact with radiolytic species.

Investigations of  $P_L$  often involve a combination of studying the magnetic field dependence and of using scavenger molecules which interfere chemically in the depolarizing process and trap the polarization before it is lost. This may involve electron scavengers which convert free or solvated electrons to less mobile radicals (e.g.  $^{\bullet}\text{CCl}_3$  from dissociative capture with  $\text{CCl}_4$ ), or hydrogen scavengers which convert Mu to diamagnetic products. Figure 3 displays an example of a study using aqueous solutions of sodium nitrate which reacts with Mu atoms with a rate constant of  $1.5 \times 10^9 \text{ M}^{-1} \text{ s}^{-1}$  under formation of a diamagnetic product [7]. In a 1 M sodium nitrate solution the chemical lifetime of Mu thus amounts to 0.6 ns. It is clearly seen that  $P_D$  is highly dependent on magnetic field. At high scavenger concentration Mu is converted efficiently to a diamagnetic state, and

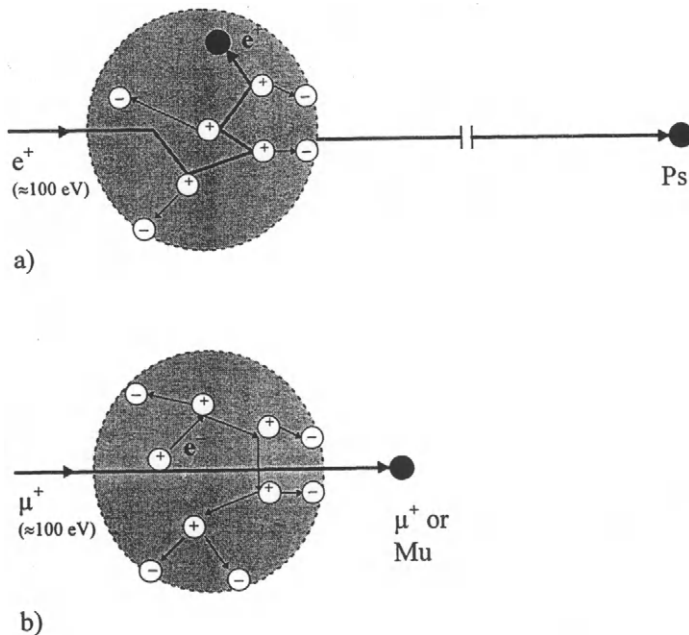


Figure 2. Schematic representation of the last spurs (shaded areas) in the tracks of (a) a positron or of Ps, and (b) of a muon or Mu, respectively (Reproduced with permission: Adapted from [16] to take account of [15]). The signs denote the charges of the  $e^-$  and  $\text{H}_2\text{O}^+$  primary ionization products.

high fields with concomitant fast evolution of spin polarization are necessary to produce significant depolarization during the short Mu lifetime.

Another technique makes use of olefins to spin-trap short-lived Mu and make it observable in muonated free radicals. In this way it was possible to prove that Mu is formed also in liquid chloroform or acetonitrile where it was never directly detected. This is shown in Figure 4 which presents Fourier spectra of the FID that was obtained with 0.2 M solutions of 2,3-dimethylbutadiene-1,3 (DMBD) in different solvents. At this concentration, DMBD can trap Mu on a time scale of ca. 40 ps in  $\text{CHCl}_3$  [17]. The spin trap adduct is the 1,1,2-trimethylallyl radical which has the Mu atom substituted in the *exo*-methyl group. It shows up in the spectrum by two muon precession frequencies, denoted  $R$ , which are the equivalent of the electron-nuclear double resonance (ENDOR) transitions in conventional magnetic resonance of free radicals.

A similar experiment using Mu trapping with pyrogallol in a wide range of aqueous solutions gave evidence of a non-homogeneous distribution of the paramagnetic products near the end of a muon thermalization track [18].

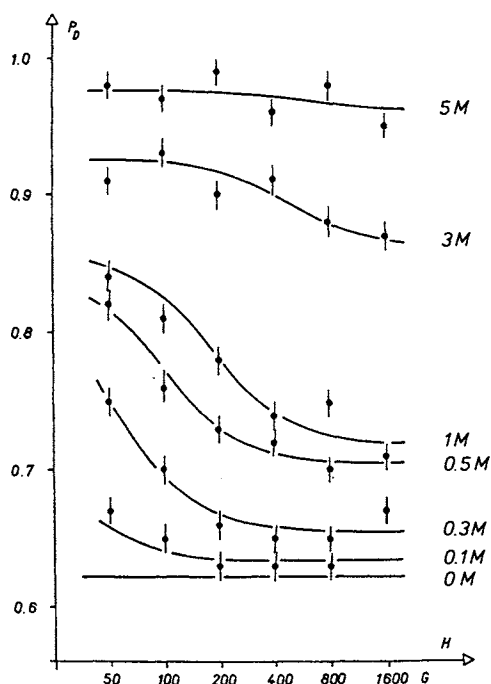


Figure 3. Muon polarization in sodium nitrate solutions as a function of magnetic field (Reprinted from [7] with permission from Elsevier Science).

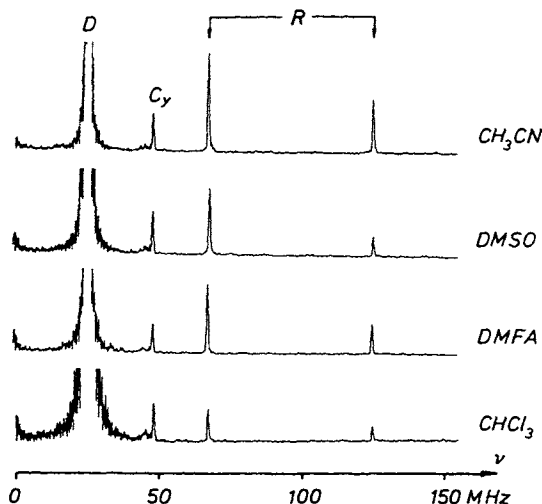


Figure 4.  $\mu$ SR frequency spectra obtained with 0.2 M solutions of DMBD in four organic solvents in a transverse magnetic field of 2000 G. *D* denotes muons in a diamagnetic environment, *Cy* is a background signal at the cyclotron frequency, and *R* is the radical formed by spin-trapping Mu ([17], reprinted with permission).

While most studies of radiation chemistry track effects have been carried out in condensed phase, and particularly in liquids, evidence of  $P_L$  due to interaction with track electrons or other paramagnetic species (e.g.  $N_2^+$ ) has also been seen in gases at high pressures and as well near the critical point in ethane [19].

At this point it is interesting to note that the distribution of muon polarization between Mu, diamagnetic compounds and the lost fraction may depend significantly on the state of the sample. For carbon tetrachloride, for example,  $P_D$  and  $P_{Mu}$  are both 0.5 in gaseous  $CCl_4$  near atmospheric pressure,  $P_D$  then changes to 1.0 in the bulk liquid or plastic crystalline phase, whereas in the rigid crystalline phase there are two components of the diamagnetic signal with different relaxation rates [20].

More recently, an alternative method has been developed which takes advantage of an applied static electric field designed to pull the muon and electron apart before they combine to form Mu near the end of the muon track [21]. The result of a typical experiment as a function of the applied field is shown in Figure 5 which gives the asymmetries (un-normalized polarizations) of Mu and D species in solid  $\alpha$ - $N_2$ . It is obvious that the field interferes in the distribution of muons, and most remarkably, the behavior is not symmetric with respect to zero field. This means that the muon does not come to rest in the center of a

probability distribution of radiolysis electrons but that, following the last ionization event, it has sufficient kinetic energy available to escape the last spur and come to rest of the order of 50 nm further downstream (compare Figure 2). Analogous studies have also revealed slow Mu formation by recombination of the muon with an electron from its own ionization track for various solid and liquid systems. An additional benefit of these experiments lies in the determination of reliable electron mobilities over distances where the material is homogeneous and not affected by grain boundaries in solids. A clear electric field effect was also reported and discussed for Ps formation in liquid n-alkanes and other systems [22].

A detailed piece of earlier work was also concerned with muon end-of-track radiolytical processes in acetone [23]. The muonated species observed on a microsecond time scale is the radical formed formally by Mu addition to the carbonyl oxygen. It was shown that two-thirds of the radicals were indeed formed by addition of Mu on a time scale of 0.1 ns. The remaining one-third did not involve a Mu precursor and was instead formed by direct combination of a track electron with a muon-acetone complex, or of a muon with an acetone anion, on a time scale of about 3 ns. This conclusion was based on an analysis of the observed initial phases of muon precession as a function of the applied magnetic field, and it takes advantage of the fact that the muon in a diamagnetic environment precesses in the opposite direction, and with a different precession frequency compared with the muon in Mu.

The above experiments show clearly that there are means to intercept end-of-track processes which occur on a time scale of tens of picoseconds to tens of nanoseconds. This has served to cool down vivid earlier discussions about the

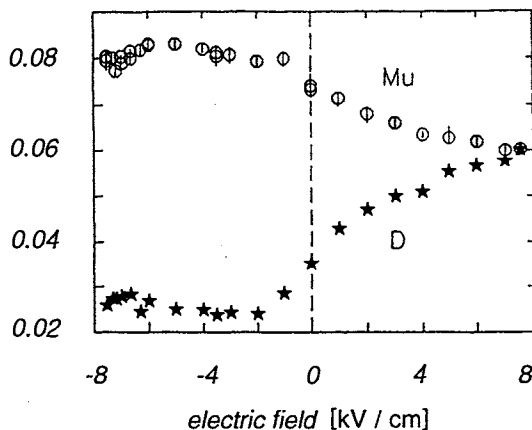


Figure 5. Electric field dependence of D and Mu asymmetries in  $\alpha$ -N<sub>2</sub> at T = 20 K (adapted from [21]).

importance of "hot" versus "thermal" contributions to the formation of muon containing species in condensed phase. Hot processes were generally understood to occur at energies far above thermal, and thus they should be too fast to be interceptable. It is believed that epithermal processes play a significant role in the gas phase whereas at lower densities spurs and tracks have no physical meaning [19].

### **2.3 Comparison of muonium with positronium and hot tritium**

Since positrons, muons and tritons are all end-of-track probes with single positive charge it is tempting to compare the results of corresponding studies and analyze them in terms of the different masses. While early ideas about hot processes were related much to those used in recoil tritium studies it is obvious that the new picture emerging for muonium formation has benefited from the spur model of positronium formation. It is nevertheless non-trivial to work out a convincing correlation between the experimental parameters which are extracted from Ps, Mu and T studies. The reason for this is to some extent due to the fact that Ps escapes its last spur largely unaffected (Figure 2), but Mu and T come to rest close to the last spur so that they can react with it, and furthermore it is due to the very different time scales on which the experiments view the end of the tracks of the three probes. Positrons are short-lived and probe time scales on the order of one nanosecond [6]. Mu experiments yield direct information over what is available on a microsecond time scale where spurs have dissipated to a large extent [16]. Only indirectly, via the above trapping and electric field experiments do we have access to earlier times [21, 23], but the correct answer is obtained only when the analysis is based on the correct chemical model. Recoil tritium experiments require that reaction products are extracted and treated radiochromatographically, a process that takes minutes or hours, before the activity of the individual components is determined. While in muon experiments Mu and radicals which have escaped the spurs are directly observed they have all reacted to diamagnetic products quantitatively on the time scale of tritium experiments.

The distribution of cyclohexadienyl radical isomers formed from toluene by addition of Mu, thermal or nominally hot T is very similar, suggesting that the conditions of formation are not significantly different (Table 1). In all cases addition in the ortho position occurs with higher than statistical probability, at cost of the other positions. The methyl substituent in toluene thus has a clear ortho-directing effect. Cl, F and CF<sub>3</sub> are meta-directing, and phenoxy, COCl and CN are para-directing [12]. For hot atom reactions one normally expects a statistical distribution.

Table 1:  
Distribution of isomers in the addition of Mu and T to toluene

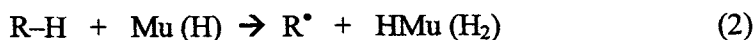
isomer	Mu [9]	thermal T [24]	"hot" T [25]
ortho	48(1)%	45.7%	46.0%
meta	35(1)%	41.2%	35.0%
para	17(2)%	13.1%	19.0%

### 3 MUONIUM REACTIONS AND KINETIC ISOTOPE EFFECTS

Primary kinetic isotope effects (KIE) are those in which a bond to the isotope is either formed or broken. They are normally found to be much more pronounced than secondary KIE where the isotope is not directly involved in the reaction.

Two types of quantum effects contribute to kinetic isotope effects, *vibrational zero-point energy shifts*, and *quantum tunneling* through energy barriers. They contribute to a different extent, depending on the nature of the reaction, and their effect on the KIE is often in opposite directions.

A zero-order approach treats chemical reactions in a simplified one-dimensional picture in which only a single degree of freedom, the reaction coordinate is taken into account. In the transition state, the reaction coordinate gets a special treatment, and therefore it is only the zero-point energy of the reactants which is relevant. A familiar example is the reaction pair



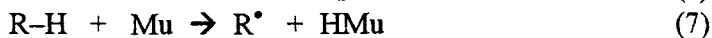
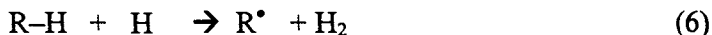
in which the abstraction of H is favored over that of D, but the attacking atom is the same for both reactions, and thus its effect cancels in the ratio of rate constants.

At the same level of approximation the reaction barrier is simply the electronic potential which is independent of isotopic masses. For identical barriers tunneling is strongly favored for the lower mass. Thus, because of tunneling, the reaction of Mu is expected to be faster than that of H or D, and this will be particularly pronounced for exo-energetic reactions which often have narrow and not too high barriers, as for example in additions to olefins (Ol)





A more complete treatment includes the other degrees of freedom. The vibrations orthogonal to the reaction coordinate now contribute with their zero-point energies to the barrier along the reaction path. This leads to a higher barrier for the reaction involving the lighter isotope, and it distinguishes between the abstraction reactions



which have the same activation energies in the zero-order approach.

Vibrational zero-point energy is an inherent contribution to the total energy, and it is therefore also the vibrational adiabatic barrier which is relevant for the extent of tunneling. The increased barrier height for the lighter isotope thus reduces significantly the tunneling probability in comparison with that expected based on a one-dimensional approach.

Thus, the lower mass of Mu compared with its heavier isotopes has the counteracting effects that its rate constants are lower because of zero-point energy effects in the transition state, and that they are higher because of tunneling. Which of the two effects wins depends on the details of the potential energy surface. It is in general found that for H abstractions Mu is slower than H by up to 2-3 orders of magnitude, and in addition reactions it is faster than H again by up to 2-3 orders of magnitude. Two typical examples are given below, others are found in literature [26, 27].

Mu addition to benzene in the gas phase ( $\text{N}_2$  moderator, 1.5 bar, representing the high pressure limit) is faster than H addition, as shown in Figure 6. While the activation energy for H amounts to  $18.6 \text{ kJ mol}^{-1}$  it is only  $6 \text{ kJ mol}^{-1}$  for Mu [28, 29]. At the same time, the pre-exponential factor for Mu is lower than that of the H reactions. Both effects are clear indicators for a KIE which is dominated by tunneling.

The behavior observed for H abstraction from  $\text{HCO}_2^-$  in aqueous solution is displayed in Figure 7 [30]. Here we have the case where Mu is clearly slower than H or D, and its activation energy is higher.

Both examples demonstrate that Mu is far more susceptible to KIE than H or D, and it is therefore an extremely sensitive probe of reaction theories and in particular of potential energy surfaces.

A particularly illustrative example of the sensitivity of Mu to kinetic isotope effects is its addition to  $\text{O}_2$ , in comparison with  $\text{H} + \text{O}_2$  [31]. In the low pressure regime at room temperature, Mu is slower than H by a factor of ca. 7, but there appears to be a cross-over at a pressure of several hundred bar, and in the high

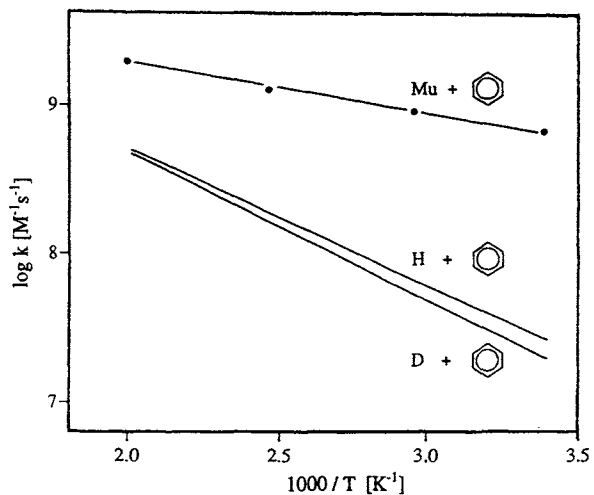


Figure 6. Arrhenius plot of the Mu, H, and D addition kinetics to benzene in the gas phase, demonstrating that tunneling accelerates the Mu reaction ([29], reprinted with permission).

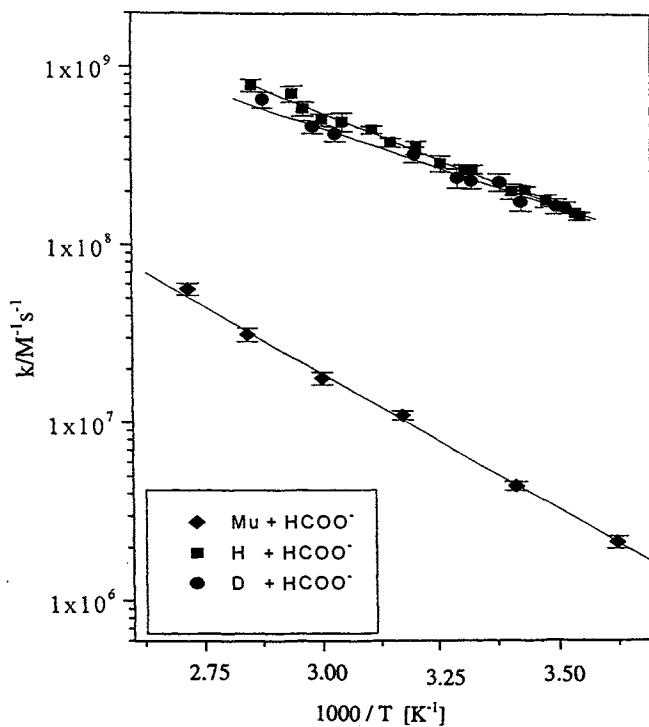


Figure 7. Arrhenius plot of the H abstraction kinetics from formate by Mu, H, and D, showing that the zero-point energy in the transition state retards the Mu reaction [30].

pressure limit Mu is predicted to be faster. A quite dramatic effect was also observed in the temperature dependence. The rate constant for the H reaction decreases with  $T^{-1.8}$  while that of Mu is essentially temperature independent. An analysis of the KIE reveals that the mass enters most effectively in the translational partition function, favoring Mu over H by a factor of 25, in the rotational partition function and in the density of vibrational states which disfavor Mu by factors of ca. 3 and 8, respectively [31]. An important role is played by a small vibrational zero-point energy barrier on top of an essentially barrier free electronic potential energy surface. Furthermore, the efficiency of energy transfer in stabilizing collisions with the moderator, a process that is theoretically not yet satisfactorily understood, appears to play a major role and seems to be subject to isotopic substitution as well [32].

## 4 SOLVATION AND DIFFUSION OF HYDROGEN ISOTOPES IN WATER

### 4.1 Equilibrium and non-equilibrium solvation

The observation that H addition to benzene is faster in aqueous solution than in the gas phase by a factor of ca. 35 [28], as shown in Figure 8, triggered a series of experimental and theoretical studies on the nature of hydrogen atoms in water. The kinetic solvent effect was explained by H atom equilibrium solvation. Atomic hydrogen in water behaves like a noble gas atom of the same polarizability, its solvation is accompanied not only by a solvation enthalpy of  $-4.1 \text{ kJ mol}^{-1}$  but in particular by a strong decrease in entropy of  $51 \text{ J mol}^{-1} \text{ K}^{-1}$  at 298 K, which is indicative of the formation of a solvent cage around a hydrophobic atom [28]. Since this is equilibrium solvation it should be nearly independent of the mass of the solvated atom. This was confirmed in recent theoretical work [33, 34].

If equilibrium solvation is the only cause of the solvent effect then the Mu reaction should also be a factor 35 faster in aqueous solution compared to the gas phase. This was not observed, the increase of its rate constant in water for addition to benzene amounts to only a factor of 3-5 (Figure 8), and it is not limited by diffusion. The difference was ascribed to a dynamic solvent effect and taken as evidence of Kramers solvent friction which increases with frequency and is thus obviously far more important for the reaction of Mu, the lighter isotope [33].

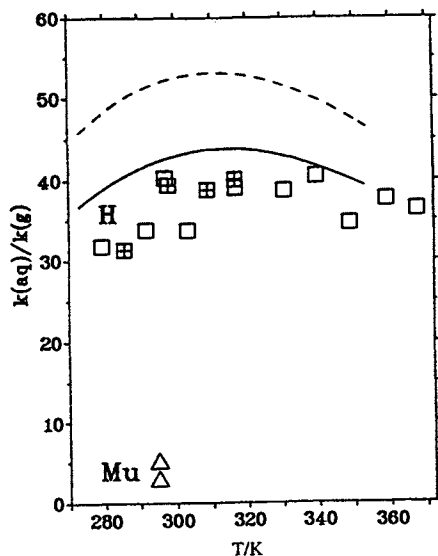


Figure 8. Aqueous solution versus gas phase ratio of rate constants for addition of H and Mu atoms to benzene. Open symbols apply to solutions using tert-butanol, crossed squares to methanol as hydroxyl radical scavengers. The broken line gives the expected values based on the positive free energy of solvation of hydrogen atoms in water, the solid line involves a further correction ([28], reprinted with permission).

#### 4.2 Break-down of the Stokes-Einstein equation

It is well-known that diffusion coefficients depend on the mass of the diffusing species in the gas phase and also in solids. In liquids, diffusion is normally described well by the Stokes-Einstein equation which depends on the hydrodynamic radius and on viscosity but not on the mass. There is no principal reason that prevents a mass dependence in solution, and many experiments have been devised to search for isotope effects [35], mostly with no clear answer. It is obvious that a comparison between Mu, H, and D should be particularly sensitive. This question has been posed long ago [16], but the answer had to await more recent results, as outlined below.

Diffusion coefficients were reported to be  $(7.0 \pm 1.5) \times 10^{-9} \text{ m}^2 \text{ s}^{-1}$  for H in  $\text{H}_2\text{O}$  and  $(5.0 \pm 1.0) \times 10^{-9} \text{ m}^2 \text{ s}^{-1}$  for D in  $\text{D}_2\text{O}$  [36]. After correction for the different viscosities of  $\text{H}_2\text{O}$  and  $\text{D}_2\text{O}$  one obtains  $D_{\text{H}}/D_{\text{D}} = 1.41 \pm 0.46$ , which is compatible with  $\sqrt{2}$  but also with unity, and it matches the presumably more accurate relative value of ca. 1.10 that was deduced by Han and Bartels from EPR dephasing rates in the reaction of the isotope with molecular oxygen [37], assuming that it is diffusion controlled. On the same basis,  $D_{\text{Mu}}/D_{\text{H}}$  was determined to be  $2.0 \pm 0.2$ , indicating that Mu diffuses in water significantly faster than H [38].

Hydrogen diffusion is nearly as fast as proton diffusion ( $D_{\text{H}^+} = 9.3 \times 10^{-9} \text{ m}^2 \text{ s}^{-1}$ ) which is normally considered to be particularly fast because of the favorable Grotthus mechanism. For atomic hydrogen, conversion of  $D_{\text{H}}$  based on the Stokes-Einstein equation,  $D = kT/4\pi\eta R_0$  in the slip limit, gives a hydrodynamic radius  $R_0$  of 0.019 nm. This is very small, less than half the Bohr radius of the atom, demonstrating clearly and not unexpectedly that the Stokes-Einstein equation breaks down for such small solutes. In this context it is interesting to be reminded of the evidence from molecular dynamics calculations as well as from the analysis of the hyperfine coupling constant that hydrogen atoms in water form a hydrophobic bubble state [39,40]. The bubble radius  $R_b$  was estimated to be about 0.23-0.25 nm, very comparable to the radius of a clathrate cage, but one order of magnitude larger than the hydrodynamic radius  $R_0$ . Based on Stokes-Einstein diffusion of the bubble the large value of  $D_{\text{H}}$  is not compatible with  $R_b$ . It means that the bubble is not dragged along in a diffusive displacement step, rather the isotope must jump to its new site which may be partially preformed by statistical fluctuations. In order to provide an isotope effect such a jump must occur more often or extend over a longer distance for the lighter atom. The situation is depicted schematically in Figure 9. It would be interesting to verify this picture with quantum molecular dynamics calculations.

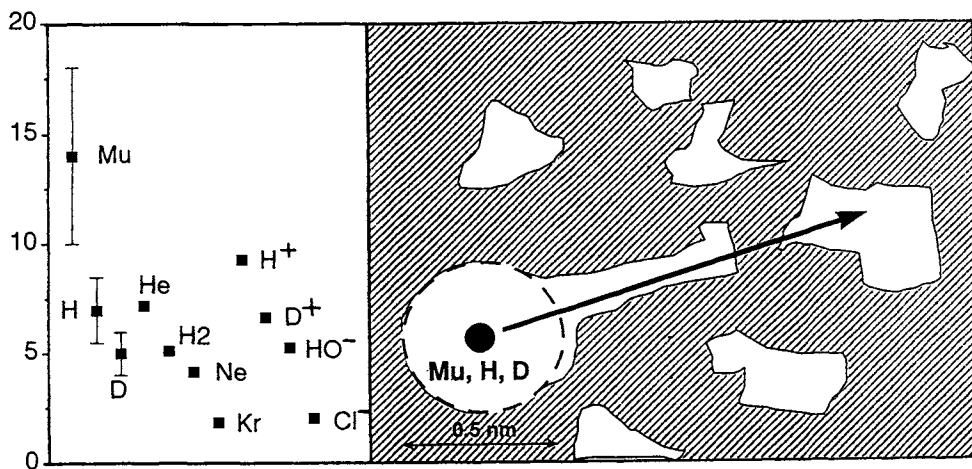


Figure 9. Diffusion coefficients in units of  $10^{-9} \text{ m}^2 \text{ s}^{-1}$  for small atoms, molecules and ions in water, and schematic representation for incoherent quantum diffusion of hydrogen isotopes in liquid water.

## 5 MUONIUM-SUBSTITUTED FREE RADICALS

### 5.1 Radical spectroscopy

Muonium-substituted free radicals contain the muon as a polarized spin label which allows its detection either by the transverse field muon spin rotation (TF- $\mu$ SR) technique or by longitudinal field avoided-level-crossing muon spin resonance (ALC- $\mu$ SR) [4].

The muon-electron hyperfine interaction,  $A_\mu$ , is obtained directly from the pair of muon nuclear precession frequencies which obey the ENDOR condition [4,12]. It is related to the structure of the radical in the same way as  $A_p$  for the proton that takes the place of the muon in conventional radical chemistry.  $A_\mu$  is obtained from  $A_p$  by scaling with the ratio of magnetic moments ( $\mu_\mu/\mu_p = 3.183$ ), but in addition there is an isotope effect of ca. 20%, favoring Mu, which is related to the anharmonicity of the bond, making C-Mu longer than C-H by ca. 5% in the vibrational average [41]. In addition, for Mu atoms substituted in methyl groups or in other environments with rotational flexibility, there is a slight preference for a conformation in which the C-Mu bond is eclipsed with the  $p_z$  orbital containing the unpaired electron - a consequence of minimization of zero-point energy [42].

ALC- $\mu$ SR spectra are scanned as a function of an applied longitudinal field. They show resonances at fields where there is an avoided crossing of magnetic energy levels which allows for additional muon relaxation. The resonance fields are related to the muon *and* nuclear hyperfine coupling constants, including their relative signs [4]; there is thus complementary information to TF- $\mu$ SR as well as to ESR. Figure 10 gives an example of both transverse field and ALC- $\mu$ SR spectra obtained with liquid 6,6'-dimethyl-fulvene [43]. The two pairs of frequencies in the transverse field spectrum (a,a' and b,b', upper part of Figure 10) show that two isomeric radicals are formed. The strong line at 40.6 MHz represents muons in diamagnetic environments. The TF- $\mu$ SR spectra give the muon coupling constant, and from the ALC- $\mu$ SR resonances in the lower part of Figure 10 we derive the proton coupling constants. The complete set of information identifies the two radicals as those formed by Mu addition to the two inequivalent ring positions, leading to the structures which are given in the inset. Both muon hyperfine coupling constants, after correction for the muon-proton ratio of magnetic moments, are larger than the coupling constants of the protons at the same carbon, giving evidence of the above mentioned hyperfine isotope effect as a consequence of bond anharmonicity.

Probably close to 300 different muonated free radicals have been observed to date. Almost all of them are derived formally by Mu addition to double or triple bonds, including C=O, C=S, and C=N bonds.

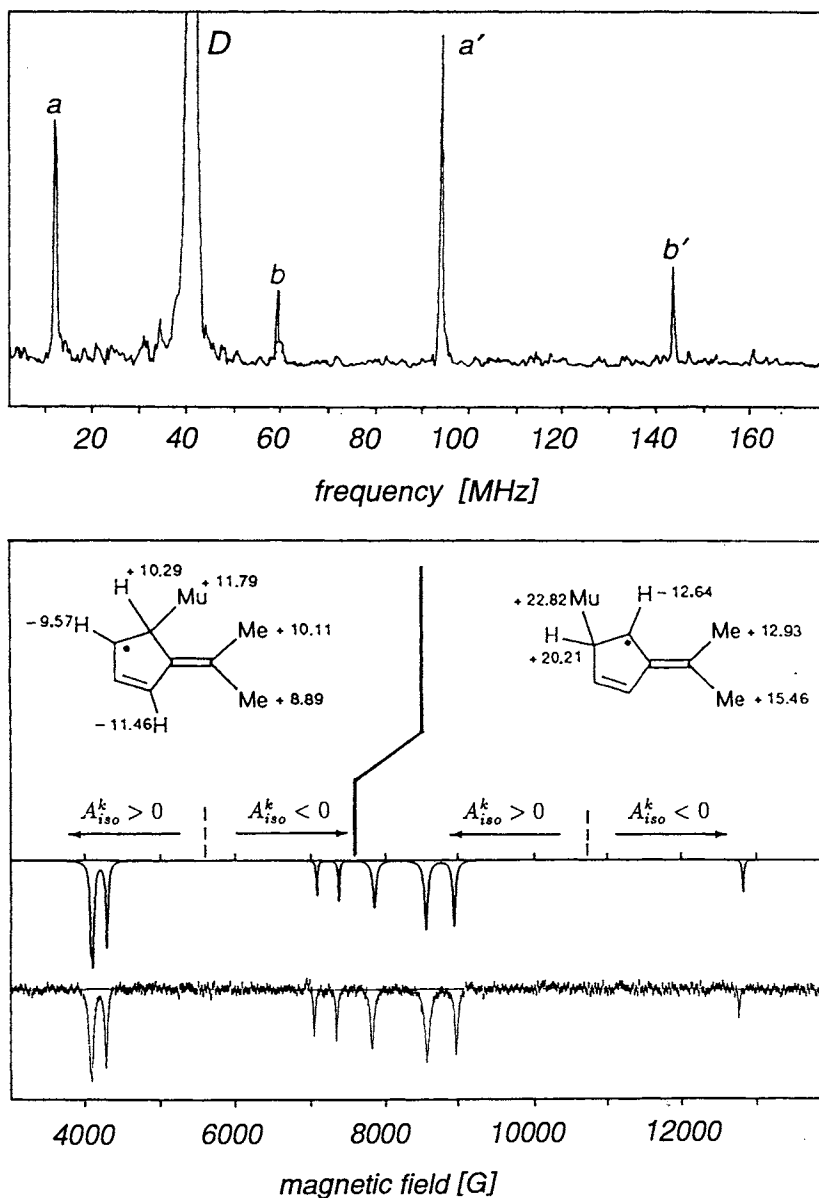


Figure 10.  $\mu$ SR spectra of the radicals formed by Mu addition to liquid 6,6'-dimethylfulvene. Transverse field muon spin rotation spectrum (upper, with lines for the radicals a and b, and for muons in diamagnetic environment D), and longitudinal field avoided level crossing spectrum (lower), simulation and experimental data based on the structures in the inset with proton coupling constants given in Gauss (adapted from [43] with permission of The Royal Society of Chemistry).

Recent work has also revealed the interaction of muonated cyclohexadienyl radicals with copper nuclei in ZSM-5 type zeolites [44]. This observation is so far unique to the  $\mu$ SR technique, and it is of potential interest for studying catalytic processes. The interaction is relatively weak with copper but appears to be much stronger with sodium and lithium ions.

## 5.2 The muon as a non-perturbing probe of radical kinetics

Mu addition to double bonds places the muon two bonds away from the radical center. Mu is thus not normally directly involved in reactions of the radical, and any kinetic isotope effects are secondary and thus small. This makes the muon a non-perturbing radical kinetics probe. Its advantage is the extraordinary sensitivity of the technique which requires only a single muon in the sample at a given time. This eliminates any radical termination reactions. With on the order of  $10^8$  muons needed for an experiment the concentration of the reaction partner does not change, and kinetics is of ideal pseudo-first order. This eliminates a number of sources for serious errors which often affect the accuracy of conventional radical kinetics.

The technique has been used to determine rate constants for a number of radical reactions in solution, notably ring closure and ring fission processes which serve as clock reactions in conventional radical kinetics [45]. As an example, the bimolecular reaction of the cyclohexadienyl radical with molecular iodine is shown in Figure 11. The straight line behavior demonstrates a pseudo-first order

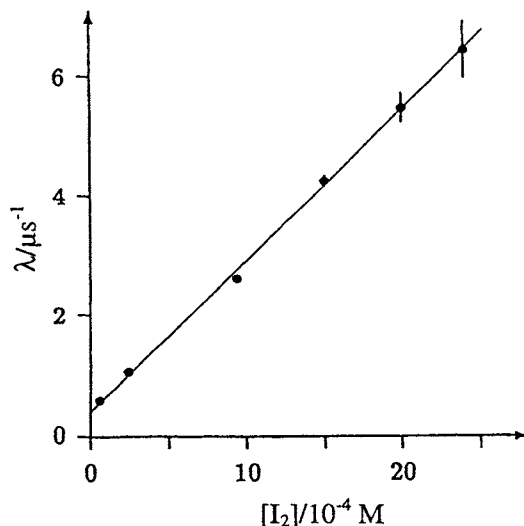


Figure 11. Kinetic plot for the reaction of  $C_6H_6\mu$  with  $I_2$  (Figure 8.4, p.77 of [12], reprinted with permission).



kinetics. The rate constant at room temperature,  $k = 2.5 \times 10^9 \text{ M}^{-1} \text{ s}^{-1}$  [12], obtained from the slope of the plot of the muon relaxation in the radical versus iodine concentration, is close to the diffusion controlled limit.

More recently, longitudinal muon spin relaxation was used to measure rate constants for the reactions of organic radicals with molecular oxygen and with NO in the gas phase [32, 46]. The reactions are important in combustion processes and for the degradation of organic pollutants in the atmosphere. Accurate determinations by conventional techniques have often proved to be non-trivial, so that the muon technique appears to be a very valuable addition to the tool box of experimental methods.

### 5.3 Probing radical reorientation dynamics on surfaces and in solids

Radicals adsorbed on surfaces can be studied by ESR as long as they are immobile. As soon as they gain translational mobility, which is when their chemistry starts to be of interest, they react with each other, and the signal disappears. Due to its high sensitivity the  $\mu\text{SR}$  technique is much more fortunate, it requires a single species at a time so that it becomes possible to study radicals also under conditions of high mobility. Advantage has been taken of this for the investigation of translational diffusion of surface adsorbed cyclohexadienyl radicals on silica [47] and of the reorientational dynamics of radicals in highly siliceous ZSM-5 zeolite [48]. Reorientation dynamics has also been studied for radicals in rotator phase solids, such as in norbornene or in fullerenes [49, 50].

There is a further particularly useful feature of ALC- $\mu\text{SR}$  which is illustrated in Figure 12. The resonances obey different selection rules, which has direct consequences as regards the appearance of the lines in the spectrum. The so-called  $\Delta_1$  resonance is the strongest one. It is present only under anisotropic conditions, mostly in solids or for strongly surface adsorbed species, while the  $\Delta_0$  resonances are allowed in all phases, but the  $\Delta_1$  is absent in liquids or gases where the anisotropy is averaged out by rapid isotropic tumbling. The critical time scale is given by the inverse of the hyperfine anisotropy and is typically 50 ns. For reorientation dynamics, particularly in the region of the critical time scale, the shape of this resonance is extraordinarily sensitive to the type of motion. For example, it disappears with increasing temperature *via broadening* for the Mu adduct to the fullerene  $C_{60}$  in its rotationally disordered phase, but *via narrowing* for the adduct to  $C_{70}$ , reflecting the fact that the lower symmetry of the latter changes the character of reorientational motion dramatically [50].

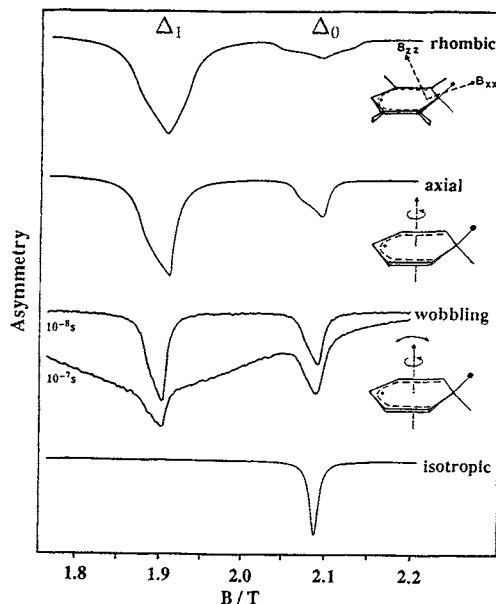


Figure 12. Selected field range of simulated ALC- $\mu$ SR spectrum of Mu substituted cyclohexadienyl radical under static conditions (rhombic environment) and for different types of reorientational dynamics (Reprinted from [48] with permission, Copyright American Chemical Society).

There are several areas in chemistry where positive muons will continue to be extraordinary probes:

- Whenever the interest is in hydrogen isotope effects of dynamic processes (reaction kinetics, diffusion), the muon or the Mu atom, owing to their low masses, are extremely sensitive probes.
- In radiation chemistry, the muon is an end-of-track probe that is suited to give unique information on radiolytic processes.
- A principal advantage of the muon that was not discussed here is due to its full polarization independent of magnetic field and temperature. This makes it an attractive magnetic probe in low or zero magnetic fields when interactions are to be studied which are quenched in higher external fields and therefore not accessible to traditional magnetic resonance. Polarization is far from thermal equilibrium, therefore independent of Boltzmann population, which is a significant advantage for muon experiments over conventional magnetic resonance.
- The muon can be implanted as a local magnetic probe in any material that does not itself contain suitable magnetic nuclei.

- There is no need for pulsing to first create coherence of spins, the time resolution of  $\mu$ SR experiments is therefore inherently higher by up to three orders of magnitude than that of ESR or NMR techniques.

Considerable recent efforts have centered on the production of muons at low energy, which allows them to be stopped near the surface of a material or in thin layers. This is attractive for example in view of studies of surface magnetism. The currently possible count rates at such beams are still somewhat low for efficient experiments, but a new generation of accelerators for high intensity neutron spallation sources which would also permit high fluxes of muons is in the planning stage. At such machines, low energy muon experiments are highly promising for a new class of applications [51].

## REFERENCES

1. W.E. Jones, S.D. MacNight, L. Teng, *Chem. Rev.* 73 (1973) 407.
2. S.F.J. Cox, *J. Phys. C: Solid State Phys.* 20 (1987) 3187.
3. A. Schenck, *Muon Spin Rotation Spectroscopy*, Hilger, Bristol, 1985.
4. E. Roduner, *Appl. Magn. Reson.* 13 (1997) 1.
5. D. Fleming and M. Senba, in *Perspectives of Meson Science*, T. Yamazaki, K. Nakai and K. Nagamine, Eds., Elsevier, Amsterdam, 1992.
6. D.M. Schrader and Y.C. Yean (eds.), *Positronium Chemistry*, Elsevier, Amsterdam, 1988.
7. P.W. Percival, E. Roduner and H. Fischer, *Chem. Phys.* 32 (1978) 353.
8. Ch. Niedermayer, I.D. Reid, E. Roduner, E.J. Ansaldo, C. Bernhard, U. Binniger, Glückler, E. Recknagel, J.I. Budnick and A. Weidinger, *Phys. Rev. B* 47 (1993) 10923.
9. E. Roduner, G.A. Brinkman and P.W.F. Louwrier, *Chem. Phys.* 73 (1982) 171.
10. P.W. Percival, J.-C. Brodovitch and K.E. Newman, *Chem. Phys. Lett.* 91 (1982) 1.
11. S.-K. Leung, J.-C. Brodovitch, P.W. Percival and D. Yu, *Chem. Phys.* 121 (1988) 393.
12. E. Roduner, *The Positive Muon as a Probe in Free Radical Chemistry. Potential and Limitation of the  $\mu$ SR Techniques. Lecture Notes in Chemistry, Vol. 49*, Springer, Heidelberg, 1988.
13. A. Mozumder, in *Advances in Radiation Chemistry*, M. Burton and J.L. Magee (eds.), Wiley, New York, 1969.
14. Farhatziz and A.J. Rodgers, Eds. *Radiation Chemistry*, VCH, Weinheim, 1987.
15. A. Seeger, *J. Phys.: Condens. Matter* 10 (1998) 10461.
16. D.C. Walker, *Muon and Muonium Chemistry*, Cambridge University Press, 1983.
17. E. Roduner, *Hyperfine Interactions* 32 (1986) 714.
18. S.-K. Leung, J.-C. Brodovitch, P.W. Percival and D. Yu, *Can. J. Phys.* 68 (1990) 947.
19. J.R. Kempton, M. Senba, D.J. Arseneau, A.C. Gonzalez, D.M. Garner, J.J. Pan, D.G. Fleming, P.W. Percival, J.-C. Brodovitch and S.-K. Leung, *J. Chem. Phys.* 94 (1991) 1046.

20. Y. Miyaka, Y. Ito, Y. Tabata and D.C. Walker, *Hyperfine Interactions* 32 (1986) 825.
21. V. Storchak, J.H. Brewer and G.D. Morris, Charge transport in solid nitrogen, in *Protons and Muons in Materials Science*, E.A. Davis and S.F.J. Cox (eds.), Taylor and Francis, London, 1996, p. 227.
22. O.E. Mogensen, *Appl. Phys.* 6 (1975) 315.
23. E. Roduner, *Radiat. Phys. Chem.* 28 (1986) 75.
24. W.A. Pryor, T.H. Lin, J.P. Stanley and R.W. Henderson, *J. Amer. Chem. Soc.* 95 (1973) 6993.
25. H.J. Ache, in: *Tritium in the Physical and Biological Sciences*, Vol. 2, Proceedings of Vienna Symposium, IAEA, Vienna, 1961.
26. E. Roduner, *Progress React. Kinet.* 14 (1986) 1.
27. D.C. Walker, *J. Chem. Soc., Faraday Trans.* 94 (1998) 1.
28. E. Roduner and D.M. Bartels, *Ber. Bunsenges. Phys. Chem.* 96 (1992) 1038.
29. E. Roduner, P.W.F. Louwrier, G.A. Brinkman, D.M. Garner, I.D. Reid, D.J. Arseneau, Senba, D.G. Fleming, *Ber. Bunsenges. Phys. Chem.* 94 (1990) 1224.
30. A. Lossack, PhD Thesis, University of Stuttgart, 1999.
31. U. Himmer, H. Dilger, E. Roduner, J.J. Pan, D.J. Arseneau, D.G. Fleming and Senba, *J. Phys. Chem. A* 103 (1999) 2076.
32. U. Himmer, PhD Thesis, University of Stuttgart, 1999.
33. B.C. Garrett and G.K. Schenter, in: *Structure and Reactivity in Aqueous Solutions*, Cramer, D.G. Truhlar (eds.), ACS Symposium Series Nr. 568; American Chemical Society, Washington D.C. 1994.
34. H. Gai and B.C. Garrett, *J. Phys. Chem.* 98 (1994) 9642.
35. H.J.V. Tyrrell and K.R. Harris, *Diffusion in Liquids*, Butterworths, London, 1984.
36. W.A. Benderskii, A.G. Krivenko and A.N. Rukin, *Chim. Vysok. Energ.* 14 (1980) 400. [English transl. *High Energy Chem.* 14 (1980) 303].
37. P. Han and D.M. Bartels, in: *Ultrafast Reaction Dynamics and Solvent Effects*, Y. Gaudel and P. Rossky (eds.), AIP Conference Proceedings 298, AIP Press, New York, 1994.
38. E. Roduner, P.L.W. Tregenna-Piggott, H. Dilger, K. Ehrensberger and M. Senba, *Chem. Soc. Faraday Trans.* 91 (1995) 1935.
39. E. Roduner, P.W. Percival, P. Han and D.M. Bartels, *J. Chem. Phys.* 102 (1995) 5989.
40. J.S. Tse and M.L. Klein, *J. Phys. Chem.* 87 (1983) 5055.
41. E. Roduner and I.D. Reid, *Israel J. Chem.* 29 (1989) 3; E. Roduner, *Faraday Discussion Chem. Soc. No. 78* (1984) 94.
42. T.A. Claxton and A.M. Graham, *J. Chem. Soc., Chem. Commun.* (1987) 1167.
43. E. Roduner, *Chem. Soc. Reviews*, 22 (1993) 337.
44. M. Stölmár and E. Roduner, *J. Amer. Chem. Soc.* 120 (1998) 583.
45. P. Burkhard, E. Roduner and H. Fischer, *Int. J. Chem. Kinetics*, 17 (1985) 186.
46. H. Dilger, M. Schwager, P.L.W. Tregenna-Piggott, E. Roduner, I.D. Reid, D.J. Arseneau, J.J. Pan, M. Senba, M. Shelley and D.G. Fleming, *J. Phys. Chem.* 100 (1996) 6561,16445.

47. M. Schwager, H. Dilger, E. Roduner, I.D. Reid, P.W. Percival and A. Baiker, *Chem. Phys.* 189 (1994) 697.
48. E. Roduner, M. Stolmár, H. Dilger and I.D. Reid, *J. Phys. Chem. A* 102 (1998) 7591.
49. E. Roduner, I.D. Reid, R. De Renzi and M. Riccò, *Ber. Bunsenges. Phys. Chem.* (1989) 1194.
50. E. Roduner, K. Prassides, R. Macrae, I.M. Thomas, C. Niedermayer, U. Binniger, Bernhard, A. Hofer and I.D. Reid, *Chem. Phys.* 102 (1995) 5989.
51. T. Prokscha, E. Morenzoni, M. Meyberg, T. Wutzke, B.E. Mathias, A. Fachat, Jungman and G. zu Putlitz, *Phys. Rev. A* 58 (1998) 3739.

## **Fundamental Processes in Gas Phase Radiation Chemistry**

**Ronald Cooper<sup>a</sup> and Stephen P. Mezyk<sup>b</sup>**

<sup>a</sup>Radiation Chemistry Group, School of Chemistry, University of Melbourne, Parkville 3052, Victoria, Australia

<sup>b</sup>Department of Chemistry, University of North Carolina at Wilmington, Wilmington, NC, 28403, United States of America

The irradiation of a simple gas generates many primary products including excited states, ions, and molecular fragments, as well as more generations of lower energy electrons. These species are formed by energetic secondary electrons, which slow down in a succession of inelastic collisions transferring energy to the components of the medium. From this cascade of events a range of chemical moieties are generated which can be used in a wide range of fundamental and applied chemical physics situations. In gases, such areas of especially useful application range from understanding atmospheric electrical phenomena, ozone depletion chemistry, and free radicals in combustion through to the modelling of electrical discharges use in waste disposal, fluorescent lighting, high voltage switching and e-beam pumped lasers.

The species generated by radiolysis in gases can also be produced by electrical discharges, however, the discharge technique used by plasma physicists is restricted to low (< 50 Torr) pressures whereas radiolysis can be used up to very high pressures (50 atm). Further, the quantitative aspects of radiation chemistry - G values via precise dosimetry - enable accurately known concentrations of species such as cations and electrons to be produced at will. Experimental developments in pulse radiolysis and associated detection techniques now allow direct observation of the reactions of radiolytically produced species from times as short as a few picoseconds. Given that at one atmosphere in a gas at ambient temperature, a gas molecule, on the average, undergoes a collision about every nanosecond then radiolytic techniques are able to make accurate temporal measurements of the kinetic parameters of gas phase reactions with time to spare!

If radiolysis is to be used as a precise source of reactive species then it is essential to ensure that the fundamental energy deposition processes do not

temporally overlap the desired chemical reaction time zones. Both experimental and theoretical studies have sought to establish time domains for the various stages of radiolysis. The defined [1] time domains are the Physical stage, where the initial irradiating particle imparts its energy to the medium; the Physico-Chemical stage which involves the relaxation of the primary species to thermally equilibrated states, and the Chemical stage which encompasses the reaction of these thermalised species to form stable products.

### **The Physical Stage**

Spencer and Fano [2] modelled the entire electron slowing down process by taking into account all possible electron energy loss mechanisms and subsequent generations of electrons. The Spencer-Fano equation is exact and determines the energy distribution of all electrons from the initial photon/particle energy down to the lowest inelastic threshold energy. However, it does not describe the evolution of the electron energy spectrum over time, nor did it attempt to describe the yield of molecular states produced in the target by the electron degradation. Inokuti and co-workers [3,4] generalised the Spencer-Fano theory to include the temporal aspects of high-energy electron energy degradation. A transport equation was written in terms of a time-dependent electron energy distribution and expressions were derived for the time-dependent yields of primary species. This time-dependent Spencer-Fano (TDSF) theory was used to calculate time-dependent yields of primary species and electron degradation spectra for the simple gases argon [3,5] hydrogen [6], mixtures of these two gases [5], and neon [7] irradiated with pulses of 2 keV electrons.

The results from these calculations proved to be very interesting. It was predicted that the initial population of primary species, such as ions and excited states, would take a finite time to evolve. At low gas pressures,  $\sim 1$  torr, the production of primary species was predicted to occur on nanosecond timescales. This prediction was verified by Burgers and Cooper [8] who used emission spectroscopy with nanosecond pulse radiolysis techniques to prove, see Figure 1, that excited states indeed show a delayed formation subsequent to the excitation pulse of high energy electrons (3 ns. from a Febetron 706). Also predicted was that for different gases at equal gas pressures, the excited states will be produced more rapidly in gases with a higher atomic number. Figure 2 shows this for the same excited state in both neon and argon. The production of the 2p state of argon is discernibly faster than that for neon. Note the excellent agreement between the smooth curve-theory, compared to the noisy curve-experimental. This is a simple demonstration of greater stopping power associated with greater  $Z$ .

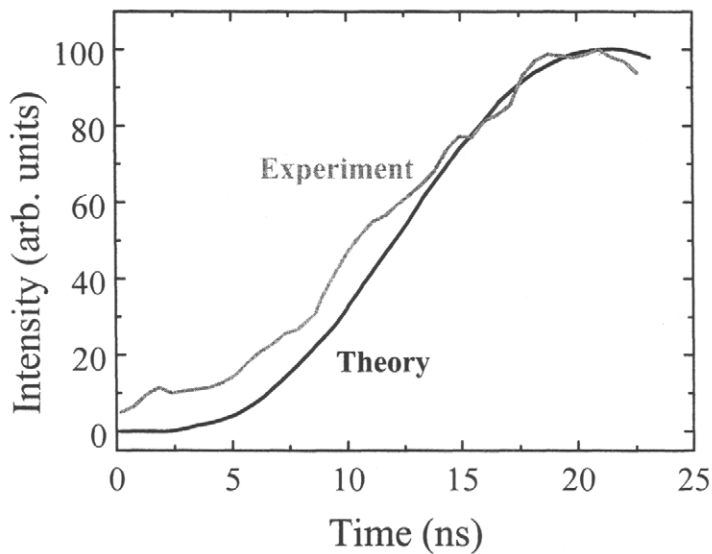


Figure 1. Comparison of experimental and predicted formation decay curves for the excited  $2p_1$  state in electron irradiated argon.

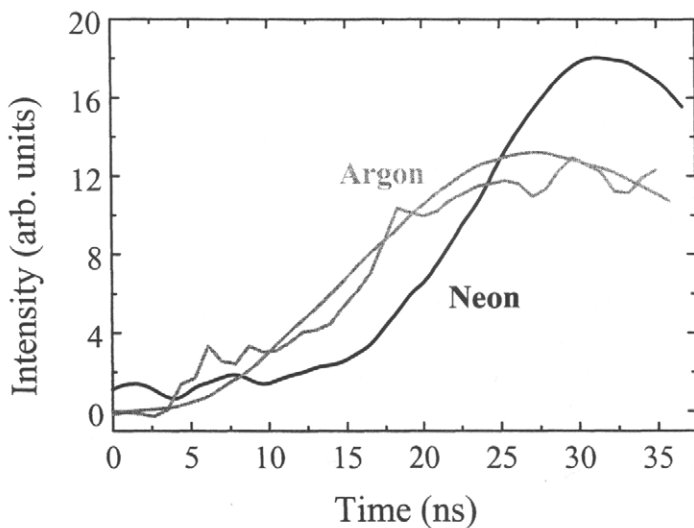


Figure 2. Emission time curves for pulse irradiated neon and argon.



Other predictions were that excited states produced in gases which are optically connected to the ground state would be found to be produced more rapidly than those for which optical transitions to the ground state are forbidden. In argon for example the production of optically forbidden states such as the  $3p^5 4p$  states ( $2p$  in Paschen notation) and the two metastable  $3p^5 4s$  states ( $1s_3$  and  $1s_5$ ) was predicted [3,5] to be delayed relative to the production of ions.

These observations are qualitatively in agreement with the predictions from the TDSF theory however, a direct comparison between theory and experiment has not yet been made for the heavier rare gases. This delay prediction was validated by the observations by Burgers [7] in irradiated neon, where the production of neutral excited states were delayed with respect to the formation of excited ions. Cooper and Sauer [9] used a picosecond pulse radiolysis technique to investigate the formation and decay kinetics of several  $2p$  states in the four rare gases neon, argon, krypton and xenon at low gas pressures ( $< 5$  Torr). They found that all these states had delayed formation.

The studies of Cooper and Sauer [9] establish a time domain for the energy degradation of a high-energy electron (and its subsequent generations of secondaries) down to an energy equal to, or less than, that of the lowest electronic level in the target atom/molecule. This secondary electron is termed a subexcitation electron and is formed within a period of the order of  $10^{-11}$  seconds in gases at one atmosphere. These studies also confirm the validity of the TDSF theory to accurately model the qualitative and quantitative aspects of electron energy degradation.

At this point in the sequence of radiolytic events, we have a plasma containing "hot", i.e. 5-20 eV, electrons. Prior to ion recombination or electron capture processes the energy needs to be further lowered to approximately thermal values.

## **Physico-Chemical Stage**

### *Subexcitation electron processes*

Subexcitation electron interactions have been observed in mixtures of gases; typically a bulk rare gas with a trace fluorescent additive. The only criterion is that the lowest electronic energy level of the bulk gas is higher than the electronic energy level of a trace probe gas. In this situation, energy from subexcitation electrons created from the bulk gas is lost by causing transitions within the probe gas. The observation of this was first made by Cooper et al. [10] and Denison et al. [11] who showed that the emission from the  $C^3\pi_u$  electronic excited state of  $N_2$  was delayed in pulse-electron irradiated, very dilute, mixtures of nitrogen in helium. The emission was observed to grow in

after the pulse and the rate was very strongly dependent on the nitrogen pressure, but only weakly dependant on the rare gas pressure which was always at least 200 times greater than that of the nitrogen. The formation decay kinetics were analysed assuming a kinetic mechanism of the form



where  $e_s^-$  is the subexcitation electron,  $e_t^-$  a thermalised electron, and  $N_2^*$  is one of the excited states of nitrogen which can be excited by  $e_s^-$ .

The weak dependence of the rate of formation of the emission on the pressure of the bulk gas was attributed to a collisional momentum transfer process between the electron and the monatomic rare gas, i.e.



where  $e_T^-$  is an electron of energy less than  $e_s^-$ .

Analysis of radiolysis data taken using a Febetron 706 pulsed electron beam system showed that the formation-decay curves could be analysed using an exponential growth and decay function since the concentration of nitrogen and helium were always very much greater than the initial concentrations of secondary electrons. The formation rate constant,  $k_i$ , was found to be pseudo first order with respect to  $N_2$  and yielded a two-body rate constant of  $5.1 \times 10^{12} \text{ dm}^3 \text{ mol}^{-1} \text{ s}^{-1}$ . Similarly, the formation rate constant was found to vary, but only weakly, with helium pressure and the derived rate constant for energy loss to helium was substantially lower. These studies were consolidated by Denison et al. [11] who used the subnanosecond pulse radiolysis facilities on the LINAC at Argonne National laboratory to study a range of fluorescent probes in rare gas buffers. The rate constant data from these studies are summarised in Table 1.

Table 1. Rate constants for the formation of emission from fluorescent additives (in  $\text{dm}^3 \text{ mol}^{-1} \text{ s}^{-1}$ ).

Bulk Gas	Fluorescent Additive			
	Anthracene	Tetracene	Terphenyl	Nitrogen
Helium	Ionisation	Ionisation	Ionisation	$5.5 \times 10^{12}$
Neon	$9.9 \times 10^{12}$	$8.1 \times 10^{12}$	$8.1 \times 10^{12}$	$5.1 \times 10^{12}$
Argon	$7.7 \times 10^{12}$	-	-	-
Krypton	$1.3 \times 10^{13}$	$1.4 \times 10^{13}$	$1.3 \times 10^{13}$	-
Xenon	$7.5 \times 10^{13}$	$7.8 \times 10^{13}$	$1.2 \times 10^{13}$	-

Table 2. Excitation levels for the rare gases.

Gas	Subexcitation level (eV)	Ionisation Potential (eV)
Helium	19.8	24.6
Neon	16.6	21.6
Argon	11.6	15.8
Krypton	9.6	14.0
Xenon	8.6	12.1

Essentially all the fluorescent probes used from simple diatomics (nitrogen) through to the complex polycyclic aromatic hydrocarbons such as anthracene, tetracene and terphenyl, showed very high rate constants for the formation of the emitting state. The singlet states of the organic scintillators were all formed with rate constants in the range  $7-13 \times 10^{12} \text{ dm}^3 \text{ mol}^{-1} \text{ s}^{-1}$ . These values are 40-100 times greater than the maximum expected for collisional rates for neutral molecular species. A further series of experiments used a trace of a heavy rare gas in an excess of a lighter one e.g. xenon in helium; again the formation of luminescence from the electronic excited states of the monatomic trace additive was delayed. The rate constant for the formation was also one to two orders of magnitude greater than the kinetic theory collisional limit. The subexcitation electron mechanism is further supported by these data which reveal that the bulk rare gas has a two to three orders of magnitude weaker effect on the excited state formation rates. These rates correlate well with values calculated from the well known energy dependent momentum transfer cross sections. Naleway et al. [12] used a monte carlo technique to successfully calculate the nitrogen-helium system assuming a subexcitation electron mechanism, and simultaneously showed that an earlier theory, the continuous slowing down approximation, CSDA, was inadequate in time dependent situations. This was due to the CSDA making no allowance for the change in the secondary electron distribution consequent to an inelastic electron-molecule interaction which resulted in a high energy loss.

The data in Table 2 shows the subexcitation level data for five rare gases. Essentially, distributions of subexcitation electrons with a maximum energy of 19.8 eV in helium down to 8.6 eV in xenon can be generated. This gives an opportunity to generate and study plasmas with a range of electron energy.

Table 3 gives data showing the energy levels of some of the fluorescent probes used in the experimental studies. All the excited levels are capable of being populated by subexcitation electrons from helium whereas with xenon as a bulk gas, only the A state of nitrogen, the B state of iodine, and the  $^1\text{S}$  state of anthracene can be produced. Note that when the energy difference between the

Table 3. Ionisation and excitation levels for some gases.

Gas	Ionisation Potential (eV)	Excitation Level (eV)	
Nitrogen	15.6	C $^3\Pi_u$	11.47
Nitrogen	15.6	A $^3\Sigma_u^+$	6.17
Iodine	9.28	B $^3\Pi_{o+u}$	2.4
Neon	21.6	2p <sub>1</sub>	18.96
Argon	15.8	2p <sub>1</sub>	12.9
Anthracene	7.55	$^1S$	3.3

subexcitation electron and the probe excited state is large, e.g. helium 19.8 eV/anthracene 3.3 eV, then little or no emission is observed since ionisation of the probe (anthracene 7.55eV) is more likely.

These kinetic data give insight into the time taken to reduce electron energies down from the subexcitation level of the order of 10-20eV - down to a few eV - i.e. the energy level of the lowest singlet state of the additive. A simple calculation can be used to give an idea of this time scale. For a mixture, say, of a rare gas and 1 Torr pressure of Nitrogen, the "half life" for subexcitation electrons would be

$$\tau_{1/2} = 0.693/[5.5 \times 10^{12} \times 5.4 \times 10^{-5}] = 2.33 \text{ ns.}$$

In 1 atmosphere of pure nitrogen this lifetime would be only 3.07 picoseconds.

In general, the effect of the monatomic rare gas, usually used as a buffer, is much weaker; the rate constant for the interaction of the subexcitation electron is of the order of  $10^9 \text{ dm}^3 \text{ mol}^{-1} \text{ s}^{-1}$ . This implies a half life for the interaction of the subexcitation electron of the order of 13 microseconds in 1 Torr of a pure rare gas, or about 20 nanoseconds at one atmosphere. However, this process only reduces the energy of the subexcitation electron to a level just below that of the lowest excited electronic state of the probe gas.

### Electron Thermalisation

The secondary electron distribution is not yet thermal. In order to measure the time taken to attain a thermal distribution, a technique sensitive to the energy of the secondary electrons is required. Warman [13,14] and co-workers have elegantly developed and utilised the a.c microwave absorption method. This technique relies on the variation of the mobility of electrons with energy and/or number density to produce a change in the absorption of energy from an applied microwave field.

The change in conductivity,  $\Delta\sigma$ , of the medium is given by

$$\Delta\sigma = \sum z_i e N_i \mu_i$$

where  $z_i$  is the charge of the ion,  $i$ , whose number density is  $N_i$  and whose mobility is  $\mu_i$ .

At constant number density, electrons are detected since their mobility is generally 1000 times greater than any atomic or molecular ion of either charge sign and hence

$$\Delta\sigma = e N_e \mu_e$$

( $\mu_e$  is a complex function of mean electron energy, collision frequency and momentum transfer cross section.)

The TRMC - Time Resolved Microwave Conductivity method - has been used successfully in pulse irradiated gases, liquids and solids by Warman and co-workers [15]. They have shown that the time required to achieve electron cooling down to thermal energies is substantially longer than that for primary electrons to enter the subexcitation energy domain. In pure helium at 1 atm pressure Scales et al. [16] found that the time taken for the secondary electron swarm to attain a mean energy within 10% of thermal was 44 ns. A wide range of di- and polyatomic gas thermalisation times have been measured by Warman and Sauer [13]; their results, see Table 4, show that for molecular gases at 1 atmosphere the thermalisation time is generally less than one nanosecond. The only exceptions are the heavier rare gases, Ar, Kr, and Xe, where the presence of the Ramsauer-Townsend effect delays electron cooling to times of the order of a microsecond.

There is some difference between various workers as to what is the definition of thermalisation time. This should be defined as the time taken for the secondary electron distribution to become a Maxwellian distribution around thermal energy. The definition seem to have been strongly biased by the limitations of the particular technique used to measure some parameter sensitive to the energy of the electron. In the earliest work, Warman and Sauer [13] used the known energy dependence of the electron capture cross section for  $\text{CCl}_4$  to analyse the decay of the electron's conductivity as it approached thermal energies. Later Warman and de Haas [14], and Scales et al. [16], used pulse radiolysis coupled with direct microwave absorption techniques to observe the changing mobility of the electron as its energy neared thermal. The characteristic time chosen was the time taken for the mobility to come within 10% of the thermal value. Suzuki and Hatano [17] used a phase shift

Table 4. Thermalisation times for electrons in gases at 1 atmosphere and 1 torr pressure.

Compound	Thermalisation time t (sec) P = 1 atm.		Thermalisation time t (sec) P = 1 Torr	
	Ar	1.71	(-6)	1.3
Ne	8.81	(-7)	6.7	(-4)
He	4.4	(-8)	3.08	(-6)
N <sub>2</sub>	1.0	(-8)	7.6	(-6)
O <sub>2</sub>	2.2	(-9)	1.7	(-6)
H <sub>2</sub>	1.97	(-9)	1.5	(-6)
CH <sub>4</sub>	2.6	(-10)	2.0	(-7)
C <sub>2</sub> H <sub>6</sub>	1.9	(-10)	1.44	(-7)
n-C <sub>6</sub> H <sub>14</sub>	1.05	(-10)	8.0	(-8)
C <sub>2</sub> H <sub>4</sub>	8.55	(-11)	6.5	(-8)
C <sub>6</sub> H <sub>6</sub>	5.0	(-11)	3.8	(-8)
N <sub>2</sub> O	4.90	(-11)	3.72	(-8)
CO <sub>2</sub>	3.81	(-11)	2.9	(-8)
NH <sub>3</sub>	3.68	(-11)	2.8	(-8)
C <sub>2</sub> H <sub>5</sub> OH	3.02	(-11)	2.3	(-8)

technique for microwave detection together with pulse radiolysis. They were able to fit the final few percent of the electron signal, as it neared a limiting thermal value, to an exponential form. From this a thermalisation "half life" was determined. This value is somewhat misleading in so much as it only applies to the final fractions of an eV energy loss by the electron. It ignores the long time taken for electrons to approach thermal energies. For example in 105 torr of xenon, the exponential approach to thermal energy of the secondary electron swarm is only observable for about 3 microseconds following a previous cooling period of 8  $\mu$ s. This early behaviour cannot be described by any simple function and does not vary simply with total pressure.

The data in Table 4 are given in terms of the time to achieve an electron swarm with a mean energy within 10% of thermal. It shows that apart from the heavier rare gases and the simple diatomic gases, the thermalisation times are all substantially less than 1 nanosecond at 1 atm pressure. Rare gases are frequently used as inert buffers for radiolytic generation of free radicals from appropriate mixtures of gases to produce stable plasmas. In the case of the heavier rare gases the thermalisation times are long since the momentum transfer cross sections for low energy electrons are very low and the influence of trace impurities must play an important role.

For some systems both thermalisation and electron capture processes are in operation. In the case of oxygen, for example, it has been found possible to resolve [18] the thermalisation process - first order in gas pressure, from the

three body capture process. Such resolution has also been achieved for helium. Figure 3 shows the time-dependence of the measured conductivity for ultrapure helium at 1 atmosphere irradiated with a 2 ns pulse of 3 MeV electrons [16]. Figure 3a shows the growth of conductivity as electrons are created and then subsequently thermalised, Figure 3b shows a stable, weakly ionised, plasma in this UHP helium sample; a further but slow growth of conductivity would be observed if Penning ionisation of impurities was occurring. Figure 3c shows the much slower decay of conductivity due to ion-electron recombination.

### Summary

One may safely assume that in 1 atmosphere of an irradiated molecular gas all primary species are created and thermalised within ~50 nanoseconds.

### The Chemical Stage

Pulse radiolysis provides a straightforward technique to initiate and study the reactions of secondary electrons, ions, free radicals and electronic excited states which are generated by ionising radiation in its primary energy deposition stage. Especially convenient is the very fast time resolution associated with this technique. Essentially the technique consists of irradiating a sample with a short and intense pulse of radiation, usually electrons, whilst monitoring some time dependent property of the system related to the composition or energy state of any new species produced.

Since gaseous samples are of low density, high current electron accelerators are needed to produce detectable quantities of reacting species. High current LINACS and Van de Graaf's are available and have been used to study gases at high (~50 atm.) pressures [19]. The advent of the field emission sources such as the Febetrans giving short intense pulses of low energy (0.6 or 2.3 MeV) electrons, enable single shot experiments to be achieved in low (down to ~1 Torr) pressure systems.

### Detection Techniques

A range of techniques are available for use in pulse radiolysis experiments. They are fully presented in several texts, see for example the compilation of Baxendale and Busi [15]. To summarise, the detection techniques used in this field are mainly D.C. and time resolved microwave conductivity (TRMC), and Optical Absorption and Emission Spectroscopy.

#### *Microwave conductivity*

The passage of microwaves through a weakly ionised medium is influenced by the number, and type, of charges present. Anything which alters

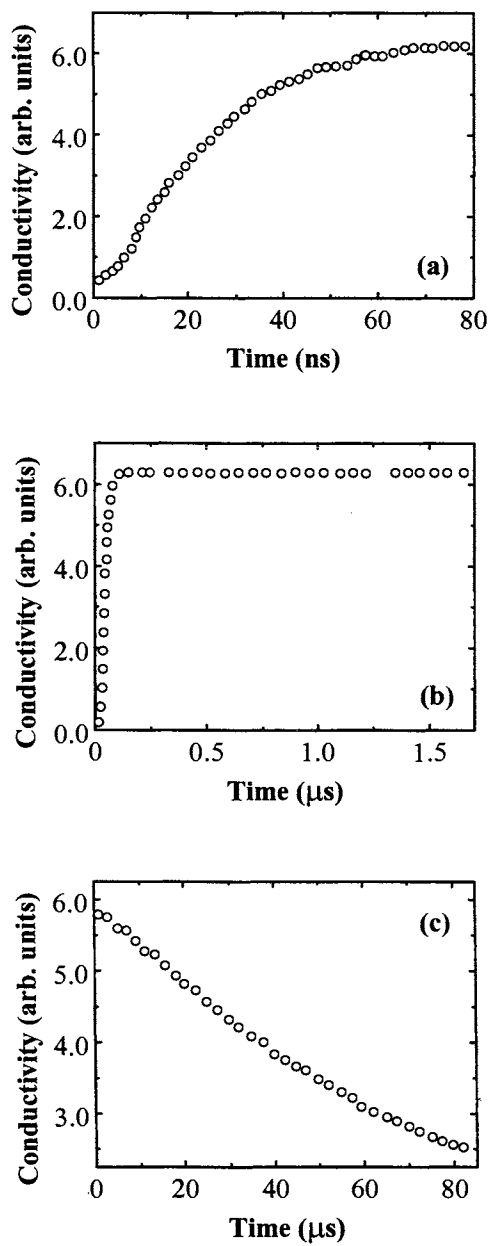


Figure 3. The extended time scale of the evolution and decay of charges in an irradiated sample of helium gas.



the dielectric constant will produce an attenuation of microwave power and hence be detectable. This technique has been extensively developed by Warman and co-workers [15] to detect charged species in the gas, liquid and solid phases with a time resolution of the order of 1 nanosecond.

In most experimental studies so far reported in gases, electrons are detected since their mobility is generally 1000 times greater than an atomic or molecular ion of either charge sign and hence

$$\Delta\sigma = e N_e \mu_e$$

This relationship may be used to define two useful limiting experimental conditions;

(1)  $N_e$  is constant

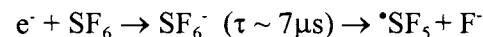
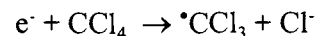
At low doses or when ion recombination is not occurring at a significant rate the change in conductivity reflects a change in the mobility of the electron. This can only occur by changes to the electron energy, for example, during thermalisation or by electron capture to produce a low mobility negative ion. These processes can hence be studied in isolation.

(2)  $\mu_e$  is constant.

When thermalisation is complete then the electron mobility attains a constant value. Any change in conductivity is then related exactly to the change in concentration of free electrons in the irradiated sample. Ion-electron recombination reactions can therefore be studied, as can electron capture and charge creation by Penning ionisation.

(i) *Electron capture:*

Typical compounds that undergo electron capture, and associated rate constants, are given in Table 5. For the two reactions:



the maximum rate constant occurs at, or close to, thermal electron energy. Based on their measured values, of the order of  $2 \times 10^{14} \text{ dm}^3 \text{ mol}^{-1} \text{ s}^{-1}$ , at 1 torr pressure the half life for capture is of the order of 100 picoseconds.

Table 5. Some electron capture agents and their capture rate constants.

Compound	Rate constant $\text{dm}^3 \text{mol}^{-1} \text{s}^{-1}$
$\text{CCl}_4$	$2.53 \times 10^{14}$
$\text{CFCl}_3$	$1.54 \times 10^{14}$
$\text{CF}_2\text{Cl}_2$	$5.1 \times 10^{11}$
$\text{CF}_4$	$< 6 \times 10^4$
$\text{CF}_3\text{I}$	$1.16 \times 10^{14}$
$\text{CF}_3\text{Br}$	$2.38 \times 10^{12}$
$\text{CH}_3\text{Br}$	$4.2 \times 10^9$
$\text{SF}_6$	$1.24 \times 10^{14}$
$\text{CO}_2$	0
$\text{N}_2\text{O}$	$3 \times 10^6$
$\text{O}_2$	$7.98 \times 10^{11}$ *
$\text{CF}_3\text{Cl}$	$6 \times 10^7$

\*  $\text{dm}^6 \text{mol}^{-2} \text{s}^{-1}$  (three body reaction,  $M = \text{O}_2$ )

Dissociative electron capture also occurs at energies greater than thermal but usually with significantly lower rate constants (cross sections) and various fragmentations. For example,  $\text{SF}_6$  at low energies forms a metastable molecular anion whereas at higher energies direct impact dissociation to  $\text{SF}_5^-$  and F occurs but with a much lower cross section.

Electron capture processes are important in determining conditions for the quenching of electrical breakdown in gases. Free electrons in gases in an electric field can be accelerated to sufficiently high energies to cause further ionization, which in turn can produce more secondary electrons and in a catastrophic avalanche lead to electrical breakdown. Chemical agents can be added to block such processes, and  $\text{SF}_6$  is widely used in high voltage applications to prevent arcing and resultant damage to switch gear.

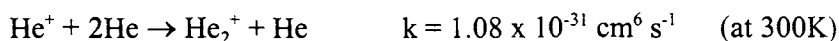
#### (ii) Ion - electron recombination

The recombination of ions and electrons in ionized gases has been studied for over 60 years. Many techniques are available for studying this recombination, all consist of a form of excitation and a method to measure the time-dependent change in electron concentration and/or other parameters. In general, most of these excitation and detection methods limit the experiments to longer timescales, usually in the millisecond range, and to low gas pressures. Under these conditions, the reaction of initially produced species with impurities becomes important. Charge transfer, electron capture, and energy transfer (Penning ionization) reactions transform impurity species into various

atomic and molecular ions. At very low pressures primary ions can diffuse to, and charge neutralize, at the surface of the vessel.

Electron pulse radiolysis technique has been well utilised for the study of ion-electron recombination in weakly ionized gases. It overcomes many of the disadvantages of discharge techniques, most notably it produces an even plasma distribution in a gas using a single pulse on very short timescales. This minimizes the effects of impurity gases and wall surface reactions. Also, very high gas pressures can be studied over a wide temperature ranges.

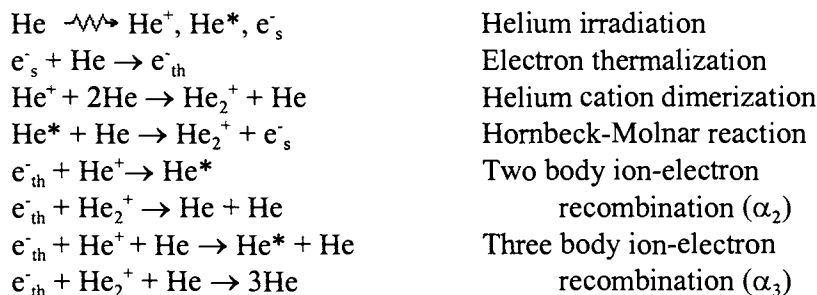
One of the most studied gas systems is helium. From the theoretical studies of Bates [20] and experimental mass spectrometry studies of Cao and Johnsen [21], it has been shown that the dominant recombining positive ion produced in irradiated helium gas is  $\text{He}_2^+$ , which is formed from the initially ionized  $\text{He}^+$  by the three-body reaction characterised by Mahan [22]



In general there will be a mixture of  $\text{He}^+$  and  $\text{He}_2^+$  undergoing recombination, depending on the timescale of measurement, the helium gas pressure, and the gas temperature.

A summary of the measured overall rate constant,  $\alpha_T$ , obtained by a range of plasma physics techniques is given in Table 6. As can be seen, at pressures below 100 Torr, the values range over two orders of magnitude; from  $\alpha_T = 0.2 \times 10^{-10}$  to  $\sim 3 \times 10^{-8} \text{ cm}^3 \text{ s}^{-1}$ .

A general irradiation/recombination mechanism for electron irradiated gaseous helium can be written as:



This mechanism would predict that the total recombination rate constant would be given by

$$\alpha_T = \alpha_2 + \alpha_3 [\text{He}]$$

Table 6. Summary of the total ion-electron recombination rate constants,  $\alpha_T$ , in ionised helium.

Workers	$\alpha_T$ ( $\text{cm}^3 \text{ s}^{-1}$ )	Analysis technique	Pressure range (Torr)
Biondi and Brown [23]	$1.7 \times 10^{-8}$	Microwave probing	< 30
Oskam and Mittlestadt [24]	$\leq 4 \times 10^{-9}$	Microwave probing	< 60
Chen et al. [25]	$8.9 \times 10^{-9}$	Optical intensity	15-30
Hinnov and Hirschberg [26]	$0.4 - 3.6 \times 10^{-10}$	Optical intensity	$\sim 10^{-3}$
Robben et al. [27]	$0.19 - 8.9 \times 10^{-10}$	Optical intensity	0.25
Born [28]	$8.9 \times 10^{-10}$ (750K) $5.9 \times 10^{-10}$ (1000K) $4.7 \times 10^{-10}$ (1250K)	Optical intensity	12-20
Berlande et al. [29]	$5 \times 10^{-10}$	Optical intensity/ Microwave probing	10-100
Johnson and Gerado [30-33]	$1 \times 10^{-8}$	Optical intensity/ Microwave probing	10-50

To overcome the limitations experienced by previous workers, van Sonsbeek et al. [34], utilized a Field Emission Corporation Febetron 706 electron pulser, which generated electron beam pulses of 0.2-0.6 MeV energy and 3ns (FWHM) duration, to investigate ion-electron recombination in helium over a large pressure range, 40-900 Torr, at electron densities of approximately  $10^{11}$ - $10^{13} \text{ cm}^{-3}$ . The a.c. microwave conductivity technique was used to directly monitor the electron concentration in the irradiation cell [14,15]. From these kinetic measurements van Sonsbeek et al. [34] were able to fully resolve both the two- and three-body helium recombination processes. Their measured rate constants exhibited excellent second order behaviour, and the pressure dependence of their measured values at 295K is given in Figure 4. The overall rate constant measured is given by

$$\alpha_T = (1.12 \pm 0.05) \times 10^{-7} + (2.20 \pm 0.25) \times 10^{-27} [\text{He}] \text{ cm}^3 \text{ s}^{-1}$$

It is important to note that at the low pressures of almost all the earlier studies the total rate constant is effectively only the two body electron-ion recombination rate constant, ( $\alpha_2$ ), with little or no contribution from three body effects ( $\alpha_3$ ). Several hundred Torr of gas pressure are required to clearly distinguish the effects of three-body recombination. In addition, the low values of  $\alpha_T$  ( $< 10^{-9} \text{ cm}^3 \text{ s}^{-1}$ ) measured by many of the early workers were almost certainly affected by impurity reactions. Electrons attached to trace impurity

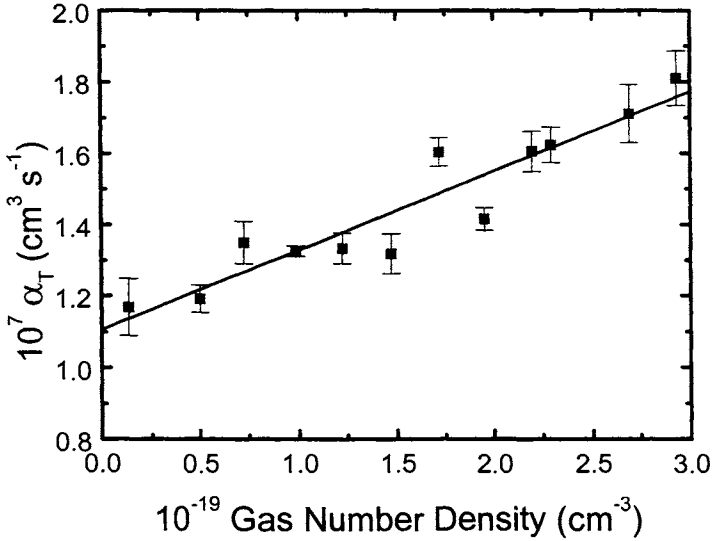


Figure 4. Pressure dependence of the ion-electron recombination rate coefficient,  $\alpha_T$  (in  $\text{cm}^3 \text{s}^{-1}$ ) in pulse irradiated helium at 295 K. Bulk gas pressures are expressed as number gas densities ( $\text{cm}^{-3}$ ).

molecules have a reduced mobility, and consequently the loss of charge in the plasma by recombination is slower.

Table 7 shows a summary of experimental determinations and theoretical calculations of  $\alpha_3$  rate constants in helium at 295K.

Table 7. Comparison of experimental and theoretical values of the three-body ion-electron recombination rate constant,  $\alpha_3$ , in helium at 295K.

Worker	Result	$10^{27} \alpha_3$ ( $\text{cm}^6 \text{s}^{-1}$ )
van Sonsbeek et al. [34]	Experimental	$2.20 \pm 0.25$
Berlande et al. [29]		$2.0 \pm 0.5$
Johnson et al. [30-33]		$20^{+28}_{-17}$
Deloche et al. [35]		$5 \pm 1$
Thompson [36]	Theoretical	0.4
Bates [37]		1.7
Whitten et al. [38]		5.4
Pitaevskii [39]		2.5

Table 8. Experimental values of van Sonsbeek et al. [34] for the two- ( $\alpha_2$ ) and three-body ( $\alpha_3$ ) ion-electron recombination rate constants in irradiated helium over the temperature range 200-295K.

Temperature (K)	$10^7 \alpha_2$ ( $\text{cm}^3 \text{s}^{-1}$ )	$10^{27} \alpha_3$ ( $\text{cm}^6 \text{s}^{-1}$ )
200	$0.48 \pm 0.03$	$5.20 \pm 0.40$
235	$0.68 \pm 0.06$	$3.33 \pm 0.30$
275	$0.79 \pm 0.06$	$1.34 \pm 0.27$
295	$1.12 \pm 0.05$	$2.20 \pm 0.25$

The experimental  $\alpha_T = (2.20 \pm 0.25) \times 10^{-27} \text{ cm}^6 \text{ s}^{-1}$  value of van Sonsbeek et al. agrees well with the previous experimental measurement of Berlande et al. [29] and favours the predictions of the Bates [37] and Pitaevskii [39] theories. The temperature dependence of electron-ion recombination in irradiated helium was also investigated by van Sonsbeek et al. [34]. A summary of their measured two- and three-body recombination rate constants over the temperature range 200-295 K is given in Table 8. The three-body recombination rate constant decreases with increasing temperature, and may be written as

$$\alpha_3 = c T^n$$

From this data, an exponent value of  $n = -2.9 \pm 1.2$  is obtained. A single-collision model for neutral-assisted three-body recombination based on the work of Thompson [36] suggests a temperature behaviour of  $T^{-2.5}$ . A later modification of this theory by Bates [40] also predicts this numerical dependence, as does the "diffusion" of electron energy in energy space model of Pitaevskii [39]. Within the experimental uncertainty, excellent agreement between experiment and theory is obtained.

In a series of subsequent experiments reported by Bhawe and Cooper [41] and Cooper et al. [42], the electron pulse irradiation/microwave conductivity investigations have been extended to determine two- and three-body recombination rate constants for the other rare gases, as well as hydrogen, methane and nitrogen. For the heavier rare gases (Ar, Kr, Xe), thermalization times become extremely long, as direct momentum transfer by electron-atom collision becomes very inefficient. This problem was overcome by including a small pressure (typically 25 Torr) of helium in the irradiation mixture. This small amount of helium ensured that electron thermalization occurred on a microsecond timescale, and any helium cations directly formed from the irradiation process resulted in charge transfer to the heavier rare gas. For all

Table 9. Summary of two- ( $\alpha_2$ ) and three-body ( $\alpha_3$ ) recombination rate constants (at 295K) determined by Cooper and co-workers [41,42] using electron pulse radiolysis and microwave conductivity.

Gas system	$\alpha_2$ ( $\text{cm}^3 \text{ s}^{-1}$ )	$\alpha_3$ ( $\text{cm}^6 \text{ s}^{-1}$ )	T dependence
Helium	$(1.12 \pm 0.05) \times 10^{-7}$	$(2.20 \pm 0.25) \times 10^{-27}$	$-2.9 \pm 1.2$
Neon	$(7.0 \pm 2.0) \times 10^{-9}$	$(1.39 \pm 0.12) \times 10^{-27}$	not consistent
Argon	$(1.1 \pm 0.2) \times 10^{-6}$	$(5 \pm 7) \times 10^{-27}$	not consistent
Krypton	$2.5 \times 10^{-7}$	$1.18 \times 10^{-26}$	not measured
Xenon	$1.5 \times 10^{-6}$	$1.17 \times 10^{-25}$	not measured
Methane	$8.2 \times 10^{-7}$	$2.04 \times 10^{-25}$	not measured
Hydrogen	$4.07 \times 10^{-7}$	$9.15 \times 10^{-27}$	not measured
Nitrogen	$(2.7 \pm 0.9) \times 10^{-7}$	$(5.1 \pm 0.2) \times 10^{-27}$	not measured

these studies, sufficient gas pressures were used to ensure cation dimerization. The recombination rate constants determined in these studies are summarized in Table 9. No consistent trend was noted with temperature in the neon or argon systems. The extremely low  $\alpha_3$  value for argon is consistent with theoretical predictions that this gas would not be a very efficient third body for the recombination process.

There has also been an optical emission study of ion-electron recombination in nitrogen, where the recombination coefficient for  $\text{N}_4^+$  was determined by observing the  $\text{C}^3\pi_u$  emissive state of  $\text{N}_2$  [43,44]. A rate constant for ion-electron recombination of  $3.3 \times 10^{-6} \text{ cm}^3 \text{ s}^{-1}$  was obtained at 298K, however, this result must be treated with some caution, as the rate was found not to vary over the pressure range 200-900 Torr.

There have also been several previous experimental investigations into electron-ion recombination in other gases using the electron pulse radiolysis technique. Warman and co-workers [45-47] used the a.c. conductivity technique to measure ion-electron recombination for pulse electron irradiated molecular gases at pressures up to several hundred Torr. A summary of their measured two- and three-body recombination rate constants is given in Table 10. It is clearly seen that the molecular gases are far more efficient at assisting ion-electron recombination, both the two- and three-body processes, relative to the rare gases. The  $\alpha_3$  values are particularly pronounced for the dipolar compounds, where it was apparent that neutral gas molecules could play a significant role in the recombination even at densities as low as  $10^{17} \text{ cm}^{-3}$ . The measured temperature dependencies for water and ammonia are seen to be consistent with the value obtained for helium,  $n = -2.9 \pm 1.2$ , although quantitative conclusions are difficult to draw due to the large experimental

Table 10. Summary of the two- and three-body recombination rate constants measured by Warman and co-workers [45-47] for molecular gases.

Gas system	$\alpha_2$ ( $\text{cm}^3 \text{s}^{-1}$ )	$\alpha_3$ ( $\text{cm}^6 \text{s}^{-1}$ )	T dependence
H <sub>2</sub> O	$4.1 \times 10^{-6}$	$2.7 \times 10^{-23}$	$-2.0 \pm 0.5$
NH <sub>3</sub>	$5.6 \times 10^{-6}$	$6.9 \times 10^{-24}$	$-2.5 \pm 0.5$
(CH <sub>3</sub> ) <sub>2</sub> CO	$6.4 \times 10^{-6}$	$5.5 \times 10^{-24}$	0
CH <sub>3</sub> Cl	$7.1 \times 10^{-6}$	$2.6 \times 10^{-24}$	
CO <sub>2</sub>	$3.9 \times 10^{-6}$	$5.8 \times 10^{-25}$	
neo-C <sub>5</sub> H <sub>12</sub>	$7.0 \times 10^{-6}$	$2.5 \times 10^{-25}$	

Table 11. Temperature dependence of electron-ion recombination rate constants for hydrated hydronium ions Leu et al. [48] in units of  $10^{-6} \text{ cm}^3 \text{ s}^{-1}$ .

T K\n	0	1	2	3	4	5	6
540	1.0±0.2	2.0±0.4	4.0±0.8				
415		2.2±0.4	4.2±0.8				
300			3.8±0.8	5.0±0.8			
205					6.6±1.2	7.5±1.5	<10

errors involved. Further corroboration, however, is also obtained from a later study of ion-electron recombination with  $\text{N}_2^+$  and  $\text{O}_2^+$ , from impurity nitrogen and oxygen ions in irradiated helium Cao and Johnson [21], where these workers also obtained a temperature exponent of  $n = -2.9$ .

The very large  $\alpha_2$  rate constants for molecular ion-electron recombination have also been reported for cluster ion studies, performed at low total gas pressures. Table 11 shows the results of measurements performed by Leu et al. [48] on gaseous ion-electron recombination involving the hydrated hydronium ion  $[\text{H}_3\text{O}^+(\text{H}_2\text{O})_n]$ . Significant increases in the recombination rate constant are seen for even a few cluster water molecules, with a value for the  $\text{H}_3\text{O}^+(\text{H}_2\text{O})_5$  cluster at 205K as high as  $7.5 \times 10^{-6} \text{ cm}^3 \text{ s}^{-1}$  obtained.

### Ion-ion recombination

Since the mobility of molecular ions, of either sign, is substantially less than that for free electrons, the a.c. conductivity technique is not sufficiently sensitive to measure ion-ion recombination. However, luminescence resulting from ion recombination has been used as a probe of the kinetics of ion recombination. Although ion-ion recombination has been studied longer even longer than ion-electron recombination, beginning with Thompson and



Rutherford [49] in 1896, very few systems have been well characterized over large pressure ranges.

The first studies to be performed over pressure ranges large enough to discern two- and three-body effects were by Schmidt et al. [50] for recombining  $SF_6^+(SF_6)_n$  and  $SF_6^-(SF_6)_m$  ions in irradiated  $SF_6$ , and Sennhauser and Armstrong [46] for  $NH_4^+(NH_3)_n$  and  $Cl^-(NH_3)_m$  ions in  $NH_3/CCl_4$  gas mixtures. In both cases  $n$  and  $m$  stand for an indeterminate number of species clustered around the recombining ions. These studies showed that the total recombination rate constant initially increased with increasing bulk pressure, but then decreased at higher pressures. However, quantitative characterization of these recombination systems was not possible due to the unknown molecularity of species involved in the measured process.

The best characterized ion recombination systems are those involving irradiated rare gases. In the mid 1970's rare gas-monohalide systems were extensively studied, due to their new-found application in u.v. exciplex lasers. Pulsed electron irradiation of these systems was the only major excitation method, as it allowed investigation under realistic laser pressure conditions of several atmospheres gas pressure. Typically these systems were investigated by monitoring of the time dependence of their characteristic peak fluorescence, as given in Table 12.

It was found, from pulse radiolysis experiments, that there were at least two temporal components to the exciplex emission, and a general mechanism for exciplex formation and decay was developed [57-67] which consists of direct reaction of electronically excited rare gas atoms with the halide source gas and ionic recombination.

Table 12. Summary of peak emission wavelengths of rare gas-monohalide exciplex species.

Species	Experimental peak (nm)	Worker
NeF*	108	Rice et al. [51]
ArF*	193	Golde [52]
ArCl*	175	Golde and Thrush [53]
ArBr*	166	Ewing [54]
KrF*	248	Brau and Ewing [55]
KrCl*	222	Golde [52]
KrBr*	206	Golde [52]
KrI*	180	Velazco and Setser [56]
XeF*	351	Golde and Thrush [53]
XeCl*	308	Golde and Thrush [53]
XeBr*	280	Golde and Thrush [53]
XeI*	253	Brau and Ewing [55]

The initial pulsed electron irradiation of a rare gas (R) produces excited states ( $R^*$ ), ions ( $R^+$ ) and a range of secondary electrons ( $e_s^-$ ) and by addition of a trace amount of a halide containing gas (AX), whose concentration is small enough that there is no direct excitation by the primary electron beam, exciplex ( $RX^*$ ) formation occurs as follows:

$R \xrightarrow{\text{e}^-} R^*, R^+, e_s^-$	Initiation
$e_s^- + R \rightarrow e_{th}^-$	Electron thermalization
$e_{th}^- + AX \rightarrow AX^-/X^-$	Thermal electron capture
$R^* + AX \rightarrow RX^* + A$	Reaction of rare gas excited states
$R^+ + 2R \rightarrow R_2^+ + R$	Cation dimerization
$R_2^+ + AX^-/X^- \rightarrow RX^* + \text{products}$	Two body ion-ion recombination
$R_2^+ + AX^-/X^- (+ R) \rightarrow RX^* + \text{products}$	Three body ion-ion recombination
$RX^* \rightarrow R + X + h\nu$	Exciplex fluorescence

Under suitable experimental conditions, for example by lowering the initial electron pulse energy, (dose), or by varying the constituent gas pressures, resolution of the excited state processes and the ionic recombination reaction can be achieved. This allows isolation, and unambiguous characterization of the ionic recombination processes in these systems.

### **Xe<sub>2</sub><sup>+</sup>/SF<sub>6</sub><sup>-</sup> ionic recombination**

The simplest exciplex system for the study of gaseous ionic recombination is from the gas system Xe/SF<sub>6</sub>. The XeF\* exciplex produced is formed solely from Xe<sub>2</sub><sup>+</sup>/SF<sub>6</sub><sup>-</sup> ion-ion recombination; there is no detectable emission from the reaction of xenon electronically excited states with SF<sub>6</sub> [68]. The emission from the coupled XeF\*(B,C) state was found to extend from 320 to 360 nm, with a peak at 351 nm.

A typical emission trace for XeF\* is shown in Figure 5a, for 500 Torr of xenon and 0.50 Torr of SF<sub>6</sub>. This curve has several components; a X-ray signal, dimer rare gas fluorescence and ionic recombination formed exciplex fluorescence. The X-ray signal followed the time profile of the 3 ns. electron pulse, and was typically only a few percent of the total emission signal. The first emission peak was also observed in irradiated pure xenon, at all wavelengths across and outside the XeF\* emission spectrum, and was therefore assigned to the broad xenon dimer, Xe<sub>2</sub>\* fluorescence. The decay of the dimer fluorescence was typically complete within several hundred nanoseconds, and its intensity varied greatly with the xenon pressure. The second peak in the emission curve was dose-dependent, and only observed across the known XeF\*

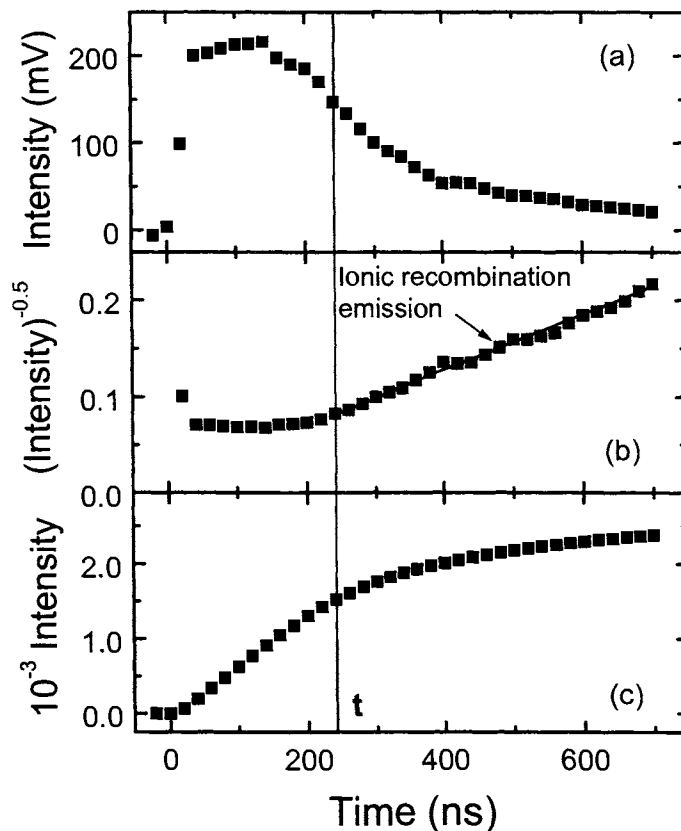


Figure 5. (a) Typical kinetic emission curve for XeF\* at 351 nm, produced by the pulse electron irradiation of 500 Torr of xenon and 0.50 Torr of SF<sub>6</sub>. (b) Transformed emission curve showing straight line analysis beginning at time *t*. (c) Integrated kinetic emission curve.

spectrum, and assigned to XeF\* emission produced by the ion-ion (Xe<sub>2</sub><sup>+</sup>/SF<sub>6</sub><sup>-</sup>) recombination processes.

An analysis of the exciplex production mechanism above [63], assuming that XeF\* is at steady state, shows that a second order plot of (Emission intensity)<sup>-1/2</sup> vs time gives a straight line at longer times, see Figure 5b. The slope of this line is readily related to the three body recombination coefficient, α<sub>3</sub>, via the absolute ion concentration which was derived from standard ozone dosimetry [69] incorporating relative stopping powers of all gases [70,71]. The ion concentration at the initial time of α<sub>3</sub> determination (time *t* in Figure 5) was obtained using an integrated kinetic trace, Figure 5c, of only the ionic

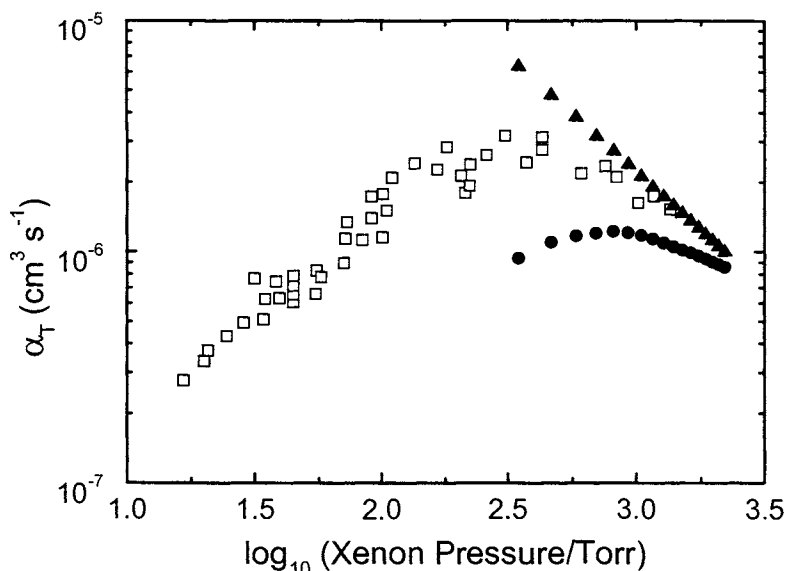


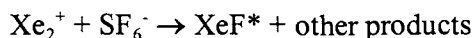
Figure 6. Xenon pressure dependence of the experimental  $\text{XeF}^*$  ionic recombination rate constants ( $\square$ ) in comparison with the Bates calculated ter-molecular ( $\bullet$ ) and Langevin-Harper ( $\blacktriangle$ ) diffusion-controlled values for  $\text{Xe}_2^+/\text{SF}_6^-$  ionic recombination in xenon.

recombination formed fluorescence. The ionic recombination fluorescence was isolated from the total measured integrated kinetic trace by subtracting out the integrated intensity belonging to the X-ray and dimer rare gas fluorescence, by normalizing an additional intensity measurement at a wavelength just outside the exciplex emission spectrum [64].

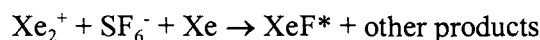
To ensure that the ion recombination process was the rate limiting step, the experimental conditions were carefully chosen. The hot electrons,  $e_s^-$ , were thermalized by both xenon and  $\text{SF}_6$ , and this process occurred typically within the duration of the electron pulse. The thermal electrons are rapidly captured by  $\text{SF}_6$ ,  $k = 2.27 \times 10^{-7} \text{ cm}^3 \text{ s}^{-1}$  [72], to form the molecular anion,  $\text{SF}_6^-$ , which was stable over the time of these experiments (0.5-2 $\mu\text{s}$ ). Fast cation dimerization of the rare gas cation was ensured by using higher xenon pressures,  $> 30$  Torr. The fluorescence lifetime of  $\text{XeF}^*$  is short ( $\sim 15$  ns) and thus the ionic recombination reaction controls the observed rate of decay of emission when the initial ion concentrations are very low.

Ionic recombination rate constants were obtained by this methodology over the xenon pressure range 18-1400 Torr, these values are given in Figure 6.

The rate constants are seen to continuously increase with increasing pressure, to a maximum value of  $\sim 4 \times 10^{-6} \text{ cm}^3 \text{ s}^{-1}$ , at  $\sim 500$  Torr, and then to decrease with higher xenon pressure. This pressure profile is attributed to the low xenon pressure recombination mechanism being two body [64]

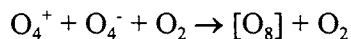


with the increasing medium xenon pressure rate constants being due to an increasing contribution of three-body recombination mechanism,

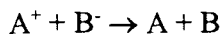


and the subsequent decrease in  $\alpha$  at higher pressures being due to the ionic recombination becoming diffusion-controlled. From the initial portion of this plot  $\alpha_3$  was determined as  $4.7 \times 10^{-25} \text{ cm}^6 \text{ s}^{-1}$ .

These ionic recombination data can also be compared to the predictions of ion-ion recombination theoretical models. The most general three-body recombination theory is from Bates [73], based on scaling of computer simulation results for the recombination coefficient pressure profile of the reaction



The Bates model predictions for  $\text{Xe}_2^+/\text{SF}_6^-$  recombination in xenon are also shown in Figure 6. It can be seen that the experimental data are always greater in magnitude than the calculated ter-molecular values, with the discrepancy being far worse at low pressures. The maximum in the experimental pressure profile is also observed at a much lower pressure than predicted. To account for this discrepancy between experiment and theory additional, two-body, mutual neutralization, ionic recombination was postulated to be occurring with a much higher efficiency than previously predicted. This additional ionic recombination mechanism is a charge exchange reaction of the form



and may be regarded as occurring through an avoided crossing between the ionic and covalent potential surfaces. The presence of a bulk gas (xenon) enhances this process by collisionally converting free ion pairs to bound ion pairs, thus allowing the avoided crossing to be traversed many more times. Although no quantitative estimate of the fraction of ions recombining by this

two-body pathway have been performed, qualitative estimates by Mezyk et al. [64] indicated that it could be as high as 50% .

At very high bulk gas pressures, the ionic recombination reaction becomes diffusion controlled. The theory of this recombination mechanism was developed by Langevin [74] and Harper [75] who obtained the relationship

$$\alpha_{LH} = 4\pi e (\mu^+ + \mu^-)$$

where  $\mu^+$  and  $\mu^-$  are the positive ( $\text{Xe}_2^+$ ) and negative ( $\text{SF}_6^-$ ) ion mobilities respectively. By substituting the average ionic mobilities for these two ions into this expression the diffusion-controlled limiting rate constant ( $\alpha_{LH}$ ) is obtained (see Figure 6). Excellent agreement at high xenon pressures is seen, with the measured data converging to the calculated diffusion-controlled limit. This implies a unit efficiency of recombination between the two ions, i.e. that the two ions always recombine to give the fluorescent  $\text{XeF}^*$  once collisions with the bulk gas have reduced the energy of the ionic system below zero, and thus formed a bound state.

### **$\text{Xe}_2^+/\text{Br}^-$ ionic recombination**

By addition of a dissociative thermal electron capturing gas such as  $\text{CH}_2\text{Br}_2$ , which quantitatively produces the atomic  $\text{Br}^-$  anion, the three body recombination process for an anion can be determined in isolation of any two-body mutual neutralization reactions. For irradiated xenon- $\text{CH}_2\text{Br}_2$  gas mixtures, the total emission at 282 nm was found to consist of X-rays, xenon dimer fluorescence, and  $\text{XeBr}^*(\text{B,C})$  exciplex fluorescence formed from both ionic recombination and xenon excited-state reaction [67]



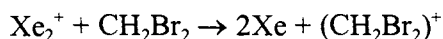
(where  $\text{Xe}^*$  represents the entire range of electronically excited xenon atoms produced by electron irradiation).

As for  $\text{XeF}^*$  the X-ray component for irradiated  $\text{Xe}/\text{CH}_2\text{Br}_2$  was negligibly small. The xenon dimer fluorescence was typically complete within 100 ns and its intensity was proportional to the xenon pressure. The exciplex fluorescence formed by the reaction of excited xenon atoms with  $\text{CH}_2\text{Br}_2$  was also observed within the first hundred nanoseconds, however its intensity was strongest at low xenon pressures. The ionic recombination formed exciplex fluorescence again had the slowest rate of production, being observed for many hundreds of nanoseconds. Its intensity was also dependent on total xenon gas pressure; being comparable to the excited-state formed fluorescence at low

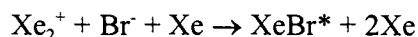
xenon pressures but accounting for nearly all of the exciplex fluorescence at high xenon pressures.

Ionic recombination rate constants were determined as described for XeF\*, by analyzing the later, linear, portion of the transformed kinetic curve and using ozone dosimetry and integrated kinetic traces. The overall exciplex fluorescence was isolated by subtraction of the X-ray and dimer xenon fluorescence intensities from the integrated fluorescence as before. However, the experimental resolution of the exciplex fluorescence yield into neutral reaction and ionic recombination components was not experimentally possible for this system. Therefore the fractional yields for each of the XeBr\* formation pathways, excited state reaction and ionic recombination, were calculated using experimental measurements of relative XeBr\* emission yields.

The selection of CH<sub>2</sub>Br<sub>2</sub> as the halide source gas was deliberate; in addition to the quantitative production of the atomic anion the ionization potential of this gas, 10.8 eV, [76], was lower than that of Xe<sub>2</sub><sup>+</sup>, 11.1 eV [77], which meant that the charge transfer reaction



occurred in competition with the recombination reaction



For ionic recombination rate constant measurements the charge transfer reaction was minimized by using a very small pressure of CH<sub>2</sub>Br<sub>2</sub>, typically 0.10 Torr, and keeping the ion concentration greater than  $3 \times 10^{13} \text{ cm}^{-3}$ .

The production of XeBr\* by only the excited state reaction could be isolated by having a sufficiently high pressure of CH<sub>2</sub>Br<sub>2</sub> to ensure complete charge transfer occurred. Figure 7 shows the total relative XeBr\* fluorescence yield dependence on CH<sub>2</sub>Br<sub>2</sub> pressure over the range 0.02-1.0 Torr, at a constant xenon pressure of 80 Torr. These relative values were determined by measuring the total emission under the entire exciplex fluorescence spectrum. The inverse plot of these yields [60] shows a limiting linear slope at higher CH<sub>2</sub>Br<sub>2</sub> gas pressures (> 0.6 Torr) where the charge transfer reaction dominates and thus all the XeBr\* fluorescence is formed by the direct reaction of xenon excited states with CH<sub>2</sub>Br<sub>2</sub>. The deviation from this linearity at lower CH<sub>2</sub>Br<sub>2</sub> pressure is due to the additional fluorescence formed by the ionic recombination reaction.

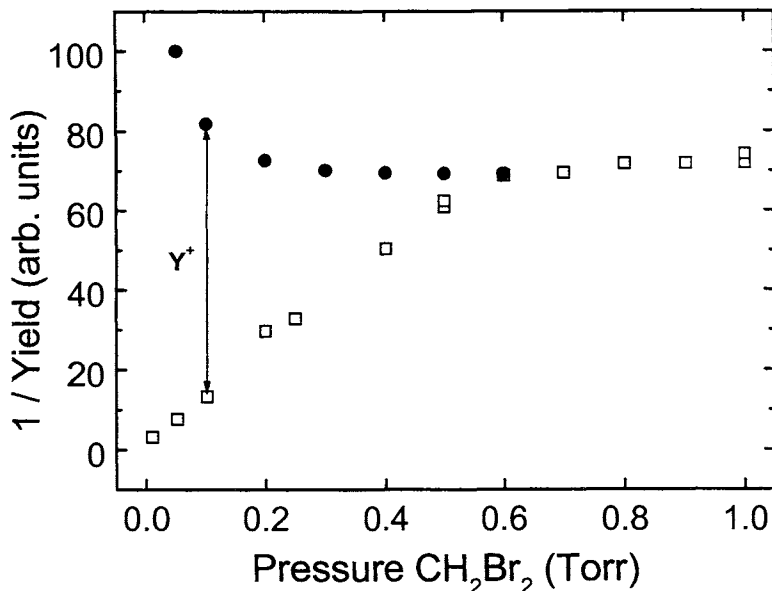
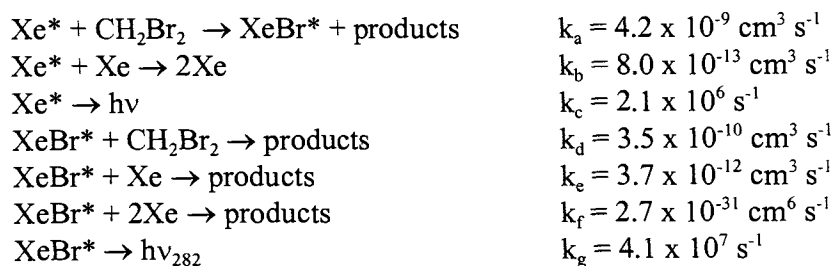


Figure 7. CH<sub>2</sub>Br<sub>2</sub> pressure dependence of the measured relative XeBr\* (□), and calculated excited-state reaction (●), yields at a constant xenon pressure of 80.0 Torr [67]. Difference at 0.10 Torr CH<sub>2</sub>Br<sub>2</sub> (Y<sub>\*</sub>) is due to additional fluorescence from Xe<sub>2</sub><sup>+</sup>/Br<sup>-</sup> ionic recombination pathway.

At CH<sub>2</sub>Br<sub>2</sub> pressures greater than 0.6 Torr exciplex fluorescence is only produced by the excited state reaction process, and can be modelled by the mechanism:



The rate constants for the first three reactions in this scheme were obtained by isolating the excited-state reaction process using low xenon pressures and initial ion concentrations [67]. For the quenching reactions of XeBr\* literature rate constants were used [78-82]. From the above reaction scheme and these rate



constants the  $\text{CH}_2\text{Br}_2$  pressure dependence of these relative fluorescence yields is given by

$$Y^* = Y_0^* \left[ \frac{R_a}{R_a + R_b + R_c} \right] \left[ \frac{R_g}{R_d + R_e + R_f + R_g} \right]$$

where  $Y_0^*$  is the maximum possible (relative) yield of excited state  $\text{XeBr}^*$  production and  $R_i$  is the rate for the  $i^{\text{th}}$  reaction in the general scheme.  $Y_0^*$  was calculated by fitting this equation to measured  $Y^*$  yields over the xenon pressure range 50-100 Torr, under the conditions where only excited-state formed fluorescence occurred (using  $\text{CH}_2\text{Br}_2$  pressures  $> 0.6$  Torr). With the calculated  $Y_0^*$  value, the  $Y^*$  fractions were then calculated as a function of  $\text{CH}_2\text{Br}_2$  gas pressure, these values are also shown in Figure 7. The difference between the measured  $Y_T$  and calculated  $Y^*$  values corresponds to the fraction of emission produced by the ionic recombination process. This relative fraction then allows calculation of the ionic recombination rate constants, as described previously for  $\text{Xe}_2^+/\text{SF}_6^-$ .

The measured  $\text{Xe}_2^+/\text{Br}^-$  recombination rate constants, as a function of xenon pressure, are shown in Figure 8. These rate constants again show the characteristic initial increase and subsequent decrease with increasing xenon pressure. Also shown in this figure are the Bates ter-molecular theoretical predictions [73] for  $\text{Xe}_2^+/\text{Br}^-$  recombination in xenon and the Langevin-Harper [74,75] diffusion controlled limit values for this recombining ion pair. Again the Bates ter-molecular predictions are seen to be always lower in magnitude, and to peak at a much higher xenon pressure, than experimentally determined. However, the limiting high pressure slope of the experimental data is again seen to converge to the  $\alpha_{\text{LH}}$  values indicating that this reaction again occurs with unit efficiency under these high-pressure conditions.

Analogous experiments utilizing electron pulse radiolysis techniques have been performed for  $\text{XeCl}^*$ ,  $\text{XeI}^*$ ,  $\text{KrF}^*$ , and  $\text{KrCl}^*$  [65-67]. Table 13 summarizes the  $\alpha_3$  rate constants obtained for these exiplexes, values ranged from  $(5 - 20) \times 10^{-25} \text{ cm}^6 \text{ s}^{-1}$ .

Although in principle one can also obtain  $\alpha_2$  values from these data by extrapolation to zero gas pressure, the large scatter in the measured rate constants at low gas pressures precluded any quantitative evaluation of this parameter. Typical values of  $\alpha_2$  were estimated to be in the range  $\sim 10^{-8}$  to  $10^{-7} \text{ cm}^3 \text{ s}^{-1}$ .

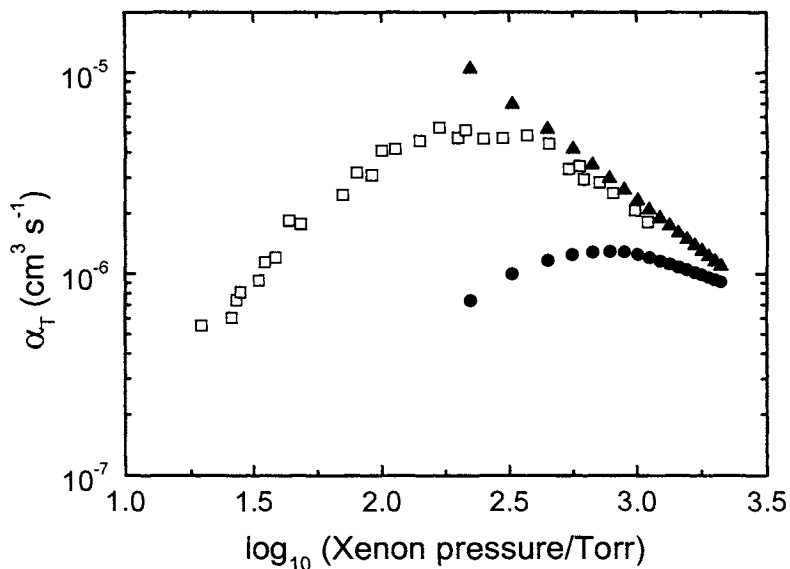


Figure 8. Xenon pressure dependence of the experimental  $\text{XeBr}^*$  ionic recombination rate constants ( $\square$ ) in comparison to the Bates calculated ter-molecular ( $\bullet$ ) and Langevin-Harper ( $\blacktriangle$ ) values for  $\text{Xe}_2^+/\text{Br}^-$  ionic recombination.

Table 13. Summary of experimental ionic recombination,  $\alpha_3$ , rate constants for xenon/krypton exciplex species.

Exciplex	Recombining ions	$\alpha_3$ $\text{cm}^6 \text{s}^{-1}$
$\text{XeF}^*$	$\text{Xe}_2^+/\text{SF}_6^-$	$(4.7 \pm 0.4) \times 10^{-25}$
$\text{XeCl}^*$	$\text{Xe}_2^+/\text{Cl}^-$	$(2.2 \pm 0.2) \times 10^{-24}$
$\text{XeBr}^*$	$\text{Xe}_2^+/\text{Br}^-$	$(1.3 \pm 0.1) \times 10^{-24}$
$\text{XeI}^*$	$\text{Xe}_2^+/\text{I}^-$	$(6.7 \pm 0.5) \times 10^{-25}$
$\text{KrF}^*$	$\text{Kr}_2^+/\text{SF}_6^-$	$(8.9 \pm 0.7) \times 10^{-25}$
$\text{KrCl}^*$	$\text{Kr}_2^+/\text{Cl}^-$	$(1.5 \pm 0.1) \times 10^{-24}$

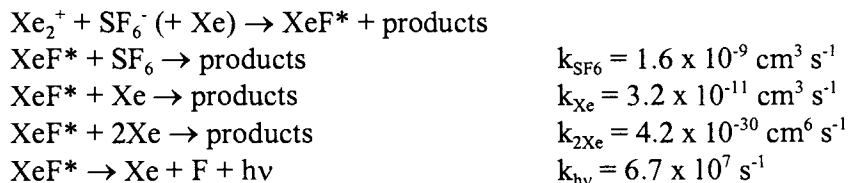
### Absolute Excitation and Emission Yields

Although radiation chemical yields in many systems are known through absorption spectroscopy and reliable extinction coefficients for radicals and ions, as well as via conductivity with known W values and ionic mobilities, yields of excitation resulting in photon emission are scarce. In e-beam and discharge pumped lasers the yields of photons from various pumping processes are not known. Recently absolute emission yields (G-values) for irradiated rare gas/halide gas mixtures have been performed. These values require the determination of both the total number of photons emitted from, and the total energy deposited in, each irradiated mixture. It is also required that the photon emission be apportioned between the various formation processes. Cooper et al. [83] have described the careful experimental procedures required to achieve reliable observations. The entire optical detection system had to be calibrated by absolute calorimetry over the wavelength range used. The optical system was free of lenses and mirrors to avoid problems with imperfections and geometry of light collection.

The number of photons emitted from an irradiated gas sample were obtained by summing the integrated emission over the exciplex spectrum, and then correcting for the dimer rare gas fluorescence and X-rays. The irradiation energy deposited was measured using conventional ozone dosimetry [69], performed under identical conditions to the emission measurements.

The results for the system xenon/SF<sub>6</sub> are shown in Figure 9. Figure 9a shows the variation in total yield, G<sub>T</sub>, for XeF\* as a function of xenon pressure, for a constant SF<sub>6</sub> pressure of 0.50 Torr. A continuous yield decrease with increasing xenon pressure was obtained over the entire pressure range studied. The dependence of SF<sub>6</sub> pressure on the XeF\* G<sub>T</sub> values (Figure 9b), at a constant Xe pressure of 50 Torr, also shows this decrease with pressure.

As the formation of the XeF\* (B,C) state fluorescence from irradiated Xe/SF<sub>6</sub> is only by ion recombination (> 95%), the decreasing emission yields with increasing component gas pressure are attributable to only the quenching reactions of XeF\*. Therefore, the G-value decreases observed in Figure 9 are described by the following reaction scheme:



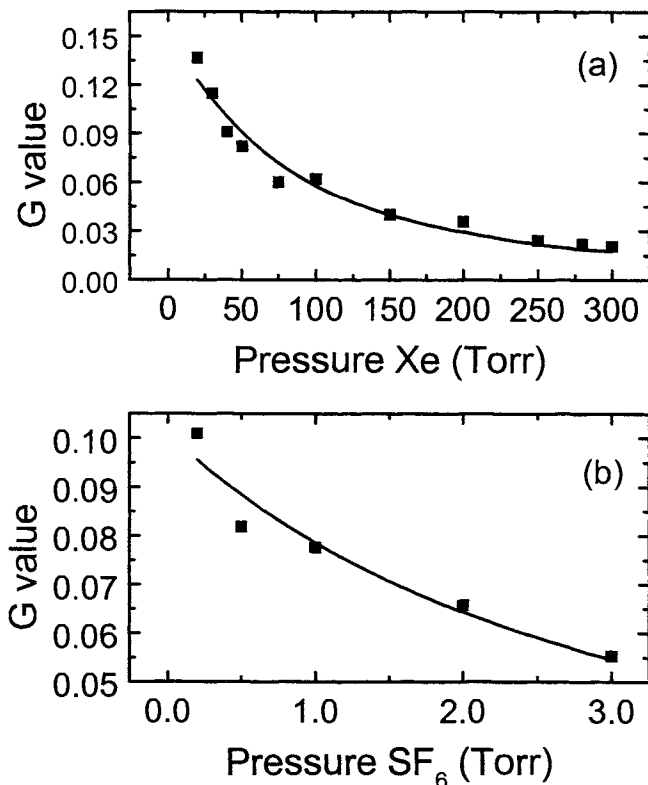


Figure 9. Variation in total XeF\*  $G_T$  values as a function of a) xenon and b) SF<sub>6</sub> gas pressure. Solid lines are calculated values based on model presented in text.

Based on this mechanism, the measured yield of XeF\* fluorescence,  $G_T$ , is given by

$$G_T = G_o^+ \left[ \frac{R_{hv}}{R_{SF_6} + R_{Xe} + R_{2Xe} + R_{hv}} \right]$$

where  $R_i$  is the rate of the  $i^{\text{th}}$  reaction in the above scheme.

Quenching rate constants for XeF\* were determined from literature data [84-89]. No literature value for SF<sub>6</sub> quenching of XeF\* ( $k_{SF_6}$ ) could be found. By globally fitting the experimental data in Figure 9 to the  $G^+$  general quenching equation, values of  $G_o^+ = 0.26 \pm 0.02$  and  $k_{SF_6} = 1.6 \times 10^{-9} \text{ cm}^3 \text{ s}^{-1}$

Table 14. Summary of the limiting, unquenched fluorescence yields for excited state,  $G_o^*$ , and ionic recombination,  $G_o^+$ , reactions for rate gas/halide gas exciplexes.

Gas system	Exciplex	$G_o^*$	$G_o^+$	$D_{A-X}$ eV
Xe/SF <sub>6</sub>	XeF*	0	0.26 ± 0.02	2.96
Xe/CCl <sub>3</sub> F	XeCl*	2.4 ± 0.6	3.2 ± 0.5	3.16
Xe/CF <sub>3</sub> Br	XeBr*	0.68 ± 0.10	3.4 ± 0.2	3.06
Xe/CF <sub>3</sub> I	XeI*	0.31 ± 0.08	4.5 ± 0.6	2.32
Kr/SF <sub>6</sub>	KrF*	0.70 ± 0.10	1.70 ± 0.10	2.96

were obtained. The calculated SF<sub>6</sub> and xenon pressure dependencies are shown as the solid lines in this figure, with very good agreement observed.

The very low derived value of  $G_o^+$ , as compared to its theoretical value of 4.5 based on the xenon W value of 22.1 ev/ion-pair [70], gives a photon yield per ion pair recombination value of 0.06. This suggests that production of the XeF\*(B,C) state is only a very minor pathway for ionic recombination in this system. It is believed that dominance of other recombination products may be due to the involvement of the molecular anion in this system [64].

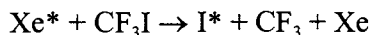
Absolute emission yields for other exciplexes have also been determined, following the methodology given for XeF\*. A summary of the limiting, unquenched fluorescence yields for excited state and ionic recombination reactions is given in Table 14.

The trends observed in these yields can be qualitatively supported by examination of the energetics of these reactions. The measured yield of  $G_o^+ = 4.5$  for the ionic recombination process in irradiated Xe/CF<sub>3</sub>I implies that, within experimental error, every ion pair formed recombines to give the fluorescent XeI\*(B,C) exciplex. The analogous yields for XeBr\* and XeCl\* are only slightly lower, about 75% of this theoretical value. However, given the accepted errors in measuring fundamental emission yields, it is doubtful whether these differences have any mechanistic significance.

The yields for these three exciplexes range over an order of magnitude, with only the value for XeCl\* in agreement with the quantitative theoretical prediction [90] of a fixed ratio between ion and excitation yields. The deduction from the experimental data in Table 14 assumes that the photon yield is equal to the total yield of excited states in the irradiated gas *and that all subsequent reactions produce the exciplex*. Although a range of xenon excited states are produced in the initial irradiation pulse, given the relatively high gas pressures and long timescales involved in these yield determinations, it can be assumed that only the longer-lived xenon metastable states, the 1s and 2p levels, with

energy ranges 8.31-9.56 and 9.58-11.14 eV, respectively [91] would be involved in exciplex formation reactions.

For XeI\* the excited-state yield is only 16% of its expected value, which implies that other reaction channels dominate. This additional process is believed to be the production of electronically excited iodine atoms by the reaction



The lowest excited state of the iodine atom has an energy of 0.9 eV [92]. However, the second lowest excited level is 6.95 eV. The addition of this latter value to the energy necessary for the appropriate bond dissociation in CF<sub>3</sub>I [93], of 2.32 eV, (see Table 14), requires that the minimum energy of the initial xenon electronically excited state to be 9.27 eV. This means that the higher 1s, as well as all the 2p, levels could participate in this dissociative reaction, thereby markedly decreasing the yield of XeI\* formed.

A similar alternative pathway may be present in the Xe/CF<sub>3</sub>Br system. For XeBr\* formation, the greater C-Br bond strength of 3.06 eV [93] and the higher second energy level for the excited state of Br\* of 8.31 eV [94] would mean that only the upper 2p levels of the excited xenon atoms would be able to produce this electronically excited halide atom. Since the population of these high excited states is lower, the amount of reaction proceeding by this pathway would be less, giving a concomitant increase in the yield of exciplex production, as observed.

In the Xe/CCl<sub>3</sub>F system, the even stronger C-Cl bond (3.16 eV, [93]), and the higher energy level of Cl\* of 9.23 eV [94] means that the excited state of xenon is required to have an energy of 12.39 eV, which is greater than the ionization potential of this atom. Thus the exit channel via Cl\* is energetically impossible, and hence the exciplex production is the only feasible channel, giving the quantitative yield experimentally observed.

For the two systems that incorporated SF<sub>6</sub> as the halide source gas, both the excited state reaction and ionic recombination limiting yields are much lower than for the xenon/atomic anion systems, suggesting that alternative pathways are dominant. This is attributed to the greater dissipation potential of the \*SF<sub>5</sub> product radical, where energy can be absorbed by further S-F bond breakage, or by additional excitement of this radical or smaller fragments. The lack of an excited-state reaction pathway for XeF\* production using SF<sub>6</sub> implies that almost all the energy of reaction is channeled into these alternative pathways, thus leaving insufficient energy to form this fluorescent exciplex. The relatively small excited state yield for KrF\* is similar to the yield measured

for XeBr\* (see Table 14) and likewise suggests that only the highest electronically excited krypton atoms have sufficient energy to form this exciplex. This is in agreement with a previous kinetic study of the Kr/SF<sub>6</sub> system [62], which showed that the very high KrF\* formation rate constant of  $2.0 \times 10^{-9} \text{ cm}^3 \text{ s}^{-1}$  was in good agreement with the observed quenching rate constants of the krypton 2p levels ( $1.5 \times 10^{-9} \text{ cm}^3 \text{ s}^{-1}$ ) but was much larger than the krypton 1s level quenching rate constant of  $3.3 \times 10^{-10} \text{ cm}^3 \text{ s}^{-1}$ .

### Summary

An overview of the fundamental early processes discussed in this section is summarized schematically in Figure 10. From this time onwards, thermal processes proceed.

### Applications of Gas Phase Radiation Chemistry

The application of gas phase pulse radiolysis to the study of homogeneous gas kinetics is well established. A full account of these applications is outside the scope of this presentation. However, a brief survey is appropriate. For further information the reader is referred to an excellent review by Jonah et al. [95].

The low electron energy, very high current, field emission devices such as Febetrons have been especially useful in this field. They enable a high dose to be deposited in a gaseous system sufficient to easily accomplish *single shot* absorption spectroscopic measurements. It has been estimated that using a Febetron 706 at its highest output, 0.6 MeV, 12 Joules of electron energy, irradiating a gas sample of, say, argon, at 2 atmospheres, would generate an ion concentration of the order of 0.1 torr! Truly "plasma conditions". Of course normal kinetics experiments would be conducted under more mild conditions.

Using such systems a variety of free radicals have been studied. Gordon and co-workers [96] have studied  $\cdot\text{NH}$ ,  $\cdot\text{NH}_2$ ,  $\cdot\text{OH}$  and  $\cdot\text{HO}_2$  radicals. In particular the formation of  $\text{HO}_2$  by a reaction  $\cdot\text{H} + \text{O}_2$  was found to be dramatically enhanced by the formation of hydrogen bonded complexes between  $\cdot\text{OH}$  and either  $\text{H}_2\text{O}$  or  $\text{NH}_3$ . The reactions of  $\cdot\text{CF}_3$  and  $\cdot\text{CCl}_3$  radicals with  $\text{NO}_2$  and  $\text{O}_2$  have been measured by Cumming et al. [97]. Bullock et al. [98] investigated ground state and vibrationally excited  $\cdot\text{CN}$  radical reactions with alkanes, alkenes,  $\text{O}_2$  and  $\text{NH}_3$ . Evidence of stepwise rate enhancement for vibrationally excited  $\cdot\text{CN}$  radicals was found. Hydroxyl ( $\cdot\text{OH}$ ) radicals have been extensively studied by several groups of workers; their reactions with  $\text{H}_2$ ,  $\text{CO}$ , alkenes, alkynes and halomethanes constitute a reliable data bank of rate constants and activation energies for combustion and environmental studies

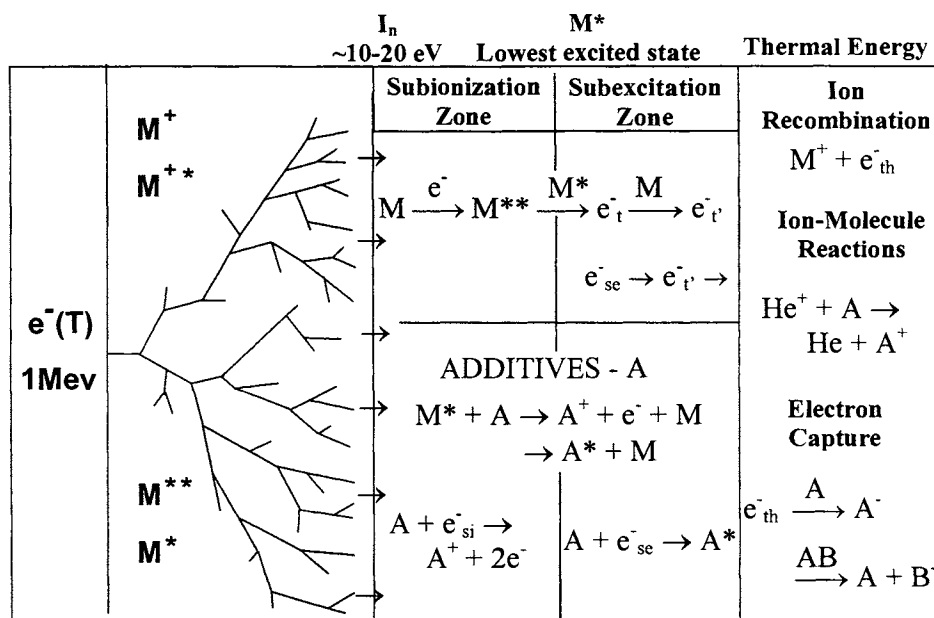


Figure 10. Overview of fundamental early processes in irradiated gases.

usage. Of especial mechanistic note is the work of Jonah et al. [99] who showed that  $\bullet OH$  addition reactions to alkenes showed a characteristic negative temperature coefficient for the rate constant indicative of inadequate energy loss processes to stabilise the  $\bullet OH$ -alkene adduct. This results in a substantial decrease in the rate, a factor of more than 10, in the range 300K to 600K. However, at very high temperatures, >700K, the reaction rate for  $\bullet OH$  radical loss dramatically increased as a high activation energy H-abstraction reaction kicked in. Research has been performed in Europe investigating the use of low energy electron beams to effect oxidative fixing of nitrogen and sulphur oxides in flue gases. Effectively, radiolysis of oxygen rich flue gases generates oxygen atoms which can convert sulphur dioxide into the trioxide, which can then be scrubbed out with ammonia giving the environmentally friendly fertiliser, ammonium sulphate. Similarly, the nitrogen oxides are worked up to ammonium nitrate rather than the oxygen depleting nitrite.

Radiation chemistry is the basic foundation for these applications.



## References:

1. R.L. Platzman, Radiation Research (Ed G. Silini). Pub. N<sup>th</sup> Holland (1967) p 20.
2. L.V. Spencer and U. Fano, Phys. Rev. (1954), 93; (1954), 1172.
3. M. Inokuti, M. Kimura and M.A. Dillon, Int. J. Quantum Chem. Symp. Series 21, (1987), 251.
4. M. Inokuti, M. Kimura and M.A. Dillon, Phys. Rev. A 38, (1988), 1217.
5. K. Kowari, M. Inokuti and M. Kimura, Phys. Rev. A 42, (1990), 795.
6. M. Inokuti, M. Kimura and M.A. Dillon, Radiat. Phys. Chem. 34, 477 (1989).
7. M. Burgers, Ph.D. Thesis "Time dependent studies in ionised gases" University of Melbourne (1993).
8. M. Burgers and R. Cooper, J. Chem. Phys. 106, (1997) 6385.
9. R. Cooper and M.C. Sauer, Jr., J. Phys. Chem. 93, (1989), 1881.
10. R. Cooper, L.S. Denison and M.C. Sauer, Jr., J. Phys. Chem. 86, (1982), 5093.
11. L.S. Denison, R. Cooper and M.C. Sauer, Jr., J. Phys. Chem. 90, (1986), 683.
12. C. Naleway, M. Inokuti, M.C. Sauer Jr, and R. Cooper, J. Phys. Chem. 90, (1986) 6154.
13. J.M. Warman and M.C. Sauer Jr., J. Chem. Phys., 62, (1975), 1971.
14. J.M. Warman and M.P. de Haas, J. Chem. Phys., 63, (1975), 2094.
15. J.M. Warman in NATO Advanced Study Institute Series, "The Study of Fast Processes and Transient Species by Electron Pulse Radiolysis", (Ed Baxendale and Busi); Pub. D. Reidel, Holland (1982), p 129; P.P. Infelta, M.P. de Haas and J.M. Warman, Radiat. Phys. Chem. 10, (1977), 353.
16. M.J. Scales, R. Cooper, J.M. Warman and M.P. de Haas, Radiat. Phys. Chem. 29, (1987), 365.
17. E. Suzuki and Y. Hatano, J. Chem. Phys. 84, (1986), 4915.
18. J.M. Warman and R. Cooper, Radiat Phys Chem. 36, (1990), 517.
19. M.C. Sauer, Jr. and L.M. Dorfman, J. Amer. Chem. Soc. (1964), 4218.
20. D.R. Bates, Phys. Rev. 77, (1950), 718.
21. Y.S. Cao and R. Johnsen, J. Phys. Chem. 94, (1991), 5443.
22. B.H. Mahan, J. Chem. Phys. 43, (1965), 3080.
23. M.A. Biondi and S.C. Brown, Phys. Rev. 76, (1949), 1697.
24. H.J. Oskam and V.R. Mittelstadt, Phys. Rev. 132, (1963), 1445.
25. C.L. Chen, C.C. Leiby and L. Goldstein, Phys. Rev. 121, (1961), 391.
26. E. Hinnov and J.G. Hirschberg, Phys. Rev. 125, (1962), 795.
27. F. Robben, W.B. Kunkel and L. Talbot, Phys. Rev. 132, (1962), 2363.
28. G.K. Born, Phys. Rev. 169, (1968), 155.
29. J. Berlande, M. Cheret, R. Deloche, A. Gonfalone and C. Manus, Phys. Rev. A. 1, (1970), 887.
30. A.W. Johnson and J.B. Gerado, Phys. Rev. Lett. 27, (1971), 835.
31. A.W. Johnson and J.B. Gerado, Phys. Rev. Lett. 28, (1972), 1096.
32. A.W. Johnson and J.B. Gerado, Phys. Rev. A 5, (1972), 1410.
33. A.W. Johnson and J.B. Gerado, Phys. Rev. A 7, (1973), 925.
34. R.J. van Sonsbeek, R. Cooper and R.N. Bhave, J. Chem. Phys. 97, (1992), 1800.
35. R. Deloche, P. Monchicourt, M. Cheret and T. Lambert, Phys. Rev. A 13, (1976), 1140.
36. J.J. Thompson, Philos. Mag. 47, (1924), 337.
37. D.R. Bates, J. Phys. B. At. Mol. Phys. 12, (1979), 35.

38. B.L. Whitten, L.W. Downes and W.E. Wells, *J. Appl. Phys.* 52, (1981), 1255.
39. L.P. Pitaevskii, *Sov. Phys. JETP* 15, (1962), 919.
40. D.R. Bates, *J. Phys. B. At. Mol. Phys.* 13, (1980), 2587.
41. R.N. Bhave and R. Cooper, *Aust. J. Phys.* 48, (1995), 503.
42. R. Cooper, R.J. van Sonsbeek, and R.N. Bhave, *J. Chem. Phys.* 98, (1993), 383.
43. M.C. Sauer Jr. and W.A. Mulac, *J. Chem. Phys.* 55, (1971), 1982.
44. M.C. Sauer Jr. and W.A. Mulac, *J. Chem. Phys.* 56, (1972), 4995.
45. J.M. Warman, E.S. Sennhauser and D.A. Armstrong, *J. Chem. Phys.* 70, (1979) 995.
46. E.S. Sennhauser and D.A. Armstrong, *J. Phys. Chem.*, 84, (1980), 123.
47. E.S. Sennhauser, D.A. Armstrong and J.M. Warman, *Radiat. Phys. Chem.* 15, (1980), 479.
48. M.T. Leu, M.A. Biondi and R. Johnsen, *Phys. Rev. A* 7, (1973), 292.
49. J.J. Thompson and E. Rutherford, *Philos. Mag.* 42, (1896), 392.
50. W.F. Schmidt, H. Jungblut, D. Hansen and H. Tagashira, *Proc. 6<sup>th</sup> Int. Conf. Gas. Dis. Applic.*, Heriot-Watt University. (1980).
51. J.K. Rice, A.K. Hay and J.R. Woodworth, *Appl. Phys. Lett.* 31, (1977), 31.
52. M.F. Golde, *J. Mol. Spectrosc.* 58, (1975), 261.
53. M.F. Golde and B.A. Thrush, *Chem. Phys. Lett.* 29, (1974), 486.
54. J.J. Ewing, *Physics Today* 31, (1978), 32.
55. C.A. Brau and J.J. Ewing, *J. Chem. Phys.* 63, (1975), 4640.
56. J.E. Velazco and D.W. Setser, *J. Chem. Phys.* 62, (1975), 1990.
57. R. Cooper, F. Grieser, and M.C. Sauer Jr., *J. Phys. Chem.* 80, (1976), 2138.
58. R. Cooper, F. Grieser, and M.C. Sauer Jr., *J. Phys. Chem.* 81, (1977), 1889.
59. M. Maeda, T. Nishirarumizu and Y. Miyazoe, *J. Jpn. Appl. Phys.* 18, (1979), 439.
60. F. Grieser and H. Shimamori, *J. Phys. Chem.* 84, (1980), 247.
61. R. Cooper and W. Mulac, *Chem. Phys. Lett.* 99, (1983), 217.
62. R. Cooper, L.S. Denison, P. Zeglinski, C.R. Roy and H. Gillis, *J. Appl. Phys.* 54, (1983), 3053.
63. R. Cooper, S.P. Mezyk and D.A. Armstrong, *Radiat. Phys. Chem.* 24, (1984), 545.
64. S.P. Mezyk, R. Cooper and J. Sherwell, *J. Phys. Chem.* 93, (1989), 8187.
65. S.P. Mezyk, R. Cooper and J. Sherwell, *J. Phys. Chem.* 95, (1990), 3152.
66. S.P. Mezyk, R. Cooper and J. Sherwell, *J. Phys. Chem.* 96, (1992), 8858.
67. S.P. Mezyk, R. Cooper and J. Sherwell, *J. Phys. Chem.* 97, (1993), 9413.
68. J.G. Young, Ph. D. Thesis, University of Melbourne. (1987).
69. C. Willis, A.W. Boyd, M.J. Young and D.A. Armstrong, *Can. J. Chem.* 48, (1970), 1505.
70. R. Cooper and R.M. Mooring, *Aust. J. Chem.* 21, (1968), 2417.
71. D.W. Huyton and T.W. Woodward, *Radiat. Phys. Chem. Rev.* 2 (1970), 205.
72. J. Sherwell, R. Cooper, D.C. Nguyen and S.P. Mezyk, *Aust. J. Chem.* 41, (1988), 1491.
73. D.R. Bates, *Advances in Atomic and Molecular Physics*, D.R. Bates and B. Bederson, Eds., Academic Press: New York, Vol. 20, (1985), p 1, and references therein.
74. P. Langevin, *Ann. Chim. Phys.* 28, (1903), 433.
75. W.R., Harper, *Proc. Cambridge Philos. Soc.* 28, (1932), 219.
76. H. Gutbier, *Z. Naturforsch* 9A, (1954), 348.
77. C.Y. Ng, D.J. Trevor, B.H. Mahan and Y.T. Loe, *J. Chem. Phys.* 66, (1977), 446.

78. W.L. Wilson Jr., R.A. Williams, R. Sauerbrey, F.K. Tittel, and G. Marowsky, *J. Chem. Phys.* 77, (1982), 1830.
79. J.K. Ku, D.W. Setser and D. Oba, *Chem. Phys. Lett.* 109, (1984), 429.
80. K. Tamagake, D.W. Setser and J.H. Kolts, *J. Chem. Phys.* 74, (1981), 4286.
81. W. Gadomski, J. Xu, D.W. Setser and T.O. Nelson, *Chem. Phys. Lett.* 189, (1992), 153.
82. A.K. Shuaibov and V.S. Shevera, *Zh. Prikl. Spektrosk.* 31, (1979), 731.
83. R. Cooper, S.P. Mezyk, J. Sherwell and J.G. Young, *J. Phys. Chem.* 100, (1996), 10634.
84. T.H. Dunning and P.J. Hay, *J. Chem. Phys.* 66, (1974), 1306.
85. C.H. Fisher and R.E. Center, *J. Chem. Phys.* 69, (1978), 2011.
86. R. Burnham and N.W. Harris, *J. Chem. Phys.* 66, (1977), 2742.
87. R.W. Waynant, *Appl. Phys. Lett.* 36, (1980), 493.
88. J.G. Eden and R.W. Waynant, *Opt. Lett.* 2, (1978), 13.
89. J.G. Eden and R.W. Waynant, *J. Chem. Phys.* 68, (1978), 2850.
90. R.L. Platzman, *Int. J. Appl. Radiat. Isot.* 10, (1961), 116.
91. C.E. Moore, Atomic energy levels as derived from the analyses of optical spectra. NBS 467, US Department of Commerce, National Bureau of Standards: Washington, D.C. Vol. 3. (1958).
92. C.E. Moore, Atomic energy levels as derived from the analyses of optical spectra. NBS 467, US Department of Commerce, National Bureau of Standards: Washington, D.C. Vol. 2. (1952).
93. R. Lide, *Handbook of Physics and Chemistry*, 71<sup>st</sup> Ed., CRC Press, Boca Raton, FL, USA, (1990)
94. C.E. Moore, Atomic energy levels as derived from the analyses of optical spectra. NBS 467, US Department of Commerce, National Bureau of Standards: Washington, DC Vol. 1. (1949).
95. C.D. Jonah, A. Liu, and W.A. Mulac, *Radiation Research; Proceedings of the 8<sup>th</sup> International Congress of Radiation Research*, Ed. Fielden, Fowler, Hendry, Scott; Pub Taylor/Francis, London (1987), p 60.
96. R.-R. Li, M.C. Sauer Jr. and S. Gordon, *J. Phys Chem.* 85, (1981), 2833.
97. J. Cumming, R. Cooper, W. Mulac and S. Gordon, *Radiat. Phys. Chem.* 16, (1980), 207.
98. G.E. Bullock and R. Cooper, *Trans. Farad. Soc.* 67, (1971), 3258.
99. C.D. Jonah, *Int. J. Chem. Kin.* 19, (1987), 25.

## High Temperature Water Radiolysis

George V. Buxton

The School of Chemistry, University of Leeds, Leeds LS2 9JT, UK.

### 1 INTRODUCTION

A knowledge of the radiation chemistry of water at high temperature became important when water-cooled nuclear power reactors came into use. These reactors are of two types, boiling water reactors (BWR) and pressurised water reactors (PWR), and the common factor is that the nuclear core is cooled by liquid water that is typically at a temperature in the range of 285 – 300 °C, depending on the particular reactor design. In BWRs the primary cooling circuit is connected directly to the steam generator, whereas in PWRs the primary cooling circuit is separate from the secondary steam generating circuit. The coolant in PWRs can be either H<sub>2</sub>O, as in the Westinghouse design, or D<sub>2</sub>O, as in the CANDU reactors. The cooling water is, of course, subjected to an intense ionising radiation field comprising low LET  $\gamma$ -rays and 2 MeV neutrons which interact with water molecules to produce high LET proton radiation.

In operational reactors it is necessary to select conditions such that the radiolytic decomposition of the water is suppressed, and this is achieved most effectively when the radiation chemistry of water under reactor conditions is understood. Thus, as with water radiolysis under normal ambient conditions, one needs to know (a) the yields (*g*-values) of the primary products formed in reaction (1):

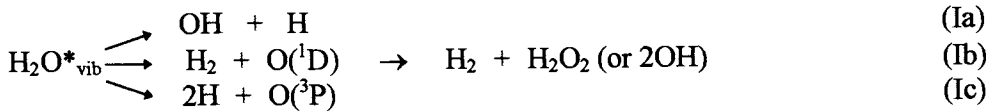
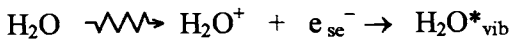


(b) the rate constants for the reactions taking place in spurs and tracks that result in these primary yields, and (c) rate constants for any solute systems that are used to determine the *G*-values, here expressed in units of mol J<sup>-1</sup>. Here the symbol *G*(*X*) is used to denote a measured yield and the symbol *g*(*X*) represents the yield of the primary products of water radiolysis when the spur reactions are complete (10<sup>-7</sup> s). The temperature dependence of rate constants over such a wide range of temperature is of more general relevance, for example in gaining insight to the chemical step in reactions that are diffusion limited at room temperature.

This chapter begins with a brief summary of the scheme for water radiolysis, followed by a description of the chemical systems used to obtain radiation chemical yields, or G-values, and rate constants at elevated temperatures that are pertinent to this scheme for both high and low LET, in H<sub>2</sub>O and D<sub>2</sub>O. Next, there is a section showing how the data can be accommodated in a simple spur diffusion model, and finally Arrhenius parameters for a number of reactions of more general interest are presented and discussed.

## 2 SCHEME FOR THE RADIOLYSIS OF WATER

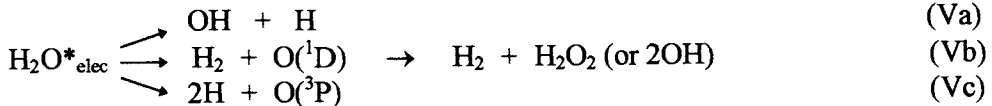
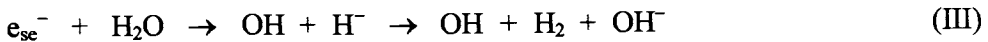
The initial processes in the radiolysis of water can be summarised as [1]:



(Ia)

(Ib)

(Ic)



(Va)

(Vb)

(Vc)

According to the model, ionisation and excitation events and the resulting products  $e_{\text{aq}}^-$ , H, H<sub>2</sub>, OH, H<sub>2</sub>O<sub>2</sub> and H<sup>+</sup> occur in clusters called spurs. For low LET radiation the spurs are separated by large distances relative to their diameter; for high LET radiation they overlap to form a continuous cylinder. The decomposition products then diffuse randomly and either react together or escape into the bulk solution. It is the competition between reaction and escape which determines the yields of the radical and molecular species extant when the spur processes are complete. The time for this completion is generally taken to be 10<sup>-7</sup> - 10<sup>-6</sup> s and the yields at this time are known as the primary yields. The spur reactions are listed in Table 1.

The requirement, then, for reactor coolant chemistry is to measure up to 300 °C in light and heavy water the primary yields for low and high LET radiation, and the rate constants of the spur reactions. It is also of intrinsic interest to test the spur-diffusion model for water radiolysis over a wide range of temperature.

TABLE 1  
Spur reaction set for the chemical stage in water radiolysis [1]

Reaction	$k/10^{10} \text{ dm}^3 \text{ mol}^{-1} \text{ s}^{-1}$	
	at 25 °C	at 300 °C
R1 $e_{\text{aq}}^- + \text{H}^+ \rightarrow \text{H}$	2.3	15
R2 $e_{\text{aq}}^- + \text{OH} \rightarrow \text{OH}^-$	2.9	11
R3 $\text{H}^+ + \text{OH}^- \rightarrow \text{H}_2\text{O}$	11.0	107
R4 $e_{\text{aq}}^- + e_{\text{aq}}^- \rightarrow \text{H}_2 + 2\text{OH}^-$	0.64	18
R5 $e_{\text{aq}}^- + \text{H} \rightarrow \text{H}_2 + \text{OH}^-$	2.1	30
R6 $\text{H} + \text{H} \rightarrow \text{H}_2$	0.54	10
R7 $\text{H} + \text{OH} \rightarrow \text{H}_2\text{O}$	1.5	6
R8 $\text{OH} + \text{OH} \rightarrow \text{H}_2\text{O}_2$	0.47	2
R9 $e_{\text{aq}}^- + \text{H}_2\text{O}_2 \rightarrow \text{OH} + \text{OH}^-$	1.4	27

### 3 MEASUREMENT OF G-VALUES

The methods adopted, pulse and steady state radiolysis, are those that have been widely used in making such measurements at room temperature. Most measurements have been made using radiation of low linear energy transfer (LET) such as  $^{60}\text{Co}$   $\gamma$ -rays or high energy (typically  $\geq 1$  MeV) electrons, but some key data have also been obtained with radiation of high LET. A limitation, of course, is the stability of the chemical system at elevated temperature. Experimentally, one only needs to be able to pressurise the reaction vessel sufficiently to prevent boiling. This requires about 20 atm at 200 °C and 100 atm at 300 °C. Under these conditions the chemical effects of pressure can be ignored.

#### 3.1 $g(e_{\text{aq}}^-)$ and $\{g(\text{H}) + g(\text{H}_2)\}$

A suitable system for the measurement of  $g(e_{\text{aq}}^-)$  and  $\{g(\text{H}) + g(\text{H}_2)\}$  up to 200 °C comprises a deaerated solution containing  $10^{-3} \text{ mol dm}^{-3}$  sodium nitrate and  $5 \times 10^{-3} \text{ mol dm}^{-3}$  sodium phosphite [2,3]. Steady-state radiolysis of this system produces nitrite ion and hydrogen, which are measured at room temperature.  $G(\text{NO}_2^-)$  provides a measure of  $g(e_{\text{aq}}^-)$  and  $G(\text{H}_2)$  is equated with  $\{g(\text{H}) + g(\text{H}_2)\}$ . Pulse radiolysis can also be used to measure  $g(e_{\text{aq}}^-)$  but a limitation is that the molar absorption coefficient,  $\epsilon$ , of the species formed has to be known at the temperature being studied since the measurable quantity is  $G\epsilon$ . Deoxygenated solutions containing 1,1'-dimethyl-4,4'-bipyridinium ion (methyl

viologen,  $MV^{2+}$ ) can be used up to 200 °C and  $g(e_{aq}^-)$  has been measured in solutions containing  $2.5 \times 10^{-4} \text{ mol dm}^{-3} MV^{2+}$  and  $10^{-2} \text{ mol dm}^{-3}$  *tert*-butanol (to scavenge OH) buffered with phosphate or borate [3]. Under these conditions  $MV^+$  is formed in reaction (2); it has  $\epsilon = 1370 \text{ m}^2 \text{ mol}^{-1}$  at 605 nm at room temperature [4] and was assumed to be temperature independent up to 200 °C [3]. Values of  $g(e_{aq}^-)$  derived from this system agree well with those obtained using the nitrate solutions described above.

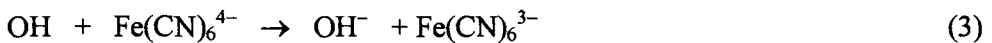


### 3.2 $g(H_2)$

A convenient way of measuring  $g(H_2)$  is by  $\gamma$ -radiolysis of degassed solutions of sodium nitrite because the nitrite ion scavenges all the primary radicals,  $e_{aq}^-$ , H and OH, very efficiently [5]. Elliot *et al.* [3] obtained  $g(H_2)$  by extrapolation of a plot of  $G(H_2)$  vs. the cube root of the nitrite ion concentration to zero concentration to allow for scavenging of the precursors of  $H_2$  in the spurs (see Table 1) [6].

### 3.3 $g(OH)$

The yield of the hydroxyl radical can readily be obtained by pulse radiolysis of aerated hexacyanateferrate(II) solution by measuring the yield of the product hexacyanateferrate(III), formed in reaction (3), whose molar absorption coefficient is well known ( $\epsilon_{420} = 104 \text{ m}^2 \text{ mol}^{-1}$  [3]):



The radicals  $e_{aq}^-$  and H are scavenged by oxygen and do not interfere. Unfortunately, hexacyanateferrate(II) solutions can only be used to measure  $g(OH)$  up to 105 °C because of their thermal instability. In order to extend the temperature range to 300 °C, Elliot *et al.* [3] measured  $G(CO_3^-)$  from aerated solutions of hydrogencarbonate where reaction (4) replaces (3):



In this case only  $G(CO_3^-)$  is measurable and it is necessary to evaluate  $\epsilon$  for  $CO_3^-$  over the whole temperature range. However, although the wavelength of maximum absorption,  $\lambda_{max} = 600 \text{ nm}$ , of the spectrum of  $CO_3^-$  is invariant with temperature, the band shows some slight broadening at elevated temperatures. Elliot *et al.* [3] concluded that the G-values were best assessed by assuming that

$\epsilon$  does not change with temperature, and they obtained good agreement with the hexacyanateferrate(II) data with  $\epsilon_{600}$  for  $\text{CO}_3^- = 193.4 \text{ m}^2 \text{ mol}^{-1}$ .

### 3.4 g(H<sub>2</sub>O<sub>2</sub>)

Measurement of the primary yield of hydrogen peroxide requires the use of a solute that scavenges  $e_{\text{aq}}^-$ , H and OH which would otherwise react to destroy the peroxide. A suitable solute is acrylamide [7] and Elliot *et al.* [3]  $\gamma$ -irradiated solutions containing  $5 \times 10^{-4} \text{ mol dm}^{-3}$  acrylamide to obtain g(H<sub>2</sub>O<sub>2</sub>) up to 100 °C. Kent and Sims [8] extended the temperature range to 270 °C by irradiating slightly alkaline solutions of N<sub>2</sub>O-saturated solutions of potassium iodide in a high-temperature loop experiment. Here the key reactions can be represented as:



and  $g(\text{H}_2\text{O}_2) = G(\text{O}_2)$  [9].

### 3.5 g-Values for other conditions

Elliot *et al.* [10] have also used some of the solute systems described above to measure primary yields in H<sub>2</sub>O irradiated under steady-state conditions with high LET radiation, specifically 23 MeV <sup>2</sup>H<sup>+</sup> and 157 MeV <sup>7</sup>Li<sup>3+</sup> ion beams. In this case it was not possible to measure g(OH) and so it was determined from the material balance equation (7):

$$g(\text{OH}) = g(e_{\text{aq}}^-) + g(\text{H}) + 2g(\text{H}_2) - 2g(\text{H}_2\text{O}_2) - 3g(\text{HO}_2) \quad (7)$$

where  $g(\text{HO}_2) = 4.1 \times 10^{-8} \text{ mol J}^{-1}$  was taken from LaVerne *et al.* [11] and assumed to be temperature independent [10]. Elliot *et al.* have also measured the primary yields in D<sub>2</sub>O for low LET radiation [3] and high LET radiation [12] under similar conditions. The data for H<sub>2</sub>O (low and high LET) are collected in Figure 1, and those for D<sub>2</sub>O (low LET only) in Figure 2.

## 4 MEASUREMENT OF RATE CONSTANTS OF SPUR REACTIONS

Measurement of the rate constants for the reactions listed in Table 1 has been achieved using pulse radiolysis up to 200 °C or 300 °C, depending on the apparatus available; the pressures needed to prevent water boiling at these temperatures are 20 atmospheres and 100 atmospheres, respectively. Where it has not been possible to make measurements at 300 °C, values of the rate



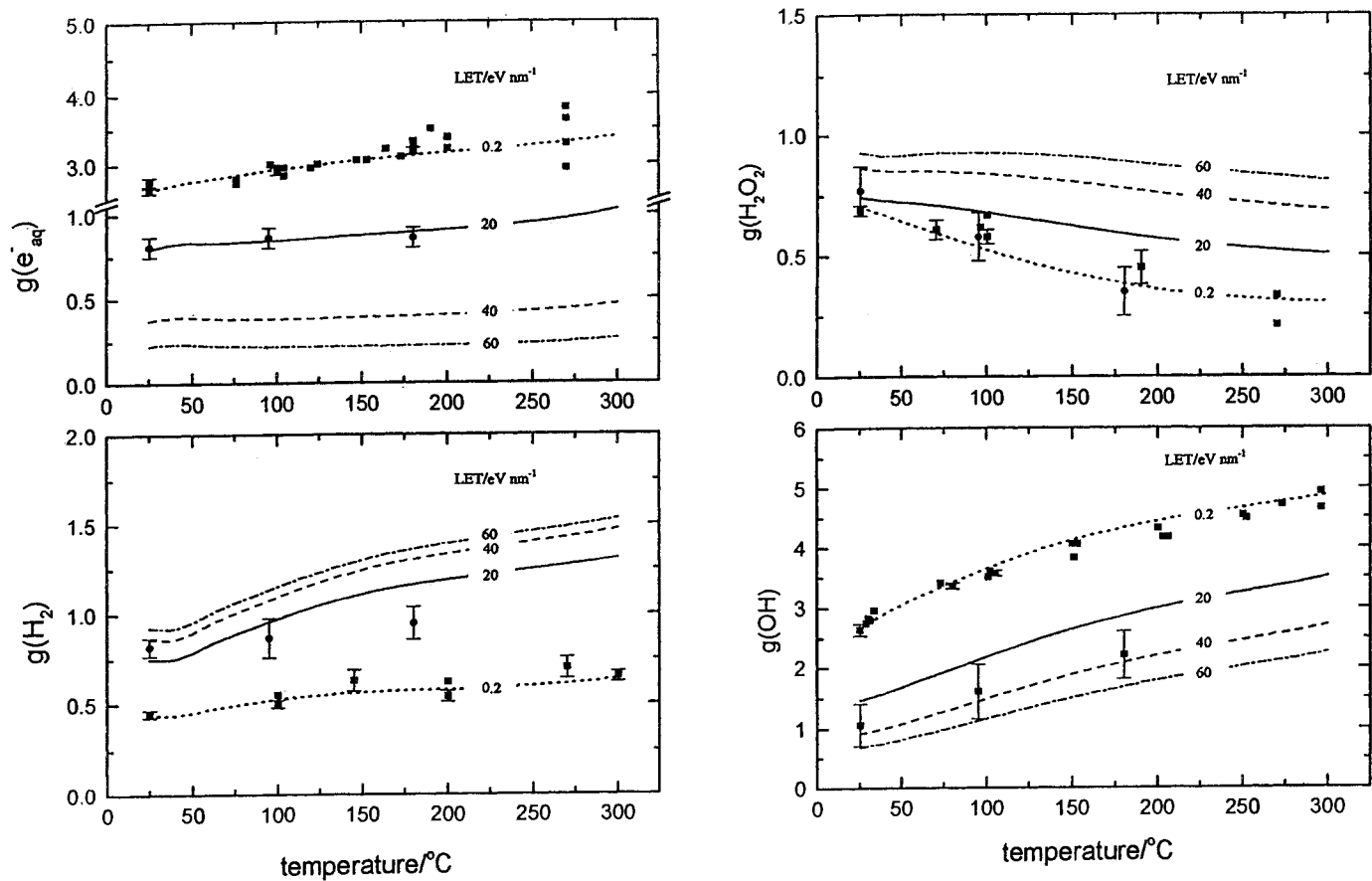


Figure 1. Values of  $g(e_{aq}^-)$ ,  $g(H_2)$ ,  $g(H_2O_2)$  and  $g(OH)$  calculated at  $1\ \mu s$  as a function of temperature and LET [1,31]. Experimental data are shown for  $0.2\ eV\ nm^{-1}$  (■) [3,8] and  $20\ eV\ nm^{-1}$  (●) [10].

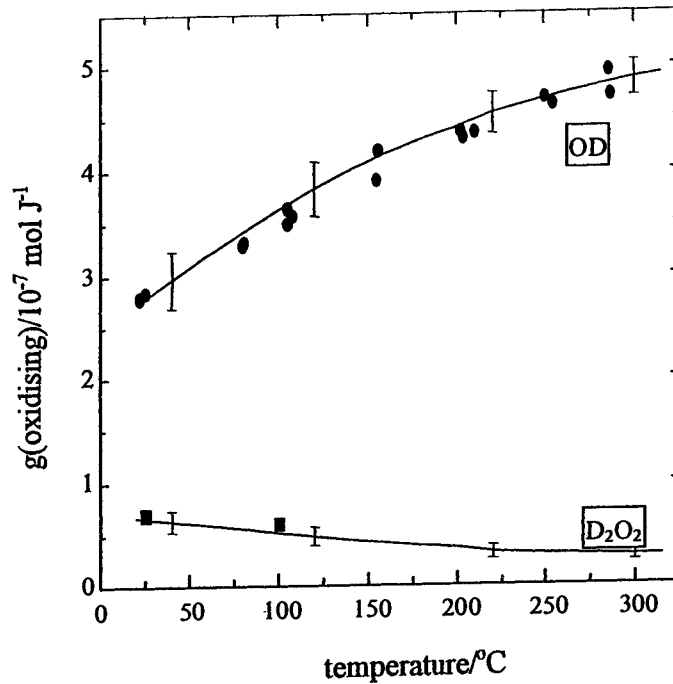
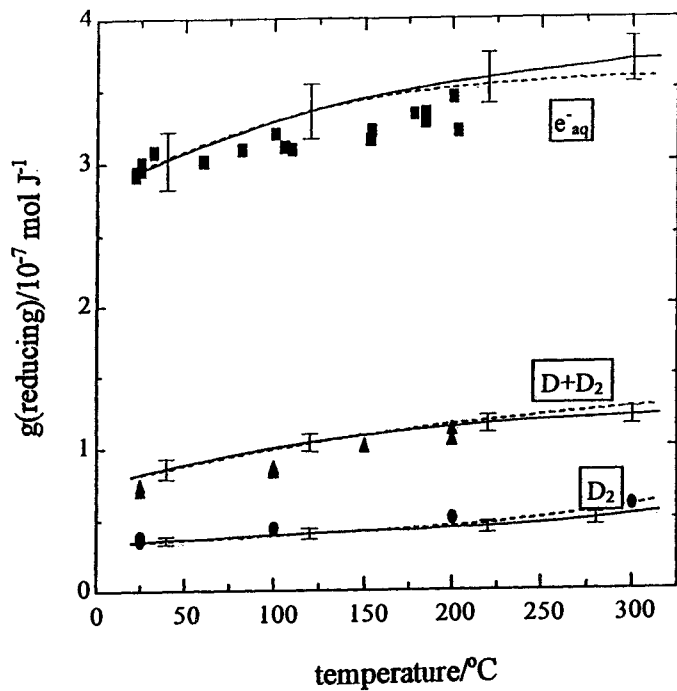


Figure 2. Primary yields (g-values) of the reducing (left hand panel) and oxidising (right hand panel) species produced in the  $\gamma$ -radiolysis of  $\text{D}_2\text{O}$ . The data points are from [3]. The solid lines are calculated as described in Section 5 [32]; the broken lines in the left hand panel are the results obtained using a linear extrapolation of the Arrhenius plot for  $k(e_{\text{aq}}^- + e_{\text{aq}}^-)$  above  $130^{\circ}\text{C}$  instead of equation (8). The sensitivity of the calculations to a 10% uncertainty in the diffusion coefficients and rate constants is shown by the error bars.

constants have been estimated from short extrapolations of Arrhenius plots as described below.

Most of the reactions listed in Table 1 are diffusion controlled at room temperature, but those involving OH as one of the reactants do not remain diffusion controlled at elevated temperatures. This is because the reaction rate becomes limited by the rate of the chemical step in the overall process of diffusion of the reactants together followed by their reaction to form products. In the general case the observed rate constant,  $k_{obs}$ , is given by equation (8) [13]:

$$k_{obs}^{-1} = k_{diff}^{-1} + k_{react}^{-1} \quad (8)$$

The temperature dependence of  $k_{diff}$  is given by the Smoluchowski equation:

$$k_{diff}(T) = 4\pi N_A D(T) r \beta f_D(T) \quad (9)$$

where  $N_A$  is Avogadro's number,  $D$  is the sum of the diffusion coefficients,  $r$  is the sum of the reaction radii,  $\beta$  is the statistical spin factor for radical-radical reactions [14] and  $f_D$  denotes the Debye factor. When the reactants are both ions  $f_D = \delta/(e^\delta - 1)$  where  $\delta$  depends on temperature through the relationship:

$$\delta = Z_A Z_B e^2 / (4\pi \epsilon_0 \epsilon(T) r k_B T) \quad (10)$$

where  $Z_A$  and  $Z_B$  are the charges on the ions,  $\epsilon_0$  is the permittivity of free space, and  $\epsilon(T)$  is the dielectric constant of water at absolute temperature,  $T$  K [15].

The Arrhenius equation (11) is used to evaluate  $k_{react}$  empirically [13]:

$$k_{react} = AT \exp(-E_{act}/RT) \quad (11)$$

#### 4.1 $k(\text{OH} + \text{OH})$

The method for evaluating rate constants outlined above is nicely illustrated by the self reaction of OH (reaction R8 in Table 1). Measured rate constants,  $k_{obs}$ , are shown in Figure 3 together with calculated values of  $k_{diff}$  and  $k_{react}$  that simulate the experimental data very well [14]. The calculated values were obtained with  $D_{OH} = 2.3 \times 10^{-9} \text{ m}^2 \text{ s}^{-1}$ ,  $\beta = 1$ ,  $r_{OH} = 0.22 \text{ nm}$ ,  $A = 3.7 \times 10^7 \text{ dm}^3 \text{ mol}^{-2} \text{ s}^{-1} \text{ K}^{-1}$  and  $E_{act} = 0 \text{ kJ mol}^{-1}$ .  $D_{OH}$  was assumed to have the same dependence on  $T$  as the self diffusion coefficient of water [16];  $r_{OH}$  was assumed to be independent of  $T$ .  $\beta$  is the statistical spin factor, which is the probability that random encounters between two doublet radicals produce a singlet state. If the spin relaxation time,  $\tau_s$ , for the radicals is longer than their encounter time,  $\tau_e$ , then  $\beta = 0.25$ ; if  $\tau_s$  is shorter than  $\tau_e$  then  $\beta = 1$ . The latter value is required to

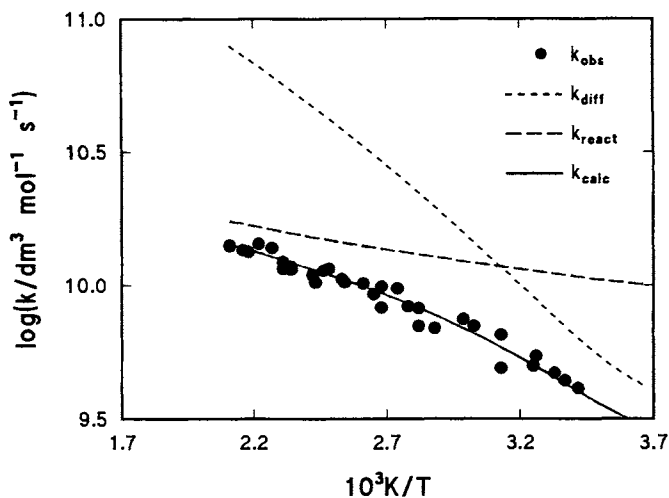


Figure 3. Arrhenius plot for  $k(\text{OH} + \text{OH})$  [14]. The solid line through the data points represents  $k_{\text{calc}}$ , the calculated value of  $k_{\text{obs}}$  obtained from equation (8). The values of  $k_{\text{diff}}$  from equation (9), and  $k_{\text{react}}$  from equation (11), are also shown.

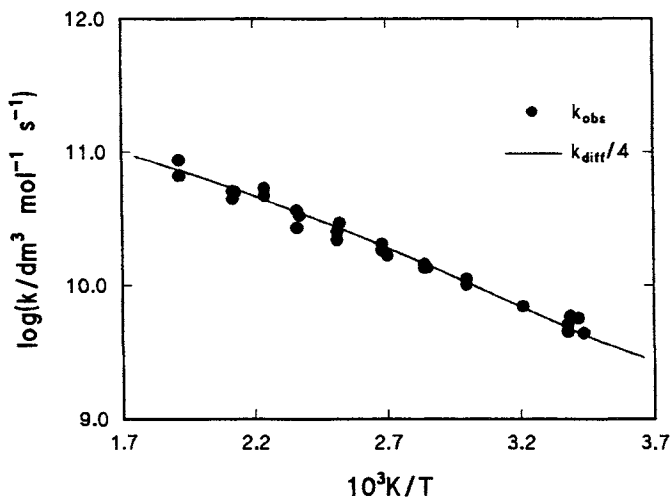


Figure 4. Arrhenius plot for  $k(\text{H} + \text{H})$ . The solid line through the data points [18] is obtained from equation (9) with  $\beta = 0.25$  [14].

simulate the data in Figure 3 and is not inconsistent with the estimate that  $\tau_e < 1$  ns for OH [17].

Before the measurements in Figure 3 were made, it had been generally assumed that spur reactions which are diffusion controlled at room temperature remained so at elevated temperatures and early modelling of the radiation chemistry of reactor coolant water was based on this premise. However, it is now evident that there is no sure substitute for experimental measurements in this field.

#### 4.2 $k(\text{H} + \text{H})$

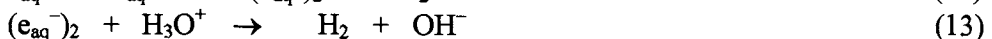
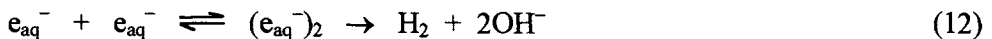
Figure 4 shows data obtained by Sehested and Christensen [18] for this reaction (R6 in Table 1). In this case the data are accurately represented by equation (9) with  $\beta = 0.25$ , taking  $D_H = 7 \times 10^{-9} \text{ m}^2 \text{ s}^{-1}$  at 25 °C [19] and  $r_H = 0.19 \text{ nm}$  [14]. Evidently this reaction is purely diffusion controlled, as would be expected for such a simple isotropic reactant, and  $\beta = 0.25$  is consistent with  $\tau_s \geq 13 \text{ } \mu\text{s}$  [20].

#### 4.3 $k(\text{H} + \text{OH})$

In measuring this rate constant, one must take into account the self reactions of OH and H which occur concurrently with their cross reaction (R7 in Table 1). Data obtained by Buxton and Elliot [14] show that  $k(\text{H} + \text{OH})$  has the same temperature dependence as  $k(\text{OH} + \text{OH})$ , with  $\beta = 1$  and  $E_{act} = 0 \text{ kJ mol}^{-1}$ , so that  $k_{react}$  has an influence on  $k_{obs}(\text{H} + \text{OH})$ . This result is qualitatively consistent with transition-state theory [21] which, for the gas phase, predicts that the reaction probability for an atom and a diatomic molecule is 10-100 times smaller than for two atoms. A comparison of  $k(\text{H} + \text{OH})$ ,  $k(\text{H} + \text{H})$  and  $k(\text{OH} + \text{OH})$  is shown in Figure 5. The similarity in the values of  $k(\text{H} + \text{H})$  and  $k(\text{OH} + \text{OH})$  at 25 °C is due mainly to the different spin factors,  $\beta$ , for the two reactions which counterbalance the difference between  $D_H$  and  $D_{OH}$ .

#### 4.4 $k(\text{e}_{aq}^- + \text{e}_{aq}^-)$

The self reaction of the hydrated electron (R4 in table 1) is an important contributor to  $\text{g}(\text{H}_2)$  in water radiolysis [1]. Its rate constant has been measured by Christensen and Sehested [22] in alkaline solution. They found that  $k_{obs}$  increased with temperature up to 150 °C and then decreased at higher temperatures, the value at 250 °C being about the same as that at room temperature. However, they also found  $k_{obs}$  at high temperature to be independent of pH (room temperature values) for  $\text{pH} \geq 10$ , but to increase sharply below pH 9. These findings were interpreted [22] in terms of reactions (12) and (13):



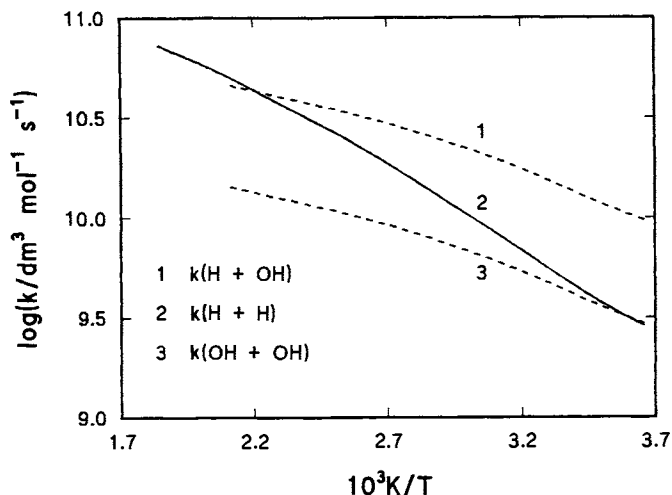


Figure 5. Comparison of the Arrhenius plots for  $k(OH + OH)$ ,  $k(H + H)$  and  $k(H + OH)$ .

with the dissociation of the dielectron,  $(e_{aq^-})_2$ , having an activation energy of more than  $125 \text{ kJ mol}^{-1}$  and reaction (13) being rapid.

Evaluation of  $k(e_{aq^-} + e_{aq^-})$  requires a knowledge of the molar absorption coefficient  $\alpha(e_{aq^-})$ . Whilst there is general agreement [23] amongst reported measurements of the temperature dependence of  $G\alpha(e_{aq^-})$  at the wavelength of maximum absorption,  $\lambda_{max}$ , Christensen and Sehested [22] took  $\epsilon_{max}$  to be independent of temperature whereas Elliot and Oullette [23] showed that it decreased according to the following relationship:

$$\epsilon_{max}(T/^\circ C)/m^2 \text{ mol}^{-1} = 2036.4 - 2.04T \quad (14)$$

Using this relationship to evaluate  $\epsilon_{max}$  results in a lower activation energy of  $20.3 \text{ kJ mol}^{-1}$  for the data up to  $150 \text{ }^\circ\text{C}$  [23]. However, attempts to model the radiolysis of water using the values of  $k(e_{aq^-} + e_{aq^-})$  in alkaline solution produces a sharp inflection in the g-values at  $150 \text{ }^\circ\text{C}$  [25] which is not observed in the measured values. This discordance between modelling and experiment suggests that the values of  $k(e_{aq^-} + e_{aq^-})$  obtained in alkaline solution are not appropriate for the acidic conditions in the spur. Support for this idea is provided by the normal behaviour of  $k(e_{aq^-} + H)$  described below.

#### 4.5 $k(e_{aq}^- + H)$

The rate constant for reaction R5 shows normal Arrhenius behaviour up to 250 °C with  $E_a = 14 \text{ kJ mol}^{-1}$  [23]. In evaluating their data, Christensen *et al.* [24] made corrections for the simultaneous occurrence of reactions R6 and R4, using the values of  $k(e_{aq}^- + e_{aq}^-)$  obtained in alkaline solution [22]. Reaction R5 is likely to proceed as follows:



Thus, in the case of reactions (12) and (13), the proposed intermediate dielectron may protonate sufficiently rapidly at the lower pH that the forward step of reaction (12) becomes rate determining. Making this assumption, Swiatla-Wojcik and Buxton [1] were able to model  $g(e_{aq}^-)$  quite accurately up to 200 °C as shown in Figure 1 and described in Section 5.

#### 4.6 $k(e_{aq}^- + OH)$

Two sets of values have been reported for  $k(e_{aq}^- + OH)$  [23,24]. In measuring this rate constant, account has to be taken of other reactions of  $e_{aq}^-$  and OH. Christensen *et al.* [24] obtained an activation energy of  $14.7 \text{ kJ mol}^{-1}$  up to 200 °C, whereas Elliot and Oullette [23] reported a value of  $7.9 \text{ kJ mol}^{-1}$  up to 150 °C. The latter value is in keeping with the activation energies obtained for the reaction of OH with itself and with H.

## 5 MODELLING OF SPUR AND TRACK PROCESSES UP TO 300 °C

Although stochastic treatments of the radiolysis of water seem the more logical approach to modelling spur and track processes, they are more complex and there are several examples to show that the essential features can be represented satisfactorily using deterministic methods and the 'average spur' concept [25-30]. As mentioned in Section 2, the spur diffusion model for low LET radiolysis of water assumes that energy deposition occurs in localised well-separated regions of spherical symmetry [25,26]. The deterministic spur diffusion model is based on the concept of an average spur with 62.5 eV deposited in it [30] producing an initial yield of electrons and ionised and excited water molecules which undergo thermalisation through random collisions with the surrounding water molecules. In pure water each spur contains a number of reactive species,  $e_{aq}^-$ , H, OH,  $H_2$ ,  $H_2O_2$ ,  $H^+$ , formed in the initial processes (I) - (V) shown in Section 2 and are

assumed to have a Gaussian distribution after thermalisation. These radiolytic products then either react within the spur as it expands by diffusion or escape into the bulk water.

Swiatla-Wojcik and Buxton [1] have applied this deterministic approach of the spur diffusion model quite successfully to water up to 300 °C, as shown by the data in Figure 1. They also extended this approach to cover high LET radiation [31] and obtained reasonable agreement with the available experimental g-values; these results are also shown in Figure 1.

The required parameters for the spur diffusion model are the initial yields,  $G^\circ$ , and the spur radii  $r_e^\rho$  for  $e_{aq}^-$ , and  $r_i^\rho = r^\rho$  for  $i = H^+$ , H, OH,  $H_2$  and  $H_2O_2$ . In their treatment, Swiatla-Wojcik and Buxton [1,31] chose these parameters to fit the extensive data available for low LET radiation at ambient temperature. The values are listed in Table 2. The values of  $G^\circ$  were then assumed to be independent of temperature and the spur radii were scaled with temperature according to the density, with the result that  $r_e^\rho$  and  $r_i^\rho$  increased by no more than 11.5% up to 300 °C. The main factors determining the temperature dependence of the g-values, therefore, are the rate constants listed in Table 1. Thus, the significant increase in  $g(OH)$  compared with  $g(e_{aq}^-)$  reflects the fact that the spur reactions of OH (R2, R7 and R8 in Table 1) become significantly slower than the diffusion-controlled rate, whereas reactions R1, R4, R5 and R9 are close to diffusion-controlled over the whole range of temperature.

The same approach has been applied successfully to heavy water for the low LET case [32] as shown in Figure 2. This was achieved by assuming that  $G^\circ(\text{ionisation})$  and  $G^\circ(\text{excitation})$  are the same as in light water (Table 2) and increasing  $r_e$  and  $r_i$  to 3.17 and 1.45 nm, respectively.

Table 2  
Initial yields and spur radii for modelling water radiolysis [1]<sup>a</sup>

entity	$H_2O^+$	$H_2O^*$	OH	$e_{aq}^-$	H	$H_2$	$H^+$	$OH^-$
$G^\circ/10^{-7} \text{ mol J}^{-1}$	5.39	0.76	5.68	4.95	0.34	0.21	5.13	0.18
$r_e =$	2.3 nm;							
$r_i =$	0.85 nm							

<sup>a</sup> In [1] and [31] G-values are expressed in units of molecules (100 eV)<sup>-1</sup>.



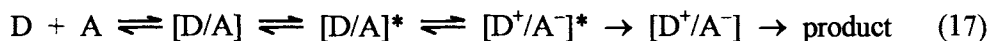
## 6 NON-LINEAR ARRHENIUS BEHAVIOUR OF RATE CONSTANTS

The development of apparatus to study the radiation chemistry of water at elevated temperatures opened the way to investigate rates of reaction of more general interest. Examples of reactions of  $e_{aq}^-$  and OH that exhibit non-linear Arrhenius behaviour are presented in the next two Sections. They show how the true chemical rate of a reaction is revealed when the diffusion limitation is lifted.

### 6.1 Some reactions of $e_{aq}^-$

In early work on the chemistry of  $e_{aq}^-$  it was found that, although the rate constants for its reactions spanned many orders of magnitude, the measured activation energies were mostly in the range 12 - 17 kJ mol<sup>-1</sup>. This led Hart and Anbar [33] to suggest that an electron transfer process with an invariant activation energy, associated with solvation shell orientation, is involved. However, measurements of rate constants up to 200 °C for the reaction of  $e_{aq}^-$  with NO<sub>2</sub><sup>-</sup>, NO<sub>3</sub><sup>-</sup>, SeO<sub>4</sub><sup>2-</sup>, S<sub>2</sub>O<sub>3</sub><sup>2-</sup>, N<sub>2</sub>O and phenol revealed that  $E_{act}$  becomes negative at elevated temperatures for each of these reactions [34]. This is exemplified by the data for NO<sub>2</sub><sup>-</sup> and SeO<sub>4</sub><sup>2-</sup> shown in Figures 6 and 7.

These reactions can be described by the following general scheme for transfer of an electron from a donor D to an acceptor A [35]:



where [D/A]\* and [D<sup>+</sup>/A<sup>-</sup>] represent the reorganised precursor and successor complexes involved in the electron transfer step. This scheme predicts that the observed activation energy for transfer can switch from positive to negative if the relaxation of [D/A]\* back to [D/A] has a larger temperature dependence than the reorganisation of [D/A] to [D/A]\*. In the case of SeO<sub>4</sub><sup>2-</sup> the calculated line in Figure 7 is obtained with values of  $E_{act}$  for these reaction steps of 46.1 and 18.8 kJ mol<sup>-1</sup>, respectively [34].

### 6.2 Reaction of OH with aromatic molecules

The reaction of OH with C<sub>6</sub>H<sub>5</sub>X (X = H, Cl, NO<sub>2</sub>, CO<sub>2</sub><sup>-</sup>, CO<sub>2</sub>H) produces the hydroxycyclohexadienyl radicals, [HOC<sub>6</sub>H<sub>5</sub>X], as shown by their absorption spectra [36]. At ambient temperature the rate of OH addition is close to diffusion controlled, but measurements up to 200 °C reveal that  $k_{obs}$  increases by less than three-fold up to 150 °C and then decreases slightly up to 200 °C, as shown in Figure 8. Evidently the electronic properties of the substituents X have little or no effect on the temperature dependence of  $k_{obs}$ , although the absolute values do differ.

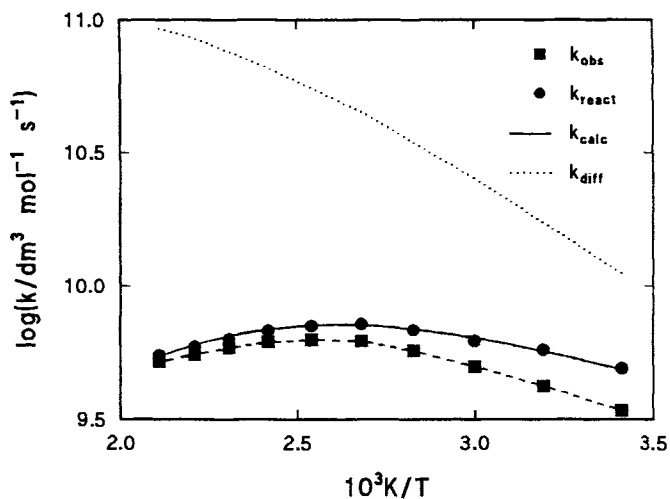


Figure 6. Arrhenius plot for  $k(e_{aq}^- + NO_2^-)$  [34]. The solid circles show the values of  $k_{react}$ , obtained from equation (8), and the solid line shows the fit of reaction scheme (16) to these data [34]. Note the influence of diffusion on  $k_{obs}$ .

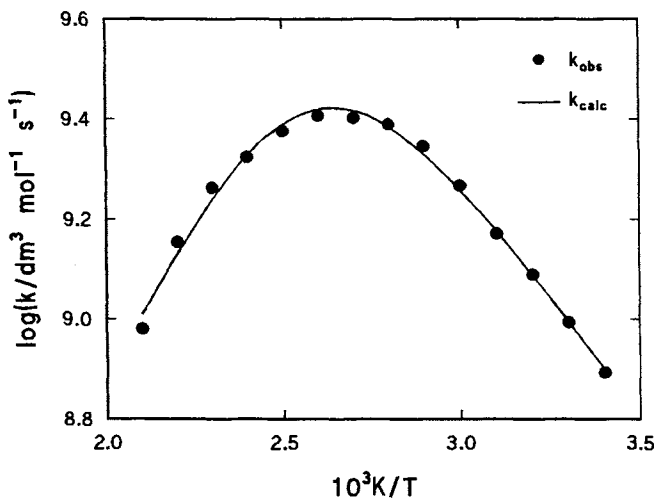


Figure 7. Arrhenius plot for  $k(e_{aq}^- + SeO_4^{2-})$  [34]. In this case the reaction rate is not influenced by diffusion so that  $k_{react} = k_{obs}$ . The solid line shows the fit of reaction scheme (16) to the data [34].

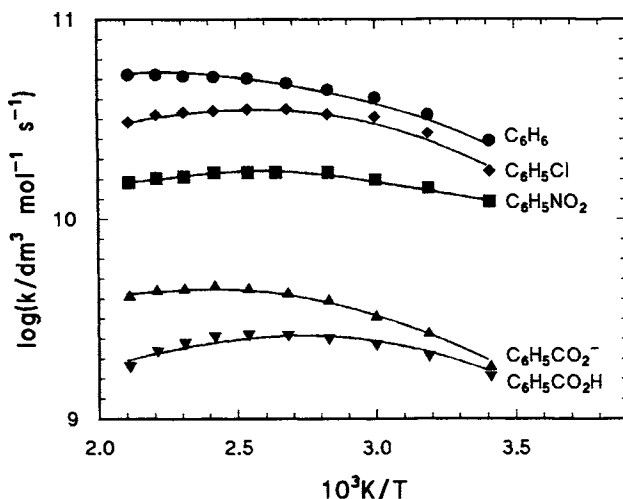


Figure 8. Arrhenius plots for the reaction of OH with some aromatic compounds.

A simple explanation [36] for these observations is that formation of the  $[\text{HO}\text{C}_6\text{H}_5\text{X}]$  radical proceeds *via* an intermediate that can dissociate back to the reactants in competition with the forward step. It has been proposed [36] that the intermediate is a  $\pi$ -complex in which the electrophilic OH interacts with the  $\pi$ -electrons of the aromatic ring as a precursor of the  $\sigma$ -bonded  $[\text{HO}\text{C}_6\text{H}_5\text{X}]$  radical. Such a mechanism has also been considered by others [37-39].

Treating the data in Figure 10 in terms of the following mechanism:



and applying the steady-state approximation to  $[\text{HO}\text{C}_6\text{H}_5\text{X}]_{\pi}$ , leads to:

$$k_{obs} = k_{18}k_{20}/(k_{19} + k_{20}) \quad (21)$$

Then, substitution of  $k_{obs}$  in equation (8) results in the parameters listed in Table 3. These show that rearrangement of the  $\pi$ -radicals to the  $\sigma$ -radicals requires little or no activation energy, whereas dissociation of the  $\pi$ -radicals has an activation energy of *ca.* 20 kJ mol<sup>-1</sup>.

Table 3

Parameters that simulate the values of  $k_{obs}$  shown in Figure 8 [36].

X	$D_{PhX}/10^{-9} \text{ m}^2 \text{ s}^{-1}$	$r/\text{nm}$	$k_{19}/10^9 \text{ s}^{-1}$	$k_{20}/10^9 \text{ s}^{-1}$	$E_{act}/\text{kJ mol}^{-1}$ for reactions	
					(19)	(20)
H	1.43	0.2	6.5	14	18	0.5
Cl	0.4	0.2	4.0	12	22	0.5
NO <sub>2</sub>	0.4	0.18	4.0	4	20	1.3
CO <sub>2</sub> <sup>-</sup>	0.6	0.18	3.8	13	21	1.0
CO <sub>2</sub> H	0.6	0.18	4.0	8	23	1.0

Values of  $k_{19}$  and  $k_{20}$  are at 25 °C.  $D_{OH} = 2.3 \times 10^{-9} \text{ m}^2 \text{ mol}^{-1}$ ;  $r_{OH} = 0.22 \text{ nm}$ .

Finally, the differences in the absolute values of  $k_{obs}$  are largely reflected in the values of  $k_{20}$ , suggesting that the electronic effects of the substituents X govern the rearrangement reaction (20).

## 7 CONCLUDING REMARKS

The most important information arising from studies of the radiolysis of water at elevated temperatures concerns rate constants. First, the temperature dependence of the rate constants of the various spur reactions account for the temperature dependence of the primary radiation chemical yields (g-values). Thus the greater changes in  $g(\text{OH})$  and  $g(\text{H}_2\text{O}_2)$  with temperature, compared with  $g(e_{aq}^-)$ ,  $g(\text{H})$  and  $g(\text{H}_2)$ , reflect the fact that the rates of the spur reactions involving OH become limited by the rate of the chemical step when restriction of the diffusion rate is lifted, whilst reactions of  $e_{aq}^-$  and H remain essentially diffusion controlled over the whole temperature range. Second, these kinetic characteristics are also observed for reactions of  $e_{aq}^-$  and OH with solutes of more general chemical interest and show that measurements of rate constants over extended high temperature ranges can provide insight to the detailed chemical mechanism.

The original impetus to measure rate constants in water at elevated temperatures was provided by the development of nuclear power reactors but, as in many other innovations, there is a spin-off of value to wider fields of research.

## REFERENCES

1. Swiatla-Wojcik and G.V. Buxton, *J. Phys. Chem.*, 99 (1995) 11464.
2. M. Haissinsky, *J. Chim. Phys.*, 62 (1965) 1141.
3. A.J. Elliot, M.P. Chenier and D.C. Oullette, *J. Chem. Soc., Faraday Trans.*, 89 (1993) 1193.
4. T. Watanabe and K. Honda, *J. Phys. Chem.*, 86 (1982) 2617.
5. G.V. Buxton, C.L. Greenstock, W.P. Helman and A.B. Ross, *J. Phys. Chem. Ref. Data*, 17 (1988) 513.
6. H.A. Mahlman, *J. Chem. Phys.*, 32 (1959) 601.
7. Z.D. Draganic and I.G. Draganic, *J. Phys. Chem.*, 73 (1969) 2571.
8. M.C. Kent and H.E. Sims, Harwell Research Report, AEA-RS-2302, 1992.
9. G.V. Buxton and F.S. Dainton, *Proc. Roy. Soc. A*, 287 (1965) 427.
10. A.J. Elliot, M.P. Chenier, D.C. Oullette and V.T. Koslowsky, *J. Phys. Chem.*, 100 (1996) 9014.
11. J.A. LaVerne, R.H. Schuler and W.G. Burns, *J. Phys. Chem.*, 90 (1986) 3238.
12. A.J. Elliot, D.C. Oullette and C.R. Stuart, AECL-11658, COG-96-390-1, 1996.
13. R.M. Noyes, *Progress in Reaction Kinetics*, G. Porter (ed.), Pergamon Press, London, 1961, p. 129.
14. G.V. Buxton and A.J. Elliot, *J. Chem. Soc., Faraday Trans.*, 89 (1993) 485.
15. G.C. Akerlof and H.I. Oshry, *J. Am. Chem. Soc.*, 72 (1950) 2844.
16. H.Z. Weingartner, *Z. Phys. Chem.*, 132 (1982) 128.
17. N.C. Verma and R.W. Fessenden, *J. Chem. Phys.*, 65 (1976) 2139.
18. K. Sehested and H. Christensen, *Radiat. Phys. Chem.*, 36 (1990) 499.
19. V.A. Benderskii, A.G. Krivenko A.N. Rukin, *High Energy Chem.*, 14 (1980) 303.
20. N.C. Verma and R.W. Fessenden, *J. Chem. Phys.*, 58 (1973) 2501.
21. S. Glasstone, K.J. Laidler and H. Eyring, *The Theory of Rate Processes*, McGraw-Hill, London, 1941.
22. H. Christensen and K. Sehested, *J. Phys. Chem.*, 90 (1986) 186.
23. A.J. Elliot and D.C. Oullette, *J. Chem. Soc., Faraday Trans.*, 90 (1994) 837.
24. H. Christensen, K. Sehested and T. Logager, *Radiat. Phys. Chem.*, 43 (1994) 527.
25. A. Mozumder and J.L. Magee, *J. Chem. Phys.*, 45 (1966) 332.
26. A. Mozumder and J.L. Magee, *Radiat. Res.*, 28 (1966) 215.
27. H.A. Schwarz, *J. Phys. Chem.*, 73 (1969) 1928.
28. W.G. Burns, H.E. Sims and J.A.B. Goodall, *Radiat. Phys. Chem.*, 23 (1984) 143.
29. J.A. LaVerne and S.M. Pimblott, *J. Phys. Chem.*, 95 (1991) 3196.
30. J.A. LaVerne and S.M. Pimblott, *J. Phys. Chem.*, 97 (1993) 3291.
31. D. Swiatla-Wojcik and G.V. Buxton, *J. Chem. Soc., Faraday Trans.*, 94 (1998) 2135.
32. D. Swiatla-Wojcik and G.V. Buxton, unpublished results.
33. E.J. Hart and M. Anbar, *The Hydrated Electron*, Wiley-Interscience, New York, 1970.
34. G.V. Buxton and S.R. Mackenzie, *J. Chem. Soc., Faraday Trans.*, 88 (1992) 2833.
35. M.D. Newton and N. Sutin, *Annu. Rev. Phys. Chem.*, 35 (1984) 437.
36. L. Ashton, G.V. Buxton and C.R. Stuart, *J. Chem. Soc., Faraday Trans.*, 91(1995) 1631.
37. B. Cercek and M. Ebert, *Adv. Chem. Ser.*, 81 (1968) 210.
38. O. Volhert and D. Schulte-Frohlinde, *Tetrahedron Lett.*, 17 (1968) 2161.
39. H.J. Van der Linde, D. Schulte-Frohlinde and F. Schworer, Per-5, Chem. Div., Atomic Energy Board, Pelidaba, S. Africa, 1976.

## **Radiation chemistry of concentrated inorganic aqueous solutions**

**Yosuke Katsumura**

Nuclear Engineering Research Laboratory,  
School of Engineering, The University of Tokyo  
2-22 Shirakata Shirane, Tokai-mura, Ibaraki, 319-1106, Japan

### **1. DIRECT AND INDIRECT ACTION OF RADIATION IN AQUEOUS SOLUTIONS**

Radiation induced reactions in dilute aqueous solutions have been studied over fifty years and, from a practical view point, almost enough knowledge has been accumulated. When the aqueous solution is irradiated with ionizing radiation, ionization and excitation take place. As a result, water decomposition products such as  $e_{aq}^-$ ,  $\bullet OH$  and  $\bullet H$  are formed and will react with solute molecules, which are consumed or converted. Here, radiation energy is mainly absorbed by water molecules and it can be said that the radiation induced reactions start from the decomposition of the water molecules. This is true only when the concentration of the solute is small. Since radiation energy is deposited through the interaction of radiation with electrons in the medium, the fraction of the energy absorbed due to the solute would be negligible in diluted solutions. Under this condition, the action of radiation on the solute is considered as an indirect one.

When the concentration of the solute is increasing, above assumption cannot hold. Let us think of a 1M  $HNO_3$  aqueous solution, as an example. The total number of electrons from  $HNO_3$  in one liter of the solution are  $(1 + 7 + 8 \times 3) \times N_A = 32 \times N_A$ , where  $N_A$  indicates the Avogadro number. On the contrary, the number from water molecules can be calculated approximately as  $(1 \times 2 + 8) \times 56 \times N_A = 560 \times N_A$ . The fraction of  $HNO_3$  is about 6%. Therefore, the direct energy deposition to the solute cannot be neglected and

should be taken into account, when the concentration of solute becomes higher. Then, the well known picture of the water radiolysis is representative for the direct action of radiation to water.

Because of the practical demands especially in nuclear technology much attention has been paid to the radiolysis of the concentrated aqueous solution. Highly concentrated nitric acid more than 3 M is used under the strong radiation field as an aqueous phase at the reprocessing of nuclear spent fuels in the so called Purex (Plутonium uranium reduction oxidation) Process [1]. Then, it is inevitably important to understand the radiation damage of the nitric acid in order to keep the operation highly efficient and safe. Similarly, perchloric acid is a useful and powerful solvent in solution chemistry because normally perchloric acid does not act as a ligand of the metal ions and therefore is not interfering with the chemistry of actinide ions, which is well understood under radiation [2]. In addition, direct processes are also closely related to the radiation effects in biology because the content of water in the living body is less than 80% and direct and indirect action on DNA damage is a typical subject [3].

When the radiolysis in concentrated aqueous solutions is concerned, the solvent H<sub>2</sub>O with an electron fraction of  $f_w$  and solute with  $f_s$  can be assumed to be separated as shown in Figure 1. Energy deposition occurs in proportional to the electron fraction of each component. The product, P, is assumed to be a sum of the products from the reaction of water decomposition product with solute and from the solute itself and, then, the G-value of the P would be described as follows.

$$G(P) = G_w f_w + G_s f_s = G_w (1-f_s) + G_s f_s \quad (1)$$

$$f_w + f_s = 1 \quad (2)$$

where  $G_w$  and  $G_s$  represent the G-values of transients from water and solute which form the product P at  $f_w = 1$  and  $f_s = 1$ , and  $f_w$  and  $f_s$  indicate electron fractions of the solvent and solute, respectively. When the product P is produced only from the solute, P is proportional to the  $f_s$  and experimental data can be plotted as closed circles in Figure 2. Typical examples are  $\text{NO}_3^\bullet$  and  $\text{SO}_4^{\bullet-}$  formation in nitrate and sulfate solutions, respectively. On the other hand, the data would be expressed as open circles in Figure 2, when the product is produced from both water and solute. Examples are the formation

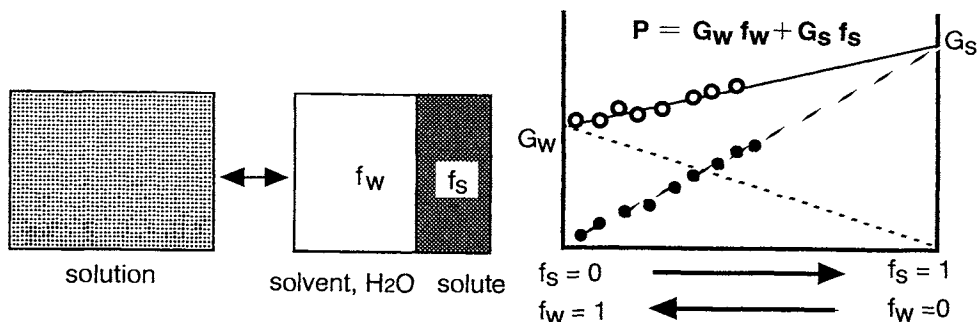


Figure 1 Schematic separation of water component with an electron fraction of  $f_w$  and solute one with  $f_s$  in concentrated solutions.

Figure 2 The change of the product yields as a function of electron fraction of solute  $f_s$  in concentrated solution. The upper line describes the sum of the products from water and solute. The lower line indicates that the product is coming only from solute.

of  $\text{NO}_3^\bullet$  and  $\text{SO}_4^{\bullet-}$  radicals not only from direct process but also from indirect reaction of  $\bullet\text{OH}$  with  $\text{HNO}_3$ , and  $\text{HSO}_4^-$  and  $\text{H}_2\text{SO}_4$  in acid solutions (see below).

Before presenting the radiolysis of several concentrated aqueous solutions, the electron fraction will be briefly discussed. While the electron fraction can be simply defined as a ratio of the number of electrons of the solute to the solution in the same volume, all electrons are not equivalent; some bind strongly to the nucleus. Then, it has been proposed that only valence electrons should be calculated [4]. But the values of the fraction from two different calculations are almost the same within a few percent not strongly dependent on the calculation, and thus the simple calculation is taken in the present chapter.

## 2. NITRIC ACID AND NITRATE SOLUTIONS

As mentioned before, radiolysis of nitric acid has been an important and complicated subject in nuclear technology and much data has been accumulated not only in low LET radiolysis but also in  $\alpha$ -radiolysis. The radiolysis study of the nitric acid started at the Oak Ridge National Laboratory in 1950s and many peculiar phenomena strongly dependent on the concentration were



observed [5]. Direct action on the nitrate has also been discussed. After the pulse radiolysis method was introduced, several groups in USA [6], Poland [7], Soviet Union [8] and Japan [9] conducted several experiments on the formation and yield measurement of  $\text{NO}_3\cdot$  radical. While the  $\text{NO}_3\cdot$  radical is one of the major transients in the radiolysis, different values reported for the absorption coefficient have opened the debate on the  $G(\text{NO}_3\cdot)$ .

In recent times interests in atmospheric chemistry have got scientists together not only from radiation chemistry but also from other fields to investigate the characteristics of the  $\text{NO}_3\cdot$  radical [10]. In addition, the treatment of the nuclear waste composed of high concentration of nitrate which has been accumulated during the development of nuclear weapons is an urgent subject. Therefore, an intensive work is in progress [11], which is also closely related the radiolysis of concentrated nitrate solutions.

When nitric acid is irradiated with an electron pulse of 10 ns duration, two formation processes, fast and slow, are observed as clearly shown in Figure 3. The fast process is completed after the duration of the pulse but the slower one grows up to 200 ns in 3 M nitric acid. If an  $\cdot\text{OH}$  scavenger is introduced, the slow component is easily reduced without the reduction of the fast component. This finding strongly suggests that the slow process is attributable to the  $\cdot\text{OH}$  radical reaction with nitric acid or nitrate ion. When the sample is replaced

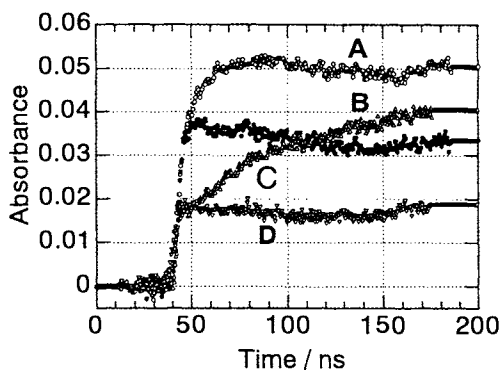


Figure 3 Time profiles of  $\text{NO}_3\cdot$  radical formation in 6 M  $\text{HNO}_3$  (A), 6 M  $\text{HNO}_3$  with 0.1M ethanol (B), 3M  $\text{HNO}_3$  (C) and 3 M  $\text{HNO}_3$  with 0.1 M ethanol (D).

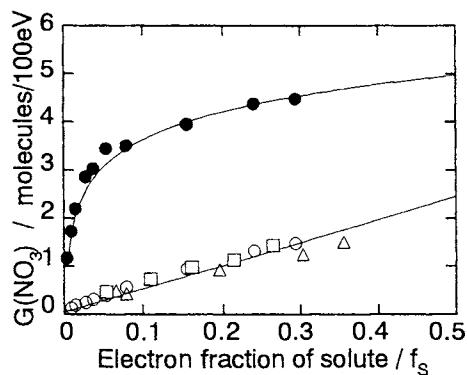


Figure 4  $G(\text{NO}_3\cdot)$  as a function of electron fraction of nitric acid or nitrate ions. Total ( $\bullet$ ) and fast ( $\circ$ ) component in  $\text{HNO}_3$  and fast one in  $\text{LiNO}_3$  ( $\square$ ) and  $\text{NaNO}_3$  ( $\triangle$ ).

with sodium nitrate solution, only the fast component is observable. This fast component is not hardly affected by the addition of the  $\bullet\text{OH}$  scavenger as observed in nitric acid. Since the  $\bullet\text{OH}$  radical is not reactive toward the nitrate ion, the slow one would be the  $\bullet\text{OH}$  reaction with undissociated nitric acid. By using the ion dissociation data of the nitric acid the experimentally determined formation rate of the radical versus concentration of the molecular nitric acid could be placed on a straight line but a curve was obtained when concentration of nitrate is taken. Then, the slow process is interpreted as a  $\bullet\text{OH}$  abstraction rather than an electron transfer reaction from molecular nitric acid as follows [9].



The yield of the  $\text{NO}_3\bullet$  can easily be evaluated if a reliable molar absorption coefficient at  $\lambda_{\text{max}}$  is known. While there have been several reported evaluations, the values are scattered. Although still a discrepancy exists, a recent value of  $\approx 1250 \text{ M}^{-1} \text{ cm}^{-1}$  at  $\lambda_{\text{max}} \approx 635 \text{ nm}$  would be acceptable [12, 13]. In Figure 4, G-values of the  $\text{NO}_3\bullet$  radical as a function of the concentration of nitrate in nitric acid and nitrate solutions are plotted. It is clear that the values of the fast component in nitrate and nitric acid are proportional to the electron fraction of the solute with  $G_s$  of 4.8. The role of  $\text{H}_2\text{O}^+$  for the  $\text{NO}_3\bullet$  formation was discussed and it seems to be a minor contribution [9].

There are several reports on  $\text{O}_2$  gas evolution. A recent report analyzed the published data and revealed that the  $\text{O}(^3\text{P})$  formation as shown below is the major origin of the  $\text{O}_2$  formation with  $G_s$ -value /  $(100 \text{ eV})^{-1}$  of 6.8 and 7.4 for  $\text{NO}_3^-$  and  $\text{HNO}_3$ , respectively [14].



Furthermore, precise measurements of  $\text{Ce}^{3+}$  formation in nitric acid and nitrate solutions in the presence and absence of  $\text{Tl}^+$  and the G-values of the

water decomposition were reported. The value is strongly dependent on the nitrate and nitric acid concentration. The value of 7.9 for  $G(-H_2O)$  was derived, which was much larger than the value of 4.08 and 4.5 in neutral and acid solutions, respectively [15]. This might be related to a fact that the nitrate ion is one of the well known efficient scavengers for the precursor of the hydrated electron [16]. A role of the nitrate ion in concentrated solution is far from complete understanding and much work is expected.

G-values of  $H_2$ ,  $HNO_3$ ,  $O_2$ ,  $H_2O_2$  have been determined by different researchers but the agreement is not satisfactory. Most of the references related to the radiolysis of nitric acid and nitrate solutions was recently summarized elsewhere [17].

### 3. SULFURIC ACID AND SULFATE SOLUTIONS

Aqueous sulfuric acid is widely used as a solvent for the Fricke dosimeter and much work has been done over these decades. The products from sulfuric acid after irradiation at various concentrations and the importance of the direct action was pointed out [18]. By using the pulse radiolysis techniques, the reaction of  $\bullet OH$  with  $HSO_4^-$  was observed and the formation of sulfate radical,  $SO_4^{\bullet -}$  with a peak position at 450 nm, was investigated at the Hahn Meitner Institute [19] and the Soviet Academy of Science [19], independently. The first report on the  $SO_4^{\bullet -}$  radical formation through direct action of radiation on sulfuric acid was reported in 1972 and the yield of  $SO_4^{\bullet -}$  was found to be proportional to the electron fraction,  $f_s(H_2SO_4)$ , with  $G_s(SO_4^{\bullet -}) = 4.3$  on the basis of the  $\epsilon(SO_4^{\bullet -}) = 1000 \text{ M}^{-1} \text{ cm}^{-1}$  [21]. Recently two distinct formation processes of the  $SO_4^{\bullet -}$  radical in sulfuric acid at different concentrations were reported; a very rapid formation of the 450 nm peak within the time duration of electron pulse (10 or 100 ns) and a slow formation strongly dependent on  $HSO_4^-$  or  $H_2SO_4$  concentration [22]. The slower one can be eliminated by the addition of the  $\bullet OH$  scavenger but the fast one is hardly affected by the scavengers. The fast formation process was identified as the direct action to the solute, sulfuric acid. Similar fast formation was also observed in sulfate solutions such as  $Na_2SO_4$  and  $Li_2SO_4$ .

Considering the acid equilibrium of  $\text{SO}_4^{2-} + \text{H}^+ \leftrightarrow \text{HSO}_4^-$  and  $\text{HSO}_4^- + \text{H}^+ \leftrightarrow \text{H}_2\text{SO}_4$ , the following reactions were determined from the growth rate of  $\text{SO}_4^{\bullet-}$ .



Using the value of  $\epsilon(\text{SO}_4^{\bullet-}) = 1600 \text{ M}^{-1}\text{cm}^{-1}$  at 450 nm [23],  $G_s(\text{SO}_4^{\bullet-}) / (100 \text{ eV})^{-1}$  was obtained to be 2.9, which is in good agreement with the one reported earlier [20] assuming  $\epsilon(\text{SO}_4^{\bullet-}) = 1000 \text{ M}^{-1}\text{cm}^{-1}$ . The above evaluation was confirmed by the measurement of the  $\text{Ce}^{4+}$  yields after the oxidation reaction of  $\text{Ce}^{3+}$  by the  $\text{SO}_4^{\bullet-}$  radical. In much higher concentrated sulfuric acid, several products such as  $\text{HSO}_3^{\bullet}$ ,  $\text{HSO}_5^{\bullet}$  as well as  $\text{SO}_4^{\bullet-}$  or  $\text{HSO}_4^{\bullet}$  were detected by pulse radiolysis measurement [24, 25] but successive reactions are not yet made clear.

#### 4. PHOSPHORIC ACID AND PHOSPHATE SOLUTIONS

Flash photolysis [26] and pulse radiolysis [27, 28] studies were carried out in phosphoric acid solutions.  $\text{H}_2\text{PO}_4^{\bullet}$ ,  $\text{HPO}_4^{\bullet-}$  and  $\text{PO}_4^{\bullet 2-}$  were identified but the evaluated absorption coefficients and acid-base equilibria seemed smaller and slightly confused, respectively. However, the accepted molar absorption coefficients and acid-base equilibrium of these transients have been established as follows [29].

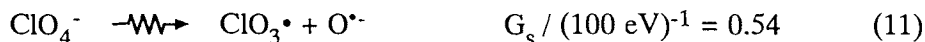
$\text{pK}_a$ 5.9	$\text{pK}_a$ 10.7	$\text{pK}_a$ value	
$\text{H}_2\text{PO}_4^{\bullet} \leftrightarrow \text{HPO}_4^{\bullet-} \leftrightarrow \text{PO}_4^{\bullet 2-}$			
520	510	530	peak position/nm
1850	1550	2150	molar absorption coefficient/ $\text{M}^{-1} \text{ cm}^{-1}$

Pulse radiolysis study on the concentrated phosphoric solutions were reported and  $\text{H}_2\text{PO}_4^{\bullet}$  radical formation was detected. Again, two formation processes of the transient, the fast and the slow, which are corresponding to

the direct one and the  $\bullet\text{OH}$  reaction with  $\text{H}_3\text{PO}_4$ , respectively, were observed [30]. The total formation yield as a function of the electron fraction of the phosphoric acid is sum of the above two processes,  $G(\text{H}_2\text{PO}_4\bullet) / (100 \text{ eV})^{-1} = 3.1 f_w + 3.4 f_s$ . The values are not consistent with recent report of  $G(\text{H}_2\text{PO}_4\bullet) = 1.6$  for 2-10 M solutions [31] in spite of the same  $1850 \text{ M}^{-1} \text{ cm}^{-1}$  was taken. The reason has not been made clear however.

## 5. PERCHLORIC ACID AND PERCHLORATE SOLUTIONS

In the radiolysis of concentrated perchloric acid the products  $\text{ClO}_3^-$ ,  $\text{ClO}_2$ ,  $\text{Cl}^-$ ,  $\text{O}_2$  and  $\text{H}_2$  were identified and measured as a function of the concentration [32-34]. G-value of the  $\text{ClO}_4^-$  decomposition was determined to be  $5.1 \pm 0.3$  [34]. The experimental results were slightly different from each other. A recent pulse and  $\gamma$ -radiolysis study evaluated the G-values for the following direct processes [35].



In the pulse radiolysis study an absorption band composed of a 350 nm peak corresponding to the  $\text{ClO}_3\bullet$  radical (next section) and a 460 nm one was clearly detected. The behavior of the latter absorption is dependent on the concentration and increased in highly concentrated condition. The band was tentatively assigned to  $\text{ClO}_4\bullet$  ( $\text{HClO}_4^{*\bullet}$ ) and it was proposed that an acid-base equilibrium brought the peculiar change. Details still remain to be solved. Furthermore, in order to reproduce the reported experimental data [34], a mathematical modelling was proposed [36].

## 6. OTHER SOLUTIONS

In spite of many reports on the direct effect on chloride solutions,

fundamental processes of  $\text{Cl}_2^{\bullet-}$  formation are not made clear yet. Sometimes, the arguments are completely opposite [37 - 39]. In LiCl solution, the yields of  $\text{Cl}_2^{\bullet-}$  and  $e^-_{\text{aq}}$  as a function of the  $\text{Cl}^-$  concentration were measured. The  $\text{Cl}_2^{\bullet-}$  yield increases with increasing  $[\text{Cl}^-]$  and it tends to decrease above 9 M, namely  $f_s > 0.20$ . At 9 M  $G(\text{Cl}_2^{\bullet-})$  was 3.4. From this data, it was concluded that direct effect on  $\text{Cl}^-$  ions gives rise to almost no  $\text{Cl}_2^{\bullet-}$  [37, 38]. On the contrary, this saturation was assumed to be caused by the electron-hole recombination due to the change of the solvent property at high concentrations of  $\text{Cl}^-$  and it was concluded that the direct action on  $\text{Cl}^-$  ions has a value of  $G_s = 7.0 \pm 0.4 / (100 \text{ eV})^{-1}$  for  $\text{Cl}_2^{\bullet-}$  formation [39]. Therefore, this is still an open question to be solved in future. In LiI solution, however, the formation of  $\text{I}_2^{\bullet-}$  and  $\text{I}_3^{\bullet-}$  are detected and the G-values of 4.8 and 7.3 are evaluated for indirect and direct effects of  $G(\text{I}_2^{\bullet-}) + 2G(\text{I}_3^{\bullet-})$  formation, respectively [40].

In chlorate solutions pulse radiolysis investigation was made and  $\text{ClO}_2^{\bullet}$  and  $\text{ClO}_3^{\bullet}$  radicals with  $G_s$ -values of 1.0 and 1.5, respectively, were measured [41]. The latter radical was observed for the first time. Later, the identification of the chlorate ( $\text{ClO}_3^{\bullet}$ ) radical was confirmed by the production of the same radical through the reaction of  $\text{SO}_4^{\bullet-}$  with  $\text{ClO}_3^-$  in laser photolysis [42]. However, the molar absorption coefficient for the  $\text{ClO}_3^{\bullet}$  radical was 4700 and 1500  $\text{M}^{-1}\text{cm}^{-1}$  in former and latter experiments, respectively. The reason for the difference is not clear.

The direct action of the radiation on solute molecules in concentrated aqueous solutions has been observed in various measurements by product analysis and pulse radiolysis, where the product yield is proportional to  $f_s$ . However, it is still not clear whether the product is formed through ionization, dissociation of the corresponding excited state or any other ultra-fast reactions. In order to grasp the details of the process, much experimental work is required. The highly time resolved experiment in a time range of ps or fs might bring the clear insight of the elementary processes of the direct effect.

In each system, the corresponding radical is formed through the direct action of the radiation and this will provide a new method to produce the corresponding radicals. Typical example is the  $\text{ClO}_3^{\bullet}$  radical observed for the

first time in concentrated solution, which was confirmed by a using different production method. In addition, this direct formation is frequently taken to measure the reactivity of the radical of interest [43, 44]. Finally, it is noted that in the concentrated aqueous solutions the micro-structure and the properties such as viscosity and dielectric constant are not the same with the bulk water any more. Therefore, the elementary processes are affected by the above factors and further analysis taking the above factors into consideration is highly expected.

### Acknowledgement

This work has been supported partly by a project of JSPS-RFTF98P00901 and Grand-In-Aid for Scientific Research (B-10480115) of the Ministry of Education, Science, Sports and Culture, Japanese Government.

### REFERENCES

- [1] M. Benedict, T. H. Pigford and H. W. Levi, Chapter 10 in Nuclear Chemical Engineering, 2nd ed., McGraw-Hill, New York, (1981).
- [2] J. J. Katz, G. T. Seaborg and L. R. Morss, Chapter 16 in The Chemistry of the Actinide Elements, 2nd ed., Chapman and Hall, New York, (1986).
- [3] M. C. Symons, Radiat. Phys. Chem., 43, 403-405 (1994).
- [4] A. J. Swallow and M. Inokuti, Radiat. Phys. Chem., 32, 185-189 (1988).
- [5] R. W. Matthews, H. A. Mahlman and T. J. Sworski, J. Phys. Chem., 76, 2680-2684 (1972) references cited herein.
- [6] M. Daniels, J. Phys. Chem., 73, 3710-3717 (1969) references cited herein.
- [7] E. Kozłowska-Milner and R. K. Broskiewics, Radiat. Phys. Chem., 11, 253-260 (1978).
- [8] A. K. Pikaev, P. Ya. Glazunov and A. A. Yakubovich, Dikl. Akade. Nauk SSSR, 215, 645-648 (1974).
- [9] Y. Katsumura, P. Y. Jiang, R. Nagaishi, T. Oishi, K. Ishigure and Y. Yoshida, J. Phys. Chem. 95, 4435-4439 (1991).
- [10] N-centered Radicals, ed. Z. B. Alfassi, John Wiley & Sons Ltd., New York (1998).
- [11] C. D. Jonah, S. Kapoor, M. S. Matheson, W. A. Mulac and D. Meisel, ANL-94/7 (1994) references cited herein.
- [12] T. Løgager, K. Sehested and J. Holcman, Radiat. Phys. Chem., 41, 539-543 (1993).
- [13] T. D. Giacco, E. Baciocchi and S. Steenken, J. Phys. Chem., 97, 5451-5456 (1993).
- [14] P. -Y. Jiang, R. Nagaishi, T. Yotsuyanagi, Y. Katsumura and K. Ishigure, J. Chem. Soc. Faraday Trans., 90, 93-95 (1994).
- [15] R. Nagaishi, P. -Y. Jiang, Y. Katsumura and K. Ishigure, J. Chem. Soc. Faraday Trans., 90, 591-595 (1994).
- [16] J. E. Aldrich, M. J. Bronskill, R. K. Wolff and J. W. Hunt, J. Chem. Phys., 55, 530-

- 539 (1971).
- [17] Y. Katsumura, Chapter 12 in *N-centered Radicals* ed. Z. B. Alfassi, John Wiley & Sons Ltd., New York (1998).
- [18] J. W. Boyle, *Radiat. Res.*, 17, 427-449 (1962) and 17, 450-464 (1962).
- [19] E. Heckel, A. Henglein and G. Beck, *Ber. Bunsenges. Phys. Chem.*, 70, 149-154 (1966).
- [20] A. K. Pikaev and V. I. Zolotarevskii, *Izv. AN SSSR*, 188-190 (1967).
- [21] B. Lesigne, C. Ferradini and J. Pucheault, *J. Phys. Chem.*, 76, 3676 (1972) and 77, 2156-2158 (1973).
- [22] P. -Y. Jiang, Y. Katsumura, R. Nagaishi, M. Domae, K. Ishikawa and K. Ishigure, *J. Chem. Soc. Faraday Trans.*, 88, 1653-1658 (1992).
- [23] O. P. Chawla and R. W. Fessenden, *J. Phys. Chem.*, 79, 2693-2700 (1975).
- [24] P.S. Polevoi, A. A. Revina, A. E. Khachaturov-Tavrizyan and S. A. Shilim, *High Energy Chemistry*, 23, 14-19 (1987).
- [25] P.S. Polevoi, A. E. Khachaturov-Tavrizian and I. N. Ivanov, *Radiat. Phys. Chem.*, 36, 99-103 (1990).
- [26] J. R. Huber and E. Hayon, *J. Phys. Chem.*, 72, 3280-3287 (1968).
- [27] E. D. Black and E. Hayon, *J. Phys. Chem.*, 74, 3199-3203 (1970).
- [28] G. Brauber, N. Getoff and Schwörer, *Int. J. Radiat. Phys. Chem.*, 5, 393-403 (1973) and 5, 405-417 (1973).
- [29] P. Maruthamuthu and P. Neta, *J. Phys. Chem.*, 82, 710-713 (1978).
- [30] P. -Y. Jiang, Y. Katsumura, M. Domae, K. Ishikawa, R. Nagaishi and K. Ishigure, *J. Chem. Soc. Faraday Trans.*, 88, 3319-3322 (1992).
- [31] A. E. Khachaturov and Yu. V. Smetannikov, *High Energy Chemistry*, 32, 171-174 (1998).
- [32] M. Cottin, *J. Chim. Phys.*, 53, 903-916 (1956).
- [33] D. Katakis and J. Konstantatos, *J. Phys. Chem.*, 72, 2054-2057 (1963) references cited herein.
- [34] Wang Wèng-hsin, L. T. Bugaenko and V. N. Belevskii, *Russ. J. Phys. Chem.*, 40, 1486-1489 (1966) references cited herein.
- [35] M. Domae, Y. Katsumura, P. Y. Jiang, R. Nagaishi, N. Chitose, K. Ishigure, T. Kozawa and Y. Yoshida, *J. Chem. Soc. Faraday Trans.*, 92, 2245-2250 (1996).
- [36] M. V. Vladimirova, *Radiat. Phys. Chem.*, 46, 575-578 (1995).
- [37] R. J. Woods, B. Lesigne, L. Gilles, C. Ferradini and J. Pucheault, *J. Phys. Chem.*, 79, 2700-2704 (1975).
- [38] J. Pucheault, C. Ferradini, R. Julien, A. Deysine, L. Gilles and M. Moreau, *J. Phys. Chem.*, 83, 330-336 (1979).
- [39] A. E. Grigor'eva, I. E. Makarov and A. K. Pikaev, *High Energy Chemistry*, 25, 172-176 (1991) references cited herein.
- [40] A. Hadjadj, R. Julien, J. Pucheault, C. Ferradini and B. Hickel, *J. Phys. Chem.*, 86, 4630-4634 (1982).
- [41] M. Domae, Y. Katsumura, P. Y. Jiang, R. Nagaishi, C. Hasegawa, K. Ishigure and Y. Yoshida, *J. Phys. Chem.*, 98, 190-192 (1994).
- [42] Z. Zuo, Y. Katsumura, K. Ueda and K. Ishigure, *J. Chem. Soc. Faraday Trans.* 93, 533-536 (1997).
- [43] P. Neta and R. E. Huie, *J. Phys. Chem.*, 90, 4644-4648 (1986).



- [44] Z. Zuo, Y. Katsumura, K. Ueda and K. Ishigure, *J. Chem. Soc. Faraday Trans.*, 93, 1885-1892 (1997).

## **Radiation Chemistry of Organic Liquids: Saturated Hydrocarbons.**

Ilya A. Shkrob, Myran C. Sauer, Jr., and Alexander D. Trifunac.

Chemistry Division , Argonne National Laboratory, Argonne, IL 60439

### **1. INTRODUCTION**

In this chapter, we examine radiolysis of neat organic liquids. The better studied and most common organic solvents are saturated hydrocarbons and alcohols. By virtue of having low dielectric constant and only C-C and C-H bonds, hydrocarbons represent an ideal medium to examine the fundamental mechanisms of radiolysis in non-polar media. For lack of space, the discussion will be limited to paraffins, branched alkanes, and cycloalkanes.

Many studies of saturated hydrocarbons have been carried out over the years; we refer the reader to previous reviews by Hummel [1], Swallow [2], and Holroyd [3]. Here we focus mainly on the last decade and discuss some of the more recent studies. Not too surprisingly, many issues examined in this chapter relate to the topics addressed in our own work; we apologize for this deficiency and hope that other reviews in this volume would complement this chapter. Specifically, we concentrate on the early stages of radiolysis and exclude from our scope chemical transformations of secondary radiolytic products, in particular, those derived from the solutes. We also limit our examination to low-LET radiation, such as UV and VUV photons, x- and  $\gamma$ -rays, and fast electrons. Significant progress has been made in understanding

the chemistry in the high-LET tracks and the omission is only due to the lack of space. Finally, we do not review the studies on dynamics and chemistry of electrons. Again, this is not to ignore excellent studies carried out over the last decade. However, our emphasis is on the bond-breaking chemical reactions. In radiolysis of hydrocarbons, these mainly occur in the excited states and solvent holes.

A brief sketch of radiation events in hydrocarbons is appropriate at this point. The ionizing radiation interacts with the solvent to produce excited solvent molecules and electron-hole pairs. Spurs containing one or several electron-hole pairs are generated in scattering events involving the primary and secondary electrons. A large fraction of the ejected electrons thermalize before they escape the Coulomb attraction of the positive charges. Few of these electrons can escape beyond the Onsager radius (at which the Coulomb attraction between the charges is  $\sim kT$ ) and the majority recombine with the holes. The distance an electron travels in the medium reflects its kinetic energy and the thermalization properties of the medium. Being non-polar, hydrocarbons are unable to "solvate" the electrons as happens in polar liquids (water, alcohols) and localized electrons remain close to the conduction band. Thermal promotion of these electrons to the conduction band leads to overall high mobility. As a result, rapid charge recombination is a dominant feature of the radiation chemistry of hydrocarbons and represents a "clock" against which all other processes compete.

The recombination of electron-hole pairs yields energetic, unstable solvent excited molecules. These excited states and pre-thermalized charges are surrounded by the solvent, and the fate of the excitation is determined by the deactivation, fragmentation, and chemical reactions of these short-lived species with the surrounding molecules. Understanding these rapid processes is the most important problem in the radiation chemistry. Unfortunately, the last decade witnessed little progress in this field. This impasse may continue since even the nature and chemistry of the lower excited states and relaxed solvent holes remains poorly understood. We believe that solving several long-standing problems in the chemistry of these species was the main achievement in the last decade. These studies provide a beachhead for the attack on the final frontier: the chemistry of highly excited neutral and charged states. Judging from the past experience, solving this "radiation chemistry" problem will require going

far beyond radiation chemistry methods such as pulse radiolysis. This is why the ultrafast laser studies on ionization and excitation in hydrocarbons, started in this decade, are so important.

While one may dream that developments in other fields would bring closure to some of the "radiation chemistry" problems, other problems can be solved only by radiation chemists themselves. Among the latter problems is the modeling of complex spur reactions. In multiple-pair spurs, many reactions occur simultaneously, resulting in tangled, inhomogeneous kinetics: charges recombine, excited solvent molecules fragment yielding radicals and neutrals, these species react with the primary ions and each other, the secondary ions react with the products, etc. Due to the high density of the reactive species, such transformations may occur in mere nanoseconds. This complexity makes the analysis of the early events a challenging task. Any understanding of the radiation chemistry will require adequately complex models of the spur processes. Development of such models has progressed significantly in this decade. Though the current computer models are still crude and primitive, they provide a benchmark against which theoretical ideas may be tested. These modeling efforts have already revitalized old discussions about the nature of radiolytic spurs. Without doubt, the future belongs to the more involved and rigorous models and, eventually, to the first-principle calculations. At the present, however, even the most elaborate computer models are as good as the parameters fed into them, and many of these parameters have not been experimentally measured.

This chapter is organized in the following way. First, studies on high-mobility solvent holes in cyclic alkanes are discussed. This topic unifies many issues in the chemistry of the solvent holes; these are examined along the way. Second, we summarize the recent advances in understanding the spur chemistry, starting from the laser and VUV studies of isolated ion pairs to modeling the multiple-pair spurs. The origins of spin effects and the importance of these effects for radiolysis are discussed in the same section. Third, we examine the studies on solvent and solute excited states in radiolysis of hydrocarbons. In the concluding section, we outline the most important problems to be addressed in the forthcoming decade.

## 2. SOLVENT HOLES WITH ANOMALOUSLY HIGH MOBILITY

*2.1 High mobility cations.* Ionization of several cycloalkane liquids - cyclohexane, methylcyclohexane, *trans*-decalin and *cis*-decalin - produces cations whose drift mobilities are 5-to-25 times greater than the mobilities of normally-diffusing molecular ions and (in some cases) thermalized electrons in these liquids [4-8]. These high-mobility cations are shown to be cycloalkane solvent holes with unusually long natural lifetimes (0.2  $\mu$ s to 5  $\mu$ s). This long lifetime and the high mobility of the cycloalkane holes makes it possible to study their reactions using microwave [7-9] or direct current (dc) [10-19] conductivity, an option that does not exist for other hydrocarbons. Indeed, in room-temperature paraffins, the solvent holes have natural lifetimes ranging from 1 ns ( $C_5$ ) to 33 ns ( $C_{16}$ ) [20,21] due to rapid dissociation of the C-C or C-H bond(s) and deprotonation,



Similarly short lifetimes are expected for branched alkanes, such as isooctane [22]. Due to these lifetime limitations, the chemical behavior of cycloalkane holes is understood in more detail than that of the solvent holes in other hydrocarbon liquids.

From conductivity studies, it is known that the cycloalkane holes rapidly react with various solutes, typically by electron or proton transfer [7-19]. These scavenging reactions establish the identity of the high-mobility cations as the solvent holes: Rapid generation of aromatic radical cations ( $A\cdot^+$ ) in reactions of the holes with aromatic solutes (A) was observed using pulse radiolysis - transient absorption spectroscopy [4,5,6,20,23-25] and, more recently, using pulse-probe laser-induced dc conductivity [26]. Rapid decay of the conductivity and transient absorbance signals from the cycloalkane holes was also observed [4-25].

It has long been speculated that the high-mobility solvent holes exist in hydrocarbons other than the four cycloalkanes. Recently, high-mobility solvent holes were observed in 2,6,10,15,19,23-hexamethyltetracosane (squalane) [24] and in cyclooctane [27]. In the squalane, rapid electron-transfer reactions of solvent holes with low-IP solutes were observed using transient absorbance spectroscopy and magnetic resonance [24]. Fast diffusion and high-rate

scavenging reactions of the squalane holes were also observed using magnetic level-crossing [28,29] and quantum beat [29] spectroscopies (see reviews [30] and [31] for the principles of these recently developed spin coherence spectroscopies). Rapid scavenging reactions were also found to account for the anomalies in the magnetic field effect observed for delayed solute fluorescence induced by VUV excitation of squalane [32,33]. In cyclooctane, high-mobility solvent holes were observed using time-dependent electric-field-modulated delayed fluorescence [27] (with this technique, the electric field is used to sort the radical ions by their drift mobilities [34]). This study supports previous observation of rapid scavenging of cyclooctane holes by aromatic solutes in the initial stage of radiolysis [35]. Both in the squalane and cyclooctane, the natural lifetime of the high mobility solvent hole is less than 20 ns [24,27-35]. It is still unclear whether this lifetime is limited by the inherent instability of the solvent holes or by their reactions with impurity. Perhaps, future work will reveal more examples of such short-lived high mobility holes. There is a recent suggestion of the presence of such holes in cyclopentane and cycloheptane; their natural lifetimes must be less than 5-10 ns [27]. Faster-than-normal scavenging of short-lived isooctane holes by diphenylsulfide and biphenyl was observed using quantum beat [36] and transient absorption spectroscopy [20]. Therefore, in addition to a few cycloalkane liquids that yield *long-lived* high-mobility solvent holes there may be many more hydrocarbon liquids that exhibit *short-lived* high-mobility holes. Importantly, not all hydrocarbon liquids can yield the high mobility solvent holes: Neither short-lived nor long-lived high-mobility cations have been found in linear alkanes.

**2.2 The solvent holes.** Previous suggestions that high-mobility cations are proton adducts or carbonium ions have been abandoned [37]. These suggestions originated by consideration of anomalous chemical and physical properties of cyclohexane and *trans*-decalin holes [38]. One of the peculiarities is that these solvent holes, while being paramagnetic species, were not observed by magnetic resonance techniques, both in neat cycloalkanes and in dilute solutions of cycloalkanes in high-IP liquids [39-48]. Instead, the resonance signals from olefin radical cations were observed (see below) [42,44,48]. This suggested a short life time for the solvent holes. The kinetic data on delayed fluorescence [49] and transient absorbance [6,20,25] in radiolysis of cyclohexane supported this conclusion. It was concluded that the lifetime of the solvent hole is only 20-30 ns [6,25], or 10 times shorter than the lifetime of the high-mobility cations

observed in the conductivity experiments. Only recently was it determined what causes the appearance of the lifetime-limited kinetics in the pulse radiolysis experiments: Some impurities in cyclohexane reversibly trap the solvent holes reducing their lifetime [11-14,25].

Another crucial finding was the realization that rapid spin-lattice ( $T_1$ ) relaxation in the high-symmetry cycloalkane radical cations precludes their detection with optically-detected magnetic resonance (ODMR) [39-48], the technique which was routinely used to study radical cations in radiolysis of hydrocarbons [38, 50]. For example, *trans*-decalin $\bullet^+$  isolated in room-temperature cyclohexane has  $T_1 \approx 7$  ns [50] while typical solute radical cations have  $T_1 \sim 1$   $\mu$ s. Since it takes several tens of nanoseconds to flip the electron spin with the microwave radiation (which is required for the magnetic resonance detection) radical cations of some cycloalkanes cannot be detected by ODMR.

The ultrafast spin-lattice relaxation is caused by dynamic averaging between the ground and excited states of the radical cations. The near degeneracy of the lower two states results through the Jahn-Teller distortion of highly symmetric radical cations [51,52]. The gap between the two lower states is greater for methylcyclohexane $\bullet^+$  and *cis*-decalin $\bullet^+$  and these two radical cations exhibit more regular magnetic resonance behavior. For cyclohexane $\bullet^+$  in hydrocarbon matrices, the dynamic averaging is so efficient that using ODMR this radical cation cannot be observed even at 4 K [39-41, 45-47, 50]. In *trans*-decalin $\bullet^+$ , the quasi-degenerate states are very close in energy (ca. 0.43 eV in the gas phase [52]) and van der Waals interaction with the host can stabilize the "excited"  $^2B_g$  state instead of the "ground"  $^2A_g$  state (see discussion in references [50,52]). Therefore, for these high-symmetry radical cations no distinction exists between the "ground" and "excited" states, especially at 300 K. For less symmetric radical cations, the state mixing was not observed.

Radiolytically-generated solvent holes have initial excess energy of several electron-volts. It is generally believed that these excited species relax to the "ground" state on a picosecond time scale or even faster [37,38,53]. Nevertheless, some authors suggest that certain excited cycloalkane holes have lifetimes in nanoseconds [54,55]. Such suggestions are not completely

groundless: in conformationally-hindered species, the structural relaxation may take a long time. For example, the twist-boat to chair transition in room-temperature cyclohexane occurs on a microsecond time scale. Perhaps, the best supported claim for such a long-lived excited solvent hole is found in the study of geminate pair dynamics in methylcyclohexane at 143 K [55,56]. Using transient absorption spectroscopy, it was concluded that the (high-mobility) solvent hole [56] has a (high-mobility) precursor with the natural lifetime of 300 ns [55]. The decay of the precursor can be accelerated upon addition of N<sub>2</sub>O; without the quencher, the precursor either fragments yielding methylcyclohexene radical cations (90 %) or relaxes (10%) [55].

It is difficult to assess the plausibility of this scenario because the data allow for more than one interpretation. N<sub>2</sub>O rapidly scavenges thermalized electrons and quenches the solvent excited states thus reducing the yield of olefins (that form by the fragmentation of these excited states) [1]. Since in some hydrocarbons the olefin radical cations may be formed in reactions of the solvent holes with the olefins in spurs (see below), the yield of these cations will decrease in the presence of N<sub>2</sub>O. Therefore, the changes observed upon the addition of N<sub>2</sub>O are not a clear-cut evidence for the involvement of the excited solvent holes.

The optical absorption spectra of the high mobility solvent holes resemble those for the radical cations isolated in freon matrices [20,22-25]. All of these spectra are bell-shaped featureless curves with maxima in the visible and/or near IR regions. In pulse radiolysis studies, the absorption signal from the solvent hole always overlaps with the signals from the fragment (and/or secondary) radical cations ("satellite ions"), even at the earliest observation times [22-25,57]. Therefore, complex deconvolutions are needed to extract the spectra of the solvent holes. This leaves large uncertainty as for the exact shape of the absorption spectra and the extinction coefficients.

*2.3 The mechanism for the high mobility.* In the early studies, the high-mobility cycloalkane holes were viewed as radical cations that undergo rapid resonant charge transfer [8]:





At any given time, the positive charge was assumed to reside on a single solvent molecule and, once in 0.5-2 ps, hop to a neighboring molecule. Reaction (2) was believed to have low activation energy due to similarity between the shapes of cycloalkane molecules and their radical cations.

This model is consistent with many observations. Dilution of cycloalkanes with high-IP alkanes (or higher-IP cycloalkanes) results in the decrease in the hole mobility that correlates with the mole fraction of the cycloalkane in the mixture: the hopping rate decreases when the density of the like molecules decreases [8,14]. The activation energies for the hole mobility, as estimated from conductivity data range from  $-(3\pm 1)$  kJ/mol for *trans*-decalin and cyclohexane to (6-7) kJ/mol for methylcyclohexane and *cis*-decalin [7,8,10]. The activation energies for the highest-rate scavenging reactions range from 4 kJ/mol to 9 kJ/mol [10]. Apparently, the migration of the solvent hole requires little thermal activation.

The occurrence of reaction (2) is firmly established experimentally. Charge transfer between  $c\text{-C}_6\text{D}_{12}\bullet^+$  and  $c\text{-C}_6\text{H}_{12}$  was observed in the gas phase, where it proceeds at  $\sim 1/3$  of the collision rate [58]. Reaction (2) was observed for radical cations and molecules of *cis*- and *trans*-decalins in dilute cyclohexane solutions (where it proceeds with a diffusion-controlled rate) [50,59]. In low-temperature solid hydrocarbons (4-30 K), the hole hopping due to reaction (2) may be observed through the time evolution of the resonance lines in ODMR spectra [39,45]; the residence time of the self-trapped holes at a given molecule is 0.1-1  $\mu\text{s}$ . At higher temperatures, the spectral diffusion caused by the rapid reaction (2) causes the ODMR spectrum to collapse to a single narrow line. For solvent holes in liquid *cis*-decalin, *trans*-decalin, and squalane, this narrow line was observed, albeit indirectly, using magnetic level-crossing and quantum beat spectroscopies [28,29,50,59]. In squalane, the residence time of the hole at the solvent molecule is relatively long, ca. 0.2-0.3 ns [24,28,29], and any mechanism of the hole migration other than reaction (2) is implausible. Thus, there is little doubt that reaction (2) occurs in liquid hydrocarbons. Nevertheless, it is doubtful that this reaction *per se* is the cause for the high mobility of the solvent holes in cycloalkanes.

Indeed, both matrix-isolation EPR experiments and quantum-mechanical calculations indicate that the neutral cycloalkanes and their ground-state radical

cations have rather different geometries [50,51,52]. For example, in *cis*- and *trans*-decalins the bridging C<sub>9</sub>-C<sub>10</sub> bond elongates from 0.153-0.156 nm in the neutral molecules to 0.19-0.21 nm in the  $^2A_1$  and  $^2A_g$  states of the radical cations, respectively [10,52]. Upon charging, the molecule undergoes considerable structural and energetical relaxation, losing at least 0.5-0.7 eV. If the charge transfer reaction (2) were a single-step process, it would require the activation energy of 1-2 eV [10].

What makes this resonant charge transfer possible? It was suggested that in the gas phase, reaction (2) proceeds through the formation of a collision complex in which the charge is shared by both of the cycloalkane molecules [58]. This sharing considerably reduces the barriers for the structural relaxation. According to MNDO calculations, the C<sub>2</sub>-symmetric cyclohexane<sub>2</sub><sup>•+</sup> dimer in which the charge is shared equally between the cyclohexane monomers, is only 150 meV higher in energy than the state in which the charge is localized on a single monomer [10]. Continuing this line of reasoning, it may be assumed that in liquid cycloalkanes the charge is shared between several solvent molecules and this sharing further reduces the hopping barrier. In such a case, the solvent hole is a small polaron whose rapid migration is caused by phonon-assisted hopping [10].

The formation of the polaron causes delocalization of the hole. Unusually large reaction radii in electron-transfer reactions of the solvent holes were first considered as evidence for such a delocalization [8]. However, more recent measurements of the hole mobility suggest that these radii were overestimated [10,14]. The best evidence for the delocalization of the solvent hole was provided by studies on dc photoconductivity in cyclohexane-methylcyclohexane mixtures [10,11]. While the addition of less than 5-10 vol % of methylcyclohexane reduces both the dc conductivity signal and its decay rate, further addition of methylcyclohexane yields little change in the conductivity signal and kinetics. The initial reduction is accounted for by rapid reversible trapping of cyclohexane holes by methylcyclohexane ( $\Delta G^0 \approx -0.11$  eV [11]). Since the isolated radical cations of methylcyclohexane in cyclohexane have normal mobility, the excess conductivity signal is proportional to the equilibrium concentration of the cyclohexane holes. At higher concentration of methylcyclohexane, the equilibrium fraction of the cyclohexane holes becomes lower. When this fraction becomes less than the ratio  $\mu_h/\mu_i$  of the mobilities of

the high mobility ( $\mu_h$ ) and normally diffusing ( $\mu_i$ ) ions, the conductivity should decrease severalfold. This decrease was not observed. We conclude that the migration of methylcyclohexane $\bullet^+$  in 5 vol % methylcyclohexane solution is as rapid as that of the solvent holes in neat methylcyclohexane. When the methylcyclohexane is diluted by *n*-hexane instead of the cyclohexane, the conductivity signal decreases proportionally to the fraction of *n*-hexane. Thus, it was cyclohexane which made the difference.

This result suggests that the methylcyclohexane holes are coupled to the solvent, forming a polaron. This coupling makes the charge migration of methylcyclohexane holes in cyclohexane as efficient as in neat methylcyclohexane. From the critical concentration of methylcyclohexane, the delocalization radius was estimated as ca. 1 nm, or 4 to 5 molecular diameters [10].

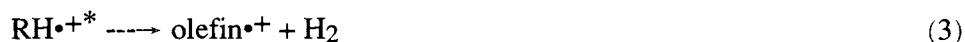
*2.4. The formation of high-mobility holes and "satellite ions".* As was briefly mentioned above, radiolysis of hydrocarbons results in the formation of several types of cationic species besides the solvent holes. Most of these "satellite ions" are generated within the first nanosecond after the radiolytic pulse.

Transient absorption spectra of some "satellite ions" closely resemble the spectra of olefin radical cations. In cyclohexane, a band centered at 270 nm (at 2 ns [22]) is observed from 250 ps [25] after the ionization event (this band overlaps with the strong 240 nm band of cyclohexyl radicals [22]). The scavenging behavior and the decay kinetics of the UV-absorbing species suggest that they are normally-diffusing radical cations [25]. In the first few nanoseconds after the ionization event, the VIS absorbance is dominated by solvent excited states [22,57]. When the thermalized electrons are rapidly scavenged using a suitable electron acceptor (halocarbons or N<sub>2</sub>O), this absorbance is much reduced and, in addition to cyclohexene $\bullet^+$ , one observes the absorption bands of cyclohexane holes (the latter may be rapidly scavenged using alcohols) and some other cations that absorb in the red [25]. The latter signals are clearly distinguishable as early as 1-5 ns after the radiolytic pulse (at earlier delay times, these signals are swamped by absorption of the excited states). The VIS spectra of the red-absorbing cations resemble those from cyclohexene dimer radical cations or cyclohexadiene radical cations. Thus,

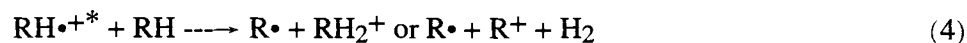
shortly after ionization of cyclohexane with fast electrons, at least three types of cation species were observed spectroscopically.

In some cases, the identity of paramagnetic "satellite ions" was established by ODMR [42,44,48]. For example, 9,10-octalin $\bullet^+$  was identified in decalins and their solutions [42]. ODMR spectra of "satellite ions" in cyclohexane were related to EPR spectra of matrix-isolated cyclohexene $\bullet^+$  (Note that in the liquid cyclohexane, cyclohexene $\bullet^+$  undergoes a fast ring-puckering motion that averages hyperfine coupling constants for equatorial and axial protons, so the the EPR spectra of cyclohexene $\bullet^+$  in liquid and solid matrices are different) [42,44,48]. In both of these cases, the olefin radical cations were formed in spurs rather than in a reaction of the solvent hole with the olefin in the solvent bulk [42] (octalins gradually accumulate as radiolytic products). Olefin "satellite ions" were also observed in squalane [24].

How do these "satellite ions" form in the early stages of radiolysis ? Two ideas were put forward [1,37,42]. First, the "satellite ions" could be generated by fragmentation of short-lived electronically- and/or vibronically-excited solvent holes formed upon the ionization of the solvent, for example



Reaction (3) is exothermic even for the ground-state alkane radical cations (0.4-0.6 eV) but requires overcoming a high potential barrier. Several authors (e.g., [22, 37]) have considered the possibility of deprotonation of the excited hole,



In cyclohexane and decalins, reaction (1) is endothermic by 0.1-0.4 eV [60] and it seems reasonable that the excitation of the hole may facilitate the proton transfer. Fragmentation of matrix-isolated hydrocarbon radical cations upon excitation with 2-4 eV photons was observed by EPR (see review [61]). For cycloalkanes, the main photoreaction is reaction (3). For radical cations of methyl-branched alkanes, the loss of CH<sub>4</sub> was also observed, while the radical cations of linear alkanes prefer to fragment to 2-butene $\bullet^+$  and the residual paraffin [60]. Thus, even the lower excited states of some radical cations are dissociative. One suggestion is that the recombination of electronically-excited

solvent holes with electrons yields strongly dissociative higher excited states of the solvent [53]. These states are likely to fragment before they relax to the lowest  $S_1$  state. In this way, it is possible to explain the low yield of the fluorescent  $S_1$  states in some hydrocarbons.

Second, the "satellite ions" could be generated in scavenging reactions of the solvent holes with radiolytic products in multiple-pair spurs [25,61-65]. The olefins are formed upon the fragmentation of excited solvent molecules generated in recombination of short-lived electron-hole pairs [1]



This mechanism would also account for rapid generation of carbonium ions in reactions of the solvent holes with radicals [65]



The results on low-temperature ODMR suggest that in some hydrocarbons, no "satellite" radical cations are formed via the dissociation of excited-state holes. No prompt generation of olefin radical cations was observed in solid paraffins, decalins, and methylcyclohexane at 4-50 K [39-41,45-47]. At these low temperatures, the holes have negligible mobility [39,45] which makes electron transfer reaction (7) slow and inefficient, as it may occur by long-range electron tunneling only. Since the excited-state holes should also be formed in the solid, these ODMR observations suggest that the "satellite" radical cations are generated mainly in ion-molecule spur reactions (at least, in some hydrocarbons).

The prompt formation of the "satellite ions" introduces ambiguity in the measurement of the hole mobility in pulse radiolysis. Indeed, the conductivity is a product of the mobility and the yield [8]. The latter quantity is poorly defined since the branching ratio  $f_h$  between the high-mobility solvent holes and the "satellite ions" is unknown.

The way around this problem is to generate solvent holes by means other than radiolysis. Since the formation of "satellite ions" is partly due to spur chemistry, in the laser multiphoton ionization of neat hydrocarbons [14-18]



(that yields isolated electron-hole pairs only) the yield of "satellite ions" would be much reduced. Another way of generating the solvent holes is by a valence-band electron transfer to the photoexcited aromatic radical cation ("hole injection") [10-13,26]



The photoexcitation of  $\text{A}\cdot^+$  may be carried out using the same UV pulse that is used to ionize the solute or using a delayed laser pulse of a different color. The latter method is preferable because by using a delay such that only free  $\text{A}\cdot^+$  exist the solvent hole can be generated without a geminate counterion. Therefore, the scavenging kinetics can be disentangled from the geminate recombination. Both of these approaches were used to study long-lived solvent holes in cycloalkanes.

Solvent holes in neat cycloalkanes were generated by multiphoton ionization ( $3 \times 4 \text{ eV}$  or  $2 \times 5 \text{ eV}$ ) of the solvent at fluxes in excess of  $0.01 \text{ J/cm}^2$  [15]. In a typical experiment, the laser-induced dc conductivity was measured as a function of the delay time with resolution better than 3 ns. A similar setup was used to observe the dc conductivity in pulse radiolysis with fast 16 MeV electrons [14]. The decay kinetics of solvent holes in cyclohexane and decalins were consistent with the value of  $f_h \approx 1$  for multiphoton laser ionization. For cyclohexane, a lower ratio of  $f_h \approx 0.5$  was needed to account for the kinetics observed in pulse radiolysis. (Note that these ratios refer to the situation at ca. 10 ns after the ionization event; the conductivity signal of the holes cannot be measured at earlier time). To be consistent with the observations, the simulations required a higher value for the mobility  $\mu_h$  of the cyclohexane holes ( $1.7 \times 10^{-2} \text{ cm}^2/\text{Vs}$  [12,14]) than previously estimated [7,8]. High yield of the "satellite ions" is not a universal property: In radiolysis of

decalins, the ratio  $f_h > 0.8-0.9$ . Apparently, the yield of the "satellite ions" varies appreciably with the hydrocarbon structure.

Knowing the absolute values of  $f_h$  is important since using the previous estimates for  $\mu_h$  led to unrealistically large reaction radii for reactions of cyclohexane and methylcyclohexane holes with low-IP solutes (2-3 nm!) [8, 14]. These radii suggested extreme delocalization of the solvent hole. Using the correct mobilities reduces these radii to ca. 1 nm which is close to a typical electron-transfer radius in a non-viscous hydrocarbon.

When reaction (11) is induced by the VIS photons (at 2.3 eV), the initial excess energy of the solvent hole is 0.7-1.2 eV (for low-IP solvents such as decalins) and the question may be raised about the occurrence of reaction (4). The pump-probe conductivity experiment outlined in reference [26] shows that after the *trans*-decalin hole produced from triphenylene $\bullet^+$ \* disappears by reacting with the triphenylene in solution, the ground-state triphenylene $\bullet^+$  is completely recovered. The kinetics of the recovery mirrors the decay kinetics of the solvent hole. These observations indicate that no "satellite ions" are formed in reaction (11). Direct photoexcitation of *trans*-decalin holes at 2.3 eV also did not result in the reduction of the conductivity signals from these holes. No cations other than  $A\bullet^+$  and high mobility solvent holes were found upon the 5 eV photoexcitation of triphenylene in *trans*-decalin, despite the high excess energy in the holes (ca. 3.8 eV) following the UV-photoinduced "hole injection". Apparently, the excited solvent hole in the *trans*-decalin is very stable; even the anticipated deprotonation does not occur. This explains the low yield of "satellite ions" in radiolysis of *cis*- and *trans*-decalins. It is presently unclear what factors control the stability of electronically-excited holes in hydrocarbon solvents.

Quantum yields  $\phi_h$  for single-photon "hole injection" for aromatic solutes in *trans*-decalin correlate well with the gas-phase IP of the aromatic solute. For triphenylene $\bullet^+$ ,  $\phi_h \approx 0.016$  was obtained for excitation with 5 eV photons (ca. 3 times the value for 2.3 eV excitation) [26].

*2.5. Ion-molecule reactions of high-mobility solvent holes.* There are several classes of such reactions:

- (i) fast irreversible electron-transfer reactions with solutes that have low adiabatic IPs (ionization potentials) and vertical IPs (such as polycyclic aromatic molecules);
- (ii) slow reversible electron-transfer reactions with solutes that have low adiabatic and high vertical IPs (such as dimethylcyclopentanes);
- (iii) fast proton-transfer reactions;
- (iv) slow proton-transfer reactions that occur through the formation of metastable complexes [9,26];
- (v) very slow reactions with high-IP, low-PA (proton affinity) solutes.

Rate constants for cyclohexane holes may be found in references [7,8,11,13,14,17], for decalin holes - in references [8,9,12,14,26], for methylcyclohexane holes - in references [12,122], for squalane holes - in references [24,30]. The data on the temperature dependence of rate constants of scavenging for the four cycloalkane holes are in reference [10]. For these holes, most of the rate constants were measured by determining the decay kinetics of the transient conductivity signals as a function of the solute concentration. The preferable way of studying the scavenging reactions is by detection of the excess dc conductivity following the "hole injection" reactions (10) and (11) [10-13,26]. In cyclohexane, the determination of the rate constants is complicated by the fact that the solvent hole is in equilibrium with an impurity in the solvent [11].

*Class (i) reactions* were observed in all four cycloalkanes that exhibit long-lived high-mobility holes [4-8,10,13,14,17]. These reactions were also observed in squalane [24, 31] and cyclooctane [26]. The reaction rates linearly scale with the hole mobility as a function of temperature (with exception of *trans*-decalin) and the fraction of cycloalkane in the solvent mixture [14]. The highest rate constants were observed for reactions of cyclohexane hole with low-IP aromatic solutes,  $(3-4.5) \times 10^{11} \text{ M}^{-1} \text{ s}^{-1}$  at 25°C [13,14]. In these irreversible reactions, a solute radical cation is generated.

*Class (ii) reactions* were directly observed for the solvent holes in cyclohexane [11] and methylcyclohexane [122]. For some solutes (SH), the equilibrium

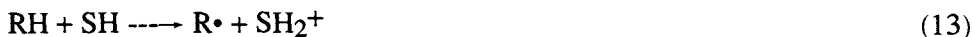




is set on the time scale of the conductivity experiment ( $> 10$  ns). In this case, the decay kinetics of the solvent holes are biexponential. Addition of 1,1-dimethylcyclopentane, *trans*-1,2-dimethylcyclopentane, and 2,3-dimethylpentane to cyclohexane or *trans*-decalin, bicyclohexyl, and *iso*-propylcyclohexane to methylcyclohexane results in such bimodal scavenging kinetics. The former two cyclopentane derivatives are present as impurity in commercial cyclohexane (10-100 ppm). For addition of methylcyclohexane to cyclohexane, the equilibrium (12) is reached so rapidly that the decay kinetics are exponential. Similar rapidly-set equilibria exist for high-mobility holes in mixtures of *cis*- and *trans*-decalins [14,38] and the decalin holes and benzene [26].

The rate constants,  $k_{12}$ , of the forward reaction (12) are an order of magnitude lower than those of the class (i) reactions, though some of the hole-trapping solutes have comparably low adiabatic IPs. The values of  $k_{12}$  did not correlate with the observed  $\Delta G^0$  of reaction (12). An explanation was proposed that the rate constants are controlled by the height of the activation barrier determined by the difference in the vertical IP of the solute and the adiabatic IP of the solvent [11]. This suggests that electron transfer to the rapidly-migrating solvent hole (as it passes by the scavenger molecule) is much faster than the relaxation time of the solute radical cations.

*Class (iii) reactions* include proton-transfer reactions of solvent holes in cyclohexane, methylcyclohexane, and squalane [4-8,10,13,14,17,26]:

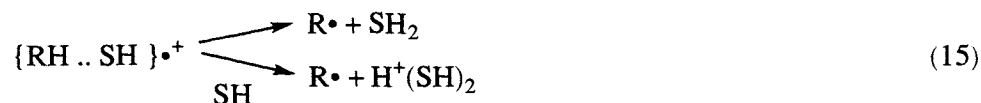


The corresponding rate constants are 10-30% of the fastest class (i) reactions and exhibit short reaction radii of 0.15-0.4 nm. Unlike the electron-transfer reactions (that may occur through space), the proton transfer requires close proximity of the donor and acceptor. Thus, short reaction radii of class (iii) reactions suggest a low degree of the solvent hole delocalization.

*Class (iv) reactions* include proton-transfer reactions in *trans*-decalin and decalin mixtures [9,12,14,26]. In neat *trans*-decalin, the reaction rates for high-IP solutes correlate poorly with the solute IP and PA [9, 12]. In binary

mixtures of *cis*- and *trans*-decalin, the mobility of the solvent hole linearly scales with the fraction of *trans*-decalin (for which  $\mu_h$  is 4.5 times higher than in *cis*-decalin) [14]. While for most of the solutes the rate constants also scale linearly with the hole mobility, for aliphatic alcohols the rate constant systematically decreases with the fraction of *trans*-decalin approaching the value of  $(5-6) \times 10^9 \text{ M}^{-1} \text{ s}^{-1}$  in neat *trans*-decalin [12,14]. This constant is only 10% of the rate constant for alcohols in *cis*-decalin.

Recently, it was demonstrated that the scavenging of *trans*-decalin holes by some alcohols proceeds through the formation of a metastable complex [26]



with a natural lifetime between 24 ns (2-propanol) to 90 ns (*tert*-butanol) at 25°C. In neat decalins, the rate of the complexation is ca. 1/2 of the highest electron-transfer rates (the reaction radius is 0.5-0.7 nm); the overall decay rate is limited by slow proton-transfer reactions (15). The rate constant of unimolecular decay of the complex is  $(5-10) \times 10^6 \text{ s}^{-1}$ . Though for other class (iii) reactions the bimodality was not observed [9,26], the basic mechanism must be the same. Only for secondary and ternary alcohols is the equilibrium (14) reached so slowly that it can be observed at 25°C on the time scale of the conductivity experiment ( $> 10 \text{ ns}$ ). For primary alcohols, the scavenging kinetics are pseudo-first order. However, for  $\text{C}_3\text{-C}_6$  alcohols the rate constants do not scale linearly with the solute concentration, betraying the fast equilibria (14). For these alcohols, PA is relatively low and the decay of the complex is mainly bimolecular. Termolecular reactions analogous to reaction (15) were observed in the gas phase, e.g., for  $c\text{-C}_6\text{H}_{12}^{\bullet+}$  and water [60].

A detailed analysis of the thermodynamics and energetics of reactions (14) and (15) is given in references [26]. Forward reaction (14) has near-zero activation energy; reaction (15) is thermally-activated (20-25 kJ/mol). The stability of the complex increases with the carbon number of the alcohol; the standard heat of the complexation decreases in the opposite direction ( $\Delta H_{298}^0$  changes from -39 kJ/mol for ethanol to -25 kJ/mol for *tert*-butanol).

Complexes of *cis*-decalin $\bullet^+$  are much more stable than complexes of *trans*-decalin $\bullet^+$  since for the former, the standard reaction entropy  $\Delta S_{298}^0$  is 35 J mol $^{-1}$  K $^{-1}$  more positive. The decrease in the entropy is small for both decalins ( $\Delta S_{298}^0 > -80$  J mol $^{-1}$  K $^{-1}$ ), approaching zero for higher alcohols [26]. Similarly small changes in the standard entropy were observed for class (ii) reactions of methylcyclohexane $\bullet^+$  [122]. Since the molecular complex formation could only reduce the degrees of freedom, to account for the small change in the entropy there must be an increase in the solvent disorder. This would be consistent with a hole being a small polaron that orders solvent molecules around it. When the positive charge is compensated, the solvent becomes disordered, and the reaction entropy increases.

Complex mechanism of class (ii) and (iii) reactions may account for the puzzling result in the studies on radiation-induced fluorescence in *cis*- and *trans*-decalins containing 3-100 mM of benzene [54], where it was concluded that on the time scale of geminate recombination of primary pairs in *trans*-decalin ( $< 1$  ns), the hole is scavenged by benzene with rate constant of  $7.7 \times 10^{10}$  M $^{-1}$  s $^{-1}$  (vs.  $(5-5.5) \times 10^9$  M $^{-1}$  s $^{-1}$  observed in the transient conductivity experiments [7,8,12,14]). This was taken as evidence for the involvement of short-lived, reactive excited solvent holes.

It is more likely that the higher rate constant corresponded to the rate constant of forward charge transfer reaction (12) or complexation reaction (14). The gas-phase IP for benzene and *trans*-decalin are very close. In *trans*-decalin solution,  $\Delta IP \approx 0.25$  eV, and benzene $\bullet^+$  readily transfers positive charge back to the solvent ( $\Delta H^0 \approx -0.27$  eV [26]). This was demonstrated through efficient generation of *trans*-decalin holes by biphotonic ionization of benzene [14] and careful analysis of scavenging kinetics [26]. The decay of the solvent hole is due to slow proton transfer reaction (13) and dimerization of benzene $\bullet^+$  with rate constant of  $5.7 \times 10^9$  M $^{-1}$  s $^{-1}$ . Since benzene $_2\bullet^+$  has 0.65 eV lower energy than benzene $\bullet^+$ , backward charge transfer from the dimer cation is inhibited, and the dimerization shifts the equilibrium (12) to the right side [26]. The forward charge transfer (or complexation) proceeds with rate constant of  $(1.1 \pm 0.1) \times 10^{11}$  M $^{-1}$  s $^{-1}$ , while  $k_{12} \approx 1.3 \times 10^8$  s $^{-1}$  (at 25°C) [26]. Therefore, while in the fluorescence studies the solvent holes were observed before the equilibrium (12) was reached (ca. 7 ns in 3 mM solution), in the conductivity studies the solvent holes were observed well after this equilibrium

was reached. Characteristically, for the low-IP solute toluene (a class (i) solute), the rate constants measured on short [54] and long time scales [9,12,14] are identical.

Although *class (iv) reactions* were observed for several high-IP, low-PA solutes [8,14,17,19,20], the kinetic data were easy to misinterpret due to traces of low-IP impurity in the inert solute (in particular, for C<sub>10</sub>-C<sub>16</sub> paraffins [20]). The only reliable data were obtained for scavenging the solvent hole in cyclohexane by cyclopropane [8,17] and for scavenging the solvent holes of cyclohexane and decalins by oxygen [14,19]. For the latter reactions, the reaction constants are  $(1-3) \times 10^8 \text{ M}^{-1} \text{ s}^{-1}$  [14], more than two orders of magnitude lower than those for class (i) reactions. Our thermochemical analysis suggests that this reaction is initiated by the H atom transfer to O<sub>2</sub> [14]. A possible mechanism for scavenging reaction with cyclopropane is the H<sub>2</sub>-transfer [8].

In concluding this section, we observe that though the nature and the migration mechanism for the high-mobility holes are not yet fully understood, a consistent picture of their chemical, dynamic, and magnetic properties begins to emerge.

### 3. SINGLE-PAIR AND MULTIPLE-PAIR SPURS

*3.1. Single-pair spurs.* Single-photon VUV or multiphoton UV ionization of neat liquid hydrocarbons results in the formation of *isolated* geminate ion pairs, reaction (9). The reaction dynamics in such pairs is less involved than the dynamics in multiple-pair spurs formed in radiolysis. The availability of synchrotron radiation in the 10-40 eV region and short-pulse UV lasers led to a rapid increase in the number of studies on "single-pair spurs". In particular, ultrafast pulse-probe laser spectroscopy was used to study ionization, geminate recombination, and generation of the solvent excited states in neat hydrocarbons [66-69]. This field is still in its infancy: Only in 1997 has the first reliable data on the geminate kinetics of electron-hole pairs been obtained [69]. Eventually, these studies will complement the studies using pulse radiolysis and VUV photoexcitation.

In these ultrafast UV laser studies, the pump energies varied between 4 eV and 5 eV, while the probe pulse energies varied between 0.55 eV and 3.1 eV. Upon biphotonic 5 eV or triphotonic 4 eV excitation, hydrocarbons (such as paraffins, isooctane, cyclopentane, cyclohexane, and *trans*-decalin) yield both the solvent excited  $S_1$  states and the electron-hole pairs [66]. Questions were raised as to the significance of the ionization channel, since more than 75% of the transient absorbance in the VIS range was from the solvent  $S_1$  states [67,68]. It is presently realized that there is a strong spectral overlap between the absorbance signals from these excited states and the primary charge carriers. The  $S_1$  state dominates the absorbance in the 1.8-3 eV region [67], while below 0.8 eV, the absorbance is from the electrons only [69]. A biphotonic 3.5-4 eV laser excitation yields the  $S_1$  states without the concurrent ionization [70]. Thus, both the  $S_1$  state dynamics and the geminate dynamics of single electron-hole pairs may be studied separately using the appropriate excitation and detection conditions. This option does not exist in pulse radiolysis studies.

The results of the ultrafast laser studies are very preliminary. The observed geminate kinetics suggest that the electron thermalization distance distribution in isolated electron-hole pairs can better be described as the exponential than the often assumed  $r^2$ -Gaussian [65]. This conclusion was supported in the studies on magnetic field dependence of hexafluorobenzene fluorescence in recombination of geminate  $C_6F_6^{\bullet-}$  - solvent hole pairs generated upon 10 eV photoionization of isooctane. One study found that even the exponential distribution law was too steep to account for the data and that a power law tail is more appropriate [71] (for radiolytic spurs, Gauss-power distributions had long been advocated [72]). The results on the solvent photoionization are in contrast with the data on multiphoton UV laser ionization of aromatic solutes in the same hydrocarbons that demonstrated good applicability of the  $r^2$ -exponential or  $r^2$ -Gaussian distributions for simulation of the geminate pair recombination and free ion yield (for example, [16]). On the other hand, no systematic studies on the pump energy dependence of the geminate kinetics in neat hydrocarbons have been carried out, while it is known from other ultrafast studies (in particular, on photoionization of liquid water [73]) that the thermalization distances strongly depend on the pump energy and the ionization mechanism.

Arguably, the greatest import of the forthcoming ultrafast studies would be assessing the role of short-lived pre-thermalized charges and highly excited states of hydrocarbons. The first step in this direction has been made: It was found that in *n*-hexane and isooctane the electron band in the near IR is shifted to lower energies in the first 2 ps after the ionization event [69]. This finding suggests that the thermalization of electrons in hydrocarbons is not as rapid as generally believed. Therefore, a considerable fraction of reactions in spurs involves pre-thermalized charge carriers.

A recent study [74] demonstrated the potential of femtosecond photoemission spectroscopy to study localization (thermalization) dynamics of electrons in hydrocarbons. The electrons were injected into *n*-heptane bilayer on Ag(111) surface (at 120 K) using a powerful 4 eV pump pulse. The electrons were then ejected to vacuum using a weaker 2 eV probe pulse. The extended and localized electron states were distinguished by the angular dependence of the kinetic energy spectrum. The lifetime of the localized electrons was ca. 1.6 ps (eventually these electrons recombine with the mirror charge). Initially, the electron is in an extended state with effective mass of 1.2  $m_e$ . The localization proceeds with rate constants between  $4 \times 10^{11} \text{ s}^{-1}$  and  $3 \times 10^{12} \text{ s}^{-1}$  depending on the electron wave vector (band energy) that determines the exothermicity of localization (which varied between 10 meV and 150 meV). Both the thermalization dynamics and energetics were studied simultaneously. Hopefully, more ultrafast photoemission studies will follow. It would be particularly interesting to carry out such observations on small-diameter jets in order to study chemical processes in the bulk of the solvent. Studies on photoelectric spectroscopy of liquid jets (water, alcohols, *n*-nonane) were recently reported [75].

*3.2. Triplet state vs. singlet state formation: spin effects.* It is commonly believed that the initial spin state of the multiple-pair spur is singlet. Shortly after the ionization event, positively and negatively charged ions recombine yielding singlet or triplet products. In the contact exchange approximation, the multiplicity of the product depends on the spin phasing at the instance of recombination [32, 76]. (Calculations with more realistic spin exchange potentials support this approximation [77]) Recombination of the initially singlet-correlated ("geminate") ion pairs yields singlet products, including the fluorescent excited states. Random cross-recombination of ions in multiple-ion

pair reduces the singlet yield and increases the triplet yield: statistically, 75% of the random-pair encounters yield the triplet excited states [76,78]. In squalane, the probability  $f_S$  of the singlet recombinations decreases from 80% at 16 eV photoexcitation to less than 40% at 120 eV photoexcitation [32]. For alkanes, the most probable energy loss is 22-24 eV [79] and the steep decrease in  $f_S$  with the photon energy follows the increasing formation of multiple-pair spurs.

Coherent spin evolution in the geminate ion pairs is the basis for several optical spectroscopies, including magnetic field effect [32,33,62-65,71,76,80], ODMR [24,39-48], magnetic level-crossing [21,28,50,59] and quantum beat spectroscopies [29-31,36,80,81]. Unpaired electrons in radical ions interact with static and microwave magnetic fields of the spectrometer (Zeeman interaction) and local magnetic fields generated by protons (hyperfine interactions). These weak magnetic interactions flip the electron spin and cause intersystem crossing in geminate pairs, eventually changing the singlet/triplet yields [76]. These spin-sorting interactions underline the magnetic and microwave field effects in radiolysis of hydrocarbons.

The importance of the magnetic and spin effects in radiolysis has been frequently discussed and we refer the reader to reviews by Brocklehurst [32,76]. There is one essential point which is seldom emphasized in the literature: Due to the very nature of quantum entanglement, the triplet and singlet channels exist *only in the context of the product formation*. In the absence of spin-sorting reactions or special initial conditions, *pairwise* spin correlations (i.e., "geminate" pairs) in many-particle spurs are forbidden by the laws of quantum mechanics. The only exceptions are single-pair spurs and spurs in which all but one pair have recombined. Given that the ion escape yield in most of hydrocarbons is < 5 %, the latter type includes most of the multiple-pair spurs that remain a few nanoseconds after the ionization event. Put together, these two types of spurs contain a large fraction of the long-lived "geminate" pairs formed in radiolysis and account for most of spin correlations observed in magnetic field and magnetic resonance experiments. As was noted by Brocklehurst [32], these long-lived pairs have a tendency to be singlet-correlated since most of the stable neutral products are singlet.

The origin of the spin effects in radiolysis has always been murky. The photoionization of the solvent could proceed directly or via short-lived highly excited solvent states. This autoionization may completely change the spur chemistry. A recent study examined the magnetic field effect on the solute fluorescence in squalane as a function of the VUV photon energy [32,62]. The magnetic field effect increased between 11 eV and 16 eV and reached the maximum corresponding to 80% singlet recombination. This probability is significantly lower than the value of 100% expected for single-pair spurs, while the photon energies do not allow one to account for the loss of spin coherence through cross-recombination. Analogous results were obtained for other systems (alcohols, benzene) [32]. Since ODMR and related studies indicate that for squalane holes the spin-lattice relaxation is longer than their decay [24,28,29], this loss of spin coherence cannot be accounted for by spin randomization of primary pairs due to magnetic interactions in the charges. It appears that the *initial state of the electron-hole pair is not purely singlet*. According to Brocklehurst [62], only direct ionization yields singlet-correlated electron-hole pairs while the autoionization results in the partial loss of spin coherence due to spin-orbital coupling in the highly excited states. This scenario is not entirely unrealistic given the possible excitonic nature of these states. However, it must be noted that the spin mixing postulated by Brocklehurst was not supported by VUV studies on solvent fluorescence [82].

Another fundamental problem is the wavefunction structure of the initial singlet state. Consider a spur consisting of two pairs,  $(e_1h_1)$  and  $(e_2h_2)$ . There are two orthogonal singlet states,  $|1\rangle = |e_1h_1\rangle_s |e_2h_2\rangle_s$  and  $|2\rangle = 1/\sqrt{3} \{ |e_1h_2\rangle_s |e_2h_1\rangle_s + |e_1e_2\rangle_s |h_1h_2\rangle_s \}$ , where  $|.. \rangle_s$  is the singlet state of the pair [77]. In the general case, the initial singlet state is a linear combination of  $|1\rangle$  and  $|2\rangle$ . It is easy to demonstrate that pairwise correlations are possible only if the initial singlet function is multiplicative (e.g., state  $|1\rangle$ ) [77]. In order to have these *pairwise* correlations *prior* to the spin-sorting recombination, the electron-hole pairs must be generated in spatially- and electronically-separated events [76,78]. While this assumption seems plausible in radiolysis of gases, in the condensed phase the excitation and charge delocalization could lead to significant mixing of the singlet wavefunctions. Another concern is that ionization events induced by low-energy secondary electrons entangle these electrons with the electron-hole pairs. Such entanglements create complex spin correlation patterns in the spur.



If the initial multiplicity of the spur is singlet, the probability  $f_S$  to form the singlet product is given by the formula [78]

$$f_S \approx \Theta + 1/4 (1-\Theta), \quad (16)$$

where  $\Theta$  is the probability of recombination of "spin-correlated geminate pairs". This expression has been used to calculate the  $f_S$  from the data on magnetic field effects [32] and quantum beats [31,80,81] in delayed solute luminescence (spin-coherence spectroscopies). Given that the premises of these methods are identical, it is understandable that the probabilities  $f_S$  determined for fast electron spurs using these spectroscopies are comparable.

A serious complication in the measurements of  $\Theta$  is the occurrence of spin relaxation in the charge carriers [33,50]. While the electrons have relatively long spin-lattice relaxation times, the solvent holes may relax on nanosecond or even subnanosecond time scales (see section 2.2). For ion pairs involving such species, the spin coherence is lost on the time scale of the singlet product formation. This problem is exacerbated when the geminate recombination is slowed down after scavenging of the primary ions by the scintillator. Even relatively slow spin relaxation induced by electron dipole-dipole coupling and anisotropic magnetic interactions in the radical cations is capable of destroying the initial spin correlation on the submicrosecond time scale [33]. This effect must be taken into account in the studies on long-lived ion pairs in viscous solvents and solids.

The common problem in studies on the efficiency of triplet and singlet recombinations is that only a fraction of the singlet/triplet products are detected. Alkane solvent holes rapidly fragment or transfer a proton which causes the loss of the solvent/solute luminescence. The recombination of pre-thermalized holes could yield other products than the lowest excited states [37,53]. In dense spurs, excited states can be quenched by radicals and radical ions. Computations show that these quenching reactions can be a significant mechanism of disappearance of the singlet excited states [65], and experimental evidence has been obtained supporting the reduced production of *solute*  $S_1$  states in spurs of 20-100 eV photons due to the quenching [32,62,65]. Shortening of the *solvent*  $S_1$  state lifetime with increasing excitation photon energy was observed in radiolysis of *cis*-decalin and *n*-dodecane with 4-to-14

keV x-rays [83]. This shortening was accounted for by quenching of the alkane  $S_1$  states by alkyl radicals generated in the same spurs.

Even more important are reactions of radiolytic products with the *precursors* of these excited states. Results from recent experiments in which the solute luminescence and magnetic field effect were compared for radiolysis of cyclohexane or isooctane with 0.5-2.2 MeV electrons, 1-5 MeV protons, and 2-20 MeV  $\alpha$ -particles suggested that the decrease in the solute luminescence and the magnetic field effect was due to both the increasing importance of cross-recombination and the "intervention of radicals or other transient species with the precursors" with the fluorescent states [63]. The effects of spin relaxation and ion-radical reactions in dense spurs were identified as likely causes for reduced magnetic field effects, fluorescence yields, and probabilities  $\Theta$  in spurs from 17-40 keV x-rays as compared to the spurs from fast electrons [80].

In short, to model the *experimentally-determined* singlet-to-triplet ratio, the initial state multiplicity, spur chemistry, and spin relaxation must be given same attention as the interplay between the cross- and geminate recombination.

*3.3. Modeling of light -particle spurs.* Many simulations of the spur kinetics in hydrocarbons have been reported over the last decade [84-89] (see reference [84] for a review). As may be anticipated, none of these simulations attained the level of complexity needed to obtain a self-consistent picture of the early radiolytic events in hydrocarbons. The threefold problem is the uncertainty about the initial spur structure, intractability of the inhomogeneous kinetics and poor understanding of spur chemistry. Due to the limited state of knowledge, the present-day simulations should be viewed as exploratory. While some researchers focus on the general aspects of spur dynamics using stochastic Monte Carlo simulations [84-88], others focus on the chemical kinetic aspects assuming simple (inhomogeneous) dynamics [23,24,89]. There are also models intended to integrate the chemical kinetics and the charge recombination dynamics [25,65]. At the present time, such models are ahead of their time, since only a few of the postulated 25-120 spur reactions have been studied experimentally.

Not having enough space to summarize all of the recent work, we will give a couple of examples. A welcome new development is the integration of energy-loss calculations [79,87] with the stochastic Monte Carlo simulations of

charge recombination in order to obtain free ion yields as a function of the primary electron energy [87]. In these calculations, the charge carriers are treated as point charges of given mobility that migrate in their mutual Coulombic field. These simplifications are justifiable since the calculations of the track structure (which yield the initial positions of the point charges) are even more simplistic. The estimated free ion yields and their energy dependence [84,85,87] correspond well to those determined experimentally for spurs from soft x-rays [90]. The import of these calculations is that the distance distribution for thermalized electron-hole pairs is independent of the primary electron energy in the keV range, while ca. 50% wider distributions are needed to account for the free ion yields for MeV electrons [87]. This unexpected result needs further verification. There is also a report on the calculations of the distance distribution in the modified model of Mozumder and Magee [88]. It was found that in single-pair spurs the distribution was much more diffuse than in the multiple-pair spurs. The significance of this result for the free ion yield calculations has not been addressed.

A detailed chemical model of hydrocarbon radiolysis was advanced in order to account for the radiolytic yields of H atoms and H<sub>2</sub> as a function of iodine concentration (the latter was used as a radical scavenger) [89]. To simplify the kinetic scheme, it was assumed that the electron-hole pairs recombine yielding only the lowest singlet and triplet states of the solvent. Although this assumption is thoroughly unrealistic (and large corrections were made to recover the balance of radiolytic hydrogen), it allows simplification of the reaction scheme to just 10 reactions, using the deterministic diffusion-kinetic approach. Time-resolved yields of H atoms, H<sub>2</sub>, radicals, olefins, and other products were estimated. From the simulation of the experimental data it appears that while the solvent S<sub>1</sub> states decay mainly via reaction (6) (the intersystem crossing was estimated to be only 10-15% efficient), the T<sub>1</sub> states decay via reactions



with relative yields between 1:1 and 3:1, depending on the cycloalkane structure.

While being useful exercises, both of these simulations were based on simplified kinetic schemes and physical models of spur dynamics. For some problems (free ion yields) these considerations may be of little importance, for other (product yields) the oversimplification leads to ambiguous results. In particular, this applies to calculations of the "singlet yields" (implicitly identified with the yields of the lowest  $S_1$  states) where the estimates entirely depend on the kinetic scheme [85,86]. Most of such calculations address only one facet of the problem: the relative significance of "geminate" recombination and cross-recombination in multiple-pair spurs. In the recent Monte-Carlo simulations [85], the initial spatial distribution of ionization events was calculated using the same approach that was used in the calculations of the free ion yield (see above). The total yield of singlet recombination for the primary pairs was estimated.

Superficially, these estimates correlate well with the energy dependence of the singlet ratio  $f_S$  determined from the magnetic field effects on the solute luminescence yield [32,64]. However, some of the latter results were obtained using low-energy photons ( $< 120$  eV) for which the stochastic Monte-Carlo calculations completely failed to reproduce the photon energy dependence of the free ion yield [64]. Radiolytic yields of the solvent  $S_1$  states and free ions upon excitation of decalins and *n*-dodecane using 4 keV to 15 keV photons have been measured [83,90]. Even in this energy regime (where the Monte-Carlo calculations gave good estimates of the free ion yield), agreement between the calculated and measured yields was observed for one solvent only, *cis*-decalin. In the same studies, significant variation of the  $S_1$  state lifetimes with the x-ray energy was observed which was a signature of quenching reactions in multiple-pair spurs [83]. Thus, the Monte-Carlo model was inadequate and the good correlation obtained between the experimental and simulated results was coincidental. Only when an understanding of the dynamics of short-lived excited states and pre-thermalized charges is reached, will development of an adequate model of the spur chemistry be possible.

#### **4. GENERATION OF SOLVENT AND SOLUTE EXCITED STATES.**

*4.1. The lower excited states.* Though excited solvent states have been discussed throughout this chapter, it is worth repeating a few points. Only the lower

excited states have been considered, the fluorescing singlet  $S_1$  state [91] and the putative, dissociative, triplet  $T_1$  state [92]. These excited states are produced mainly via charge recombination; the singlet states may also be produced by direct excitation of the solvent by secondary electrons and Cerenkov light [93]. The  $S_1$  state lives between 0.5 ns and 2 ns; this lifetime is longer (3-5 ns) for long-chain paraffins [92,94]. In multiple-pair spurs, the  $S_1$  state lifetimes are shortened due to quenching of the excited state by radiolytic products [83]. Eventually, the  $S_1$  state either fragments via reaction (6) or crosses to another excited state, possibly  $T_1$  [92] or  $S_2$  [95]; the radiative decay is very inefficient (< 1%). For homologous hydrocarbons, the quantum yield of fluorescence depends linearly on the excited state lifetime. For  $C_7$ - $C_{17}$  paraffins, the radiative rate constant is ca.  $1.3 \times 10^6 \text{ s}^{-1}$ , for alkylcyclohexanes -  $7 \times 10^6 \text{ s}^{-1}$  [94]. The fragmentation is temperature-dependent (with activation energy of 0.145-0.21 eV), while the crossing is temperature-independent [92, 95, 96]. The yield of the  $S_1 \rightarrow T_1$  (or  $S_1 \rightarrow S_2$ ) crossing for cyclo- and *n*-alkanes varies between 10% and 40%; for some branched alkanes (such as isopropylcyclohexane and 2,3-dimethylbutane) this yield approaches 50-60% [92].

Cyclohexane fluoresces in liquid, solid and vapor, with lifetimes 0.8 ns (298 K), 1.85 ns (at 225 K), and 2.07 ns (298 K), respectively (7.3 eV excitation) [95]. For liquid cyclohexane at 298 K, the rate constant of crossing is  $3.6 \times 10^8 \text{ s}^{-1}$ , the activation energy and pre-exponential factor for the fragmentation are 0.135 eV and  $1.6 \times 10^{11} \text{ s}^{-1}$ , respectively, and the quantum yield of fluorescence is ca. 0.01 at 7 eV photoexcitation [92]. For cyclohexane (and most of other saturated hydrocarbons), this quantum yield rapidly decreases with the excitation energy (to  $3.5 \times 10^{-3}$  at 8.4 eV, the onset of photoionization) [60,82,92,94]. All of the hydrocarbon  $S_1$  states have energies around 7 eV above the ground state (bottom-to-bottom) [92] and radiate between 5 eV and 6.5 eV [91]. The excited singlet states mainly dissociate to olefin/carbene +  $H_2$  or alkyl radical + H atom. For cyclohexane (*n*-hexane), the relative yields of these two fragmentation channels change from 4:1 (3:1) upon 7.6 eV photoexcitation to 2:3 (1:1) upon 11.6 eV photoexcitation [97].

The nature of the long-lived  $S_1$  states has been the subject of much speculation. Some authors view these states as liquid-phase analogs of Rydberg states in the gas phase. Others identify these states with self-trapped excitons, drawing from solid-state physics. Both of these descriptions offer no insight in

what defines the experimental properties of these states, such as their reactions, energetics, and absorption spectra. Apparently, only first-principle calculations and further spectroscopic studies (in particular, in the IR) will be useful.

The lowest triplet states lay ca. 1 eV below the  $S_1$  states [92]. These states are presumed to be extremely short lived (0.1-1 ps). The putative triplets are believed to decay via reactions (17) and (18). In paraffins and branched alkanes, the C-C bond dissociation is thought to be as efficient as the C-H bond dissociation; in alkylcyclohexanes, biradical formation was suggested [92]. Another study suggested the involvement of the  $S_2$  state that dissociates yielding the same products as reaction (17) [95].

While this much is presumed or accepted, the role of these (and other) excited states in the radiolysis remains poorly understood. The results obtained over the last decade only add to the existing uncertainties.

*4.2. Non-fluorescing excited states of alkanes.* Several relatively long-lived non-fluorescing ("dark") excited states of hydrocarbons capable of sensitizing singlet solute luminescence have been proposed in recent years.

The strongest evidence of such states is from the work of Lipsky and co-workers [98-100] who have shown that the sensitization of solute fluorescence by transfer of energy from the photoexcited solvent (cyclohexane, *n*-hexadecane, 2,3-dimethylbutane, and *cis*- and *trans*-decalins) can be explained by the participation of *two* solvent excited states: the fluorescent  $S_1$  state and a "dark" state. In *cis*-decalin containing 0.01 M of 2,5-diphenyloxazole (PPO), ca 10% of the solute luminescence is sensitized from this second singlet state. In a 20  $\mu$ M solution, ca. 70% of the solute excitations are mediated by the "dark" state, with 0.25% of such energy transfers per each 7.7 eV photon absorbed or 0.06 per "dark" state produced. In 0.01 M solutions, the "dark" state transfers energy with 97% efficiency. In experiments where a biphotonic 3.7 eV or 4 eV laser excitation was used instead of 7.6 eV light, the same "dark" states were observed [99]. These states have a quantum yield of only a few percent of the fluorescent states and do not yield the  $S_1$  states on deactivation. From the laser experiments, the conclusion was made that the "dark" states live much longer than the  $S_1$  states, though their lifetimes must be less than 10 ns. Neither this lifetime nor the efficiency of the energy transfer from the "dark" state varied with the solvent viscosity when *cis*-decalin was diluted with higher-IP alkanes

(2,3-dimethylbutane and isooctane). Lipsky and co-workers suggested that the "dark" states are exciplexes that migrate with a diffusion constant of  $4 \times 10^{-4}$  cm<sup>2</sup>/s [98]. Because the "dark" states have relatively low yield, their contribution to the solute fluorescence is most noticeable at low solute concentration.

A "dark" state capable of rapid energy transfer to aromatic solutes has been proposed in irradiated cyclohexane on the basis of experiments in which the formation of the S<sub>1</sub> state of *cis*-decalin (added as a scintillator) was measured and compared with the amount of this S<sub>1</sub> state expected from ion recombination and energy transfer from the S<sub>1</sub> state of cyclohexane [101]. A significant yield (0.8 per 100 eV) of the *cis*-decalin S<sub>1</sub> state was attributed to energy transfer from the "dark" state of cyclohexane. If one considers concentrated solutions, this "dark" state seems to be more important in the radiolysis than the "dark" state identified by Lipsky and co-workers. "Dark" exciton states were also postulated to account for the high yield of luminescence from 2,5-bis-(*tert*-butylbenzoxazolyl-2)-thiophene in picosecond pulse radiolysis of decalins and cyclohexane [102]. The radiolytic yield of this "dark" excitonic state was estimated at 1 per 100 eV and the rate of the energy transfer from these states was estimated as  $(1-3) \times 10^{11}$  M<sup>-1</sup> s<sup>-1</sup>. We are inclined to think that the observations of "dark" states in radiolysis are artifacts of data analysis. It remains to be seen whether these "dark" states are real.

*4.3. Low yields of the solvent S<sub>1</sub> states.* Radiolytic yields of the solvent S<sub>1</sub> states observed in the fast electron radiolysis of some alkanes (e.g., C<sub>3</sub>-C<sub>8</sub> paraffins) and cycloalkanes (e.g., C<sub>5</sub>-C<sub>7</sub> cycloalkanes and methylcyclohexane) are unexpectedly low (see tables IX.3-11 in reference [102] for available data). For example, in radiolysis of cyclohexane, the yield of the S<sub>1</sub> states is only  $1.45 \pm 0.15$  per 100 eV [104] (other estimates are  $1.5 \pm 0.4$  [105], 1.4-1.7 [100], and 1.75 per 100 eV [89]) while the T<sub>1</sub> states are generated at 3.4 per 100 eV [89], as estimated from the solvent luminescence yield and the product analysis, respectively. If these S<sub>1</sub> states were mainly produced in recombination of electron-hole pairs (as follows from studies of the effect of electron scavengers on the yield of solvent luminescence), the radiolytic yields would seemingly be equal to the G-value of ionization times the singlet recombination probability,  $f_S$ . For  $f_S \approx 0.5$  (see below), one obtains the ionization yield of 3 pairs per 100 eV, whereas the experimental estimates are between 4.5 and 5 pairs per 100 eV

[1]. Therefore, it appears that only 50-65% of the ionizations produce the electron-hole pairs that involve solvent radical cations.

One way to explain this deficit of solvent  $S_1$  states is to postulate the prompt formation of "satellite ions" whose recombination does not yield the solvent  $S_1$  states or any other fluorescent states [37,53]. As discussed in section 2.4, there are many results suggesting significant yield of "satellite ions" in ionization of hydrocarbons. For cyclohexane, the dc conductivity data suggest that ca. 50% of the cations observed 10 ns after the ionization event are not solvent holes. Promptly-generated cyclohexene $\bullet^+$  ions were observed by ODMR and transient absorbance spectroscopies. In the latter experiments, the "satellite ions" were observed as early as 250 ps after the ionization event. Very high yields of fragment cations in cyclohexane cannot be accounted for by scavenging reactions (7) and (8) in radiolytic spurs. For *cis*- and *trans*-decalins, where no conductivity or magnetic resonance data exists that indicate a high yield of the "satellite ions", the radiolytic yield of the  $S_1$  states is roughly twice that in cyclohexane (see below). Apparently, in some hydrocarbons there must be rapid fragmentation of pre-thermalized solvent holes. Cyclohexane is prone to such fragmentations: In gamma radiolysis of gaseous cyclohexane, the radiolytic yields of  $C_6H_{12}\bullet^+$ ,  $C_6H_{11}^+$  (-H), and  $C_6H_{10}\bullet^+$  (-H<sub>2</sub>) cations are 2.0, 0.62, and 0.35 species per 100 eV, respectively, out of the total ion pair yield of 4.4 per 100 eV [1]. In scavenging experiments with ammonia, the radiolytic yield of *c*- $C_6H_{11}^+$  cations in liquid cyclohexane was estimated as 0.7 ions per 100 eV [106].

Measurement of the effect of electron scavengers on the  $^1RH^*$  yield show that scavengers are more effective in reducing this yield than they are in scavenging electrons. A kinetic mechanism was proposed in which a fraction of the solvent holes are initially in an excited state that does not yield the solvent  $S_1$  state upon recombination [53]. The relaxation and fragmentation of the pre-thermalized solvent hole is expected to occur on the time scale of a few picoseconds.

*4.4. Estimates of excited state generation by final product analysis.* We have already mentioned the product analysis studies on the yield of the solvent excited states and the products of their decomposition [89]. Using iodine scavenging, the radiolytic yields of H<sub>2</sub>, olefins and radicals were determined



for C<sub>5</sub>-C<sub>8</sub> cycloalkanes as a function of LET [89,107]. To obtain the observed yield of H<sub>2</sub>, a high yield of promptly generated H<sub>2</sub> (0.75 molecules per 100 eV for cyclohexane) was postulated. As discussed above, this hydrogen is likely to be from reaction (6). Therefore, it is instructive to compare the data on cyclohexane with such data for decalins, which seem to yield more stable excited solvent holes. Decalins also yield relatively stable highly excited states, since quantum yields of fluorescence vary little with the photon excitation energy [82]. This suggests efficient relaxation to the lowest S<sub>1</sub> state.

A recent study has provided the needed information [108]. Product yields from the S<sub>1</sub> state of *cis*- and *trans*- decalins were determined in 7.6 eV photolysis. Only 40-50% of these states were found to fragment (which is an unusually low dissociation yield for a saturated hydrocarbon). The yields of the solvent S<sub>1</sub> states in 3 MeV β-radiolysis were determined and, combined with the photolysis results, were used to estimate the fraction of radiolytic products that originate from the S<sub>1</sub> states. The rest of the products were assigned to the T<sub>1</sub> states. Table 1 summarizes the results. As seen from this table, for *cis*- and *trans*-decalins the probabilities  $f_s$  of singlet recombination are close to 0.5. This probability is in fair agreement with the recently corrected estimate of  $f_s \approx 0.65$  obtained from the measurements of absolute fluorescence yields [109]. According to Table 1, the S<sub>1</sub> yields in decalins are roughly twice that in cyclohexane while the T<sub>1</sub> yields for all three of the cycloalkanes are comparable. We conclude that highly excited states of neutral and charged decalins, unlike those of cyclohexane and many other hydrocarbons, exhibit low yields of fragmentation.

TABLE 1.

Radiolytic yields of solvent excited states in decalins (3 MeV electrons) [108] and cyclohexane (<sup>60</sup>Co γ-radiolysis) [89] estimated from product analysis.

yield per 100eV	<i>cis</i> - decalin	<i>trans</i> - decalin	cyclo- hexane
S <sub>1</sub> state	3.4	2.8	1.75
T <sub>1</sub> state <sup>a</sup>	3.0	3.2	3.40
$f_s$ <sup>b</sup>	0.53	0.47	0.34

prompt H <sub>2</sub>	c	c	0.75
H <sub>2</sub> from S <sub>1</sub>	1.43	1.40	1.49
H <sub>2</sub> from T <sub>1</sub>	2.47	3.00	1.9 <sup>d</sup>

- a) before S<sub>1</sub>→T<sub>1</sub> conversion [89];  
 b) probability of singlet recombination for electron-hole pairs;  
 c) not included in the kinetic scheme;  
 d) reaction (18) only.

While product analysis is an important source of information on the early stages of radiolysis, this approach has a serious problem: For all of the alkanes studied, the yield of primary decomposition estimated from the total product yields significantly exceed the ionization yield: 6 to 6.5 per 100 eV vs. 4.5 to 5 per 100 eV [1]. This suggests that some of the products were counted twice: i.e., that fragmentation of the excited states is more extensive than was assumed. For example, instead of H<sub>2</sub> elimination, the excited state may eliminate two H atoms. Such decompositions were observed in gaseous methane (see discussion in reference [110]). In the fast-electron radiolysis of dilute solutions of methane in liquefied noble gases, the prompt yield of free H atoms is ca. 5 times higher than the prompt yield of methyl radicals. Using time-resolved EPR, these species were detected several tens of nanoseconds after their generation, and the yield of the methyl radicals was unaffected by cross-recombination (extremely long thermalization distances in the simple liquids make the kinetics homogeneous from the onset [110]). These results suggest that in a large fraction of recombination/excitation events involving methane and its cations, a methylene and two H atoms are generated. The implications of such fragmentations in radiolysis of neat hydrocarbons are obvious.

Alkyl radicals are one of the most chemically-important products of hydrocarbon radiolysis [1-3,60]. Their generation is very fast; e.g., for cyclohexyl radicals, the rise time of the formation is < 20 ps [22]. It is generally believed, that the radicals are generated in dissociation of the T<sub>1</sub> states or higher singlet states, in rapid reactions of "hot" H atoms and in "slow" reactions of thermalized H atoms generated in reaction (16) with hydrocarbons (the relaxed H atoms have lifetime of ca. 10 ns). Other pathways include deprotonation of solvent holes (reactions (1) and (4)) and neutralization of proton adducts and carbonium ions [37]. Radiolytic yields of radicals were

estimated from the product analysis: the yield of cross-linking products, halocarbons generated upon scavenging the radicals with TI and I<sub>2</sub>, and from the isotope sampling [1-3]. For long-chain paraffins, this analysis is complicated by uncertainties about the significance of hydrogen  $\beta$ -shifts and radical disproportionation [111]. Promptly generated radicals (< 100 ns) may be observed using time-resolved EPR; on this short timescale the secondary radical reactions are unimportant and one can directly measure the absolute and relative yields of neutral radicals [112,113]. Interestingly, these prompt yields change little upon addition of electron scavengers [113], which suggests that radicals might be generated on time scales faster than charge recombination (e.g., via reaction (4)).

For paraffins, the ratio of yields of penultimate and interior -H radicals is 20% higher than expected from the abundance of the corresponding C-H bonds (this was observed using both by the product analysis [111] and EPR [112]). Since the C-H bond dissociation energies for carbon-2 bonds are higher than those for interior carbon atoms, this preference cannot be explained through the abstraction by H atoms. One way to explain the observed preference is to assume the occurrence of reaction (4): it is known that in low-temperature solid paraffins reaction (1) yields mainly terminal and penultimate radicals [114]. In addition to the -H radicals, paraffins exhibit high yield of radicals formed upon C-C scissions, preferably for interior carbon atoms [3].

For branched alkanes, the fragmentation patterns could be very complex [3, 111]. The prompt yield of the -H radicals is always minor; the highest yields are of the radicals formed by scission of skeletal C-C bonds next to the branches. For example, in radiolysis of isooctane only 15% of the radicals are of the -H type, the rest being *tert*-butyl and 2-propyl radicals [111]. In radiolysis of 2,3-dimethylbutane, 70% of radicals are 2-propyl and 30% are -H radicals (2,3-dimethyl-2-butyl). It is not known what species dissociate (singlets? triplets? excited holes? excited radicals?) and what controls these fragmentation patterns.

**4.5. Generation of solute excited states.** In radiolysis of hydrocarbon solutions of aromatic scintillators (A), a significant fraction of solute fluorescence in the first several nanoseconds is sensitized by the energy transfer from the solvent S<sub>1</sub> state



Direct excitation of A is usually unimportant, but excitation of A by Cerenkov light is not negligible [49]. For many solutes, reaction (19) has large reaction radii (1-1.5 nm) and low activation energy (~ 50 meV).

Solute fluorescence is also induced by charge scavenging followed by radical ion pair recombination



Triplet solute states ( ${}^3\text{A}^*$ ) are formed only in these reactions. Since, typically, electron scavenging reaction (20) is faster than hole scavenging reaction (21), reactions (22) and (23) account for most of the delayed solute fluorescence. In the first few nanoseconds, only reactions (19) and (22) are important. Reaction (24) is important only in the studies on solute photoionization in hydrocarbons. The  ${}^3\text{A}^* + {}^3\text{A}^*$  annihilation is a minor source of delayed fluorescence, though there have been reports to the contrary.

Radiolytic yields of solute  ${}^1\text{A}^*$  states have been determined in several laboratories by measuring the fluorescence from solutions of aromatic scintillators on the subnanosecond time scale [49,100,101,109,115-118]. At Argonne [49,118], the motivation was to compare the experimental values with stochastic Monte-Carlo simulations using a single ion-pair model in order to determine whether the experimental kinetics could be matched by this model. The approximate correspondence between the experimental and simulated kinetics appeared to be possible only by making the assumption that the solvent holes were unstable on the time scale of the fluorescence measurement, undergoing a transformation that partially "disabled" reaction (22). This assumption allowed fair agreement with the *shapes* of the fluorescence kinetics for 1, 10 and 50 mM solutions of the aromatic scintillator, but the agreement

with the absolute radiolytic yields was poor, and the magnitude of the disagreement varied with solute concentration.

A factor which contributes to the complexity of the analysis is the occurrence of reaction (19) which accounts for a large fraction of the  $^1A^*$  states. For cyclohexane, this process can be accounted for with reasonable certainty. For *n*-hexane, the simulation is less satisfactory because the yield of the solvent  $S_1$  state has not been accurately measured ( $1.6 \pm 0.5$  per 100 eV [119]), and the estimates of its lifetime vary from 0.3 ns [95] to 0.7 ns [94].

Here we examine again what is perhaps the most puzzling aspect of the results, i.e., rapid leveling of the  $^1A^*$  yield in dilute scintillator solutions ( $\sim 1$  mM). Qualitatively, simulations show that production of  $^1A^*$  by energy transfer from the solvent  $S_1$  state has a time profile very similar to the observed kinetics. The question is why does not the yield of  $^1A^*$  continuously increase after 2 ns despite the occurrence of reactions (21) and (22)? Since the cyclohexane hole has long lifetime, the flatness of the kinetics must be due to something else than the hole instability. For *n*-hexane, a re-examination of the results indicates that the occurrence of reaction (22) is needed to explain the kinetics observed; the latter can be simulated assuming that 50% of recombinations (22) yield  $^1A^*$ . However, the calculated  $G(^1A^*)$  at 5 ns is larger than the experimental value of 0.07 per 100 eV by a factor of  $\approx 1.8$ , so quantitatively, the situation with *n*-hexane is not settled.

While it is an open question whether the quenching reactions in multiple-pair spurs and sensitization of solute fluorescence by "dark" states can explain the discrepancies, it seems more likely that the loss of the solute luminescence is due to some irregularity in the behavior of cyclohexane holes. One possibility is that rapid electron spin-relaxation in these holes randomizes  $\{RH^+ A^{\bullet-}\}$  geminate pairs and reduces the  $^1A^*$  yield (see section 2.2). The occurrence of such randomization does not contradict the experimental estimates of  $f_S \approx (0.5-0.6)$  for recombination of secondary pairs: these estimates were obtained in concentrated solutions ( $>0.1$  M) of the scintillator in which the solvent hole was scavenged prior to the spin relaxation (see below). Alternatively, one may speculate that for cyclohexane, reaction (22) does not produce solute excited states or at least does so with reduced efficiency.

4.6. *Time-resolved measurements of the singlet recombination probability.* For saturated hydrocarbons irradiated with fast electrons and  $\gamma$ -rays, the estimates of singlet recombination probability  $f_S$  obtained using spin coherence methods (such as magnetic field effect and quantum beat spectroscopy) are between 0.4 and 0.65 [31,32,80,81]. These probabilities were estimated from the fraction  $\Theta$  of spin-correlated geminate pairs by implementation of formula (16). Importantly, this fraction was determined for *secondary* radical-ion pairs. To prevent the loss of spin coherence due to spin relaxation in the solvent holes, both the solvent hole and the electron were scavenged in less than 1 ns, using 0.12 M diphenylsulfide and 1 mM *para*-terphenyl, respectively [80,81]. Still, the estimates of  $\Theta$  were compromised by involvement of pairs that included "satellite" ions, such as olefin radical ions [81]. In the latter species, the electron spin is strongly coupled to protons. This speeds up the spin dephasing of the geminate pair. Thus, the reported values of  $\Theta$  are the low-limit estimates [31].

Given that the validity of formula (16) and the premises of the spin-coherence methods are not obvious, it was important to determine  $f_S$  for secondary ion pairs in a direct way. The time dependence of the  $^1A^*$  and  $^3A^*$  yields in 0.1 M solutions of biphenyl and naphthalene in cyclohexane, *n*-hexane, and isooctane was measured [118]. In these solutions, reactions (19), (20), and (21) was over in a fraction of a nanosecond, and reaction (23) was the only source of  $^1A^*$  and  $^3A^*$  states between 1 ns and 70 ns. From the derivatives of the G-values of  $^3A^*$  and  $^1A^*$ , the time-dependent probability  $f_t=1-f_S$  of triplet recombination was obtained. This probability was  $0.5\pm 0.1$  regardless of the delay time. Surprisingly, no experimentally significant decrease in  $f_S$  during the first 10 ns after the ionization event (due to spin mixing in the secondary geminate pairs, e.g., by hyperfine interaction in the radical ions) was found. Thus, the spin-coherence methods seem to give reliable estimates of  $f_S$ .

In the same work, the probability  $f_t$  for long-lived secondary pairs was estimated by time-resolved measurements of  $G(^3A^*)$  and  $G(A^{\bullet-})$  over the solute concentration range 1 mM to 0.1 M and for times out to 1  $\mu$ s. Corrections were made to take into account dimerization of  $A^{\bullet+}$ ,  $^1A^* \rightarrow ^3A^*$  crossing, triplet-triplet annihilation, reactions of  $^1A^*$  and  $A^{\bullet-}$  with cyclohexyl radicals, etc. [118]. No provisions were made to account for spin dephasing in secondary pairs, though this dephasing is not negligible on the long time scale. It was

found that the kinetics simulated using  $f_t \approx 0.5-0.7$  were in a reasonable agreement with the experimental ones, and the fit quality was not improved by allowing  $f_t$  to vary with time.

An interesting result that still awaits theoretical explanation is a remarkable similarity in the formation kinetics for  $^1A^*$  and  $^3A^*$  states observed between 60 ps to 5 ns in concentrated solutions of aromatic scintillators in *n*-hexane (0.05-0.1 M) [49,118]. At these concentrations, the electrons are scavenged in  $< 10$  ps and the formation of the solvent  $S_1$  states is much reduced, so that reaction (19) is relatively unimportant. Thus, most of the  $^1A^*$  states are formed in the same reaction as the  $^3A^*$  states, via recombination of the solvent holes (reaction (22)) and "satellite ions" with  $A^{\bullet-}$ . The similarity of the formation kinetics for the  $^1,^3A^*$  states suggests that on the short time scale the probability of cross-recombinations and geminate recombinations are very similar. It was concluded that "the spurs are made of a collection of negative and positive ions instead of separate geminate pairs" [118]. As was emphasized above, this view (the loss of pairwise spin correlations in multiple-pair spurs) does not contradict the occurrence of spin coherence phenomena in radiolysis. Whether this result can be explained using the conventional Monte-Carlo models of the spur kinetics needs to be determined.

## 5. CONCLUDING REMARKS

Radiation chemistry of saturated hydrocarbons is far from being well understood, and is a province of numerous controversies and speculations. No closure is in sight. At the same time, no other medium with exception of liquid water has been studied as comprehensively as liquid alkanes and cycloalkanes. Below, we provide our list of the most important and challenging problems in the radiation chemistry of saturated hydrocarbons:

- *The chemistry of "hot" intermediates:* pre-thermalized charges, highly excited solvent states, energetic fragments (such as "hot" H atoms). What is the nature of these states? What role do they play in radiolysis? How do they relax and react? *What happens to the heat dissipated in radiolytic reactions?* What is the mechanism for vibrational deactivation of the products? Could the heat be

dissipated through the formation of unusual conformers and what chemical consequence would that have?

- *Understanding the spur structure* as a function of the electron energy, especially below 1 keV. What is the relative significance of ionization and autoionization processes? What is the origin of the observed spin effects ?
- *First-principle simulations of the excitation dynamics, charge localization, and charge transport in liquid hydrocarbons.* Are there excitons, Rydberg states, and exciplexes in liquid hydrocarbons? What are the mechanisms for localization of electrons and holes in non-polar liquids? What is the mechanism for rapid diffusion of holes and excited states? What determines the fragmentation pathways of triplet and singlet excited states?
- *The role of "silent" species,* in particular, hydrogen atoms, "dark" states, proton adducts, and carbonium ions. How do these species form and interact with each other, excited states, and primary and secondary ions? Are there chemically-significant short-lived intermediates, such as carbenes and biradicals or some other unrecognized species?

This list may be expanded to include most of the issues discussed in this chapter. A lot of these problems stem from insufficient knowledge of short-lived intermediates and the complexity of spur dynamics. The use of traditional methods of radiation chemistry, such as product analysis or transient absorption and fluorescence spectroscopies, has its limitations. The "real action" in radiolysis takes place within the first few tens of picoseconds, when the hot species form, relax, fragment, and react. The existing pulse radiolysis facilities provide the time resolution to 20-30 ps. A new generation of laser-coupled linacs will push this time resolution to 500 fs [120]. The linac at the Osaka University already provides pulses of 800 fs with 2 nC charge (3 ps time resolution). Tabletop accelerators that use intense laser light ( $> 10^{18}$  W/cm<sup>2</sup>) to generate  $\sim 1$  nC of photoelectrons with energies up to 30 MeV have been demonstrated [121,123]; with this technique, 50-100 fs electron pulses will be available. Thus, the time resolution will soon be improved. Will this improvement bring the closure?

Several decades ago, picosecond pulse radiolysis was as eagerly anticipated as the femtosecond pulse radiolysis today. Knowing what followed thereafter



suggests that, by itself, the improved time resolution would not solve many outstanding problems: Though quite a few of the intermediates in radiolysis of hydrocarbons (e.g., solvent holes and solvent  $S_1$  states) live for nanoseconds, their nature remains elusive and their formation and decay mechanisms undetermined. The most daunting task in the development of ultrafast pulse radiolysis is not only in the generation of short electron pulses. Rather, it is the development of better detection techniques (see reference [120], p. 17). Transient absorption spectroscopy was proven inadequate on the time scales of picoseconds or nanoseconds; there is no reason to expect that it would fare better on the shorter time scales. Actually, the situation would be worse since there are fewer sufficiently fast reactions to sort out light-absorbing species by their reactivity. Separating the overlapping absorbance signals from excited states, charge carriers, and fragments would be impossible given that none of these species have distinctive absorption bands. Most of techniques that complemented transient absorption spectroscopy on longer time scales (magnetic resonance, conductivity, fluorescence spectroscopy, etc.) cannot be used on the picosecond and subpicosecond time scales.

We conclude that putting the emphasis on the time resolution without offering adequate spectroscopic base would ensure a new stalemate. Therefore, *the development of fast, highly selective and sensitive techniques for detection of short-lived intermediates in spurs is the most urgent experimental problem in radiolysis of liquids*. Ultrafast laser spectroscopy must be utilized to prepare the ground for the ultrafast pulse radiolysis with the development of better detection techniques.

This work was performed under the auspices of the Office of Basic Energy Sciences, Division of Chemical Science, US-DOE under contract number W-31-109-ENG-38.

## REFERENCES

1. A. Hummel, in *The Chemistry of Alkanes and Cycloalkanes*, S. Patai and Z. Rappoport (eds.), John Wiley, New York, 1992, p. 743.
2. A. J. Swallow, in *Radiation Chemistry: Principles and Applications*, Farhatziz and M. A. J. Rodgers (eds.), VCH Publishers, 1987, p. 351.

3. R. A. Holroyd in *Fundamental Processes in Radiation Chemistry*, P. Ausloos (ed.), Interscience, New York, p. 413.
4. G. Beck and J. K. Thomas, *J. Phys. Chem.* 76 (1972) 3856.
5. A. Hummel and L. H. Luthjens, *J. Chem. Phys.* 59 (1973) 654.
6. E. Zador, J. M. Warman and A. Hummel, *J. Chem. Phys.* 62 (1975) 3897; *Chem. Phys. Lett.* 23 (1973) 363; *J. Chem. Soc. Farad. Trans. I*, 75 (1979) 914.
7. M. P. de Haas, J. M. Warman, P. P. Infelta and A. Hummel, *Chem. Phys. Lett.* 31 (1975) 382; *ibid.* 43 (1976) 321; *Can. J. Chem.* 55 (1977) 2249.
8. J. M. Warman, *The Study of Fast Processes and Transient Species by Electron-Pulse Radiolysis*; J. H. Baxendale and F. Busi (eds.), Reidel, The Netherlands, 1982, p. 433.
9. J. M. Warman, H. C. de Leng, M. P. de Haas and O. A. Anisimov, *Radiat. Phys. Chem.* 36 (1990) 185.
10. I. A. Shkrob, A. D. Liu, M. C. Sauer, Jr., K. H. Schmidt and A. D. Trifunac, *J. Phys. Chem.* 102 (1998) 3363.
11. I. A. Shkrob, A. D. Liu, M. C. Sauer, Jr., K. H. Schmidt and A. D. Trifunac, *J. Phys. Chem.* 102 (1998) 3371.
12. A. D. Liu, I. A. Shkrob, M. C. Sauer, Jr. and A. D. Trifunac, *J. Phys. Chem.* 51 (1998) 273.
13. I. A. Shkrob, M. C. Sauer, Jr., K. H. Schmidt, A. D. Liu, J. Yan and A. D. Trifunac, *J. Phys. Chem.* 101 (1997) 2120.
14. M. C. Sauer, Jr., I. A. Shkrob, J. Yan, K. H. Schmidt and A. D. Trifunac, *J. Phys. Chem.* 100 (1996) 11325.
15. A. D. Liu, M. C. Sauer, Jr. and A. D. Trifunac, *J. Phys. Chem.* 97 (1993) 11265.
16. K. H. Schmidt, M. C. Sauer, Jr., Y. Lu and A. Liu, *J. Phys. Chem.* 94 (1990) 244.
17. M. C. Sauer, Jr. and K. H. Schmidt, *Radiat. Phys. Chem.* 32 (1988) 281.
18. M. C. Sauer, Jr., K. H. Schmidt and A. Liu, *J. Phys. Chem.* 91 (1987) 4836.
19. M. C. Sauer, Jr., A. D. Trifunac, D. B. McDonald and R. Cooper, *J. Phys. Chem.* 88 (1984) 4096.
20. R. Mehnert, in *Radical Ionic Systems, Properties in Condensed Phase*, A. Lund and M. Shiotani (eds.), Kluwer, Dordrecht, 1991, p. 231; R. Mehnert, O. Brede and W. Naumann, *Ber. Bunsenges. Phys. Chem.* 89 (1985) 1031; O. Brede, J. Bös, W. Naumann and R. Mehnert, *Radiochem. Radioanal. Lett.* 35 (1978) 85.
21. F. B. Sviridenko, D. V. Stass and Yu. N. Molin, *Chem. Phys. Lett.* 297 (1998) 343.
22. S. Tagawa, N. Hayashi, Y. Yoshida, M. Washio and Y. Tabata, *Radiat. Phys. Chem.* 34 (1989) 503.

23. I. A. Shkrob, M. C. Sauer, Jr., J. Yan and A. D. Trifunac, *J. Phys. Chem.* 100 (1996) 6876.
24. I. A. Shkrob, M. C. Sauer, Jr. and A. D. Trifunac, *J. Phys. Chem.* 100 (1996) 5993; I. A. Shkrob and A. D. Trifunac, *J. Phys. Chem.* 100 (1996) 14681.
25. I. A. Shkrob, M. C. Sauer, Jr. and A. D. Trifunac, *J. Phys. Chem.* 100 (1996) 7237.
26. I. A. Shkrob, M. C. Sauer, Jr. and A. D. Trifunac, *J. Phys. Chem. B* 103 (1999) 4773; *ibid.*, B 104 (2000) 3752 and 3760.
27. V. I. Borovkov, S. V. Anishchik and O. A. Anisimov, in *Proceedings of the 21st Miller Conference on Radiation Chemistry, April 24-29, 1999, Doorwerth, The Netherlands*, p. 31.
28. B. M. Tadjikov, D. V. Stass, O. M. Usov and Yu. N. Molin, *Chem. Phys. Lett.* 273 (1997) 25.
29. O. M. Usov, D. V. Stass, B. M. Tadjikov and Yu. N. Molin, *J. Phys. Chem. A* 101 (1997) 7711.
30. A. V. Veselov, O. A. Anisimov and Yu. N. Molin, in *Pulse Radiolysis*, Y. Tabata (ed.), CRC Press, Boston, 1991, p. 27.
31. Yu. N. Molin, *Bull. Korean Chem. Soc.* 20 (1999) 7.
32. B. Brocklehurst, *Radiat. Phys. Chem.* 50 (1997) 213.
33. B. Brocklehurst, *J. Chem. Soc. Farad. Trans.* 93 (1997) 1079; M. Okazaki, Y. Tai, K. Nunome and K. Toriyama, *Chem. Phys.* 161 (1992) 177.
34. V. I. Borovkov, S. V. Anishchik and O. A. Anisimov, *Chem. Phys. Lett.* 270 (1997) 327.
35. A. Hummel, private communication.
36. V. M. Grigoryants, B. M. Tadjikov, O. M. Usov and Yu. N. Molin, *Chem. Phys. Lett.* 246 (1995) 392.
37. M. C. Sauer, Jr., D. W. Werst, C. D. Jonah and A. D. Trifunac, *Radiat. Phys. Chem.* 37 (1991) 461; A. D. Trifunac, M. C. Sauer, Jr. and C. D. Jonah, *Chem. Phys. Lett.* 113 (1985) 316.
38. A. D. Trifunac, M. C. Sauer, Jr., I. A. Shkrob and D. W. Werst, *Acta Chem. Scand.* 51 (1997) 158.
39. I. A. Shkrob and A. D. Trifunac, *J. Phys. Chem.* 98 (1994) 13262.
40. D. W. Werst, M. G. Bakker and A. D. Trifunac, *J. Am. Chem. Soc.* 112 (1990) 40.
41. A. D. Trifunac, D. W. Werst and L. T. Percy, *Radiat. Phys. Chem.* 34 (1989) 547.
42. D. W. Werst and A. D. Trifunac, *J. Phys. Chem.* 92 (1988) 1093.
43. D. W. Werst, L. T. Percy and A. D. Trifunac, *Chem. Phys. Lett.* 153 (1988) 45.

44. J. P. Smith, S. Lefkowitz and A. D. Trifunac, *J. Phys. Chem.* 86 (1982) 4347.
45. B. M. Tadjikov, N. N. Lukzen, O. A. Anisimov and Yu. N. Molin, *Chem. Phys. Lett.* 171 (1990) 413.
46. B. M. Tadjikov, V. I. Melekhov, O. A. Anisimov and Yu. N. Molin, *Radiat. Phys. Chem.* 34 (1989) 353.
47. V. I. Melekhov, O. A. Anisimov, V. A. Veselov and Yu. N. Molin, *Chem. Phys. Lett.* 127 (1986) 97.
48. V. I. Melekhov, O. A. Anisimov, V. A. Saik and Yu. N. Molin, *Chem. Phys. Lett.* 112 (1984) 106.
49. M. C. Sauer, Jr., C. D. Jonah and C. A. Naleway, *J. Phys. Chem.* 95 (1991) 730.
50. B. M. Tadjikov, D. V. Stass and Yu. N. Molin, *J. Phys. Chem. A* 101 (1997) 377.
51. A. Lund, M. Lindgren, S. Lunell and J. Maruani, in *Molecules in Physics, Chemistry, and Biology*, vol. 3, J. Maruani (ed.), Kluwer, Dordrecht, 1989, p. 259; P. Wang, M. Shiotani and S. Lunell, *Chem. Phys. Lett.* 292 (1998) 110, and references therein.
52. V. I. Melekhov, O. A. Anisimov, L. Sjöqvist and A. Lund, *Chem. Phys. Lett.* 174 (1990) 95.
53. C. D. Jonah and M. C. Sauer, Jr., *Radiat. Phys. Chem.* 46 (1989) 497.
54. D. B. Johnston, Y.-M. Wang and S. Lipsky, *Radiat. Phys. Chem.* 38 (1991) 583.
55. R. E. Bühler, *Res. Chem. Intermed.* 25 (1999) 259; R. E. Bühler and Y. Katsumura, *J. Phys. Chem. A* 102 (1998) 111.
56. Y. Katsumura, T. Azuma, M. A. Qadir, A. S. Domazou and R. E. Bühler, *J. Phys. Chem.* 99 (1995) 12814.
57. M. A. Lewis and C. D. Jonah, *Radiat. Phys. Chem.* 33 (1989) 1; B. C. Le Motais and C. D. Jonah, *Radiat. Phys. Chem.* 33 (1989) 505.
58. S. G. Lias, P. Ausloos and Z. Horvath, *Int. J. Chem. Kinet.* 8 (1976) 725.
59. D. V. Stass, N. N. Lukzen, B. M. Tadjikov, V. M. Grigoryants and Yu. N. Molin, *Chem. Phys. Lett.* 243 (1995) 533.
60. P. Ausloos, R. E. Rebbert, F. P. Schwartz and S. G. Lias, *Radiat. Phys. Chem.* 21 (1983) 27.
61. E. Haselbach and T. Bally, *Pure Appl. Chem.* 56 (1984) 1203 and references there.
62. B. Brocklehurst, *Radiat. Phys. Chem.* 50 (1997) 393.
63. J. A. LaVerne and B. Brocklehurst, *Radiat. Phys. Chem.* 47 (1996) 71; *J. Phys. Chem.* 100 (1996) 1682.
64. B. Brocklehurst, *Chem. Phys. Lett.* 211 (1993) 31.

65. B. Brocklehurst, *J. Chem. Soc. Farad. Trans.* 88 (1992) 167 and 2823.
66. H. Miyasaka and N. Mataga, in *Pulse Radiolysis*, Y. Tabata (ed.), CRC Press, Boston, 1991, p. 173; *Radiat. Phys. Chem.* 32 (1988) 177; *Chem. Phys. Lett.* 134 (1987) 480, *ibid.* 126 (1986) 219.
67. M. U. Sander, U. Brummund, K. Luther and J. Troe, *J. Phys. Chem.* 97 (1993) 8378.
68. F. H. Long, H. Lu and K. B. Eisenthal, *J. Phys. Chem.* 99 (1995) 7436.
69. L. D. A. Siebbeles, U. Emmerichs, A. Hummel and H. J. Bakker, *J. Chem. Phys.* 107 (1997) 9339.
70. G. Orlandi, L. Flamingi, F. Barigiletti and S. Dellonte, *Radiat. Phys. Chem.* 21 (1983) 113.
71. V. O. Saik and S. Lipsky, *Chem. Phys. Lett.* 264 (1997) 649; V. O. Saik, A. E. Ostafin and S. Lipsky, *J. Chem. Phys.* 103 (1995) 7347.
72. J. P. Dodelet, K. Shinsaka and G. Freeman, *Can. J. Chem.* 54 (1976) 744.
73. R. A. Crowell and D. M. Bartels, *J. Phys. Chem.* 100 (1996) 17940.
74. N.-H. Ge, C. M. Wong, R. L. Lingle, Jr., J. D. McNeill, K. J. Gaffney and C. B. Harris, *Science* 279 (1998) 202 [also see their review in *J. Phys. Chem. B* 103 (1999) 282].
75. M. Faubel, B. Steiner and J. P. Toennis, *J. Chem. Phys. A* 106 (1997) 9013.
76. B. Brocklehurst, *Radiat. Phys. Chem.* 21 (1983) 57; *J. Chem. Soc. Farad. Trans. II*, 72 (1976) 1869; *Nature* 221 (1969) 921.
77. C. E. Bolton and N. J. B. Green, *J. Phys. Chem.* 100 (1996) 8807.
78. W. M. Bartczak, M. Tachiya and A. Hummel, *Radiat. Phys. Chem.* 36 (1990) 195.
79. J. A. LaVerne and S. M. Pimblott, *J. Phys. Chem.* 99 (1995) 10540.
80. S. V. Anishchik, O. M. Usov, O. A. Anisimov and Yu. N. Molin, *Radiat. Phys. Chem.* 51 (1998) 31.
81. O. M. Usov, V. M. Grigoryants, B. M. Tadjikov and Yu. N. Molin, *Radiat. Phys. Chem.* 49 (1997) 237.
82. A. E. Ostafin and S. Lipsky, *J. Chem. Phys.* 98 (1993) 5408.
83. R. A. Holroyd, J. M. Preses and J. C. Hanson, *J. Phys. Chem. A* 101 (1997) 6931; *Radiat. Res.* 135 (1993) 312.
84. W. M. Bartczak and A. Hummel, *J. Radioanal. Nucl. Chem.* 232 (1998) 7.
85. L. D. A. Siebbeles, W. M. Bartczak, M. Terrisol and A. Hummel, in *Microdosimetry. An Interdisciplinary Approach*, D. T. Goodhead, P. O'Neill and H. G. Menzel (eds.), The Royal Society of Chemistry, Special Publ. No. 204, Cambridge, 1997, p. 11.

86. W. M. Bartczak and A. Hummel, *Chem. Phys. Lett.* 208 (1993) 232; *Radiat. Phys. Chem.* 39 (1992) 29.
87. L. D. A. Siebbeles, W. M. Bartczak, M. Terrisol and A. Hummel, *J. Phys. Chem. A* 101 (1997) 1619; W. M. Bartczak and A. Hummel, *J. Phys. Chem.* 97 (1993) 1253.
88. L. Musolf, W. M. Bartczak, M. Wojcik and A. Hummel, *Radiat. Phys. Chem.* 47 (1996) 83.
89. J. A. LaVerne, S. M. Pimblott and L. Wojnárovits, *J. Phys. Chem. A* 101 (1997) 1628.
90. R. A. Holroyd and T. K. Sham, *Radiat. Phys. Chem.* 51 (1998) 37; *J. Phys. Chem.* 89 (1985) 2909; R. A. Holroyd, T. K. Sham, B.-X. Yang and X.-H. Feng, *J. Phys. Chem.* 96 (1992) 7438.
91. F. Hirayama and S. Lipsky, *J. Chem. Phys.* 51 (1969) 3616; F. Hirayama, W. Rothman and S. Lipsky, *Chem. Phys. Lett.* 5 (1969) 296; W. Rothman, F. Hirayama and S. Lipsky, *J. Chem. Phys.* 58 (1973) 1300.
92. L. Wojnárovits and G. Földiák, *Triplet States of Alkanes*, in *Proceedings of the 5th Working Meeting on Radiat. Interact.*, H. Mai, O. Brede and R. Mehnert (eds.), *ZFI-Mitteilungen*, Leipzig, 1991, p. 64.
93. M. C. Sauer, Jr., C. D. Jonah, B. C. Le Motais and A. C. Chernovitz, *J. Phys. Chem.* 92 (1988) 4099.
94. R. Hermann, R. Mehnert, and L. Wojnárovits, *J. Lumin.* 33 (1985) 69; Y. Katsumura, Y. Yoshida, S. Tagawa and Y. Tabata, *Radiat. Phys. Chem.* 21 (1983) 103.
95. M. A. Wickramaaratchi, J. M. Preses, R. A. Holroyd and R. E. Weston, Jr., *J. Chem. Phys.* 82 (1985) 4745.
96. J. M. Preses and R. A. Holroyd, *J. Chem. Phys.* 92 (1990) 2938; S. Dellonte, L. Flamingi, F. Bargaletti, L. Wojnárovits and G. Orlandi, *J. Phys. Chem.* 88 (1984) 58.
97. F. P. Schwarz, D. Smith, S. G. Lias, and P. Ausloos, *J. Chem. Phys.* 75 (1981) 3300.
98. T. S. R. Krishna and S. Lipsky, *J. Phys. Chem. A* 102 (1998) 496.
99. Y.-M. Wang, D. B. Johnston and S. Lipsky, *J. Phys. Chem.* 97 (1993) 403 and references 3 to 10 therein.
100. L. Walter and S. Lipsky, *Int. J. Radiat. Phys. Chem.* 7 (1975) 175.
101. L. H. Luthjens, H. C. de Leng, L. Wojnárovits and A. Hummel, *Radiat. Phys. Chem.* 26 (1985) 509.
102. V. M. Grigoryants and V. V. Lozovoy, *High Energy Chem.* 30 (1996) 38.
103. Y. Tabata, Y. Ito, and S. Tagawa, *CRC Handbook of Radiation Chemistry*, CRC Press, Boston, 1991.
104. H. T. Choi, D. Askew and S. Lipsky, *Radiat. Phys. Chem.* 19 (1982) 373.
105. L. Wojnárovits and G. Földiák, *Acta Chim. Acad. Sci. Hung.* 105 (1980) 27.

106. T. Wada, S. Shida and Y. Hatano, *J. Phys. Chem.* 79 (1975) 561; S. Shida and Y. Hatano, *Int. J. Radiat. Phys. Chem.* 8 (1974) 171.
107. L. Wojnárovits and J. A. LaVerne, *J. Radioanal. Nucl. Chem.* 232 (1998) 19; *J. Phys. Chem.* 99 (1995) 3168; *J. Phys. Chem.* 98 (1994) 6046; J. A. LaVerne and L. Wojnárovits, *Radiat. Phys. Chem.* 47 (1996) 353; L. Wojnárovits and J. A. LaVerne, G. Földiák, M. Roder and L. Wojnárovits, *Hung. Magy. Kem. Foly.* 100 (1994) 184; *J. Radioanal. Nucl. Chem.* 165 (1992) 385; *ibid.* 164 (1992) 29.
108. A. Hummel, H. C. de Leng, L. H. Luthjens and L. Wojnárovits, *J. Chem. Soc. Farad. Trans.* 90 (1994) 2459.
109. L. H. Luthjens, H. C. de Leng, W. R. S. Appleton and A. Hummel, *Radiat. Phys. Chem.* 36 (1990) 213; L. H. Luthjens, P. Dorenbos, J. T. M. de Haas, A. Hummel and C. W. E. van Eijk, *Radiat. Phys. Chem.*, in press.
110. I. A. Shkrob and A. D. Trifunac, *Radiat. Phys. Chem.* 50 (1997) 227; *J. Phys. Chem.* 99 (1995) 11122.
111. B. Tilquin and T. Baudston, *Radiat. Phys. Chem.* 37 (1991) 23.
112. I. A. Shkrob and A. D. Trifunac, *Radiat. Phys. Chem.* 46 (1995) 83.
113. D. W. Werst and A. D. Trifunac, *Chem. Phys. Lett.* 137 (1987) 475.
114. K. Toriyama, M. Iwasaki, Fukaya, H. Muto and K. Nunome, *J. Chem. Soc. Chem. Commun.* (1982) 1293; *J. Phys. Chem.* 89 (1985) 5278.
115. V. V. Lozovoy, V. M. Grigoryants, O. A. Anisimov, Generation of Excited States of Solutes in Radiolysis of Dilute Hydrocarbons, *Inst. Chem. Kinet. & Combustion, Novosibirsk, Russia, Preprint 28, 1988 (in Russian)*; V. M. Grigoryants, V. V. Lozovoy, Yu. D. Chernousov, I. É. Shebolaev, V. A. Arutyunov, O. A. Anisimov and Yu. N. Molin, *Radiat. Phys. Chem.* 34 (1989) 349.
116. Y. Yoshida, S. Tagawa, M. Washio, H. Kobayashi and Y. Tabata, *Radiat. Phys. Chem.* 34 (1989) 493; *ibid.* 30 (1987) 83; Y. Katsumura, Y. Yoshida, S. Tagawa and Y. Tabata, *Radiat. Phys. Chem.* 21 (1983) 103; S. Tagawa, Y. Katsumura, and Y. Tabata, *Radiat. Phys. Chem.* 19 (1982) 125.
117. L. Wojnárovits, L. H. Luthjens, H. C. de Leng and A. Hummel, *J. Radioanal. Nucl. Chem.* 101 (1986) 349.
118. M. C. Sauer, Jr. and C. D. Jonah, *Radiat. Phys. Chem.* 44 (1994) 281.
119. L. Wojnárovits and G. Földiák, *ZFI-Mitteilungen (Leipzig)* 43a (1981) 243.
120. Research Needs and Opportunities in Radiation Chemistry, US-DOE Office of Science, BES-CHEM, Chesterton, Indiana, April 19-22, 1998, p. 13.
121. G. A. Mourou, C. P. J. Barty and M. D. Perry, *Physics Today* 51 (1998) 22; S. J. Matthews, *Laser Focus World* 35 (1999) 155.
122. I. A. Shkrob, A. D. Liu, M. C. Sauer, Jr., and A. D. Trifunac, *J. Phys. Chem. B*, in press.

123. N. Saleh, K. Flippo, K. Nemoto, D. Umstadter, R. A. Crowell, C. D. Jonah, A. D. Trifunac, *Rev. Sci. Instr.* 71 (2000) 2305.



## **Radiation chemistry of organic halides in aqueous solution**

**Hari Mohan and Jai P.Mittal<sup>†</sup>**

Radiation Chemistry and Chemical Dynamics Division,  
Bhabha Atomic Research Centre, Trombay, Mumbai 400 085, India.

### **1 INTRODUCTION**

Halogenated organic compounds are frequently employed as solvents, pesticides and refrigerants and for the study of electron transfer reactions in radiation and electrochemical investigations [1-8]. Many of these compounds are hazardous and toxic in nature if metabolized in living species and cause environmental and toxicological problems [8-11]. The toxic action of these compounds is associated with the generation of free radicals during their metabolism and cause cell damage due to high oxidizing behavior [12-15]. The reaction of these free radicals in biological systems is difficult to study due to many possible reaction pathways. However, in radiation chemical studies, selective free radicals can be generated and their reactions with biological model compounds can be investigated. Similarity in product pattern between metabolic and free radical degradation has been observed for certain halogenated organic compounds [16-18]. These compounds are also known to have important role in the depletion of tropospheric ozone [19]. The degradation of the compounds in atmosphere is by the reaction with  $\cdot\text{OH}$  radicals. The tropospheric life time of these compounds would depend on the rate constant of the reaction of  $\cdot\text{OH}$  radicals. A significant attention is focused to obtain the kinetic data for halogenated compounds.

The identity and reactivity of the transient species produced on radiolysis and photolysis of halogenated organic compounds has been the subject of recent interest [20-24]. The recent advances in the methods of generation and detection of transient intermediates have made the radical ion chemistry an active area of research both in the gas and condensed phase [25-28]. The nature and reactions

---

<sup>†</sup> Also affiliated as Honorary Professor with the Jawaharlal Nehru Centre for Advanced Scientific Research Bangalore, India.

of the transient species can be investigated by time resolved studies employing the technique of pulse radiolysis and laser flash photolysis [29-39]. Most of the studies are carried out in aqueous solutions in which the primary radiolytic species of water ( $\cdot\text{OH}$ ,  $\cdot\text{H}$ ,  $e_{\text{aq}}^-$ ) and secondary radicals ( $\text{SO}_4^{\cdot-}$ ,  $\text{N}_3$ ,  $\text{Cl}_2^{\cdot-}$ ) are used to generate different types of reactive species [40-43]. In order to understand the physico-chemical properties of the halogenated organic compounds, it is therefore necessary to know the identity and reactivity of the transient species generated under different experimental conditions.

At room temperature, the life-time of the transient species is generally very small. However, in the solid state at sufficiently low temperature (77 K) the reaction of transients can be slowed down so much that they can be observed over periods of minutes or hours and could be conveniently studied by optical absorption investigations in glassy matrix of 3-methylpentane (3MP), 2-methyltetrahydrofuran and by electron spin resonance measurements [44-50]. With the availability of pulse radiolysis technique, the identity of transients can be investigated at room temperature [29-39].

$\gamma$ -radiolysis of water gives us three highly reactive species ( $e_{\text{aq}}^-$ ,  $\cdot\text{OH}$ ,  $\cdot\text{H}$ ) in addition to the formation of less reactive or inert molecular products ( $\text{H}_2\text{O}_2$ ,  $\text{H}_2$ ) [40]. One can study the reaction of any of these species with halogenated organic compounds under different conditions. The reaction of  $\cdot\text{OH}$  radicals is investigated in  $\text{N}_2\text{O}$ -saturated conditions, where  $e_{\text{aq}}^-$  is quantitatively converted to  $\cdot\text{OH}$  radicals with  $G(\cdot\text{OH}) = 5.6$  ( $G$  denotes the number of species per 100 eV of absorbed energy). The reaction of  $\cdot\text{H}$  atoms can be investigated in  $\text{N}_2$ -saturated neutral solutions with  $G(\cdot\text{H}) = 0.6$ , in presence of *t*-butyl alcohol to scavenge  $\cdot\text{OH}$  radicals. *t*-Butyl alcohol acts as a weak  $\cdot\text{H}$  atom and strong  $\cdot\text{OH}$  radical scavenger. The reaction of  $\cdot\text{H}$  atoms can also be investigated in acidic solutions with  $G(\cdot\text{H}) = 3.2$  as under these conditions,  $e_{\text{aq}}^-$  would be converted to  $\cdot\text{H}$  atoms. The reaction of  $\text{O}^-$  can be studied in highly alkaline ( $\text{pH} = 13$ ) solutions where  $\cdot\text{OH}$  radicals are converted to  $\text{O}^-$  with a  $\text{pK}_a$  value of 11.9. The reaction of  $e_{\text{aq}}^-$  is investigated in  $\text{N}_2$ -saturated solutions in presence of *t*-butyl alcohol to scavenge  $\cdot\text{OH}$  radicals with  $G(e_{\text{aq}}^-) = 2.7$ .

The specific one-electron oxidants ( $\text{Cl}_2^{\cdot-}$ ,  $\text{Br}_2^{\cdot-}$ ,  $\text{I}_2^{\cdot-}$ ,  $\text{N}_3$ ,  $\text{SO}_4^{\cdot-}$ ,  $\text{Ti}^{2+}$ ) and reductants ( $\text{COO}^-$ ,  $\alpha$ -hydroxyalcohol radicals) are generated on reaction of primary radiolytic species of water radiolysis with standard solutes under conditions such that primary radiolytic species don't react with the substrate initially. The one-electron oxidants and reductants would then react with the

substrate [43,51,52]. The nature of the transient species has been investigated by employing the technique of pulse radiolysis [53-57].

The radiation chemistry of organic halides in aqueous solution, particularly the formation of transient species, has been discussed in detail in this chapter. However, a brief introduction on the radiation chemistry of organic halides in hydrocarbons and matrix isolation technique for the investigation of transient species has also been mentioned here. Radiolysis of hydrocarbons with high energy electrons result in the formation of positive ions and electrons. While in liquid phase, positive ions have high probability of reaction with an electron giving rise to a G value of 0.1 - 0.2 for electrons, more electrons escape prompt recombination with high value of trapped electron (0.8 - 3, depending on the nature of the solvent) at 77 K. Due to the high mobility of electrons and positive holes produced on  $\gamma$ -radiolysis of hydrocarbons (3MP) at 77 K, electrons and positive holes react with the organic compounds present in the hydrocarbon matrix and generate cations and anions. The ionization potential of halogenated organic compounds is lower than that of 3MP (10.08 eV), and the migrating positive charge can be efficiently trapped by these compounds. The nature of the intermediates is investigated with known hole and electron scavengers. The assignment of the transient absorption bands to solute cation is based on the following facts. (1) The absorption bands were suppressed in the presence of hole scavengers. (2) These bands remained insensitive to electron scavengers. (3) The insensitivity to photobleaching of these absorption bands also suggests that the bands are due to cations and not due to anions because the electrons are easily photodetached from anions whereas cations may not be easily photobleached [58-62].

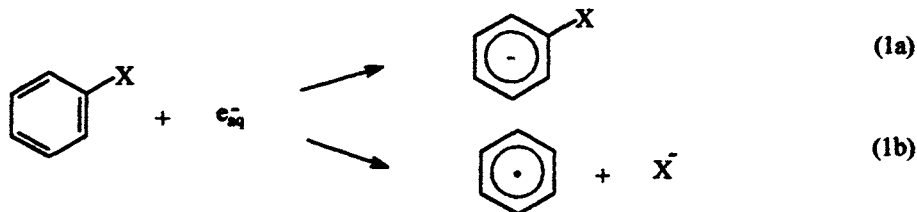
The reactivity of trapped electrons in aqueous and organic glassy matrix at 77 K has been investigated and found to react with the solute by tunneling mechanism [63-65]. The nature of the transient intermediates and stable products formed on  $\gamma$ -radiolysis of halogenated organic compounds in hydrocarbon matrix have been investigated in detail [66-72]. The aggregation of alkyl halides in non-polar matrix of 3MP at 77 K was observed to play an important role on the nature of transients and stable products formed on radiolysis. The aggregation of the polar solutes in non-polar solvents at 77 K, such as halogenated organic compounds in 3MP, can be affected by the nature of freezing of the sample [58]. The variation in the products yield on  $\gamma$ -radiolysis of  $\text{CHI}_3$  in 3MP at 77 K was explained as due to the formation of solute aggregates [66]. The linear variation in the products yield, as a function of solute concentration, was observed at 300 K whereas the yield was appreciably high at high solute concentration at 77 K. Benzene, which is known to lessen

aggregation of alkyl halides due to charge transfer complex formation, was observed to affect the distribution pattern of stable products. The matrix isolation studies are very useful in studying the transient properties of the solute cation. The radiation chemical studies on halogenated compounds in hydrocarbon matrix at room temperature have been investigated in detail and the  $\gamma$ -dose-rate-dependent formation of stable products was explained as being due to a chain reaction [73,74].  $\gamma$ -radiolysis of aerated aqueous solutions of  $\text{CH}_3\text{I}$  has shown the formation of hydrogen peroxide and methyl hydroperoxide with G values comparable to the primary species of water radiolysis. It is also shown that the reaction of  $e_{\text{aq}}^-$  with  $\text{CH}_3\text{I}$  is dissociative in nature and  $\text{CH}_3\text{I}^-$  does not react with  $\text{H}^+$  [75,76].

## 2 FORMATION OF TRANSIENT SPECIES

### 2.1 Reaction with $e_{\text{aq}}^-$

The reaction of  $e_{\text{aq}}^-$  with halogenated organic compounds is dissociative in nature due to the high electron affinity of the halogen. In case of aromatic compounds ( $\text{ArX}$ ), the electron capture may involve the  $\pi$  orbital of the aromatic moiety equation (1a) or the substituent halogen atom equation (1b). In gas phase, the former process generally has electron capture energy threshold whereas the latter process has either lower or no threshold depending on the aromatic ring and the substituent [77]. The equation (1b) gives an aryl radical and halide ion from a repulsive state formed as electron enters a strongly antibonding orbital. On the other hand, molecular anion formed in equation (1a) is a bound state and depending upon the relative magnitudes of the bond energy of C-X bond, presence of substituents and electron affinity of halogen, may cross over to the repulsive state leading to dissociation similar to equation (1b) [78,79]. Most of the fluoro compounds form molecular anions in gas phase as well as in the condensed phase, whereas the chloro, bromo and iodo aromatic compounds on electron capture give intermediate bound state which may cross over to a repulsive state resulting in the scission of C-X bond.



Scheme 1

The rate of fluoride elimination from radical anion depends on the orbital occupied by the unpaired electron. If the unpaired electron occupies an orbital that has a significant  $\sigma$  character, a rapid rate is expected. A relatively slow rate is expected for a  $\pi$  radical as it requires an intramolecular electron transfer to the orthogonal  $\sigma$  orbital of the C-F bond [80-83]. The presence of a substituent with high electron affinity would further reduce the rate. The fluoride ion yield was equal to  $G(e_{aq}^-)$  for higher fluorinated compounds ( $C_6F_6$ ) and much lower yields were found for the reaction of  $e_{aq}^-$  with mono and difluorobenzenes indicating that scavenging of an electron by fluorobenzene may not necessarily lead the elimination of a fluoride ion [77]. The transient optical absorption spectra ( $\lambda_{max} = 280, 390 \text{ nm}$ ,  $k = 1 \times 10^{10} \text{ dm}^3 \text{ mol}^{-1} \text{ s}^{-1}$ ) obtained on reaction of  $e_{aq}^-$  with deprotonated form of pentafluorophenol is assigned to H-adduct formed via equations (2, 3) [84-88]. In the case of iodopentafluoro benzene, the reaction of  $e_{aq}^-$  has not shown any defluorination and the transient absorption bands are assigned to the radical anion, which can protonate to form the H-adduct via equations (4, 5) [88].



The nature of the transient species formed from the reaction of  $e_{aq}^-$  with perfluorobenzene can be determined from electron transfer studies with a suitable electron acceptor. Based on these studies it was concluded that the reaction of  $e_{aq}^-$  with perfluoroacetophenone or perfluorobenzaldehyde formed radical anions whereas the reaction with hexafluorobenzene, pentafluorophenol or pentafluoroaniline resulted in the formation of a radical species with fluoride ion elimination. Similarly, the reaction of electron with alkyl halides (RX) lead to the formation of the alkyl radical and the halide ion.

## 2.2 Formation and reaction of peroxy radicals

Except for fluorinated organic compounds, the radical species (alkyl, phenyl) generated on dissociative electron capture process have absorption bands at  $\lambda < 300 \text{ nm}$ . The peroxy radicals generated on addition of oxygen also have absorption bands at  $\lambda < 300 \text{ nm}$  except for phenyl peroxy radicals which show absorption band in 400 - 600 nm region [89-92]. Phenyl peroxy radicals ( $PhOO^{\cdot}$ ,  $E^{\circ} \sim 0.7 \text{ V}$  vs NHE) are much more reactive than alkyl peroxy radicals

(ROO $\cdot$ ) and halogen substitution in the aromatic ring further increase the reactivity [89-96]. Halogenated alkyl peroxy radicals are much more reactive than their non-halogen analogues. The reactions of these peroxy radicals with organic compounds are investigated from the formation kinetic studies and the reactions of a large number of peroxy radicals with a variety of compounds have been investigated [97-104]. The bimolecular rate constant values for the reaction of a number of peroxy radicals with a variety of organic compounds have been compiled and are found to vary linearly with Taft's ( $\sigma^*$ ) inductive parameter [97, 105-108]. Recent studies have shown that (1) the reaction of alkyl peroxy radicals increase with the number of halogen atoms in the alkyl group (CCl<sub>3</sub>OO $\cdot$  > CHCl<sub>2</sub>OO $\cdot$  > CH<sub>2</sub>ClOO $\cdot$  > CH<sub>3</sub>OO $\cdot$ ). (2) The alkyl peroxy radicals having a halogen with high electron affinity are more reactive (Cl > Br > I). (3) The peroxy radicals of chloromethanes are more oxidative in nature than those of chloroethanes. (4) In the case of chloroethanes, the oxidative power of peroxy radicals is found to be independent of the position of the chlorine atom, i.e., the oxidative power for peroxy radical of 1,1,1-trichloroethane and 1,1,2-trichloroethane are almost the same. (5) The peroxy radical of CF<sub>2</sub>Cl<sub>2</sub> is more oxidative in nature than that from CH<sub>2</sub>Cl<sub>2</sub> [98-104].

### 2.3 Reaction of $\cdot$ OH radicals

The radiation chemical investigations on the nature of  $\cdot$ OH radical reaction with organic halides has been the subject of current interest [109,110] particularly with aromatic halides containing electron donating substituents [111-136]. The measurement of the rate constants, the oxidation of OH-adduct by various

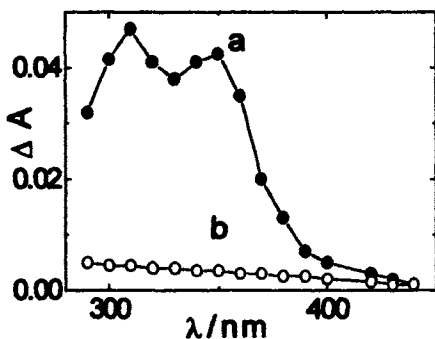


Figure 1. Transient absorption spectra obtained on pulse radiolysis of N<sub>2</sub>O-saturated neutral aqueous solution ( $1 \times 10^{-3}$  mol dm<sup>-3</sup>) of CH<sub>3</sub>I - (a) and CF<sub>3</sub>CH<sub>2</sub>I - (b).

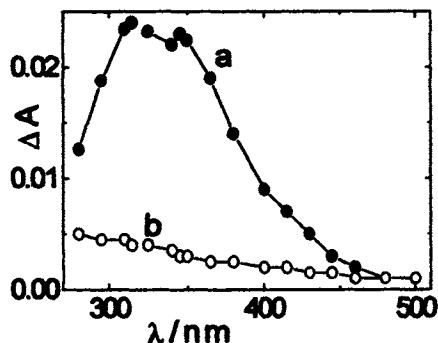


Figure 2. Transient absorption spectra obtained on pulse radiolysis of N<sub>2</sub>O-saturated neutral aqueous solution ( $1 \times 10^{-3}$  mol dm<sup>-3</sup>) of Cl(CH<sub>2</sub>)<sub>3</sub>I - (a) and ClCH<sub>2</sub>I - (b).

Table 1

Kinetic parameters of the transient species formed on reaction of  $\cdot\text{OH}$  radicals with alkyl halides in neutral aqueous solution

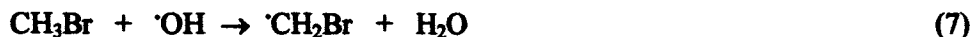
Reaction	$\lambda_{\text{max}} / \text{nm}$	$\epsilon / 10^3 \text{ dm}^3 \text{ mol}^{-1} \text{ cm}^{-1}$	$k / 10^9 \text{ dm}^3 \text{ mol}^{-1} \text{ s}^{-1}$	$k_d / 10^5 \text{ s}^{-1}$
$\text{CH}_3\text{I} + \cdot\text{OH}$	310, 350	4.6	2.2	0.69
$\text{Cl}(\text{CH}_2)_3\text{I} + \cdot\text{OH}$	315, 345	2.5	4.7	1.50
$\text{Br}(\text{CH}_2)_4\text{I} + \cdot\text{OH}$	310, 350	---	2.5	0.53
$\text{Cl}(\text{CH}_2)_4\text{I} + \cdot\text{OH}$	315, 360	1.9	4.7	5.20
$\text{C}_2\text{H}_5\text{Br} + \cdot\text{OH}$	< 280	---	---	---
$\text{C}_3\text{H}_7\text{Cl} + \cdot\text{OH}$	< 290	---	---	---
$\text{ClCH}_2\text{I} + \cdot\text{OH}$	< 290	---	---	---
$\text{CF}_3\text{CH}_2\text{I} + \cdot\text{OH}$	< 290	---	---	---
$\text{Br}(\text{CH}_2)_4\text{Cl} + \cdot\text{OH}$	< 290	---	---	---

oxidants and stable product analysis have been commonly employed for radiation chemical studies. The reaction of  $\cdot\text{OH}$  radicals are most extensively studied as they can undergo a variety of reactions i.e., addition, abstraction and electron transfer. The nature of the reaction is influenced both by the halogen and the substitution in halogenated organic compounds. Therefore, it is very important to know the nature of the transient species generated both from aromatic and aliphatic organic compounds as this knowledge is also required for evaluating the reactivity of the transient species generated from halogenated organic compounds.

#### 2.4 Reaction with alkyl halides in neutral solutions

The reaction of  $\cdot\text{OH}$  radicals with alkyl halides is observed to depend on the halogen. In alkyl iodides, the transient absorption bands at 310 and 350 nm formed on pulse radiolysis of  $\text{N}_2\text{O}$ -saturated neutral aqueous solution of  $\text{CH}_3\text{I}$  (Fig 1) are assigned to OH-adduct equation (6) [22,137-139], whereas  $\cdot\text{OH}$  radicals react by  $\cdot\text{H}$  atom abstraction with alkyl bromides equation (7) forming a carbon centered radical with absorption at  $\lambda < 280 \text{ nm}$  [137]. The transient absorption spectrum (Fig 1) decayed by first order kinetics with  $k = 6.9 \times 10^4 \text{ s}^{-1}$ . The bimolecular rate constant ( $k_6$ ) determined by formation kinetic studies at 350 nm gave a value of  $2.2 \times 10^9 \text{ dm}^3 \text{ mol}^{-1} \text{ s}^{-1}$ , close to that obtained by

competition kinetic studies ( $1.2 \times 10^9 \text{ dm}^3 \text{ mol}^{-1} \text{ s}^{-1}$ ) using KSCN as the standard solute. The absorbance of the transient spectrum remained independent of solute concentration ( $0.7 - 6 \times 10^{-3} \text{ mol dm}^{-3}$ ) and the molar absorptivity at 350 nm was determined to be  $4.6 \times 10^3 \text{ dm}^3 \text{ mol}^{-1} \text{ cm}^{-1}$ .



The pulse radiolysis studies have been carried out with a number of alkyl halides (Figs 1, 2, Table 1) [22,23,139-148] and it can be concluded that (1) the transient absorption bands in the region of 310 and 350 nm formed on reaction of  $\cdot\text{OH}$  radicals with alkyl iodides are due to OH-adduct, forming a 3-electron bonded species between iodine and oxygen. (2) The transient species formed on reaction of  $\cdot\text{OH}$  radicals with alkyl bromides and alkyl chlorides showed very little absorption in 300 - 700 nm region and assigned to a carbon centered radical formed on abstraction of  $\cdot\text{H}$  atom, which has an absorption band at  $\lambda < 280 \text{ nm}$ . The OH-adduct is probably not formed. (3) The nature of the transient species formed on reaction of  $\cdot\text{OH}$  radicals is observed to depend on the nature of additional halogen and its relative position with respect to iodine in alkyl iodide. In 1,*n*-chloroiodoalkanes, OH-adduct with absorption bands in 310 and 350 nm region is formed only if  $n \geq 3$ . With  $n \leq 2$ ,  $\cdot\text{OH}$  radicals react with the formation of a transient species having absorption band at  $\lambda < 280 \text{ nm}$  (Fig 2).

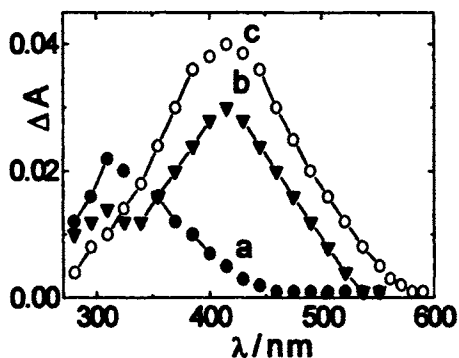


Figure 3. Transient absorption spectra obtained on pulse radiolysis of  $\text{N}_2\text{O}$ -saturated aqueous ( $\text{pH} = 3$ ) solution of  $\text{CH}_3\text{I}$  ( $1 \times 10^{-4} \text{ mol dm}^{-3}$ ) - (a),  $1 \times 10^{-3} \text{ mol dm}^{-3}$  - (b) and  $8 \times 10^{-3} \text{ mol dm}^{-3}$  - (c).

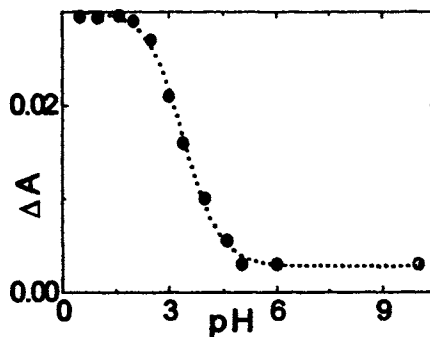


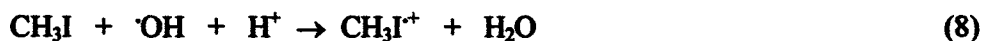
Figure 4. Variation of absorbance at 415 nm formed on pulse radiolysis of aerated aqueous solution of  $\text{CH}_3\text{I}$  ( $8 \times 10^{-3} \text{ mol dm}^{-3}$ ) as a function of pH.



The same is true for 1,n-bromochloroalkanes. (4)  $C_2H_5I$  on reaction with  $\cdot OH$  radicals showed absorption bands in 310 and 350 nm region whereas in  $CF_3CH_2I$ , the absorption is observed only below 280 nm (Fig 1b).

## 2.5 Reaction with alkyl halides in acidic solutions

In acidic aqueous solutions of alkyl iodides, the transient absorption spectrum obtained on reaction of  $\cdot OH$  radicals is observed to depend on the solute concentration. In dilute solutions of  $CH_3I$  ( $1 \times 10^{-4} \text{ mol dm}^{-3}$ ,  $pH = 3$ ), the transient absorption spectrum (Fig 3a) is assigned to the solute radical cation equation (8). The bimolecular rate constant for the reaction of  $\cdot OH$  radicals with



$CH_3I$  to form a solute radical cation is determined by formation kinetic studies at 310 nm and the value is  $4.5 \times 10^9 \text{ dm}^3 \text{ mol}^{-1} \text{ s}^{-1}$ . The competition kinetic studies using KSCN as the standard solute also gave similar value ( $5.2 \times 10^9 \text{ dm}^3 \text{ mol}^{-1} \text{ s}^{-1}$ ). The molar absorptivity at 310 nm is determined to be  $3.9 \times 10^3 \text{ dm}^3 \text{ mol}^{-1} \text{ cm}^{-1}$ . As the solute concentration is increased, the transient absorption at 310 nm decreased (Fig 3b) with a simultaneous increase in the absorbance at 415 nm (Fig 3b). The absorption at 415 nm saturated at  $8 \times 10^{-3} \text{ mol dm}^{-3}$ . At this concentration, only one band at 415 nm is observed (Fig 3c). Since the

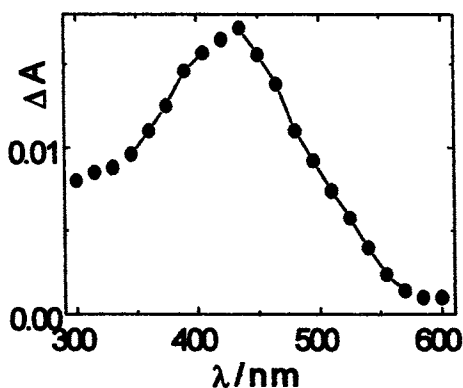


Figure 5. Transient absorption spectrum obtained on pulse radiolysis of aerated acidic [ $HClO_4 = 7.8 \text{ mol dm}^{-3}$ ] aqueous solution of  $C_3H_7Br$  ( $1.2 \times 10^{-2} \text{ mol dm}^{-3}$ ).

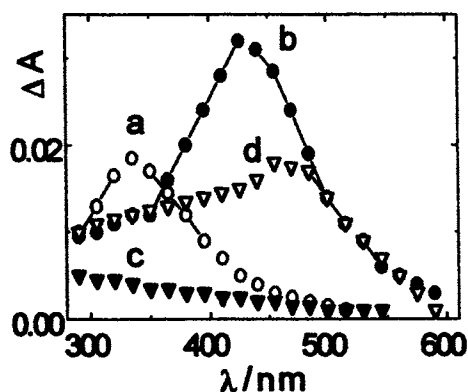


Figure 6. Transient absorption spectrum obtained on pulse radiolysis of aerated acidic aqueous solution of ( $ClC_3H_2I = 1.2 \times 10^{-4} \text{ mol dm}^{-3}$ ,  $pH = 2$ ) - (a); ( $ClC_3H_2I = 6 \times 10^{-3} \text{ mol dm}^{-3}$ ,  $HClO_4 = 6 \text{ mol dm}^{-3}$ ) - (b); ( $ClCH_2I = 4 \times 10^{-3} \text{ mol dm}^{-3}$ ,  $pH = 2$ ) - (c) and ( $ClCH_2I = 4 \times 10^{-3} \text{ mol dm}^{-3}$ ,  $HClO_4 = 6 \text{ mol dm}^{-3}$ ) - (d).

Table 2

Kinetic parameters of the transient species formed on reaction of  $\cdot\text{OH}$  radicals with alkyl halides in acidic aqueous solution

RX	$\text{RX}^+$			$(\text{RX})_2^{+\cdot}$		
	$\lambda_{\text{max}}/\text{nm}$	$k_f/10^9$ $\text{dm}^3\text{mol}^{-1}\text{s}^{-1}$	$\epsilon/10^3$ $\text{dm}^3\text{mol}^{-1}\text{cm}^{-1}$	$\lambda_{\text{max}}/\text{nm}$	$k_f/10^9$ $\text{dm}^3\text{mol}^{-1}\text{s}^{-1}$	$\epsilon/10^3$ $\text{dm}^3\text{mol}^{-1}\text{cm}^{-1}$
$\text{CH}_3\text{I}$	310	4.8	3.9	415	3.5	6
$\text{IC}_4\text{H}_9\text{I}$	435 <sup>a</sup>	—	4.7	—	—	—
$\text{C}_2\text{H}_5\text{Br}$	—	—	—	410	—	6.7
$\text{BrC}_4\text{H}_9\text{Br}$	400 <sup>b</sup>	6.5	4.8	—	—	—
$\text{C}_3\text{F}_7\text{I}$	—	—	—	420	—	—
$\text{CF}_3\text{CH}_2\text{I}$	340	—	—	435	1.7	—
$\text{BrC}_2\text{H}_4\text{Cl}$	—	—	—	430	4.5	—
$\text{BrC}_4\text{H}_9\text{Cl}$	380 <sup>c</sup>	—	—	—	—	—
$\text{BrC}_4\text{H}_9\text{I}$	440 <sup>d</sup>	2.2	—	—	—	—
$\text{ClC}_4\text{H}_9\text{I}$	420 <sup>e</sup>	3.5	5.5	—	—	—
$\text{ClC}_3\text{H}_7\text{I}$	—	—	—	430	2.1	—
$\text{ClC}_3\text{H}_6\text{I}$	345	—	—	430	—	—

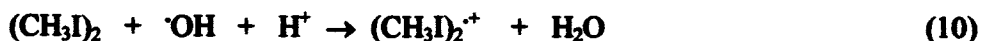
a- intra-molecular monomer radical cation ;  $\text{I}\cdot\text{I}^+$ ; b- intra-molecular monomer radical cation ;  $\text{Br}\cdot\text{Br}^+$ ; c- intra-molecular monomer radical cation ;  $\text{Br}\cdot\text{Cl}^+$ ; d- intra-molecular monomer radical cation ;  $\text{Br}\cdot\text{I}^+$ ; e- intra-molecular monomer radical cation ;  $\text{I}\cdot\text{Cl}^+$

absorbance and the life time of this band was observed to increase with solute concentration, it is assigned to dimer radical cation formed according to the following equilibrium.



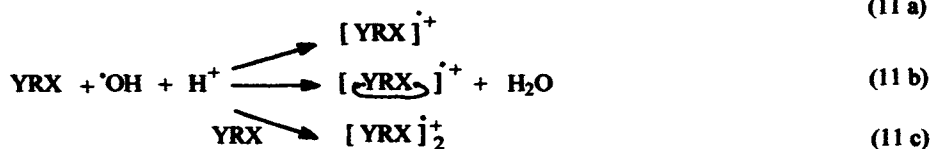
The assignment of solute monomer and dimer radical cation has been assessed from conductivity and electron transfer studies. The bimolecular rate constant for the reaction of  $\cdot\text{OH}$  radical with  $\text{CH}_3\text{I}$ , forming a dimer radical cation is determined by formation kinetic studies at 415 nm and the value is  $3.5 \times 10^9 \text{ dm}^3 \text{ mol}^{-1} \text{ s}^{-1}$ . The competition kinetic studies using KSCN as the standard solute also gave similar results. The formation of 415 nm band was not observed to follow the decay of 310 nm band, indicating that dimer radical cations are formed in the overall reaction (9) and not on decay of  $\text{CH}_3\text{I}^+$ . The variation of absorbance at 415 nm as a function of pH (Fig 4) gave an inflection point at pH

= 3.5. Since the absorbance at 415 nm reached saturation when the solute concentration was in the range of  $(6 - 8) \times 10^{-3} \text{ mol dm}^{-3}$ , the molar absorptivity at 415 nm was calculated to be  $6 \times 10^3 \text{ dm}^3 \text{ mol}^{-1} \text{ cm}^{-1}$ . At high solute concentration,  $\cdot\text{OH}$  radicals can react with  $\text{CH}_3\text{I}$  in acidic solutions according to reaction (9) or with solute dimers according to reaction (10). The pulse radiolysis of acidic aqueous solution of  $\text{CH}_3\text{I}$  has not shown any variation in the nature of the transient spectrum in the presence of benzene, which is known to affect the aggregation of  $\text{CH}_3\text{I}$ , and thus excluding the possibility of reaction (10).



The pulse radiolysis studies in acidic aqueous solutions have been carried out for a variety of alkyl halides (Figs 5, 6, Table 2). It is observed that the nature of the  $\cdot\text{OH}$  radical reaction depends (1) on the nature of halogen. Alkyl iodides form monomer and dimer radical cations in low and high solute concentrations respectively (Fig 4). Alkyl bromides form only dimer radical cations (Fig 5). The transient absorption in 300 - 700 nm region was not observed with alkyl chlorides. (2) In the presence of an additional halogen atom, the nature of the  $\cdot\text{OH}$  radical reaction depends not only on the nature of halogen but also on the relative distance between two halogens. In the case of 1,n-diiodoalkanes and 1,n-dibromoalkanes, intra-molecular monomer radical cation is observed only when the chain length between two halogen atoms ( $n = 3 - 5$ ) provide appreciable p-orbital overlap. In the absence of sufficient p-orbital overlap ( $n \leq 2, > 5$ ), dimer radical cation is observed instead of intra-molecular monomer radical cation. (3) The site of radical cation, in alkylhalides containing two different halogen atoms, is the halogen with lower electronegativity i.e., iodine in the case of chloroiodoalkanes and bromoiodoalkanes and bromine in bromo chloroalkanes. (4) Intra-molecular monomer radical cation between two dissimilar halogen atoms is formed if sufficient p-orbital overlap is provided and the difference in the electronegativity between two halogen atoms is small. Alternatively, dimer radical cations are formed (Table 2). (5) The concentration of  $\text{H}^+$  required for the acid-catalyzed oxidation of alkyl halides is found to depend on the electronegativity of the halogen. The solute radical cations of alkyl iodides are observed at  $\text{pH} < 3$  whereas in the case of alkyl bromides, it was possible only when  $[\text{HClO}_4] > 2 \text{ mol dm}^{-3}$ . The required concentration of  $\text{H}^+$  is also observed to depend on the chain length. Lower concentration of  $\text{H}^+$  is required for the oxidation of  $\text{C}_4\text{H}_9\text{Br}$  as compared to  $\text{C}_2\text{H}_5\text{Br}$ . The required

concentration of  $H^+$  increases if the solute contains more than one halogen atom. Based on these results, acid catalyzed oxidation of alkyl halides can be represented by equation (11) and is discussed below.



X = I, Br ; Y = H, I, Br, Cl

### Scheme 2

(1) Alkyl iodides result in the formation of iodine-centered monomer, dimer radical cation at low and high solute concentration respectively (equations 11a, 11c). (2) Intra-molecular radical cations are formed with 1,n-diiodoalkanes and 1,n-dibromoalkanes (equation 11b). (3) Iodine-centered intra-molecular radical cation is formed with chlorine and bromine if sufficient orbital overlap is provided between oxidized iodine and the other halogen atom (equation 11b). (4) Bromine-centered intra-molecular radical cation is formed between oxidized bromine and chlorine under favorable conditions (equation 11b). The equilibrium, in the formation of radical cation of alkyl halides is affected by the

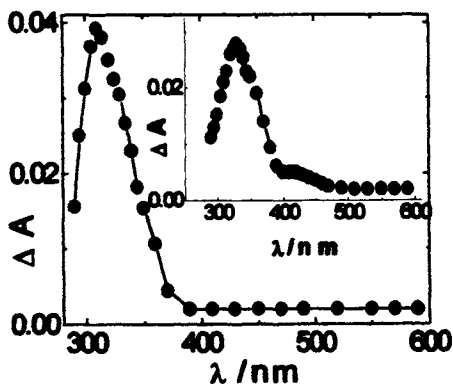


Figure 7. Transient optical absorption spectra obtained on pulse radiolysis of  $N_2O$ -saturated neutral aqueous solution ( $1 \times 10^{-3}$  mol  $dm^{-3}$ ) of 1-fluoro-4-iodobenzene and of 1-chloro-3-iodobenzene in the inset.

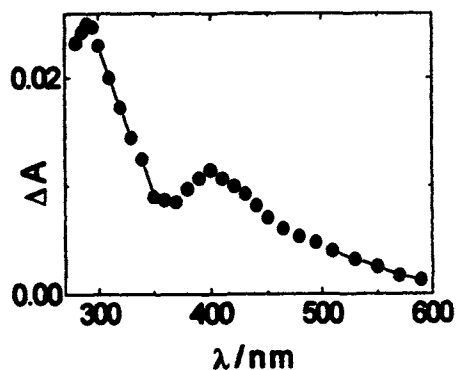


Figure 8. Transient optical absorption spectrum obtained on pulse radiolysis of  $N_2O$ -saturated neutral aqueous solution of pentafluoroiodobenzene ( $1 \times 10^{-3}$  mol  $dm^{-3}$ ).

Table 3

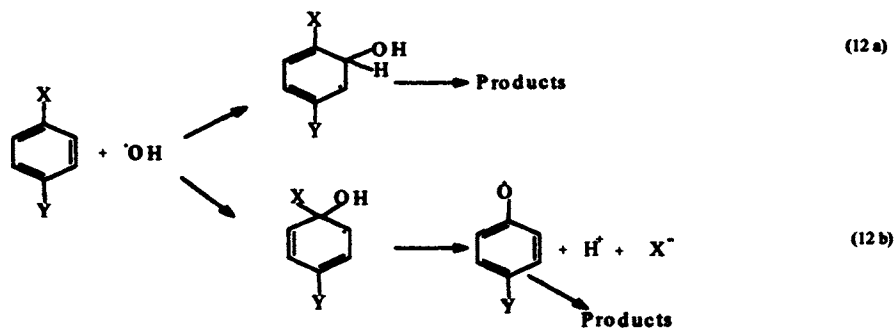
Kinetic and spectral parameters of the OH-adduct formed on reaction of  $\cdot\text{OH}$  radicals with halogenated benzenes in  $\text{N}_2\text{O}$ -saturated neutral aqueous solution

Solute	$\lambda_{\text{max}}$ / nm	$k /$ $10^9 \text{ dm}^3$ $\text{mol}^{-1} \text{ s}^{-1}$	$\sigma_{\text{cal}}$	probable site of $\cdot\text{OH}$ attack	$\epsilon / 10^3$ $\text{dm}^3 \text{ mol}^{-1}$ $\text{cm}^{-1}$	$2k / 10^9$ $\text{dm}^3 \text{ mol}^{-1}$ $\text{s}^{-1}$
$\text{C}_6\text{H}_5\text{F}$	310	5.7	-0.07	4	3.2	1.1
$\text{C}_6\text{H}_5\text{Cl}$	330	3.2	0.11	4	6.2	1.0
$\text{C}_6\text{H}_5\text{Br}$	325	5.2	0.15	4	4.5	2.2
$\text{C}_6\text{H}_5\text{I}$	325	2.7	0.14	4	4.5	3.4
$\text{CH}_3\text{C}_6\text{H}_4\text{Cl}$ (2)	325	6.5	-0.17	2	3.6	5.0
$\text{CH}_3\text{C}_6\text{H}_4\text{Cl}$ (3)	330	3.5	-0.11	4	4.2	1.1
$\text{CH}_3\text{C}_6\text{H}_4\text{Cl}$ (4)	310	5.5	-0.31	4	4.0	4.7
$\text{C}_6\text{H}_4\text{Cl}_2$ (1,2)	325	2.5	0.2	1,2	—	—
$\text{C}_6\text{H}_4\text{Cl}_2$ (1,3)	330	2.2	0.31	4,6	—	—
$\text{CH}_3\text{C}_6\text{H}_3\text{Cl}_2$ (3,4)	325	1.7	-0.11	4	1.4	0.6
$\text{CH}_3\text{C}_6\text{H}_3\text{Cl}_2$ (2,6)	320	2.5	0.23	2,6	—	—
$\text{OCH}_3\text{C}_6\text{H}_4\text{Cl}$ (3)	340	9.3	-0.58	4	5.1	3.7
$\text{CH}_2\text{ClC}_6\text{H}_3\text{Cl}_2$ (3,4)	330	2.5	0.34	4	3.5	1.8
$\text{CHCl}_2\text{C}_6\text{H}_3\text{Cl}_2$ (2,6)	325	4.9	—	—	1.5	0.7
$\text{CF}_3\text{C}_6\text{H}_4\text{Cl}$ (3)	320	2.0	0.72	4	2.7	0.7
$\text{ClC}_6\text{H}_4\text{COCl}$ (2)	315	4.1	0.1	5	2.8	1.9
$\text{CH}_3\text{C}_6\text{H}_4\text{Br}$ (2)	330	1.7	-0.17	2	—	—
$\text{CH}_3\text{C}_6\text{H}_4\text{Br}$ (3)	330	4.9	-0.10	4	5.3	2.3
$\text{CH}_3\text{C}_6\text{H}_4\text{Br}$ (4)	315	2.9	-0.31	5	—	—
$\text{C}_6\text{H}_4\text{Br}_2$ (1,2)	330	2.3	0.21	1,2	—	—
$\text{C}_6\text{H}_4\text{Br}_2$ (1,3)	330	1.9	0.36	4,6	—	—
$\text{C}_6\text{H}_4\text{Br}_2$ (1,4)	325	2.8	0.15	1,4	—	—
$\text{CH}_3\text{C}_6\text{H}_4\text{I}$ (2)	325	1.7	-0.17	2	2.1	1.1
$\text{CF}_3\text{C}_6\text{H}_4\text{I}$ (2)	325	0.8	—	—	2.4	1.3
2-Cl-6-F- $\text{C}_6\text{H}_3\text{CH}_3$	330	4.2	0.4	2	2.9	3.1
1-Cl-3-F- $\text{C}_6\text{H}_4$	320	4.8	0.13	6	3.0	3.1
1-Br-2-Cl- $\text{C}_6\text{H}_4$	330	2.0	0.2	1	3.2	1.6
1-Br-3-F- $\text{C}_6\text{H}_4$	310	3.5	—	—	2.8	2.5
1-F-3-I- $\text{C}_6\text{H}_4$	315	3.0	0.14	4	—	—
1-F-4-I- $\text{C}_6\text{H}_4$	310	4.2	-0.07	4	4.2	3.4
1-Br-3-Cl- $\text{C}_6\text{H}_4$	325	2.3	0.32	6	—	—
1-Br-4-Cl- $\text{C}_6\text{H}_4$	320	2.9	0.11	1	—	—
1-Br-4-I- $\text{C}_6\text{H}_4$	325	2.6	0.14	1	1.6	0.9
1-Cl-4-I- $\text{C}_6\text{H}_4$	320	3.0	0.11	4	2.5	0.8
1-Br-2-F- $\text{C}_6\text{H}_4$	315	4.1	0.21	2	3.0	2.6
1-F-2-I- $\text{C}_6\text{H}_4$	310	3.2	0.14	3	2.1	2.9
1-Cl-2-F- $\text{C}_6\text{H}_4$	305	2.1	0.2	2	—	—

nature of halogen. High concentrations of  $H^+$  are required for halogens with higher electronegativity. At low  $H^+$  concentration, hydration of solute radical cation is very fast and solute radical cations are not observed.

## 2.6 Reaction with aromatic halides in neutral solutions

The reaction of  $\cdot OH$  radicals in the neutral aqueous solutions of halogenated benzenes showed the formation of a transient optical absorption band with  $\lambda_{max}$  in 300 - 340 nm region (Fig 7, Table 3). The transient optical absorption spectrum was not observed in the presence of t-butanol ( $0.5 \text{ mol dm}^{-3}$ ), an efficient  $\cdot OH$  radical and weak  $\cdot H$  atom scavenger, indicating that the transient absorption spectra (Figs 7, 8, Table 3) are due to the reaction of  $\cdot OH$  radicals with the solute and the contribution of  $\cdot H$  atom reaction is negligible. The bimolecular rate constant for the reaction of  $\cdot OH$  radicals with halogenated benzenes was determined by monitoring the growth of the transient absorption at  $\lambda_{max}$  as a function of solute concentration  $(1 - 8) \times 10^{-4} \text{ mol dm}^{-3}$  and the value was in the range of  $(1 - 8) \times 10^9 \text{ dm}^3 \text{ mol}^{-1} \text{ s}^{-1}$ . The absorbance remained independent of solute concentration  $(0.6 - 2) \times 10^{-3} \text{ mol dm}^{-3}$ , indicating that the entire yield of  $\cdot OH$  radicals have reacted with the solute. The molar absorptivity of the transient species is in the range of  $(1.5 - 6.2) \times 10^3 \text{ dm}^3 \text{ mol}^{-1} \text{ cm}^{-1}$ . The band was observed to decay by second order kinetics with a bimolecular rate constant ( $2k$ ) in the range of  $(0.6 - 5) \times 10^9 \text{ dm}^3 \text{ mol}^{-1} \text{ s}^{-1}$ . In most cases, only one transient absorption band with  $\lambda_{max}$  in 300 - 340 nm region (Table 3) is observed. The band is assigned to the OH-adduct formed on addition of  $\cdot OH$  radical to the benzene ring forming a cyclohexadienyl radical (12a, scheme 3) [77,80,89-91,124-130].



$X = Y = H, Cl, Br, I$   
Scheme 3

Table 4

Kinetic and spectral parameters of the OH-adduct formed on reaction of  $\cdot\text{OH}$  radicals with halogenated benzenes in  $\text{N}_2\text{O}$ -saturated neutral aqueous solution

Solute	$\lambda_{\text{max}} / \text{nm}$	$k / 10^9 \text{ dm}^3 \text{ mol}^{-1} \text{ s}^{-1}$	$\sigma_{\text{cal}}$	probable site of $\cdot\text{OH}$ attack	$\epsilon / 10^3 \text{ dm}^3 \text{ mol}^{-1} \text{ cm}^{-1}$	$2k / 10^9 \text{ dm}^3 \text{ mol}^{-1} \text{ s}^{-1}$
1-Br-2-I- $\text{C}_6\text{H}_4$	320	1.7	0.21	1,2	2.9	4.6
1-Cl-4-F- $\text{C}_6\text{H}_4$	300	4.5	-0.07	1	4.4	2.2
1-Br-3-I- $\text{C}_6\text{H}_4$	330	2.8	0.21	1	2.9	1.6
1-Cl-2-I- $\text{C}_6\text{H}_4$	320	2.7	0.20	2	3.3	3.9
1-Cl-3-I- $\text{C}_6\text{H}_4$	330	2.1	0.32	4	3.0	1.5
$\text{C}_6\text{F}_5\text{I}$	290,400	1.2	---	---	3.0 <sup>a</sup>	5.2

a- 290 nm

The addition of  $\cdot\text{OH}$  radicals at the ipso position would result in the formation of phenoxyl radical and halide ion (12b, scheme 3). The phenoxyl radicals have absorption in 360 - 430 nm region [77] and the small absorption observed in this region on reaction of  $\cdot\text{OH}$  radicals with 1-chloro-3-iodobenzene (inset of Fig 7) may be due to the formation of phenoxyl radical. The absorption in this region is observed only for halogenated benzenes shown in Table 4. Using the molar absorptivity of the phenoxyl radicals at  $\lambda_{\text{max}} = 1.5 \times 10^3 \text{ dm}^3 \text{ mol}^{-1} \text{ cm}^{-1}$ , the maximum fraction of  $\cdot\text{OH}$  radicals forming phenoxyl radicals was for 1-chloro-3-iodobenzene (~ 20%). For other derivatives, it was much less, except for  $\text{C}_6\text{F}_5\text{I}$  for which only phenoxyl radicals were formed. In the case of pentafluoroiodobenzene, the transient absorption spectrum showed bands at 290 and 400 nm (Fig 8) and were quite different from those obtained for other halogenated benzenes (Table 3). In this case, addition of  $\cdot\text{OH}$  radical at any position would result in the formation of phenoxyl radicals. Hexafluoro benzene has also shown the formation of phenoxyl radicals alone in contrast to the formation of OH-adduct with monofluoro benzene.

The hydroxyl radicals behave as an electrophile and the substituent effect can be correlated by the Hammett equation. It is reported that the ortho and para positions are more favored for  $\cdot\text{OH}$  radical attack with substituted benzenes [124-128]. The algebraic sum of the Hammett constants ( $\sigma_{\text{p}}^+$  or  $\sigma_{\text{m}}^+$ ) for para and meta substituents and Taft's constant ( $\sigma^*$ ) for ortho substituent has been used to determine the more probable site of  $\cdot\text{OH}$  radical attack where  $\sigma$  value ( $\sigma_{\text{cal}}$ ) is expected to be minimum [105-108]. The minimum  $\sigma_{\text{cal}}$  values for

different compounds are shown in Table 3. The distribution pattern for  $\cdot\text{OH}$  radical attack can be estimated by assuming that the site with maximum  $\sigma$  value has zero probability and the site with minimum  $\sigma$  value has more probable site of attack. However, only from steady state analysis of product distribution, direct evidence for the probable site of  $\cdot\text{OH}$  radical attack can be obtained. The rate constant values for diffusion-controlled reactions are not normally expected to obey the Hammett relationship as was seen from the leveling of  $\log k$  vs  $\sigma_{\text{cal}}$  plot for the oxidation of OH-adduct by  $\text{IrCl}_6^{2-}$  and  $\text{Fe}(\text{CN})_6^{3-}$ . A good linear relationship is observed only for  $\log k$  values between 9.3 and 9.5 and the slope ( $\rho^+$ ) calculated from the Hammett plot is found to be between -0.4 and -0.6. The plot of  $\log k$  vs  $\sigma_{\text{cal}}$  values (Fig 9) for different compounds (Table 3) has not shown a good linear relationship in the entire range. However, in a narrow range of  $\log k$  value between 9.3 and 9.5, the slope ( $\rho^+$ ) was calculated to be -0.6, which is in good agreement with the reported values of -0.52, -0.5, -0.4 for some of the substituted benzenes [121, 124-126]. For  $\log k$  values  $> 9.5$ , the linear relationship was not good indicating that the Hammett relationship is not valid in this region and  $\log k$  values remained nearly independent of  $\sigma_{\text{cal}}$  values.

### 2.7 Reaction with aromatic halides in acidic solutions

In spite of the high oxidation potential of  $\cdot\text{OH}$  radicals (2.8 V vs NHE at pH = 0), one-electron oxidation has been reported only for the compounds containing electron releasing substituents [110, 129-135]. Even in the reaction with  $\text{SO}_4^{\cdot-}$ ,

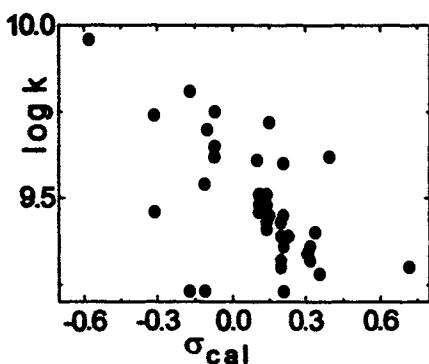


Figure 9. Variation of  $\log k$  vs  $\sigma_{\text{cal}}$  for various halogenated aromatic compounds (Table 3).

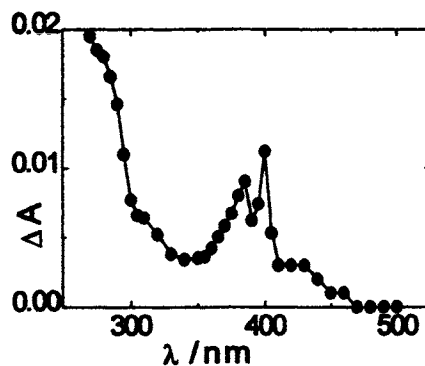


Figure 10. Transient optical absorption spectrum obtained on pulse radiolysis of aerated acidic ( $\text{HClO}_4 = 5.9 \text{ mol dm}^{-3}$ ) aqueous solution of fluorobenzene ( $1 \times 10^{-3} \text{ mol dm}^{-3}$ ).



the radical cation is not stable and undergoes hydration to form the OH-adduct. The main reason for not observing the radical cation of halogenated aromatic compounds is due to the fact that the hydration of the radical cation is a veryfast process under normal pH conditions. On the basis of the photoionization studies on benzene, the lifetime of the benzene radical cation was estimated to be  $\sim 20$  ns [110]. In the presence of electron-donating substituents, ( $-\text{CH}_3$ ) the lifetime of the radical cation of toluene is 30 ns at pH = 5 - 6 and increases at lower pH. With methoxy substituents, the stability of the radical cation is high enough and it could be observed even at pH = 6 - 7 [130, 159]. Considering the increase in the lifetime of the radical cation at lower pH, we have carried out the pulse radiolysis studies of halogenated benzenes, in highly acidic solutions, and the transient absorption bands observed in the visible region were assigned to the solute radical cation. The acid-catalyzed dehydration of the OH-adduct of halogenated benzenes ( $\text{C}_6\text{H}_5\text{X}$ ; X = F, Cl, Br, I) showed the formation of transient optical absorption bands with  $\lambda_{\text{max}} = 630$  (I), 550 (Br), 475 (Cl), 395 nm (F) and assigned to solute radical cation (Figs 10 - 13) (scheme 4). In the presence of high  $\text{H}^+$  concentration, the reaction (13) shifts towards right and the solute radical cation is stabilized. The yield of the radical cation was observed to increase with  $[\text{H}^+]$  reaching a saturation value at high  $[\text{H}^+]$  and the amount of  $\text{H}^+$  concentration required for the acid-catalyzed dehydration of OH-adduct was observed to depend on the electronegativity of the halogen. For  $\text{C}_6\text{H}_5\text{I}$ , the saturation value was attained at pH = 1 and for  $\text{C}_6\text{H}_5\text{Br}$ , it was observed when

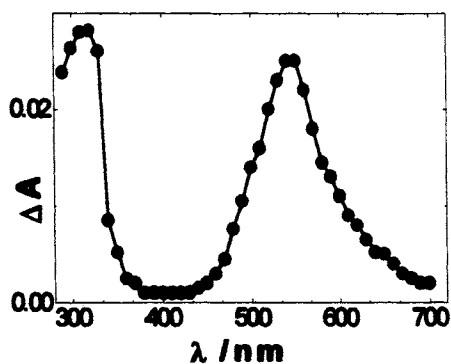


Figure 11. Transient optical absorption spectrum obtained on pulse radiolysis of aerated acidic ( $\text{HClO}_4 = 7.8 \text{ mol dm}^{-3}$ ) aqueous solution of bromobenzene ( $1 \times 10^{-3} \text{ mol dm}^{-3}$ ).

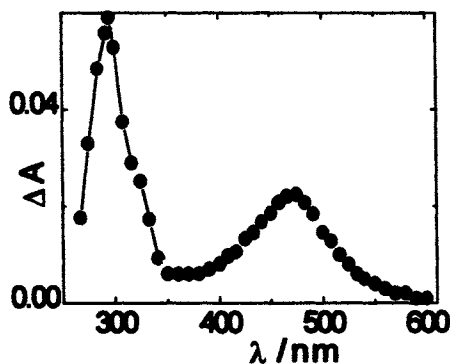
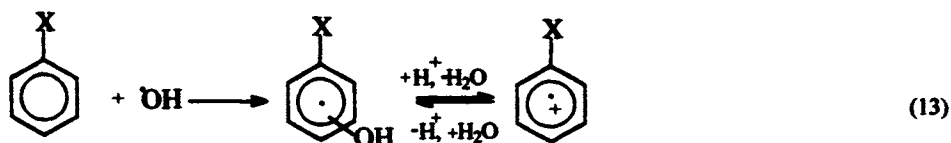


Figure 12. Transient optical absorption spectrum obtained on pulse radiolysis of aerated acidic ( $\text{HClO}_4 = 7.8 \text{ mol dm}^{-3}$ ) aqueous solution of chlorobenzene ( $1 \times 10^{-3} \text{ mol dm}^{-3}$ ).

$\text{HClO}_4$  concentration was close to  $10 \text{ mol dm}^{-3}$ . For  $\text{C}_6\text{H}_5\text{Cl}$ , the saturation value could not be attained even at the highest available concentration of  $\text{HClO}_4$ . Although the electronegativity of fluorine is very high (4.1 eV), the concentration of  $\text{HClO}_4$  required ( $2 \text{ mol dm}^{-3}$ ) for the acid-catalyzed dehydration of OH-adduct of  $\text{C}_6\text{H}_5\text{F}$  and the concentration of  $\text{HClO}_4$  for the saturation value ( $6 \text{ mol dm}^{-3}$ ) was low and does not follow the linear relationship (Fig 14) [160]. The unusual behavior of fluorine may be due to strong electron withdrawing by the field inductive effect and the weak electron pair donating nature [69,87,161,162].



X = F, Cl, Br, I  
Scheme 4

The formation of transient absorption bands on pulse radiolysis of aqueous solutions of halogenated organic compounds in highly acidic conditions is due to the reaction of  $\cdot\text{OH}$  radical with the solute and not due to any other factors as discussed below. (1) The transient absorption bands were not observed in the presence of t-butanol, an efficient  $\cdot\text{OH}$  radical scavenger. (2) The bands are not

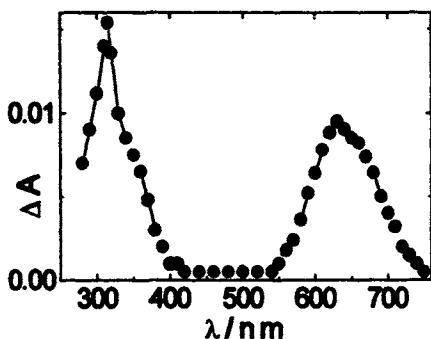


Figure 13. Transient optical absorption spectrum obtained on pulse radiolysis of aerated acidic (pH = 1) aqueous solution of iodobenzene ( $1 \times 10^{-3} \text{ mol dm}^{-3}$ ).

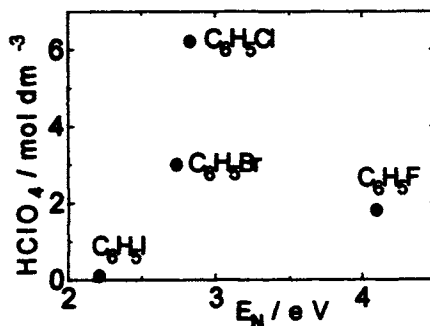


Figure 14. Variation of  $[\text{HClO}_4]$  required for the acid catalyzed dehydration of OH-adduct of halogenated benzenes as a function of electronegativity of halogen.

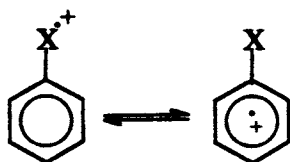
due to the transient species generated from radiolysis of  $\text{HClO}_4$ , as these species have absorption at 350 nm. Pulse radiolysis of concentrated acidic solutions of  $\text{HClO}_4$  had shown the formation of transient absorption band with low yield and molar absorptivity and were assigned to  $\text{ClO}_3$  radicals [163, 164]. The transient bands were also not observed in the absence of the solute.  $\text{HClO}_4^{\cdot+}$  with  $\lambda_{\text{max}} = 440$  nm is formed only when  $[\text{HClO}_4]$  was more than  $10 \text{ mol dm}^{-3}$ . (3) These bands are also not due to the reaction of these species with halogenated organic compounds as the transient bands of solute radical cations were also generated in the presence of an other acid ( $\text{H}_2\text{SO}_4$ ). (4) The halogenated organic compounds are stable in highly acidic conditions within the experimental time. (5) The reaction of the transient absorption bands generated from halogenated organic compounds showed electron transfer reactions with inorganic ions, confirming the cationic nature of the transient absorption bands. (6) The bands are neither due to  $\cdot\text{H}/\text{HO}_2$  radicals nor due to their reaction with the solute, as the studies in the presence of t-butanol have not shown the formation of any transient absorption bands and  $\cdot\text{H}/\text{HO}_2$  radicals absorb well below 300 nm [41]. The redox potential value of the  $\text{HO}_2$  radicals is quite low ( $\sim 1.0$  V) and even stronger one-electron oxidants failed to produce one-electron oxidation of the halogenated organic compounds [165]. (7) The bands are not due to the high ionic strength of  $\text{HClO}_4$  as the transient absorption bands were not produced on pulse radiolysis of neutral aqueous solution of  $\text{NaClO}_4$  ( $7.8 \text{ mol dm}^{-3}$ ) containing low concentration of halogenated organic compounds. (8) The transient absorption bands are due to solute radical cations as similar transient absorption spectra were also observed on matrix isolation studies of halogenated benzenes in 3-methyl pentane at 77 K and also in 1,2-dichloroethane [166].

Pulse radiolysis of aerated acidic aqueous solution of benzene showed the formation of a transient absorption band at 310 nm with a broad absorption in 350 - 500 nm region [167]. Although the position of the main band at 310 nm matched with that observed in neutral solutions, the redox properties were different and it is assigned to solute radical cation. The radical cation site of these aromatic compounds is expected to be the halogen atom as the position of the absorption maxima was very different and a different concentration of  $\text{HClO}_4$  was required in each case. It is possible that halogen centered radical cation may then undergo resonance stabilization with the aromatic ring (equation 14, scheme 5). The OH-adduct of halogenated benzenes was observed to undergo acid-catalyzed dehydration to form the solute radical cation. Unlike OH-adduct formed in neutral solutions, the nature of the transient optical absorption spectrum formed in acidic solutions was observed to depend on the

Table 5

Kinetic and spectral parameters of the radical cation formed on reaction of  $\cdot\text{OH}$  radicals with halogenated benzenes in aerated acidic ( $\text{HClO}_4 = 7.8 \text{ mol dm}^{-3}$ ) aqueous solution

Solute	$\lambda_{\text{max}} / \text{nm}$	$k / 10^9 \text{ dm}^3 \text{ mol}^{-1} \text{ s}^{-1}$	$G\epsilon / 10^4 \text{ dm}^3 \text{ mol}^{-1} \text{ cm}^{-1}$	Minimum $[\text{HClO}_4]$ for radical cation formation / $\text{mol dm}^{-3}$
$\text{C}_6\text{H}_5\text{F}$	395	6.1	—	1.8
$\text{C}_6\text{H}_5\text{Cl}$	295, 475	1.7	1.33	6.1
$\text{C}_6\text{H}_5\text{Br}$	320, 550	8.9	1.63	3.1
$\text{C}_6\text{H}_5\text{I}$	310, 650	4.7	2.1	0.1
$\text{CH}_3\text{C}_6\text{H}_4\text{Cl}$ (2)	295, 470	2.2	1.14	3.8
$\text{CH}_3\text{C}_6\text{H}_4\text{Cl}$ (3)	295, 495	3.2	1.20	3.6
$\text{CH}_3\text{C}_6\text{H}_4\text{Cl}$ (4)	300, 485	2.0	1.56	4.1
$\text{C}_6\text{H}_4\text{Cl}_2$ (1,2)	315, 520	0.8	1.98	6.5
$\text{C}_6\text{H}_4\text{Cl}_2$ (1,3)	325, 520	1.0	0.72	6.8
$\text{CH}_3\text{C}_6\text{H}_3\text{Cl}_2$ (3,4)	305, 485	2.2	1.08	6.4
$\text{CH}_3\text{C}_6\text{H}_3\text{Cl}_2$ (2,6)	300, 525	2.0	0.81	5.9
$\text{OCH}_3\text{C}_6\text{H}_4\text{Cl}$ (3)	<290, 470	5.1	1.81	3.9
$\text{CH}_2\text{ClC}_6\text{H}_3\text{Cl}_2$ (3,4)	320, 525	1.1	0.60	6.9
$\text{CHCl}_2\text{C}_6\text{H}_3\text{Cl}_2$ (2,6)	320, 530	1.1	0.42	7.2
$\text{CF}_3\text{C}_6\text{H}_4\text{Cl}$ (2)	315, 470	0.7	0.36	7.5
$\text{ClC}_6\text{H}_4\text{COCl}$ (2)	310, 470	1.5	1.07	5.1
$\text{CH}_3\text{C}_6\text{H}_4\text{Br}$ (2)	290, 520	—	1.14	2.1
$\text{CH}_3\text{C}_6\text{H}_4\text{Br}$ (3)	295, 545	3.4	1.26	2.1
$\text{CH}_3\text{C}_6\text{H}_4\text{Br}$ (4)	310, 525	1.3	1.9	1.5
$\text{C}_6\text{H}_4\text{Br}_2$ (1,2)	310, 540	1.3	1.6	5.1
$\text{C}_6\text{H}_4\text{Br}_2$ (1,3)	310, 550	1.1	1.1	5.9
$\text{C}_6\text{H}_4\text{Br}_2$ (1,4)	310, 500	—	0.4	—
$\text{CH}_3\text{C}_6\text{H}_4\text{I}$ (2)	310, 640	1.9	1.7	0.1
$\text{CF}_3\text{C}_6\text{H}_4\text{I}$	320, 650	3.3	1.8	0.1
$\text{C}_6\text{F}_5\text{I}$	310, 660	5.5	—	1.1



$\text{X} = \text{F}, \text{Cl}, \text{Br}, \text{I}$   
Scheme 5

(14)

Table 6

Kinetic and spectral parameters of the radical cation formed on reaction of  $\cdot\text{OH}$  radicals with halogenated benzenes in aerated acidic ( $\text{HClO}_4 = 7.8 \text{ mol dm}^{-3}$ ) aqueous solution

Solute	$\lambda_{\text{max}} / \text{nm}$	$k / 10^9 \text{ dm}^3 \text{ mol}^{-1} \text{ s}^{-1}$
1-Cl-3-F-C <sub>6</sub> H <sub>4</sub>	300, 485	4.5
1-Br-2-I-C <sub>6</sub> H <sub>4</sub>	310, 650	3.2
1-Br-2-Cl-C <sub>6</sub> H <sub>4</sub>	300, 530	4.1
2-Cl-6-F-CH <sub>3</sub> C <sub>6</sub> H <sub>4</sub>	290, 490	2.7
1-Br-3-F-C <sub>6</sub> H <sub>4</sub>	300, 540	2.9
1-F-3-I-C <sub>6</sub> H <sub>4</sub>	310, 650	3.5
1-Br-3-Cl-C <sub>6</sub> H <sub>4</sub>	305, 545	4.2
1-Br-4-Cl-C <sub>6</sub> H <sub>4</sub>	315, 540	5.3
1-Br-4-I-C <sub>6</sub> H <sub>4</sub>	310, 645	4.9
1-Cl-4-I-C <sub>6</sub> H <sub>4</sub>	310, 640	3.8
1-F-4-I-C <sub>6</sub> H <sub>4</sub>	305, 640	2.6
1-Cl-2-I-C <sub>6</sub> H <sub>4</sub>	320, 645	3.9

nature of the halogen and its relative position with respect to the other halogen in dihalogenated benzenes. Pulse radiolysis studies have been carried out for a number of dihalogenated benzenes in acidic aqueous solutions. Table 5 shows the kinetic and spectral parameters for dihalogenated benzenes containing two similar halogen atoms. It is clear from this that (1) the  $[\text{HClO}_4]$  required for the formation of the transient absorption band of the solute radical cation increased with the number of halogen atoms and other electron withdrawing groups ( $\text{CF}_3$ ) present in the molecule. (2) Decreased with the presence of electron donating substituents ( $\text{CH}_3$ ,  $\text{OCH}_3$ ). (3) The bimolecular rate constant values, determined by formation kinetic studies, were observed to vary in  $(0.7 - 5.1) \times 10^9 \text{ dm}^3 \text{ mol}^{-1} \text{ s}^{-1}$ . The nature of the transient absorption spectrum remained same. The transient absorption spectrum obtained on pulse radiolysis of acidic aqueous solution of 2-chloro-benzoylchloride was similar to that obtained for chlorobenzene (Fig 12). Similarly, the transient absorption spectrum of pentafluoroiodobenzene matched with that of iodobenzene (Fig 13). The bimolecular rate constant for the reaction of OH-adduct with  $\text{H}^+$  is very fast and could not be measured, except for fluorobenzene for which the value is  $1.4 \times 10^5 \text{ dm}^3 \text{ mol}^{-1} \text{ s}^{-1}$ . In the case of dihalogenated benzenes containing two different halogens, the nature of the transient absorption spectra depends strongly on the nature of the halogen. Studies carried out on a number of dihalogenated benzenes containing two different halogens (Table 6) revealed that the amount

of  $\text{HClO}_4$  required for the formation of solute radical cation was more than monohalogenated benzene and the position of the transient absorption band matched with the halogen having lower electronegativity. A typical example of the transient absorption spectrum obtained on pulse radiolysis of 1-bromo-2-chlorobenzene, identical to that obtained from bromobenzene, is shown in Fig 15. The transient absorption spectrum similar to that of fluorobenzene could not be obtained from dihalogenated benzene containing fluorine. This could be due to higher electronegativity of fluorine. When out of two halogens, one is fluorine and the other halogen is at the ortho position, the nature of the transient absorption spectrum was different under different acidic conditions. Figure 16 shows the transient absorption spectra obtained on pulse radiolysis of 1-chloro-2-fluorobenzene under two different acidic conditions. At low concentration of  $\text{HClO}_4$  ( $5.9 \text{ mol dm}^{-3}$ ) the transient spectrum is identical to that of fluorobenzene and at high  $\text{HClO}_4$  concentration ( $9.8 \text{ mol dm}^{-3}$ ) the transient spectrum is same to that of chlorobenzene. Dihalogenated benzenes, which showed two different transient absorption spectra under two different acidic conditions are shown in Table 7. The transient absorption spectrum obtained on pulse radiolysis of aerated acidic aqueous solution of 1-fluoro-2-iodobenzene showed the formation of transient absorption band of fluorobenzene (390 nm) and iodobenzene (630 nm) radical cations. The transient absorption bands corresponding to fluorobenzene and chlorobenzene are observed on pulse radiolysis of aerated acidic aqueous solution of 1-chloro-2-fluorobenzene. Although the yield of radical cation of fluorobenzene, observed in the case of 1-fluor-2-iodobenzene is low, the distinct absorption of fluorobenzene radical cation could be seen.

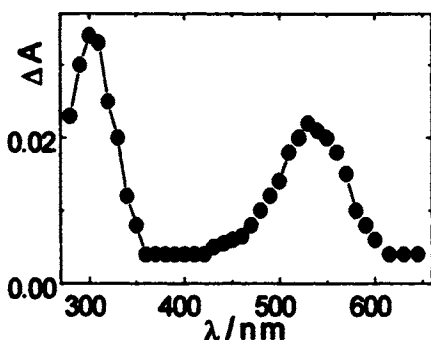


Figure 15. Transient absorption spectrum obtained on pulse radiolysis of aerated acidic ( $\text{HClO}_4 = 7.8 \text{ mol dm}^{-3}$ ) aqueous solution of 1-bromo-2-chlorobenzene ( $2 \times 10^{-3} \text{ mol dm}^{-3}$ )

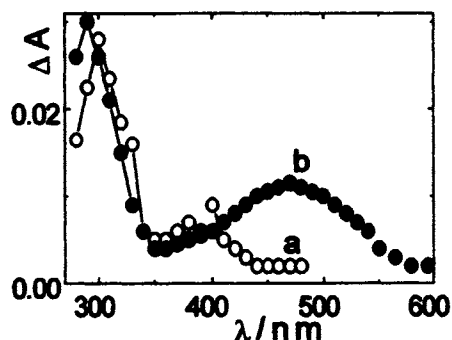


Figure 16. Transient absorption spectra obtained on pulse radiolysis of aerated acidic aqueous solution of 1-chloro-2-fluorobenzene ( $2 \times 10^{-3} \text{ mol dm}^{-3}$ ),  $\text{HClO}_4 = 5.9 \text{ mol dm}^{-3}$  - (a) and  $9.8 \text{ mol dm}^{-3}$  - (b).

**Table 7**  
**Kinetic and spectral parameters of the radical cation formed on reaction of**  
 **$\cdot\text{OH}$  radicals with halogenated benzenes in aerated acidic aqueous solution**

Solute	$\text{HClO}_4 / \text{mol dm}^{-3}$	$\lambda_{\text{max}} / \text{nm}$	$k / 10^9 \text{ dm}^3 \text{ mol}^{-1} \text{ s}^{-1}$
1-Br-2F- $\text{C}_6\text{H}_4$	3.9	310, 380	0.6
	7.8	300, 520	3.1
1-Cl-2-F- $\text{C}_6\text{H}_4$	5.9	305, 395	0.3
	9.8	290, 470	2.5
1-F-2-I- $\text{C}_6\text{H}_4$	0.1	390,	0.2
		310, 620	4.7

### 3 OXIDATION POTENTIAL OF SOLUTE RADICAL CATIONS

The OH-adduct of benzene and substituted derivatives can be oxidized by oxidants such as  $\text{Fe}(\text{CN})_6^{3-}$ . The radical cation of halogenated benzenes are observed to be oxidizing in nature. The transient absorption band of the solute radical cation showed accelerated decay on addition of low concentration of inorganic ions such as  $\text{I}^-$ ,  $\text{Br}^-$ ,  $\text{SCN}^-$  and the bimolecular rate constant values are in the diffusion-controlled limits. One-electron oxidants such as  $\text{I}_2^-$ ,  $\text{Br}_2^-$  failed to undergo electron-transfer reactions with halogenated benzenes. On the other hand, halogenated benzenes are able to transfer electron to strong one-electron oxidants such as  $\text{Cl}_2^-$  and  $\text{SO}_4^-$  and the redox potential value for the radical cations of halogenated benzenes is estimated to be in 2 - 2.4 V range.

### 4 CONCLUSIONS

Hydroxyl radicals are able to undergo electron transfer reaction with halogenated organic compounds in highly acidic conditions. The concentration of the acid required depends directly on the electronegativity of the halogen. In the case of aromatic halogenated compounds, the  $\lambda_{\text{max}}$  of the solute radical cation depends strongly on the nature of the halogen i.e., 630 nm for I, 550 nm for Br, 475 nm for Cl and 395 nm for F. The transient absorption spectrum remains identical in dihalogenated benzenes containing the same halogen atoms. If the halogen atoms are different, the position of the transient absorption band depends strongly on the nature as well as on the relative positions of halogen atoms. The transient absorption band matches with that halogen having lower electronegativity and the transient absorption spectra similar to both the

halogens, under two different conditions, is observed only if one of the halogens is fluorine and is ortho to the other halogen.

In the case of alkyl halides, only iodides and bromides are able to undergo electron-transfer reaction. In contrast, chlorides can not transfer an electron even in highly acidic conditions. Iodine-centered monomer radical cations have well defined absorption band around 310 nm and is able to form dimer radical cation. Bromine-centered monomer radical cations are highly unstable and are converted to dimer radical cation. Oxidized iodine and bromine are able to form an intra-molecular radical cation on p-orbital overlap with another halogens (iodine, bromine, chlorine) under favorable geometrical considerations. The acid-catalyzed oxidation of OH-adduct is a diffusion-controlled process, except for fluorobenzene. In the case of fluorobenzene, the decay of the OH-adduct is affected in the presence of  $H^+$ , accompanied by the formation of the solute radical cation with  $k = 1.4 \times 10^5 \text{ dm}^3 \text{ mol}^{-1} \text{ s}^{-1}$ .

## REFERENCES

1. Z.B. Alfassi, S. Mosseri and P. Neta, *J. Phys. Chem.*, 93 (1989) 1380.
2. S.S. Emmi, G. Beggiato and G. Casalbore-Miceli, *Radiat. Phys. Chem.*, 33 (1989) 29.
3. T. Sumiyoshi, S. Sawamura, Y. Koshikawa and M. Katayama, *Bull. Chem. Soc. Japan.*, 55 (1982) 2346.
4. C.A.M. Vanden Ende, L.H. Luthjens, J.M. Warmen and A. Hummel, *Radiat. Phys. Chem.*, 19 (1982) 455.
5. J. Grodkowski and P. Neta, *J. Phys. Chem.*, 88 (1984) 1205.
6. L.C.T. Shoute and P. Neta, *J. Phys. Chem.*, 94 (1990) 2447.
7. L.C.T. Shoute and P. Neta, *J. Phys. Chem.* 94 (1990) 7181.
8. J. Mönig, D. Bahnemann and K.-D. Asmus, *Chem. Biol. Interact.*, 47 (1983) 15.
9. E.S. Reynolds, M.T. Moslen, *Free Radical in Biology*, W.A. Pryor (ed), Academic Press, New York, 4 (1980) 49.
10. T.F. Slater, *Free Radical, Lipid Peroxidation and Cancer*, D.C.H. McBrien, T.F. Slater (eds), Academic Press, London, 1982.
11. R.O. Recknagel, E.A. Glende and A.M. Hruszkevycz, *Free Radicals in Biology*; W.A. Pryor (ed), Academic Press, New York, 3 (1977) . 97.
12. T.L. McDonald, *CRC Crit. Rev. Toxic.*, 11 (1983) 85.
13. J.E. Packer, J.S. Mahood, R.L. Wilson and B.S. Wolfenden, *Int. J. Radiat. Biol.*, 39 (1981) 135.
14. J.E. Packer, T.F. Slater and R.L. Wilson, *Life Sciences*, 23 (1978) 2617.
15. A. Tomasi, S. Billing, A. Garner, T.F. Slater and E. Albano, *Chem. Biol. Inter.*, 46 (1983) 353.
16. K.-D. Asmus, D. Bahnemann, K. Krischer, M. Lal and J.Mönig, *Life Chem. Rep.*, 3 (1985) 1.
17. J. Mönig and K.-D. Asmus, *J. Chem. Soc., Perkin Trans.,2*, (1984) 2057.
18. M. Lal, J. Mönig and K.-D. Asmus, *Free. Rad. Res. Commun.*, 1 (1986) 235.



19. Y.J. Kime, D.C. Driscoll and P.A. Dowben, *J. Chem. Soc., Faraday Trans.*, 2, 83 (1987) 403.
20. G.I. Khaikin, Z.B. Alfassi and P. Neta, *J. Phys. Chem.*, 99 (1995) 11447.
21. M. Lal, C. Schöneirch, J. Mönig and K.-D. Asmus, *Int. J. Radiat. Biol.*, 54 (1988) 773.
22. H. Mohan and K.-D. Asmus, *J. Chem. Soc., Perkin Trans.*, 2, (1987) 1795.
23. H. Mohan, D.K. Maity and J.P. Mittal, *J. Chem. Soc., Faraday Trans.*, 89 (1993) 477.
24. G. Merga, B.S.M. Rao, H. Mohan and J.P. Mittal, *J. Phys. Chem.*, 98 (1994) 9158.
25. R.W. Holman, C.D. Warner, R.N. Hayes and M.L. Gross, *J. Am. Chem. Soc.*, 112 (1990) 3362.
26. K. Walter, R. Weinkauff, U. Boesi and E.W. Schlag, *Chem. Phys. Letter*, 155 (1989) 8.
27. D.A. Dougherty, *Science*, 271 (1996) 163.
28. H. Koppel, *Chem. Phys. Letter*, 205 (1993) 361.
29. K.-D. Asmus and E. Janata, *The Study of Fast Processes and Transient Species by Electron Pulse Radiolysis*, J.H. Baxendale and F. Busi (eds), D. Reidel, Boston, 1982.
30. J.P. Keene, *Nature*, 188 (1960) 843.
31. E.J. Land, *Primary Photo Processes in Biology and Medicine*, R.V. Bensasson, E.J. Land and T.G. Truscott (eds), NATO, ASI Series, A : Life Sciences, 85 (1985) 35.
32. J.W. Boag and E.J. Hart, *Nature*, 197 (1963) 45.
33. M. Ebert, J.P. Keene, A.J. Swallow and J.H. Baxendale (eds), *Pulse Radiolysis*, Academic Press, London, 1965.
34. M.S. Matheson and L.M. Dorfman, *Pulse Radiolysis*, MIT Press, Cambridge, 1969.
35. R.V. Bensasson, E.J. Land and T.G. Truscott, *Flash Photolysis and Pulse Radiolysis*, Pergamon Press, London, 1983.
36. M.A.J. Rodgers, *Radiation Chemistry*, VHC Publishing Co., New York 1987.
37. C. von Sonntag, *The Chemical Basis of Radiation Biology*, Taylor and Francis, London, 1987.
38. R.V. Bensasson, E.J. Land and T.G. Truscott, *Excited States and Free Radicals in Biology and Medicine*, Oxford University Press, 1993.
39. J. Butler, B.M. Hoey and J.S. Lea, *Free Radicals, Methodology and Concepts*, C. Rice-Evans and B. Halliwell (eds), Richelieu Press, London, 1988.
40. J.W. Spinks and R.J. Woods, *An Introduction to Radiation Chemistry*, John Wiley, New York, 1990.
41. G.L. Hug, NSRDS-NBS 69, Govt. Printing Office, Washington, 1981.
42. G.V. Buxton, C.L. Greenstock, W.P. Helman and A.B. Ross, *J. Phys. Chem. Ref. Data*, 17 (1988) 513.
43. P. Wardman, *J. Phys. Chem. Ref. Data*, 18 (1989) 1637.
44. W.H. Hamill, *Ionic Processes in  $\gamma$ -Irradiated Organic Solids at  $-196^\circ$ , Radical Ions*, L. Kevan (ed), Interscience, New York, (1967) 321.
45. J.E. Willard, *Organic Compounds in the Solis State, Fundamental Processes in Radiation Chemistry*, P. Ausloos (ed), Interscience, N. Y., (1968) 599.
46. M.C.R. Symons, *J. Chem. Soc., Perkin Trans.*, 2, (1974) 1618.
47. B.C. Gilbert, D.K.C. Hodgeman and R.O.C. Norman, *J. Chem. Soc., Perkin Trans.*, 2, (1973) 1748.
48. F.C. Adams, G.E. Smith and A.J. Elliot, *Can. J. Chem.*, 56 (1978) 1856.
49. W. Gordy, *Radiat. Res. Suppl.*, 1 (1959) 491.
50. M. Shirom and J.E. Willard, *J. Phys. Chem.*, 772 (1968) 1702.

51. P. Neta and R.E. Huie, *J. Phys. Chem. Ref. Data*, 17 (1988) 1027.
52. P.S. Rao and E. Hayon, *J. Am. Chem. Soc.*, 96 (1974) 1295.
53. K.I. Priyadarsini, D.B. Naik, P.N. Moorthy and J.P. Mittal, *Proc. 7th Tihany Symposium on Radiation Chemistry, Hungarian Chem. Soc., Budapest, (1991) 105.*
54. S.N. Guha, P.N. Moorthy, K. Kishore, D.B. Naik and K.N. Rao, *Proc. Indian Acad. Sci., (Chem.Sci.)*, 99 (1987) 261.
55. E.M. Fielden, *The Study of Fast Processes and Transient Species by Electron Pulse Radiolysis*, J.H. Baxendale and F. Busi (eds), D. Reidel, Boston, (1984) 59.
56. M.S. Panajkar, P.N. Moorthy and N.D. Shirke, *BARC Report*, 1410 (1988).
57. M.S. Panajkar, P.N. Moorthy and N.D. Shirke, *BARC Report*, 1470 (1989).
58. S.K. Saha and R.M. Iyer, *Radiat. Phys. Chem.*, 36 (1978) 219.
59. P.N. Bajaj, H. Mohan and R.M. Iyer, *Radiat. Phys. Chem.*, 26 (1985) 253.
60. J.P. Mittal and W.H. Hamill, *J. Am. Chem. Soc.*, 89 (1967) 5749.
61. L.C.T. Shoute and J.P. Mittal, *Radiat. Phys. Chem.*, 24 (1985) 459.
62. L.C.T. Shoute and J.P. Mittal, *Spectro. Chimica Acta*, 45A (1989) 863.
63. G. Girija and C. Gopinathan, *Radiat. Phys. Chem.*, 17 (1981) 41.
64. S. Kapoor and C. Gopinathan, *Radiat. Phys. Chem.*, 27 (1986) 199.
65. K.N. Rao and P.N. Moorthy, *National Acad. Sci.*, (1980) 1.
66. H. Mohan, K.N. Rao and R.M. Iyer, *Radiat. Phys. Chem.*, 26 (1985) 57.
67. P.N. Bajaj and R.M. Iyer, *Radiat. Phys. Chem.*, 16 (1980) 21.
68. L.C.T. Shoute and J.P. Mittal, *Radiat. Phys. Chem.*, 24 (1984) 209.
69. L.C.T. Shoute and J.P. Mittal, *Radiat. Phys. Chem.*, 30 (1987) 105.
70. S.R. Hunter, J.G. Carter and L.G. Christophorous, *Chem. Phys.*, 86 (1987) 693.
71. M.B. Yim and D.E. Wood, *J. Am. Chem. Soc.*, 98 (1976) 2053.
72. M.C.R. Symons, R.C. Selby, I.G. Smith and S.W. Bratt, *Chem. Phys. Lett.*, 48 (1977) 100.
73. A.D. Belapurkar and R.M. Iyer, *Radiat. Effect Lett.*, 43 (1979) 25.
74. H. Mohan and R.M. Iyer, *Radiat. Effects*, 39 (1978) 97.
75. J. Shankar, K.V.S. Rao and L.V. Shastri, *J. Phys. Chem.*, 75 (1969) 52.
76. K.V.S.R. Rao, D. Prasad and J. Shankar, *Indian J. Chem.*, 11 (1973) 1045.
77. R. Koster and K.-D. Asmus, *J. Phys. Chem.*, 77 (1973) 749.
78. W.F. Wentworth, R.S. Becker and R. Tung, *J. Phys. Chem.*, 71 (1967) 1652.
79. L.G. Christophorou, M.W. Grant and D.L. McCorkle, *Advances in Chemical Phys.*, I. Prigogine and S.A. Rice (eds), John Wiley, New York, 36 (1977) 413.
80. D. Behar and P. Neta, *J. Am. Chem. Soc.*, 103 (1981) 2280.
81. J.P. Bays, S.T. Blumer, S. Baral-Tosh, D. Behar and P. Neta, *J. Am. Chem. Soc.*, 105 (1983) 320.
82. A.B. Pierini and J.S. Duca, Jr., *J. Chem. Soc., Perkin Trans.*, 2, (1995) 1821.
83. P. Neta and D. Behar, *J. Am. Chem. Soc.*, 103, (1981) 103.
84. L.C.T. Shoute, J.P. Mittal and P. Neta, *J. Phys. Chem.*, 100 (1996) 3016.
85. L.C.T. Shoute and J.P. Mittal, *J. Phys. Chem.*, 100 (1996) 14022.
86. L.C.T. Shoute, J.P. Mittal and P. Neta, *J. Phys. Chem.*, 100 (1996) 11355.
87. L.C.T. Shoute and J.P. Mittal, *J. Phys. Chem.*, 97 (1993) 379.
88. H. Mohan and J.P. Mittal, *J. Phys. Chem.*, 99 (1995) 12559.
89. Z.B. Alfassi, G.I. Khaikin and P. Neta, *J. Phys. Chem.*, 99 (1995) 265.
90. Z.B. Alfassi, S. Marguet and P. Neta, *J. Phys. Chem.*, 98 (1994) 8019.

91. Z.B. Alfassi and L.C.T. Shoute, *Int. J. Chem. Kinetics*, 25 (1993) 79.
92. G.I. Khaikin, Z.B. Alfassi and P. Neta, *J. Phys. Chem.*, 99 (1995) 11447.
93. J.E. Packer, R.L. Wilson, D. Bahnemann and K.-D. Asmus, *J. Chem. Soc., Perkin Trans.*, 2, (1980) 296.
94. Z.B. Alfassi, S. Mosseri and P. Neta, *J. Phys. Chem.*, 91 (1987) 3383.
95. Z.B. Alfassi, R.E. Huie, M. Kumar and P. Neta, *J. Phys. Chem.*, 96 (1992) 767.
96. R. Mertens, C. von Sonntag, *Angew. Chem. Int. Ed. Engl.*, 33 (1994) 1262.
97. P. Neta, R.E. Huie and A.B. Ross, *J. Phys. Chem. Ref. Data.*, 19 (1990) 413.
98. J. Mönig, K. Krischer and K.-D. Asmus, *Chem. Biol. Interact.*, 48 (1983) 43.
99. H. Mohan and P.N. Moorthy, *Radiat. Phys. Chem.*, 36 (1990) 805.
100. H. Mohan and C. Gopinathan, *Radiat. Phys. Chem.*, 36 (1990) 801.
101. S. Kapoor and C. Gopinathan, *Int. J. Chem. Kinetics*, 24 (1992) 1035.
102. P. Neta, R.E. Huie, S. Mosseri, L.V. Shastri, J.P. Mittal, P. Maruthamuthu and S. Steenken, *J. Phys. Chem.*, 93 (1989) 4099.
103. L.C.T. Shoute, Z.B. Alfassi, P. Neta and R.E. Huie, *J. Phys. Chem.*, 98 (1994) 5701.
104. Z.B. Alfassi, R.E. Huie, P. Neta and L.C.T. Shoute, *J. Phys. Chem.*, 94 (1990) 8800.
105. R. Taft, *J. Chem. Phys.*, 26 (1957) 93.
106. R. Taft, *J. Am. Chem. Soc.*, 75 (1953) 4231.
107. J. March, *Advanced Organic Chemistry Reaction Mechanism and Structure*, McGraw Hill, (1968) 241.
108. J. Hine, *Physical Organic Chemistry*, McGraw Hill, (1962) 97.
109. P. Neta and A. Harriman, *Photoinduced Electron Transfer*, M.A. Fox and M. Chanon, (eds), Elsevier, Amsterdam, (1988) 110.
110. S. Steenken, *J. Chem. Soc., Faraday Trans.*, 1, 83 (1987) 113.
111. P. Neta and M. Dorfman, *Adv. Chem. Ser.*, 81 (1968) 222.
112. M.K. Eberhardt, *J. Phys. Chem.*, 79 (1975) 1930.
113. M.K. Eberhardt, *J. Phys. Chem.*, 81 (1977) 1051.
114. M.K. Eberhardt and M.I. Martinez, *J. Phys. Chem.*, 79 (1975) 1917.
115. K. Bhatia and R.H. Schuler, *J. Phys. Chem.*, 78 (1974) 2335.
116. K. Bhatia, *J. Phys. Chem.*, 79 (1975) 1032.
117. G.W. Klein, K. Bhatia, V. Madhavan and R.H. Schuler, *J. Phys. Chem.*, 79 (1975) 1767.
118. X. Chen and R.H. Schuler, *J. Phys. Chem.*, 97 (1993) 421.
119. M. Anbar, D. Meyerstein and P. Neta, *J. Phys. Chem.*, 70 (1966) 2660.
120. S. Solar, W. Solar and N. Getoff, *Radiat. Phys. Chem.*, 28 (1986) 229.
121. G.V. Buxton, J.R. Langan and J.R.L. Smith, *J. Phys. Chem.*, 90 (1986) 6309.
122. S. Steenken, N.V. Raghavan, *J. Phys. Chem.*, 83 (1979) 3101.
123. P.B. Draper, M.A. Fox, E. Pelizzetti and N. Serpone, *J. Phys. Chem.*, 93 (1989) 1918.
124. H. Mohan, J.P. Mittal, M. Mudalier, C.T. Aravindakumar and B.S.M. Rao, *J. Chem. Soc., Perkin Trans.*, 2, (1991) 1387.
125. S. Steenken, *Free Radicals in Synthesis and Biology*, E. Minisci (ed) NATO ASI Series C-260, Kluwer Acad., Dordrecht, The Netherlands, (1989) 213.
126. G. Merga, C.T. Aravindakumar, H. Mohan, B.S.M. Rao and J.P. Mittal, *J. Chem. Soc., Faraday Trans.*, 90 (1994) 597.
127. G. Merga, H.-P. Schuchmann, B.S.M. Rao and C. von Sonntag, *J. Chem. Soc., Perkin Trans.*, 2, (1996) 551.

128. G. Merga, H.-P. Schuchmann, B.S.M. Rao and C.von Sonntag, *J. Chem. Soc., Perkin Trans., 2*, (1996) 1097.
129. P. Neta, V. Madhavan, H. Zemel and R.W. Fessenden, *J. Am. Chem. Soc.*, **99** (1977) 163.
130. P. O'Neill, S. Steenken and D. Shulte-Frohlinde, *J. Phys. Chem.*, **79** (1975) 2773.
131. M. Jonson, J. Lind, T. Reitberger, T.E. Eriksen and G. Merenyi, *J. Phys. Chem.*, **97** (1993) 11278.
132. M. Bonfacic and K.-D. Asmus, *J. Phys. Chem.*, **80** (1976) 2426.
133. K. Schested, H. Corfitzen, H.C. Christensen and E.J. Hart, *J. Phys. Chem.*, **79** (1975) 310.
134. H. Zemel and R.W. Fessenden, *J. Phys. Chem.*, **82** (1978) 2670.
135. N. Zevos and K. Schested, *J. Phys. Chem.*, **82** (1978) 138.
136. K. Schested and E.J. Hart, *J. Phys. Chem.*, **79** (1975) 1639.
137. J.K. Thomas, *J. Phys. Chem.*, **71** (1967) 1919.
138. U. Brühlmann, H. Büchler, F. Marchetti and R.E. Bühler, *Chem. Phys. Lett.*, **21** (1973) 412.
139. H. Mohan and K.-D. Asmus, *J. Am. Chem. Soc.*, **109** (1987) 4745.
140. H. Mohan and K.-D. Asmus, *J. Phys. Chem.*, **92** (1988) 1297.
141. H. Mohan and P.N. Moorthy, *J. Chem. Soc., Perkin Trans., 2*, (1990) 277.
142. H. Mohan, D.K. Maity and J.P. Mittal, *Chem. Phys. Lett.*, **194** (1992) 135.
143. H. Mohan, D.K. Maity and J.P. Mittal, *Chem. Phys. Lett.*, **220** (1994) 455.
144. D.K. Maity and H. Mohan, *Chem. Phys. Lett.*, **230** (1994) 351.
145. H. Mohan and J.P. Mittal, *J. Chem. Soc., Perkin Trans., 2*, (1992) 1731.
146. D.K. Maity, H. Mohan, S. Chattopadhyay and J.P. Mittal, *J. Phys. Chem.*, **99** (1995) 12195.
147. D.K. Maity, H. Mohan, S. Chattopadhyay and J.P. Mittal, *Radiat. Phys. Chem.*, **49** (1997) 21.
148. H. Mohan, D.K. Maity, S. Chattopadhyay and J.P. Mittal, *Chem. Phys. Lett.*, **300** (1999) 493.
149. H. Mohan, M. Mudaliar, C.T. Aravindakumar, B.S.M. Rao and J.P. Mittal, *J. Chem. Soc., Perkin Trans., 2*, (1991) 1387.
150. H. Mohan, M. Mudaliar, B.S.M. Rao and J.P. Mittal, *Radiat. Phys. Chem.*, **40** (1992) 513.
151. H. Mohan and J.P. Mittal, *Chem. Phys. Lett.*, **263** (1996) 263.
152. H. Mohan, *Radiat. Phys. Chem.*, **49** (1997) 15.
153. S.C. Choure, M. Bamataraf, B.S.M. Rao, R. Das, H. Mohan and J.P. Mittal, *J. Phys. Chem., A*, **101** (1997) 10012.
154. H. Mohan and J.P. Mittal, *J. Chem. Soc., Faraday Trans.*, **91** (1995) 2121.
155. H. Mohan and J.P. Mittal, *J. Phys. Chem.*, **99** (1995) 6519.
156. H. Mohan and J.P. Mittal, *Chem. Phys. Lett.*, **235** (1995) 444.
157. H. Mohan and J.P. Mittal, *Res. Chem. Intermed.*, **25** (1999) 367.
158. H. Mohan and P.N. Moorthy, *Radiat. Phys. Chem.*, **33** (1989) 211.
159. J. Holcman and K. Sebested, *J. Phys. Chem.*, **80** (1976) 1642.
160. F.A. Cotton and G. Wilkinson, *Advanced Inorganic Chemistry*, Interscience Publishers, London, 1966.

161. C.R. Brundle, M.B. Robin, N.A. Kuebler and H. Busch, *J. Am. Chem. Soc.*, **94**, (1972) 1451.
162. Y. Kobayashi and I. Kumadaki, *Acc. Chem. Res.*, **14** (1981) 76.
163. M. Domae, Y. Katsumura, P.-Y. Jiang, R. Nagishi, K. Ishigure, T. Kozawa and Y. Yoshida, *J. Chem. Soc., Faraday Trans.*, **92** (1996) 2245.
164. M. Domae, Y. Katsumura, P.-Y. Jiang, R. Nagishi, C. Hasegawa, K. Ishigure and Y. Yoshida, *J. Phys. Chem.*, **98** (1994) 190.
165. B.H.J. Bielski, R.L. Arudi and M.W. Sutherland, *J. Biol. Chem.*, **258** (1983) 1748.
166. Y. Kadera and T. Hikida, *Spectroscopy Lett.*, **22** (1989) 1229.
167. H. Mohan and J.P. Mittal, *J. Phys. Chem.*, **103** (1999) 379.

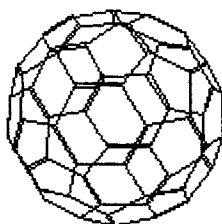
## Radiation Chemistry of Fullerenes

Dirk M. Guldi

University of Notre Dame, Radiation Laboratory, Notre Dame, IN 46556  
GULDI.1@ND.EDU

### 1. INTRODUCTION

The 3-dimensional icosahedral structure of [60]fullerene gives rise to a point group of high symmetry ( $I_h$ ) (1). This, in turn, leads to a five-fold degeneracy of the 30 doubly-occupied  $\pi$ -orbitals, accommodating the 60  $\pi$ -electrons. In the ground state the five-fold degenerate  $4h_u$  orbital is the highest occupied molecular orbital (HOMO) with an energy of -7.32 eV (2). This orbital is, based on the complete population, well resonance stabilized. Semiempirical calculations regarding the electron distribution of [60]fullerene reveal a three-fold degenerate lowest-unoccupied molecular orbital (LUMO), namely,  $5t_{1u}$  (-4.34 eV). In particular, these are the  $t_{1u-x}$ ,  $t_{1u-y}$  and  $t_{1u-z}$  orbitals. The moderate HOMO-LUMO gap of ca. 1.8 eV makes the 3-dimensional [60]fullerene an excellent electron acceptor, comparable to those of 2-dimensional planar moieties (quinones etc.) (3).



[60]Fullerene

Based on the fullerene's high electron affinity, [60]fullerene forms anions of the general  $A_3C_{60}$  and  $A_6C_{60}$  type with a number of alkali and alkali earth metals (4-6). The primarily occurring population of the  $5t_{1u}$  levels shifts the associated Fermi energies to smaller values. A half-filled occupation of the three-fold degenerate  $5t_{1u}$  levels, which corresponds to a three-electron reduction process, results in a  $A_3C_{60}$  type composition. These composites are characterized by a metallic behavior and display superconductivity below temperatures of around 33 K ( $Rb_3C_{60}$ ). A further filling of the  $5t_{1u}$  LUMO produces the completely filled  $A_6C_{60}$  phase, which is, however, insulating. Besides alkali

metals, doping of [60]fullerene has been probed with a number of alkali earth metals ( $\text{Ca}_5\text{C}_{60}$ ,  $\text{Sr}_6\text{C}_{60}$  and  $\text{Ba}_6\text{C}_{60}$ ). Hereby, a partial occupation of the likewise three-fold degenerate  $2t_{1g}$ -orbitals (LUMO + 1; -3.18 eV) is noticed.

In electrochemical studies, a reversible one-electron reduction step around -0.44 V *versus* SCE with anodic-cathodic peak separation of ca. 0.05 mV is noted in deaerated dichloromethane solutions (7,8). This process corresponds to the fullerene's first reduction and clearly underlines the small energy gap between valence ( $4h_u$ ) and conduction band ( $5t_{1u}$ ). Another five reversible one-electron steps follow the first step and, eventually, complete the population of the fullerene  $5t_{1u}$  level. The formation of the hexaanion,  $\text{C}_{60}^{6-}$ , is in good resemblance with the three-fold degeneration of the  $5t_{1u}$  orbitals. It is interesting to note that all six one-electron reduction steps are energetically equally separated from each other, which points to the electron delocalization within the fullerene carbon network. In contrast to the reduction of [60]fullerene, oxidation, which corresponds to the removal of an electron from the fully-occupied  $4h_u$  HOMO, is made more difficult by the resonance stabilization of this orbital and is limited to two one-electron oxidation steps. Only the first oxidation step is found to be reversible at a potential of +1.26 *versus* Fc /  $\text{Fc}^+$  in tetrachloroethylene. The potential difference between the oxidation and the first reduction processes for [60]fullerene is 2.32 V which provides a good measure for the energy difference between the  $4h_u$  HOMO and  $5t_{1u}$  LUMO in solution. Finally it should be added that in the case of [70]fullerene, which is easier to oxidize by 0.06 V (+1.20 V *versus* Fc /  $\text{Fc}^+$ ), a second, but irreversible oxidation process is reported at a potential of +1.76 V *versus* Fc /  $\text{Fc}^+$ .

A powerful technique to detect paramagnetic radical species, such as the one-electron reduced  $\pi$ -radical anions ( $\text{C}_{60}^{\cdot-}$ ) and oxidized  $\pi$ -radical cation ( $\text{C}_{60}^{\cdot+}$ ) is electron spin resonance (ESR) (9,10). Studies, regarding the characterization of fullerene intermediates *via* employing the ESR technique are, however, still somewhat controversial. Absorption spectrophotometry, on the other hand, is been successfully employed in matrix irradiation, silver mirror reduction in tetrahydrofuran (THF), and detection of transients in time-resolved laser photolysis and pulse radiolysis (10,11).

The scope of the following review is to summarize the radiation chemical studies that are concerned with the radical-induced redox, excitation and alkylation reaction of fullerenes. In particular, the reactivity of fullerenes and functionalized fullerene derivatives are compared in homogeneous and also heterogeneous systems, including micelles, vesicles and guest-host complexes.

## 2. [60], [70], [76], [78] AND [84]FULLERENES

In light of aspects involving charge transfer and radical addition processes, the unambiguous characterization and identification of  $\pi$ -radical anions,  $\pi$ -radical cations and

radical adducts of [60]fullerene is of fundamental importance. It is expected that this sheds light into a better understanding of functionalized fullerene derivatives and, in addition, as a data set for covalently linked, fullerene containing donor-bridge-acceptor dyads and triads.

### 2.1. Fullerenes in homogeneous systems

**Reduction:** Typical fullerene solvents are organics of low or medium polarity, such as toluene, benzonitrile, chlorinated hydrocarbons and CS<sub>2</sub>. In contrast, fullerenes are poorly soluble in polar solvents, including various alcohols. In polar solvents a spontaneous and irreversible cluster formation is noticed, yielding aggregates of various sizes. In aqueous solutions, [60]fullerene and its higher homologous, are practicable insoluble. It should be noted that most of the listed solvents cannot *per se* be employed for radiation-induced reduction studies.

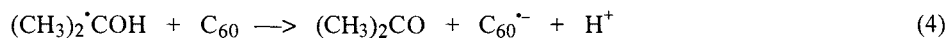
Accordingly, a concept was developed, that involves one of the organic compounds, e.g., toluene as a fullerene-dissolving medium (12,13). The systematic fullerene reduction was then obtained *via* addition of adequate co-solvents, namely, acetone and 2-propanol. Acetone was chosen as an efficient electron scavenger to hinder a reaction between solvated electrons and toluene. Followed by a fast protonation a radical species with a reducing character is formed. In addition, the (CH<sub>3</sub>)<sub>2</sub>•COH species is identical with the main product of the radiolysis of the second co-solvent, 2-propanol.



Upon pulse radiolytic reduction of an oxygen-free [60]fullerene solution, containing toluene, acetone and 2-propanol in a 8:1:1 v/v ratio, strong absorption changes were noted throughout the visible part of the spectrum. A net decrease of the absorption around 300 nm, a region which is dominated by strong fullerene ground state absorption suggests consumption of the fullerene as a result of a reaction with (CH<sub>3</sub>)<sub>2</sub>•COH radicals according to equation 4. Spectral analysis in the NIR region gave further evidence for the nature of the product. In particular, the detection of a maximum around 1080 nm (Figure 1) is in excellent agreement with an independently performed CNDO/S calculation regarding the electronic structure of the fullerene π-radical anion, C<sub>60</sub><sup>•-</sup> (10). A bimolecular rate constant of 8.5 × 10<sup>8</sup> M<sup>-1</sup>s<sup>-1</sup> was determined for the [60]fullerene



reduction in a toluene/2-propanol/acetone solvent mixture (8:1:1 v/v) which is close to the diffusion controlled limit in this solvent composite ( $k_{\text{diff}} = 4.5 \times 10^9 \text{ M}^{-1}\text{s}^{-1}$ ).



Similar observations were made in radiolytic experiments with  $\text{N}_2\text{O}$  or  $\text{N}_2$ -saturated 2-propanol solutions of [60]fullerene, despite the poor fullerene solubility. Radiolysis of  $\text{N}_2\text{O}$  / 2-propanol solutions leads also to a single reactive species, namely,  $(\text{CH}_3)_2\dot{\text{C}}\text{OH}$  and the fullerene reduction proceeds similar to the one outlined in the toluene/2-propanol/acetone solvent mixture (13). In  $\text{N}_2$ -saturated 2-propanol solutions the solvated electron ( $e^-_{\text{sol}}$ ), existing beside the  $(\text{CH}_3)_2\dot{\text{C}}\text{OH}$  radical, reduces the [60]fullerene with a rate constant of  $1.0 \times 10^{10} \text{ M}^{-1}\text{s}^{-1}$ :

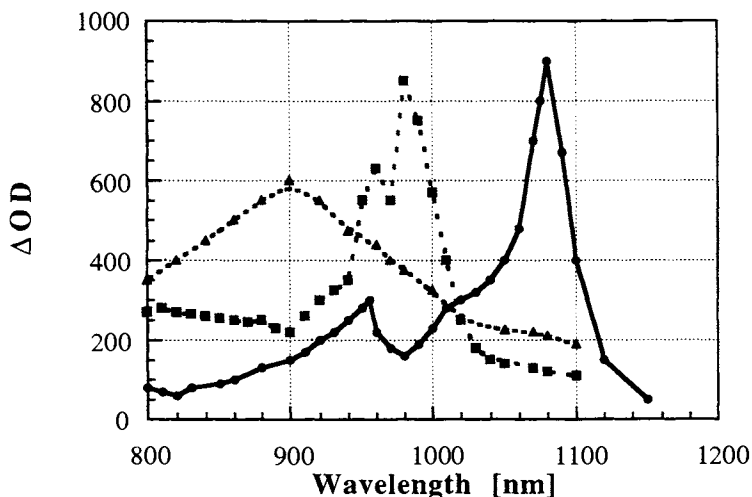
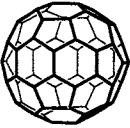
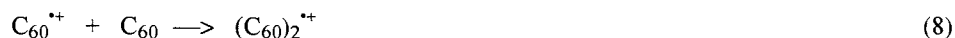


Figure 1: Differential absorption spectrum in the near-IR region of the  $\pi$ -radical anion (●),  $\pi$ -radical cation (■) and radical adduct (◆) obtained upon radiolysis of  $\text{C}_{60}$  (12,13).

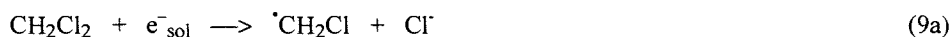
Table 1: Rate Constant for the Radiation-Induced Reduction of C<sub>60</sub> in Organic Solvents (12,13)

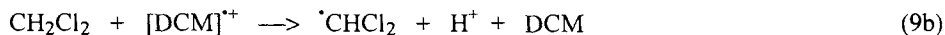
COMPOUND	MEDIUM	REAGENT	RATE CONSTANT [10 <sup>10</sup> M <sup>-1</sup> s <sup>-1</sup> ]	PRODUCT; MAXIMUM [nm]
 C <sub>60</sub> (I <sub>h</sub> )	Toluene/Acetone 2-Propanol	(CH <sub>3</sub> ) <sub>2</sub> •COH	0.085	C <sub>60</sub> <sup>•-</sup> ; 1080
	2-Propanol	e <sub>sol</sub> <sup>-</sup>	1.0	C <sub>60</sub> <sup>•-</sup> ; 1080
	2-Propanol	(CH <sub>3</sub> ) <sub>2</sub> •COH	0.05	C <sub>60</sub> <sup>•-</sup> ; 1080

**Oxidation:** The radiation-chemically induced ionization of chlorinated hydrocarbons, i.e., dichloroethane (DCE) leads to the initial generation of the corresponding solvent radical cation, [DCE]<sup>•+</sup>. The electron affinity of the latter is sufficient to oxidize the fullerene moiety ([60]fullerene: E<sub>1/2</sub> = +1.26 *versus* Fc / Fc<sup>+</sup>). Pulse radiolytic experiments with [60]fullerene in nitrogen-saturated or aerated DCM solutions yielded a doublet with maxima at 960 and 980 nm (Figure 1) (12-18). This fingerprint is identical to that detected in photolytic oxidation experiments and that computed in CNDO/S calculations. Rate constants for the [60]fullerene oxidation are typically very fast with estimated values k<sub>7</sub> > 2 x 10<sup>10</sup> M<sup>-1</sup>s<sup>-1</sup>. The π-radical cation is short-lived and decays *via* a concentration-dependent bimolecular dimerization reaction with a ground state molecule (k<sub>8</sub> = 6 x 10<sup>9</sup> M<sup>-1</sup>s<sup>-1</sup>) (13).



**Radical Addition:** The radiolysis of DCE or dichloromethane (DCM) leads, beside the above mentioned solvent radical cation [DCM]<sup>•+</sup>, to the carbon centered •CH<sub>2</sub>Cl and •CHCl<sub>2</sub> radicals. These are formed *via* dissociative electron capture and subsequent H<sup>+</sup>/Cl<sup>-</sup> dissociation. In oxygenated solvents the radical formation is followed by a rapid reaction with molecular oxygen, yielding the respective •OOCH<sub>2</sub>Cl and •OOCHCl<sub>2</sub> peroxy radicals.





It should be noted that the surface curvature of the carbon network exerts a profound impact on the reactivity of the fullerene core. The most striking consequence is the pyramidalization of the individual carbon atoms. Influenced by the curvature, the  $\text{sp}^2$  hybrids, which exist in truly 2-dimensional planar carbon networks, adopt a  $\text{sp}^{2.278}$  hybridization with p-orbitals that possess a s-character of 0.085 (19). Accordingly, the exterior surface is much more reactive than planar analogues, and becomes comparable to those of electron deficient polyolefines. This, in turn, rationalizes the high reactivity of the fullerene core towards many photolytically generated carbon- and heteroatomic-centered radicals (20).

In this light, a simple addition, rather than a redox reaction, was expected to dominate the reaction of [60]fullerene with the above mentioned radiolytically generated carbon- and heteroatomic-centered radicals (12-18,21,22). Spectrophotometric evidence for the postulated adduct formation stems from the broad 900 nm absorption band (Figure 1), substantially different from those of the singly reduced or oxidized fullerene, i.e. the  $\pi$ -radical anion (1080 nm) and  $\pi$ -radical cation (960 / 980 nm), respectively (12,13).

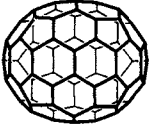


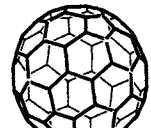


Complementary experiments with  $\cdot\text{CH}_3$ ,  $\cdot\text{CH}_2\text{CH}_2\text{Cl}$ ,  $\cdot\text{CH}_2\text{C}(\text{CH}_3)_2(\text{OH})$  and  $\cdot\text{CH}_2\text{Br}$  radicals corroborated this assignment. The generated radical adducts have different electronic configuration and, in turn, give rise to characteristic shifts of the absorption maxima, ranging from 890 to 920 nm. In conclusion, the position of  $\lambda_{\text{max}}$  of the different fullerene adducts can be rationalized as a function of the electron inducing or withdrawing effects of the covalently bonded substituents. This is an important parameter, which helps to interpret the observations made for functionalized fullerene derivatives, which are discussed later. The corresponding rate constants for the adduct formation are between  $1.7 - 4.8 \times 10^9 \text{ M}^{-1}\text{s}^{-1}$ .

With the help of steady-state radiolysis radical-induced multiple addition reactions were carried out. Via chromatographic separation the complete degradation of the hydrophobic educt, e.g., [60]fullerene was monitored during the course of the irradiation. An intermediate formation of a transient eventually leads to a quite polar product. Unspecific UV absorption and the high radical concentration both suggest a

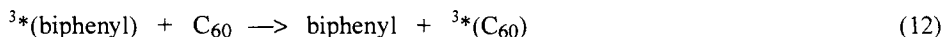
highly functionalized fullerene derivative. A complete characterization of the intermediate and the final product has not yet been achieved.

Table 2: Rate Constant for the Radiation-Induced Reduction of C<sub>70</sub>, C<sub>76</sub>, C<sub>78</sub> and C<sub>84</sub> in Organic Solvents (23-26)

COMPOUND	MEDIUM	REAGENT	RATE CONSTANT [10 <sup>10</sup> M <sup>-1</sup> s <sup>-1</sup> ]	PRODUCT; MAXIMUM [nm]
 C <sub>70</sub> (D <sub>5h</sub> )	Toluene/Acetone 2-Propanol	(CH <sub>3</sub> ) <sub>2</sub> •COH	0.08	C <sub>70</sub> <sup>•-</sup> ; 880
	H <sub>2</sub> O/Triton	e <sub>aq</sub> <sup>-</sup>	3.9	C <sub>70</sub> <sup>•-</sup> ; 880
	H <sub>2</sub> O/Triton	(CH <sub>3</sub> ) <sub>2</sub> •COH	0.03	C <sub>70</sub> <sup>•-</sup> ; 880
 C <sub>76</sub> (D <sub>2</sub> )	Toluene/Acetone 2-Propanol	(CH <sub>3</sub> ) <sub>2</sub> •COH	0.13	C <sub>76</sub> <sup>•-</sup> ; 905
	H <sub>2</sub> O/Triton	e <sub>aq</sub> <sup>-</sup>	3.3	C <sub>76</sub> <sup>•-</sup> ; 920
	H <sub>2</sub> O/Triton	(CH <sub>3</sub> ) <sub>2</sub> •COH	0.071	C <sub>76</sub> <sup>•-</sup> ; 920
 C <sub>78</sub> (C <sub>2v</sub> ')	Toluene/Acetone 2-Propanol	(CH <sub>3</sub> ) <sub>2</sub> •COH	0.16	C <sub>78</sub> <sup>•-</sup> ; 975
	H <sub>2</sub> O/Triton	e <sub>aq</sub> <sup>-</sup>	3.6	C <sub>78</sub> <sup>•-</sup> ; 980
	H <sub>2</sub> O/Triton	(CH <sub>3</sub> ) <sub>2</sub> •COH	0.072	C <sub>78</sub> <sup>•-</sup> ; 980
 C <sub>84</sub> (D <sub>2</sub> )	Toluene/Acetone 2-Propanol	(CH <sub>3</sub> ) <sub>2</sub> •COH	0.1	C <sub>84</sub> <sup>•-</sup> ; 960

Identical reaction pathways for the reduction, oxidation and radical addition, were established for the higher fullerene homologues (23-26). It is interesting to note that the associated symmetries of the higher fullerenes have a large impact on (i) the relative position of the corresponding  $\pi$ -radical anion and  $\pi$ -radical cation absorption bands, (ii) their relative intensity and (iii) equally important on the electrochemically determined reduction potentials (Table 2). As a direct consequence of the smaller HOMO-LUMO energy difference, higher fullerenes are proposed to be better electron acceptor moieties than [60]fullerene. Faster rate constants of  $1.3 \times 10^9 \text{ M}^{-1}\text{s}^{-1}$  and  $1.6 \times 10^9 \text{ M}^{-1}\text{s}^{-1}$  for the radiation induced reduction of [76]- and [78]fullerene with  $(\text{CH}_3)_2\dot{\text{C}}\text{OH}$  radicals, respectively, relative to [60]fullerene ( $8.5 \times 10^8 \text{ M}^{-1}\text{s}^{-1}$ ) are in perfect agreement with this hypothesis. Electrochemically determined oxidation potentials reveal a similar trend, e.g., lower oxidation potentials for the higher homologues. This has an important consequence for the stability of the  $\pi$ -radical cations. Specifically, an increasing fullerene size correlates well with a higher stability of the  $\pi$ -radical cations. The rate constants ( $k_8$ ) for the reaction of a fullerene  $\pi$ -radical cation with another non-oxidized fullerene molecule are  $6 \times 10^9 \text{ M}^{-1}\text{s}^{-1}$  ([60]fullerene),  $6 \times 10^9 \text{ M}^{-1}\text{s}^{-1}$  ([70]fullerene),  $9.8 \times 10^8 \text{ M}^{-1}\text{s}^{-1}$  ([76]fullerene) and  $7.9 \times 10^8 \text{ M}^{-1}\text{s}^{-1}$  ([78]fullerene). In summary, higher fullerenes are both better electron acceptors and better electron donors than [60]fullerene.

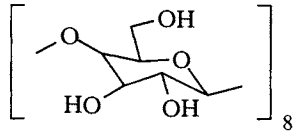
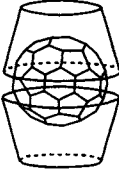
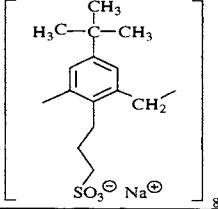
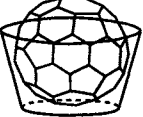
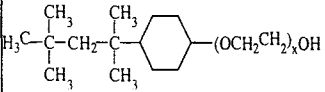
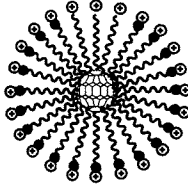
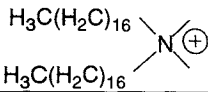
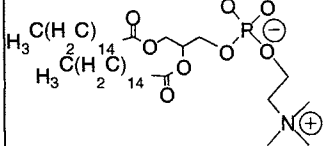
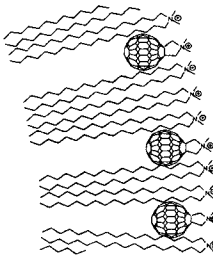
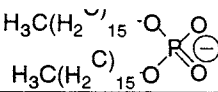
**Triplet Excited States:** Pulse radiolysis has also been shown to generate the triplet excited state of various fullerenes and a large number of functionalized fullerene derivatives *via* triplet-triplet energy transfer from an energetically high lying triplet sensitizer (27-32). The triplet excited state of, for example, biphenyl, with an energy level ( $E_T = 2.74 \text{ eV}$ ) sufficiently above typical fullerene triplets ( $E_T \approx 1.50 \text{ eV}$ ), can be produced efficiently during the radiolysis of oxygen-free toluene or benzene solutions containing high concentrations of biphenyl (0.02 M). Rate constants ( $k_{12}$ ) for the proposed energy transfer are nearly diffusion controlled (ca.  $1.0 \times 10^{10} \text{ M}^{-1}\text{s}^{-1}$ ), in line with an exchange mechanism (27).



In general, the underlying rate constants differ only slightly from fullerene to fullerene. This independence can be ascribed to the large energy gap between the triplet sensitizer, e.g., biphenyl and the various fullerenes. This technique is particularly useful for the investigation of higher fullerenes, e.g., [76]fullerene ( $\Phi \approx 0.05$ ) and [78]fullerene ( $\Phi \approx 0.12$ ), that are subject to a moderate intersystem crossing yield relative to the much higher effectiveness of [60]fullerene ( $\Phi \approx 1$ ), with respect to quantum yields, extinction coefficients and lifetimes (24).

## 2.2. Fullerenes in heterogeneous guest host structures

Table 3: Watersoluble Host-Guest Structures for the Incorporation of Fullerenes

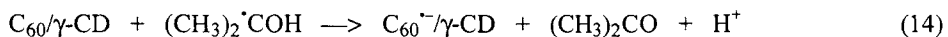
COMPOUND	HOSTSTRUCTURE	COMPLEXATION	GUEST
<u><math>\gamma</math>-Cyclodextrin</u>			C60 monofunctionalized derivatives
<u>Calix[8]arene</u>			C60, C70 monofunctionalized derivatives
<u>Triton X-100</u> (reduced Form)			C60, C70, C76, C78 monofunctionalized derivatives bisfunctionalized derivatives
Cetyltrimethyl- ammonium chloride	$\text{CH}_3(\text{CH}_2)_{15}\text{N}^+(\text{CH}_3)_3$		C60, C70, C76, C78 monofunctionalized derivatives
<u>DABCO</u>			C60, C70 monofunctionalized derivatives
<u>Lecithin</u>			C60, C70 monofunctionalized derivatives
<u>DHP</u>			C60, C70 monofunctionalized derivatives

The insolubility of pristine fullerenes in polar solvents provokes a variety of complex questions. A viable concept to overcome this solubility problem involves the incorporation of pristine fullerenes into the hydrophobic cavity of water soluble host structures. Table 3 shows a survey of host structures, which were successfully employed to accommodate [60]fullerene etc. and, in turn, to dissolve fullerenes in aqueous media. The large van-der Waals radius of fullerenes, with typical values of  $5 \pm 1.5 \text{ \AA}$ , limits the selection of adequate host complexes. This will be discussed in more details in the following.

Prior to the herein described investigations, concerns were raised whether fullerene reduction can be actually achieved, because of the shielding induced by the different host structures. Furthermore, these studies were helpful to highlight the beneficial role of the heterogeneous system in stabilizing charge-separated radical pairs or even to preserving the optical properties relative to a homogenous organic solution.

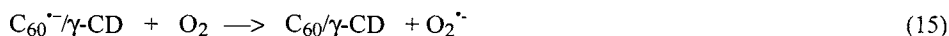
**Cyclodextrin:** Cyclodextrines, e.g., alpha ( $\alpha$ ), beta ( $\beta$ ) and gamma ( $\gamma$ ), are cyclic oligosaccharides with hydrophilic cavities. A consideration regarding the right balance between cavity radius and fullerene size leads to the assumption that  $\gamma$ -CD should be the most promising candidate to host [60]fullerene. Molecular modeling suggests, nevertheless, that a full incorporation, in form of a 1:1 complex, is practically impossible to achieve. Despite this apparent size mismatch, an incorporation of a single [60]fullerene molecule between the cavities of two  $\gamma$ -cyclodextrin molecules has been postulated and later confirmed by various spectroscopic techniques (33,34). Parallel experiments attempting to incorporate [60]fullerene into  $\alpha$ - or  $\beta$ -cyclodextrin failed.

Radiation-induced reaction of the  $C_{60}/\gamma$ -CD complex with hydrated electrons ( $e^-_{aq}$ ) in aqueous solutions ( $N_2$ -saturated, at neutral pH) led to strong UV-VIS changes, resembling those described for the reduction experiments in the toluene/2-propanol/acetone solvent mixture (8:1:1 v/v) (12,13,35,36). More importantly, differential absorption changes in the NIR region showed unequivocally the  $C_{60}^{\cdot-}$  fingerprint at 1080 nm. This demonstrates the successful reduction of the  $\gamma$ -CD-incorporated fullerene core by hydrated electrons (eq. 13). To obtain further evidence for the fullerene reduction various  $\alpha$ -hydroxyl radicals namely,  $\cdot CH_2OH$ ,  $CH_3\cdot CHO$  and  $(CH_3)_2\cdot COH$  were also probed. The rate constants for the underlying  $C_{60}/\gamma$ -CD reduction follow the strength of these  $\alpha$ -hydroxyl radicals.



The reduction experiments disclose a noticeable slow-down of the  $C_{60}/\gamma\text{-CD}$  reduction ( $k_{14} = 2.7 \times 10^8 \text{ M}^{-1}\text{s}^{-1}$ ), initiated by the bulky  $(\text{CH}_3)_2\text{COH}^\bullet$  radicals, relative to a bimolecular reaction in homogeneous systems ( $k_4 = 8.5 \times 10^8 \text{ M}^{-1}\text{s}^{-1}$ ). In conclusion, the fullerene core is not completely shielded from the aqueous phase and, thus, can be efficiently reduced *via* hydrated electrons and various  $\alpha$ -hydroxyl radicals.

Under anaerobic conditions the singly reduced  $C_{60}^{\bullet-}/\gamma\text{-CD}$  is quite stable and reacts only slowly with molecular oxygen (37).



Addition of base or acid had, however, a significant impact on the stability and yield of the characteristic 1080 nm absorption band. A semilogarithmic correlation between the proton concentration and the intensity of the fullerene  $\pi$ -radical anion band (1080 nm) is observed in anaerobic aqueous solutions. This observation has been ascribed to a reversible protonation of  $C_{60}^{\bullet-}/\gamma\text{-CD}$ . Experimental proof for this assumption was brought forward by the fact that the 1080 nm absorption, in an alkaline solution (pH 10), diminished upon acidifying (pH 3) and was completely restored upon addition of base (pH 10). The reversible protonation process gives rise to a  $\text{pK}_a$  of 4.5.



Based on the depicted equilibrium and the observed lifetime a rate constant for the forward reaction of  $10^3 \text{ M}^{-1}\text{s}^{-1}$  was estimated. The slow protonation rate of the one-electron reduced fullerene  $\pi$ -radical anions can be understood in terms of the charge delocalization and also the hybridization of the generated carbanion. Furthermore, the heterogeneous and hydrophobic environments of the host's interior can be assumed to be beneficial for the slow-down of the protonation dynamics. In homogeneous aqueous solutions the protonation rate should be faster, a hypothesis that was substantiated by recent radiolytic experiments with bisfunctionalized fullerene derivatives. The latter compounds are soluble in aqueous solutions without employing a solubilizer (host) and give rise to protonation rate constants of  $3 \times 10^4 \text{ M}^{-1}\text{s}^{-1}$  (38).

Radiolytic experiments of  $C_{60}/\gamma\text{-CD}$  under conditions that generate carbon-centered radicals, such as  $^\bullet\text{CH}_3$ , were in line with a radical addition mechanism. It is interesting to note that a reaction of [60]fullerene even with the strongly oxidizing  $\text{Cl}_2^{\bullet-}$  radicals (oxidation potential of +2.3 V *versus* SCE) give an absorption that suggests a  $(C_{60}\text{-Cl})^\bullet$  adduct. This is in contrast to a prediction that is purely based on the



thermodynamic driving force, which would rather predict an oxidation of the fullerene core. No spectral evidence was, however, obtained in support of the formation of  $C_{60}^{•+}/\gamma$ -CD (38).



In addition to the radical-induced reduction of the  $\gamma$ -CD incorporated [60]fullerene, even the formation of  $C_{60}$ -radical adducts were demonstrated to occur. Considering the configuration of the  $\gamma$ -CD/ $C_{60}/\gamma$ -CD complex, a reaction with radical species is only possible through the two caps of the cyclodextrin moieties and should thus be restricted to small radicals. In light of this aspect, a reaction with a bulky radical species such as  $\dot{C}H_2(CH_3)_2COH$  should be made more difficult or even be ruled out. In fact, the lack of any spectral evidence for a  $(C_{60}\text{-}CH_2(CH_3)_2COH)^{\bullet}$  adduct supports this view.

Finally, the reaction with the two remaining primary radical species that are generated during the course of the radiolysis of water, e.g.,  $H^{\bullet}$  and  $\dot{O}H$  radicals, should be discussed. However, due to their rapid reaction with the  $\gamma$ -CD host molecule, such reactions with the fullerene core are practically precluded and, accordingly, could not be observed (35).

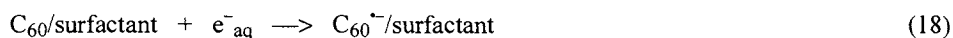
**Calixarenes:** Calix[8]arene host structures give rise to a significantly increased hydrophobic cavity with a mean diameter of nearly 8.6 Å relative to the above discussed cyclodextrin. In this context, the diameter of [60]fullerene of 7.1 Å should be emphasized. Corresponding attempts to incorporate [60]fullerene and also [70]fullerene into calix[8]arene were successful (39), but radiation-induced reduction by hydrated electrons or  $\dot{C}H_2OH$ ,  $CH_3\dot{C}HOH$  and  $(CH_3)_2\dot{C}OH$  radicals failed (40). Spectral analysis of the differential absorption changes, recorded upon radiolysis in anaerobic aqueous solutions, suggests that the aromatic arene units of the calix[8]arene scavenge the generated hydrated electrons and  $\alpha$ -hydroxyl radicals. A subsequent electron transfer reaction from the reduced host molecule to the fullerene host could, however, not be substantiated.

**Surfactants:** Two other classes of host molecule, with, however, flexible cavities, are amphiphilic micellar and vesicular assemblies. In a simple view, these molecules bear a hydrophilic headgroup (e.g., ionic, zwitter ionic, or non-ionic) and a hydrophobic tail (carbon hydrogen chain). Depending on the solvent environment they organize in 3-dimensional surface-active assemblies. For example, in aqueous solutions their alignment

creates a hydrophobic core, comprised by the hydrophobic tails. These domains are capable of accommodating water-insoluble entities including hydrophilic fullerenes. A very intriguing aspect is the structural flexibility of micellar and vesicular assemblies, which should enable them to host, in contrast to the rigid cyclodextrins and calix[8]arenes, even higher fullerenes ([70], [76], [78] and [84]fullerenes) (41-49).

A variety of surfactants, ranging from non-ionic Triton X-100, Tween 20 and BRIJ 35 to cationic cetyltrimethylammonium chloride, were successfully shown to host the hydrophobic fullerene moieties. Well resolved absorption bands throughout the UV-VIS-NIR part, in close resemblance with organic solutions, and the lack of any significant light scattering, points to the monomeric dissolution of the fullerene moieties within freshly prepared surfactant ensembles. Of particular interest is the possibility of dissolving [76]- and [78]fullerenes, and even nanotubes for investigation in aqueous solutions (42).

The pulse radiolytically induced reduction of the fullerene were followed in N<sub>2</sub>O-saturated aqueous solution containing 1% of the micelle and 10% 2-propanol (42). In such systems, similar to the homogenous solution, the only reactive species formed is the (CH<sub>3</sub>)<sub>2</sub>•COH radical. The differential absorption spectrum recorded after the completion of the reaction resembles the one obtained in neat 2-propanol, including the NIR fingerprint ( $\lambda_{\text{max}}$  1075 nm). Hence the reaction can be ascribed to the formation of the C<sub>60</sub><sup>-</sup> radical anion generated *via* the reaction between the incorporated [60]fullerene and (CH<sub>3</sub>)<sub>2</sub>•COH radicals. A bimolecular rate constant of  $k = 6.1 \times 10^8 \text{ M}^{-1}\text{s}^{-1}$  has been derived from the respective absorption time-profile throughout the UV-VIS-NIR. The rate resembles that in homogeneous solution. Complementary reduction experiments with hydrated electrons, namely, in N<sub>2</sub> rather than N<sub>2</sub>O saturated solutions, led to spectral changes superimposable to those described for the (CH<sub>3</sub>)<sub>2</sub>•COH system. More importantly, the comparison between the rate constants for the fullerene reduction by hydrated electrons in the surfactant incorporated system ( $2.6 \times 10^{10} \text{ M}^{-1}\text{s}^{-1}$ ) with the  $\gamma$ -CD-incorporated ensemble ( $1.8 \times 10^{10} \text{ M}^{-1}\text{s}^{-1}$ ) leave little doubt about monomeric fullerenes. Under anaerobic conditions C<sub>60</sub><sup>-</sup> is stable over the experimental time scale of the pulse radiolysis.



**Vesicular Systems:** Vesicular solutions of [60]fullerene in DODAB (positively charged head group), DHP (negatively charged) and lecithin (zwitter ionic) all showed yellow-brownish colors rather than the magenta color of C<sub>60</sub> in toluene or dichloromethane (41,50). The spectral features, e.g., absorption bands at 220 nm, 260 nm and 340 nm, confirm the incorporation of the fullerene into these lipid bilayer

membranes. One of the most significant results emerges with respect to the [60]fullerene 334 nm UV band which is subject to remarkable changes in the vesicular environment as compared to homogeneous organic solutions or micellar aqueous systems. The UV bands are generally red-shifted with increasing  $[C_{60}]/[\text{vesicle}]$  concentration ratio with the extent depending strongly on the nature of the vesicle. Furthermore, the spectral shifts are accompanied by light scattering and significantly decreasing extinction coefficients. These concentration-dependent changes in the spectral characteristics of the fullerene UV band (334 nm) are suggested to indicate the aggregation of hydrophilic [60]fullerene cores located within the interior of the lipid bilayer membranes.

The aggregation of fullerenes in these heterogeneous systems can be rationalized in terms of their strong intermolecular  $\pi$ - $\pi$  association forces. This phenomenon will be discussed in further details below. Additional experiments, characterizing the fullerene triplet lifetime in the DODAB, DHP and lecithin systems gives further proof for the proposed aggregation. Specifically, reduced triplet lifetimes ( $\tau < 0.2 \mu\text{s}$ ), relative to a fullerene monomer ( $\tau \approx 100 \mu\text{s}$ ), indicate an enhanced contribution of triplet-triplet or triplet-singlet ground state annihilation to the triplet deactivation.

[60]fullerene, incorporated into the three types of vesicles discussed, was successfully reduced to  $C_{60}^{\cdot-}$   $\pi$ -radical anions by hydrated electrons ( $e_{\text{aq}}^-$ ) and  $(\text{CH}_3)_2\dot{\text{C}}\text{OH}$  radicals. The latter reaction was monitored in pulse radiolysis experiments with  $\text{N}_2\text{O}$ -saturated, aqueous solutions of the respective [60]fullerene-containing vesicles in the presence of 2-propanol. The experiment revealed differential absorption changes with respect to the bleaching of the [60]fullerene UV band at the respective  $\lambda_{\text{max}}$  (around 340 nm) and formation of a new transient absorption in the NIR, as reported in homogeneous solutions. The yields of the [60]fullerene reduction in the vesicles, as calculated from the measured changes in absorption (340 nm) and the respective extinction coefficients of [60]fullerene are unequivocally highest for the positively charged DODAB vesicle and lowest for the negatively charged DHP vesicle. This finding suggests that the transfer of an electron from the 2-propanol radical through the vesicle surface to the [60]fullerene is most favored for the charge-wise least repelling head group barrier, namely, positively charged DODAB vesicle.



Detection of an NIR band for DODAB, lecithin, and DHP solutions of [60]fullerene confirmed our earlier report, which was based on differential absorption changes in the Vis region. Interestingly, the characteristic NIR-band of  $C_{60}^{\cdot-}$  within these lipid materials reveals a blue shift with a maximum centered around 1020 nm as compared to organic solutions of [60]fullerene and aqueous  $C_{60}/\gamma$ -CD where the

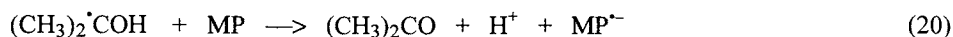
maximum was recorded at 1080 nm and remained unaffected by the host material. The 1020 nm band is also substantially broadened and, consequently, attributed to fullerene aggregation.

In summary, incorporation of [60]fullerene into artificial bilayer membranes, despite being successful in principle, nevertheless, disclosed a number of unexpected complications. The most dominant parameter, in this view, is the strong aggregation forces among the fullerene cores. The lack of appropriately structured domains within the vesicular hosts, which could assist in keeping the fullerene units apart, is believed to be the reason for the instantaneous cluster formation. The incorporation of a number of suitably functionalized derivatives, which on their own bear hydrophobic and hydrophilic substructures, will be discussed further below.

### 2.3. Intermolecular electron transfer with fullerenes

The combination of a high degree of electron delocalization within the fullerene's  $\pi$ -system and their effective sizes prompts to the application of this carbon material as new electron accepting moieties. More importantly, the total reorganization energy upon reduction has been shown to be relative small. Hence, fullerenes became very appealing spheres for inter- and intramolecular electron transfer processes under the aspect of energy conversion and energy storage. In the following two examples are described which demonstrate the participation of fullerenes in reductive and oxidative electron transfer reactions with a variety of electron donor (one-electron reduced metalloporphyrins) and electron acceptor moieties (one electron oxidized arenes), respectively.

**Intermolecular electron transfer between radiolytically-reduced metalloporphyrins and [60]fullerene (51,52)** Metalloporphyrins were reduced in a radiolytical experiment carried out in a similar solvent mixture described above for the reduction of fullerenes, e.g., containing toluene, acetone and 2-propanol in a 8:1:1 v/v ratio. Again, the solely reducing species in this solvent mixture is the radical derived from 2-propanol by hydrogen-abstraction, i.e.  $(\text{CH}_3)_2\dot{\text{C}}\text{OH}$  radical. This radical is known to reduce a number of metalloporphyrins (MP) quite rapidly.



Pulse irradiation of oxygen-free solutions containing various metalloporphyrins, MP, resulted in the formation of broad absorption in the 600-800 nm range. These

absorptions are ascribed to the  $\pi$ -radical anions, resulting from the reduction of the porphyrin ligands. In the absence of other electron acceptors the  $\pi$ -radical anions decay slowly *via* a sequence of disproportionation and protonation reactions. The lifetimes of the  $\pi$ -radical anions have been shown to depend strongly on the medium and on the reduction potential of the respective metalloporphyrin.

Addition of various concentrations of [60]fullerene, for example, to a ZnTPP solution, resulted in an accelerated decay of the  $\pi$ -radical anion (ZnTPP $^{\cdot-}$ ). The observed rate was linearly dependent on the [60]fullerene concentration, which, in turn, has led to the assumption that the ZnTPP  $\pi$ -radical anion reacts with [60]fullerene. To confirm a probable electron transfer, the formation of the characteristic C<sub>60</sub> $^{\cdot-}$  absorption in the NIR ( $\lambda_{\text{max}} = 1080 \text{ nm}$ ) was also monitored. The grow-in rate of the C<sub>60</sub> $^{\cdot-}$  absorption at various wavelengths in the 980-1060 nm range was nearly identical to the decay rate of the MP $^{\cdot-}$  absorption at 650-750 nm. For example, in the case of ZnTPP  $\pi$ -radical anion (ZnTPP $^{\cdot-}$ ), a bimolecular rate constant of  $(2.5 \pm 1.0) \times 10^9 \text{ M}^{-1} \text{ s}^{-1}$  was derived from the ZnTPP $^{\cdot-}$  decay (720 nm) and  $(1.4 \pm 1.0) \times 10^9 \text{ M}^{-1} \text{ s}^{-1}$  from the C<sub>60</sub> $^{\cdot-}$  formation (970 nm). These two values are in reasonable agreement and confirm unmistakably the electron transfer from the one-electron reduced metalloporphyrin (ZnTPP) to the singlet ground state of the fullerene:



The rate constants for electron transfer from various metalloporphyrin  $\pi$ -radical anions to [60]fullerene are found to be in the range of  $(1-3) \times 10^9 \text{ M}^{-1} \text{ s}^{-1}$ , despite the large variation in one-electron reduction potentials for the examined metalloporphyrins between  $E_{1/2} \text{ ZnP/ZnP}^{\cdot-} = -1.35 \text{ V}$  and  $E_{1/2} \text{ SnP/SnP}^{\cdot-} = -0.8 \text{ V}$  *versus* SCE. This lack of dependence of the rate constant on the driving force for the reaction probably reflects the fact that the investigated porphyrins and [60]fullerene experience already electronic interactions in the ground state which lead to nearly diffusion-controlled reactions ( $k_{\text{diff}} = 3.5 \times 10^9 \text{ M}^{-1} \text{ s}^{-1}$ ). It should be noted, however, that no ground state charge transfer interactions were detectable, e.g. as perturbation of the ground state absorption. The latter appears simply a good superimposition of the two different components (metalloporphyrin and fullerene).

Tin-(IV) porphyrins (Sn<sup>IV</sup>P) are very easily reduced to their long-lived  $\pi$ -radical anions. Because their reduction potential is only slightly more negative than that of [60]fullerene, it was expected that the electron transfer between these two species, if sufficiently rapid as compared with the decay of the radicals, may lead to the observation of equilibrium conditions. Indeed, we found such an equilibrium with a tin-(IV) porphyrin (Sn<sup>IV</sup>(Ph)<sub>3</sub>(Py)P). Reduction of this porphyrin resulted in formation of the characteristic  $\pi$ -radical anion with absorption in the 700-800 nm range.

Upon addition of various [60]fullerene concentrations, the rate of decay of this  $\pi$ -radical anion increased linearly with  $C_{60}$ . However, the rate of decay was also found to increase upon raising the porphyrin concentration at constant [60]fullerene concentrations. Such a dependence of the rate of reaction upon both concentrations is indicative of an equilibrium process. To confirm this tentative assignment and, furthermore, to determine the equilibrium constant, we measured the rate constant with a series of different  $\text{Sn}^{\text{IV}}\text{P}$  and [60]fullerene concentrations. The results show the expected linear dependence. The kinetic plot gives  $k_{22} = 3.2 \times 10^9 \text{ M}^{-1}\text{s}^{-1}$ ,  $k_{-22} = 2.1 \times 10^8 \text{ M}^{-1}\text{s}^{-1}$ , and  $K_{22} = 15$ . In good agreement with this figure, the absorbance plot gives  $K_{22} = 13$ . Thus the average equilibrium constant ( $K_{22}$ ) from these plots is  $14 \pm 3$ .



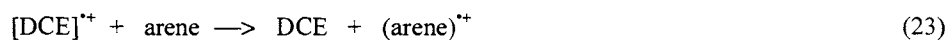
In contrast, one-electron reduction of  $\text{Cr}^{\text{III}}\text{MSP}$ ,  $\text{Ni}^{\text{II}}\text{TPP}$ , and  $\text{Cu}^{\text{II}}\text{TPP}$  is known to occur at the metal center yielding  $\text{Cr}^{\text{II}}\text{MSP}$ ,  $\text{Ni}^{\text{I}}\text{TPP}$ , and  $\text{Cu}^{\text{I}}\text{TPP}$ , respectively. Reduction of the metal center results in only minor spectral shifts of the metalloporphyrins Soret- and Q-bands, and lacks, in particular, the intense absorption in the 600-800 nm region. The decay of these species upon reaction with [60]fullerene was monitored in the 500 nm range, where the reduced metalloporphyrin absorbs more intensely than the parent compound. The rate constants for these reactions were derived from the linear dependence of the decay rate upon [60]fullerene concentration.

These rate constants ( $0.68 - 2.4 \times 10^8 \text{ M}^{-1}\text{s}^{-1}$ ) are substantially lower than those measured for the reduction by the  $\pi$ -radical anions despite the similarity in the reduction potentials ( $E_{1/2} \text{Cr}^{\text{III}}\text{P}/\text{Cr}^{\text{II}}\text{P} = -1.14 \text{ V}$ ;  $E_{1/2} \text{Ni}^{\text{II}}\text{P}/\text{Ni}^{\text{I}}\text{P} = -1.18 \text{ V}$ ;  $E_{1/2} \text{Cu}^{\text{II}}\text{P}/\text{Cu}^{\text{I}}\text{P} = -1.2 \text{ V}$  versus SCE). Possibly, the small size of the reactive metal center, versus the large size of that in the porphyrin  $\pi$ -radical anions, i.e. geometric constrains, may be the cause for the decreased rate constants.

Extending the studies on the reductive electron transfer from reduced metalloporphyrin states to [60]fullerene into aqueous media requires employment of a water-soluble form of [60]fullerene. Therefore, a micellar assembly consisting of the fullerene incorporated into Triton X-100 was investigated. The electron transfer does indeed occur across the interface of the micellar assembly. The rates exhibit a considerable slow-down compared to the homogeneous systems but, on the other hand, show a clear dependence on the reduction potential of the water-soluble metalloporphyrin.

**Intermolecular electron transfer between radiolytically-oxidized arenes and [60]fullerenes** (25,51) Oxidative electron transfer from [60]fullerene to various organic radical cations was studied in  $\text{CH}_2\text{Cl}_2$  (DCM) as a solvent. The kinetic study makes use of the unequally sized reaction partners, e.g., a large-sized electron donor and small-sized electron acceptor couple, and benefit from the low viscosity of the DCM, both elevating the diffusion-controlled limit.

In analogy to the fullerene oxidation, the arene radical cations were generated in deoxygenated DCM solutions containing ca.  $2 \times 10^{-2}$  M of the respective arenes. As a convenient means to probe the formation and the lifetime of the generated  $(\text{arene})^{+\bullet}$  the respective absorptions in the UV-VIS region were monitored.



To study the electron transfer from [60]fullerene to the arene radical cation, deoxygenated DCM solutions of, for example, m-terphenyl were irradiated in the presence of variable [60]fullerene concentrations ( $0.7 - 6.0$ )  $\times 10^{-5}$  M. The short life-time of some of the  $(\text{arene})^{+\bullet}$ , in combination with the unfavorably high ionization potential of [60]fullerene limited the ability to measure the electron transfer process to, however, only a few  $(\text{arene})^{+\bullet}$ . Formation of the electron transfer product, namely,  $\text{C}_{60}^{+\bullet}$  was confirmed spectroscopically by measuring the NIR fingerprint at  $\lambda_{\text{max}} = 980$  nm, which resembles that found upon direct oxidation of [60]fullerene.

The rate constants  $k_{24}$  for biphenyl, t-stilbene, m-terphenyl, and naphthalene vary between  $2.5 \times 10^9 \text{ M}^{-1}\text{s}^{-1}$  and  $7.9 \times 10^9 \text{ M}^{-1}\text{s}^{-1}$  (Table 4). The driving forces ( $-\Delta G$ ) of the bimolecular electron transfer, calculated on the basis of the difference in the respective arenes' and fullerenes' ionization potentials ( $-\Delta G = \Delta \text{IP} = \text{IP}_{\text{arene}} - \text{IP}_{\text{fullerene}}$ ), show no linear correlation with the measured rate constants for the electron transfer reactions. In fact, it is interesting to note that these results indicate even a decrease of the rate constant at higher  $\Delta \text{IP}$ 's.

The substantially reduced ionization potentials of [76]fullerene ( $\text{D}_2$ ) ( $\text{IP} = 7.1$  eV) and [78]fullerene ( $\text{C}_{2v}$ ) ( $\text{IP} = 7.05$  eV) relative to [60]fullerene ( $\text{I}_h$ ) ( $\text{IP} = 7.59$  eV) are beneficial for following the envisaged intermolecular electron transfer processes, for a significantly increased number of suitable electron accepting substrates.

Similar to the [60]fullerene case, addition of [76]fullerene and [78]fullerene in the  $10^{-5}$  M concentration range resulted in an accelerated decay of the arene radical cation's UV-VIS absorption, with rates linearly depending on the fullerene concentration. At the same time, formation of the fullerene radical cations became observable in the NIR

confirming the underlying process to be, indeed, an intermolecular electron transfer according to reaction 24. Bimolecular rate constants could be measured for a large number of arenes with ionization potentials ranging from 7.21 eV (9-anthracenemethanol) to 8.2 eV (durene).

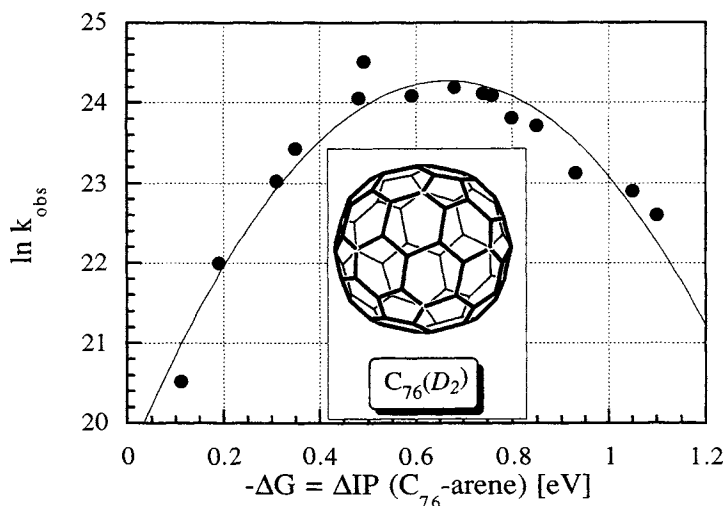


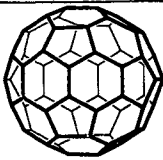
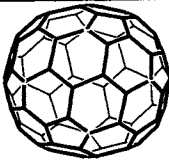
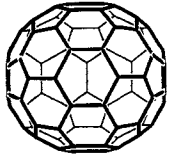
Figure 2: Plot of  $\ln k_{obs}$  for electron transfer from [76]fullerene ( $D_2$ ) to  $(arene)^{++}$  in DCM at room temperature as a function of the free energy changes for the reactions (25).

A pronounced parabolic dependency is noticed (Figure 2), including a decrease of the rate constants with increasing free energy towards the highly exothermic region. Maxima are found around 0.6 eV corresponding to total reorganization energy of  $13.8 \text{ kcal mol}^{-1}$ . These values are in excellent agreement with those calculated from the classical dielectric continuum model for the different arenes, with  $\lambda_s$  ranging from 11.14 to  $16.33 \text{ kcal mol}^{-1}$ .

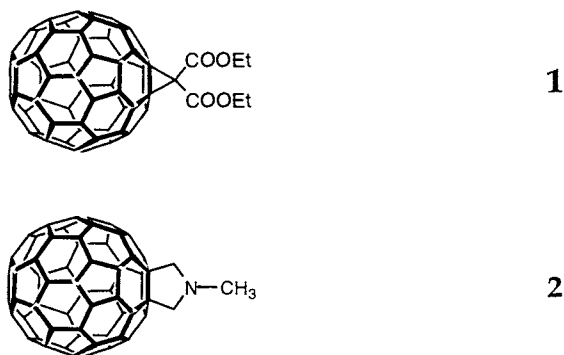
These relatively low values together with minor vibrational differences in the fullerene oxidized state relative to its ground state, are both consequences of the large degree of delocalization within the resonance structure of the fullerenes  $\pi$ -system. Furthermore, the relatively low reorganization energy is clearly beneficial for the possibility of establishing a Marcus-inverted region as it facilitates reaching the maximum of the exothermic electron transfer process at lower  $-\Delta G$ . In the light of these findings the limited set of data obtained with [60]fullerene may now also be viewed as, at least, qualitative evidence for a Marcus-inverted behavior as well.



Table 4: Rate Constant for Electron Transfer from C<sub>60</sub>, C<sub>76</sub> and C<sub>78</sub> to Various (Arene)<sup>•+</sup> in Dichloromethane at Room Temperature (25, 51)

COMPOUND	IP [eV]			
		C <sub>60</sub> (I <sub>h</sub> ) k <sub>obs</sub> [10 <sup>10</sup> M <sup>-1</sup> s <sup>-1</sup> ]	C <sub>76</sub> (D <sub>2</sub> ) k <sub>obs</sub> [10 <sup>10</sup> M <sup>-1</sup> s <sup>-1</sup> ]	C <sub>78</sub> (C <sub>2v</sub> ) k <sub>obs</sub> [10 <sup>10</sup> M <sup>-1</sup> s <sup>-1</sup> ]
durene	8.2		0.66	0.69
naphthalene	8.15	0.25	0.89	0.93
m-terphenyl	8.01	0.38	1.1	1.5
biphenyl	7.95	0.79	2.0	2.5
hexamethylbenzene	7.9		2.1	2.0
triphenylene	7.86		2.9	2.3
phenanthrene	7.85		3.0	2.5
fluorene	7.78		3.2	2.9
trans-Stilben	7.7	0.68		
9-anthraldehyde	7.69		2.9	3.0
chrysene	7.59		4.5	4.2
9,10-dibromoanthracene	7.58		2.8	2.7
anthracene	7.45		1.5	1.7
pyrene	7.41		1.0	1.1
coronene	7.29		0.36	
9-anthracenemethanol	7.21		0.078	0.2

### 3. MONOFUNCTIONALIZED FULLERENE DERIVATIVES



Scheme 1

The unique reactivity and the predominantly hydrophobic nature of [60]fullerene, stimulated broad and interdisciplinary interest to modify its polyfunctional structure which contains 30 reactive double bonds located at the junctions of two hexagons *via* an extended number of addition reactions (53-58). Covalent attachment of a large number of addends at the hydrophobic fullerene core has been shown to lead to novel and innovative materials with unique properties ranging from drug delivery to advanced nanostructured devices. In the following sections, studies are reviewed that focus on time-resolved and steady-state experiments with functionalized fullerene derivatives.

**C<sub>60</sub>C(COOEt)<sub>2</sub> (1) and C<sub>60</sub>(C<sub>4</sub>H<sub>9</sub>N) (2):** Pulse irradiation of an oxygen-free toluene, acetone and 2-propanol solution (8:1:1 v/v) containing C<sub>60</sub>C(COOEt)<sub>2</sub> resulted in the formation of a distinct absorption pattern in the NIR. This band is ascribed to the  $\pi$ -radical anion formed in the general reaction (59,60):

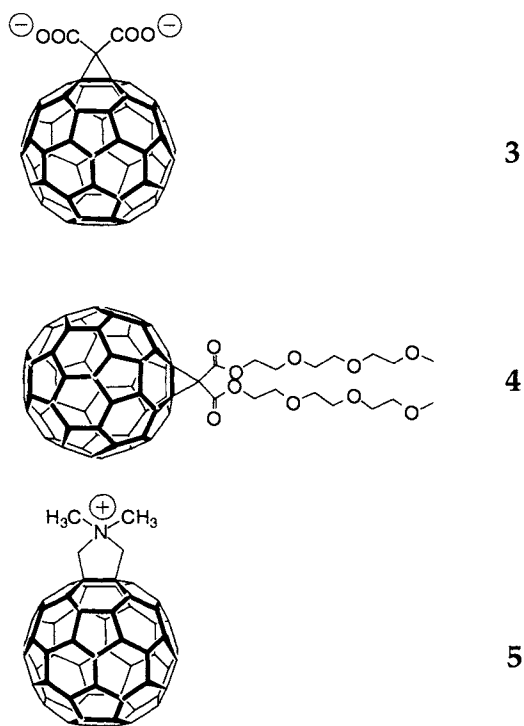


The differential absorption spectrum obtained upon pulse radiolysis of C<sub>60</sub>C(COOEt)<sub>2</sub> exhibits a maximum at 1040 nm, hypsochromically shifted by 40 nm relative to the 1080 nm  $\pi$ -radical anion band of [60]fullerene. A corresponding blue-shift was also observed for the  $\pi$ -radical anion of C<sub>60</sub>(C<sub>4</sub>H<sub>9</sub>N) (61). This reflects the

perturbation of the fullerene HOMO's and LUMO's in the monoadduct relative to those of [60]fullerene. For example, the molecular orbitals of  $C_{60}C(COOEt)_2$  show a significant electron deficit in the HOMO, especially in the equatorial area. Reduction, by means of an addition into a vacant LUMO leads to an electron distribution with a notable localization in the equatorial area. This may serve as supportive evidence to explain the substantial optical differences between ground state, reduced state and excited state spectra of [60]fullerene and  $C_{60}C(COOEt)_2$  derivatives.

### 3.1. Hydrophilic Addends

Functionalization of the fullerene core with hydrophilic groups (Scheme 2) has emerged as an important goal, which if successfully reached, enables the pulse radiolytic investigation in aqueous media without the necessity of employing solubilizing host molecules.



Scheme 2

**C<sub>60</sub>C(COO<sup>-</sup>)<sub>2</sub> (3)**: Surprisingly, no evidence was found for any reduction of the functionalized fullerene dicarboxylate, C<sub>60</sub>C(COO<sup>-</sup>)<sub>2</sub> (Scheme 2), in aqueous solution (62). This emerged from pulse radiolysis experiments with an aqueous solution containing a wide concentration range of this fullerene derivative. The absorption attributable to the hydrated electron remained virtually unaffected upon addition of C<sub>60</sub>C(COO<sup>-</sup>)<sub>2</sub> and the characteristic NIR-absorption of the fullerene radical anion was completely lacking. Similarly, any attempt to achieve reduction by <sup>•</sup>CH<sub>2</sub>OH, CH<sub>3</sub><sup>•</sup>CHOH, (CH<sub>3</sub>)<sub>2</sub><sup>•</sup>COH and (CH<sub>3</sub>)<sub>2</sub><sup>•</sup>CO<sup>-</sup> failed.

This finding is explained by a micellar aggregation of the C<sub>60</sub>C(COO<sup>-</sup>)<sub>2</sub> derivative in water as a result of its amphiphilic structure. These clusters are considered to contain an inward oriented hydrophobic fullerene moiety and a hydrophilic layer of carboxylate head groups, which prevent penetration of the electron. This conclusion is corroborated by corresponding experiments in solvents with lower polarity where the carboxylate groups become neutralized and facilitate the fullerene reduction again. Evidence for clustering in aqueous and alcoholic systems is also provided by the ground state spectra. In particular, the visible region is dominated by strong dynamic light scattering.

The incorporation of the functionalized fullerene into a host molecule, such as a  $\gamma$ -cyclodextrin or surfactants is an elegant way to bypass the aggregation of C<sub>60</sub>C(COO<sup>-</sup>)<sub>2</sub>. As demonstrated in studies with [60]fullerene this host can accommodate only a single fullerene molecule, which still has access to the solvent phase. The ground state spectrum of this guest-host complex shows the same narrow bands as, for example, monomeric C<sub>60</sub>C(COOEt)<sub>2</sub> or C<sub>60</sub>/ $\gamma$ -CD and clearly differs from the presumed {C<sub>60</sub>C(COO<sup>-</sup>)<sub>2</sub>}<sub>n</sub> cluster.

Pulse radiolysis of C<sub>60</sub>C(COO<sup>-</sup>)<sub>2</sub>/ $\gamma$ -CD in aqueous media leaves no doubt that this nonaggregated fullerene complex is rapidly reduced by the hydrated electron. Variation of the fullerene concentration resulted in an accelerated formation of the characteristic fullerene radical anion in the near NIR band, which maximizes at 1040 nm, and decay of the hydrated electron absorption around 760 nm. Both rates are linearly dependent on the fullerene concentration, and in excellent agreement with each other, suggesting that the observed reaction can be ascribed to an electron induced reduction of the C<sub>60</sub>C(COO<sup>-</sup>)<sub>2</sub>/ $\gamma$ -CD complex. The rate constant amounts to  $9.8 \times 10^9 \text{ M}^{-1}\text{s}^{-1}$ , and is only slightly lower than the one found for [60]fullerene encapsulated in  $\gamma$ -CD. This trend parallels the electrochemically determined reduction potentials of [60]fullerene and various monofunctionalized fullerene derivatives. It is also in line with the fact that, saturation of a C=C double bond of the fullerene core usually raises the LUMO energy and, in turn, shifts the reduction potentials to more negative values.

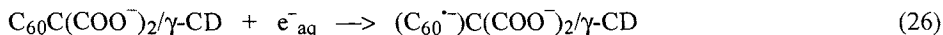
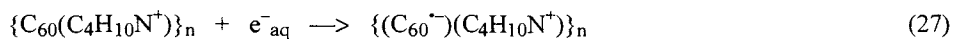


Table 5: Rate Constant for the Radiation-Induced Reduction of C<sub>60</sub> and Monofunctionalized Fullerene Derivatives in Various Solvents (50,59-64).

COMPOUND	MEDIUM	REAGENT	RATE CONSTANT [10 <sup>10</sup> M <sup>-1</sup> s <sup>-1</sup> ]	PRODUCT; MAXIMUM [nm]
C <sub>60</sub> /γ-CD	H <sub>2</sub> O	e <sub>aq</sub> <sup>-</sup>	1.8	C <sub>60</sub> <sup>·-</sup> ; 1080
	H <sub>2</sub> O	(CH <sub>3</sub> ) <sub>2</sub> <sup>·</sup> COH	0.027	C <sub>60</sub> <sup>·-</sup> ; 1080
C <sub>60</sub> C(COOEt) <sub>2</sub> (1)	Toluene/Acetone 2-Propanol	(CH <sub>3</sub> ) <sub>2</sub> <sup>·</sup> COH	0.11	C <sub>60</sub> <sup>·-</sup> ; 1040
C <sub>60</sub> C(COO <sup>-</sup> ) <sub>2</sub> (3)	H <sub>2</sub> O/Triton	e <sub>aq</sub> <sup>-</sup>	1.7	C <sub>60</sub> <sup>·-</sup> ; 1015
	H <sub>2</sub> O/Triton	(CH <sub>3</sub> ) <sub>2</sub> <sup>·</sup> COH	0.054	C <sub>60</sub> <sup>·-</sup> ; 1015
C <sub>60</sub> C(COO <sup>-</sup> ) <sub>2</sub> /γ-CD (3)	H <sub>2</sub> O	e <sub>aq</sub> <sup>-</sup>	0.98	C <sub>60</sub> <sup>·-</sup> ; 1040
	H <sub>2</sub> O	(CH <sub>3</sub> ) <sub>2</sub> <sup>·</sup> COH	0.036	C <sub>60</sub> <sup>·-</sup> ; 1040
C <sub>60</sub> [C(OCH <sub>2</sub> CH <sub>2</sub> ) <sub>3</sub> CH <sub>3</sub> ] <sub>2</sub> (4)	H <sub>2</sub> O/Triton	e <sub>aq</sub> <sup>-</sup>	1.3	C <sub>60</sub> <sup>·-</sup> ; 1010
	H <sub>2</sub> O/Triton	(CH <sub>3</sub> ) <sub>2</sub> <sup>·</sup> COH	0.061	C <sub>60</sub> <sup>·-</sup> ; 1010
C <sub>60</sub> [C(OCH <sub>2</sub> CH <sub>2</sub> ) <sub>3</sub> CH <sub>3</sub> ] <sub>2</sub> /γ-CD (4)	H <sub>2</sub> O	e <sub>aq</sub> <sup>-</sup>	0.92	C <sub>60</sub> <sup>·-</sup> ; 1030
	H <sub>2</sub> O	(CH <sub>3</sub> ) <sub>2</sub> <sup>·</sup> COH	0.052	C <sub>60</sub> <sup>·-</sup> ; 1030
C <sub>60</sub> (C <sub>3</sub> H <sub>7</sub> N) (2)	Toluene/Acetone 2-Propanol	(CH <sub>3</sub> ) <sub>2</sub> <sup>·</sup> COH	0.098	C <sub>60</sub> <sup>·-</sup> ; 1025
C <sub>60</sub> (C <sub>4</sub> H <sub>10</sub> N <sup>+</sup> ) (5)	H <sub>2</sub> O	e <sub>aq</sub> <sup>-</sup>	0.36	C <sub>60</sub> <sup>·-</sup> ; 1010
	H <sub>2</sub> O	(CH <sub>3</sub> ) <sub>2</sub> <sup>·</sup> COH	0.09 *	C <sub>60</sub> <sup>·-</sup> ; 1010
	H <sub>2</sub> O/Triton	e <sub>aq</sub> <sup>-</sup>	3.5	C <sub>60</sub> <sup>·-</sup> ; 1015
	H <sub>2</sub> O/Triton	(CH <sub>3</sub> ) <sub>2</sub> <sup>·</sup> COH	0.077	C <sub>60</sub> <sup>·-</sup> ; 1015
	vesicle	e <sub>aq</sub> <sup>-</sup>	3.2	C <sub>60</sub> <sup>·-</sup> ; 1015
C <sub>60</sub> (C <sub>4</sub> H <sub>10</sub> N <sup>+</sup> )/γ-CD (5)	H <sub>2</sub> O	e <sub>aq</sub> <sup>-</sup>	2.8	C <sub>60</sub> <sup>·-</sup> ; 1030

**C<sub>60</sub>[C(OCH<sub>2</sub>CH<sub>2</sub>)<sub>3</sub>CH<sub>3</sub>]<sub>2</sub> (4)**: To discriminate the contribution that stems from a potential charge repulsion between the hydrated electrons and the charged fullerene core a fullerene derivative was probed that bears a solubilizing triethylenglycol chain (C<sub>60</sub>[C(OCH<sub>2</sub>CH<sub>2</sub>)<sub>3</sub>CH<sub>3</sub>]<sub>2</sub>) (Scheme 2) (63). From the pulse radiolytic experiments however the concern emerged that, beside the charge repulsion, clustering has possibly the comparatively stronger effect on the fullerene reactivity. This assumption correlates, in fact, with the ground state and excited state properties of an aqueous solution of C<sub>60</sub>[C(OCH<sub>2</sub>CH<sub>2</sub>)<sub>3</sub>CH<sub>3</sub>]<sub>2</sub>: Strong light scattering of the absorption spectrum and a very short triplet lifetime substantiate the fullerene clustering. In essence, only the surfactant-capped or  $\gamma$ -CD incorporated complex revealed the expected ease of radiolytic reduction.

**C<sub>60</sub>(C<sub>4</sub>H<sub>10</sub>N<sup>+</sup>) (5)**: Finally in an attempt, not only to overcome the Columbic charge repulsion, but, more importantly, to attract a reaction of the hydrated electrons with a charged fullerene core, a positively charged pyrrolidinium salt, e.g., C<sub>60</sub>(C<sub>4</sub>H<sub>10</sub>N<sup>+</sup>) (Scheme 2), was probed (64). Despite the also unequivocally occurring clustering in aqueous media, attachment of a pyrrolidinium group enhanced the rate for reduction of these clusters by hydrated electrons and (CH<sub>3</sub>)<sub>2</sub><sup>•</sup>COH radicals as compared to the negatively charged system {C<sub>60</sub>C(COO<sup>-</sup>)<sub>2</sub>}<sub>n</sub>.



The NIR fingerprint indicated also significant differences relative to the reduced  $\gamma$ -CD-incorporated monomer ((C<sub>60</sub><sup>•-</sup>)(C<sub>4</sub>H<sub>10</sub>N<sup>+</sup>)/ $\gamma$ -CD). The spectral features of the fullerene cluster, for example, are much broader. This is further corroborated by lower yields of the reduced cluster compared to the reduced monomer.

Concerning the reduction of C<sub>60</sub>(C<sub>4</sub>H<sub>10</sub>N<sup>+</sup>)/surfactant and C<sub>60</sub>(C<sub>4</sub>H<sub>10</sub>N<sup>+</sup>)/ $\gamma$ -CD by hydrated electrons a significant rate enhancement over [60]fullerene and negatively charged C<sub>60</sub>C(COO<sup>-</sup>)<sub>2</sub> (surface-capped or  $\gamma$ -CD-incorporated) is noticed (Table 5). This can be understood in terms of the Columbic forces which decelerate a reaction between hydrated electrons and the negatively charged fullerenes while they facilitate reduction of the positively charged fullerene. On the other hand, electron transfer rates from uncharged (CH<sub>3</sub>)<sub>2</sub><sup>•</sup>COH radicals, which should be less affected by the surface charge of the respective functionalized fullerene derivative, still follow the trend observed for reactions of the hydrated electron. This suggests, in line with the quenching rates, an anodic shift of the reduction potential of C<sub>60</sub>(C<sub>4</sub>H<sub>10</sub>N<sup>+</sup>) relative to C<sub>60</sub>C(COO<sup>-</sup>)<sub>2</sub> and [60]fullerene.

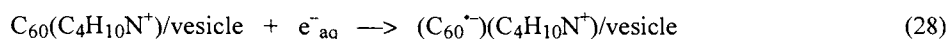
In summary, functionalization of C<sub>60</sub> shows that a single hydrophilic addend is not sufficient to prevent the strong hydrophobic 3-dimensional interactions among the fullerene moieties and the resulting tendency to form aggregates. This precludes formation of stable monomers of monofunctionalized fullerene derivatives in aqueous solution and leads to the irreversible formation of clusters.

### 3.2. Vesicular Systems

The systematic variation of the functionalizing addends, covalently linked to the fullerene core, has also been used to facilitate their incorporation into different vesicular matrices, and to probe these systems in electron transfer studies (50).

Functionalized fullerene derivatives in lipid bilayer materials exhibited the characteristic fullerene ground state absorption. In particular, the 213, 259, 324, and 426 nm bands are fingerprints for mono-functionalized fullerene derivatives (C<sub>60</sub>(C<sub>4</sub>H<sub>10</sub>N<sup>+</sup>) and C<sub>60</sub>[C(OCH<sub>2</sub>CH<sub>2</sub>)<sub>3</sub>CH<sub>3</sub>]<sub>2</sub>) evolving from their partially broken C<sub>2v</sub> symmetry. Obstruction of cluster formation in case of C<sub>60</sub>(C<sub>4</sub>H<sub>10</sub>N<sup>+</sup>) and C<sub>60</sub>[C(OCH<sub>2</sub>CH<sub>2</sub>)<sub>3</sub>CH<sub>3</sub>]<sub>2</sub> derivatives points to an amphiphilic behavior. These compounds contain addends that may establish strong interaction with either the polar head group of the hosting matrix or the surrounding aqueous phase. It should be pointed out that the pyrrolidinium group in C<sub>60</sub>(C<sub>4</sub>H<sub>10</sub>N<sup>+</sup>) resembles the head group structure of DODAB and lecithin. On the other hand, the triethylenglycol chains in C<sub>60</sub>[C(OCH<sub>2</sub>CH<sub>2</sub>)<sub>3</sub>CH<sub>3</sub>]<sub>2</sub> should implement interaction, through the polar interface, with the aqueous medium.

Electron transfer to the electron-accepting fullerene moieties was probed by pulse radiolysis under strictly reductive conditions. The experiments showed significantly reduced lifetimes of the hydrated electron absorption around 700 nm suggesting reaction 28 to occur. Characteristic changes were also observed with respect to the fullerene  $\pi$ -radical anion band in the NIR.



The shape and, more importantly, the yield of the  $\pi$ -radical anion absorption depend mainly on the charge of the vesicle head group. The data demonstrate that, regardless of the derivative, the most efficient fullerene reaction takes place within the positively charged DODAB vesicle, while the least effective reduction was found to occur in the negatively charged DHP systems. This trend suggests that variation of the head group charge impacts the dynamics of the associated electron transfer process. A possible rationale is based on charge attraction or repulsion exposed to the negative electrons by the oppositely or equally charged vesicle interface, respectively.

The rate constants for the reduction of  $C_{60}(C_4H_{10}N^+)/DODAB$  and  $C_{60}[C(OCH_2CH_2)_3CH_3]_2/DODAB$  systems by hydrated electrons amount to  $3.2 \times 10^{10} M^{-1}s^{-1}$  and  $1.7 \times 10^{10} M^{-1}s^{-1}$ , respectively. They are in excellent agreement with those established for the corresponding  $\gamma$ -CD inclusion complexes and fullerene surfactant solutions (see Table 5).

In conclusion, structurally balanced fullerene derivatives were successfully incorporated into various vesicular matrices. Truly monomeric immersion of amphiphilic  $C_{60}(C_4H_{10}N^+)$  and  $C_{60}[C(OCH_2CH_2)_3CH_3]_2$  derivatives into the polar head group anchored the fullerene core still close enough to the lipid bilayer interface to facilitate very efficient reductions by hydrated electrons and  $\cdot CH_2OH$  radicals.

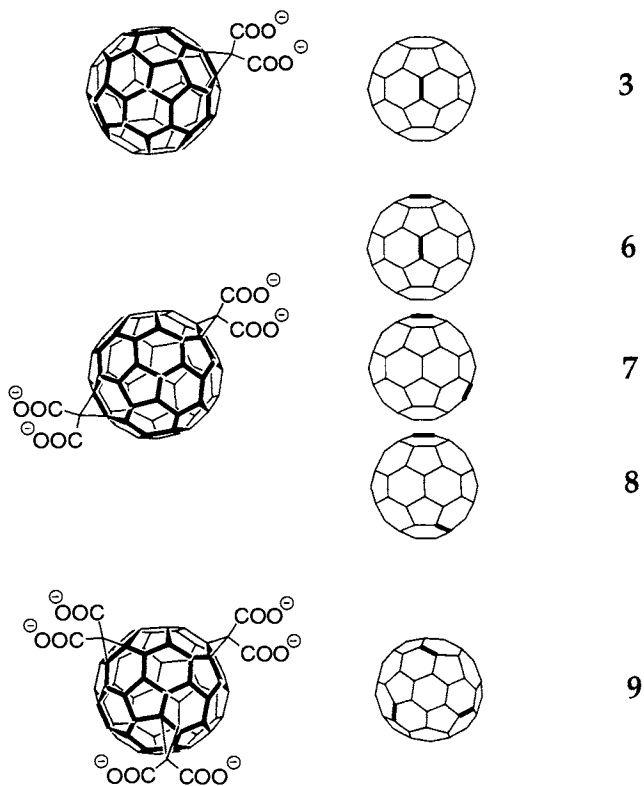
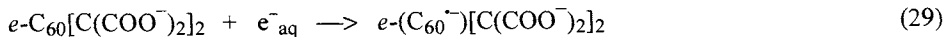
#### 4. MULTIPLY FUNCTIONALIZED FULLERENE DERIVATIVES

Introduction of a second and, subsequently, a third hydrophilic ligand to the fullerene core leads to materials, which, in essence, display an enhanced surface coverage of the hydrophobic fullerene surface. It was expected that fullerene aggregation may be impacted to a noticeable extent and that micellar aggregation does not play a role in the reactivity of these functionalized fullerenes. It should be noted that these water-soluble derivatives are important alternatives to the  $\gamma$ -incorporated and surfactant-capped fullerenes.

**$C_{60}[C(COO^-)_2]_2$  (6-8) and  $C_{60}[C(COO^-)_2]_3$  (9):** A series of water-soluble multiplyfunctionalized fullerenes, namely, *e*- $C_{60}[C(COO^-)_2]_2$  (**6**), *trans*-3- $C_{60}[C(COO^-)_2]_2$  (**7**), *trans*-2- $C_{60}[C(COO^-)_2]_2$  (**8**), and *e, e, e*- $C_{60}[C(COO^-)_2]_3$  (**9**) (Scheme 3) were probed in radical-induced studies and compared to those of  $\{(C_{60})C(COO^-)_2\}_n$  clusters from the monofunctionalized fullerenes (**65**). Ground state absorption spectra, recorded up to  $1.0 \times 10^{-4} M$ , show no deviation from the Lambert Beer law and thus speak against any clustering. The strongly enhanced triplet lifetime ( $\approx 40 \mu s$ ) relative to  $\{(^3C_{60})C(COO^-)_2\}_n$  clusters ( $\tau = 0.4 \mu s$ ) also indicates a truly monomeric appearance of these bis- and trisfunctionalized fullerenes in aqueous solutions.

Pulse radiolytic reductions were conducted without employing a hydrophilic host molecule. Radical-induced reduction of *e*- $C_{60}[C(COO^-)_2]_2$  in  $N_2$ -purged aqueous solution showed that the expected formation of the diagnostic NIR transition band occurs synchronously with the decay of the electron absorption. The fullerene  $\pi$ -radical anion, absorbs at 1055 nm, which is 5 nm blue-shifted relative to the analogous reduced ester derivative.









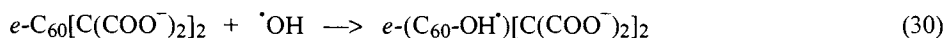
Scheme 3

From the first-order rate constant *versus* concentration dependency a bimolecular rate constant of  $2.9 \times 10^9 \text{ M}^{-1}\text{s}^{-1}$  was derived for reaction 29. All bisfunctionalized fullerene derivatives investigated were successfully reduced by means of hydrated electrons ( $(0.75 - 3.4) \times 10^9 \text{ M}^{-1}\text{s}^{-1}$ ) and  $(\text{CH}_3)_2\dot{\text{C}}\text{OH}$  radicals ( $(0.9 - 2.2) \times 10^8 \text{ M}^{-1}\text{s}^{-1}$ ) (Table 6). These values are, however, significantly lower than those for the reduction of  $\text{C}_{60}$ /surfactant ( $\text{C}_{60}\text{C}(\text{COO}^-)_2$ )/surfactant and the respective  $\gamma$ -CD encapsulated complexes. Such an effect reflects the perturbation of the fullerene  $\pi$ -system caused by placing two functional negatively charged appendices onto the fullerene core.

Table 6: Rate Constant for the Radiation-Induced Reduction of Various Bisfunctionalized Fullerene Derivatives in Homogeneous (H<sub>2</sub>O, 10 vol % 2-propanol, pH 9.7) and Heterogeneous (5% Triton X-100) Aqueous Solutions (65).

COMPOUND	MEDIUM	REAGENT	RATE CONSTANT [10 <sup>10</sup> M <sup>-1</sup> s <sup>-1</sup> ]	PRODUCT; MAXIMUM [nm]
 <i>e</i> -C <sub>60</sub> [C(COO <sup>-</sup> ) <sub>2</sub> ] <sub>2</sub> (6)	H <sub>2</sub> O	e <sub>aq</sub> <sup>-</sup>	0.29	(C <sub>60</sub> <sup>•-</sup> )R; 1040
	H <sub>2</sub> O	(CH <sub>3</sub> ) <sub>2</sub> COH <sup>•</sup>	0.022	(C <sub>60</sub> <sup>•-</sup> )R; 1040
	H <sub>2</sub> O/Triton	e <sub>aq</sub> <sup>-</sup>	0.34	(C <sub>60</sub> <sup>•-</sup> )R; 1040
	H <sub>2</sub> O/Triton	(CH <sub>3</sub> ) <sub>2</sub> COH <sup>•</sup>	0.021	(C <sub>60</sub> <sup>•-</sup> )R; 1040
 trans-3-C <sub>60</sub> [C(COO <sup>-</sup> ) <sub>2</sub> ] <sub>2</sub> (7)	H <sub>2</sub> O	e <sub>aq</sub> <sup>-</sup>	0.19	(C <sub>60</sub> <sup>•-</sup> )R; 995
	H <sub>2</sub> O	(CH <sub>3</sub> ) <sub>2</sub> COH <sup>•</sup>	0.011	(C <sub>60</sub> <sup>•-</sup> )R; 995
	H <sub>2</sub> O/Triton	e <sub>aq</sub> <sup>-</sup>	0.26	(C <sub>60</sub> <sup>•-</sup> )R; 995
	H <sub>2</sub> O/Triton	(CH <sub>3</sub> ) <sub>2</sub> COH <sup>•</sup>	0.024	(C <sub>60</sub> <sup>•-</sup> )R; 995
 trans-2-C <sub>60</sub> [C(COO <sup>-</sup> ) <sub>2</sub> ] <sub>2</sub> (8)	H <sub>2</sub> O	e <sub>aq</sub> <sup>-</sup>	0.34	(C <sub>60</sub> <sup>•-</sup> )R; 880
	H <sub>2</sub> O	(CH <sub>3</sub> ) <sub>2</sub> COH <sup>•</sup>	0.019	(C <sub>60</sub> <sup>•-</sup> )R; 880
	H <sub>2</sub> O/Triton	e <sub>aq</sub> <sup>-</sup>	0.32	(C <sub>60</sub> <sup>•-</sup> )R; 880
	H <sub>2</sub> O/Triton	(CH <sub>3</sub> ) <sub>2</sub> COH <sup>•</sup>	0.02	(C <sub>60</sub> <sup>•-</sup> )R; 880
 <i>e,e,e</i> -C <sub>60</sub> [C(COO <sup>-</sup> ) <sub>2</sub> ] <sub>3</sub> (9)	H <sub>2</sub> O	e <sub>aq</sub> <sup>-</sup>	0.075	(C <sub>60</sub> <sup>•-</sup> )R; 1020
	H <sub>2</sub> O	(CH <sub>3</sub> ) <sub>2</sub> COH <sup>•</sup>	0.009	(C <sub>60</sub> <sup>•-</sup> )R; 1020

Bisfunctionalized  $C_{60}$  carrying negatively charged carboxyl groups,  $C_{60}[C(COO^-)_2]_2$ , or positively charged quaternary ammonium groups,  $C_{60}(C_4H_{10}N^+)_2$ , have been shown to exhibit high water-solubility without cluster formation. This renders them excellent target molecules for free radical attack in aqueous environment. Absolute rate constants on the order of  $8 \times 10^9 \text{ M}^{-1}\text{s}^{-1}$  and  $1.5 \times 10^9 \text{ M}^{-1}\text{s}^{-1}$  have been measured for the addition of  $\cdot\text{OH}$  radicals to the fullerene core for a variety of bisfunctionalized stereoisomers. Water-soluble polyfunctionalized fullerenes, namely, *e,e,e*- $C_{60}[C(COO^-)_2]_3$ ,  $C_{60}[(CH_2)_4SO_3H]_6$ , and  $C_{60}(\text{OH})_{18}$  exhibited, however, a lower reactivity towards  $\cdot\text{OH}$  radicals (66). Polyfunctionalization reduces the number of reactive sites on the fullerene surface due to  $sp^{2.278}$ -carbon hybridization, and eventually leads to fullerene derivatives that show little resemblance to the original [60]fullerene.

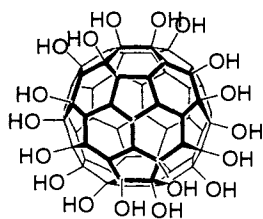


In the case of  $C_{60}/\gamma\text{-CD}$ ,  $C_{60}C(COO^-)_2/\gamma\text{-CD}$ , and  $C_{60}[C(\text{OCH}_2\text{CH}_2)_3\text{CH}_3]_2/\gamma\text{-CD}$  the supramolecular host ( $\gamma\text{-CD}$ ) may, as shown for the example of  $\cdot\text{OH}$ -radicals, serve as an efficient radical trap. It even seems to prevent a consecutive transfer of the radical site created at the host to the fullerene guest.

**$C_{60}(\text{OH})_{18}$  (10):** Polyhydroxylation (Scheme 4) of the hydrophobic [60]fullerene core enhances the water solubility of this carbon allotrope up to  $4.0 \times 10^{-2} \text{ M}$  (67). The  $\pi$ -radical anion,  $(C_{60}^{\bullet-})(\text{OH})_{18}$ , generated by electron transfer from hydrated electrons and  $(\text{CH}_3)_2\dot{\text{C}}\text{OH}$  radicals, absorbs with maxima at 870, 980 and 1050 nm. The bimolecular rate constant for a reaction with hydrated electrons is  $4.5 \times 10^8 \text{ M}^{-1}\text{s}^{-1}$ . Based on electron transfer studies with suitable electron donor / acceptor substrates, the reduction potential of the  $C_{60}(\text{OH})_{18}/(C_{60}^{\bullet-})(\text{OH})_{18}$  couple was estimated to be in the range between -0.358 V and -0.465 V *versus* NHE.



In conclusion, the extended and highly delocalized  $\pi$ -system experiences a gradual destruction. Specifically, a perturbation is noticed which depends strongly on i) the degree of functionalization, ii) the relative distance of the individual addends to each other, and iii) the electronic structure of the substituent.



10

Scheme 4

## 5. CONCLUDING REMARKS

Radiation chemical techniques were employed to characterize transient intermediates and stable products following the one-electron reduction and oxidation of fullerenes and functionalized fullerene derivatives. In particular, these techniques are excellently suited for conducting energy transfer and alkylation reactions with fullerenes in homogenous and heterogeneous environments. The NIR fingerprint of all the different fullerene products (e.g.,  $\pi$ -radical anion,  $\pi$ -radical cation, triplet excited states and alkyl adduct radicals) proved to be a powerful means to differentiate between the different reaction pathways. A fundamental advantage of pulse radiolysis, for example, is the low solute concentration, at which a meaningful experiment can be performed. This is an important aspect in view of the generally poor solubility of fullerenes. This allowed, beside the spectral identification of transients and the determination of the individual reaction rate constants for intermolecular reactions between fullerenes and a variety of reducing / oxidizing radicals and stable  $\pi$ -radical anion /  $\pi$ -radical cations with high accuracy. Furthermore, the spectral and kinetic parameters determined helped to gain a comprehensive mechanistic view of the formation and deactivation of fullerene intermediates.

Two findings are particularly noteworthy. First, the experiments in which the reactivity of water-soluble fullerene derivatives in aqueous media was probed (62-64): Not only, that the intermolecular reactions with hydrated electron and various radicals provided unequivocally evidence for the presence of fullerene clusters. But, furthermore, these investigations helped, in reference to the kinetics of the fullerene monomers, to estimate the agglomeration number for, for example, the mono pyrrolidinium salt in the respective fullerene cluster. Secondly, the intermolecular electron transfer reactions between radiolytically generated arene  $\pi$ -radical cations and higher fullerenes (25,51): The noted parabolic dependence of the rate constants on the thermodynamic driving force is one of the rare confirmations of the existence of the "Marcus-Inverted" region in forward electron transfer.

More recently, pulse radiolysis started to play a major role in the characterization of photolytically generated ( $A^{\cdot-}-D^{\cdot+}$ ) radical pairs in a variety of fullerene containing donor-bridge-acceptor dyads (68,69). While the latter evolve from photoinduced intramolecular electron transfer reactions complementary employment of pulse radiolysis allowed to generate the reduced and oxidized entities in separate experiments and to superimpose the features of the two reactive moieties. In this context, it should be noted that conventional methods, such as cyclic voltammetry, due to their unfavorable time resolution, fail to contribute to the radical pair characterization.

## 6. ACKNOWLEDGMENT

This work was supported by the Office of Basic Energy Sciences of the Department of Energy (contribution No. NDRL-4133 from the Notre Dame Radiation Laboratory).

## 7. REFERENCES

1. R. C. Haddon, L. E. Brus and K. Raghavachari, *Chem. Phys. Lett.*, 131 (1986) 165.
2. M. K. Kelly, P. Etchegoin, D. Fuch, W. Krätschmer and K. Fostiropulos, *Phys. Rev. B*, 46 (1992) 4963.
3. A. Y. Saito, H. Shinohara, M. Kato, H. Nagashima, M. Ohkohchi and Y. Ando, *Chem. Phys. Lett.*, 186 (1992) 236.
4. P. W. Stephens, L. Mihaly, P. L. Lee, R. L. Whetten, S.-M. Huang, R. Kaner, F. Diederich and K. Holczer, *Nature*, 351 (1991) 632.
5. M. J. Rosseinsky, *J. Mater. Chem.*, 5 (1995) 1497.
6. J. H. Weaver, *Acc. Chem. Res.*, 25 (1992) 143.
7. L. Echegoyen and L. E. Echegoyen, *Acc. Chem. Res.*, 31, 593-601 (1998).
8. P. L. Boulas, M. Gomez-Kaifer and L. Echegoyen, *Angew. Chem. Int. Ed. Engl.*, 37 (1998) 216.
9. D. Dubois, K. M. Kadish, S. Flanagan, R. E. Haufler, L. P. F. Chibante and L. J. Wilson, *J. Am. Chem. Soc.*, 113 (1991) 4364.
10. T. Kato, T. Kodama, T. Shida, T. Nakagawa, Y. Matsui, S. Suzuki, H. Shiromaru, K. Yamauchi and Y. Achiba, *Chem. Phys. Lett.*, 180 (1991) 446.
11. M. Baumgarten, A. Gügel and L. Ghergel *Adv. Mater.*, (1993) 5 458.
12. D.M. Guldi, H. Hungerbühler, E. Janata and K.-D. Asmus, *J. Chem. Soc., Chem. Commun.*, (1993) 84.
13. D.M. Guldi, H. Hungerbühler, E. Janata and K.-D. Asmus, *J. Phys. Chem.*, 97 (1993) 11258.
14. N. Dimitrijevic, *Chem. Phys. Lett.*, 194 (1992) 457.

15. Z.R. Lian, S.D. Yao, W.Z. Lin, W.F. Wang and N.Y. Lin, *Radiat. Phys. Chem.*, 50 (1997) 245.
16. H.-Q. Hou, C. Luo, Z.-X. Liu, D.-M. Mao, Q.-Z. Qin, Z.-R. Lian, S.-D. Yao, W.-F. Wang, J.-S. Zhang and N.-Y. Lin, *Chem. Phys. Lett.*, 203 (1993) 555.
17. S.-D. Yao, Z.-R. Lian, W.-F. Wang, J.-S. Zhang, N.-Y. Lin, H.-Q. Hou, Z.-M. Zhang and Q.-Z. Qin, *Chem. Phys. Lett.*, 239 (1995) 112.
18. S.D. Yao, W.Z. Lin, Z.R. Lian, W.F. Wang and N.Y. Lin, *Radiat. Phys. Chem.*, 50 (1997) 249.
19. R. C. Haddon, *Acc. Chem. Res.*, 21 (1988) 243.
20. J. R. Morton, F. Negri and K. F. Preston, *Acc. Chem. Res.*, 31 (1998) 63.
21. N.M. Dimitrijevic, P.V. Kamat and R.W. Fessenden, *J. Phys. Chem.*, 97 (1993) 615.
22. H.N. Ghosh, H. Pal, A.V. Sapre, T. Mukherjee and J.P. Mittal, *J. Chem. Soc., Faraday Trans.*, 92 (1996) 941.
23. D.M. Guldi, H. Hungerbühler, M. Wilhelm and K.-D. Asmus, *J. Chem. Soc. Faraday Trans.*, 90 (1994) 1391.
24. D.M. Guldi, D. Liu and P.V. Kamat, *J. Phys. Chem. A*, 101 (1997) 6195.
25. D.M. Guldi and K.-D. Asmus, *J. Am. Chem. Soc.*, 119 (1997) 5744.
26. P.V. Kamat, G. Sauve, D.M. Guldi and K.-D. Asmus, *Research on Chemical Intermediates*, 23 (1997) 575.
27. N.M. Dimitrijevic and P.V. Kamat, *J. Phys. Chem.*, 96 (1992) 4811.
28. D. K. Palit, H. Mohan and J.P. Mittal, *J. Phys. Chem. A*, 102 (1998) 4456.
29. D.K. Palit, H. Mohan, P.B. Birkett and J.P. Mittal, *J. Phys. Chem.*, 101 (1997) 5418.
30. K.I. Priyadarsini, H. Mohan, P.B. Birkett and J.P. Mittal, *J. Phys. Chem.*, 100 (1996) 501.
31. R.V. Bensasson, E. Bienvenüe, C. Fabre, J.-M. Janot, E.J. Land, S. Leach, V. Leboulaire, A. Rassat, S. Roux and P. Seta, *Chem. Eur. J.*, 4 (1998) 270.
32. R.V. Bensasson, E. Bienvenüe, J.-M. Janot, S. Leach, P. Seta, D.I. Schuster, S.R. Wilson and H. Zhao, *Chem. Phys. Lett.*, 245 (1995) 566.
33. M. Sundahl, T. Andersson, K. Nilsson, O. Wennerstrom, and G. Westman, *Synth. Met.*, 55 (1993) 3252.
34. T. Andersson, K. Nilsson, M. Sundahl, G. Westman, and O. Wennerström, *J. Chem. Soc., Chem. Commun.*, (1992) 604.
35. K.I. Priyadarsini, H. Mohan, J.P. Mittal, D.M. Guldi and K.-D. Asmus, *J. Phys. Chem.*, 98 (1994) 9565.
36. N.M. Dimitrijevic and P.V. Kamat, *J. Phys. Chem.*, 97 (1993) 7623.
37. V. Ohlendorf, A. Willnow, H. Hungerbühler, K.-D. Asmus and D.M. Guldi, *J. Chem. Soc., Chem. Commun.*, (1995) 759.
38. D.M. Guldi, to be published.
39. R. M. Williams and J. W. Verhoeven, *Recl. Trav. Chim. Pays-Bas*, 111(1992) 531.
40. D.M. Guldi, *Research on Chemical Intermediates*, 23 (1997) 653.

41. H. Hungerbühler, D.M. Guldi and K.-D. Asmus, *J. Am. Chem. Soc.*, 115 (1993) 3386.
42. D.M. Guldi, *J. Phys. Chem. B*, 101 (1997) 9600.
43. A. Beeby, J. Eastoe, and E. R. Crooks, *Chem. Commun.*, (1996) 901.
44. J. Eastoe, E. R. Crooks, A. Beeby, and R. K. Heenan, *Chem. Phys. Lett.*, 245 (1995) 571.
45. Y. N. Yamakoshi, T. Yagami, K. Fukuhara, S. Sueyoshi, and N. Miyata, *J. Chem. Soc., Chem. Commun.*, (1994) 517.
46. S. Niu and D. Mauzerall, *J. Am. Chem. Soc.*, 118 (1996) 5791.
47. K. C. Hwang and D. C. Mauzerall, *Nature*, 361 (1993) 138.
48. K. C. Hwang and D. C. Mauzerall, *J. Am. Chem. Soc.*, 114 (1992) 9705.
49. R. V. Bensasson, E. Bienvenue, M. Dellinger, S. Leach and P. Seta, *J. Phys. Chem.*, 98 (1994) 3492.
50. D.M. Guldi and H. Hungerbühler, *Research on Chemical Intermediates*, 25 (1999) 00000.
51. D.M. Guldi, P. Neta and K.-D. Asmus, *J. Phys. Chem.*, 98 (1994) 4617.
52. D.M. Guldi, P. Neta and K.-D. Asmus, In *Progress in Fullerene Research*, H. Kuzmany, J. Fink, M. Mehring and S. Roth, Eds., World Scientific, (1994) 37.
53. A. Hirsch, *The Chemistry of the Fullerenes* (Georg Thieme Verlag, Stuttgart, 1994).
54. M. Prato and M. Maggini, *Acc. Chem. Res.*, 31 (1998) 519.
55. H. Imahori and Y. Sakata, *Adv. Mater.*, 9 (1997) 537.
56. M. Prato, *J. Mater. Chem.*, 7 (1997) 1097.
57. N. Martín, L. Sánchez, B. Illescas and I. Pérez, *Chem. Rev.*, 98 (1998) 2527.
58. F. Diederich and C. Thilgen, *Science*, 271 (1996) 317.
59. D.M. Guldi, H. Hungerbühler and K.-D. Asmus, *J. Phys. Chem.*, 99 (1995) 9380.
60. D.M. Guldi and K.-D. Asmus, *J. Phys. Chem. A*, 101 (1997) 1472.
61. D.M. Guldi and M. Maggini, *Gaze. Ital. Chim.*, 127 (1998) 779.
62. D.M. Guldi, H. Hungerbühler and K.-D. Asmus, *J. Phys. Chem.*, 99 (1995) 13487.
63. D.M. Guldi, *J. Phys. Chem. A*, 101 (1997) 3895.
64. D.M. Guldi, H. Hungerbühler and K.-D. Asmus, *J. Phys. Chem. A*, 101 (1997) 1783.
65. D.M. Guldi, H. Hungerbühler and K.-D. Asmus, *J. Phys. Chem.*, 103 (1999) 1444.
66. D.M. Guldi and K.-D. Asmus, submitted.
67. H. Mohan, D.K. Palit, J.P. Mittal, L.Y. Chiang, K.-D. Asmus and D.M. Guldi, *J. Chem. Soc., Faraday Trans.*, 94 (1998) 359.
68. A. Polese, S. Mondini, A. Bianco, C. Toniolo, G. Scorrano, D.M. Guldi and M. Maggini, *J. Am. Chem. Soc.*, 121 (1999) 3446.
69. M. Maggini, D.M. Guldi, S. Mondini, G. Scorrano, F. Paolucci, P. Ceroni and S. Roffia, *Chem. Eur. J.*, 4 (1998) 1992.

## Radiation chemistry of quinones

Tulsi Mukherjee

Radiation Chemistry & Chemical Dynamics Division, Chemistry Group,  
Bhabha Atomic Research Centre, Trombay, Mumbai 400 085, India

### 1. INTRODUCTION

Quinones, having at least two carbonyl groups in the para-position of a ring, are known to act as very efficient electron accepting agents [1-4] and have evoked strong interest as a separate class of compounds during the second half of the twentieth century. Since 1955, the National Cancer Institute (USA) has screened over 2000 potential drugs for antitumour activity [5,6]. Many potential drugs have been identified. Out of these, majority are quinones (Figure 1), the first being the simple quinone, 2-methyl-p-benzoquinone.

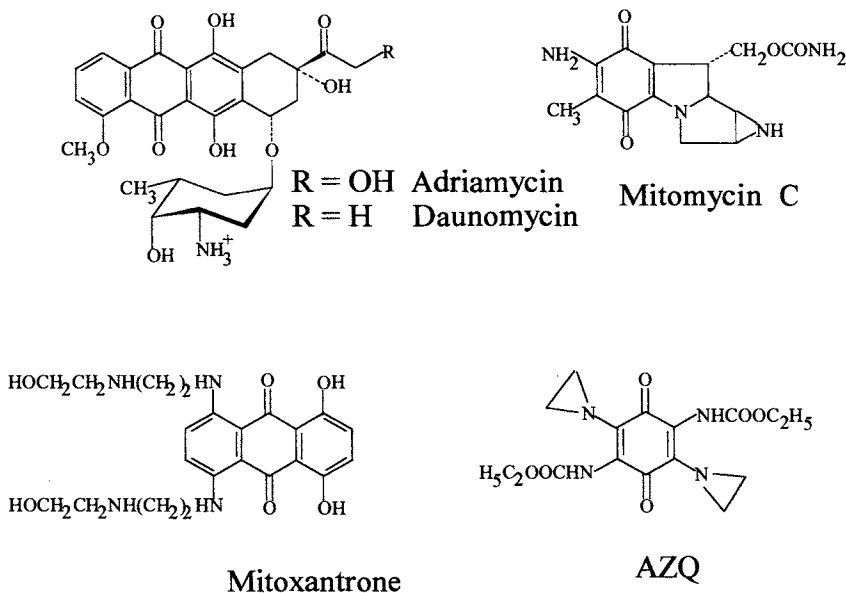


Figure 1. Structure of some quinone antitumour agents.



A considerable amount of research has gone into elucidating the molecular mechanism of action of these antitumour quinones. While several mechanisms are possible, a single mechanism may not fully explain all of the observed cytotoxic effects. One of the objectives of the NCI and other studies elsewhere has been to determine if there were any structure-activity relationships within the major structural groups ranging from the simplest benzoquinones to the complex multiple heteroatom quinones. One of the main conclusions from these studies was that the most active compounds were mitomycin C, the 3,6-diaziridinylbenzoquinones with 2,5-alkylamino substituents, adriamycin (doxorubicin), daunomycin (daunorubicin) and AZQ (Figure 1).

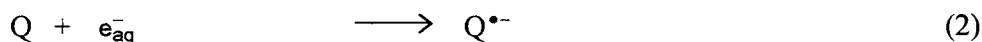
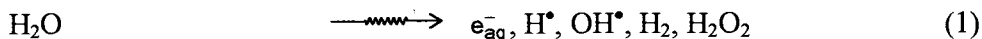
It can be seen that the only apparent similarity in these structures is that all of them contain a quinone group. The number of such compounds that has been studied by advanced techniques of pulse radiolysis and flash photolysis is increasing rapidly over nearly last three decades. Around the main objectives cited above, a large number of studies [7-12] have simply been made on the structure-property relationship.

Anthraquinone derivatives also constitute a commercially important class of vat dyes for dyeing synthetic fibres [13]. Many anthraquinones are used as photoinitiator for crosslinking or degradation of polyethylene. In the present article, an effort is made to capture the essence of these studies in quinones and also point out some future prospects.

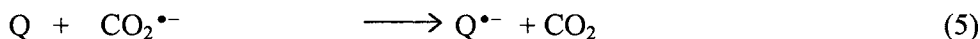
During the last 27 years, a number of excellent monographs [7-12] have appeared in the literature on the subject topic, the first being in 1974 and the last being in 1999. While efforts will be made to minimise overlap, a certain extent of commonality will be inevitable, as a vast amount of research in the subject area has been credited to this author's research schools at Manchester (U.K.) and BARC (India).

## 2. FORMATION OF SEMIQUINONES IN AQUEOUS SOLUTIONS

Quinones are capable of reacting with a large number of radiation-produced primary species like  $e_{aq}^-$ ,  $H^\bullet$  and  $OH^\bullet$  [14-16]. While  $e_{aq}^-$  and  $H^\bullet$  may reduce quinones by one-electron reduction process to the semiquinone,  $OH^\bullet$  may either add to the ring or some suitable substituent position and give rise to one-electron oxidation to some form of transient. Formation of semiquinones by  $\gamma$ -radiolysis has been discussed in detail in earlier monographs [7,9,17-19] and will not be included here. Pulse radiolysis kinetic spectrophotometry technique [20,21] has opened up new scope for detailed studies [8-12,15,16,22-25] on semiquinones. On pulse radiolytic one-electron reduction of quinones, semiquinones may be formed as follows :-

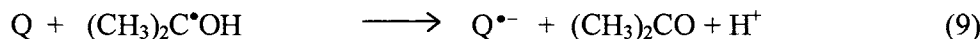
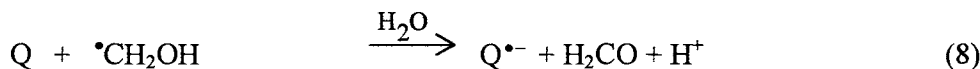
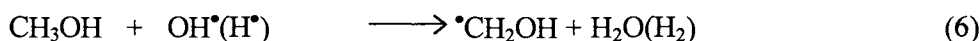


In aqueous solutions containing sodium formate, the reaction may be:



As reaction (2) also takes place, yield of  $\text{Q}^{\bullet-}$  increases in this case.

In aqueous alcoholic solutions containing either methanol or 2-propanol, following reactions take place.

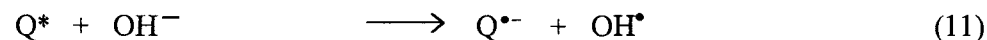


Higher alcohols may also be used. However, more branched radicals, e.g.  $\bullet\text{CH}_2(\text{CH}_3)_2\text{COH}$  (formed by reactions of  $\text{OH}^\bullet/\text{H}^\bullet$  with tert-butanol) are normally unreactive.

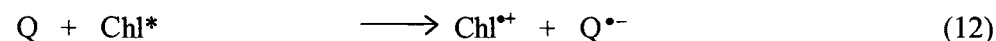
Semiquinones are also formed photolytically from quinones by abstraction of a hydrogen atom from the solvent by the triplet state of the quinone.



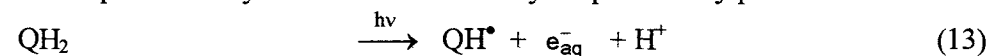
The organic radical formed may give more semiquinone by reaction (9). Excited quinones may also abstract electrons from suitable donors.



Quinones may also be reduced by excited states of other molecules by electron transfer reaction



Semiquinones may also be formed from hydroquinones by photoionisation.



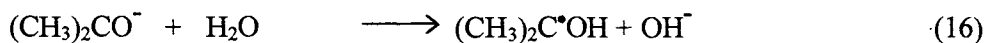
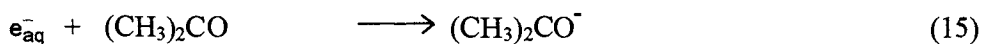
Excited dye molecule ( $D^*$ ) can oxidise hydroquinone ( $QH_2$ ) to the semiquinone.



We will confine ourselves mostly to radiation-induced generation of semiquinones.

In most cases, an aqueous solution of the quinone has been used for radiation chemical studies. However, the reaction sequence depends entirely on the added scavengers like sodium formate, methanol, 2-propanol, tert-butanol or others. In our own work, we have extensively used a relatively novel solvent system comprising of a mixture of 2-propanol ( $5 \text{ mol dm}^{-3}$ ) and acetone ( $1 \text{ mol dm}^{-3}$ ) in water ( $32.5 \text{ mol dm}^{-3}$ ). The advantage of this system, over and above solubilizing quinones insoluble in water, lies in the chemistry involved [26,27], so that  $(CH_3)_2C^*OH$  radical is produced as an exclusive reducing agent.

In our aqueous-organic mixed solvent system, reactions (2),(3),(7) and (9) are supplemented with reactions (15) and (16).



The solute quinone (Q) is reduced to its semiquinone by any combination of the above reductants (reactions 2, 3, 5, 8 and 9).

### 3. CHARACTERISTICS OF SEMIQUINONES

#### 3.1 Optical absorption characteristics

Study of physical chemistry of semiquinones relies heavily on knowledge of optical absorption characteristics of the free radicals, namely, absorption maxima and molar extinction coefficients. As radiation dose can be calculated fairly accurately, the yield of free radicals can be easily estimated. From the observed absorbance at a given dose, molar extinction coefficient of the semiquinone can be calculated.

The observed absorbance ( $\Delta A$ ) after an electron pulse is given to the solution containing quinone and a suitable additive, will constitute a difference absorption spectrum given by:

$$\Delta A = (\epsilon_{\text{semiquinone}} - \epsilon_{\text{quinone}}) \cdot \Delta C_{\text{quinone}} \cdot l \quad (17)$$

where,  $l$  = optical path length,  $\Delta C_{\text{quinone}}$  is the amount of quinone converted into the semiquinone and  $\epsilon$  terms are the respective molar extinction coefficients.

Three cases may arise at a particular wavelength  $\lambda_{\text{obs}}$  :-

- (i)  $\epsilon_{\text{semiquinone}} = \epsilon_{\text{quinone}} ; \Delta A = 0$
- (ii)  $\epsilon_{\text{semiquinone}} > \epsilon_{\text{quinone}} ; \Delta A = +ve$
- (iii)  $\epsilon_{\text{semiquinone}} < \epsilon_{\text{quinone}} ; \Delta A = -ve$

The case (iii) denotes depletion and will occur in the wavelength region where the parent quinone absorbs more strongly than its semiquinone. The corresponding (semiquinone-quinone) difference absorption spectrum shows a depletion region (Figure 2). As  $\epsilon_{\text{quinone}}$  is known at all wavelengths, and  $\Delta C_{\text{quinone}}$  can be easily calculated at a given dose (as G-value is known under different experimental conditions),  $\epsilon_{\text{semiquinone}}$  can be calculated at any given wavelength by using equation (18).

$$\epsilon_{\text{semiquinone}} = \epsilon_{\text{quinone}} + \frac{\Delta A_{\text{obs}} \times (G \epsilon)_{\text{dosimeter}}}{A_{\text{dosimeter}} \times G_{\text{semiquinone}}} \quad (18)$$

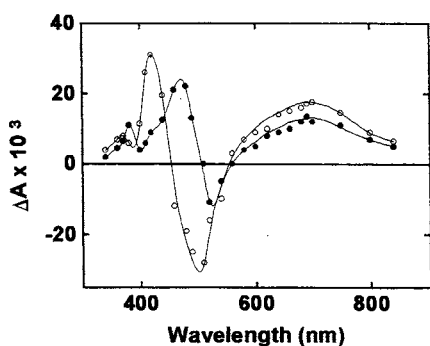


Figure 2. Semiquinone-quinone difference absorption spectra for adriamycin at (o) pH 1.1 mol dm<sup>-3</sup> formic acid + H<sub>2</sub>SO<sub>4</sub>; (●) pH 9.1 (10<sup>-1</sup> mol dm<sup>-3</sup> formate + borate buffer). Dose = 5.5 Gy.

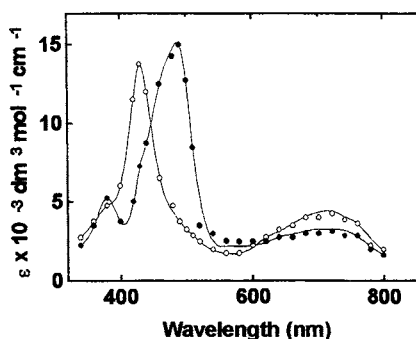


Figure 3. Absolute absorption spectra of adriamycin semiquinone obtained from data of Figure 2, (o) pH 1.1, (●) pH 9.1. (Figures 2 and 3 are reproduced from reference [41] with permission.)

Table 1  
Comparison of spectroscopic characteristics and pK(1) of quinones.

Quinone	$\lambda_{\max}$ nm ( $\epsilon / 10^3 \text{ dm}^3 \text{ mol}^{-1} \text{ cm}^{-1}$ )		pK(1) of QH*	Ref
	QH*	Q*		
Benzoquinone (BQ)	415(4.7) <sup>a</sup> , 410 (3.8) <sup>b</sup>	425(6.9) <sup>a</sup> , 430 (3.6) <sup>b</sup>	4.0 <sup>a</sup> , 4.7 <sup>b</sup>	9 <sup>a</sup> , 28 <sup>b</sup>
1,4-Naphthoquinone(NQ)	370 (7.2) <sup>a</sup> , 370 (8.1) <sup>b</sup>	390(12.5) <sup>a</sup> ,375 (7.8)	4.1 <sup>a</sup> , 4.3 <sup>b</sup>	9 <sup>a</sup> ,28 <sup>b</sup> 29 <sup>b</sup>
2,3-Dimethyl-NQ	380(7.3)	400(11.4)	4.25	9
2-Hydroxy-NQ (Lawsone)	370 (5.9) <sup>a</sup>	390 (6.3) <sup>a</sup>	4.7 <sup>a</sup>	9,29
5-Hydroxy-NQ (Juglone) <sup>a</sup>	370 (12.6)	385 (12.2)	3.65	29,30
5,8-Dihydroxy-NQ (Naphthazarin) <sup>a</sup>	380 (11.8), 760 (2.7)	380 (10.5)	2.7	29,31
9,10-Antraquinone (AQ)	375 (9.8) <sup>ac</sup> 380 (8.9) <sup>b</sup>	395(7.0) <sup>ac</sup> ,480(6.5) <sup>ac</sup> 385 (6.7) <sup>b</sup> , 490 (5.2) <sup>b</sup>	5.3 <sup>a</sup> 4.4 <sup>b</sup>	9 <sup>a</sup> 28 <sup>b</sup> , 29,32
AQ-1-sulphonate <sup>a,c</sup>	385 (10.7)	400 (7.2), 500 (7.2)	5.4	32,33
AQ-2-sulphonate <sup>a,c</sup>	390 (11.2)	400 (7.3), 500 (7.3)	3.25	32,34
AQ-1,5-disulphonate <sup>a</sup>	385 (8.4)	390 (5.6), 500 (5.7)	6.1	32
AQ-2,6-disulphonate <sup>a</sup>	388 (9.5)	396 (6.4), 515 (8.3)	3.0	31
1-Amino-AQ <sup>b</sup>	400 (10.5)	390 (6.7)	5.8	35
1-Hydroxy-AQ <sup>b</sup>	470 (2.9),650 (2.0) 390 (10.5)	480 (10.3), 740 (2.0) 390 (8.1)	4.6	35
1-Amino-4-hydroxy-AQ <sup>b</sup>	520 (1.1),620 (1.4) 410 (6.8)	445 (7.9), 730 (1.7) 390 (6.3)	6.3	36
1,4-Diamino-AQ <sup>b</sup>	490 (4.7),700 (2.5) 390 (6.5)	500 (13.1), 740 (3.4) 385 (6.0)	7.9	36
1,4-Dihydroxy-AQ (Quinizarin) <sup>b</sup>	490 (8.0),720 (2.2) 410 (11.6)	510 (14.4), 740 (3.3) 388 (5.8)	3.3	26,37
Quinizarin 2-sulphonate <sup>a</sup>	680 (3.0),720 (2.7) 425 (12.4)	475 (13.7), 720 (1.8) 390 (6.4), 475 (17.2)	2.2	37
Quinizarin 6-sulphonate <sup>a</sup>	680 (3.0) 420 <sup>b</sup> (12.4)	700 (2.6), 780 (2.3) 390 (6.4), 475 (17.2)	2.2	37
5-Methoxy-quinizarin <sup>b</sup>	680 (3.0) 370 (6.6), 420 (12.1)	700 (2.6), 780 (2.3) 375 (6.5), 480 (16.9)	3.65	35
1,5-Dihydroxy -AQ <sup>b</sup>	620 (2.2) 410 (12.4)	440 (13.0), 720 (1.4) 390 (8.0),	3.65	38
1,8-Dihydroxy-AQ <sup>b</sup>	620 (3.4) 400 (15.8)	450 (14.7), 720 (1.8) 380 (8.5)	3.95	38
1-Chloro-AQ	620 (3.4) 380 (8.9)	450 (14.7), 720 (1.8) 390 (5.0), 500 (5.4)	4.2	39
1,5-Dichloro-AQ <sup>b</sup>	380 (8.0)	390 (4.7), 520 (4.8)		39
1,8-Dichloro-AQ <sup>b</sup>	375 (9.9)	390 (5.1), 530 (6.0)	3.9	39
2-Hydroxy-AQ <sup>b</sup>	380 (6.6)	400 (6.6), 450 (4.4)	4.7	40
2,6-Dihydroxy-AQ <sup>b</sup>	390 (11.0)	410 (9.0), 450 (4.5)	5.4	40

Table 1 Continued....

Comparison of spectroscopic characteristics and pK(1) of quinones.				
Adriamycin/Daunomycin <sup>a</sup>	420 (13.2)	380 (5.0)	2.8	41
	720 (4.2)	480 (14.8), 720 (3.4)		
5,12-Naphthacene quinone <sup>b</sup>	390	390 (3.3), 460 (2.6)	6.0	28

a :  $10^{-1}$  mol dm<sup>-3</sup> sodium formate in water; b: 5 mol dm<sup>-3</sup> 2-propanol + 1 mol dm<sup>-3</sup> acetone in water; c: corrected  $\epsilon$  - values[32].

A plot of  $\epsilon_{\text{semiquinone}}$  vs  $\lambda$  will constitute a corrected absorption spectrum of the semiquinone (Figure 3). Numerous studies have been made and corrected absorption spectra of the semiquinones have been determined ( Table 1).

A close examination of Table 1 reveals few interesting trends. For example, most neutral semiquinones generated from naphthoquinone and anthraquinone derivatives absorb strongly around 370-390 nm region, while their anions absorb at longer wavelength with higher molar extinction coefficients. Except for naphthoquinone and 2-hydroxynaphthoquinone, they all have molar extinction coefficient in the vicinity of  $12,000 \text{ dm}^3 \text{ mol}^{-1} \text{ cm}^{-1}$ . In the case of dihydroxy-substituted quinones, a weak and broad absorption band was observed at 700-760 nm region. Unsubstituted or sulphonated anthrasemiquinone radical anions have two distinct absorption peaks around 400 and 500 nm with comparable molar extinction coefficients For other substituted anthrasemiquinones , on the other hand, molar extinction coefficients of these two bands differ widely. Dihydroxy-anthrasemiquinone derivatives show weak absorption bands (molar extinction coefficient  $\sim 6,000 \text{ dm}^3 \text{ mol}^{-1} \text{ cm}^{-1}$ ) around 380-390 nm and stronger absorption bands (molar extinction coefficient  $\sim 13,000\text{-}17,000 \text{ dm}^3 \text{ mol}^{-1} \text{ cm}^{-1}$ ) around 475 nm. The exact nature of the red band is still a matter of intense speculation. The effect of matrix (i.e. change of solvent) on the absorption characteristics has been very minimal in general, showing that in most cases intramolecular stabilisation is predominant.

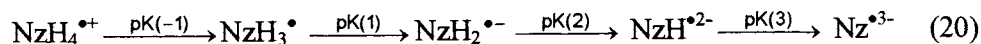
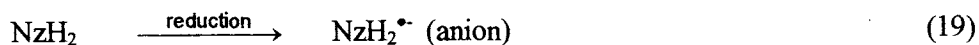
A close examination of the formation of semiquinone from quinone shows that the parent quinone structure changes to aromatic in the semiquinone. All UV-visible absorptions are thus considered as due to  $\pi\text{-}\pi^*$  transitions. As the shift in  $\lambda_{\text{max}}$  between the neutral semiquinone and its anion is usually small, it is safely assumed that the orbitals involved in the absorption process are not significantly affected by protonation. Similar arguments hold good for substituted quinones, where the effect of ring substitution on  $\lambda_{\text{max}}$  has been seen to be very small (see Table 1). However, for-OH substitution, the effect is more prominent due to stronger intramolecular hydrogen bonding [42].

While determining extinction coefficient, it is essential to establish that formation of the semiquinone is complete. Otherwise a lower extinction coefficient will result (CAUTION!).

Some researchers have argued [43] that a semiquinone may exist in an associated form ( $Q \dots Q^{\bullet}$ ). This is possible in specific cases if the parent quinone is aggregated. Unless more comprehensive work is done, it is premature to have a discussion on this issue. In dilute aqueous solutions, however, the probability of dimerisation is indeed very small and can be neglected.

### 3.2 Acid-base dissociation constants

Semiquinone radical anions can undergo protonation steps to form neutral semiquinone or in very strongly acidic solution, a semiquinone cation radical. On the other hand, semiquinone radical anions containing ionisable H can undergo deprotonation to form dianion, trianion or even polyanion. An example is the case of naphthazarin (5,8-dihydroxy-1,4-naphthoquinone)(NzH<sub>2</sub>) [31] where 5 different states of protonation of the semiquinone radicals are possible.



Studies on pK(-1) are rare [44]. It is probably believed that in very strong acidic solutions, semiquinone radicals can remain in the cationic form. Except some ESR studies [45-47], very little research has been oriented to this direction. Irradiation of p-benzoquinone in a CFC<sub>3</sub> matrix at 77 K and subsequent ESR studies [48] established a symmetric  $\sigma$ -radical cation. In situ UV photolysis of p-benzoquinone in CF<sub>3</sub>COOH at room temperature apparently gave a symmetric  $\pi$ -cation radical [49,50]. The question of the nature of the radical cation still remains unresolved.

Mayer and Kraslukianis [44] carried out pulse radiolysis of p-benzoquinone, 1,4-naphthoquinone, naphthazarin, 9,10-anthraquinone and quinizarin, in freon 113 (CF<sub>2</sub>Cl-CFCl<sub>2</sub>) solution at room temperature. Blue shifted UV-visible absorption spectra were assigned to the radical cations. High formation rate constants ( $\sim 10^{10} \text{ dm}^3 \text{ mol}^{-1} \text{ s}^{-1}$ ) have been reported. The value of pK(1) is the most important parameter as pK(2) and pK(3) are normally measurable in very strongly alkaline solutions only [31].

As the absorption spectra of neutral and anionic semiquinones differ considerably, it has been possible to estimate pK(1) and in many cases, even pK(2), by choosing appropriate wavelengths and a modified Hendersen's equation [40]:

$$A_{obs} = \frac{A_{QH_3}}{1 + 10^{pK(1)-pH} + 10^{pK(1)+pK(2)-2pH}} + \frac{A_{QH_2^{\bullet-}}}{1 + 10^{pH-pK(1)} + 10^{pK(2)-pH}} + \frac{A_{QH^{\bullet 2-}}}{1 + 10^{2pH-pK(1)-pK(2)} + 10^{pH-pK(2)}} \quad (21)$$

A representative plot of  $\Delta A$  vs pH is shown in Figure 4. However, wherever such intramolecular stabilisation effect is not present, the  $pK(1)$  value goes up, e.g. 9,10-anthraquinone-1,5-disulphonate; 1,4-diamino-9,10-anthraquinone; 1-amino-4-hydroxy-9,10-anthraquinone; 5,12-naphthacene quinone, etc.

In the case of benzo-semiquinone the  $pK(1)$  value is 4.1 in aqueous solution [9] and 4.7 in the aqueous-organic mixed solvent [28]. However, in substituted quinones, especially OH-substituted quinones, the anion is more stabilized due to the intramolecular H-bonding. As a result,  $pK(1)$  values are lower, as shown in Table 1.

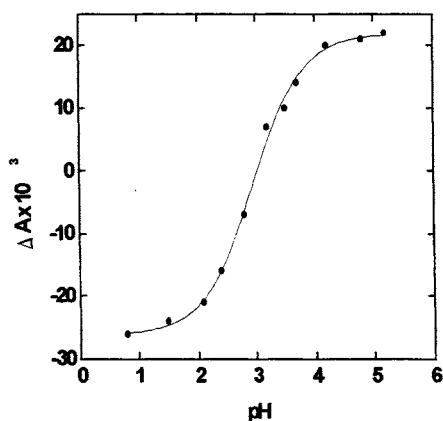


Figure 4. Variation with pH of change in absorbance at 475 nm produced by pulse,  $[\text{adriamycin}] = 5.6 \times 10^{-5} \text{ mol dm}^{-3}$ . The solid line is a computed best fit with  $pK(1) = 2.9$ . [Reproduced from reference [41] with permission]

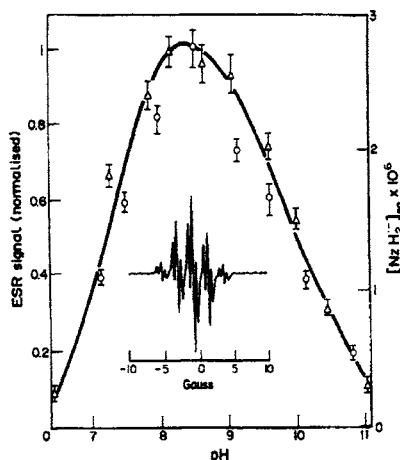


Figure 5. Normalised ESR signal (o) and  $[\text{NzH}_2^{\bullet}]$  at equilibrium as obtained from optical pulse radiolysis ( $\Delta$ ). [Reproduced from reference [52] with permission.]

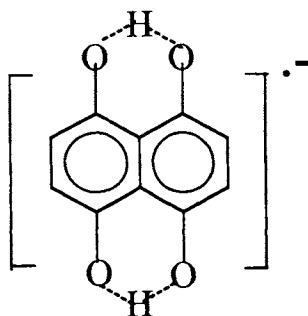
### 3.3 Charge on the semiquinone

One important aspect of chemistry of semiquinones is determination of the charge on the molecule. Conventional ionic salt effect studies in the absence of



any buffer often gives indication of the net charge at near neutral pH [31]. However, we have shown that by a judicious use of ionic salt effect studies, together with pulsed conductance studies and electron spin resonance spectroscopy, one can identify the ionic charge on the molecule without any doubt [51,52]. Once charge on a transient species at a given pH is known, charge on the species at other pH values can be ascertained by knowing the pK values of the transient.

Mukherjee et al [51,52] demonstrated the efficacy of the above methods by comparing the yield of the semiquinone derived from naphthazarin with the normalised ESR signal. Not only an extremely good correlation was obtained (Figure 5), but the unique chemical structure of the semiquinone, with the odd electron delocalised over the entire structure, could also be established.



Another advantage demonstrated is that all those semiquinones, which show some stability over a pH zone, can be generated *in situ* cleanly by a combination of micellar solubilisation and photolytic irradiation [51,52].

### 3.4 Rate constants for formation of semiquinones

Quinones are electron attracting type of molecules and can be reduced by a large variety of reducing radicals. Typically, rate constants for formation of semiquinones due to reactions with  $e_{aq}^-$  (or,  $e_{solv}^-$ ) are virtually diffusion-controlled and fall around  $(1-3) \times 10^{10} \text{ dm}^3 \text{ mol}^{-1} \text{ s}^{-1}$  (see Table 2). These rate constants are normally directly calculated from a  $\Delta A$  versus  $t$  plot at  $\sim 720 \text{ nm}$ , representing decay of  $e_{aq}^-$ , and correcting for the matrix. Alternatively, competition kinetics with another solute may also be used. In the presence of substituents, the electron affinity of the molecule changes. However, it has been difficult to have a direct correlation between  $e_{aq}^-$  rate constants and substitution effects.

Table 2

Formation rate constants of transients formed by one-electron reduction of some representative quinones<sup>e</sup> ( $k$  in  $10^9 \text{ dm}^3 \text{ mol}^{-1} \text{ s}^{-1}$ )

Quinone	$e_{aq}^-$ (pH)	$\text{CO}_2^{\bullet-}$ (pH)	$(\text{CH}_3)_2\text{C}^{\bullet}\text{OH}$ (pH)	$\text{H}^{\bullet}$ (pH)	Ref
Benzoquinone (BQ)	i	I	5.0 (2.5) 2.3 (8.0), 3.0 (c)	i	28
1,4-Naphthoquinone (NQ)	i	I	1.7 (2.5) 2.6 (7.0), 2.3 (c)	i	28, 29
2-Hydroxy-NQ (Lawsone)	i	I	3.9(1.8),1.0(6.7) 1.3 (10.3) 2.3 (13.0),1.0(c)	i	29
5-Hydroxy-NQ (Juglone) <sup>a</sup>	28(6.4),21(10.5)	4.4 (1.2) 3.8(6.4),1.3(10.5)	3.1(2.0),2.9(7.0) 1.7 (10.4) 1.4 (13.0),3.1(c)	2(1.2)	29, 30
5,8-Dihydroxy-NQ (Naphthazarin) <sup>a</sup>	31.0 (5.8) 24.0(9.2),22(13)	5.1 (5.8) 2.2(9.2),1.4(13)	1.5(1.3),2.0(5.2) 1.5 (7.0),1.5(11)	8.9 (1.2)	29, 31
9,10-Anthraquinone (AQ) <sup>d</sup>	i	i	2.7(2.0),1.8(8.0) 1.6 (12.0),1.9(c)	i	28, 29, 32
1-Amino-AQ <sup>b</sup>	i	i	3.0(2.0),3.2(8.0) 2.8 (12.0),0.9(c)	i	35
1-Hydroxy-AQ <sup>b</sup>	i	i	3.2(2.0),2.8(8.0) 1.5 (12.0),2.0(b)	i	35
2-Hydroxy-AQ <sup>b</sup>	8.0 (11.0)	1.0 (11.0)	1.3(1.5),1.3(7.0) 0.9 (13.0),1.3(c)	----	30
1,4-Diamino-AQ	i	i	0.9 (5.5)	i	36
1-Amino-4-hydroxy-AQ <sup>b</sup>	50.0(11),53(~14)	1.1(11),1.3(~14)	1.6 (8.8)	----	36
1,4-Dihydroxy-AQ (Quinizarin, QZ) <sup>f</sup>	i	i	3.3(1.2),3.2(5.4) 1.5(10.4) 1.8(~14)	i	26, 37
Methoxy-QZ (QZOMe)					
1,5-Dihydroxy -AQ	45.0(11.0) 53.0(~14)	1.0 (11.0) 0.27 (~14)	2.2 (---)	----	38
1,8-Dihydroxy-AQ	34.0(11.0) 38.0(~14)	1.7 (11.0) 0.37 (~14)	2.0 (---)	----	38
2,6-Dihydroxy-AQ	14.0(11.0)	1.0 (11.0)	2.3(1.5),1.2(7.0) 0.7 (13.0),0.7(c)	----	40
AQ-1,5-disulphonate	17.0 (8.4)	10.0 (8.4)	----	2.4 (2.0)	32
AQ-2,6-disulphonate	10.0 (7.0)	0.8 (7.0)	----	3.0 (1.4)	32
QZ-2-sulphonate	27.0 (6.5)	3.1 (1.1),3.2 (5.7)			37
(QZ-6-sulphonate)	18.0(11.7)	1 (10.4),0.2 (~14)	----	----	

Table 2 Continued

Formation rate constants of transients formed by one-electron reduction of some representative quinones <sup>e</sup> ( $k$  in  $10^9 \text{ dm}^3 \text{ mol}^{-1} \text{ s}^{-1}$ ).

1-Chloro-AQ	i	i	2.5(2.0),2.4(9.0) 1.6 (c)	i	39
1,5-Dichloro-AQ	i	i	2.2(2.0),2.0(9.0) 1.7 (c)	i	39
1,8-Dichloro-AQ	i	i	2.9(2.0),2.6(9.0) 2.2 (c)	i	39
5,12-Naphthacenequinone	i	i	3.1(2.0),1.7(8.0) 2.1 (c)	i	28
Adriamycin	25.0 (6.5) 15.0(11.5)	3.5 (1.1),3.4 (6.5) 0.18 (11.5)	-----	2.9 (1.1)	41

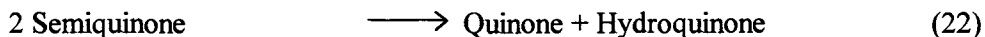
a, b, c : as in Table 1, e : excludes those reported in reference [8], i : not determined due to insolubility in water, d :  $k$  with  ${}^{\bullet}\text{CH}_2\text{OH}$   $2.1 \times 10^8 \text{ dm}^3 \text{ mol}^{-1} \text{ s}^{-1}$  [53] (in alkaline methanol solution), f :  $k$  with  ${}^{\bullet}\text{CH}_2\text{OH}$  (acidic solution) =  $7.5 \times 10^8 \text{ dm}^3 \text{ mol}^{-1} \text{ s}^{-1}$  [54].

A few general (but not universal) observations are as follows.

- In alkaline solutions  $k$  values are lower, obviously due to the Coulombic repulsion between the negative charges on the two reactants. However, the difference in  $k$ -values is not very significant. A number of specific examples have been discussed in reference [12]. Others are observable in Table 2.
- Where a negatively charged substituent is attached to the molecule (say,  $-\text{SO}_3^-$ ), the rate constant increases with substitution, due to the electron withdrawing ability of the  $-\text{SO}_3^-$  group from the aromatic ring, stabilising the radical anion.
- Reducing agents other than  $e_{\text{aq}}^-$  always react much slower, typically by an order of magnitude. Same trend as in (a) above was observed in such cases too.
- Neutral radicals (e.g.  $(\text{CH}_3)_2\text{C}^{\bullet}\text{OH}$ ) react at a slower rate than the anionic radicals ( $\text{CO}_2^{\bullet-}$ ,  $\text{CH}_2\text{O}^{\bullet-}$ ).
- At acidic pH, rate constants for H atom reactions are much higher than for bulkier radicals like  ${}^{\bullet}\text{COOH}$ ,  ${}^{\bullet}\text{CH}_2\text{OH}$  etc.).

### 3.5 Disproportionation reactions of semiquinones

In de-oxygenated aqueous solutions, a semiquinone normally undergoes a bimolecular disproportionation reaction, forming the parent quinone and the corresponding two- electron reduced hydroquinone.



Typical rate constants fall in the range of  $10^8$ - $10^9$   $\text{dm}^3\text{mol}^{-1}\text{s}^{-1}$ . However, in cases where substituents are present, an equilibrium of the type of reaction (23) has been observed over a range of intermediate pH values.



Especially in the case of hydroxy-substituted naphthoquinones [30,31] and anthraquinones [26,35-38], such equilibrium was seen to lie heavily to the left, showing exceptional stability of the semiquinones. In case of naphthazarin [26,37], for example, we could preserve a de-oxygenated solution containing high concentration of the naphthazarin semiquinone for months !

It was conclusively established that such exceptional stability was due to the nearness of the  $E^1$  (one-electron reduction potential),  $E^2$  (second one-electron reduction potential) and  $E^m$  (two-electron reduction potential) values of the quinone and the characteristic changes of  $E^1$ ,  $E^2$  and  $E^m$  as a function of pH as a consequence of the pK values of the quinones, semiquinones and hydroquinones. These are discussed later in the section dealing with redox potentials.

Mayer [12] has discussed a very interesting case from our studies [32] involving anthraquinone sulphonates (mono- and di-), where the mono-sulphonate showed an increase in the value of  $\log K_{\text{eq}}$  for the reaction (23) on either side of pH of about 8.5, while the di-sulphonates showed a continuous drop in  $\log K_{\text{eq}}$  with pH, ending in a plateau at pH ~14. These observations could also be explained on the basis of the redox characteristics.

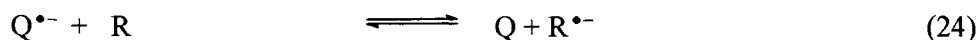
As pointed out by Mayer [12] from our studies [30,51], stable juglone semiquinones could not be formed and the semiquinones decayed by a second-order process. The importance of redox potentials falling close to one another in an intermediate pH range, for extra stability, is further exemplified by this observation.

Mukherjee et al attempted [26,41] to quantify the observed stability of semiquinones as a function of pH, by correlating the  $K_{\text{eq}}$  values with pK values of the species involved and their redox characteristics (Figures 6 and 7). As the details may be out of scope for this review, readers are encouraged to see our work on quinizarin and adriamycin [26,41].

### 3.6 One-electron reduction potentials

The reduction potentials for semiquinones are those for formation from the parent quinones, i.e. the one-electron reduction potential of the parent quinone,  $E(Q/Q^{\bullet-})$ , and for reduction to hydroquinone, i.e. the second one-electron reduction potential,  $E(Q^{\bullet-}/Q^{2-})$  for addition of the second electron to the quinone. These reduction potentials depend on pH as Q,  $Q^{\bullet-}$  and  $Q^{2-}$  can all be protonated.

Pulse radiolysis has been established as possibly the “cleanest” method for determining these potentials [16,55]. After the anionic form of a semiquinone has been formed at low concentration by the action of an appropriate electron-donating reducing agent, it is possible to establish an equilibrium of the type



with a reference redox couple  $R/R^{\bullet-}$ , under ideal chemical conditions, before  $Q^{\bullet-}$  can disappear by disproportionation or other chemical reactions. Measurement

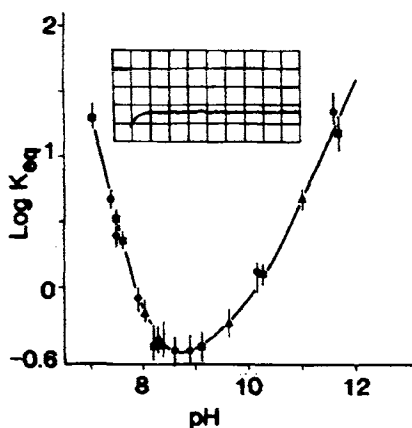


Figure 6. Variation of  $\log K_{eq}$  with pH for solutions containing adriamycin(•)or daunomycin (■)or both(▲). Solid line indicates the computer best fit. (Figures 6 and 7 are reproduced from reference [58], with permission.)

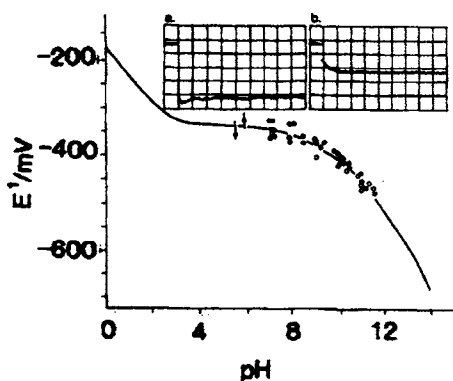


Figure 7. Variation with pH of one- electron reduction potentials of adriamycin (•)and daunomycin (o). A single best fit line is calculated on the basis of  $E^1 = -365$  mV at pH 8.5,  $pK(1) = 2.8$ ,  $pK(2) = 9.2$  and  $pK(3) > 14$ . The insets show changes of optical transmittance with time for daunomycin at pH 9.2.

of equilibrium optical absorbance can then give the equilibrium constant  $K$  for the reaction (24). If the reduction potential  $E(R/R^{\bullet-})$  is known, the value of  $E(Q/Q^{\bullet-})$  at 25°C vs NHE can easily be derived as

$$E^1(Q/Q^{\bullet-}) = E^1(R/R^{\bullet-}) - 59.16 \log K \quad (25)$$

where all  $E$  values are in mV. The reduction potential  $E(Q^{\bullet-}/Q^{2-})$  is obtained from:

$$E^2(Q^{\bullet-}/Q^{2-}) = 2E^m(Q/Q^{2-}) - E^1(Q/Q^{\bullet-}) \quad (26)$$

where  $E^m(Q/Q^{2-})$  is the known two-electron potential of the quinone.

It is imperative to have an accurate  $E^1$  value for the reference from the literature [55]. Care has to be taken about solvent also, as Mukherjee et al [27] have demonstrated. For example, the  $E^1(MV^{2+}/MV^{•+})$  is - 450 mV in aqueous system while it is - 330 mV in 2-propanol-acetone-aqueous (mixed) solvent.

Table 3  
Redox potentials of several quinone/semiquinones systems

Quinone	$E^1_7 / \text{mV}$	$E^2_7 / \text{mV}$	$E^m_7 / \text{mV}$	Ref
Benzoquinone (BQ) <sup>b</sup>	-30	-	-	28
1,4-Naphthoquinone (NQ) <sup>b</sup>	-200	-	-	28
NQ-2-sulphonate	-60	+300	+120	56
2,3-Dimethyl-NQ	-240	-	-	56
2-Hydroxy-NQ <sup>b</sup>	-350	-	-	29
5-Hydroxy-NQ	-95 <sup>a</sup> , -125 <sup>b</sup>	+157 (pH 2) <sup>a</sup>	+69 (pH 2) <sup>a</sup>	29,30
5,8-Dihydroxy-NQ	-109 <sup>a</sup> , -115 <sup>b</sup>	-15 <sup>a</sup>	-62 <sup>a</sup>	29,21
9,10-Anthraquinone (AQ)	-445 <sup>b</sup> , (-266)	-	-	28
AQ-1-sulphonate <sup>a</sup>	-415	-	-	32,33
AQ-2-sulphonate <sup>a</sup>	-380	-76	-228	32-34
AQ-1,5-disulphonate <sup>a</sup>	-418	-283	-350	32
AQ-2,6-disulphonate <sup>a</sup>	-215	-	-	32
1-Amino-AQ <sup>b</sup>	-435	-	-	35
1-Hydroxy-AQ <sup>b</sup>	-385	-	-	35
1-Amino-4-hydroxy-AQ <sup>b</sup>	-408 <sup>b</sup>	-348 <sup>b</sup>	-388 <sup>b</sup>	36
1,4-Diamino -AQ <sup>b</sup>	-410	-329	-380	36
1,4-Dihydroxy-AQ (quinizarin) <sup>b</sup>	-249 <sup>b</sup> , (-326)	-188	-229	26,37
Quinizarin 2-sulphonate <sup>a</sup>	-270 <sup>a</sup> , -298 <sup>b</sup>	-246	-258	37
Quinizarin 6-sulphonate <sup>a</sup>	-249 <sup>a</sup>	-213	-231	37
5-Methoxyquinizarin <sup>b</sup>	-333	-192	-263	26
1,5-Dihydroxy-AQ <sup>b</sup>	-326, -306 <sup>b</sup>	-273	-300	38
1,8-Dihydroxy-AQ <sup>b</sup>	-298 (pH 7), -377 (pH 11)	-345, -325 <sup>b</sup>	-415, -380	38
1-Chloro-AQ <sup>b</sup>	-360	-	-	39
1,5-Dichloro-AQ <sup>b</sup>	-370	-	-	39
1,8-Dichloro-AQ <sup>b</sup>	-410	-	-	39
2-Hydroxy-AQ <sup>b</sup>	-440	-	-	40
2,6-Dihydroxy-AQ <sup>b</sup>	-400	-	-	40
Adriamycin/Daunomycin <sup>a</sup>	-341	-260	-300	57,58
Mitomycin C	-310 <sup>a</sup>	-	-	59
AZQ <sup>a</sup>	-70 <sup>a</sup>	-	-	5
BZQ <sup>a</sup>	-376 <sup>A</sup>	-	-	5
5,12-Naphthacene quinone <sup>b</sup>	-380	-	-	28

(Abbreviations as in Table 1.)

Over last two decades a large number of  $E^1$  values have been determined accurately by this simple method. Some chosen values are shown in Table 3. When only a single ionisation of the semiquinone is considered,  $E^1(Q/Q^{\bullet-})$  is related to pH as:

$$E^1(Q/Q^{\bullet-}) = E^1(Q/Q^{\bullet-})_7 + 59.16 \log (K+[H^+]) / (K+10^{-7}) \quad (27)$$

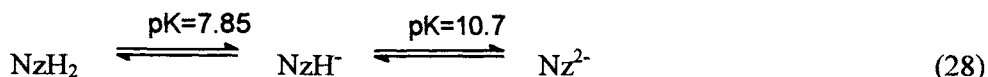
where  $K$  is the ionisation constant of the semiquinone. Thus in the pH-independent region ( $\text{pH} > \text{pK}$ ), the redox process is the simple addition of an electron, whereas in the acidic region, it involves addition of a proton (i.e.  $Q + H^+ + e_{\text{aq}}^- \rightarrow QH^{\bullet}$ ). More complex correlation between  $E^1$  and pH has been done and experimentally verified [57,58].

### 3.7 Anthracyclines and their model quinones

#### 3.7.1 First one-electron step

The most basic structural model for anthracyclines adriamycin (doxorubicin) and daunomycin (daunorubicin) was considered to be the strongly intramolecularly hydrogen-bonded naphthazarin (5,8-dihydroxy-1,4-naphthoquinone) (Section 3.2). It is usually customary to study the way in which such simple quinones form radicals in order to gain insight into the way more complex quinones might produce toxic and other effects. This is more so as the radical centres in the complex molecules are usually located in these simpler model structures. Treatment of naphthazarin will also demonstrate how various data may be compiled and compared.

In aqueous solution, naphthazarin ( $\text{NzH}_2$ ) can exist in the fully protonated form ( $\text{NzH}_2$ ), anionic form ( $\text{NzH}^-$ ) or dianionic form ( $\text{Nz}^{2-}$ ) depending on the pH.



Pulse radiolytic one-electron reduction of naphthazarin in aqueous formate/formic acid solution [31] leads to various protonated forms of the semiquinone. Change in absorbance at chosen wavelengths of the semiquinone absorption spectra, plotted as a function of pH, allowed three of the four forms to be identified, with  $\text{pK}_1$  and  $\text{pK}_2$  values of 2.7 and  $>13.8$ , respectively. The charge on the semiquinone at  $\text{pH} \sim 5$  was confirmed to be -1, based on ionic strength effect on the disproportionation rate. The semiquinone at this pH was thus assigned the structure  $\text{NzH}_2^{\bullet-}$ . The transition  $\text{NzH}_3^{\bullet} \rightarrow \text{NzH}_2^{\bullet-}$  was assigned the  $\text{pK} = 2.7$ . The reduction in pK value by 1.4 units over that of simple 1,4-naphthoquinone was easily attributed to the strong intramolecular hydrogen

bonding in  $NzH_2^{\bullet-}$ . Pulsed conductance studies and ESR studies further confirmed structural assignments [51,52]. It may be mentioned here that the stability of the  $NzH_2^{\bullet-}$  form of naphthazarin semiquinone over a pH range of 11.1 units is the best known example of stabilisation due to intramolecular hydrogen bonding.

The ESR studies also established that the  $pK \geq 13.8$  could be assigned to the transition  $NzH_2^{\bullet-} \rightarrow NzH^{2-}$ , and that the structure of the semiquinone was a strongly intramolecularly hydrogen-bonded highly symmetric structure where the unpaired electron is delocalised over the entire ring structure (Section 3.2).

The one-electron reduction potential ( $E^1$ ) values were calculated at several pH values using several redox standards. From these measurements,  $E^1 = -109$  mV vs NHE at  $25^\circ\text{C}$  was established. A  $E^1$  versus pH plot shows a region independent of pH, i.e. no proton involved in the reduction process, confirming the above structural assignments.

### 3.7.2 Second one-electron step

In many cases, semiquinones are present at appreciable concentrations in solutions containing quinones and the corresponding hydroquinone. In the case of naphthazarin, the  $NzH_2^{\bullet-}$  form was found to be extremely stable in the weakly alkaline solutions unlike at the two extremes of the pH range when the disproportionation of the semiquinone was complete. The reaction (23) was studied over the entire pH range 1-14. Within pH  $\sim 6$  to 11, the disproportionation was incomplete and the semiquinone was stable over hundreds of milliseconds at least. The equilibrium concentration of the semiquinone was measured and the equilibrium constant  $K_{eq}$  was calculated. Such stability constants were related to the one-electron reduction potentials for the quinone and the semiquinone (at  $25^\circ\text{C}$ ) via the expression:

$$E^1(\text{Quinone/Semiquinone}) - E^2(\text{Semiquinone/Hydroquinone}) = -59.16 \log K_{eq} \quad (29)$$

The two one-electron reduction potentials are related in turn to the two-electron reduction potential of the quinone (equation 26),

$$E^1(\text{Quinone/Semiquinone}) + E^2(\text{Semiquinone/Hydroquinone}) = 2E^m(\text{Quinone/Hydroquinone}) \quad (30)$$

Extremely good correlation was obtained among the measured and the calculated physical parameters, establishing a complete chemistry of naphthazarin semiquinones. The hydroquinones were actually formed in-situ in the cell in the



pulse radiolysis set-up, by giving a large number of electron pulses to the solution and measuring the absorbance immediately [60]. The close proximity of  $E^1$ ,  $E^2$  and  $E^m$  vs pH over a small pH range (Figure 8) gives physicochemical explanation about the exceptional stability of the naphthazarin semiquinones.

### 3.7.3 Quinone antitumour drugs

Several quinones are used clinically in the chemotherapy of cancer [61,62]. Some examples are adriamycin (doxorubicin), daunomycin (daunorubicin), mitomycin C and more recent diaziridinyl benzoquinones and diamino anthraquinones [5]. Physiological enzyme based reduction of these quinones caused by xanthine oxidase, cytochrome P450 reductase etc.[63], leads to the formation of semiquinone and hydroquinone forms. Pulse radiolysis can generate and characterise these intermediates and products [10].

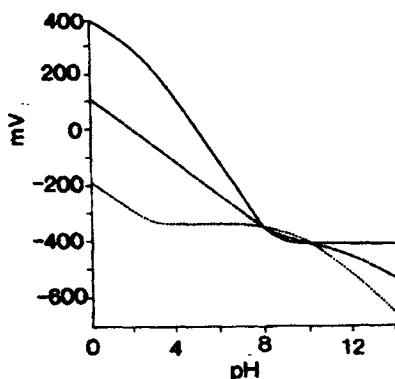


Figure 8. Variation with pH of reduction potentials of adriamycin and daunomycin. First one-electron reduction potential  $E^1$  (...); second one-electron reduction potential  $E^2$  (—); two-electron reduction potential  $E^m$  (---). (Reproduced from reference [58] with permission).

Mitomycin C undergoes reduction in hypoxic tumour cells to form damaging adducts with DNA bases by aziridine ring opening. Steady state studies are rather inadequate to answer all the puzzling aspects of the mechanisms involved. For example : how to account for the number of different products which are produced when Mitomycin C undergoes one-electron reduction by characteristic enzyme systems. By combining the techniques of pulse radiolysis, HPLC and enzyme assay, it has been established that only three initial products are formed by the reduction of Mitomycin C and two of them are isomers [64]. Many other products observed by other workers will have been formed by further reduction of the initial products. It is presumed that the ring opening process must occur at the one-electron reduction to the semiquinone state. The Mitomycin C

semiquinones have now been studied for times as long as several seconds using very low doses of radiation and a 10 cm capillary cell. The only reaction observable is the dismutation reaction [64].

Aziridine ring opening was observed to occur after the hydroquinone had been formed. Further proof that the reactions do not occur at the semiquinone stage was obtained from analysis of yields of products formed from radiation dose from a linac, favouring dismutation of the semiquinone, and a  $^{137}\text{Cs}$  source, favouring prolonged lifetime of the semiquinone. The yields of products were the same in the two cases, further confirming that they are formed from the hydroquinone. Final confirmation of the complete mechanism came from pulse radiolysis data over time scales of between 0.1 s and 1 minute. The most interesting aspect is the intramolecular oxidation and rearrangement of the hydroquinone of Mitomycin C forming a modified quinone, observed using pulse radiolysis over time scales of 33 s / division. However, the authors did not account for the Brownian motion.

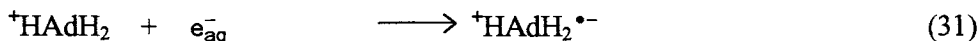
Clinically most successful antitumour drug, adriamycin undergoes redox cycling reactions producing also some toxic side effects. When adriamycin is reduced by one-electron reducing enzymes, the daunosamine moiety is liberated. As in Mitomycin C, it was believed that the process occurred at the semiquinone stage.

Radiation chemistry of adriamycin and daunomycin could be studied on the basis of the studies made on naphthazarin. These anthracyclines are much complex molecules and a larger number of combination of pK values leads to several states of overlapping protonation over a narrow pH range [65].

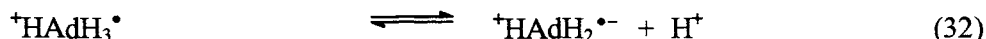
A large number of protonation, namely  $^+\text{HAdH}_2$ ,  $\text{AdH}_2$ ,  $^+\text{HAdH}$ ,  $\text{AdH}$ ,  $\text{Ad}^{2-}$  etc (Ad = adriamycin core without two ionisable H) are possible with pK values like 8.22, 9.01, 9.36, 10.1 and 13.2 [65]. Closeness of these pK values makes study with anthracyclines a very complex proposition. In the above formulation, fully protonated adriamycin was represented as  $^+\text{HAdH}_2$  where the first H refers to the amino-sugar  $\text{NH}_2$  and the other two to those on the hydroquinone.

Pulse radiolysis of aqueous solution of adriamycin under reducing conditions leads to semiquinone radicals in their various protonated forms [41,57,58,66-68]. In the acidic region, a semiquinone pK of 2.9 fit the data. Daunomycin semiquinone showed the same pK within experimental error.

The one-electron reduction potential of adriamycin and daunomycin was estimated as a function of pH [58] as in the case of naphthazarin. Within experimental error limit,  $E^1$  of both anthracyclines were treated as identical (as shown in the  $E^1$  vs pH curve in Figure 7). Around pH 7,  $E^1$  was independent of pH, showing that the one-electron reduction process does not involve either an uptake or liberation of a proton around this pH. A number of experiments confirm that the reduction process in this region is :



The pK of 2.9 thus corresponds to

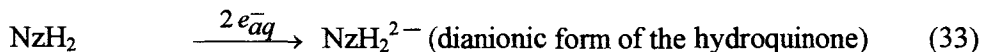


We could get a best fit of  $E^1$  versus pH at pH > 7 only when a pK = 9.2 for the ( $\text{NH}_3^+ \rightarrow \text{NH}_2 + \text{H}^+$ ) ionisation at the sugar moiety of the semiquinone was implicated. A series of experiments gave a  $E^1_7 = -341$  mV vs NHE at 25°C for the two anthracyclines. Later on, similar values were reported for other structurally related anthracycline derivatives [5].

Analogous to the naphthazarin semiquinone, the initial absorption decays in a second-order manner due to disproportionation reaction of the semiquinone. The equilibrium was much more to the semiquinone. Figure 7 shows the variation of log  $K_{\text{eq}}$  with pH. The  $K_{\text{eq}}$  values, in conjunction with  $E^1$  values at a given pH, yielded  $E^2$  and  $E^m$  values at the same pH. Over a narrow range  $E^1$ ,  $E^2$  and  $E^m$  values were very close, demonstrating exceptional stability. However, in this case, deglycosylation of the initially formed hydroquinone to form the quinone methide tautomer, wherein the absorption characteristics are virtually indistinguishable, was established. There has been no evidence for the liberation of daunosamine at the semiquinone stage. For these drugs, however, the presence of the equilibrium (23) even at neutral pH indicates that loss from the semiquinone and the hydroquinone will be indistinguishable. The rate constant of deglycosylation reaction was established as  $1.1 \text{ s}^{-1}$  and the rate constant for the quinone methide to 7-deoxy-adriamycinone (having similar absorption characteristics as that of the parent quinone) reaction was  $1.5 \times 10^{-2} \text{ s}^{-1}$ , at pH 7 [69]. It may be stated here that many unexplained observations are available in the case of anthracyclines and a complete mechanism of action is far from established.

### 3.8 Two-electron reduction

Land et al [60] have shown how pulse radiolysis can be used to generate 2-electron reduced species from parent quinones. A significant difference in behaviour of reduced naphtho- and anthraquinones was established during our subsequent studies. Naphthoquinones generated corresponding hydroquinones by complete 2-electron reduction. The fully reduced species readily reacted with oxygen to generate the parent quinone, e.g. naphthazarin.



Depending on pK values, neutral or anionic forms of the hydroquinone are formed. Then,



This reaction is quite slow in the case of naphthazarin. However, it becomes faster when oxygen is bubbled, or, in the alkaline solutions. Same reaction in the case of anthraquinone and higher derivatives gives rise to a reduced species which does not react with oxygen, or, reacts infinitesimally slowly. It was inferred that the reduced species could not be a normal hydroquinone. Several studies led to the proposal that a dihydroquinone type of molecule was generated.

An interesting observation in the two-electron reduction of quinones [37] has been the loss of sulphonate ( $-\text{SO}_3^-$ ) group from the fully reduced quinizarin-2-sulphonate when reduction takes place at  $\text{pH} < 7$  and the solution is made alkaline. Such  $-\text{SO}_3^-$  loss was not observed when reduction took place in the alkaline solutions or when quinizarin-6-sulphonate was used. On re-oxidation, quinizarin (and not its 2-sulphonate) was generated. Alkali was ruled out as cause of the  $-\text{SO}_3^-$  loss. Two alternative mechanisms involving tautomerisation and/or base-induced  $\beta$ -elimination of  $-\text{SO}_3^-$  were proposed for this very interesting and rare observation.

### 3.9 Reactivity with oxygen

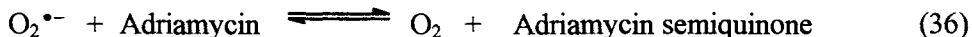
When an electron pulse is given to a solution which contains known quantity of oxygen, initially both semiquinone and  $\text{O}_2^{\bullet-}$  (superoxide radical) are produced depending on the relative concentrations and rate constants. However, in all cases studied so far, the following reaction



occur, with equilibrium, if any, established within a few hundred microseconds. The exact course of reaction depends entirely on the relative one-electron reduction potential of  $\text{O}_2/\text{O}_2^{\bullet-}$  system ( $E^1 = -155 \text{ mV}$  at  $25^\circ\text{C}$  vs NHE, when oxygen concentration is expressed in  $\text{mol dm}^{-3}$  unit) and  $\text{Q}/\text{Q}^{\bullet-}$  system (see Table 3 for some representative values).

A close look on Table 3 will show that naphthoquinones may be reduced to their semiquinones with  $\text{O}_2^{\bullet-}$  as  $E(\text{O}_2/\text{O}_2^{\bullet-}) < E(\text{Q}/\text{Q}^{\bullet-})$ . On the other hand,  $\text{O}_2^{\bullet-}$  radicals are preferentially formed by the reaction of anthrasemiquinones with  $\text{O}_2$  as  $E(\text{Q}/\text{Q}^{\bullet-}) < E(\text{O}_2/\text{O}_2^{\bullet-})$ .

The rate constant for the important reaction



could be determined pulse radiolytically [41] as  $3.5 \times 10^8 \text{ dm}^3 \text{ mol}^{-1} \text{ s}^{-1}$ . If one assumes  $E^1(\text{O}_2/\text{O}_2^{\bullet-}) = -155 \text{ mV}$  and  $E^1(\text{adriamycin/adriamycin semiquinone}) = -341 \text{ mV}$ , one can calculate the equilibrium constant as  $7.04 \times 10^{-4}$  at pH 7. In the acidic pH, upto pH  $\sim 5$ , the K value does not change much. At pH  $< 5$ ,  $\text{HO}_2^\bullet$  forms from  $\text{O}_2^{\bullet-}$ . At pH  $> 7$ , the equilibrium is even more to the left. This consideration clearly shows that superoxide radicals are formed by reaction of the semiquinone with  $\text{O}_2$ , a finding of great biomedical significance.

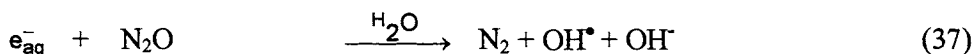
Presence of oxygen in the vicinity of enzymatically produced anthracycline semiquinones leads to predominant formation of  $\text{O}_2^{\bullet-}$ , sometime leading to concomitant  $\text{OH}^\bullet$  formation, causing cardiotoxicity and cytotoxicity. The equilibrium reaction (36) may be used in calculating  $E^1(\text{Q}/\text{Q}^{\bullet-})$  system by either measuring equilibrium concentrations or by measuring rate constants. Results are in agreement with the Marcus theory of electron transfer reactions.

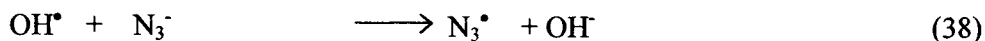
### 3.10 Radiation chemistry of orthoquinones

Most radiation chemical studies on quinones involve 1,4- or para-quinones. Recently, orthoquinones have assumed renewed significance in melanoma-related studies [70]. It was interesting to note that limited stability of anisyl-3,4-quinone [71] prompted the authors to prepare anisyl-3,4-semiquinone by one-electron oxidation of anisyl -3,4-hydroquinone, and not by one-electron reduction of the quinone. The transient absorption spectrum showed a maximum at  $\sim 320 \text{ nm}$  and a smaller maximum at  $\sim 400 \text{ nm}$  ( $k = 4.7 \times 10^9 \text{ dm}^3 \text{ mol}^{-1} \text{ s}^{-1}$ ). This semiquinone was shown to form an equilibrium involving the parent quinone,  $\text{O}_2$  and  $\text{O}_2^{\bullet-}$ . The favoured direction is  $\text{O}_2^{\bullet-}$  reducing the quinone to its semiquinone. Calculations led to  $E^1 \geq +77 \text{ mV}$ . The authors set a limit of  $E^1 \gg +100 \text{ mV}$ . The corresponding  $E^1_7$  for the structurally related but unstable 1,2-benzoquinone [9] was estimated to be  $+210 \text{ mV}$  pulse radiolytically. Such studies have physiological significance in explaining the cytotoxicity mechanism associated with the administration of 4-hydroxyanisole in the treatment of malignant melanoma.

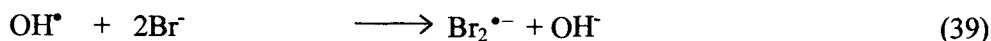
## 4. OXIDATION OF QUINONES

As the hydroxyl radical ( $\text{OH}^\bullet$ ) is a non-selective oxidising agent, it is normally converted into some secondary radical by using a suitable chemical.





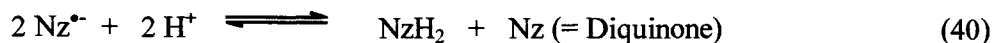
$\text{N}_3^-$  may be replaced by halides, thiocyanate etc. e.g.



Simple quinones undergo  $\text{OH}^\bullet$  addition to the ring as an oxidation reaction. On the other hand, hydroxy-substituted quinones can undergo additional oxidation reaction at the -OH site, first by addition to form cyclohexadienyl type radicals, followed by water elimination to form semi-oxidised quinones as free radicals [72]. Such oxidation reactions of 1,4-dihydroxyquinones assume special significance in view of these compounds being the central functional chromophoric centre of the quinonoid antitumour drugs, e.g. one-electron oxidation of adriamycin has been implicated by ESR studies [73]. However such oxidation reactions are more complex than one-electron oxidation of juglone [29], of dihydroxy-anthraquinones and their sulphonate derivatives [38,74] which have been characterised by using  $\text{OH}^\bullet$  and other more selective oxidants:  $\text{N}_3^\bullet$ ,  $\text{Br}_2^{\bullet-}$ ,  $\text{SO}_4^{\bullet-}$ ,  $^\bullet\text{CH}_2\text{CHO}$  ( $^\bullet\text{CHCHO}$ ), etc. As in the case of one-electron reduced species, one can measure the difference absorption spectrum (Figure 9) and corrected spectrum (Figure 10) for the one-electron oxidised substrate. Rate constants for the formation reactions are within the range  $10^9$ - $10^{10} \text{ dm}^3 \text{ mol}^{-1} \text{ s}^{-1}$ . It may be noted that, unlike in the case of the reduced semiquinones, quinonoid character is retained in the semi-oxidised quinones. Some representative spectroscopic data are given in Table 4 while rate constants are given in Table 5.

As in the case of the reduced quinones, the difference and absolute absorption spectra of the one-electron oxidised species have been studied in most of the above-named quinones. Two such typical difference and corrected spectra are shown in Figures 9 and 10, respectively, representing the neutral and anionic forms of one-electron oxidised quinizarin 2-sulphonate.

Mukherjee et al [72] have shown that the decay of the one-electron oxidized naphthazarin ( $\text{NzH}^\bullet$  and  $\text{Nz}^{\bullet-}$ ) proceeds by a complicated mechanism not fully understood in spite of extensive studies. At low dose condition, there was no visible change in the concentration of naphthazarin. The pK of the semi-oxidised naphthazarin was shown as  $< 4$ . The most interesting observation was the evidence for the disproportionation (40) proceeding to an equilibrium level in favour of the semi-oxidised quinone, accompanied by reaction (41). The possibility of dimerisation of the one-electron oxidised species was not fully explored.





Contrary to the naphthazarin case, dihydroxyanthraquinones (QH<sub>2</sub>) form semi-oxidised quinones which undergo simple bimolecular disproportionation to the diquinone and parent quinone [74]. Both the above reactions have been wrongly given due to "printers' devil" type error in a recent review [12]. The pK for the semi-oxidised anthraquinone derivatives was measured and shown to be around ~ 8.

The third aromatic ring in the anthraquinone derivatives possibly renders all secondary reactions very slow in comparison with the timescale for radical decay. Hydroxyl radicals react with OH-substituted quinones or other hydroquinones mainly by addition, followed by acid or base catalysed water elimination [55,72].

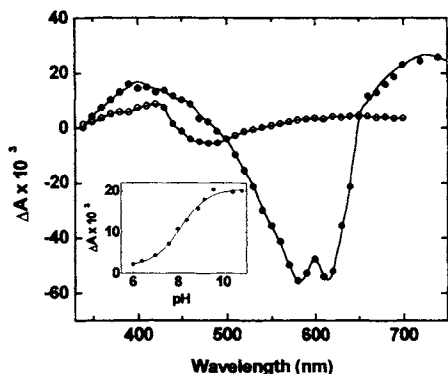
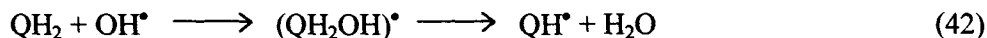


Figure 9. Difference absorption spectra of the semi-oxidised 1,4-QH<sub>2</sub>-2S at *ca.* pH 1 (o) and 11 (●). The oxidising agents were  $\dot{\text{C}}\text{H}_2\text{CHO}$  (*ca.* pH 1) and  $\text{N}_3^\bullet$  (pH 11). Inset: Variation of absorbance with pH at 720 nm (using  $\text{N}_3^\bullet$  as the oxidising agent.)

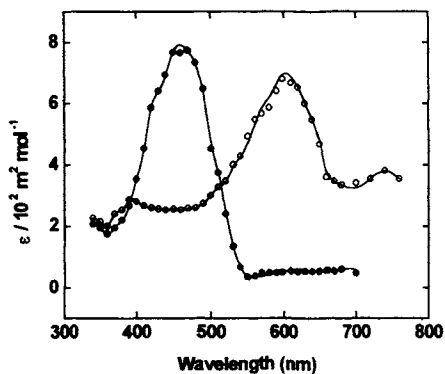


Figure 10. Corrected absorption spectra of the semi-oxidised 1,4-QH<sub>2</sub>-2S at *ca.* pH 1 (o) and pH 11 (●). (Figures 9 and 10 are reproduced from reference [74] by permission of the Royal Society of Chemistry.)

Table 4

Comparison of spectroscopic characteristics and pK of one-electron oxidised quinones in aqueous solution

Quinone	$\lambda_{\max} / \text{nm}$		pK	Ref
	$(\epsilon / 10^3 \text{ dm}^3 \text{ mol}^{-1} \text{ cm}^{-1})$			
	neutral	anionic		
2-Hydroxy-NQ(Lawsone)	340(3.4), 450(2.8)	-		29
5-Hydroxy-NQ (Juglone)	420(2.8), 540(3.1)	-		29
5,8-Dihydroxy-NQ (Naphthazarin)	390(3.2), 500(4.8) ~800(broad) (0.7)	440(3.4) 770(4.5), 870(3.9)	<3.5	72
1,4-Dihydroxy-AQ (Quinizarin)	i	390(3.0), 540(7.0)	i	74
1,5-Dihydroxy-AQ	i	472(10.5)	i	74
1,8-Dihydroxy-AQ	i	482(8.3)	i	74
Quinizarin 2-sulphonate	465(8.0)	390(2.9), 610(7.0)	8.0	74
Quinizarin 6-sulphonate	468(7.4)	420(4.0), 600(5.8)	7.9	74

i: Very poor solubility of the quinone at pH <10.5. No measurements

Table 5

Formation rate constants of transients formed by one-electron oxidation of some representative quinones ( $k$  in  $10^9 \text{ dm}^3 \text{ mol}^{-1} \text{ s}^{-1}$ ) in aqueous solution

Quinone	$\text{OH}^\bullet$ (pH)	$\text{N}_3^\bullet$ (pH)	$\text{O}^{\bullet-}$ (pH)	Ref
2-Hydroxy-NQ	11.0 (7.5)	6.0 (7.0)	7.4 (12.5)	29
5-Hydroxy-NQ	2.6 (10.4)	3.9 (10.4)	1.3 (13.0)	29
5,8-Dihydroxy-NQ	3.4 (5.3), 6.7 (9.2)	0.5 (5.8) 4.0 (9.1), 4.8 (~13)	1.0 (~13.0)	72
1,4-Dihydroxy-AQ(Quinizarin)	13.0(11.0)	6.5(11), 7.0(~14)	3.7 (~14)	74
1,5-Dihydroxy -AQ	41.0 (11.0)	12 (11), 14 (~14)	14.0 (~14)	74
1,8-Dihydroxy-AQ	21.0 (11.0)	10 (11), 10 (~14)	5.0 (~14)	74
Quinizarin 2-sulphonate	9.7 (11.0)	1.4 (6.0) 4.4 (11), 4.4 (~14)	1.7 (~14)	74
Quinizarin 6-sulphonate	11.0 (11.0)	1.3 (6.0) 5.6 (11), 5.7 (~14)	1.5 (~14)	74

## 5. TRIPLET EXCITED STATES

Phototendering and fading of anthraquinonoid dyes are believed to involve the triplet excited states. Apart from known photochemical excitation techniques, irradiation of quinone solutions in nonpolar solvents give rise to triplet states of quinones via the geminate recombination of initially formed ion pairs. Most popular solvents for such studies involve acetonitrile and cyclohexane, having no abstractable hydrogen atoms. In polar solvents like alcohols, initially formed triplets will react with the solvents by hydrogen atom abstraction to form semiquinone radicals [75-80].



In many cases where direct photo-generation of the triplet states of quinones is not very facile, pulse radiolysis offers a viable route, e.g. ubiquinone [81,82]. By choosing either a suitable donor or acceptor, as the case may be, and energy transfer method described by Bensasson and Land [83], the characteristics of the triplet excited states, eg. T-T absorption spectra, extinction coefficient, quantum yield and kinetic parameters have been determined for a number of quinones [75-80,84-87].

Anthracycline antibiotic and their derivatives have been shown to photosensitise the formation of singlet oxygen via their triplet state [86].

## 6. CURRENT SCOPE AND FUTURE PROSPECTS

It is amazing that quinones have sustained interest of radiation chemists for over three decades. The basic radiation chemistry of simple quinones and their simple derivatives is now well-understood. Therefore, efforts have to be diverted to complex derivatives of quinones, as the characteristics of the parent as well as the semiquinones will depend heavily on the perturbing groups/rings present. The accumulated data will give a clear insight into the perturbation effect of the overall substitution.

In the present scenario of protection of product development rights, it is expected that a large number of new products, based on the basic anthracycline structure, will be developed for anti-tumour trials. While basic radiation chemistry may not differ significantly from what we already know, it will be very interesting to know how the redox properties change with new structures [88]. The most important characteristics for either anti-tumour action or toxicity is the redox potential values. We should be able to put substituents at will to have a desired redox potential of the substrate. This is extremely important from the research point of view. However, no concerted efforts have been made in this direction.

A large number of studies are expected towards understanding the chemistry of the metabolites derived from complex biological quinones. Right now the field is barren, mainly because the facility of pulse radiolysis is not available openly to scientists the world over.

In the basic research areas, a very wide scope exists towards understanding the characteristics of the excited  $S_1/T_1$  states and their reactivities. Quinones, by virtue of their electronegativity, form ideal partners for electron transfer. A number of studies have begun where quinone moiety is bridged with another moiety through methylene bridges, e.g. prophyrin-quinone bridged systems [89,90]. Presently, only basic data may be collected on excitation and electron transfer. In few years' time, such systems may find wide application in

photodynamic therapy, where light will be absorbed by the prophyrin, electron transfer will take place and the semiquinone developed will participate in the anti-tumour activity. This may be a wishful thinking - but then, man's innovative eagerness knows no bounds !!

In a biological environment, the redox properties of the quinone/semiquinone system will be profoundly affected by solvation as well as by complexation with other surrounding molecules, and also by availability of large number of free and bound protons. Semiquinones are capable of complexing with quinones, other semiquinones, as well as hydroquinones. They can also complex with metal ions [91,92]. Even in the simplest case of  $\text{Cu}^{2+}$ /benzosemiquinone system, the latter substitute for a water molecule in the co-ordination sphere of the metal ion. Although the reduction potential of benzoquinone is +99 mV and that of  $\text{Cu}^{2+}$  is +153 mV, no rapid inner-sphere electron transfer is seen.

Micellar systems and microemulsions provide useful biological models for specific studies. We have demonstrated the generation of a large number of semiquinones in cationic, anionic and neutral micelles by simple light irradiation. It will be interesting to study chemistry of the semiquinones of water-insoluble complex biologically important quinones dissolved in micelles and microemulsions.

Finally, a word of caution ! Looking back at the work on semiquinones, the author finds a large number of simple facts, yet unexplained. These studies have to be taken up seriously on a full scale. Simple questions like exceptional stability over a narrow pH zone, loss of a  $-\text{SO}_3^-$  group on reduction, unusual phenomena observed in the steady-state irradiation of anthracyclines [93] etc. are not yet fully explained.

In short, there is ample scope for furtherence of knowledge of radiation chemistry of quinones.

### ACKNOWLEDGEMENTS

The author wishes to thank Dr. M. C. Rath and Ms. J. Pandya for meticulously typing and formatting the manuscript. Help received from many colleagues in India and abroad is gratefully acknowledged.

### REFERENCES

1. S. Patai (ed.) "The Chemistry of Quinonoid Compounds", Wiley, New York, 1972.
2. G. E. W. Wolstenholme and M. O'Conner (ed.) "Quinones in Electron Transport", J & A Churchill Ltd., London, 1961.
3. T. Itoh, Chem. Rev., 95 (1995) 2351.

4. K. Hamanoue and T. Nakayama, *Proc. Indian Acad. Sci., (Chem. Sci.)*, 104 (1992) 219.
5. J. Butler and B.M. Hoey, *British J. Cancer*, 55 (suppl-III) (1987) 53.
6. J. S. Driscoll, G. F. Hazard, H. B. Wood and A. Goldin, *Cancer Chem. Rep.*, 2 (1974) 1.
7. J. H. Fendler and E. J. Fendler, in S. Patai (ed.), "The Chemistry of the Quinonoid Compounds (Part1)", John Wiley, New York; 1974; p.539.
8. A. J. Swallow, *Prog. Reaction Kin.*, 9 (1978) 238.
9. A. J. Swallow, in B. J. Trumppower (ed.) "Functions of Quinones in Energy Conserving Systems", Academic Press, New York, 1982, p.59.
10. R. Bensasson, E. J. Land and T. J. Truscott, "Excited States and Free Radicals in Biology and Medicine", Oxford University Press, Oxford, 1993, Ch.11.
11. P. Neta, in S. Patai and Z. Rappoport (eds.), "The Chemistry of the Quinonoid Compounds (Vol.2)", John Wiley, New York, 1989, p.879.
12. J. Mayer, in J. Mayer (ed.), "Properties and Reactions of Radiation Induced Transients: Selected Topics", Polish Scientific Publishers PWN, Warszawa, 1999, p.205.
13. *Colour Index*, 4th edition (1992), Society of Dyers and colourists, Bradford, U.K.
14. A. J. Swallow, "Radiation Chemistry: An Introduction", Longman, London, 1973.
15. R. Bensasson, E.J. Land and T.J. Truscott, "Flash Photolysis and Pulse Radiolysis", Oxford University Press, Oxford, 1983.
16. J. H. Baxendale and F. Busi (eds.), "The Study of Fast Processes and Transient Species by Electron Pulse Radiolysis", Reidel, Dordrecht, 1982.
17. J. Perkowski and J. Mayer, *J. Radioanal. Nucl. Chem.*, 132 (1989) 269.
18. J. Perkowski and J. Mayer, *J. Radioanal. Nucl. Chem.*, 172 (1993) 19.
19. J. Perkowski and J. Mayer, *J. Radioanal. Nucl. Chem.*, 173 (1993) 339.
20. P. Wardman, *Rep. Progr. Phys.*, 41 (1978) 259.
21. Farhatziz and M. A. J. Rodgers (eds.) "Radiation Chemistry, Principles and Applications", VCH, New York, 1987.
22. T. Mukherjee, in "Atomic, Molecular and Cluster Physics", ed. S.A. Ahmed, Narosa, New Delhi, 1997, p. 299.
23. P. S. Rao and E. Hayon, *J. Phys. Chem.*, 77 (1973) 2274.
24. E. Hayon, T. Iabata, N. N. Lichtin and M. Simic, *J. Phys. Chem.*, 76 (1972) 2072.
25. P. S. Rao and E. Hayon, *J. Am. Chem. Soc.*, 96 (1974) 1287 & 1295.

26. T. Mukherjee, A.J. Swallow, P.M. Guyan and J.M. Bruce, *J. Chem. Soc., Faraday Trans.*, 86 (1990) 1483.
27. H. Pal and T. Mukherjee, *J. Indian Chem. Soc.*, 70 (1993) 409.
28. M. C. Rath and T. Mukherjee, *Radiat. Phys. Chem.*, 49 (1997) 29.
29. M. C. Rath, H. Pal and T. Mukherjee, *J. Chem. Soc., Faraday Trans.*, 92 (1996) 1891.
30. T. Mukherjee, *Radiat. Phys. Chem.*, 29 (1987) 455.
31. E. J. Land, T. Mukherjee, A. J. Swallow and J. M. Bruce, *J. Chem. Soc., Faraday Trans. 1*, 79 (1983) 391.
32. H. Pal, D. K Palit, T. Mukherjee and J. P. Mittal, *Radiat. Phys. Chem.*, 37 (1991) 227.
33. B. E. Hulme, E. J. Land and G. O. Phillips, *J. Chem. Soc., Faraday Trans. 1*, 68 (1972) 1992.
34. D. Meisel and P. Neta, *J. Am. Chem. Soc.*, 97 (1975) 5198.
35. H. Pal, T. Mukherjee and J. P. Mittal, *Radiat. Phys. Chem.*, 44 (1994) 603..
36. H. Pal, D. K Palit, T. Mukherjee and J. P. Mittal, *Radiat. Phys. Chem.*, 40 (1992) 529.
37. T. Mukherjee, E. J. Land, A. J. Swallow, P. M. Guyan and J. M. Bruce, *J. Chem. Soc., Faraday Trans. 1*, 84 (1988) 2855.
38. H. Pal, D. K Palit, T. Mukherjee and J. P. Mittal, *J. Chem. Soc., Faraday Trans.*, 87 (1991) 1109.
39. M. C. Rath, H. Pal and T. Mukherjee, *Radiat. Phys. Chem.*, 47 (1996) 221.
40. H. Pal, T. Mukherjee and J. P. Mittal, *J. Chem. Soc., Faraday Trans.*, 90 (1994) 711.
41. E. J. Land, T. Mukherjee, A. J. Swallow and J. M. Bruce, *British J. Cancer*, 51 (1985) 515.
42. T. Mukherjee and J. M. Brice, *Indian J. Chem.*, 33A (1994) 386.
43. E. Mc Alpine, R. S. Sinclair, T. G. Truscott and E. J. Land, *J. Chem. Soc., Faraday Trans. 1*, 74 (1978) 597.
44. J. Mayer and R. Krasluklanis, *J. Chem. Soc., Faraday Trans.*, 87 (1991) 2943.
45. G. A. Russel and F. A. Neugebauer, *Org. Magn. Reson.*, 1 (1969) 125.
46. B. Venkataraman, B. G. Segal and G. K. Fraenkel, *J. Chem. Phys.*, 30 (1959) 1006.
47. T. Mukherjee and N. J. F. Dodd, *Biochem. Pharmacol.*, 33 (1984) 379.
48. H. Chandra, L. Portwood and M. C. R. Symons, *J. Chem. Soc., Faraday Trans.*, 1, 85 (1989) 1801.
49. M. C. Depew, Z. -L. Liu and J. K. S. Wan, *J. Am. Chem. Soc.*, 105 (1983) 2480
50. Z. -L. Liu, L. -M. Wu and Y. -C. Liu, *Magn. Reson. Chem.*, 26 (1988) 577.

51. N. J. F. Dodd and T. Mukherjee, *Biochem. Pharmacol.*, 33 (1984) 379.
52. T. Mukherjee, B. Cercek, N. J. F. Dodd and A. J. Swallow, *Radiat. Phys. Chem.*, 30 (1987) 271.
53. J. Mayer and R. Krsiukianis, *Radiat. Phys. Chem.*, 36 (1990) 169.
54. J. Mayer and R. Krsiukianis, *Radiat. Phys. Chem.*, 37 (1991) 273.
55. P. Wardman, *J. Phys. Chem. Ref. Data*, 18 (1989) 1637.
56. K. B. Patel and R. L. Willson, *J. Chem. Soc., Faraday Trans.*, 69 (1973) 814.
57. E. J. Land, T. Mukherjee, A. J. Swallow and J. M. Bruce, *Archives Biochem. Biophys.*, 225 (1983) 116.
58. T. Mukherjee, E. J. Land, A. J. Swallow and J. M. Bruce, *Archives Biochem. Biophys.*, 272 (1989) 450.
59. J. Butler and B. M. Hoey, *J. Free Rad. Biol. Med.*, 2 (1986) 77.
60. E. J. Land, T. Mukherjee, A. J. Swallow and J. M. Bruce, *J. Chem. Soc., Faraday Trans. 1*, 79 (1983) 405.
61. F. Arcamone, "Doxorubicin Anticancer Antibiotics," *Medicinal Chemistry Monograph*, Vol. 17, Academic Press, New York, 1981.
62. M. S. El-Khadem (ed.), "Anthracycline Antibiotics", Academic Press, New York, 1982.
63. S. S. Pan, P. A. Andrews, C. J. Glover and N. R. Bachur, *J. Biol. Chem.*, 259 (1984) 959.
64. B. Hoey, J. Butler and A. J. Swallow, *Biochem.*, 27(1988) 2608.
65. R. J. Sturgeon and S. G. Schulman, *J. Pharmaceut. Sci.*, 66 (1977) 958.
66. C. Houee-Levin, M. Gardes-Albert, A. Rouscilles, C. Ferradini and B. Hickel, *Biochem.*, 30 (1991) 8216.
67. B. A. Svingen and G. Powis, *Arch. Biochem. Biophys.*, 209 (1981) 209.
68. C. Houee-Levin, M. Gardes-Albert, C. Ferradini, M. Faraggi and M. Klapper, *FEBS Lett.* 179 (1985) 46.
69. J. S. Lea, F. A. P. Rushton, E. J. Land and A. J. Swallow, *Free Rad. Res. Commun.*, 8 (1990) 241.
70. C. Lambert, J. N. Chacon, M. R. Chedekel, E. J. Land, P. A. Riley, A. Thompson and T. G. Truscott, *Biochim. Biophys. Acta*, 993 (1989) 12.
71. C. J. Cooksey, E. J. Land, P. A. Riley, T. Sarna and T. G. Truscott, *Free Radic. Res. Commun.*, 4 (1987) 131.
72. T. Mukherjee, E. J. Land, A. J. Swallow, J. M. Bruce, P. C. Beaumont and B. Parsons, *J. Chem. Soc., Faraday Trans. 1*, 84 (1988) 3423.
73. D. D. Pietronigro, J. E. McGuinness, M. J. Koren, R. Gippa, M. L. Seligman and H.B. Demopoulos, *Physiol. Chem. Phys.*, 11 (1979) 405.
74. H. Pal, D. K. Palit, T. Mukherjee and J. P. Mittal, *J. Chem. Soc., Faraday Trans.*, 88 (1992) 681.

75. D. K. Palit, T. Mukherjee and J. P. Mittal, *J. Indian Chem. Soc.*, 63 (1986) 35.
76. D. K. Palit, H. Pal, T. Mukherjee and J. P. Mittal, *J. Photochem.*, 37 (1987) 95.
77. D. K. Palit, H. Pal, T. Mukherjee and J. P. Mittal, *J. Photochem. Photobiol. A : Chem.*, 43 (1988) 59.
78. D. K. Palit, H. Pal, T. Mukherjee and J. P. Mittal, *J. Photochem. Photobiol. Sec A: Chem.*, 52 (1990) 375. (Corrigendum : *ibid* 54 (1990) 271.
79. H. Pal, D. K. Palit, T. Mukherjee and J. P. Mittal, *J. Photochem. Photobiol. Sec A : Chem.*, 62 (1991) 183.
80. H. Pal, D. K. Palit, T. Mukherjee and J. P. Mittal, *Indian J. Chem.*, 31A (1992) 811.
81. R. Bensasson C. Chachaty, E. J. Land and C. Salet, *Photochem. Photobiol.*, 16 (1972) 27.
82. E. Amoayal, R. Bensasson and E. J. land, *Photochem, Photobiol.*, 20 (1974) 415.
83. R. Bensasson and E. J. Land, *Trans. Faraday Soc.*, 67 (1971) 1904.
84. B. E. Hulme, E. J. Land and G. O. Phillips, *J. Chem. Soc. Faraday Trans. 1*, 68 (1972b) 2003.
85. E. J. Land E. McAlpine, R. S. Sinclair and T. G. Truscott, *J. Chem. Soc., Faraday Trans. 1*, 72 (1976) 2091.
86. A. Andreoni, E. J. Land, V. Malatesa, A. J. McLean and T. G. Truscott, *Biochim. Biophys. Acta*, 990 (1989) 190.
87. T. Nakayama, K. Ushida, K. Hamanoue, M. Washio, S. Tagawa and Y. Tabata *J. Chem. Soc. Faraday Trans.*, 86 (1990) 95.
88. M. C. Rath, R. T. Pardasani, P. Pardasani, S. Muktawat, R. Ghosh and T. Mukherjee, *Res. Chem. Intermed.* (in print).
89. G. Bhaskar Maiya, Private Communication
90. E. J. Land, D. Lexa, R. V. Liddell and G. A. Nemeth, *J. Phys. Chem.*, 91 (1987) 4831.
91. S. Das, P. C. Mandal, M. C. Rath and T. Mukherjee, *Res. Chem. Intermed.*, 25 (1999) 351.
92. S. Das, P. C. Mandal, M. C. Rath and T. Mukherjee, (to be published).
93. T. Mukherjee, (to be published).

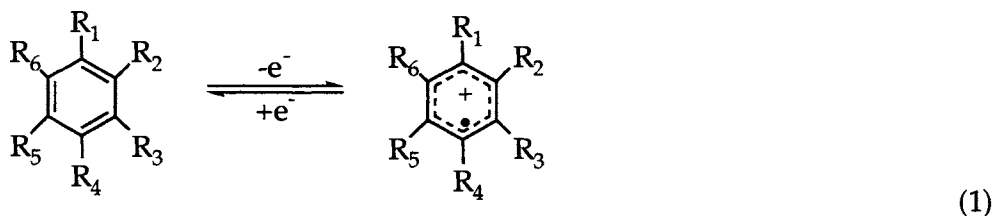
## Redox Chemistry and Energetics of Radical Cations of Substituted Benzenes

Mats Jonsson

Department of Chemistry, Nuclear Chemistry, Royal Institute of Technology, SE - 100 44 Stockholm, Sweden

### 1. INTRODUCTION

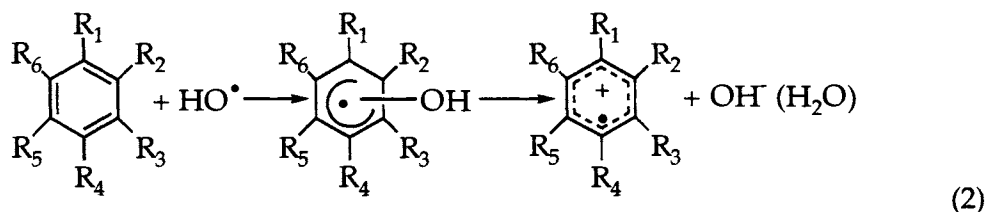
Numerous synthetic, technical and natural processes involve formation of aromatic radical cations as reaction intermediates.[1,2] In general, aromatic radical cations are formed upon ionization, e.g., by direct photolysis or radiolysis, or one-electron oxidation of aromatic compounds (reaction 1).



These radical cations are usually very reactive and the two main modes of reaction are side-chain fragmentation and attack by nucleophiles. The reactivity patterns of radical cations in general have recently been reviewed by Schmittel and Burghart.[1] For many reactions, there is a correlation between the thermodynamic stability of the radical cation and the kinetics of the reaction.

Pulse radiolysis has proven to be a very useful and versatile method for studies of both the kinetics and the thermochemistry of substituted benzene radical cations in aqueous solution. In aqueous solution, most substituted benzenes and benzene itself are oxidized by  $\text{SO}_4^{\bullet-}$  ( $E^\circ = 2.4$  V vs. NHE).[3] Other oxidants, such as  $\text{Br}_2^{\bullet-}$  and  $\text{N}_3^{\bullet-}$ , can also oxidize benzene substituted with strongly electron donating groups. The hydroxyl radical, another potent oxidant frequently used in radiation chemical studies, initially forms a hydroxycyclohexadienyl radical when reacting with substituted benzenes. This radical can decompose into the

corresponding aromatic radical cation and  $\text{OH}/\text{H}_2\text{O}$  (reaction 2) provided the thermochemical conditions are favorable, i.e., in principle that the one-electron reduction potential of the radical cation is lower than that of the hydroxyl radical (which is always the case if  $\text{H}^+$  catalysis is included). The rate of the reaction between the hydroxyl radical and substituted benzenes is diffusion controlled and, thus, does not vary significantly with the substituent. However, in the gas-phase, the rate constant depends on the substituent pattern and thereby, as will be shown later, also on the ionization potential of the substituted benzene.[4]



The life-time of the intermediate hydroxycyclohexadienyl radical strongly depends on the substituent pattern.

Substituted benzene radical cations are also susceptible to attack by nucleophiles such as  $\text{OH}$  or  $\text{H}_2\text{O}$  and thus, in aqueous solution they will eventually become hydrolyzed yielding a hydroxycyclohexadienyl radical. The kinetics for the nucleophilic addition to benzene radical cations, and thereby also the life time of the radical cations in aqueous solution, is also very sensitive to the substituent pattern.\* The rate of nucleophilic addition has been shown to depend on the one-electron reduction potential of the radical cation (determined by the substituent pattern) and also on the nucleophilicity of the nucleophile.[8-10]

During the last two decades, the redox and acidity properties and the reactivity of substituted benzene radical cations in aqueous solution and organic solvents have been extensively studied by pulse radiolysis, electrochemical techniques and photochemical techniques.[1,2,5-20]

Both the redox and acidity properties, and hence also the X-H bond dissociation energies, have been found to depend on the substituent pattern. In the majority of cases, the substituent effects have been shown to follow linear free energy relationships, even for

\* It should be noted that the isomeric product distribution of the hydroxycyclohexadienyl radicals is not necessarily identical for the two isoelectronic reaction pathways. The product pattern seems to be governed by the charge distribution on the radical cation and the electron density distribution on the corresponding substituted benzene. [5-7]



multisubstituted radical cations.[13] Recently, electrochemical studies have also revealed that solvent effects on the redox properties of radical cations can be described by linear solvation energy relationships.[21,22] The aim of this paper is to give a unified picture of these findings which form the very basis for understanding the redox chemistry and energetics of radical cations of substituted benzenes in solution. The gas-phase properties of substituted benzenes will be used as a reference system throughout the paper.

## 2. THERMOCHEMISTRY

The thermochemical property that best reflects the reactivity or stability of a radical cation in solution is the one-electron reduction potential,  $E^\circ$ . The corresponding gas-phase property is the ionization potential,  $IP$ , of the corresponding neutral molecule. The latter can be considered as the intrinsic solvent independent one-electron reduction potential of the radical cation. The solvent independent ionization potential and the solvent dependent one-electron reduction potential are approximately related via equation (3) where the constant, 4.44 ( $\pm 0.02$ ) eV,[23] is the absolute potential of the hydrogen electrode in water.[24]

$$IP \approx 4.44(\pm 0.02) + E^\circ + \frac{\Delta G^\circ_{\text{solv}}(\text{Ar}) - \Delta G^\circ_{\text{solv}}(\text{Ar}^{\bullet+})}{F} \quad (3)$$

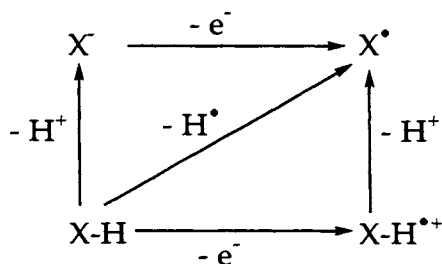
$\Delta G^\circ_{\text{solv}}(\text{Ar})$  and  $\Delta G^\circ_{\text{solv}}(\text{Ar}^{\bullet+})$  are the free energies of solvation of the neutral molecule and the radical cation, respectively, and  $F$  is the Faraday constant. It should be noted that the ionization potential is the enthalpy of ionization at 0 K; thus, the ionization entropy and the temperature correction are neglected in equation (3). However, these corrections are assumed to be fairly small.

Aromatic radical cations containing -XH substituents, e.g., in the simplest case, phenol, aniline and toluene, can deprotonate to form the corresponding neutral radicals. This is the simplest type of radical cation fragmentation reaction. Thus, the stability of these radical cations in solution is also reflected by the  $pK_a$  (reaction 4).



The corresponding gas-phase property is the proton affinity, or more correctly the gas-phase basicity, of the neutral radical.\*

For any species containing -XH groups there is a relationship between the redox and acidity properties and the homolytic X-H bond dissociation enthalpy as illustrated by the thermochemical cycle in scheme 1.



Scheme 1. Thermochemical cycle for X-H dissociation.

Consequently, the homolytic gas-phase X-H bond dissociation enthalpy,  $D_{X-H}$ , for the corresponding neutral molecule can be calculated using Hess' law and the one-electron reduction potential of the radical cation ( $X\text{-H}^{\bullet+}$ ) in combination with the  $\text{p}K_a$  of the radical cation or the one-electron reduction potential of the radical ( $X^\bullet$ ) in combination with the  $\text{p}K_a$  of the neutral molecule ( $X\text{-H}$ ). This results in equation 5 where C is a constant that depends on the family of compounds and the solvent.[25]

$$D_{X-H} = 96.5E^\circ + 5.70\text{p}K_a + C \quad (\text{kJ mol}^{-1}) \quad (5)$$

This relationship can also be used to calculate any of the thermochemical properties included, provided that the other two are known.

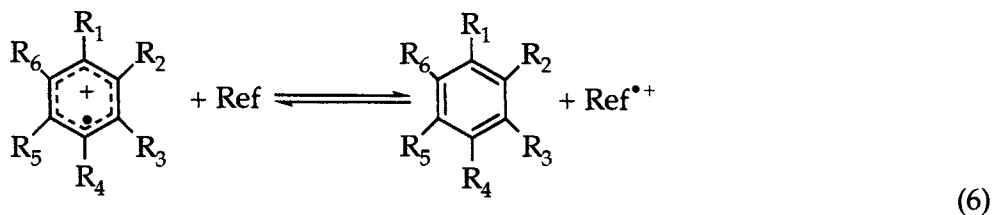
\* The proton affinity is the enthalpy while the gas-phase basicity is the free energy for the reaction  $\text{R}^\bullet + \text{H}^+$ .

### 3. EXPERIMENTAL TECHNIQUES

There are two main techniques used for measurement of one-electron reduction potentials in solution; pulse radiolysis and cyclic voltammetry. They both have their advantages and disadvantages which will be discussed here. The acidity of substituted benzene radical cations have been studied mainly by pulse radiolysis but a few measurements using laser flash photolysis have also been reported.

#### 3.1. Pulse radiolysis

The technique has been described in detail elsewhere.[26] In short, a pulse of high energy electrons induces a series of chemical reactions that can be monitored, e.g., using time resolved UV-vis spectroscopy. The reaction of interest is usually induced by a reaction between a radical formed from radiolysis of the solvent (usually water) and a solute molecule. The primary radiolysis products in aqueous solution are  $\text{HO}^\bullet$ ,  $e_{\text{aq}}^-$ ,  $\text{H}^\bullet$ ,  $\text{H}_2\text{O}_2$ ,  $\text{H}_2$  and  $\text{H}_3\text{O}^+$ . The major radical species,  $\text{HO}^\bullet$  and  $e_{\text{aq}}^-$ , are formed in equimolar concentrations,  $0.28 \mu\text{mol/J}$  each, on electron or  $\gamma$ -irradiation.[27] As can be seen in reaction 2, the hydroxyl radical does not yield a benzene radical cation instantly upon reaction with a substituted benzene. For this reason, secondary oxidants, such as  $\text{SO}_4^{\bullet-}$ ,  $\text{Br}_2^\bullet$  and  $\text{N}_3^\bullet$ , are usually used to generate benzene radical cations. To determine one-electron reduction potentials of radical cations, the redox equilibrium between the radical cation of interest and a redox couple with a known one-electron reduction potential is studied. The equilibrium constant can be derived from the rate constants of the electron-transfer reaction and the back reaction and/or the equilibrium concentrations of the two redox couples (reaction 6).[28]



The one-electron reduction potential of interest is then calculated from the equilibrium constant and the one-electron reduction potential of the redox reference couple using Nernst's equation ( $\Delta E^\circ = 0.0591 \log K$ ). While electrochemical techniques often yield irreversible oxidation potentials, pulse radiolysis usually yields thermodynamically correct one-electron reduction potentials, provided the reactions are fast

enough and that no other reactions occur within the time-scale of the experiment. The error margin is typically  $\pm 20$  mV for potentials determined by pulse radiolysis. A disadvantage of this method is that it can only be used with high accuracy for aqueous solutions where the radiation chemical processes are well-established.

The  $pK_a$  of radical cations can be determined by measuring the radical cation concentration at various pH.[12,13] This can be done since there are spectral differences between a radical cation and the corresponding neutral radical. The concentration (or absorbance) is then plotted against the pH, resulting in a typical  $pK_a$ -curve from which the radical cation  $pK_a$  can be obtained. This method has also been used successfully with laser flash photolysis.[20]

### 3.2. Cyclic voltammetry

The technique, which is a standard electrochemical technique for measurement of oxidation- and reduction potentials, has been described in great detail elsewhere.[29] In short, a standard three electrode set-up is used and the potential of the working electrode is scanned from a potential  $E_1$  to  $E_2$  and back to  $E_1$  again giving rise to an oxidation current and a reduction current. For a completely reversible system the oxidation current is equal to the reduction current and the half-wave potential ( $E_{1/2} = \frac{E_{red} + E_{ox}}{2}$ ) is identical to the thermodynamical one-

electron reduction potential of the oxidized species. However, for a large number of substituted benzene radical cations, radical-radical and radical-solvent reactions are very rapid which results in irreversible oxidation of the substrate and consequently, the thermodynamical one-electron reduction potential of the substituted benzene radical cation cannot be determined. For a series of structurally similar compounds, the irreversible peak oxidation potentials usually reflect the relative one-electron reduction potentials of the radical cations. The advantages of using cyclic voltammetry are that a wide variety of solvents can be used and that the measurements are relatively simple to perform.

## 4. REDOX PROPERTIES

### 4.1. Aqueous Solution

In table 1, the one-electron reduction potentials of some mono- and multisubstituted benzene radical cations measured by pulse radiolysis (or estimated) in aqueous solution are given. The one-electron reduction potentials of monosubstituted benzene radical cations range from

slightly below 1 V vs. NHE to slightly below 3 V vs. NHE, i.e., from moderately to strongly oxidizing. As can be seen, electron-donating substituents lower the reduction potential compared to unsubstituted benzene while electron-withdrawing substituents increase it. The stability of a radical cation usually increases with decreasing one-electron reduction potential as the charge becomes more delocalized. The charge delocalization implies decreased reactivity towards nucleophiles and thereby increased life time in aqueous solution.

Substituent effects on the properties or reactivity of substituted benzenes are often best described by the Hammett equation using the Hammett substituent constant,  $\sigma_p$ . For substituted benzene radical cations, the Brown substituent constant,  $\sigma_p^+$ , has been found to describe substituent effects somewhat better than the Hammett constant.[30,31] The use of linear free energy relationships is very convenient both for systematizing the thermochemical information and for predictions when experimental data are lacking. As can be seen in figure 1, the one-electron reduction potential of benzene radical cations in aqueous solution depends linearly on the Brown substituent constant. The linear correlation is given by equation (7).

$$E^\circ = (2.24 \pm 0.04) + (0.84 \pm 0.05)\sigma_p^+ \quad (R^2 = 0.98) \quad (7)$$

The intercept of equation (7),  $2.24 \pm 0.04$  V vs. NHE, corresponds to the one-electron reduction potential of the unsubstituted benzene radical cation. Due to its very short life-time in solution, the thermodynamical one-electron reduction potential for this radical cation has not been possible to measure directly by pulse radiolysis or any other technique. The values given for the unsubstituted benzene radical cation in table 1 are thermochemical estimates giving the upper and lower limits. Recently, the limiting values were confirmed by Mohan and Mittal based on a pulse radiolysis study.[18]

Equation (7) also constitutes a basis for further empirical modeling of substituent effects on benzene radical cations since it gives the intercepts for the linear relationships between one-electron reduction potentials of 1,4-substituted benzene radical cations and  $\sigma_p^+$  of the 4-substituent given a specific 1-substituent. The 1-substituent defines the family, e.g., phenol, anisole, aniline, etc. Since the 1,4-substituents can belong to either the 1-substituent family or the 4-substituent family, the general empirical relationship must be symmetrical, i.e., the resulting one-electron reduction potential must be the same regardless of choice of family.

TABLE 1  
One-electron Reduction Potentials of Some Substituted Benzene Radical Cations in Aqueous Solution.

Substituted benzenes	$E^\circ$ (V vs. NHE)	Substituted benzenes	$E^\circ$ (V vs. NHE)
Monosubstituted benzenes		Anilines	
$C_6H_6 \bullet^+$	2.1[24], 2.4[32]	2,4-( $CH_3$ ) <sub>2</sub>	0.89[13]
$C_6H_5NO_2 \bullet^+$	2.9[24]	3,4-( $CH_3$ ) <sub>2</sub>	0.89[13]
$C_6H_5CH_3 \bullet^+$	1.98[24]	3,5-( $CH_3$ ) <sub>2</sub>	0.98[13]
$C_6H_5NH_2 \bullet^+$	1.02[12], 1.03[33]	2- $CH_3O$	0.90[13]
$C_6H_5N(CH_3)_2 \bullet^+$	0.86[33]	4- $CH_3O$	0.79[12]
$C_6H_5OH \bullet^+$	1.5[34]	2,4-( $CH_3O$ ) <sub>2</sub>	0.72[13]
$C_6H_5OCH_3 \bullet^+$	1.62[9]	3,4-( $CH_3O$ ) <sub>2</sub>	0.78[13]
$C_6H_5Br$	2.31±0.15[17]	3,5-( $CH_3O$ ) <sub>2</sub>	1.04[13]
Anisoles		4-R- $C_6H_5-S-CH_3 \bullet^+$	
2- $CH_3O$	1.44[9]	( $CH_3$ ) <sub>2</sub> N	0.65[14]
2,3-( $CH_3O$ ) <sub>2</sub> C	1.42[9]	$CH_3O$	1.43[14]
2,4-( $CH_3O$ ) <sub>2</sub>	1.13[9]	$CH_3$	1.42[14]
4- $CH_3O$	1.30[9]	H	1.45[14]
3- $CH_3O$	1.55[9]	$CF_3$	1.45[14]
MPP <sup>§</sup>	1.40[9]	4-R- $C_6H_5-Se-CH_3 \bullet^+$	
Anilines		( $CH_3$ ) <sub>2</sub> N	0.60[14]
4- $NH_2$	0.59[12]	$CH_3O$	1.09[14]
4-( $CH_3$ ) <sub>3</sub> C	0.94[12]	$CH_3$	1.07[14]
4- $CH_3CO$	1.14[12]	H	1.09[14]
4-I	1.02[12]	$CF_3$	1.20[14]
4-CN	1.32[12]	4-R- $C_6H_5-Te-CH_3 \bullet^+$	
2- $CF_3$	1.30[13]	$CH_3O$	0.73[14]
3- $CF_3$	1.27[13]	$CH_3$	0.72[14]
4- $CF_3$	1.28[12]	H	0.74[14]
2- $CH_3$	1.01[13]	$CF_3$	0.75[14]
4- $CH_3$	0.92[12]		

The linear relationship for an arbitrary family is then given by the equation (8)

$$E^\circ = (2.2 + 0.8\sigma_{p1}^+) + f(\sigma_{p1}^+)\sigma_{p4}^+ \quad (8)$$

where  $f(\sigma_{p1}^+)$  is the slope of the Hammett plot, given a specific 1-substituent. On empirical grounds,  $f(\sigma_{p1}^+)$  was found to be:

$$f(\sigma_{p1}^+) = 0.79 + 0.42\sigma_{p1}^+ \quad (9)$$

<sup>§</sup> 3-(2-methoxyphenoxy)-1,2-propanediol

Incorporating equation (9) into equation (8) we obtain equation (10).[9]

$$E^\circ = 2.2 + 0.8(\sigma_{p1}^+ + \sigma_{p4}^+) + 0.4\sigma_{p1}^+\sigma_{p4}^+ \quad (10)$$

which is indeed symmetrical.

Interestingly, the effects of the two substituents are not additive, which is shown by the so called cross-interaction constant[35] of 0.4. From equation (10), we can also see that 1-substituted benzene radical cations with low one-electron reduction potentials are less sensitive to 4-substitution than 1-substituted benzene radical cations with high one-electron reduction potentials.

Equation (10) has also been extended to hold for multisubstituted benzene radical cations (equation 11):[13]

$$E^\circ = 2.2 + 0.8\left(\sigma_{p1}^+ + \sum_{i=2}^6 \sigma_i^+\right) + 0.4\sigma_{p1}^+ \sum_{i=2}^6 \sigma_i^+ \quad (11)$$

In this equation, position 1 is always that of the substituent with the lowest substituent constant. In other words, the identity of the radical cation is determined by the most electron-donating substituent.

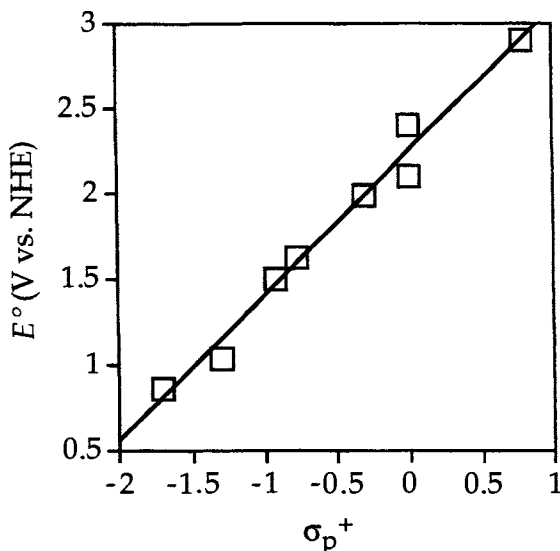


Figure 1. One-electron reduction potentials of monosubstituted benzene radical cations plotted against the substituent  $\sigma_p^+$  values.

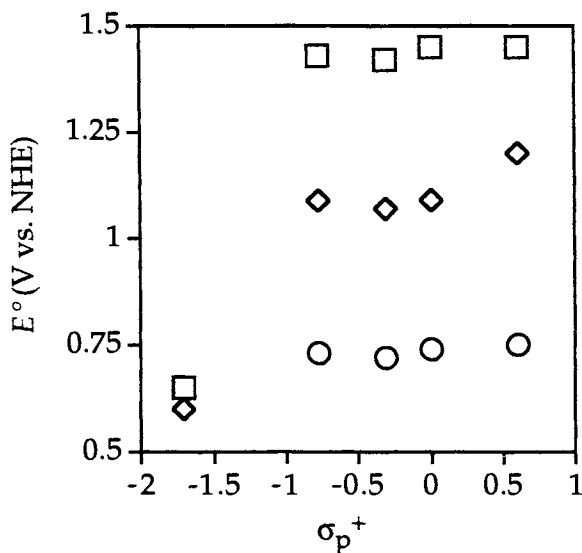


Figure 2. One-electron reduction potentials of, from top to bottom, 4-substituted  $C_6H_5-S-CH_3^{+\bullet}$ ,  $C_6H_5-Se-CH_3^{+\bullet}$  and  $C_6H_5-Te-CH_3^{+\bullet}$  plotted against the substituent  $\sigma_p^+$  values.

The substituent constants to be used in equation (11) are  $\sigma_p^+$  for substituents in position 1 and 4,  $\sigma_m^+$  for substituents in position 3 and 5 and a conditional *ortho* scale for substituents in position 2 and 6 ( $\sigma_o^+ = 0.73\sigma_p^+$ ).[13] A similar conditional *ortho* scale has also been derived for phenoxy radicals.[36] Furthermore, a comparison of the effects of *ortho* and *para* substituents on the gas-phase ionization potentials of substituted benzenes confirms that the effect of a given substituent in the *ortho* position is ca. 70 % of the effect of the same substituent in the *para* position.[37]

Interestingly, equation (10) does not hold for radical cations with the general structure  $4-R-C_6H_4-X-CH_3^{\bullet+}$  where X is S, Se or Te.[14] In these species, the charge seems to be localized to the heteroatom which is reflected by the almost negligible effects of 4-substitution on the one-electron reduction potential (figure 2). The one-electron reduction potentials of these radical cations is governed by the ionization potential of the heteroatom rather than by the substituent effects as described by the substituent constants.

An interesting observation here is that for strongly electron donating substituents like  $-N(CH_3)_2$ , the one-electron reduction potential drops dramatically. This can be interpreted as a change in the character of the



radical cation where the charge becomes delocalized on the benzene ring. Electrochemical studies reveal the same trend for these compounds.[19]

#### 4.2. Gas-Phase

The gas-phase ionization potentials have been measured for a large number of substituted benzenes. A comprehensive and continuously updated review can be found in ref. [37].

In table 2, the ionization potentials of a number of monosubstituted benzenes are given. As can be seen in figure 3, the ionization potential of monosubstituted benzenes also depends linearly on the Brown substituent constant. The linear correlation is given by equation (12).

$$IP = (9.10 \pm 0.05) + (0.97 \pm 0.06)\sigma_p^+ \quad (R^2 = 0.95) \quad (12)$$

As for benzene radical cations in solution, substituents containing S and Se deviate from the general trend. Interestingly, also the halogenated benzenes (except  $C_6H_5F$ ) follow the same trend as the S- and Se-substituted benzenes, i.e., the ionization potential of the substituent halogen atom rather than the substituent effect as described by the substituent constant governs the ionization potential.

If we treat the substituent effects on the ionization potential of 1,4-substituted benzenes in the same way as the one-electron reduction potentials in aqueous solution we obtain equation (13) (based on data from ref. [37]).

TABLE 2  
Ionization potentials of monosubstituted benzenes.

Substituted Benzene	IP (eV)	Substituted Benzene	IP (eV)
$C_6H_6$	9.24 [38]	$C_6H_5I$	8.79 [46]
$C_6H_5OH$	8.51 [39]	$C_6H_5SCH_3$	7.93 [47]
$C_6H_5NH_2$	7.74 [40]	$C_6H_5SeCH_3$	7.4 [48]
$C_6H_5CH_3$	8.83 [41]	$C_6H_5SH$	8.3 [49]
$C_6H_5OCH_3$	8.25 [42]	$C_6H_5SeH$	7.7 [48]
$C_6H_5CF_3$	9.7 [43]	$C_6H_5N(CH_3)_2$	7.15 [47]
$C_6H_5COH$	9.35 [44]	$C_6H_5NH(CH_3)$	7.38 [50]
$C_6H_5NO_2$	9.67 [44]	$C_6H_5OCH_2CH_3$	8.6 [51]
$C_6H_5CN$	9.73 [45]	$C_6H_5CH_2CH_3$	8.77 [15]
$C_6H_5F$	9.20 [46]	$C_6H_5CH(CH_3)_2$	8.72 [52]
$C_6H_5Cl$	9.08 [46]	$C_6H_5C(CH_3)_3$	8.69 [53]
$C_6H_5Br$	9.00 [46]	$C_6H_5C(O)CH_3$	9.28 [54]

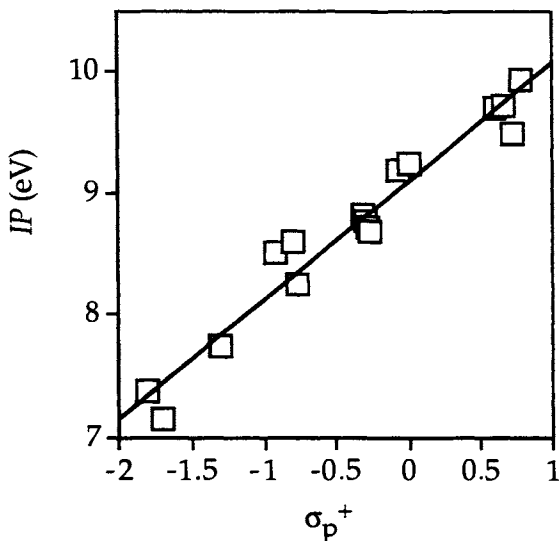


Figure 3. Ionization potentials of monosubstituted benzenes plotted against the substituent  $\sigma_p^+$  values.

$$IP = 9.1 + 1.0(\sigma_{p1}^+ + \sigma_{p4}^+) + 0.2\sigma_{p1}^+\sigma_{p4}^+ \quad (13)$$

If we compare equation (12) and (13) to equation (7) and (10), we see that the gas-phase ionization potential is more sensitive to substitution than the one-electron reduction potential in aqueous solution. This can be attributed to solvation effects, i.e., that the difference in solvation free energy between the neutral molecule and the corresponding radical cation depends on the nature of the substituted benzene. Furthermore, the effect of 1,4-disubstitution is closer to additivity in the gas-phase than in solution. This is reflected by the smaller cross-interaction constant in equation (13) compared to equation (10), i.e., 0.2 and 0.4, respectively.

#### 4.3. Solvent Effects

To understand how solvation affects the redox properties of radical cations, it is convenient to take a closer look at equation (3). The solvation term,  $\Delta\Delta G_{solv}^\circ$ , determines the one-electron reduction potential of a given radical cation in a given solvent. The solvation term will mainly depend on the solvation of the radical cation since the solvation free energy of the corresponding neutral molecule is comparatively small. It has previously been suggested that the higher the gas-phase ionization potential, the more localized is the charge on

the radical cation which, in turn, leads to more exergonic solvation of the cation.[55] This was confirmed in a recent electrochemical study where it was also found that the variation in solvation free energy for a given radical cation between different solvents increases for strongly solvated species.[22] The solvent effects on the one-electron reduction potential of a given radical cation can be described by a reduced Kamlet-Taft expression:

$$E^\circ = A + s\pi^* + h\delta_H \quad (14)$$

where  $A$ ,  $s$  and  $h$  are solvent-independent coefficients depending on the radical cation and  $\pi^*$  and  $\delta_H$  are the solvent dipolarity/polarizability and the Hildebrand solubility parameter, respectively. The latter parameter is a measure of the solvent-solvent interactions that are interrupted when a cavity is created for the solute.[56] Both  $s$  and  $h$  increase with increasing ionization potential of the molecule.[22] For rough estimates, the magnitude of the solvent effects can simply be described as  $\frac{\Delta E^\circ}{\Delta \pi^*}$ . In table 3, the magnitude of the solvent effects for some different radical cations are given along with the gas-phase ionization potential of the corresponding molecules. In figure 4, the magnitude of the solvent effects are plotted against the gas-phase ionization potential. The linear trend is given by equation (15).

$$\frac{\Delta E^\circ}{\Delta \pi^*} = 2.8(\pm 0.6) - 0.46(\pm 0.08)IP \quad (R^2 = 0.82) \quad (15)$$

TABLE 3

Solvent effects on the one-electron reduction potential of some radical cations.[22]

Radical cation	$IP$	$\frac{\Delta E^\circ}{\Delta \pi^*}$
$\text{CH}_3\text{OC}_6\text{H}_5^{*\cdot}$	8.2	-1.12
$1,2\text{-(CH}_3\text{O)}_2\text{C}_6\text{H}_4^{*\cdot}$	7.8	-0.74
$1,4\text{-(CH}_3\text{O)}_2\text{C}_6\text{H}_4^{*\cdot}$	7.56	-0.82
$1,2,4\text{-(CH}_3\text{O)}_3\text{C}_6\text{H}_3^{*\cdot}$	7.5	-0.68
DABCO $^{*\cdot}$	7.32	-0.38
TMPD $^{*\cdot}$	6.1	-0.10
$(\text{C}_6\text{H}_5)_2\text{NH}^{*\cdot}$	7.19	-0.64
$\text{C}_6\text{H}_5\text{NHCH}_3^{*\cdot}$	7.32	-0.45
$\text{C}_6\text{H}_5\text{NH}_2^{*\cdot}$	7.72	-0.76

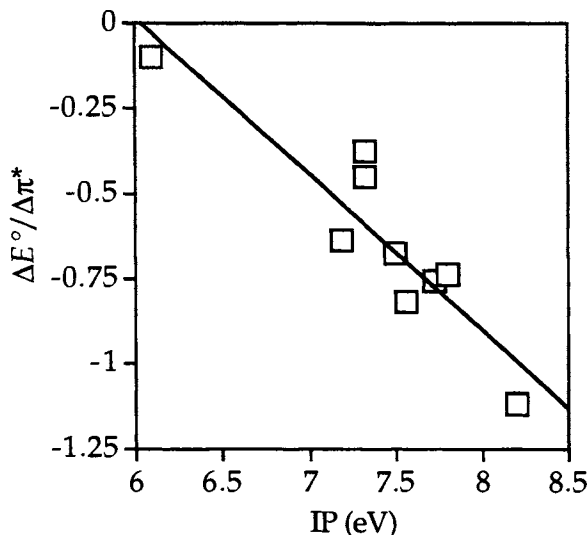


Figure 4. The magnitude of the solvent effects on the one-electron reduction potentials of radical cations plotted against the gas-phase ionization potentials of the corresponding neutral molecules.

As for the substituent effects on the one-electron reduction potentials of substituted benzenes, the magnitude of the solvent effects increase linearly with the gas-phase ionization potential of the corresponding molecule. In conclusion, the more stable the radical cation is (i.e., the more delocalized the charge is), the less sensitive it is to its environment.

## 5. ACIDITY PROPERTIES

### 5.1. Aqueous Solution

The  $pK_a$  of monosubstituted benzene radical cations vary from 7 for  $C_6H_5NH_2^{+\cdot}$  to -2 for  $C_6H_5OH^{+\cdot}$ .  $C_6H_5CH_3^{+\cdot}$  is even more acidic but the  $pK_a$  has not been determined experimentally. In table 4, the  $pK_a$ s of a number of substituted phenol- and aniline radical cations are given. The  $pK_a$ s of aniline radical cations have been determined by pulse radiolysis as previously described [12,13,57,58] and the  $pK_a$ s of phenol radical cations have been measured by ESR in mixtures of sulphuric acid and water. [59,60]

As for the one-electron reduction potentials, the  $pK_a$ s of substituted aniline radical cations seem to be linearly dependent on the Brown substituent constant. In figure 5, the  $pK_a$ s of 4-substituted aniline radical

cations are plotted against  $\sigma_p^+$ . The linear dependence can be described by equation (16).

$$pK_a(4-R-C_6H_4NH_2^{*+}) = (7.1 \pm 0.1) - (3.8 \pm 0.2)\sigma_p^+ \quad (R^2 = 0.98) \quad (16)$$

This equation can also be extended to hold for multisubstituted aniline radical cations.[13]

Judging from the data on phenol radical cation acidity, the  $pK_a$  of the phenol radical cation is relatively insensitive to substitution. The reason for this is that the  $pK_a$  is largely governed by the difference in solvation between the phenol radical cation and the phenoxyl radical. In aqueous solution, the phenol radical cation is strongly solvated since most of the positive charge is localized to the phenolic hydrogen which can coordinate water in a way analogous to the strong solvation of small metal ions in water. It should be noted that the phenol radical cation is much more acidic in DMSO ( $pK_a = -8.1$ ).[61]

In principle, the  $pK_a$  of the toluene radical cation can be estimated from the one-electron reduction potential of the radical cation and the C-H bond dissociation enthalpy for toluene ( $368 \text{ kJ mol}^{-1}$ )[62] using equation (5). The resulting  $pK_a$  is ca -10, i.e., considerably more acidic than the phenol radical cation. Nicholas and Arnold have estimated the  $pK_a$  of the toluene radical cation to between -9 and -13 in acetonitrile which is well in line with the estimate given here.[32] Since the C-H bond dissociation enthalpies of substituted toluenes seem to be almost invariant with substituent,[63-66] the substituent effect on the  $pK_a$  of

TABLE 4

$pK_a$  Values of Some Substituted Benzene Radical Cations in Aqueous Solution.

Phenols	$pK_a$	Anilines	$pK_a$
H	-2.0[59]	4-(CH <sub>3</sub> ) <sub>3</sub> C	8.2±0.2[12]
2-CH <sub>3</sub>	-1.8[59]	4-CH <sub>3</sub> CO	6.1±0.2[12]
3-CH <sub>3</sub>	-1.9[59]	4-I	7.1±0.2[12]
4-CH <sub>3</sub>	-1.6[59]	4-CF <sub>3</sub>	4.8±0.2[12]
4-NO <sub>2</sub>	-1.79[60]	4-CN	4±0.5[12]
4-COCH <sub>3</sub>	-1.86[60]	2-CF <sub>3</sub>	4.5±0.3[13]
4-F	-1.59[60]	3-CF <sub>3</sub>	5.5±0.3[13]
4-CF <sub>3</sub>	-1.46[60]	2-CH <sub>3</sub>	7.9±0.2[13]
4-Cl	-1.30[60]	2,4-(CH <sub>3</sub> ) <sub>2</sub>	8.0±0.2[13]
Anilines		3,4-(CH <sub>3</sub> ) <sub>2</sub>	8.6±0.2[13]
H	7.05[57]	3,5-(CH <sub>3</sub> ) <sub>2</sub>	8.1±0.2[13]
4-SO <sub>3</sub> <sup>-</sup>	5.8±0.2[58]	2-CH <sub>3</sub> O	8.4±0.2[13]
4-NH <sub>2</sub>	12±0.5[12]	2,4-(CH <sub>3</sub> O) <sub>2</sub>	10.8±0.2[13]
4-CH <sub>3</sub> O	9.6±0.2[12]	3,4-(CH <sub>3</sub> O) <sub>2</sub>	10.3±0.2[13]
4-CH <sub>3</sub>	8.5±0.2[12]	3,5-(CH <sub>3</sub> O) <sub>2</sub>	8.1±0.2[13]

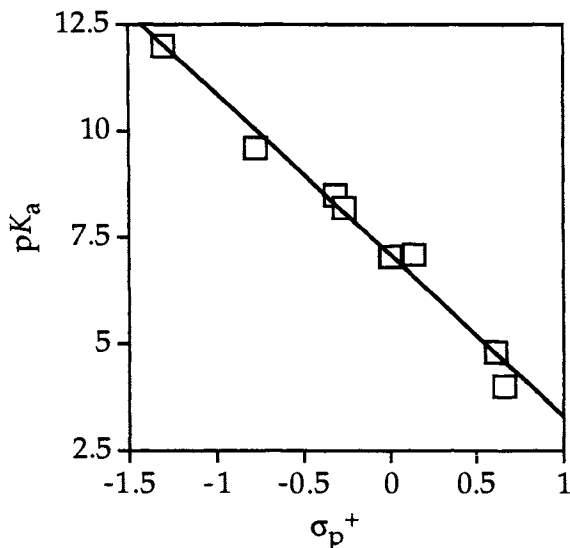


Figure 5.  $pK_a$ s of 4-substituted aniline radical cations plotted against the Brown substituent constant,  $\sigma_p^+$ .

toluene radical cations can be estimated from the substituent effect on the one-electron reduction potential of toluene radical cations. In view of this, we obtain the following approximate equation for 4-substituted toluene radical cations.

$$pK_a(4-R-C_6H_4CH_3^{\bullet+}) = -10 - 11\sigma_p^+ \quad (17)$$

The strong substituent effect on the acidity of toluene radical cations is also reflected by the effect of substitution on the rate of deprotonation from the radical cations.[8]

The  $pK_a$  of the unsubstituted benzene radical cation itself can also be estimated from the estimated one-electron reduction potential, 2.2 V vs. NHE, and the C-H bond dissociation enthalpy in benzene, 465.3 kJ mol<sup>-1</sup>, using equation (5).[67] The resulting  $pK_a$  is ca. 3. In practice, however, the benzene radical cation will not deprotonate in aqueous solution to form a phenyl radical since hydrolysis of the radical cation is extremely rapid.

## 5.2 Gas-Phase

The gas-phase proton affinity ( $\Delta H$ ) and the gas basicity ( $\Delta G$ ) are available for the aniliny-, phenyl-, benzyl- and phenoxy radicals. These values are displayed in table 5.

TABLE 5

Proton affinity and gas basicity of some neutral aromatic radicals.[68]

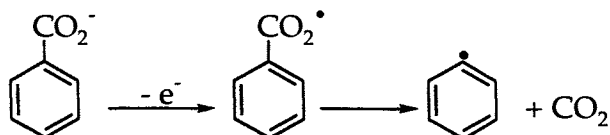
Radical	Proton Affinity kJ mol <sup>-1</sup>	Gas Basicity kJ mol <sup>-1</sup>
C <sub>6</sub> H <sub>5</sub> NH <sup>•</sup>	948.9	917.4
C <sub>6</sub> H <sub>5</sub> <sup>•</sup>	884	851.5
C <sub>6</sub> H <sub>5</sub> CH <sub>2</sub> <sup>•</sup>	857.7	827
C <sub>6</sub> H <sub>5</sub> O <sup>•</sup>	831.4	800.7

Clearly, there is no direct correlation between the gas-phase acidity and the pK<sub>a</sub>s in aqueous solution. This is mainly due to differences in solvation, especially for radical cations which can form strong hydrogen bonds to the solvent. Judging from the gas-phase properties, the phenol radical cation should be more acidic than the other three types of radical cations. The fact that it is much less acidic than the toluene radical cation can be accounted for by the stabilization of the phenol radical cation due to the strong solvation.

## 6. REACTIVE SIDE-CHAINS

For a number of different substituted benzenes, the substituents are involved themselves in the redox chemistry. Among these substituent-active compounds, we find phenolic substances, aromatic amines, chalcogenide substituted benzenes, benzylic substances, benzoic acids, thiobenzoic acids and benzyl alcohols. As has already been discussed, phenol radical cations, aniline radical cations and toluene radical cations are more or less acidic and can deprotonate to form the corresponding neutral radical. Chalcogenide substituted benzenes (S, Se and Te) are usually characterized by the fact that their redox properties are determined by the chalcogenides rather than by the substituent pattern.

One-electron oxidation of benzoic and thiobenzoic acids usually results in the formation of neutral radicals rather than CO<sub>2</sub><sup>-</sup> or COS<sup>-</sup> substituted benzene radical cations.[69-72] For benzoic acids with strongly electron-donating substituents, the character of the radical becomes more zwitterionic.[69,73]



(18)

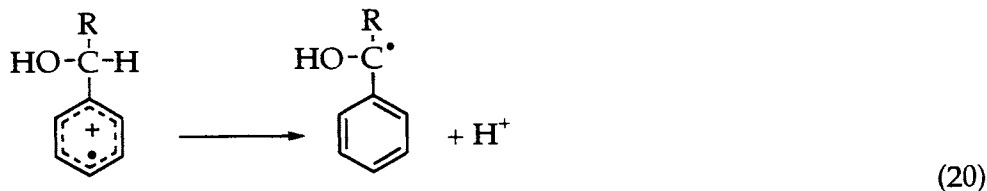
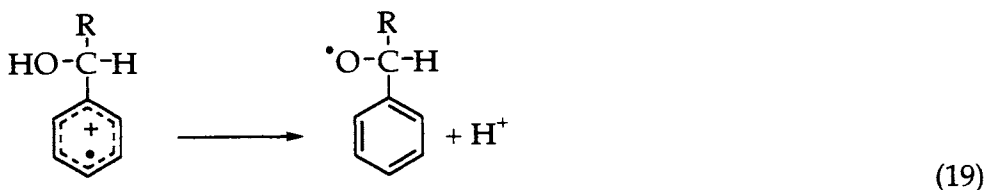
TABLE 6

One-electron reduction potentials of benzoylthiyl radicals

Radical	$E^\circ$ (V vs. NHE)
4-CH <sub>3</sub> C <sub>6</sub> H <sub>4</sub> COS <sup>•</sup>	1.19[72]
4-CH <sub>3</sub> OC <sub>6</sub> H <sub>4</sub> COS <sup>•</sup>	1.17[72]
C <sub>6</sub> H <sub>5</sub> COS <sup>•</sup>	1.21[71]
4-CF <sub>3</sub> C <sub>6</sub> H <sub>4</sub> COS <sup>•</sup>	1.28[72]
4-CNC <sub>6</sub> H <sub>4</sub> COS <sup>•</sup>	1.23[72]

These neutral radicals rapidly expel CO<sub>2</sub> and COS. The expulsion of CO<sub>2</sub> is faster than the expulsion of COS and for this reason, the one-electron reduction potentials of oxidized benzoic acids are practically impossible to measure while the potentials of a few oxidized thiobenzoic acids have been measured by pulse radiolysis. These values are given in table 6.

As for other substituted benzenes containing chalcogenides, the one-electron reduction potentials change very little with the substituent. One-electron oxidized benzyl alcohols, which are of vital importance for the understanding of lignin chemistry, display some very interesting properties since they can deprotonate to form two different types of radicals.[74]



At pH ≤ 5 the radical cation undergoes α-C-H deprotonation and at pH 10 the radical cation undergoes O-H deprotonation.[75] The oxyl radical thus formed is suggested to undergo a formal 1,2 hydrogen atom shift to give the thermodynamically more stable C-centered radical or undergo β-cleavage to yield benzaldehyde. The side-chain fragmentation of arylalkanol radical cations has been studied quite extensively.[76,77] Judging from the difference in homolytic bond dissociation enthalpy



between an O-H bond and a benzylic C-H bond, the  $pK_a$  for O-H deprotonation from the radical cation should be more than 10 units higher than the  $pK_a$  for  $\alpha$ -C-H deprotonation. Consequently, O-H deprotonation is kinetically favored at high pH. The formation of the oxyl radical was first postulated since no direct evidence for its formation was available. However, by using 4-methoxycumyl alcohol (4- $\text{CH}_3\text{OC}_6\text{H}_4\text{C}(\text{CH}_3)_2\text{OH}$ ), Baciocchi et al. were able to study the formation of the 4-methoxycumyloxyl radical formed upon O-H deprotonation of the radical cation.[75] The oxyl radical was identified spectroscopically by its relatively unique UV-vis spectra. It has been suggested that deprotonation from O-H initially results in the formation of a zwitterion followed by intramolecular electron transfer to give the neutral oxyl radical. However, the existence of such an intermediate or transition state is highly questionable since the increased O-H acidity of the radical cation compared to the neutral molecule is in itself already the result of a change in the electron configuration. It is more likely that the O-H deprotonated species has zwitterionic character which is also indicated by the spectral red-shift on going from nonaqueous to aqueous solvents.[75]

## 7. CONCLUDING REMARKS

The redox properties of substituted benzene radical cations in aqueous solution appear to stand on a fairly solid ground. The structure-activity relationships derived from experimental data provide a useful tool for prediction of unknown one-electron reduction potentials and also give a systematic picture of the effects of ring substituents on the one-electron reduction potentials of benzene radical cations. Further experimental studies on the one-electron reduction potentials of simple substituted benzene radical cations are not expected to give any new significant insights. By using the linear solvation energy relationships derived for radical cations, the one-electron reduction potential can be estimated in virtually any solvent where determination of the thermodynamical potential would be impossible for practical reasons. The future challenge in this field is to study the thermochemistry of more complex benzene radical cations containing reactive side-chains and multifunctional groups, e.g., arylalkanol radical cations and aromatic hydroxylamines. The thermochemistry of these species is not straightforward to study experimentally due to the variety of possible side reactions.

**Acknowledgment.** The author thanks the Swedish Natural Science Research Council for financial support.

## REFERENCES

- 1 M. Schmittel and A. Burghardt, *Angew. Chem. Int. Ed. Engl.* 1997, 36, 2550
- 2 O. Hammerich and V. D. Parker, *Adv. Phys. Org. Chem.* 1984, 20, 55 and references therein
- 3 R. E. Huie, C. L. Clifton and P. Neta, *Radiat. Phys. Chem.* 1991, 38, 477
- 4 F. Witte, E. Urbanik and C. Zetzsch, *J. Phys. Chem.* 1986, 90, 3251
- 5 M. K. Eberhardt, *J. Org. Chem.*, 1977, 42, 832
- 6 C. Walling, D. M. Camaioni and S. S. Kim, *J. Am. Chem. Soc.*, 1978, 100, 4814
- 7 M. Jonsson, *One-Electron Oxidized Substituted Benzenes - Thermochemistry and Kinetics*, Ph.D. Thesis, ISSN 0349-6465, Stockholm, 1995
- 8 K. Sehested and J. Holcman, *J. Phys. Chem.* 1978, 82, 651
- 9 M. Jonsson, J. Lind, T. Reitberger, T. E. Eriksen and G. Merényi, *J. Phys. Chem.* 1993, 97, 11278
- 10 M. S. Workentin, L. J. Johnston, D. D. M. Wayner and V. D. Parker, *J. Am. Chem. Soc.* 1994, 116, 8279 and references therein
- 11 S. Steenken, *J. Chem. Soc., Faraday Trans. 1* 1987, 83, 113 and references therein
- 12 M. Jonsson, J. Lind, T. E. Eriksen and G. Merényi, *J. Am. Chem. Soc.* 1994, 116, 1423
- 13 M. Jonsson, J. Lind, G. Merényi and T. E. Eriksen, *J. Chem. Soc. Perkin Trans. 2* 1995, 61
- 14 M. Jonsson, J. Lind, G. Merényi and T. E. Eriksen, *J. Chem. Soc. Perkin Trans. 2* 1995, 67
- 15 J. O. Howell, J. M. Goncalves, C. Amatore, L. Klasinc, R. M. Wightman and J. K. Kochi, *J. Am. Chem. Soc.* 1984, 106, 3968
- 16 Kochi, J. K. *Acc. Chem. Res.* 1992, 25, 39 and references therein
- 17 H. Mohan and J. P. Mittal, *J. Phys. Chem.* 1995, 99, 6519
- 18 H. Mohan and J. P. Mittal, *J. Phys. Chem. A*, 1999, 103, 379
- 19 L. Engman, J. Persson, C. M. Andersson and M. Berglund, *J. Chem. Soc. Perkin Trans. 2*, 1992, 1309
- 20 M. Jonsson, *Recent Res. Devel. in Physical Chem.*, 1997, 1, 475
- 21 M. Jonsson, D. D. M. Wayner and J. Luszytk, *J. Phys. Chem.* 1996, 100, 17539
- 22 M. Jonsson, A. Houmam, G. Jocsy and D. D. M. Wayner, *J. Chem. Soc. Perkin Trans. 2*, 1999, 425
- 23 S. Trasatti, *Pure Appl. Chem.* 1986, 58, 955
- 24 R. G. Pearson, *J. Am. Chem. Soc.* 1986, 108, 6109
- 25 L. Ebersson, *Acta Chem. Scand.* 1963, 17, 2004
- 26 For a more thorough description of pulse radiolysis see *Pulse Radiolysis*, Tabata, Y. Ed., CRC Press, Boston, 1991
- 27 J. W. T. Spinks and R. J. Woods, *Introduction to Radiation Chemistry*, 3rd ed., John Wiley & Sons, New York, 1990
- 28 P. Wardman, *J. Phys. Chem. Ref. Data* 1989, 18, 1637

- 29 See for example: R. Greef, R. Peat, L. M. Peter, D. Pletcher and J. Robinson, *Instrumental Methods in Electrochemistry*; Kemp, T. J., Ed.; Ellis Horwood Limited: Chichester, U.K., 1985
- 30 C. Hansch, A. Leo and R. W. Taft, *Chem. Rev.* 1991, 91, 165
- 31 C. Hansch and H. Gao, *Chem. Rev.* 1997, 97, 2995
- 32 A. M. P. Nicholas and D. R. Arnold, *Can. J. Chem.* 1982, 60, 2165
- 33 R. E. Huie and P. Neta, *J. Phys. Chem.* 1988, 92, 134
- 34 Calculated from data given in J. Lind, X. Shen, T. E. Eriksen and G. Merényi, *J. Am. Chem. Soc.* 1990, 112, 479
- 35 J. -E. Dubois, M. -F. Ruasse and A. Argile, *J. Am. Chem. Soc.* 1984, 106, 4840
- 36 M. Jonsson, J. Lind, T. E. Eriksen and G. Merényi, *J. Chem. Soc. Perkin Trans. 2* 1993, 1567
- 37 Data taken from NIST Standard Reference Database Number 69 - November 1998 Release
- 38 G. I. Nemth, H. L. Selze and E. W. Schlag, *Chem. Phys. Lett.* 1993, 215, 151
- 39 R. J. Lipert and S. D. Colson, *J. Chem. Phys.* 1990, 92, 3240
- 40 J. T. Meek, E. Sekreta, W. Wilson, K. S. Viswanathan and J. P. Reilly, *J. Chem. Phys.* 1985, 82, 1741
- 41 K. -T. Lu, G. C. Eiden and J. C. Weisshaar, *J. Phys. Chem.* 1992, 96, 9742
- 42 D. A. Ponomarev, O. V. Arapov, Y. L. Sergeev and A. B. Chistyakov, *Izv. Vyssh. Uchebn. Zaved., Khim. Khim. Tekhnol.* 1986, 29, 107
- 43 J. B. Peel and E. I. von Nagy-Felsobuki, *J. Mol. Struct.* 1987, 159, 195
- 44 L. Klasinc, B. Kovac and H. Gusten, *Pure Appl. Chem.* 1983, 55, 289
- 45 M. Araki and S. -I. Sato, *J. Phys. Chem.* 1996, 100, 10542
- 46 S. Fujisawa, K. Ohno, S. Masuda and Y. Harada, *J. Am. Chem. Soc.* 1986, 108, 6505
- 47 J. M. Behan, R. A. W. Johnstone and T. W. Bentley, *Org. Mass Spectrom.* 1976, 11, 207
- 48 A. D. Baker, G. H. Armen and Y. Guang-di, *J. Org. Chem.* 1981, 46, 4127
- 49 J. D. Faulk, R. C. Dunbar and C. Lifshitz, *J. Am. Chem. Soc.*, 1990, 112, 7893
- 50 M. Mautner (Meot-Ner), S. F. Nelsen, M. R. Willi and T. B. Frigo, *J. Am. Chem. Soc.*, 1984, 106, 7384
- 51 D. H. Williams, R. G. Cooks and I. Howe, *J. Am. Chem. Soc.*, 1968, 90, 6759
- 52 R. G. McLoughlin, J. D. Morrison and J. C. Traeger, *Org. Mass Spectrom.* 1979, 14, 104
- 53 I. N. Domnin, A. M. Lakshin, A. D. Misharev, V. M. Orlov and V. V. Takhistov, *J. Org. Chem. USSR*, 1985, 21, 1149
- 54 R. G. McLoughlin and J. C. Traeger, *Org. Mass Spectrom.*, 1979, 14, 434
- 55 D. D. M. Wayner, B. A. Sim and J. J. Dannenberg, *J. Org. Chem.* 1991, 56, 4853
- 56 M. J. Kamlet, J.-L. M. Abboud, M. H. Abraham and R. W. Taft, *J. Org. Chem.* 1983, 48, 2877
- 57 L. Qin, G. N. R. Tripathi and R. H. Schuler, *Z. Naturforsch.* 1985, 40a, 1026
- 58 D. Behar and B. Behar, *J. Phys. Chem.* 1991, 95, 7552
- 59 W. T. Dixon and D. Murphy, *J. Chem. Soc. Faraday Trans. 2* 1976, 72, 1221
- 60 D. M. Holton and D. Murphy, *J. Chem. Soc. Faraday Trans. 2*, 1979, 75, 1637
- 61 F. G. Bordwell and J. -P. Cheng, *J. Am. Chem. Soc.*, 1989, 111, 1792
- 62 W. A. Pryor, D. F. Church, F. Y. Tang and R. H. Tang, in *Frontiers of Free Radical Chemistry*, Ed. Pryor, W. A., Academic, New York, 1980, p 355

- 63 X. -M. Zhang, F. G. Bordwell, J. E. Bares, J. -P. Cheng and B. C. Petrie, *J. Org. Chem.* 1993, 58, 3051
- 64 M. Jonsson, J. Lind, G. Merényi and T. E. Eriksen, *J. Chem. Soc. Perkin Trans. 2*, 1994, 2149
- 65 Y. -D. Wu, C. -L. Wong, K. W. K. Chan, G. -Z. Ji and X. -K. Jiang, *J. Org. Chem.* 1996, 61, 746
- 66 T. Fox and P. A. Kollman, *J. Phys. Chem.*, 1996, 100, 2950
- 67 J. Berkowitz, G. B. Ellison and D. Gutman, *J. Phys. Chem.*, 1994, 98, 2744
- 68 E. P. Hunter and S. G. Lias, *J. Phys. Chem. Ref. Data* (to be published), 1998
- 69 H. Zemel and R. W. Fessenden, *J. Phys. Chem.*, 1978, 82, 2670
- 70 J. Chateaufneuf, J. Lusztyk and K. U. Ingold, *J. Am. Chem. Soc.*, 1988, 110, 2877 and 2886
- 71 R. Zhao, J. Lind, G. Merényi and T. E. Eriksen, *J. Am. Chem. Soc.*, 1998, 120, 2811
- 72 R. Zhao, J. Lind, G. Merényi, M. Jonsson and T. E. Eriksen, to be published
- 73 G. N. R. Tripathi and Y. Su, *J. Am. Chem. Soc.*, 1996, 118, 2235
- 74 E. Baciocchi, M. Bietti and S. Steenken, *J. Am. Chem. Soc.* 1997, 119, 4078
- 75 E. Baciocchi, M. Bietti, O. Lanzalunga and S. Steenken, *J. Am. Chem. Soc.*, 1998, 120, 11516
- 76 E. Baciocchi, *Acta Chem. Scand.*, 1990, 44, 645
- 77 E. Baciocchi, M. Bietti, L. Putignani and S. Steenken, 1996, 118, 5952

## **Heteroatom-Centered Free Radicals Some Selected Contributions by Radiation Chemistry**

**Klaus-Dieter Asmus**

Radiation Laboratory and Department of Chemistry & Biochemistry,  
University of Notre Dame, Notre Dame, IN 46556, U.S.A.

### **1 INTRODUCTION**

One of the topics to which Radiation Chemistry has made many significant and highly visible contributions is that of “free radical chemistry”. An interesting group within organic radicals is that where the spin is located on a heteroatom. Such radicals often exhibit quite different properties as compared to C-centered radicals owing to the influence of lone electron pairs on their overall electronic structure. Research on these transients flourished particularly since the advent of time-resolved techniques such as pulse radiolysis and flash photolysis which allowed their direct detection on real time. Because of their electronic structure hetero-centered radicals most often exhibit intense and thus easily detectable optical absorptions in the UV, visible and near-IR.

This article will and cannot make an attempt to review all the fine work which has been conducted over the years on heteroatom-centered radicals in radiation laboratories, let alone in free radical chemistry, in general. There are excellent and comprehensive reviews and books available, e.g. in a series on heteroatom-centered radicals edited by Alfassi<sup>1-3</sup> or a NATO-Science edition on sulfur-centered species.<sup>4</sup> This essay will rather present and discuss some specially selected examples from solution (mainly aqueous) studies, and highlight some of the general achievements and basic concepts emerging therefrom. Two important groups of radicals belonging to the heteroatom-centered category will deliberately not or only briefly be mentioned, namely, those derived from purines and pyrimidines, and also the entire family of oxygen-centered radicals. Both are covered in other articles in this book.

Before focusing in on the examples a brief word may be appropriate why radiation chemical techniques and which ones, in particular, have turned out to be so useful and successful for radical research, in general. Most importantly,

radical yields can be determined very accurately, allowing quantification of yield-dependent parameters such as extinction coefficients or absolute second order radical-radical termination rate constants. As far as particular detection techniques are concerned, the vast majority of studies rely on time-resolved optical pulse radiolysis covering time windows from the pico- to millisecond range. Such investigations enabled the identification and chemical characterization of a large number of transients. Reasonably strong optical absorptions ( $\epsilon > 10^3 \text{ M}^{-1} \text{ cm}^{-1}$ ), furthermore, provide the possibility to perform resonance Raman spectroscopy with radicals.<sup>5</sup> If applied in a time-resolving manner, information can be extracted from such experiments which pertains primarily to vibrational modes, electronic transitions and molecular structure, but also allows conclusions on many other parameters such as electron density distributions within radicals, or protonation sites and pK values in transients with acid/base properties. Among other time-resolved detection techniques developed over the years, also conductivity deserves particular mention.<sup>6-8</sup> It enables quantification of processes involving changes of overall conductance and is, therefore, a very suitable approach whenever radical ions are under investigation, particularly when they don't show any absorption. Another significant benefit radiation chemistry has to offer for the study of radicals derived from heteroatom-containing compounds is the ease by which these can often be generated through one-electron redox processes owing to the presence of the heteroatom lone electron pairs.

The first topic to be dealt with in this article dates back to the early days of pulse radiolysis and is concerned with intermediates generated from organic nitro and nitroso compounds in some elementary redox processes. This will be followed by a presentation of some most recent results on aminyl radicals derived from amino acids, exemplifying the diversity of possible reactions of a seemingly simple type of radicals. The third example on aniline and anilino radicals aims to demonstrate the potential of time-resolved resonance Raman spectroscopy. A common message of all these studies on N-centered radicals hints at the importance of acid/base properties of radicals. The aniline system, in particular, also draws attention to spin and charge distribution, and possible implications to the chemistry of radical species.

The major part of the second section is devoted to thiyl radicals. This species has long been viewed as relatively uninteresting with respect to its chemistry since its only fate was thought to be dimerization to the respective disulfide. Like the aminyl radicals, thiyl radicals can engage in a large variety of reactions. Radiation chemical studies have identified and quantified reactions in which thiyl radicals act as hydrogen abstraction agent, showed their involvement in reversible addition and displacement reactions and, last but not

least, characterized thiyl radicals as reasonably good oxidants. Complementary information on perthiyl and sulfuranyl radicals closes this section which points, in particular, to the significance of equilibria and consequences thereof for the entire redox chemistry of thiol and disulfide containing systems.

Sulfur- and other heteroatom-centered radical cations from organic compounds are the subject of the third section. The fact that such species could exhibit relatively long lifetimes of up to milliseconds was an initially somewhat surprising but most welcome property for their investigation. The present survey summarizes some of their optical and redox properties, and reveals parameters controlling their decay.

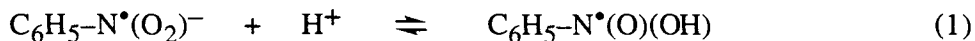
Emerging from the studies on sulfur-centered radical cations, derived especially from organic sulfides, a most interesting class of radicals caught the attention of the entire community interested in radical chemistry, namely, those with an odd number of electrons shared by two or more interacting heteroatoms. An important clue is that in, for example, the most frequently observed three- and five-electron bonds one of the electrons is antibonding in nature and thus reduces the bond order compared to the next lower even-electron bond. The final and largest section focuses exclusively on these fascinating kind of transients. It outlines the general concept of odd-electron bonds, shows how sensitively their optical absorptions reflect electronic and molecular structures, and surveys some important thermodynamic and reactivity parameters. Particularly the examples where two different heteroatoms are involved in such bonds reveal the broad potential as well as the limits of this concept which, in general terms, provides insight into the process of bond breakage and formation, and the transition between single and double bonds.

## **2 SOME SELECTED RADICALS AND RADICAL IONS FROM N-ORGANIC COMPOUNDS**

### **2.1 One-electron reduced organic nitro and nitroso compounds**

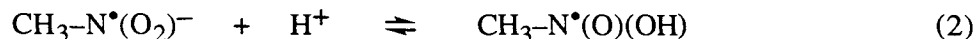
The question whether or not radical ions are formed upon irradiation of liquids and stabilized enough for detection or engagement in bimolecular chemical reactions has moved radiation chemists ever since the early days of this research field. This was particularly exciting with respect to low polarity solvents, but even for aqueous solutions conclusions had to rely mainly on indirect evidence. A real breakthrough came with the experimental discovery of the hydrated electron and other powerful one-electron reductants (e.g.,  $\alpha$ -hydroxyalkane radicals such as  $(\text{CH}_3)_2\text{C}^*\text{OH}$ ). Applying these new tools a large number of organic radical anions were detected and characterized with respect to their optical and chemical properties, particularly by pulse radiolysis.

Among the early examples were the reduction of organic nitro and nitroso compounds which yielded relatively long-lived nitrogen-centered radical anions. One of the questions raised in those days, especially by electrochemists, was whether the reduced nitro moiety existed exclusively in an anionic form or could establish an acid/base equilibrium as formulated in eq. 1 for the nitrobenzene case.



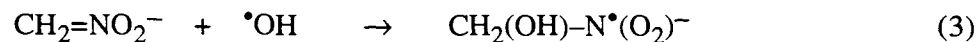
It was radiation chemistry which provided an unambiguous answer and established the  $\text{pK}_a = 3.2$  based on the different optical absorptions of the two conjugates.<sup>9</sup>

Substitution of the aromatic phenyl by the aliphatic methyl, incidentally, does not cause too much of a change with respect to the  $\text{pK}$ . It shifted by just about one order of magnitude to  $\text{pK}_a = 4.4$  for equilibrium 2.<sup>10</sup>



The influence of the aromatic  $\pi$ -system becomes much more visible in the spectral characteristics of the respective transients, particularly in their molar extinction coefficients. While the main UV bands of  $\text{C}_6\text{H}_5\text{-N}^*(\text{O}_2)^-$  and  $\text{C}_6\text{H}_5\text{-N}^*(\text{O})(\text{OH})$  exhibit  $\epsilon = 1.4 \times 10^4$  (at  $\lambda_{\text{max}}$  285 nm) and  $9.25 \times 10^3 \text{ M}^{-1} \text{ cm}^{-1}$  (275nm), respectively, the corresponding data for  $\text{CH}_3\text{-N}^*(\text{O}_2)^-$  and  $\text{CH}_3\text{-N}^*(\text{O})(\text{OH})$  are significantly lower, namely,  $\epsilon = 2.8 \times 10^3$  (270 nm) and  $2.0 \times 10^3 \text{ M}^{-1} \text{ cm}^{-1}$  (250nm).

Aliphatic nitro compounds are characterized by another interesting and mechanistically important property. Based on tautomeric and protolytic equilibria the stable form of nitromethane in basic solution is that of a double bonded *aci*-nitromethane anion,  $\text{CH}_2=\text{NO}_2^-$ , which becomes ready target for electrophilic radical additions. An example, studied by pulse radiolysis, is its reaction with hydroxyl radicals as formulated in eq. 3.<sup>11</sup>

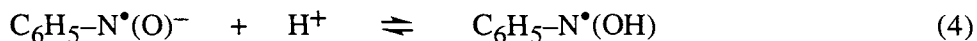


Incidentally, this process was investigated not only by means of optical detection ( $\epsilon = 1.9 \times 10^3$  at 280 nm) but also by time-resolved ESR ( $a_{\text{N}}$  24.6 G;  $a_{\text{H}}$  8.9 G),<sup>12</sup> serving as an instructive example for the value of complementary experimental approaches.

A similar study as in case of nitrobenzene was also conducted with nitrosobenzene.<sup>13</sup> It revealed an acid/base equilibrium of the one-electron



reduced radical form with, however, a dramatically different  $pK_a$  as compared to the reduced nitrobenzene, namely 11.7 for equilibrium 4.



The reaction of nitrosobenzene with  $\cdot\text{OH}$  radicals resulted in the conjugate radical pair  $\text{C}_6\text{H}_5\text{-N}^*(\text{O}_2)^- / \text{C}_6\text{H}_5\text{-N}^*(\text{O})(\text{OH})$  (depending on pH), clearly establishing the intermediate redox state of these radical transients between the stable nitro and nitroso compounds.

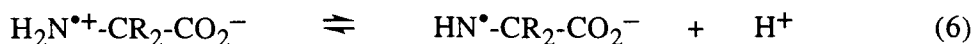
While the above mentioned reactions had caught the attention of radiation chemists in the sixties in order to contribute to some fundamental aspects in the redox and acid/base chemistry of nitro compounds, focus turned again on this class of chemicals in the late seventies and early eighties in connection with their potential as radiosensitisers and chemotherapeutics. Chemically, the parameter of interest in this context was the one-electron reduction potential of  $\text{RNO}_2 / \text{RN}^*(\text{O}_2)^-$  couples<sup>14</sup> which, in the majority of cases, afforded accurate determination of the radical concentrations. We shall not elaborate on further details and general considerations because that will be done in other chapters of this book. It should just be mentioned that the underlying radiation chemical studies were particularly concerned with nitrobenzenes, nitrofurans, 2-, 4- and 5-nitroimidazoles, nitroazaindoles, nitroacridines, and quite a number of other nitroaryl compounds.

## 2.2 Aminyl radicals from amino acids

As becomes apparent from the last remarks in the above section, radiation chemistry enjoys a very fruitful interaction with life sciences. One of the important classes of compounds with biological activity are amino acids. Since real life conditions include exposure to free radicals the associated chemistry becomes, consequently, of interest. Within the amino acid molecules, the  $\alpha$ -amino- $\alpha$ -carboxyl moiety is a preferred target of radical attack. Reaction with, for example,  $\cdot\text{OH}$  and other one-electron oxidants leads to appreciable yields of N-oxidation and, wherever possible, cleavage of a  $\text{C}_{\alpha}\text{-H}$  bond. These primary processes are the starting point of quite complex and, in part, competitive reaction schemes. Their detailed nature depends on the respective protonation state of the two functional groups, i.e., on the pH of their environment.<sup>15-19</sup>

Recent radiation chemical research has mainly focused on basic solutions in which the amino nitrogen carries a free electron pair which, upon oxidation, may suffer simple loss of an electron or convert via an addition/elimination process into the  $\text{H}_2\text{N}^{\bullet+}\text{-CR}_2\text{-CO}_2^-$  radical zwitterion ( $\text{R} = \text{H}$ , alkyl).<sup>18,19</sup> This species is prone for fast decarboxylation and rate constant

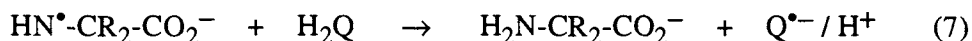
estimates of  $>10^8 \text{ s}^{-1}$ , possibly  $\approx 10^{11} - 10^{12} \text{ s}^{-1}$  have been forwarded for the expulsion of  $\text{CO}_2$  (eq. 5). This process, in principle, has to compete with deprotonation to yield the aminyl radical (forward reaction in eq. 6).



Although this is basically a simple scheme, several interesting aspects emerged and still a number of challenges remain. For example, while both  $\bullet\text{CH}_2\text{NH}_2$  and  $\text{HN}^{\bullet}\text{-CR}_2\text{-CO}_2^-$  have been identified (at least indirectly), their relative yield remains unchanged up to at least  $\text{pH} \approx 13$ , i.e., even  $\text{OH}^-$  bulk concentrations of 0.1 M are not sufficient to accelerate reaction 6 at the expense of reaction 5. It appears that the deprotonation of the radical zwitterion can successfully compete only at proton acceptor concentrations  $>1\text{M}$ . Such a situation is given, for example, in the initial cage of  $\{\text{H}_2\text{N}^{\bullet+}\text{-CR}_2\text{-CO}_2^- / \text{OH}^-\}$  or  $\{\text{H}_2\text{N}^{\bullet+}\text{-CR}_2\text{-CO}_2^- / 4\text{-CB}^{\bullet-}\}$  ion pairs as they are generated in the  $\bullet\text{OH}^-$ - or  $^3(4\text{-CB})$ -triplet-induced oxidation of  $\text{H}_2\text{N-CR}_2\text{-CO}_2^-$ , respectively.<sup>20,21</sup> Formation of the aminyl radical by H-atom abstraction should also be considered.

Decarboxylation (corresponding to eq. 5) occurs, incidentally, also quite readily from N-alkyl substituted zwitterionic radical cations.<sup>18</sup> An N-attached phenyl substituent, on the other hand, seems to slow down this process significantly.<sup>22</sup> This leaves interesting questions concerning the effect of electronic resonance and, possibly, molecular structure.

While the short lifetime of the  $\text{H}_2\text{N}^{\bullet+}\text{-CR}_2\text{-CO}_2^-$  zwitterion with respect to decarboxylation practically prevents it from any engagement in bimolecular redox processes, its deprotonated form  $\text{HN}^{\bullet}\text{-CR}_2\text{-CO}_2^-$ , on the other hand, is long-lived enough to effectively act as an oxidant, e.g., towards hydroquinone (eq.7). (Although stoichiometrically representing an H-atom transfer, this reaction is most likely based on an electron transfer).<sup>19,23</sup>



A representative rate constant is  $7.4 \times 10^7 \text{ M}^{-1} \text{ s}^{-1}$  for the reaction of the corresponding glycine radical  $\text{HN}^{\bullet}\text{-CH}_2\text{-CO}_2^-$  at pH 11. (At this pH the hydroquinone is partially deprotonated,  $\text{H}_2\text{Q} : \text{HQ}^- : \text{Q}^{2-} = 6 : 71 : 23$ , and the rate constant is, accordingly, a weighted one over all three forms).

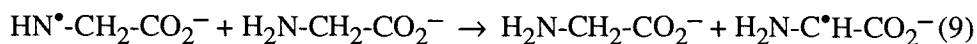
An open question is still the  $\text{pK}_a$  of  $\text{H}_2\text{N}^{\bullet+}\text{-CR}_2\text{-CO}_2^-$ . Estimates range from a negative value to about 3-4 with the latter probably being the more realistic target.<sup>19,24</sup> Unfortunately, direct titration is impossible due to the

short lifetime of the radical zwitterion. An interesting finding is that protonation of  $\text{HN}^\bullet\text{-CR}_2\text{-CO}_2^-$  can be achieved quite effectively, even in basic solution, by suitable proton donors,  $\text{BH}^+$ , (eq. 8).



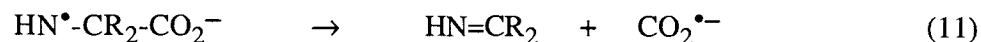
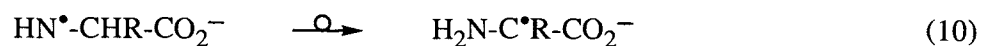
Experimental data have been evaluated for the reactions of the aminyl radicals from glycine ( $\text{R} = \text{H,H}$ ), alanine ( $\text{R} = \text{H,CH}_3$ ) and  $\alpha$ -methylalanine ( $\text{R} = \text{CH}_3,\text{CH}_3$ ) with  $\text{BH}^+ = \text{H}_2\text{PO}_4^-$ ,  $\text{HPO}_4^{2-}$  and the respective unoxidized zwitterions of the amino acids,  $\text{AA}^\pm$ . Rate constants (in the  $10^5 - 10^8 \text{ M}^{-1} \text{ s}^{-1}$  bracket) increase in the order of the three amino acids as listed, are naturally the highest for  $\text{H}_2\text{PO}_4^-$  as proton donor, and lower and almost equal for  $\text{HPO}_4^{2-}$  and  $\text{AA}^\pm$ .<sup>19,23</sup>

Aminyl radicals are also capable of abstracting H-atoms. This process is of particular interest if the original amino acids themselves are the target molecules since it may completely change the redox properties of the system. As formulated in eq. 9 for glycine, for example, the oxidizing  $\text{HN}^\bullet$ - radical is converted into a reducing  $\alpha$ -amino- $\alpha$ -carboxyl radical.



Rate constants are, however, relatively low ( $3.0 \times 10^4$  and  $1.7 \times 10^5 \text{ M}^{-1} \text{ s}^{-1}$  for the glycine and alanine system, respectively) and become of significance, therefore, only at high concentrations of the amino acid anions.<sup>19,23</sup> The higher bond dissociation energy of N-H ( $415 \text{ kJ mol}^{-1}$ ) as compared to that of  $\text{C}_\alpha\text{-H}$  ( $365 \text{ kJ mol}^{-1}$ ) can be forwarded as a major contributor to the driving force of this process.

In addition to these bimolecular reactions, two unimolecular processes further enlarge the picture, namely, a 1,2-hydrogen shift (eq. 10) and a  $\beta$ -scission (eq. 11). Both reactions find their analogy in alkoxy radical chemistry.<sup>25,26</sup>

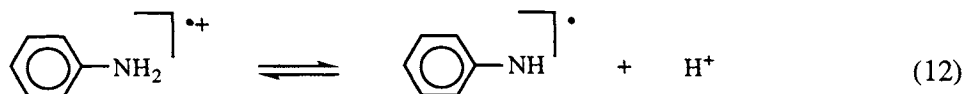


The shift reaction requires, of course, the presence of at least one hydrogen at  $\text{C}_\alpha$ . From the few available absolute data it appears that the shift occurs, however, considerably slower in the aminyl as compared to the oxy radical.<sup>19,27,28</sup> For comparison, rate constants estimates have been derived which are on the order of  $10^3$  and  $10^6 \text{ s}^{-1}$ , respectively.

$\beta$ -Scission has been proven unambiguously for the aminyl radicals from  $\alpha$ -methylalanine and alanine through a specific reaction of the scission product radical  $\text{CO}_2^{\bullet-}$  with 4-carboxybenzophenone. Rate constants for reaction 11 have been determined for  $\text{HN}^{\bullet}\text{-C}(\text{CH}_3)_2\text{-CO}_2^-$  ( $7.3 \times 10^4 \text{ s}^{-1}$ ) and  $\text{HN}^{\bullet}\text{-CH}(\text{CH}_3)\text{-CO}_2^-$  ( $2.3 \times 10^4 \text{ s}^{-1}$ ).<sup>23</sup> This result parallels findings with oxyl radicals that fragmentation is facilitated by branched molecular structures. In case of the aminyl radical from glycine,  $\text{HN}^{\bullet}\text{-CH}_2\text{-CO}_2^-$ , distinction between  $\beta$ -scission and H-shift has been difficult owing to low yields under feasible experimental conditions. Unambiguous assignment and deconvolution of an extrapolated first order rate constant of  $1.2 \times 10^3 \text{ s}^{-1}$  must await further investigations.

### 2.3 Aniline radical cations and anilino radicals

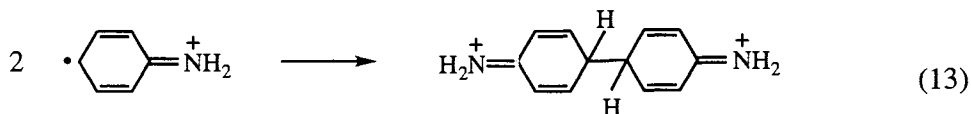
The following is an excellent example where a special technique, in this case time-resolved resonance Raman spectroscopy added significant information which simple optical absorption measurements could not provide. The system of interest is aniline and its radicals generated upon oxidation (e.g., by  $\text{N}_3^{\bullet}$ ). The latter are the radical cation and its deprotonated form existing in equilibrium 12 with a pK of 7.04.<sup>29</sup>



Both conjugates exhibit optical absorptions in the near UV, the radical cation having its strongest band at 430 nm ( $\epsilon \approx 4500 \text{ M}^{-1} \text{ cm}^{-1}$ ). The anilino radical also absorbs in this wavelength region although with about three to four times lower extinction coefficients. Complications with respect to unambiguous assignments arise in part from this overlap but also from strong absorptions of subsequently formed products. Resonance raman studies circumvent these problems as the vibrational spectra of the species involved are clearly distinguishable from each other and also sensitively respond to deuteration.<sup>29-32</sup>

One of the informative results obtained is the high C-N stretching mode frequency ( $1494 \text{ cm}^{-1}$ ) in the radical cation, quite in contrast to the much lower frequency of the same bond in  $^1\text{A}_1$  ground state aniline ( $1274 \text{ cm}^{-1}$ ). The C-N bond in the radical cation thus has assumed a strong double bond character which, by comparison with other systems such as *p*-phenylenediamine radical cations, exceeds the value of 1.5 in bond order. This finding implies the radical cation to be mainly C-centered rather than N-centered which is, in fact, corroborated by the observed major termination product of

the aniline radical cation benzidine (eq. 13). In general terms, this example draws attention to charge and spin distribution in radicals, particularly in molecular structures with inherent resonance possibilities.



The Raman spectrum of the neutral anilino radical is very similar with respect to the vibrational frequencies, e.g., the C–N mode is at  $1505 \text{ cm}^{-1}$ . This shows that the loss of a proton does not lead to any significant structural changes. The fact that the C–N frequency is even slightly higher than that of the radical cation has been suggested to reflect a somewhat decreased coupling between the C–N stretching and N–H bending motion. A second interesting result is that even at pH 10.4, i.e., way beyond the pK of the aniline radical cation the latter can still be detected on the time scale of Raman resolution ( $\approx 100 \text{ ns}$ ). The neutral anilino radical is only formed as a result of the radical cation's reaction with  $\text{OH}^-$  (estimated rate constant:  $5 \times 10^{10} \text{ M}^{-1} \text{ s}^{-1}$ ).

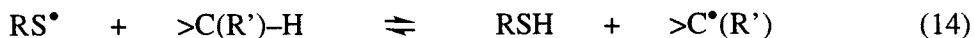
### 3 S-CENTERED RADICALS AND RADICAL ANIONS

#### 3.1 Thiyl radicals

The great attention sulfur-organic compounds and their radicals have achieved has many reasons, one of them undoubtedly being their relevance to biology, life sciences and many fields within chemistry.<sup>3,4</sup> In the early radiation chemical studies the focus was, however, limited to mainly thiols and the way they could serve as repair agents for C-centered radicals (back reaction in eq. 14).<sup>33,34</sup> The associated formation of thiyl radicals, on the other hand, received less attention, probably because dimerization to the respective disulfide was long considered to be the only follow-up process of significance. However, this view changed with the discovery and quantification of other properties of the thiyl, as they will be presented and discussed with respect to their general significance in the following.

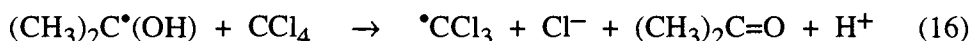
##### 3.1.1 Thiyl radicals as H-atom abstracting agent

A most important finding was the reversibility of the above mentioned repair reaction, i.e., the establishment of an equilibrium between C- and S-centered radicals:<sup>35-37</sup>



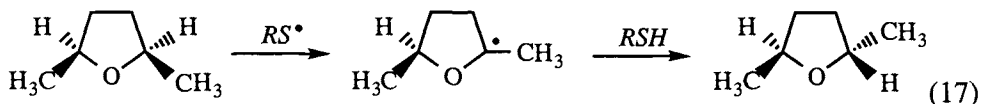
The equilibrium constant is strongly dependent on the nature of  $R'$ , which serves an activating function on the C-H bond to be cleaved in the forward reaction and also affects the degree of resonance stabilization in the C-centered radical. Extensive radiation chemical studies on this equilibrium have been conducted, in particular, with alcohols and ethers as reaction partner for the thiyl radical. Rate constants for the forward reaction in these systems typically range from  $10^3 - 10^4 \text{ M}^{-1} \text{ s}^{-1}$  while the back process occurs about four orders of magnitude faster ( $10^7 - 10^8 \text{ M}^{-1} \text{ s}^{-1}$ ). Equilibrium constants are, accordingly, of the order of  $10^{-4}$ .

Although these figures clearly identify the back ("repair") reaction as dominating process and the thiyl radicals as the prevailing radical species in the equilibrium, the reaction may, nevertheless, be driven completely to the right hand side whenever the C-centered radical engages in an irreversible process. This is the case when, for example, penicillamine thiyl radicals,  $\text{PenS}^{\bullet}$ , are generated in system containing 2-propanol and carbon tetrachloride.<sup>35</sup> While a direct reaction of  $\text{PenS}^{\bullet}$  with  $\text{CCl}_4$  does not occur, a stoichiometric removal of the thiyl radical and reduction of the halocarbon is, nevertheless, achieved. The mechanism is based on the equilibration of  $\text{PenS}^{\bullet}$  with the  $\alpha$ -hydroxyl radical (eq. 15), and irreversible reaction of the latter with carbon tetrachloride (eq. 16).

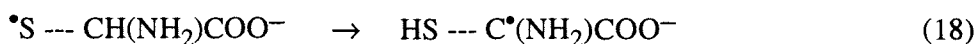


Since  $\cdot\text{CCl}_3$  and particularly its conjugate peroxy form  $\cdot\text{OOCCL}_3$  readily attack cellular membranes<sup>38</sup> the above systems may well be the basis for a thiyl radical induced lipid peroxidation, and can also account for the chemistry behind the action of  $\text{CCl}_4$  as a potent liver toxin.

An instructive example for hydrogen abstraction by thiyl radicals, in this case from an ether, has been reported by Akhlaq *et al.*<sup>39</sup> Experimental evidence is a racemisation of 2,5-dimethyl-tetrahydrofuran according to a reaction sequence which involves an intermediate planar radical site at the carbon  $\alpha$  to the ether's oxygen.



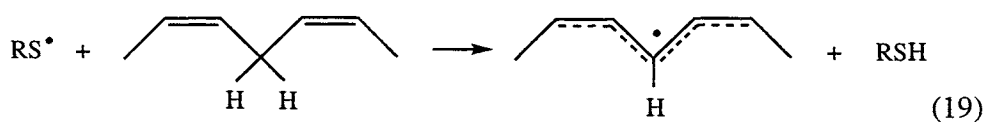
Some further examples involving radiation chemical studies deal with an intramolecular  $RS^\bullet$ -induced hydrogen atom abstraction from  $\alpha$ -amino activated C–H bonds. Thus Zhao *et al.*<sup>40</sup> report on the formation of C-centered reducing radicals



within the anionic form of several amino acids. The measured rate constants for this reaction ( $2.5 \times 10^4 \text{ s}^{-1}$  for cysteine,  $2.2 \times 10^5 \text{ s}^{-1}$  for homocysteine, and  $1.8 \times 10^5 \text{ s}^{-1}$  for glutathione) indicate that this H-transfer may well compete with other reactions of the thiol functionality. A practically identical value ( $1.2 \times 10^5 \text{ s}^{-1}$ ) has been obtained for the glutathione system by Grierson, *et al.*<sup>41</sup> It is noted that the highest rate constant, observed for homocysteine, involves the most favorable 5-membered ring arrangement, while glutathione requires a 9-ring, and cysteine has to cope with the least favorable 4-ring structure.

Intermolecular H-atom abstraction by cysteine thiol radicals from the  $\alpha$ -C–H groups in the amino acids glycine and alanine occurs with rate constants of  $7.5 \times 10^5 \text{ M}^{-1} \text{ s}^{-1}$  and  $3.2 \times 10^5 \text{ M}^{-1} \text{ s}^{-1}$ , respectively, i.e., about an order of magnitude faster than the above cited corresponding abstractions from alcohols.<sup>40</sup> This nicely coincides with the trend in C–H bond dissociation energy in  $NH_2C(H)(CO_2^-)H$  (363 kJ/mol) and  $(CH_3)_2C(OH)H$  (381 kJ/mol).

All these examples clearly identify the difference in bond dissociation energy between C–H and S–H as a major factor determining the extent to which  $RS^\bullet$ -induced H-abstraction occurs. The most striking case is the reaction of thiol radicals with polyunsaturated fatty acids (PUFA) (eq. 15).<sup>36,37,42</sup> The strength of the bisallylic C–H bonds in the latter is on the order of  $\approx 300$  kJ/mol, i.e., considerably smaller than that of the S–H bond in thiols (340–365 kJ/mol).



The resulting pentadienyl-type radical is easily identifiable through its strong optical absorption at 280 nm. Its lifetime, under pulse radiolysis conditions, is quite long and even at  $10^{-2} \text{ M}$  thiol no decay of the signal is observed on the lower millisecond time scale, meaning that the back reaction (repair reaction) is practically negligible.

Rate constants for the above H-atom abstraction process are on the order of  $10^7 \text{ M}^{-1} \text{ s}^{-1}$  with the actual values depending both on the nature of the thiyl and the PUFA. For a given thiyl radical the measured rate increases with the number of bisallylic hydrogens. The reaction of glutathiyl radicals,  $\text{GS}^\bullet$ , with PUFAs, for example, occurs with the following rate constants:  $0.8 \times 10^7 \text{ M}^{-1} \text{ s}^{-1}$  (linoleic acid, 18:2, two double bonds in one bisallylic functionality),  $1.9 \times 10^7 \text{ M}^{-1} \text{ s}^{-1}$  (linolenic acid, 18:3, three double bonds in two bisallylic functionalities), and  $3.1 \times 10^7 \text{ M}^{-1} \text{ s}^{-1}$  (arachidonic acid, 20:4, four double bonds in three bisallylic functionalities). As to be expected, the mere length of the aliphatic chain does not play any role as is indicated by identical rate constants for the 18:3 and 22:3 PUFAs. Practically no reaction ( $k < 10^5 \text{ M}^{-1} \text{ s}^{-1}$ ) is observed with oleic acid (18:1, one double bond) which lacks bisallylic hydrogens.

One further aspect besides H-atom abstraction must, however, be considered in the reactions of thiyl radicals with PUFAs, namely, the possibility of concurrent  $\text{RS}^\bullet$  additions to the double bonds. By analyzing a particular system in which the thiyl radical from mercaptoethanol had reacted with linolenic acid, Schöneich *at al.*<sup>37</sup> came to the conclusion that the abstraction of bisallylic hydrogen and thiyl addition occur with comparable rates. The C-centered adduct radical formed in the addition reaction is, of course, prone for repair in the presence of thiols, i.e., will subsequently regenerate thiyl radicals via the back reaction of equilibrium 14. These, in turn, will re-enter into the abstraction / addition competition cycle and eventually all of the thiyl radicals will appear to have reacted via the abstraction route. Experimentally, overall efficiencies of up to 85 % have been measured and the difference to the limiting 100% efficiency may be accounted for by side and termination processes. But looking into the details, the situation is, in fact, even more complex. As shown by Schwinn *at al.*<sup>43</sup>, there is still another process which readily occurs within the  $\text{RS}^\bullet$ -adducts to the double bonds, namely, cis-trans isomerization. Quantification of this is of imminent interest for the biological community.

### 3.1.2 Reversible oxygen addition to thiyl radicals

A second important finding radiation chemistry has provided for the understanding of thiyl chemistry in chemical and biological systems is the reversibility of oxygen addition.

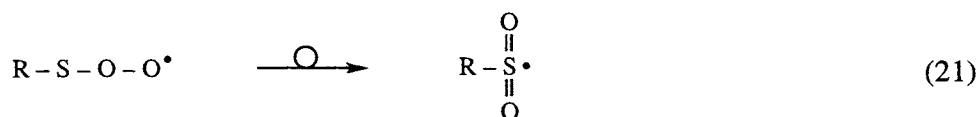


Rate constants of the order of several  $10^9 \text{ M}^{-1} \text{ s}^{-1}$  and  $10^5$ - $10^6 \text{ s}^{-1}$  for the

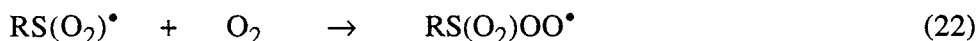


forward and back reactions, respectively, yield equilibrium constants of  $10^3$ - $10^4$  M<sup>44-46</sup> indicating quite an appreciable stability for the thioperoxy radical. It should be noted, however, that in air-saturated solutions ( $[O_2] \approx 2.5 \times 10^{-4}$  M) its formation occurs with a rate ( $t_{1/2} \approx 1 \mu s$ ) which is of the same magnitude as that for its re-dissociation. Consequently, both  $RS^\bullet$  and  $RSOO^\bullet$  will be present under this condition and may prevent unambiguous identification of follow-up reactions. Two of the overall still small number of systems for which accurate measurements are available deal with the respective thiyl and thioperoxy radicals of mercaptoethanol and glutathione. In case of the mercaptoethanol derived thioperoxy radical, investigations have been facilitated by a weak but distinct optical absorption of  $RSOO^\bullet$  with  $\lambda_{max}$  near 550 nm ( $\epsilon \approx 200 - 400 \text{ M}^{-1} \text{ cm}^{-1}$ ).<sup>47,48</sup>

With respect to a discussion of the thioperoxy properties it is interesting to note that the terminal oxygen appears to carry just about half of the spin density while 40% reside on the inner oxygen and 8% even on the sulfur. This may directly be connected with the relative ease by which the thioperoxy radical is, presumably irreversibly, transformed into the fully sulfur-centered sulfonyl radical.<sup>49</sup>

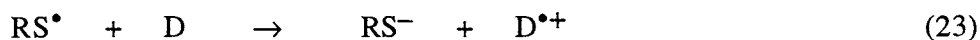


All these processes, and the possible pick-up of another oxygen molecule to yield the sulfonyl peroxy radical,<sup>50</sup> reveal further challenges for radiation chemical research on these systems.



### 3.1.3 Thiyl radicals as oxidants

Another important property of thiyl radicals is their capacity to act as an oxidant. Redox potentials on the order of +0.75 to +1.35 V (vs. NHE) have been measured or calculated for  $RS^\bullet/RS^-$  and  $RS^\bullet, H^+/RSH$  couples, respectively.<sup>51</sup> Electron transfer via the general reaction



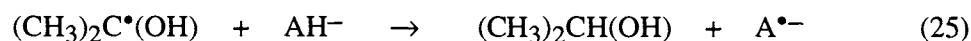
has been established, for example, for  $RS^\bullet$  from cysteine, cysteamine, penicillamine, glutathione and other thiols with ascorbate, phenols,  $\alpha$ -tocopherol and

various phenothiazines as donor molecules.<sup>52,53</sup> ( $D^{\bullet+}$  represents the one-electron oxidized form of the donor, irrespective of the actual overall charge). Absolute rate constants of up to the order of  $10^8 - 10^9 \text{ M}^{-1} \text{ s}^{-1}$  identify these processes as quite efficient ones. In principle, reaction 23 is reversible.

For some of these reactions, such as the thiyl reaction with ascorbate ( $AH^-$ ) (eq. 24) the question may be raised whether this is perhaps not an oxidation induced by electron transfer but rather a hydrogen atom transfer.



Forni and Willson<sup>54</sup>, by isotope effect studies and also by comparison with the much lower rate for a true H-transfer reaction (eq. 25),



could, however, convincingly demonstrate that the ascorbate oxidation is, indeed, best explained in terms of an electron transfer. The same mechanistic consideration probably applies for the thiyl induced oxidation of phenols.

#### 3.1.4 Thiyl / disulfide radical anion conjugation

The electrophilic nature of thiyl radicals expresses itself also in a pronounced tendency to couple the unpaired electron at sulfur with free electron pairs of another heteroatom. The most prominent example is the reaction of thiyl with thiolate and the establishment of an equilibrium with disulfide radical anions, formulated in eq. 26.



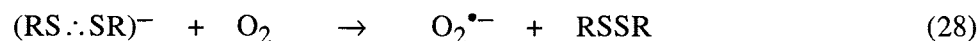
The actual electronic structure of  $(RSSR)^{\bullet-}$  is especially interesting. Key feature is a  $2\sigma/1\sigma^*$  bond between the two sulfur atoms, rendering  $[RS \cdot SR]^-$  an even more appropriate and informative notation.<sup>55,56</sup> While further details on this three-electron bond will be dealt with in the "odd electron bonds" section (*vide infra*), the following is of immediate interest. The combined effect of the two bonding  $\sigma$ -electrons and the one antibonding  $\sigma^*$  electron affords a formal bond order of 1/2. This, in turn, provides the rationale for the above equilibrium and relative ease of redissociation of the newly formed sulfur-sulfur bond. The same  $[RS \cdot SR]^-$  species is, incidentally, formed in the reduction of disulfides by hydrated electrons. Thiyl radicals and disulfide radical anions thus are two conjugate forms of the one-electron redox intermediate between thiols and disulfides.

The inherent lifetime of  $(RS \cdot SR)^-$  with respect to dissociation into  $RS^\bullet$  and  $RS^-$  is generally very short ( $\approx 200$  ns in aqueous solution for systems with  $R = \text{alkyl}$ ). With equilibrium constants on the order of  $K_{26} \approx 10^3$  M,<sup>57</sup> and a thiolate concentration of  $\leq 10^{-5}$  M, as they are generated in a typical pulse radiolysis experiment, the half-life for the re-association amounts to a comparatively long  $20 \mu\text{s}$ . Accordingly, the two entities,  $RS^\bullet$  and  $RS^-$ , once formed will diffuse apart and become available for other reactions, practically undisturbed by the equilibrium. It is easy to recognise, however, that the formation of freely diffusing thiyl radicals is not possible upon reduction of a disulfide bridge which is held together by a linking backbone as, for example, in lipoic acid and several cyclic disulfides. The radical anions generated from such compounds exhibit lifetimes of over  $100 \mu\text{s}$ , even in the absence of free thiolate.<sup>58-62</sup>

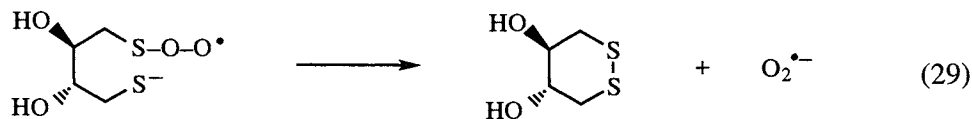
The possibility to control the lifetime of the two conjugate radicals, particularly that of the disulfide radical anion, through equilibrium 26 allows targeted follow-up reactions. An example is an electron transfer reaction involving lipoic acid and cystamine as formulated in eq. 27.<sup>58</sup>



Of even greater importance appear to be the consequences of equilibrium 26 with respect to the redox properties. As has been stated already, thiyl radicals are oxidants. Disulfide radical anions, on the other hand, are reductants ( $E^\circ \approx -1.5$  V).<sup>51</sup> The transfer of their antibonding electron to oxygen is of particular interest, especially in biological systems.<sup>63,65</sup>



In certain systems this sequence may even spare the  $(RS \cdot SR)^-$  intermediate. In the case of dithiothreitol, for example, the possible involvement of oxygen is discussed already at the  $RS^\bullet$  level according to eq. 29, with formation of a transient thioperoxy.<sup>46,66</sup>



Most disulfide radical anions lose their relative stability in acidic environment. In simple aliphatic systems the protonated form of the disulfide radical

anion,  $[\text{RSS}(\text{H})\text{R}]^{\bullet-}$ , is basically hypothetical and immediately dissociates into its thiyl and thiol components (eq. 30)



Backbone linkage, however, is again able to hold the two sulfurs together and may, in fact, render these processes reversible. A particularly nice example for this is the reduced form of lipoic acid where not only the anion,  $\text{Lip}(\text{S} \cdot \cdot \text{S})^{\bullet-}$ , (as mentioned before) but also the protonated form,  $\text{Lip}(\text{S} \cdot \cdot \text{S}, \text{H})$ , are relatively long-lived and unambiguously distinguishable through their different optical absorptions.<sup>67</sup> The same considerations apply for the one-electron oxidation product of dithiothreitol.<sup>51</sup>

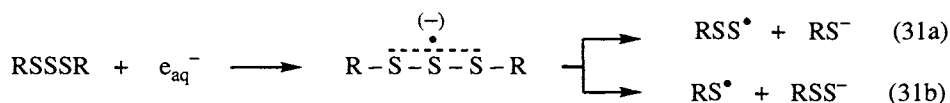
### 3.1.5 Optical properties

Non-aromatic thiyl radicals typically display an absorption band in the UV with  $\lambda_{\text{max}}$  around 330 nm and extinction coefficients of usually less or about  $500 \text{ M}^{-1} \text{ cm}^{-1}$ . The only exceptions reported with respect to the latter refer to the thiyl radicals derived from penicillamine and glutathione,  $\text{PenS}^{\bullet}$  and  $\text{GS}^{\bullet}$ , which for some as yet unidentified reason have a higher  $\epsilon$  of  $\approx 1200$  and  $800 \text{ M}^{-1} \text{ cm}^{-1}$ , respectively.<sup>68</sup> Aromatic thiyl radicals, on the other hand, show a much more pronounced absorption pattern in the UV/vis as they benefit from the resonance interaction of the unpaired electron at sulfur with the aromatic  $\pi$ -system. For example, a broad and asymmetric band between 400 and 510 nm and an even stronger band with  $\lambda_{\text{max}}$  at 295 nm, with maximum  $\epsilon$ -values of 2,500 (at 460 nm) and  $10,000 \text{ M}^{-1} \text{ cm}^{-1}$  (at 295 nm) are the particular optical characteristics of the phenyl thiyl radical,  $\text{C}_6\text{H}_5\text{S}^{\bullet}$ .<sup>69,70</sup> Interesting structural characteristics of this species have been obtained by applying resonance Raman spectroscopy.<sup>70</sup>

The disulfide radical anions  $(\text{RS} \cdot \cdot \text{SR})^{\bullet-}$  are characterized by a relatively strong and thus easily detectable optical absorption. Depending on the nature of R absorption maxima range from 380 to 430 nm (for more details see section dealing with “odd electron bonds”) and extinction coefficients are about  $(8\text{-}9) \times 10^3 \text{ M}^{-1} \text{ cm}^{-1}$ .<sup>71</sup>

## 3.2 Perthiyl radicals

Much of what has been outlined above for thiyl radicals also holds for perthiyl radicals,  $\text{RSS}^{\bullet}$ . A most convenient way to generate them radiation chemically is via reduction of organic trisulfides. As depicted in eq. 31 the incoming electron is initially accommodated in an antibonding orbital, like in reduced disulfides, but here extending over the entire trisulfide bridge.



Subsequently, two pathways may be entered, one leading to perthiyl (plus thiolate), while the other results in thiyl radicals (plus perthiolate). An example shedding light on the strong influence of structural parameters on the relative yields of these two options has been described by Everett *et al.*<sup>72</sup> who report reaction 31a to dominate for penicillamine derivative ( $\geq 95\%$ ), as opposed to an only  $\approx 20\%$  yield of this process in the reduction of cysteine trisulfide. A similarly striking difference between these two trisulfides was found with respect to the  $\bullet\text{OH}$ -induced formation of perthiyl radicals (63% for R=Pen and 10% for R=Cys).

RSS $^\bullet$  radicals exhibit a reasonably strong UV absorption band with an apparent common maximum at 374 nm irrespective of the nature of R. Most interestingly, also the respective extinction coefficients appear to be the same for all RSS $^\bullet$ , namely,  $\epsilon \approx 1700 \text{ M}^{-1} \text{ cm}^{-1}$ .<sup>72-74</sup> This specifically includes the penicillamine species (PenSS $^\bullet$ ) the thiyl analogue of which (PenS $^\bullet$ ) behaved so differently in this respect relative to the other RS $^\bullet$ .

The reactivity of perthiyl is generally reduced as compared with that of thiyl, reflecting the higher degree of resonance stabilization. The measured rate constant for the reaction of the penicillamine-derived perthiyl radical with oxygen (eq. 32), for example, amounts to  $5.1 \times 10^6 \text{ M}^{-1} \text{ s}^{-1}$ . Generally, oxygen addition to RSS $^\bullet$  occurs 2-3 orders of magnitude slower than to RS $^\bullet$ .<sup>72</sup>



It is likely, although it still needs experimental proof, that this reaction is reversible as in the thiyl radical case.

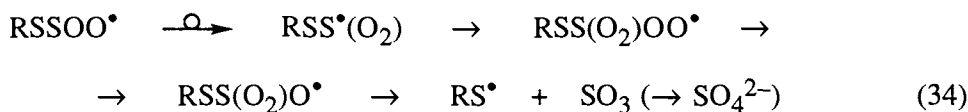
Like thiyl, also perthiyl radicals exhibit oxidizing properties.<sup>72</sup> They readily react, for example, with ascorbate. This process occurs by about two orders of magnitude slower than the RS $^\bullet$  induced one (e.g.,  $4.1 \times 10^6 \text{ M}^{-1} \text{ s}^{-1}$  vs.  $4.9 \times 10^8 \text{ M}^{-1} \text{ s}^{-1}$  for the reaction of ascorbate with PenSS $^\bullet$  and PenS $^\bullet$ , respectively).

Another interesting result worth mentioning concerns the reversible H-atom transfer with alcohols, with the actual data presented here referring to 2-(3-aminopropyl-amino) ethanepersulfide (also known as the persulfide analogue of the radioprotector drug WR-1065).<sup>75</sup>



The forward (“repair”) reaction occurs with  $2.4 \times 10^9 \text{ M}^{-1} \text{ s}^{-1}$  and the back reaction with  $3.8 \times 10^3 \text{ M}^{-1} \text{ s}^{-1}$  which are about one order of magnitude faster and slower, respectively, than the corresponding reactions involving RSH and  $\text{RS}^\bullet$ .

Finally, an avenue linking organic with inorganic chemistry is opened in the reaction of perthiyl radicals with oxygen which, depending on the nature of R, yields more or less significant amounts of sulfate.<sup>72</sup> The mechanism leading from  $\text{RSSOO}^\bullet$  to  $\text{SO}_4^{2-}$  has been suggested to involve a rearrangement, oxygen addition to the resulting S-centered radical, followed by typical peroxy chemistry and  $\beta$ -scission (eq. 34). Further work is, however, necessary for verification of all suggested intermediate steps.



### 3.3 Sulfuranyl radicals

A limited number of radiation chemical results pertains to sulfuranyl radicals. The simplest of these three-coordinate sulfur-centered radicals, namely,  $\text{R}_3\text{S}^\bullet$  are very short-lived ( $t_{1/2} < 1 \mu\text{s}$ ) and so far escaped direct detection. Their transitory formation can, however, be deduced from a fast, close to diffusion controlled, reduction of the corresponding sulfonium salts by hydrated electrons and scavenging of the radicals cleaved as an overall result of reaction sequence 35.



In case of cyclic sulfonium salts (two of the three substituents backbone-linked) the results indicate that sulfur-carbon cleavage leading to ring opening seems to prevail over expulsion of the open chain alkyl group.<sup>76</sup>

Better candidates for stabilization of a sulfuranyl type intermediate appear to be those which offer the possibility for resonance and electron delocalization. Reduction of 1-methyl-1,2-dithiolanium, for example, results in a transient with  $t_{1/2} \approx 10 \mu\text{s}$  and  $\lambda_{\text{max}} 396 \text{ nm}$  which can be assigned to a structure **1** but in the light of all the findings concerning three-electron bonded species (*vide infra*) is probably even better represented by structure **2**.<sup>77</sup>



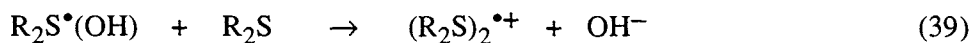
One of them is depicted in structure 3.<sup>80</sup> It has a half-life of about 10  $\mu$ s, long enough to study and quantify bimolecular reactions of this species with a variety of substrates, e.g. molecular oxygen. The latter reaction, incidentally, yields a hydroxythioperoxyl radical in the first instance.

## 4 SULFUR- AND OTHER HETEROATOM-CENTERED RADICAL CATIONS

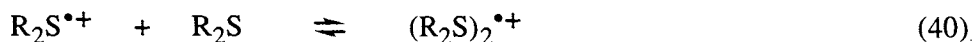
### 4.1 Molecular sulfide radical cations

An early example for a sulfur-centered radical cation in aqueous solution has been described by Meißner *et al.* who observed a relatively long-lived transient absorption ( $\lambda_{\text{max}}$  465 nm) when dimethylsulfide ( $\text{Me}_2\text{S}$ ) was oxidized by  $\cdot\text{OH}$  radicals.<sup>82</sup> This longevity was, to some extent, surprising since it had generally been assumed that radical cations would suffer fast deprotonation or nucleophilic attack and thus escape direct detection. However, with the advent of time-resolved pulse radiolysis conductivity techniques, unambiguous evidence emerged about the cationic character of these transients.<sup>83</sup>

In the simplest mechanistic approach, the transient sulfide radical cation could have been the molecular radical cation, i.e.,  $\text{Me}_2\text{S}^{\bullet+}$  formed via electron transfer or  $\cdot\text{OH}$ -addition/ $\text{OH}^-$ -elimination. Variation of the solute concentration, however, indicated that the absorbing species was, in fact, a dimer, namely,  $(\text{Me}_2\text{S})_2^{\bullet+}$ .<sup>82</sup> Later studies on this and corresponding species obtained upon oxidation of a large variety of other thia compounds revealed several new and interesting features.<sup>71,83-88</sup> To begin with, the formation of the  $\text{OH}^-$ /radical cation pair is not the result of a simple electron transfer mechanism but proceeds, indeed, via an intermediate  $\cdot\text{OH}$ -adduct to the sulfur moiety. This subsequently transfers into the dimer radical cation via the generalized overall displacement formulated in eq. 39.



Secondly, it was established that the dimer and molecular radical cations exist in an equilibrium (eq. 40) in which the dimer typically is the comparatively less reactive partner.

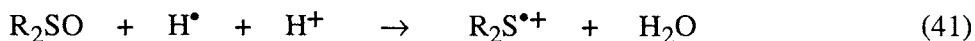


The most important feature of the dimer radical cation is, however, its molecular structure in which the two sulfide entities are linked together via a



newly established sulfur-sulfur bond containing an odd number of electrons. This aspect will be discussed in depth in the “odd electron bonds” section below.

An alternative, although less versatile, method to generate molecular sulfide radical cations is based on the reduction of sulfoxides by hydrogen in very acid solution (eq. 41).<sup>89,90</sup>



An advantage of this method is that it does not require the presence of sulfide in the solution and, therefore, avoids fast conversion of  $\text{R}_2\text{S}^{\bullet+}$  into its dimer complex according to eq. 40.

## 4.2 Physico-chemical properties

### 4.2.1 Absorption spectra

All the sulfur-centered radical cations mentioned above exhibit moderate to strong optical absorptions allowing convenient detection and study of their properties by pulse radiolysis. In case of  $(\text{R}_2\text{S})_2^{\bullet+}$  and  $(\text{RSSR})^{\bullet+}$  the main absorption bands are located in the near UV and visible part of the spectrum. Since they are related to the special features of the odd-electron bonds it is again appropriate to present and discuss further details later.

In this section we will just briefly touch on the  $\text{R}_2\text{S}^{\bullet+}$ -type species. In case of aliphatic sulfides these molecular sulfide radical cations typically exhibit one major transition around 300 nm (285 nm for R = methyl; 310 nm for R = *t*-butyl).<sup>89,91</sup> Aromatic radicals, on the other hand, show a variety of UV/vis absorption bands, based on transitions within the aromatic  $\pi$ -system and involving the non-bonding electrons at sulfur (e.g., 360 and 740 nm for  $(\text{C}_6\text{H}_5)_2\text{S}^{\bullet+}$ , and 310, 530 and possibly 740 nm for  $\text{C}_6\text{H}_5\text{-S}^{\bullet+}\text{-CH}_3$ ).<sup>92-94</sup> In their very elaborate study on a variety of thioanisole derivatives, Iolele, Steenken and Baciocchi<sup>93</sup> provided also information on extinction coefficients, being typically on the order of  $1 \times 10^4$  and  $6 \times 10^3 \text{ M}^{-1} \text{ cm}^{-1}$  for the UV and visible band, respectively. Dimerization to the corresponding  $(>\text{S} \cdot \cdot \text{S} <)^+$  could not be achieved in most cases, due to solubility limitations preventing sufficiently high solute concentration for overcoming the relatively high internal, resonance based stabilization energies of the monomer radical cations.

### 4.2.2 Reduction potentials

The monomeric radical cations are generally excellent oxidants, better than their dimeric conjugates. Even the resonance stabilized aromatic ones are still powerful enough to initiate oxidation reactions. Two values have been

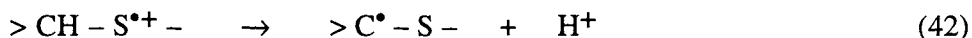
reported for the redox potential of the  $(\text{C}_6\text{H}_5\text{-S}^{\bullet+}\text{-CH}_3) / \text{C}_6\text{H}_5\text{SCH}_3$  couple, namely, +1.45 and +1.53 V (vs. NHE).<sup>93,94</sup> Estimates for aliphatic  $\text{R}_2\text{S}^{\bullet+}$  are of the same order of magnitude ( $> +1.4$  V), based on the observation that these sulfide radical cations readily oxidize disulfides.<sup>95</sup> An exact value (+1.66 V) has been evaluated for  $(\text{CH}_3)_2\text{S}^{\bullet+}$ .<sup>96</sup>

#### 4.2.3 Deprotonation, disproportionation, and nucleophilic attack

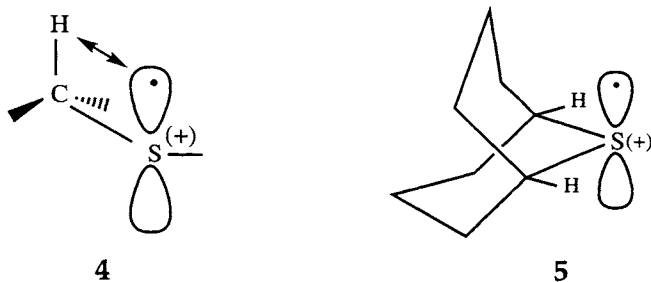
In the absence of suitable redox partners sulfide and disulfide radical cations decay mainly by disproportionation or deprotonation. Considering their positive charge they are also prone for nucleophilic attack. Examples for the latter are the reaction of  $\text{R}_2\text{S}^{\bullet+}$  with  $\text{OH}^-$ , leading to sulfuranyl radicals  $\text{R}_2\text{S}^{\bullet}(\text{OH})$ , or with halide ions, yielding sulfur-halide coupled radicals. Both these product radical species will be dealt with in more detail in separate sections.

Disproportionation has been assumed primarily from the observed second order decay kinetics. This applies, in particular, to most disulfide radical cations and to those sulfide radical cations which do not deprotonate at all or not fast enough. Little is known so far on mechanistic details and products as result of the disproportionation, except that the  $\text{R}_2\text{S}^{2+}$  product dication seems to account for most of the sulfoxide formed upon the  $\bullet\text{OH}$ -induced oxidation of sulfides in aqueous solution.<sup>83,97</sup>

Deprotonation generally only involves hydrogens residing on aliphatic carbons, affording formation of an  $\alpha$ -(alkylthio)alkyl type radical as shown in reaction (42). The rate can be accelerated by proton acceptors such as phosphate.<sup>86</sup>



The possibility for deprotonation strongly depends on the molecular structure of the radical cation or, to be more specific, on the relative alignment of the singly occupied sulfur p-orbital with the C-H  $\sigma$ -bond to be cleaved. A very fast deprotonation is observed, for example, for the *i*-Pr<sub>2</sub>S<sup>•+</sup> radical cation ( $k = 2.7 \times 10^5 \text{ s}^{-1}$ ).<sup>86</sup> This can be envisaged by a high probability of parallel alignment of the sulfur-p- and C-H- $\sigma$ -orbitals, presumably facilitated by the steric influence of the two methyl groups in combination with the free rotation around the C-S bond (structure 4). In the radical cation from 9-thia-bicyclo-[3.3.1]-nonane (5), on the other hand, the neighboring C-H bonds are fixed in a configuration perpendicular to the sulfur p-orbital. This practically prevents deprotonation, and 5 decays by a pure second order process under pulse radiolysis conditions ( $\approx 10^{-5}$  M radical concentration).<sup>56,98</sup>



### 4.3 Selenium- and tellurium-centered radicals

Most aspects mentioned above for sulfur-centered radical species apply to heteroatom-centered analogues as well. At this point only some specific findings concerning Se- and Te-centered radical cations and  $\cdot\text{OH}$  adducts shall be highlighted.

Radical cations of the general type  $\text{Ar}_2\text{Se}^{\bullet+}$  and  $\text{Ar}_2\text{Te}^{\bullet+}$ , like their  $\text{Ar}_2\text{S}^{\bullet+}$  analogues, receive their stability from the resonance of the unpaired Se- or Te-p-electron with the aromatic  $\pi$ -system. A pulse radiolysis study, concerned with the evaluation of one-electron reduction potentials, gave values of +1.54 V, +1.37 V, and +1.14 V for  $(\text{C}_6\text{H}_5)_2\text{S}^{\bullet+}/(\text{C}_6\text{H}_5)_2\text{S}$ ,  $(\text{C}_6\text{H}_5)_2\text{Se}^{\bullet+}/(\text{C}_6\text{H}_5)_2\text{Se}$ , and  $(\text{C}_6\text{H}_5)_2\text{Te}^{\bullet+}/(\text{C}_6\text{H}_5)_2\text{Te}$  couples, respectively.<sup>92</sup> Another noteworthy quantification refers to the formation of these radical cations by reduction of the respective oxides. This becomes increasingly efficient within the series of S-, Se-, and Te-compounds, corroborating results obtained most recently on the reduction of methionine and selenomethionine.<sup>99</sup> Finally, the chalcogenide investigations revealed interesting information on chalcogen-oxygen bonds. While the strength of double bonds decreases in going from  $>\text{S}=\text{O}$ , to  $>\text{Se}=\text{O}$  and  $>\text{Te}=\text{O}$ , that of a single bond within the corresponding  $\cdot\text{OH}$ -adduct increases in the series  $>\text{S}^{\bullet}-\text{OH}$ ,  $>\text{Se}^{\bullet}-\text{OH}$ , and  $>\text{Te}^{\bullet}-\text{OH}$ .<sup>92</sup> In view of the odd-electron bond concept discussed below, this can possibly be rationalized in terms of a decreasing antibonding, i.e., bond weakening character of the radical electron as the difference in electronegativity increases between the chalcogen and oxygen.

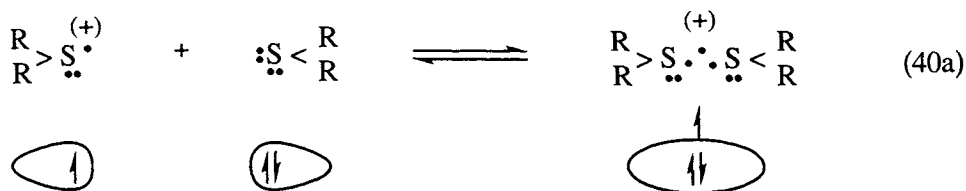
## 5 ODD-ELECTRON BONDS

Odd-electron bonded species represent a very special class of radicals with unique characteristics. Many of them, perhaps even the majority have been evaluated using radiation chemical, particularly pulse radiolysis methods.

It is, however, only fair to acknowledge the vital input this field has received from complementary studies conducted especially with photochemical, ESR, electrochemical and theoretical means. Sulfur-centered radicals and radical ions turned out to be probably the most informative species in this respect and, accordingly, will serve as basis for the following evaluation of the characteristic features of such bonds. In general, the principles to be presented and discussed for the sulfur-centered species apply, however, also to any heteroatom-heteroatom interaction as will be shown for selected examples with Group III and Group V-VII elements.

### 5.1 Sulfur-centered radicals from mono- and polythia compounds

The basic feature of the sulfur-sulfur bond in the dimer radical cation  $(R_2S)_2^{\bullet+}$  introduced above is that it contains three electrons, namely, two bonding  $\sigma$ -electrons and one antibonding  $\sigma^*$ -electron. Formally, it can be viewed as resulting from an interaction of a singly occupied p-orbital of the sulfur-centered radical cation,  $R_2S^{\bullet+}$ , and the p-lone pair of a second non-oxidized sulfur.<sup>56,85</sup> This is depicted in eq. 40a and associated orbital pictorial.



A most important consequence of the  $2\sigma/1\sigma^*$  structure arises from the antibonding electron, specifically its bond-weakening influence. As can easily be appreciated from the MO diagram (Figure 1a), the overall formal bond order is only 0.5, rendering it prone for easy dissociation.

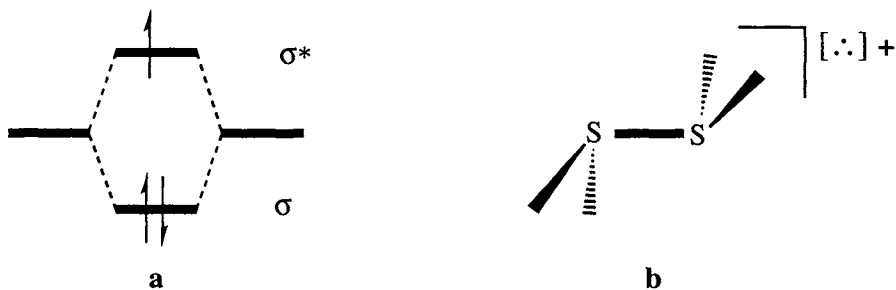


Figure 1 a) MO diagram for  $2\sigma/1\sigma^*$  bond  
b) preferred (lowest energy) structure of  $(R_2S\cdot:SR_2)^+$

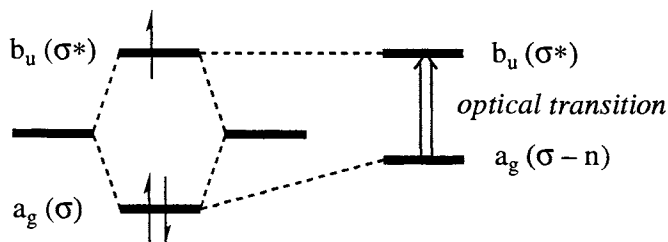
This is, in fact, the rationale behind the above formulated equilibrium between the three-electron bonded species and its conjugate monomeric radical cation. The “ $\cdot$ ” notation for this type of bond, incidentally, has been introduced by us and is now generally accepted and widely used.

Most of the physico-chemical characterization of the sulfur-centered S $\cdot$ :S-bonded species has been provided by time-resolved optical pulse radiolysis studies (*vide infra*). However, in the early days of investigations unambiguous assignment benefitted very much from ESR measurements although this technique has some obvious limitations associated with the lack of nuclear spin at the sulfur’s main isotope,  $^{32}\text{S}$ . With the help of Fenton-type chemistry conducted under steady-state flow conditions, for example,<sup>100</sup> the  $\{(\text{CH}_3)_2\text{S}\cdot\text{S}(\text{CH}_3)_2\}^+$  dimeric radical cation was shown to exhibit the splittings of twelve equivalent protons. The antibonding character of the unpaired electron could also be concluded from low temperature experiments<sup>101-103</sup> and an analogue selenium-centered radical cation produced in an irradiated halocarbon matrix containing dimethyl selenide.<sup>104</sup> Later, there has been quite important input also from theoretical and gas phase studies.<sup>105-115</sup> They clearly confirmed the electronic concept and, in addition, provided quantitative information on a number of thermodynamic parameters (for further details see below) and structures.

The perpendicular alignment of the p-orbitals relative to the C–S–C plane and possible steric constraints lead to the preferred conformation of  $(\text{R}_2\text{S}\cdot\text{SR}_2)^+$ , as depicted in Figure 1b.

### 5.1.1 Optical absorptions

The probably most informative property of the  $2\sigma/1\sigma^*$  three-electron bonded species is their optical absorption. Structureless bands peaking in the visible exhibit extinction coefficients of  $\approx 6 (\pm 1) \times 10^3 \text{ M}^{-1} \text{ cm}^{-1}$  and are characterized by a considerable broadness ( $\approx 1.0 \pm 0.2 \text{ eV}$ ) indicating that the transition is an allowed one.<sup>71,83</sup>



The actual transition occurs between the uppermost doubly occupied orbital,

which essentially is the  $\sigma$  energy level disturbed by the non-bonding sulfur electrons and other molecular electronic influences, and the singly occupied  $\sigma^*$  energy level which is practically not affected as shown in the above simplified pictorial drawn on the basis of a theoretical study by Clark.<sup>106</sup>

### 5.1.2 Effect of substituents on $\lambda_{max}$

The optical transition energies for  $(R_2S \cdots SR_2)^+$  depend strongly on the nature of the substituent R and are a sensitive probe for the geometric and electronic structure of the  $2\sigma/1\sigma^*$  species. For example,  $\lambda_{max} = 370$  nm for R = H,<sup>116</sup> 465 nm for R = CH<sub>3</sub>, 555 nm for R = (CH<sub>3</sub>)<sub>2</sub>CH,<sup>71</sup> and 600 nm for a mixedly substituted with one CH<sub>3</sub>- and three (CH<sub>3</sub>)<sub>3</sub>C-groups.<sup>90</sup> These dramatic shifts can, to a significant extent, be rationalized by a linear free energy correlation between the transition energies (in terms of eV) as a function of Taft's inductive parameter (for mixed systems this parameter has been weighted) in Figure 2.

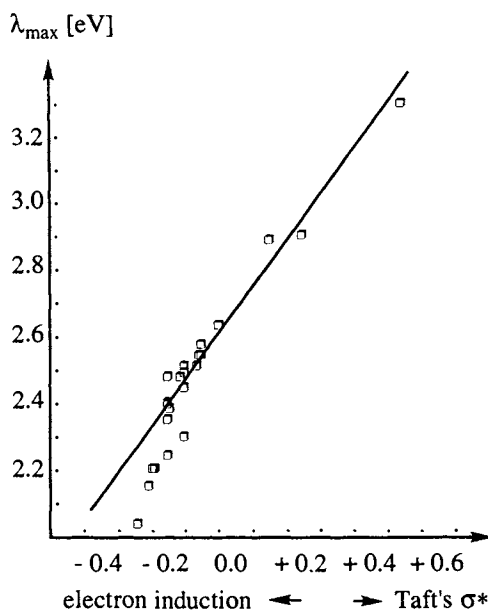


Figure 2. Linear free energy correlation between optical transition energies in  $(R_2S \cdots SR_2)^+$  as a function of Taft's inductive parameter  $\sigma^*$ , weighted over all substituents R.

Electron density release from the substituents into the antibonding orbital weakens the sulfur-sulfur bond, increases the distance between these two atoms

and causes a correspondingly smaller difference between the  $\sigma$  and  $\sigma^*$  energy levels. In particular it appears that, by and large, the optically relevant  $a_g$  ( $\sigma$ -n) energy level is proportionally affected.

However, looking at the data in detail, electron induction is not the only contributing parameter. While most of the measured data are well described (within experimental error limits) by a linear correlation<sup>71,90</sup>

$$\lambda_{\max} [\text{eV}] = 1.4 (\sigma^*) + 2.63$$

it is noted that for low transition energies the corresponding points fall below the straight line, i.e.,  $\lambda_{\max}$  is more red-shifted than the inductive parameter alone can account for. All these deviations refer to ( $>S \cdot S <$ )<sup>+</sup> radical cations carrying especially bulky substituents (branched alkyl groups, particularly *t*-butyl). Therefore, steric constraints affecting the p-orbital orientation and overlap in the sulfur-sulfur bond are forwarded as a rationale. An extreme example is the all-*t*-butyl substituted (*t*-Bu)<sub>2</sub>S $\cdot$ :S(*t*-Bu)<sub>2</sub><sup>+</sup> which, in fact, cannot be stabilized anymore in aqueous solution.

Two further results support this conclusion. The first is that no steric effects are observed for the earlier mentioned (RS $\cdot$ :SR)<sup>-</sup> radical anions which carry only one substituent per sulfur.<sup>71</sup> In this case an excellent straight line is obtained for the entire series with R varying from H to *t*-butyl indicating that here the substituents become effective only through their electronic impact. The second result sheds even some light on how the steric strain operates. There is a marked difference in  $\lambda_{\max}$  between (*t*-Bu)<sub>2</sub>S $\cdot$  $\cdot$ SMe<sub>2</sub>)<sup>+</sup> (545 nm) and (Me,*t*-BuS $\cdot$  $\cdot$ SMe,*t*-Bu)<sup>+</sup> (510 nm) although they carry the same number of methyl and *t*-butyl groups.<sup>90</sup> The presence of two bulky *t*-butyl substituents on one side of the S $\cdot$  $\cdot$ S bridge appears to distort an optimal arrangement significantly more, thereby lowering the ( $\sigma$ -n)/ $\sigma^*$  energy difference, than if they were placed one each on either sulfur.

### 5.1.3 Intramolecular S $\cdot$ :S (2 $\sigma$ /1 $\sigma^*$ ) three-electron bonded radical cations

The steric parameter becomes even more pronounced, and in fact dominant, for radical cations with *intramolecular* sulfur-sulfur coupling. Most examples, studied by radiation chemical (but also other) methods, have been observed in the oxidation of cyclic and open chain dithia compounds.<sup>84,85,117-123</sup> The two extreme situations with respect to the most (left) and least favorable (right) orbital alignment are depicted in Figure 3. The former is closest realized upon one-electron oxidation of 1,5-dithiacyclooctane, **6**, and was first described in conventional ESR work by W. K. Musker.<sup>119-121</sup> It exhibits an optical absorption with  $\lambda_{\max}$  at 400 nm and, incidentally, consti-

tutes the most blue-shifted example known (except for the all-hydrogen substituted  $(\text{H}_2\text{S}\cdot\cdot\text{SH}_2)^+$  which absorbs at 370 nm).<sup>84</sup> Stabilization of **6** is facilitated by the establishment of two five-membered rings on either side of the transannular  $\text{S}\cdot\cdot\text{S}$  bridge.

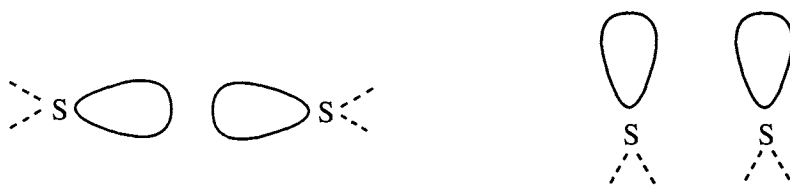
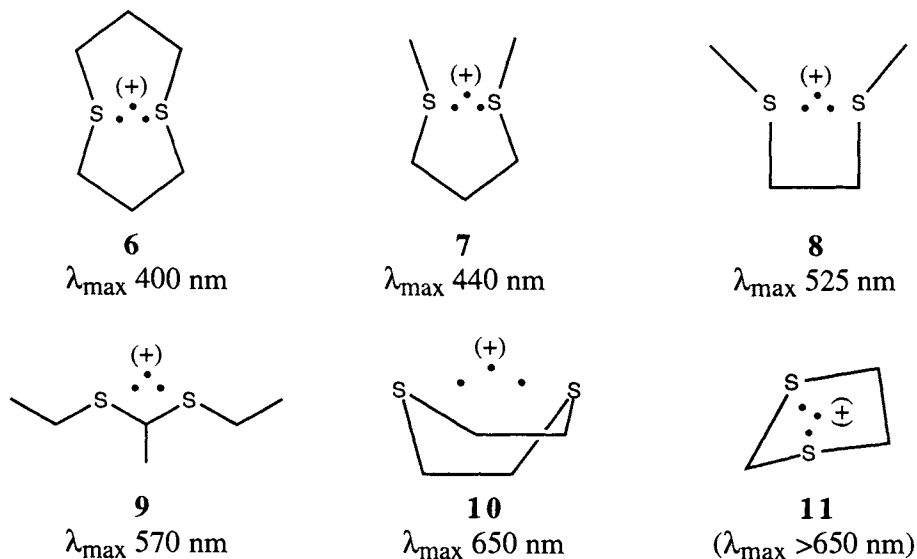


Fig. 3 Most (left) and least (right) favorable alignment of sulfur p-orbitals for establishment of a  $2\sigma/1\sigma^*$  three-electron bond.

The other extreme is given for the radical cation of 1,3-dithiacyclopentane (**11**).<sup>123</sup> In this rigid molecule the sulfur p-orbitals are aligned more or less perpendicular to the ring plane (only very slight envelope structure) which prevents any appreciable overlap for  $\sigma$ -bond formation. Only a very weak and very red-shifted absorption ( $>650$  nm) is indicated upon oxidation of this compound, and assignment to a three-electron bonded radical cation remains, in fact, ambiguous.



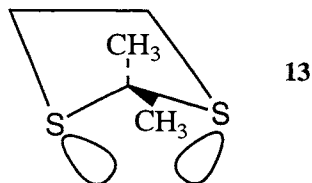
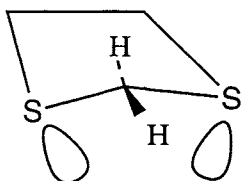
Radical cations **7-9** are generated from open chain dithia compounds, and **10** from 1,4-dithiane. They represent a series with decreasing extent of



possible p-orbital interaction along the sulfur-sulfur axis. With the sulfur p-orbitals being aligned practically perpendicular to the C-S-C plane their orientation relative to each other gradually changes from the left to the right hand side of the picture given in Figure 3. As to be expected, **7** (from 2,6-dithiaheptane) has the most blue-shifted optical absorption besides **6** since it is the only other radical cation in this series which can assume a five-membered ring configuration. Steric strain in the four-membered and three-membered rings in the radical cations from 2,5-dithiahexane (**8**), 3,5-dithia-4-methylheptane (**9**) and 1,4-dithiane (**10**), respectively, results in weaker S••S bonds and, consequently, red-shifted absorptions (525, 570 and 650 nm, respectively). These considerations hold for all *intramolecular* radical cations generated from dithia compounds R-S-(CH<sub>2</sub>)<sub>n</sub>-S-R, and for *transannular* sulfur-sulfur interaction upon oxidation of cyclic dithia compounds (as in **6**).<sup>84,85,124</sup> Note the boat configuration of **10** in which the energy gained upon S••S formation clearly overcomes the energetic demand for converting the ground state chair into the boat.

#### 5.1.4 Optical parameters as sensitive probe for stereoelectronics

As indicated already, the optical transition energy are an extremely sensitive probe for the electronic and steric properties of the three-electron-bonded species and their respective relative contributions. However, the effect of substituents on the optical transitions becomes of much lesser importance in *intramolecular* radical cations derived from open-chain dithianes (type **7-9**). Changing the terminal substituents in R-S-(CH<sub>2</sub>)<sub>3</sub>-S-R from methyl to *iso*-propyl results in a just 15 nm change (440 vs. 455 nm), i.e., structure clearly appears to be the dominating parameter. This is fully corroborated by the pulse radiolysis results on 2-substituted-1,3-dithiacyclopentanes.<sup>123</sup> As mentioned already, the radical cation (**11**), derived from 1,3-dithiacyclopentane (**12**), is very unstable if formed at all ( $\lambda_{\text{max}} > 650$  nm). The analogous radical cation generated upon oxidation of 1,3-dithia-2,2-dimethylcyclopentane (**13**), on the other hand, exhibits a pronounced and blue-shifted absorption at 610 nm as well as a considerable kinetic and thermodynamic stability.



Since the electron inductive influence exerted by the methyl groups should result in bond weakening, i.e., a red-shift in absorption and, furthermore, substitution in the 4-position does not lead to any comparable stabilization, the observed effect in the 2-substituted species can, indeed, only be explained in terms of steric reasons specific to the C-2 position. It has been proposed that the shift in  $\lambda_{\max}$  reflects the *gem-dialkyl* effect which causes a structural distortion favoring p-orbital interactions with respect to  $2\sigma/1\sigma^*$  bond formation to a relatively larger extent.<sup>123</sup> This aspect is depicted in structures **12** and **13**.

### 5.1.5 Thermodynamic stability of $2\sigma/1\sigma^*$ bonds

The difference in energy between  $\sigma$  and  $\sigma^*$  relates to the thermodynamic stability of the  $2\sigma/1\sigma^*$  bond. One of the parameters of interest in this respect is the stability constant for equilibrium 40/40a. Early measurements, based on the observable yields of  $(R_2S \cdot \cdot SR_2)^+$  in pulsed aqueous solutions of some sulfides, suggested  $K = [(R_2\dot{S} \cdot \cdot SR_2)^+]/[R_2S^{\bullet+}][R_2S]$  to be of the order of  $10^3$ - $10^4$  M<sup>-1</sup>.<sup>83</sup> Later studies revealed, however, that this was only a crude estimate which lacked quantitative consideration of the complex deprotonation kinetics of the  $R_2S^{\bullet+}$  radical cations and the influence of the initial short-lived ( $t_{1/2} \leq 1$   $\mu$ s) adduct precursor radical,  $R_2S^{\bullet}(OH)$ . Taking these aspects into consideration much more reliable stability constants were derived which, furthermore, could be confirmed by the independent sulfoxide reduction method (see above, in context of eqs. 39 and 41).<sup>86,90</sup> The following two values, namely,  $2.0 \times 10^5$  M<sup>-1</sup> and  $5.4 \times 10^2$  M<sup>-1</sup> for  $(CH_3)_2S \cdot \cdot S(CH_3)_2^+$  and  $(i-C_4H_9)_2S \cdot \cdot S(i-C_4H_9)_2^+$ , respectively, nicely reflect the destabilizing effect the *iso*-propyl group exerts on the three-electron bond relative to the methyl group.

The actual bond energies, on the other hand, do not seem to differ very much.  $D(S \cdot \cdot S)$  have been evaluated to 100-120 kJ mol<sup>-1</sup> and 80-90 kJ mol<sup>-1</sup> for the above two species from experimental data obtained in aqueous environment,<sup>86</sup> while for the  $(H_2S \cdot \cdot SH_2)^+$  an estimate of 120-130 kJ mol<sup>-1</sup> has been reported from theoretical calculations.<sup>105,109</sup> Later experiments conducted in the gas phase at elevated temperatures (506-576 K), and also supported by calculations, gave, in fact, almost the same values of  $117 \pm 5$  kJ mol<sup>-1</sup> for the all-H-, CH<sub>3</sub>- and C<sub>2</sub>H<sub>5</sub>-substituted species.<sup>114,115</sup> These results show two things. First, the presence of the antibonding electron does, indeed, significantly lower the sulfur-sulfur bond strength relative to that of a normal 2-electron  $\sigma$ -bond which in a disulfide is about 240 kJ mol<sup>-1</sup>. Second, and confirming a statement made already above in the context of mixedly substituted systems, the optical transition energies do not allow a linear extrapolation to the bond energies as originally proposed. The reason is that these two

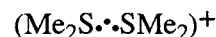
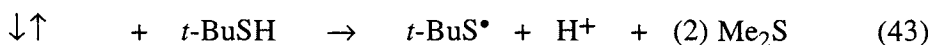
parameters are based on two different energy levels, the electronically disturbed  $\sigma$ -n and the undisturbed  $\sigma^*$ -level, respectively.

The low bond order in S.:S is also indicated in stretching frequency of this three-electron bond. With  $276\text{ cm}^{-1}$ , measured by resonance Raman spectroscopy,<sup>125-127</sup> it is almost half of that for the regular S–S  $\sigma$ -bond ( $507\text{ cm}^{-1}$ ).

### 5.1.6 Kinetic stability and involvement in redox processes

The stability constants for the  $2\sigma/1\sigma^*$  species seem to be mainly controlled by the activation energies and, in turn, rate constants for the dissociation of the three-electron bond (back reaction of eq. 40/40a). The respective values, for the two systems with all-methyl and all-*i*-propyl substitution are  $57$  and  $17\text{ kJ mol}^{-1}$ , and  $1.5 \times 10^4\text{ s}^{-1}$  and  $5.6 \times 10^6\text{ s}^{-1}$ .<sup>86</sup> The latter are certainly in line with the S.:S bond energies but, again, a direct correlation is not justified because in aqueous solution the reaction of interest is not simply the dissociation of the 3-e-bond but, in fact, a displacement process which involves also a water molecule. (See section on “sulfur-oxygen interactions”).

Chemically, the  $(>\text{S}:\text{S}<)^+$  radical cations are less reactive than their conjugate  $(>\text{S})^{\bullet+}$  counterparts, reflecting the respective internal stabilization energies. This is illustrated, for example, in the oxidation of *t*-butyl mercaptane by the radical cations from dimethyl sulfide.<sup>69</sup>

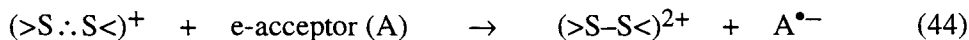


The measured rate constants for the *t*-BuS $^\bullet$  formation decrease with increasing Me<sub>2</sub>S concentration, i.e., increasing shift of the equilibrium to the side of the 3-e-species.

Being cationic species, both conjugates are susceptible to reactions with nucleophiles such as halide ions (to form S.:Hal radicals) or hydroxide ions (to yield  $>\text{S}^\bullet\text{-OH}$  sulfuranyl radicals). (For more details on these product species see corresponding later sections).

With respect to redox properties, the  $>\text{S}^{\bullet+}$  radical cations are stronger oxidants than  $(>\text{S}:\text{S}<)^+$ , e.g.,  $+1.66\text{ V}$  vs.  $+1.40\text{ V}$  for the species derived from Me<sub>2</sub>S.<sup>96</sup> In general, the three-electron bonded radical cations could, however, even be ambivalent. While they may act as an oxidant towards

suitably strong electron donors -- although this is often difficult to verify in view of the generally much higher reactivity of the  $>S^{\bullet+}$  conjugate -- their action as reductant should also be envisaged. For the sulfur-centered species, however, only one such reaction has been reported in solution, namely, that between the *intramolecular* radical cation **6** with iodine.<sup>119-121</sup> In general terms, this leads to the formation of dications as formulated in eq. 44.



Considering the electronic nature of a  $2\sigma/1\sigma^*$  bond radical cation **6** may, in fact, be the most suitable species to lose the antibonding electron because it is prone for optimal p-orbital interaction and, consequently, a high lying  $\sigma^*$  energy level.

The higher the  $\sigma^*$  energy level, the lower should be the ionization energy for the antibonding electron. This expectation, although not established so far in solution chemistry, was verified in a double mass spectrometry experiment<sup>128-130</sup> in which a series of *intramolecular* radical cations were mass selected and subjected to collisional ionization in the overall process:



( $M = O_2$ ) The results, listed in Table I for radical cations **7**, **8** and **10**, show that the species with the most favorable p-orbital overlap (indicated by the most blue-shifted optical absorption) requires, indeed, the least energy to remove the  $\sigma^*$  electron. The highest ionization energy, on the other hand, has been measured for the radical cation with the lowest lying  $\sigma^*$  energy level and most red-shifted absorption. These findings are an excellent proof of the underlying  $\sigma/\sigma^*$  concept.

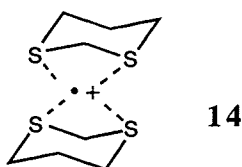
TABLE I  
Ionization energy (IP) of  $[>S\cdot\cdot S<]^+$  in relation to  $\lambda_{\max}$ <sup>128-130</sup>

$[>S\cdot\cdot S<]^+$	IP (eV)	$\lambda_{\max}$ (nm)
<b>7</b>	12.3	440
<b>8</b>	13.3	525
<b>10</b>	15.0	650

### 5.1.7 Multi-center radical cations

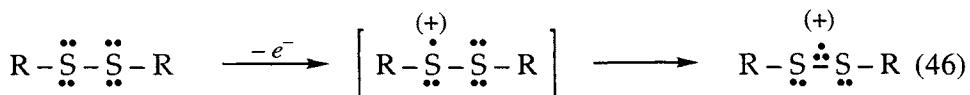
A short remark on tri- and polythia compounds: Several such substrates (1,3,5-trithiane, 1,4,7-trithiacyclononane, 1,4,7,10-tetrathiacyclodecane, and 1,5,8,12-tetrathiacyclotetradecane) have been subjected to one-electron oxidation.<sup>117,122,131</sup> The common feature of the optical absorptions attributable to the intramolecular radical cations derived from these compounds indicates that interaction occurs mainly between two of the sulfur atoms. For example,  $\lambda_{\max} = 600$  and  $610$  nm for the radical cations from 1,3-dithiane and 1,3,5-trithiane, respectively. For the two transients derived from 2,5-dithiaheptane and 1,4,7-trithiacyclononane, respectively, even the same  $\lambda_{\max} = 525$  nm has been measured. Some tailing on the low energy side and broadening of the absorption bands in the trithia systems suggests, however, some small additional influence by the other sulfurs on the electronic energy levels. This conclusion is fully in line with photoelectron spectroscopy data.<sup>132</sup>

An interesting aspect emerged when radical cations from dithia (but also some trithia) compounds were generated in hydrocarbon solutions.<sup>117,122</sup> At high solute concentrations (e.g.,  $10^{-2}$  M) a new infrared absorption showed up with  $\lambda_{\max} \approx 750$  nm. It was particularly pronounced in case of 1,3-dithiane, and assigned to a complex between the molecular radical cation and a second unoxidized molecule in which interaction is not limited to an intermolecular  $>S \cdot \cdot S<$  bond of just two sulfurs but where all four sulfurs from both molecules could be involved. Such a multi-atom interaction requires a favorable geometry, e.g., in kind of a sandwich structure **14**, which may be stabilized only in aprotic and low dielectric environment.



## 5.2 Disulfide radical cations

Disulfide radical cations are an example for a 5-electron bond. As depicted in eq. 46, removal of a sulfur-p-electron in the initial oxidation step formally leads to a radical cation site at one of the sulfurs. This situation stabilizes by electron, spin and charge sharing, and accommodation of the unpaired electron as well as the lone p-electron pair of the other sulfur in the sulfur-sulfur bridge.<sup>55</sup>



In essence, two of these three electrons form a  $\pi$ -bond, on top of the existing  $\sigma$ -bond, and the remaining electron is placed into an antibonding  $\pi^*$ -orbital. The sulfur-sulfur bond thus assumes a partial  $\pi$ -double bond character.<sup>133,134</sup> As direct consequence, the rotation becomes restricted and, particularly in cyclic disulfides, molecular structures tend to flatten. Even the possible formation of *cis*- and *trans*-isomers of  $(\text{MeSSMe})^{\bullet+}$  could recently be verified through identification of two distinct vibrational stretching frequencies evaluated from time-resolved resonance Raman spectroscopy measurements. Both frequencies (557 and 591  $\text{cm}^{-1}$ ) clearly exceed that of a single S-S  $\sigma$ -bond (507  $\text{cm}^{-1}$ ). These findings were also supported by corresponding calculations.<sup>126,127,135</sup>

Formation of the  $(\text{RSSR})^{\bullet+}$  radical cations can be achieved by oxidation of disulfides with  $\bullet\text{OH}$  radicals.<sup>136,137</sup> In the case of simple aliphatic disulfides the yields of  $(\text{RSSR})^{\bullet+}$  amount, however, to only about 50% and drop even further for more functionalized disulfides such as cysteine, cysteamine, and others. Higher yields of up to 100% are generated upon oxidation of simple aliphatic disulfides by typical one-electron oxidants like  $\text{Ag}^{2+}$ ,  $\text{Tl}^{2+}$ ,  $\text{SO}_4^{\bullet-}$ ,  $\text{Br}_2^{\bullet-}$ ,  $\text{RI}^{\bullet+}$ ,  $(\text{RI}:\text{IR})^+$ , and  $(\text{R}_2\text{S}:\text{SR}_2)^+$  radical cations.<sup>95,138</sup> Rate constants for these electron transfer reactions are on the order of about  $10^9 \text{ M}^{-1} \text{ s}^{-1}$ , i.e., about one order of magnitude lower than for the  $\bullet\text{OH}$ -induced process ( $\approx 10^{10} \text{ M}^{-1} \text{ s}^{-1}$ , depending on R). Within the series of aliphatic RSSR, their rate of oxidation decreases in going from  $\text{R}=\text{Me}$  to  $\text{R}=\textit{t}\text{-Bu}$ , e.g., from  $3.0 \times 10^9$  to  $0.4 \times 10^9 \text{ M}^{-1} \text{ s}^{-1}$ , respectively, for oxidation by  $\text{MeI}^{\bullet+}/(\text{MeI}:\text{IME})^+$ . It is interesting to note that this trend does not follow the first gas phase ionization potentials (8.97 and 8.17 eV for  $\text{MeSSMe}$  and  $\textit{t}\text{-BuSS}\textit{t}\text{-Bu}$ , respectively) but rather a trend in torsional CS-SC angles (which is larger for the *di-t*-butyl than for the dimethyl disulfide,  $110^\circ$  vs.  $84.7^\circ$ ). Stereo-electronic parameters thus appear to be the deciding factors.

The aliphatic  $(\text{RSSR})^{\bullet+}$  radical cations exhibit reasonably strong optical absorptions in the near UV/vis with  $\lambda_{\text{max}}$  ranging from 440 nm to 410 nm for  $\text{R}=\text{Me}$  to  $\textit{t}\text{-Bu}$ , respectively, and extinction coefficients of about  $2 \times 10^3 \text{ M}^{-1} \text{ cm}^{-1}$ . As may be noticed, the trend between  $\lambda_{\text{max}}$  and the electron releasing power of the substituent is opposite to that for the  $(\text{R}_2\text{S}\cdot\text{SR}_2)^+$  radical cations from monosulfides.<sup>137</sup> This can, however, also be rationalized as a direct consequence of the electronic concept. The more electron density is released from the substituents into the  $\pi^*$ -level, the smaller becomes the overall  $\pi$ -

character, and typically this coincides with higher optical excitation energies, i.e., blue-shifted absorptions. Exact reduction potentials have been determined for (RSSR)<sup>•+</sup>/RSSR couples of CH<sub>3</sub>SSCH<sub>3</sub> (+1.391 V), lipoic acid (+1.135 V), and lipoate (+1.10 V) (all vs. NHE).<sup>139</sup>

### 5.3 Dynamics of three-electron bond formation

The mechanism of three-electron bond formation by addition of the anti-bonding electron to an existing  $\sigma$ -bond is trivial in the sense that in this case the dynamics are simply controlled by the kinetics of an electron reacting with, or transferred to the accepting molecule (example: one-electron reduction of disulfides). The same consideration applies to the *intermolecular* coupling of the heteroatom-centered radical electron with the lone pair of another heteroatom in a separate molecule. Examples are the coupling of RS<sup>•</sup> with RS<sup>-</sup> (eq. 26) or R<sub>2</sub>S<sup>•+</sup> with R<sub>2</sub>S (eq. 40/40a).

But what about the *intramolecular* coupling process or, to take a particular example, what are the dynamics of the two sulfurs in 1,3-bis(methylthio)propane to yield radical cation **7** after one of the sulfurs has been oxidized? All attempts to follow the presumed molecular folding in any of the dithia compounds with sulfur-sulfur separations of up to five carbon atoms, i.e., to resolve the S $\cdots$ S formation from the initial oxidation of one of the sulfurs on the conventional pulse radiolysis time scale (> 10 ns) have failed. The answer to this puzzle could only be provided indirectly by other techniques which, incidentally, emphasizes the value of complementary experimental approaches.

One hint comes from photoelectron spectroscopy which indicates, through spectral splitting, prevalence of sulfur-sulfur interaction already in the unoxidized ground state of the dithia compounds.<sup>132</sup>

Even better corroborating information is provided by the electrochemical method of cyclic voltammetry.<sup>140,141</sup> The following data in Table II on the first oxidation peak potentials of various MeS(CH<sub>2</sub>)<sub>n</sub>SMe with n=1-4, together with the  $\lambda_{\max}$  of the respective *intramolecular* (S $\cdots$ S)<sup>+</sup> radical cations illustrate the issue.

First of all, the electrochemical oxidation of the dithia compounds occurs at significantly lower potentials than that of a monosulfide, clearly indicating some neighboring group influence on this process. Secondly, within the dithia compound series the oxidation peak potentials parallel the trend observed for the optical transition energies of the *intramolecular* three-electron bonded radical cations, with the lowest E<sub>p</sub> coinciding with the most blue-shifted  $\lambda_{\max}$ .

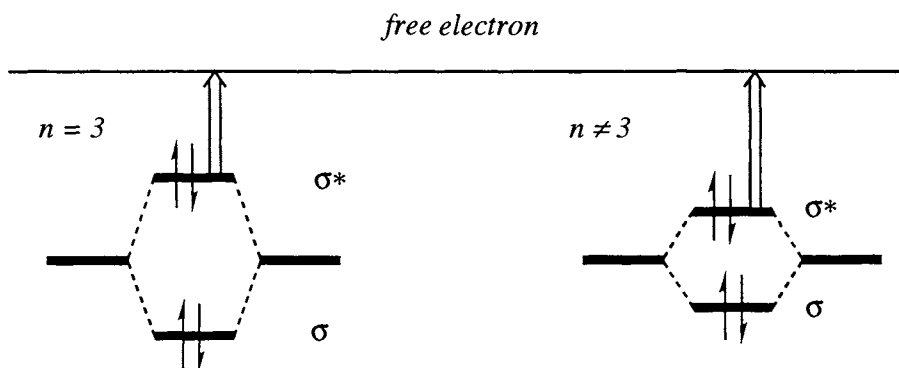
TABLE II

First oxidation peak potentials for  $\text{Me}_2\text{S}$  and various  $\text{MeS}(\text{CH}_2)_n\text{SMe}$  with  $n=1-4$ , together with the  $\lambda_{\text{max}}$  of the respective *intramolecular*  $(\text{S}\cdots\text{S})^+$  radical cations.

compound	1. oxid. peak ( $E_p$ ), V	$\lambda_{\text{max}}$ , nm
$\text{Me}_2\text{S}$	1.450	
-----		
-S-1-S-	1.130	660
-S-2-S-	1.095	525
-S-3-S-	0.742	440
-S-4-S-	0.900	460

( $E_p$  measured in acetonitrile with 0.1 N TEAP against 0.1 N  $\text{Ag}/\text{AgNO}_3$ )

This fact, namely, that characteristic features of the one-electron oxidation product are reflected already in a process involving the still unoxidized molecule can only be rationalized under the assumption of a preexisting sulfur-sulfur interaction in the ground state. As shown in the following simplified scheme for  $\text{RS}(\text{CH}_2)_n\text{SR}$  with  $n = 3$  and  $n \neq 3$ , the two interacting sulfur lone pairs generate  $\sigma$  and  $\sigma^*$  energy levels, both doubly occupied. Their separation is highest and oxidation (i.e., removal of a  $\sigma^*$ -electron), accordingly, requires the least energy when the molecular structure facilitates optimal sulfur p-orbital overlap. This is the case for  $n = 3$ . The principle relationship with the optical transitions (*vide supra*) is obvious.



While this clearly explains the failure to observe an *intramolecular* coupling by diffusion or folding on the ns- $\mu\text{s}$  pulse radiolysis time scale, some molecular relaxation is, nevertheless, bound to occur in the radical cation after



one of the antibonding electrons has been removed in the oxidation process. But this happens at a much shorter times, requiring different observation techniques.

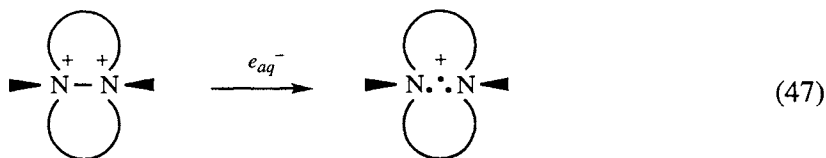
Sulfur-sulfur interaction dynamics involving folding of a molecular structure and taking place on a relatively long time scale becomes observable, however, for larger molecular units in which both sulfurs are located very far from each other. Most recently, Bobrowski *et al.* observed such a process when oxidizing polypeptides in which two methionine units were linked by up to four proline spacers.<sup>142</sup>

#### 5.4 Odd-electron bonds between other identical heteroatoms

All of what has been described for sulfur-centered radicals and ions applies, in principle, to corresponding species with other heteroatoms as radical site. Whether it is three- or five-electron bonds, the basis of their establishment is always the interaction of a singly occupied orbital with a lone pair orbital and promotion of one of the electrons into the lowest lying antibonding orbital. The following gives a brief survey on examples with heteroatoms other than sulfur.

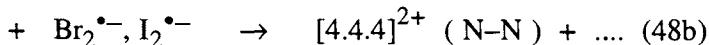
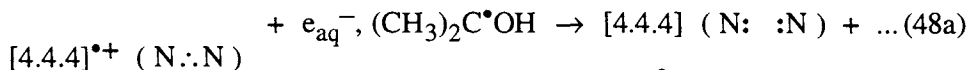
*Group III:* There are even odd-electron bonds involving Group III elements although they lack the lone electron pair. An example is the one-electron bonded  $[(\text{MeO})_3\text{B}\cdot\text{B}(\text{OMe})_3]^-$  radical anion.<sup>143</sup> From a formal electronic point of view, such bonds originate by coupling of a half-filled orbital with an empty orbital, and the bonding glue between the two boron atoms is provided by the one  $\sigma$ -electron and the negative charge they share. With respect to bond strength the one-electron  $1\sigma$  bond thus resembles that of a three-electron  $2\sigma/1\sigma^*$  bond.

*Group V:* Among the odd-electron species involving interaction of identical Group V elements only a limited number of species have been studied. Concerning nitrogen, stabilization of  $\text{N}\cdot\text{N}$  bonds could be achieved especially for radical cations in which the nitrogen atoms were held together by two, or better even three backbone linkages. An example of their generation is the reduction of cyclic hexaalkyl hydrazine dications by hydrated electrons as formulated in eq. 47 for a bicyclic system.<sup>144</sup> Radical cations of this type with 5- and six-membered rings typically absorb in the 450 - 500 nm region. Reduction of these alkyl hydrazine dications by  $e_{\text{aq}}^-$  occurs with rate constants  $>10^{10} \text{ M}^{-1} \text{ s}^{-1}$ .



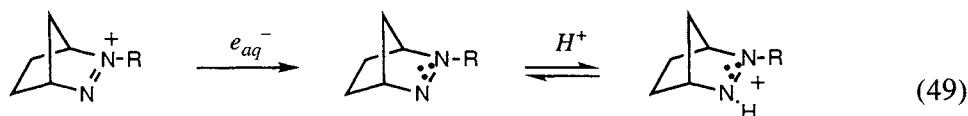
In this context it is interesting that the reduction could not be achieved, however, with  $(\text{CH}_3)_2\text{C}^\bullet\text{OH}$  radicals despite an estimated overall exothermicity of the reaction. A substantial steric effect on the rate of electron transfer has been suspected.

A particularly stable  $\text{N}:\text{N}$  bonded radical cation prevails in a tricyclic system with four methylene groups in each of the three  $\text{N},\text{N}$ -linking bridges as in the 1,6-diazabicyclo[4.4.4] dodecane radical cation (abbreviated,  $[\text{4.4.4}]^{\bullet+}$ ). In fact, as tetrafluoroborate salt it is persistent and can be bottled. This enabled a convenient study of its reactions with radiation chemically generated highly reactive species.<sup>145</sup> The results on these radical-radical reactions are consistent with the features of shorter-lived  $\text{N}:\text{N}$ -bonded radical cations which otherwise could only be studied with respect to reactions with non-radical partners. The finding that  $[\text{4.4.4}]^{\bullet+}$  is easily reduced (e.g., by  $e_{aq}^-$  and some  $\alpha$ -hydroxyalkyl radicals) as well as oxidized (e.g., by  $\text{Br}_2^{\bullet-}$  and  $\text{I}_2^{\bullet-}$ ) (eqs. 48a,b) with almost equal rates reflects, at least to some extent, that both products, the diamine and the hydrazine dication, are similarly stable molecules.  $[\text{4.4.4}]^{\bullet+}$  is, however, not only engaged in redox processes but reacts also very efficiently with H-atom abstracting radicals such as  $^\bullet\text{OH}$ ,  $^\bullet\text{CH}_3$ ,  $\alpha$ -hydroxyalkyl radicals (in competition with eq. 48a), and even  $(\text{CH}_3)_3\text{S}^\bullet$ . These close to diffusion controlled reactions can only be rationalized in terms of a highly labile  $\text{C-H}$  bond which receives its activation through the neighboring  $2\sigma/1\sigma^*$  bond.



Analogues to the five-electron bonded  $2\sigma/2\pi/1\pi^*$  disulfide radical cations in nitrogen-based systems, namely, hydrazine radical cations could be generated by one-electron reduction of trialkyl diazenium salts (eq. 49) and subsequent equilibration of the neutral product radical with its protonated form. The  $\text{pK}$  of the  $\text{R}=\textit{t}$ -butyl substituted species, incidentally, is 7.0, 2.6 units below that of the parent hydrazine compound. The results emphasize the importance of structural parameters, in particular those which control orbital orientation and overlap.<sup>146,147</sup> The alternative possibility to generate such

radical species would be a radical-induced one-electron oxidation of hydrazine derivatives ( $>N-N<$ ). Corresponding studies<sup>148</sup> using  $\bullet OH$  radicals as oxidant yielded, however, ambiguous results for reasons of competing processes and overlapping optical absorptions.



Concerning other Group V elements, some low temperature (77 K) ESR radiation studies have verified the existence of  $2\sigma/1\sigma^*$  radical cations with P: $\cdot$ P and As: $\cdot$ As bonds.<sup>149,150</sup> In solution, only one mention has been made, namely, on  $(Et_3P:\cdot PEt_3)^+$ .<sup>151</sup> In this case assignment was made on the basis of a transient optical absorption at 385 nm obtained upon reaction of  $\bullet OH$  radicals with triethyl phosphine in pulse irradiated aqueous solution at pH >7. The high pH was necessary to prevent the phosphorus from protonation and keep the phosphorus lone pair available for both, one-electron oxidation and P-P orbital coupling.

*Group VI:* No room temperature example has been reported for oxygen-oxygen three-electron bonds. They are apparently extremely unstable. In case of the hypothetical  $(H_2O:\cdot OH_2)^+$ , as opposed to the relatively stable  $(H_2S:\cdot SH_2)^+$ , theory has provided a special clue in that the thermodynamically favored species is not the three-electron bonded species but a  $(H_3O^+ \cdot OH)$  ion-radical couple.<sup>109,110</sup>

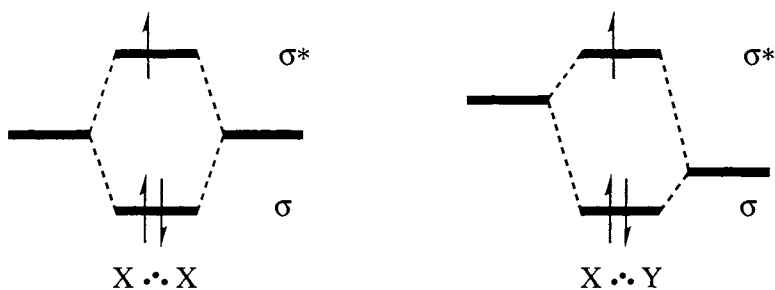
For all other species mentioned here, theory clearly supports the three-electron concept. Generally, the higher the heteroatoms are located in the periodic table, i.e., the more versatile and softer the electronic structure of the heteroatom becomes, the greater the thermodynamic stability of the  $2\sigma/1\sigma^*$  bonds is predicted to be. It must be emphasized, however, that so far only a limited number of reliable experimental verifications have been made. Optically, a series of aliphatic *intra*- and *intermolecular*  $(>Se:\cdot Se<)^+$  radical cations exhibit very similar  $\lambda_{max}$  as their sulfur-analogues, particular with respect to the trends discussed at length for the sulfur-centered species.<sup>126,140</sup> A significant difference becomes, however, apparent with respect to the kinetic stability of the selenium based radical cations. They seem to be considerably more stable than their sulfur analogues, and under pulse radiolysis conditions their decay is dominated by second order processes, presumably disproportionation.

*Group VII:* The dependence of stability as a function of the heteroatom's positioning in the periodic table becomes even more visible for halogen-based  $(RHal \cdot \cdot HalR)^+$  radical cations. While *intra-* as well as *intermolecular* examples have been described for  $Hal = I$ ,<sup>152,153</sup> (again with general physico-chemical features and trends as for S- and Se-based species) no corresponding radical cations have been reported for organic bromides, chlorides and fluorides ( $Hal = Br, Cl, F$ ). In this context, it should be noted that the inorganic  $(Hal)_2^{\bullet-}$  radical anions are also  $2\sigma/1\sigma^*$  three-electron bonded with the thermodynamic stability evidently decreasing in the  $I_2^{\bullet-} > Br_2^{\bullet-} > Cl_2^{\bullet-}$  series and  $F_2^{\bullet-}$  not stabilized at all anymore in solution.

## 5.5 Three-electron bonds between different heteroatoms

### 5.5.1 $S \cdot \cdot X$ species with $X = N, P, Se, Cl, Br,$ and $I$

The concept of  $\sigma^*$  or  $\pi^*$  odd-electron bonds implies that, in principle, they may be established between any heteroatoms irrespective of whether these are of the same or different kind. Experimental evidence has been gathered, in particular, for  $X \cdot \cdot Y$  ( $2\sigma/1\sigma^*$ ) coupled cationic, neutral and anionic radicals with one of the heteroatoms being sulfur and the other N, P, O, Se, Cl, Br, or I. A first important consideration concerning this kind of species is that the thermodynamic stability of an  $X \cdot \cdot Y$  bond is generally not as high as that of a symmetric  $X \cdot \cdot X$  system since the energy levels of X and Y are usually different and consequently the gain in bond energy upon interaction becomes smaller. This can be rationalized from the corresponding MO diagrams in the following scheme.



A substantial number of investigations has been devoted to sulfur-halogen interactions, particularly neutral  $R_2S \cdot \cdot X$  radicals.<sup>56,122,154,155</sup> For  $X =$  iodine and bromine such species can be generated via oxidation of the sulfide and subsequent association of  $R_2S^{\bullet+}$  with the halide anion, or via ligand

displacement within an  $S \cdot : S \rightleftharpoons S \cdot : X$  equilibrium (eqs. 50/51). Alternatively, the halide may first be oxidized to the  $X_2^{\bullet -}$  radical anion which then enters into ligand exchange equilibrium (52).

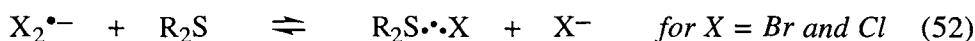
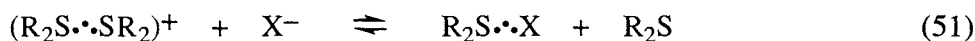
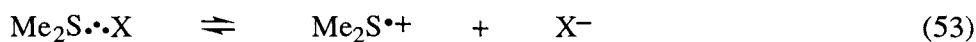


Table III lists some informative data concerning the neutral  $Me_2S \cdot \cdot I$ ,  $Me_2S \cdot \cdot Br$ , and  $Me_2S \cdot \cdot Cl$  radicals. Their optical absorptions, for example, are seen to vary slightly with the nature of the halogen and to lie between those of  $(Me_2S \cdot \cdot SMe_2)^+$  (465 nm) and the respective  $X_2^{\bullet -}$ . Particularly interesting are the equilibrium constants  $K_{53}$  and  $K_{54}$ , referring to ionic (eq. 53) and atomic (eq. 54) dissociation since they again shed some light on general electronic features of  $X \cdot : Y$  three-electron bonds.



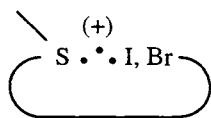
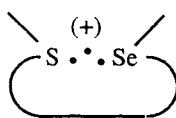
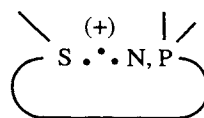
Not surprisingly, ionic dissociation increases with increasing difference in electronegativity between S and X. Accordingly,  $Me_2S \cdot \cdot Cl$  is the least stabilized in this respect. Atomic dissociation, on the other hand, is most favored for  $Me_2S \cdot \cdot I$ . In fact, this is also the only system in which atomic dissociation dominates over ionic dissociation ( $K_{54} > K_{53}$ ) and in this context it is noted that iodine is the only halogen with a lower electronegativity than sulfur (2.4 vs. 2.5). Generally, one should expect that, upon dissociation of the three-electron bond, two of the electrons stay with the more electronegative heteroatom while the third electron remains unpaired at the more electropositive one. The above data make, accordingly, a lot of sense, not only with respect to their qualitative trend but also from the quantitative point of view. As such, they serve as an excellent example for the potential of pulse radiolysis to generate highly accurate and thus meaningful data in mechanistically complex reaction systems.

TABLE III

Optical data and equilibrium constants concerning  $\text{Me}_2\text{S} \cdot \cdot \text{X}$  radicals

$\text{Me}_2\text{S} \cdot \cdot \text{X}$	$\lambda_{\text{max}}$ , nm	$K_{53}$	$K_{54}$
$\text{Me}_2\text{S} \cdot \cdot \text{I}$	410	$< 10^{-7}$	$4.4 \times 10^{-5}$
$\text{Me}_2\text{S} \cdot \cdot \text{Br}$	400	$8.2 \times 10^{-6}$	$4.2 \times 10^{-10}$
$\text{Me}_2\text{S} \cdot \cdot \text{Cl}$	390	$1.2 \times 10^{-2}$	$< 10^{-11}$

Examples for anionic species are rare and only some  $(\text{RS} \cdot \cdot \text{Br})^-$  have been observed.<sup>156</sup> Radical cations have, however, been detected much more frequently. They include, for example, *intramolecular* sulfur-bromine, -iodine, -selenium, -nitrogen, and -phosphorus species of the general types **15**, **16**, and **17**.<sup>140,151,157-161</sup>

**15****16****17**

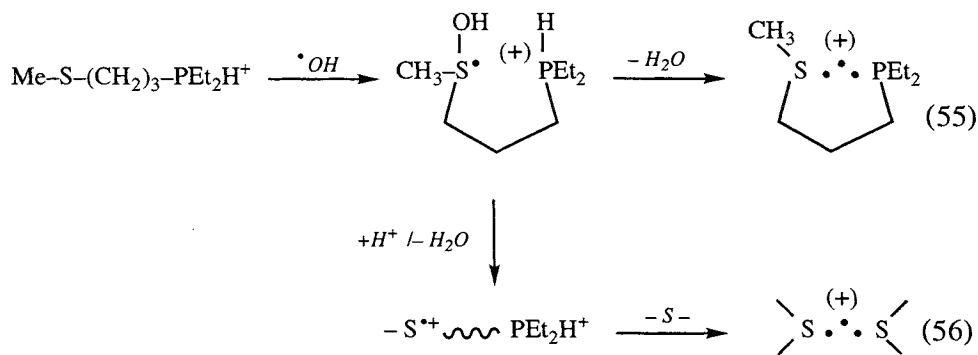
With regard to optical absorptions, influence of substituents and molecular structure all observed trends follow the same rules as outlined for the  $(\text{S} \cdot \cdot \text{S})^+$  radical cations. The most stable  $(\text{S} \cdot \cdot \text{X})^+$  radical cations are those *intramolecular* species which attain five-membered ring structures, i.e., those with, for example, three linking carbons between the two heteroatoms. Particularly interesting are the  $\text{S} \cdot \cdot \text{Br}$  bonded systems since they represent a rare example of bromine-based cationic species in organic chemistry.

### 5.5.2 Site of oxidative attack

For all the molecules with two different heteroatoms the question arises at which of them the initial oxidation actually occurs. In the most simple-minded approach, one expects this to be the atom with the lowest ionization energy. However, this is not necessarily the case and probably applies only to systems where the two heteroatoms are, in fact, prevented from establishing an *intramolecular* three-electron bond and constitute completely isolated targets. In these cases only *intermolecular* coupling needs to be considered.

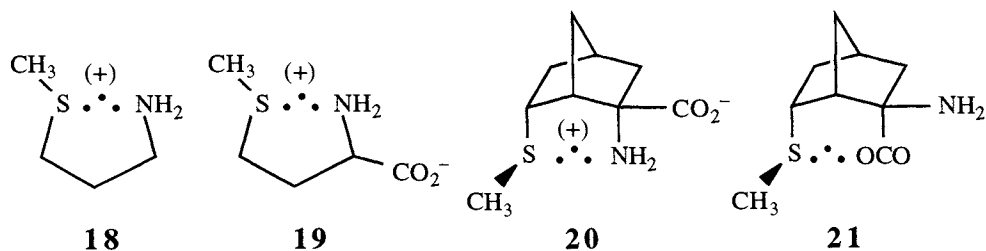
For all other cases two specific situations can be addressed. The first is concerned with systems where the three-electron bonds are readily formed despite the lack of a free electron pair on one of the heteroatoms. The second deals with the oxidation of compounds where both heteroatoms do provide free electron pairs but their individual ionization potentials become, nevertheless, irrelevant.

An example for the first category is the  $\cdot\text{OH}$ -induced formation of an S:P coupled radical cation in aqueous solutions at a pH at which the phosphine functionality is protonated, i.e., present as phosphonium.<sup>140</sup> The only target for oxidation in this case is sulfur and the mechanism can only proceed via an  $\cdot\text{OH}$ -addition to this atom. This is then followed by *intramolecular* water elimination, as schematically depicted in eq. 55 for the oxidation of 1-(methylthio)-3-(diethylphosphino)propane. The active involvement of the phosphonium proton becomes apparent upon lowering the pH to  $\leq 3$  where external bulk protons can successfully compete for the removal of hydroxide from the  $>\text{S}^+\text{OH}$  function. As a result, the S:P absorption (385 nm) is replaced by the S:S absorption ( $\approx 485$  nm) of the *intermolecular* dimer radical cation (eq. 56).



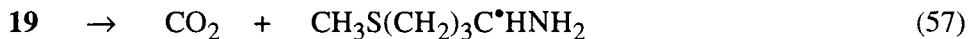
The second situation has already been dealt with in the section on the "Molecular dynamics of three-electron bond formation". Whenever both heteroatoms provide a free electron pair in the ground state (e.g., for the above example in basic solution) there will be "lone pair - lone pair" interaction already prior to oxidation, and the latter will then take place from the joint used, doubly occupied  $\sigma^*$  level. The question at which heteroatom the initial oxidation occurs becomes, therefore, irrelevant.

The radiation chemical study of sulfur-nitrogen coupled analogues have found special interest in quite a variety of other fields and triggered off many complementary investigations.



Radical cation **18**, exhibiting a strong absorption at 385 nm and a long lifetime in the upper microsecond domain,<sup>161</sup> for example, proved an excellent target for time-resolved resonance Raman spectroscopy. The fundamental vibrational S: $\cdot$ N stretching frequency of 290 cm<sup>-1</sup> is considerably smaller than that of a normal S–N  $\sigma$ -bond which, by analogy with an S–S bond in disulfides, should be on the order of 500 cm<sup>-1</sup>.<sup>126,127</sup> Density functional theory (UB3LYP / 6-311G(d,p)) revealed that there may be two possible and energetically close conformers for which, respectively, frequencies of 256 and 265 cm<sup>-1</sup>, S: $\cdot$ N distances of 2.581 and 2.586 Å, and  $\lambda_{\max}$  372 and 367 nm were calculated.<sup>162</sup> All these data clearly support the  $\sigma^*$  structure.

The overall zwitterionic radical **19** derived from methionine turned out to be a transient of general importance in the free-radical-induced oxidation of amino acids as it is the species which leads to decarboxylation.<sup>160</sup>



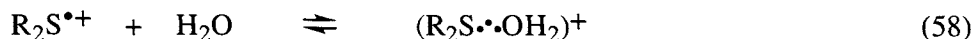
The significance of this process, in terms of free radical chemistry, is that the decarboxylation results in the formation of  $\alpha$ -amino radicals which are powerful reductants and cause a drastic change in the system's redox capacity.<sup>163</sup> The lifetime of **19** with respect to reaction 57 is very short ( $t_{1/2} \approx 200$  ns). However, the  $\cdot\text{OH}$  or one-electron induced decarboxylation of simple amino acids occurs much faster, presumably on the picosecond time scale (as mentioned above in the section on "aminyl radicals").<sup>20,21</sup> The presence of the sulfide function in methionine thus not only offers a possibility for initiation of the decarboxylation at a location originally remote from the amino acid moiety, it also allows this process at a pH where the amino group is protonated (according to a mechanism outlined, in principle, in eq. 55). But most importantly, the S: $\cdot$ N coupling slows down the actual decarboxylation by many orders of magnitude. In this context it is interesting to note that seleno analogue of **19** (Se: $\cdot$ N) has even a lifetime of close to 100  $\mu\text{s}$ , serving as another experimental example for the increase in stability of the three-electron bond with increasing atomic number.<sup>99,164</sup>



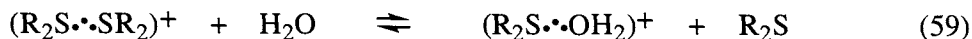
A valid question which may be posed in connection with the methionine example is whether the initially oxidized sulfur couples only with nitrogen or possibly also with an oxygen from the carboxylate function. An answer to this was provided by synthesis of two norbornane-based stereo isomers in which the amino and carboxylate groups were fixed in their position relative to sulfur.<sup>165</sup> The respective transients **20** and **21** formed upon oxidation exhibit maxima at 400 and 340 nm and lifetimes of about 1 and 25  $\mu$ s, respectively. These data clearly speak for an S $\cdot$ :N coupling in the methionine system. Furthermore, **20** decarboxylates directly, while **21** rather appears to deprotonate (at carbon adjacent to sulfur).

### 5.5.3 Sulfur-oxygen interaction

The  $>\text{S}\cdot\cdot\text{O}(\text{O})\text{C}^-$  species touches on another aspect of general interest, namely, the establishment of a three-electron bond between two elements of very different electronegativity. Any sulfur-oxygen interaction, in principle, constitutes an extreme situation with respect to an asymmetry in the MO energy diagram. One of the most relevant examples is probably the association of a water molecule to an oxidized sulfur radical cation, as formulated in eq. 58.<sup>56</sup>



The strength of the sulfur-oxygen bond in this species has been estimated to *ca* 70 kJ mol<sup>-1</sup>,<sup>113</sup> allowing to view the  $\text{R}_2\text{S}^{\bullet+}$  radical cation in aqueous solution as a well defined bimolecular species. The magnitude of the bond strength would also nicely explain why the presumably weakest of all dimer sulfide complexes, namely, the all-*t*-butyl substituted  $(t\text{-Bu}_2\text{S}\cdot\cdot\text{S}t\text{-Bu}_2)^+$  could not be detected in aqueous environment. Its extrapolated S $\cdot\cdot$ S bond strength becomes smaller than that for the  $(t\text{-Bu}_2\text{S}\cdot\cdot\text{OH}_2)^+$  radical and equilibrium 59 is completely shifted to the right hand side.



In view of  $(\text{R}_2\text{S}\cdot\cdot\text{OH}_2)^+$  being a distinct species it would not be unreasonable to also formulate the  $\cdot\text{OH}$ -adduct to a sulfide function, i.e.,  $\text{R}_2\text{S}^{\bullet}(\text{OH})$  as three-electron bonded radical  $\text{R}_2\text{S}\cdot\cdot\text{OH}$ . However, being a neutral species, the latter cannot benefit anymore from any stabilization due to charge delocalization. The unpaired electron will, therefore, be driven towards the more electro-positive sulfur by the full impact of electronegativity difference between the two heteroatoms and, therefore, the sulfuranyl notation,  $>\text{S}^{\bullet}-\text{OH}$ , may thus

describe the actual electronic situation more accurately. In line with these considerations, also species **21** may not contain a true  $2\sigma/1\sigma^*$  bond but instead perhaps be better described by a coulombic interaction between the oxidized sulfur and the carboxylate group,  $>S^{\bullet+} \leftrightarrow -OOC^-$ .<sup>166</sup>

There are a few more sulfur-oxygen linked radicals which have been characterized by pulse radiolysis and may reasonably be addressed as S...O bonded species. They all require very rigid conditions for their stabilization and depend on the steric forces which hold the two interacting atoms in close proximity.<sup>166,167</sup>

Clearly, with the sulfur-oxygen interactions we are approaching the limits of the  $2\sigma/1\sigma^*$  concept.

## 6 CONCLUDING REMARKS AND OUTLOOK

Radiation, when impacting on matter, causes physical and chemical changes. Ionizations and radical formation are the main chemical consequences and, accordingly, it has been Radiation Chemistry's most legitimate initial task in the wake of the discovery of these effects to study and quantify them in detail. With the maturing of the field, however, the Free Radical Chemistry community increasingly, in a way, turned the argument around and took advantage of the great potential radiation chemical methods offered as a powerful tool for the investigation of free radicals and ions, in general. For Radiation Chemistry itself this provided the chance to significantly widen its impact horizon. The fact that many research fields have benefitted from the contribution made from radiation chemical laboratories could hopefully be indicated by the selected examples concerning heteroatom-centered radicals in this article. As pointed out in the introductory section it could not nor was it intended to provide a comprehensive review but focused only on some basic concepts which emerged from these studies. However, these are an important aspect for the understanding and further research of complex chemical reaction mechanism, with the radical related DNA chemistry perhaps serving as one of the most prominent examples. But also the odd-electron bond concept, presented here in the context of heteroatom-centered radicals, clearly has its implications on quite a variety of parameters such as bond breakage, bond formation, control of redox properties, neighboring group participation, transfer and parking of reactivity, and long range electron transfer. A major role in all this is played or based on phenomena related to heteroatom-centered radicals.

As for future research and perspectives concerning heteroatom-centered radicals in general, there are still many gaps to fill and interesting questions to

follow up as mentioned and outlined at various places in the context of the examples discussed above. A general challenge is to test the principles, which have emerged from the relatively elementary studies, in complex molecular systems. Such investigations will become of increasing importance particularly for material and bio sciences which direct their focus more and more to larger molecules and molecular assemblies.

## 7 ACKNOWLEDGEMENT

The support received from the Office of Basic Energy Sciences of the U.S. Department of Energy is gratefully acknowledged. This is document No. NDRL-4156 of the Notre Dame Radiation Laboratory.

## 8 REFERENCES

1. Z. B. Alfassi (ed.), Peroxyl Radicals, John Wiley & Sons, Chichester, New York, Weinheim, Brisbane, Singapore, Toronto, 1996.
2. Z. B. Alfassi (ed.), N-Centered Radicals, John Wiley & Sons, Chichester, New York, Weinheim, Brisbane, Singapore, Toronto, 1996.
3. Z. B. Alfassi (ed.), S-Centered Radicals, John Wiley & Sons, Chichester, New York, Weinheim, Brisbane, Singapore, Toronto, 1996.
4. C. Chatgililoglu and K.-D. Asmus (eds.), Sulfur-Centered Reactive Intermediates in Chemistry and Biology, NATO-ASI Vol 197, Plenum Press, New York, London, 1990.
5. G. N. R. Tripathi, In: Time-Resolved Spectroscopy, R. J. H. Clark and R. E. Hester (eds.), John Wiley & Sons: Chichester, New York, Brisbane, Toronto, Singapore, 1989; Vol. 18, pp 157.
6. G. Beck, Int. J. Radiat. Phys. Chem., 1 (1969) 361.
7. K. H. Schmidt and W. L. Buck, Science, 171 (1966) 70.
8. K.-D. Asmus and E. Janata, In: The Study of Fast Processes and Transient Species by Electron Pulse Radiolysis, J. H. Baxendale and F. Busi (eds.), D. Reidel, Dordrecht, 1982, pp 91.
9. K.-D. Asmus, A. Wigger and A. Henglein, Ber. Bunsenges. Phys. Chem., 70 (1966) 862.
10. K.-D. Asmus, A. Henglein and G. Beck, Ber. Bunsenges. Phys. Chem., 70 (1966) 459.
11. K.-D. Asmus and I Taub, J. Phys. Chem., 72 (1968) 3382.
12. K. Eiben and R. W. Fessenden, J. Phys. Chem., 72 (1968) 3387.
13. K.-D. Asmus, G. Beck, A. Henglein and A. Wigger, Ber. Bunsenges. Phys. Chem., 70 (1966) 869.

14. P. Wardman, *J. Phys. Chem. Ref. Data*, 18 (1989) 1637.
15. J. Kapoldova, J. Liebster and A. Babicky, *Int. J. Appl. Radiat. Isot.*, 13 (1962) 617.
16. H. Paul and H. Fischer, *Helv. Chim. Acta*, 54 (1971) 485.
17. P. Neta and R. W. Fessenden, *J. Phys. Chem.*, 75 (1971) 738.
18. J. Mönig, R. Chapman and K.-D. Asmus, *J. Phys. Chem.*, 89 (1985) 3139.
19. M. Bonifačić, I. Štefanić, G. L. Hug; D. A. Armstrong and K.-D. Asmus, *J. Am. Chem. Soc.*, 120 (1998) 9930.
20. G. L. Hug, M. Bonifačić, K.-D. Asmus, D. A. Armstrong, *J. Phys. Chem. B*, 104 (2000) 6674.
21. M. Bonifačić and K.-D. Asmus, to be published.
22. M. Canle L., J. A. Santaballa and S. Steenken, *Chem. Eur. J.*, 5 (1999) 1192.
23. M. Bonifačić, D. A. Armstrong, I. Carmichael and K.-D. Asmus, *J. Phys. Chem. B*, 104 (2000) 643-649.
24. D. A. Armstrong, A. Rauk and D. Yu, *J. Chem. Soc., Perkin Trans.*, 2 (1995) 553.
25. C. von Sonntag and H.-P. Schuchmann, *Angew. Chem.*, 103 (1991) 1255.
26. K.-D. Asmus and M. Bonifačić, In: *Exercise and Oxygen Toxicity*; C. K. Sen, L. Packer and O. Haenninen (eds), Elsevier, Amsterdam, 1994, pp 1.
27. B. C. Gilbert, R. G. G. Holmes, H. A. H. Laue and R. O. C.; Norman, *J. Chem. Soc., Perkin Trans. 2*, (1967) 1047.
28. H.-P. Schuchmann and C. von Sonntag, *J. Photochem.*, 16 (1981) 289.
29. L. Qin, G. N. R. Tripathi and R. H. Schuler, *Z. Naturforsch. A*, 409 (1985) 1026.
30. G. N. R. Tripathi and R. H. Schuler, *J. Chem. Phys.*, 86 (1987) 3795.
31. G. N. R. Tripathi and R. H. Schuler, *Chem. Phys. Lett.*, 110 (1984) 542.
32. G. N. R. Tripathi, R. H. Schuler and L. Qin, In: *Time-Resolved Vibr. Spectrosc.*, Proc. Int. Conf. Emil-Warburg Symp., A. Lauberau and M. Stockberger (eds), Springer, Vol. Proc. Phys. 4, 1985, pp 183.
33. R. L. Willson, In: *Radioprotectors and Anticarcinogens*, O. F. Nygaard and M. G. Simic (eds), Academic Press: New York, 1983, pp 1.
34. C. von Sonntag, *The Chemical Basis of Radiation Biology*; Taylor and Francis, London, 1987.
35. C. Schöneich, M. Bonifačić and K.-D. Asmus, *Free Rad. Res. Comms.*, 6 (1989) 393.
36. C. Schöneich, M. Bonifačić, U. Dillinger and K.-D. Asmus, In: *Sulfur-Centered Reactive Intermediates in Chemistry and Biology*, C. Chatgililoglu and K.-D. Asmus (eds.), NATO-ASI Vol 197, Plenum Press, New York, London, 1990, pp 367.
37. C. Schöneich, U. Dillinger, F. von Bruchhausen and K.-D. Asmus, *Arch. Biochem. Biophys.*, 292 (1992) 456.
38. T. F. Slater, *Free Radicals Mechanism in Tissue Injury*, Pion Ltd., London, 1972.
39. M. S. Akhlaq, H.-P. Schuchmann and C. von Sonntag, *Int. J. Radiat. Biol.*, 51 (1987) 91.
40. R. Zhao, J. Lind, G. Merényi and T. Eriksen, *J. Am. Chem. Soc.*, 116 (1994) 12010.
41. L. Grierson, K. Hildenbrand and E. Bothe, *Int. J. Radiat. Biol.*, 62 (1992) 265.

42. C. Schöneich, K.-D. Asmus, U. Dillinger and F. von Bruchhausen, *Biochem. Biophys. Res. Commun.*, 161 (1989) 113.
43. J. Schwinn, H. Sprinz, K. Drößler, S. Leistner and O. Brede, *Int. J. Radiat. Biol.*, 74 (1998) 359.
44. M. Tamba, G. Simone and M. Quintiliani, *Int. J. Radiat. Biol.*, 50 (1986) 595.
45. X. Zhang, N. Zhang, H.-P. Schuchmann and C. von Sonntag, *J. Phys. Chem.*, 98 (1994) 6541.
46. H.-P. Schuchmann and C. von Sonntag, In: *Peroxy Radicals*, Z. B. Alfassi (ed.), John Wiley & Sons, Ltd, New York, 1997, pp 439.
47. G. G. Jayson, D. A.; Stirling and A. J. Swallow, *Int. J. Radiat. Biol.*, 19 (1971) 143.
48. Y. Razskazovskii and M. Y. Mel'nikov, *Sov. J. Chem. Phys. (Engl. Transl.)*, 10 (1992) 148.
49. M. D. Sevilla, D. Becker and M. Yan, *Int. J. Radiat. Biol.*, 57 (1990) 65.
50. C. Chatgililoglu, C. Schöneich and K.-D. Asmus, unpublished results.
51. D. A. Armstrong, In: *Sulfur-Centered Reactive Intermediates in Chemistry and Biology*, C. Chatgililoglu and K.-D. Asmus (eds.), NATO-ASI Vol 197, Plenum Press, New York, London, 1990, pp 121.
52. L. G. Forni, J. Mönig, V. O. Mora-Arellano and R. L. Willson, *J. Chem. Soc., Perkin Trans. 2*, (1983) 961.
53. C. Dunster and R. L. Willson, In: *Sulfur-Centered Reactive Intermediates in Chemistry and Biology*, C. Chatgililoglu and K.-D. Asmus (eds.), NATO-ASI Vol 197, Plenum Press, New York, London, 1990, pp 377.
54. L. F. Forni and R. L. Willson, *Biochem. J.*, 240 (1986) 897.
55. K.-D. Asmus, In: *Radioprotectors and Anticarcinogens*, O. F. Nygaard and M. Simic (eds.), Academic Press, New York, London, Paris, San Diego, San Francisco, Sao Paulo, Sydney, Tokyo, Toronto, 1983, pp 23.
56. K.-D. Asmus, In: *Sulfur-Centered Reactive Intermediates in Chemistry and Biology*, C. Chatgililoglu and K.-D. Asmus (eds.), NATO-ASI Vol 197, Plenum Press, New York, London, 1990, pp 155.
57. S. P. Mezyk, *J. Phys. Chem.*, 100 (1996) 8295.
58. M. Bonifačić and K.-D. Asmus, *Int. J. Radiat. Biol.*, 46 (1984) 35.
59. R. L. Willson, *Chem. Commun.*, (1970) 1425.
60. M. Z. Hoffman and E. Hayon, *J. Am. Chem. Soc.*, 94 (1972) 7920.
61. M. Faraggi, J. L. Redpath and Y. Tal, *Radiat. Res.*, 64 (1975) 452.
62. C. von Sonntag, In: *Sulfur-Centered Reactive Intermediates in Chemistry and Biology*, C. Chatgililoglu and K.-D. Asmus (eds.), NATO-ASI Vol 197, Plenum Press, New York, London, 1990, pp 359.
63. J. P. Barton and J. E. Packer, *Int. J. Radiat. Phys. Chem.*, 2 (1970) 159.
64. P. C. Chan and B. H. J. Bielski, *J. Am. Chem. Soc.*, 95 (1973) 5504.

65. O. I. Micic, V. M. Markovic and M. T. Nenadovic, *Bull. Soc. Chim. Beograd*, 40 (1975) 277.
66. N. Zhang, H.-P. Schuchmann and C. von Sonntag, *J. Phys. Chem.*, 95 (1991) 4718.
67. M. Bonifačić, private communication.
68. M. Z. Hoffman and E. Hayon, *J. Phys. Chem.*, 77 (1973) 990.
69. M. Bonifačić, J. Weiss, S. A. Chaudhri and K.-D. Asmus, *J. Phys. Chem.*, 89 (1985) 3910.
70. G. N. R. Tripathi, Q. Sun, D. A. Armstrong, D.M. Chipman and R. H. Schuler, *J. Phys. Chem.*, 96 (1992) 5344.
71. M. Göbl, M. Bonifačić and K.-D. Asmus, *J. Am. Chem. Soc.*, 106 (1984) 5984.
72. S. A. Everett, C. Schöneich, J. H. Stewart and K.-D. Asmus, *J. Phys. Chem.*, 96 (1992) 306.
73. G. H. Morine and R. R. Kuntz, *Photochem. Photobiol.*, 33 (1981) 1.
74. Z. Wu, T. G. Back, R. Ahmad, R. Yamdagni and D. A. Armstrong, *J. Phys. Chem.*, 86 (1982) 4417.
75. S. A. Everett, L. K. Folkes, P. Wardman and K.-D. Asmus, *Free Rad. Res.*, 20 (1994) 387.
76. M. Bonifačić and E. Anklam, *J. Chem. Soc., Perkin Trans. 2*, (1991) 243.
77. E. Anklam, private communication.
78. M. Bonifačić and K.-D. Asmus, *J. Phys. Chem.*, 88 (1984) 6286.
79. M. Göbl and K.-D. Asmus, *J. Chem. Soc., Perkin Trans. 2*, (1984) 691.
80. K. Bobrowski and C. Schöneich, *J. Chem. Soc., Chem. Commun.*, (1993) 795.
81. K. Bobrowski, G. L. Hug, B. Marciniak, B. Miller and C. Schöneich, *J. Am. Chem. Soc.*, 119 (1997) 8000.
82. G. Meissner, A. Henglein and G. Beck, *Z. Naturforsch. B*, 22 (1967) 13.
83. M. Bonifačić, H. Möckel, D. Bahnemann and K.-D. Asmus, *J. Chem. Soc., Perkin Trans. 2*, (1975) 675.
84. K.-D. Asmus, D. Bahnemann, C.-H. Fischer and D. Veltwisch, *J. Am. Chem. Soc.*, 101 (1979) 5322.
85. K.-D. Asmus, *Acc. Chem. Res.*, 12 (1979) 436.
86. J. Mönig, R. Goslich and K.-D. Asmus, *Ber. Bunsenges. Phys. Chem.*, 90 (1986) 115.
87. K.-D. Asmus, *Nukleonika*, 45 (2000) 3.
88. K.-D. Asmus and M. Bonifačić, In: *S-Centered Radicals*, Z. B. Alfassi (ed.), John Wiley & Sons Ltd., New York, 1999, pp 141.
89. S. A. Chaudhri, M. Göbl, T. Freyholtz and K.-D. Asmus, *J. Am. Chem. Soc.*, 106 (1984) 5988.
90. S. A. Chaudhri, H. Mohan, E. Anklam and K.-D. Asmus, *J. Chem. Soc., Perkin Trans. 2*, (1996) 383.
91. E. Janata, D. Veltwisch and K.-D. Asmus, *Radiat. Phys. Chem.*, 16 (1980) 43.
92. L. Engman, J. Lind and G. Merényi, *J. Phys. Chem.*, 98 (1994) 3174.

93. M. Iolele, S. Steenken and E. Baciocchi, *J. Phys. Chem.*, 101 (1997) 2979.
94. H. Mohan and J. P. Mittal, *J. Phys. Chem.*, 101 (1997) 10012.
95. M. Bonifačić and K.-D. Asmus, *J. Phys. Chem.*, 80 (1976) 2426.
96. G. Merenyi, J. Lind and L. Engman, *J. Phys. Chem.*, 100 (1996) 8875.
97. C. Schöneich, A. Aced and K.-D. Asmus, *J. Am. Chem. Soc.*, 115 (1993) 11376.
98. S. F. Nelsen and K.-D. Asmus, unpublished results.
99. A. Assmann, M. Bonifačić, K. Briviba, H. Sies and K.-D. Asmus, *Free Rad. Res.*, 32 (2000) 371.
100. B. C. Gilbert, D. K. C. Hodgeman and R. O. C.; Norman, *J. Chem. Soc., Perkin Trans. 2*, (1973) 1748.
101. M. C. R. Symons, *J. Chem. Soc., Perkin Trans. 2*, (1974) 1618.
102. R. L. Peterson, D. J. Nelson and M. C. R. Symons, *J. Chem. Soc., Perkin Trans. 2*, (1978) 225.
103. W. B. Gara, J. R. M. Giles and B. P. Roberts, *J. Chem. Soc., Perkin Trans. 2*, (1980) 1444.
104. K. Nishikada and Ff. Williams, *Chem. Phys. Lett.*, 34 (1975) 302.
105. T. Clark, *J. Comput. Chem.*, 2 (1981) 261.
106. T. Clark, *J. Comput. Chem.*, 3 (1982) 112.
107. T. Clark, *J. Comput. Chem.*, 4 (1983) 404.
108. T. Momose, T. Susuki and T. Shida, *Chem. Phys. Letters*, 107 (1984) 568.
109. T. Clark, *J. Am. Chem. Soc.*, 110 (1988) 1672.
110. P. M. W. Gill and L. Radom, *J. Am. Chem. Soc.*, 110 (1988) 4931.
111. P. M. W. Gill, P. Weatherhall and L. Radom, *J. Am. Chem. Soc.*, 111 (1989) 2782.
112. A. J. Illies, P. Livant and M. L. McKee, *J. Am. Chem. Soc.*, 110 (1988) 7980.
113. T. Clark, In: *Sulfur-Centered Reactive Intermediates in Chemistry and Biology*, C. Chatgililoglu and K.-D. Asmus (eds.), NATO-ASI Vol 197, Plenum Press, New York, London, 1990, pp 13.
114. Y. Deng, A. J. Illies, M. A. James, M. L. McKee and M. Peschke, *J. Am. Chem. Soc.*, 117 (1995) 420.
115. M. A. James, M. L. McKee and A. J. Illies, *J. Am. Chem. Soc.*, 118 (1996) 7836.
116. S. A. Chaudhri and K.-D. Asmus, *Angew. Chem., Int. Ed. Engl.*, 20 (1981) 672.
117. K.-D. Asmus, H. A. Gillis and G. G. Teather, *J. Phys. Chem.*, 82 (1978) 2677.
118. D. Bahnemann and K.-D. Asmus, *J. Chem. Soc., Chem. Commun.*, (1975) 238.
119. W. K. Musker and T. L. Wolford, *J. Am. Chem. Soc.*, 98 (1976) 3055.
120. W. K. Musker, T. L. Wolford and B. P. Roush, *J. Am. Chem. Soc.*, 100 (1978) 6416.
121. W. K. Musker, *Acc. Chem. Res.*, 13 (1980) 200.
122. K.-D. Asmus, D. Bahnemann, M. Bonifačić and H. A. Gillis, *Faraday Discussions*, 63 (1978) 213.
123. M. Bonifačić and K.-D. Asmus, *J. Org. Chem.*, 51 (1986) 1216.
124. E. Anklam, K.-D. Asmus and H. Mohan, *J. Phys. Org. Chem.*, 3 (1990) 17.

125. R. Wilbrandt, N. H. Jensen, P. Pagsberg, A. H. Sillesen, K. B. Hansen and R. E. Hester, *J. Raman Spectrosc.*, 11 (1981) 24.
126. T. Tobien, PhD thesis, Technical University Berlin, Berlin, Germany, 1997.
127. G. N. R. Tripathi, T. Tobien, I. Carmichael and K.-D. Asmus, unpublished results.
128. T. Drewello, C. B. Lebrilla, K.-D. Asmus and H. Schwarz, *Angew. Chem., Int. Ed. Engl.*, 28 (1989) 1275.
129. T. Drewello, C. B. Lebrilla, K.-D. Asmus and H. Schwarz, *Angew. Chem.*, 101 (1989) 1247.
130. D. Sülzle, T. Drewello and H. Schwarz, In: *Sulfur-Centered Reactive Intermediates in Chemistry and Biology*, C. Chatgililoglu and K.-D. Asmus (eds.), NATO-ASI Vol 197, Plenum Press, New York, London, 1990, pp 185.
131. Sanaulah; H. Hungerbühler, C. Schöneich, M. Morton, D. G. Vander Felde, G. S. Wilson, K.-D. Asmus and R. S. Glass, *J. Am. Chem. Soc.*, 119 (1997) 2134.
132. K.-D. Asmus, unpublished results.
133. G. A. Russell and W. C. Law, In: *Sulfur-Centered Reactive Intermediates in Chemistry and Biology*, C. Chatgililoglu and K.-D. Asmus (eds.), NATO-ASI Vol 197, Plenum Press, New York, London, 1990, pp 173.
134. H. Bock, V. Stein and A. Semkov, *Chem. Ber.*, 113 (1980) 3208.
135. I. Carmichael, et al., unpublished results.
136. H. Möckel, M. Bonifačić and K.-D. Asmus, *J. Phys. Chem.*, 78 (1974) 282.
137. M. Bonifačić, H. Möckel, K. Schäfer and K.-D. Asmus, *J. Phys. Chem.*, 79 (1975) 1496.
138. H. Mohan and K.-D. Asmus, *J. Phys. Chem.*, 92 (1988) 118.
139. M. Bonifačić and K.-D. Asmus, *J. Chem. Soc., Perkin Trans. 2*, (1986) 1805.
140. T. Tobien, H. Hungerbühler and K.-D. Asmus, *Phosphorus, Sulfur, and Silicon*, 95/96 (1994) 249.
141. B. R. Coleman, R. S. Glass, W. N. Setzer, U. D. G. Prabhu and G. S. Wilson, *Adv. Chem. Ser.*, 201 (1982) 417.
142. K. Bobrowski, C. Schöneich and G. L. Hug, private communication.
143. R. L. Hudson and Ff. Williams, *J. Am. Chem. Soc.*, 99 (1977) 7714.
144. S. F. Nelsen, R. W. Alder, R. B. Sessions, K.-D. Asmus, K.-O. Hiller and M. Göbl, *J. Am. Chem. Soc.*, 102 (1980) 1429.
145. R. W. Alder, M. Bonifačić and K.-D. Asmus, *J. Chem. Soc., Perkin Trans. 2*, (1986) 277.
146. S. F. Nelsen, W. P. Parmelee, M. Göbl, K.-O. Hiller, D. Veltwisch and K.-D. Asmus, *J. Am. Chem. Soc.*, 102 (1980) 5606.
147. S. F. Nelsen, J. M. Buschek, M. Göbl and K.-D. Asmus, *J. Chem. Soc., Perkin Trans. 2*, (1984) 11.
148. E. Hayon and M. Simic, *J. Am. Chem. Soc.*, 94 (1972) 42.
149. A. R. Lyons and M. C. R. Symons, *J. Chem. Soc., Faraday Trans. 2*, 68 (1972) 1589.



150. T. Gillbro, C. M. L. Kerr and Ff. Williams, *Mol. Phys.*, 28 (1974) 1225.
151. H. Hungerbühler, S. N. Guha and K.-D. Asmus, *J. Chem. Soc., Chem. Commun.*, (1991) 999.
152. H. Mohan and K.-D. Asmus, *J. Am. Chem. Soc.*, 109 (1987) 4746.
153. H. Mohan and K.-D. Asmus, *J. Chem. Soc., Perkin Trans. 2*, (1987) 1795.
154. M. Bonifačić and K.-D. Asmus, *J. Chem. Soc., Perkin Trans. 2*, (1980) 758.
155. K.-O. Hiller and K.-D. Asmus, *Int. J. Radiat. Biol.*, 40 (1981) 583.
156. J. E. Packer, *J. Chem. Soc., Perkin Trans. 2*, (1984) 1015.
157. E. Anklam, H. Mohan and K.-D. Asmus, *Helv. Chim. Acta*, 70 (1987) 2110.
158. E. Anklam, H. Mohan and K.-D. Asmus, *J. Chem. Soc., Chem. Commun.*, (1987) 629.
159. W. K. Musker, P. S. Surdhar, R. Ahmad and D. A. Armstrong, *Can. J. Chem.*, 62 (1984) 1874.
160. K.-O. Hiller, B. Masloch, M. Göbl and K.-D. Asmus, *J. Am. Chem. Soc.*, 103 (1981) 2734.
161. K.-D. Asmus, M. Göbl, K.-O. Hiller, S. Mahling and J. Mönig, *J. Chem. Soc., Perkin Trans. 2*, (1985) 641.
162. I. Carmichael, *Acta Chem. Scand.*, 51 (1997) 567.
163. K.-O. Hiller and K.-D. Asmus, *J. Phys. Chem.*, 87 (1983) 3682.
164. K.-D. Asmus and M. Bonifačić, to be published.
165. K. Steffen, R. S. Glass, M. Sabahi, G. S. Wilson, C. Schöneich, S. Mahling and K.-D. Asmus, *J. Am. Chem. Soc.*, 113 (1991) 2141.
166. S. Mahling, K.-D. Asmus, R. S. Glass, M. Hojjatie and G. S. Wilson, *J. Org. Chem.*, 52 (1987) 3717.
167. R. S. Glass, M. Hojjatie, G. S. Wilson, S. Mahling, M. Göbl and K.-D. Asmus, *J. Am. Chem. Soc.*, 106 (1984) 5382.

## **Zeolite catalysis studies by radiation chemical methods†**

**D. W. Werst and A. D. Trifunac**

Chemistry Division, Argonne National Laboratory, Argonne, Illinois 60439

### **1 INTRODUCTION**

Ionizing radiation has found applications in the study of heterogeneous catalysis primarily as a means of producing unstable species and reactive intermediates, many of them paramagnetic, whose study can elucidate fundamental issues of structure, mechanisms, transport and reactivity. Fast detection techniques are needed to observe short-lived species and measure their kinetics. However, solid catalysts and microporous solids, by virtue of specific surface-adsorbate interactions, geometric constraints and strong ionic character, possess the ability to stabilize highly reactive species. Thus radiolysis has been used to produce a variety of paramagnetic species that can be characterized by non-time-resolved methods, and in particular, electron paramagnetic resonance (EPR) spectroscopy, at ambient and sub-ambient temperatures.

Intermediates in high-temperature processes have been stabilized at low temperature after  $\gamma$  irradiation of metal oxides and zeolites. Important early examples were oxygen anions,  $O^-$ ,  $O_2^-$  and  $O_3^-$ .<sup>1-3</sup> Some of their reactions with small molecules were also elucidated by EPR. Metal cluster ions have also been produced by radiolysis and stabilized in zeolites. Examples include alkali metal cation clusters<sup>3,4</sup> in faujasites and silver cation clusters<sup>5-8</sup> in zeolite A and in silicoaluminophosphate molecular sieves. Detailed information was obtained from EPR studies about their structure, thermal stability and formation of adducts.

Radical cations can be stabilized inside zeolites and on some amorphous metal oxide surfaces. This was recognized early by the EPR observation of radical cations generated spontaneously upon exposure of certain solid catalysts to easily oxidized species such as aromatic hydrocarbons and certain olefins.<sup>9-13</sup> These observations reveal the presence of electron acceptor sites and, whether or not

---

†Work at Argonne performed under the auspices of the Office of Basic Energy Sciences, Division of Chemical Science, US-DOE under contract number W-31-109-ENG-38.

the radical cations are actual intermediates in catalysis, their detection can shed light on reaction mechanisms.

Similarly, radiolytically produced radical cations can be stabilized in zeolites and related materials. This possibility was exploited by spectroscopists to study the EPR of radical cations and some neutral radicals even before the development of inert matrices such as rare gases and freons for radical cation stabilization.<sup>14,15</sup> Recently, work in our laboratory has developed the use of inert zeolites as microreactors to control radical cation reactions and to study radiation chemistry in heterogeneous systems.<sup>16-26</sup> In the case of active catalysts, radiolysis can potentially produce radical cations of products as well as starting material.<sup>23,27,28</sup> Thus, like the spontaneous oxidation process described above, radiolysis combined with EPR permits a method of post-reaction analysis of products by *in situ* spectroscopy.

It is not practical to cover every topic in this review in which radiation chemical techniques have contributed to the understanding of catalyst function or catalytic reactions. With this introduction as a cursory guide to relevant topics, we move on to a discussion of the radiolytic spin labeling technique for analyzing products of catalytic reactions in zeolites, which has been the main thrust of experiments directed at fundamental aspects of catalysis in our laboratory.

## 2 SPIN LABELING BY IONIZATION

Radiolytic spin labeling of molecules adsorbed in zeolites occurs by ionization to form radical cations and by formation of H-adduct radicals by H atom addition.<sup>26-28</sup> Ionization of adsorbed molecules is a two-step process, equations (1) and (2). Because the adsorbate loading used in experiments is low (typically one percent or less by weight), energy is absorbed by the matrix and not directly by the adsorbate. Holes ( $Z^{**}$ ) created in the zeolite lattice migrate to adsorbate (A) by charge transfer. Stabilization of radical cations is made possible at low temperature by sequestration in the zeolite pores and by trapping of electrons by the matrix.



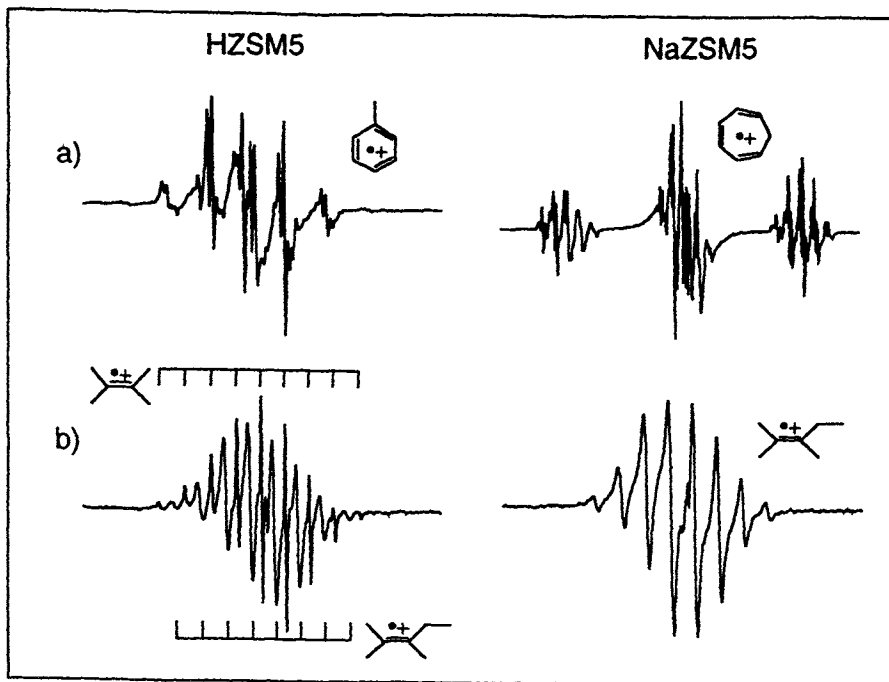


Figure 1. Radiolysis/EPR results for a) 1,3,5-cycloheptatriene and b) 2,3-dimethyl-2-pentene on HZSM5 and NaZSM5. The radical cations of catalytic products, toluene and tetramethylethylene, were observed only on the acidic zeolite and not on NaZSM5.

It sounds simple, but as mass spectroscopists know, ionization as an analysis technique creates very reactive species. It is not enough to be able to detect ions; one must also have knowledge of how the ions react. Fortunately, many radical cations are quite stable in selected zeolites at low temperature. For example, the excellent stability of radical cations of simple aromatic hydrocarbons and olefins in MFI zeolites has contributed to the successful application of the radiolytic spin labeling technique to catalytic processes of considerable importance to the fuels and petrochemical industries - hydrocarbon transformations in zeolite ZSM5.<sup>23,27,28</sup>

How is it possible to distinguish radical cation reactions from genuine transformations catalyzed by the zeolite, and what types of processes tend to intrude on the identification of products of catalysis? To answer the first question, we rely on the ion-exchangeability of zeolites. Zeolites are crystalline aluminosilicates, natural or man-made, that can adopt a remarkable range of channel-type and cage-type lattice architectures, depending on the

connectivity of ring structures built from  $(\text{SiO}_4)^{4-}$  and  $(\text{AlO}_4)^{5-}$  tetrahedra.<sup>29</sup> Extraframework cations are present in stoichiometric amounts to charge balance the negative lattice. Ion exchange is an important method of varying the acid/base character of zeolites and of incorporating other metal centers (for example, transition metal ions) with catalytic function. In this chapter we limit our discussion to the proton- and  $\text{Na}^+$ -exchanged zeolites. The former derive catalytic activity from bridging hydroxyl groups ( $\equiv \text{AlO}(\text{H})\text{Si} \equiv$ ), that are strong Bronsted acid sites and the latter are inert adsorbents.

The availability of both active and inactive, isomorphous zeolites provides a direct control experiment for the radiolytic spin labeling technique because the radical cation reactions can be elucidated on the inactive zeolite. This is best explained by example and two cases are illustrated in Figure 1. In the first example, radiolysis of an HZSM5 sample exposed at room temperature to 1,3,5-cycloheptatriene gave rise to the EPR spectrum of the toluene radical cation, and in the second, the tetramethylethylene radical cation was observed on HZSM5 loaded with 2,3-dimethyl-2-pentene. Alongside each result on the active catalyst the result for the same hydrocarbon loaded on the inactive NaZSM5 is shown. In each case, the EPR spectrum on the inactive zeolite shows only the radical cation of the starting material. Clearly, the transformations observed on HZSM5, ring contraction and cracking, are caused by acid catalysis since the radical cations do not undergo these reactions.

When the parent radical cation of a catalysis product is not stabilized, more knowledge is needed to interpret the results of catalysis. For example, adsorption of 1,3- or 1,4-cyclohexadiene on H-Beta gave, upon radiolysis, the EPR spectrum of benzene radical cation (Figure 2a). Control experiments for both olefins on Na-Beta also gave benzene radical cation and no cyclohexadiene radical cation. Proof of catalytic dehydrogenation of cyclohexadiene to give benzene, involving intermolecular hydrogen transfer, an important step in aromatization on zeolites, was revealed by changes in the EPR spectrum upon annealing the samples. In the H-Beta experiment, the benzene radical cation decayed and was replaced by benzene dimer radical cation upon raising the temperature above 120 K (Figure 2b). The exact same behavior was observed on Na-Beta loaded with benzene. In Na-Beta loaded with cyclohexadiene, the benzene dimer radical cation did not appear upon sample annealing - there is no neutral benzene to react with benzene radical cations. From this behavior it can be deduced that extensive conversion of olefin to benzene occurs on H-Beta (catalytically), whereas on Na-Beta only those molecules that are ionized undergo  $\text{H}_2$  elimination.

When the primary species (products of catalysis) must be deduced from knowledge of the radical cation chemistry, interpretation becomes more

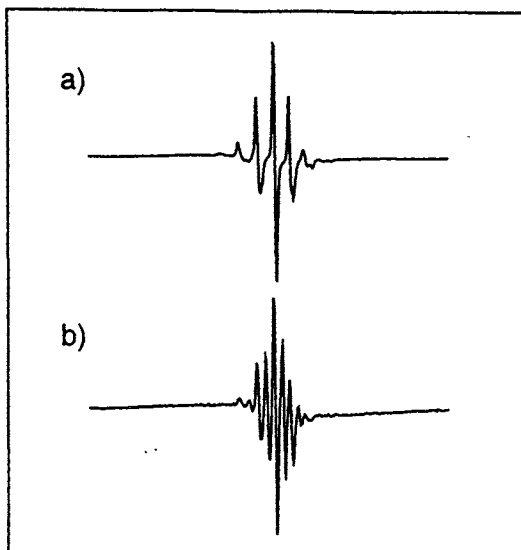


Figure 2. Radiolysis/EPR result after reaction of 1,3-cyclohexadiene on H-Beta. a) Radiolysis at 77 K gave the benzene radical cation,  $a = 4.5$  G. b) Annealing the sample above approximately 120 K caused the transformation of benzene radical cations to benzene dimer radical cations,  $a = 2.2$  G.

challenging. Not in every case, however, will the radical cation reaction mimic the catalytic reaction as in the preceding example. A last caveat regards quantitative estimates of relative product yields. Since ionization is used as the detection method, then charge migration can skew the representation of relative product yields in the EPR spectrum. That is, hole transfer among different products favors stabilization of radical cations of those species with the lowest ionization potential. We have investigated hole transfer in some detail in mixtures, both in zeolites and in frozen solutions.<sup>24</sup> The degree of bias can be estimated in this way, but the occurrence of hole transfer ultimately makes radiolysis a somewhat selective labeling technique.

### 3 RADIOLYSIS/EPR METHOD

The advantages of the radiolysis/EPR method for studying mechanisms of zeolite catalysis are due to the sensitivity and structural specificity of EPR, surpassing that of other *in situ* spectroscopies, such as FTIR and NMR, and the ability to identify products at low temperature. It is often the case that at high temperatures needed to evolve products from the zeolite for *ex situ* analysis, a

complex sequence of reactions has already occurred. Therefore, elucidation of the elementary reactions of the sequence necessitates *in situ* analysis at low temperatures. In addition, product selectivity can be more pronounced for reactions carried out under mild conditions. Product studies under these conditions allow deeper insights into the subtle details of zeolite-reactant interactions.

The radiolysis/EPR experiment can be succinctly described as follows. The zeolite powder is first activated to approximately 450°C under vacuum for several hours in a 4 mm o.d. suprasil tube. Under such activation conditions, no Lewis acid sites are created to give rise to spontaneous oxidation of adsorbed species. No EPR signals are observed in loaded zeolites prior to radiolysis. The adsorbate is quantitatively transferred via a glass vacuum manifold to the tube containing zeolite and the tube is sealed. The sealed tube is equilibrated at some temperature  $T_{eq}$  for a time  $t_{eq}$ . At the end of the reaction period, transfer of the sample tube to a liquid nitrogen storage dewar quenches any further chemistry.

Radiolysis is carried out at 77 K and EPR spectra are collected between 4 K and room temperature. Catalytic transformations can be arrested after formation of a single product or the evolution to many products can be dissected into a sequential development of different intermediates and products by systematically varying  $T_{eq}$  and  $t_{eq}$ . Taking snapshots of the material composition on the zeolite as it incrementally changes greatly aids the interpretation of multicomponent EPR spectra. Increasing multiplicity of products will eventually defeat any chance of deconvolving the EPR spectrum and one must resort to alternative (*ex situ*) techniques. However, in the study of isobutene reactions on HZSM5 (*vide infra*), five different species, including starting material, were identified.<sup>27</sup>

#### 4 REACTIONS OF ACYCLIC OLEFINS ON ZSM5

The investigation of reactions of isobutene and related acyclic olefins on HZSM5 provides a good basis for comparison of the radiolysis/EPR technique and other *in situ* spectroscopies, such as FTIR,<sup>30</sup> NMR<sup>32,33</sup> and EPR without radiolysis.<sup>34-41</sup> Results obtained by the different techniques are in general agreement, but advantages of the radiolysis/EPR method can be noted. A chief advantage was the ability to distinguish and identify structurally similar products.

The loss of isobutene starting material and the build-up of C<sub>8</sub> and C<sub>6</sub> products, reflecting dimerization, isomerization and cracking processes, were all evident in radiolysis/EPR experiments on HZSM5 at room temperature and

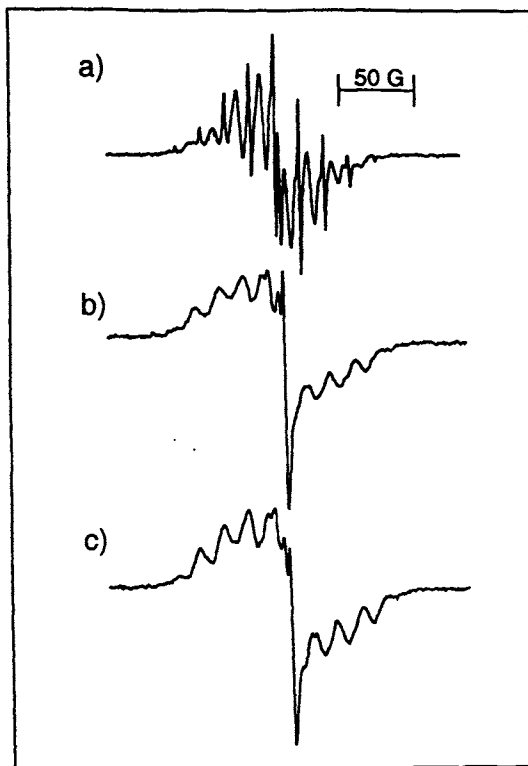


Figure 3. Radiolysis/EPR results after reaction of isobutene on HZSM5 a) for 16 h at 295 K and b) for 16 h at 338 K. c) Radiolysis/EPR result after reaction of propene on HZSM5 for 16 h at 338 K.

below.<sup>27</sup> Above room temperature, products larger than  $C_8$  began to form. By appropriate variation of  $T_{eq}$  and  $t_{eq}$ , the sequence of appearance of products could be partially deduced, adding important chemical insight into the identity of the products.

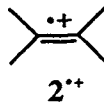
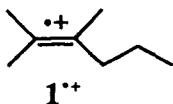
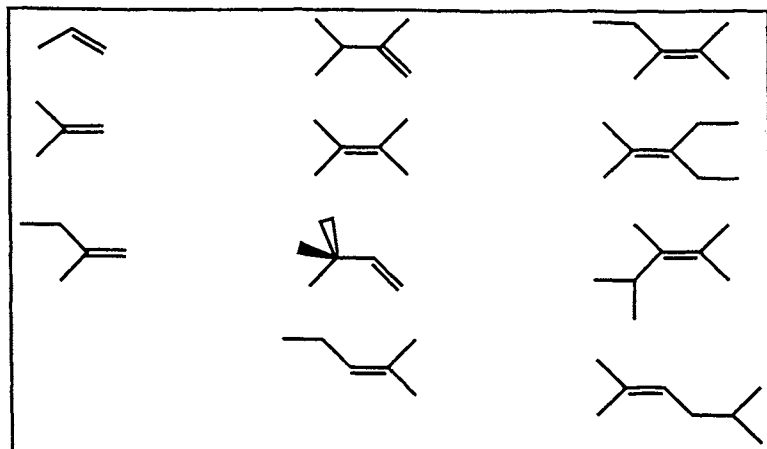


Figure 3 shows just two "EPR snapshots" of the evolving material composition on the catalyst loaded with isobutene. The EPR spectrum observed after 16 h equilibration at 295 K consisted of signals from two radical cations with structures  $1^{*+}$  (broad lines,  $a = 17$  G) and  $2^{*+}$  (sharp lines,



Table 1

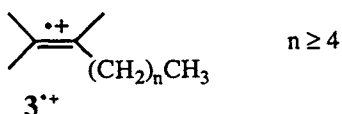
Acyclic olefins included in radiolysis/EPR studies of reactions on HZSM5



a = 17 G). There was no evidence of any remaining monomeric starting material; by this stage, it has been consumed in dimerization reactions followed by isomerization and cracking.

The radiolysis/EPR study of isobutene was supported by experiments on  $C_3$ - $C_8$  olefins on both HZSM5 and NaZSM5 (Table 1). This allowed screening for possible radical cation reactions (minimal for these compounds), and the survey of related compounds aided spectroscopic assignment and tested the catalytic reaction steps from different starting points. For example, **2** was also formed from  $C_7$  and  $C_8$  feed molecules, corroborating the conclusion that **2** can be formed from isobutene by cracking the dimer as opposed to addition of  $C_4$  and  $C_2$  units.

After reaction at higher temperatures (approximately 338 K), the resulting EPR spectrum evolved from that in Figure 3a into that in Figure 3b. The hyperfine structure indicates a radical cation with structure analogous to **1<sup>•+</sup>** and the sequence of formation of this product suggests that it is a higher molecular weight species. It is clearly a polymeric radical cation, or combination of radical cations, with structure **3<sup>•+</sup>**. Discrimination of different length polymers,  $n \geq 4$ , from the EPR data was not possible.



A general observation and one that clearly points out the advantage of following catalytic reactions under very mild conditions, was that the radiolysis/EPR result for samples equilibrated for an hour or more at 338 K began to be indistinguishable regardless of feed molecule (for all cases studied, C<sub>3</sub>-C<sub>8</sub>). For comparison, the result for propene on HZSM5, equilibrated under the same conditions as the sample in Figure 3b, is shown in Figure 3c. After extensive reaction, the hydrocarbon composition on the catalyst essentially loses memory of the starting material. Experiments under such reaction conditions do not lead to an understanding of the elementary reactions steps, reaction sequence or differences that can account for reaction selectivity.

Our conclusions are in general agreement with previous NMR<sup>32,33</sup> and FTIR<sup>30</sup> studies of olefin reactions on HZSM5. In particular, isobutene isomerization was observed as low as 143 K by NMR. The average size range of C<sub>8</sub>-C<sub>12</sub> was reported for reaction up to 300 K, but no evidence of cracking was cited under these conditions. Discrimination of C<sub>6</sub>, C<sub>8</sub> and C<sub>12</sub> species by NMR or FTIR is considerably less certain than by EPR. While chemical shift and vibrational spectra allow the estimation of relative amounts of aliphatic and olefinic protons, vinyl vs. methylene C-H bonds, etc., assignments of unique chemical structures, especially in mixtures, from such data is usually not possible.

Finally, radiolysis/EPR results forced the reinterpretation of literature spanning more than 25 years on EPR studies of olefin reactions on zeolites in the presence of Lewis acid sites.<sup>34-41</sup> Spontaneous oxidation of olefins and products of their Bronsted acid-catalyzed reactions on dehydroxylated (to form Lewis acid sites) ZSM5 and Mordenite (*vide infra*) provides an alternative method of spin labeling, and the technique gives results mostly consistent with those from radiolysis/EPR. However, in the spontaneous oxidation method, the limited degree of control over the ionization process and progress of the catalysis has led to erroneous conclusions (mainly in the earlier work). Interpretation of the radiolysis/EPR experiments is greatly aided by the ability to methodically vary the relative contribution of different products to the EPR spectrum.

## 5 SHAPE SELECTIVITY: ZSM5 AND MORDENITE

One of the paramount advantages of microporous reactors is the influence of geometry/spatial constraints on the reactions of guest species. This gives rise to shape selectivity which is vividly displayed in the products of cyclic olefin reactions on zeolites ZSM5 and Mordenite.<sup>28</sup> The largest contrast is that Mordenite, with its system of 12-ring channels (Table 2), is capable of

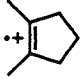
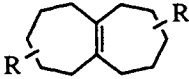
Table 2

Diameters of elliptical channels in ZSM5 and Mordenite [ref. 42]

		<u>Diameter (Å)</u>
ZSM5	10-ring, straight channels	5.3 x 5.6
	10-ring, sinusoidal channels	5.1 x 5.5
Mordenite	12-ring	6.5 x 7.0
	8-ring	2.6 x 5.7

Table 3

Major products formed from cyclic precursors on ZSM5 and Mordenite

<u>Catalyst</u>	<u>Precursor</u>	<u>Major Product</u>
HZSM5	5-, 6-, 7-member ring $C_7H_{12}$	
H-Mordenite	5-, 6-, 7-member ring $C_6H_{10}$ , $C_7H_{12}$	 R = H or $CH_3$

accommodating products that are too large to fit in the 10-ring channels of ZSM5.

Reaction of cyclic olefins on HZSM5 below 340 K is limited to unimolecular rearrangement. For example, a family of seven different compounds with 5-, 6- and 7-member rings and the empirical formula  $C_7H_{12}$  all reacted to give 1,2-dimethylcyclopentene (Figure 4a).<sup>28</sup> Such transformations - hydrogen and alkyl shifts, ring contraction, ring expansion - are well-known processes involving Bronsted acid catalysis.<sup>43,44</sup> Using the carbenium ion formalism, one such transformation is shown in Scheme 1, which depicts the intermediacy of a protonated cyclopropane ring. A question currently debated is whether free carbenium ions exist on zeolite catalysts. The question really is how acidic are zeolite catalysts, are they super acids? Evidence suggests that most reactive

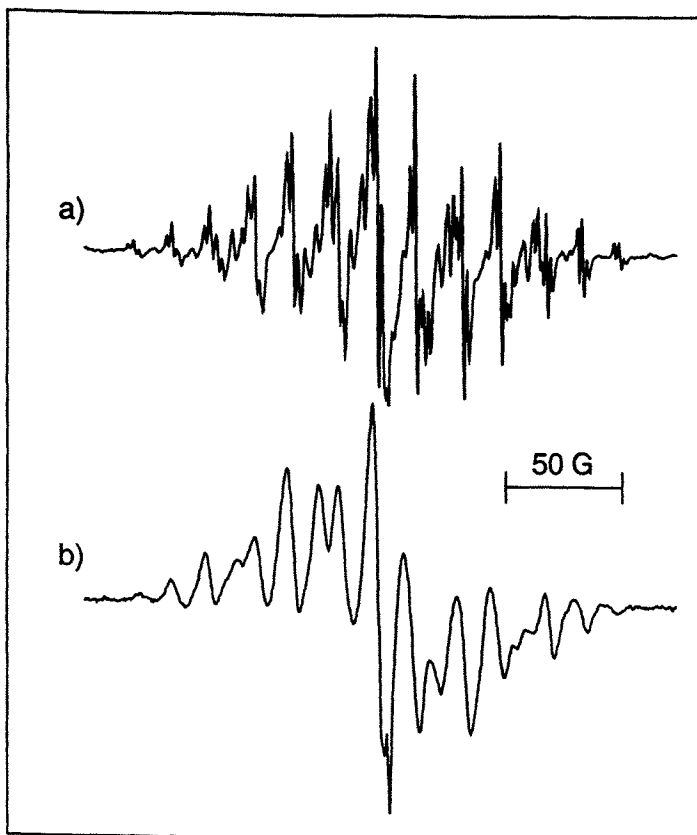
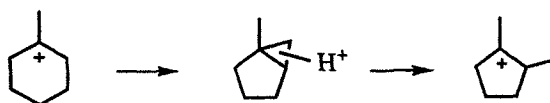


Figure 4. a) Radiolysis/EPR result after reaction of 1,5-dimethylcyclopentene on HZSM5 for 16 h at 318 K. b) Radiolysis/EPR result after reaction of cyclohexene on H-Mordenite for 16 h at 295 K. The spectrum is assigned to the bicyclo[5.5.0] dodecene radical cation.

intermediates are framework-bonded species,<sup>45-48</sup> but zeolite catalysis can nevertheless involve transition states with enough ionic character such that rules governing carbenium ion reactions are obeyed to some degree within the geometry constraints imposed by the zeolite.

Scheme 1: Carbenium ion mechanism of ring contraction and methyl side-chain generation



Bimolecular reaction products were more prevalent when cyclic olefins were reacted on H-Mordenite.<sup>28</sup> These products (Table 3, Figure 4) reflected dimerization and ring expansion processes. The exception, 1,2-dimethylcyclopentene, suggests that factors other than size exclusion are also important. This molecule was stable, even up to 318 K (16 h), whereas another C<sub>7</sub> compound (1-methylcyclohexene) was converted to the more typical bicyclic dimer product.

Another exception, cyclohexene, showed greater resistance to ring contraction on HZSM5 than methylcyclohexenes or cycloheptene. The carbenium ion-type mechanism does not disfavor the ring contraction in the case of cyclohexene, and the thermodynamic benefit of going from a secondary carbenium ion to a tertiary carbenium ion (methylcyclopentyl) should be a strong driving force for ring contraction. The greater acidity of secondary carbenium ions, such as cyclohexyl, compared to tertiary ions, such as methylcyclohexyl, could partly underlie the stability of cyclohexene on HZSM5. However, that suggests that cycloheptene should also be slow to undergo ring contraction, which was not the case. Furthermore, H-mordenite, a comparable acid to HZSM5, is able to activate the conversion of cyclohexene to the dimer product at equally low temperatures.

## 6 H/D EXCHANGE

Certain observations of reaction selectivity, such as those described in the preceding paragraphs, suggest that the carbenium ion paradigm - that is, the direct analogy to reactions of olefins in superacid solutions - is a simplistic model for Bronsted acid catalysis in zeolites. The carbenium ion formalism can account for most of the products, but glosses over the specific characteristics of zeolite catalysis, such as volume constraints, relative acidity and possible bifunctional nature of zeolite catalysts owing to the proximity of basic oxygen atoms adjacent to the acid site.

An experimental test for the intermediacy of carbenium ions in zeolite catalysis is isotope exchange. One such experiment from our laboratory involved the oligomerization of acetylene-d<sub>2</sub> on HZSM5 at room temperature.<sup>23</sup> The benzene product of the Bronsted acid-catalyzed trimerization of acetylene was detected as benzene radical cation. The EPR spectrum showed that the oligomerization of acetylene proceeds without exchange with zeolitic protons. While it is conceivable for H/D exchange to occur without the formation of a free ion, the lack of H/D exchange seems strong negative evidence for the intermediacy of free carbenium ions. This example fits with the growing experimental and theoretical evidence that zeolites are not superacids and that

intermediates involved in many catalytic reactions retain some degree of covalent bonding to the lattice.

Scrambling of the isotope label on benzene did not occur under the conditions used to study acetylene trimerization, but we have shown by radiolysis/EPR that benzene does undergo H/D exchange on HZSM5 at higher temperatures.<sup>25</sup> Beck et al. determined the activation energy (14.4 kcal/mol) for this reaction by NMR.<sup>49</sup> This fundamental reaction is itself an important test of theoretical calculations of zeolite acidity and reaction mechanisms. An interesting and remaining puzzle regarding H/D exchange in benzene on HZSM5 is the observation by radiolysis/EPR that the exchange is very nonstatistical; some of the benzene undergoes extensive exchange and some of the benzene exchanges very little.<sup>25</sup> This observation could not be attributed to a fraction of the benzene residing on the external surface of the zeolite.

## 7 CONCLUSION

Radiation chemical methods, when coupled with appropriate detection techniques, can be used to study many different aspects of solid heterogeneous catalysis. Ionizing radiation can be used to generate reactive intermediates, to change the oxidation state of metal ions or clusters, to create reactive defects in the solid lattice and to spin label reaction products. When radiolysis and EPR are used together, products of catalysis can be identified *in situ* and at low temperatures with the excellent structural specificity and sensitivity inherent in the EPR method.

As always, exceptions to the rule can offer greater insights into chemical mechanisms. Subtle structure/reactivity dependences revealed by radiolysis/EPR experiments carried out under very mild conditions provide interesting examples to theorists in their attempts to learn more about the intimate details of the steric factors and specific interactions of reactant molecules with the catalytically active site.

## Acknowledgements

We acknowledge the generosity of Chemie Uetikon of Switzerland for the gift of the zeolite materials used in most of our research.

## REFERENCES

1. M. Narayana, R. Janakiraman and L. Kevan, Chem. Phys. Lett. **90** 235 (1982).
2. J. H. Lunsford, Catal. Rev. **8** 135 (1973).

3. P. H. Kasai and R. J. Bishop, *Zeolite Chemistry and Catalysis*, J. A. Rabo, ed., American Chemical Society, Washington, DC, 1976, Chapter 6.
4. K.-K. Iu, X. Liu and J. K. Thomas, *J. Phys. Chem.* **97** 8165 (1993).
5. J. Michalik, M. Zamadics, J. Sadlo and L. Kevan, *J. Phys. Chem.*, **97** 10440 (1993).
6. J. Michalik, T. Wasowicz, J. Sadlo, E. J. Reijerse and L. Kevan, *Radiat. Phys. Chem.*, **47** 75 (1995).
7. J. Michalik, N. Azuma, J. Sadlo and L. Kevan, *J. Phys. Chem.*, **99** 4679 (1995).
8. H. Yahiro, K. Manabe, Y. Itagaki and M. Shiotani, *J. Chem. Soc., Faraday Trans.*, **94** 805 (1998).
9. J. J. Rooney and R. C. Pink, *Trans. Faraday. Soc.*, **58** 1632 (1962).
10. F. R. Dollish and W. K. Hall, *J. Phys. Chem.*, **71** 1005 (1967).
11. N. H. Sagert, R. M. L. Pouteau, M. G. Bailey and F. P. Sargent, *Can. J. Chem.*, **50** 2041 (1972).
12. Y. Kurata, T. Sonoda and M. Sato, *J. Catal.*, **19** 82 (1970).
13. P. L. Corio and S. Shih, *J. Catal.*, **18** 126 (1970).
14. P.-O. Kinell, A. Lund and A. Shiizu, *J. Phys. Chem.*, **73** 4175 (1969).
15. T. Komatsu, A. Lund and P.-O. Kinell, *J. Phys. Chem.*, **76** 1721 (1972).
16. X.-Z. Qin and A. D. Trifunac, *J. Phys. Chem.*, **94** 4751 (1990).
17. X.-Z. Qin and A. D. Trifunac, *J. Phys. Chem.*, **95** 6466 (1991).
18. M. V. Barnabas and A. D. Trifunac, *Chem. Phys. Lett.*, **187** 565 (1991).
19. M. V. Barnabas and A. D. Trifunac, *J. Chem. Soc., Chem. Commun.* 813 (1993).
20. M. V. Barnabas, D. W. West and A. D. Trifunac, *Chem. Phys. Lett.* **204**, 435 (1993).
21. M. V. Barnabas, D. W. Werst and A. D. Trifunac, *Chem. Phys. Lett.* **206**, 21 (1993).
22. D. W. Werst, E. E. Tartakovsky, E. A. Piosos and A. D. Trifunac, *J. Phys. Chem.*, **98** 10249 (1994).
23. E. A. Piosos, D. W. Werst and A. D. Trifunac, *J. Phys. Chem.*, **100** 8408 (1996).
24. D. W. Werst, P. Han and A. D. Trifunac, *Chem. Phys. Lett.*, **269** 333 (1997).
25. D. W. Werst, P. Han and A. D. Trifunac, *Radiat. Phys. Chem.*, **51** 255 (1998).
26. D. W. Werst, P. Han, S. C. Choure, E. I. Vinokur, L. Xu and A. D. Trifunac, *J. Phys. Chem.*, in press.
27. E. A. Piosos, P. Han and D. W. Werst, *J. Phys. Chem.*, **100** 7191 (1996).
28. D. W. Werst and P. Han, *Catal. Lett.*, **45** 253 (1997).
29. D. W. Breck, *Zeolite Molecular Sieves*, John Wiley, New York, 1974.
30. G. Spoto, S. Bordiga, G. Ricchiardi, D. Scarano, A. Zecchina and E. Borello, *J. Chem. Soc., Faraday Trans.*, **90** 2827 (1994).
31. K. Domen, J. N. Kondo and F. Wakabayashi, *Res. Chem. Intermed.*, **24** 411 (1998).
32. N. D. Lazo, B. R. Richardson, P. D. Schettler, J. L. White, E. J. Munson and J. F. Haw, *J. Phys. Chem.*, **95** 9420 (1991).
33. J. P. van den Berg, J. P. Wolthuizen, A. D. H. Clague, G. R. Hays, R. Huis and J. H. C. van Hoof, *J. Catal.*, **80** 130 (1983).

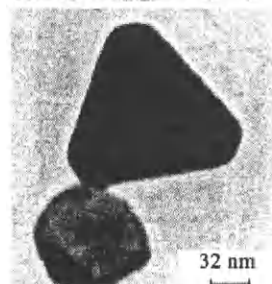
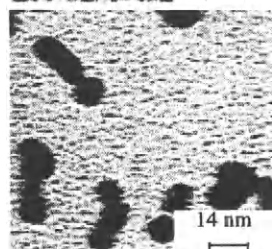
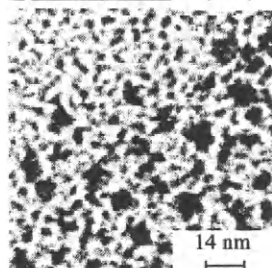
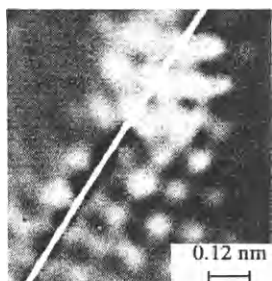
34. I. R. Leith, *J. Chem. Soc., Chem. Commun.*, 1282 (1972).
35. S. Shih, *J. Catal.*, **36** 238 (1975).
36. A. V. Kucherov and A. A. Slinkin, *Kinet. Katal.*, **23** 1172 (1982).
37. A. V. Kucherov and A. A. Slinkin, *Kinet. Katal.*, **24** 947 (1983).
38. A. V. Kucherov and A. A. Slinkin, *Kinet. Katal.*, **24** 955 (1983).
39. T. Ichikawa, M. Yamaguchi and H. Yoshida, *J. Phys. Chem.*, **91** 6400 (1987).
40. J.-P. Lange, A. Gutsze and H. G. Karge, *J. Catal.*, **114** 136 (1988).
41. E. Roduner, L.-M. Wu, R. Crockett and C. J. Rhodes, *Catal. Lett.*, **14** 373 (1992).
42. W. M. Meier, D. H. Olson and Ch. Baerlocher, *Zeolites*, **17** 1 (1996).
43. D. M. Brouwer, *Chemistry and Chemical Engineering of Catalytic Processes*, R. Prins and G. C. A. Schuit, eds., Sijthoff and Noordhoff, Amsterdam, 1980, p. 137.
44. P. A. Jacobs and J. A. Martens, *Stud. Surf. Sci. Catal.*, **58** 445 (1991).
45. T. Xu and J. F. Haw, *J. Am. Chem. Soc.*, **116** 10188 (1994).
46. P. Viruela-Martin, C. M. Zicovich-Wilson and A. Corma, *J. Phys. Chem.*, **97** 13713 (1993).
47. R. A. van Santen and G. J. Kramer, *Chem. Rev.*, **95** 637 (1995).
48. V. B. Kazansky, *Acc. Chem. Res.*, **24** 379 (1991).
49. L. W. Beck, T. Xu, J. B. Nicholas and J. F. Haw, *J. Am. Chem. Soc.*, **117** 11594 (1995).



## Radiation chemistry of nanocolloids and clusters

J. Belloni and M. Mostafavi

Laboratoire de Chimie Physique, UMR 8000 CNRS, Université Paris-Sud, 91405 Orsay, France.



For more than two decades, extensive research work has been devoted to the unique properties of clusters. They are made of a small number (or nuclearity) of atoms or molecules only, and therefore constitute a new state of matter, or mesoscopic phase, between the atom or molecule and the crystal. New methods have been developed in physics and chemistry for their synthesis, their direct observation, the study of their properties, and of their crucial role in number of processes, such as phase transition, catalysis, surface phenomena, imaging. Owing to its specific approach, radiation chemistry offered first the opportunity to reveal the existence of nuclearity-dependent properties of clusters and has then proven to be a powerful method to study the mechanisms of cluster formation and reactivity in solution.

### 1. INTRODUCTION

One century ago, X rays discovered by W. Roentgen,<sup>1</sup> then radiation of radioactive elements discovered by H. Becquerel,<sup>2</sup> were detected through their effects on the material they traversed, specially reduction of silver ions of the photographic plates and ion pair formation in irradiated air. Both effects were therefore used from the origin of the study of ionizing radiation to indirectly detect their presence and calibrate their intensity, even if the molecular processes of cluster formation in the photo-

Figure 1. Radiation-induced metal clusters under various conditions. From top :  $\text{Ag}_7^{3+}$  with  $n = 4$ , stabilized by PA (partial reduction at  $4 \text{ kGy h}^{-1}$ ),<sup>3</sup> alloyed  $(\text{AgAu})_n$ , PA with  $n \approx 5 \times 10^2$  (at  $8 \text{ MGy.h}^{-1}$ ),<sup>4</sup> alloyed  $(\text{AgAu})_n$ , PVA with  $n \approx 10^5$  (at  $35 \text{ kGy h}^{-1}$ ),<sup>4</sup> and  $\text{Ag}_n$  with  $n \approx 10^8$  (partial reduction at  $3 \text{ kGy h}^{-1}$  and then developed by EDTA)<sup>5</sup> (see text).

graphic latent image or the effects of radiation were at that time unexplained. Progressively, the complexity of the specific absorption of high-energy radiation by matter, including the non-homogeneous spatial distribution of initial ions and radicals, was better understood, at least in aqueous solutions.

In particular, various metal ions were used widely as radical scavengers and redox indicators in the reduction or oxidation processes induced indirectly by the short-lived primary radiolytic species, allowing their identification and the calibration of their formation yield.<sup>6,7,8</sup> Metal ions such as those of gold or silver irradiated in solutions by  $\gamma$ -<sup>9</sup> or pulse radiolysis<sup>10</sup> underwent reduction to the zero-valence metal, to form colloids and then precipitates.<sup>7,11</sup>

The radiolytic method of reduction allowed, owing to the accurate knowledge of the dose used, a control of the progressive extent of the reduction and an instantaneous distribution of the reducing agent formed throughout the solution. However, quite often, puzzling data were reported when the zero-valent metal was formed, such as an induction time for precipitation, radiolytic yields sensitive to the initial presence or absence of added particles, and only weakly reproducible.<sup>12,13</sup> Moreover, oxidation of silver atoms by molecular oxygen was observed, though the process was thermodynamically improbable for a noble metal like silver.<sup>10</sup> The explanation of some oxidation observed of newly formed zero-valent silver (latent image regression) in nuclear photographic plates used for long in particle track detection was also a difficult question.<sup>12</sup>

It was observed, in 1973, that the metal that was expected to arise from the reduction of  $\text{Cu}^+$ , was not found when these ions were used as electron scavengers in the radiolysis of liquid ammonia, despite the fast reduction of metal ions by solvated electrons.<sup>14</sup> Instead, molecular hydrogen was evolved. These results were explained by assigning to the "quasi-atomic state" of the nascent metal specific thermodynamical properties distinct from those of the bulk metal that is stable under the same conditions.<sup>14</sup> This concept implied that, as soon as formed, atoms and small clusters of a metal, even a noble metal, may exhibit much stronger reducing properties than the bulk metal, and may be spontaneously corroded by the solvent with simultaneous hydrogen evolution. It also implied that for a given metal the thermodynamics depended on the particle nuclearity (number of atoms reduced per particle), and allowed that to provide rationalized interpretation of other previous data, for example that on the spontaneous oxidation of nascent radiolytic silver by oxygen in water, or its higher stability when produced at the surface of added particles.<sup>10,14</sup> Soon, experiments on the photoionization of silver atoms in solution demonstrated that their ionization potential was much lower than that of the bulk metal.<sup>15</sup> Also, it was shown that the redox potential of isolated silver atoms in water must be lowered relative to that of the silver electrode  $E^\circ(\text{Ag}^+/\text{Ag}_{\text{met}}) = 0.79 \text{ V}_{\text{NHE}}$ , by the sublimation energy of the metal equal to 2.6 V and  $E^\circ(\text{Ag}^+/\text{Ag}^0) = -1.8 \text{ V}_{\text{NHE}}$ .<sup>16</sup> In early eighties, an increasing number of experimental works emphasized, for metal or semiconductor particles prepared by various ways in the gaseous and condensed phases, the nuclearity-dependent properties of clusters of atoms or molecules,<sup>17</sup> theoretically predicted earlier by Kubo.<sup>18</sup>

Nuclearity-dependent properties of semiconductor particles may be studied by radiolysis too. For example, a soluble anion-cation couple is transformed by electron scavenging into a pair of low solubility product.<sup>1</sup>

The radiation-induced method, in the  $\gamma$ - or pulse regime, provides a particularly powerful means to understand the exotic phenomena which occur any time a new phase of oligomeric particles is formed in the bulk of a homogeneous mother phase,<sup>20-24</sup> phenomena which are thus rather frequent in physics and chemistry.

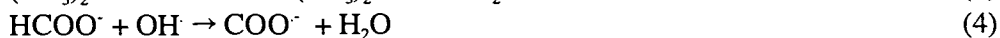
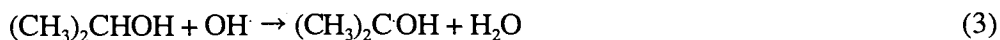
## 2. PRINCIPLES

### 2.1. Metal cation reduction

The atoms are produced in deaerated solution by radiation-induced reduction of the metal ion precursors. The species solvated electrons  $e_{aq}^-$ , and H atoms arising from the radiolysis of water<sup>25</sup> are strong reducing agents ( $E^\circ(H_2O/e_{aq}^-) = -2.87 V_{NHE}$  and  $E^\circ(H^+/H) = -2.3 V_{NHE}$ ). They easily reduce metal ions up to the zero-valent state :



where  $M^+$  is the symbol of monovalent metal ions possibly complexed by a ligand. Similarly, multivalent ions are reduced by multistep reactions, also including disproportionation of intermediate valencies. Such reduction reactions have been observed directly by pulse radiolysis for a lot of metal ions.<sup>26</sup> Most of their rate constants are known and the reactions are often diffusion controlled. In contrast, OH radicals, which are also formed in water radiolysis<sup>25</sup> are able to oxidize the ions or the atoms into a higher oxidation state and thus to counterbalance the previous reductions (2) and (3). For that reason, the solution is generally added with a scavenger of OH radicals. Among various possible molecules, the preferred choice is for solutes whose oxidation by OH yields radicals which are unable to oxidize the metal ions but in contrast exhibit themselves strong reducing power such as the radicals of secondary alcohols or of formate anion.

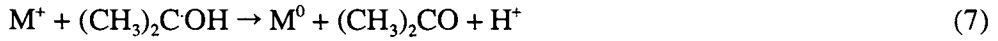


H atoms ( $E^\circ(H/H_2) = +2.3 V_{NHE}$ ) oxidize these molecules as well :

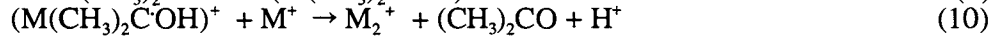


The radicals  $(CH_3)_2C\dot{O}H$  and  $COO^-$  are almost as powerful reducing agents as H atoms:  $E^\circ((CH_3)_2C\dot{O}H/(CH_3)_2COH) = -1.8 V_{NHE}$ <sup>27</sup> at pH 7 and  $E^\circ(CO_2/COO^-)$

= - 1.9 V<sub>NHE</sub>,<sup>28</sup> respectively. In some cases they can reduce directly metal ions into lower valencies or into atoms for monovalent cations:



In other cases, the reduction proceeds *via* complexation of the ion with the radical :



Then the charged dimer is formed.

## 2.2. Metal atom coalescence

The atoms are formed with a homogeneous distribution throughout the solution. The binding energy between two metal atoms is stronger than the atom-solvent or atom-ligand bond energy. Therefore the atoms dimerize when encountering or associate with excess ions. Then, by a cascade of coalescence process these species progressively coalesce into larger clusters:



where  $m$ ,  $n$ , and  $p$  represent the nuclearities, *i.e.* the number of reduced atoms they contain,  $x$ ,  $y$  and  $z$  the number of associated ions. The radicals  $(CH_3)_2C\cdot OH$ , or  $COO\cdot^-$  also reduce  $M_{n+1}^+$  as  $e_{aq}^-$  in reaction (15). The radius of  $M_n$  increases as  $n^{1/3}$  (Figure 1). The fast reactions (12) and (13) of ion association with atoms or clusters play an important role in the cluster growth mechanism. Firstly, the homolog charge of clusters slow down their coalescence (reaction (14)). Secondly, the subsequent reduction of the ions fixed on the clusters (reactions (13) and (15)) favors their growth rather than the generation of new isolated atoms (reactions (1, 7, 8)). The competition between reduction of free ions (1, 7, 8) and of absorbed ions (15) is controlled by the rate of reducing radical formation. Coalescence reactions (11) or (14) obey second order kinetics. Therefore, the cluster formation by direct reduction (1, 7, 8) followed by coalescence (11) is predominant at high irradiation dose rate.

However, almost in the early steps of the growth, the redox potential of the clusters, which decreases with the nuclearity, is quite negative. Therefore, the growth process undergoes another competition with a spontaneous corrosion by the solvent which may even prevent the formation of clusters, as mostly in the case of non noble metals. Monomeric atoms and oligomers of

these elements are so fragile to reverse oxidation by the solvent and radiolytic protons that  $H_2$  is evolved and the zerovalent metal is not formed.<sup>14</sup>



For that reason, it is preferable in these systems to scavenge the protons by adding a base to the solution and to favor the coalescence by a reduction faster than the oxidation which obeys first order kinetics (§ 4.2)

### 2.3. Semiconductor cluster formation

Nanoparticles of semiconductor compounds  $(MA)_n$  may be formed from scavenging of radiolytic species produced by irradiation. The cationic part  $M^+$  is for example provided by a soluble salt, while the anionic part  $A^-$  is generated by cleavage after electron attachment to a soluble electrophile substitute RA as a precursor.  $M^+$  and  $A^-$  are selected for their very low solubility product :



Other semiconductor monomers are formed from  $A^-$  provided by a soluble salt and  $M^+$  resulting from the radiolytic reduction (for instance by  $e_{aq}^-$ ) of a higher valency metal ion :



Similarly, reaction (22) is followed by the formation reactions (19 - 21) of the  $(MA)_n$  cluster. Adsorption of precursor ions  $M^+$  (or  $A^-$ ) on clusters confer them identical charges which slow down the coalescence due to electrostatic repulsion. But it favors their growth by further reaction with  $A^-$  (or  $M^+$ ) (ripening) :



Nucleation by reactions (19, 20) is in competition with growth by (23, 24) and is favored by fast  $A^-$  generation, thus at high dose rate. Multivalent anionic  $A^-$  and cationic  $M^{x+}$  precursors react also by successive ion fixation on the growing cluster according to the stoichiometry and yield eventually  $(M_y A_x)_n$  clusters.

### 2.4. Cluster stabilization

Metal atoms or semiconductor monomers formed by irradiation or any other method tend to coalesce into oligomers which themselves progressively

grow into larger clusters and eventually into precipitates, as found in early radiolytic experiments. However, for studying stable clusters or for applications, the coalescence must be limited, by adding a polymeric molecule acting as a cluster stabilizer. Functional groups with high affinity for the metal ensure the anchoring of the molecule at the cluster surface while the polymeric chain protects the cluster from coalescing with the next one and thus inhibits at an early stage further coalescence through electrostatic repulsion or steric hindrance. Some of these polymeric systems are at the same time the stabilizer and the reducing agent used to chemically synthesize the metal clusters. When metal or semiconductor clusters are to be prepared by irradiation, the stabilizing polymers must be selected instead for their inability to directly reduce the ions before irradiation. Poly(vinyl alcohol) (PVA),<sup>29</sup> sodium dodecyl sulfate (SDS),<sup>29,30</sup> sodium poly(vinylsulfate) (PVS),<sup>31</sup> poly(acrylamide) (PAM)<sup>32,33</sup> or poly(N-methylacrylamide) (PNPAM),<sup>32</sup> carbo-wax,<sup>34</sup> poly(ethyleneimine) (PEI),<sup>35,36</sup> polyphosphate (PP),<sup>37</sup> gelatin,<sup>38,39</sup> do not reduce ions and fulfill the conditions for the stabilization. Some functional groups such as alcohol are OH scavengers and may contribute to the reduction under irradiation. The final size of metal clusters stabilized by these polymers lies in the nanometer range. Sodium polyacrylate (PA) is a much stronger stabilizer which allows the formation of long-lived metal oligomers (Figure 1).<sup>3,40</sup>

Some ligands (e.g. CN,<sup>41</sup> or EDTA<sup>5</sup>) are able by themselves to stabilize small sized particles (Figure 1). The coalescence of atoms into clusters may also be restricted by generating the atoms inside confined volumes of microorganized systems<sup>42</sup> or in porous materials. The ionic precursors are included *prior* to penetration of radiation. The surface of solid supports adsorbing metal ions is a strong limit to the diffusion of the nascent atoms formed by irradiation at room temperature, so that quite small clusters can survive.<sup>43</sup> The stabilization of radiation-induced clusters at the smallest sizes by a polymer or a support is the way to benefit the specific properties appearing for the lowest nuclearities.

### 3. METAL CLUSTER NUCLEATION AND GROWTH

#### 3.1. Cluster nucleation

As the early species produced after reduction such as atoms, dimers and oligomers are short-lived, time-resolved observations of the reactions of these transients are carried out by the pulse radiolysis method, coupled with optical absorption or conductivity.<sup>25</sup> Generally, kinetics are studied in the absence of oxygen or stabilizer unless their specific interaction has to be known. The earliest<sup>10,11,16</sup> and most complete data<sup>38,44,45,46</sup> on the nucleation mechanism were obtained on silver clusters. Indeed, silver may be considered as a model system owing to the one-step reduction of the monovalent silver ions, hydrated or complexed with various ligands, and to the intense absorption bands of the transient oligomers and final clusters. As for other metal oligomers, the specific feature of the spectral properties is to be nuclearity-dependent. The wavelengths of the absorption band maxima of the atom Ag<sup>0</sup> and of the

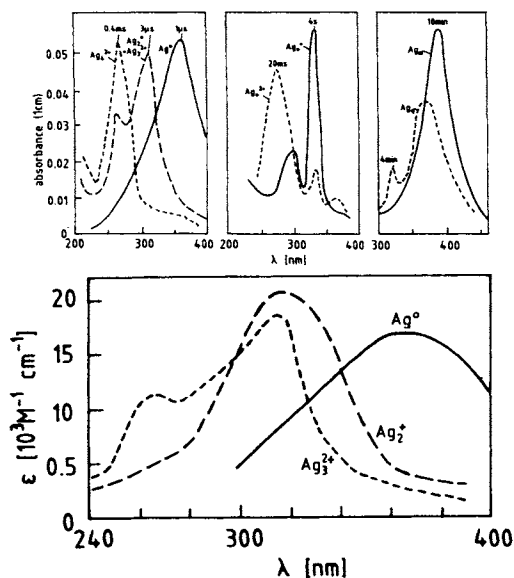


Figure 2. Optical properties of hydrated silver clusters. Top : Transient absorption spectra of silver oligomers.<sup>22</sup> Bottom : Calibrated absorption spectra of  $\text{Ag}^0$ ,  $\text{Ag}_2^+$  and  $\text{Ag}_3^{2+}$  in water obtained by pulse radiolysis.<sup>47</sup>

charged dimer  $\text{Ag}_2^+$  (Figure 2), and the rate constants of their formation (reactions 1 and 12, respectively) in aqueous solutions are given in Table 1.  $\text{Ag}_3^{2+}$  is formed by reaction of  $\text{Ag}_2^+$  with an additional  $\text{Ag}^+$  cation (Figure 2). Atoms and charged dimers of other metals are formed by homolog reactions (Table 1).

Table 1

Formation rate constants ( $\text{mol l}^{-1} \text{s}^{-1}$ ) and optical absorption maxima of metal atoms, hydrated or complexed, and of the corresponding charged dimers in water.

Metal ions	$k_{M^+ + e_{aq}^-}$	$\lambda$ (nm) of $M^0$	$k_{M^0 + M^+}$	$\lambda$ (nm) of $M_2^+$
$\text{Ag}^+$	$3.6 \times 10^{10}$	$360^{16,47}$	$8 \times 10^9$	290, 315 <sup>16,47</sup>
$\text{Tl}^+$	$3 \times 10^{10}$	$450, 260^{48,49}$	$1.4 \times 10^9$	700, 420, 245 <sup>48,49</sup>
$\text{In}^+$	-	$500^{60}$	$1.5 \times 10^9$	$310, 460^{60}$
$\text{Ag}(\text{CN})_2^-$	$5 \times 10^9$	$450, 500^{56}$	$2 \times 10^{10}$	$350, 410, 490^{56}$
$\text{Ag}(\text{EDTA})^{3-}$	$1.7 \times 10^9$	$400, 450^{56}$	$1.6 \times 10^9$	$310, 340, 400, 475^{56}$
$\text{Ag}(\text{NH}_3)_2^+$	$3.2 \times 10^{10}$	$350,^{11} 385^{57}$	-	$315, 340^{58}$
$\text{Au}(\text{CN})_2^-$	$1.1 \times 10^{10}$	$420^{50,59}$	-	-
$\text{Ag}^1, \text{PA}$	$3.6 \times 10^9$	$360^{51}$	$8.9 \times 10^9$	$310, 450^{51}$
$\text{Ag}^1, \text{gelatin}$	$1.1 \times 10^{10}$	$360^{38}$	$1.1 \times 10^{10}$	$290, 315, 308, 325^{38}$
$\text{Cu}(\text{Cl})_3^{2-}$	$2.7 \times 10^{10}$	$380^{60}$	$4.9 \times 10^7$	$360^{60}$

The band maxima of metal species are different in the gaseous and condensed phases. The absorption bands of  $\text{Ag}^0$  and  $\text{Ag}_2^+$  are highly dependent on the environment.<sup>52</sup> They are red-shifted with the decreasing polarity of the solvent as in EDA and liquid  $\text{NH}_3$ , where they appear at a longer wavelength than in water.<sup>53</sup> Moreover, the maximum in  $\text{NH}_3$  is red-shifted with increasing the temperature. Electron spin echo modulation analysis of  $\text{Ag}^0$  in ice or methanol glasses has concluded to a charge transfer character to solvent (CTTS) of the absorption band.<sup>54</sup> As shown in Table 1 and Figure 3, the interaction of ligands  $\text{CN}^-$ ,  $\text{NH}_3$ , or EDTA with the atom or the dimer has also a strong influence on the absorption spectra.<sup>55</sup>

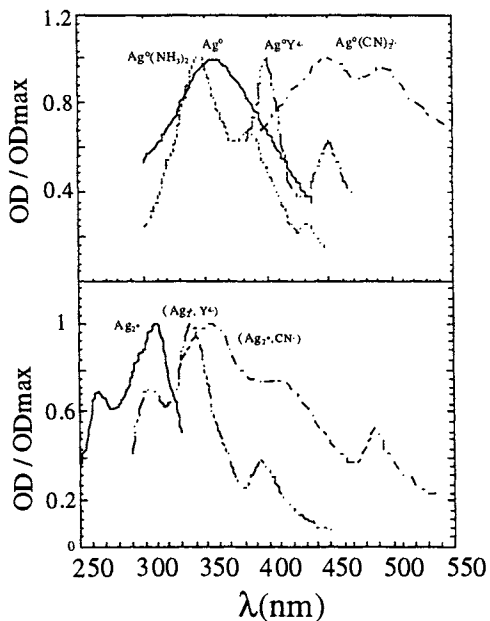


Figure 3. Absorption spectra of silver atom  $\text{Ag}^0$  (top) and charged dimer  $\text{Ag}_2^+$  (bottom) complexed by  $\text{CN}^-$ ,<sup>56</sup> EDTA,<sup>56</sup> and  $\text{NH}_3$ <sup>57,58</sup> in solution. The spectra of uncomplexed  $\text{Ag}^0$  and  $\text{Ag}_2^+$  are shown for comparison.<sup>47</sup>

The transient product of the reduction of complexed silver ions is not the isolated atom but a complexed silver atom,  $\text{Ag}^0(\text{CN})_2$ ,<sup>56</sup>  $\text{Ag}^0(\text{NH}_3)_2$ ,<sup>57</sup> or  $\text{Ag}^0(\text{EDTA})$ ,<sup>56,58</sup> respectively, as well as for  $\text{Au}^0(\text{CN})_2$ <sup>2-,59</sup> or  $\text{CuCl}_3^{3-}$ .<sup>60</sup> Though less complete, the results on the reduction of other monovalent metals cations into atoms,<sup>26</sup> such as  $\text{Tl}^0$ ,  $\text{In}^0$ ,  $\text{Au}^0(\text{CN})_2^{2-}$ ,  $\text{Cu}^0\text{Cl}_3^{3-}$ , are comparable with silver (Table 1).

The multistep reduction mechanism of multivalent cations are also partially known from pulse radiolysis studies.<sup>26</sup> For example, the reduction of  $\text{Au}^{\text{III}}\text{Cl}_4^-$  into  $\text{Au}^{\text{II}}\text{Cl}_3^-$  and the disproportionation of  $\text{Au}^{\text{II}}$  into  $\text{Au}^{\text{I}}$  and  $\text{Au}^{\text{III}}$  have been directly observed and the rate constants determined.<sup>61</sup> However, the last step of reduction of  $\text{Au}^{\text{I}}$  complexed by  $\text{Cl}^-$  into  $\text{Au}^0$  is not observed by pulse radiolysis because the  $e_{\text{aq}}^-$  scavenging by the precursors  $\text{Au}^{\text{III}}$  is more efficient. Moreover, the disproportionation of  $\text{Au}^{\text{I}}$  or of other monovalent cations is thermodynamically hindered by the quite negative value of  $E^\circ(\text{M}^{\text{I}}/\text{M}^0)$  (§ 4).

### 3.2. Cluster growth

After reactions (1-12), the reaction of  $\text{Ag}_2^+$  with  $\text{Ag}^+$  yielding  $\text{Ag}_3^{2+}$  ( $\lambda_{\text{max}} = 315$  and  $260$  nm)<sup>47</sup> or its dimerization into  $\text{Ag}_4^{2+}$  ( $\lambda_{\text{max}} = 265$  nm) and the multi-step coalescence of oligomers result in clusters of increasing nuclearity



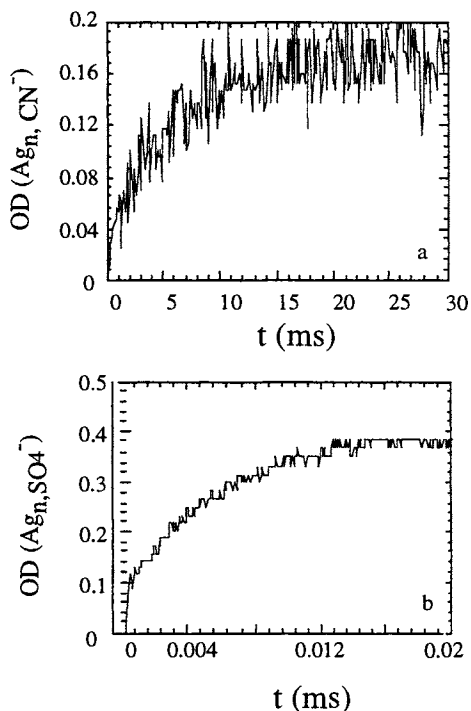


Figure 4. Growth kinetics of silver clusters observed through their absorbance at 400 nm in the presence of (a) cyanide or (b) sulfate.<sup>65</sup>

atom  $\epsilon = 1.5 \times 10^4 \text{ l mol}^{-1}\text{cm}^{-1}$  beyond  $n = 13$ .<sup>64</sup> Then, the coalescence into larger clusters is still continuing, though the spectrum is unchanged. Note that the coalescence rate constant depends on the ligand as shown in Figure 4.<sup>65</sup> At the same initial concentration of atoms, the plateau is reached at almost  $10^3$  longer time for  $\text{Ag}_n(\text{CN}^-)$  than  $\text{Ag}_n(\text{SO}_4^{2-})$ .

#### 4. TRANSIENT METAL CLUSTER REACTIVITY

The determination of the redox potential of short-lived oligomers is accessible only by kinetics methods using pulse radiolysis. In the couple  $\text{M}_n^+/\text{M}_n$ , reducing properties of  $\text{M}_n$  as electron donor as well as oxidizing properties of  $\text{M}_n^+$  as electron acceptor are deduced from the occurrence of an electron transfer reaction with a reference reactant of known potential. The unknown potential  $E^\circ(\text{M}_n^+/\text{M}_n)$  is derived in comparing the action of several reference systems of different potential. Number of rate constants for reactions of transients from metal ions and metal complexes were determined by pulse radiolysis.<sup>66</sup>

$\text{Ag}_n$  (reaction 14). The absorption spectrum is shifted to the surface plasmon band at 380-400 nm (§ 5). It is known indeed according to Mie theory<sup>62</sup> and its extension<sup>63</sup> that the interaction of light with the electrons of small metal particles results in an absorption band whose shape and intensity depend on the complex dielectric constant of the metal, the cluster size and the environment. During the coalescence, the total amount of silver atoms formed by the pulse is constant, but they are aggregated into clusters of increasing nuclearity with a decreasing concentration. Thus the absorbance increase observed at 400 nm (Figure 4) is assigned to the increase with the nuclearity of the extinction coefficient *per* silver atom. It was shown from the kinetics analysis that the plasmon band is totally developed with the constant value per

#### 4.1. Redox potentials of metal atoms and dimers

Oxidation reactions of  $\text{Ag}^0$  and  $\text{Ag}_2^+$ ,<sup>10,67</sup> or of  $\text{Au}^0(\text{CN})_2^{2-}$ ,<sup>59</sup> or of  $\text{Tl}^0$  and  $\text{Tl}_2^+$ ,<sup>48,68</sup> by even *mild oxidizing* molecules ( $\text{O}_2$ ,  $\text{CCl}_4$ ,  $\text{CH}_3\text{NO}_2$ ,  $\text{N}_2\text{O}$ ,  $\text{Fe}^{\text{III}}$ , for example) were observed by pulse radiolysis and the high rate constants found indicate the strong electron donating character of atomic silver, gold or thallium. This confirms the evaluation of  $E^\circ(\text{Ag}^+/\text{Ag}^0) = -1.8 V_{\text{NHE}}$  and  $E^\circ(\text{Tl}^+/\text{Tl}^0) = -1.9 V_{\text{NHE}}$  which was derived from the difference between the metal electrode potential,  $E^\circ(\text{M}^+/\text{M}_{\text{met}})$ , and the metal sublimation energy<sup>16,48</sup> (Table 2). More generally, due to the high value of the sublimation energy, the potential of any metal  $E^\circ(\text{M}^+/\text{M}^0)$  is expected to be quite negative.

According to reaction (1), the redox potential values of all metal atoms are higher than that of  $E^\circ(\text{H}_2\text{O}/e_{\text{aq}}^-) = -2.87 V_{\text{NHE}}$ . However, some complexed ions are *not reducible* through reaction (7)<sup>41</sup> and thus  $E^\circ(\text{M}^+\text{L}/\text{M}^0\text{L}) < -2.1 V_{\text{NHE}}$  which is the potential value of alcohol radicals under basic conditions (Table 2). The results were confirmed by SCF calculations of  $\text{Ag}^+\text{L}$  and  $\text{Ag}^0\text{L}$  structures associated with the solvation effect given by the cavity model for  $\text{L} = \text{CN}^-$ <sup>69</sup> or  $\text{NH}_3$ ,<sup>57</sup> respectively.

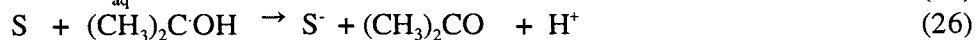
Table 2.

Redox potentials ( $V_{\text{NHE}}$ ) of the hydrated and complexed  $\text{M}^+/\text{M}^0$  couple in water.

Couple	$\text{Au}^+/\text{Au}^0$	$\text{Cu}^+/\text{Cu}^0$	$\text{Tl}^+/\text{Tl}^0$	$\text{Ag}^+/\text{Ag}^0$	$\text{Ag}(\text{CN})_2^-/\text{Ag}^0(\text{CN})_2^{2-}$	$\text{Ag}(\text{NH}_3)_2^+/\text{Ag}^0(\text{NH}_3)_2$	$\text{Ag}(\text{EDTA})^{3-}/\text{Ag}^0(\text{EDTA})^{4-}$
$E^\circ$	-1.4 <sup>49</sup>	-2.7 <sup>16</sup>	-1.9 <sup>48</sup>	-1.8 <sup>16</sup>	-2.6 <sup>41,69</sup>	-2.4 <sup>57</sup>	-2.2 <sup>56</sup>

#### 4.2. Redox potentials of oligomeric metal clusters

For clusters of higher nuclearity too, the kinetics method for determining the redox potential  $E^\circ(\text{M}_n^+/\text{M}_n)$  is based on the electron transfer, for example, from *mild reductants* of known potential which are used as reference systems, towards charged clusters  $\text{M}_n^+$ . Note that the redox potential differs from the microelectrode potential  $E^\circ(\text{M}^+/\text{M}_n)$  by the adsorption energy of  $\text{M}^+$  on  $\text{M}_n$  (except for  $n = 1$ ). The principle (Figure 5) is to observe at which step  $n$  of the cascade of coalescence reactions (14), a reaction of electron transfer, occurring between a donor  $\text{S}^-$  and the cluster  $\text{M}_n^+$  could compete with (14). Indeed  $n$  is known from the time elapsed from the end of the pulse and the start of coalescence. The donor  $\text{S}^-$  is produced by the same pulse as the atoms  $\text{M}^0$ , the radiolytic radicals being shared between  $\text{M}^+$  (reactions 1,7,8) and  $\text{S}$  (reactions 25, 26).



The transfer requires that  $E^\circ(\text{M}_n^+/\text{M}_n)$  which increases with  $n$  becomes higher than the reference  $E^\circ(\text{S}^-/\text{S})$ , thus fixing a critical nuclearity  $n_c$  (Figure 5). Therefore the given total amount of reducing equivalents provided by the pulse

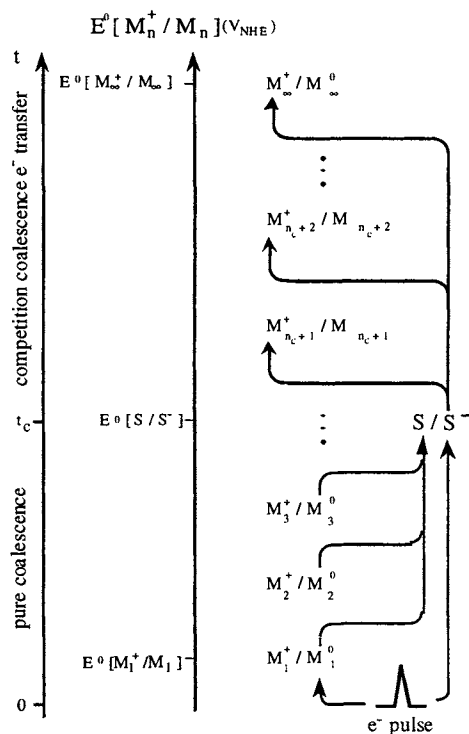


Figure 5. Principle of the determination of short-lived cluster redox potential by kinetics method. The reference electron donor  $S^-$  of given potential and the metal atoms are generated by the same single pulse. During the cluster coalescence the redox potential of the couple  $E^\circ(M_n^+/M_n)$  progressively increases, so that an effective transfer is observed after a critical time when the cluster potential becomes higher than that of the reference imposing a threshold ( $n \geq n_c$ ). The subcritical clusters  $M_n$  ( $n < n_c$ ) may be oxidized by  $S^-$ .<sup>44, 70</sup>

is shared between direct reduction into  $M^0$  (1,7,8) and indirect reduction *via*  $S^-$  (27, 29) when  $n \geq n_c$ :



As far as  $n < n_c$ , the coalescence occurs as in the absence of  $S^-$  (reactions 1, 7-14). The process is followed by the evolution of the system  $S/S^-$ , which is also selected for its intense optical absorption properties, which allows a detailed kinetics study. If  $S^-$  concentration is high, the indirect reduction (27-29) is faster than the coalescence (10-14). The clusters grow now mostly by successive additions of supplementary reduced atoms (electron plus ion). It has been shown that once formed, a critical cluster, of silver for example<sup>44,70</sup>, behaves indeed as a growth nucleus. Alternate reactions of electron transfer (27, 29) and adsorption of surrounding metal ions (28) make its redox potential more and more favorable to the transfer (Figure 6), so that an autocatalytic growth is observed.<sup>44</sup> The branching ratio between direct and indirect reduction of  $M^+$  is fixed by the  $M^+$  and  $S^-$  concentration ratio. Therefore, for a given final amount of atoms, the ratio controls their

distribution in isolated atoms yielding the nuclei and the atoms formed by  $S^-$  collected in growing centers. It is clear that the distribution of final sizes is totally governed by this competition. At increasing  $S$  concentration, less nuclei are formed and they are developed to larger sizes.<sup>44</sup>

The observation of an effective transfer from  $S^-$  to  $M^+$  implies that the potential of the critical cluster is at least slightly more positive than that of the electron donor system, i.e. :  $E^\circ(M_n^+/M_n) > E^\circ(S/S^-)$ .

The value of the critical nuclearity allowing the transfer from the monitor depends on the redox potential of this selected donor  $S^-$ . The donor decay and the correlated increase of supplementary atoms from reaction (27) start systematically after a critical time  $t_c$  (Figure 6). The critical time and the donor decay rate depend both on the initial concentrations of metal atoms and of the donor.<sup>71</sup> The critical nuclearity  $n_c$  corresponding to the potential threshold imposed by the donor and the transfer rate constant  $k_{27}$ , which is supposed to be independent of  $n$ , are derived from the fitting between the kinetics of the experimental donor decay under various conditions and numerical simulations through adjusted parameters.<sup>44,71</sup> By changing the reference potential in a series of redox monitors, the dependence of the silver cluster potential on the nuclearity was obtained (Table 5).

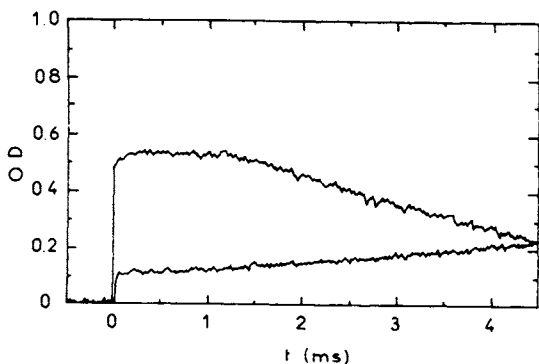


Figure 6. Transient optical absorption signals of the electron donor decay (reduced form of sulfonato-propyl viologen SPV $^-$  at 650 nm) and of the autocatalytic growth of silver clusters (at 420 nm), after a critical time. Single pulse in a mixed solution of silver ions and SPV.<sup>44</sup>

Clusters  $M_n^+$  may also behave as electron donors when formed in the presence of *oxidizing* reactants. For example, as far as  $n < n_c$ , the electron transfer from  $M_n$  to  $S$  is possible since  $E^\circ(M_n^+/M_n) < E^\circ(S/S^-)$  :



This cascade of reactions (corrosion process) is generally slow with respect to (27-29) due to the step of  $M^+$  release (31). However, it is observed when the coalescence (14) is also slow. For example, it was found that during the very slow coalescence of  $Ag_n$  in a Nafion membrane, controlled by the slow diffusion between the cavities ( $10^4 \text{ l mol}^{-1} \text{ s}^{-1}$ )<sup>72</sup>, the smallest clusters could be

Table 3

Nuclearity-dependence of  $E^\circ(M_n^+/M_n)$  (in  $V_{\text{NHE}}$ )<sup>24</sup>

Reference system (electron donor)	$E^\circ(S/S^-)$ (ref. couple)	Metal cluster (electron acceptor)	$n_c$ (reduced atoms/cluster)
Ni <sup>+</sup>	- 1.9	Ag <sub>n</sub>	1
(CH <sub>3</sub> ) <sub>2</sub> C <sup>•</sup> OH (pH	- 1.8	Ag <sub>n</sub>	1
SPV <sup>-•</sup>	- 0.41	Ag <sub>n</sub>	4
Cu <sup>+</sup>	0.16	Ag <sub>n</sub>	11
Q <sup>-•</sup> (pH = 4.8)*	0.22	Ag <sub>n</sub>	85 ± 5
Q <sup>-•</sup> (pH = 3.9)	0.33	Ag <sub>n</sub>	500 ± 30
MV <sup>•+</sup>	- 0.41	Ag <sub>n,CN</sub> <sup>-</sup>	5 - 6
MV <sup>•+</sup>	- 0.41	Ag <sub>n,PA</sub>	4
MV <sup>•+</sup>	- 0.41	Cu <sub>n,Cl</sub> <sup>-</sup>	6 ± 1

\* Q<sup>-•</sup> is the semiquinone of naphthazarin.

oxidized, particularly when the dose *per* pulse is low, by the protons H<sub>3</sub>O<sup>+</sup>, which are highly concentrated at the surface of cavities ( $k_{\text{corr}} = 0.5 \text{ l mol}^{-1} \text{ s}^{-1}$ ). In contrast, when clusters reach by coalescence the critical nuclearity for which their potential is higher than  $E^\circ(\text{H}_3\text{O}^+/\text{H}_2) = 0 V_{\text{NHE}}$ , they escape corrosion and are observed by optical absorption. The numerical simulation of the kinetic signal including the cascade of coalescence reactions (14) and of oxidation reactions (30-32) yields the value  $n = 8$  for the upper limit of nuclearity of silver clusters oxidized by H<sub>3</sub>O<sup>+</sup> in the Nafion cavities.<sup>72</sup> Therefore,  $E^\circ(\text{Ag}_8^+/\text{Ag}_8) > E^\circ(\text{H}_3\text{O}^+/\text{H}_2) = 0 V_{\text{NHE}}$ . Note that such a corrosion by H<sub>3</sub>O<sup>+</sup> is not observed under conditions of free diffusion of the clusters as in Ag<sup>+</sup> solutions,<sup>53</sup> because the coalescence let grow much faster the clusters up to the supercritical nuclearities.

When silver or gold atoms are generated from Ag<sup>I</sup>(CN)<sub>2</sub><sup>-</sup> or Au<sup>I</sup>(CN)<sub>2</sub><sup>-</sup> in the presence of the methylviologen redox couple MV<sup>2+</sup>/MV<sup>•+</sup>, oxidation of the smallest clusters is also observed, because coalescence in cyanide solutions is slow.<sup>65,73</sup> While supercritical silver clusters ( $n > 6 \pm 1$ ) (Table 3) accept electrons from MV<sup>•+</sup> with a progressive increase of their nuclearity (reactions (25-27)), the subcritical clusters undergo a progressive oxidation by MV<sup>2+</sup> through reactions (28-30). Reaction (30) ( $n < n_c$ ) is the reverse of reaction (25) ( $n > n_c$ ). If cyano silver clusters require a higher nuclearity than aquo clusters to react with MV<sup>•+</sup> (Table 3), it means that the ligand CN<sup>-</sup> lowers the redox potential at a given  $n$ , as it is the case for the bulk metal. Actually, the reduced ions MV<sup>•+</sup> so produced act as an electron relay favoring the growth of large clusters at the expense of the small ones. The coexistence of reduction by MV<sup>•+</sup> and oxidation by MV<sup>2+</sup> is observed because the coalescence in the

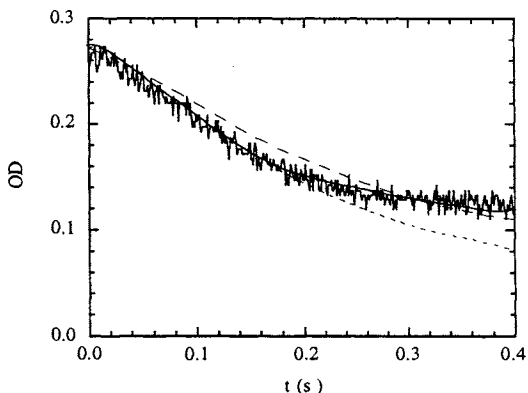


Figure 7. Comparison between simulated and experimental decay of  $MV^+$  in the presence of growing clusters  $Ag_n(CN^-)$  including oxidation of subcritical oligomers by  $MV^{2+}$  and development of supercritical clusters by  $MV^+$ . The best fit yields  $n_c = 5$ .<sup>65</sup>

presence of ligand  $CN^-$  is quite slow (Figure 7). In the case of gold clusters complexed by cyanide, the coalescence is still slower and oxidation of  $Au_n(CN^-)$  by  $MV^{2+}$  is observed alone.<sup>73</sup> Figure 8 compares the nuclearity effect on the redox potentials<sup>44,70</sup> of hydrated  $Ag^+$  clusters  $E^\circ(Ag_n^+/Ag_n)_{aq}$  together with the effect on ionization potentials  $IP_g(Ag_n)$  of bare silver clusters in the gas phase.<sup>74,75</sup> The asymptotic value of the redox potential is reached at the nuclearity around  $n = 500$  (radius  $\approx 1$  nm), which thus represents for the system the transition between the mesoscopic and the macroscopic phase of the bulk metal. The density of values available so far is not sufficient to prone the existence of odd-even oscillations like for  $IP_g$ . However, it is obvious from this figure that the variations of  $E^\circ$  and  $IP_g$  do exhibit opposite trends vs.  $n$ , for the solution (Table 5) and the gas phase, respectively.

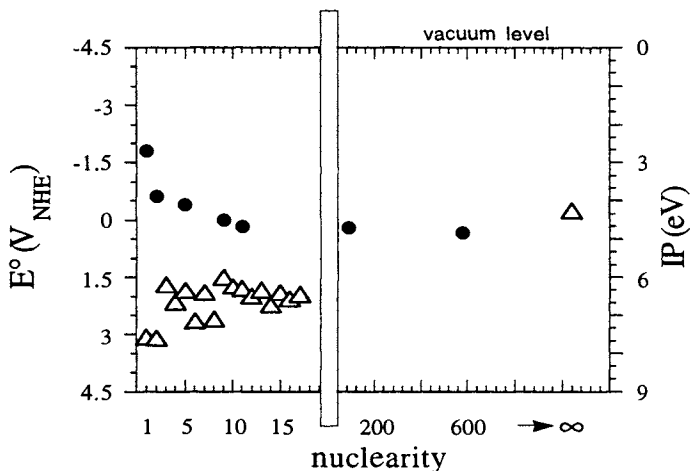


Figure 8. Size-dependence of the redox potential of silver clusters in water ( $\bullet$ )<sup>70</sup> and in the gas phase ( $\Delta$ ).<sup>74,75</sup> The redox potentials refer to the normal hydrogen electrode whose Fermi potential is at 4.5 eV.

The difference between ionization potentials of bare and solvated clusters decreases with increasing  $n$  and corresponds fairly well to the solvation free energy deduced from the Born model<sup>52</sup> (for the single atom, the difference of 5 eV represents the solvation energy of the silver cation).<sup>44</sup>

A variation of  $E^\circ(\text{Cu}_n^+/\text{Cu}_n)$ , similar to that of silver, is expected for copper since the atom potential is  $E^\circ(\text{Cu}^+/\text{Cu}^0) = -2.7 \text{ V}_{\text{NHE}}$ <sup>16</sup> (Table 2), that of  $\text{Cu}_7$  is  $E^\circ(\text{Cu}_7^+/\text{Cu}_7) = -0.4 \text{ V}_{\text{NHE}}$ <sup>76</sup> (Table 5), and the bulky electrode potential is at  $0.52 \text{ V}_{\text{NHE}}$ .

Some calculations<sup>77</sup> have been made also to derive the microelectrode potential  $E^\circ(\text{M}^+, \text{M}_{n-1}/\text{M}_n)$  for silver and copper from the data in the gas phase (nuclearity-dependent  $\text{M}-\text{M}_n$  bond energy and  $\text{IP}_g(\text{M}_n)$ ). The potential  $E^\circ(\text{M}^+, \text{M}_{n-1}/\text{M}_n)$  presents odd-even oscillations with  $n$ , (more stable for  $n$  even) as for  $\text{IP}_g$ , but again the general trends are opposite, and an increase is found in solution due to the solvation energy.

## 5. SYNTHESIS OF MONOMETALLIC NANOCLUSTERS

The quite negative value of  $E^\circ(\text{M}^1/\text{M}^0)$  and the dependence of the cluster redox potential on the nuclearity have crucial consequences in the formation of early nuclei, their possible corrosion or their growth. As an example, the faster the coalescence, the lower is the probability of corrosion by the medium. Another consequence is that when clusters of different sizes encounter, even if they are prevented from coalescing by a polymer coating, the smaller, which has a more negative potential, can still donate successively electrons to the ions adsorbed on the larger one, up to the complete oxidation of the former.<sup>53</sup> The process results in a narrower size dispersity but also to a further growth. However, various applications require the synthesis of small clusters and the coalescence should be somewhat prevented by a stabilizer or a support.

### 5.1. Metal oligomers

Metal oligomers are stabilized at quite small nuclearity when formed at low dose in the presence of polyacrylate PA.<sup>40</sup> From pulse radiolysis of  $\text{Ag}^+$ -PA solutions, it appears that the very slow ( $10^5 \text{ l mol}^{-1} \text{ s}^{-1}$ ) dimerization of  $\text{Ag}_4^{2+}$  silver clusters.<sup>51,78</sup> (275 and 350 nm) results into a blue cluster ( $n = 4$ ) absorbing at 292 nm and 800 nm<sup>79</sup> and stable in air for years. The 800 nm absorption band is assigned to a cluster-ligand PA interaction.<sup>51</sup> The results have been recently confirmed.<sup>80</sup> Clear images by STM show flat clusters of 0.7 nm with atoms spaced by 0.25 nm (Figure 1).<sup>3</sup> Each cluster contains seven nuclei (possibly with an eighth atom in the central position). Since 4 atoms only were reduced, they correspond to the stoichiometry  $\text{Ag}_7^{3+}$  (or  $\text{Ag}_8^{4+}$ ). Though the clusters are protected from coalescence, they undergo fast growth by successive electron transfer reactions from  $\text{MV}^+$  and cation adsorption. Once developed they absorb at 400 nm and their size may reach tens of nm. In the presence of gelatin, complexation of silver with methionine groups slows down the oligomer growth and small oligomers are stabilized.<sup>38</sup>

Similarly, when  $\text{PtCl}_6^{4-}$  ions are irradiated in the presence of PA which prevents coalescence, most of Pt atoms are found by STM imaging in the form of very small *platinum* oligomers of 3-7 atoms only.<sup>81</sup> In the presence of PP,  $\text{PtCl}_6^{4-}$  irradiated solutions present a UV band with a maximum at 215 nm.<sup>82</sup> About 20 % of the initial signal is lost by oxidation when the sample is exposed to air, the rest being stable. This result again confirms that the redox potential of the smallest clusters is markedly shifted to the negative values.

When  $\text{CuSO}_4$  solutions are  $\gamma$ -irradiated with PA at pH 10, new absorption bands at 292, 350 and 455 nm are observed provided the reduction of copper ions is partial.<sup>83</sup> At increasing dose, the intensity of the peaks assigned to small stabilized *copper oligomers* decreases correlatively with the plasmon band increase which develops at 570 nm. The UV species are very sensitive to oxygen. Under acidic conditions, large clusters are observed but not the UV oligomers. A pulse radiolysis study of monovalent  $\text{Cu}^+$  ions, complexed in the presence of a high concentration of  $\text{Cl}^-$ , without polymeric stabilizer, has shown that short-lived states of reduced copper corresponding to the early steps of growth also absorb in the range 355-410 nm.<sup>84</sup>

Among the non-noble metals that can be synthesized by radiation-induced reduction in solution, nickel raises some difficulties since the atom formation and aggregation processes undergo the competition of oxidation reactions of highly reactive transients, such as monovalent  $\text{Ni}^+$  ion, Ni atom and the very first *nickel* oligomers. Nevertheless, in the presence of PA, a new absorption band develops at 540 nm with increasing dose. The formation of the same absorption band was observed by pulse radiolysis. It increases simultaneously with the formation of the very first Ni atoms and it is assigned to a cluster-ligand interaction. Due to the high reactivity of nickel oligomers, the band disappears within 24 hours, even when solutions are preserved from oxygen, through a spontaneous reaction with the solvent.<sup>85</sup>

## 5.2. Molecular metal clusters

When the irradiation of metal ion solutions is done in the presence of the ligands CO or  $\text{PPh}_3$ , metal reduction, ligandation and aggregation reactions compete, leading to reduced metal complexes and then to stable molecular clusters.<sup>23,86</sup> Increasing the [metal precursor]/[ligand] ratio favors higher nuclearities. Chini clusters  $[\text{Pt}_3(\text{CO})_6]_m^{2-}$  with  $m = 3-10$  (*i.e.* 9-30 Pt atoms) have been obtained by irradiating  $\text{K}_2\text{PtCl}_4$  under CO in a water/2-propanol solution.<sup>86,87</sup> The oxidation degree is  $-2/3m$ . The  $m$  value is deduced from the very specific UV-visible and IR absorption spectra (Figure 9).

The synthesis is selective and  $m$  is controlled by adjusting the dose ( $m$  decreases at high doses). The mechanism of the reduction has been observed recently by pulse radiolysis.<sup>88</sup> Reduction by pulse-induced radicals of all  $[\text{Pt}_3(\text{CO})_6]_6^{2-}$  clusters yields the transient  $[\text{Pt}_3(\text{CO})_6]_6^{3-}$ , which then quickly dimerizes into  $[\text{Pt}_3(\text{CO})_6]_{12}^{6-}$  before undergoing cleavage into  $3 \times [\text{Pt}_3(\text{CO})_6]_4^{2-}$ . If the initial reduction is only partial, further addition of  $[\text{Pt}_3(\text{CO})_6]_4^{2-}$  with excess  $[\text{Pt}_3(\text{CO})_6]_6^{2-}$  leads to  $2 \times [\text{Pt}_3(\text{CO})_6]_5^{2-}$  which is also the product observed by  $\gamma$ -radiolysis. Molecular clusters  $[\text{Pt}_3(\text{CO})_6]_5^{2-}$  have been observed by STM.<sup>89</sup>



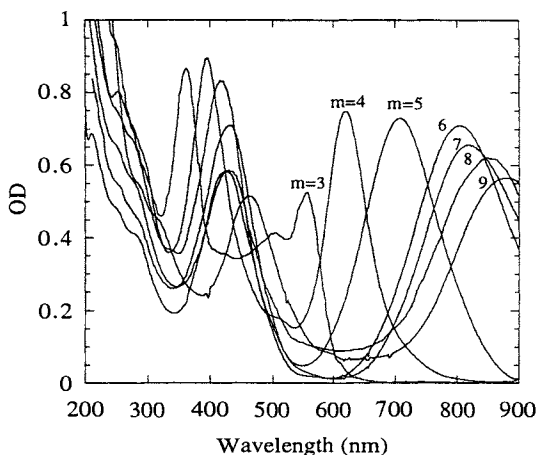


Figure 9. UV/VIS spectra of clusters  $[\text{Pt}_3(\text{CO})_6]_m^{2-}$  of different nuclearity  $m$  produced in  $\gamma$ -irradiated solutions of  $\text{K}_2\text{PtCl}_4$  in equivolumic  $\text{H}_2\text{O}$ -2-propanol solvent under 1 atm CO with various doses.

$m = 9$  : 0.1 kGy, 8 : 0.20, 7 : 0.40, 6 : 0.80, 5 : 1.60, 4 : 3.20, 3 : 10 kGy.<sup>88</sup>

Other molecular metal clusters have been obtained by  $\gamma$ -radiolysis, such as  $\text{Ru}_3(\text{CO})_{12}$  and  $\text{H}_2\text{Ru}_6(\text{CO})_{18}$ , or  $\text{Fe}(\text{CO})_5$  and  $\text{Fe}_3(\text{CO})_{12}$  at higher  $[\text{M}]/[\text{L}]$  ratio. Similarly,  $\text{Co}_2(\text{CO})_8$ ,  $[\text{Os}_5(\text{CO})_{15}]^2$  and  $[\text{HOs}_5(\text{CO})_{15}]$ ,<sup>90</sup>  $\text{Rh}_6(\text{CO})_{16}$ ,<sup>91</sup>  $[\text{Rh}_{12}(\text{CO})_{30}]^2$ ,<sup>92</sup> may be generated by irradiation. Some mixed bi- or tri-nuclear carbonyl clusters have been also synthesized such as  $\text{FeRu}_2(\text{CO})_{12}$ ,  $\text{RuOs}_2(\text{CO})_{12}$  or  $\text{Ru}_2\text{Os}(\text{CO})_{12}$ .<sup>91</sup>

### 5.3. Nanometric metal clusters

Most of mono or multivalent metals, except alkaline metals, have been prepared by  $\gamma$ -radiolysis in the form of small clusters (Table 4). They are stabilized with respect to further coalescence by polymers or simply ligands (Figure 1). The final size depends on the type of polymer or ligand, on the ratio metal/polymer but also on the dose rate. Indeed, sudden generation of a high concentration of isolated atoms at high dose rate and thus the formation by coalescence of more numerous and smaller nuclei yields clusters of 1-2 nm. Instead, the reduction of adsorbed ions at the surface of clusters which is predominant at low dose rate contributes to development of less numerous growth centers and results in larger clusters. In both cases, however, the nuclei generation being strictly reproducible, the distribution of long-term sizes presents an exceptional homodispersity.

Table 4 presents the maximum wavelength of the cluster surface plasmon absorption. The particles are most often spherical. Nevertheless, some of these clusters, which are generated in solution and then deposited on a grid for HRTEM and electron diffraction observations exhibit clearly pentagonal shapes with a fcc structure, which suggests the formation of twin fcc crystallites growing from the faces of an icosahedral nucleus. The noble metal clusters are generally stable in air, which makes them useful in numerous applications. Phase imaging in tapping mode AFM is a powerful tool for the characterization of clusters stabilized by polymer matrices as shown recently in observing silver and gold samples<sup>93</sup> and helps to discriminate between amorphous polymer and metal clusters.

Table 4.  
Radiation-induced metal clusters. Optical absorption properties.

Metal	$\lambda_{\max}$ (nm)	Ref.	Metal	$\lambda_{\max}$ (nm)	Ref.	Metal	$\lambda$	Ref.
Co	UV	94,95	Pd	205	39,96,97,99	Ir	UV	43,98
Ni*	UV	94,99,100,101	Ag*	380	11,44,47,64	Pt*	215	81,102,103,104
Cu*	570	39,60,82,96,105	Cd*	260	39,106,107	Au*	520	50,59,61,108,109,110
Zn	UV	94	In*	270	60	Hg*	500	60,94
Mo	UV	94	Sn	200	94,111	Tl*	300	48,49,60,68,112
Ru	UV	94	Sb	UV	94	Pb*	220	60,94,113,114
Rh	UV	94	Os	UV	94	Bi	253	60,94,115

The symbol \* indicates that the earliest steps of the cluster formation have been studied by pulse radiolysis.

Non noble metal clusters are considerably more fragile to corrosion by the solvent than are noble metal clusters. Therefore the production of stable small particles results from a compromise between the smallest size and the longest stability.

Long-lived clusters  $\text{Cu}_n$ ,  $\text{Ni}_n$ ,  $\text{Co}_n$ ,  $\text{Sn}_n$ ,  $\text{Tl}_n$ ,  $\text{Pb}_n$  (Table 4) may be formed in deaerated basic medium, but  $\text{Zn}_n$  clusters are oxidized into zinc hydroxide within a few weeks even in the absence of  $\text{O}_2$ . Clusters  $\text{Cd}_n$  are better stabilized by gelatin.<sup>39</sup>  $\text{Ni}_n$  or  $\text{Co}_n$  clusters display ferromagnetic behaviour. Whereas all of these non-precious metal clusters are easily oxidized in solution by  $\text{O}_2$ , they may be stabilized in air after drying under inert atmosphere.

Adsorption of ions or molecules on metal clusters affect markedly their optical properties. It was shown that the intensity and the shape of the surface plasmon absorption band of silver nanometric particles which is close to 380 nm change upon adsorption of various substances.<sup>116</sup> The important damping of the band generally observed is assigned to the change of the electron density of the thin surface layer of the particle where electrons are for instance injected by adsorbed electrophilic anions.<sup>22</sup> This is followed by a red shift of the damped band corresponding to loose agglomeration of the clusters.<sup>117</sup> Silver particles covered by  $\text{I}^-$  become particularly sensitive to oxidation in air since the Fermi level is shifted to a more negative potential by the electron donation.<sup>22</sup>

#### 5.4. Developed clusters

Actually, the kinetics study of the cluster redox potential (§ 4.2) mimics the process of the photographic development, except clusters are free in the solution (not fixed on AgBr crystals) and, beyond the critical nuclearity, they

receive electrons without delay from the developer already present. However, the processes present similar features in both cases. The critical nuclearity depends on the donor potential and then the autocatalytic growth does not stop until the reaction is complete. Consequently, the same mechanism (Figure 5) based on the nuclearity-dependence of the cluster redox potential was also proposed<sup>44</sup> to explain the existence of a critical size in the photographic development, the threshold being imposed by the developer potential. The amplification of the cluster size by the development is from tens of nm ( $n = 3-5$ ) to the AgBr crystal size of  $1 \mu\text{m}$  ( $n = 10^{8-9}$ ), while in solution it depends on the concentration ratio between critical nuclei and the rest of metal ions reduced by the electron donor.

The development process may be used to select the cluster final size but it occurs also spontaneously any time an even mild reducing agent is present during the radiolytic synthesis. The specificity of this method is to combine the ion reduction successively :

i) by radiolytic reduction. The atoms independently formed in the bulk coalesce into oligomers (reactions 1, 7-14);  
 ii) by chemical reduction beyond a certain oligomer nuclearity, for which the redox potential allows electron transfer from a conventional donor  $S$  (reactions 25-27). This chemical agent is generally unable thermodynamically to reduce directly the ions into atoms (§ 4.1), but it achieves the reduction of the rest of the ions after they have been adsorbed on the radiation-induced clusters acting as nuclei of catalytic reduction and growth. Note that (i) the presence of a polymer restricts the coalescence process but (ii) does not prevent at all the electron transfer from the donor. As in § 4.2, the redox threshold  $E^\circ(S/S')$  fixed by the donor imposes a critical nuclearity  $n_c$  for the growth process. Adjusting the respective parts of ions radiolytically and chemically reduced allows to control the cluster concentration (equal to that of nuclei) and their final size after development with an excellent homodispersity. Note also that for multivalent precursors the very negative potential between the transient monovalent  $M^+$  and free atoms  $M^0$  often inhibits the last step of  $2M^+$  disproportionation into  $M^{2+}$  and  $M^0$ , whereas  $M^+$  is reduced into  $M^0$  by the radiolytic radicals. However, when clusters are already formed radiolytically, the disproportionation occurs at their surface because the potential of the couple  $M_n, M^+/M_{n+1}$  is shifted to much higher values. This process also contributes to the cluster development.

The final *silver* cluster diameter increases, at a given initial  $\text{Ag}^+$  concentration, for example from 15 nm to 50 nm ( $n$  50 times larger) when the part of reduction is increasingly achieved by the donor  $\text{SPV}^-$  rather than by radiolytic radicals.<sup>44</sup> A red shift correlates with the growth in size in the final optical surface plasmon band. Non irradiated solutions of EDTA silver complex are stable because EDTA does not reduce directly the ions. However, after the appearance of the 400 nm spectrum of silver clusters formed in a partially radiation-reduced solution (spherical particles of 10-15 nm diameter),

the band intensity increases for days as a post-effect and the silver ions are totally reduced.<sup>5</sup> The post-irradiation reduction is assigned to the lone pair N atom electrons of the EDTA ligand, provided the silver ions are fixed on clusters formed by irradiation acting as nuclei. Once the development is over, the absorption band is red-shifted (large particles of 100-150 nm ) (Figure 1). It is clear that this unusual growth occurs preferentially in a planar way favoring the 111 surface.

*Nickel* oligomers prepared in the presence of PA ( $\lambda_{\max} = 540 \text{ nm}$ ) (§ 5.1) may act also as catalysts for the reduction of  $\text{Ni}^{2+}$  by hypophosphite ions. This requires, as shown by pulse radiolysis, a critical nuclearity, while free  $\text{Ni}^{2+}$  cannot be directly reduced by  $\text{H}_2\text{PO}_2^-$ . Very low radiation dose conditions, just initiating the formation of a few supercritical nuclei, will lead to large particles of nickel.<sup>84</sup>

When trivalent chloro *gold* ions  $\text{Au}^{\text{III}}\text{Cl}_4^-$  are  $\gamma$ -irradiated at increasing doses, the reduction occurs by successive steps (reduction into the unstable bivalent state  $\text{Au}^{\text{II}}$  then disproportionation of  $\text{Au}^{\text{II}}$  into  $\text{Au}^{\text{III}}$  and  $\text{Au}^{\text{I}}$ ). However,  $\text{Au}^{\text{I}}$  ions are not reduced as far as  $\text{Au}^{\text{III}}$  ions are more concentrated than  $\text{Au}^{\text{I}}$ , nor do they disproportionate because the redox potential involving the single atom  $E^\circ(\text{Au}^{\text{I}} / \text{Au}^{\text{0}})$  is quite negative (Table 2). Thus  $\text{Au}^{\text{I}}\text{Cl}_2^-$  ions accumulate and the cluster appearance is delayed by an induction time (Figure 10).<sup>109</sup> With higher doses,  $\text{Au}^{\text{I}}$  ions become more abundant than  $\text{Au}^{\text{III}}$  and are also reduced into atoms and clusters. In the presence of alcohols or of preformed clusters,  $\text{Au}^{\text{I}}$  ions do not accumulate because the potential order of  $(\text{Au}^{\text{I}} / \text{Au}^{\text{0}})$  and  $(\text{Au}^{\text{II}} / \text{Au}^{\text{I}})$  couples is now inverted due to complexation or adsorption, respectively.  $\text{Au}^{\text{I}}$  ions are thus allowed to disproportionate giving rise to clusters. In addition, a very slow chemical reduction by the alcohol is found, which occurs exclusively at the surface of the clusters formed by irradiation so that all gold ions may be reduced, whatever the initial dose.<sup>109</sup> As seen by AFM observations, the cluster size remains constant and their concentration increases with dose during the  $\gamma$ -irradiation, while during the post-irradiation reduction by alcohol the size increases at constant density of particles. The lower the dose, the larger the final size of the homodisperse cubic crystallites which may range from 10 to 500 nm, depending on the respective parts of radiolytic and chemical types of reduction.

Gold ions  $\text{Au}^{\text{I}}(\text{CN})_2^-$  are not reducible in solution by alcohol radicals owing to their much lower redox potential in the complexed form<sup>59</sup> than in the hydrated form (§ 4.1 and Table 2). This has been recently confirmed<sup>110</sup> by the observation of a quite long induction time before the appearance of the plasmon band of gold clusters generated by a low amount of solvated electrons only.

However, the complexed ions are reduced when adsorbed at a particle surface where the potential is shifted to more positive values. Indeed such a radiolytic reduction of  $\text{Au}(\text{CN})_2^-$  by alcohol radicals on conventional gold

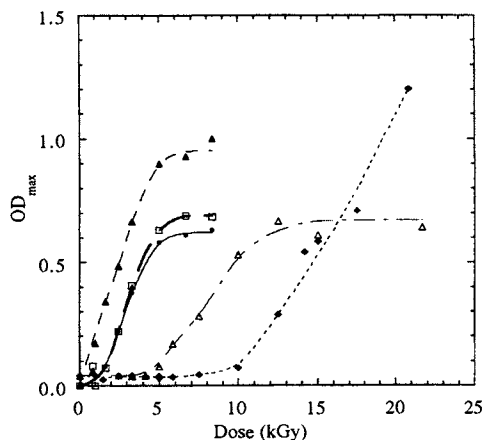


Figure 10. Evolution of the absorbance of gold clusters at 520 nm vs dose in  $\text{Au}^{\text{III}}$  solutions without additives at  $10^{-3} \text{ mol.l}^{-1}$  ( $\Delta$ ),  $2 \times 10^{-3} \text{ mol.l}^{-1}$  ( $\blacklozenge$ ), and with PVA ( $\bullet$ ), 2-propanol ( $\blacktriangle$ ), PVA and 2-propanol ( $\square$ ).<sup>109</sup>

clusters results in their development into larger clusters to an extent depending on added gold ion amount. A stabilization of low valencies of metals and an induction time before cluster formation have been observed as well in the case of iridium,<sup>98</sup> platinum,<sup>99</sup> palladium,<sup>118</sup> copper<sup>83</sup> or nickel.<sup>100</sup>

The time-resolved studies of the cluster formation achieved by pulse radiolysis techniques allow one to better understand the main kinetics factors that affect the final cluster size found, not only in the radiolytic method but also in other reduction (chemical or photochemical) techniques. A general scheme of nucleation and growth of clusters generated in solution is presented in Figure 11. Metal ions are reduced by radiolytic radicals at each encounter. The role of polymeric surfactants is to prevent coalescence beyond a certain limit of nuclearity even at long time. For a given polymer and given conformation and chain length, this limit decreases with the ratio between metal atoms/polymer concentrations and is also affected by the type of metal. It seems that all the atoms which interact with the same single polymeric chain coalesce easily while the protection against interchain coalescence of the nucleus, then the cluster, by the coiled polymer chain is strong. Because the nucleation rate is controlled by the dose rate, the smallest size limit at a given ratio of atom/polymer is obtained when the irradiation is as sudden as possible (Figure 11a).

By contrast, a slower irradiation favors adsorption of ions not yet reduced onto atoms or small clusters formed at the start of irradiation and this process is not prevented by the polymer nor is the reduction *in situ* of the ions by electron transfer from the reducing radicals. Likewise, electrons from small clusters can be transferred to larger ones coated with adsorbed ions and polymer. The final size may thus be much higher than the above limit imposed by the polymer when just coalescence occurs and the size increases with the irradiation time required for the reduction (therefore at decreasing dose rate) (Figure 11b).

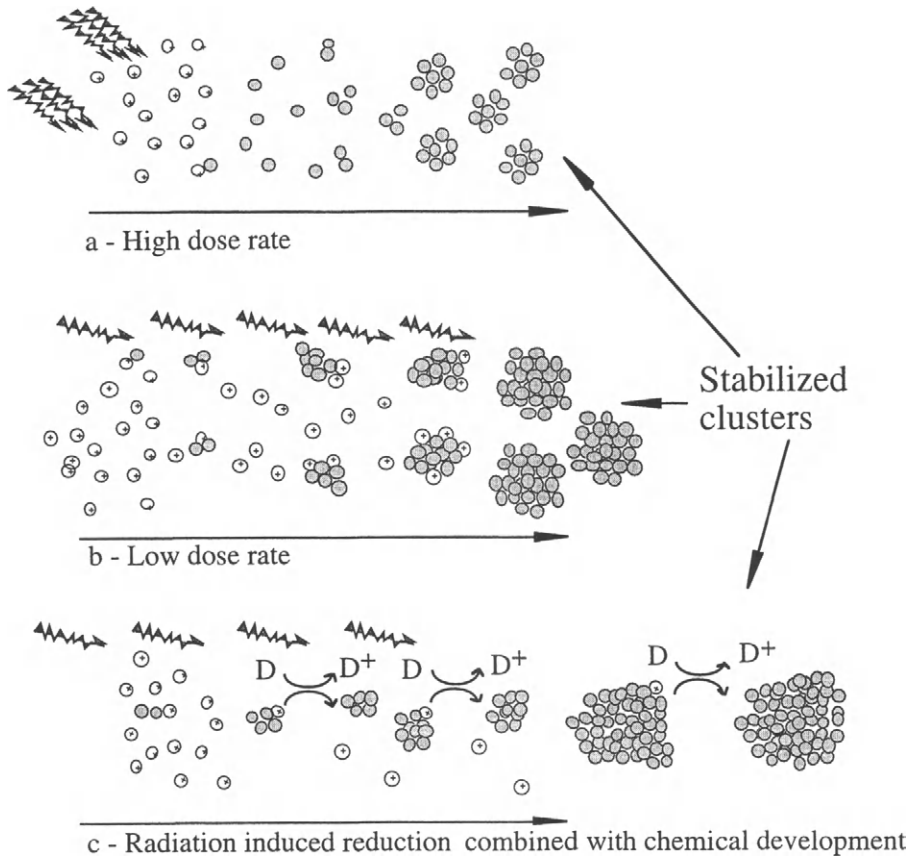


Figure 11. Nucleation and growth of clusters generated by radiolytic radicals at various dose rates, with or without electron donor D. The stabilizing effect of the polymer prevents exclusively coalescence beyond a certain limit of nuclearity but does not prevent successive ion and electron transfers (from the radicals at low dose rate and from the donor) which let develop the cluster up to much larger sizes.

An extreme case of the size development occurs, despite also the presence of the polymer, when the nucleation induced by radiolytic reduction is followed by a chemical reduction. Because the donor potential is more positive than that of the ion/atom couple, the donor D does not create new nuclei and the electron transfer towards adsorbed ions starts exclusively after radiolytic reduction and coalescence have produced clusters of critical nuclearity. Then the final size depends on the ratio between the concentration

of ions chemically reduced and that of supercritical nuclei (fixed by the dose and the donor redox potential) (Figure 11c). The shape also may be different from that resulting from coalescence if ions are preferentially adsorbed on a specific face of the growing nanocrystal<sup>5</sup> (Figure 1).

Conversely, under conditions of slow reduction and coalescence, oxidation of the smallest clusters is possible by  $O_2$ ,  $H^+$  or even by the oxidized form of the donor,  $D^+$ .

Generally reducing chemical agents are thermodynamically unable to reduce directly metal ions into atoms (§ 4) unless they are complexed or adsorbed on walls or particles. Therefore we explain the higher sizes and the broad dispersity obtained in this case by *in situ* reduction on fewer sites.

### 5.5. Supported and confined nanoclusters

The radiolytic synthesis consists in i) either preparing first nanometric metal clusters in solution which are then put in contact with the support (possibly by filtration), or ii) irradiating *in situ* the ionic precursors after their adsorption onto the supporting material.

Positively charged metal ions easily diffuse into the cavities of a Nafion *polymeric membrane* by ion-exchange of the counter cations of the constitutive sulfonic groups. (§ 4.2) The size of channels and cavities is controlled by the proportion of alcohol in aqueous solution which also governs the final size of silver or nickel clusters. During irradiation of a solution of metal ions (silver, palladium or nickel) containing PVA, the ion reduction occurs simultaneously with the cross-linking of the polymer.<sup>23</sup> Finally, after drying, the clusters formed are trapped in a polymeric film. In the case of nickel, the thin film is ferromagnetic. Irradiation of reverse *micelles* containing gold ions in the aqueous phase generates small gold clusters.<sup>42</sup> Silver oligomers ( $n < 10$ ) in AOT micelles absorb in the UV.<sup>119</sup>

Colloidal support such as small  $SiO_2$  particles restrict interparticle diffusion of silver atoms when formed by radiolysis of the ions at their surface. The silver oligomers absorbing at 290 and 330 nm are observed by pulse radiolysis. They are stable with respect to coalescence but they are oxidized by  $MV^{2+}$ ,  $O_2$ ,  $Cu^{2+}$  and  $Ru(NH_3)_6^{3+}$ .<sup>120</sup> *Alumino-silica* gels with silver ions give after irradiation optically clear xerogels containing silver clusters from 2.5 to 4.5 nm.<sup>121,122</sup>

Irradiation by ionizing radiation able to penetrate into a *zeolite* material exchanged by metal ions allows to generate metal atoms and clusters *in situ* in the cavities.<sup>123,124</sup> The observation of irradiated faujasite (Na-Y zeolite) by optical absorption spectroscopy at increasing doses and at low silver content demonstrates the formation of two bands at 265 and 305 nm which have been assigned to the charged trimer  $Ag_3^{2+}$ . Then, the ESR observation after a dehydration step indicates the reduction of this species into  $Ag_3^0$ .<sup>125</sup> Irradiation of  $H_2PtCl_6$  solution included in mesoporous channels of molecular sieves induces nanowires of platinum.<sup>126</sup>

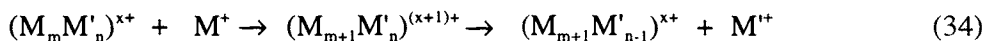
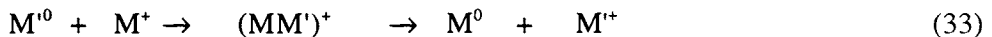
Pulse radiolysis studies of the reactivity of 25 nm *AgI* particles with  $e_{aq}^-$  in the presence of alcohol have shown that first the semiconductor spectrum at 360 nm is bleached, then silver atoms and clusters at 450-600 nm are formed.<sup>127,128</sup> The electron transfer between the couple  $MV^{2+}/MV^+$  and  $Ag_n$  clusters formed on an *AgCl* crystallite was studied by pulse radiolysis.<sup>129</sup> The coalescence of Ag atoms at the *AgCl* surface is slow so that, as in the presence of  $CN^-$ , an electron transfer from subcritical clusters to  $MV^{2+}$  precedes the electron transfer from  $MV^+$  to supercritical  $Ag_n^+$ .

## 6. BIMETALLIC CLUSTERS

Composite clusters, alloyed or bilayered, are of great interest because they enlarge the number of the possible types of clusters. It is therefore important to be able to select the conditions of the synthesis of composite metal clusters containing  $M^0$  and  $M'^0$  in variable proportions, with either an alloyed or a core/shell structure. Actually, when a mixed solution of two ionic precursors  $M^+$  and  $M'^+$  is irradiated or chemically reduced, both situations of alloyed or bilayered cluster formation may be encountered without clear prediction.<sup>130</sup>

### 6.1. Core-shell clusters formation

In many cases, even though  $M^+$  and  $M'^+$  are both readily reduced by radiolytic radicals (reactions (1,7,8)), a further electron transfer from the more electronegative atoms (for example  $M'$ ) to the more noble ions  $M^+$  ( $E^\circ(M^+/M^0) < E^\circ(M'^+/M'^0)$ ) systematically favors the reduction into  $M^0$ .



If the ionic precursors are plurivalent, an electron transfer is possible as well between the low valencies of both metals, so increasing the probability of segregation.<sup>131</sup> Reaction (33) has been observed directly by pulse techniques for some systems<sup>44,132,133</sup> and the transient cluster  $(MM')^+$  sometimes identified such

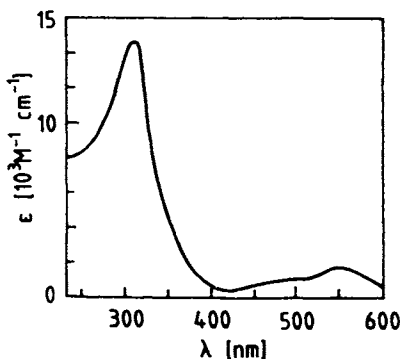


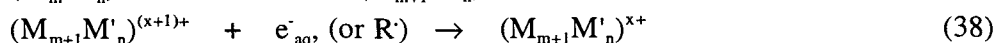
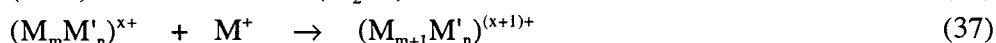
Figure 12. Absorption spectrum of  $(AgCo)^{2+}$  obtained by pulse radiolysis of a mixed solution containing  $2.5 \times 10^{-4}$  M  $Co^{2+}$ ,  $10^{-3}$  M  $Ag^+$  and 0.1 M propanol-2.<sup>133</sup>



as  $(\text{AgTl})^+$  or  $(\text{AgCo})^{2+}$  (Figure 12).<sup>133</sup> The less noble metal ions act as an electron relay towards the precious metal ions. Thus monometallic clusters  $M_n$  are formed first and then, when  $M^+$  ions are exhausted,  $M'^+$  ions are reduced afterwards at the surface of  $M_n$ . The final result is a core-shell cluster  $M_m/M'_n$  where the more noble metal  $M$  is coated by the second  $M'$ .

## 6.2. Alloyed clusters formation

In some other cases, the intermetal electron transfer does not occur even during hour-long irradiations.<sup>99</sup> The initial reduction reactions (1) are followed by mixed coalescence and association of atoms and clusters with ions as in (33, 34). Besides dimerization of atoms of the same metal into  $M_2$  and  $M'_2$ , coalescence of both types of atoms occurs twice more frequently :



Then alternate association (37) and reduction reactions (38) progressively build bimetallic alloyed clusters according to the statistics of encounters, therefore to the relative initial ion abundance.<sup>53</sup>

## 6.3. Dose rate effects

The possible formation of an alloyed or a core-shell cluster depends on the kinetic competition between, on one hand, the irreversible release of the metal ions displaced by the excess ions of the more noble metal after electron transfer (reactions (33, 34) and, on the other hand, the radiation-induced reduction of both metal ions (reactions (1, 7, 8, 38)) which depends on the dose rate (Table 5). Once the reduction of both metal ions is complete, any further intermetallic electron transfer is unlikely at room temperature. A pulse-radiolysis study of a mixed system<sup>73</sup> suggested that a very fast and total reduction by the means of a powerful and short irradiation delivered for instance by an electron beam (EB) should produce alloyed clusters. Indeed such a decisive effect of the dose rate has been demonstrated.<sup>4</sup> However, the competition imposed by the intermetal electron transfer is more or less serious, since, depending on the couple of metals, the process may not occur,<sup>99</sup> or on the contrary lasts hours, only minutes or even seconds.<sup>4</sup>

The alloyed or layered character of a small bimetallic cluster structure is generally quite difficult to conclude experimentally.<sup>4, 134</sup> Even if the surface plasmon transitions of both pure metals are specific (with one possibly in the UV), the unknown spectra of alloyed or bilayered clusters are both expected in the same intermediate region. The structure of the composite cluster is derived indeed from the evolution observation of the absorption spectrum at increasing dose.<sup>4, 143</sup> Because the spectrum is due to surface phenomena, it changes with dose when electron transfer occurs. The composition of the bilayered cluster

surface is shifted at increasing dose from the spectrum of the more noble metal to that of a cluster coated by the second. In contrast, the spectrum shape of alloyed clusters is unchanged at increasing dose while their intensity increases. X-ray analysis of clusters at partial reduction (low dose) clearly indicates whether atoms of one only or of both types of metals are present in the particles.<sup>4</sup> Electron and X-diffraction methods may reveal superlattices which correspond to a perfectly ordered atom arrangement in the case of an alloyed cluster.<sup>4,99,140</sup> Provided the lattice constants of the metals are somewhat different, the distances between atomic plans in HRTEM images indicate the possible alloyed character of the clusters. A transverse analysis of a single cluster in a scanning transmission electron microscope equipped with a field emission gun and X-ray detector provides also decisive information on the cluster composition in depth.<sup>134</sup>

The spectra of silver and gold are intense and distinct (Table 4). They are thus particularly suitable to detect the evolution of a cluster composition during its construction. Actually, pulse radiolysis of a mixed system of monovalent cyano-silver and gold ions<sup>73</sup> provided the time-resolved observation of an intermetallic displacement (Figure 13). The atoms  $\text{Ag}^0$  and  $\text{Au}^0$  are formed readily after the pulse and coalesce into an alloyed oligomer.

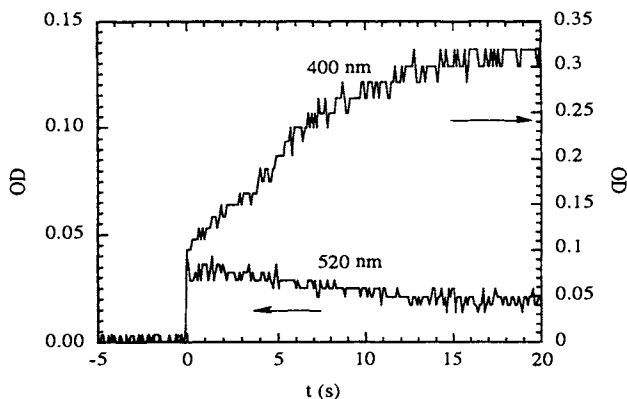


Figure 13. Correlated signals at 400 nm and 520 nm with a single pulse in equimolar mixed solution of gold and silver cyanide,  $\text{Ag}(\text{CN})_2^-$  and  $\text{Au}(\text{CN})_2^-$ , in the presence of 2-propanol.<sup>73</sup>

But, due to a slow electron transfer (within seconds) from  $\text{Au}^0$  atoms of the alloy to the unreduced ions  $\text{Ag}^1$ , a supplementary formation of  $\text{Ag}^0$  correlates with the complete dissolution of  $\text{Au}^0$ . By  $\gamma$ -radiolysis at increasing dose, the spectrum of pure silver clusters, more noble due to the  $\text{CN}^-$  ligand, is seen first at 400 nm. Then the spectrum is red-shifted when gold is reduced at the surface of silver clusters in a bilayered structure,<sup>4</sup> as when the cluster is formed in a two-step operation<sup>139</sup> (Table 5). However, when the same system is irradiated at high dose rate with an electron beam, allowing the sudden (out of redox thermodynamics equilibrium) and complete reduction of all the ions prior to the metal displacement, the band maximum of the alloyed clusters is at 420 nm.<sup>4</sup>

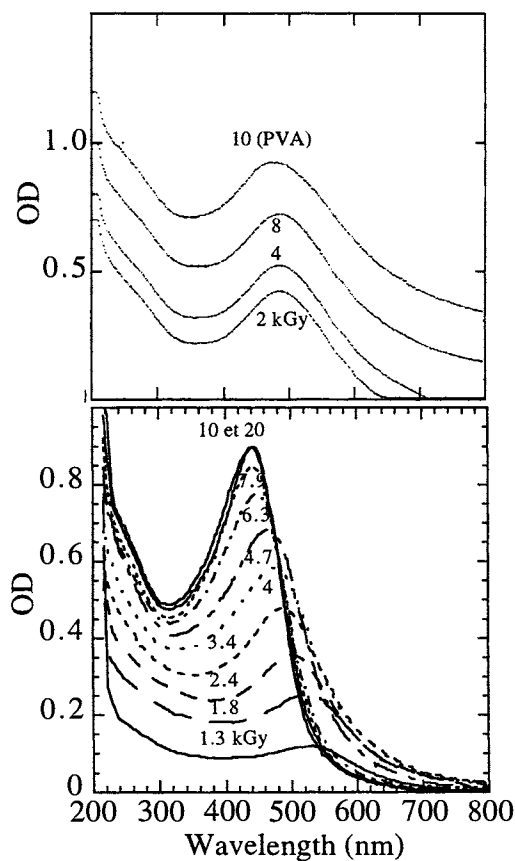


Figure 14. Absorption spectrum evolution with irradiation dose of same mixed solutions of  $\text{Au}^{\text{III}}$  and  $\text{Ag}^{\text{I}}$  at two different dose rates. Bottom : 3.8  $\text{kGy}\cdot\text{h}^{-1}$ . Top : 35  $\text{kGy}\cdot\text{h}^{-1}$ .<sup>4</sup>

Similarly, for the couple  $\text{Au}^{\text{III}}\text{Cl}_4^-$ ,  $\text{Ag}^+$ , at moderate dose rate, gold appears at first at 520 nm. Therefore,  $\text{Ag}^+$  ions act essentially as an electron scavenger, and as an electron relay toward more noble gold ions as far as gold ions are not totally reduced. Then silver-coated gold clusters are formed (Figure 14).<sup>4</sup> But at higher  $\gamma$ - or EB dose rate (irradiation time of a few seconds), the electron transfer is too slow to compete with coalescence and the spectrum of alloyed clusters develops without any shift from the lowest doses (Figure 14). Once this quenching radiolytic reduction has consumed all the ions, the intermetal displacement becomes by the fact excluded at room temperature. The maximum of the alloyed cluster surrounded by  $\text{Cl}^-$  is now at 480 nm. In both cases the profiles of local analysis by combined STEM-X-ray detection confirm the structures, bilayered and alloyed.<sup>134</sup> Noteworthy is that the clusters are particularly homodisperse and that the mean size is markedly smaller ( $< 3$  nm) than for  $\gamma$ -induced clusters, as shown by the TEM micrographs of bi-metallic samples prepared by EB irradiation (8  $\text{MGy}\cdot\text{h}^{-1}$ ). (Figure.1).

This is likely to be due to a much higher concentration of single atoms suddenly produced in the solution; these atoms act as many individual centers of nucleation and further coalescence (in contrast with low dose rate irradiation conditions under which fewer nuclei adsorb excess ions which are then reduced *in situ*).<sup>4,23</sup> The same evolution of the absorption spectrum with the dose has been found at high dose rate for various values of the Ag and Au ion fraction in the initial solution. Clusters  $\text{Ag}_{1-x}\text{Au}_x$  are alloyed with the same composition. The maximum wavelength  $\lambda_{\text{max}}$  and the extinction coefficient  $\epsilon_{\text{max}}$  of the alloy depend on  $x$ . The experimental spectra are in good agreement with

the surface plasmon spectra calculated from Mie model at  $x$  values for which optical data are available.<sup>4</sup> Similar calculations have been done for the alloy  $\text{Ag}_x\text{Pd}_{1-x}$  obtained at moderate dose rate.<sup>140</sup> Other examples of bimetallic clusters are presented in Table 5. They are formed either by irradiating a mixed solution of ionic precursors or in two steps by reducing the second metal at the surface of preformed clusters of the first metal. The process of the progressive building of alloyed clusters results from coalescence between reduced atoms and clusters, and also from the *in situ* reduction of mixed charged oligomers after association with ions (reaction 26), both processes resulting from the statistics of encounters.<sup>53</sup>

Table 5  
Synthesis and irradiation conditions of multimetallic clusters

Mixed Salts, or *Cluster, Salt	Dose rate ( kGy h <sup>-1</sup> ) Irradiation source	Particle structure (Ref.)
$\text{Ag}_n, \text{Au}(\text{CN})_2^-$	$\gamma$ , 0.9	Ag/Au, Bilayer <sup>135</sup>
$\text{Ag}(\text{CN})_2^-, \text{Au}(\text{CN})_2^-$	$\gamma$ , 35	Ag/Au, Bilayer <sup>4</sup>
$\text{Ag}(\text{CN})_2^-, \text{Au}(\text{CN})_2^-$	EB, $7.9 \times 10^3$	AgAu, Alloy <sup>4</sup>
$\text{Ag}^+, \text{AuCl}_4^-$	$\gamma$ , 3.8	Au/Ag, Bilayer <sup>4</sup>
$\text{Ag}^+, \text{AuCl}_4^-$	$\gamma$ , 35; EB, $7.9 \times 10^3$	AgAu, Alloy <sup>4</sup>
$\text{Ag}^+, \text{Cd}^{2+}$	$\gamma$ , 0.87	Ag/Cd, Bilayer <sup>136</sup>
$\text{Ag}_n, \text{Cu}^{2+}$	$\gamma$ , 0.87	Ag/Cu, Bilayer <sup>137,138</sup>
$\text{Ag}_n, \text{In}^{3+}$	$\gamma$ ,	Ag/In, Bilayer <sup>139</sup>
$\text{Ag}^+, \text{Pd}^{2+}$	$\gamma$ , 35	AgPd, Alloy <sup>140</sup>
$\text{Pd}_n, \text{Ag}(\text{CN})_2^-$	$\gamma$ , 0.87	Pd/Ag, Bilayer <sup>141</sup>
$\text{Ag}^+, \text{PtCl}_6^{2-}$	$\gamma$ , 30	AgPt, Alloy <sup>142</sup>
$\text{Ag}^+, \text{Tl}^+$	$\gamma$ , 0.6	Ag/Tl, Bilayer <sup>112</sup>
$\text{AuCl}_4^-, \text{PtCl}_6^{2-}$	EB, $7.9 \times 10^3$ ; $\gamma$ , 0.5-40	Au/Pt, Bilayer <sup>143</sup>
$\text{Au}(\text{CN})_2^-, \text{PtCl}_6^{2-}$	EB, $7.9 \times 10^3$ ; $\gamma$ , 0.5-40	Pt/Au, Bilayer <sup>143</sup>
$\text{Au}_n, \text{Pb}^{2+}$	$\gamma$ , 0.4, 0.87	Au/Pb, Bilayer <sup>144,145</sup>
$\text{Au}_n, \text{Pb}^{2+}, \text{Cd}^{2+}$	$\gamma$ , 0.87	Au/Pb/Cd Tri-layer <sup>145</sup>
$\text{Au}_n, \text{Cd}^{2+}$	$\gamma$ , 0.4	Au/Cd, Bilayer <sup>145</sup>
$\text{Au}_n, \text{Tl}^+$	$\gamma$ , 0.4	Au/Tl, Bilayer <sup>145</sup>
$\text{Au}_n, \text{Sn}^{2+}$	$\gamma$ , 0.4	AuSn, Alloy <sup>111</sup>
$\text{Cu}^{2+}, \text{Cd}^{2+}$	$\gamma$ , 0.42, 0.48	CuCd, Alloy <sup>39,146</sup>
$\text{Cu}^{2+}, \text{Pd}^{2+}$	$\gamma$ , 30	CuPd, Alloy <sup>99</sup>

\*The ions of  $M'$  are introduced in a second step after the formation of the cluster  $M_n$ , and are then reduced by  $\gamma$ -irradiation.

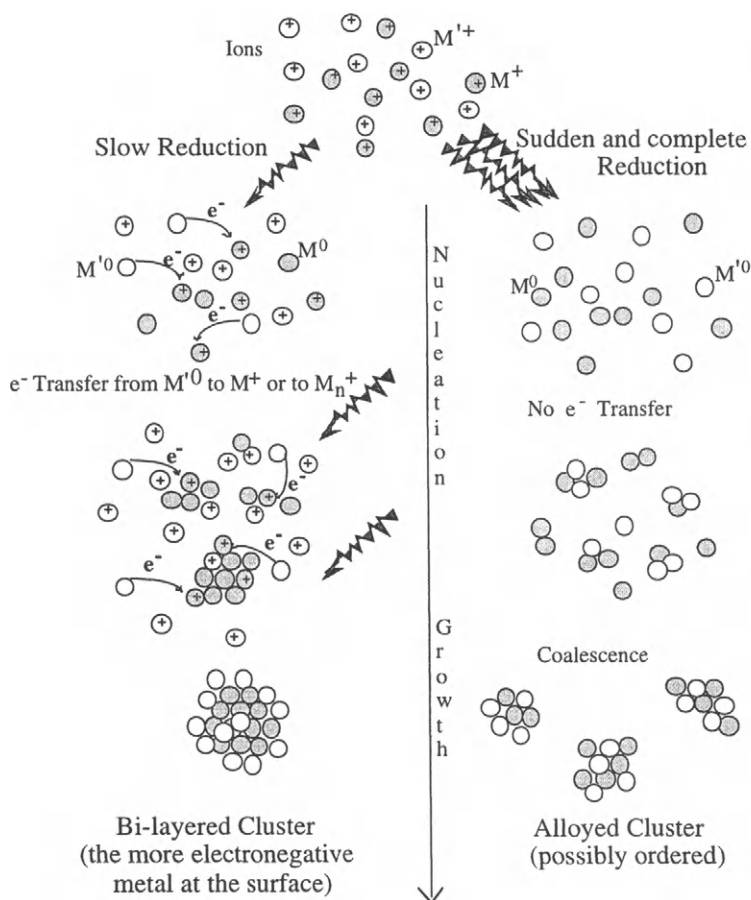


Figure 15. Scheme of the influence of the dose rate on the competition between the inter-metal electron transfer and the coalescence processes during the radiolytic reduction of mixed metal ion solutions.

High dose rates favor alloying whereas low dose rates favor segregation of the metals in the clusters.

Depending on the rate of the intermetal electron transfer competing with the dose rate-dependent coalescence (Figure 15 and Table 5), alloying :

i) may occur spontaneously, even at low reduction rate ( $\gamma$ -irradiation with low dose rate)<sup>99</sup>, as for alloyed  $Cu_3Pd$ ,  $CuPd$ ,  $Ni-Pt$ ,  $CuAu$ ,  $Ag_xPd_{1-x}$  and  $Ag-Pt$  clusters,

ii) may require higher  $\gamma$ -dose rates<sup>4</sup> as for  $Ag_xAu_{1-x}(Cl^-)$ ,

iii) is only obtained through a short and intense irradiation provided by an electron accelerator<sup>4</sup> as for  $Ag_xAu_{1-x}(CN^-)$ ,

iv) is even not obtained. In extreme cases, the electron transfer is achieved within times shorter than the irradiation time required for complete reduction (a few seconds with EB) and metals are segregated in spite of the very fast reduction ( $Au/Pt$ ,  $Ag/Cu$ ).<sup>146</sup> For multivalent ion precursors, intermetal electron transfer reactions may also occur between the transient lower valency ions.

## 6.4. Alloyed cluster development

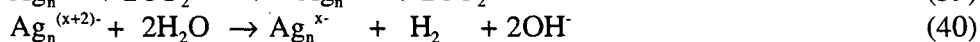
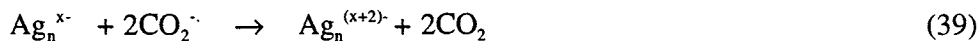
Another way to favor the statistical reduction leading to alloyed particles is to let the clusters grow more rapidly, before any observable intermetal transfer, and consequently to let their redox potential increase in order to lower the risk of the displacement. This can be achieved through a fast chemical reduction by a donor  $S^-$  at an alloyed nucleus surface as for monometallic clusters (§ 4.2). The reaction competing with the intermetal exchange is now the chemical reduction which can be very fast provided nuclei are present. In a pulse radiolysis study, the transient reduced viologen formed by an electron pulse has been observed to react with the small alloyed  $(AuAg)_{n,CN^-}$  clusters and the developed alloyed clusters are stable towards segregation. Their final size is quite large because the ions reduced by the donor are concentrated on a small number of nuclei. Moreover, it was found<sup>73</sup> that the redox potential of such critical alloyed AgAu clusters is almost the same ( $-0.4 V_{NHE}$  at  $n_c = 6$ ) as that of the more noble metal (silver in cyanide environment).<sup>65</sup>

## 7. CATALYTIC PROPERTIES OF METAL CLUSTERS

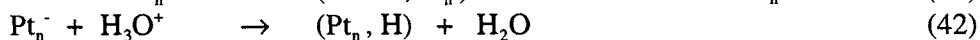
One of the important applications of metal clusters is to be used as catalysts. The cluster potential and its dependence on the nuclearity or adsorbed molecules play a crucial role in the catalysis of electron transfer. The cluster is able to relay efficiently electrons from a donor to an acceptor, provided the potential value is intermediate between those of the reactants.<sup>53</sup> This optimum range is adjustable by the size.<sup>70</sup>

### 7.1. Clusters in solution

The catalytic role of metal clusters such as  $Tl_n$ ,<sup>1132</sup>  $Ag_n$ ,<sup>147</sup>  $Pt_n$ ,<sup>148</sup>  $Au_n$ ,<sup>109,149</sup>  $Ir_n$ ,<sup>20</sup> concerning the electron transfer from radiation-induced free radicals such as  $CO_2^{\cdot-}$  or  $(CH_3)_2C^{\cdot}OH$  to a substrate, after the complete reduction of the metal ions, has been demonstrated. Electrons donated from the radicals are first stored on clusters as charge pools<sup>20</sup> and then are transferred again for example pairwise to water producing molecular hydrogen:



Pulse radiolysis allows one to observe directly some catalytic electron transfer reactions other than the autocatalytic growth (reactions (25-27)). Indeed the clusters are so small that they may be considered as diffusing molecular systems. The electron transfer from  $MV^+$  to protons in water requires the presence of a catalyst, for example radiolytically formed gold<sup>149</sup> or platinum<sup>148</sup> clusters:





For a given metal amount, the transfer rate increases linearly with the particle concentration. The initial electron transfer step (41) between one  $\text{MV}^+$  radical and one  $\text{Pt}_n$  cluster of  $n = 35\text{-}50$  atoms is diffusion controlled and the rate determining step of the process is clearly, as on  $\text{Au}_n$ , the desorption step after the intra- or inter-particle formation (43) of the molecular hydrogen.<sup>148,149</sup>

The catalytic role of the metal clusters may be explained again by their influence on the reaction thermodynamics. Actually, the direct electron transfer from  $\text{MV}^+$  ( $E^\circ(\text{MV}^{2+}/\text{MV}^+) = -0.41 \text{ V}_{\text{NHE}}$ ) to  $\text{H}_3\text{O}^+$  ( $E^\circ(\text{H}_3\text{O}^+/\text{H}) = -2.3 \text{ V}_{\text{NHE}}$ ) is thermodynamically unfavored if they are both in solution, and in contrast the reverse reaction from  $\text{H}$  to  $\text{MV}^{2+}$  is fast. However, the redox potential of  $\text{H}_3\text{O}^+/\text{H}$  when adsorbed on a nanometric cluster  $E^\circ(\text{H}_3\text{O}^+/\text{H}, \text{Pt}_n)$  is shifted to values higher than that of  $E^\circ(\text{MV}^{2+}/\text{MV}^+)$  and the transfer (39-41) becomes possible. The evolution of molecular hydrogen catalyzed by clusters from radicals such as  $\text{CO}_2^{\cdot-}$  or  $(\text{CH}_3)_2\text{COH}$  which are also in solution less strong reducing agents than  $\text{H}$  radicals may be similarly explained.

The catalysis of the disproportionation of the superoxide anion  $\text{O}_2^{\cdot-}$  by  $\text{Pt}_n$  clusters, in subcolloidal solutions or supported on colloidal  $\text{TiO}_2$  particles, has also been studied by time-resolved techniques.<sup>150</sup> The decay of  $\text{O}_2^{\cdot-}$  obeys first order kinetics with respect to both  $\text{O}_2^{\cdot-}$  and  $\text{Pt}_n$  clusters because the catalysis is governed indeed by the proton concentration adsorbed at the cluster surface.

## 7.2. Supported clusters

Metal clusters supported on solid supports are easier to use as catalysts. However, the mechanism of their action is inferred mostly indirectly from their efficiency. Multimetallic clusters are known to present enhanced catalytic properties relative to pure metals, specially when the catalyzed reaction process includes several steps. The method of radiation-induced reduction provides a powerful way to obtain homodisperse, small and alloyed clusters.

Small clusters of iridium supported on  $\text{Al}_2\text{O}_3$ <sup>151</sup> or  $\text{TiO}_2$ <sup>150</sup> and of platinum, iridium, ruthenium or rhodium supported on  $\text{SnO}_2$  counter electrodes<sup>152,153</sup> were radiolytically prepared and displayed efficient catalytic properties for hydrazine decomposition and electron transfer, respectively. The radiolytic method was also used to graft metal nanoaggregates upon *anodes* or *cathodes* involved in the chlorine-soda process.<sup>154</sup> A drastic decrease of overpotential and an increase of the electrocatalytic efficiency relative to unmodified electrodes was obtained once bimetallic nanoparticles of Pt-Ru and Ni-Ru, were grafted onto bulk metal electrodes (*Ti* or *Ni*).

Special processes of diffusion transfer in silver *photographic emulsions* require diffusion of silver ions of the positive image and their catalytic reduction around added development centers such as metal clusters, small enough to ensure a high resolution and no loss of transparency. Added  $\gamma$ -induced silver clusters have a strong efficiency. However, alloyed clusters of Au-Cu and Ni-Pt and mostly of Ag-Au, Ag-Cu, and Ag-Cu-Pd, prepared under

high dose rate conditions, exhibit the best activity owing to their small size and the presence of the different metal atoms at the surface.<sup>155</sup>

Metal clusters-carbon composites are of high interest in making electrodes for fuel cells. Homogeneously dispersed  $Pt_x(CO)_y$  clusters anchored to carbon fibers and powders are electroactive in methanol or hydrogen oxidation and in oxygen reduction.<sup>89</sup> In order to enhance the methanol electrooxidation currents at lower potentials and to extend the catalyst lifetime, bimetallic Pt-Ru, Pt-Sn and trimetallic Pt-Ru-Sn clusters were prepared by radiation-induced reduction in solution with CO and then impregnated onto carbon powder at high loading. Actually, clusters synthesized by electron beam irradiation at high dose rate are markedly more active catalytically, mostly Pt-Ru-Sn, than those prepared by  $\gamma$ -radiolysis, which suggests that all metals cooperate in the reaction at the surface of the alloyed clusters.<sup>23</sup>

## 8. SEMICONDUCTOR CLUSTER NUCLEATION AND REACTIVITY

The specificity of ionizing radiation (deep penetration even in turbid system owing to their high energy) is used either to study the nucleation mechanism of small semiconductor clusters or the electron transfer between the particles and the surrounding molecules.<sup>19</sup> In the latter case, pulse radiolysis allows the production of radicals in the bulk of the solution. One can then observe the reactions with the cluster, providing complementary information to the direct excitation of the semiconductor by laser sources. The increasing knowledge of the mechanisms allows the extension of radiolysis to application purposes.

### 8.1. Mercury halide

It has long been known that the reduction of mercuric chloride by  $\gamma$ -irradiation leads to the formation of  $Hg_2Cl_2$  precipitates as the final product.<sup>156</sup> By pulse radiolysis, the  $HgCl$  monomer was observed<sup>157</sup> as the first transient in the crystal formation (reaction (19)). It absorbs at 330 nm and dimerizes into  $Hg_2Cl_2$ . The ESR signal of the monomer has been detected at 77 k.<sup>158</sup>

Table 6

Spectral data of  $HgX$  and formation and dimerization rate constants ( $l\ mol^{-1}\ s^{-1}$ )<sup>159</sup>

X	$k(HgX_2 + e_{aq}^-)$	$k(HgX_2 + (CH_3)_2COH)$	$\lambda_{max}$ (nm) of $Hg^I X$	$2k(2HgX)$
Cl <sup>-</sup>	$4.0 \times 10^{10}$	$2.0 \times 10^9$	330	$4.5 \times 10^9$
Br <sup>-</sup>	$3.4 \times 10^{10}$	$2.4 \times 10^9$	350	$2.2 \times 10^9$
I <sup>-</sup>	$3.0 \times 10^{10}$	$2.0 \times 10^9$	355	$1.4 \times 10^9$
SCN <sup>-</sup>	$4.5 \times 10^{10}$	$2.2 \times 10^9$	415	$2.8 \times 10^9$
CN <sup>-</sup>	$1.6 \times 10^{10}$	-	285	$3.1 \times 10^9$



The reduction of other mercuric halides or pseudohalides  $\text{HgX}_2$  ( $\text{X} = \text{Br}^-$ ,  $\text{I}^-$ ,  $\text{CN}^-$ , or  $\text{SCN}^-$ , respectively) by hydrated electrons or alcohol radicals yields as well transient  $\text{HgX}$  monomers.<sup>160</sup> They dimerize except  $\text{HgCN}$  which disproportionates. It was found that the  $\text{Hg}_2\text{X}_2$  absorption spectra are at shorter wavelengths than those of  $\text{HgX}$  (Table 6). The monomers are strong electron donors towards  $\text{O}_2$ , tetranitromethane and p-benzoquinone. On the contrary, in diluted solutions of  $\text{HgCl}_2$ , added with more concentrated salts such as  $\text{Cd}^{2+}$ ,  $\text{Zn}^{2+}$ ,  $\text{Sn}^{2+}$ ,  $\text{Pb}^{2+}$ ,  $\text{Fe}^{2+}$  or  $\text{Mn}^{2+}$ , electrons are transferred from the monovalent state of the ions to  $\text{Hg}^{\text{I}}$  which is indirectly reduced into  $\text{Hg}_2\text{Cl}_2$ .<sup>161</sup>

## 8.2. Silver halides

As early as in 1969, before the size-dependence of cluster properties was suspected, pulse radiolysis was used to form  $\text{AgCl}$  monomers and to observe the precipitation of growing particles.<sup>19</sup> The anions  $\text{Cl}^-$  reacting with silver ions (reaction (18)) were formed through the capture of electron by chloroacetic acid (reaction (17)). The kinetics of light scattering increase presented an induction period assigned to the nucleation process in supersaturated solutions before precipitation.<sup>19</sup> Also, the induction time of the nanometric  $\text{AgCl}$  particles appearance has been found<sup>162</sup> to decrease with the dose.

From the progressive evolution of transient absorption spectra after the pulse, the growth mechanism of  $\text{AgI}$  clusters from oligomers to nanoparticles was proposed.<sup>163</sup> The band maximum in the UV is red-shifted at increasing time according to the nuclearity-dependence of the cluster spectra (Figure 15).

Similarly, the  $\text{AgBr}$  monomer was observed ( $\lambda_{\text{max}} = 295 \text{ nm}$ ) as the first step of  $(\text{AgBr})_n$  cluster formation. This short-lived molecule ( $< 1 \mu\text{s}$ ) dimerizes into  $(\text{AgBr})_2$ , which absorbs at  $285 \text{ nm}$  (Figure 16). Then the coalescence continues and the nanometric clusters are formed in the range of seconds<sup>164</sup>.

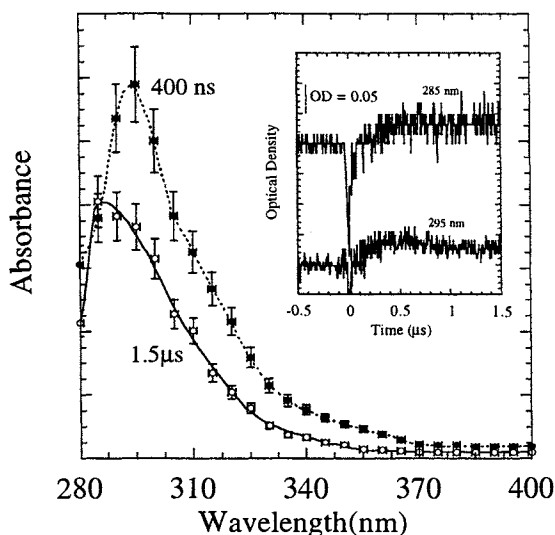


Figure 16. : Transient absorption spectra of  $(\text{AgBr})_1$  and  $(\text{AgBr})_2$  obtained after a 3 ns pulse. The insert shows the kinetics at 295 and 285 nm.<sup>164</sup>

AgBr nanoclusters have been also synthesized by  $\gamma$ -radiolysis under various conditions of irradiation dose and dose rate.<sup>164</sup> The final cluster size is governed by the competition between two mechanisms of particle growth, one by the coalescence (controlled by second order kinetics and dose rate sensitive):



the second by the ripening or successive addition of monomers (controlled by pseudo-first order kinetics of  $\text{Ag}^+$  adsorption on  $(\text{AgBr})_n$ ):



At the end of irradiation with a given dose, the cluster nuclearity decreases ( $\lambda_{\text{max}}$  blue-shifted) with increasing the dose rate.

### 8.3. Metal sulfide

The  $\gamma$ -radiolytic method has been also used to produce CdS clusters by dissociative electron attachment onto thiol molecules releasing  $\text{SH}^-$  in the presence of  $\text{Cd}^{2+}$  cations (reaction (18)).<sup>165</sup> The authors emphasize that under given conditions of pH and stabilizer concentration, the cluster nuclearity is controlled by the total dose of irradiation. At increasing dose, the absorption and fluorescence bands are red-shifted and the predominant cluster size increases. A pulse radiolysis study of the mechanism showed that the  $(\text{CdS})_n$  growth control is provided by the competition between  $\text{RS}^-$  and  $\text{HS}^-$  for the  $\text{Cd}^{2+}$  ions at the surface of the growing particle.<sup>166</sup> It was shown recently<sup>167</sup> that high dose rates favor the formation of small nuclearity  $(\text{CdS})_n$  clusters (Figure 17) as for  $(\text{AgBr})_n$ . In fact, at a given dose generating a given amount of  $\text{SH}^-$ , the competition between the mechanisms of coalescence and ripening (as in (44) and (45-47), respectively) is controlled by the dose rate. Higher the formation rate of  $\text{SH}^-$ , higher is the formation rate of nuclei in solution and, after a cascade of coalescence reactions, smaller is the mean nuclearity of  $(\text{CdS})_n$  clusters. The observation of isosbestic points in series of spectra obtained at various dose rates suggests that some specific sizes with absorption spectra peaking at 270, 280 and 320 nm appear successively in filiation. They coalesce very slowly ( $100 \text{ l mol}^{-1} \text{ s}^{-1}$ ) because of the presence of the strong complexing thiol agent. Thus, radiolysis under high dose rate conjugated with low dose conditions allows the production of a monodisperse population of extremely small  $(\text{CdS})_n$  clusters (radius of 0.6 nm). At moderate dose rate, though larger, the clusters still display an exceptional monodispersity. Besides, the observations of the cluster formation by radiolysis demonstrate that they grow progressively from monomers and oligomers with size-dependent spectra and that they do not arise suddenly from the precipitation of a supersaturated solution.  $\gamma$ -Irradiation has been also used to synthesize CdS clusters included in gels.<sup>121</sup>

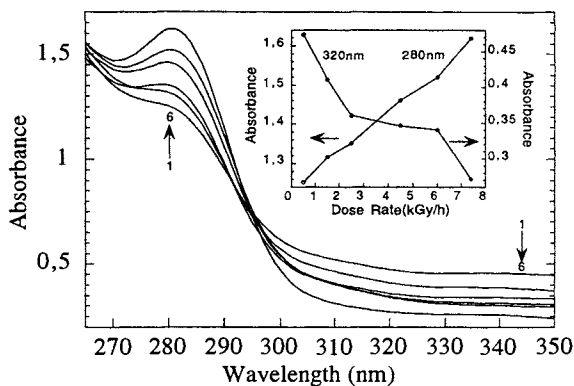


Figure 17. Absorption spectra of CdS clusters in solutions of  $\text{CdSO}_4$  and  $\text{HO}(\text{CH}_2)_2\text{SH}$ . 1-6 correspond to 0.5, 1.0, 2.0, 4.5, 6.0, 7.4  $\text{kGy h}^{-1}$ . Inset: Evolution of the optical density at 282 nm and 320 nm as a function of the dose rate.<sup>167</sup>

Pulse radiolysis provides also means to determine the size of chemically prepared CdS clusters in measuring their reaction rate with OH radicals.<sup>168</sup> The mechanisms of such an electron transfer process from the surface of CdS,<sup>169</sup> CdTe and ZnTe,<sup>170</sup> PbS<sup>171</sup> semiconductor particles to OH radicals, and from solvated electrons or alcohol radicals to the particle were studied. The absorption spectrum of CdS with an excess electron is blue-shifted. Colloidal nanoparticles (2 nm) of chalcopyrite  $\text{CuFeS}_2$  are oxidized in their first monolayer by  $\text{Fe}^{\text{III}}$  ions induced by a pulse.<sup>172</sup>

Radiolytic reduction of ethanol-water solutions of elemental sulfur in the presence of  $\text{Ag}^+$  or  $\text{Cu}^{2+}$  yields  $\text{Ag}_2\text{S}$  or  $\text{CuS}$  particles, respectively.<sup>173</sup> Selenium particles of 8-17 nm were produced from irradiation of solutions.<sup>174</sup>

#### 8.4. Metal oxides and silica

Nanosized particles of metal oxides  $\text{Cu}_2\text{O}$ ,<sup>175</sup>  $\text{Cr}_2\text{O}_3$ ,<sup>176</sup> and  $\text{MnO}_2$ ,<sup>177</sup> are produced by irradiation under reductive conditions of  $\text{CuSO}_4$ ,  $\text{Cr}_2\text{O}_7^{2-}$ ,  $\text{MnO}_4^-$ , respectively. Pure nanocrystalline  $\text{Fe}_3\text{O}_4$  magnetite particles are prepared by  $\gamma$ -irradiation of ferric hydroxide sol.<sup>178</sup> The oxide  $\alpha\text{-Fe}_2\text{O}_3$  and to a lesser extent  $\text{Fe}_3\text{O}_4$  are reduced by  $(\text{CH}_3)_2\text{COH}$  radicals into  $\text{Fe}^{2+}$  which are dissolved in the aqueous solution.<sup>179</sup>

Nanomeric  $\text{TiO}_2$  particles accept electrons from radiation-induced organic radicals and are partly reduced at the surface into  $\text{Ti}^{\text{III}}$ .<sup>180</sup> The rate constant of the electron transfer to colloidal  $\text{TiO}_2$  or  $\alpha\text{-Fe}_2\text{O}_3$  particles from  $\text{MV}^+$  ( $E^\circ(\text{MV}^{2+}/\text{MV}^+) = -0.41 \text{ V}_{\text{NHE}}$ ), which are produced by pulse radiolysis and observed at 600 nm, increases correlatively with the potential of the semiconductor conduction band when the pH decreases ( $-0.1 \text{ V}_{\text{NHE}}$  at pH 0).<sup>181</sup> Time-resolved microwave conductivity technique has been used to observe the life-time of charges created inside pulse-irradiated particles of high- $T_c$  superconductor  $\text{DyBa}_2\text{Cu}_3\text{O}_{7-x}$  or of  $\text{CdS}$ <sup>182</sup> and in nanoparticles of  $\text{Al}_2\text{O}_3$ ,  $\text{MgO}$ , and  $\text{TiO}_2$ .<sup>183,184</sup> The conductivity signal of  $\text{TiO}_2$  samples increases with the particle radius since shallow trapping of electrons at the surface is favored by a high specific area. The signal decay after the pulse is accelerated by surface platinum clusters due to their fast collection of electrons, whereas the signal

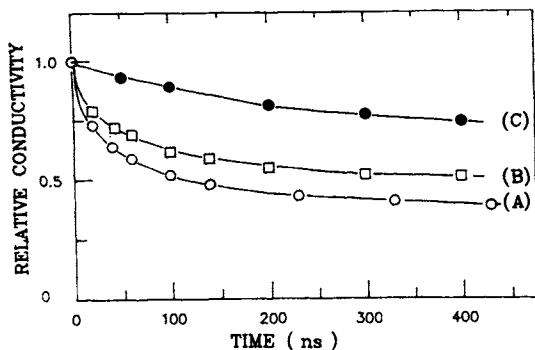


Figure 18. Microwave conductivity signals observed on irradiation of Degussa P25  $\text{TiO}_2$  powder using 20 ns, 45 nC pulses of 3 MeV electrons. The traces refer to (A) air equilibrated material, (B) a sample heated at  $60^\circ\text{C}$  in a vacuum oven for a week, (C) sample (B) to which  $20\mu\text{L}$  of iso-propanol has been added in the perspex holder. The traces have been normalized to the same end-of-pulse height.<sup>183</sup>

elongation in the presence of 2-propanol at the interface results from scavenging of holes followed by electron injection from the alcohol radical (Figure 18). For samples doped in the bulk by  $\text{Cr}^{3+}$ , the signal becomes negligible presumably due to a very fast recombination of the charge carriers induced by the defect centres.

Increasing attention is paid to microheterogeneous radiation-assisted processes and to the mechanism of organic molecules degradation at the surface of colloidal oxides. Radiolytic destruction of EDTA is enhanced by the presence of  $\text{TiO}_2$ <sup>185</sup>, while the electron transfer reactions between solvated electrons or OH radicals and organic molecules adsorbed on  $\text{SnO}_2$  are one order of magnitude slower than in solution.<sup>186</sup> Dechlorination of hexachlorobenzene into penta- and tetrachlorobenzene has been achieved through  $\gamma$ -ray induced charge separation and transfer process on  $\text{Al}_2\text{O}_3$  surface where molecules are adsorbed.<sup>187</sup>

Energy deposited from irradiation by a pulsed electron beam in 7-22 nm  $\text{SiO}_2$  particles crosses the solid-liquid interface and appears as solvated electrons in the aqueous phase.<sup>188,189</sup>

## 9. FUTURE TRENDS

Radiation chemistry methods have been proven to have a potential to induce and to study the dynamics of nucleation and growth of metal and semiconductor clusters from the monomer to the stable nanoparticle. Pulse radiolysis provides also the means to observe directly by the time-resolved technique their reactivity, thus to determine during the growth their nuclearity-dependent properties, such as the redox potential, which is of crucial importance in certain catalytic reactions. Actually, the very general concept of size effects on cluster properties was pointed out first in radiolytic experiments. The radiolytic radicals used to produce the monomers have strong reducing potentials and can be provided with dose rates from slow to quasi-sudden regimes. Therefore monomers are formed without energetic

barrier and owing to the high density of nuclei the final cluster size can be limited at most and is of exceptional homodispersity.

The kinetics mechanism explaining the properties of the final particles from the conditions of the radiolytic synthesis has been exploited to guide the procedure of obtaining clusters with definite size. But the mechanism is not specific to the radiation-induced method and will be helpfully extended to other ways of chemical or photochemical synthesis. The understanding of the detailed mechanism of bimetallic cluster synthesis has permitted also the control of conditions favoring alloying, possibly with ordered atom arrangement or segregation in a core-shell structure.

However, the variety of composite materials to be elaborated by the method is still scarcely explored. For example bi- and multi-metal or semiconductor nanoparticles, included in different matrices (polymeric membranes, porous supports, ...) have promising applications. New methods of cluster characterization at this extremely low size scale are developed and will improve their study.

As shown by a few recent examples, pulse radiolysis is also a powerful tool, as an alternative to other pulse techniques, to study reactions at the interface between clusters and solution, such as fast heterogeneous catalytic processes, or transfer of the charges generated inside the particle.

Moreover, the interpretation of experimental data on clusters in solution requires more elaborated theoretical models to include solvation effects around the structure of a small metal or semiconductor cluster. New kinetics models are also to be developed to describe nucleation which governs the phase transition from a solute to a small solid phase.

## REFERENCES

1. W.C. Roentgen, *Sitzungs-ber. Phys-Medizin. Ges., Wuerzburg*, (1896) 11.
2. H. Becquerel, *C. R. Acad. Sci.*, 122 (1896) 420.
3. S. Remita, J. M. Orts, J. M. Feliu, M. Mostafavi and M.O. Delcourt, *Chem. Phys. Letters*, 218 (1994) 115.
4. M. Treguer, C. de Cointet, H. Remita, J. Khatouri, M. Mostafavi, J. Amblard, J. Belloni and R. de Keyser, *J. Phys. Chem.*, 102 (1998) 4310.
5. S. Remita, M. Mostafavi and M.O. Delcourt, *New J. Chem.*, 18 (1994) 581.
6. H. Fricke, *J. Chem. Phys.*, 2 (1934) 556.
7. M. Haïssinsky and A.M. Pujo, *C.R. Acad. Sci.*, 240 (1955) 2530.
8. M. Haïssinsky, *La chimie nucléaire et ses applications*, Masson & Cie, Paris, (1957).
9. A.M. Koulkes-Pujo and S. Rashkov, *J. Chim. Phys.*, 64 (1967) 534.
10. J.H. Baxendale, E.M. Fielden, J.P. Keene and M. Ebert, in *Pulse Radiolysis*, J.P. Keene, A. Swallow, J.H. Baxendale (eds.), Acad Press, London, (1965) 207.
11. J. Von Pukies, W. Roebke and A. Henglein, *Ber.Bunsenges. Phys.Chem.*, 72 (1968) 842.
12. M. Haïssinsky in *Radiation Chemistry*, J. Dobo, P. Hedwig (eds.), Akad. Kiado Budapest, 2 (1972) 1353 and following discussion.
13. J. Belloni, in *Actions chimiques et biologiques des Radiations*, M. Haissinsky (ed.), Masson et Cie, Paris, (1971) 47.
14. M.O. Delcourt and J. Belloni, *Radiochem. Radioanal. Lett.*, 13 (1973) 329.

15. N. Basco, S.K. Vidyarthi and D.C. Walker, *Can. J. Chem.*, 51 (1973) 2497.
16. A. Henglein, *Ber. Bunsenges. Phys. Chem.*, 81 (1977) 556.
17. W.H. Halperin, *Rev. Mod. Phys.*, 58 (1986) 533.
18. R. Kubo, *J. Phys. Soc. Japan*, 17 (1962) 975.
19. R. Schiller and M. Ebert, *Int. J. Radiat. Phys. Chem.* 1 (1969) 111.
20. A. Henglein, *Chem. Rev.*, 89 (1989) 1861.
21. J. Belloni, J. Amblard, J.L. Marignier, M. Mostafavi, in *Clusters of atoms and Molecules*, H. Haberland (ed.), Springer-Verlag, 2 (1994) 290.
22. A. Henglein, *Ber. Bunsenges. Phys. Chem.*, 99 (1995) 903.
23. J. Belloni, M. Mostafavi, H. Remita, J.L. Marignier and M.O. Delcourt, *New J. Chem.*, 22 (1998) 1239.
24. J. Belloni and M. Mostafavi, in *Metal Clusters in Chemistry*, P. Braunstein, R. Oro and J. Raithby (eds.), Wiley (1999), 1213.
25. J.H. Baxendale, F. Busi, *The Study of fast Processes and transient Species by Electron Pulse Radiolysis*, NATO ASI Series 86, D. Reidel (1982).
26. G.V. Buxton, C.L. Greenstock, W.P. Helman and A.B. Ross, *J. Phys. Chem. Ref. Data*, 17 (1988) n<sup>o</sup>2.
27. J. Elliott and A.S. Simon, *Radiat. Phys. Chem.*, 24 (1984) 229.
28. H.A. Schwarz and R.W. Dodson, *J. Phys. Chem.*, 93 (1989) 409.
29. A. Henglein, *J. Phys. Chem.*, 83 (1979) 2209.
30. Yingjie Zhu, Yitai Qian, Manwei Zhang, Zuyao Chen, Bin Lu and Changsui Wang, *Materials Letters*, 17 (1993) 314.
31. C.D. Jonah, M.S. Matheson and D. Meisel, *J. Phys. Chem.*, 81 (1977) 1805.
32. R. Rafaeloff, Y. Haruvy, J. Binenboym, G. Baruch and L.A. Rajbenbach, *J. Molec. Catal.*, 22 (1983) 219.
33. Yingjie Zhu, Yitai Qian, X J Li and Manwei Zhang, *Chem. Comm.*, 12 (1997) 1081.
34. M. Graetzel, *Acc. Chem. Res.*, 14 (1981) 376.
35. B.G. Ershov, *Russ. Chem. Bull.*, 43 (1994) 16.
36. T. Sosebee, M. Giersig, A. Holzwarth and P. Mulvaney, *Ber. Bunsenges. Phys. Chem.*, 99 (1995) 40.
37. A. Henglein, *Chem. Phys. Letters*, 154 (1989) 473.
38. S. Kapoor, D. Lawless, P. Kennepohl, D. Meisel and N. Serpone, *Langmuir*, 10 (1994) 3018.
39. M. Kumar, S. Kapoor and C. Gopinathan, *Radiat. Phys. Chem.*, 50 (1997) 465.
40. M. Mostafavi, N. Keghouche, M.O. Delcourt and J. Belloni, *Chem. Phys. Letters*, 167 (1990) 193.
41. I. Texier and M. Mostafavi, *Radiat. Phys. Chem.*, 49 (1997) 459.
42. K. Kurihara, J. Kizling, P. Stenius and J.H. Fendler, *J. Am. Chem. Soc.*, 105 (1983) 2574.
43. J. Belloni, M.O. Delcourt and C. Leclere, *Nouv. J. Chim.*, 6 (1982) 507.
44. M. Mostafavi, J.L. Marignier, J. Amblard and J. Belloni, *Radiat. Phys. Chem.*, 34 (1989) 605.
45. E. Janata, J. Lilie and M. Martin, *Radiat. Phys. Chem.*, 43 (1994) 353.
46. E. Janata, *Radiat. Phys. Chem.*, 44 (1994) 449.
47. E. Janata, A. Henglein and B.G. Ershov, *J. Phys. Chem.*, 98 (1994) 10888.
48. J. Butler and A. Henglein, *Radiat. Phys. Chem.*, 15 (1980) 603.
49. B. Cercek, M. Ebert and A.J. Swallow, *J. Chem. Soc. A*, (1966) 612.
50. Ghosh-Mazumdar and E.J. Hart, *Adv. Chem. Ser.*, 81 (1968) 193.
51. M. Mostafavi, M.O. Delcourt, N. Keghouche and G. Picq., *Radiat. Phys. Chem.*, 40 (1992) 445.
52. J. Belloni, J. Khatouri, M. Mostafavi, J. Amblard, in *Ultrafast reaction dynamics and solvent effects*, P.J. Rossky and Y. Gauduel (eds), *Am. Inst. Phys.*, (1993) 541.

53. J. Belloni, M.O. Delcourt, J.L. Marignier and J. Amblard, in *Radiation Chemistry*, P. Hedwig, L. and R. Schiller (eds.), Akad. Kiado, Budapest, (1987) 89.
54. L. Kevan, *J. Phys. Chem.*, 85 (1981) 1828.
55. M. Mostafavi and J. Belloni, *Recent Res. Devel. Phys.Chem.*, 1 (1997) 459.
56. S. Remita, M. Mostafavi and M.O. Delcourt, *J. Phys. Chem.*, 100 (1997) 10187.
57. I. Texier, S. Remita, P. Archirel and M. Mostafavi, *J. Phys. Chem.*, 100 (1996) 12472.
58. M. Mostafavi, S. Remita, M.O. Delcourt and J. Belloni, *J. Chim. Phys.* 93 (1996) 1828.
59. S. Mosseri, A. Henglein and E. Janata, *J. Phys. Chem.*, 93 (1989) 6791.
60. B.G. Ershov and N.L. Sukhov, *Radiat. Phys. Chem.*, 36 (1990) 93.
61. Gosh-Mazumdar and E.J. Hart, *Int. J. Rad. Phys. Chem.*, 1 (1969) 165.
62. G. Mie, *Ann. Phys.*, 25 (1908) 377.
63. J.A. Creighton and D.J. Eadon, *J. Chem. Soc. Faraday Trans.*, 87 (1991) 3881.
64. A. Henglein and R. Tausch-Treml, *J. Coll. Interf. Sci.*, 80 (1981) 84.
65. C. de Cointet, M. Mostafavi, J. Khatouri and J. Belloni, *J. Phys. Chem.*, 101 (1997) 3512.
66. G.V. Buxton, Q.G. Mulazzani and A.B. Ross, *J. Phys. Chem. Ref. Data*, 24 (1995) n°3.
67. R. Tausch-Treml, A. Henglein and J. Lilie, *Ber. Bunsenges. Phys. Chem.*, 82 (1978) 1335.
68. P.S. Rao and E. Hayon, *J. Phys. Chem.*, 79 (1975) 865.
69. S. Remita, P. Archirel and M. Mostafavi, *J. Phys. Chem.*, 99 (1995) 13198.
70. J. Khatouri, M. Mostafavi and J. Belloni, in *Photochemistry and Radiation Chemistry*, J. Wishart J and D. Nocera (eds.), *Adv. Chem. Ser. ACS Washington*, 254 (1998) 293.
71. J. Khatouri, J. Ridard, M. Mostafavi, J. Amblard and J. Belloni, *Z. Phys. D*, 34 (1995) 57.
72. O. Platzler, J. Amblard, J. L. Marignier and J. Belloni, *J. Phys. Chem.*, 96 (1992) 2334 and 2340.
73. C. de Cointet, J. Khatouri, M. Mostafavi and J. Belloni, *J. Phys. Chem.*, 101 (1997) 3517.
74. C. Jackschath, I. Rabin and W. Schulze, *Z. Phys. D*, 22 (1992) 517.
75. G. Alameddin, J. Hunter, D. Cameron and M.M. Kappes, *Chem. Phys. Letters*, 192 (1992) 122.
76. J. Khatouri, M. Mostafavi, J. Amblard and J. Belloni, *Z. Phys. D*, 26 (1993) 82.
77. A. Henglein, *J. Phys. Chem.*, 97 (1993) 5457.
78. M. Mostafavi, M.O. Delcourt and G. Picq, *Radiat. Phys. Chem.*, 41 (1992) 453.
79. M. Mostafavi, N. Keghouche and M.O. Delcourt, *Chem. Phys. Letters*, 169 (1990) 81.
80. B.G. Ershov and A. Henglein, *J. Phys. Chem.*, 102 (1998) 667 and 10663.
81. B.Keita, L. Nadjo, C. de Cointet, J. Amblard and J. Belloni, *Chem. Phys. Letters*, 249 (1996) 297.
82. A. Henglein, B.G. Ershov and M. Malow, *J. Phys. Chem.*, 99 (1995) 14129.
83. J. Khatouri, M. Mostafavi, J. Amblard and J. Belloni, *Chem. Phys. Letters* 191 (1992) 351.
84. N.L. Sukhov, M.A. Akinshin and B.G. Ershov, *Khim. Vys. Energii*, 20 (1986), 292.
85. Ming-Zhang Lin and J.L. Marignier, to be published
86. H. Remita, R. Derai and M.O. Delcourt, *Radiat. Phys. Chem.*, 37 (1991) 221.
87. Le Gratiel B., Remita H., Picq G. and M.O. Delcourt, *Radiat. Phys. Chem.*, 47 (1996) 263.
88. M. Treguer, H. Remita, J. Khatouri and J. Belloni, *J. Phys. Chem.*, (2001) in press.
89. B. Le Gratiel, H. Remita, G. Picq and M.O. Delcourt, *J. Catal.*, 164 (1996) 36.
90. H. Remita, R. Derai and Delcourt M.O., *J. Chim. Phys.*, 88 (1991) 845.
91. M.M. Bettahar and M.O. Delcourt, *Radiat. Phys. Chem.*, 32 (1988) 779.
92. R. Derai, H. Remita and M.O. Delcourt, *Radiat. Phys. Chem.*, 38 (1991) 483.
93. B. Keita, L. Nadjo, E. Gachard, H. Remita, J. Khatouri and J. Belloni, *New J. Chem.*, 21 (1997) 851.
94. J. Belloni, J.L. Marignier, M.O. Delcourt and M. Minana, US Patent N° 4 629 709 (1986). CIP N° 4 745 094 (1987).

95. Yunping Liu, Yingjie Zhu, Y H Zhang, Yitai Qian, Manwei Zhang, L. Yang and Changsui Wang, *J. Mater. Chem.*, 7 (1997) 787.
96. B.G. Ershov, N.L. Sukhov and D.I. Troitskii, *Russ. J. Phys. Chem.*, 68 (1994) 734.
97. M. Michaelis and A. Henglein, *J. Phys. Chem.*, 96 (1992) 4719.
98. G. Mills and A. Henglein, *Radiat. Phys. Chem.*, 26 (1985) 391.
99. J.L. Marignier, J. Belloni, M.O. Delcourt and J.P. Chevalier, *Nature* 317 (1985) 344.
100. J.L. Marignier and J. Belloni, *J. Chim. Phys.*, 85 (1988) 21.
101. N. Fujita, C. Matsuura, D. Hiroishi and K. Saigo, *Radiat. Phys. Chem.*, 53 (1998) 603.
102. Ghosh-Mazumdar and E.J. Hart, *Int. J. Radiat. Phys. Chem.*, 1 (1969) 165.
103. J. Von Pukies, W. Roebke and A. Henglein, *Ber. Bunsenges. Phys. Chem.*, 82 (1978) 1335.
104. M.O. Delcourt, J. Belloni, J.L. Marignier, C. Mory and C. Colliex, *Radiat. Phys. Chem.*, 23 (1984) 485.
105. B.G. Ershov, E. Janata, M. Michaelis and A. Henglein, *J. Phys. Chem.*, 95 (1991) 8996.
106. A. Henglein and J. Lilie, *J. Phys. Chem.*, 85 (1981) 1246.
107. A. Henglein, M. Gutierrez, E. Janata and B.G. Ershov, *J. Phys. Chem.*, 96 (1992) 4598.
108. J. Westerhausen, A. Henglein and J. Lilie, *Ber. Bunsenges. Phys. Chem.*, 85 (1981) 182.
109. E. Gachard, H. Remita, J. Khatouri, J. Belloni, B. Keita and L. Nadjo, *New J. Chem.*, 22 (1998) 1257.
110. A. Henglein and D. Meisel, *Langmuir*, 14 (1998) 7392.
111. A. Henglein and M. Giersig, *J. Phys. Chem.*, 98 (1994) 6931.
112. G.V. Buxton, T. Rhodes and R. Sellers, *J. Chem. Soc. Faraday Trans.1*, 78 (1982) 3341.
113. M. Breitenkamp, A. Henglein and J. Lilie, *Ber. Bunsenges. Phys. Chem.*, 80 (1976) 973.
114. A. Henglein, E. Janata and A. Fojtik, *J. Phys. Chem.*, 96 (1992) 4734.
115. M. Gutierrez and A. Henglein, *J. Phys. Chem.*, 100 (1996) 7656.
116. A. Henglein, P. Mulvaney and T. Linnert, *Faraday Discuss.*, 92 (1991) 31.
117. F. Strelow and A. Henglein, *J. Phys. Chem.*, 99 (1995) 11834.
118. M. Michaelis and A. Henglein, *J. Phys. Chem.*, 96 (1992) 4719.
119. J.L. Marignier, A. Dokuchaev, S. Hauteclouque and D. Grand, *Proc. 7th Int. Symp. Small Part. Inorg. Clusters*, (1994) 189.
120. D. Lawless, S. Kapoor, P. Kennepohl, D. Meisel and N. Serpone, *J. Phys. Chem.*, 98 (1994) 9616.
121. T. Gacoin, F. Chaput, J.P. Boilot, M. Mostafavi and M.O. Delcourt, in *Eurogel 91*, S. Vilminot, R. Nass and H. Schmidt (eds.), E-MRS, North Holland. (1991) 159.
122. Xingjie Zhu, Yitai Qian, Manwei Zhang, Zuyao Chen and Guien Zhou, *J. Mater. Chem.*, (1994) 1619.
123. Guohong Zhang, Xinsheng Liu and J.K. Thomas, *Radiat. Phys. Chem.*, 51 (1998) 135.
124. J. Michalik, N. Azuma, J. Sadlo and L. Kevan, *J. Phys. Chem.*, 99 (1995) 4679.
125. E. Gachard, J. Belloni and M.A. Subramanian, *J. Mater. Chem.* 6 (1996) 867.
126. M. Sasaki, M. Osada, N. Higashimoto, T. Yamamoto, A. Fukuoka, and M. Ishikawa, *J. Molec. Catal. A: Chem.*, 141 (1999) 223.
127. M.I. Vucemilovic and O.I. Micic, *Radiat. Phys. Chem.*, 32 (1988) 79.
128. O.I. Micic, M. Meglic, D. Lawless, D.K. Sharma and N. Serpone, *Langmuir*, 6 (1990) 487.
129. J.L. Marignier, Ashokkumar and M. Mostafavi, *Proc. 50th Annual IS&T Conf. on Silver Halides*, (1997) 67.
130. J. Belloni, *Curr. Opinion Coll. Interf. Sci.*, 1 (1996) 184.
131. A. Malkov and J. Belloni, *J. Chim. Phys.*, 89 (1992) 885.
132. B.G. Ershov, E. Janata and A. Henglein, *J. Phys. Chem.*, 98 (1994) 7619 and 10891.
133. B.G. Ershov, E. Janata and A. Henglein, *Radiat. Phys. Chem.*, 47 (1996) 59.
134. A. De Vyt, R. Gijbels, H. Davock, C. Van Roost and I. Geuens, *J. Anal. Atom. Spectrum.* 14 (1999) 499.



135. P. Mulvaney, M. Giersig and A. Henglein, *J. Phys. Chem.*, 97 (1993) 7061.
136. A. Henglein, *J. Phys. Chem.*, 96 (1992) 2411.
137. T. Sosebee, M. Giersig, A. Holzwarth and P. Mulvaney, *Ber. Bunsenges. Phys. Chem.*, 99 (1995) 40.
138. J. Khatouri, M. Mostafavi, J. Amblard and J. Belloni, *Z. Phys. D*, 26 (1993) 82.
139. A. Henglein, P. Mulvaney, A. Holzwarth, T.E. Sosebee and A. Fojtik, *Ber. Bunsenges. Phys. Chem.*, 96 (1992) 754.
140. H. Remita, J. Khatouri, M. Treguer, J. Amblard and J. Belloni, *Z. Phys. D*, 40 (1997) 127.
141. M. Michaelis, A. Henglein and P. Mulvaney, *J. Phys. Chem.*, 98 (1994) 6212.
142. S. Remita, M. Mostafavi and M.O. Delcourt, *Radiat. Phys. Chem.*, 47 (1996) 275.
143. S. Remita., G. Picq, J. Khatouri and M. Mostafavi, *Radiat. Phys. Chem.*, 54 (1999) 463.
144. P. Mulvaney, M. Giersig and A. Henglein, *J. Phys. Chem.*, 96 (1992) 10419.
145. F. Henglein, A. Henglein and P. Mulvaney, *Ber. Bunsenges. Phys. Chem.*, 98 (1994) 180.
146. M. Kumar, S. Kapoor and C. Gopinathan, *Radiat. Phys. Chem.*, 54 (1999) 39.
147. A. Henglein, *J. Phys. Chem.*, 83 (1979) 2209.
148. M.O. Delcourt, N. Keghouche and J. Belloni, *Nouv. J. Chim.*, 7 (1983) 131.
149. D. Meisel, W.A. Mulac and M.S. Matheson, *J. Phys. Chem.*, 85 (1981) 179.
150. J. Belloni and A. Lecheheb, *Radiat. Phys. Chem.*, 29 (1987) 89.
151. J. Belloni, M.O. Delcourt and C. Leclere, *Nouv. J. Chim.*, 6 (1982) 507.
152. J. Bruneaux, H. Cachet, M. Froment, J. Amblard, J. Belloni and M. Mostafavi, *Electrochim. Acta*, 32 (1987) 1533.
153. J. Bruneaux, H. Cachet, M. Froment, J. Amblard and M. Mostafavi, *J. Electroanal Chem.*, 269 (1989) 375.
154. J. Amblard, O. Platzer and J. Belloni, *J. Chim. Phys.*, 88 (1991) 835.
155. Agfa GV Patent, EP 95 203 1706, Nov. 20th (1995) .
156. G. Stein, R. Watt and J. Weiss, *Trans. Faraday. Soc.*, 48 (1952) 1030.
157. N. B. Nazhat and K. D. Asmus, *J. Phys. Chem.*, 77 (1973) 614.
158. S. Fujita, H. Horii, T. Mori and S. Taniguchi, *Bull. Chem. Soc. Japan*, 48 (1975) 3067 and 49 (1976) 1250.
159. A.I. Aleksandrov and B.G. Ershov, *Russ. Chem. Bull.*, (1976) 249.
160. H. Jungbluth, J. Beyrich and K.D. Asmus, *J. Phys. Chem.* 80 (1976) 1049.
161. A. Malkov and J. Belloni, *J. Chim. Phys.*, 89 (1992) 885.
162. B.G. Ershov, N.L. Sukhov and D.I. Troitskii, *Radiat. Phys. Chem.*, 39 (1992) 123.
163. K.H. Schmidt, R. Patel and D. Meisel, *J. Am. Chem. Soc.*, 110 (1988) 4882.
164. H.G. Zhang and M. Mostafavi, *J. Phys. Chem.*, 101 (1997) 8443.
165. D. Hayes, O.I. Micic, M.T. Nenadovic, V. Swayambunathan and D. Meisel, *J. Phys. Chem.*, 93 (1989) 4603.
166. V. Swayambunathan, D. Hayes, K.H. Schmidt, Y.X. Liano and D. Meisel, *J. Am. Chem. Soc.*, 112 (1990) 3831.
167. M. Mostafavi, Yun-Ping Liu, P. Pernot and J. Belloni, *Radiat. Phys. Chem.*, 59 (2000) 49.
168. S. Baral, A. Fojtik, H. Weller and A. Henglein, *J. Am. Chem. Soc.*, 108 (1986) 375.
169. A. Henglein, A. Kumar, E. Janata and H. Weller, *Chem. Phys. Letters*, 132 (1986) 133.
170. U. Resch, H. Weller and A. Henglein, *Langmuir*, 5 (1989) 10015.
171. S. Gallardo, M. Gutierrez, A. Henglein and E. Janata., *Ber. Bunsenges. Phys. Chem.*, 93(1989) 10080.
172. E. Silvester, F. Grieser, T.W. Healy, D. Meisel and J.C. Sullivan, *J. Chem. Soc. Faraday Trans.*, 90 (1994) 3301.
173. F.J. Johnston, *Radiat. Phys. Chem.*, 33 (1989) 113.
174. Yingjie Zhu, Yitai Qian, H. Huang and Manwei Zhang, *Mater. Lett.*, 18 (1996) 119.

175. Yingjie Zhu, Yitai Qian, Manwei Zhang, Zuyao Chen, Dengfeng Xu, Li Yang and Guien Zhou, *Materials Res. Bull.*, 29 (1994) 377.
176. Yingjie Zhu, Yitai Qian and Manwei Zhang, *Materials Sci. Eng. B*, 41 (1996) 294.
177. Yunping Liu, Yitai Qian, Y.H. Zhang, Manwei Zhang, Changsui Wang and Li Yang, *Materials Res. Bull.*, 32 (1997) 1055.
178. Shizhong Wang, Houwen Xin and Yitai Qian, *Mater. Lett.*, 33 (1997) 113.
179. G.V. Buxton, T. Rhodes and R.M. Sellers, *Nature*, 295 (1982) 583. *J. Chem. Soc., Trans. Faraday I*, 79, (1983) 2961.
180. A. Henglein, *Ber. Bunsenges. Phys. Chem.*, 86 (1982) 241.
181. N.M. Dimitrijevic, D. Savic, O.I. Micic and A.J. Nozik, *J. Phys. Chem.*, 88 (1984) 4278.
182. J.M. Warman, M.P. de Haas and H.M. Wentinck, *Radiat. Phys. Chem.*, 34 (1989) 581.
183. J.M. Warman, M.P. de Haas, P. Pichat, T.P.M. Koster, E.A. van der Zouwen-Assink, A. Mackor and R. Cooper, *Radiat. Phys. Chem.*, 37 (1991) 433.
184. J.M. Warman, M.P. de Haas, P. Pichat and N. Serpone, *J. Phys. Chem.*, 95 (1991) 8858.
185. Y. Su, Y. Wang, J.L. Daschbach, T.B. Fryberger, M.A. Henderson, J. Janata and C.H.F. Peden, *J. Adv. Oxid. Technol.*, 3 (1998) 63.
186. D. Liu and P.V. Kamat, *Langmuir*, 12 (1996) 2190.
187. G.A. Zacheis, K.A. Gray and P.V. Kamat, *J. Phys. Chem. B*, 103 (1999) 2142.
188. T. Schatz, A.R. Cook and D. Meisel, *J. Phys. Chem. B*, 102 (1998) 7225.
189. N.M. Dimitrijevic, A. Henglein and D. Meisel, *J. Phys. Chem. B*, 103 (1999) 7073.

## Radiation Chemical Studies of Porphyrins and Metalloporphyrins

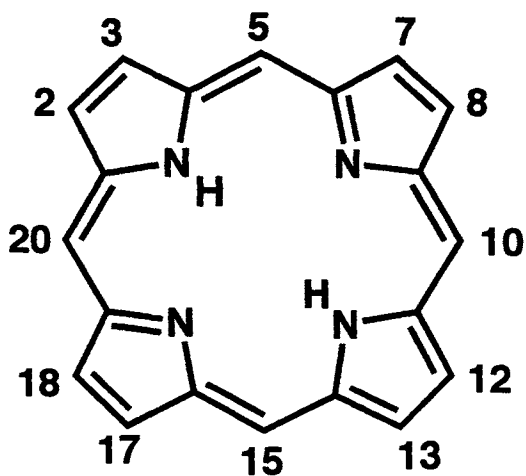
P. Neta

Physical and Chemical Properties Division, National Institute of Standards and Technology, Gaithersburg, Maryland 20899, USA

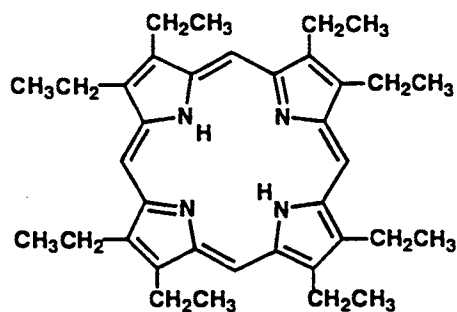
### 1 INTRODUCTION

Porphyrins (P) are tetrapyrrole macrocyclic compounds with an extended  $\pi$ -system. The peripheral carbons are numbered as shown below:

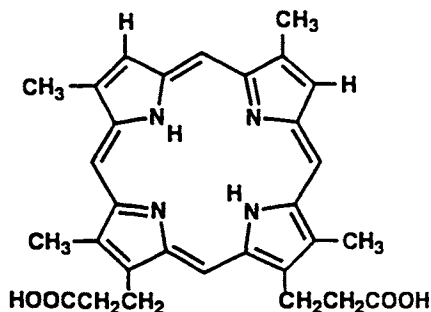
Because the four nitrogens form an optimal cavity, porphyrins can bind a wide variety of metal ions to form metalloporphyrins (MP). Iron porphyrins are found in many biological systems and act as electron transfer mediators (cytochromes) or oxygen transfer agents (hemoglobin). Modified porphyrins are found in nature also in the form of chlorophylls and vitamin B<sub>12</sub> and related compounds. These natural compounds bear various substituents at the  $\beta$ -pyrrole positions (2,3,7,8,12,13,17,18).



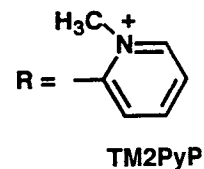
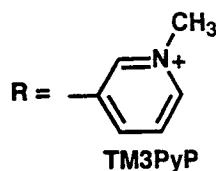
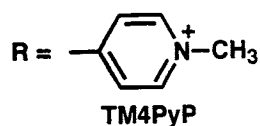
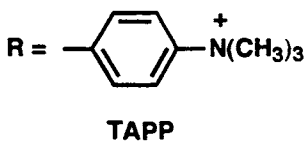
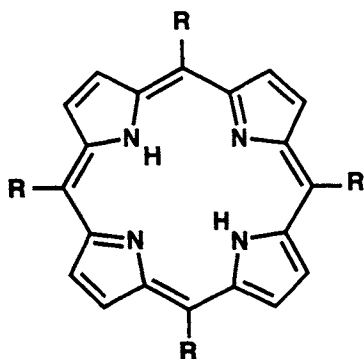
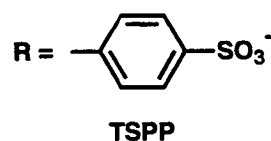
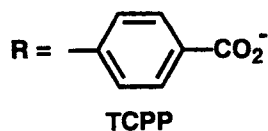
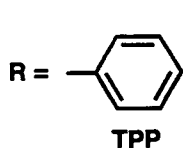
Many synthetic porphyrins have been prepared which are substituted at the meso positions (5,10,15,20). Porphyrins that have only alkyl or aryl substituents are insoluble in water. Water soluble porphyrins are made by introducing charged groups, such as carboxylate, sulfonate, trimethylammonium, or pyridinium. Some common synthetic porphyrins and their abbreviated notations are shown below.



OEP



DP



OEP = 2,3,7,8,12,13,17,18-octaethylporphyrin, DP = deuteroporphyrin D  
 TPP = 5,10,15,20-tetraphenylporphyrin or *meso*-tetraphenylporphyrin, TCP  
 = *meso*-tetrakis(4-carboxyphenyl)porphyrin, TSPP = *meso*-tetrakis(4-sulfonat  
 phenyl)porphyrin, TAPP = *meso*-tetrakis[4-(N,N,N-trimethylamino)phenyl]  
 porphyrin, TMXPyP = tetrakis(N-methyl-X-pyridyl)porphyrin. For uniformit  
 of notation, the charges of these substituted porphyrins are generally disregarde  
 in the abbreviations and in subsequent discussion, unless necessary for clarifi  
 of discussion.

Because of their extended  $\pi$ -system, porphyrins and related compounds absorb visible light. Therefore, their potential application as chromophores for harvesting solar energy, as a means to mimic the natural role of chlorophyll, has been under intense study. In addition, porphyrins can act as mediators of electron transfer, both as oxidants and as reductants. Therefore, the role of porphyrins as catalysts for various reductions and oxidations also has been studied by many authors.

Metal-free porphyrins can undergo several steps of reduction and oxidation at the macrocyclic ring  $\pi$ -system. Metalloporphyrins may undergo reduction and oxidation reactions both at the porphyrin  $\pi$ -system and at the central metal ion. The site and rate of such redox reactions strongly depend on the porphyrin structure, the nature of the central metal ion, and the environment. Many of the fundamental reactions of porphyrins and metalloporphyrins have been studied by radiation chemical methods; these studies are reviewed in this chapter.

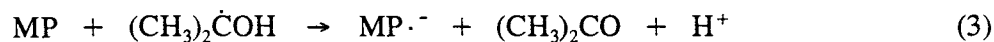
## 2 REDUCTION OF THE PORPHYRIN LIGAND

The porphyrin macrocycle contains conjugated double bonds that form an 18-membered  $\pi$ -electron system. This  $\pi$ -system can accept several electrons in a stepwise manner. The addition of one electron forms a porphyrin  $\pi$ -radical anion. Such  $\pi$ -radical anions have been prepared from metalloporphyrins and from metal free porphyrins and related compounds by irradiation in various environments.

Most studies have been carried out in aqueous or aqueous-alcohol solutions and the intermediate and final products have been followed by spectrophotometry.<sup>1-8</sup> All porphyrins react with the hydrated electron with diffusion-controlled rate constants ( $k \approx 10^{10} \text{ L mol}^{-1} \text{ s}^{-1}$ ) to form the  $\pi$ -radical anions.



They are also reduced by  $\cdot\text{CO}_2^-$  and by  $\alpha$ -hydroxyalkyl radicals, e.g.

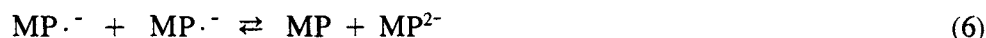


The rate constants in these cases depend on the reduction potential of the porphyrin and the radical and can vary from  $< 10^7$  to  $> 10^9 \text{ L mol}^{-1} \text{ s}^{-1}$ .<sup>9</sup> The radical anions formed in these reactions generally exhibit intense absorption

bands at in the region of 600 nm to 800 nm so that their formation and subsequent reactions can be easily monitored.

The radical anions are stable in aprotic media in the absence of oxidants but decay rapidly in protic solvents. The stability of porphyrin radical anions in aqueous solutions was found to depend very strongly upon the nature of the substituents on the ring and the nature of the metal center.

A dramatic difference was observed in the behavior of porphyrin radical anions that contain phenyl *vs.* pyridinium substituents at the meso positions.<sup>6</sup> It was suggested that the radical anions decay either via protonation, to form a neutral radical, or disproportionation, to form a dianion, which then protonates very rapidly. The dianion can take-up a proton at a meso site to form a phlorin anion or take up two protons at a pyrrole ring to form a chlorin.



Since the pyridyl groups have a stronger electron withdrawing effect than the phenyl groups, they decrease the electron density on the ring  $\pi$ -system and thus retard protonation and inhibit decay. Furthermore, a dramatic difference was found between the stability of the radical anions derived from the three isomeric TMPyP ligands, i.e. TM2PyP, TM3PyP, and TM4PyP. In TM2PyP, protonation is strongly inhibited because the positive charge is very close to the porphyrin  $\pi$ -system and because the steric effects of the methyl groups inhibit deformation of the ring. Therefore, the radical anion of TM2PyP is much longer-lived than those of TM3PyP or TM4PyP and is exceptionally stable in alkaline solutions.<sup>10</sup> The inductive and steric effects discussed above also influence the distribution of final products, i.e. production of chlorin *vs.* phlorin anion.<sup>11</sup>

The nature of the central metal ion also exerts a strong influence on the electron density at the porphyrin ring and, consequently, affects the reactivity of reduced porphyrins. The lifetime of the radical anions of various TM4PyP complexes was found to vary by many orders of magnitude for different central metal ions. The stability decreased in the order  $\text{Sb}^{\text{V}}$ ,  $\text{Sn}^{\text{IV}}$ ,  $\text{In}^{\text{III}}$ ,  $\text{Ge}^{\text{IV}}$ ,  $\text{Ga}^{\text{III}}$ ,  $\text{Al}^{\text{III}}$ ,  $\text{Zn}^{\text{II}}$ , which was also the order of the porphyrin one-electron reduction potentials

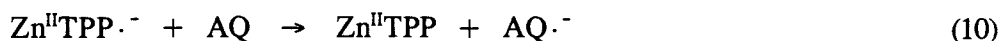
under similar experimental conditions.<sup>8</sup> The observed correlation between reduction potential and radical anion stability confirms that the major factor influencing the reactivity of these reduced porphyrins is the relative electron density on the ring. With a strongly electronegative metal cation and an electron-withdrawing substituent at the porphyrin meso-position, as found with Sn<sup>IV</sup>TM4PyP, the radical anion is stable in the absence of air, due to retardation of protonation, even in acidic solution.<sup>8</sup>

It should be noted that the radical anions of metal-free porphyrins (H<sub>2</sub>P<sup>·-</sup>) were observed in alkaline solutions but in neutral solutions they underwent protonation at a pyrrolic nitrogen to form the neutral radicals (H<sub>3</sub>P<sup>·</sup>).

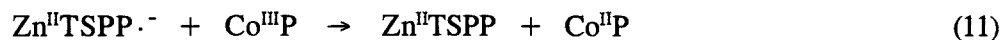


The pK<sub>a</sub> values for such radicals were determined from changes in absorption spectra and found to be in the mildly alkaline range.<sup>2</sup> On the other hand, metalloporphyrin radical anions cannot protonate on the nitrogen unless this leads to demetallation (see below). They may protonate on a carbon atom, but such species have not been shown to exist in the microsecond time scale under ambient conditions. Therefore, the above disproportionation mechanism is likely to be driven by protonation of the dianion rather than protonation of the radical anion.

Aside from disproportionation and protonation, porphyrin π-radical anions can engage in electron transfer to other compounds, such as quinones, methyl viologen, fullerenes, and other porphyrins. For example, the radical anions of H<sub>2</sub>TPP and Zn<sup>II</sup>TPP in 2-propanol transfer an electron to anthraquinone with rate constants *ca.* 2 × 10<sup>9</sup> L mol<sup>-1</sup> s<sup>-1</sup>, the radical anion of H<sub>2</sub>TCPP in water transfers an electron to methyl viologen with a similar rate constant and to anthraquinone-2-sulfonate somewhat more slowly, but when the radical anion is protonated it donates an electron about an order of magnitude more slowly.<sup>2</sup>

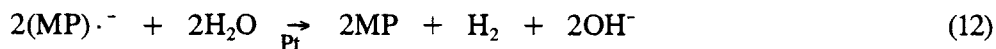


In another study, the radical anion of Zn<sup>II</sup>TSPP was found to transfer an electron to Co<sup>III</sup>TSPP, Co<sup>III</sup>TAPP, and Co<sup>III</sup>TM4PyP with rate constants of 2.0 × 10<sup>7</sup>, 5.5 × 10<sup>8</sup>, and 1.4 × 10<sup>9</sup> L mol<sup>-1</sup> s<sup>-1</sup>, respectively, in line with changes in the reduction potentials of the acceptors.<sup>3</sup>



More recently, rate constants were determined for electron transfer from a number of metalloporphyrin radical anions to C<sub>60</sub> and were found to be quite

rapid ( $k$  ca.  $2 \times 10^9$  L mol<sup>-1</sup> s<sup>-1</sup>); only the radical anion of Sb<sup>V</sup>OEP, which has a very low reduction potential, reacted much more slowly with C<sub>60</sub> ( $k < 10^7$  L mol<sup>-1</sup> s<sup>-1</sup>).<sup>12</sup> Porphyrin radical anions also can donate an electron to metal catalysts, such as colloidal Pt in water, to lead to formation of H<sub>2</sub>.<sup>13</sup>



Although most radiolytic studies on the reduction of porphyrins were done in aqueous or alcohol solutions, a number of studies were carried out in other organic media. For example, the radical anion of chlorophyll a was observed in solutions of tetrahydrofuran by pulse radiolysis and in a 2-methyltetrahydrofuran glass at 77 K following  $\gamma$ -irradiation.<sup>14</sup> The radical anions of copper and vanadyl porphyrins were observed by optical and ESR spectroscopy following  $\gamma$ -irradiation in MTHF glass.<sup>15</sup>

Pulse radiolysis of porphyrins in benzene permitted the observation of porphyrin triplet states and provided a more accurate method than laser photolysis to determine their molar absorption coefficients.<sup>16</sup>

### 3 OXIDATION OF THE PORPHYRIN LIGAND

The porphyrin  $\pi$ -system can donate a number of electrons to form the radical cation, dication, etc. Pulse radiolysis has been used to oxidize porphyrins to the  $\pi$ -radical cations both in aqueous solutions<sup>3,5</sup> and in organic solvents. In aqueous solutions, the  $\cdot\text{OH}$  radical is not a good oxidant for porphyrins because it adds to the double bonds. However, oxidizing radicals such as  $\text{Cl}_2\cdot^-$ ,  $\text{Br}_2\cdot^-$ ,  $\text{N}_3\cdot^-$ ,  $\text{CCl}_3\text{O}_2\cdot^-$ , and  $\cdot\text{CH}_2\text{CHO}$  are suitable for this purpose.<sup>3,5</sup> For example, oxidation by  $\text{Br}_2\cdot^-$  takes place with rate constants in the range of  $10^9$  L mol<sup>-1</sup> s<sup>-1</sup>.



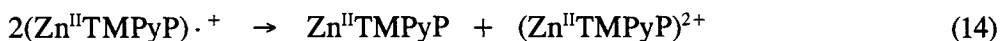
The azide and dichloride radicals react more rapidly and the organic radicals shown above react more slowly. Many water-soluble metalloporphyrins were oxidized by these reactions, and radical cations were generated from Zn<sup>II</sup>, Cd<sup>II</sup>, Cu<sup>II</sup>, Pd<sup>II</sup> and Sn<sup>IV</sup>-porphyrins.<sup>5</sup> Other metalloporphyrins were subsequently studied.

The resulting porphyrin  $\pi$ -radical cations exhibit a fairly strong absorptior band around 650-700 nm. The exact position of this band is dependent upon the nature of the porphyrin ligand.<sup>3,5</sup> With a positively charged ligand (Zn<sup>II</sup>TM4PyP), the spectrum of the radical cation was also slightly dependent



on the anion used to form the oxidizing radical, suggesting some binding of the anion to the highly charged (+5) radical cation.<sup>17</sup>

In most cases, the radical cations were unstable and decayed within milliseconds. The rate of decay was greatly influenced by the nature of the substituents on the porphyrin ring, as outlined earlier for the various radical anions. Thus, the tetranegative  $\text{Zn}^{\text{II}}\text{TSP}$  gave a relatively long-lived radical cation, with half-life  $\sim 7$  s at pH 7. In contrast, the tetrapositive  $\text{Zn}^{\text{II}}\text{TMPyP}$  complexes gave very short-lived radical cations. They decay via disproportionation to form a dication,

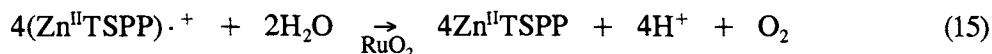


which then reacts with water to form stable products. Comparison with other water-soluble zinc porphyrins showed<sup>18,19</sup> that the stability of the radical cation depended upon the ability of the meso-substituent to donate electronic charge to the porphyrin ring. In fact, it was found that the substituent influences both the potential for one-electron oxidation of the porphyrin and the half-life of the porphyrin radical cation. Substituents that raise the electron density on the porphyrin ring lower the oxidation potential and stabilize the radical cation. Thus factors stabilizing the radical anions appear to destabilize the radical cations.

The influence of the central metal ion upon the reactivity of porphyrin radical cations in water was also studied.<sup>20</sup> As described for the porphyrin radical anions, the electronegativity of the central metal ion was found to exert a pronounced effect on the rate of decay of the cations. For a given type of porphyrin ring, the stability of the porphyrin radical cation decreased in the order  $\text{Pb}^{\text{II}}$ ,  $\text{Mg}^{\text{II}}$ ,  $\text{Cd}^{\text{II}}$ ,  $\text{Zn}^{\text{II}}$ ,  $\text{Pd}^{\text{II}}$ ,  $\text{V}^{\text{IV}}\text{O}$ ,  $\text{Fe}^{\text{III}}$ , and again there was a good correlation between stability and oxidation potential. For example,  $\text{Mg}^{\text{II}}\text{TSP}$ , because of the electropositive  $\text{Mg}^{\text{II}}$  ion, formed a particularly stable radical cation. In neutral aqueous solution the first half-life for decay of  $(\text{Mg}^{\text{II}}\text{TSP})\cdot^+$  was about 37 s, although it decreased at higher pH due to deprotonation of the axially-bound water molecule.

The interest in the properties of metalloporphyrin radical cations in water relates to their potential use as oxidants in solar energy storage schemes. In particular, the oxidation of water to oxygen by highly-oxidized metalloporphyrins has been considered as a model for photosynthesis. The pulse radiolytic studies outlined above provided good understanding of the factors that influence the stability of the radical cations in water. A critical point is the correlation between stability of a porphyrin radical cation and the redox potential for oxidation of the porphyrin. Consequently, porphyrins with a sufficiently high oxidation potential to be useful oxidants of water have short-

lived radical cations. Therefore, oxidation of water has to be attempted with less stable species and thus requires highly effective catalysts. Colloids of  $\text{RuO}_2$ <sup>21</sup> and  $\text{IrO}_x$ <sup>22,23</sup> were found to be efficient catalysts for the oxidation of water to  $\text{O}_2$ . For example, the radical cations of  $\text{Mg}^{\text{II}}\text{TSPP}$  and  $\text{Zn}^{\text{II}}\text{TSPP}$ , with reduction potentials  $E_{1/2} = 0.7 \text{ V}$  and  $0.9 \text{ V}$  vs. NHE, respectively, and with relatively long lifetime in water, can accept an electron from colloidal  $\text{RuO}_2$  to result in water oxidation.

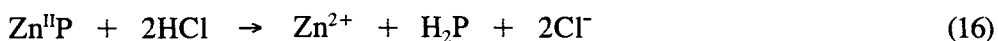


This reaction is thermodynamically feasible only in alkaline solutions. It is advantageous, however, to be able to oxidize water to oxygen in neutral solutions. To achieve this task it is necessary to use metalloporphyrins with higher oxidation potentials.  $\text{Zn}^{\text{II}}\text{TM4PyP}$  has a higher oxidation potential than  $\text{Zn}^{\text{II}}\text{TSPP}$  but the radical cation  $\text{Zn}^{\text{II}}\text{TM4PyP}\cdot^+$  was much less effective than  $\text{Zn}^{\text{II}}\text{TSPP}\cdot^+$  in production of  $\text{O}_2$ . This difference was ascribed to the overall charge of these "radical cations". TSPP has four negatively charged sulfonate groups and thus is repelled from the colloidal oxide particles, which are generally negatively charged. TM4PyP, on the other hand, has four positively charged pyridinium groups and thus is strongly attracted to the particles. As a result, the  $\text{Zn}^{\text{II}}\text{TSPP}$  radical cation transfers its charge to the colloidal particle and moves away, permitting the particle to accumulate charge and then discharge it by oxidizing water. On the other hand, the  $\text{Zn}^{\text{II}}\text{TM4PyP}$  radical cation reacts much more rapidly with the colloidal particle but remains attached, causing the particle to discharge its accumulated positive charge back into the porphyrin and thus the porphyrin was found to be oxidized instead of water. Preparation of positively charged colloids, by using a positively charged stabilizing polymer, allowed oxygen production by  $\text{Zn}^{\text{II}}\text{TM4PyP}$  but did not provide high yields. Therefore, to improve the efficiency of  $\text{O}_2$  production, other TSPP complexes with higher oxidation potentials have been studied. The potential was raised either by adding electron withdrawing groups on the porphyrin ring or changing the central metal ion. The best results were obtained with  $\text{Pd}^{\text{II}}\text{TSPP}$  ( $E_{1/2} = 1.1 \text{ V}$  vs NHE) and it was concluded that further increase in potential may not improve the overall efficiency of  $\text{O}_2$  production.<sup>24</sup>

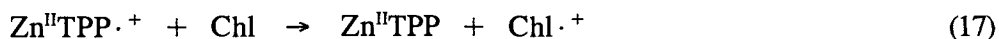
Aqueous micellar solutions were utilized for pulse radiolysis studies of chlorophylls and porphyrins that are insoluble in water. Chlorophyll, bacteriochlorophyll, and pheophytin in aqueous solutions containing Triton X 100 were oxidized by  $\text{N}_3\cdot$ ,  $\text{Br}_2\cdot^-$ , and  $(\text{SCN})_2^-$  with rate constants of the order of  $10^9 \text{ L mol}^{-1} \text{ s}^{-1}$ , and by certain other radicals more slowly.<sup>25</sup> The spectra of the radical cations were determined. In subsequent studies under similar

conditions, rate constants for electron transfer from chlorophylls to carotene radical cations were determined.<sup>26</sup> The rate constants in micelles were found to be about two orders of magnitude lower than those in homogeneous solutions and the effect was ascribed to slow migration of chlorophyll inside the micelle. Studies in micellar solutions were also carried out on the oxidation and reduction of Zn<sup>II</sup>TPP and chlorophyll.<sup>27</sup> Rate constants were determined for both the ground states and the excited states of these compounds and found to be much higher for the latter species.

Radical cations of water insoluble porphyrins were studied in chlorinated organic solvents. Pulse radiolysis in dichloroethane led to production of the radical cations of several metalloporphyrins, but an additional process was observed in the case of Mg<sup>II</sup> and Zn<sup>II</sup> complexes.<sup>28</sup> It was found that this second process was due to demetallation of these complexes by the HCl formed in the radiolysis.



Complexes of Ni<sup>II</sup> and Co<sup>II</sup>, for example, do not undergo demetallation but complexes of Zn<sup>II</sup> and Mg<sup>II</sup> do so very readily. To prevent demetallation, either a base (pyridine) was added to neutralize the HCl,<sup>29</sup> or the solvent was changed to CCl<sub>4</sub>,<sup>30</sup> where HCl is not produced. By using dichloroethane/pyridine solutions rate constants could be determined for the electron transfer from Co<sup>II</sup>TPP and from chlorophyll a to the radical cations of various metalloporphyrins.



The rate constants were found to be mostly in the range of  $3 \times 10^8$  to  $5 \times 10^8$  L mol<sup>-1</sup> s<sup>-1</sup> despite large differences in reduction potentials. Since these values are much lower than the diffusion-controlled limit, it was suggested that the reaction rate is restricted by steric effects or by axial ligand exchange. The rate constants for oxidation of Co<sup>II</sup>TPP by various metalloporphyrin radical cations were somewhat lower in CCl<sub>4</sub>/pyridine than in dichloroethane/pyridine, probably due to the lower solvent polarity, but they were much lower in the absence of pyridine, due to the change in the Co<sup>II</sup>/Co<sup>III</sup> reduction potential with and without pyridine as an axial ligand.<sup>31</sup>

Rate constants for oxidation of Zn<sup>II</sup>TPP by the CCl<sub>3</sub>O<sub>2</sub>· radical were determined in various organic solvents containing CCl<sub>4</sub> as the radical source and found to decrease by two orders of magnitude upon going from hydrocarbon

solvents to DMSO or pyridine. The results indicated that the rate constant was not dependent on solvent polarity but on the ability of the solvent to attach as an axial ligand to the  $Zn^{II}TPP$ . To explain the results, it was suggested that the reaction involves an inner sphere mechanism, whereby the peroxy radical attaches to the Zn before electron transfer.<sup>32</sup>

Porphyrin radical cations were also produced by  $\gamma$ -irradiation in frozen organic media at 77 K. In hydrocarbon solvents, both the radical anion and the radical cation were formed from the porphyrin, but addition of a small amount of  $CCl_4$  eliminated the radical anion. Other experiments were carried out in chlorinated hydrocarbons. In this manner, the optical absorption spectra and the ESR spectra were recorded for the radical cations of chlorophyll,<sup>33</sup>  $Pb^{II}TPP$ ,<sup>34</sup>  $Cu^{II}OEP$ ,<sup>35</sup> and  $V^{IV}OTPP$ .<sup>36</sup> The observed spectra led to the conclusion that in all these metalloporphyrins the species observed is the radical cation, i.e. the unpaired spin is predominantly on the porphyrin ring. Other metalloporphyrins, however, can be oxidized or reduced at the metal center. Such process are discussed below.

#### 4 REDUCTION OF THE METAL CENTER

In the previous two sections we discussed the one-electron reduction and oxidation of the porphyrin ring to form radical anions and cations. In the case of metal-free porphyrins and with  $Zn^{II}$ ,  $Mg^{II}$ ,  $Cd^{II}$ ,  $Al^{III}$ , and similar ions as the metal center, these are the only possible redox processes. However, with transition metal ions that have a variety of stable oxidation states, the porphyrin complexes can undergo reduction or oxidation reactions at the central metal rather than on the porphyrin ring. Certain transition metal porphyrins, such as those of Fe, Co, and Mn, undergo redox processes which involve the principal oxidation states of the metal center practically under any conditions and with any porphyrin ligand. In several metalloporphyrins, however, such as those of Ni and Cr, redox reactions involving the metal center may take place with nearly the same potential as those involving the porphyrin ligand, and the actual mode of reaction becomes critically dependent on the structure of the porphyrin and even on the medium which can act as an axial ligand. Some of these studies were carried out by pulse radiolysis and are summarized below.

Usually, it is easy to identify the site of reaction from the absorption spectra of the products; reduction or oxidation at the porphyrin ring causes large changes in the absorption spectrum, frequently forming intense bands in the near IR region, whereas reduction or oxidation at the central metal gives more subtle changes, generally only minor shifts (10-30 nm) in the absorption peaks and no major absorptions in the near IR region.

Radiolytic studies in aqueous solutions demonstrated reduction of  $\text{Fe}^{\text{III}}\text{P}$  to  $\text{Fe}^{\text{II}}\text{P}$ ,<sup>37-39</sup> of  $\text{Co}^{\text{III}}\text{P}$  to  $\text{Co}^{\text{II}}\text{P}^{3-6}$  to  $\text{Co}^{\text{I}}\text{P}$ ,<sup>40</sup> of  $\text{Mn}^{\text{III}}\text{P}$  to  $\text{Mn}^{\text{II}}\text{P}$ ,<sup>41</sup> and in 2-propanol reduction of  $\text{Rh}^{\text{III}}\text{P}$  to  $\text{Rh}^{\text{I}}\text{P}$  via an unstable  $\text{Rh}^{\text{II}}\text{P}$ .<sup>42</sup> Trivalent metalloporphyrins generally contain a halide ion and/or a solvent molecule as axial ligands. Reduction of these complexes to form the divalent metal center often is accompanied by release of the axial ligands.

When radiolytic reduction of  $\text{Mn}^{\text{III}}$  and  $\text{Co}^{\text{III}}$  porphyrins was carried out in frozen MTHF at 77 K, the anionic axial ligands could not diffuse away and thus the optical and ESR spectra of the reduced complexes were quite different from those of the equilibrated reduced products.<sup>43,44</sup> On the other hand, when the complexes were dissolved in alcohol, the halide axial ligand was exchanged with a solvent molecule; and when these solutions were frozen and irradiated, the reduced species were identical with the equilibrated stable products.<sup>45</sup>

Reduction of the metal center forms a metal ion with a larger radius. In certain cases, because of the limited size of the porphyrin cavity, the reduced complexes are unstable and undergo demetallation. The demetallation can be catalyzed by acid. Since the oxidized form is stable, and since the reduction step can be very rapid, pulse radiolysis can be utilized to measure the rate of demetallation. Thus, radiolytic reduction of  $\text{Ag}^{\text{II}}\text{TSPP}$  to  $\text{Ag}^{\text{I}}\text{TSPP}$  was followed by rapid demetallation,<sup>46</sup> to form  $\text{H}_2\text{TSPP}$  in neutral solutions, and radiolytic reduction of several  $\text{Mn}^{\text{III}}$ -porphyrins produced the corresponding  $\text{Mn}^{\text{II}}$ -porphyrins, which underwent demetallation in acidic solutions.<sup>47</sup> The rate of demetallation of  $\text{Mn}^{\text{II}}\text{TSPP}$  was a complex function of the acid concentration and was much higher than the rate of demetallation of  $\text{Mn}^{\text{II}}\text{TM4PyP}$ . Demetallation was also used as an indicator of the porphyrin reduction product. For example,  $\text{Cu}^{\text{II}}$ -porphyrins are reduced to give species that exhibit the characteristic absorptions of the  $\pi$ -radical anions, but these species were found to undergo demetallation in acidic solutions, suggesting a partial  $\text{Cu}^{\text{I}}$  character.<sup>48</sup>

Porphyrin complexes of certain metal ions have reduction potentials for the ligand and the metal center that are sufficiently close to lead to uncertainties in the site of reduction. The outcome of the reaction can be determined from the optical absorption spectrum of the product (transient or stable). The site of reduction is dependent on the electron affinity of the ligand and, therefore, complexes of pyridylporphyrins or  $\text{TMPyP}$  are more likely to be reduced at the ligand than complexes of  $\text{TPP}$  or  $\text{OEP}$ . This was found to be the situation with  $\text{Ni}^{\text{II}}$ -porphyrins,<sup>49</sup> where several complexes were reduced to  $\text{Ni}^{\text{I}}\text{P}$  but the presence of a single *meso*-pyridyl group was sufficient to direct the reduction toward the ligand to form  $\text{Ni}^{\text{II}}\text{P}^{\cdot -}$ . However, all one-electron reduction products were unstable in water and decayed to form the  $\text{Ni}^{\text{II}}$ -chlorin or phlorin.

The site of reduction of  $\text{Cr}^{\text{III}}$ -porphyrins was found to be dependent also on the medium, because the medium can be involved in axial ligation. For the

complexes  $L_1L_2Cr^{III}P$ , where  $L_1$  and  $L_2$  are axial ligands, the site of reduction was dependent on the nature of  $L$ ; stronger ligands donate electron density to the metal and increase the likelihood of porphyrin ring reduction.<sup>50</sup>

The effect of the axial ligand is very strong in the case of  $CN^-$  and shifts the site of reduction for a  $Co^{III}$ -porphyrin. Thus, the complex  $(CN)_2Co^{III}TM4PyP$  is the only example in which a  $Co^{III}$ -porphyrin is found to be reduced at the ligand rather than at the metal.<sup>51</sup>

Reduction of  $Fe^{II}$ -porphyrins leads to production of  $Fe^I$ -porphyrins.<sup>52,53</sup> These products are unstable in aqueous solutions and are oxidized back to the ferrous state, probably by the solvent. Only the sterically hindered  $Fe^{II}TM2PyP$  formed an  $Fe^I$  complex which was stable in alkaline solutions, although it decayed rapidly in acidic solutions.<sup>54</sup> Because  $Fe^I$ -porphyrins are known to be stable in organic solvents, and because they have been shown to be reduced to  $Fe^0$ -porphyrins, which then react with protons, it was suggested that the observed decay of the  $Fe^I$  complex is not via direct reaction with a proton but rather via disproportionation to form an equilibrium mixture with  $Fe^{II}$  and  $Fe^0$  and the latter species is the one reacting with the proton.

The interest in these highly reduced states stems from their potential use as catalysts for the electrochemical or photochemical reduction of  $CO_2$  to  $CO$ .<sup>54,55</sup> The mechanism involves binding of  $CO_2$  as an axial ligand to the reduced metalporphyrin followed by two-electron transfer.  $Fe^I$  and  $Co^I$  porphyrins do not react with  $CO_2$  but when they are reduced to the  $M^0$  oxidation state they react rapidly.

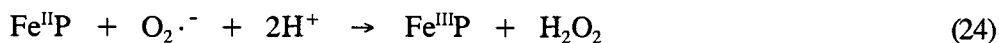


The  $CO_2$ -adducts can decompose to  $CO$  by reaction with a proton or by reaction with  $CO_2$  or other acids. The same  $CO_2$ -adducts can be formed in the pulse radiolysis by reaction of  $Fe^I P$  or  $Co^I P$  with  $\cdot CO_2^-$ , but their subsequent decomposition appeared to be very fast and did not permit characterization of these adducts.

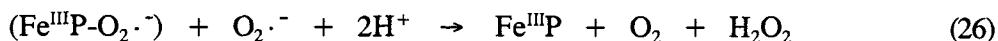
Other reduced metalporphyrins have been shown to catalyze the reduction of  $O_2$ , alkyl halides, nitrate ions, and other compounds. Some of these processes will be discussed in a later section.

A catalytic reaction of particular interest in biochemistry is that of superoxide

dismutase. Several radiolytic studies were carried out on model compounds, i.e. on metalloporphyrins that can catalyze the dismutation of  $O_2\cdot^-$  into  $O_2$  and  $H_2O_2$ .<sup>56-59</sup> Such activity requires that one oxidation state of the metalloporphyrin reacts rapidly with  $O_2\cdot^-$  via oxidation and the other state reacts rapidly via reduction. For example,



Another possible mechanism involves inner sphere reactions, i.e. the superoxide radical binds to the metalloporphyrin and the resulting complex reacts with another superoxide to form the products.



Metalloporphyrins of  $Zn^{II}$ ,  $Cu^{II}$ , and  $Ni^{II}$  did not catalyze superoxide dismutation to any observable extent, whereas metalloporphyrins of  $Co^{III}$ ,  $Fe^{III}$ , and  $Mn^{III}$  were reactive; the order of reactivity for several complexes was  $Fe^{III}TM4PyP \gg Mn^{III}TM4PyP > Co^{III}TM4PyP \sim Mn^{III}TAPP > Fe^{III}TSP$ . From considerations of the measured rate constants it was concluded that the last four metalloporphyrins react via the outer sphere mechanism, while the most reactive,  $Fe^{III}TM4PyP$ , reacts via an inner sphere mechanism.<sup>58</sup> For the latter porphyrin, evidence was presented for the formation of a superoxide complex.<sup>57</sup> A subsequent study was carried out with a water-soluble picket-fence iron porphyrin,  $Fe^{III}PFP$  (in which the four phenyl groups of  $Fe^{III}TPP$  contain an N-methylisonicotinamido group at the ortho position). Reactivities were compared for the complexes containing water, 1-methylimidazole, or cyanide as the axial ligands. Despite the finding that the aquo complex was two orders of magnitude more reactive toward superoxide than the other complexes, no evidence for an inner sphere reaction was found, and it was argued that all these complexes react via the outer sphere mechanism.<sup>59</sup>

## 5 OXIDATION OF THE METAL CENTER

Porphyrin complexes containing transition metal ions at the lower oxidation states, e.g.  $Mn^{II}$ ,  $Fe^{II}$ ,  $Co^{II}$ , are easily oxidized to the higher oxidation states. In the presence of strong axial ligands, such as water or pyridine, these complexes

are oxidized even by exposure to  $O_2$ . Rate constants for oxidation of such porphyrins by several oxidizing radicals were measured by pulse radiolysis. For example, the rate constants for oxidation of  $Co^{II}TSPP$  by  $Br_2^{\cdot -}$  ( $1 \times 10^9 \text{ L mol}^{-1} \text{ s}^{-1}$ ) and by  $\cdot CH_2CHO$  ( $2 \times 10^9 \text{ L mol}^{-1} \text{ s}^{-1}$ )<sup>3</sup> and for oxidation of  $Mn^{II}TM4PyP$  by  $Br_2^{\cdot -}$  ( $8.5 \times 10^9 \text{ L mol}^{-1} \text{ s}^{-1}$ ) and by  $Cl_2^{\cdot -}$  ( $1.5 \times 10^{10} \text{ L mol}^{-1} \text{ s}^{-1}$ ) are all very high.<sup>41</sup> Oxidation by the dihalide radicals was suggested to take place via an inner sphere mechanism to form a product in which a halide ion is attached to the oxidized metal ion as an axial ligand.

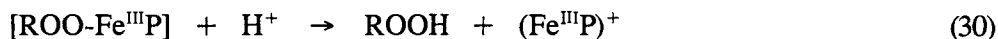
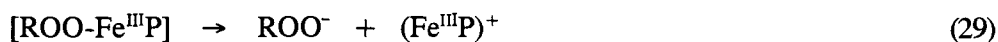


Oxidation of several  $Mn^{III}$ -porphyrins by the same radicals take place slightly more slowly.<sup>41</sup> When the oxidation is carried out in neutral or alkaline solutions the products are  $Mn^{IV}$ -porphyrins, but when the oxidation is carried out in acidic solutions the products were suggested to be the  $\pi$ -radical cations  $Mn^{III}P^{\cdot +}$ .<sup>60</sup> Both of these products were unstable and were reduced by the solvent back to the  $Mn^{III}P$ . The  $Mn^{IV}P$ , however, was sufficiently long-lived in highly alkaline solutions to permit observation of its subsequent radiolytic oxidation with  $Br_2^{\cdot -}$  ( $k$  near  $10^9 \text{ L mol}^{-1} \text{ s}^{-1}$ ).<sup>60</sup> And again, the product of oxidation was  $Mn^V P$  at very high pH but  $Mn^{IV}P^{\cdot +}$  at lower pH. This change in product occurred around pH 12 to 13, depending on the porphyrin structure; with  $Mn^{IV}TM4PyP$  being oxidized to the  $\pi$ -radical cation even at pH 14. Decay of these highly oxidized manganese porphyrins did not lead to production of  $O_2$ . Even when  $RuO_2$  was added as a catalyst, only small amounts of  $O_2$  were formed.

Oxidation of  $Fe^{III}$ -porphyrins was studied extensively as a model for cytochrome  $P_{450}$  and peroxidases. One-electron oxidation may lead to formation of either  $Fe^{IV}P$  or  $Fe^{III}P^{\cdot +}$ . Various results led to different conclusions concerning the site of oxidation, but most likely the site of oxidation depends on the porphyrin structure, axial ligand, solvent, and pH. Pulse radiolysis studies provided rate constants for the oxidation of  $Fe^{III}P$  by various peroxy radicals in aqueous alcohol solutions and the observed transient spectra were interpreted in terms of oxidation at the porphyrin  $\pi$ -system.<sup>61</sup> The rate constants were in the range of  $10^7$  to  $10^8 \text{ L mol}^{-1} \text{ s}^{-1}$  and decreased in the order  $CF_3OO\cdot > CBr_3OO\cdot > CCl_3OO\cdot > CHCl_2OO\cdot > CH_2ClOO\cdot > CF_3CHClOO\cdot >> CH_3OO\cdot$ .<sup>61,62</sup> The increase in rate constant with increasing degree of halogenation was interpreted to be in line with an expected electron transfer mechanism, but the unexpected order for the three  $CX_3OO\cdot$  radicals remains unclear (although it was observed in the oxidation of other compounds as well). The peroxy radicals derived from methanol and 2-propanol oxidized  $Fe^{III}P$  more slowly than the halogenated radicals. Probably because of the slowness of this reaction, kinetic evidence was obtained for the intermediate



formation of a complex,  $[\text{ROO-Fe}^{\text{III}}\text{P}]$ , which then decomposes to products via two parallel pathways.<sup>63</sup>



Despite uncertainties concerning the site of the first one-electron oxidation of  $\text{Fe}^{\text{III}}\text{P}$ , the second oxidation is thought to form a ferryl species,  $\text{O}=\text{Fe}^{\text{V}}\text{P}$ , which can oxidize or hydroxylate various organic compounds. In parallel with this chemistry of iron porphyrins, the oxidation of ruthenium and osmium porphyrins was studied by radiation chemical methods.

$\text{Ru}^{\text{II}}$ -porphyrins are generally stabilized with a CO molecule as an axial ligand. Thus the radiolytic oxidation of  $(\text{CO})\text{Ru}^{\text{II}}\text{OEP}$  and  $(\text{CO})\text{Ru}^{\text{II}}\text{TPP}$  in aerated  $\text{CH}_2\text{Cl}_2$  solutions was found to lead first to the radical cation  $(\text{CO})\text{Ru}^{\text{II}}\text{P}\cdot^+$ , and this species reacts with  $\text{Cl}^-$  ( $k = 1 \times 10^5 \text{ L mol}^{-1} \text{ s}^{-1}$ ) to form  $(\text{Cl})(\text{CO})\text{Ru}^{\text{II}}\text{P}\cdot^+$ .<sup>64</sup> In the presence of  $\text{CN}^-$  the  $\text{Ru}^{\text{II}}$  porphyrin became  $(\text{CN})(\text{CO})\text{Ru}^{\text{II}}\text{P}$ . Oxidation of this complex with  $\text{CCl}_3\text{O}_2\cdot$  also produced the radical cation  $(\text{CN})(\text{CO})\text{Ru}^{\text{II}}\text{P}\cdot^+$ , but this species underwent a first order transformation ( $k = 5 \times 10^3 \text{ s}^{-1}$ ) into  $(\text{CN})\text{Ru}^{\text{III}}\text{P}$ . When  $\text{OH}^-$  is bound as an axial ligand, oxidation also takes place at the metal center, but in the alkaline solutions the  $(\text{HO})_2\text{Ru}^{\text{III}}\text{P}$  is unstable and forms  $\text{Ru}^{\text{IV}}$  products, probably by disproportionation. The product was suggested to be the  $\mu$ -oxo dimer  $[(\text{HO})\text{Ru}^{\text{IV}}\text{P}]_2\text{O}$ .

Radiolytic oxidation of  $(\text{CO})\text{Os}^{\text{II}}\text{P}$  in  $\text{CH}_2\text{Cl}_2$  formed  $\text{Os}^{\text{III}}\text{P}$  products with various axial ligands, with no indication of a radical cation.<sup>65</sup> Oxidation in alkaline solutions led directly to  $\text{Os}^{\text{IV}}\text{P}$  products, the  $\text{Os}^{\text{III}}\text{P}$  being an unstable intermediate in this case.

Radiolytic oxidation of  $\text{Cr}^{\text{III}}$ -porphyrins in alkaline solutions also led to the formation of oxo- $\text{Cr}^{\text{IV}}$ -porphyrins.<sup>66</sup> Further irradiation led to production of oxo- $\text{Cr}^{\text{V}}$ -porphyrins. Pulse radiolysis studies indicated that  $\text{Cr}^{\text{III}}\text{P}$  under all conditions is oxidized first to the  $\pi$ -radical cation,  $\text{Cr}^{\text{III}}\text{P}\cdot^+$ . This radical cation is unstable in aqueous solutions and undergoes disproportionation, but in  $\text{CH}_2\text{Cl}_2$  it is stabilized by the HCl (produced by the radiolysis). The radical cation was further oxidized by irradiation and the product was suggested to be a dication,  $\text{Cr}^{\text{III}}\text{P}^{2+}$ , also stabilized by the HCl. Furthermore, it was found that addition of base to  $\text{Cr}^{\text{III}}\text{P}\cdot^+$  converts this species into  $\text{Cr}^{\text{IV}}\text{P}$ , and the process can be reversed by the addition of acid.

One-electron oxidation of  $\text{Ni}^{\text{II}}$ -porphyrins produced either  $\text{Ni}^{\text{II}}\text{P}\cdot^+$  or  $\text{Ni}^{\text{III}}\text{P}$ ,

depending on the porphyrin and the conditions.<sup>67</sup> The results were interpreted in terms of an inner sphere oxidation by peroxy radicals or dihalide radicals to form initially X-Ni<sup>III</sup>P (X = ROO<sup>-</sup>, Br<sup>-</sup>, etc.). In non-polar solvents this remains the final product. However, under conditions that enhance charge separation of the X<sup>-</sup> (water, electrolytes, negatively charged porphyrin ligand) the product rearranges to Ni<sup>II</sup>P<sup>·+</sup>. Both products were observed at short time scales by pulse radiolysis, were distinguished through their optical absorption spectra, and decayed to give stable products that were Ni<sup>II</sup> complexes of oxidized porphyrins.

Thus the site of oxidation, whether at the metal or at the porphyrin ligand, depends on the reduction potential of the metal center relative to that of the porphyrin ligand and also on the coordination sphere of the metal and on the medium. Because the species formed by one-electron oxidation are often unstable, pulse radiolysis has been a crucial technique for observing these species and for determining the kinetics of their subsequent transformation or decay. The structural assignments were based on optical absorptions spectra, which generally are quite different for the two possible products. Nevertheless, these assignments remain tentative in certain cases and must await independent confirmation.

## 6 ORGANOMETALLIC CHEMISTRY OF PORPHYRINS

In addition to the studies on reduction and oxidation of metalloporphyrins, radiolytic methods have been used to investigate reactions of radicals with metalloporphyrins that lead to formation of metal-carbon bonds. Formation of metal-carbon bonds has been implicated in various catalytic reactions and in biological systems. Therefore, numerous studies have been carried out on the formation and decomposition of such bonds involving porphyrin complexes of Fe,<sup>38,53,62,68-70</sup> Co,<sup>40</sup> Rh,<sup>71,72</sup> and other metals,<sup>73,74</sup> as well as complexes of related macrocycles, such as Co-phthalocyanine<sup>75,76</sup> and Co-B<sub>12</sub>.<sup>77,78</sup> Certain oxidation states of transition metal ions react with free radicals by attachment to form organometallic products, some of which are stable but others are short-lived. Pulse radiolysis has been used to investigate the formation and decay of such species.

Organometallic complexes can be formed via different routes. Let us consider a complex M<sup>III</sup>P as a general example, assume that M<sup>III</sup>P does not react with radicals via addition at the metal, and that it can be reduced to M<sup>II</sup>P which does react.





If  $\text{M}^{\text{II}}\text{P}$  is further reduced to  $\text{M}^{\text{I}}\text{P}$ , this may react directly with  $\text{RX}$  to form the same organometallic product.



Both of these paths can be studied by pulse radiolysis when selective reductants can be used to reduce the metal complex or the radical source. For example, one can use hydrated electrons to reduce  $\text{RX}$  (present in excess over  $\text{M}^{\text{III}}\text{P}$ ) and  $\cdot\text{CO}_2^-$  radicals to reduce  $\text{M}^{\text{III}}\text{P}$ . On the other hand, if  $\cdot\text{CO}_2^-$  is the sole reducing radical in the system, since this does not react rapidly with  $\text{RX}$ , one can prepare  $\text{M}^{\text{I}}\text{P}$  and follow its subsequent reaction with  $\text{RX}$ . Of course,  $\text{R}\cdot$  can be prepared also by reactions of various precursors other than  $\text{RX}$ .

The early radiolytic studies on iron porphyrins were aimed at understanding the biological function of cytochrome  $\text{P}_{450}$  in the detoxification of organic halides. By using iron deuteroporphyrin IX as a model compound in aqueous solutions, it was found that  $\text{Fe}^{\text{III}}\text{P}$  does not react with  $\cdot\text{CCl}_3$  radicals ( $k \leq 10^6 \text{ L mol}^{-1} \text{ s}^{-1}$ ) but  $\text{Fe}^{\text{II}}\text{P}$  reacts with several chlorinated methyl radicals with rate constants near  $2 \times 10^9 \text{ L mol}^{-1} \text{ s}^{-1}$ .<sup>38</sup> The spectra of the  $\text{R-Fe}^{\text{III}}\text{P}$  species were found to change over milliseconds in a first order process which was ascribed to reorganization of the coordination sphere. A subsequent study on the  $\text{CF}_3\dot{\text{C}}\text{HCl}$  radical (produced from the anesthetic agent halothane,  $\text{CF}_3\text{CHClBr}$ ) also demonstrated a rapid reaction with  $\text{Fe}^{\text{II}}\text{P}$  but detected no reaction with  $\text{Fe}^{\text{III}}\text{P}$ .<sup>69</sup>

In contrast with these halogenated alkyl radicals, the  $\cdot\text{CH}_3$  radical reacted rapidly both with  $\text{Fe}^{\text{II}}\text{P}$  ( $4 \times 10^9 \text{ L mol}^{-1} \text{ s}^{-1}$ ) and with  $\text{Fe}^{\text{III}}\text{P}$  ( $2 \times 10^9 \text{ L mol}^{-1} \text{ s}^{-1}$ ).<sup>68</sup> The product of the former reaction,  $\text{CH}_3\text{Fe}^{\text{III}}\text{P}$ , was stable under anaerobic conditions, but the product of the latter reaction,  $\text{CH}_3\text{Fe}^{\text{IV}}\text{P}$ , was unstable. The spectral changes observed upon decay of this product were interpreted as hydrolysis by  $\text{OH}^-$  to form  $\text{CH}_3\text{OH}$  and  $\text{Fe}^{\text{II}}\text{P}$ , followed by a methyl transfer reaction of the  $\text{Fe}^{\text{II}}\text{P}$  with  $\text{CH}_3\text{Fe}^{\text{IV}}\text{P}$  to form  $\text{CH}_3\text{Fe}^{\text{III}}\text{P}$  and  $\text{Fe}^{\text{III}}\text{P}$ .

A subsequent study<sup>62</sup> compared the reactions of  $\cdot\text{CF}_3$  and  $\cdot\text{CBr}_3$  radicals to the reactions discussed above. Whereas  $\cdot\text{CBr}_3$  behaved similarly with  $\cdot\text{CCl}_3$ , i.e. reacted with  $\text{Fe}^{\text{II}}\text{P}$  but not with  $\text{Fe}^{\text{III}}\text{P}$ , the behavior of the  $\cdot\text{CF}_3$  radical resembled that of  $\cdot\text{CH}_3$  in this respect. The rate constant for reaction of  $\cdot\text{CF}_3$  with  $\text{Fe}^{\text{II}}\text{P}$  was  $2 \times 10^9 \text{ L mol}^{-1} \text{ s}^{-1}$  and with  $\text{Fe}^{\text{III}}\text{P}$  was  $5 \times 10^8 \text{ L mol}^{-1} \text{ s}^{-1}$ .

However, unlike  $\text{CH}_3\text{Fe}^{\text{III}}\text{P}$ , which is stable,  $\text{CF}_3\text{Fe}^{\text{III}}\text{P}$  was found to be reduced by  $\text{Fe}^{\text{II}}\text{P}$  to form the carbene,  $\text{CF}_2\text{Fe}^{\text{II}}\text{P}$ , which then hydrolyzed to form the carbonyl complex,  $\text{COFe}^{\text{II}}\text{P}$ .<sup>62</sup>

The reactions of ferrous porphyrins with hydroxyalkyl radicals also take place by addition. The  $\alpha$ -hydroxyalkyl radicals derived from methanol, ethanol, and 2-propanol,  $\cdot\text{CR}_1\text{R}_2\text{OH}$ , are known to act as reducing radicals. However, they reacted rapidly with  $\text{Fe}^{\text{II}}\text{P}$  ( $2.5$  to  $6 \times 10^8 \text{ L mol}^{-1} \text{ s}^{-1}$ ) to form the adducts,  $\text{HO}\text{CR}_1\text{R}_2\text{-Fe}^{\text{III}}\text{P}$ , which decomposed in a first order process ( $\sim 3 \times 10^2 \text{ s}^{-1}$ ) to yield the oxidized product  $\text{Fe}^{\text{III}}\text{P}$ .<sup>53</sup> The mechanism was suggested to involve heterolytic bond cleavage, using a proton from water to form the original alcohols. By comparison,  $\beta$ -hydroxyalkyl radicals also reacted rapidly with  $\text{Fe}^{\text{II}}\text{P}$  to form similar adducts, which decayed slightly more slowly ( $80 \text{ s}^{-1}$  for  $\cdot\text{CH}_2\text{CH}_2\text{OH}$ ) via a  $\beta$ -hydroxy elimination to form  $\text{Fe}^{\text{III}}\text{P}$  and the olefin.<sup>70</sup>

The reactions of  $\alpha$ -hydroxyalkyl radicals with  $\text{Co}^{\text{II}}\text{P}$  also took place via addition to the metal but, unlike the case of  $\text{Fe}^{\text{II}}\text{P}$ , the adducts were found to undergo heterolysis leading to reduction of the porphyrin to  $\text{Co}^{\text{I}}\text{P}$ .<sup>40</sup> Another difference between the iron and cobalt porphyrins is in the stability of the methyl adduct;  $\text{CH}_3\text{Co}^{\text{III}}\text{P}$  was found to be stable even in the presence of  $\text{O}_2$ . Related studies were carried out on the reactions of alkyl radicals with  $\text{Co}^{\text{II}}$ -tetrasulphophthalocyanine (tspc)<sup>75,76</sup> and with  $\text{B}_{12}$ .<sup>77,78</sup> Several cobalt-carbon adducts have been observed and in many cases they were found to decompose to yield the oxidized  $\text{Co}^{\text{III}}$ -complex. However, in the reaction of  $\text{Co}^{\text{II}}$ tspc with the radical derived from *t*-BuOH, the oxidized product was formed in neutral solutions but the reduced product,  $\text{Co}^{\text{I}}$ tspc, was formed in alkaline solutions.

Radiolytic studies on rhodium porphyrins<sup>71</sup> in aqueous solutions led to production of  $\text{CH}_3\text{Rh}^{\text{III}}\text{P}$  by various reactions and this product was more resistant to oxidation than the methyl derivatives of the iron and cobalt porphyrins. Furthermore, the hydride  $\text{HRh}^{\text{III}}\text{P}$  was also observed and its spectrum was very similar to that of  $\text{CH}_3\text{Rh}^{\text{III}}\text{P}$ . This is in contrast with the cases of the iron and cobalt porphyrins, where the corresponding hydrides were not observed. It should be pointed out that in the same study on RhP a reduced product was observed in alkaline solutions which was assumed to be the dimeric species,  $(\text{Rh}^{\text{II}}\text{P})_2$ . Although such species are known to exist, it is now clear that the observed product in alkaline aqueous solutions was, in fact,  $\text{Rh}^{\text{I}}\text{P}$ . A recent radiolytic study<sup>72</sup> on Rh-porphyrins in alcohol solutions also identified the  $\text{HRh}^{\text{III}}\text{P}$  in acidic solutions and the  $\text{Rh}^{\text{I}}\text{P}$  in alkaline solutions, as well as alkylrhodium(III) porphyrins. It was further found that one-electron reduction of  $\text{CH}_3\text{Rh}^{\text{III}}\text{P}$  takes place at the porphyrin ligand to form  $\text{CH}_3\text{Rh}^{\text{III}}\text{P}\cdot^-$ , which in alkaline solutions eliminates  $\cdot\text{CH}_3$  to form  $\text{Rh}^{\text{I}}\text{P}$  but in acidic solutions disproportionates and protonates at the macrocycle to form methylrhodium chlorin,  $\text{CH}_3\text{Rh}^{\text{III}}\text{PH}_2$ .

Studies on chromium porphyrins<sup>73</sup> found that both  $\text{Cr}^{\text{II}}\text{P}$  and  $\text{Cr}^{\text{III}}\text{P}$  react with alkyl radicals to form relatively stable  $\text{RCr}^{\text{III}}\text{P}$  and  $\text{RCr}^{\text{IV}}\text{P}$ , more stable than analogous products from chromium cyclam or aqueous chromium ions. Both of these products are slowly oxidized by  $\text{O}_2$ , the former producing  $\text{Cr}^{\text{III}}\text{P}$  and the latter forming a product oxidized at the porphyrin ring.

In contrast with the stability of the alkyl-metalloporphyrins discussed above, pulse radiolytic studies on nickel<sup>74,79</sup> and manganese porphyrins<sup>74</sup> indicated that reactions of alkyl radicals with these porphyrins yield very unstable species. Both  $\text{Ni}^{\text{I}}\text{P}$  and  $\text{Ni}^{\text{II}}\text{P}$  react very rapidly with alkyl radicals to form Ni-C bonds. The only Ni-C bond that was found to be stable was that of  $\text{CF}_3\text{Ni}^{\text{II}}\text{P}$ . Other  $\text{RNi}^{\text{II}}\text{P}$  decayed with half lives of the order of seconds to yield  $\text{Ni}^{\text{II}}\text{P}$ .  $\text{RNi}^{\text{III}}\text{P}$  decayed even more rapidly, within milliseconds, also forming  $\text{Ni}^{\text{II}}\text{P}$ . It was suggested that the reaction between  $\text{R}\cdot$  and  $\text{Ni}^{\text{II}}\text{P}$  is an equilibrium reaction forming  $\text{RNi}^{\text{III}}\text{P}$  and that the decay of this species is through the dimerization of  $\text{R}\cdot + \text{R}\cdot$ . The reaction of alkyl radicals with  $\text{Mn}^{\text{II}}\text{P}$  is also rapid and probably occurs via addition to the metal, but the adduct immediately decomposes to yield  $\text{Mn}^{\text{III}}\text{P}$ . These wide variations in the stability of the metal-carbon bonds in the various alkyl-metalloporphyrins have been rationalized in terms of the radius of the metal ion relative to the size of the porphyrin cavity and in terms of the number of d electrons in the metal center.<sup>74</sup>

## 7 CONCLUDING REMARKS

The studies discussed above demonstrate the utility of radiation chemical methods for investigating fast reactions of porphyrins. The reactions studied include one-electron reduction and oxidation, formation and decomposition of metal-carbon bonds, as well as demetallation reactions. Pulse radiolysis has been a very useful tool for observing unstable intermediates and for elucidating mechanisms, and thus provided considerable insight into the chemistry of porphyrins and metalloporphyrins. Most studies have been carried out with homogeneous solutions, several studies involved micellar systems, and one study involved a porphyrin-cyclodextrin complex.<sup>80</sup> Related macrocyclic compounds also have been studied by pulse radiolysis, including the phthalocyanines and  $\text{B}_{12}$  briefly mentioned above,<sup>75-78</sup> as well as other compounds. For example, studies with the porphyrin isomers, porphycenes<sup>81,82</sup> and corphycenes,<sup>83</sup> examined the effect of cavity size on the stability of the various metal oxidation states and it was shown that by proper tuning of the size of the macrocycle cavity to the radius of the ion it is possible to stabilize metal ion oxidation states that may be unstable in regular porphyrins. A very recent study examined the redox behavior of metallotetraphyrins, pentadentate porphyrin analogues, and in particular the

Gd<sup>III</sup> complex, which is a radiation sensitizer.<sup>84</sup> Many studies have been done on simpler macrocyclic complexes such as cyclam, too numerous to mention in this brief review.

Pulse radiolysis has been used to study elementary reactions of importance in photosynthesis. Early experiments provided rate constants for electron transfer reactions of carotenoid radical cations and radical anions with chlorophyll pigments.<sup>26,85,86</sup> More recent experiments dealt with intramolecular electron transfer in covalently bound carotenoid-porphyrin and carotenoid-porphyrin-quinone compounds.<sup>87</sup> Intramolecular electron transfer reactions within metalloproteins have been studied by various authors; much of that work has been reviewed by Buxton,<sup>88</sup> and more recent work has been published.<sup>89,90</sup> Pulse radiolysis was also used to study charge migration in stacked porphyrins<sup>91</sup> and phthalocyanines.<sup>92</sup> Most of these studies were carried out by pulse radiolysis because this technique allowed proper initiation of the desired processes and permitted determination of very high reaction rate constants. The distinct character of radiolysis to initiate reactions with the medium, in contrast with the case of photolysis, and the recent developments in pulse radiolysis techniques promise continued application of this technique for the study of porphyrins and of more complex chemical systems.

## ACKNOWLEDGEMENTS

I thank Dr. Peter Hambright for many helpful discussions and the Division of Chemical Sciences, Office of Basic Energy Sciences, US Department of Energy, for financial support.

## REFERENCES

1. Y. Harel and D. Meyerstein, On the Mechanism of Reduction of Porphyrins. A Pulse Radiolytic Study, *J. Am. Chem. Soc.*, 96 (1974) 2720.
2. P. Neta, A. Scherz, and H. Levanon, Electron Transfer Reactions Involving Porphyrins and Chlorophyll a, *J. Am. Chem. Soc.*, 101 (1979) 3624.
3. P. Neta, One-Electron Transfer Reactions Involving Zinc and Cobalt Porphyrins in Aqueous Solutions, *J. Phys. Chem.*, 85 (1981) 3678.
4. R. Bonnet, R.J. Ridge, E.J. Land, R.S. Sinclair, D. Tait, and T.G. Truscott, Pulse Irradiation of Water-Soluble Porphyrins, *J. Chem. Soc., Faraday Trans. 1*, 78 (1982) 127.
5. A. Harriman, M.C. Richoux, and P. Neta, Redox Chemistry of Metalloporphyrins in Aqueous Solutions, *J. Phys. Chem.*, 87 (1983) 4957.

6. S. Baral, P. Neta, and P. Hambright, Spectrophotometric and Kinetic Studies of the Radiolytic Reduction of Several Pyridylporphyrins and Their Metal Complexes, *Radiat. Phys. Chem.*, 24 (1984) 245.
7. S. Baral, P. Hambright, and P. Neta, One- and Two-Electron Reduction of Aluminum and Tin Pyridylporphyrins. A Kinetic Spectrophotometric Study, *J. Phys. Chem.*, 88 (1984) 1595.
8. M.C. Richoux, P. Neta, A. Harriman, S. Baral, and P. Hambright, One- and Two-Electron Reduction of Metalloporphyrins. Radiation Chemical, Photochemical, and Electrochemical Studies. Kinetics of the Decay of  $\pi$ -Radical Anions, *J. Phys. Chem.*, 90 (1986) 2462.
9. P. Neta, J. Grodkowski, and A. B. Ross, Rate Constants for Reactions of Aliphatic Carbon-Centered Radicals in Aqueous Solutions, *J. Phys. Chem. Ref. Data*, 25 (1996) 709.
10. S. Mosseri, G.S. Nahor, P. Neta, and P. Hambright, Radiolytic Reduction of Tetrapyridylporphyrins. Formation of a Stable Radical Anion from Tetrakis(N-methyl-2-pyridyl)porphyrin, *J. Chem. Soc. Faraday Trans.*, 87 (1991) 2567.
11. T.P.G. Sutter, R. Rahimi, P. Hambright, J.C. Bommer, M. Kumar, and P. Neta, Steric and Inductive Effects on the Basicity of Porphyrins and on the Site of Protonation of Porphyrin Dianions: Radiolytic Reduction of Porphyrins and Metalloporphyrins to Chlorins or Phlorins, *J. Chem. Soc. Faraday Trans.*, 89 (1993) 495.
12. D.M. Guldi, P. Neta, and K.-D. Asmus, Electron Transfer Reactions Between  $C_{60}$  and Radical Ions of Metalloporphyrins and Arenes, *J. Phys. Chem.*, 98 (1994) 4617.
13. Z. Abou-Gamra, A. Harriman, and P. Neta, Redox Chemistry of Gold(III) Porphyrins in Water, *J. Chem. Soc., Faraday Trans. 2*, 82 (1986) 2337. See also references therein.
14. H. Seki, S. Arai, T. Shida, and M. Imamura, Transient Absorption Spectra of the Chlorophyll a Anion and Cation, *J. Am. Chem. Soc.*, 95 (1973) 3404.
15. M. Hoshino, S. Konishi, S. Watanabe, and Y. Hama, Absorption Spectroscopic and ESR Studies on One-Electron Reduction Products of Copper(II) and Oxovanadium(IV) Tetraphenyl-porphyrins Produced by  $\gamma$ -Radiolysis in 2-Methyltetrahydrofuran Solutions at 77 K, *Chem. Phys. Lett.*, 110 (1984) 205.
16. R. Bonnett, A.A. Charalambides, E.J. Land, R.S. Sinclair, D. Tait, and T.G. Truscott, Triplet States of Porphyrin Esters, *J. Chem. Soc., Faraday Trans. 1*, 76 (1980) 852.
17. P. Neta and A. Harriman, Zinc Porphyrin  $\pi$ -Radical Cations in Aqueous Solutions. Formation, Spectra and Decay Kinetics, *J. Chem. Soc. Faraday Trans. 2*, 81 (1985) 123.
18. M.C. Richoux, P. Neta, P.A. Christensen, and A. Harriman, Formation and Decay of Zinc Tetrakis(N-methyl-3-pyridyl)-porphine  $\pi$ -Radical Cation in Water, *J. Chem. Soc. Faraday Trans. 2*, 82 (1986) 235.

19. P. Neta, M.C. Richoux, A. Harriman, and L.R. Milgrom, Resonance Stabilisation of Zinc Porphyrin  $\pi$ -Radical Cations, *J. Chem. Soc. Faraday Trans. 2*, 82 (1986) 209.
20. A. Harriman, P. Neta, and M.C. Richoux, Reactions of Magnesium Porphyrin Radical Cations in Water. Disproportionation, Oxygen Production, and Comparison with Other Metalloporphyrins, *J. Phys. Chem.*, 90 (1986) 3444.
21. P.A. Christensen, A. Harriman, G. Porter, and P. Neta, A Pulse Radiolytic and Photochemical Study of the Oxidation of Water by Zinc Porphyrin  $\pi$ -Radical Cations, *J. Chem. Soc. Faraday Trans. 2*, 80 (1984) 1451.
22. A. Harriman, G.S. Nahor, S. Mosseri, and P. Neta, Iridium Oxide Hydrosols as Catalysts for the Decay of Zinc Porphyrin Radical Cations in Water, *J. Chem. Soc., Faraday Trans. 1*, 84 (1988) 2821.
23. G.S. Nahor, S. Mosseri, P. Neta, and A. Harriman, Polyelectrolyte-Stabilized Metal Oxide Hydrosols as Catalysts for the Photooxidation of Water by Zinc Porphyrins, *J. Phys. Chem.*, 92 (1988) 4499.
24. G.S. Nahor, P. Neta, P. Hambright, A.N. Thompson, Jr., and A. Harriman, Metalloporphyrin-Sensitized Photooxidation of Water to Oxygen on the Surface of Colloidal Iridium Oxides. Photochemical and Pulse Radiolytic Studies, *J. Phys. Chem.*, 93 (1989) 6181.
25. J.-P. Chauvet, R. Viogy, R. Santus, and E.J. Land, One-Electron Oxidation of Photosynthetic Pigments in Micelles. Bacteriochlorophyll a, Chlorophyll a, Chlorophyll b, and Pheophytin a, *J. Phys. Chem.*, 85 (1981) 3449.
26. J.-P. Chauvet, R. Viogy, E.J. Land, R. Santus, and T.G. Truscott, One-Electron Oxidation of Carotene and Electron Transfer Involving Carotene Cations and Chlorophyll Pigments in Micelles, *J. Phys. Chem.*, 87 (1983) 592.
27. H. Levanon and P. Neta, Electron Transfer Reactions of Chlorophyll a and Porphyrin Triplets with Radicals in Aqueous Micellar Solutions, *J. Phys. Chem.*, 86 (1982) 4532.
28. H. Levanon and P. Neta, One-Electron Oxidation and Demetallation of Metalloporphyrins and Chlorophyll a in Dichloroethane Solutions as Studied by Pulse Radiolysis, *Chem. Phys. Lett.*, 70 (1980) 100.
29. P. Neta, V. Grebel, and H. Levanon, One-Electron Oxidation of Chlorophyll a and (Tetraphenylporphyrinato)cobalt(II) by Various Metalloporphyrin Cation Radicals. Kinetic Spectrophotometric Studies, *J. Phys. Chem.*, 85 (1981) 2117.
30. J. Grodkowski and P. Neta, One-Electron Oxidation in Irradiated Carbon Tetrachloride Solutions of ZnTPP, TMPD, and Phenols, *J. Phys. Chem.*, 88 (1984) 1205.
31. J. Grodkowski, J.H. Chambers, Jr., and P. Neta, Kinetics of Electron Transfer from Cobalt(II) Porphyrins to Various Metalloporphyrin  $\pi$ -Radical Cations in Irradiated Carbon Tetrachloride Solutions, *J. Phys. Chem.*, 88 (1984) 5332.



32. Z.B. Alfassi, A. Harriman, S. Mosseri, and P. Neta, Rates and Mechanisms of Oxidation of ZnTPP by  $\text{CCl}_3\text{O}_2$  Radicals in Various Solvents, *Int. J. Chem. Kinet.*, 18 (1986) 1315.
33. M. Hoshino, K. Ikehara, M. Imamura, H. Seki, and Y. Hama, Optical Absorption and Electron Spin Resonance Spectra of Cation Radicals of Dimeric Chlorophyll a in Low-Temperature Matrices, *Photochem. Photobiol.*, 34 (1981) 75.
34. M. Hoshino, S. Konishi, K. Ito, and M. Imamura, Optical and ESR Spectra of One-Electron Oxidized Lead(II) Tetraphenylporphyrin Produced by  $\gamma$ -Radiolysis and Photolysis in 1,1,2,2,-Tetrachloroethane Solutions at 77 K, *Chem. Phys. Lett.*, 88 (1982) 138.
35. S. Konishi, M. Hoshino, and M. Imamura, Triplet ESR Spectrum of the Copper Porphyrin Cation Radical, *J. Am. Chem. Soc.*, 104 (1982) 2057.
36. M. Hoshino, S. Konishi, M. Imamura, S. Watanabe, and Y. Hama, Optical Absorption and Triplet ESR Spectra of Oxovanadium(IV) Tetraphenylporphyrin Cation Radical, *Chem. Phys. Lett.*, 102 (1983) 259.
37. J. Butler, G.G. Jayson, and A.J. Swallow, One-Electron Reduction of a Ferrihaem, *J. Chem. Soc., Faraday Trans. 1*, 72 (1976) 1391.
38. D. Brault, C. Bizet, P. Morliere, M. Rougee, E.J. Land, R. Santus, and A.J. Swallow, One-Electron Reduction of Ferrideuteroporphyrin IX and Reaction of the Oxidized and Reduced Forms with Chlorinated Methyl Radicals, *J. Am. Chem. Soc.*, 102 (1980) 1015.
39. P.C. Wilkins and R.G. Wilkins, Rapid Pulse Radiolytic Reduction of Iron(III) Complexes of Tetrakis(4-sulfonatophenyl)porphine Anion and Tetrakis(N-methylpyrid-4-yl)porphine Cation, *Inorg. Chem.*, 25 (1986) 1908.
40. S. Baral and P. Neta, Reduction and Alkylation of Cobalt(II) Tetrakis(4-sulfonatomethyl)porphyrin in Aqueous Solutions. A Kinetic Spectrophotometric Study, *J. Phys. Chem.*, 87 (1983) 1502.
41. K.M. Morehouse and P. Neta, Redox Reactions of Manganese Porphyrins in Aqueous Solutions. Steady-State and Pulse Radiolysis Spectrophotometric Studies, *J. Phys. Chem.*, 88 (1984) 1575.
42. J. Grodkowski, P. Neta, and P. Hambright, Radiolytic Reduction of Rhodium Porphyrins. Chain Reaction in Alakline 2-Propanol, *J. Phys. Chem.*, 99 (1995) 6019.
43. S. Konishi, M. Hoshino, K. Yamamoto, and M. Imamura, ESR and Optical Detection of the Constrained Complexes of Co(II) Tetraphenylporphyrin, *Chem. Phys. Lett.*, 72 (1980) 459.
44. S. Konishi, M. Hoshino, and M. Imamura, Constrained Complexes of Manganese(II) Tetraphenylporphyrin in Rigid Solution, *J. Phys. Chem.*, 86 (1982) 1412.
45. M. Hoshino, S. Konishi, and M. Imamura, Solvent Effects on Optical and ESR Spectra of One-Electron Reduced Species of Cobalt(III) and Manganese(III) Tetraphenylporphyrins Produced by  $\gamma$ -Radiolysis at 77 K, *Bull. Chem. Soc. Jpn.*, 57

- (1984) 1713.
46. A. Kumar and P. Neta, Reduction and Demetallation of Silver Porphyrins in Aqueous Solutions, *J. Phys. Chem.*, 85 (1981) 2830.
  47. K.M. Morehouse and P. Neta, Kinetics of Demetallation of Manganese(II) Porphyrins in Aqueous Solutions, *J. Phys. Chem.*, 88 (1984) 3118.
  48. M. Kumar, P. Neta, T.P.G. Sutter, and P. Hambright, One-Electron Reduction and Demetallation of Copper Porphyrins, *J. Phys. Chem.*, 96 (1992) 9571.
  49. G.S. Nahor, P. Neta, P. Hambright, L.R. Robinson, and A. Harriman, Site of One-Electron Reduction of Ni(II) Porphyrins. Formation of Ni(I) Porphyrins or Ni(II) Porphyrin  $\pi$ -Radical Anion, *J. Phys. Chem.*, 94 (1990) 6659.
  50. D.M. Guldi, P. Hambright, D. Lexa, P. Neta, and J.-M. Saveant, One-Electron Reduction of Chromium(III) Porphyrins. Formation of Chromium(II) Porphyrins or Chromium(III) Porphyrin  $\pi$ -Radical Anions, *J. Phys. Chem.*, 86 (1992) 4459.
  51. S. Mosseri, P. Neta, A. Harriman, and P. Hambright, Reduction Reactions of Water Soluble Cyano-Cobalt(III)-Porphyrins: Metal Versus Ligand Centered Processes, *J. Inorg. Biochem.*, 39 (1990) 93.
  52. D. Brault, R. Santus, E.J. Land, and A.J. Swallow, One-Electron Reduction of Iron(II) Porphyrin and Characterization of Iron(I) Porphyrin in Aqueous Medium. Steady-State and Pulse Radiolysis Studies, *J. Phys. Chem.*, 88 (1984) 5836.
  53. Y. Soreq, H. Cohen, and D. Meyerstein, Reactions of Iron(II) Protoporphyrin with Strongly Reducing Free Radicals in Aqueous Solutions. A Pulse Radiolytic Study, *J. Chem.*, *Faraday Trans. 1*, 81 (1985) 233.
  54. J. Grodkowski, D. Behar, P. Neta, and P. Hambright, Iron-Porphyrin Catalyzed Reduction of CO<sub>2</sub>. Photochemical and Radiation Chemical Studies, *J. Phys. Chem. A*, 101 (1997) 248.
  55. D. Behar, T. Dhanasekaran, P. Neta, C.M. Hosten, D. Ejeh, P. Hambright, and E. Fujita, Cobalt Porphyrin Catalyzed Reduction of CO<sub>2</sub>. Radiation Chemical, Photochemical, and Electrochemical Studies, *J. Phys. Chem. A*, 102 (1998) 2870.
  56. Y. Ilan, J. Rabani, I. Fridovich, and R.F. Pasternack, Superoxide Dismuting Activity of An Iron Porphyrin, *Inorg. Nucl. Chem. Lett.*, 17 (1981) 93.
  57. D. Solomon, P. Peretz, and M. Faraggi, Chemical Properties of Water-Soluble Porphyrins. 2. The Reaction of Iron(III) Tetrakis(4-N-methylpyridyl)porphyrin with the Superoxide Radical Dioxygen Couple, *J. Phys. Chem.*, 86 (1982) 1842.
  58. P. Peretz, D. Solomon, D. Weintraub, and M. Faraggi, Chemical Properties of Water-Soluble Porphyrins. 3. The Reaction of Superoxide Radicals with Some Metalloporphyrins, *Int. J. Radiat. Biol.*, 42 (1982) 449.
  59. M. Faraggi, P. Peretz, and D. Weintraub, Chemical Properties of Water-Soluble Porphyrins. 4. The Reaction of a Picket-Fence-Like Iron(III) complex with the Superoxide Oxygen Couple, *Int. J. Radiat. Biol.*, 49 (1986) 951.

60. A. Harriman, P.A. Christensen, G. Porter, K. Morehouse, P. Neta, and M.-C. Richoux, Decay of High-Valent Manganese Porphyrins in Aqueous Solution and Catalyzed Formation of Oxygen, *J. Chem. Soc., Faraday Trans. 1*, 82 (1986) 3215.
61. D. Brault and P. Neta, Reactions of Iron(III) Porphyrins with Peroxyl Radicals Derived from Halothane and Halomethanes, *J. Phys. Chem.*, 88 (1984) 2857.
62. D. Brault and P. Neta, Reactions of Iron Porphyrins with  $\cdot\text{CF}_3$ ,  $\text{CF}_3\text{O}_2\cdot$ , and  $\text{CBr}_3\text{O}_2\cdot$  Radicals, *J. Phys. Chem.*, 91 (1987) 4156.
63. D. Brault and P. Neta, Oxidation of  $\text{Fe}^{\text{III}}$  Porphyrins by Peroxyl Radicals Derived from 2-Propanol and Methanol. Evidence for Acid-Dependent and Acid-Independent Pathways, *Chem. Phys. Lett.*, 121 (1985) 28.
64. S. Mosseri, P. Neta, and P. Hambright, Radiolytic Studies of the Redox Reactions of Ruthenium Porphyrins, *J. Phys. Chem.*, 93 (1989) 2358.
65. S. Mosseri, P. Neta, P. Hambright, D.Y. Sabry, and A. Harriman, Redox Reactions of Osmium Porphyrins, *J. Chem. Soc. Dalton Trans.* (1988) 2705.
66. D.M. Guldi, P. Neta, and P. Hambright, Oxidation of Chromium(III) Porphyrins to Their  $\pi$ -Radical Cations or to Oxochromium(IV) Porphyrins, *J. Chem. Soc. Faraday Trans.*, 88 (1992) 2013.
67. G.S. Nahor, P. Neta, P. Hambright, and L.R. Robinson, One-Electron Oxidation of Nickel Porphyrins. Effect of Structure and Medium on Formation of Nickel(III) Porphyrin or Nickel(II) Porphyrin  $\pi$ -Radical Cation, *J. Phys. Chem.*, 95 (1991) 4415.
68. D. Brault and P. Neta, Reactions of Iron Porphyrins with Methyl Radicals, *J. Am. Chem. Soc.*, 103 (1981) 2705.
69. D. Brault and P. Neta, One-Electron Reduction of Ferriporphyrins and Reactions of Ferric and Ferrous Porphyrins with a Halothane-Derived Radicals, *J. Phys. Chem.*, 86 (1982) 3405.
70. Y. Sorek, H. Cohen, and D. Meyerstein, Kinetics of the  $\beta$ -Hydroxy Elimination Reactions from the Protoporphyrin Iron(III)- $\text{CHRCH}_2\text{OH}$  Complexes in Aqueous Solutions. A Pulse Radiolysis Study, *J. Chem. Soc., Faraday Trans. 1*, 82 (1986) 3431.
71. S. Baral, P. Hambright, A. Harriman, and P. Neta, Radiolytic Studies of the Redox Reactions and Alkylation of Rhodium Tetrakis(4-sulfonatophenyl)porphyrin in Aqueous Solutions, *J. Phys. Chem.*, 89 (1985) 2037.
72. J. Grodkowski, P. Neta, Y. Abdallah, and P. Hambright, Reduction and Alkylation of Rhodium Porphyrins in Alcohol Solutions. Radiation Chemical and Photochemical Studies, *J. Phys. Chem.*, 100 (1996) 7066.
73. D.M. Guldi, P. Neta, and P. Hambright, Reaction of Alkyl Radicals with Chromium Porphyrins, *J. Chem. Soc. Faraday Trans.*, 88 (1992) 2337.
74. D.M. Guldi, M. Kumar, P. Neta, and P. Hambright, Reactions of Alkyl and Fluoroalkyl Radicals with Nickel, Iron, and Manganese Porphyrins, *J. Phys. Chem.*, 96 (1992) 9576.

75. Y. Soreq, H. Cohen, W.A. Mulac, K.H. Schmidt, and D. Meyerstein, Reaction of  $\cdot\text{CH}_2\text{C}(\text{CH}_3)_2\text{OH}$  Radicals with Cobalt(II) Tetrasulfophthalocyanine in Aqueous Solutions. A Pulse Radiolytic Study, *Inorg. Chem.*, 22 (1983) 3040.
76. Y. Soreq, H. Cohen, and D. Meyerstein, Mechanistic Study of  $\beta$ -Hydroxy Elimination from [Tetrasulfophthalocyanine  $\text{Co}^{\text{III}}\text{-CR}_7\text{R}_2\text{CR}_3\text{R}_4\text{OH}$ ] in Aqueous Solutions. A Pulse Radiolysis Study, *J. Chem. Soc., Faraday Trans. 1*, 85 (1989) 1169.
77. R. Blackburn, M. Kyaw, G.O. Phillips, and A.J. Swallow, Free Radical Reactions in the Coenzyme B12 System, *J. Chem. Soc., Faraday Trans. 1*, 71 (1975) 2277.
78. W.A. Mulac and D. Meyerstein, Reactions of  $\text{B}_{12r}$  with Aliphatic Free Radicals: A Pulse Radiolysis Study, *J. Am. Chem. Soc.*, 104 (1982) 4124.
79. D.M. Guldi, P. Neta, P. Hambright, and R. Rahimi, Ring Reduction of [N-Methyltetrakis(4-sulfonatophenyl)-porphinato]cobalt(III), -nickel(II), and -copper(II) and Subsequent Methyl Group Migration. Reversible Reaction between Methyl Radicals and  $\text{Ni}^{\text{II}}\text{TSP}$ , *Inorg. Chem.*, 31 (1992) 4849.
80. S. Mosseri, J.C. Mialocq, B. Perly, and P. Hambright, Porphyrins-Cyclodextrin. 1. Photooxidation of Zinc Tetrakis(4-sulfonatophenyl)porphyrin in Cyclodextrin Cavities: The Characterization of ZnTSP Dication. Photolysis, Radiolysis, and NMR Studies, *J. Phys. Chem.*, 95 (1991) 2196.
81. D.M. Guldi, P. Neta, and E. Vogel, Radiolytic Reduction of Tetrapropylporphycene and Its Iron, Cobalt, Nickel, Copper, and Tin Complexes, *J. Phys. Chem.*, 100 (1996) 4097.
82. D.M. Guldi, J. Field, J. Grodkowski, P. Neta, and E. Vogel, One-Electron Oxidation of Metalloporphycenes as Studied by Radiolytic Methods, *J. Phys. Chem.*, 100 (1996) 13609.
83. D.M. Guldi, P. Neta, A. Heger, E. Vogel, and J.L. Sessler, Octaethylcorrphycene and Its metal Complexes. Radiolytic Reduction Studies. *J. Phys. Chem. A*, 102 (1998) 960.
84. J.L. Sessler, N.A. Tvermoes, D.M. Guldi, T.D. Mody, and W.E. Allen, One-Electron Reduction and Oxidation Studies of the Radiation Sensitizer Gadolinium(III) Texaphyrin (PCI-0120) and Other Water Soluble Metallotexaphyrins, *J. Phys. Chem. A*, 103 (1999) 787.
85. J. Lafferty, T.G. Truscott, and E.J. Land, Electron Transfer Reactions Involving Chlorophylls a and b and Carotenoids, *J. Chem. Soc., Faraday Trans. 1*, 74 (1978) 2760.
86. J. McVie, R.S. Sinclair, D. Tait, T.G. Truscott, and E.J. Land, Electron Transfer Reactions Involving Porphyrins and Carotenoids, *J. Chem. Soc., Faraday Trans. 1*, 75 (1979) 2869.
87. E.J. Land, D. Lexa, R.V. Bensasson, D. Gust, T.A. Moore, A.L. Moore, P.A. Liddell, and G.A. Nemeth, Pulse Radiolytic and Electrochemical Investigations of Intramolecular Electron Transfer in Carotenoporphyrins and Carotenoporphyrin-

- Quinone Triads, *J. Phys. Chem.*, 91 (1987) 4831.
88. G.V. Buxton, Pulse Radiolysis Studies on Metalloproteins and Metalloporphyrins, in: *Advances in Inorganic and Bioinorganic Mechanisms*, A.G. Sykes, ed., Academic Press, Orlando, FL, 1984, Vol. 3, p. 131.
  89. M. Faraggi and M.H. Klapper, Intramolecular Long-Range Electron Transfer in the  $\alpha$ -Hemoglobin Subunit, *J. Am. Chem. Soc.*, 110 (1988) 5753.
  90. M. Faraggi and M.H. Klapper, Intramolecular Long-Range Electron Transfer in the Hemerythrin Monomer: A Pulse Radiolysis Study, *Biochem. Biophys. Res. Commun.*, 166 (1990) 867.
  91. P.G. Schouten, J.M. Warman, M.P. de Haas, M.A. Fox, and H.-L. Pan, Charge Migration in Supramolecular Stacks of Peripherally Substituted Porphyrins, *Nature*, 353 (1991) 736.
  92. J.M. Warman, M.P. de Haas, J.F. van der Pol, and W. Drenth, Charge Separation and Recombination in Pulse Irradiated Columnar Aggregates of Peripherally Octa-n-alkoxy-Substituted Phthalocyanines, *Chem. Phys. Lett.*, 164 (1989) 581.

## Carbohydrates

**C. von Sonntag and H.-P. Schuchmann**

Max-Planck-Institut für Strahlenchemie  
P.O. Box 101365, Stiftstrasse 34-36, D-45470 Mülheim an der Ruhr, Germany

### 1. INTRODUCTION

The initial impetus for the study of the chemical behaviour of carbohydrates under the influence of ionizing radiation consisted in the hope that the power of the new sources of radioactivity might provide a practical way of transforming abundant natural carbohydrates, especially cellulose which is relatively difficult to deal with chemically or enzymatically, into other useful chemicals [1-3], and in the need to examine the chemical effect of radiation sterilization of carbohydrate-containing foods with respect to its wholesomeness after such treatment [4, 5]; it has been observed that carbohydrate-derived compounds carrying additional keto functions [6] can be mutagenic [7], similar to various aldehydes [8]. A second major incentive was originally derived from radiation-protection considerations. In order to evaluate possible chemical protective strategies it was necessary to obtain mechanistic information on the production of radiation-induced DNA damage such as the formation of strand breaks and the release of nucleobases [9]. The latter processes originate from radicals generated at the deoxyribose moiety of DNA whose backbone is a chain consisting of 2-deoxyribose units bridged by phosphate groups at the positions 3' and 5'. The use of various carbohydrate model compounds, among them functionalized ones, in the detailed mechanistic studies of the radiation-induced damage of its sugar moiety proved to be crucial since DNA offers a variety of reactive sites for free-radical attack, notably the nucleobases whose reactivity in this situation tends to overshadow the reactivity shown by the deoxyribose moiety as such [10]. Thus, for a better understanding of the mechanistic principles that lead to DNA strand breakage and base release, a large number of low-molecular-weight carbohydrate systems have been investigated [11].

Ionizing radiation is in fact a convenient means to induce free-radical chemistry such as can be set in motion, for instance, by oxidative processes.

Thus, the free-radical-induced degradation of hyaluronic acid, another carbohydrate biopolymer, is a major aspect of rheumatoid arthritis, which has provoked radiation-chemical studies to elucidate the kinetics of its depolymerization (the lubricating property of hyaluronic acid in a joint is rapidly lost when its molecular weight is decreased).

Most of such radiation-chemical studies of carbohydrates have been carried out in aqueous solution. Besides, there are crystalline-state studies which in some cases show interesting examples of solid-state chain reactions (*cf.* [2]). Some of the paths traced by the radical function as the reaction propagates through the crystal can be inferred on the basis of X-ray crystallography (*cf.* [12, 13]).

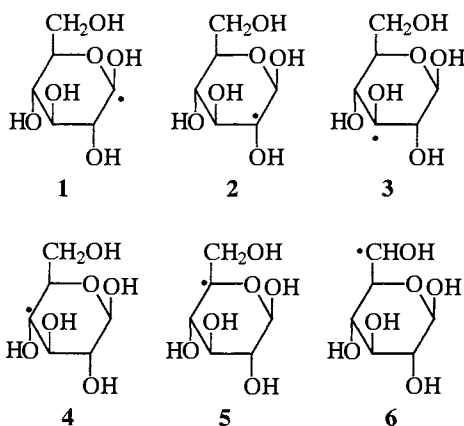
## 2. AQUEOUS SOLUTIONS

Carbohydrates (many of them being at the same time polyhydric alcohols) and those of their derivatives that are of interest in the above context are usually water soluble (notable exceptions, the biopolymers cellulose and chitin). Good water solubility has allowed to study the radiation chemistry of their aqueous solutions without the difficulties that are encountered in the case of poorly soluble substrates. Difficulties are mainly of a product-analytical nature. It is relatively easy to determine the low-molecular weight carbohydrate products that are formed via the unimolecular transformation of the starting radical, while it is very difficult to analyse completely the complex mixtures of the dehydro dimers which arise from the substrates under anoxic conditions as several different primary radicals intercombine and, in addition, different stereochemical options exist for each combination.

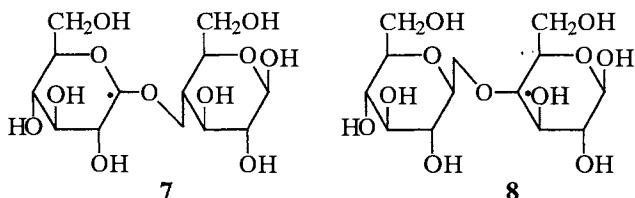
The formation of the primary radicals in these systems is governed by H-abstraction reactions, effected by  $\text{OH}^\cdot$  and  $\text{H}^\cdot$  since the substrates usually exist mainly in the hemiacetal form (or acetal form in the case of disaccharides and polysaccharides). The hydrated electron  $e_{\text{aq}}^-$  is essentially non-reactive in the absence of the free carbonyl function (there are exceptions with certain glycosides when the glycosidic group upon elimination can form a stabilized radical) [14, 15]. In radiation-chemical experimentation  $e_{\text{aq}}^-$  is usually transformed into the  $\text{OH}^\cdot$  radical with  $\text{N}_2\text{O}$ . Due to the much lower bond dissociation energy of the C-H bond compared to the O-H bond, practicality only carbon-centred radicals are formed. For the  $\text{OH}^\cdot$  radical, the reaction rate constants are typically near  $2 \times 10^9 \text{ dm}^3 \text{ mol}^{-1} \text{ s}^{-1}$ , and about one to two orders of magnitude slower for the H atom [16]. Generally, there is no pronounced regioselectivity [17], *i.e.* in D-glucose, radicals 1-6 are formed in comparable

yields [18]. Higher selectivity is observed with other H-atom abstractors, *e.g.* the sulfate radical anion [19].

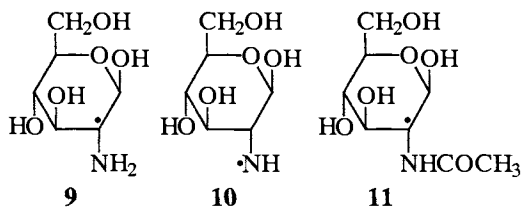
Considering the type of chemistry they undergo, the primary radicals from regular carbohydrates may be divided into several groups (that may partially overlap), *e.g.*, 1,2-diol-type radicals such as **1-4**, 2-alkoxy-hydroxyalkyl radicals such as **4** and **6**, and ether-type radicals such as **1** and **5**.



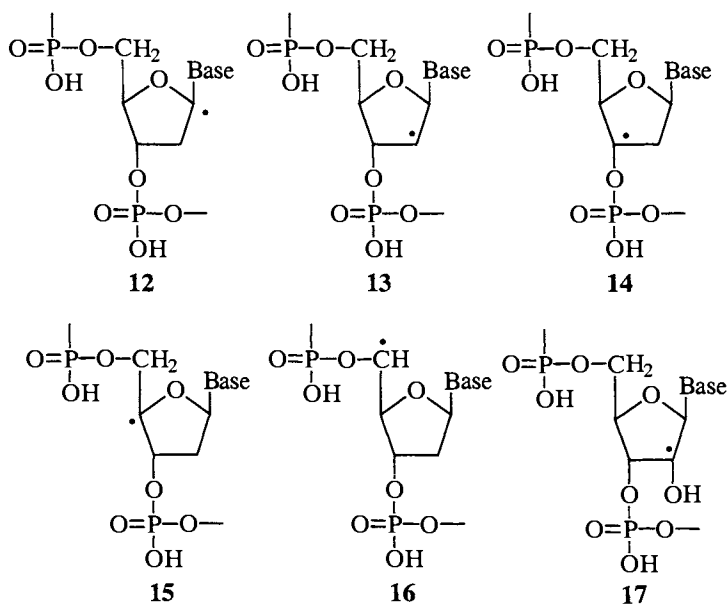
In disaccharides and polymeric carbohydrates, the ether-type radicals such as **7** and **8** have the radical site proximate to the glycosidic linkage and therefore play a major role in its scission (see below). In glucosamine [20] and *N*-acetylglucosamine [21] as well as in their related polymers chitin, chitosan and hyaluronic acid, one must further consider radicals of the type **9-11**. Thus, one may expect that in addition to the behaviour shown by the prototypical carbohydrate radicals, reactions such as are observed with amino acids (*cf.* [22]) and peptides (*cf.* [23-25]), may also play a role.







In DNA, five different radicals may be formed at the sugar moiety. The radical site in **12** is proximate to the *N*-glycosidic linkage and can give rise to base release [26]. Radical **13** appears to behave in the way of an alkyl-type radical. Radicals **14** and **16** have phosphate groups in  $\alpha$ -position, while radical **15** has these groups in a  $\beta$ -position linked to an oxygen atom which makes heterolytic cleavage possible (see below).  $\alpha$ -Phosphato radicals such as **14** and **16** do not show phosphoester release [27]. In RNA and *ribo*-polynucleotides which lack the deoxy function one must take radical **17** into consideration which regarding the ease of phosphoester release resembles **15**.

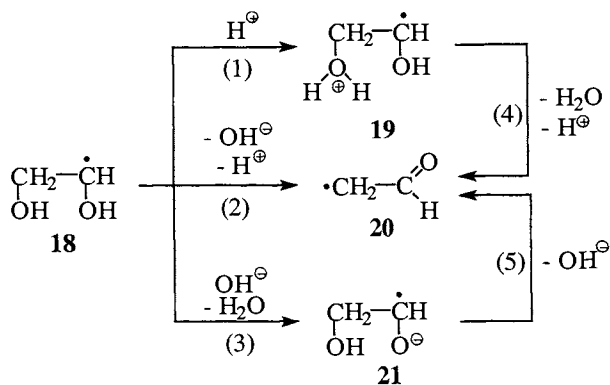


It has been mentioned above that in these systems the radiation chemistry is mainly governed by the free-radical chemistry of the nucleobases, and much of the knowledge about their chemistry has to come from model studies.

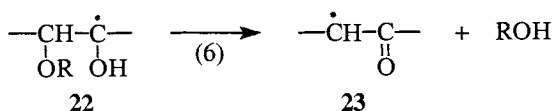
As discussed below, there are two types of unimolecular reaction pathway open to all of these carbohydrate radicals, *i.e.* “ionic” elimination, and cleavage of a carbon-oxygen bond  $\beta$  to the free-radical site. Depending on whether the substituent is a hydroxyl group, an ester, ether, or other hetero function, preference will lie toward one or the other reaction channel.

### 2.1. Elimination of water or alcohol

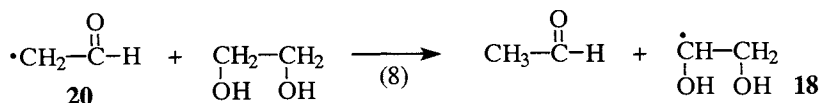
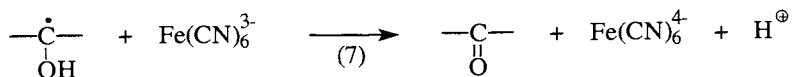
Many carbohydrates have the structural element  $-\text{CHOH}-\text{CHOH}-$ . Radicals such as **1** – **4**, just like **18**, generated by H-abstraction from such sites can eliminate water [28]. This reaction occurs at a relatively slow rate spontaneously (“water-catalyzed”), but faster upon acid or base catalysis [reactions (1)-(3)].



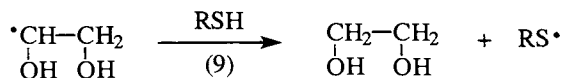
Carbinol ROH can be similarly eliminated [reaction (6)] (this reaction has been studied in a variety of model compounds [29, 30]; *cf.* further [31, 32] and references therein); this reaction as well converts the exocyclic glucose-derived radical **6** into a  $\beta$ -ketoalkyl radical. The elimination of ammonia from  $\beta$ -amino- $\alpha$ -hydroxyalkyl radicals has also been reported [33].



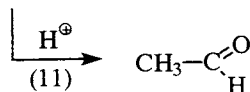
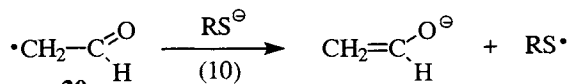
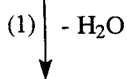
While  $\alpha$ -hydroxyalkyl radicals are of a reducing nature [*cf.* reaction (7)] [17, 34], the resulting  $\beta$ -ketoalkyl radicals have oxidizing properties. The latter can effect (slow) H-abstraction from the substrate [reaction (8)] which in the case of ethylene glycol leads to a short chain reaction [35].



Interestingly, the reaction of the (reducing)  $\alpha$ -hydroxyalkyl radicals with thiols [reaction (9)] is relatively fast while the (oxidizing) formylmethyl radical does not react with thiols at an appreciable rate [36]. In contrast, in basic solution where the thiolate form predominates, a rapid reduction, by electron transfer, of the formylmethyl radical is observed [reaction (10)] [36].



**18**



In carbohydrates (and polyhydric alcohols), the importance of the water-elimination reaction is reflected in the mix of products. Deoxy compounds dominate among the products (*cf.* Table 1). A full material balance has been obtained in the case of ethylene glycol, the prototype of this group [35]. However, already in the case of the monomeric carbohydrates

Table 1 -  $\gamma$ -Radiolysis of D-glucose in N<sub>2</sub>O [37] and N<sub>2</sub>O/O<sub>2</sub>-saturated [18] solutions. Products and their G values.

Product	N <sub>2</sub> O	N <sub>2</sub> O/O <sub>2</sub>
D-Gluconic acid	0.15	0.90
D- <i>arabino</i> -Hexosulose	0.15	0.90
D- <i>xylo</i> -Hexos-3-ulose	0.10	0.57
D- <i>xylo</i> -Hexos-4-ulose	0.08	0.50
D- <i>xylo</i> -Hexos-5-ulose	0.18	0.60
D-gluco-Hexodialdose	0.95	1.55
2-Deoxygluconic acid	0.95	absent
D-Glucuronic acid	absent	0.05*
5-Deoxy-4-keto-glucose	} 0.08	absent
2-Deoxy-5-keto-glucose		
5-Deoxy- <i>xylo</i> -hexodialdose	} 0.25	absent
3-Deoxy-4-keto-glucose		
4-Deoxy-5-keto-glucose		
3-Deoxy-glucosone	} 0.05	absent
6-Deoxy-5-keto-glucose		
D-Arabinose	0.01	0.07
D-Xylose	< 0.005	0.01
Ribose	< 0.005	
<i>xylo</i> -Pentodialdose	absent	0.07
2-Deoxy-ribose	0.04	absent
3-Deoxy-pentulose	< 0.005	absent
D-Arabinonic acid	absent	0.03
D-Erythrose	0.01	0.01
L- <i>threo</i> -Tetrodialdose	absent	0.20
Butan-2-one-1,4-diol	0.02	absent
D-Erythronic acid	absent	0.01
D-Glyceraldehyde	absent	0.06
D-Glyceric acid	absent	0.07
Dihydroxyacetone	0.03	absent
Glyoxal	absent	0.11
Glyoxylic/glycolic acids	absent	0.4
Formaldehyde	absent	0.12
Formic acid	absent	0.6
Hydrogen peroxide		3.0
Glucose consumption	5.6	

\*secondary product

Table 2

Approximate values for rate constants of phosphate release from some  $\alpha$ -methoxy- $\beta$ -phosphatoalkyl radicals according to [38].

Radical	Rate constant / s <sup>-1</sup>
$\cdot\text{CH}(\text{OCH}_3)\text{CH}_2\text{OPO}_3\text{H}_2$	$10^6$
$\cdot\text{CH}(\text{OCH}_3)\text{CH}_2\text{OPO}_3\text{H}^\cdot$	$10^3$
$\cdot\text{CH}(\text{OCH}_3)\text{CH}_2\text{OPO}_3^{2-\cdot}$	0.1 – 1
$\cdot\text{CH}(\text{OCH}_3)\text{CH}_2\text{OPO}_3(\text{CH}_2\text{CH}_2\text{OCH}_3)\text{H}$	$10^7$
$\cdot\text{CH}(\text{OCH}_3)\text{CH}_2\text{OPO}_3(\text{CH}_2\text{CH}_2\text{OCH}_3)^\cdot$	$10^3 - 10^4$
$\cdot\text{CH}(\text{OCH}_3)\text{CH}_2\text{OPO}_3(\text{CH}_2\text{CH}_2\text{OCH}_3)_2$	$4 \times 10^7$

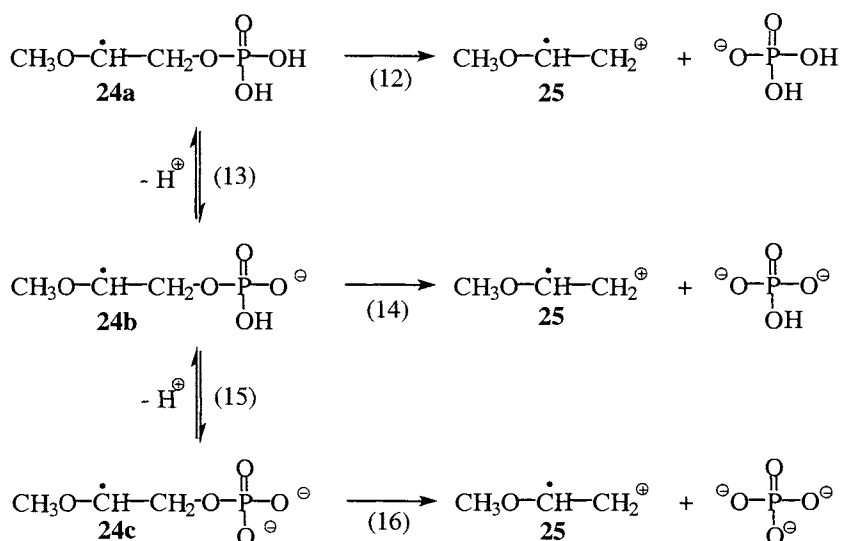
such as glucose the number of the products becomes fairly large so that at a given dose the amount of a particular product tends to be small; both reasons contribute to making the analysis of the products difficult. Thus it has not been possible in the case of glucose and other carbohydrates of similar molecular size to determine the dimer fraction, in contrast to the disproportionation products. This leads to a sizeable deficit in the elemental balance (with respect to, say, carbon compared to the amount of OH radicals and H atoms produced which is known from their  $G$  value and the applied dose), as can be seen from Table 1. In contrast, the formation of the dimeric products is suppressed in the presence of  $\text{O}_2$ , which permits a better balance to be achieved (*cf.* Table 1).

## 2.2. $\beta$ -Elimination of anionic leaving groups: phosphate

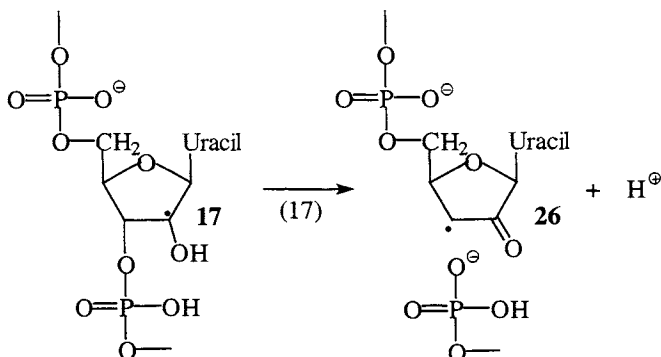
In the case of good anionic leaving groups, such as phosphate *cf.* [38], sulfate [39], or halogen [40], these can be eliminated directly by bond heterolysis. These eliminations can be very fast even in the absence of base catalysis, the rate depending on the state of protonation of the leaving group (Table 2).

In  $\alpha$ -hydroxy- $\beta$ -phosphatoalkyl radicals, phosphate elimination and hydroxyl proton loss may occur in a concerted manner. In the glycerol phosphates, the elimination occurs within a few microseconds [27, 41, 42]. This type of reaction plays a role in the nucleobase-radical-induced strand breakage of poly(U) [*cf.* reaction (17)]. In this reaction, a radical at C(2') **17** is generated. In DNA, strand

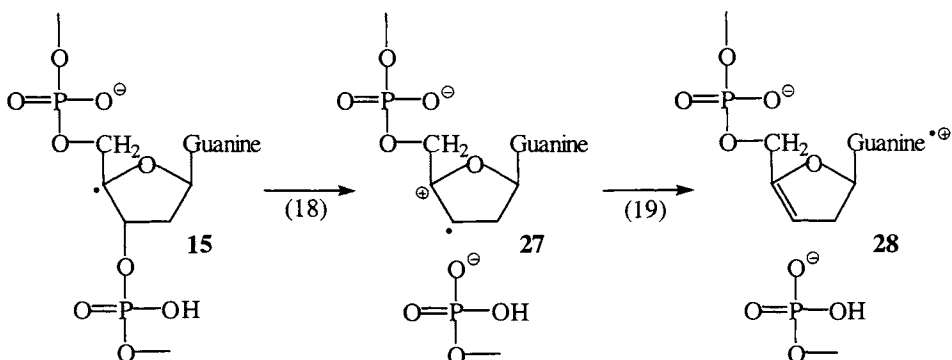
breakage occurs from the C(4') radical **15** [43]. In this case, however, the rate of strand breakage depends strongly on the pH. This is due to a change in mechanism. As has been shown in model systems (*cf.* Table 2) the rate of phosphate elimination is very fast when the leaving phosphate group is neutral [reaction (12)]; it drops by three orders of magnitude when it is mono-negatively charged [reaction (14)] and again in about the same proportion upon further deprotonation [reaction (16)]. This is a strong indication that a radical cation must be formed in this reaction which subsequently undergoes hydrolysis.



The free-radical chemistry of carbohydrate phosphates exhibits the same characteristics [*e.g.* reaction (17)], with the additional option that if the free-radical site materializes  $\alpha$  to the carbohydrate-ring oxygen atom, ring cleavage may occur (see below). Ribose-5-phosphate [44-49] provides an example for this kind of behaviour.



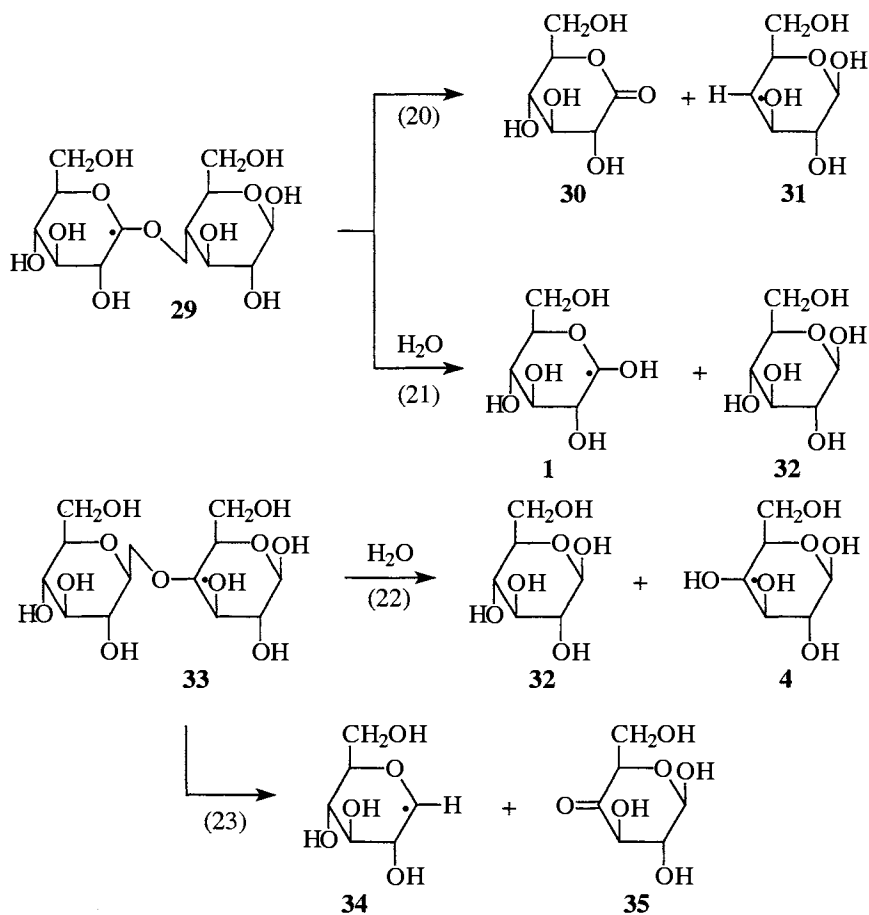
Further reaction pathways may be opened up in more highly substituted carbohydrates, *e.g.* nucleosides. Radical cations are strong oxidants, and it has been shown recently that the radical cation **27** formed in reaction (18) can oxidize the neighbouring guanine residue [reaction (19)] [50, 51].



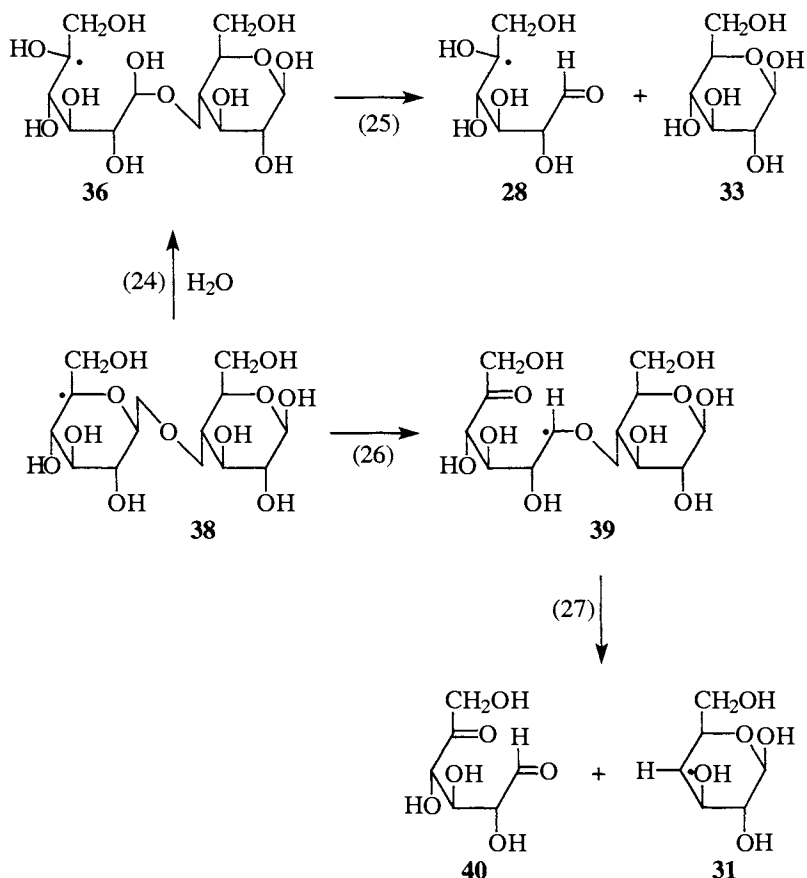
### 2.3 Scission of the glycosidic linkage and ring cleavage

In the radiation chemistry of polysaccharides, the scission of the glycosidic linkage is the most conspicuous process as it leads to the reduction of their molecular weight. There are alternative pathways to this process, as well as to ring cleavage (which is observed, of course, already in monosaccharides) which in some cases may precede glycosidic scission: (i) homolytic transfer of the radical site, to end up on the opposite side of the bond to be cleaved (radical  $\beta$  cleavage), (ii) hydrolysis of the carbon-alkoxyl bond  $\beta$  to the radical site which does not remove. Radical  $\beta$  cleavage has been observed in prototypical  $\alpha$ -alkoxyalkyl radicals (*cf.* [52]); the ease of this reaction depends on the degree of stabilization of the ensuing radical (an OH group as in  $\alpha$ -hydroxyalkyl confers

some stability). Radical  $\beta$  cleavage [reactions (20), (26) and (27); conceivably reaction (23) also occurs, but the products resulting from **34** have not yet be found] can be concurrent with hydrolysis [reactions (22) and (24)] of the radical; these reactions are shown here for the case of cellobiose; similar reactions are observed with other disaccharides [53, 54] (see also [14, 55, 56]).

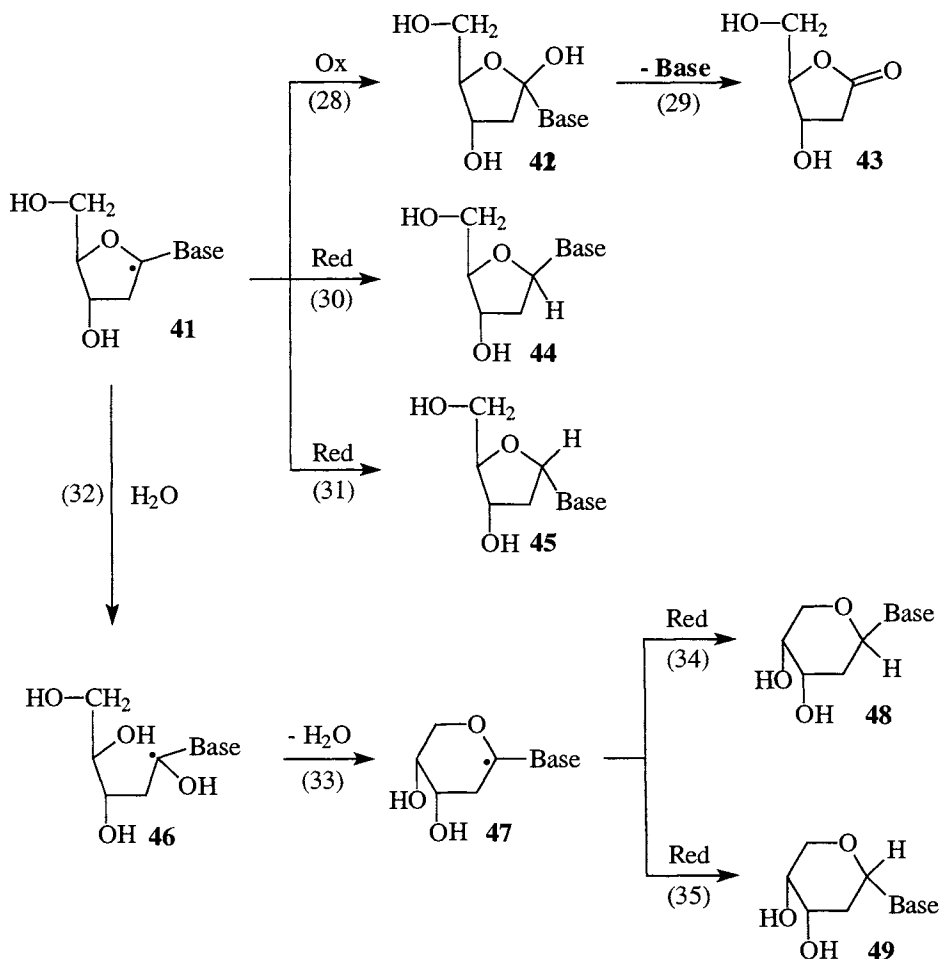




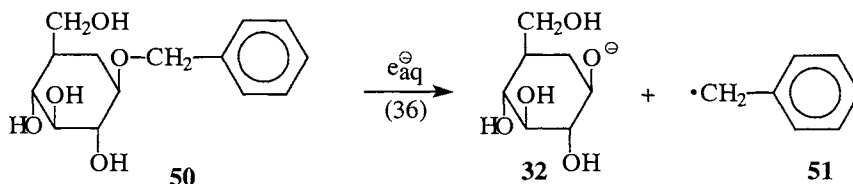


The scission of the glycosidic linkage may occur not only on the free-radical, but also on the product level. When the free-radical site becomes isolated from the glycosidic function, or removed through a free-radical termination reaction or oxidation, the ensuing hemiacetal-like or orthocarbonic-acid-like structures undergo hydrolysis relatively fast, *e.g.* reaction (25). A more complex process leading to this type of scission is conceivable in radicals such as **29**, *via* ring cleavage, acyl migration in the ensuing ester [57], and hydrolysis when the labile C(1) acetal-ester form materializes [58] (though in the case of cellobiose, no product was detected that bears the trace of the corresponding (C4) radical formed upon the ring-opening of **29**, therefore reaction not shown). Similarly in the case of DNA and related compounds, oxidation of the (C1') radical leads to the formation of the orthoester-amide structure **42** [reaction (28)] which subsequently eliminates the base [reaction (29)] [59]. These reactions may occur

in competition with other reactions, including rearrangements that eventually lead to isomerization at (C1') [reactions (30)-(35)] [60, 61].

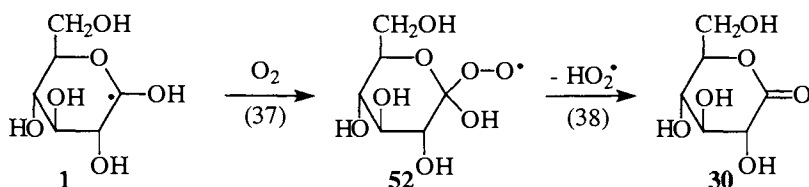


It has been mentioned that under favourable conditions, *e.g.* with benzyl glycosides, the glycosidic linkage is readily broken also by the action of the solvated electron whose attachment to the aglycon moiety [15] leads to rapid scission of the glycosidic linkage, in competition with the protonation of the electron adduct by water. The driving force for reaction (36) is the formation of the highly-stabilized benzyl radical **51**.



#### 2.4. Reactions with molecular oxygen

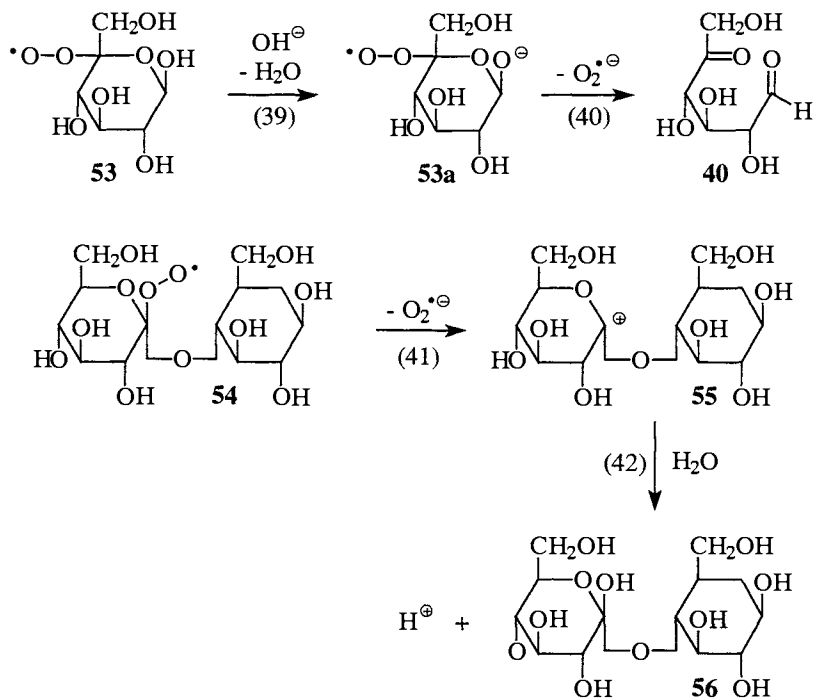
The carbon-centered radicals generally react very fast with oxygen [*e.g.* reaction (37)], so that under conditions of air saturation many of the elimination reactions discussed above are forestalled. This gives rise to the corresponding peroxy radicals (for reviews on peroxy radicals in aqueous solution see [62, 63]). Among them, the  $\alpha$ -hydroxyalkylperoxy radicals stand out, one, because they outnumber the others, and two, because this kind of radical is known relatively easily to eliminate  $HO_2^\cdot$  [*e.g.* reaction (38)].



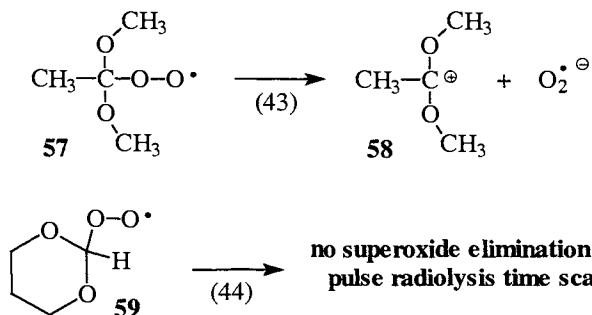
This spontaneous  $HO_2$ -elimination is thought to be a concerted process [64]. The rate of the  $HO_2$ -elimination reaction depends strongly on the nature of neighbouring groups (electronic and steric effects). In carbohydrates the situation becomes rather complex mechanistically [65] as there are several kinds of  $\alpha$ -hydroxyalkylperoxy radical present. The  $HO_2$ -elimination reaction is of the type that is also undergone by other compounds that carry the structural element  $-C(X)OH-$  where X is a good leaving group, such as gem-halohydrins (*cf.* [66-68]).

In basic solution, deprotonation at the hydroxyl group (typically) leads to a very rapid elimination of the superoxide radical anion [65, 69]. The deprotonation reaction was found to be the rate-limiting step in all of those cases where the kinetics were studied in sufficient detail. The peroxy radical derived from a carbon-centered radical such as 53 apparently eliminates superoxide in a similar fashion [18]; this probably happens following the pathway (39), (40).

In the case of glycosides, this pathway is blocked, and alternatives such as reaction (41) may be envisaged.



Evidence for this type of superoxide elimination exists in similar “non- $\alpha$ -hydroxyl” systems [70], with rates apparently varying across a wide range. Thus, the half-time of reaction (43) is 30  $\mu\text{s}$  [71] whereas that of reaction (44) is at least three orders of magnitude longer [72].



It seems that these rates are strongly dependent on the flexibility of the acetalic structure. In the present case, the rate is expected to be relatively slow. This means that such peroxy radicals may competitively undergo bimolecular

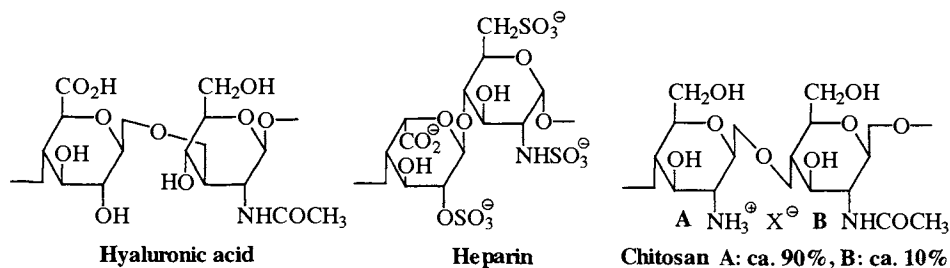
termination, giving rise to tertiary oxyl radicals that are prone to fragmentation [62, 63], in which the glycosidic linkage may likewise be cleaved. This pathway cannot materialize in monosaccharides which have the faster deprotonation-superoxide elimination pathway (OH group geminal to peroxy group, reaction (38)) open to them [65].

For D-glucose, the complete set of reactions (not shown) is not excessively cumbersome to be written out, and the products compiled in Table 1 not only give a complete material balance with respect to the yield of the initiating OH radicals, but also indicates that fragmentation products are formed in very minor yields. The fact that 5-keto-glucose is a major product shows that an  $\text{HO}_2/\text{O}_2^-$ -elimination must have occurred also in the case of the C(5)-peroxy radical. This is expected to be much slower than the other  $\text{HO}_2^-$ -elimination reactions, and the formation of 5-keto-glucose proceeds *via* deprotonation at the C(1)-OH group, followed by the elimination of  $\text{O}_2^-$  [reactions (39) and (40)].

Apart from dioxygen, free radicals may also be oxidized by other oxidants, such as transition metal ions in higher valence states, mostly in complexed form [*cf.* reaction (7)] [34], or nitro compounds (see for instance [72, 73]). These reactions do not necessarily proceed *via* direct electron transfer but apparently mostly through the intermediacy of an adduct. The finer details remain to be elucidated.

## 2.5. Degradation of polymeric carbohydrates

From among the natural carbohydrate polymers, we mention here cellulose, chitin and its deacetylated form chitosan, hyaluronic acid (hyaluronan), and heparin. Apart from cellulose, the monomer-unit sequences are not strictly regular, but the structures given below are representative. Chitosan, hyaluronic acid, and heparin are water-soluble because they carry electrically-charged functions. Since cellulose and chitin are insoluble in water, most of their radiation chemistry has been done in the solid state, as discussed below. Yields of molecular-weight reduction have usually been determined by viscosimetry and, more recently, by the laser light-scattering technique.



The free-radical-induced reduction of the molecular weight of polymeric carbohydrates must occur *via* the scission of a glycosidic linkage, or *via* phosphate release in DNA and related polymers. Mechanistic aspects of these reactions have been discussed above. An additional aspect comes into play on account of the action of shear which tends to enhance the importance of polymer-chain scission by free-radical transfer [*cf.* reactions (20) – (27)], versus the other reaction pathways open to the radicals involved, compared with the unstressed situation in, *e.g.*, disaccharides, because of the drastic weakening of the chemical bonds  $\beta$  to the radical site. In polymers, the resulting products are difficult to characterize chemically as each cleavage produces two chemically modified ends per a large number of unmodified units, although this has been achieved for DNA [10]. It is, however, relatively easy to determine the kinetics of the cleavage process by pulse radiolysis, using conductometry (in the case of charged polymers) and low-angle laser light-scattering (charged and non-charged polymers). Where the polymer is charged, a fraction of the counter-ions is condensed onto the polymer due to the high electric field exerted locally by the charged groups along the polymer chain. As the broken ends diffuse apart upon free-radical-induced chain scission, the force of the electric field exerted by the fragments near the cleavage site weakens and some of the counter-ions diffuse into the bulk of the solution. As a consequence of this, the conductance increases above that observed before the irradiation impulse. In contrast to processes where protons (and anions) are released and the conductance increases in the acid pH range but decreases in the basic range as the proton is neutralized and thus both  $H^+$  and  $OH^-$  disappear, fragmentation-induced counter-ion release always leads to an increase of conductance, irrespective of pH. Such experiments, originally carried out with poly(U) [74], have been done in the carbohydrate series proper with hyaluronic acid [75, 76] and with chitosan (*cf.* Figure 1).

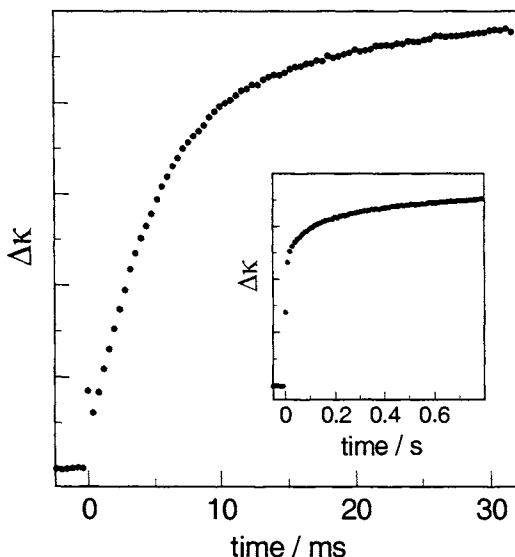


Figure 1. Pulse radiolysis of chitosan in  $\text{N}_2\text{O}$ -saturated aqueous solutions. Kinetics of chain scission as detected by changes in conductance [77].

In Fig. 1, the kinetics of counter-ion release are shown for the chitosan system. It is evident that these kinetics cannot be described by a single first-order process. This also holds for hyaluronic acid [75, 76]. This is in fact not to be expected because here more than one kind of radical may contribute to chain breakage (*cf.* scission of the glycosidic linkage in disaccharides discussed above). At present, it is not yet possible to correlate a given reaction with a specific time frame of the kinetic experiment. However, the counter-ion release experiment yields quantitative data which can be set in relation to the observed decrease of the molecular weight (chain scission). From such data it has been calculated that close to 8 counter-ions are released per chain break [78]. Such values vary somewhat with the system, as they depend on the linear density of electrical charge along the polymer molecule.

In the presence of oxygen, such conductometry experiments cannot be carried out with confidence because of the copious formation of superoxide in these systems (see above). Its relatively rapid decay (*e.g.* by reaction of  $\text{O}_2^{\cdot-}$  with polymer-bound peroxy radicals) itself causes a conductance change. Therefore under those conditions, the kinetics of chain scission must be followed by low-angle laser light-scattering [75]. As it turns out, these reactions are no longer kinetically of first order, but the rates observed depend strongly on the strength of the pulse, *i.e.* there are important second-order contributions [75]. The chain-breaking reactions that occur in the presence of oxygen are less well understood

(for a model system study see [79]) as those in the absence of oxygen, but it is evident that the fixation of radicals by oxygen that in its absence cause chain scission, reduces the yield of chain breakage considerably [73, 75, 76]. This is in contrast to other, non-carbohydrate polymers where a chain scission only becomes noticeable in the *presence* of oxygen (see for instance [80]). Nevertheless, some polymers such as poly(acrylic acid) and poly(methacrylic acid) undergo effective chain scission (*via* a  $\beta$ -fragmentation process) also in the *absence* of oxygen [81, 82].

Thus, ionizing radiation provides an excellent tool to reduce the molecular weight of a carbohydrate polymer whenever required for medicinal application, *e.g.* in the case of chitosan [83-85]. On the other hand, an increased stability against free-radical induced depolymerization might be required. This may be achieved by chemically crosslinking the native linear polymer; the radiolytic behaviour of cross-linked hyaluronic acid, called hylan, has been studied [86].

The free-radical-induced degradation of heparin in aqueous solution is reported to proceed without the formation of free sulfate [87] which would suggest that the initial radical attack occurs exclusively at positions C(1) and/or C(4). In puzzling contrast, NMR data regarding the reduced-molecular-weight heparin fragments seem to indicate an increasing loss of sulfate from the fragments as the dose increases and the fragments get smaller [88]. In view of the fact that sulfate is a good  $\beta$ -elimination leaving group (see above), this is in agreement with expectation.

### 3. RADIOLYSIS IN THE SOLID STATE

In close analogy to the radiolysis of water which produces the free electron and the water radical cation which in turn gives rise to the OH radical and a proton, the radical cations generated in neat carbohydrates, polyhydroxy compounds, will likewise deprotonate at oxygen yielding oxyl radicals and protons. The latter may react with the electron, forming an H atom which abstracts the carbon-bound hydrogen yielding molecular hydrogen. The oxyl radicals can undergo  $\beta$ -fragmentation or H-abstraction from neighbouring carbohydrate molecules (the 1,2-H shift of  $\alpha$ -hydrogen-containing oxyl radicals [89-91] seems to be restricted to aqueous solutions). The major part of the radicals remain immobilised in the crystal matrix and only interact with one another when the irradiated sample is dissolved in water for analysis. For instance, the products which are observed after the  $\gamma$ -radiolysis of D-glucose [92] are compiled in Table 3.



Table 3

$\gamma$ -Radiolysis of crystalline D-glucose. Products and their *G* values [92]. Further (as yet not quantified) products are: glucosone, 3-keto-glucose, 4-keto-glucose, 5-keto-glucose and gluconic acid.

Product	<i>G</i> value
Dihydroxyacetone	0.05
3-Deoxytetrose	0.015
1,4-Dideoxy-2-pentulose	0.05
2,4-Dideoxypentose	0.09
Threose / Erythrose / Erythrulose / Erythronic acid	0.04
1-Deoxy-2-pentulose	0.005
2-Deoxyribose	0.25
3-Deoxypentosulose	0.02
3,5-Dideoxyhexonic acid	0.02
2,3-Dideoxyhexonic acid	0.01
Arabinose	0.25
Ribose / Ribonic acid	0.02
2-Deoxy-2-C-hydroxymethylpentonic acid	0.06
5-Deoxygluconic acid / 2-Deoxy-5-keto-glucose	0.02
2-Deoxygluconic acid / 2-Deoxy-5-keto-glucose	0.1
3-Deoxyglucosone / 3-Deoxygluconic acid / 3-Deoxy-4-keto-glucose	0.2
3-Deoxy-4-keto-glucose / 2-Deoxy-3-keto-glucose	0.19
Hydrogen	5.75

It can be seen that in contrast to its radiolysis in aqueous solution (see Table 1), in the solid state there is a larger contribution from fragmentation products which we attribute to the participation of oxyl radicals under these conditions. As expected, hydrogen is a major product and the material balance is poor despite the fact that a large number of products have been quantified (Table 3). Again, the missing complement should mainly consist of dimers which would escape analysis.

Table 4.

$\gamma$ -Radiolysis of crystalline D-fructose. Products and their  $G$  values. Further (as yet not quantified) products are: glyceraldehyde, 3-butanone-1,2-diol, 2- and 3-deoxyhexodiuloses [92].

Product	$G$ value
2-Deoxytetrose	0.5
Threose / Erythrose / Erythulose	0.65
3-Deoxypentonic acid / 3-Deoxypentosulose	0.3
Arabonic acid	0.1
Ribonic acid	0.05
6-Deoxy-D-threo-2,5-hexodiulose	40
Hydrogen	4.75

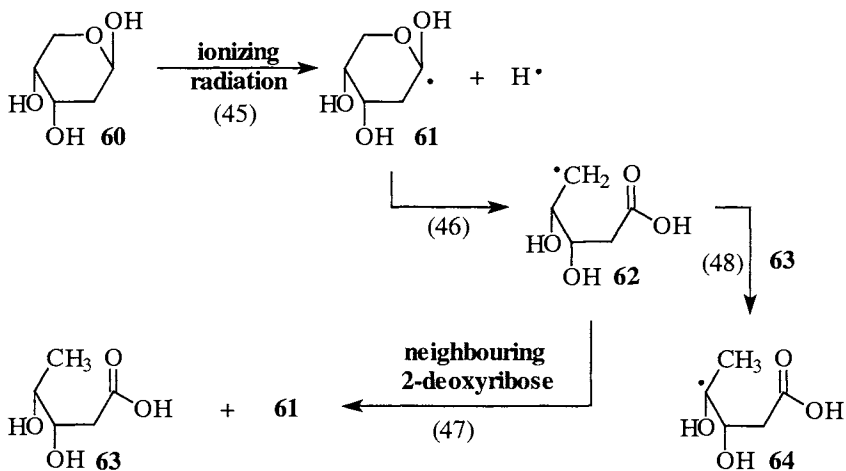
Table 5

Radiation-induced chain reactions in some crystalline carbohydrates. The chain products and their *G* values.

Substrate	Product	<i>G</i> value	Ref.
2-Deoxy-D-ribose	2,5-Dideoxypentonic acid	650	[13, 93]
α-Lactobiose • H <sub>2</sub> O	2-Deoxylactobionolactone	20	[94, 95]
	5-Deoxylactobionic acid	40	
	4-Deoxy-D-glucose + Galactonolactone	4.5	
D-Fructose	6-Deoxy-D- <i>threo</i> -hexodiulose	40	[12, 92, 96]
<i>N</i> -Acetylglucosamine	2-Acetylamino-2,5-L- <i>threo</i> -dideoxyhexo-dialdose	1.1	[97]

If a similar situation were always to exist with all crystalline carbohydrates, *i.e.* major amounts of hydrogen, a large number of minor products and a considerable unresolved dimer fraction, the attention that this field has found would perhaps have been undeserved. Interestingly, however, radiation-induced chain reactions were observed in the case of several crystalline carbohydrates (see Tables 4 and 5; note also the dominance of the chain product (6-deoxy-D-*threo*-2,5-hexodiulose) compared to the fragmentation products, in Table 4). The chain reaction which often leads to an isomer of the substrate molecule or its dehydration product is governed by the crystal structure, as it is no longer observed in crystals of the same compound, but with a different structure.

The most effective chain reaction is observed with 2-deoxy-D-ribose in the 2-deoxy-β-D-*erythro*-pentopyranose form [reactions (45) - (47)] [13, 93]. The chain comes to a halt when the propagating radical **62** abstracts an H atom from the product molecule just formed [reaction (48)]. The resulting radical **64** is hence trapped between two product molecules and has been identified by EPR as the most persistent radical in this system [98]. The crystal structure clearly shows the pathway taken through the crystal. In the pristine crystal the distance between the sites of reaction is ≤ 3.3 Å [13], and upon rearrangement these two centres might come closer to one another in order for reaction (47) to proceed.

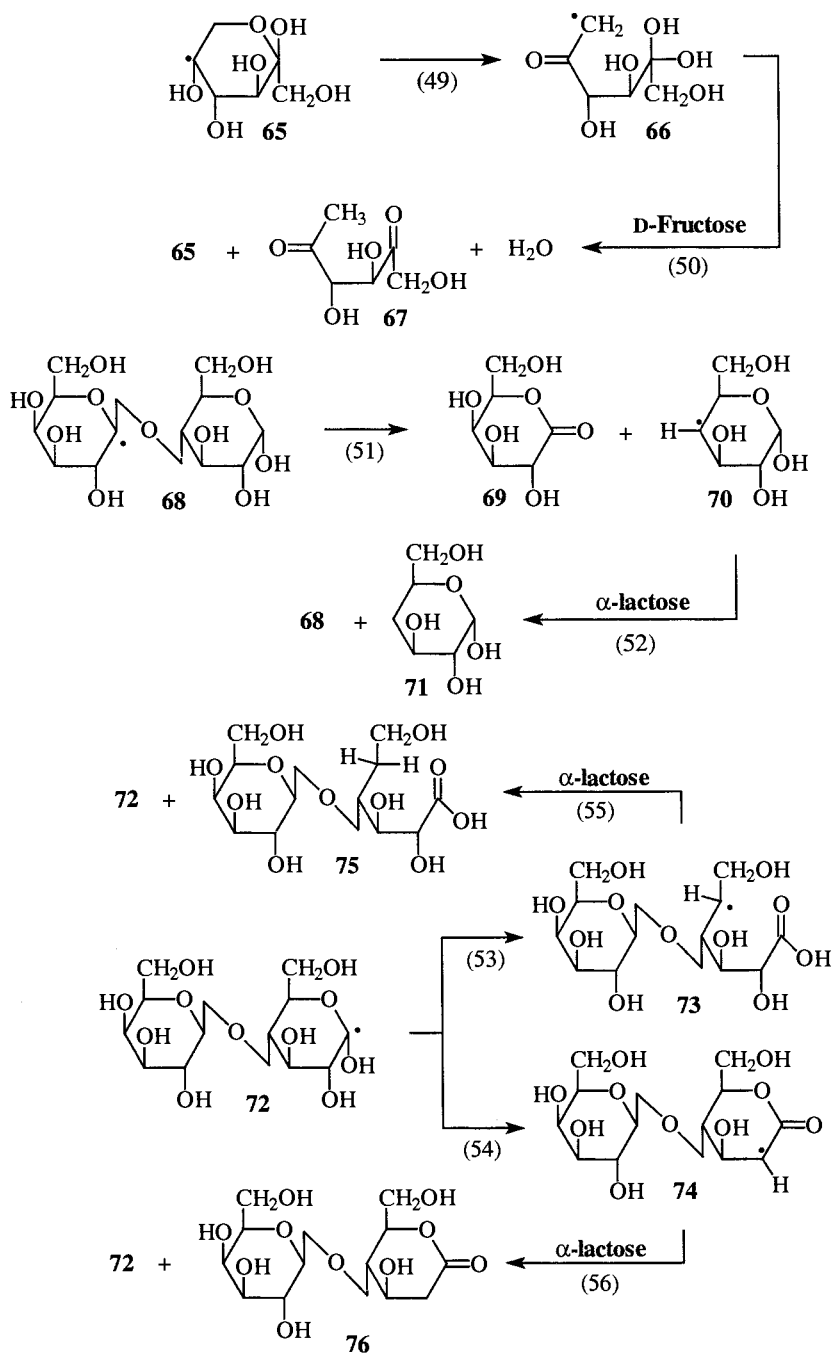


A similar distance has been calculated for the crystal structure of  $\beta$ -D-fructose for the H-transfer in the propagating step (see below) [12]. The  $G$  value drops with increasing dose indicating that termination reactions are favoured by imperfections. There is also a characteristic change of the irradiated 2-deoxyribose crystal: it turns highly hygroscopic at moderate doses.

The sequence involved in the chain reaction traversing D-fructose is depicted by reactions (49) and (50).

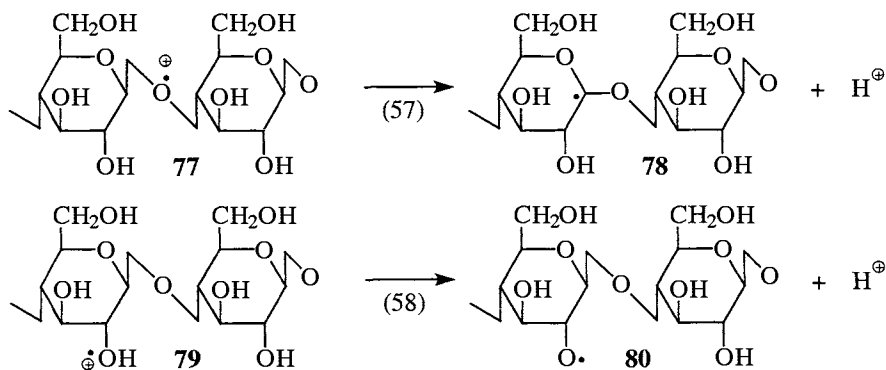
In  $\alpha$ -lactose monohydrate, several chain reactions are observed at the same time, yielding 4-deoxy-D-glucose plus galactonolactone, 5-deoxylactobionic acid and 2-deoxylactobionolactone [reactions (51) – (56) [94, 95].  $\gamma$ -Radiolysis of  $\alpha$ -lactobiose monohydrate is the easiest way to prepare 5-deoxylactobionic acid [94], because it is readily isolated from the irradiated material by ion exchange chromatography.

*N*-Acetylglucosamine is listed in Table 5: even though the  $G$  value of the corresponding product appears quite small, it is large compared to typical non-chain products (*cf.* Table 3); this is taken as an indicator for a short chain reaction. Some aspects of the pathway to 2-acetylamino-2,5-L-*threo*-dideoxyhexodialdose are fairly well understood: the chain must start from the radical at C(6) with subsequent carbinol elimination [*cf.* reaction (6)] which here implies ring opening followed by H-abstraction from a neighbouring *N*-actylglucosamine molecule.



A considerable amount of work has been devoted to the action of ionizing radiation on polymeric carbohydrates in the solid state, in particular with regard to its effect on the mechanical properties even though some chemical effects have also emerged. For a recent review see [99]. Of these polymers, cellulose has been the most studied (*cf.* [99, 100]). Native cellulose is locally crystalline. Determination of chain breakage by radiolysis has usually been done after dissolution through complexation, *e.g.* as the copper-ammine complex (Schweizer's reagent), or the cadmium-ethylenediamine complex.

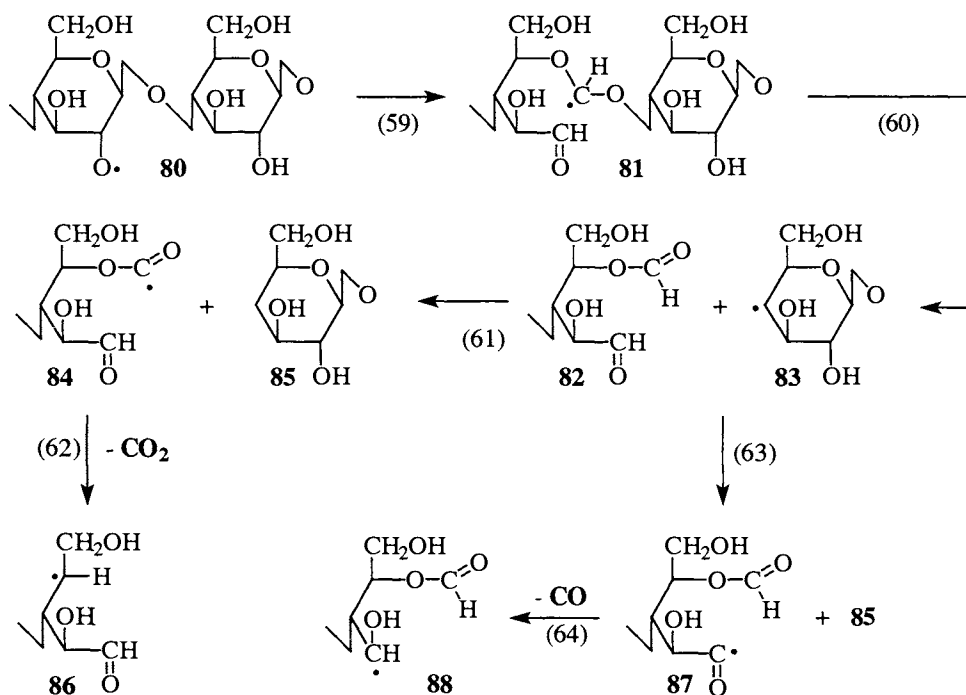
In contrast to aqueous-dissolved systems where the OH radical and the H atom are the main initiators, radical cations plus electrons and excited states are formed in the solid state. This is also the case with cellulose dispersed in water [101]. The radical cations are transformed by deprotonation [*e.g.* reactions (57) and (58)]. These suffer fragmentation such as reactions (20) – (23), as discussed above, or, for example, reaction (59).



When cellulose is irradiated *in vacuo*  $G(\text{H}_2) \approx 3$ ,  $G(\text{CO}_2) \approx 6$  and  $G(\text{CO}) \approx 1 \times 10^{-7} \text{ mol J}^{-1}$  have been observed [99]. The gaseous products CO and  $\text{CO}_2$  are ascribed to the decay of highly excited states (excited radical cations). It is noted that CO formation is also of some importance in the radiolysis of alcohols in the liquid and frozen state [102, 103]. However, for  $\text{CO}_2$  and CO, a free-radical pathway starting with the  $\beta$ -fragmentation of the oxyl radical **80** [reaction (59)] is also conceivable, as one expects the radicals in the solid to have a long lifetime due to a reduced mobility, which could selectively permit reactions (60) – (64) to occur.

Values for  $G(\text{chain scission})$  of chitin ( $1.1 - 1.8 \times 10^{-7} \text{ mol J}^{-1}$ ) are lower than of (solid) heparin ( $\sim 3 \times 10^{-7} \text{ mol J}^{-1}$ ) and cellulose ( $\sim 6 \times 10^{-7} \text{ mol J}^{-1}$ ) [99]. Cellulose degradation  $G$  values in wood are lower by half or more, presumably

because the affinity of the lignin for electrons and holes is greater than of the cellulose fiber [99].



## REFERENCES

1. G.O. Phillips, *Adv. Carbohydr. Chem. Biochem.*, 16 (1961) 13.
2. G.O. Phillips, in: *The Carbohydrates*, Vol. IB, W. Pigman, D. Horton and J.D. Wander (eds.), Academic Press, New York, 1980 p. 1217.
3. N.K. Kochetkov, L.I. Kudrjashov and M.A. Chlenov, in: *Radiation Chemistry of Carbohydrates*, G.O. Phillips (transl. ed.), Pergamon Press, Oxford, 1979.
4. J.F. Diehl and H. Scherz, *Int. J. Appl. Radiat. Isotopes*, 26 (1975) 499.
5. J. Schubert, in: *Improvement of Food Quality by Irradiation*, Int. Atomic Energy Agency Vienna, 1974, p. 1.
6. J.W. Baynes, in: *Drugs, Diet and Disease*, C. Ioannides (ed.), Pergamon Press, London, 1996 p. 201.
7. Y. Nishi, Y. Miyakawa and K. Kato, *Mutation Res.*, 227 (1989) 117.

8. V.J. Feron, H.P. Til, F. de Frijer, R.A. Woutersen, F.R. Cassee and P.J. van Bladeren, *Mutation Res.*, 259 (1991) 363.
9. C. von Sonntag, *Int. J. Radiat. Biol.*, 46 (1984) 507.
10. C. von Sonntag, *The Chemical Basis of Radiation Biology*, Taylor and Francis, London, 1987.
11. C. von Sonntag, *Adv. Carbohydr. Chem. Biochem.*, 37 (1980) 7.
12. M. Dizdaroglu, J. Leitich and C. von Sonntag, *Carbohydr. Res.*, 47 (1976) 15.
13. M.N. Schuchmann, C. von Sonntag, Y.H. Tsay and C. Krüger, *Z. Naturforsch.*, 36b (1981) 726.
14. N.K. Kochetkov, L.I. Kudryashov and M.A. Chlenov, *J. Gen. Chem. USSR*, 38 (1968) 76.
15. N.S. Fel', L.I. Nedoborova, L.I. Kudryashov, P.I. Dolin and N.K. Kochetkov, *High Energy Chem.*, 5 (1971) 215.
16. G.V. Buxton, C.L. Greenstock, W.P. Helman and A.B. Ross, *J. Phys. Chem. Ref. Data*, 17 (1988) 513.
17. J.S.B. Park, P.M. Wood, B.C. Gilbert and A.C. Whitwood, *J. Chem. Soc. Perkin Trans. 2*, (1999) 923.
18. M.N. Schuchmann and C. von Sonntag, *J. Chem. Soc. Perkin Trans. II*, (1977) 1958.
19. B.C. Gilbert, J.R. Lindsay Smith, P. Taylor, S. Ward and A.C. Withwood, *J. Chem. Soc. Perkin Trans. 2*, (1999) 1631.
20. A.G.W. Bradbury and C. von Sonntag, *Z. Naturforsch.*, 31b (1976) 1274.
21. A.G.W. Bradbury and C. von Sonntag, *Carbohydr. Res.*, 62 (1978) 223.
22. M. Bonifacic, I. Stefanic, G.L. Hug, D.A. Armstrong and K.-D. Asmus, *J. Am. Chem. Soc.*, 120 (1998) 9930.
23. O.J. Mieden and C. von Sonntag, *J. Chem. Soc. Perkin Trans. 2*, (1989) 2071.
24. O.J. Mieden and C. von Sonntag, *Z. Naturforsch.*, 44 b (1989) 959.
25. O.J. Mieden, M.N. Schuchmann and C. von Sonntag, *J. Phys. Chem.*, 97 (1993) 3783.
26. M. Dizdaroglu, D. Schulte-Frohlinde and C. von Sonntag, *Int. J. Radiat. Biol.*, 32 (1977) 481.
27. M.N. Schuchmann, M.L. Scholes, H. Zegota and C. von Sonntag, *Int. J. Radiat. Biol.*, 68 (1995) 121.
28. A.L. Buley, R.O.C. Norman and R.J. Pritchett, *J. Chem. Soc. (B)*, (1966) 849.
29. S. Steenken, M.J. Davies and B.C. Gilbert, *J. Chem. Soc. Perkin Trans. II*, (1986) 1003.



30. L.R. Karam, M.G. Simic and M. Dizdaroglu, *Int. J. Radiat. Biol.*, 49 (1986) 67.
31. O. I. Shadyro, *Homologous Series of Transformability in Biology and Chemistry*, Izdatelstvo Universitetskoye, Minsk, 1987.
32. E. P. Petryaev, and O. I. Shadyro, *Radiation Chemistry of Bifunctional Organic Compounds*, Izdatelstvo Universitetskoye, Minsk, 1986.
33. O.I. Shadyro, A.A. Sosnovskaya and O.N. Vrublevskaya, *High Energy Chem.*, 33 (1999) 94.
34. G.E. Adams and R.L. Willson, *Trans. Faraday Soc.*, 65 (1969) 2981.
35. C. von Sonntag and E. Thoms, *Z. Naturforsch.*, 25b (1970) 1405.
36. M.S. Akhlaq, S. Al-Baghdadi and C. von Sonntag, *Carbohydr. Res.*, 164 (1987) 71.
37. M. Dizdaroglu, D. Henneberg, G. Schomburg and C. von Sonntag, *Z. Naturforsch.*, 30b (1975) 416.
38. G. Behrens, G. Koltzenburg, A. Ritter and D. Schulte-Frohlinde, *Int. J. Radiat. Biol.*, 33 (1978) 163.
39. G. Koltzenburg, E. Bastian and S. Steenken, *Angew. Chem. Int. Ed. Engl.*, 27 (1988) 1066.
40. G. Koltzenburg, G. Behrens and D. Schulte-Frohlinde, *J. Am. Chem. Soc.*, 104 (1982) 7311.
41. A. Samuni and P. Neta, *J. Phys. Chem.*, 77 (1973) 2425.
42. S. Steenken, G. Behrens and D. Schulte-Frohlinde, *Int. J. Radiat. Biol.*, 25 (1974) 205.
43. M. Dizdaroglu, C. von Sonntag and D. Schulte-Frohlinde, *J. Am. Chem. Soc.*, 97 (1975) 2277.
44. L. Stelter, C. von Sonntag and D. Schulte-Frohlinde, *Int. J. Radiat. Biol.*, 29 (1976) 255.
45. L. Stelter, C. von Sonntag and D. Schulte-Frohlinde, *Int. J. Radiat. Biol.*, 25 (1974) 515.
46. L. Stelter, C. von Sonntag and D. Schulte-Frohlinde, *Z. Naturforsch.*, 30b (1975) 609.
47. L. Stelter, C. von Sonntag and D. Schulte-Frohlinde, *Z. Naturforsch.*, 30b (1975) 656.
48. N.K. Kochetkov, L.I. Kudrjashov, M.A. Chlenov and L.P. Grineva, *Carbohydr. Res.*, 53 (1977) 109.
49. N.K. Kochetkov, L.I. Kudrjashov, M.A. Chlenov and L.P. Grineva, *Carbohydr. Res.*, 35 (1974) 235.
50. E. Meggers, D. Kusch, M. Spichty, U. Wille and B. Giese, *Angew. Chem. Int. Ed.*, 37 (1998) 460.

51. E. Meggers, M.E. Michel-Beyerle and B. Giese, *J. Am. Chem. Soc.*, 120 (1998) 12950.
52. S. Steenken, H.-P. Schuchmann and C. von Sonntag, *J. Phys. Chem.*, 79 (1975) 763.
53. C. von Sonntag, M. Dizdaroglu and D. Schulte-Frohlinde, *Z. Naturforsch.*, 31b (1976) 857.
54. H. Zegota and C. von Sonntag, *Z. Naturforsch.*, 32b (1977) 1060.
55. N.K. Kochetkov, L.I. Kudryashov, S.M. Yarovaya and E.I. Bortsova, *J. Gen. Chem. USSR*, 35 (1965) 1195.
56. N.K. Kochetkov, L.I. Kudryashov, S.M.B. Yarovaya and O.S. Chizhov, *J. Gen. Chem. USSR*, 38 (1968) 2297.
57. M.L. Wolfrom and W. Szarek, in: *The Carbohydrates*, W. Pigman and D. Horton (eds.), Academic Press, New York, 1972, p. 217.
58. S. Vanwetswinkel, V. Carlier, J. Marchand-Brynaert and J. Fastrez, *Tetrahedron Lett.*, 37 (1996) 2761.
59. M. Dizdaroglu, K. Neuwald and C. von Sonntag, *Z. Naturforsch.*, 31b (1976) 227.
60. N. Mariaggi, R. Teoule, J. Cadet, H. Dickie and E. Hughes, *Radiat. Res.*, 79 (1979) 431.
61. M. Berger and J. Cadet, *Z. Naturforsch.*, 40b (1985) 1519.
62. C. von Sonntag and H.-P. Schuchmann, *Angew. Chem. Int. Ed. Engl.*, 30 (1991) 1229.
63. C. von Sonntag and H.-P. Schuchmann, in: *Peroxy Radicals*, Z.B. Alfassi (ed.), Wiley, Chichester, 1997, p. 173.
64. E. Bothe, G. Behrens and D. Schulte-Frohlinde, *Z. Naturforsch.*, 32b (1977) 886.
65. E. Bothe, D. Schulte-Frohlinde and C. von Sonntag, *J. Chem. Soc. Perkin Trans. II*, (1978) 416.
66. N. Latif, P. O'Neill, D. Schulte-Frohlinde and S. Steenken, *Ber. Bunsenges. Phys. Chem.*, 82 (1978) 468.
67. R. Mertens, C. von Sonntag, J. Lind and G. Merenyi, *Angew. Chem. Int. Ed. Engl.*, 33 (1994) 1259.
68. P. Dowideit, R. Mertens and C. von Sonntag, *J. Am. Chem. Soc.*, 118 (1996) 11288.
69. E. Bothe, M.N. Schuchmann, D. Schulte-Frohlinde and C. von Sonntag, *Photochem. Photobiol.*, 28 (1978) 639.
70. M.N. Schuchmann and C. von Sonntag, *Z. Naturforsch.*, 42b (1987) 495.
71. R.A. Cardona, C.M. King and J.L. Redpath, *Cancer Res.*, 35 (1975) 2007.
72. C. Nese, M.N. Schuchmann, S. Steenken and C. von Sonntag, *J. Chem. Soc. Perkin Trans. 2*, (1995) 1037.

73. D.J. Deeble, P. Myint, B.J. Parsons, G.O. Phillips, H. Starnes and C. von Sonntag, *Int. J. Radiat. Biol.*, 62 (1992) 105.
74. E. Bothe and D. Schulte-Frohlinde, *Z. Naturforsch.*, 37c (1982) 1191.
75. D.J. Deeble, E. Bothe, H.-P. Schuchmann, B.J. Parsons, G.O. Phillips and C. von Sonntag, *Z. Naturforsch.*, 45c (1990) 1031.
76. D.J. Deeble, G.O. Phillips, E. Bothe, H.-P. Schuchmann and C. von Sonntag, *Radiat. Phys. Chem.*, 37 (1991) 115.
77. P. Ulanski and C. von Sonntag, *J. Chem. Soc. Perkin Trans 2*, (2000) 2022.
78. M. Adinarayana, E. Bothe and D. Schulte-Frohlinde, *Int. J. Radiat. Biol.*, 54 (1988) 723.
79. M.N. Schuchmann and C. von Sonntag, *Int. J. Radiat. Biol.*, 34 (1978) 397.
80. P. Ulanski, E. Bothe, K. Hildenbrand, J.M. Rosiak and C. von Sonntag, *J. Chem. Soc. Perkin Trans. 2.*, (1996) 23.
81. P. Ulanski, E. Bothe, K. Hildenbrand and C. von Sonntag, *J. Chem. Soc. Perkin Trans. 2*, (1996) 13.
82. P. Ulanski, E. Bothe and C. von Sonntag, *Nuclear. Instr. Meth. Phys. Res. B.*, 151 (1999) 350.
83. P. Ulanski and J. Rosiak, *Radiat. Phys. Chem.*, 39 (1992) 53.
84. J.M. Rosiak, P. Ulanski, M. Kucharska, J. Dutkiewicz and L. Judkiewicz, *J. Radioanal. Nucl. Chem. (Articles)*, 159 (1992) 87.
85. P. Ulanski, A. Wojtasz-Pajak, J.M. Rosiak and C. von Sonntag, in: *Advances in Chitin Science*, Vol. 4, M.G. Peter, R.A.A. Muzzarelli and A. Domard (eds.), (2000) 420.
86. S. Al-Assaf, G.O. Phillips, D.J. Deeble, B. Parsons, H. Starnes and C. von Sonntag, *Radiat. Phys. Chem.*, 46 (1995) 207.
87. F. Jooyandeh, J.S. Moore, R.E. Morgan and G.O. Phillips, *Radiat. Res.*, 45 (1971) 455.
88. Z. Liu and A.S. Perlin, *Carbohydrate Res.*, 255 (1994) 183.
89. V.M. Berdnikov, N.M. Bazhin, V.K. Fedorov and O.V. Polyakov, *Kinet. Catal. (Engl. Transl. )*, 13 (1972) 986.
90. B.C. Gilbert, R.G.G. Holmes, H.A.H. Laue and R.O.C. Norman, *J. Chem. Soc. Perkin Trans. II*, (1976) 1047.
91. H.-P. Schuchmann and C. von Sonntag, *J. Photochem.*, 16 (1981) 289.
92. M. Dizdaroglu, D. Henneberg, K. Neuwald, G. Schomburg and C. von Sonntag, *Z. Naturforsch.*, 32b (1977) 213.
93. C. von Sonntag, K. Neuwald and M. Dizdaroglu, *Radiat. Res.*, 58 (1974) 1.
94. M. Dizdaroglu, C. von Sonntag, D. Schulte-Frohlinde and W.V. Dahloff, *Liebigs Ann. Chem.*, (1973) 1592.
95. C. von Sonntag and M. Dizdaroglu, *Z. Naturforsch.*, 28b (1973) 367.
96. S. Kawakishi, Y. Kito and M. Namiki, *Agr. Biol. Chem.*, 39 (1975) 1897.

97. A.G.W. Bradbury and C. von Sonntag, *Z. Naturforsch.*, 32b (1977) 725.
98. J. Hüttermann and A. Müller, *Z. Naturforsch.*, 24b (1969) 463.
99. B.G. Ershov, *Russian. Chem. Rev.*, 67 (1998) 315.
100. B.G. Ershov and A.S. Klimentov, *Russ. Chem. Rev.*, 53 (1984) 1195.
101. J. Lind, G. Merényi and N.O. Nilvebrant, *J. Wood Chem. Technol.*, 17 (1997) 111.
102. J.H. Baxendale and P. Wardman, *NSRDS-NBS*, 54 (1975) 1.
103. G.R. Freeman, in: *Actions Chimiques et Biologiques des Radiations*, M. Haissinsky (ed.), Masson, Paris, 1970, p. 73.

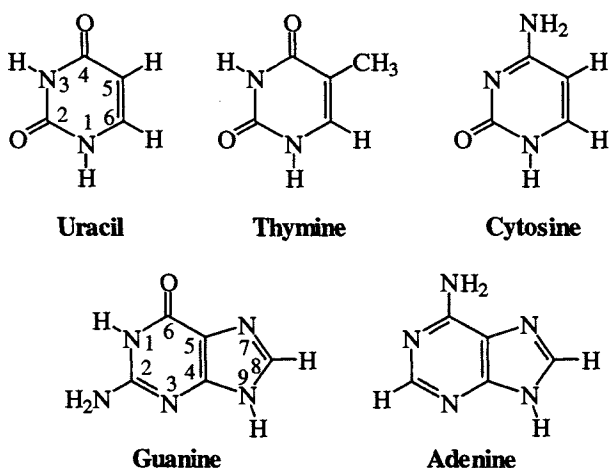
## Radiation Chemistry of the Nucleobases

C. von Sonntag and H.-P. Schuchmann

Max-Planck-Institut für Strahlenchemie  
P.O.Box 101365, Stiftstrasse 34-36, D-45470 Mülheim an der Ruhr, Germany

### 1. INTRODUCTION

Five heterocyclic compounds, the so-called nucleobases, namely the three pyrimidine-dione derivatives uracil, thymine and cytosine ("pyrimidines"), and the two purine derivatives guanine and adenine ("purines"), stand out from the vast number of other heteroaromatic compounds because life has evolved making use of them in its coding systems (DNA, RNA). For this reason, intense interest has been devoted to the study of their chemical transformations which in the biological context are in general to be regarded as detrimental. Perhaps unavoidably in view of their biological function which presupposes chemical sensitivity, these compounds are relatively easily attacked by a range of chemical species, in particular free radicals that are a constant presence in biological systems, owing to the cells' metabolism, but also owing to the action of ionizing radiation which pervades the natural and man-made environments.



The free-radical chemistry of the nucleobases has been reviewed in the past [1-5]. The goal of this Chapter is to present an update in a more general sense; a more detailed discussion of the topic will be published in a different context [6]. The present Chapter is centered on the radiation-induced free-radical chemistry of the nucleobases and some of their derivatives which comprise, on the one hand, the nucleosides and nucleotides, and on the other hand, model compounds such as some methylated nucleobases.

The major effect of ionizing radiation on cellular systems, *e.g.* reproductive cell death, is caused by its interaction with the cellular DNA either by the absorption of the energy in the DNA (direct effect), or by the reaction of the DNA with the water-derived radicals (OH radical, hydrogen atom, and solvated electron), generated by the ionising radiation in the aqueous medium in the immediate neighbourhood of the DNA strand [4]. It has been estimated that the direct effect contributes about 40% to the cellular-DNA radiation damage, while the effect of the water radicals, notably the OH radical, amounts to about 60% [4]. Thus there is a long-standing interest in the radiation chemistry of DNA and its constituents in aqueous solutions. The reactions of the water radicals with the nucleobases merit particular attention since, owing to the higher reactivity toward the water radicals compared to the DNA sugar moiety (for some aspects of the radiation-induced reactions of the sugar moiety see the Chapter on carbohydrates), these reactions prevail on a quantitative basis, although potentially more severe types of damage (*e.g.* strand breakage) are initiated by radical attack on the sugar moiety.

One can say that the radiolytic studies of the nucleobases, apart from satisfying a chemical curiosity with respect to these compounds as such, are carried out toward two goals. One is to establish a kinetic image of the interplay of the processes that are induced by the action of radiation, the other is to find out which are the products that are generated. Viewing this in the context of radiolytic or free-radical damage to DNA, knowledge of the kinetics might in principle point toward a way to offset or neutralize (the concept of chemical radioprotection [7-10]), or even enhance (through radiation sensitizers in, *e.g.*, cancer therapy [11, 12]) this damage at an early stage. An exact knowledge of the products (corresponding to the damaged sites in DNA) might ultimately allow to locate the damaged site (*e.g.*, immunoassay [13-19]) and facilitate its repair.

The effect of other inorganic radicals on the nucleobases, apart from the "water radicals" mentioned above, has repeatedly been studied, for instance the sulfate radical which has been used to generate nucleobase radical cations with the aim to mimic the direct effect of ionizing radiation on DNA. Carbon-centred

radicals and peroxy radicals also react with these compounds but exhibit a lower reactivity. These reactions will not be discussed in detail here but have been reviewed elsewhere [4] Moreover, a forthcoming book will offer a comprehensive update of these and other aspects of nucleobase free-radical chemistry [6].

In aqueous solution, the nucleobases react with the OH radical and the solvated electron at close to diffusion-controlled rates, while the H atom reacts one order of magnitude more slowly (Table 1). In nucleosides and nucleotides, of these three species only the OH radical shows a moderate inclination of reacting with the sugar moiety, typically in the range of 10 to 20% of the total.

The nucleobases, like all unsaturated systems, react with the water radicals OH and H mostly by addition (with  $e_{aq}^-$ , of course, exclusively so). As one would expect, the reactivity pattern (regarding the various positions within the molecule) shown by the bicyclic purines is considerably more complex than in the case of the pyrimidines. It is therefore useful to divide the discussion and start with the simpler pyrimidines.

Table 1.

Rate constants for the reactions of OH radicals, H atoms and solvated electrons with the nucleobases. Guanine being very poorly water-soluble, the corresponding data for guanosine are listed here instead. *Source:* [20]

Substrate	$\cdot\text{OH}$	$\text{H}\cdot$	$e_{aq}^-$
Adenine	$6.1 \times 10^9$	$1.0 \times 10^8$	$9.0 \times 10^9$
Cytosine	$6.3 \times 10^9$	$9.2 \times 10^7$	$1.3 \times 10^{10}$
Guanosine	$7.8 \times 10^9$	$5.0 \times 10^8$	$6.0 \times 10^9$
Thymine	$6.4 \times 10^9$	$6.8 \times 10^8$	$1.8 \times 10^{10}$
Uracil	$5.7 \times 10^9$	$4.7 \times 10^8$	$1.5 \times 10^{10}$

## 2. PYRIMIDINES

### 2.1. The reactions of the OH radical

The OH radical, being electrophilic, prefers to attach to the C(5)-C(6) double bond [reactions (1) and (2)] (see Table 2) at the site of relatively high electron density, C(5) [reaction (1)], where negative charge tends to accumulate owing to N(1)-iminium-C(5)-carbanion mesomerism. Both kinds of the resulting

radicals can be relatively easily titrated since, as it happens, they differ markedly in their redox behaviour [regrettably for the researcher, in most free-radical systems, *e.g.* the purines (see below) this is not the case]. The C(6)-centered radical is of reducing nature due to the interaction with the lone pair at the neighbouring nitrogen, and its yield can be readily determined in pulse radiolysis by its rapid reaction with tetranitromethane which produces the strongly absorbing nitroform anion [reaction (4)]. On the other hand, the C(5)-centered radical has oxidizing properties (note its mesomerism with the radical site at  $O^4$ ). Its yield can be determined with the help of *N,N,N',N'*-tetramethylphenylenediamine [reaction (5)]. These OH-adduct radicals can also be observed by EPR (see *e.g.* [21-23]).

The allylic radical formed in moderate to small yield by H-abstraction from the methyl group in, *e.g.*, thymine [*cf.* reaction (2)], has neither reducing nor oxidizing properties, and its yield may be deduced from the difference of the sum of reducing and oxidizing radicals with respect to the total OH-radical yield; H-atom abstraction at pyrimidine *N*, amino *N*, and methine *C* is negligible. The proportion of these radicals for the pyrimidine nucleobases and some of their homologues are compiled in Table 2.

Table 2.

Reactions of OH radicals with some pyrimidines. Yields of addition at C(5) and C(6), and of allylic H-abstraction where applicable. *Source*: [24-26].

Pyrimidine	Addition at C(5)	Addition at (C6)	H-Abstraction
Uracil	82	18	—
Thymine	60	30	10
6-Methyluracil	88	12	little
Isoorotic acid	63	37	—
Orotic acid	86	14	—
1,3-Dimethyluracil	80	20	little
Cytosine	87	10	—
1-Methylcytosine	87	8	—
2-Methylcytosine	92	10	—
5-Methylcytosine	65	22	13
5-Carboxycytosine	82	24	—



## 2.2. Water elimination and rearrangement

The OH-adduct radicals can become deprotonated at nitrogen. As a consequence of this, water is eliminated from the adduct. This reaction results in the formation of a heteroatom-centered, oxidizing radical [*e.g.* reaction (11)]; this may also be formed directly from the deprotonated nucleobase at higher pH [reaction (10)]. At high pH, this radical can undergo a second deprotonation [reaction (12)]. However, this radical anion is not the thermodynamically favoured species under these conditions, and is subsequently reprotonated at carbon (*i.e.* the heteroatom-protonated acid has a lower  $pK_a$  value than its carbon-protonated isomer) [reaction (14)]. The hydroxyl group can also be eliminated by acid catalysis, which gives rise to a radical cation. These reactions will be discussed below in a separate section.

## 2.3. Products in the absence of oxygen

Detailed studies concerning the products that are formed after OH-radical attack (radiolysis of  $N_2O$ -saturated solutions) have been carried out for uracil [27], thymine [28, 29], cytosine [30] and 1,3-dimethyluracil [26]. In addition, the radiolysis of uracil in deoxygenated solutions (in the absence of  $N_2O$ ) has also found attention [31, 32]. Under such conditions, however, not only do the OH-radical-induced reactions play a role, but also the electron-adduct radical with all the ensuing mechanistic complications contribute to the products.

The nucleobases carry a hydrogen atom at  $N(1)$  which can take part in disproportionation reactions, which will lead to the formation of the pyrimidines in a different tautomeric form. These isopyrimidines rearrange to the normal,  $N(1)$ -H form (for their reactions see below). The product 5-hydroxycytosine from the radiolysis of cytosine (Table 3) may largely be formed in this way. The hydrogen atom (at  $N(1)$ ) involved in the disproportionation reaction is not available in nucleosides that are closer models to the DNA. No detailed studies are available to date for pyrimidine nucleosides. 1,3-Dimethyluracil is a compound which is much easier to handle analytically than nucleosides but which retains the major aspects of the base moiety of uracil- and thymine-containing nucleosides. Thus, the results from a study on the  $\gamma$ -radiolysis of 1,3-dimethyluracil in  $N_2O$ -saturated solutions (*cf.* Table 4) may give useful indications as to the reactions that one might have to expect in the nucleosides and also in DNA. It has been seen above that OH-radical attack gives rise to two kinds of radicals, whereby OH-addition at  $C(5)$  dominates over that at  $C(6)$ . This is also the case in 1,3-dimethyluracil [reactions (15) and (16)] where the major product is formed from the recombination of the  $C(5)$ -OH-adduct radicals [reaction (17)]. In competition, these radicals may disproportionate, thereby

yielding the hydrate and the enol form of 1,3-dimethylisobarbituric acid [reaction (18)]. The glycol is an intriguing product. It has been proposed that it could be formed in an electron transfer reaction. Due the considerable activation energies associated with solvent rearrangement in direct electron transfer reactions as compared with radical recombination reactions, it is now thought that this reaction might occur via an addition/elimination process [reactions (19) and (20)], similar to what has been found in other systems [33].

Table 3.

$\gamma$ -Radiolysis of  $N_2O$ -saturated aqueous solutions of cytosine. Products and their  $G$  values. *Source*: [30]

Product	$G / 10^{-7} \text{ mol J}^{-1}$
Dimers	3.3
5-Hydroxycytosine*	1.5
5,6-Dihydroxycytosine	0.2
5,6-Dihydro-5,6-dihydroxyuracil	0.15
6-Hydroxycytosine	0.08
5,6-Dihydro-5,6-dihydroxycytosine	0.05
Uracil	0.02
Cytosine consumption	5.8

\*some of this may be a secondary product formed in the workup through the dehydration of cytosine glycol

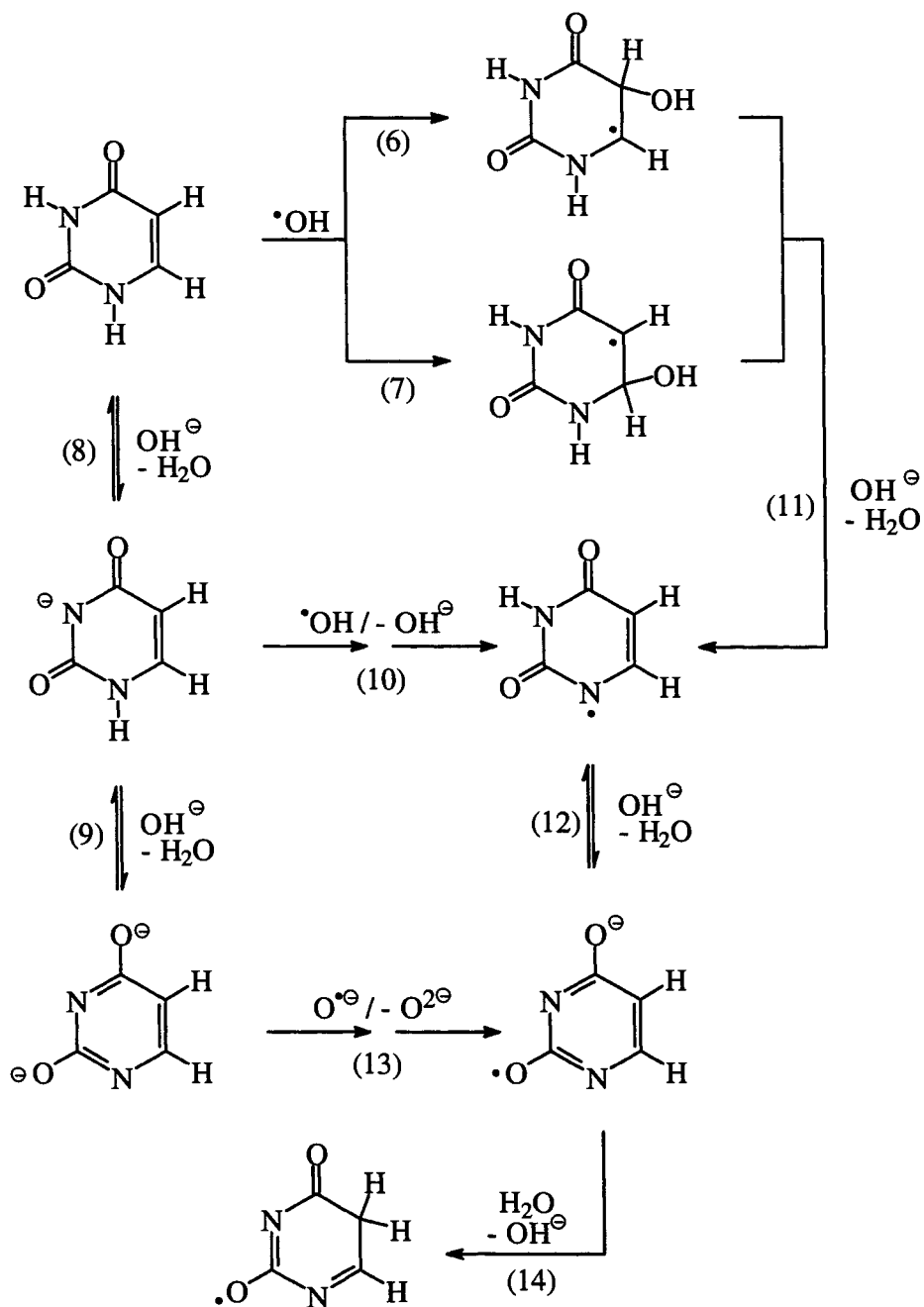
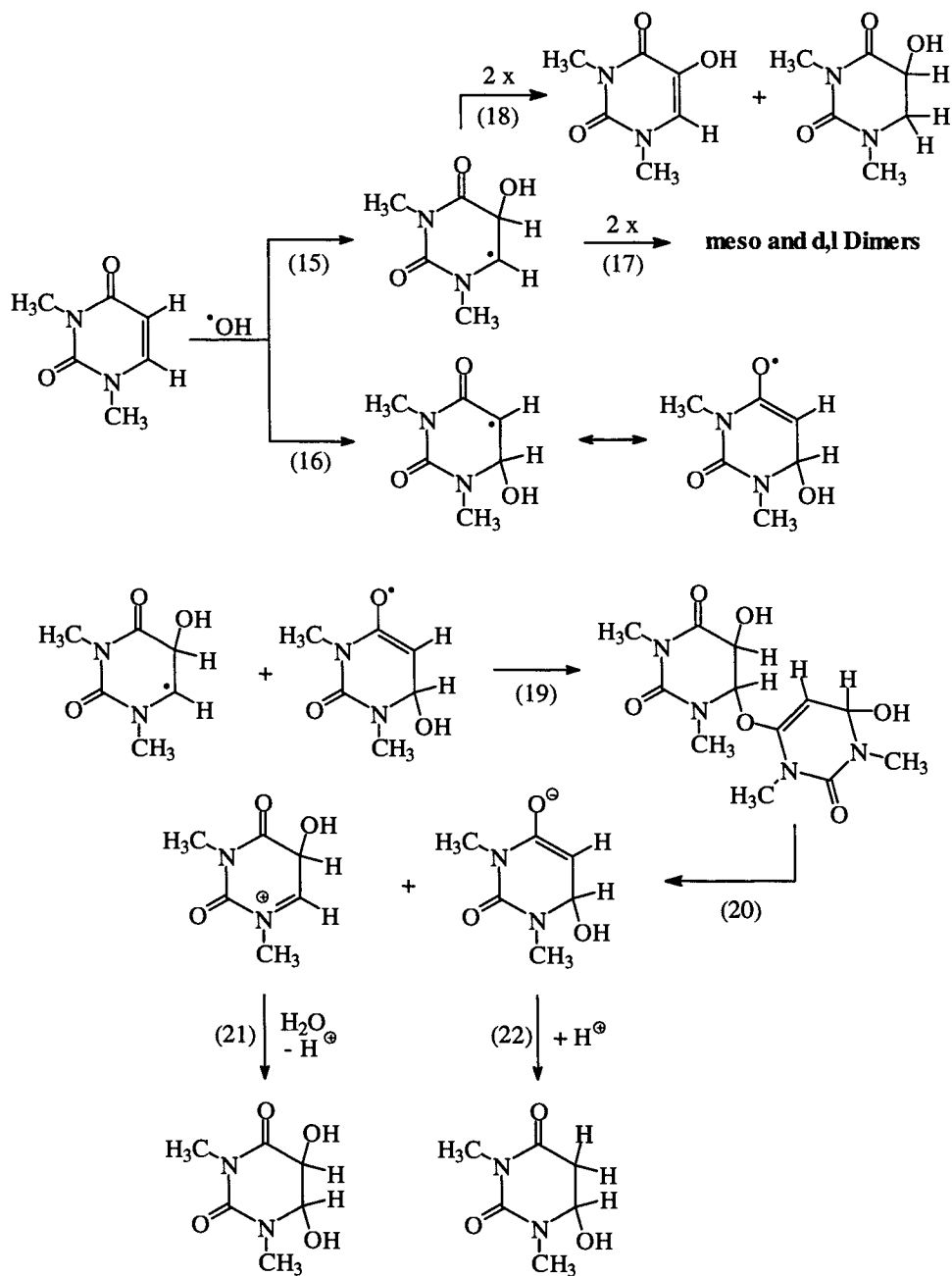


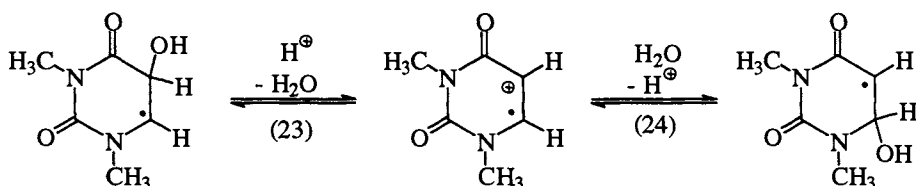
Table 4.  $\gamma$ -Radiolysis of  $N_2O$ -saturated aqueous solutions (*i.e.* OH-radical attack) of 1,3-dimethyluracil. Products and their  $G$  values in units of  $10^{-7}$  mol  $J^{-1}$ . *Source*: [26].

Product	pH 3	pH 6.5	pH 10.4
5,6-Dihydro-5-hydroxy-1,3-dimethyluracil	0.4	0.8	0.6
5,6-Dihydro-6-hydroxy-1,3-dimethyluracil	< 0.1	0.2	<0.1
1,3-Dimethylisobarbituric acid	0.15	0.1	$\leq 0.1$
5,6-Dihydro-5,6-dihydroxy-1,3-dimethyluracil	1.6	0.9	0.85
Dimers (of 6-yl radicals, in monomer units)	1.8	3.5	3.3
Dimers (involving H-adduct radicals)	<0.1	0.2	<0.1
1,3-Dimethyluracil consumption	4.0	5.9	5.3

As can be seen from Table 4, there is practically no change evident in the product yields when neutral and basic solutions are compared. However, the yield of the dimers is drastically reduced in acid solutions, while the yield of the glycol is enhanced. Altogether, the  $G$  value of consumption is also reduced which points to an increase of the importance of disproportionation reactions. This has been explained by an acid-catalyzed transformation of the reducing 6-yl radical into an oxidizing 5-yl radical [reactions (23)-(24)]. This interpretation would indicate that the oxidizing radical is thermodynamically favoured over the reducing radical.



In fact, the dominant radical seen by EPR when uracil is  $\gamma$ -irradiated in low-temperature sulfuric-acid glasses, is the 5-yl one [34], which supports this contention under the assumption that the nucleobase is not protonated under these conditions.



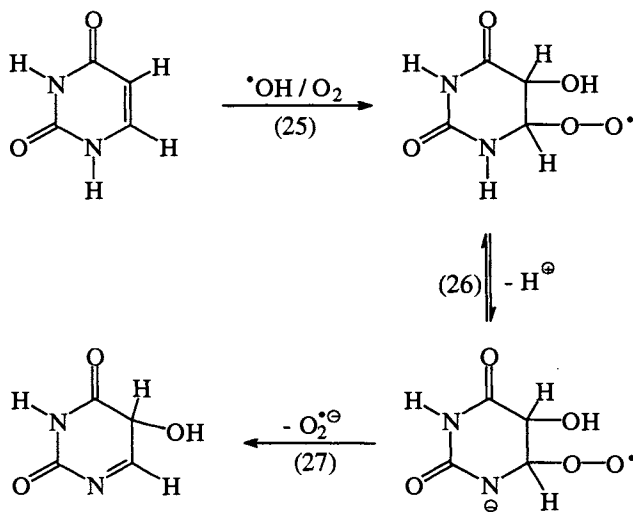
In the presence of a thiol, the OH-adduct can be reduced, the reducing C(5)-OH-C(6)-yl radical, paradoxically, apparently more readily than the oxidizing C(6)-OH-C(5)-yl one. Nevertheless, the rate of this reaction must be very slow, as in the radiolysis of  $\text{N}_2\text{O}$ -saturated solution of 5'-thymidylic acid in the presence of 5% cysteamine, thioethers *i.e.* the recombination products of a cysteamine-derived thiyl radical with a 5'-thymidylic-acid-derived OH-adduct radical, are formed with a  $G$  value as high as  $1.5 \times 10^{-7} \text{ mol J}^{-1}$  [35] in a competitive reaction [36].

#### 2.4. Products in the presence of oxygen

In the presence of  $\text{O}_2$ , most radicals are converted into the corresponding peroxy radicals [37, 38], with the notable exception of heteroatom ( $O$ ,  $N$ )-centered radicals which do not productively react with  $\text{O}_2$  at an appreciable rate [39]. In this context it should be noted that even though peroxy radical reactions may dominate in radiomimetic systems, *e.g.* the reactions induced by the autoxidation of Fe(II)EDTA or Fe(II)NTA, the subsequent reactions seem to be considerably modified by the presence of the transition metal ion, *i.e.* product ratios are found in these reactions differ from those observed under ionizing radiation in the absence of Fe(II)/Fe(III) in the case of 2'-deoxynucleosides [40]. A basis for the understanding of these differences may be in the various redox reactions that peroxy radicals may undergo with Fe(II)/Fe(III) (*cf.* [41]).

The OH-adduct radicals of the pyrimidines react with oxygen at close to diffusion-controlled rates, yielding the corresponding peroxy radicals. In basic solutions, but also in neutral solutions provided that these peroxy radicals have a sufficiently long lifetime, the C(5)-OH,C(6)-peroxy radicals can undergo superoxide elimination after deprotonation at N(1) [reactions (26) and (27)]

[42]. Details of this kind of superoxide elimination, including the determination of the  $pK_a$  value of the peroxy radical, have been elucidated in a very similar system, glycine anhydride [43]. An isopyrimidine (see below) is formed in reaction (27).



In acid solutions, but also in neutral solutions at high steady-state radical concentrations, the superoxide elimination becomes too slow compared with the bimolecular decay of these peroxy radicals [reactions (28)-(31)]. This leads to a very different product distribution, as seen in Table 5. There is evidence that in their bimolecular decay peroxy radicals can give rise to the formation of oxyl radicals which may undergo fragmentation (see, *e.g.*, [37, 38]) [*e.g.*, reaction (30)], leading to products with the pyrimidine cycle destroyed (*e.g.*, 1-*N*-formyl-5-hydroxyhydantoin). Other pyrimidine-ring cleavage reactions are conceivable but at present not supported by product data).

However, if non-tertiary, oxyl radicals in aqueous solution are capable of undergoing a rapid 1,2-H-shift [44-46] [reaction (34)] in competition with fragmentation. Then after addition of oxygen, superoxide is eliminated [reaction (36)]. Thus under these conditions also, superoxide radicals are likely intermediates which are expected to react with peroxy radicals, reducing them to the corresponding hydroperoxides. These are abundant, though somewhat unstable, products in the radiolysis of air-saturated pyrimidine solutions. They are considered to be important precursors of the pyrimidine glycols observed under various conditions [1].

Table 5.

$\gamma$ -Radiolysis of  $N_2O/O_2$ -saturated solutions of uracil ( $2 \times 10^{-4}$  mol  $dm^{-3}$ ) under various pH conditions. Products and their  $G$  values (in units of  $10^{-7}$  mol  $J^{-1}$ ). Source: [42].

Product	pH 3.0	pH 6.5	pH 10.0
5,6- <i>cis</i> -Dihydroxy-5,6-dihydrouracil	0.6	0.9 <sub>5</sub>	1.4 <sub>5</sub>
5,6- <i>trans</i> -Dihydroxy-5,6-dihydrouracil	0.5	1.1	1.0
Isobarbituric acid	0	0.2	1.2 <sub>5</sub>
1- <i>N</i> -Formyl-5-hydroxyhydantoin	1.6 <sub>5</sub>	1.4 <sub>5</sub>	0.2
Dialuric acid	0.9 <sub>5</sub>	0.4	0.2
Isodialuric acid	0.1	0.2	0.1
5-Hydroxyhydantoin	0.4	0.4	0.3
Unidentified products	0.9 <sub>5</sub>	0.6	0.9 <sub>5</sub>
Hydrogen peroxide	n.d.	3.0	n.d.
Oxygen consumption	n.d.	5.0	n.d.
Uracil consumption	5.1	5.5	5.4

n.d. = not determined

### 2.5. Formation and properties of isopyrimidines

Isopyrimidines are short-lived intermediates formed in the reactions of C(6)-radicals of pyrimidines which carry an H-atom at  $N(1)$ . Such radicals can be oxidized *via* the peroxy radical [cf. reactions (26) and (27)] but also by oxidants such  $Fe(CN)_6^{3-}$  directly to the radical cation [reactions (37) and (41)]. The isopyrimidines undergo rearrangement and hydration reactions. Some rate constants are compiled in Table 6.



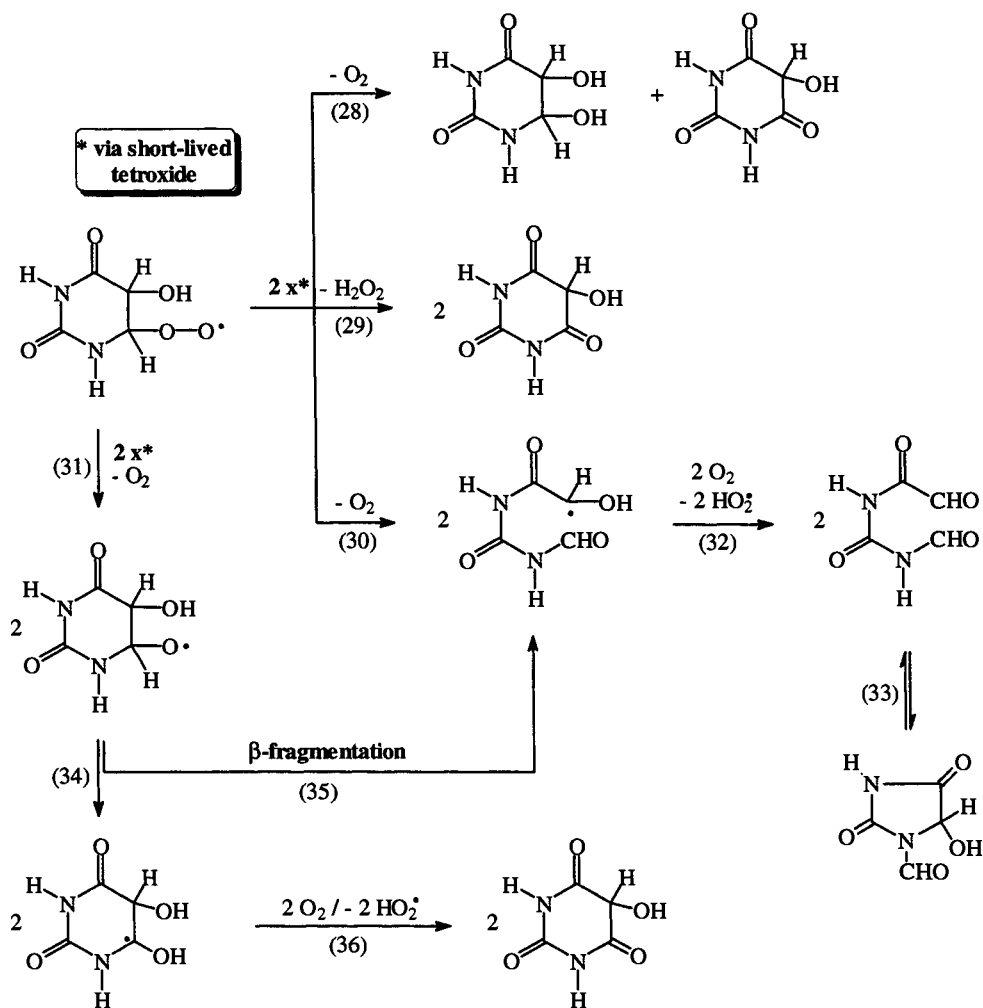


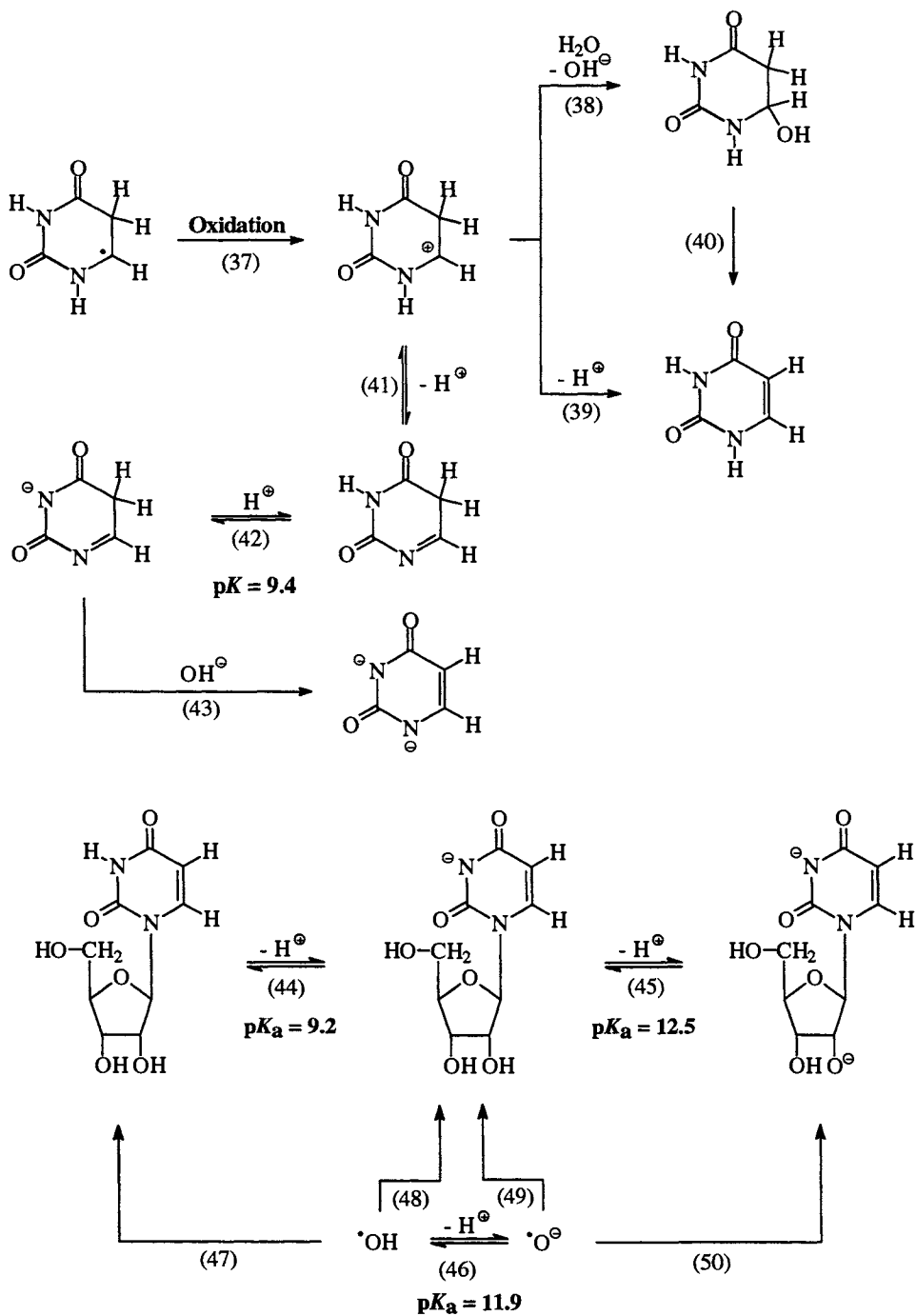
Table 6.

Rate constants of isopyrimidine  $\rightarrow$  pyrimidine rearrangements at 20 °C. *Source:* [49]

Isopyrimidine	Neutral spont. $s^{-1}$	Neutral $H^+$ -catal. $dm^3 mol^{-1} s^{-1}$	Neutral $OH^-$ -catal. $dm^3 mol^{-1} s^{-1}$	Anion spont. $s^{-1}$	Anion $OH^-$ -catal. $dm^3 mol^{-1} s^{-1}$
Isouracil	3000	$1.8 \times 10^7$	absent	50	$4.9 \times 10^5$
3-Methylisouracil	2500	$1.1 \times 10^7$	$2.7 \times 10^7$	absent	absent
5-Hydroxyisouracil	2000	$2.6 \times 10^7$	absent	< 50	$2.2 \times 10^5$

## 2.6. Reactions of the $O^-$ radical

It had been observed early on [47] that  $G(\text{base release})$  in nucleosides increases drastically at high pH, and it was suggested that this was due to a base-induced transformation of a base OH-adduct radical into a sugar-centered radical which then gave rise to the release of unaltered base. It was later [48] shown, however, that this enhancement of base release at high pH is in fact due to the involvement of the basic form of the OH radical,  $O^-$ . In contrast to the electrophilic OH radical which adds preferentially to the base moiety, the *nucleophilic*  $O^-$  radical no longer undergoes this reaction very efficiently but rather abstracts an H atom from the sugar moiety. Some of these sugar-derived radicals will release the base. Reactions (44)-(50) show the various  $pK_a$  values involved, for instance, in the uridine system.



## 2.7. The reactions with the H atom and the solvated electron

Similar to the OH radical, the H-atom acts as an electrophilic radical, and in its additions to C=C double bonds it has a preference for the electron-rich site. Thus, in the pyrimidine series an addition to the C(5)-position is the preferred reaction [*cf.* reaction (52) and Table 7]. The same kind of radical is formed by H-atom abstraction from 5,6-dihydropyrimidines [*cf.* reaction (54)][50], as can be inferred from the data compiled in Table 8. Regarding the behaviour of the H-atom-adduct peroxy radicals one would start from the dihydropyrimidines while it would be impractical to study it in the pyrimidine system.

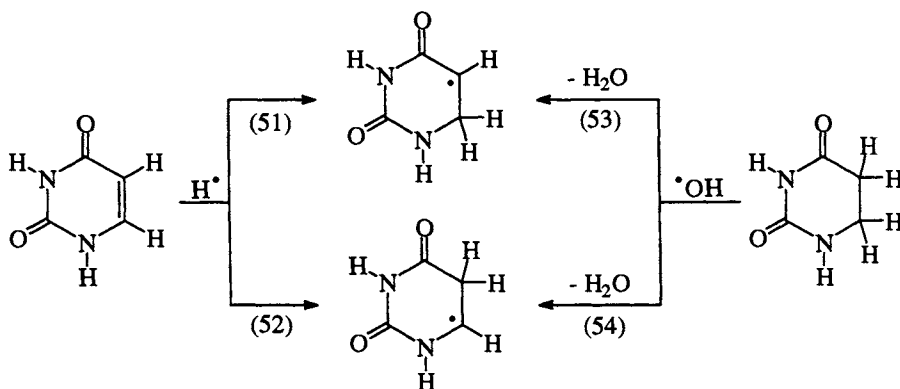


Table 7.

Sites of H-attack (in %) in uracil and some of its derivatives. *Source:* [51]

Substrate	C(5)	C(6)	Methyl group
6-Methyluracil	87	13	nil
1,3-Dimethyluracil	71	29	nil
Uracil	69	31	—
Thymine	37	59.5	3.5
Thymidine	32	62.5	5.5*
1,3-Dimethylthymine	25	73	2.0

\* including H abstraction at the carbohydrate moiety

Table 8.

Pattern of OH-radical attack (in %) on 5,6-dihydrouracil and some of its methyl derivatives. The OH-radical balance is sometimes significantly below 100%, partly due to the inefficiency of the method for the detection of oxidizing C(5)-radicals. *Source:* [50]

Substrate	C(5)	C(6)	Methyl	Total
5,6-Dihydrouracil	5	90	—	95
1-Methyl-5,6-dihydrouracil	≈ 2	61	29	92
3-Methyl-5,6-dihydrouracil	≈ 2	72	10	84
1,3-Dimethyl-5,6-dihydrouracil	≈ 2	≈ 62	30*	94
5-Methyl-5,6-dihydrouracil	4	74	6	84
6-Methyl-5,6-dihydrouracil	≈ 2	84	6	92

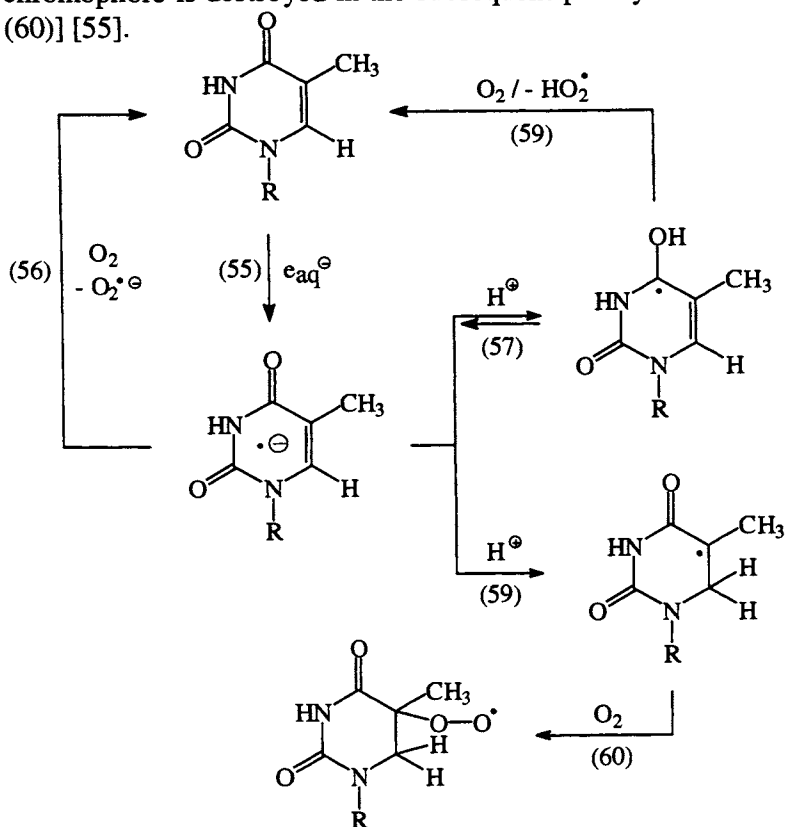
\* ≈ 22% at  $N(1)CH_3$ , 8% at  $N(3)CH_3$

Due to the much lower rate of allylic H-abstraction by the H-atom as compared to the OH radical, this process is generally of small importance (*cf.* Table 7). In so far as the base is methylated at carbon, the pattern of site preference exhibited by the H atom is influenced by the position of the methyl group in ways different from the OH radical (Table 1). It may be the effect of hyperconjugation that appears to enhance the relative attraction for the hydrogen atom to become attached, *cf.* the pronounced preference for addition at C(5) in 6-methyluracil, and the reversal of the preference in thymine, as compared to uracil.

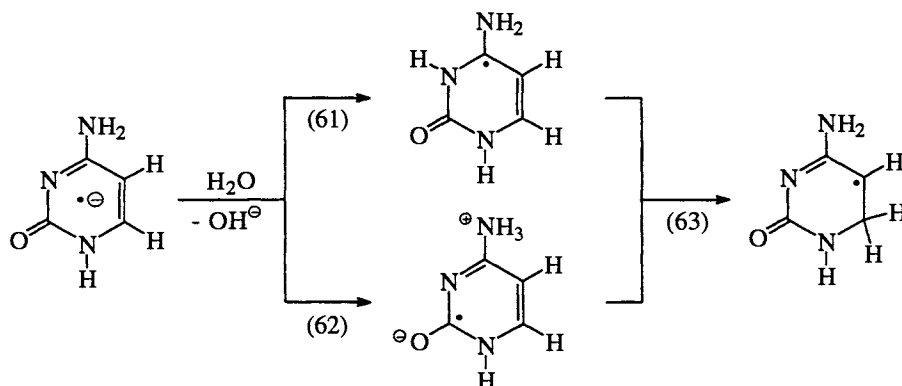
The pyrimidines react with the solvated electron at practically diffusion-controlled rates. The ensuing reactions are well understood in uracil and thymine, while in the case of cytosine more questions remain unresolved.

Thymine and uracil behave similar to typical carbonyl compounds, *i.e.* the first intermediate is a radical anion [reaction (55)] which is in equilibrium with its oxygen-protonated conjugated acid [reaction (57)]. The other functional groups, especially the second carbonyl function, withdraw electron density, and hence the  $pK_a$  values of these oxygen-protonated radical anions are much lower (thymine:  $pK_a = 6.9$  [52]) than those of the corresponding radicals from simple carbonyl compounds. However, the C(6)-protonated isomers [*cf.* reaction (58)]

are thermodynamically more stable. Since protonation at carbon is usually a much slower process than protonation at a heteroatom, the conversion of the radical anion and its oxygen-protonated conjugate acid into the carbon-protonated acid [reactions (57) and (58)] can be observed on the pulse radiolysis time scale only when sufficient buffer is added to speed up the protonation/deprotonation reactions [53, 54]. Upon the change of the protonation site, the redox properties of the radicals change dramatically. While the radical anions and their conjugate, *oxygen*-protonated acids are good reducing agents, the C(6)-protonated electron adduct has oxidizing properties. This is also reflected in the way they react with oxygen. The radical anion and its conjugate, *oxygen*-protonated acid rapidly eliminate superoxide, thereby restoring the pyrimidine [reactions (56) and (59)] [55]. On the other hand, when oxygen reacts with the C(6)-protonated electron adducts, the pyrimidine chromophore is destroyed in the subsequent peroxy radical reactions [reaction (60)] [55].



The cytosine electron adduct is rapidly protonated by water [reactions (61) and/or (62);  $t_{1/2} \leq 200$  ns [56];  $t_{1/2} \leq 20$  ns [57]], either at *N*(3) at or at the amino group [58, 59].



The resulting heteroatom-protonated electron adduct(s) must have a  $pK_a$  value  $\geq 11$ , as shown by conductance measurements in pulse radiolysis [56]. The absence of any noticeable change in the absorption spectrum of the (protonated) electron adduct of cytidine in the pH range 6-13 suggests that its  $pK_a$  value is even larger than 13 [60]. Like the situation in the corresponding thymine system, the heteroatom-protonated species is thermodynamically disfavoured and subsequent (irreversible) protonation occurs at carbon [reaction (63)], albeit with a rate constant too low [61] to be measured by pulse radiolysis.

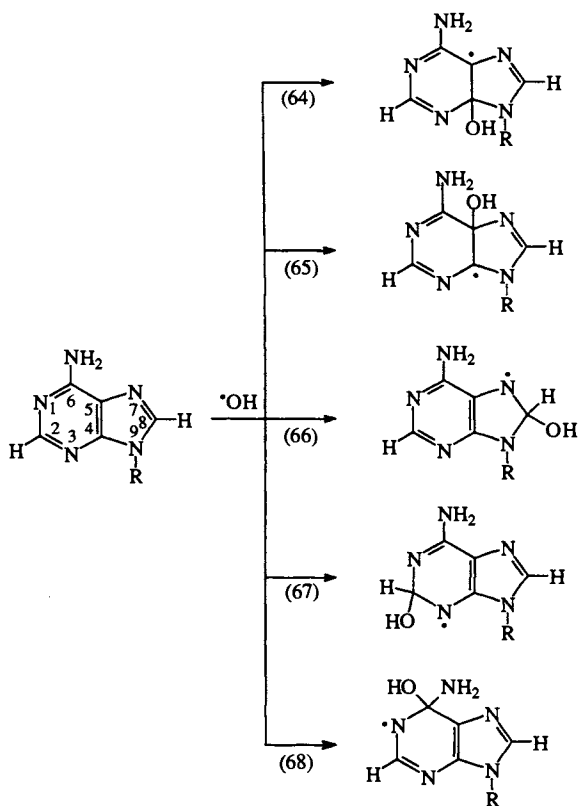
### 3. PURINES

#### 3.1. The reactions of the OH radical

Just as in the case of the pyrimidines, OH-radical attack is by addition to a ring double bond targeting a carbon atom (but not the guanine carbonyl carbon), to the practical exclusion of H-atom abstraction reactions. However in the purines, the relative importance of the target sites is more difficult to assess for two reasons. First, the five (adenine) or four (guanine) OH-adducts that are formed in reactions (64)-(72) do not show a pronounced difference in their redox behaviour as the two (for each) pyrimidine-derived ones do.

Also in these larger and highly-conjugated systems, mesomerism tends to "smear out" the radical site more across the molecule [just one representative is written out in each of the reactions (64)-(72)]. In addition, the OH-adducts can

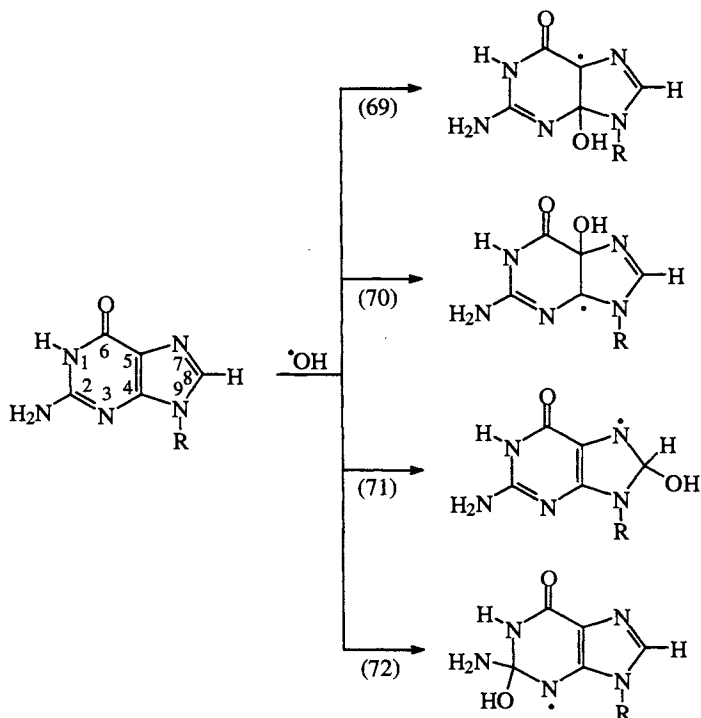
undergo a number of rapid water-elimination and ring-opening reactions. It has been suggested [5, 62-64] that in the case of 2'-deoxyadenosine, 30% add to the C(4) position, 37% to the C(8) position [reactions (64) and (66)] while for guanine the corresponding yields are reported at 50% and 16% [reactions (69) and (71)]. The ammonia yields determined right after irradiation in  $N_2O$ -saturated solutions suggest that OH-addition at C(6) in 2'-deoxyadenosine [reaction (68)] and at C(2) in 2'-deoxyguanosine [reaction (72)] should not materially exceed 1% in 2'-deoxyadenosine (2% after heating), or 0.5% in 2'-deoxyguanosine (1.5% after heating) [65]. It must be noted that some of the product data reported in the literature refer to products that are apparently formed in a complex sequence of reactions whose conditions may in practice not have been precisely controlled. Therefore it cannot be ruled out that these values may have to be revised as more information becomes available.



The reactivity of adenine, adenosine, and guanosine toward  $\cdot O^-$  is reported to be almost an order of magnitude smaller than that of OH [66], paralleling the

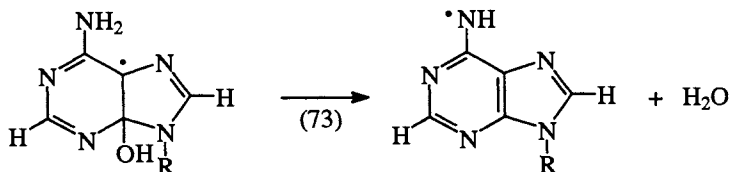


behaviour observed in the pyrimidines [48]. In adenine (which exists as the anion under these conditions), the lower tendency of  $\cdot\text{O}^-$  to add to a double bond appears to make H-atom abstraction at the amino group somewhat competitive.

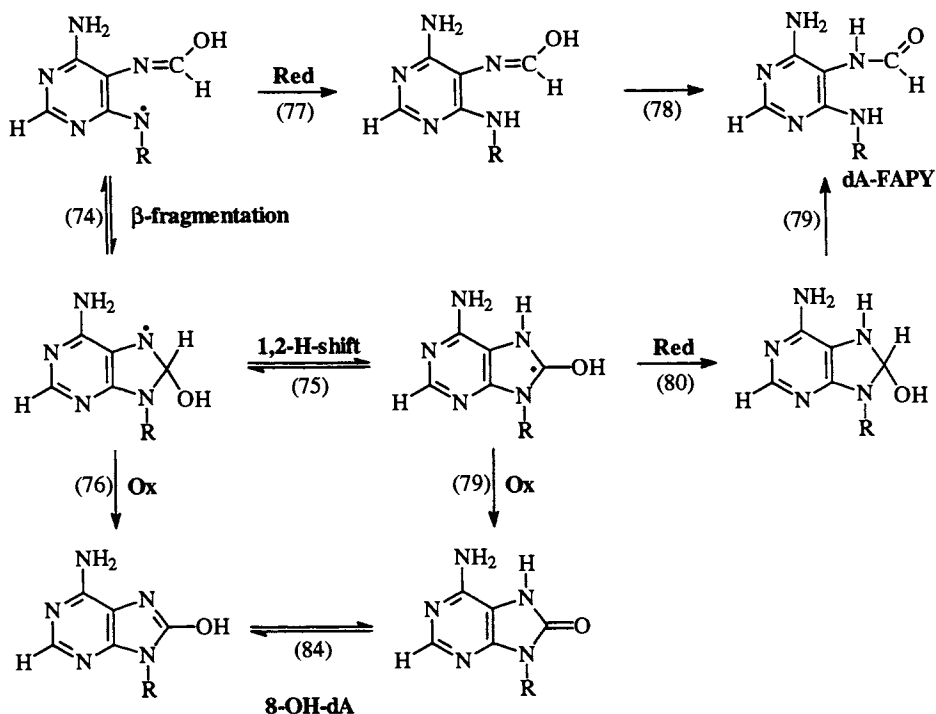


### 3.2. Water elimination and rearrangement reactions

While OH radicals readily add to double bonds, they undergo electron transfer reactions with reluctance. This implies that, since there is evidence that heteroatom-centered radicals are formed from guanine and adenine derivatives (see also below), the precursor of the intermediates must under these conditions be an OH-adduct radical rather than the radical cation. Rapid transformation has been observed with adenosine and guanosine. Part of this is attributed to solvent-catalyzed water elimination such as in reaction (73) [5]. In the case of acid catalysis, the intermediate is a radical cation (see below). It can be seen that OH-adducts with OH attached in several different positions lead to a single anhydro radical.



It appears that the OH-adduct radicals to the pyrimidinic cycle are denied the option of undergoing fragmentation of the purine skeleton since this would require the transformation of a  $\pi$  radical into a  $\sigma$  radical.



This barrier does not exist for the C(8)-OH adduct [cf. reaction (74)]. This radical can moreover undergo the 1,2-H-shift reaction (75), leading to a species whose reduction [reaction (80)] gives rise [reaction (79)] to a product that can hydrolyze to an amino-formamidopyrimidine, FAPY. These are well-documented purine radiolysis products. In the presence of an oxidant, e.g.  $\text{Fe}(\text{CN})_6^{3-}$ , these transformation reactions (ring-opening and/or 1,2-H-shift) can

be suppressed [*e.g.* reactions (76) and (79)]. The resulting product is the corresponding 8-hydroxypurine derivative. In the case of 2'-deoxyguanosine, the maximum attainable yield of the 8-hydroxy compound ( $G = 1.3 \times 10^{-7} \text{ mol J}^{-1}$ ) is reached in the presence of  $5 \times 10^{-4} \text{ mol dm}^{-3} \text{ Fe(CN)}_6^{3-}$  in  $\text{N}_2\text{O}$ -saturated solutions in the acid pH range [67], in fair agreement with the aforementioned proportion of 16 per cent estimated for the C(8)-OH adduct. Apparently, oxygen does not oxidize the intermediate radicals in the same way since the yield of 2'-deoxy-8-hydroxyguanosine remains comparatively low (at  $2.5 \times 10^{-4} \text{ mol dm}^{-3} \text{ O}_2$ ,  $G = 0.3 \times 10^{-7} \text{ mol J}^{-1}$ ) under otherwise equal conditions (but increases toward neutrality) [67].

### 3.3. Products in the absence of oxygen

The product yields that are observed in the absence of oxygen are usually quite low (there are exceptions under certain conditions, see below), and an adequate material balance has not been established (*cf.* Table 9), in contrast to the situation in the case of pyrimidines, *e.g.* uracil. Typically, much less than 50% of the primary OH radicals can be accounted for by corresponding purine-derived products. Dehydrodimers have never been observed. In our laboratory it has been observed that in the case of 2'-deoxyguanosine during analysis, the HPLC column tends to clog up after injection of irradiated samples, possibly by accumulating oligomeric material on the surface on the chromatographic support. Also, the very low 2'-deoxyguanosine-consumption  $G$  value of  $1.6 \times 10^{-7} \text{ mol J}^{-1}$  suggests that in this case, large-scale restitution of substrate accompanied by the sacrificial destruction of some product(s) is taking place during the irradiation.

The formation of 2'-deoxy-5',8-cyclonucleosides (and 5',8-cyclonucleotides from nucleotides *cf.* [68-75]) and compounds such as the 5'-aldehydes [these are "two-electron-oxidized" with respect to the starting nucleoside *cf.* reactions (85) - (87)] derived from the purine 2'-deoxynucleosides, has traditionally been explained by assuming a primary OH-attack at the sugar moiety, *i.e.* at C(5'). However, recent studies [75, 76] on 2'-deoxyadenosine have shown that it is essentially base-sited radicals that are the precursors of the 5'-radicals. The way to these products is by no means straightforward. Their yields appear strongly pH-dependent; they peak at  $G$  values of about  $3 \times 10^{-7} \text{ mol J}^{-1}$  near pH 9.5 and sharply drop towards higher pH [75, 76]. Remarkably, at pH 9.5 the consumption of 2'-deoxyadenosine is twice the primary OH-radical yield [67] which implies damage amplification. The behaviour of the yields as the pH is changed over the range from acidic to neutral suggests that a reactive intermediate forms a complex (base-stacked, hydrogen-bonded ?) with the

substrate whose stability and conformation is strongly affected by protonation equilibria. The surprising finding that in its maximum the yield of these two products combined approaches the OH-radical yield implies that the base-radical attack takes place practically exclusively at C(5') even though radical transfer is thought to be intermolecular not intramolecular as the 2'-deoxyadenosine disappearance is double that of the OH yield. These are preliminary results of a study which is underway [76]. The reduction products have so far not been tracked down.

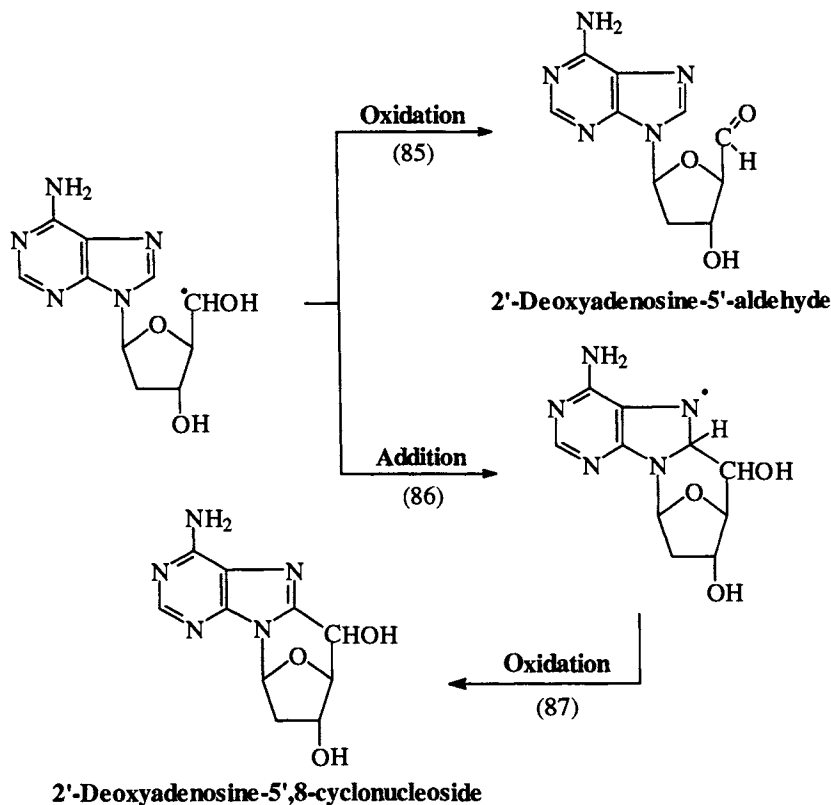


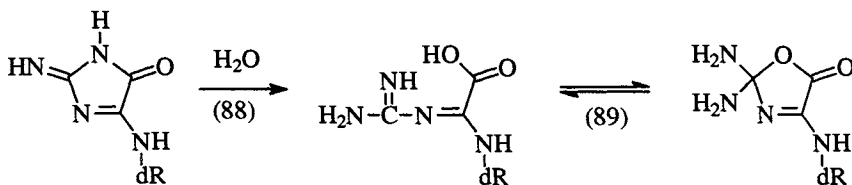
Table 9.  $\gamma$ -Radiolysis of 2'-deoxyguanosine ( $5 \times 10^{-3}$  mol dm<sup>-3</sup>) in deaerated and N<sub>2</sub>O-saturated solutions. Products derived from an attack at the base and their G values (in units of 10<sup>-7</sup> mol J<sup>-1</sup>). *Source*: [77]. Products involving initial attack at the sugar moiety have been omitted.

Product	N <sub>2</sub>	N <sub>2</sub> O
N <sup>6</sup> -(2'-Deoxyribo)-2,6-diamino-5-formamidopyrimid-4-one (FAPY)	0.36	0.36
5'-8-Cyclo-2',5'-dideoxyguanosine	0.05	0.06
8-Hydroxy-2'-deoxyguanosine	-	0.25
9-(2'-Deoxy- $\beta$ -D- <i>erythro</i> -pento-1',5'-dialdo-1',4'-furanosyl)-guanine	0.07	0.08
2'-Deoxyguanosine consumption	0.83	1.6

### 3.4. Products in the presence of oxygen

Owing to the possibility of water elimination from the OH-adduct radicals, one expects the formation of two families of peroxy radicals. At sufficiently high oxygen concentrations, the OH-adduct radicals can in principle be intercepted by oxygen. But the reactivity toward oxygen of both the OH-adducts and their dehydrated offspring is more or less diminished, even to the limit of apparent non-reactivity, by the fact that by mesomerism each of them exhibits heteroatom-centered-radical character (a similar situation exists in, *e.g.*, phenoxy radicals [38]). Reversibility of oxygen addition [78] may also play a role. The peroxy radicals that *do* eventually form have the possibility to intramolecularly add to a double bond, with subsequent fragmentation of this endoperoxide radical species. Repetition of the sequence of peroxy radical formation and fragmentation leads to the progressive degradation, or rearrangement, of the purinic skeleton. Bimolecular reactions of the peroxy radicals may give rise to oxyl radicals which may similarly undergo fragmentation. It is apparent that the number of conceivable products is large, which contributes to the difficulty of achieving a satisfactory elemental balance.

The radiation chemistry of these oxygenated systems is therefore complex. One of the products, a triaminooxazolone compound, has been identified in the degradation of 2'-deoxyguanosine [79-81].

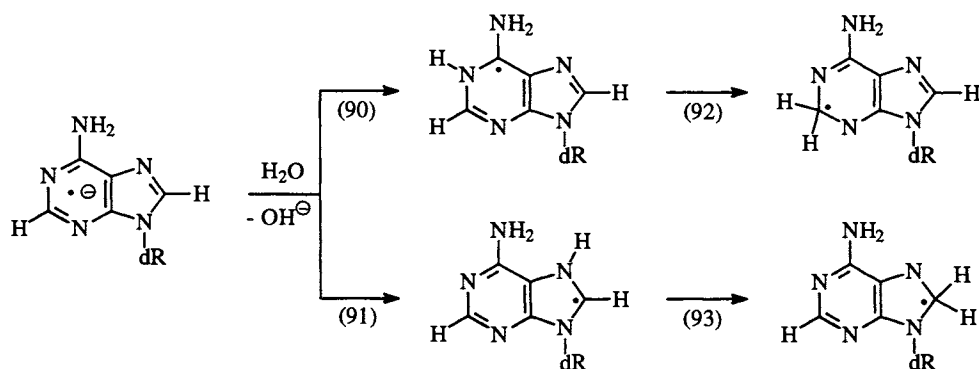


The mechanism leading to this product is not understood. Its formation is suppressed by  $\text{Ti}^+$  [82] which captures the OH radical; the  $\text{Ti}^{2+}$  then oxidizes the guanine moiety to the radical cation. Thus the latter, or the ensuing heteroatom-centered radical, cannot be this product's precursor. Superoxide is required as the formation of the product is suppressed in the presence of superoxide dismutase. The maximum yield, about 1/6 of the OH-radical yield [82], is obtained in  $\text{O}_2$ -saturated solutions where both OH-adduct radicals and superoxide are abundant. In this context it is of interest to note that the  $\text{O}_2$ -consumption [83] induced by the guanine OH-adduct radicals is low under the experimental conditions employed. The drastic pH dependence of the yields of certain products *in the absence* of oxygen (that can be quite high, see preceding section), suggests that the pH should be an important parameter in oxygenated solutions as well.

### 3.5. Reactions with the solvated electron and the H atom

The solvated electron and the H atom both react at close to diffusion-controlled rates. The properties of the radical anions of the purines formed by their reaction with the solvated electron are very different from those of *e.g.* the thymine radical anion, but show some resemblance to those of the cytosine radical anion. The radical anion is in equilibrium with its conjugate acids, *i.e.* various radicals tautomeric with the purine H-atom adducts, with one or the other of them predominating. Protonation is usually fastest at the position of a heteroatom [84-89]. This does not rule out further fast proton transfer from heteroatom to carbon [88]. For example, the 2'-deoxyadenosine radical anion protonates with a rate of at least  $1.4 \times 10^8 \text{ s}^{-1}$  [85] at a heteroatom, *e.g.* reactions (90) and (91) (note that protonation can also occur at other nitrogen atoms). Base radical anions and also their heteroatom-protonated conjugate acids have reducing properties and thus react readily with oxidants such as *p*-nitroacetophenone [84] and methylviologen [87]. Interestingly, the oxidation by *p*-nitroacetophenone does not fully restore 2'-deoxyadenosine, but a product is formed of a  $\text{pK}_a$  of 8.8. It has been suggested that this product might be formally a hydrate of the substrate [84]. Regarding the transient, it had been observed

early on in pulse-radiolytic studies of the reaction of purines with the solvated electron that there is a considerable change in the recorded UV absorption spectra which occurs toward high pH near pH 10.5 [90]. That this is not due to a deprotonation reaction was eventually proved by pulse radiolysis using conductometric detection, where it was established that this does not involve a change of the charge status of the transient [84]. This suggested a rearrangement of a heteroatom-protonated radical anion into a carbon-protonated radical anion [reactions (92) and/or (93)] which is apparently favoured on thermodynamic grounds.



In guanosine after the rapid protonation of the electron adduct by water [86, 88] at the heteroatom [at O<sup>6</sup>, N(3) or N(7);  $k \geq 10^7 \text{ s}^{-1}$ ], a rapid transformation occurs which is catalysed by phosphate buffer and which has been attributed to a protonation at C(8) [88]. This assignment is based upon solid-state EPR data [91], where the C(8)-H-adduct radical appears as the thermodynamically most stable H-adduct radical. The high solvent-kinetic-isotope effect of  $k_{\text{H}}/k_{\text{D}} = 8$  is a strong indication that a proton is transferred in the rate-determining step. The magnitude of the rate of phosphate buffer catalysis points to a protonation at carbon (for a similar reaction observed with the thymine radical anion see above). Other purines, *e.g.* hypoxanthine/inosine, behave in a similar way [89].

Little is known about the reactions of the H atom in the purine systems. However, being an electrophilic radical also, the position-specificity for the addition of the H atom is expected to be similar to that of the OH radical in so far as the carbon atoms of the purine skeleton are concerned. In contrast to the OH radical, however, the H atom may in principle also attach to a ring imino nitrogen atom even though this mode of reaction is apparently of minor importance. Also, it should be emphasized that on a pulse radiolysis time scale the

group of H-atom adducts is not identical as to the structure and the relative quantitative importance of its members, with the group of the protonated electron adducts. An approach similar to the one taken in the pyrimidines which have a single reactive double bond, *viz.* to produce these species by H-atom abstraction from dihydropurines, is infeasible as the various dihydropurines are practically unavailable.

## 4. NUCLEOBASE RADICAL CATIONS

### 4.1. Formation of radical cations

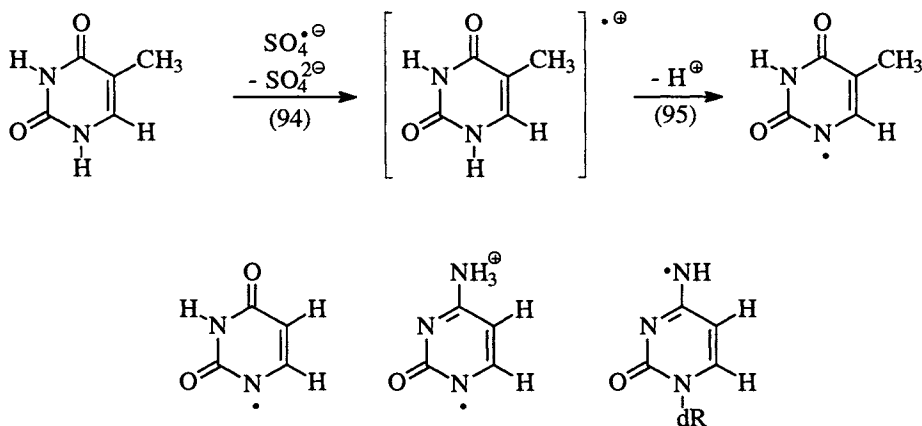
In this context, in the narrow sense the term nucleobase radical cation signifies a species identical to that which is produced upon one-electron oxidation of the base. Its deprotonation leads to a radical whose unpaired spin is largely heteroatom-sited. Reprotonation of this radical could in principle give rise to radical cations that are not identical but tautomeric to the original radical cation.

Radical cations are the primary products when the energy of ionizing radiation is deposited in the DNA molecule ("direct effect"). For this reason, their chemical behaviour is of considerable interest. In aqueous solution, nucleobase radical cations, or their conjugate bases, may be produced by hydroxide, or water, elimination from the OH-adduct radicals. The method of choice to produce them for the purpose of their study is to react the nucleobases or their derivatives with strongly oxidizing radicals. The rate of reaction of the strongest of their number which is at the same time easy to utilize in aqueous solution,  $\text{SO}_4^{\cdot-}$ , with them is fast in all cases, while less strongly oxidizing radicals may only react with nucleobases that have a relatively low oxidation potential, notably guanine. In the reactions of these oxidizing radicals, short-lived adducts may be formed as intermediates, and it cannot therefore always be strictly ruled out that processes observed at very short times and attributed to the reactions of radical cations, may in fact be due to such intermediates. Stable sulfate-adduct radicals have been observed the case of the reaction of sulfate radicals with maleic acid [92]. Radical cations are also assumed to be intermediates in the reactions of photosensitization reactions with menadione [93-95] and riboflavin [79]. Obviously, photoionization (*e.g.* by 193 nm light) and laser multi-photon excitation will equally lead to such species [96-98].



## 4.2. Pyrimidines

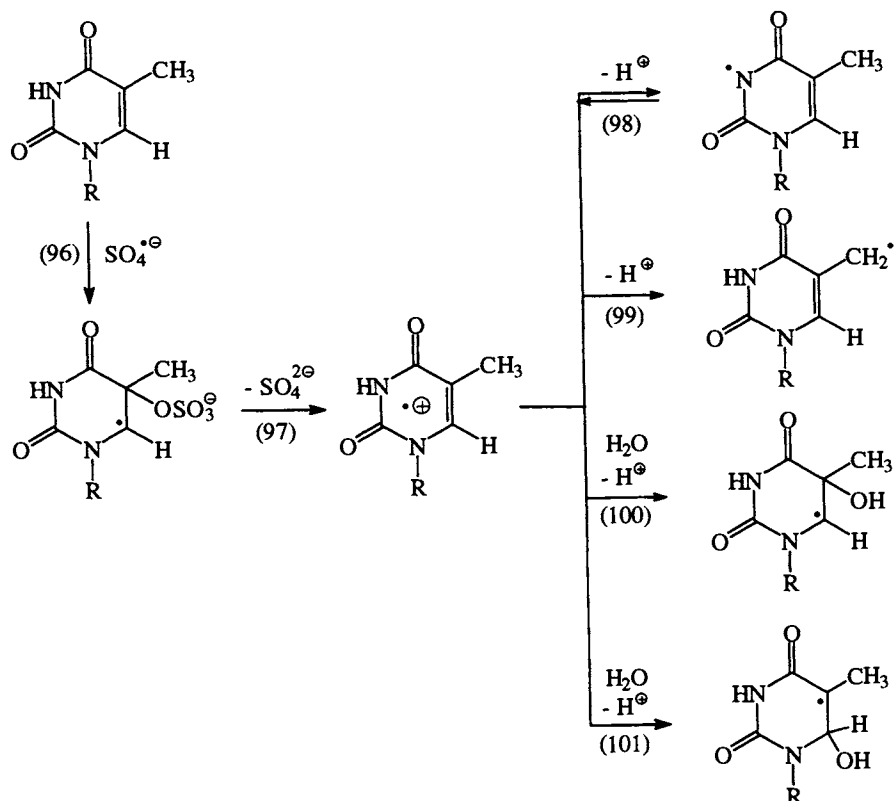
The observation of heteroatom-centered radicals by EPR from the nucleobases uracil, thymine [*cf.* reactions (94) and (95)], cytosine [23, 99] as well as 2'-deoxycytidine [21, 99] is evidence that a radical cation is indeed a likely intermediate in the reaction of the sulfate radical with pyrimidines.



As an electrophile, the sulfate radical adds preferentially to an electron-rich position of the substrate, C(5) in the case of pyrimidines [reaction (96)]. It is generally thought that the transformation of the pyrimidine-sulfate-radical-adduct into the radical cation [*e.g.* reaction (97)] is fast (the pyrimidine sulfate-radical adduct has escaped detection by EPR), and that the transient accessible to observation is the radical cation [100], even though evidence has recently been claimed [101] for a relative longevity of some sulfate-radical adducts which are thought to mimic the behaviour otherwise expected of the pyrimidine radical cations (*e.g.*, strongly-oxidative behaviour, non-reactivity toward oxygen). Crucially in this context, in the presence of phosphate anion the phosphate-adduct radical is formed [102] when the reaction is initiated by the sulfate radical. This strongly suggests the intermediacy of a radical cation to which the phosphate ion attaches.

Behaviour similar to that of  $SO_4^{\bullet-}$  is expected of the phosphate radical anion. In the latter case, however, an adduct radical *is* observed by EPR. The fact that this is the C(6)-adduct not the C(5) one was explained through the assumption that a rapid 5,6-shift follows the initial addition at C(5), which leads to the thermodynamically more stable C(6)-phosphate adduct [102]. At pH > 6.5 the

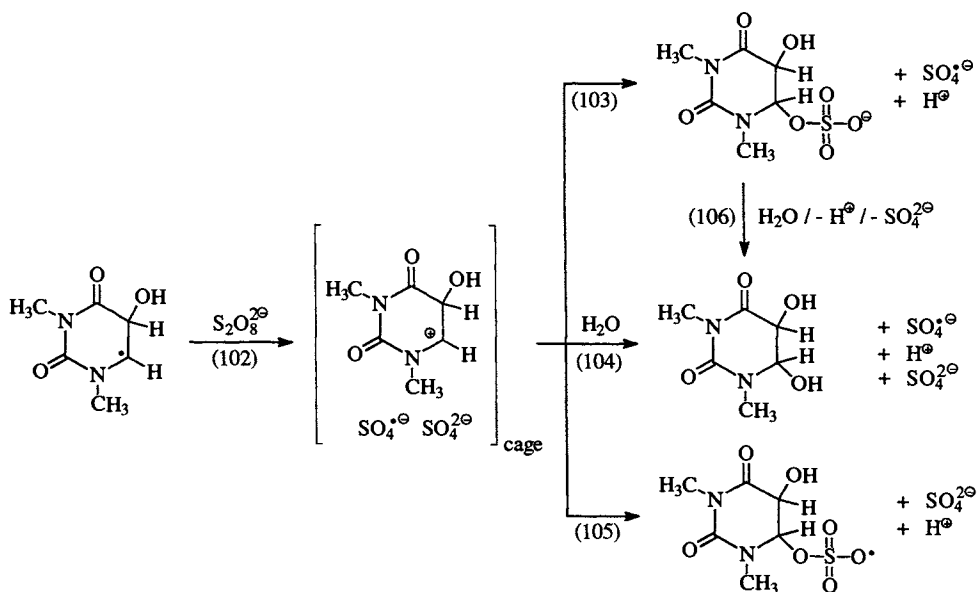
5,6-shift is sufficiently slow to allow the interception the C(5)-phosphate adduct by a spin trap [103].



Pulse radiolysis shows that the pyrimidine radical cations are fairly strong acids and rapidly deprotonate at a heteroatom [reaction (98)]. As protonation/deprotonation reactions at heteroatoms are easily reversible, the radical cations are regenerated upon reprotonation. Deprotonation at carbon or reaction with water yields the final free-radical products [reactions (99) - (101)]. It is noted that in thymidine [23] and 5'-thymidylic acid [104] the allylic thymine radical is observed by EPR and there is very little question that its precursor is the thymine radical cation. The identification of the C(6)-OH-5-yl radical by EPR supports the view [100] that reaction with water competes with the deprotonation at methyl. Due to the ready oxidation of the (reducing) C(5)-OH-6-yl by peroxodisulfate, this type of radical is only observed at low peroxodisulfate concentrations in these systems, *i.e.* the (oxidizing) C(6)-OH-5-yl radicals are correspondingly enriched under conditions favourable to a chain reaction [22]. In the case of 1,3-dimethyluracil the interesting characteristics of

this kind of chain reaction have been closely investigated [105]. It is nearly independent of the peroxodisulfate concentration, but shows a marked dependence on the 1,3-dimethyluracil concentration. Thus it appears that the rate determining step, *i.e.* the reaction of the reducing C(5)-OH adduct radical with peroxodisulfate ( $k = 2.1 \times 10^5 \text{ dm}^3 \text{ mol}^{-1} \text{ s}^{-1}$ ), does not just yield exclusively sulfate, the glycol (*via* hydrolysis of the ensuing carbocation) and a new sulfate radical (the trivial case, *cf.* [106, 107]), but that a "sluggish" radical is created as well. In the case of 1,3-dimethyluracil this suggests that the 1,3-dimethyluracil carbocation, the sulfate radical and the sulfate dianion, formed within the cage [reaction (102)], have three options to react.

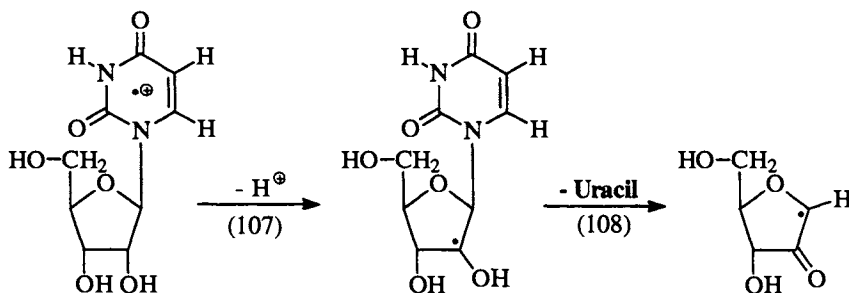
The carbocation may recombine with either of the two anions or react with water [reactions (103)-(105)]. When the carbocation combines with the sulfate radical [reaction (105)], an oxidizing species is formed which, however, is not as reactive as the sulfate radical but nevertheless contributes to the propagation of the chain with a slow rate ( $k = 1.2 \times 10^4 \text{ dm}^3 \text{ mol}^{-1} \text{ s}^{-1}$ ), and thus the chain length becomes dependent on the 1,3-dimethyluracil concentration.



In the case of 1,3,6-trimethyluracil, the same type of chain reaction is observed [108] with one minor difference: while in 1,3-dimethyluracil the glycol is the only pyrimidine chain product, there are *two* chain products in 1,3,6-trimethyluracil, namely the glycol and 1,3,6-trimethylisobarbituric acid, formed

in a ratio of 2:1. The latter is believed to arise from the glycol monosulfate by the elimination of  $\text{H}_2\text{SO}_4$ . It is noted that a deprotonation at C(6)-methyl does not take place, in contrast to the situation in 1,3-dimethylthymine (C(5)-methyl) and other thymine systems discussed above. In pulse radiolysis upon sulfate radical attack on uridine and its derivatives (but not with 2'-deoxyuridine), UV-spectral behaviour is observed [109] that is untypical for sulfate radical reactions with pyrimidine bases. On the basis of EPR experiments [23, 104] these observations can be interpreted by an intramolecular H-transfer and deprotonation, giving rise to the C(2')-radical [reaction (107)] and corresponding base release [reaction (108)].

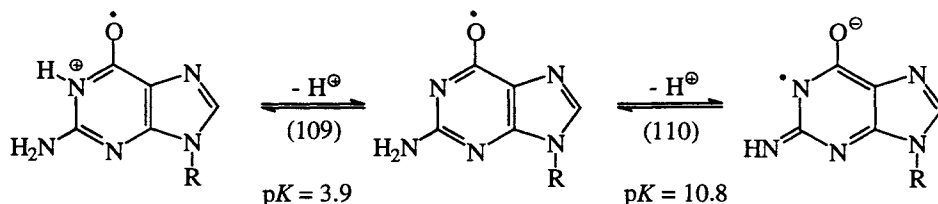
This type of reaction occurs with even higher yields in the case of cytidine [99]. As in other cases, in the presence of peroxodisulfate the reaction turns into a chain reaction, and base release yields strongly depend on the dose rate [110]. However, with 2'-deoxyuridine and thymidine, the C(5)-OH-6-yl radicals are observed upon sulfate-radical attack whereas with 2'-deoxycytidine an N-centered radical is formed. [21, 99]



### 4.3. Purines

Among the nucleobases, guanine has the lowest ionization potential [111] and hence is most readily oxidized. This is of importance in DNA where the "positive hole" created in the direct effect tends to become localized at a guanine moiety. One-electron oxidation of guanine (neutral base) is achieved by the usual oxidants such as  $\text{Ti}^{2+}$ ,  $\text{SO}_4^{\ominus}$  and  $\text{Br}_2^{\ominus}$  and produces the radical cation. Weaker oxidants such as  $\text{N}_3^{\cdot}$  [112] and the dimeric tetramethylthiourea radical cation [113] are capable of oxidizing guanine only at high pH, *i.e.* in its anionic form, and produce the guanyl radical. It is likely that depending on the nature of the oxidant, oxidation can take place by direct electron transfer as well as by addition-elimination. The radical cation formed in these reactions is an acid [114] ( $\text{p}K_a = 3.9$ ; [115] and readily deprotonates at a heteroatom to yield the corresponding neutral radical [equilibrium (109)]. Since the parent compound

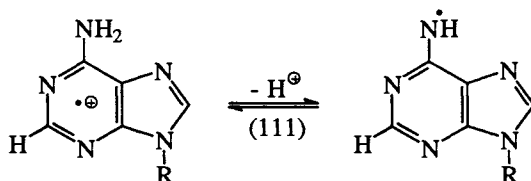
deprotonates at  $N(1)$  ( $pK_a = 9.4$ ), it is not unlikely that the radical cation deprotonates at the same position. At high pH the neutral heteroatom-centered radical deprotonates further [equilibrium (110),  $pK_a = 10.8$  [116]].



The guanyl radical is readily reduced by electron donors such as  $N,N,N',N'$ -tetramethyl-*p*-phenylenediamine, ascorbate, ABTS [117] or bisbenzimidazole derivatives, *e.g.* the *Hoechst* group of fluorescent dyes [118]. The good linear relationship between the rate of electron transfer from the reductant to the heteroatom-centered guanyl radical is evidence [117], but not proof (*cf.* [119, 120]) that this reaction proceeds *via* an outer-sphere electron transfer. At high pH, when the guanyl radical is deprotonated, poorer reductants no longer are capable of reducing this intermediate [117]. As an important facet of guanine free-radical chemistry, at around pH 10 the guanyl radical derived from 2'-deoxyguanosine is not stable and slowly decays by a unimolecular process (in competition with its bimolecular decay) [110, 112]. The products of this reaction are unknown. The guanine radical cation ( $pK_a = 3.9$ ) is a weaker acid than the protonated parent ( $pK_a = 2.4$ ) but a stronger one than its corresponding neutral parent ( $pK_a = 9.4$ ).

Due to the high spin density at the heteroatoms and a correspondingly low one at carbon, the guanyl radical does not react with  $O_2$  on the pulse radiolysis time scale [75]. This low reactivity is further supported by the observation that even at the low dose rates of  $\gamma$ -radiolysis there is merely a small uptake of  $O_2$  [ $G(-O_2) = 0.7 \times 10^{-7} \text{ mol J}^{-1}$ ] when the heteroatom-centered 2'-deoxyguanosine radicals are generated by  $Tl^{2+}$  in  $N_2O/O_2$ -saturated solution [121].

Adenine has a considerably higher oxidation potential than guanine [111], and for this reason it is not as readily oxidized, even by strongly oxidizing radicals,  $SO_4^{\cdot-}$  excepted. The  $pK_a$  of the adenine radical cation, at less than 1 [5], lies below that of its guanine analogue.



**REFERENCES**

1. R. Téoule and J. Cadet, in: *Effects of Ionizing Radiation on DNA*, A.J. Bertinchamps, J. Hüttermann, W. Köhnlein and R. Téoule (eds.), Springer, Berlin, 1978, p. 171.
2. C. von Sonntag, *Radiat. Phys. Chem.*, 30 (1987) 313.
3. C. von Sonntag and H.-P. Schuchmann, *Int. J. Radiat. Biol.*, 49 (1986) 1.
4. C. von Sonntag, *The Chemical Basis of Radiation Biology*, Taylor and Francis, London, 1987.
5. S. Steenken, *Chem. Rev.*, 89 (1989) 503.
6. C. von Sonntag and K.M. Prise, *Free-Radical-Induced DNA Damage and Repair. A Chemical and Biological Perspective*, Springer Verlag, Heidelberg, in preparation.
7. G.A. Hospers, E.A. Eisenhauer and E.G. de Vries, *Br. J. Cancer*, 80 (1999) 629.
8. K.M. Prise, N.E. Gillies and B.D. Michael, *Int. J. Radiat. Biol.*, 74 (1998) 53.
9. J.F. Weiss, *Environ. Health Perspect.*, 105 (1997) 1473.
10. E.A. Bump and K. Malaker (eds.), *Radioprotectors: Chemical, Biological, and Clinical Perspectives*, CRC Press, Boca Raton, USA, 1997.
11. P. Wardman, *Radiat. Phys. Chem.*, 24 (1984) 293.
12. P. Wardman, *Curr. Top. Radiat. Res. Quart.*, 11 (1977) 347.
13. A.F. Fuciarelli, F.Y. Shum and J.A. Raleigh, *Radiat. Res.*, 110 (1987) 35.
14. A.F. Fuciarelli, G.G. Miller and J.A. Raleigh, *Radiat. Res.*, 104 (1985) 272.
15. H. Kasai and S. Nishimura, *Environ. Health Perspect.*, 67 (1986) 111.
16. H.L. Lewis, D.R. Muhleman and J.F. Ward, *Radiat. Res.*, 75 (1978) 305.
17. H.L. Lewis and J.F. Ward, in: *DNA Repair Mechanisms*, P.C. Hanawalt, E.C. Friedberg and C.F. Fox (eds.), Academic Press, New York, 1978, p. 35.
18. R. Rajagopalan, R.J. Melamede, M.F. Laspia, B.F. Erlanger and S.S. Wallace, *Radiat. Res.*, 97 (1984) 499.
19. H. Waller, E. Friess and J. Kiefer, *Radiat. Environ. Biophys.*, 19 (1981) 259.
20. G.V. Buxton, C.L. Greenstock, W.P. Helman and A.B. Ross, *J. Phys. Chem. Ref. Data*, 17 (1988) 513.
21. K. Hildenbrand, G. Behrens, D. Schulte-Frohlinde and J.N. Herak, *J. Chem. Soc. Perkin Trans. 2*, (1989) 283.

22. D. Schulte-Frohlinde and K. Hildenbrand, in: *Free Radicals in Synthesis and Biology*, F. Minisci (ed.), Kluwer, Dordrecht, 1989, p. 335.
23. H. Catterall, M.J. Davies and B.C. Gilbert, *J. Chem. Soc. Perkin Trans. 2*, (1992) 1379.
24. S. Fujita and S. Steenken, *J. Am. Chem. Soc.*, 103 (1981) 2540.
25. D.K. Hazra and S. Steenken, *J. Am. Chem. Soc.*, 105 (1983) 4380.
26. M. Al-Sheikhly and C. von Sonntag, *Z. Naturforsch.*, 38b (1983) 1622.
27. K.M. Idris Ali and G. Scholes, *J. Chem. Soc. Faraday Trans. I*, 76 (1980) 449.
28. G.A. Infante, P. Jirathana, J.H. Fendler and E.J. Fendler, *J. Chem. Soc. Faraday Trans. I*, 69 (1973) 1586.
29. S. Nishimoto, H. Ide, T. Wada and T. Kagiya, *Int. J. Radiat. Biol.*, 44 (1983) 585.
30. M. Dizdaroglu and M.G. Simic, *Radiat. Res.*, 100 (1984) 41.
31. G.A. Infante, P. Jirathana, E.J. Fendler and J.H. Fendler, *J. Chem. Soc. Faraday Trans. I*, 70 (1974) 1162.
32. P.C. Shragge, A.J. Varghese, J.W. Hunt and C.L. Greenstock, *Radiat. Res.*, 60 (1974) 250.
33. C. Nese, M.N. Schuchmann, S. Steenken and C. von Sonntag, *J. Chem. Soc. Perkin Trans. 2*, (1995) 1037.
34. H. Riederer and J. Hüttermann, *J. Phys. Chem.*, 86 (1982) 3454.
35. S.A. Grachev, E.V. Kropachev and G.I. Litvyakova, *Bull. Acad. Sci USSR, Chem. Ser.*, (1983) 1595.
36. S.A. Grachev, E.V. Kropachev and G.I. Litvyakova, *Bull. Akad. Sci. USSR Chem. Ser.*, 10 (1986) 2178.
37. C. von Sonntag and H.-P. Schuchmann, *Angew. Chem. Int. Ed. Engl.*, 30 (1991) 1229.
38. C. von Sonntag and H.-P. Schuchmann, in: *Peroxyl Radicals*, Z.B. Alfassi (ed.), Wiley, Chichester, 1997 p. 173.
39. H.-P. Schuchmann and C. von Sonntag, in: *Peroxyl Radicals*, Z.B. Alfassi (ed.), Wiley, Chichester, 1997 p. 439.
40. N. Murata-Kamiya, H. Kamiya, M. Muraoka, H. Kaji and H. Kasai, *J. Radiat. Res.*, 38 (1998) 121.
41. I.L. Yurkova, H.-P. Schuchmann and C. von Sonntag, *J. Chem. Soc. Perkin Trans. 2*, (1999) 2049.
42. M.N. Schuchmann and C. von Sonntag, *J. Chem. Soc. Perkin Trans. II*, (1983) 1525.
43. O.J. Mieden, M.N. Schuchmann and C. von Sonntag, *J. Phys. Chem.*, 97 (1993) 3783.

44. V.M. Berdnikov, N.M. Bazhin, V.K. Fedorov and O.V. Polyakov, *Kinet. Catal. (Engl. Transl.)*, 13 (1972) 986.
45. B.C. Gilbert, R.G.G. Holmes, H.A.H. Laue and R.O.C. Norman, *J. Chem. Soc. Perkin Trans. II*, (1976) 1047.
46. H.-P. Schuchmann and C. von Sonntag, *J. Photochem.*, 16 (1981) 289.
47. S. Fujita, *Int. J. Radiat. Biol.*, 45 (1984) 371.
48. M.L. Scholes, M.N. Schuchmann and C. von Sonntag, *Int. J. Radiat. Biol.*, 61 (1992) 443.
49. M.N. Schuchmann, M. Al-Sheikhly, C. von Sonntag, A. Garner and G. Scholes, *J. Chem. Soc. Perkin Trans. II*, (1984) 1777.
50. M.N. Schuchmann, S. Steenken, J. Wroblewski and C. von Sonntag, *Int. J. Radiat. Biol.*, 46 (1984) 225.
51. S. Das, D.J. Deeble and C. von Sonntag, *Z. Naturforsch.*, 40c (1985) 292.
52. E. Hayon, *J. Chem. Phys.*, 51 (1969) 4881.
53. S. Das, D.J. Deeble, M.N. Schuchmann and C. von Sonntag, *Int. J. Radiat. Biol.*, 46 (1984) 7.
54. D.J. Deeble, S. Das and C. von Sonntag, *J. Phys. Chem.*, 89 (1985) 5784.
55. D.J. Deeble and C. von Sonntag, *Int. J. Radiat. Biol.*, 51 (1987) 791.
56. A. Hissung and C. von Sonntag, *Int. J. Radiat. Biol.*, 35 (1979) 449.
57. K.J. Visscher, H.J.W. Spoelder, H. Loman, A. Hummel and M.L. Hom, *Int. J. Radiat. Biol.*, 54 (1988) 787.
58. M.C.R. Symons, *Int. J. Radiat. Biol.*, 58 (1990) 93.
59. J. Hüttermann, J. Ohlmann, A. Schaefer and W. Gatzweiler, *Int. J. Radiat. Biol.*, 59 (1991) 1297.
60. S. Steenken, J.P. Telo, H.M. Novais and L.P. Candeias, *J. Am. Chem. Soc.*, (1992) 4701.
61. C. Nese, Z. Yuan, M.N. Schuchmann and C. von Sonntag, *Int. J. Radiat. Biol.*, 62 (1992) 527.
62. A.J.S.C. Vieira and S. Steenken, *J. Am. Chem. Soc.*, 112 (1990) 6986.
63. P. O'Neill, *Radiat. Res.*, 96 (1983) 198.
64. A.J.S.C. Vieira, L.P. Candeias and S. Steenken, *J. Chim. Phys.*, 90 (1993) 881.
65. R. Flyunt, R. Wagner and C. von Sonntag, unpublished results.
66. M.S. Vinchurkar, B.S.M. Rao, H. Mohan and J.P. Mittal, *Res. Chem. Intermed.*, 25 (1999) 471.
67. R. Wagner, U. Westhoff, H.-P. Schuchmann and C. von Sonntag, unpublished results.
68. U. Hagen, K. Keck, H. Kröger, F. Zimmermann and T. Lücking, *Biochim. Biophys. Acta*, 95 (1965) 418.



69. K. Keck, U. Hagen and H. Friebolin, *Naturwiss.*, 53 (1966) 304.
70. J.A. Raleigh, W. Kremers and R. Whitehouse, *Radiat. Res.*, 65 (1976) 414.
71. N. Mariaggi, J. Cadet and R. Teoule, *Tetrahedron*, 32 (1976) 2385.
72. J.A. Raleigh and B.J. Blackburn, *Biochem. Biophys. Res. Commun.*, 83 (1978) 1061.
73. T.P. Haromy, J. Raleigh and M. Sundaralingam, *Biochemistry*, 19 (1980) 1718.
74. J.A. Raleigh and A.F. Fuciarelli, *Radiat. Res.*, 102 (1985) 165.
75. C. von Sonntag, *Int. J. Radiat. Biol.*, 66 (1994) 485.
76. R. Wagner, M. Hess, H.-P. Schuchmann and C. von Sonntag, unpublished results.
77. M. Berger and J. Cadet, *Z. Naturforsch.*, 40b (1985) 1519.
78. X. Fang, X. Pan, A. Rahmann, H.-P. Schuchmann and C. von Sonntag, *Chem. Eur. J.*, 1 (1995) 423.
79. G.W. Buchko, J. Cadet, J.-L. Ravanat and P. Labataille, *Int. J. Radiat. Biol.*, 63 (1993) 669.
80. S. Raoul, M. Berger, G.W. Buchko, P.C. Joshi, B. Morin, M. Weinfeld and J. Cadet, *J. Chem Soc. Perkin Trans. 2*, (1996) 371.
81. D. Gasparutto, J.-L. Ravanat, O. Gérot and J. Cadet, *J. Am. Chem. Soc.*, 120 (1999) 10283.
82. R. Wagner, H.-P. Schuchmann and C. von Sonntag, in preparation
83. M. Isildar, M.N. Schuchmann, D. Schulte-Frohlinde and C. von Sonntag, *Int. J. Radiat. Biol.*, 41 (1982) 525.
84. A. Hissung, C. von Sonntag, D. Veltwisch and K.-D. Asmus, *Int. J. Radiat. Biol.*, 39 (1981) 63.
85. K.J. Visscher, M.P. de Haas, H. Loman, B. Vojnovic and J.M. Warman, *Int. J. Radiat. Biol.*, 52 (1987) 745.
86. C. von Sonntag, In: *Physical and Chemical Mechanisms in Molecular Radiation*, W.A. Glass and M.N. Varma (eds.), Plenum, New York, 1991, p. 287.
87. L.P. Candeias and S. Steenken, *J. Phys. Chem.*, 96 (1992) 937.
88. L.P. Candeias, P. Wolf, P. O'Neill and S. Steenken, *J. Phys. Chem.*, 96 (1992) 10302.
89. C.T. Aravindakumar, H. Mohan, M. Mudaliar, B.S.M. Rao, J.P. Mittal, M.N. Schuchmann and C. von Sonntag, *Int. J. Radiat. Biol.*, 66 (1994) 351.
90. P.N. Moorthy and E. Hayon, *J. Am. Chem. Soc.*, 97 (1975) 3345.

91. B. Rakvin, J.N. Herak, K. Voit and J. Hüttermann, *Radiat. Environ. Biophys.*, 26 (1987) 1.
92. R.O.C. Norman, P.M. Storey and P.R. West, *J. Chem. Soc. (B)*, (1970) 1087.
93. J. Cadet, C. Decarroz, L. Voituriez, J.R. Wagner and G.J. Fisher, in: *Proc. Seventh Congr. Radiat. Res. Amsterdam 1983*, J.J. Broerse, G.W. Barendsen, H.B. Kal and A.J. van der Kogel (eds), Martinus Nijhoff, Amsterdam, 1983, p. A 3.
94. C. Decarroz, J.R. Wagner and J. Cadet, *Free Radical Res. Commun.*, 2 (1987) 295.
95. C.M. Krishna, C. Decarroz, J.R. Wagner, J. Cadet and P. Riesz, *Photochem. Photobiol.*, 46 (1987) 175.
96. L.P. Candeias and S. Steenken, *J. Am. Chem. Soc.*, 115 (1993) 2437.
97. H. Görner, *J. Photochem. Photobiol. B: Biol.*, 26 (1994) 117.
98. D.H. Giamalva, D.F. Church and W.A. Pryor, *J. Am. Chem. Soc.*, 108 (1986) 6646.
99. H. Niehaus and K. Hildenbrand, *J. Chem. Soc. Perkin Trans. 2* (2000) 947.
100. D.J. Deeble, M.N. Schuchmann, S. Steenken and C. von Sonntag, *J. Phys. Chem.*, 94 (1990) 8186.
101. R. Lomoth, S. Naumov and O. Brede, *J. Phys. Chem. A*, 103 (1999) 6571.
102. G. Behrens, K. Hildenbrand, D. Schulte-Frohlinde and J.N. Herak, *J. Chem. Soc. Perkin Trans. II* (1988) 305.
103. K. Hildenbrand, *J. Chem. Soc. Perkin Trans. 2* (1995) 2153.
104. K. Hildenbrand, *Z. Naturforsch.*, 45c (1990) 47.
105. H.-P. Schuchmann, D.J. Deeble, G. Olbrich and C. von Sonntag, *Int. J. Radiat. Biol.*, 51 (1987) 441.
106. H.-P. Schuchmann and C. von Sonntag, *Radiat. Phys. Chem.*, 32 (1988) 149.
107. P. Ulanski and C. von Sonntag, *J. Chem. Soc. Perkin Trans. 2* (1999) 165.
108. R. Rashid, F. Mark, H.-P. Schuchmann and C. von Sonntag, *Int. J. Radiat. Biol.*, 59 (1991) 1081.
109. E. Bothe, D.J. Deeble, D.G.E. Lemaire, R. Rashid, M.N. Schuchmann, H.-P. Schuchmann, D. Schulte-Frohlinde, S. Steenken and C. von Sonntag, *Radiat. Phys. Chem.*, 36 (1990) 149.
110. C.T. Aravindakumar, M.N. Schuchmann B.S.M. Rao, J. von Sonntag and C. von Sonntag, in preparation
111. S. Steenken and S.V. Jovanovic, *J. Am. Chem. Soc.*, 119 (1997) 617.

112. M. Farraggi and M.H. Klapper, *J. Chim. Phys.*, 91 (1994) 1062.
113. M.N. Schuchmann, H.-P. Schuchmann, W. Knolle, J. von Sonntag, S. Naumov, W.-F. Wang and C. von Sonntag, *Nukleonika*, 45 (2000) 55.
114. R.L. Willson, P. Wardman and K.-D. Asmus, *Nature*, 252 (1974) 323.
115. K.-D. Asmus, D.J. Deeble, A. Garner, K.M. Idriss Ali and G. Scholes, *Br. J. Cancer Suppl. III*, 37 (1978) 46.
116. L.P. Candeias and S. Steenken, *J. Am. Chem. Soc.*, 111 (1989) 1094.
117. P. O'Neill and P.W. Chapman, *Int. J. Radiat. Biol.*, 47 (1985) 71.
118. A. Adhikary, E. Bothe, C. von Sonntag and V. Jain, *Radiat. Res.*, 148 (1997) 493.
119. S. Steenken, in: *Free Radicals: Chemistry, Pathology and Medicine*, C. Rice-Evans and T. Dormandy (eds.), Richelieu Press, London, 1988, p. 53.
120. V. Jagannadham and S. Steenken, *J. Am. Chem. Soc.*, 110 (1988) 2188.
121. M. Al-Sheikhly, *Radiat. Phys. Chem.*, 44 (1994) 297.

## Radiation chemistry of proteins

Chantal Houée-Levin and Cécile Sicard-Roselli

L. P. C. R., UMR 8610 Université Paris-Sud-CNRS, Bât. 350, Centre Universitaire,  
F-91405 Orsay cedex, France

Radiation chemistry of proteins has been studied for more than 30 years. This field leads to numerous applications. For instance it is a basis for improving protocols of radiosterilization of food (1), drugs, etc... It has been recognized as a very powerful tool for exploring structure-reactivity relationships in proteins (2, 3). Protein radical chemistry is also essential for the understanding of development of several important pathologies related to oxidative stress (4, 5), ageing, neurodegenerative diseases (6), radiobiology (7)... and in signal transduction processes (8). In addition, disconnected with any interaction of ionizing or UV irradiation, protein free radicals play roles in cellular life since they are part of many enzymatic systems (9).

Several reviews were already published about radiolysis of amino acids (7, 10), proteins in the solid state (11) or in aqueous solutions (2, 3, 7, 12). In this review, our aim is not only to present most recent data but also to give an overview of the unknown aspects in protein radiation chemistry as well as in some of the expected biological consequences of protein radiolytic modifications.

### 1. RADIOLYSIS OF PROTEINS IN THE SOLID STATE

Under irradiation, proteins are affected by direct and indirect effects of ionizing radiations. When these macromolecules are in liquid solution, direct effects can be neglected and the indirect effects are predominant. On the contrary, in solid state, proteins are ionized mainly by direct interaction (11).

Proteins in solid state can be found in different forms, lyophilized or in frozen aqueous solution. Under irradiation, lyophilized proteins mostly aggregate, as was shown for egg-white lysozyme irradiated at room temperature (13, 14, 15, 16). On the contrary, irradiation of frozen protein solutions gives rise to fragmentation (11, 16 and references therein). Rupture of the N-C $\alpha$  bond of the polypeptide chain seems to be responsible for fragmentation, as it was observed for homopolymers irradiated at 77K (17).

In sodium dodecyl sulfate-polyacrylamide gel electrophoresis (SDS-PAGE), bands of determined apparent molecular mass appear. Thus fragmentation can be specific or non-specific, depending on the conditions of irradiation. The presence of hole scavengers increases the formation of specific breaks. For example, irradiation of lysozyme at 195 K, under nitrogen atmosphere and in the presence of tris-hydroxymethyl-aminomethane buffer, produces 11 specific fragments (16). Using SDS-PAGE analysis, the mass of these fragments were determined between 2650 and 11250 Da. In addition, sequencing analysis revealed that all the fragmentation sites are located at the surface of lysozyme at the loops and turns. This result is in agreement with that of aspartate transcarbamylase, for which fragmentation was localized in the connecting loop of the protein (18). The importance of the tertiary structure of a protein for the radiation-induced fragmentation was investigated more precisely (19). Proteins whose tertiary structure is well-known, and which undergo a conformational change were studied. For example, citrate synthase was irradiated in the presence or in the absence of substrates or cofactors such as oxaloacetate, acetylcoenzyme A, or citrate. Native, molten globule and denatured lactalbumin was also irradiated. It then appeared that a more compact protein has a higher resistance to radiations (quantified here with the D37 value). Indeed, under denaturing conditions, for example in the presence of urea, the fragmentation is found random. Breaking of the polypeptidic chain seems to be a surface phenomenon. The origin might be electron and/or hole localization at the surface, coming or not from migration from the inside of the protein. A participation of the solvent during redissolution for analysis cannot be excluded. However nothing is known concerning side chain modifications.

Interestingly, irradiation of polymeric proteins in the frozen state, induces fragmentation of the subunits but no dissociation of the oligomeric structure (20). Miller et al. (20) reported the effects of radiation on dimeric, tetrameric and hexameric proteins at - 135 °C. After irradiation of protein frozen solutions, size-exclusion chromatography and SDS-PAGE analysis revealed no appreciable dissociation, indicating that monomers are not released. Then, high dose of irradiation can cause fragmentation of several subunits, but only very little dissociation of the protein structure.

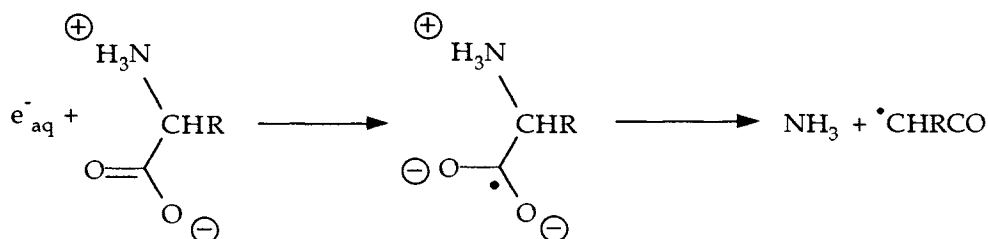
Garrison (10) proposed that this fragmentation involves dry electrons which react with the carbonyl groups of the protein, leading to a breakage of the CO-NH bond. Symons (21) and Sevilla's group (22) proposed a mechanism in which the first radical is localized on C $\alpha$  (or  $\beta$ ). It then undergoes a scission of the N-C $\alpha$  bond in agreement with experimental results of Morishima and Hatano (17). This hypothesis has suggested theoretical studies by quantum mechanics methods, of C-H and C-C bond dissociation energies and reduction potentials of several amino-acids (23, 24, 25). The authors show a marked increase in the ease of abstraction of H in the C $\alpha$  radical in the series Ala, Ser and Thr.

## 2. REACTIONS OF WATER PRIMARY RADICALS

Proteins react very efficiently with primary water free radicals.  $e^-_{aq}$  and  $OH^\bullet$  free radicals may react with many targets and hence various forms of modifications are expected: of the polypeptidic backbone (dimerizations and polymerizations, fragmentations), and of residues. These reactions have been studied extensively, especially those of  $^\bullet OH$  free radicals because of their importance in biological oxidative disorders (5, 7).

### 2.1. Reduction by hydrated electron

It is known that hydrated electrons react with the carbonyl groups of peptidic bonds. Consequences seem to be fragmentation and ammonia liberation in amino-acids. This cleavage is supposed to take place at the free radical level :



G-values of ammonia were measured after reduction of amino-acids and peptides (7, 9), and of some proteins such as histones that contain relatively low amount of sulfur residues and histidines (26). They may reach the  $G(e^-_{aq})$  value. The high reactivity of  $e^-_{aq}$  toward peptidic bonds is also responsible for the progression of the rate constant with the number of carbonyl groups in small peptides (table 1). The deaminated radical was observed by pulse radiolysis (absorption maximum around 430 nm, extinction coefficient at this wavelength ca.  $1100 \text{ mol}^{-1} \text{ l cm}^{-1}$ ) (3).

$e^-_{aq}$  reacts with almost all amino-acids. The reaction is faster with protonated histidine than with its unprotonated form. The fastest reaction is with disulfide groups (table 2). Free radicals are easily identified by their absorption spectra in pulse radiolysis (table 3). Thus reactions of  $e^-_{aq}$  with proteins are always very fast (table 2), with rate constants equal or above the diffusion limited rate constant value in water (ca.  $2 \times 10^{10} \text{ mol}^{-1} \text{ l s}^{-1}$ ). This rate constant decreases with increasing pH (27). In horse heart myoglobin, this variation was interpreted as coming from interaction of  $e^-_{aq}$  with protonated histidines (28). Identified final compounds include fragments and proteins reduced at disulfide bonds. However, the probability of reaction with a determined site (e. g. disulfide bond) is not related to the rate constant of reaction of the corresponding amino-acid. It has been shown long ago, for instance, that for ribonuclease in the native state (29), disulfide groups do not react with hydrated electron whereas they do in the denatured protein. Similarly, the reactivity of histidine groups was followed by pulse radiolysis (30, 31). The authors reported a lack of reactivity for some

Table 1

Rate constants of reactions of  $e^-_{aq}$  with some aliphatic amino-acids and some peptides.

Amino-acid or peptide	Rate constant ( $\text{mol}^{-1} \text{l s}^{-1}$ )
Gly	$8.2 \times 10^6$
Gly-Gly	$3.7 \times 10^8$
Gly-Gly-Gly	$1.8 \times 10^9$
Ala	$9.0 \times 10^6$
Ala-Ala	$2.0 \times 10^8$
Ala-Ala-Ala	$4.9 \times 10^8$
(Ala) <sub>4</sub>	$1.2 \times 10^9$
(Ala) <sub>5</sub>	$1.9 \times 10^9$
(Ala) <sub>12</sub>	$6.1 \times 10^9$
(Ala) <sub>20</sub>	$1.2 \times 10^{10}$

Data are taken from: G. V. Buxton, C. L. Greenstock, W. P. Helman and A. B. Ross, J. Phys. Chem. Ref. Data 17 (1988) 513.

proteins like lysozyme, although this residue was on surface. Thus the reactivity of a target is not only controlled by its accessibility.

When the protein contains a reducible prosthetic group (metal ion, flavin, quinone...) this group can be reduced with a yield strongly dependent on the protein. As an example, reduction of flavoproteins was extensively studied. In some of them the flavin is the most probable target (32). In others, the flavin is partly or totally non-reactive (33, 34). In flavoproteins, the flavin is almost always inside the protein matrix and contact with the solvent is limited. The degree of reactivity is thus not only related to its accessibility and the reduction might be due to intramolecular electron transfer (see 5).

In haemeproteins, the target is not  $\text{Fe}^{3+}$  ion but the porphyrin itself (35). Thus the reduction is very little affected by the oxidation state of the metal ion, or even its presence or absence (36).

### 2.3. Oxidation by Hydroxyl Radical and Hydrogen atoms

Reactions of hydroxyl radical are of particular importance because of their probable involvement in many pathological processes related to oxidative stress.

Table 2  
Rate constants of reactions of  $e^-_{aq}$  with some amino-acids and proteins.

Compound	Rate Constant ( $\text{mol}^{-1} \text{dm}^3 \text{s}^{-1}$ )
Amino-acids	
Tyrosine	$1.6 \times 10^9$
Protonated Histidine	$7 \times 10^9$
Cysteine	$8.7 \times 10^9$
Cystine	$1.3 \times 10^{10}$
Proteins without prosthetic group	
$\alpha$ -chymotrypsin	$2.0 \times 10^{10}$
trypsin	$3.0 \times 10^{10}$
lysozyme	$4.6 \times 10^{10}$
Proteins with metallic prosthetic group	
ceruloplasmin	$9 \times 10^{10}$
azurin	$1.0 \times 10^{11}$
catalase	$2.0 \times 10^{11}$
cytochrome c	$1.0 \times 10^{10}$
ferredoxin, 2Fe-2S	$9.7 \times 10^9$
superoxyde dismutase	$1.3 \times 10^{10}$

Data are taken from: G. V. Buxton, C. L. Greenstock, W. P. Helman and A. B. Ross, J. Phys. Chem. Ref. Data 17 (1988) 513.

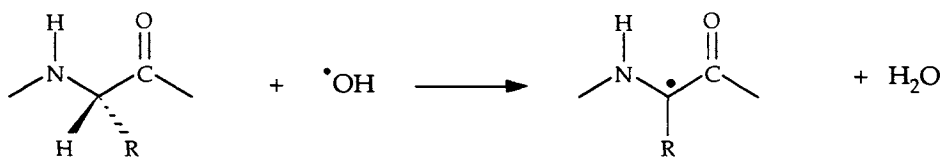
$\text{OH}^\bullet$  radicals would be produced in vivo mostly by the Fenton system ( $\text{Fe}^{2+} + \text{H}_2\text{O}_2$ ) (5). Reactions of H atom are poorly known compared to those of  $\text{OH}^\bullet$ ; however, they are believed to have similar mechanisms.

$\text{OH}^\bullet$  free radicals do not react with the peptidic bond, but they may withdraw an H atom to the  $\alpha$ -carbon. In the absence of oxygen, the fate of this free radical is not well known. In amino-acids, decarboxylation occurs (37), thus it might end up with protein fragmentation. In the presence of oxygen, a peroxy radical is



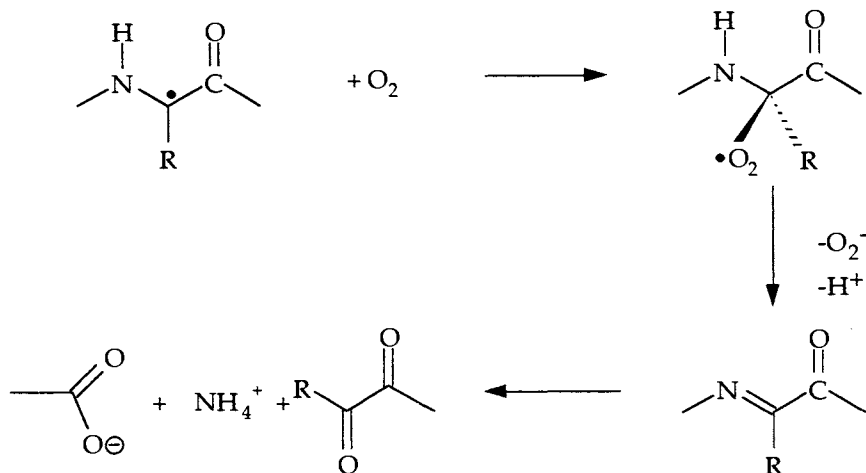
Table 3  
Spectral properties of some important amino-acid free radicals in peptides and proteins.

Free Radical	Absorption maxima in nm (average extinction coefficient $\text{mol}^{-1} \text{l cm}^{-1}$ )	Reference
Reduced amino-acids		
disulfide anion	420-440 (6000-8000)	(38)
protonated disulfide	400-410 (1000-1300)	(38)
histidyl	360 (2000)	(39)
Oxidized amino-acids		
thiyl	320-340 (300)	(40)
methionyl S-N bonded	390-400 (6600)	(41)
S-O bonded	390-400 (3900)	(42)
S-S bonded	490 (5000-7000)	(43)
tyrosinyl	410 (2600)	(44)
tryptophanyl	510 (1800)	(45)



formed which releases superoxide. The process leads also to polypeptide chain fragmentation (10, 46, 47, 48).

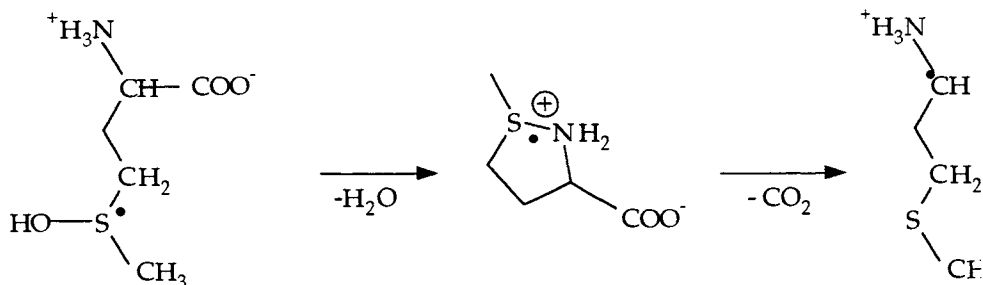
In cyclic dipeptides  $\text{cyclo}(\text{Gly})_2$  and  $\text{cyclo}(\text{Ala})_2$  a single type of radical is formed, in each case by abstracting a carbon-bound H atom at the ring (49). In  $\text{N}_2\text{O}-\text{O}_2$  atmosphere, peroxy radicals eliminate superoxide ions in a base-catalyzed reaction. The main products are 3-hydroxy-2,5-dioxopiperazine, 2,3,5-trioxopiperazine and 2,5-dioxo-2,3,4,5-tetrahydropyrazine.



OH free radicals react with almost all amino-acids. For aliphatic residues, rate constants are correlated with the strength of the X-H bond (X = S, C or N) (1). Thus the reaction is relatively slow with glycine ( $k = 1.7 \times 10^7 \text{ mol}^{-1} \text{ l s}^{-1}$ ) and fast with the -SH function of cysteine ( $k = 1.9 \times 10^{10} \text{ mol}^{-1} \text{ l s}^{-1}$ ). The thiyl radical formed upon oxidation of cysteine, whose spectral properties are in table 3, is formed but a carbon-centered radical is also present (50, 51). In the presence of oxygen, thiyl radical fixes  $\text{O}_2$  giving peroxy radicals (52). These radicals may photoisomerize into sulfonyl radicals  $\text{RSO}_2\cdot$  (53). In small molecules, disulfide groups can also be oxidized. This reaction was not demonstrated in proteins, but cannot be neglected. A disulfide radical cation is formed (54). Final compounds are not known.

Reactions are fast with aromatic residues ( $k \approx 10^9 \text{ mol}^{-1} \text{ l s}^{-1}$ ). They begin by OH addition to the ring. With phenylalanine, addition occurs preferentially on the ortho position relative to  $-\text{CH}_2\text{CHCONH}$  group (55). For tyrosine, addition takes place mostly at the ortho position relative to the phenol function. However, in both cases additions can also be expected on other positions. In tryptophan, the indole ring is more reactive than the phenyl one. OH-adducts may release OH $^-$  giving phenoxyl (from tyrosine) or indolyl (from tryptophan) radicals whose absorption spectra are well characterized (table 3).

Oxidation of methionine residues has been widely studied. Reaction of OH is fast ( $k \approx 10^{10} \text{ mol}^{-1} \text{ l s}^{-1}$ ) and proceed via formation of an OH-adduct  $>\text{S-OH}$ , the hydroxy sulfuranyl radical (42). This radical eliminates water, yielding the monomeric radical cation  $>\text{S}^{\bullet+}$  which then stabilizes through formation of  $>\text{S-X}$  radical species, X = N, O or S (56). In methionine amino-acid, the free radical undergoes ring closure with the amine function to give cyclic  $>\text{SN}$  radical (57) which then gets decarboxylated. Final compound seems to be methionine sulfoxide. When methionine is in a peptide, the fate of the hydroxy sulfuranyl radical is strongly dependent on the position of methionine in the peptide,



neighbouring residues, the conformation and the pH. In Ser-Met and Thr-Met, it leads to side chain fragmentation of Ser and Thr into aldehyde function (58). Formation of aldehyde requires an N-terminal Ser or Thr residue and the presence of methionine in the sequence. An intermediate is  $>SN$  radical. The most sensitive step is cyclization of the free radical. Preferentially 5- or 6-membered cycles are formed. Cyclization may involve N-terminal or carboxylate groups. If such functions are not available in a sterically favourable site, dimerization with a non-oxidized peptide occurs which gives either disulfide radical cation,  $S-N^{\bullet+}$  or  $S-O^{\bullet+}$  radical cations (59, 60). Decarboxylation seems to arise from intramolecular electron transfer between  $>S^{\bullet+}$  and the C-terminal and/or interaction between  $>S-OH$  or  $>S-N$  bond and a protonated amino group positioned  $\alpha$  to a carboxyl group (61, 62).

The main identified final products of oxidation of residues by OH radicals, are listed in table 4. From this table, it appears that, whereas the nature of the free radicals formed upon oxidation of residues is well known, on the other hand identification of the final compound is far from being complete. Goals are nevertheless important, since this knowledge is crucial for the understanding of biological disorders related to oxidative stress. Some of these identified compound are used as markers of oxidative stress in vivo (5).

Knowledge of the one-electron reduction potentials is essential to predict chemical properties of protein free radicals. Some of them were measured in model compounds and peptides, because of difficulties to deal with proteins. They are listed in table 5. Values do not change much with neighbouring amino-acid in small peptides. However, they might change considerably in proteins. As an example, some two-electron reduction potentials of disulfide/thiol systems were measured in a few proteins involved in thiol-disulfide exchange and their values do vary with the protein (63). Prütz and coworkers (64) proposed that by decreasing oxidation strength, one may expect

Met/ $SN^{\bullet+}$  (Met/ $SS^{\bullet+}$ )  $>$  Trp $\bullet$   $>$  TyrO $\bullet$   $>$  thiol  $>$  RSSR $\bullet$   $\approx$  carbon-centered radical.

Limited data is available concerning G-values of amino-acid modifications in proteins. However, as it is for hydrated electrons, the yield of oxidation of amino-acids is not only related to the rate constant of the reaction of the amino-acid free

Table 4  
Main identified final products formed by oxidation of some amino-acids by  $\bullet\text{OH}$  radicals.

Amino-acid	Products	References
Histidine	asparagine	(65)
	aspartate	(66)
	2-oxo histidine *	(67)
Phenylalanine	o-tyrosine	(46, 68, 69, 70)
	m-tyrosine	
	p-tyrosine	
	dimers	(71)
Tyrosine	2, 2' bityrosine	(70, 72, 73, 74)
	dihydroxy-phenylalanine (DOPA)**	(75)
Leucine	$\gamma$ -hydroxyleucine***	(76)
	$\delta$ -hydroxyleucine***	
Valine	$\beta$ -hydroxy valine***	(77)
	2-amino-3-hydroxy-3-methyl butanoic acid***	
	$\gamma$ -hydroxyvaline***	
Tryptophan	N-formyl kynurenine	(55, 78)
	kynurenine	
	hydroxy tryptophans	
Proline	glutamate?	(64)
Cysteine	disulfide	(7, 12)
	sulfonate*	(79)
	sulfenic acid*	(78)
Methionine	methionine sulfoxide	(80)

\* in the presence of oxygen

\*\* isolated with  $\bullet\text{OH}$  formed by the Fenton system

\*\*\* in the presence of oxygen. Precursor is the corresponding hydroperoxide.

in solution with OH. The most sensitive ones seem to be the aromatic residues and thiol groups. The main problem encountered with the measure of G-values

Table 5  
One-electron reduction potentials of amino-acids and model compounds.

redox couple	Compound	E° (V)	Reference
TyrO•/TyrOH	amino-acid in solution	0.94	(81)
	small peptides	0.87-0.91	(82)
Trp•/Trp	amino-acid in solution	1.05	(81)
	small peptides	0.99-1.15	(82)
RSSR•+/RSSR	lipoate	1.1	(54)
RSSR/RSSR•-	cystine*	-1.7	(83)
	β-mercaptoethanol	-1.5	(84)
	oxidized*		(84)
	lipoamide*	-1.6	
RS•/RS-	cysteine	1.1	(83)
RS•/RSH	β-mercaptoethanol	1.35	(84)
Met/SN•+	Met-Gly	1.4	
His•+/His	amino-acid in solution	1.17	(85)

\* calculated.

of oxidation, is the instability of aromatic amino-acids in conditions of analysis, and the lack of experimental methods avoiding destruction of residues. Table 6 gives the G-values of destruction of some amino-acids in histone H2A in an atmosphere of N<sub>2</sub>O (86). Considering that G(•OH)≈0.58 μmol J<sup>-1</sup>, the stoichiometry is far from being observed.

Table 6  
G-values of destruction of some amino-acids of histone H2A, after reaction with •OH in an atmosphere of N<sub>2</sub>O (86).

G(-His) μmol J <sup>-1</sup>	G(-Tyr) μmol J <sup>-1</sup>	G(-Phe) μmol J <sup>-1</sup>
0.02	0.023	0.010

In conclusion, oxidation of proteins by •OH free radicals gives birth to modified proteins, dimers, polymers and/or fragments. As for metalloproteins, a variable proportion of OH radicals reacts with the metal center. For instance, in ferrocycytochrome c, Fe<sup>2+</sup> is oxidized with a yield of ca. 5% (87) whereas in

ferricytochrome c,  $\text{Fe}^{3+}$  is reduced with a yield of 25-50% (87). The mechanisms of these two reactions are poorly known and involve intramolecular steps. These mechanisms are still being studied because of their tremendous importance in biology.

### 2.3 Reactions of superoxide anion

Despite their increasing biological importance, reactions of superoxide anion and of its acidic form, hydroperoxyl radical, with proteins, are little understood. More generally speaking, the chemical basis of biological role of superoxide is still questioned (88).

It is known that superoxide reacts very slowly with all amino-acids since all rate constants are below  $100 \text{ mol}^{-1} \text{ l s}^{-1}$  (89). Hence its reactivity with proteins without prosthetic group is low (89). One exception seems to be collagen, in which proline residues are oxidized into hydroxyproline (90). On the other hand, superoxide reacts efficiently with free radicals such as tryptophanyl radical (91). Reaction is fast with metalloproteins. It proceeds mostly by oxidizing or reducing the metal center. Some characteristics and rate constants of reactions with metalloproteins are given in table 7. It is obvious that products are often unknown and that the mechanism is sometimes unclear. It seems that there is no reaction with transferrin (92) and horseradish and lacto-peroxidase compounds II (93). The reason is unknown.

$\text{O}_2^{\bullet-}$  reacts with various forms of hemoglobin: hemoglobin is oxidized to methemoglobin and methemoglobin is reduced to hemoglobin (94). Both reactions have rate constants of the same order of magnitude (ca.  $10^3 \text{ mol}^{-1} \text{ l s}^{-1}$  (95)).  $\text{O}_2^{\bullet-}$  seems to accelerate autoxidation of hemoglobin. In addition, the protein gets polymerized (96).

Superoxide ion reduces  $\text{Fe}^{3+}$ -cytochrome c ( $k = 2.6 \times 10^5 \text{ mol}^{-1} \text{ l s}^{-1}$  (97)) but can also oxidize  $\text{Fe}^{2+}$ -cytochrome c. The free radical seems to attack one of the edges of the heme and the kinetic control is due to electrostatic guidance to the heme.

The most striking reaction of  $\text{O}_2^{\bullet-}$  is with the family of superoxide dismutases (98, 99, 100). That with Cu-Zn SOD was specially studied. Rate constants can be higher than  $10^9 \text{ mol}^{-1} \text{ l s}^{-1}$  with Cu-Zn superoxide dismutase and somewhat smaller with other SODs (ca.  $10^7 \text{ mol}^{-1} \text{ l s}^{-1}$ ). The reaction is controlled by electric potential surrounding the macromolecule and more precisely by lysine residues of the active site (101). The guidance of superoxide to the active site is so efficient that 10% of the collisions lead to reaction (102). At physiological ionic strength, the invariant Arg141 is essential in determining the electrostatic forces facilitating the diffusion of the substrate towards the active site (103, 104). A recent characterization of the functional properties of Cu-Zn SOD of *P. leiognathi* has shown that this enzyme has of  $8.5 \times 10^9 \text{ mol}^{-1} \text{ l s}^{-1}$  (105). A mutant of this enzyme E59Q in which a glutamate close to the active site has been charged neutralized to glutamine, is even more efficient ( $1 \times 10^{10} \text{ mol}^{-1} \text{ l s}^{-1}$ ) (106).

Table 7  
Reactions of superoxide anion with some metalloproteins.

enzyme	Rate constant (mol <sup>-1</sup> s <sup>-1</sup> )	Products and comments	Ref.
Fe <sup>3+</sup> peroxydase C	N. D.	no H <sub>2</sub> O <sub>2</sub> formed after reaction	(107)
peroxidase A2	< 10 <sup>3</sup>		(108)
peroxidase C	N. D.	oxidized protein, perhaps Fe <sup>III</sup>	
Cu(I) thionein	7.5 × 10 <sup>6</sup>	no oxidation of copper, little Cu <sup>II</sup> released	(108)
lactoperoxidase compound I	N. D.	reduction to compound II	(109)
indoleamine 2, 3 dioxygenase	8 × 10 <sup>6</sup>	formation of the oxygenated enzyme, protein activated	(110)
catalase compound I	5 × 10 <sup>6</sup>	reduction to compound II	(111)
catalase myeloperoxidase-Fe <sup>3+</sup>		formation of compound III formation of compound III	(112)
- horse	8 × 10 <sup>6</sup>		
- human	5 × 10 <sup>6</sup>		
lactate dehydrogenase - NADH (complex)	1.0 × 10 <sup>5</sup>	Disappearance of NADH via chain reaction	(113)

Brownian dynamics simulation suggests that such a high value is due to an enhanced substrate attraction by the modified electric field distribution. The reaction with Mn SOD was less deeply studied. The proposed mechanism involves adducts Mn<sup>2+</sup>(O<sub>2</sub><sup>•-</sup>) (114).

### 3. INSIGHT INTO MECHANISMS: REACTIONS OF OTHER FREE RADICALS

The water primary radicals reactions occur on many targets and therefore study of the mechanisms of their reaction is difficult. First, upon attack of a specific amino-acid, several free radicals may be formed. As a consequence, many final compounds appear. Their yields are strongly dependent on conditions of irradiation (temperature, ionic strength, pH...). Second, the attack usually concerns several amino-acids. Third, the initial reaction is often followed by intramolecular rearrangements (see section 4). However some selectivity is

Table 8.  
Rate constants of reactions of the most used oxidizing secondary radicals, with amino-acids, peptides and proteins.

Free Radical	Reactant	Rate constant (mol <sup>-1</sup> l s <sup>-1</sup> )
Br <sub>2</sub> <sup>•-</sup>	Cysteine	1.8 × 10 <sup>8</sup>
	glutathione oxidized	7 × 10 <sup>7</sup>
	Histidine	1.9 × 10 <sup>7</sup>
	Methionine	(1.7-2) × 10 <sup>9</sup>
	Tryptophan	7.0 × 10 <sup>8</sup>
	Tryptophan in small peptides	(1-5) × 10 <sup>9</sup>
	Tyrosine	2 × 10 <sup>8</sup>
	Tyrosine in small peptides	(4.6-10) × 10 <sup>7</sup>
	Proteins	(4-10) × 10 <sup>9</sup>
NO <sub>2</sub> <sup>•</sup>	Cysteine	>5 × 10 <sup>8</sup>
	Tryptophan	<5 × 10 <sup>5</sup>
	Tyrosine	1 × 10 <sup>6</sup>
	Tyrosine in small peptides	2.9 × 10 <sup>7</sup>
N <sub>3</sub> <sup>•</sup>	Cysteine	1.4 × 10 <sup>7</sup>
	Methionine	<1 × 10 <sup>6</sup>
	Tryptophan	4.1 × 10 <sup>9</sup>
	Tryptophan in small peptides	> 3 × 10 <sup>9</sup>
	Tyrosine	1.0 × 10 <sup>8</sup>
	Tyrosine in small peptides	(1-2) × 10 <sup>8</sup>
	Proteins	(6-60) × 10 <sup>8</sup>

Data are taken from: P. Neta and R. E. Huie, J. Phys. Chem. Ref. Data 17 (1988) 1027.

observed. To get a better understanding of the free radical reactions and of the subsequent rearrangements, more specific secondary radicals towards amino-acids are used (115). Some rate constants of reaction of free radicals with amino-acids are given in table 8.

The chemistry of NO<sub>2</sub><sup>•</sup> was reviewed (116). Few data concern reactions of NO<sub>2</sub><sup>•</sup> with proteins. It seems to react only with tyrosine (117). Since NO<sub>2</sub><sup>•</sup> seems to be formed in the course of peroxyxynitrite decay (118), its reactions with proteins are of great interest.

In agreement with the rate constants measured for amino-acids in solution, azide radicals attack primarily mostly tryptophan whereas halides like dibromide may also react with methionine. Thiocyanate radicals are also specific of tryptophan residues. However this process is a reversible equilibrium between lysozyme (119).



In peptides and proteins, oxidation of tryptophan is followed by tryptophanyl radical reduction by tyrosine, leading to tyrosinyl radical. This reaction was shown first by Prütz and co-workers (120). Azide radicals are very convenient for this study. This process is easily visualized by pulse radiolysis since both free radicals absorb at different wavelengths (table 3) and the time scale for this reaction goes to microsecond for small peptides to millisecond for proteins. This reaction may occur by intramolecular step and thus it constitutes an excellent model to investigate long range intramolecular electron transfer. These results will be discussed further (see 5.1).

Organic carbon-centered radicals from alcohols seem to react mostly with thiol functions in amino-acids (cysteine) or small peptides such as glutathione (121). The reaction is the so-called "repair process"



in which thiol groups trap oxidized free radicals. For similar reaction in proteins one should take into account conformational changes induced by large amounts of organic compounds in the solution, and side effects due to reactions of radiolysis products such as aldehydes or ketones.

As for reduction processes,  $CO_2^{\cdot-}$  free radicals were shown to react specifically with disulfide bonds (122). They were extensively used to study the redox properties of disulfide bonds, thiol and disulfide free radicals in proteins. This is discussed in paragraph 5. However, they do react with thiol functions also (37). For proteins containing a prosthetic group, the reduction concerns also oxidized valencies of metals and flavins, Flavin adenine dinucleotide (FAD) or Flavin Mononucleotide (FMN). The proportion of reduced disulfide/reduced prosthetic group varies considerably with the protein. For instance, lipoamide dehydrogenase contains one disulfide bond close to a flavin (FAD). Free radicals can reduce only the flavin, although both are in the active site (123). In chicken egg white riboflavin binding protein, competitive formation of both disulfide and semireduced flavin is observed (124).

Other reducing radicals were used. Reduction of flavodoxin was performed using methyl- or benzyl viologen (125). The authors show that the reduction process is driven by conformational change in agreement with earlier suggestions (126). Benzoate radicals can reduce the flavin in D-amino acid oxidase whereas hydrated electrons cannot (127). N-methylnicotinamide or 5-deazalumiflavin radicals were used to investigate the reduction of milk xanthine oxidase (128). The authors show the role of the iron-sulphur centers in mediating electron transfer between the molybdenum and flavin centers of the enzyme. Phosphite radicals reduce disulfide bond of lipoate in very basic medium (129) and thus can be expected to do the same with the proteins that can bear to be in such basic media. Isopropyl radicals also reduce peptide disulfide bonds, however one should be careful of reactions of acetone with protein residues.

Pulse radiolysis was also used to elucidate the mechanism of catalytic action of monodehydroascorbate reductase, an enzyme containing FAD and using Nicotinamide adenine dinucleotide (NADH) as reductant. The substrate is dehydroascorbate radical produced by pulse radiolysis (130). The authors show that this radical reacts with the protein to give the  $FADH\cdot$  radical and that the



Table 9.  
Some characteristics of the reaction of reduction of disulfides in proteins.

Protein	Mass (kDa)	nb. disulfide bonds - in the protein - reducible	k(protein + CO <sub>2</sub> <sup>•-</sup> ) mol <sup>-1</sup> l s <sup>-1</sup> (pH 8)	Reference
Neo Carzinostatin (apo)	10.7	2 1	0.4 x 10 <sup>8</sup>	37
Immunoglobulin G	164	16 16	1.4 x 10 <sup>8</sup>	37
Riboflavin Binding Protein (apo)	29.2	9 9	1.7 x 10 <sup>8</sup>	(137)
Hen egg-white lysozyme	14.3	4 1	2.5 x 10 <sup>8</sup>	(137)
Thioredoxin	12	1 1	6.4 x 10 <sup>8</sup>	(138)

couple and accessibility of the thiol group in the protein. A systematic study of the properties of disulfide free radicals was performed using proteins without thiol functions. Some results are given in tables 9 and 10.

The number of disulfide bonds that can be reduced varies considerably from one protein to another. The case of hen egg-white lysozyme was specially studied (139). The reactive 6-127 disulfide bond was identified by NMR after alkylation of the thiol functions. This bond is in the vicinity of the positively charged end of arginine 5 whereas the others are surrounded by aromatic rings, hence the radical anion is electrostatically stabilized. Modelization by quantum chemistry methods indicates that the most stable geometry of Arginine-disulfide radical anion is close to that of parent protein, indicating that the reorganization energy following reduction should be low.

In table 10, some properties of disulfide radical anions are summarized. Examination of tables 9 and 10 leads to striking conclusions: the rate  $c$  (table 10) vary much more than those of formation. As a consequence, end products also vary: according to the protein, one gets reduced dithiol protein, dimers or others, such as fragment. In lysozyme, the fragmentation might be initiated by electron localization on Arg5 (137). Absorption spectra of disulfide anions are similar, although some differences in extinction coefficients are noticed.

Thioredoxin behaves differently from other proteins. Because of the great interest of the sulphur function in this enzyme (it is the active site of this thiol-disulfide oxidoreductase), the reduction of oxidized thioredoxin was studied in detail (139, 140). The disulfide radical is much more acidic than in other proteins, and its decay leads only to the reduced protein. Site-directed mutagenesis was used to modify selectively two amino-acids, Asp30 and Trp35, in order to observe the modulation of the redox properties of the sulphur functions. It was thus shown that both residues play a role in the proton transfer associated to electron transfer, although differently: for instance, removal of W35 increases the pK<sub>a</sub> of

Table 10  
Some properties of disulfide radicals in proteins

Protein	pK <sub>a</sub>	Maximum absorption (extinction coefficient mol <sup>-1</sup> l cm <sup>-1</sup> )	Decay: ‡ second-order (mol <sup>-1</sup> l s <sup>-1</sup> ) ‡‡ first-order (s <sup>-1</sup> ) (pH 8)	End products	Ref.
Neo Carzinostatin (apo)	5.7	425 (1500)	‡ 1.1 × 10 <sup>4</sup> ‡‡ 5.2	P/(SH) <sub>2</sub> * ?	37
Immunoglobulin G	6.5, 5.5, 4.4	440 (3300)	‡ no ‡‡ 94.3 and 14.3	P/(SH) <sub>2</sub> * HL, H, L** chains	37
Riboflavin Binding Protein (apo)	5.0	425 (3900)	‡ 3.3 × 10 <sup>5</sup> ‡‡ 2.7	P/(SH) <sub>2</sub> * dimers	(138)
Hen egg-white lysozyme	4.6	425 (6600)	‡ 5 × 10 <sup>6</sup> ‡‡ 25.0	P/(SH) <sub>2</sub> * dimers fragment	(137)
Thioredoxin	<3	440 (6750)	‡ 4.0 × 10 <sup>5</sup> ‡‡ 6.7	P/(SH) <sub>2</sub> * only	(140)

\*P/(SH)<sub>2</sub> denotes the reduced dithiol protein.

\*\*H= heavy chain, L = light chain, HL = heavy-light dimer

the disulfide free radical by ca. 2 units but renders the protein less reactive; removal of D30 makes the protein thiyl radical more oxidant towards formate.

## 5. LONG RANGE INTRAMOLECULAR ELECTRON TRANSFER IN PROTEINS

Long Range Intramolecular Electron Transfer (LRET) across peptides and proteins was suggested ca. 30 years ago (141, 142). Now this hypothesis has been verified by numerous observations in model compounds, peptides, natural and modified proteins (for reviews, see 115, 143, 144, 145 and references therein). This phenomenon has biological significance in photosynthesis and respiration, and at a biochemical level, probably in all enzyme-catalyzed redox reactions. It has also been the subject of numerous theoretical treatments based upon Marcus Theory (146, 147, 148 and references therein). It is generally admitted that the rate constant depends on the driving force  $\Delta_r G^\circ$ , a nuclear reorganization parameter ( $\lambda$ ), and the electronic-coupling between the redox centers  $H_{AB}$ . LRET rate reaches its maximum value for  $-\Delta_r G^\circ = \lambda$ . The coupling efficiency depends on the distance between donor and acceptor. The rate constant decays exponentially with distance (149) and an estimation of 1.4 Å<sup>-1</sup> for parameter value of this

exponential decay was first proposed, based on the reactions in bacterial photosynthetic center (150).

### 5.1. LRET in model peptides

Several types of donor-acceptor pairs were used: tyrosine-tryptophan, methionine-tyrosine and pairs of metal complexes. Spacer was specially designed peptides.

The model of intramolecular reduction of tryptophyl radical by tyrosine was first developed by Land and co-workers (151, 152). The process is easily visualized by the use of azide radicals (see 3). Peptides were specially designed for this study. Pioneering work on this reaction was done on flexible oligoglycine peptides as spacers (151, 153, 154). Oligoprolines were then chosen since they are particularly appropriate as more rigid spacers. The donor and acceptor are thus held apart, the distance increases regularly with the number of prolines and a conformational analysis makes possible the determination of the donor-acceptor distance distribution. The number of prolines varied between 1 to 5 (155, 156, 157). The rate constant does fall off exponentially by increasing the number of prolines; however, the decay is more pronounced in Trp-(Pro)<sub>n</sub>-Tyr than in Tyr-(Pro)<sub>n</sub>-Trp, indicating a directionnal effect (156).  $\beta$  values were calculated by two methods, each assuming through-space pathway : (i) assuming each added proline equals 3.1Å, the authors found 0.37 and 0.25 Å<sup>-1</sup> for Trp-(Pro)<sub>n</sub>-Tyr and Tyr-(Pro)<sub>n</sub>-Trp respectively (156); (ii) by conformational analysis of the peptides, authors found 0.28 Å<sup>-1</sup> for Trp-(Pro)<sub>n</sub>-Tyr (157). Activation parameters were also determined in both groups.

Recently, the conformational dynamics of the same peptides was taken into account and relative rate constants averaged over all the conformers were calculated for two assumed competitive pathways: through space (TS) or through the peptide backbone (TB) (158). The authors conclude that in shorter peptides, transfer occurs predominantly by TS pathway whereas it would take place by TB one for longer peptides.  $\beta$  value would be equal to 2.5 nm<sup>-1</sup> for TB pathway.

The role of proton transfer was also investigated. The rate constant of LRET decreases with increasing pH between pH 4 to 6 and then is constant between pH ~7 and 11 (156). No chain-end effect is observed by adding lysine residues at both ends of the peptides. Replacing tryptophan by N-methyl tryptophan, the rate of LRET becomes one order of magnitude higher, however the  $\beta$  value is the same (159). The authors conclude that proton transfer is not rate-determining.

Methionine radicals (Met/S-Br) can oxidize tyrosine or tryptophan residues in peptides by an intramolecular process (160, 161). Mean values of distances between Tyr and Met were calculated by conformational analysis of Met-enkephalin analogs using molecular mechanics and Monte-Carlo techniques (162). A good correlation between distances and rate constants was found.

The group of Isied measured pulse radiolytically initiated LRET from Os(II) to Co(III) (163) and from Os(II) to Ru(III) (164). The rates and activation parameters were determined. Shanze and coworkers worked with a Ru(II) complex linked through polyproline to a p-quinone (165) and with a Re(I) complex-benzoate pair

(166, 167). Initiation of electron transfer was made by excitation of the metal complex with UV-visible light. Although there are main differences between these systems, the obtained results have common features. For instance the rate constant always decreases exponentially with the distance in agreement with theory, but the  $\beta$  values are different : for instance  $\beta = 0.65 \text{ \AA}^{-1}$  for Os-(Pro)<sub>n</sub>- Ru peptides (163). Some of these experimental values were tabulated (145). They range between 0.2 and 2.1  $\text{\AA}^{-1}$ .

In conclusion, it seems that no common value can be taken for  $\beta$ , even when identical spacers are used. It might be that the pathway is not only determined by the spacer.

## 5.2. Reduction of Tryptophan radicals by Tyrosine in proteins

The Trp-Tyr model was also investigated in proteins. The most widely studied one was hen egg-white lysozyme about which LRET was first observed (168). This protein has several advantages, among which a well-known three dimensional structure in crystal and in aqueous solution. However, the drawback is that the protein contains six tryptophan and three tyrosine residues. The rate constant of LRET is equal to  $130 \pm 10 \text{ s}^{-1}$  at room temperature and at pH 7 (169), thus lower than that observed for Trp-(Pro)<sub>5</sub>-Tyr. Its pH-dependence is different from that in Trp-(Pro)<sub>n</sub>-Tyr : it exhibits a maximum near pH 5.4 and decreases both in acidic and basic media. Globally the pH dependence is similar to that of lysozyme inactivation by azide radicals (170). The plot of rate constant vs pH between pH 5 and 7.4 might reflect protonation of Glu35 (171), which is part of the active site. The important participation of the active site in this process is also confirmed by temperature effect : Arrhenius plot of the rate constant at pH 5-6 shows a sharp break at  $\sim 303\text{K}$  like the trend for enzymatic activity (170, 172). The most exposed tryptophan residues are indeed close to the active site (62, 63 and 108). Selective oxidation of Trp62 to N<sup>1</sup>-formylkynurenine caused a large drop in the initial yield of Trp<sup>•</sup> radical, a relatively low decrease of the rate constant, but a pronounced effect on the temperature dependence (172). The authors conclude that Trp62 is one of the major targets of azide radicals. An attempt to identify the involved tyrosine residues was made by use of the program Pathways (173, 174) which attempts to calculate electronic coupling between two residues. This program identifies Trp62/Tyr53, Trp63/Tyr53 and Trp123/Tyr23 as possible pairs involved in the electron transfer (172).

Both groups observe a discrepancy between the yields of Trp<sup>•</sup> radicals (equal to G(N<sub>3</sub><sup>•</sup>) within experimental uncertainty) and that of Tyr<sup>•</sup> radicals which is ca 25% lower. This discrepancy is even more pronounced with one-electron oxidation of other lysozymes (175). These authors tried to identify the final oxidized amino-acids. Among tryptophans, it seems that Trp62 and Trp63 are unaffected, whereas Trp108 and/or Trp111 stayed oxidized. These results are pertinent to the studies of Adams and co-workers who observed inactivation due to oxidation of Trp108 (176). Tyr53 and Tyr20 would be oxidized to dityrosine indicating that Trp62/Tyr53 and Trp63/Tyr53 would be partners in LRET, as proposed in (172). In addition, the process initiates also fragmentation of the polypeptidic chain between residues 13 and 104. Thus it appears that LRET would not be total, and that the concerned residues are not only tyrosines.

### 5.3 LRET in modified metalloproteins

Wild-type metalloproteins were the subject of numerous studies by pulse radiolysis. For instance, one should mention the pioneering work on Cytochrome c (177, 178). Using secondary radicals, it appeared that the reactions with the metal centers almost always involved LRET. Thus several groups tried to modify these proteins in order to bring elements to the determination of electron pathways.

Azurins are "blue" single-copper proteins that mediate electrons in the energy conversion system of several bacteria strains. All sequenced azurins contain a disulfide bridge at one end of a  $\beta$  sandwich structure, 2.6 nm from the copper binding site present at the opposite end of the barrel-shaped protein. The role of the disulfide is probably only structural and the redox center is the copper-containing domain. The disulfide was reduced using  $\text{COO}^{\bullet-}$  free radicals and the resulting disulfide anion decays by LRET to copper (179, 180). Rate constants are typically equal to ca.  $40 \text{ s}^{-1}$ . To investigate the role of medium in LRET, the authors have investigated the reaction on four different wild-type proteins and constructed mutants at single site by site-directed mutagenesis spanning a large range of redox potentials (181, 182). Details of the results were summarized (183, 184).

Most of the mutations have little effect, indicating that the microenvironment was little modified and the reorganization energies are roughly the same. The authors have also temptatively interpreted their results by the use of the program Pathways. The experimental rates correlate well with pathway distance and driving force as predicted by Marcus theory, using a through bond mechanism.

Comparing the rate constants in wild type proteins, it seemed that the presence of a tryptophan residue in position 48 in *P. Aeruginosa* azurin enhances the rate constant. However, mutation of W48 did not change the rate constant (185). Conversely mutation V31W enhanced the rate constant by a factor of  $\sim 4$ . It is suggested that aromatic residues placed in appropriate positions may enhance LRET by a more effective coupling. Recently, the same group has expressed an azurin mutant in which the blue type 1 copper site is replaced by the purple  $\text{Cu}_A$  site of *Paracoccus denitrificans* cytochrome c oxidase (186). The rate constant of LRET between disulfide anion and copper is ca. 3-fold faster than in wild type enzyme in spite of a smaller driving force (0.69 V instead of 0.76V) (187). It is proposed that the higher rate constant would be due to lower reorganization energy.

Another group modified azurin from *Pseudomonas aeruginosa*, by replacing Met121 by His. This His residue was used to complex Ru cation (188). The  $\text{Cu}^+$  to  $\text{Ru}^{3+}$  rate constant yielded a  $\beta$  value of  $1.1 \text{ \AA}^{-1}$  and the LRET is activationless.

[2Fe-2S] Ferredoxins of *Anabaena variabilis* were modified by attachment of Ru(III) complex to the surface histidine 16 (189). The Fe(II)Fe(III)Ru(III) state was formed by pulse radiolysis reduction of  $(\text{Fe(III)})_2\text{Ru(III)}$ . despite a driving force of ca. 0.5 V, no LRET is observed of Fe(II)Fe(III) to Ru(III). The reduced Fe is on the remote side of the [2Fe-2S] cluster from the site of attachment of Ru. The edge-to-edge distance is 16.1  $\text{ \AA}$  but the pathway distance calculated using the program Pathways should be 37.1  $\text{ \AA}$ .

Intramolecular oxidation and reduction in cytochrome c complexes covalently modified was studied by several groups (for review see 190). Histidines (191, 192, 193) and cysteines (194) were used to attach covalently Ruthenium complexes to Fe- or Zn-substituted cytochrome c. Most of the experiments were done using laser flash photolysis. In each series of experiments, the distance was considered as constant and determined by molecular modelling. The free energies span between  $\sim 0.5$  to  $\sim 1.4$  V. The LRET rate constants do vary with the driving force as expected. However the reactions proceed with rate constants lower than those expected on the basis of results obtained on peptides. Results were all analyzed using Marcus theory.  $\lambda$  and  $H_{AB}$  were considered as adjustable parameters. Each series of experimental data was fitted separately (3 to 6 points). In all these papers,  $\lambda$  values go from 1.15 to 1.22 eV and  $H_{AB}$  vary from 0.1 to 0.24  $\text{cm}^{-1}$ . Activation volumes were also measured (195). It seems that the transition state is more compact than the reactant state in both intra- and inter-molecular steps.

#### 5.4 *De novo* design of redox proteins

The role of the very common  $\alpha$  helical structure was investigated as "conducting" structure (196, 197, 198). Conclusions are unclear and rather disappointing : the  $\alpha$  helix structure appears very little conductive. The electron transfer seems to occur through space.

However maquettes for the design of redox proteins were proposed, based on a three helix bundle with a capping Co(III) (bipyridine)<sub>3</sub> electron acceptor at the N-terminus and an electron donor at the C-terminus (199, 200). These proteins were tested for LRET. The  $\alpha$ -helical percent was adjusted by addition of urea or trifluoroethanol (201, 202). Intriguingly, studies of one of the proteins (16-mer-three helix bundle) shows a 2-fold higher LRET rate constant when the percent of helicity is 77% than when it is 0% (denatured in urea). However authors indicate that the kinetics is not a simple first-order one in the presence of urea. They interpret these data as coming from different donor-acceptor distances. The distribution of distances was determined by fluorescence lifetimes fit. Both when helicity is 0% or 77%, distributions peak around 18 Å for the Ru(II) (16-mer)<sub>3</sub>-A (where A=5-(((2-acetyl)amino)ethyl)amino)-naphthalene-1sulfonic acid). Actually the distance appears 0.7Å shorter for  $\alpha$ -helix which is found consistent with the increased rate constant, by the authors.

Other approaches were used to create *de novo* proteins, which are summarized in ref. (195), but none of them has yet been tried for LRET to our knowledge. Another group is focusing on  $\beta$ -pleated sheets (203). Such attempts will indeed bring new elements to the understanding of LRET in proteins.

## 6. BIOLOGICAL CONSEQUENCES

### 6.1. Modifications of the polypeptidic backbone

It was said that reduction as well as oxidation of proteins lead to polypeptidic backbone modifications, fragmentation, dimerization or polymerization. Three



mechanisms leading to dimerization (polymerization) were identified: (i) formation of intermolecular disulfide bonds coming from thiol oxidation; (ii) nitrosylation formation coming from tyrosine oxidation; (iii) dimerization of phenylalanine residues in peptides (71). All these mechanisms intervene in the radiolysis of proteins in the absence of oxygen (74, 204). Oxidations of the peptidic bond were also proposed (205). However intramolecular electron migrations to specific places in of the backbone could also happen (139). The amount of fragmentation versus dimerization increases if irradiation takes place in the presence of oxygen (48, 206). In the presence of oxygen, one mechanism of fragmentation is known, oxidation of C $\alpha$  as detailed earlier (see 2.2). Probably other mechanisms still unknown, are involved.

## 6.2. Enzyme inactivation

Inactivation of enzymatic activity after irradiation has already been reviewed (7, 12, 207). It appeared that inactivation yield produced by radicals of water is small (ca. 5 to 10 % for OH $\cdot$  for example). This inactivation can be the consequence of different effects.

First, the damage of a crucial amino-acid located in the active site of an enzyme can be responsible for inactivation. On papain, inactivation yields were calculated for different irradiation conditions. Oxidation of Cys 25 was shown to be predominantly responsible for the inactivation of papain (79). The authors distinguished "repairable and non-repairable" inactivation processes. Hydrogen peroxide was found to be responsible for the main repairable inactivation. On the contrary, e $_{aq}^{-}$ , OH $\cdot$  and O $_2^{-}$  radicals cause non-repairable inactivation of papain. OH $\cdot$  and O $_2^{-}$  radicals oxidize Cys25 (208). Solvated electron does not appear to react with Cys25 and thus its mechanism of inactivation is attributed to other unidentified modifications. As for lactate dehydrogenase, the radiation inactivation is accompanied by a loss of sulfhydryl groups (probably Cys165 at the active site) (209). Binding of the coenzyme protects the enzyme.

Identification of the amino-acid implicated in the loss of activity can be used to localize the active site of a protein. For dihydroorotate dehydrogenase, oxidation by specific free radicals (Br $_2^{\cdot-}$ , I $_2^{\cdot-}$  and (SCN) $_2^{\cdot-}$ ) shows that Tyr and Cys residues are involved in its catalytic activity (210). In the case of xanthine oxidase, oxidative damage using N $_3^{\cdot}$  and Br $_2^{\cdot-}$ , is initiated by a Trp radical, transferred to a Tyr, itself transferred to a Cys residue. Finally, EPR studies showed that inactivation of that enzyme arises mainly from the alteration of an Iron/sulfur center I of the enzyme (211). Inactivation of ribonuclease is initiated by a tyrosine radical that is transferred to a very important histidine residue for catalytic activity (152). The radical transfer of a residue to another allows interception of the radical by other species. Thus oxygen was shown to protect several enzymes against radiation induced-inactivation (152, 212). Cu-Zn SOD reacts with 1-hydroxyethyl radicals with a rate constant of  $6.8 \times 10^5 \text{ mol}^{-1} \text{ l s}^{-1}$  but is inactivated with a slower apparent rate constant ( $1.3 \times 10^4 \text{ mol}^{-1} \text{ l s}^{-1}$ ) (213). The ratio of these two rate constants might represent the fraction of area covered by the active site.

Second, inactivation can be due to a conformational change of the enzyme (214). For example, chymotrypsin inactivation by OH radical, which can be protected by the presence of oxygen, is pH-dependent (212). This pH dependence,

which is not expected to influence much radical yields, is proposed to be due to changes of the tertiary structure of the enzyme.

Finally, inactivation of an enzyme can be due to the rupture of a covalent bonding. The rate of inactivation of lysozyme by OH is of ca. 15%, and the result of that oxidation is the formation of fragments, dimers and trimers (215).

An application of radiation induced-inactivation, is the determination of the size of the enzyme (216, 217). Nevertheless, care should be taken when using this method as secondary damage due to free radicals generated in the local environment of an enzyme, can influence the apparent target size determined (218). Also, it might be that radiation damage is a surface phenomenon thus not dependent on the volume of the protein but on its surface (19).

### **6.3. Modifications in more biological systems : expected consequences at the cellular level**

Attempts to study protein radiolytic modifications in systems closer to biological media were done. Few experiments were done in reverse micelles (219, 220, 221) and they only concern reactions of  $e_{aq}^-$  with haemeproteins. Radiation-induced chemical degradations of transmembrane  $\alpha$  helices of human erythrocyte glucose transporter were studied at 77 K (222). Results were interpreted in terms of target size determination. The target size is 10-12 times larger than that of each transmembrane helix, demonstrating significant energy transfer in the absence of covalent linkage. Radiolytic inactivation of ion channels formed by gramicidin A is due to oxidation of the 4 tryptophan residues (223). The main radiolytic effect would be cleavage of the peptidic backbone leading to immediate closure of an open channel. Monoamine oxidase which undergoes fragmentation induced by  $OH^\bullet + O_2$ , is protected by lipids in submitochondrial particles (224). Irradiation of cartilage fragments leads to peptidic bond cleavage in proteoglycans with liberation of chondroitin sulfate (225).

Structural and antigenic properties of proteins are expected to change after one-electron redox processes whatever they are. Such effect was demonstrated using ovalbumin and bovine serum albumin (226). Antigenicity was decreased by irradiation. This change could be related to that measured by circular dichroism at 222 nm. The authors suggest that the main part of conformation-dependent antigenic structure is lost by irradiation.

Radiolysis of DNA is modified in the presence of proteins. DNA-binding proteins induce DNA radioprotection toward double strand breaks (227, 228). Proteins such as bovine serum albumin (229, 230) lead to DNA-protein adducts under anaerobic as well as aerobic conditions. A similar result is obtained with chromatin (231). DNA double strand breaks also occur. However  $OH^\bullet$  radicals do not crosslink DNA with lysozyme (232). Tyrosine and tryptophan residues are involved in the crosslinking process (233).

Modified proteins do exhibit new chemical properties of possible biological importance since they participate in damaging reactions and signal induction (4 and references therein). However studies show that oxidized proteins are recognized by protease systems and thus their degradation would be accelerated (234, 235). Some pathways were identified (236, 237).

## 7. CONCLUSION

Protein radiation chemistry has been studied for more than 30 years and a wealth of data has been accumulated. In the solid phase, only modifications of the polypeptidic backbone were shown. They concern the surface. More precisely it seems that weak points are turns and loops. Nothing is known concerning modifications of residues. The knowledge about radiation chemistry of membrane proteins is also extremely poor. Efforts in this field would be relevant for biology. Let us mention that one of the most important free radical producer systems of living cells is partly buried in a membrane (NADPH oxidase) (see for instance 238).

In aqueous solution, the first step is the reaction of free radicals. This reaction proceeds with a rate constant that varies with the nature of the free radical, but very little with the protein. The chemical nature of the resulting odd-electron site(s) can be hypothesized but prediction of its location is still difficult : the reactivity of residues depends on many factors, including accessibility, neighbouring residues, electrostatic guidance... A major role is probably played by reorganization energy following electron transfer. Similarly, the behaviour of this free radical site is highly dependent on the protein. Such a dependence was already known for e. g.  $pK_a$  of residues, reduction potentials.... For instance, a difference of more than 3-4 units may exist between the  $pK_a$  of an amino-acid in solution and that of the corresponding residue in a protein matrix (238). It is thus not surprising to find that residue free radicals can exhibit a similar variety in their chemical properties.

Data concerning final compounds resulting from free radical reactions, are lacking. Reasons are numerous : protein analytical chemistry is difficult and long; some residues, like aromatics, are unstable in analytical conditions; some others, like methionine, get easily oxidized and thus artifacts may take place. However, there is a need for a better understanding of the entire process of one-electron exchange with proteins, because of the involvement of these reactions in many important pathologies (5). Now free radical processes in biology are universally recognized as important at the cellular level, and radiolysis methods provide a unique way of studying their chemical basis.

There is a general interest in the understanding of long range intra-molecular electron transfer mechanisms. The aims are numerous : increase of knowledge about redox processes in life; design of new peptides with specified conducting properties. The process obeys to Marcus theory in the driving force and distance dependences of the rate constant. However it seems that the key parameters ( $\beta$  and  $H_{AB}$ ) have values that vary with the donor-acceptor pair and with the protein. Moreover, up to now, only one process was followed to completion (175) and it appeared that the electron conduction may have "leaks". Thus, a good question is to what extent these processes are really known.

## REFERENCES

1. M. G. Simic, *Agric. Food Chem.* 26 (1976) 6.

2. A. Shafferman and G. Stein, *Biochim. Biophys. Acta* 416 (1975) 287.
3. M. H. Klapper and M. Faraggi, *Quart. Rev. Biophysics* 12 (1979) 465.
4. E. R. Stadtman *Trends Biochem. Sci.* 11 (1986) 11.
5. O. I. Aruoma and B. Halliwell, *Molecular Biology of Free Radicals in Human Diseases*. OIKA International Ltd London (1999).
6. W. R. Markesbery, *Free Radic. Biol. Med.* 23 (1997) 134.
7. C. Von Sonntag *The Chemical Basis of Radiation Biology*, Taylor and Francis, London (1987).
8. Y. J. Suzuki, H. J. Forman and A. Sevanian, *Free Radic. Biol. Med.* 22 (1997) 269.
9. J. Stubbe, and W. A. Van der Donck, *Chem. Rev.* 98 (1998) 705.
10. W. M. Garrison, *Chem. Rev.* 87 (1987) 381.
11. E. S. Kempner, *Quart. Rev. Biophysics* 26 (1993) 27.
12. C. Houée-Levin *J. Chim. Phys.* 91 (1994) 1107.
13. C. O. Stevens, J. L. Long and D. Upjohn, *Proceed. Soc. Exp. Biol. Med.*, 132 (1969) 951.
14. D. J. Marciani and B. M. Tolbert, *Biochim. Biophys. Acta*, 271 (1972) 431.
15. F. Friedberg, *Radiat. Res.*, 38 (1969) 34.
16. A. Filali-Mouhin, M. Audette, M. St-Louis, L. Thauvette, L. Denoroy, F. Penin, X. Chen, N. Rouleau, J-P. Le Caer, J. Rossier, M. Potier and M. Lemaire, *Int. J. Radiat. Biol.* 72 (1997) 63.
17. H. Morishima and H. Hatano, *Bull. Inst. Chem. Res. Kyoto*, 53 (1975) 15.
18. M. Le Maire, L. Thauvette, B. De Foresta, A. Viel, G. Beauregard and M. Potier, *Biochem. J.*, 267 (1990) 431.
19. M. Audette, X. Chen, C. Houée-Levin, M. Potier, and M. Le Maire, *Int. J. Radiat. Biol.* in press (1999).
20. J. H. Miller, D. A. Fedoronko, B. D. Hass, M. Myint and E. S. Kempner, *Arch. Biochem. Biophys.*, 352 n°2 (1998) 281.
21. M. C. R. Symons, *Radiat. Phys. Chem.*, 45 (1995) 837.
22. M. D. Sevilla, J. M. D'Arcy and K. Morehouse, *J. Phys. Chem.* 83 (1979) 2887.
23. D. A. Armstrong, D. Yu and A. Rauk, *Can. J. Chem.* 74 (1996) 1192.
24. M. Jonsson, D. D. M. Wayner, D. A. Armstrong, D. Yu and A. Rauk, *J. Chem. Soc. Perkin Trans. 2* (1998) 1967.
25. A. Rauk, D. Yu, and D. A. Armstrong, *J. Am. Chem. Soc.* 119 (1997) 208.
26. O. Inanami, M. Kubawara, M. Hayashi, G. Yoshi, B. Syuto and F. Sato, *Int. J. Radiat. Biol.* 49 (1986) 47.
27. J. Wilting, H. Nauta, and R. Braams, *FEBS Lett.* 16 (1971) 147.
28. V. Le Tilly, S. Pin, B. Hickel, and B. Alpert, *J. Am. Chem. Soc.* 119 (1997) 10810.
29. R. Braams and M. Ebert, *Int. J. Radiat. Biol.* 13 (1967) 195.
30. M. Faraggi, M. H. Klapper, and L. M. Dorfman, *J. Phys. Chem.* 82 (1978) 508.
31. J. P. Steiner, M. Faraggi, M. H. Klapper, and L. M. Dorfman, *Biochemistry* 24 (1985) 2139.
32. K. Kobayashi, T. Iyanagi, H. Ohara and K. Hayashi, *J. Biol. Chem.* 263 (1988) 7493.

33. A. J. Elliot, P. L. Munk, K. J. Stevenson, and D. A. Armstrong, *Biochemistry* 19 (1980) 4945.
34. K Kobayashi, K. Hirota, H. Ohara, K. Hayashi, R. Miura and T. Yamano *Biochemistry* 22 (1983) 2239.
35. S. Pin, B. Hickel, B. Alpert, and C. Ferradini, *Biochim. Biophys. Acta* 994 (1989) 47.
36. B. B. Hasinoff and I. Pecht, *Biochim. Biophys. Acta* 743 (1983) 310.
37. J. Mönig, R. Chapman, and K. D. Asmus, *J. Phys. Chem.* 89 (1985) 3139.
38. V. Favaudon, H. Tourbez, C. Houée-Levin and J-M. Lhoste, *Biochemsitry* 29 (1990) 10978.
39. M. Faraggi and M. Klapper, *Radiat. Res.* 71 (1977) 311.
40. M. Z. Hoffmann, and E. Hayon, *J. Phys. Chem.* 77 (1973) 990.
41. K. O. Hiller, B. Masloch and K. D. Asmus, *J. Am. Chem. Soc.* 103 (1981) 2734.
42. K. Bobrowski and J. Holcman, *J. Phys. Chem.* 93 (1989) 6381.
43. K. D. Asmus, *Acc. Chem. Res.* 12 (1979) 436.
44. K. M. Bansal and R. W. Fessenden, *Radiat. Res.* 67 (1987) 7099.
45. E. J. Land, and W. A. Prütz, *Int. J. Radiat. Biol. Relat. Stud.* 36 (1979) 75.
46. S. P. Wolff, A. Garner, and R. T. Dean, *TIBS* 11 (1986) 27.
47. E. R. Stadtman, *Annu. Rev. Biochem.* 62 (1993) 3051.
48. H. Schüssler and A. Herget, *Int. J. Radiat. Biol.* 37 (1980) 71.
49. L. Grierson, K. Hildebrand and E. Bothe, *Int. J. Radiat. Biol.* 62 (1992) 265.
50. L. Sjöberg and T. Eriksen, *Radiat. Res.* 89 (1982) 255.
51. T. E. Eriksen and G. Fransson, *Radiat. Phys. Chem.* 32 (1988) 163.
52. M. Tamba, G. Simone and M. Quintiliani, *Int. J. Radiat. Biol.* 50 (1986) 595.
53. M. D. Sevilla, D. Becker and M. Yan, *Int. J. Radiat. Biol.* 57 (1990) 65.
54. M. Bonifacic and K. D. Asmus, *J. Chem. Soc. Perkin Trans. II* (1986) 1805.
55. N. Getoff, *Amino Acids* 2 (1992) 195.
56. M. Göbl, M. Bonifacic and K. D. Asmus, *J. Am. Chem. Soc.* 106 (1984) 5984.
57. K. O. Hiller, B. Masloch, M. Göbl and K. D. Asmus, *J. Am. Chem. Soc.* 103 (1981) 2734.
58. C. Schöneich, F. Zhao, K. P. Madden and K. Bobrowski, *J. Am. Chem. Soc.* 116 (1994) 4641.
59. K. Bobrowski and J. Holcman, *J. Phys. Chem.* 93 (1989) 6381.
60. K. Bobrowski, C. Schöneich, J. Holcman, and K. D. Asmus, *J. Chem. Soc. Perkin Trans. 2* (1991) 353.
61. K. Bobrowski, C. Schöneich, J. Holcman and K. D. Asmus, *J. Chem. Soc. Perkin Trans. 2* (1991) 975.
62. K. Bobrowski and C. Schöneich, *Radiat. Phys. Chem.* 47 (1996) 507.
63. F. Siedler, S. Rudolph-Böhner, M. Doi, H-J. Musiol and L. Moroder, *Biochemistry* 32 (1993) 7488.
64. W. A. Prütz, J. Butler, E. J. Land, and A. J. Swallow, *Int. J. Radiat. Biol.* 55 (1989) 539.
65. E. R. Stadtman, *Free Radic. Biol. Med.* 9 (1990) 315
66. R. T. Dean, S. P. Wolff and M. A. McElligott, *Free Rad. Res. Comm.* 7 (1989) 97.

67. K. Uchida and S. Kawakishi, *FEBS* 332 (1993) 208
68. G. Boguta and A. M. Dancewicz, *Studia Biophys.* 73 (1978) 149.
69. I. Cudina and L. Josimovic, *Radiat. Res.* 109 (1987) 206.
70. Z. Maskos, J. D. Rush and W. H. Koppenol, *Arch. Biochem. Biophys.* 296 (1992) 521.
71. H.J. Kim, L. K. Mee, S. J. Adelstein, I. A. Taub, S. A. Carr and V. N. Reinhold, *Radiat. Res.* 100 (1984) 30.
72. S. Solar, W. Solar and N. Getoff, *J. Phys. Chem.* 88 (1984) 2091.
73. S. P. Gieseg, J. A. Simpson, T. S. Charlton, M. W. Duncan and R. T. Dean, *Biochemistry* 32 (1993) 4780.
74. K. J. A. Davies, M. E. Delsignore and S. W. Lin, *J. Biol. Chem.* 262 (1987) 9902
75. G. Cohen, S. Yakushin and D. Dembiec-Cohen, *Anal. Biochem.* 263 (1998) 232.
76. S. L. Fu, and R. T. Dean, *Biochem. J.* 324 (1997) 41.
77. S. Fu, L. A. Hick, M. M. Hick, M. M. Sheil and R. T. Dean, *Free Radic. Biol. Med.* 19 (1995) 281.
78. R. Langlois, H. Ali and J. Van Lier, *J. Chim. Phys.* 90 (1993) 985.
79. W. S. Lin, M. Lal, G. M. Gaucher and D. A. Armstrong, *Faraday Disc. Chem. Soc.* 63 (1978) 226.
80. W. Vogt, *Free Radic. Biol. Med* 18 (1995) 93.
81. M. R. deFelippis, C. R. Murphy, M. Faraggi and M. H. Klapper, *Biochemistry* 28 (1989) 4847.
82. M. R. DeFelippis, C. P. Murthy, F. Broitman, D. Weiraub, M. Faraggi and M. H. Klapper, *J. Phys. Chem.* 95 (1991) 3416.
83. R. Ahmad and D. A. Armstrong, *Can. J. Chem.* 62 (1984) 171.
84. P. S. Surdhar and D. A. Armstrong, *J. Phys. Chem.* 91 (1987) 6532.
85. S. Navaratnam and B. J. Parsons, *J. Chem. Soc. Faraday Trans.* 94 (1998) 2577.
86. L. Mee and S. J. Adelstein, *Radiat. Res.* 110 (1987) 155.
87. W. H. Koppenol and J. Butler, *Israel J. Chem.* 24 (1984) 11.
88. M. Faraggi and C. Houée-Levin, *J. Chim. Phys.* 96 (1999) 71.
89. B. H. J. Bielski, D. E. Cabelli and R. L. Arudi, *J. Phys. Chem. Ref. Data* 14 (1985) 1041.
90. J-C. Monboisse, M. Gardès-Albert, A. Randoux, J-P. Borel and C. Ferradini, *Biochim. Biophys. Acta* 965 (1988) 29.
91. R. Santus, L. K. Patterson and M. Bazin, *Free Radic. Biol. Med.* 19 (1995) 837.
92. G.R. Buettner, *J. Biol. Chem.* 262 (1987) 11995.
93. K. Kobayashi, K. Hayashi and A.J. Swallow, *Biochemistry* 29 (1990) 2080.
94. C. C. Winterbourn, B. M. Mc Grath and R. W. Carell, *Biochem. J.* 155 (1976) 493.
95. C. Ferradini, J. Foos, L. Gilles, D. Haristoy and J. Pucheault *Photochem. Photobiol.* 28 (1978) 851.
96. J. Thillet and A. M. Michelson, *Free Radic. Res. Commun.* 1 (1985) 89.
97. J. Butler, W. H. Koppenol and E. Margoliash, *J. Biol. Chem.* 257 (1982) 10747.

98. G. Rotilio, R. C. Bray and E. M. Fielden, *Biochim. Biophys. Acta* 268 (1972) 605.
99. J. M. Mc Cord and I. Fridovich, *J. Biol. Chem.* 244 (1969) 6049.
100. E. M. Fielden, P. B. Roberts, R. C. Bray, D. J. Lowe, G. N. Mautner, G. Rotilio and L. Calabrese, *Biochem. J.* 139 (1974) 49.
101. A. Cudd and I. Fridovich, *J. Biol. Chem.* 257 (1982) 11443.
102. K. Sharp, R. Fine and B. Honig, *Science* 236 (1987) 1460.
103. C. L. Fisher, D. E. Cabelli, J. A. Tainer, R. A. Hallewell and E. D. Getzoff, *Proteins* 19 (1994) 24.
104. F. Polticelli, A. Battistoni, P. O'Neill, G. Rotilio and A. Desideri, *Protein Sci.* 7 (1998) 2354.
105. M. E. Stropollo, M. Sette, P. O'Neill, F. Polizio, M. T. Cambria and A. Desideri, *Biochemistry* 37 (1998) 12287.
106. S. Foscarelli, F. Venerini, A. Battistoni, P. O'Neill, G. Rotilio and A. Desideri, *Biochem. Biophys. Res. Commun.* 256 (1999) 425.
107. N. Shimizu, K. Kobayashi and K. Hayashi, *Biochim. Biophys. Acta* 995 (1989) 133.
108. K. Felix, E. Lengfelder, H. J. Hartmann and U. Weser, *Biochim. Biophys. Acta* 1203 (1993) 104.
109. L. Gebicka and J. L. Gebicki, *Int. J. Radiat. Biol.* 63 (1993) 565.
110. K. Kobayashi, K. Hayashi and M. Sono, *J. Biol. Chem.* 264 (1989) 15280.
111. L. Gebicka, D. Metodiewa and J. L. Gebicki, *Int. J. Radiat. Biol.* 55 (1989) 45.
112. A. J. Kettle, D. F. Sangster, J. L. Gebicki and C. C. Winterbourn, *Biochim. Biophys. Acta* 956 (1988) 58.
113. B. H. J. Bielski and P. C. Chan, *J. Biol. Chem.* 250 (1976) 318.
114. D. E. Cabelli, *Adv. Chem. Ser. Photochem. Radiat. Chem.* 254 (1998) 247.
115. R. V. Bensasson, E. J. Land and T. G. Truscott, *Excited states and free radicals in Biology and Medicine* Oxford Univ. Press (1993).
116. R. E. Huie, *Toxicology* 89 (1994) 193.
117. W. A. Prütz, H. Monig, J. Butler and E. J. Land, *Arch. Biochem. Biophys.* 243 (1985) 125.
118. G. Merenyi and J. Lind, *Chem. Res. Toxicol.* 11 (1998) 243.
119. R. H. Bisby, R. B. Cundall, S. Movassaghi, G. E. Adams, M. L. Posener and P. Wardman, *Int. J. Radiat. Biol.* 42 (1982) 163.
120. W. A. Prütz, J. Butler, E. J. Land and A. J. Swallow, *Biochem. Biophys. Res. Commun.* 96 (1980) 408.
121. M. Lal, *Radiat. Phys. Chem.* 43 (1994) 595.
122. G. E. Adams, J. L. Redpath, R. H. Bisby and R. B. Cundall, *Isr. J. Chem.* 10 (1972) 1079.
123. A. J. Elliot, P. L. Munk, K. J. Stevenson and D. A. Armstrong, *Biochemistry* 19 (1980) 4945.
124. M. H. Klapper and M. Faraggi, *Biochemistry* 22 (1983) 4067.
125. J. W. Van Leeuwen, C. Van Dijk and C. Veeger, *Eur. J. Biochem.* 135 (1983) 601.
126. M. Faraggi and M. Klapper, *J. Biol. Chem.* 254 (1979) 8139.

127. K. Kobayashi, K. Hirota, H. Ohara, K. Hayashi, R. Miura and T. Yamano, *Biochemistry* 22 (1983) 2239.
128. R. Hille and R. F. Anderson, *J. Biol. Chem.* 266 (1991) 5608.
129. K. Schäfer and K. D. Asmus, *J. Phys. Chem.* 84 (1980) 2156.
130. K. Kobayashi, S. Tagawa, S. Sano and K. Asada, *J. Biol. Chem.* 270 (1995) 27551.
131. A. Hollaender and C. Doherty, *Radiation Damage and Sulfhydryl Compounds*, International Atomic Energy Agency, Vienna, 1969.
132. P. Wardman and C. Von Sonntag, in *Biothiols, Part A, Methods in Enzymology* 251 (1995) 31.
133. Z. Abedinzadeh, *J. Chim. Phys.* 94 (1997) 262.
134. J. R. Clement, D. A. Armstrong and N. V. Klassen, *Can. J. Chem.* 50 (1972) 2833.
135. X. Fang, J. Wu, G. Wei, H. P. Schuchmann and C. Von Sonntag, *Int. J. Radiat. Biol.* 68 (1995) 459.
136. A. J. Elliot, A. S. Simson and F. C. Sospchyshin, *Radiat. Phys. Chem.* 23 (1984) 377.
137. V. Favaudon, H. Tourbez, C. Houée-Levin and J-M. Lhoste, *J. Chim. Phys.* 88 (1991) 993.
138. C. ElHanine Lmoumene, D. Conte, J-P. Jacquot and C. Houée-Levin, submitted (1999).
139. J. Bergès, E. Kassab, D. Conte, E. Adjadj and C. Houée-Levin, *J. Phys. Chem. A* 101 (1997) 7809.
140. C. ElHanine Lmoumene, D. Conte, J-P. Jacquot and C. Houée-Levin, *Res. Chem. Intermed.* 25 (1999) 313.
141. L. I. Grossweiner, *Curr. Top. Radiat. Res.* 11 (1979) 141.
142. M. H. Klapper and M. Faraggi, *Q. Rev. Biophysics* 12 (1979) 465.
143. G. McLendon, *Acc. Chem. Res.* 21 (1988) 160.
144. H. B. Gray and B. G. Malmstrom, *Biochemistry* 28 (1989) 7499.
145. M. Faraggi and M. H. Klapper, in "Excess Electrons in Dielectric Media", C. Ferradini and J-P. Jay-Gerin Eds CRC Press (1991) 397.
146. R. A. Marcus and N. Sutin, *Biochim. Biophys. Acta* 811 (1985) 265.
147. D. S. Wuttke, M. J. Bjerrum, J. R. Winkler and H. B. Gray, *Science* 256 (1992) 1007.
148. G. A. Mines, B. E. Ramirez, H. B. Gray and J. R. Winkler, *Adv. Chem. Ser. Photochem. Radiat. Chem.* 254 (1998) 51.
149. J. J. Hopfield, *Proc. Natl. Acad. Sci. USA* 71 (1974) 3640.
150. C. C. Moser, J. M. Keske, K. Warnke, R. S. Farid and P. L. Dutton, *Nature* 355 (1992) 796.
151. W. A. Prütz and E. J. Land, *Int. J. Radiat. Biol.* 36 (1979) 513.
152. W. A. Prütz, J. Butler, E. J. Land and A. J. Swallow, *Biochem. Biophys. Res. Commun.* 96 (1980) 408.
153. W. A. Prütz, E. J. Land and R. W. Sloper, *J. Chem. Soc. Faraday Trans. 1* 77 (1981) 281.
154. J. Butler, E. J. Land, W. A. Prütz and A. J. Swallow, *J. Chem. Soc. Chem. Commun.* (1986) 348.



155. K. Bobrowski, K. L. Wierzchowski, J. Holcman and M. Ciurak, *Studia Biophysica* 122 (1987) 23.
156. M. R. DeFelippis, M. Faraggi and M. H. Klapper, *J. Am. Chem. Soc.* 112 (1990) 5640.
157. K. Bobrowski, J. Holcman, J. Poznanski, M. Ciurak, and K. L. Wierzchowski, *J. Phys. Chem.* 96 (1992) 10036.
158. K. Bobrowski, J. Poznanski, J. Holcman and K. L. Wierzchowski, *Adv. Chem. Ser. Photochem. Radiat. Chem.* 254 (1998) 131.
159. A. Mishra, R. Chandrasekar, M. Faraggi and M. H. Klapper, *J. Am. Chem. Soc.* 116 (1994) 1414.
160. K. Bobrowski, K. L. Wierzchowski, J. Holcman and M. Ciurak, *Int. J. Radiat. Biol.* 57 (1990) 919.
161. K. Bobrowski, K. L. Wierzchowski, J. Holcman and M. Ciurak, *Int. J. Radiat. Biol.* 62 (1992) 507.
162. B. Vestermans, K. Bobrowski, J. Betins, G. V. Nikiforovich and K. L. Wierzchowski, *Biochim. Biophys. Acta* 1079 (1991) 39.
163. S. S. Isied, A. Vassilian, R. H. Magnusson and H. A. Schwartz, *J. Am. Chem. Soc.* 107 (1985) 7432.
164. A. Vassilian, J. F. Wishart, B. van Hemelryck, H. Schwartz and S. S. Isied, *J. Am. Chem. Soc.* 112 (1990) 7278.
165. K. S. Shanze and K. Sauer, *J. Am. Chem. Soc.* 110 (1988) 1180.
166. K. S. Shanze and L. A. Cabana, *J. Phys. Chem.* 94 (1990) 2740.
167. L. A. Cabana and K. S. Shanze, in *Electron transfer in Biology and the solid state*, M. K. Johnson, R. B. King, D. M. Kurtz, C. Kutal, M. L. Norton and R. A. Scott eds. *Adv. Chem. Ser.* 226 (1990) 101.
168. J. Butler, E. J. Land, W. A. Prütz and A. J. Swallow, *Biochem. Biophys. Res. Commun.* 96 (1982) 150.
169. M. Weinstein, Z. B. Alfassi, M. R. DeFelippis, M. H. Klapper and M. Faraggi, *Biochim. Biophys. Acta* 1076 (1991) 173.
170. M. Faraggi, E. Bettelheim and M. Weinstein, *J. Chim. Phys.* 94 (1997) 356.
171. K. Bobrowski, J. Holcman, J. Poznanski, and K. L. Wierzchowski, *Biophys. Chem.* 63 (1997) 153.
172. K. Bobrowski, J. Holcman, and K. L. Wierzchowski, *Free Rad. Res. Commun.* 6 (1989) 235.
173. D. Beratan, J. N. Betts, and J. N. Onuchic, *Science* 252 (1991) 1285.
174. J. N. Betts, D. Beratan and J. N. Onuchic, *J. Am. Chem. Soc.* 114 (1992) 4043.
175. M. Audette, Y. Blouquit, M. Faraggi, and C. Houée-Levin, submitted.
176. G. E. Adams, R. L. Willson, J. E. Aldrich and R. B. Cundall, *Int. J. Radiat. Biol.* 16 (1969) 333.
177. E. J. Land and A. J. Swallow, *Arch. Biochem. Biophys.* 145 (1971) 365.
178. M. Faraggi and I. Pecht, *FEBS Lett.* 13 (1971) 221.
179. O. Farver and I. Pecht, *Proc. Natl. Acad. Sci. USA* 86 (1989) 6968.
180. O. Farver and I. Pecht, *J. Am. Chem. Soc.* 114 (1992) 5764.
181. O. Farver, L. K. Skov, M. Van de Kamp, G. W. Kanters and I. Pecht, *Eur. J. Biochem.* 210 (1992) 399.

182. O. Farver, L. K. Skov, T. Pasher, B. G. Karlsson, M. Nordling, L. G. Lundberg, T. Vanngard and I. Pecht, *Biochemistry* 32 (1993) 7317.
183. O. Farver, L. K. Skov, G. Gilardi, G. van Pouderoyen, G. W. Canters, S. Wherland and I. Pecht, *Chem. Phys.* 204 (1996) 271.
184. I. Pecht, and O. Farver, *Adv. Chem. Ser. Photochem. Radiat. Chem.* 254 (1998) 65.
185. O. Farver, L. K. Skov, S. Young, N. Bonander, B. G. Karlsson, T. Vanngard and I. Pecht, *J. Am. Chem. Soc.* 119 (1997) 5453.
186. M. Hay, J. H. Richards and Y. Lu, *Proc. Natl Acad. Sci USA* 93 (1996) 461.
187. O. Farver, Y. Lu, M. C. Ang and I. Pecht, *Proc. Natl. Acad. Sci. USA* 96 (1999) 899.
188. R. Lange, I-J. Chang, J. P. Germanas, J. H. Richards, J. R. Winkler and H. B. Gray, *Science* 268 (1995) 1733.
189. E. Lloyd, N. P. Tomkinson, G. A. Salmon and A. G. Sykes, *Biochim. Biophys. Acta* 1202 (1993) 113.
190. S. S. Isied, in *Electron transfer in Biology and the solid state*, M. K. Johnson, R. B. King, D. M. Kurtz, C. Kutal, M. L. Norton and R. A. Scott eds. *Adv. Chem. Ser.* 226 (1990) 91.
191. T. J. Meade, H. B. Gray and J. R. Winkler, *J. Am. Chem. Soc.* 111 (1989) 4353.
192. B. E. Bowler, T. J. Meade, S. L. Mayo, J. H. Richards and H. B. Gray, *J. Am. Chem. Soc.* 111 (1989) 8757.
193. M. J. Therien, M. Selman, H. B. Gray, I. J. Chang and J. R. Winkler, *J. Am. Chem. Soc.* 112 (1990) 2420.
194. J. L. Wright, K. Wang, L. Geren, A. J. Saunders, G. J. Pielak, B. Durham and F. Millett, *Adv. Chem. Ser. Photochem. Radiat.* 254 (1998) 99.
195. J. F. Wishart, R. van Eldik, J. Sun, C. Su and S. S. Isied, *Inorg. Chem.* 31 (1992) 3986.
196. S. S. Isied and A. J. Vassilian, *J. Am. Chem. Soc.* 106 (1984) 1726.
197. Y. Inai, M. Sisido and Y. Imanishi, *J. Phys. Chem.* 95 (1991) 3847.
198. H. Lee, M. Faraggi and M. H. Klapper, *Biochim. Biophys. Acta* 1159 (1992) 286.
199. M. Lieberman and T. Sasaki, *J. Am. Chem. Soc.* 113 (1991) 1470.
200. M. R. Ghadiri, C. Soares and C. Choi, *J. Am. Chem. Soc.* 114 (1992) 825.
201. M. M. Muntz, G. L. Mc Lendon, J. F. Wishart, E. R. Gaillard and A. F. Corin, *Proc. Natl. Acad. Sci. USA* 93 (1996) 9521.
202. M. M. Muntz, J. F. Wishart and G. L. Mc Lendon, *Adv. Chem. Ser. Photochem. Radiat.* 254 (1998) 145.
203. M. Y. Ogawa, A. B. Gretchikine, S. D. Soni and S. M. Davis, *Inorg. Chem.* 34 (1995) 6423.
204. G. Boguta and A. M. Dancowitz, *Int. J. Radiat. Biol.* 43 (1983) 249.
205. M. Puchala and H. Schüssler, *Int. J. Radiat. Biol.* 64 (1993) 149.
206. C. Capeilliere-Blandin, T. Delaveau and B. Descamp-Latscha, *Biochem. J.* 277 (1991) 175.
207. A. Saha, P. C. Mandal and S. M. Bhattacharyya, *Radiat. Phys. Chem.* 46 (1995) 123.
208. D. A. Armstrong and J. D. Buchanan, *Photochem. Photobiol* 28 (1978) 743.

209. J. D. Buchanan and D. A. Armstrong, *Int. J. Radiat. Biol.* 30 (1976) 115.
210. A. Saha, P. C. Mandal and S. M. Bhattacharyya *Radiat. Res.* 132 (1992) 7.
211. R. F. Anderson, R. Hille and K. B. Patel *Int. J. Radiat. Biol.* 68 (1995) 535.
212. G. E. Adams, K. F. Baverstock, R. B. Cundall and J. L. Redpath 1973, *Radiat. Res.*, 54, 375.
213. D. Santiard, C. Ribière, C. Houée-Levin and R. Nordmann, *Free Radic. Biol. Med.* 19 (1995) 121.
214. K. J. A. Davies and M. E. Delsignore *J. Biol. Chem.* 262 (1987) 9908.
215. E. Franzini, H. Sellak, J. Hakim and C. Pasquier, *Biochem. Biophys. Acta*, 1203 (1993) 11.
216. M. A. A. Parnaik, M. Davis, S. Kaufman and E.S. Kempner *FEBS* 449 (1999) 49.
217. E. S. Kempner *TIBS* 18 (1993) 236.
218. D. C. Eicher, L. P. Solomonson, M. J. Barber, M. J. McCreery and G. C. Ness, *J. Biol. Chem.* 262 (1987) 9433.
219. A. J. W. G. Visser and J. H. Fendler, *J. Phys. Chem.* 86 (1982) 947.
220. C. Petit, P. Brochette and M-P. Pileni, *J. Phys. Chem.* 90 (1986) 6517.
221. L. Gebicka and J. L. Gebicki, *J. Radionanal. Nucl. Chem.* 189 (1995) 175.
222. E. Jhun, B. H. Jhun, L. R. Jones and C. Y. Jung, *J. Biol. Chem.* 266 (1991) 9403.
223. L. Kunz, U. Zeidler, K. Haegele, M. Przybylski and G. Stark, *Biochemistry* 34 (1995) 11895.
224. R. T. Dean, S. M. Thomas and A. Garner, *Biochem. J.* 240 (1986) 489.
225. R. T. Dean, C. L. Roberts and L. G. Forni, *Biosc. Rep.* 4 (1984) 1017.
226. T. Kume and T. Matsuda, *Radiat. Phys. Chem.* 46 (1995) 225.
227. V. Isabelle, J. Franchet-Beuzit, R. Sabattier, B. Laine, M. Spothem-Maurizot and M. Charlier, *Int. J. Radiat. Biol.* 63 (1993) 749.
228. J. Franchet-Beuzit, M. Spothem-Maurizot, R. Sabattier, B. Blazy-Baudras and M. Charlier, *Biochemistry* 32 (1993) 2104.
229. H. Schüssler and H. Hartmann, *Int. J. Radiat. Biol. Relat. Stud. Phys. Chem. Med.* 52 (1987) 269.
230. H. Schüssler, L. Distel and R. Sieber, *Int. J. Radiat. Biol.* 71 (1997) 543.
231. L. K. Mee and S. J. Adelstein, *Int. J. Radiat. Biol. Relat. Stud. Phys. Chem. Med.* 36 (1979) 359.
232. H. Werbin and C. J. Cheng, *Carcinogenesis* 6 (1985) 1689.
233. J. R. Casas-Finet, J-R. Toulme, R. Santus, J. Butler, E. J. Land and A. J. Swallow, *Int. J. Radiat. Biol. Relat. Stud. Phys. Chem. Med.* 45 (1984) 119.
234. K. J. A. Davies and S. W. Lin, *Free Radic. Biol. Med.* 5 (1988) 215.
235. R. T. Dean, *FEBS* 220 (1987) 278.
236. K. J. A. Davies and S. W. Lin, *Free Radic. Biol. Med.* 5 (1988) 225.
237. R. E. Pacifici and K. J. A. Davies in *Oxidative damage and repair. Chemical, biological and medical aspects*, K. J. A. Davies, ed. Pergamon press, Oxford (1991) 364.
238. D. Voet and J. G. Voet, *Biochemistry*, second edition, Wiley, New York (1995).

## Radiation-induced damage in DNA

P. O'Neill

Medical Research Council, Radiation & Genome Stability Unit, Harwell,  
Didcot, Oxfordshire, OX11 0RD, United Kingdom

### 1. INTRODUCTION

The radiation chemistry of deoxyribose nucleic acid (DNA) has generally been studied to gain a detailed understanding of the chemical modifications induced in DNA by ionising radiation. The various biological effects *in vivo* of ionising radiation are thought to be as a consequence of these chemical modifications to DNA [1,2]. Cells have well developed repair systems to deal with DNA damage, essential to maintain the integrity of the genome [3-6]. There is significant information on the various repair pathways which cells utilise to cope with DNA damage. However the recognition and processing of DNA damage does not always occur with total fidelity [3] so that some DNA damages lead to chromosomal aberrations which, if transmissible, may lead to mutations, radiation induced carcinogenesis or to reproductive cell death. More recently radiation-induced DNA damage has been implicated in cell signalling processes [7], such as apoptosis, a process for preventing the propagation of genetically aberrant cells which contain significant levels of DNA damage. Cell killing, radiation mutagenesis, radiation carcinogenesis and genome instability are some of the biological effects which have been suggested to arise from radiation-induced changes to DNA. Two of the main research areas to which knowledge of radiation-induced modifications to DNA has contributed significantly is Radiation Oncology and Radiation Protection. These two fields rely upon close interactions between biophysicists, chemists and (molecular) biologists who are researching to unravel the mechanisms leading to the biological consequences of ionising radiation. Knowledge of the free radical processes leading to radiation-induced DNA damage, the chemical identity of the damage and quantification of the damage  $\text{cell}^{-1} \text{Gy}^{-1}$  provides a) essential information for the development of models to predict the biological effects of radiation at low dose and dose rate for radiation protection, b) links between DNA damage, biochemical processes and radiosensitivity and c) useful leads towards the development of agents, which

may modulate the damage to DNA and may be used as adjuncts in cancer therapy [see Wardman chapter]. The development of radiosensitisers and more recently bioreductive agents as anti-cancer agents for killing of hypoxic regions of tumours is based on radiation-chemical principles and is presented in more detail in another chapter [Wardman]. Further, radiation-chemical studies of DNA have provided the majority of quantitative information on free radical processes, such as rate constants for interaction of water radicals with DNA [8] and spectral information on the resulting DNA radicals. Such information has been essential for the understanding of the mechanisms of action of reactive oxygen species, implicated, for example, in many degenerative diseases and ageing [9].

To date the majority of the information on radiation-induced DNA damage comes from the use of low linear energy transfer (LET) radiations, such as  $\gamma$ -radiation, hard X-rays and high energy electrons. The latter type of radiation is generated by accelerators and is generally used in the technique of pulse radiolysis which has provided most of the quantitative information on the reactivity and types of DNA radicals. Pulse radiolysis has provided the majority of information on the interactions of water radicals with DNA [8]. Other techniques and in particular electron spin resonance (esr) [10] have provided the majority of information on the types of damage produced by direct energy deposition in DNA. Although there have been significant advances in the detection of DNA damage using analytical techniques such as high performance liquid chromatography [11] and gas chromatography with mass spectrometry [12,13], these analytical techniques have been complemented through the use of specific enzymes [5] which recognise certain types of DNA damage. The use of these base excision repair enzymes from *E. Coli* will be discussed later in more detail.

More recently, data using high linear energy transfer (LET) radiations are appearing on the chemical characteristics of DNA damage. This information should provide useful insights into the identification of 'novel' lesions produced by high LET radiation, since the biological effectiveness of ionising radiation increases with increasing LET of the radiation [15]. Although any 'unique' lesions produced by high LET radiation may contribute to the enhanced biological severity of high LET radiation, it is thought that this increase reflects the increased ionisation density of high LET radiations, such as  $\alpha$ -particles [16,17]. Therefore track structural considerations are fundamental to understanding radiation induced, cellular DNA damage. LET is defined as the average energy deposited through interactions per unit distance traversed by the radiation track. Radiation chemistry and its dependence on track structure is reviewed in another chapter. The major focus of this chapter is the chemistry of DNA damage, how the DNA structure may alter the chemistry and distribution

of products compared with the simpler model systems generally studied [1,2,14] and to give an idea on how this damage may influence the biological effects of ionising radiation.

## 2. STRUCTURE OF DNA

The chemical composition of DNA, a long chained biopolymer, consists of a 2'-deoxyribose phosphate backbone with the four bases, namely adenine and guanine, the two purines, and thymine and cytosine, the two pyrimidines, attached through the C(1)' position of the 2'-deoxyribose group by a  $\beta$ -glycosidic bond. The primary structure of one of the strands of DNA is shown in Figure 1. In its biological form DNA is double stranded and the two strands

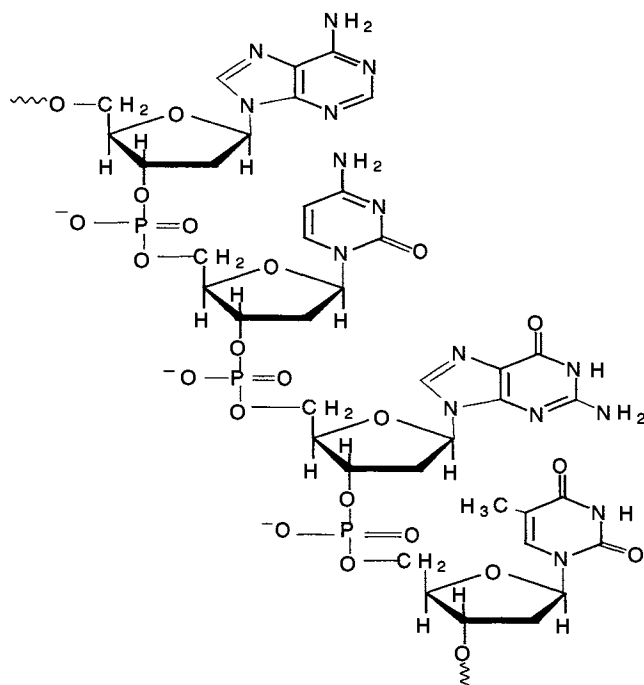


Figure 1. The structure of one strand of DNA

are held together in the Watson and Crick structure by hydrogen bonding of the complementary bases. Adenine is hydrogen bonded with its complementary base, thymine and guanine with cytosine. The binding of the guanine/cytosine pair is through three H-bonds and is stronger than that of the adenine/thymine pair which has only two H-bonds. Water plays a significant role in stabilising DNA's secondary and tertiary structures [18]. The primary hydration shell

consists of ~10 water molecules per nucleotide with about 5 water molecules associated with each phosphate group. Hydrogen bonding between water and the nucleobases determines the assembly of DNA. 'Dry' DNA is in the A-form which is converted into the B-form on full hydration of the DNA. Fully hydrated DNA has ~20 water molecules per nucleotide. These water molecules have different properties to that of bulk water. The double strandedness of DNA is required for its replication in cells so that at mitosis two cells are formed which carry identical genetic information. DNA damage may prevent cell division, reproductive cell death or, if the damage is transmissible, then the daughter cell will contain a mutation, a change in the genetic make-up of the cell.

The double stranded structure of DNA may also influence the site of interaction of diffusible water radicals through reduced accessibility to certain sites [19-21]. For instance, C-5 and C-6 of thymine and cytosine and C-5 and C-8 of adenine and guanine face into the major groove of DNA and are therefore solvent accessible. The distribution of radical attack at the different carbon atoms of the nucleobases may be different to that determined with the mononucleotides. In section 4.3, the influence of the accessibility of the minor groove to the hydroxyl (OH) radical on H-atom abstraction from the various carbon sites of sugar moiety is discussed.

### **3. CELLULAR DNA DAMAGE INDUCED BY IONISING RADIATION**

Ionising radiation randomly induces a variety of damages to cellular DNA. The most frequent types of DNA damage produced are single (ssb) and double (dsb) strand breaks, base and sugar modifications and DNA-protein crosslinks [1,2,22,23]. Typical yields of these types of cellular DNA damages induced by low LET radiation under aerobic conditions are shown in Table 1. Over the years considerable evidence has accumulated showing that OH radical scavengers afford considerable protection to cells from ionising radiation as shown in Table 2. From these studies it is thought that radiation-induced damage to cellular DNA is due to direct energy deposition in DNA and its associated water of hydration or by indirect effects involving diffusible water radicals and in particular the OH radical. The indirect effect involves OH radicals that are formed within about 3-4 nm of the DNA [24], diffuse and upon interaction with DNA cause damage. For low LET radiation the indirect effect contributes about 60% to the overall effect but considerably less for high LET radiations. Therefore in the cell it is considered that DNA and its surrounding water molecules are a potentially critical target, damage to which initiates the biological effects of radiation.

Since many of the damages are recognised and removed by the cell's repair systems resulting in restitution of genome stability [3], it is thought that non-repaired dsb are major lesions leading to reproductive, cell death. Other types of clustered DNA damage (Section 7), in which two or more DNA lesions are produced within a few tens of base pairs on either strand of the DNA, should not be overlooked as major DNA modifications which may contribute to the biological severity of radiation. In fact, the majority of studies on cellular DNA damage have focussed on strand breakage [23,25,26], although more recent experimental data are becoming available on clustered DNA damage [27,28]. The biological role of clustered DNA damage has been hypothesised in the light of the increased biological effectiveness of high LET radiations [15] and from track structure simulations of DNA damage [16,29, Section 4.5].

The yield of radiation-induced DNA damage is also critically dependent upon the cellular environment. In eukaryotic cells, nuclear DNA is associated with histone and non-histone proteins in a chromatin complex [30]. These histones

Table 1

The yield (damage Gy<sup>-1</sup> cell<sup>-1</sup>) of various lesions produced in human mammalian cells irradiated under aerobic conditions

<u>DNA damage</u>	<u>lesions</u> Gy <sup>-1</sup> cell <sup>-1</sup>	<u>cell type</u>	<u>Radiation</u>	<u>reference</u>
single strand break	1000			
double strand break	23-37	various	<sup>60</sup> Co γ-rays	[23]
DNA-protein crosslinks	46	V79-4 cells	<sup>60</sup> Co γ-rays	[134]
thymine glycol	486	human lung carcinoma cells	<sup>137</sup> Cs γ-rays	[54]
8-oxo-7,8-dihydroguanine	119	monocytes	<sup>60</sup> Co γ-rays	[57]
Fpg sensitive sites	264	monocytes	<sup>60</sup> Co γ-rays	[57]
endonuclease III sensitive sites	295	monocytes	<sup>60</sup> Co γ-rays	[57]
Fpg + endonuclease III sensitive sites	500	human lymphoblast cells	250 kv X-rays	[56]



**Table 2**  
 Percentage Protection by Radical Scavengers on a Variety of Biological Endpoints Under Aerobic Conditions

Cells and Conditions	% Protection	Biological Endpoint	ref
CHO/DMSO	62	Survival, ssb	[135]
L 5178Y/Variou alcohols	71	ssb	[24]
L 5178Y/Variou alcohols	65	survival	[24]
V79/glycol or DMSO	65-67	ssb, survival	[136]
V79/DMSO	~60	Survival	[137]
V79/DMSO	44	dsb	[137]
V79/DMSO/LET KeV/ $\mu$ m	120 ~30%	dsb, Survival	[138]
V79/DMSO/LET KeV/ $\mu$ m	180 ~56	Survival	[139]

may partially protect the DNA from diffusible radicals produced in its vicinity [30]. The chromatin structure (cellular DNA packaging) has also been proposed to increase the probability of producing large, non-randomly produced DNA deletions up to several tens to thousands of base pairs in length, particularly for high LET radiations [31]. The reader is directed to the following reviews on chromatin effects [32,33]. The influence of the chemical environment of cellular DNA is demonstrated in the different radiosensitivity of cells in the presence of oxygen and thiols. For instance, in the presence of oxygen, cells are more radiosensitive to low LET radiation as compared with cells under hypoxia [2, 15, see chapter by Wardman]. The oxygen enhancement ratio (OER) is generally around 3 for cell killing, i.e. the dose required to give the same extent of cell inactivation is 3x less for irradiation under aerobic compared with hypoxic conditions, and is slightly higher for strand break induction for low LET radiations. Endogenous thiols protect cells to varying degrees from the deleterious effects of radiation, especially under hypoxic conditions [2]. As

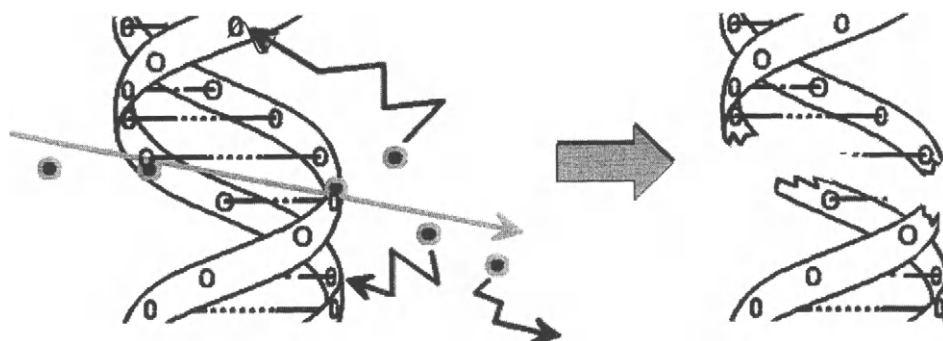


Figure 2 Schematic representation of the formation of a DNA double strand break as the radiation track deposits energy (circles). The zigzag arrows represent random diffusion of the water radicals.

these agents, oxygen and thiols, have to be present at the time of irradiation [34], it is believed that free radical processes are involved in these interactions as distinct from the generally slower biochemical processes. Agents that could mimic the effects of oxygen but have no effect on aerobic cells when irradiated led to the development of radiosensitisers and bioreductive agents (see Chapter by Wardman). Rapid mix experiments have provided convincing evidence for the biological effects of ionising radiation in the presence of radiosensitisers, arising through fast free radical processes initiated by the radiation.

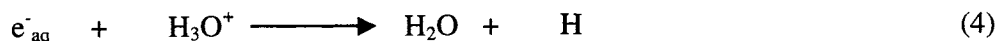
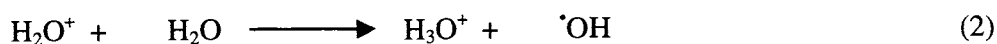
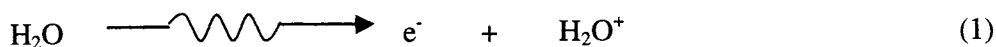
The deposition of energy by ionising radiation occurs as a succession of energy loss events as the photon/particle progresses through the medium/cell. The biophysics of the track are described elsewhere [35]. The biological consequences of a given dose of radiation also vary depending on whether the radiation used is high or low LET. Increasing the LET of the radiation leads to an increase in the effectiveness of the radiation to cause cell inactivation, mutations and cancer [15]. This increased effectiveness of high LET radiations is thought to reflect the higher ionisation density of the track as it passes through and deposits energy near to or in the DNA to produce DNA damage [35,36] by both the indirect and direct pathways. The effects of this spatial distribution of DNA lesions resulting from energy deposition in small volumes within DNA or its immediate environs is the formation of clustered DNA damage (also referred to as multiple damaged sites), which are a fingerprint of the radiation track (Figure 2). A clustered DNA damage is the formation of two or more lesions, as described above, within a few tens of base pairs on either strand of the DNA. A DNA dsb is a specific type of lesion contributing to the spectrum of clustered

DNA damages. Clustered DNA damage is a special feature of ionising radiation and may compromise the ability of the cellular repair machinery to recognise and process the damage faithfully. This concept of the spatial distribution of the lesions reflecting the structure of the radiation track is an important feature of ionising radiation-induced damage to DNA, as distinct from the more isolated type of damages caused by reactive oxygen species (ROS) [9]. Although many of the elementary chemical modifications of DNA induced by ROS and ionising radiation are similar, it is important to appreciate that the spatial distribution of radiation-induced DNA damages makes it distinct from oxidative damage. Generally isolated damages are processed efficiently by the cell whereas more complex damages may present a challenge. At present there is little direct, experimental evidence for the presence of clustered damage in cells, with the exception of dsb, and the identification of clustered damage will provide an analytical challenge for chemists.

#### 4. EARLY PROCESSES IN RADIATION-INDUCED DNA DAMAGE

The various processes that contribute to the absorption of ionising radiation are described elsewhere [37]. In general most of the energy is deposited by secondary electrons which are formed from ionisation events that produce a positive ion and an electron, ejected with sufficient energy to cause further ionisations and excitations. For a 10 MeV electron about 76% of the energy is deposited as isolated spurs (energy deposited between 6-100 eV) and 8% and 16% of its energy as blobs (energy deposited between 100-500 eV) and short tracks (energy deposited between 0.5-5 keV) respectively. The partition of these track entities into specific energy domains is purely arbitrary. Indeed DNA dsb are produced predominantly by the low, energy secondary electrons (blobs and short tracks) of the radiation track for low LET radiation [25]. Since the biological effects of radiation result from direct and indirect effects and the cell contains ~80 % water, it is thought for low LET radiations that the majority of the indirect effect arises from diffusible water radicals. In the radiolysis of water the main species produced are OH radicals, H-atoms and hydrated electrons,  $e_{-aq}$  [38]. A small quantity of molecular products are formed namely hydrogen peroxide and hydrogen. The yield of OH radicals and hydrated electrons are similar whereas the yield of H-atoms is only ~10% of the overall yield of water radicals. The following reactions (1-4) show the main features of the radiolysis of water. The rate constants for reaction of the OH radical,  $e_{-aq}$  and H-atoms with polynucleotides and single and double stranded DNA are compiled in the following reference [8] and are of the order of  $10^8 - 10^9 \text{ dm}^3 \text{ mol}^{-1} \text{ s}^{-1}$ . The OH radicals interact with either the sugar phosphate by H-atom abstraction or by addition to the nucleobases. About 20% of the interactions of

the OH radical occur at the sugar phosphate and about 80% at the bases. H-atoms and  $e^-_{aq}$  interact predominantly by addition to the nucleobases [2].



It is important to bear in mind that in the cell the DNA radicals formed on interaction with water radicals occur within a few nanoseconds based on the mean diffusion distance of water radicals of  $\sim 4$  nm in the cell. However, the DNA radicals formed in the cell may persist for tens of milliseconds even extending to seconds at ambient temperatures. It is during this period that the DNA free radicals are susceptible to chemical interactions with additives or indeed may undergo hydration reactions. These interactions may change the distribution of the types of persistent DNA damage observed or their amounts resulting ultimately in different biological effects, for instance the effect of oxygen on damage modification. Another consideration is the possibility that the DNA radicals may undergo secondary reactions which are not generally observed in studies using the mononucleotides(sides). These differences may for instance be due to the DNA structure and the influence of the complementary base to undergo proton transfer through the hydrogen bond and to the extended lifetime of the radicals when in DNA.

The interactions of water radicals with the free bases, (deoxy)nucleosides, (deoxy)nucleotides, oligo(deoxy)nucleotides and DNA and the interactions of the resulting bio-radicals with oxygen have been extensively documented [1,2,14,39] and are described in detail in an accompanying chapter by von Sonntag. The following sections therefore give only a brief synopsis of these interactions concentrating on the OH radical which is considered to be the main water radical leading to strand breakage and base modifications, although the contribution of  $e^-_{aq}$  to base modifications should not be overlooked.

#### 4.1. OH radical-induced base damage

The OH radical is electrophilic in nature so it interacts by addition with unsaturated systems at sites of high electron density. Therefore with the nucleobases which contain a  $\pi$ -system (see Figure 1), the OH radical interacts predominantly by addition. With pyrimidines, the OH radical interacts with the C(5)=C(6) double bond to produce the radicals shown in Figure 3. These two

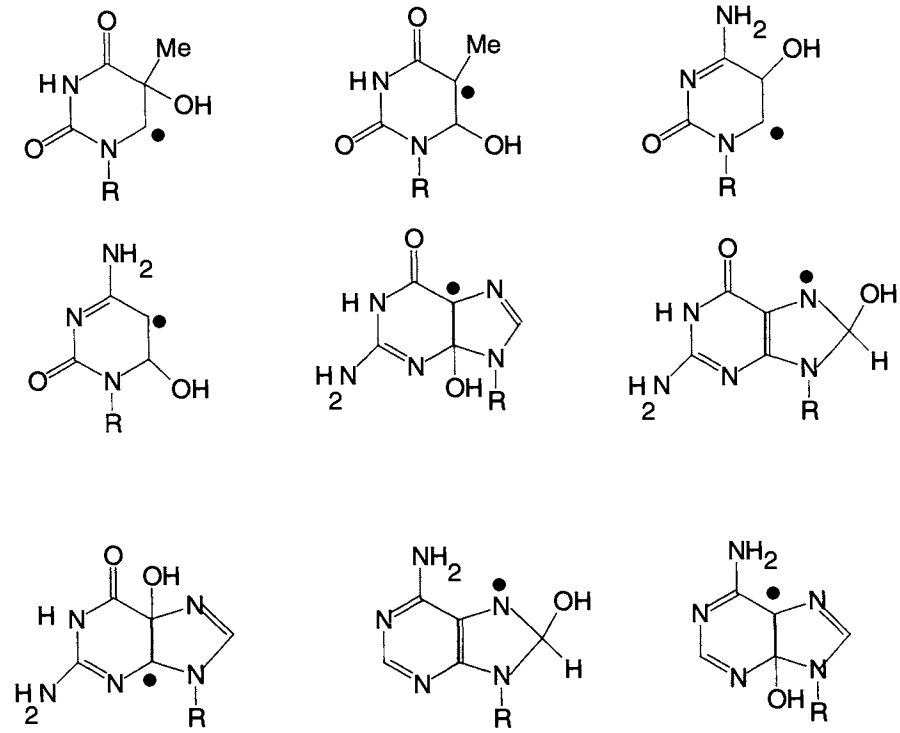


Figure 3. Some of the main OH-adducts formed on interaction of the OH radical with the nucleobases.

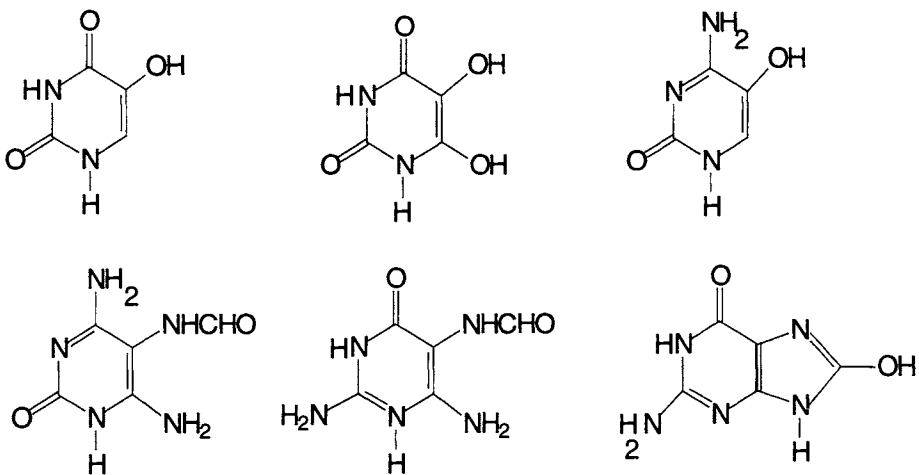


Figure 4. Some of the major products detected in irradiated DNA [2,13].

radicals are readily distinguished through their different redox properties where the 5-hydroxy-6-yl radical is reducing and the 6-hydroxy-5-yl radical is oxidising [40,41]. The relative yields of these radicals are presented in Table 3. With thymine a minor radical is formed by H-atom abstraction from its methyl group. In the presence of oxygen, these pyrimidine radicals interact with oxygen by addition to produce the corresponding peroxy radical adducts [2]. Some of the major products that have been detected in irradiated DNA in cells are shown in Figure 4.

The interaction of OH radicals with the purines, guanine and adenine, are also shown in Figure 3. The OH radical adds preferentially to positions C(4) and C(8) of the purine ring [14,42,43]. Addition to C(5) of the purine is a minor process. Both the C(4) and C(8) radicals of adenine undergo unimolecular transformations. The C(4) adduct of adenine undergoes a dehydration reaction to yield a radical, which has strong oxidising properties [44,45]. In the absence of oxygen the C(8) radical of adenine, which is strongly reducing undergoes

Table 3

Yields of oxidising and reducing radicals produced on interaction of the OH radical with mononucleotides (side)

OH-adduct	Yield of radicals <sup>1</sup>		
	reducing	oxidising	References
Guanine			
C(4)-OH +			
C(5)-OH		51-59	[42,43]
C(8)-OH	>16	7	[43]
Adenine			
C(4)-OH		30	[44]
C(5)-OH		<5	[43]
C(8)-OH	37		[43]
Cytosine			
C(5)-OH	88		[40]
C(6)-OH		10	
Thymine			
C(5)-OH	64		[41]
C(6)-OH/CU <sub>2</sub> -T		-30	

<sup>1</sup>expressed as a percentage of the OH radical yield.

ring-opening in the absence of oxygen, to yield the 5-formamido-pyrimidine radical. However in the presence of oxygen, the C(8)-OH adduct of adenine is oxidised to yield 8-hydroxyadenine [14]. Similar reactions occur involving the corresponding OH adducts of guanine. The C(4)-OH adduct of guanine dehydrates to yield a radical, which has oxidising properties. The C(8)-OH adduct of guanine ring-opens in a unimolecular process in the absence of oxygen to yield the 5-formamido-6-amino-pyrimidine radical. In the presence of oxidants or oxygen, the C(8)-OH adduct of guanine is oxidised to yield 8-oxo-7,8-dihydroguanine, an important product, the presence of which is a probe for oxidative DNA damage. The major permanent products formed from the purine bases on irradiation of DNA are shown in Figure 4.

Many of the products formed from OH radical interactions with DNA in aqueous solution have been well documented [12,14]. However with DNA, not all the ring carbons of the bases are solvent accessible so that the product distribution in DNA may differ to that for the mononucleotides. Furthermore, the reactions of the OH-induced base radicals in DNA may have additional routes of reaction not available in the monomers. For instance, an interesting reaction that may occur in DNA is the intra-molecular oxidation of guanine by the dehydrated adenine radical, if they are in close proximity. In fact there is substantial evidence for such a transfer initiated by one-electron oxidation of DNA (see Section 6). Radiation-induced damage transfer is an example of a reaction which occurs efficiently in DNA but which is very inefficient when involving an inter-molecular electron transfer between deoxynucleotides [47]. A further example is the formation of tandem lesions in  $\gamma$ -irradiated oligonucleotides containing thymine and guanine [48-50]. That these tandem lesions arise from two primary radicals is discounted based on the dose dependence for their formation. The mechanism of their formation is not known but it was suggested that the C(6)-OH adduct of thymine interacts with oxygen and that the resulting peroxy radical is reduced by the neighbouring guanine. The resulting one-electron oxidised guanine radical is known to yield 8-oxo-7,8-dihydroguanine in the presence of oxygen. These tandem lesions represent an amplification of damage by an electron transfer process. If formed in double stranded DNA, such tandem lesions may pose a challenge to the repair machinery, although they would be on the same strand. A recent study [51] showed that a synthetically inserted, tandem damage is excised by *E. Coli* formamidopyrimidine-DNA glycosylase (Fpg) and with *E. Coli* endonuclease III, the formylamido-damage is excised but not 8-oxo-7,8-dihydroguanine. The formylamido-damage is alkali labile but not the 8-oxo-7,8-dihydroguanine. Interestingly, the 3' and 5' exonuclease activity of snake venom and calf spleen phosphodiesterase are inhibited by this tandem damage. Another example of damage amplification is presented in Section 4.3 where the OH-radical adducts

of the bases may lead to strand breakage in DNA in the absence or presence of oxidants through transfer of the radical site from the base moiety to an adjacent sugar phosphate in the DNA backbone.

The majority of the information on DNA base damage has come from irradiated DNA in solution and there are few studies on cellular DNA damage. At present the background levels of base damage determined in cellular DNA are relatively high presumably due to their formation in the extensive work-up required to quantify the damage [11,13,52]. In fact one of the major purine modifications in the DNA is the formation of 8-oxo-7,8-dihydroguanine, which may also be formed on oxidation of guanine under the conditions of the work-up. The accurate quantification of the yields of 8-oxo-7,8-dihydroguanine and the other base products in the absence of artefacts remains a challenge for the analytical chemists. The importance of the accurate detection of 8-oxo-7,8-dihydroguanine is in its use as a potential bio-marker of oxidative damage in cells. A further problem is the large doses required to produce sufficient product for analytical detection. For instance, the products formed may alter the reaction pathways occurring in DNA of irradiated cells. For instance 8-oxo-7,8-dihydroguanine is more readily oxidised than guanine [53] and therefore when formed could subsequently interfere in radiation-induced electron migration in DNA (see Section 6). An additional, future challenge is therefore the detection of DNA base modifications by analytical methods which at present lack the sensitivity required for detection at biological relevant doses of ~1-2 Gy. A method based on immuno-chemical recognition coupled with capillary electrophoresis and laser-induced fluorescence detection [54] has reduced the detection limit several orders of magnitude. For instance,  $3 \times 10^{-21}$  moles of radiation-induced thymine glycol have been detected in human cells using a dose of only 0.05 Gy. The yield of thymine glycol produced by irradiation of A549 cells is 0.9 per  $10^7$  bases per Gy. Some typical yields of radiation-induced DNA base damages determined from cells irradiated with low LET radiation are shown in Table 1. Some caution must be exercised in using these values since several of the presently used analytical techniques may produce oxidised DNA products upon work-up or the enzyme probes may be <100% efficient at excising the damages which they recognise.

More recently, various biochemical methods have been used based on enzymes which recognise specific base damages. The enzymes are capable of excising specifically damaged bases by hydrolysis of the N-glycosidic bond linked to the modified base. The resulting abasic site is cleaved by the associated AP lyase activity to convert the abasic site to a strand break as shown in Figure 5 for Fpg and endonuclease III, the two most generally used enzymes. There are several extensive reviews of the activity of these proteins and the specific lesions they recognise and excise [3-5,55]. Endonuclease III and Fpg have been used to



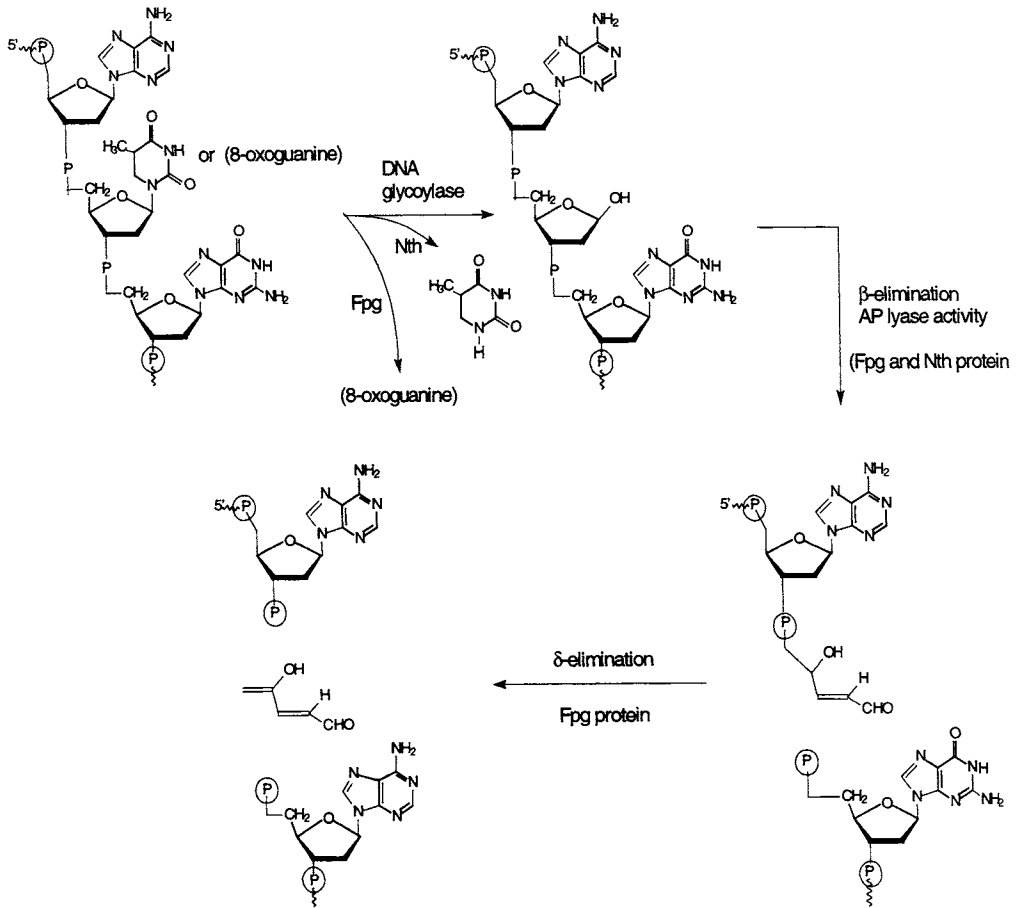


Figure 5. Excision of a damaged DNA base by endonuclease III and Fpg proteins followed by  $\beta,\delta$  elimination of the AP site.

determine the yields of base damage induced by radiation in a variety of cells [56,57] (see Table 1). The advantage of this enzymatic approach is the use of biologically relevant doses to induce DNA damage. However it has not been established that they efficiently remove all the damage that they recognise [58]. Each glycosylase is specific to the types of lesions they recognise. In general, endonuclease III recognises pyrimidine products in which the 5-6 double bond is saturated such as thymine glycol, 5,6-dihydrothymine, uracil glycol, 5,6-dihydrouracil, 5-hydroxy-6-hydrothymine, 5-hydroxy-6-hydrouracil, abasic sites and ring-opened and degraded pyrimidines. In contrast, Fpg recognises oxidised purine damages such as 8-oxo-7,8-dihydroguanine, formamido-pyrimidines and abasic sites. Whether Fpg recognises 8-oxo-7,8-dihydroadenine remains open to

question.

These enzymatic approaches have also been used to study the mechanisms of base damage induction in DNA through determination of the yields of enzyme sensitive sites induced in plasmid DNA. Plasmid DNA has proven to be extremely useful for detecting damage following irradiation of aqueous solutions containing different concentrations of radical scavengers. Briefly, plasmid DNA is circular DNA which is in the supercoiled form (closed circular). If a ssb (either prompt ssb or an induced ssb through subsequent treatment of the irradiated DNA) is induced in the supercoiled form, the plasmid DNA is converted into the relaxed circular form (open circular). If a dsb is induced, the plasmid DNA is linearised as shown schematically in Figure 6. These different forms of the plasmid have different mobilities and are readily distinguished by agarose gel electrophoresis, so that the system is sufficiently sensitive that only ONE ssb is readily detected. The various forms may be quantified using fluorescent dye staining and fluorescence imaging. OH radical scavengers are added to the plasmid DNA solutions so that the cell conditions with respect to radical diffusion distances may be mimicked. Therefore a plasmid DNA solution containing radical scavengers has the following advantages:-

- i) the scavenger concentration establishes the lifetime of the radicals in solution and as such determines the mean diffusion distance of the water radicals. From cellular studies, it is established that the mean diffusion distance of OH radicals in the cell is about 4 nm, which corresponds to a scavenging capacity of  $\sim 10^9 \text{ s}^{-1}$  and
- ii) the yield of ssb ( prompt or enzyme sensitive sites) per DNA molecule per Gy is readily determined.

Therefore, under conditions where the majority of the damage is induced by isolated OH interactions with DNA (e.g. scavenging capacity  $< 5 \times 10^7 \text{ s}^{-1}$ ), the yields of enzyme sensitive sites relative to the yield of prompt ssb under aerobic conditions are about 0.6 for endonuclease III sites and 1.0 for Fpg sites [59-61]. These yields of base damage are compared with the combined yield of prompt and heat-labile ssb. The ratio (1:1.6) of the yields of endonuclease III sites to Fpg sites, where the latter are predominantly due to purine damages, is similar to the analytically determined ratio of 1:1.5 for the yields of oxidised pyrimidines to oxidised purines [62]. The predominant purine damage induced by ionising radiation is 8-oxo-7,8-dihydroguanine. Since heat-labile ssb contribute  $\sim 30\%$  of the total yield of prompt and heat-labile ssb [63], it is estimated that the yield of base damage induced by OH radicals and recognised as enzyme sensitive sites is about 2-2.5 x the yield of prompt ssb. The yield of base damage induced in cells by low LET radiation is significant compared with the yield of prompt ssb.

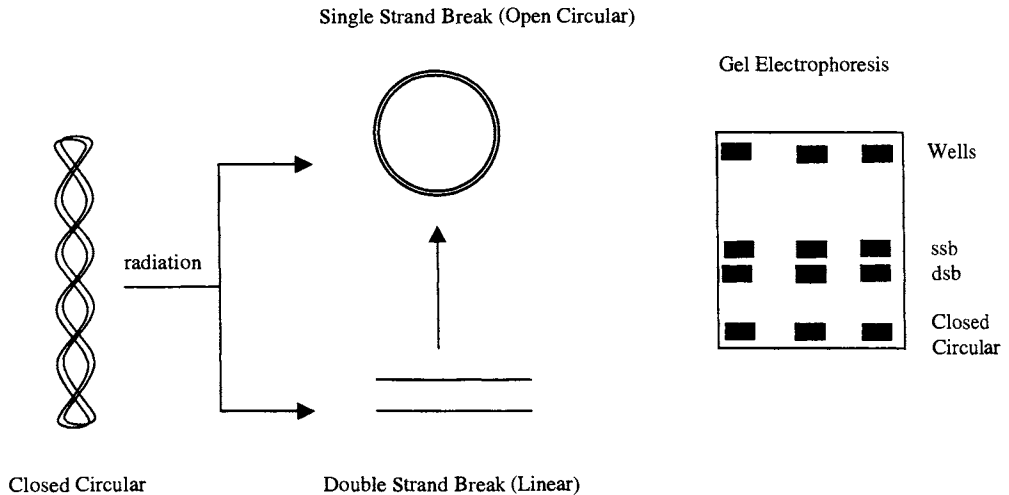


Figure 6. Electrophoretically distinct forms of plasmid DNA after irradiation. Gel electrophoresis used to distinguish and quantify the various forms.

#### 4.2. Base damage by direct effects

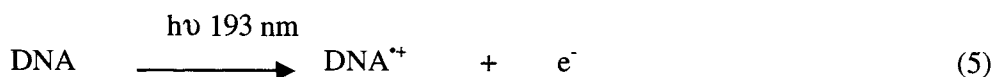
There is less information on the types of base damage produced by the direct deposition of energy in DNA. The majority of the information on free radical intermediates produced in DNA by ionising radiation has come from electron spin resonance (esr) studies and has been reviewed in detail elsewhere [10]. The DNA samples are generally irradiated in frozen, aqueous solutions at 77K and the free radical intermediates characterised by esr. Irradiation at 77K ensures that the DNA species are produced by direct effects, since reactions with diffusible water radicals, which occur at 310K, are 'frozen-out'. Effectively two major radicals were observed; the guanine radical cation and the cytosine/thymine radical anion. Since all the bases absorb energy and ionised to produce their corresponding radical cation (electron hole centre) and an electron, the guanine radical cation is therefore formed through migration to and localisation of the electron hole centres at guanine. This process is thermodynamically favoured since guanine has the lowest oxidation potential ( $E$  1.24V, [64]) of all the DNA bases. The ejected electrons migrate and become localised at the pyrimidines, the bases with the highest reduction potentials [65]. The most recent findings are interpreted in terms of formation of the electron adduct of cytosine [66]. Since ionisation of the water of hydration in the first solvent shell of DNA may also occur to produce  $H_2O^{+*}$  at 77K, it is suggested that  $H_2O^{+*}$  subsequently oxidises its associated base thereby transferring the damage into DNA in competition with its conversion into an OH radical. There is some evidence for the formation of OH radicals in the outer hydration shells

of DNA [67]. At present there is little evidence for the formation of sugar radicals or phosphorus radicals with low LET radiation at these temperatures however they probably are formed but are difficult to detect. Irradiation of DNA under these conditions but with a high LET  $^{16}\text{O}^{8+}$  ion beam has shown that carbon-centred radicals are formed, indicative of sugar radicals and that a low yield of phosphorus-centred radicals are produced [68].

These esr studies were essentially the first to show that ionisation events in DNA lead to charge migration in DNA. More recently, charge migration in DNA has been confirmed at ambient temperatures through photochemical induced one-electron oxidation of DNA and the use of 193 nm light [69] which is capable of ionising DNA but not water in monophotonic processes. Radiation-induced charge migration in DNA is discussed in Section 6.

As shown in Section 4.1, there is a vast literature on the interactions of water radicals with DNA at ambient temperatures whereas there is little information on direct damage induced in DNA in an aqueous environment by ionising radiation at ambient temperatures. The problem is the overwhelming contribution of water radical damage to DNA in aqueous solution. The major approaches to simulate the direct effects in DNA in an aqueous environment are i) the use of one-electron oxidants such as  $\text{SO}_4^{\cdot-}$  [1,70], ii) the use of laser light of appropriate wavelength to ionise DNA [69,71,72] or iii) the use of photo-oxidants [73-76]. These approaches give chemical information on one-electron oxidation of DNA, essential to understand the types of species produced. These approaches are biased to the types of damage induced in the bases since interactions at the sugar moiety are minor processes, if they occur at all. The use of one-electron oxidants and chiefly  $\text{SO}_4^{\cdot-}$  has shown that the major species produced in DNA is one-electron oxidised guanine [70]. As guanine is the most easily oxidised base in DNA, a limitation is that the interactions may occur only at guanine. Further, other reactions such as addition and H-atom abstraction by  $\text{SO}_4^{\cdot-}$  have complicated interpretations using this approach, as reviewed extensively elsewhere [1].

The use of 193 nm light has been reviewed [69] but more recently it has been confirmed that guanine is the major site for localisation of the oxidative damage [72,77], consistent with the findings from esr studies. 193 nm light ionises DNA in aqueous solution with a quantum yield of  $\sim 0.05$  as shown in equation 5.



The solutions generally contain oxygen to scavenge the hydrated electron, which is readily observed optically at early times [72,78]. Although all the bases will

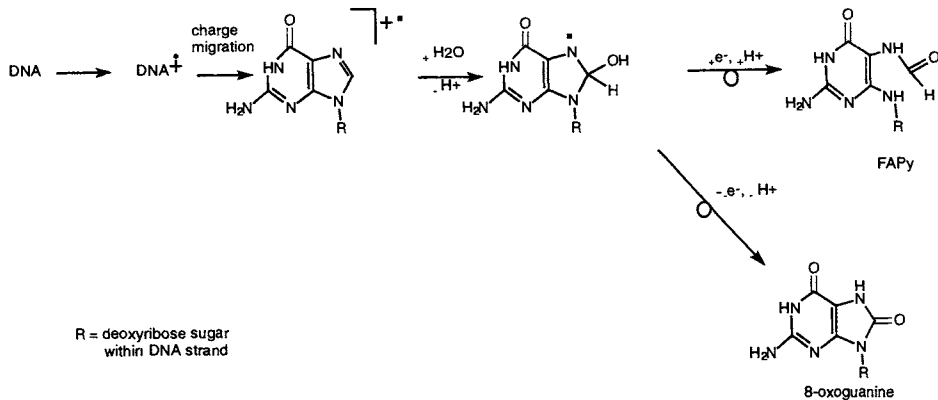


Figure 7. Reaction pathways leading to radiation-induced DNA damage by direct energy deposition in DNA.

be ionised to varying degrees depending on their extinction coefficients at 193 nm and their quantum yields of photo-ionisation [79], the major species observed at early times is the guanine radical cation. The lifetime of the guanine radical cation in DNA is  $\sim 0.05$  s [80], however the loss of the cation does not lead to ssb. It is assumed that hydration of the guanine radical cation occurs on this time scale, a reaction that occurs with the guanine radical cation in DNA but not in the mononucleotide [43]. Much of the earlier literature from the esr studies had assumed that the guanine radical cation is a precursor to ssb, however this assumption is not confirmed by solution studies [80,81]. Sequencing gel electrophoresis [82] has been used to identify the sites of base damage induced by 193 nm light and is able to resolve, at the single nucleotide level, damage in a DNA fragment, typically 20-300 bp long, provided the damaged base is converted into a ssb. Since many of the base damages and in particular 8-oxo-7,8-dihydroguanine are not particularly alkali-labile [81] to give a ssb, the use of specific enzymes which recognise and excise the damage to give a ssb have been used as discussed for OH-radical induced base damage in Section 4.1. It was confirmed that the majority of the base damage induced by 193 nm light is localised at guanine [77]. The yield of guanine base damage is 20-30x that prompt ssb; the latter only represents  $\sim 1-2\%$  of the photo-ionisation events [84]. The use of enzymes which recognise photo-products do not result in significant yields of single strand breakage. Similar distributions of DNA damage are produced in the absence of oxygen, an important observation since superoxide or singlet oxygen could have been responsible for the damage [83]. These studies are consistent with the esr studies that ionising radiation results in the formation of electron loss centres in DNA by direct effects and that these

electron loss centres migrate and become localised at guanine, a 'hotspot' for directly induced damage in the DNA bases. Figure 7 summarises the reaction pathways induced by direct effects in DNA.

The major radiation-induced DNA radicals produced by the direct effects are localised at guanine (oxidative damage) and the electron at cytosine. The major, persistent damage was identified as 8-oxo-7,8-dihydroguanine in irradiated DNA under condition where the DNA is fully hydrated (22 water molecules/nucleotide) at ambient temperatures but no bulk water is present [85]. Under these conditions, the radiation effect simulates the direct effect. Minor yields of FapyGua, 8-oxo-7,8-dihydroadenine, pyrimidine glycols and some other very minor products are produced from the oxidative pathway. Similarly, using photo-oxidants which oxidise DNA, the major product is 8-oxo-7,8-dihydroguanine [62]. Using photo-oxidants, the yield of pyrimidine products is minor compared with the yield of 8-oxo-7,8-dihydroguanine. The reductive pathway results predominantly in formation of dihydrothymine but in significantly lower yields than that of the oxidative products [85]. Therefore the major chemical modifications of the bases resulting from the direct effects of ionising radiation are oxidised guanine and pyrimidine products from electron trapping. Whether these product distributions change for high LET radiation remains a challenge for the future. Since the probability of multiple ionisations occurring within a few base pairs is greater for high LET radiation, other pathways may become available for localisation of the damage, if several radicals are produced within a few base pairs.

### 4.3. OH radical-induced DNA strand breakage

In order to produce a prompt ssb in DNA by radiation, the radical site must be ultimately located on the sugar phosphate moiety. The OH radical interacts with the sugar moiety by H-atom abstraction with rate constants of about  $2 \times 10^9 \text{ dm}^3 \text{ mol}^{-1} \text{ s}^{-1}$  [8]. The OH radical produces different radicals depending on the site of H-atom abstraction. In the presence of oxygen, these radicals interact with oxygen to give their corresponding peroxy radicals. The interaction of OH radicals with the sugar moiety and the pathways to strand breakage have been discussed in several reviews [2,20,86] and in the Chapter by von Sonntag. In DNA, the interaction of the OH radical with the various H-atoms at the different sugar carbon atoms results in a different distribution compared with the chemistry known for deoxyribose. The hydrogen atoms attached to the carbon atoms of the deoxyribose moiety are designated H-1', H-2', H-2'', H-3', H-4', H-5' and H-5''. The OH radical interacts predominantly with the H-4', which is in the minor groove of the double helix, and with the two hydrogens at the 5' position [19,21]. H-5'' is also in the minor groove of the double helix whereas H-5' is on the edge of the groove. Variations in the DNA sequence influence

the accessibility to the minor groove, thereby affecting the abstraction of H-4' and H-5'' but not H-5'. This change of accessibility for the OH radical due to minor groove variations has been related to the sequence dependent probability of ssb, with a reduced probability of ssb occurring at runs of A/T [19,87]. It was proposed that ssb induced in DNA arise equally from the 4'-pathway and the 5'-pathway (see later for mechanisms). The 4'- and 5'-hydrogens of DNA are the most readily accessible to diffusible OH radicals. H-1' is buried in the minor groove so its accessibility and probability of reaction with the OH radical is very low. Similarly, the 2' hydrogens are thought not to be readily accessible or have lower reactivity with the OH radical. H-3' is in the major groove of the double helix but is thought not to contribute significantly to strand breakage. The abstraction of an H-atom from the various positions in the deoxyribose moiety described above was supported by deuterium isotope studies on double stranded oligonucleotides [21].

As alluded to above, the major precursors to OH radical induced ssb are the C-4' radical and the C-5' radical resulting from H-atom abstraction of H-4' and H-5'/H-5'' respectively [2]. From irradiation of plasmid DNA in aqueous solution under aerobic conditions, it is estimated that the probability of prompt ssb formation on interaction with the OH radical is ~13% [88]. To measure prompt ssb it is essential to irradiate and subsequently maintain the DNA at 4 °C during electrophoresis to avoid the formation of heat-labile sites. The yield of heat labile sites is ~30% of the yield of prompt ssb [63]. Further, DNA should be retained at near neutral pH to avoid the formation of alkali-labile sites. For instance, if C-1' radicals are produced in DNA by OH radicals or direct effects, these C-1' radicals lead to abasic sites with the formation of deoxyribonolactone, an alkali-labile site [89,90]. In the presence of oxygen, the C-1' radical forms a peroxy radical adduct which decomposes into a carbocation at C-1' and the superoxide radical anion.

There now exists substantial evidence that the C-4' radical in DNA is a precursor to prompt ssb. The pathway to ssb formation is shown in Figure 8. The seminal studies of von Sonntag and Schulte-Frohlinde [2] showed that in the absence of oxygen, the C-4' radical undergoes a  $\beta$ -elimination of one of the phosphates. The resulting radical cation undergoes hydration followed by a second  $\beta$ -elimination of the other phosphate. The rate constant for hydration of the radical cation is estimated to be  $6 \times 10^7 \text{ s}^{-1}$  [91]. This pathway yields DNA ssb in which there is a gap representing loss of a nucleoside [92] and the ssb termini are 3'- and 5'- phosphates in the absence of oxygen [93]. An alternative reaction of the radical cation of the sugar, if there is an adjacent guanine, is oxidation of the guanine leaving an enol ether end termini [94]. The rate constant for this oxidation process is estimated to be  $>10^8 \text{ s}^{-1}$  in order to compete with the hydration reaction of the radical cation. In the presence of oxygen the

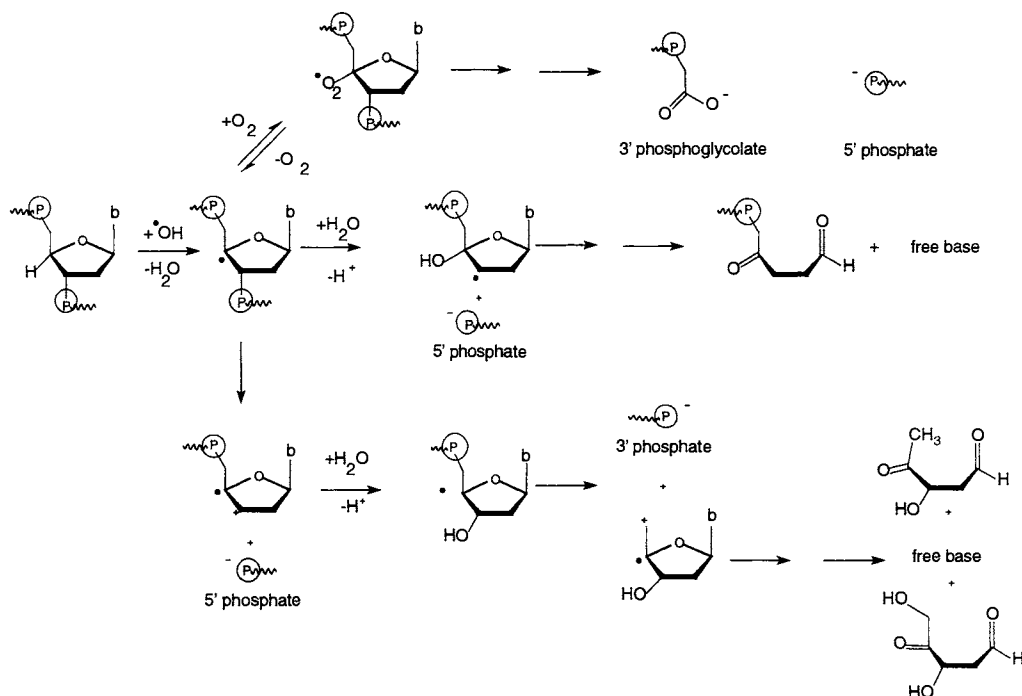


Figure 8. C-4' mechanism for single strand break formation.

C-4' radical interacts with oxygen to form a peroxy radical. This peroxy radical may then interact with another peroxy radical to produce a tetroxide which, following homolytic cleavage, undergoes a  $\beta$ -elimination reaction. Whether the formation of a tetroxide occurs in duplex DNA however is as yet not known. The end-group termini of the ssb in the presence of oxygen are 5'-phosphate and 3'-phosphoglycolate [93,95,96] and the base is eliminated as a base propanal. In single stranded DNA, the peroxy radical undergoes a reversible release of oxygen unless trapped by the presence of H-atom donors so that ssb are induced via the anaerobic pathway [94].

Less is known about the mechanism of ssb arising from the C-5' radical. A possible mechanism involves formation of a ssb gap with 5'- and 3'-phosphate termini. However irradiation of DNA under aerobic conditions with  $\gamma$ -radiation yields ssb with a 5'-phosphate and either a 3'-phosphoglycolate or a 3'-phosphate termini as shown from the different mobilities of fragments with the same number of nucleotides on a sequencing gel [95]. These two 3'-end termini are produced in about equal yield. It is important to stress that a radiation-induced ssb is distinctly different from a simple, single stranded nick involving cleavage of the phosphate-ester linkage by specific enzymes. Whereas a radiation-induced ssb involves a gap representing loss of a base, a nick does not



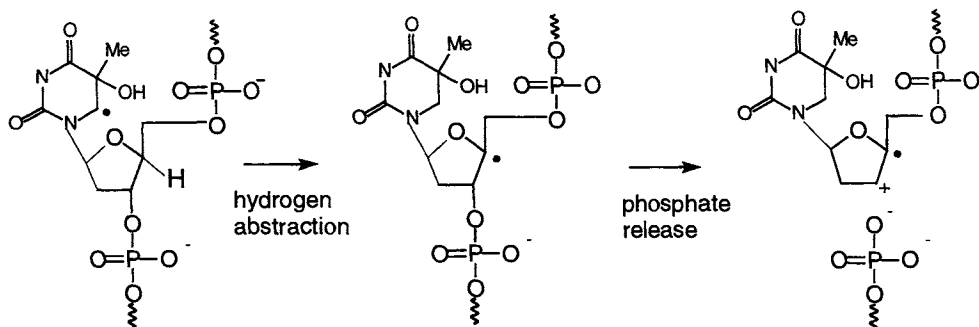


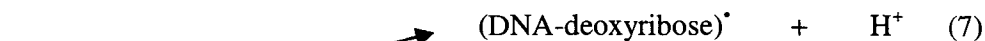
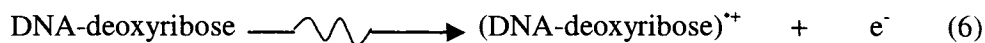
Figure 9. Transfer of the radical site from a DNA base radical to the sugar moiety.

lead to base loss and importantly the end termini are 5'-phosphate and 3'-hydroxy groups. These end termini are substrates for ligase, an enzyme which reseals the nick. In contrast, a radiation-induced ssb has to be processed by the cellular enzymes before the ssb can be sealed by ligase. Firstly the ends need to be cleaned up, followed by a polymerase step to fill in the gap and finally a ligase step. If two ssbs are formed within about 10 bp of each other but on different strands of the duplex, a double strand break is formed which is thought to be more difficult to repair biochemically and therefore is biologically of more consequence.

An additional pathway to ssb in DNA is transfer of the radical site from a hydroxyl radical adduct of the base to the adjacent sugar involving a rate determining H-atom abstraction [97-99], as shown in Figure 9. This reaction involves H-atom abstraction from an adjacent sugar [100] by the OH radical adduct of the base or its corresponding peroxy radical, formed on reaction with oxygen. The rate constant for this reaction in single stranded DNA under aerobic conditions is  $\sim 5\text{-}8\text{ s}^{-1}$  [1]. In the absence of oxygen, this reaction involves the OH radical adducts of the DNA bases with reducing properties. This transfer of the radical site to the deoxyribose sugar was also observed from the 5,6-dihydrothymidine-5-peroxy radical generated by photochemical methods using photo-active groups which generate specific radicals [101,102]. This peroxy radical abstracts a H-atom from the C-1' position of the 5' adjacent nucleotide. This pathway would be the same as that initiated by H-atom abstraction. As discussed above, the C-1' radical does not lead to prompt strand breakage but to a ssb resulting from scission of an alkali-labile site. The importance of this type of pathway to ssb formation, if it occurs in duplex DNA [103], is an amplification of damage. The ssb is formed next to a sugar containing a modified base formed in the H-atom abstraction process. As mentioned earlier, clustered damage in DNA is thought to present a greater challenge to the repair machinery of the cell.

#### 4.4. DNA single strand breaks by direct effects

The majority of the detailed mechanistic chemistry on DNA ssb is derived from studies with OH radicals. In the cell, about 40% of the ssb are induced by the direct effects of radiation. Although esr studies [10] indicate that the major radicals formed are located at the bases, it is established that the guanine radical cation does not lead to ssb by radical transfer to the sugar moiety. There is little mechanistic information on ionisation of the sugar phosphate backbone of DNA. Direct energy deposition in the deoxyribose moiety will cause ionisation provided the energy is sufficient to cause ionisation as shown in reactions (6-8).



If the radical cation of the sugar deprotonates, then the corresponding sugar radicals, namely C-1' - C-5', will be produced. The chemistry of these radicals would correspond with those discussed in Section 4.3 and in the Chapter by von Sonntag. The C-4' and C-5' radicals would lead to strand breakage. The end termini of ssb induced under direct effects are 3'- and 5'-phosphates [104] with no evidence for the formation of 3'-phosphoglycolates. A recent study on ionisation of the phosphate group [105] has shown that with ribose-5-phosphate the phosphate radical, produced on ionisation, may rapidly abstract a H-atom at C-4' involving a six-membered transition state ( $k = >5 \times 10^7 \text{ s}^{-1}$ ). In DNA, the resulting C-4' radical would give rise to a ssb as shown in Figure 8. This mechanism involving H-atom abstraction by the phosphate radical may explain the pathway to prompt ssb in DNA induced by 193 nm light and why the phosphate radical, due to its short lifetime, is not observed in esr studies with low LET radiation [10]. This H-atom abstraction by the phosphate radical cation may cause strand breakage in competition with oxidation of the base moiety as shown in reaction 8. A base oxidation process would be very dependent on the oxidation potential of the base, since guanine is more readily oxidised than the other bases of DNA. As discussed in Section 4.3, the radical cation resulting from  $\beta$ -elimination of the phosphate from the C-4' sugar radical may oxidise guanine in competition with its hydration [94]. The evidence so far indicates that the guanine oxidised is on the complementary strand. A detailed understanding of the chemistry of ionisation of the sugar phosphate backbone and the persistent damage produced resulting from ionisation awaits further experimentation.

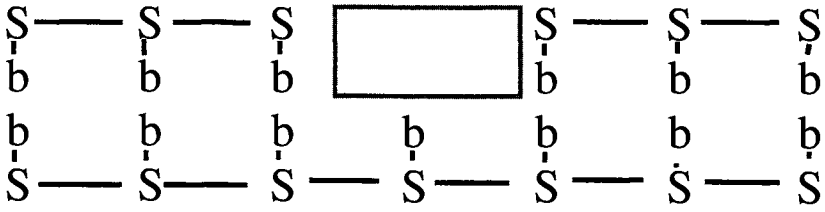
#### 4.5. Track structure simulations of ssb distributions

Over the years, damage to DNA has been simulated using track structure approaches and more recently the chemistry of the water radicals has been included as they diffuse and interact with DNA [16,106]. A detailed discussion of these approaches is outside the scope of this chapter. The idea of this Section is to highlight the DNA damage aspects of these theoretical approaches. The rationale for these simulations is to understand the effects of a single track of radiation, the lowest possible dose that may be delivered to a cell. This information is important in the development of mechanisms relating to the biological consequences of ionising radiation at low dose and dose rate, of prime importance in radiological protection. Much higher doses are generally used in experimental studies, so requiring extrapolation to low doses.

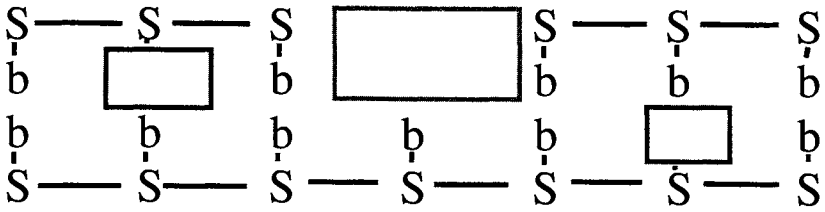
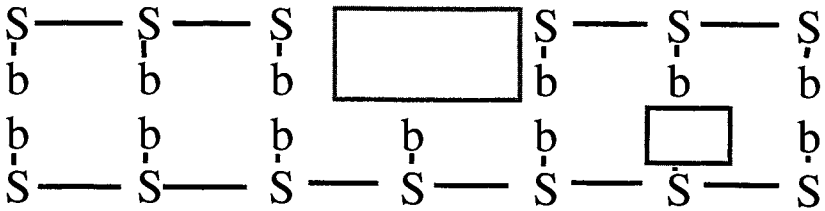
Several different track structure codes have been used to simulate the effects of both low and high LET radiations. These simulations are based upon accurately scoring all the energy deposition events as the radiation track intersects the DNA and its surrounding environment [35,36,107]. Several different models of DNA have been used ranging from a solid voxel model [108] to more molecular models of DNA. The exact base or sugar phosphate moiety in which the energy event occurs is recorded together with the amount of energy deposited. The track events which occur in the vicinity of the DNA and assumed to be in water, are converted into water radicals [35,36]. The water radicals are diffused and either react with other radicals formed in the track and are removed or interact with DNA if they reach the DNA. If an interaction occurs at DNA the exact sugar/base moiety is recorded so that together with the damage produced by direct interactions with DNA, a complete picture of the initial damage is obtained. With knowledge of the number of tracks within a given volume and the amount of DNA, these damages are converted into damages/Gy/base pair. The majority of these studies [35,36,108] use various assumptions based on

- i) the amount of energy deposited in DNA required to give a ssb and dsb
- ii) the distribution of water radical interactions with the base and sugar moieties, usually based on the 80 to 20% distribution between base and sugar phosphate respectively and
- iii) the probability of the OH radical abstracting an H-atom from the sugar moiety to give ultimately a ssb.

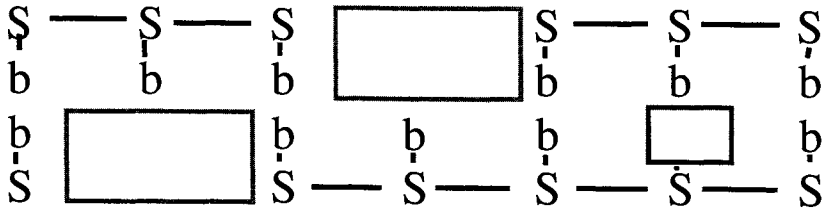
The models are based on a significant amount of information derived from radiation chemistry. The reader is directed to the studies of Nikjoo *et al* [35] and Otterlenghi *et al* [107] for a more detailed description of the assumptions and approaches on scoring the DNA damage. An important outcome from these simulations on DNA damage for the experimentalist is an indication of the single strand break spatial distribution of lesions produced in DNA ranging from isolated ssb to more complex DNA lesions. A compilation of some of the



examples of clustered damage



Double strand break



base damage

Figure 10. Schematic representation of examples of clustered DNA damage.

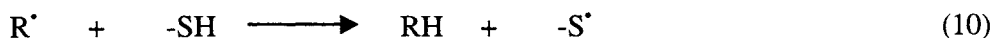
various types of lesions formed in DNA from these simulations are presented in Figure 10. As mentioned in Section 3, the concept of clustered DNA damage arose from these biophysical approaches [16]. An important observation is the formation of a ssb with an associated ssb within about 20 bp. Of the dsb formed about 30% are associated with another strand break lesion within a few base pairs [35]. As the LET of the radiation increases the complexity of the DNA damage increases so that at high LET ~70% of dsb are associated with at least one other lesion within the complex damage [109]. Therefore, there exists the possibility of producing various types of clustered DNA lesions which may not be formed or are rare for low LET radiation. It is from these types of simulations that the increase in complexity of DNA damage with increasing LET of the radiation was suggested to be a reflection of the biological severity of the different radiations.

Many of these simulations do not at present include base modifications although their inclusion in the simulations of damage complexity is beginning to appear [109]. The complexity of DNA damage is significantly increased on inclusion of base damage. Although there is little experimental evidence for clustered DNA damage (not including those described above derived from a single radical), dsb, which are a simple form of complex DNA damage, are produced in irradiated cells [23,25,26]. The cellular yields of dsb determined experimentally are in reasonable agreement with those determined from simulations under conditions which simulate the cellular environment [110]. Other types of radiation induced cluster DNA damage have not been detected in cells and this presents a significant challenge to the experimenters. Using cell extracts to rejoin DNA ssb induced by irradiation of plasmid DNA in solution [27,28,111], evidence was obtained for the formation of complex ssb especially by  $\alpha$ -particles and ultrasoft X-ray irradiation. It was estimated that the majority of ssb are associated with at least one other lesion, either a base damage or an additional ssb. The biological consequences of clustered damage are presented in Section 7.

## 5. EFFECT OF CHEMICAL MODIFIERS OF DNA DAMAGE

Many agents are known to interact with the initially produced free radicals of DNA and modify these radicals to yield different types of products or even modify the product distribution. Thiols and other H-atom donors have been thought to act as radioprotectors through their ability to interact with DNA radicals [112]. As discussed above, many of the radicals e.g. sugar radicals and OH adducts of the bases, especially those with reducing properties, interact with oxygen to produce peroxy radicals as shown in reaction (9) where R $\cdot$  represents a DNA radical. If R $\cdot$  is a C-4' sugar radical this reaction competes with its

interaction with a H-atom donor such as a thiol as shown in reaction (10) [2].



Under normal aerobic conditions, the interaction of DNA sugar radicals with oxygen ( $10^8$ - $10^9$  dm<sup>3</sup> mol<sup>-1</sup> s<sup>-1</sup>) is much more efficient than the reaction with the thiol ( $10^4$ - $10^6$  dm<sup>3</sup> mol<sup>-1</sup> s<sup>-1</sup>) [1,2,112]. In the presence of oxygen, this reaction leads to fixation of damage leading to a ssb as discussed in Section 4.3. In many cells *in vivo*, the oxygen tension is low so that the competitive interactions between oxygen and an endogenous thiol may occur leading to protection against a DNA strand break [113]. This competition involving reactions (9) and (10) has been proposed to explain the OER of about 3-4 for ssb induction in cells. There is less evidence for the interaction of thiols with the DNA bases although in the monomers this reaction occurs. For instance, the OH adduct of guanine with oxidising properties interact with thiolate and other reducing agents by electron transfer [42]. That DNA base radicals are less susceptible to interactions with thiols compared to the monomers may be a reflection of the DNA structure inhibiting accessibility.

Since hypoxic cells are less sensitive to ionising radiation, much research was invested in the development of radiosensitisers. These agents were developed to mimic the effects of oxygen in hypoxic cells. The chemistry of radiosensitisers and the more recent developments, which arose out of this earlier research, of agents which are toxic to hypoxic cells following redox activation is discussed in the Chapter by Wardman. Briefly, radiosensitisers enhance the radiosensitivity of cells under conditions of hypoxia and the efficiency of the radiosensitiser is related to its ease of reduction, e.g. its one electron reduction potential. As with oxygen, these agents must be present within a few milliseconds of the radiation [34], thus leading to the concept that the radiosensitisers interacted with a bio-radical [refer to Chapter by Wardman]. Since DNA damage is modified by these agents, it was thought that the interaction involved DNA radicals, although the mechanism is still to be elucidated by which the redox dependence of the chemical reactions between radiosensitisers and bioradicals reflects that seen for cell inactivation.

Radiosensitisers are typically nitroaromatics which are good oxidants. Although the mechanism of sensitisation remains unclear, there are some indications from studies looking at the interactions of DNA radicals with a variety of oxidants (radiosensitisers). Nitroaromatics have been shown to interact with alcohol radicals and ether radicals initially through the formation of

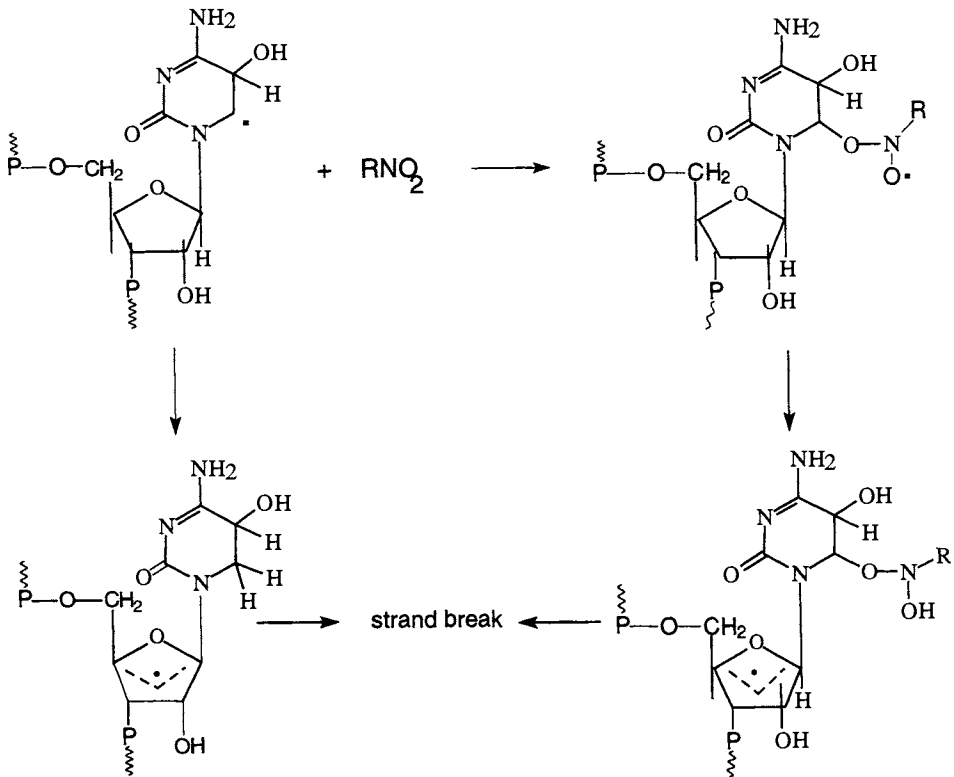


Figure 11. Pathways to formation of single strand breaks by reaction of OH adducts of DNA bases with nitro-aromatics.

a nitroxyl adduct which are long-lived in the case of the ethers [114-116]. However the redox dependence of the rate constants for adduct formation is  $\sim 3\text{-}4\text{ V}^{-1}$  compared with the value of  $\sim 8\text{-}9\text{ V}^{-1}$  for the rate limiting step seen for radiosensitisation of cell killing under hypoxia. Formation of an adduct with the nitro-aromatics is thought to mimic the formation of a peroxy radical by oxygen.

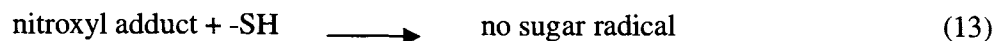
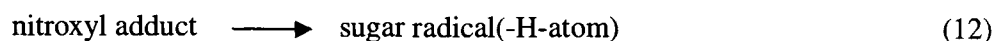
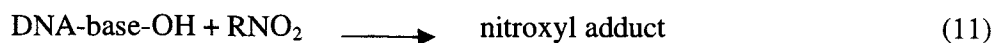
### 5.1. Reaction with nitro-aromatics

DNA base radicals induced by OH radicals are also a possible target for interactions with nitro-aromatics [117]. For instance, the OH adducts of the nucleobases with reducing properties interact with nitro-aromatics to form nitroxyl adducts [118]. The rate constants for this interaction show only a weak dependence on the one electron reduction potential of the nitro-aromatic. However, using poly C as a model for a biopolymer, the nitroxyl radical adducts formed through addition of nitrofurantoin to the C-6 position of the C(5)-OH

adduct of the cytosine moiety is able to abstract a H-atom, presumed to be from an adjacent sugar [118]. If this abstraction from the sugar occurs at a carbon site which is a precursor to ssb (see Section 4.3), then a strand break is formed as shown in Figure 11. Interestingly, the adducts appear to be very long lived since the rate constant for the H-atom transfer from the sugar is  $\sim 2\text{-}3\text{ s}^{-1}$ . It is not known whether this H-atom abstraction reaction in Figure 11 shows a strong dependence on the redox potential of the nitro-aromatic. Therefore nitroaromatics mimic the effects of oxygen in that they may lead to ssb on interaction with OH radical adducts of the nucleobases. As stated earlier though, some caution is required on the accessibility of the base radicals in DNA by these experiments.

If quinones are used as the oxidant, the reaction of the OH radical adducts of the nucleobases proceeds by outer sphere electron transfer to yield a carbocation but not an adduct [118]. The rate constant for this interaction shows a strong dependence on the one-electron reduction potential of the quinone. This reaction does not lead to ssb induction in poly C in the presence of benzoquinone but to a reduction in the yield of ssb.

The mechanism of ssb enhancement and radiosensitisation may be related in some way to those oxidants which form adducts with the DNA radicals. With the nitroaromatics a plausible enhancement of ssb is the possible H-atom abstraction by the base nitroxyl radical. The reactivity of the nitroxyl adducts with thiols or other reductants has not been studied in detail as there are at least two possible interactions where competition between the nitro-aromatic and a thiol may occur as shown in reactions (11-15).



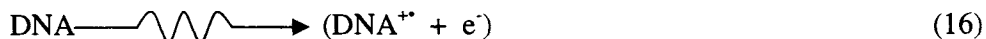
The type of ssb end group termini induced by irradiation of DNA under hypoxic conditions in the presence of misonidazole, a nitroaromatic, is an aerobic type damage, namely a 3'-phosphoglycolate [93]. That the yield of ssb was not enhanced by misonidazole in an aqueous solution is an indirect indication that the pathway to ssb in cellular DNA may involve a competition for the precursor radical between the nitroaromatic and a thiol or some other protective agent.



This scenario is identical to that for the lack of an oxygen effect on ssb induction with irradiated plasmid DNA in aqueous solution and in the absence of thiols.

## 6. RADIATION-INDUCED CHARGE TRANSFER IN DNA

There is significant evidence that direct energy deposition in DNA results in radiation-induced charge transfer in DNA as discussed in section 4.2. Direct energy deposition may lead to ionisation of the DNA as shown in reaction (16).



The migration of the ejected electron has been discussed in detail and the reader is referred to reference [1] and Section 4.2. Briefly, from addition of additives to DNA, the ejected electron migrates ~ 25 base pairs (for review see [1]). In contrast, the migration of the hydrated electron after addition to DNA occurs over ~5 base pairs [1]. From esr studies on DNA at 77K, it has been proposed that the ejected electron only migrates ~3 base pairs. The radiation-induced ionisation events are produced randomly in the DNA and the ejected electron may tunnel and/or undergo hopping processes which are in competition with irreversible trapping of the adduct, possibly involving protonation at carbon. Indeed, the dihydrothymine-5-yl is the major electron gain centre observed by esr at higher temperatures replacing the initially observed cytosine radical anion at 77K [10]. As discussed below for migration of oxidative damage, tunnelling mechanisms may involve short migration distances whereas larger distances, which require an electron trap for detection, involve a hopping mechanism. In a hopping process, high mobility electron carriers would not be observed.

There has been a resurgence of interest in the transfer of oxidative damage to guanine in DNA and the distance over which this transfer occurs. From the earlier esr data [10], it was not necessary to invoke long range transfer of the radiation-induced electron loss centre to guanine in DNA at 77K. That the electron loss centre localises at guanine is predicted from its oxidation potential in relationship to that of the other bases [64]. Some sequence dependent effects are to be expected as GG sites in DNA are preferred sites for localisation of the oxidative damage [119] since, from theoretical calculations, these sites are more readily oxidised in DNA. The use of 193 nm light has shown that guanine is the preferred site of damage localisation in DNA at ambient temperatures [72]. This finding was emphasised by the use of enzymes which excise the base damage (see section 4.2 for discussion and mechanism) [77]. Several other studies have used photo-oxidants and showed the importance of guanine as a 'hotspot' of damage localisation [73-76]. Since ionising radiation or 'free' photo-oxidants

**Table 4**  
Photo-induced charge migration in DNA: Distance dependence

<u>Oligonucleotide length/bp<sup>a)</sup></u>	<u><math>\beta/A^{-1}</math><sup>b)</sup></u>	<u>migration/bp</u>	<u>Reference</u>
$\leq 53$	0.7	15	[125]
7 <sup>e)</sup>	0.64		[121]
$\leq 14$	$\sim 1$	8	[75]
63		55-60	[120]
25		11	[76]
	0.2		[74]
Calf Thymus DNA	0.9 - 1.4	3	[73]
Theoretical Prediction	1.2 - 1.6		[123]

produce oxidative damage randomly, it is difficult to comment on the distance of charge migration.

More recently, photo-oxidants (e.g. ruthenium and rhodium donor complexes [75, 120], anthraquinones [76], stilbene dicarboxamides [121]) which are tethered to one end of short fragments of DNA of known sequence or form a bridge connecting the two complementary strands, have been used to initiate guanine oxidation. From the known sites of guanine damage at various distances, in terms of base pairs from the photo-oxidant, it has been possible to obtain distances over which the electron may migrate. The initial studies indicated that the charge does not migrate long distances in photo-oxidised DNA. If the charge transfer occurs by an electron tunnelling process, the following dependence for charge migration previously developed in proteins [75, 122] applies. The  $\beta$ -values, obtained from the dependence shown in equation (17), are given in Table 4.

$$k_{et} = A \exp\{-\beta(R)\} \quad (17)$$

In equation (17), the rate constant for electron tunnelling is  $k_{et}$ ,  $R$  the distance between donor and acceptor and  $\beta$  a distance dependent constant. This electron tunnelling type of mechanism indicates that the rate of electron transfer decreases by about one order of magnitude per base pair, since the typical value of  $\beta$  is in the range 1-1.5  $A^{-1}$  [123]. As shown in Table 4 typical values of  $\beta$  for

electron transfer by tunnelling in DNA is  $0.6-0.7 \text{ A}^{-1}$ . This value represents a rapid decrease in the rate constant for electron transfer with distance so that the charge is predicted to transfer over short distances. However, findings from other studies [120, 124, 125] indicated considerably longer distances as shown in Table 4. Although there is conflict on the distance migration of the oxidative damage, it has recently been rationalised based on theoretical considerations, that these longer distances involve an electron hopping mechanism [126]. It was proposed that the electron may tunnel over short distances but the longer distances involve a hopping mechanism. Such hopping is influenced by the local DNA sequence and the proximity of the nearest guanine. For instance, runs of AT bases are inhibitors to hole migration [120,121]. A further consideration with the hopping mechanism is the depth of the trap will determine the detrapping rate and this detrapping process must compete with irreversible chemistry of the radical cation. These competing processes would include hydration of the radical cation [80] and proton transfer processes involving the complementary base [127].

In all of these photochemical studies the following points of caution need to be remembered. Firstly, the sites of damage from sequencing gels assume that the damages are revealed by treatment of the irradiated DNA with piperidine. Several of the oxidative damages are not labile to piperidine treatment, one of which is 8-oxoguanine [81]. Therefore sites which may be damaged may not be revealed by this approach so could lead to over emphasis on the alkali-labile sites. Secondly, back electron transfer with the photo-oxidant may influence the quantity of cleavage within a few base pairs of the photo-oxidant due to back electron transfer. Notwithstanding these limitations, radiation-induced charge migration occurs in DNA has significant implications for not only damage localisation/repair but for the possibility of signalling damage over several base pairs and the ability to move energy along the DNA. The field of DNA as a charge carrier is opening up novel areas of research and applications in health and diagnostics. Recently, proteins, which bind to DNA, have been shown to modulate electron transfer in DNA [128]. This area of research should provide interesting insights into the ability of DNA to be used as a medium to transfer energy.

## **7. CLUSTERED DNA DAMAGE**

Although clustered DNA damage induced by radiation has been mentioned several times in this chapter (especially in Section 4.5), it seems appropriate to bring together the implications of this type of damage to the biological effects of radiation. In the sections above, the radiation mechanisms by which ssb and base damages are formed have been presented including the possible role of

DNA acting as a medium to facilitate charge transfer. The distance of charge transfer on the whole is probably limited otherwise the fingerprint of the radiation track, especially at high LET, would be lost and consequently the enhanced radiosensitivity of high LET radiation. The two types of clustered DNA damage discussed are

- i) when several fundamental lesions are produced within a few tens of base pairs as discussed above from simulations (see section 4.5) and
- ii) the formation of two clustered damaged sites within a few 100's of base pairs especially for high LET radiation. These later damages are called regionally damaged sites [129].

Experimental evidence for clustered DNA damage is scarce. Indirect evidence comes from the increased efficiency of forming a dsb per ssb as the LET of the radiation increases [23,25,26]. This increase in the probability of producing a dsb per ssb has been seen with plasmid DNA irradiated with  $\alpha$ -particles in the presence of high concentrations of scavenger to mimic the mean diffusion distance of an OH radical in cells [130]. The number of radiation-induced dsb remaining after a repair period of a few hours in the cell increases as the LET of the radiation increases [26, 131]. Cell extracts have been used to rejoin radiation-induced ssb in plasmid DNA (see Section 4.5). Under 'cell mimetic' conditions and using high LET radiation to initiate ssb formation, the number of ssb which could be rejoined was reduced drastically [27,28,112]. This difference in the extent of ssb rejoining was interpreted to reflect an increased probability of a ssb being associated with another lesion (base damage or another ssb on the same strand) as the LET of the radiation increases.

The importance of clustered DNA damage from a biological viewpoint is that it may compromise repair pathways. Observations on dsb rejoining in cells added credence to the hypothesis from track structure simulation (see Section 4.5) on the biological significance of clustered DNA damage. Indeed, evidence that the repairability of cluster DNA lesions is reduced was also obtained [132,133] from model systems in which synthetic damages, containing a base damage opposite an abasic site or a ssb, were treated with base excision repair enzymes (see section 4.1). The efficiency of processing of these synthetic, clustered DNA damages is critically dependent upon the number of base pairs intervening between the two damages. If the damage persists, it may result in a mutation. Evidence for the presence of clustered DNA damage using chemical detection methods and for the influence of clustered DNA damage on its recognition and repair by proteins are topics for future research (see Section 3). Although the majority of cellular studies have focused on the determination of dsb (a complex lesion), it is apparent that the yield of other non-dsb complex lesions may predominate. Future areas of research will focus on the challenge and biological consequences that clustered DNA damage present to the cellular repair

machinery and to signalling processes.

## ACKNOWLEDGEMENTS

This work is supported by the Medical Research Council. I am grateful to my colleagues past and present who have contributed significantly to research on radiation induced DNA damage. I thank Anne Johnson and Jon Fulford for help in compilation of this chapter.

## REFERENCES

1. P. O'Neill and E. Martin Fielden, *Adv. Radiat. Biol.*, 17 (1993) 53.
2. C. von Sonntag, *The Chemical Basis of Radiation Biology*. Taylor & Francis (1987).
3. E.C. Friedberg, G.C. Walker and W. Siede, *DNA Repair Mutagenesis*. ASM Press, Washington D.C. (1995).
4. R.D. Wood, *Annu. Rev. Biochem.*, 65 (1996) 135.
5. S.S. Wallace, *Environ. Mol. Mutagen.*, 12 (1988) 431-477.
6. B. Demple and L. Harrison, *Annu. Rev. Biochem.*, 63 (1994) 915-948.
7. D.P. Lane, *Nature*, 358 (1992) 15.
8. G.V. Buxton, C.L. Greenstock, W.P. Helman and A.B. Ross, *J. Phys. Chem. Ref. Data*, 17 (1988) 513-886.
9. B. Halliwell and O.I. Aruoma, *DNA and Free Radicals*, Ellis Horwood, Chichester, (1993).
10. D. Becker and M.D. Sevilla, *Adv. Radiat. Biol.*, 17 (1993) 121-180.
11. T Douki, T. Delatour, F. Bianchini and J. Cadet, *Carcinogenesis*, 17 (1996) 347.
12. S.G. Swarts, M.D. Sevilla, D. Becker, C.J. Tokar and K.T. Wheeler, *Radiat. Res.*, 129 (1992) 333.
13. T. Mori and M. Dizdaroglu, *Radiat. Res.*, 140 (1994) 85.
14. S. Steenken, *Chem. Rev.*, 89 (1989) 503.
15. E.J. Hall, *Radiobiology for the Radiologist*, Lippincott Williams & Wilkins, (Fourth Edition) (1994).
16. D.T. Goodhead, *Int. J. Radiat. Biol.*, 65 (1994) 7.
17. J.F. Ward, *Radiat. Res.*, 104 (1985) S103.
18. W. Saenger, *Principles of Nucleic Acid Structure*, Springer NY, 1984.
19. D. Sy, C. Savoye, M. Begusova, V. Michalik, M. Charlier and M. Spothem-Maurizot, *Int. J. Radiat. Biol.*, 72 (1997) 147.
20. W. K. Pogozelski and T.D. Tullius, *Chem. Rev.* 98 (1998) 1089.
21. B. Balasubramanian, W.K. Pogozelski and T.D. Tullius, *Proc. Natl. Acad. Sci.*, 95 (1998) 9738.
22. M. Frankenberg-Schwager, *Radiother. Oncol.*, 14 (1989) 307-320.
23. K.M. Prise, G. Ahnstrom, M. Belli, J. Carlson, D. Frankenberg, J. Kiefer, M. Löbrich, B.D. Michael, J. Nygren, G. Simone and B. Stenerlow, *Int. J. Radiat. Biol.*, 74 (1998) 173.
24. R. Roots and S. Okada, *Radiat. Res.*, 64 (1975) 306.
25. S.W. Botchway, D.L. Stevens, M.A. Hill, T.J. Jenner and P.O'Neill, *Radiat. Res.*, 148 (1997) 317.

26. T.J. Jenner, C.M. deLara, P. O'Neill and D.L. Stevens, *Int. J. Radiat. Biol.*, 64 (1993) 265.
27. P.S. Hodgkins, P. O'Neill, D. Stevens and M.P. Fairman, *Radiat. Res.*, 146 (1996) 660.
28. P.S. Hodgkins, M.P. Fairman and P. O'Neill, *Radiat. Res.*, 145 (1996) 24.
29. D.T. Goodhead, P. O'Neill and H.G. Menzel (eds), *Microdosimetry-An Interdisciplinary Approach*, The Royal Society of Chemistry, 1997.
30. R.L. Warters and B.W. Lyons, *Radiat. Res.*, 130 (1992) 309.
31. M. Löbrich, P.K. Cooper and B. Rydberg, *Int. J. Radiat. Biol.*, 70 (1996) 493.
32. N.L. Oleinick, U. Balasubramaniam, L. Xue and S. Chiu, *Int. J. Radiat. Biol.*, 66 (1994) 523.
33. N.L. Oleinick and S.-M. Chiu, *Radiat. Prot. Dosim.* 52 (1994) 353.
34. M.E. Watts, R.J. Hodgkiss, N.R. Jones, D.S. Sehmi and M. Woodcock, *Int. J. Radiat. Biol.*, 43 (1983) 329.
35. H. Nikjoo, P. O'Neill, D.T. Goodhead and M. Terrissol, *Int. J. Radiat. Biol.*, 71 (1997) 467.
36. V.V. Moiseenko, R.N. Hamm, A.J. Waker and W.V. Prestwich, *Int. J. Radiat. Biol.*, 74 (1998) 533.
37. A.Chatterjee, In: *Radiation Chemistry Principles and Applications*, Farhatziz and M.A.J. Rodgers (eds), (1987) pp1-28.
38. G.V. Buxton, In *Radiation Chemistry Principles and Applications*, Faratatziz and M.A.J. Rodgers (eds), VCH Publishers, NY, (1987) pp.321-349.
39. C.J. Burrows and J.G. Muller, *Chem. Rev.*, 98 (1998) 1109.
40. D.K. Hazra and S. Steenken, *J. Amer. Chem. Soc.*, 105 (1983) 4380.
41. S. Fujita and S. Steenken, *J. Amer. Chem. Soc.*, 103 (1981) 2540.
42. P. O'Neill, *Radiat. Res.*, 96 (1983) 198.
43. A.J.S.C. Vieira, L.P. Candeias and S. Steenken, *J. Chim. Phys.*, 90 (1993) 881.
44. P. O'Neill, P.W. Chapman and D.G. Papworth, *Life Chem. Rep.*, 3 (1985) 62.
45. A.J.S.C. Vieira and S. Steenken, *J. Amer. Chem. Soc.*, 112 (1990) 6986.
46. A.F. Fuciarelli, B.J. Wegher, W.F. Blakely and M. Dizdaroglu, *Int. J. Radiat. Biol.*, 58 (1990) 397.
47. L.P. Candeias and S. Steenken, *J. Amer. Chem. Soc.*, 115 (1993) 2437.
48. H.C. Box, H.G. Freund, E.E. Budzinski, J.C. Wallace and A.E. Maccubbin, *Radiat. Res.* 141 (1995) 91.
49. H.C. Box, E.E. Budzinski, J.B. Dawidzik, J.S. Gobey and H.G. Freund, *Free Radical Biol. Med.*, 23 (1997) 1021.
50. H.C. Box, E.E. Budzinski, J.B. Dawidzik, J.C. Wallace and H. Iijima, *Radiat. Res.*, 149 (1998) 433.
51. A.-G. Bourdat, D. Gasparutto and J. Cadet, *Nucl. Acids Res.*, 27 (1999) 1015.
52. J. Cadet, T. Douki and J.-L. Ravanat, *Environ. Health Pers.*, 105 (1997) 1034.
53. Z.A. Doddridge, P.M. Cullis, G.D.D. Jones and M.E. Malone, *J. Amer. Chem. Soc.*, 120 (1998) 10998.
54. X. Chris Le, J.Z. Xing, J. Lee, S.A. Leadon and M. Weinfeld, *Science*, 280 (1998) 1066.
55. A.R. Collins, S.J. Duthie and V.L. Dobson, *Carcinogenesis*, 14 (1993) 1733.
56. J.P. Banáth, S.S. Wallace, J. Thompson and P.L. Olive, *Radiat. Res.*, 151 (1999) 550.
57. J.-P. Pouget, J.-L. Ravanat, T. Douki, M.-J. Richard and J. Cadet, *Int. J. Radiat. Biol.*, 75 (1999) 51.
58. S. Boiteux, E. Gajewski, J. Laval and M. Dizdaroglu, *Biochem.*, 31 (1992) 106.
59. M. Haering, H. Ruediger, B. Demple, S. Boiteux and B. Epe, *Nucl. Acids Res.*, 22

- (1994) 2010.
60. J.R. Milligan, J.A. Aguilera, T-T.D. Nguyen, J.F. Ward, Y.W. Kow, B. He R.P. Cunningham, *Radiat. Res.*, 151 (1999) 334.
  61. T. Roldán-Arjona and B. Sedgwick, *Molecular Carcinogenesis*, 16, (1996) 188.
  62. T. Douki and J. Cadet, *Int. J. Radiat. Biol.*, 75 (1999) 571.
  63. G.D.D. Jones, T.V. Boswell and J.F. Ward, *Radiat. Res.*, 138 (1994) 291.
  64. S. Steenken and S.V. Jovanovic, *J. Amer. Chem. Soc.*, 119 (1997) 617.
  65. S. Steenken, J.P. Telo and L.P. Candeias, *J. Amer. Chem. Soc.*, 114 (1992) 4701.
  66. M.D. Sevilla, D. Becker, M. Yan and S.R. Summerfield, *J. Phys. Chem.*, 95 (1991) 3409.
  67. T. La Vere, D. Becker and M.D. Sevilla, *Radiat. Res.*, 145 (1996) 673.
  68. D. Becker, Y. Razskazovskii, M.U. Callaghan and M.D. Sevilla, *Radiat. Res.*, 146 (1996) 361.
  69. H. Görner, *J. Photochem. Photobiol. B: Biol.*, 26 (1994) 117.
  70. P. Wolf, G.D.D. Jones, L.P. Candeias and P. O'Neill, *Int. J. Radiat. Biol.*, 64 (1993) 7.
  71. I.E. Kochevar and L.A. Buckley, *Photochem. Photobiol.*, 51 (1990) 527.
  72. T. Melvin, M.A. Plumb, S.W. Botchway, P. O'Neill and A.W. Parker, *Photochem. Photobiol.*, 61 (1995) 653.
  73. A.M. Brun and A. Harriman, *J. Amer. Chem. Soc.*, 114 (1992) 3656; *id* 116 (1994) 10383.
  74. C.J. Murphy, M.R. Arkin, Y. Jenkins, N.D. Ghatlia, N.D. Bossmann and J.K. Barton, *Science*, 262 (1993) 1025.
  75. T. J. Meade and J.F. Kayyem, *Angew. Chem. Int. Ed. Engl.* 34 (1995) 352.
  76. S.M. Gasper and G.B. Schuster, *J. Amer. Chem. Soc.*, 119 (1997) 12762.
  77. T. Melvin, S.M.T. Cunniffe, P. O'Neill, A.W. Parker and T. Roldan-Arjona, *Nucl. Acids Res.*, 26 (1998) 4935.
  78. L.P. Candeias, P. O'Neill, G.D.D. Jones and S. Steenken, *Int. J. Radiat. Biol.*, 61 (1992) 15.
  79. L.P. Candeias and S. Steenken, *J. Amer. Chem. Soc.*, 114 (1992) 699.
  80. T. Melvin, S.W. Botchway, A.W. Parker and P. O'Neill, *J. Amer. Chem. Soc.*, 118 (1996) 10031.
  81. P.M. Cullis, M.E. Malone and L.A. Merson-Davies, *J. Amer. Chem. Soc.* 118 (1996) 2775.
  82. J. Sambrook, E.F. Fritsch and T. Maniatis, *Molecular Cloning: A Laboratory Manual*, 2nd Edition Cold Spring Harbor, NY (1989).
  83. T. Melvin, S. Cunniffe, D. Papworth, T. Roldan-Arjona and P. O'Neill, *Photochem. Photobiol.*, 65 (1997) 660.
  84. T.P.A. Devasagayam, S. Steenken, M.S.W. Obendorf, W.A. Schulz and H. Sies, *Biochem.*, 30 (1991) 6284.
  85. S.G. Swarts, D. Becker, M. Sevilla and K.T. Wheeler, *Radiat. Res.*, 145 (1996) 304.
  86. A.P. Breen and J.A. Murphy, *Free Rad. Biol. Med.*, 18 (1995) 1033.
  87. F. Barone, M. Belli and F. Mazzei, *Radiat. Environ. Biophys.*, 33 (1994) 23.
  88. J.R. Milligan, J.A. Aguilera and J.F. Ward, *Radiat. Res.*, 133 (1993) 158.
  89. C. Chatgililoglu and T. Gimisis, *Chem. Commun.*, (1998) 1249.
  90. C.J. Emanuel, M. Newcomb, C. Ferreri and C. Chatgililoglu, *J. Amer. Chem. Soc.*, 121 (1999) 2927.
  91. E. Meggers, D. Kusch, M. Spichty, U. Wille and B. Giese, *Angew. Chem. Int. Ed.*, 37 (1998) 460.

92. E.S. Henle, R. Roots, W.R. Holley and A. Chatterjee, *Radiat. Res.*, 143 (1995) 144.
93. G.W. Buchko and M. Weinfeld, *Biochem.*, 32 (1993) 2186.
94. A. Dussy, E. Meggers and B. Giese, *J. Amer. Chem. Soc.*, 120 (1998) 7399.
95. W.D. Henner, S.M. Grunberg and W.A. Haseltine, *J. Biol. Chem.*, 257 (1982) 11750.
96. W.D. Henner, S.M. Grunberg and W.A. Haseltine, *J. Biol. Chem.*, 258 (1983) 15198.
97. G.D.D. Jones, P. O'Neill, *Int. J. Radiat. Biol.*, 57 (1990) 1123.
98. G.D.D. Jones and P. O'Neill, *Int. J. Radiat. Biol.*, 59 (1991) 1127.
99. T. Melvin, P. O'Neill and G.D.D. Jones, *Int. J. Radiat. Biol.*, 66 (1994) 499.
100. L.R. Karam, M. Dizdaroglu and M.G. Simic, *Radiat. Res.*, 116 (1988) 210.
101. M.M. Greenberg, M.R. Barvian, G.P. Cook, B.K. Goodman, T.J. Matray, C. Tronche and H. Venkatesan, *J. Amer. Chem. Soc.*, 119 (1997) 1828.
102. C. Tronche, B.K. Goodman and M.M. Greenberg, *Chem. Biol.*, 5 (1998) 263.
103. K.M. Prise, N.E. Gillies and B.D. Michael, *Int. J. Radiat. Biol.*, 74 (1998) 53.
104. P.M. Cullis, G.D.D. Jones, M. Sweeney, M.C.R. Symons and B.W. Wren, *Free Rad. Res. Commun.*, 6 (1989) 149.
105. S. Steenken and L. Goldbergerova, *J. Amer. Chem. Soc.*, 120 (1998) 3928.
106. H. Nikjoo, P. O'Neill, M. Terrissol and D.T. Goodhead, *Int. J. Radiat. Biol.*, 66 (1994) 453.
107. A. Ottolenghi, F. Monforti and M. Merzagora, *Int. J. Radiat. Biol.*, 72 (1997) 505.
108. D.E. Charlton, H. Nikjoo and J.L. Humm, *Int. J. Radiat. Biol.*, 56 (1989) 1.
109. H. Nikjoo, P. O'Neill, M. Terrissol and D.T. Goodhead, *Radiat. Environ. Biophys.*, 37 (1999) 31.
110. P. O'Neill, S.M.T. Cunniffe, D.L. Stevens, S.W. Botchway and H. Nikjoo, In *Microdosimetry-An Interdisciplinary Approach*, D.T. Goodhead, P. O'Neill and H.G. Menzel (eds), The Royal Society of Chemistry (1997) pp 81-84.
111. S.M.T. Cunniffe and P. O'Neill, *Radiat. Res.*, 152 (1999) 421.
112. P. Wardman, In *Biothiols in Health and disease*, L. Packer and E. Cadenas(eds), Marcel Dekker NY, 1995.
113. M. Liphard, E. Bothe and D. Schulte-Frohlinde, *Int. J. Radiat. Biol.*, 58 (1990) 589.
114. V. Jagannadham and S. Steenken, *J. Amer. Chem. Soc.*, 110 (1988) 2188.
115. P. Wardman and E.D. Clarke, In *New Chemo and Radiosensitizing Drugs*, A. Breccia and J.F. Fowler (eds) lo Scarabeo, Bologna, 1985, p.21.
116. C. Nese, M.N. Schuchmann, S. Steenken and C. von Sonntag, *J. Chem. Soc., Perkin Trans. 2*, (1995) 1037.
117. V. Jagannadham and S. Steenken, *J. Phys. Chem.*, 92 (1988) 111.
118. M.M.M. Bamatraf, P. O'Neill and B.S.M. Rao, *J. Amer. Chem. Soc.*, 120 (1998) 11852.
119. H. Sugiyama and I. Saito, *J. Amer. Chem. Soc.*, 118 (1996) 7063.
120. M.E. Núñez, D.B. Hall and J.K. Barton, *Chem. Biol.*, 6 (1999) 85.
121. F.D. Lewis, T. Wu, Y. Zhang, R.L. Letsinger, S.R. Greenfield and M.R. Wasielewski, *Science*, 277 (1997) 673.
122. H.B. Gray and J.R. Winkler, *Ann. Rev. Biochem.*, 65 (1996) 537.
123. S. Priyadarshy, S.M. Risser and D.N. Baratan, *J. Phys. Chem.*, 100 (1996) 17678.
124. D.B. Hall, S.O. Kelley and J.K. Barton, *Biochem.*, 37 (1998) 15933.
125. E. Meggers, M.E. Michel-Beyerle and B. Giese, *J. Amer. Chem. Soc.*, 120 (1998) 12950.
126. J. Jortner, M. Bixon, T. Langenbacher and M.E. Michel-Beyerle, *Proc. Natl. Acad. Sci.*, 95 (1998) 12759.
127. S. Steenken., *Free Rad. Res. Commun.* 16 (1992) 349.



128. S.R. Rajski, S. Kumar, R.J. Roberts and J.K. Barton, *J. Amer. Chem. Soc.*, 121 (1999) 5615.
129. W.R. Holley and A. Chatterjee, *Radiat. Res.*, 145 (1996) 188.
130. G.D.D. Jones, J.R. Milligan, J.F. Ward, P.M. Calabro-Jones and J.A. Aguilera, *Radiat. Res.*, 136 (1993) 190.
131. D. Bloetcher, *Int. J. Radiat. Biol.*, 54 (1988) 761.
132. M.A. Chaudhry and M. Weinfeld, *J. Mol. Biol.*, 249 (1995) 914.
133. L. Harrison, Z. Hatahet, A. Purmal and S.S. Wallace, *Nucl. Acids Res.*, 26 (1998) 932.
134. T.J. Jenner, S.M.T. Cunniffe, D.L. Stevens and P. O'Neill, *Radiat. Res.*, 150 (1998) 593.
135. J.D. Chapman, A.P. Reuvers, J. Borsa and C.L. Greenstock, *Radiat. Res.*, 56 (1973) 291.
136. B.C. Millar, O. Sabora, E.M. Fielden and P.S. Loverock, *Radiat. Res.*, 86 (1981) 506.
137. O. Sabora, F. Barone, M. Belli, A. Maggi, M. Quintiliani and M.A. Tobocchini, *Int. J. Radiat. Biol.*, 60 (1991) 467.
138. C.M. deLara, T.J. Jenner, K.M.S. Townsend, S.J. Marsden and P. O'Neill, *Radiat. Res.*, 144 (1995) 43.
139. R. Roots, A. Chatterjee, E. Blakely, P. Chang, K. Smith and C. Tobias, *Radiat. Res.*, 92 (1982) 245.

## Free radical mechanisms in anti-cancer drug research

P. Wardman

Gray Laboratory Cancer Research Trust, P.O. Box 100, Mount Vernon Hospital,  
Northwood, Middlesex HA6 2JR, United Kingdom

### 1 INTRODUCTION

A chapter in an earlier compilation [1] bringing together fundamentals and applications of radiation chemistry illustrated applications to biochemistry and radiobiology. That chapter mainly described studies of redox processes in proteins and biomolecules. It therefore seemed appropriate to focus instead a major part of the present review on free radicals derived from xenobiotic molecules, especially drugs of interest in cancer therapy.

As was noted in the earlier chapter, radiation chemistry in this context is used as a tool rather than as a means to understand radiation effects. It is a powerful tool. Intermediate free radicals from drug oxidation *or* reduction can be readily produced, in known concentrations, in a microsecond or so, and their reactions followed directly. The tool is well established, and not very expensive if the capital investment is depreciated over the lifetime of the equipment, or if skills are available to refurbish accelerators after their economic life in radiotherapy centres.

The present chapter naturally concentrates on chemical properties and chemical mechanisms in anti-cancer drug research, although a brief outline of the biological basis for some outstanding problems in cancer therapy is included, together with an overview of redox characteristics of drugs and radicals. For brevity, only illustrative examples of specific studies that have utilized radiation-chemical techniques are included, and the bibliography concentrates on reviews where possible. Some earlier reviews outline in a broader context redox mechanisms of some anti-cancer and other redox-active drugs [2-8].

'Ged' Adams was a pioneer in the application of radiation chemistry to cancer research, particularly directed towards the development of drugs which might be useful in therapy, and his Failla Memorial Lecture [9] reviews the principles and key examples of the development of redox-sensitive drugs for use in cancer

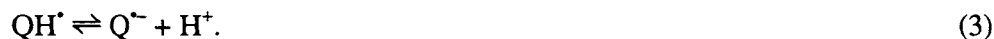
therapy. He was also the senior editor of a volume of papers at a NATO Advanced Research Workshop on 'Selective Activation of Drugs by Redox Processes' [10], which provides an excellent overview of the field.

## 2 REDOX CHARACTERISTICS OF DRUGS AND RADICALS

### 2.1 Reduction potentials as a measure of ease of reduction or of oxidation of drugs

A compilation of reduction potentials of one-electron couples involving free radicals in aqueous solution (mainly organic couples) includes an introductory outline of the quantitative basis for expressing redox properties by means of reduction potentials, which the reader may find useful [11]. Other compilations concentrate on inorganic couples [12] or include data on the kinetics of electron-transfer equilibria [13].

For simplicity consider first reduction of a drug such as a quinone Q, or oxidation of a hydroquinone QH<sub>2</sub>, by one or two electrons. Some examples of quinones that are drugs or biologically-active substances are shown in Figure 1, 1 – 7. One-electron reduction of Q (equation (1)) or oxidation of QH<sub>2</sub> (equation (2)) generates the same intermediate, the free radical Q<sup>•-</sup>/QH<sup>•</sup>, which may be involved in prototropic equilibria such as equation (3):



The ease of reduction of Q may be quantified by the reduction potential of the couple Q/Q<sup>•-</sup>, usually denoted by *E* and expressed in volts relative to the Normal Hydrogen Electrode (NHE). Only if both oxidant Q and reductant Q<sup>•-</sup> are in their thermodynamic standard states will the potential *E* equate to the standard reduction potential of the couple and symbolized as *E*<sup>o</sup> or *E*<sup>o</sup>. In the present context, interest is focused on effective potentials under physiological conditions, i.e. in water at pH values close to 7. Reduction potentials such as polarographic half-wave potentials obtained in non-aqueous media, especially aprotic solvents such as dimethylformamide or acetonitrile and relative to a standard calomel electrode (for example), will be numerically quite different. *E*<sup>o</sup> should not be confused with a *formal potential* *E*<sub>0</sub>, which is usually defined as the potential when the ratio of the total concentrations of oxidized and reduced

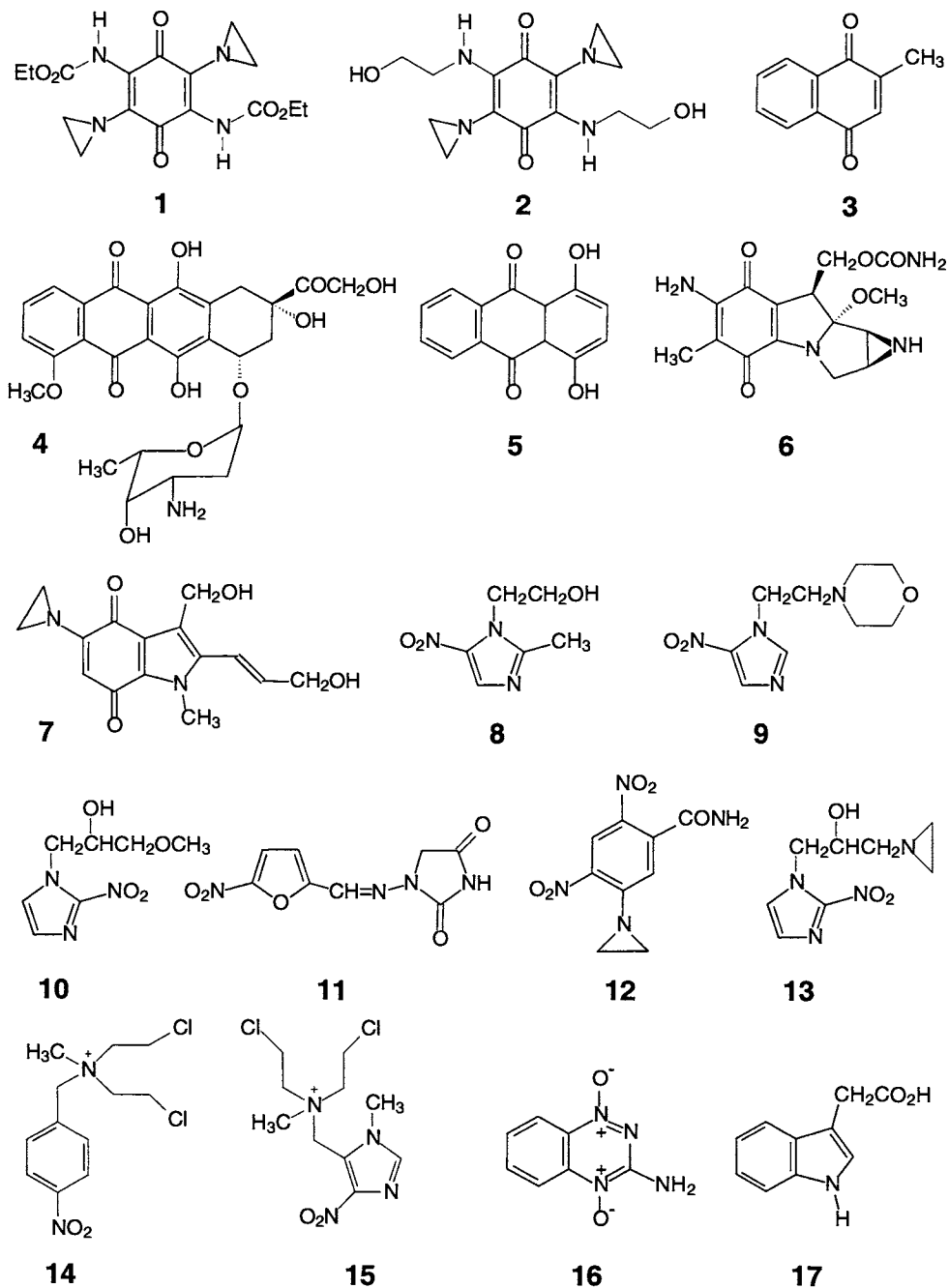


Figure 1. Structures of some drugs and other chemicals discussed in the text.

species is unity and  $H^+$  is at unit activity ( $pH = 0$ ) [14]. If protonation of the semiquinone  $Q^{\cdot-}$  only occurs at  $pH$  values  $\ll 7$  ( $pK_3 \ll 7$ ), then the mid-point potential at  $pH$  7,  $E_{m7}$ , will approximate to  $E^\circ(Q/Q^{\cdot-})$ . Common quinones typically exhibit values of  $pK_3$  of 4.0 – 5.5 [15], and at  $pH$  values  $pH$ ; approaching or below  $pK_3$  the mid-point reduction potential is best denoted as  $E_{mi}(Q, H^+/QH^{\cdot-})$  to indicate the significant participation of protons in the couple; the value will increase by  $\sim 0.06$  V per decreasing  $pH$  unit below  $pK_3$  ( $0.06$  V  $\approx 2.303 RT/nF$ , where the number of electrons,  $n = 1$ ,  $F$  is the Faraday constant,  $R$  the gas constant and  $T$  the absolute temperature). The *standard* potential  $E^\circ(Q, H^+/QH^{\cdot-})$  is higher than  $E^\circ(Q/Q^{\cdot-})$  by the factor  $\sim 0.06 \times pK_3$  volts [11].

The higher the numerical value of  $E_{m7}(Q/Q^{\cdot-})$ , the easier  $Q$  is to reduce (more powerful the oxidant). Drugs discussed below include some quinones, such as derivatives of 1,4-benzoquinone or 1,4-naphthoquinone ( $E^\circ(Q/Q^{\cdot-}) \equiv E_{m7}(Q/Q^{\cdot-})$  since  $pK_3 \approx 4.1$ ), and the common cancer therapeutic agent, adriamycin (doxorubicin, Figure 1, 4). The latter structure can be considered to be based on 1,4-dihydroxy-9,10-anthraquinone (quinizarin, Figure 1, 5); indolequinones are also of interest (e.g. EO9, Figure 1, 7).

Nitroarenes, especially heteroarenes such as imidazoles and furans, are quite widely used in medicine as agents with selective toxicity towards anaerobic organisms, and have also attracted attention as hypoxic cell radiosensitizers (see below); typical examples include metronidazole (Figure 1, 8), nimorazole (9), misonidazole (10) and nitrofurantoin (11). Since protonation of either the nitro group or the unsubstituted imidazole nitrogen in the radical-anions of nitroimidazoles only occurs at  $pH$  values rather less than 7, the radical obtained on one-electron reduction of many nitroarenes are largely unprotonated at  $pH$  7 and for convenience can be symbolized as  $ArNO_2^{\cdot-}$ . Functional groups of side chains/substituents may of course be protonated, with  $pK$  values differing in ground state and radical; an example was shown in the introduction to the compilation [11] and also in a review of the chemistry of nitroarene radicals [16]. The latter review also compared nitroarene radicals with those obtained on reduction of some aromatic  $N$ -oxides, especially that from the 1,2,4-benzotriazine-1,4-dioxide, tirapazamine (Figure 1, 16), now in clinical trial as an adjunct to chemotherapy with selective toxicity towards hypoxic tumour cells (see below).

Table 1 lists some reduction potentials of the drugs mentioned above (or simpler models), including the potentials for oxygen. Two values of the latter are listed. The first is the standard potential,  $E^\circ(O_2(1 \text{ atm})/O_2^{\cdot-})$ , where oxygen is at its thermodynamic standard state of unit fugacity (essentially one atmosphere partial pressure); the second is the mid-point potential  $E_{m7}(O_2(1 \text{ mol dm}^{-3})/O_2^{\cdot-})$ , where both oxygen and superoxide are at unit concentration/activity [17].

TABLE 1

Reduction potentials of drugs/biomolecules or their radicals, in water at pH 7, vs. NHE (numbers in bold type refer to the structures in Figure 1)

Couple (oxidant/reductant, for one-electron reduction)	$E_{m7} / V$
Ascorbate radical-ion/ascorbate ion	+ 0.33
Benzoquinone AZQ ( <b>1</b> )/AZQ radical-anion	- 0.09
Benzoquinone BZQ ( <b>2</b> )/BZQ radical-anion	- 0.38
Doxorubicin (adriamycin, <b>4</b> )/doxorubicin radical-anion	- 0.36
Flavin mononucleotide/flavosemiquinone radical	- 0.33
Flavosemiquinone radical/dihydroflavin	- 0.11
Indolequinone EO9 ( <b>7</b> )/EO9 radical-anion	- 0.27
Indolyl-3-acetate radical/indole-3-acetate ( <b>17</b> )	+ 0.97
Menadione ( <b>3</b> )/menadione radical-anion	- 0.23
Misonidazole ( <b>10</b> )/misonidazole radical-anion	- 0.41
Metronidazole ( <b>8</b> )/metronidazole radical-anion	- 0.51
Nimorazole ( <b>9</b> )/nimorazole radical-anion	- 0.46
Nitrofurantoin ( <b>11</b> )/nitrofurantoin radical-anion	- 0.28
Oxygen (1 mol dm <sup>-3</sup> O <sub>2</sub> )/superoxide radical-anion	- 0.18
Oxygen (1 atm O <sub>2</sub> )/superoxide radical-anion	- 0.35
Tirapazamine ( <b>16</b> )/tirapazamine radical-anion	- 0.45

Values are from [11,18-20], corrected for adjustment to reference potentials [21].

The latter value is most appropriate for comparing the relative electron affinities of oxygen and drugs in aqueous solutions. This property is reflected in the position of the equilibrium, equation (4), which is a general example of redox equilibria involving one-electron transfer (5):



It can be shown [11] that the difference in reduction potentials,  $\Delta E_5 = E(B/B^{\cdot-}) - E(A/A^{\cdot-})$  is related to  $K_5$  by:

$$\log K_5 \approx (nF/2.3RT) \Delta E_5 \quad (6)$$

and therefore an order of magnitude change in  $K_5$  is reflected by a change in the difference in the potentials  $\Delta E_5$  of  $\sim 0.06$  V. The importance of using the appropriate value for the oxygen/superoxide couple is easily seen. For example, Table 1 gives a value of  $E_{m7}(Q/Q^{\cdot-}) \approx -0.36$  V for doxorubicin (Figure 1, **4**);

using the *standard* reduction potential for the  $O_2/O_2^{\cdot-}$  couple, when  $O_2$  is at 1 atm, one would wrongly conclude that  $K_4 \approx 1$  since the potentials of both quinone and oxygen are similar. In fact, if we use instead the value  $E_{m7}(O_2(1 \text{ mol dm}^{-3})/O_2^{\cdot-}) = -0.18 \text{ V}$ , we can correctly estimate that  $K_4 \approx 10^3$  since  $\log K_4 \approx (-0.18 + 0.36)/0.06 \approx 3$ , i.e. oxygen is considerably more electron-affinic than this quinone.

In older literature, ease of oxidation is sometimes quantified by oxidation potentials, but it is much better practice to use reduction potentials exclusively, i.e. the couple characterized by equation (7) rather than equation (2):



Thus the ease of oxidation of a hydroquinone drug  $QH_2$  is reflected in the reduction potential of the radical  $QH^{\cdot}$ , or at pH 7 the mid-point potential  $E_{m7}(QH^{\cdot}, H^+/QH_2)$  since most hydroquinones do not dissociate significantly (to  $QH^-$  or  $Q^{2-}$ ) at this pH. The higher the value of this reduction potential of the radical, the more difficult  $QH_2$  is to oxidize. Included in Table 1 are the reduction potential of the radical obtained on oxidation of indole-3-acetic acid (Figure 1, 17), and that of the ascorbate (vitamin C) radical. A radical from a drug higher up the reduction potential scale (or 'pecking order' [22]) will oxidize ascorbate. Thus the radical-cation/indolyl radical obtained on oxidation of indole-3-acetic acid reacts rapidly with ascorbate [23].

Values of reduction potentials for the two-electron couple (quinone/hydroquinone):



are related to the individual one-electron steps by:

$$2 E_{mi}(Q, 2H^+/QH_2) = E_{mi}(Q, H^+/QH^{\cdot}) + E_{mi}(QH^{\cdot}, H^+/QH_2). \quad (9)$$

Further, the 'semiquinone formation constant', i.e. the propensity for mixtures of quinone and hydroquinone to form semiquinone radicals, equation (10), is related to the reduction potentials by equation (11) [11]:



$$E_{mi}(Q, H^+/QH^{\cdot}) = E_{mi}(Q, 2H^+/QH_2) - (RT/2F) \ln K_{10}. \quad (11)$$

Hence if either of the one-electron potentials (quinone/radical or radical/hydro-

quinone) is known, together with that of the quinone/hydroquinone couple, it is possible to calculate  $K_{10}$ . Plots of this equilibrium constant as a function of pH for several illustrative redox systems are in the earlier review [1].

## 2.2 Redox properties of radiation-produced radicals useful in producing drug radicals

The application of radiation chemistry to drug research [24,25] is conceptually simple and greatly facilitated by the ready availability of authoritative compilations of kinetic information obtained by radiation chemists [26], especially computer-searchable databases [27] and those accessible on the Internet (<http://allen.rad.nd.edu/>).

In studies of free radicals of drugs, the desire is frequently to produce selected drug radicals, usually involving one-electron oxidation or reduction, which are putative intermediates in drug activation or metabolism. The redox properties of likely activating enzymes are thus of interest, but of most importance is the selectivity of reaction.

Thus oxidizing drugs by  $\cdot\text{OH}$  radicals is seldom useful, because the sites of reaction with typical drugs will be multiple. More selective oxidants are used, such as the secondary radicals derived from halide or pseudohalide oxidation by  $\cdot\text{OH}$ . Reducing radicals are less of a problem, since the radicals from scavenging  $\cdot\text{OH}$  by formate or 2-propanol usually reduce oxidants to produce the same radicals as cellular reduction systems (even if short-lived intermediate adducts are involved).

Table 2 lists some common 'scavenging' systems useful in drug research, along with the reduction potentials of the reactive couples in water at pH 7. Typically, the main radical scavenger will be added at around  $0.1 \text{ mol dm}^{-3}$  with the drug at (say)  $1\text{--}2 \text{ mmol dm}^{-3}$  so that few primary water radicals from radiolysis react directly with the drug.

To study reactions of drug radicals with oxygen or other biomolecule (equation (4) for example), concentrations of the third solute would be selected to avoid reactions with both primary water radicals and the secondary reducing or oxidizing radical. Experimental design requires only the simple concepts of kinetic competition and a large database of rate constants with the molecules of interest, or ones sufficiently similar for these purposes, which radiation chemistry has now provided.

Two illustrative reactions (equations (12) and (13)) exemplify much of the work in drug research exploiting radiation-chemical generation of radicals, involving reduction or oxidation, respectively, of drugs (D). Examples of suitable reductants and oxidants can be found in Table 2.



TABLE 2

Some radicals useful in reducing or oxidizing drugs by radiolysis of aqueous solutions

Solute	Water radicals scavenged	Redox couple generated at pH 7	Reducing/oxidizing	$E_{m7} / V$ vs. NHE †
$N_2O$	$e_{aq}^-$	$\cdot OH, H^+ / H_2O$	oxidizing*	+ 2.32
$HCO_2^-$	$\cdot OH, H^+$	$CO_2 / CO_2^{\cdot -}$	reducing	- 1.90
$(CH_3)_2CHOH$	$\cdot OH, H^+$	$(CH_3)_2CO, H^+ / (CH_3)_2C^{\cdot}OH$	reducing	- 1.39
$Br^-$	$\cdot OH$	$Br_2^{\cdot -} / 2 Br^-$	oxidizing	+ 1.66
$N_3^-$	$\cdot OH$	$N_3^{\cdot -} / N_3^-$	oxidizing	+ 1.33
$SCN^-$	$\cdot OH$	$(SCN)_2^{\cdot -} / 2 SCN^-$	oxidizing	+ 1.33
$S_2O_8^{2-}$	$e_{aq}^-$	$SO_4^{\cdot -} / SO_4^{2-}$	oxidizing	+ 2.43

\* Usually used in conjunction with other scavengers to 'convert'  $e_{aq}^-$  to  $\cdot OH$  and thence to more selective oxidants, rather than as a direct oxidant. † Data from [11,12].



### 3 REDOX CHARACTERISTICS OF TUMOURS COMPARED TO NORMAL TISSUES

#### 3.1 Lower oxygen levels (hypoxia) in tumours

The microenvironment of human tumours is characterized by several features that distinguish it from that of surrounding normal tissue [28]. Perhaps foremost of these from the chemical viewpoint is the relatively poor vascularization, which is accompanied by oxygen gradients. Regions of both chronic and acute hypoxia occur. The former type was recognized almost half a century ago by Gray and colleagues to be a factor in the success of radiotherapy [29].

Hypoxia can now be detected and quantified by microelectrodes and the binding of reactive, reduced metabolites of nitroimidazoles, which reflect oxygen levels (because the radical-anion reduction intermediate is oxygen reactive) [30]. A new fibre-optic probe for tissue oxygenation, now available commercially, relies on measurements of emission from a ruthenium probe, which has an oxygen-dependent excited-state lifetime [31]. Acute or fluctuating hypoxia, which has features in common with ischaemia/reperfusion and therefore with myocardial infarction and stroke, can be detected by vascular stains such as bisbenzimidazole intercalators with different fluorescent characteristics. These can be administered intravenously a few minutes apart;

the 'mismatch' of colours of sections under the fluorescence microscope reveals temporal variations in vascular delivery. Laser doppler techniques, measuring the velocity of red blood cells, quantify these variations directly.

The importance associated with tumour hypoxia stems from the decreased radiosensitivity of hypoxic cells: up to three-fold higher radiation doses are required to kill anoxic cells compared to well-oxygenated ones [32]. Cellular proliferation and resistance to cytotoxic drugs may also be influenced by hypoxia. There is now absolutely no question that hypoxic regions frequently occur in common human tumours and that treatment outcome, i.e. survival, is directly related [28].

### 3.2 Some enzymes catalysing chemical reduction in tumours

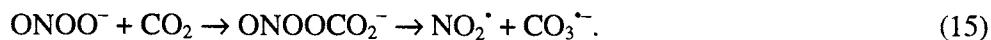
The reductive chemistry of drugs outlined below is initiated in biology by cellular *reductases*. These drugs are described as 'bioreductively-activated' and provide a rationale for therapeutic gain if *either* the reductase enzymes are elevated in tumours compared to normal tissue, *or* the tumour microenvironment (particularly low oxygen levels) is conducive to selective reduction in tumours. In favourable instances, both conditions may be met. Two key flavoproteins involved are NADPH:cytochrome P-450 reductase (which reduces simple nitroarenes, for example, to their oxygen-sensitive radical-anions [33]), and DT-diaphorase (or NAD(P)H:(quinone-acceptor) oxidoreductase, which reduces quinones to hydroquinones without direct semiquinone formation). Over-expression of either may provide selective toxicity if drugs are activated by these enzymes [34-36], the basis for enzyme-directed bioreductive drug development [37].

### 3.3 Some enzymes catalysing chemical oxidation in tumours

The major oxidative or nitrosative stress in tumours probably arises from infiltrating macrophages, which can produce both superoxide and nitric oxide radicals [38,39] via an NADPH-oxidase and inducible nitric oxide synthase (NOS) respectively. NOS activity is elevated in some common tumours compared to adjacent, normal tissue [40,41], and the implications of nitric oxide production in cancer therapy have been reviewed [42,43]. (NOS is a flavoprotein which can also reduce oxygen to superoxide if the normal substrate (L-arginine) is depleted [44].)

The NADPH-oxidase of human phagocytes can produce superoxide at rates of 15 fmol/cell/min [45]; even averaged over a nominal cellular volume of 1 pL this corresponds to a production of 250 micromolar superoxide *per second*, and higher if averaged over the smaller phagocytic intercompartmental space. Superoxide, via hydrogen peroxide and chloride (in a reaction catalysed by

myeloperoxidase), can be the source of the reactive oxidant, hypochlorous acid (HOCl) [46]. This oxidant can also produce hydroxyl radicals by Fenton-type chemistry [47,48]). Superoxide and  $\text{NO}^\bullet$  react at a diffusion-controlled rate [49], forming peroxynitrite, precursor to hydroxyl, nitrogen dioxide and carbonate radicals:



The chemistry summarized by these two equations is complex and has been the subject of intensive, ongoing studies [50-62]. For the present we note merely that many early studies utilizing radiation chemistry to quantify reactions of nitrogen oxides [63-69] subsequently became of considerable interest in a biological context two decades later, and that the generation of carbonate radical via equation (15) provides immediate biological interest for the 222 rate constants for this species in the current NDRL-NIST database [27].

Myeloperoxidase is only one of the peroxidases in mammalian tissues utilizing hydrogen peroxide as the cofactor. The peroxidase content in cells from rat mammary tumours induced by 7,12-dimethylbenz(a)anthracene was much higher in tumours compared to normal tissue [70].  $\text{H}_2\text{O}_2$  production rates by human tumour cells, initially around  $10 \mu\text{mol dm}^{-3} \text{s}^{-1}$  if the cell volume is nominally 1 pL, were reported to be comparable (over a 4 h period) to the levels produced by stimulated neutrophils in the 'respiratory burst' [71]. Since peroxidases are capable of catalysing the oxidation of many potential drugs [72], this oxidative activity is the basis for a new approach to the 'oxidation therapy' of cancer [73], as discussed below.

## 4 DRUGS ENHANCING CELLULAR RADIOSENSIVITY

### 4.1 Introduction

Drugs to enhance radiation sensitivity are of clinical value only if there is selectivity towards the tumour compared to normal tissues unavoidably included in the radiation field in radiotherapy. The drugs discussed briefly below – hypoxic cell radiosensitizers – present such selectivity mainly because oxygen is such an efficient radiosensitizer that in well-oxygenated tissues its effect is virtually at a maximum, and added 'oxygen-mimetic' drugs have very little additional effect.

## 4.2 The identification of 'oxygen-mimetic' radiosensitizers

The identification of drugs that might overcome the problem of the reduced radiation sensitivity of sub-populations of tumour cells at low oxygen tensions was a triumph of radiation chemistry [9]. Several pieces of evidence pointed to the possibility that the radiosensitizing effect of oxygen involved short-lived DNA free radicals and that chemical substitutes for oxygen could be found that might be therapeutically useful.

Firstly, the 'oxygen effect' was approximately constant at around three in dose-modifying terms (the radiation dose required for constant biological effect) in cells which varied enormously in their absolute radiation sensitivities. Thus human cancer cells in anoxia might be killed (by a factor  $1/e \approx 37\%$  survival) at doses of the order of 3 Gy, whereas bacterial spores might require 400 times this dose; however, both sensitivities are enhanced by oxygen by about the same effect – a factor of 2.2 to 3.0.

Secondly, rapid-mix techniques, in both the liquid and gas/liquid phases, indicated that oxygen had no radiosensitizing effect if the oxygen exposure occurred only a few milliseconds after the radiation [74]. This clearly indicated that short-lived species, probably free radicals, were involved.

Thirdly, DNA was shown to be an important target using external radiation beams with very shallow penetration, or by intracellular incorporation of radionuclides with known penetration characteristics in nucleus or membrane. (Recently, considerable progress has been made in developing radiation beams with micron and sub-micron spatial resolution ('microbeams'), which are more sophisticated tools to probe sites of cellular radiosensitivity [75].)

By 1963, a considerable number of rate constants for reactions of the hydrated electron were available, and it was recognized by Adams and Dewey that some substances that increased the radiosensitivity of anoxic bacteria were highly reactive towards  $e_{aq}^-$ , i.e. were 'electron-affinic'. The radiosensitizing efficiencies in anoxic bacterial spores of acetone, 1,4-benzoquinone and 4-nitroacetophenone were in the same ranking order as the stepwise electron transfer observed directly by pulse radiolysis, and there was a broad correlation between radiosensitizing efficiency in this system and reduction potential. Nitrobenzenes, particularly 4-nitroacetophenone, were shown to be effective in mammalian cells, and substituted nitrobenzenes showed a gradation of efficacy that enabled a structure-activity relationship correlating radiosensitizing efficiency with the Hammett sigma substituent 'constant' to be established in 1973. Since the nitrobenzene derivatives reacted with  $e_{aq}^-$  with rate constants at or close to the diffusion-controlled limit, and reactive substances such as nitrous oxide are ineffective radiosensitizers, it was by then apparent that electron scavenging was not the mechanism of radiosensitization (see earlier reviews [76-79]).

### 4.3 Quantitative structure-activity relationships (QSARs) for hypoxic cell radiosensitizers

Radiation chemistry played a key role in extending the Hammett relationships for nitroarene radiosensitizers to be independent of aromatic moiety. By 1973, pulse radiolysis was being used to establish the positions of one-electron transfer equilibria involving unstable free radicals and hence reduction potential differences, equations (5) and (6) [15,80,81]. Baxendale and colleagues had (20 years earlier) measured the semiquinone formation constant ( $K_{10}$ ) for duroquinone at high pH, where a large fraction of quinone/hydroquinone is present as semiquinone. Hence it was possible to calculate  $E_{m7}(Q/Q^{\cdot-})$  for duroquinone/durosemiquinone, and using a measurement of  $K_4$  (from pulse radiolysis [15]), the reduction potential of the oxygen/superoxide couple was derived [81,82].

Reduction potentials of nitroarene/nitroarene radical-anion couples were similarly estimated by generating radicals by pulse radiolysis and measuring  $K_5$  with e.g. A = a nitroarene and B (the reference indicator) = duroquinone or 9,10-anthraquinone-2-sulphonate [80]. Viologens were found to be very useful alternatives to quinone redox indicators in this type of study [83] partly because the stable radical-cations permit electrochemical measurements of the oxidant/radical couples of these redox indicators, although dimerization of benzyl viologen radical-cation (in particular) can introduce error [11,21,84]. Different viologens  $V^{2+}$  provide a wide range of redox indicators,  $E^{\circ}(V^{2+}/V^{\cdot+})$  spanning the range  $\sim -0.1$  to  $-0.83$  V [85-87].

The reduction potentials of metronidazole, nimorazole, misonidazole, and nitrofurantoin (Figure 1, **8**, **9**, **10** and **11** respectively) and analogues of these nitroarene radiosensitizers were thus measured and compared with the concentrations  $C$  of the compounds needed to achieve a defined radiosensitizing effect in mammalian cells. QSARs of the form:

$$\log (1/C) = \text{intercept} + [\text{slope} \times E_{m7}(ArNO_2/ArNO_2^{\cdot-})] \quad (16)$$

were established [88]. An example is shown in Figure 2. These studies provided a critical test of model systems which sought to describe the underlying mechanisms of radiosensitization: the models had to show a redox dependence of the rate-limiting step of around  $8-9$  V<sup>-1</sup> when the kinetic data were fitted to a form similar to equation (16), with rate constant replacing  $1/C$ .

There are two caveats to such an argument. Firstly, analysis of the radiosensitization data for different levels of effect showed that the slope of equation (16) varied with effect. This implies two (or more) mechanisms, with different redox dependencies, are involved. Secondly, the experimental

measurements relate to extracellular concentrations in the medium, and for some compounds, extracellular:intracellular concentrations gradients were observed. In particular, weak acids or bases were expected, and found [89,90], to result in pH-controlled concentration gradients. These gradients explained apparently enhanced radiosensitization by basic radiosensitizers [91]. Fluorescence quenching [92,93] or hplc measurements [94] after disrupting intracellular pH gradients revealed intracellular concentration gradients. For meaningful comparisons of biological and chemical data, we need to know concentrations at the target site.

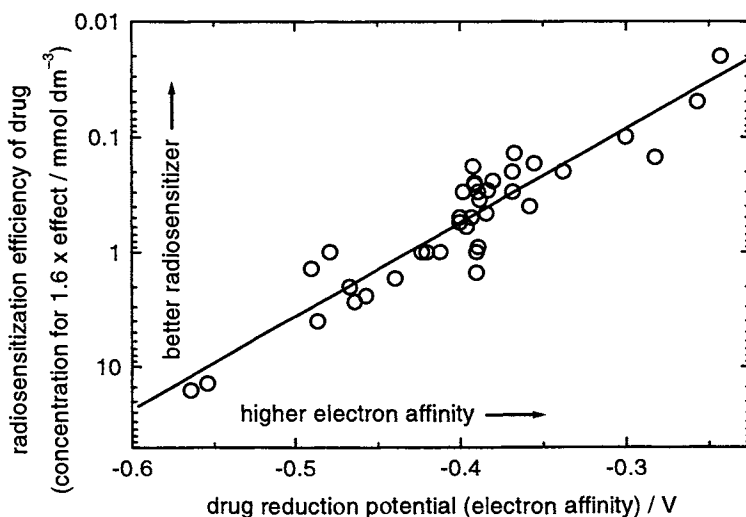


Figure 2. Relationship between efficiency in radiosensitizing hypoxic mammalian cells *in vitro* and the reduction potential of nitroarenes. Data from [88].

In spite of these problems, the QSAR shown in Figure 2 was of great importance in the search for improved radiosensitizers. Multivariate analysis showed drug lipophilicity was of relatively little importance in mammalian cells *in vitro* [88], whereas reductions in neurotoxic side-effects were achieved *in vivo* by reducing the lipophilicity (and the drugs' capacities to cross the blood/brain or other lipophilic barriers) [95]. Equally importantly, the pulse radiolysis measurements of reduction potential were applied to data for the cytotoxicity of the radiosensitizers *in vitro*, in the presence [96] or absence [97] of oxygen, and quantitatively similar relationships between effect and redox property were demonstrated as had been derived for radiosensitization. This pointed to the

difficulty of a strategy of improving efficacy merely by increasing reduction potential.

Although activity in the search for improved hypoxic cell radiosensitizers has decreased, the contribution of radiation chemistry in defining the range of reduction potentials which are needed for effective radiosensitizers was seminal.

#### 4.4 Redox-controlled reactions of nitroarene radiosensitizers in chemical systems

Nitroarenes can react with reducing radicals in two general pathways, radical-addition or outer-sphere electron-transfer, although electron transfer can proceed via adducts in an inner-sphere addition/elimination reaction [98]. Prototypical behaviour was established from electron paramagnetic resonance (epr) experiments [99], which showed that hydroxymethyl radicals reduced nitrobenzene via an intermediate adduct, relatively stable in acid but which underwent base-catalyzed heterolysis:



Reactions of nitroarenes with both sugar and base radicals have been studied in some depth by several groups, summarized in earlier reviews [77-79,93,100]. Thus a radical that clearly forms adducts, such as that derived from an ether, reacted with nitroimidazoles with a redox relationship three times 'shallower' than observed for radiosensitization of mammalian cells [100]:



$$\log k_{18} = 9.77 + 2.7 [E_{m7}(\text{ArNO}_2/\text{ArNO}_2^{\bullet-})/V]. \quad (19)$$

The rate constant for adduct formation by  ${}^{\bullet}\text{CH}_2\text{OH}$  with different nitrobenzenes was also weakly-redox-controlled, equation (20) [101], but the heterolysis of the adducts formed with  $\text{CH}_3\text{C}^{\bullet}\text{HOH}$  was influenced by reduction potential to a greater extent, equation (21) [102]:

$$\log k = 9.1 + 3.3 [E_{m7}(\text{ArNO}_2/\text{ArNO}_2^{\bullet-})/V] \quad (20)$$

$$\log k = 6.9 + 7.9 [E_{m7}(\text{ArNO}_2/\text{ArNO}_2^{\bullet-})/V]. \quad (21)$$

More recent studies have provided interesting new information. A comparison was made of the reactions of 4-nitrobenzonitrile or oxygen with  $\alpha$ -alkoxyalkyl radicals, models for DNA *sugar* radicals, produced via reaction of  ${}^{\bullet}\text{OH}$  with e.g.

1,4-dioxane and the sensitizer [103]. It was concluded that long-lived adduct radicals could be reduced by ascorbate in competition with both homolytic or heterolytic fragmentation of the *N*-alkoxyaminoxyl radicals. The 1,4-dioxan-2-yl radicals yielded the same products with either nitrobenzotrile or oxygen as the 'adding' molecule. Ascorbate [104] or  $\alpha$ -tocopherol [105] reduced the radiosensitization efficiency of misonidazole *in vitro*, provided endogenous glutathione had been depleted. (Since most mammalian cell cultures *in vitro* lack ascorbate, the importance of cellular reductants could be underestimated from the *in vitro* models.)

The question as to whether an adduct radical between a DNA *base* radical and a nitroarene or other radiosensitizer could abstract hydrogen from a sugar and lead to strand breaks (*cf.* base peroxy radicals as the rate-limiting step in strand break formation [106]) has been addressed in another recent study [107]. The possibility of a nitroarene/pyrimidine-6-yl adduct radical abstracting hydrogen from a sugar was discussed in an earlier review [108] but it was recognized in the recent study that hydrogen abstraction would most likely be from an adjacent sugar moiety, not the sugar in the same nucleotide. Importantly, it is now clear that heterolysis of the adducts is *very* slow if the base is substituted at N(1), so that the adducts could be sufficiently long-lived in DNA for even quite slow hydrogen-abstraction reactions to occur.

The redox dependence of hydrogen abstraction from sugars by base/nitroarene radical-adducts (nitroxyl radicals) in DNA has not yet been characterized, and it is quite possible that nitroarenes form adducts at *both* base and sugar sites. A detailed molecular understanding of the mechanisms of radiosensitization of hypoxic cells therefore remains elusive. For a complete picture it will be necessary to include an appreciation of the structure and accessibility of the target sites.

## 5 DRUGS SELECTIVELY TOXIC TOWARDS HYPOXIC CELLS

### 5.1 Introduction

An alternative strategy to overcoming the radioresistance of hypoxic tumour cells is to identify drugs selectively toxic towards this sub-population. This goal has been pursued for many years [109] but has been stimulated recently by the increasing sophistication of enzyme-directed therapy [110]. Selectivity of action relies in part on the kinetics of fast, free-radical reactions which have been studied by radiation-chemical methods [111]. There are two general approaches [112]. In the first, reducible chemical functions deactivate the prodrug (Figure 3); in the second, prodrug reduction releases an active entity (Figure 4).



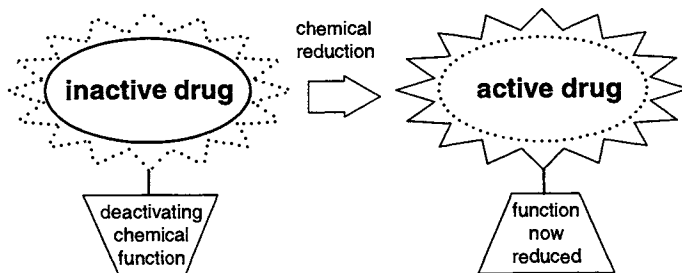


Figure 3. Principle of action of prodrugs activated by reduction to form an active drug without involving fragmentation.

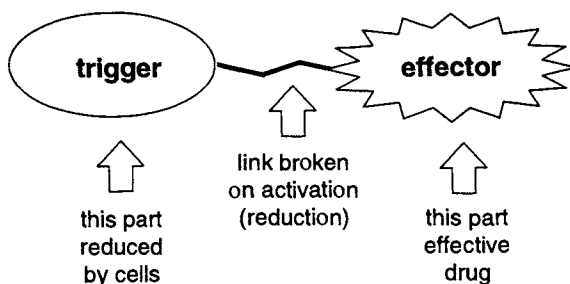
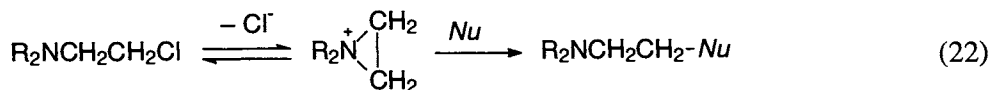


Figure 4. Principle of action of prodrugs which fragment upon reduction, thus releasing the active drug moiety.

## 5.2 Activation of prodrugs in hypoxia or anoxia by chemical reduction without fragmentation

### 5.2.1 'Mustard'-type alkylating agents

Alkylating agents have been of interest in cancer therapy for many years [113,114]. A typical aliphatic 'nitrogen mustard' rapidly forms an aziridinium ion in aqueous solution, reactive towards nucleophiles such as DNA bases (and, in competition, water, thiols, etc.):



In the dinitrobenzenecarboxamide, CB1954 or the quinones AZQ/BZQ (Figure 1, **12**, **1** or **2** respectively), the aziridine moiety is deactivated by the electron-withdrawing nitro substituents or the electron-deficient quinone system respectively. However, on reduction the  $pK_a$  of the aziridine nitrogen increases, activating the site towards reaction with nucleophiles.

Even in RSU-1069 (Figure 1, **13**), a nitroimidazole with an N-1 substituent terminating in an aziridine but 'insulated' from the aromatic moiety by a 3-carbon chain, the inductive effect of the nitroimidazole group is sufficient that reduction of the nitro group activates the alkylating function.

### 5.2.2 Indolequinones

The indolequinone moiety is of interest: (i) as the activating nucleus of aziridine alkylating substituents and/or alkylating functionality through an iminium derivative produced in a C-3 elimination process [115-118], and (ii) as a vehicle for oxygen-sensitive, bioreductively-activated drug delivery [119,120] (see below).

There are some parallels with the reductive activation of mytomyacin C (Figure 1, **6**) [121], a compound which has been evaluated extensively in both laboratory and clinic [122-125], including radiolysis studies [126]. A summary of the latter studies is included in a recent review [8].

Another related indolequinone which entered Phase II clinical trials was EO9 (Figure 1, **7**). This aziridinylindolequinone can potentially cross-link to DNA when activated, through both the 5-aziridinyl moiety and the 3-methide function produced on reduction to the hydroquinone. Pulse radiolysis was used to measure the reduction potential of the quinone/semiquinone couple of EO9 [18] and related quinones [127], as well as the rate constants of the important electron-transfer reactions between semiquinone and oxygen (see below). While the clinical results with EO9 were disappointing [128], it was pointed out [129] that single-agent trials of a hypoxia-selective drug (i.e. without treatment of oxic cells) is generally inappropriate.

### 5.2.3 Nitroarenes forming reactive nitroso or hydroxyamino derivatives

Most nitroarenes or nitroheteroarenes are reduced in a stepwise manner, forming nitroso (+ 2  $e^-$ ), hydroxyamino (+ 4  $e^-$ ) or amino (+ 6  $e^-$ ) derivatives through disproportionation reactions. Amine formation can be viewed as a detoxifying/excretion route, but the reduction intermediates are potentially cytotoxic because they can react with nucleophiles such as protein thiol groups and DNA bases.

Nitrosoarenes react with cellular thiols with half-lives typically a few milliseconds [130]; the environmental pollutant and carcinogen, nitropyrene, forms adducts with DNA at guanine sites upon reduction [131]. Radical intermediates are certainly involved in the first two reduction steps [16,111].

### 5.2.4 Heteroarene-*N*-oxides

There are several parallels in the reduction chemistry of nitroarenes and aromatic *N*-oxides, such as similar kinetics of electron transfer reactions of the radical-anions and the effects of prototropic equilibria on radical lifetimes in aqueous solution [16]. The benzotriazine di-*N*-oxide, tirapazamine (Figure 1, 16) is currently in Phase III clinical trial as a hypoxic cell cytotoxin in conjunction with cisplatin [132]. The mechanism of its action appears to involve the one-electron reduction product [133] cleaving DNA [134], probably also sensitizing the damage by a radical-addition step [135-138].

Steady-state radiolysis was used to study the efficiency of tirapazamine radicals in abstracting hydrogen from alcohols or sugars, by measuring the chain length in reaction sequences such as:



where T = tirapazamine or other *N*-oxides and TH<sub>2</sub> = the mono *N*-oxide (in the case of tirapazamine) [111,139]. As with the earlier study [134] involving formate as hydrogen donor, a short chain length with 2-propanol or deoxyribose as donor was indicative of reactions such as (25), the pH-dependent chain length being interpreted as evidence that the protonated radical TH\* (*pK*<sub>a</sub> ≈ 6) was the reactive form.

Hydrogen abstraction rate constants of only a few hundred dm<sup>3</sup> mol<sup>-1</sup> s<sup>-1</sup> were derived assuming the pH-dependent equation (26) was the single chain-terminating reaction:



### 5.3 Release of active drug by reductive fragmentation of a prodrug

This concept (Figure 4) offers the most promise for the general delivery of active drugs to hypoxic tissues [140,141]. A prototypical pulse radiolysis study built on pointers from earlier work, indicative of leaving group elimination [142], to measure the rate of release of halide leaving groups from nitrobenzyl halide radical-anions [143]. The leaving groups were eliminated in times ranging from a few microseconds to > 0.1 s depending on structure. Pulse radiolysis measurements of the elimination of a mustard from various nitroarenes (with a quaternary nitrogen substituent) showed the behaviour varied

with different aromatic moieties. Thus radicals from 2- or 4-nitrobenzene derivatives (e.g. Figure 1, **14**) decayed by bimolecular processes, whereas nitroimidazole or nitropyrrole derivatives (e.g. Figure 1, **15**) eliminated the mustard with half-lives of ~ 90 or 70  $\mu$ s respectively [144].

Leaving group properties also influence the chemistry. 1-Methyl-2-nitroimidazole substituted with bromomethyl at the 5-position eliminated bromide unimolecularly in < 1ms, whereas in the analogous compound with bromide replaced by salicylate linked through the carboxylate moiety there was a marked reduction in elimination rate [145]. However, measurements of the stoichiometry of release indicated elimination from the 4-electron reduction product, the 2-hydroxyaminoimidazole, did occur. The quantitative basis for radiolytic radical production is a valuable feature of this type of study, since it is indicative of the release mechanism.

An interesting project to exploit this chemistry to activate prodrugs by *radiation* rather than cellular enzymes is in progress [146]. The strategy aims to use the radiotherapy beam itself to activate the prodrugs to release a cytotoxic mustard or other agent. In this case the reduction potential can be chosen to be so low that cellular enzymes do not activate the drugs in normal tissues (see below), since radiation-produced primary or secondary reducing radicals have reduction potentials which are much lower than cellular enzymes.

Indolequinones substituted with appropriate leaving groups can also be used as the basis for oxygen-sensitive, bioreductively-activated drug delivery [119,120]. It is evident that kinetic factors control the efficiency and oxygen-sensitivity of drug delivery [120]. Important factors are the rates and redox dependencies of drug activation and competing electron-transfer reactions, as discussed below.

#### **5.4 Reduction potential as a predictor of drug activation rates**

Some of the flavoproteins which catalyse the reduction of bioreductive drugs show redox-controlled catalysis. The most important of these is probably NADPH:cytochrome P-450 reductase, a one-electron donor [147]. At the simplest level, such proteins can be modelled by reduced flavin mononucleotide, FMNH<sub>2</sub> [148].

Xanthine oxidase is another flavoprotein which can catalyse nitroreduction in hypoxia with redox-controlled rates [149,150]. Figure 5 shows that the redox dependencies of nitroreduction by free flavin or by three different flavoprotein enzymes are not very different, and of the same order as that expected for electron-transfer reactions [100,151]. Cytotoxicity has a similar redox dependence, in both oxic [96] and hypoxic [97] conditions.

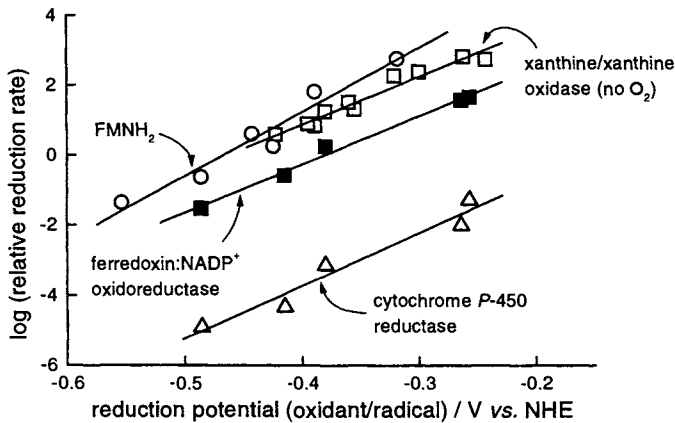


Figure 5. Relative reduction rates of nitroarenes/heteroarenes at pH  $\sim 7$  are controlled by the substrate reduction potential. Data from [147-149].

### 5.5 Reduction potential as a predictor of reactivity of radical-anions with oxygen

As shown in Table 1, most nitroarenes, and many quinones, have reduction potentials lower than that of oxygen ( $1 \text{ mol dm}^{-3}$ ), i.e. equilibrium (4) is over to the right. The rate of electron transfer from the radical to oxygen is redox-controlled, as shown in Figure 6 for nitroarenes/heteroarenes. However, it is important to note that quinone radicals are much more reactive towards oxygen as nitro compounds or *N*-oxides of the same reduction potential [111,152] (the benzotriazine, tirapazamine behaves kinetically as a nitroarene [16]).

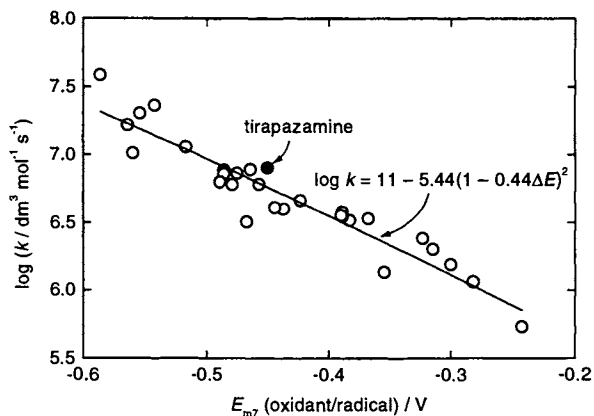


Figure 6. Rate constants for electron transfer from nitro radical-anions or tirapazamine radical to oxygen. Data mainly from [134,153], and unpublished measurements by Mr. E. D. Clarke.

### 5.6 Kinetics controlling bioreductive drug selectivity towards hypoxic cells

It is evident from Figures 5 and 6 that drugs with the highest reduction potentials are activated to their radical-anions fastest, but are slowest in the protective, competing electron transfer to oxygen, which restricts activation to hypoxic tissues. For a given series of compounds, i.e. nitroarenes, quinones, *N*-oxides, etc., there will be an optimum balance (shown in Figure 7) between activation and oxygen tensions that confer protection of oxic tissues. Further, where drug activation involves leaving group elimination – either to activate the drug or to release the ‘effector’ – the rate of elimination must be balanced to radical reactivity towards oxygen, and reactivity/diffusion of the putative cytotoxin within or between cells [111,120,139].

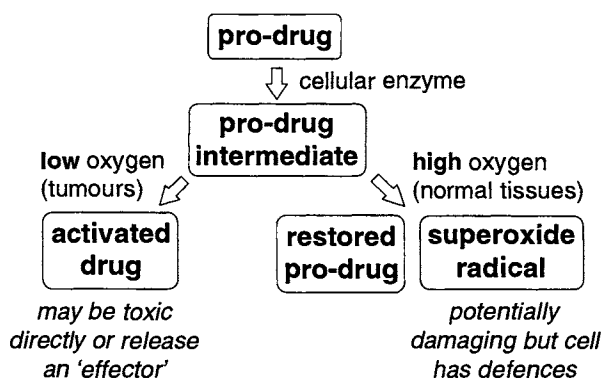


Figure 7. Basis for selectivity of action towards hypoxic cells of bioreductively-activated drugs which involve oxygen-reactive intermediates.

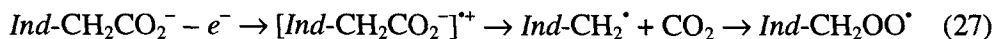
## 6 DRUGS ACTIVATED BY OXIDATIVE REACTIONS

### 6.1 Introduction

There has been much less work directed to exploiting endogenous or targeted oxidative reactivity in tumours, compared to work on bioreductive drugs. Glucose oxidase or hypoxanthine/xanthine oxidase has been explored as sources of hydrogen peroxide or superoxide radicals [154,155], and the effects on tumour growth of ischaemia/reperfusion (which leads to a superoxide ‘burst’) has been studied [156,157].

As discussed above, there is some evidence for enhanced peroxidase activity in one tumour model [70]. Reports of radical fragmentation of indole-3-acetic acid (Figure 1, 17) following peroxidase-catalysed oxidation [72] prompted the

present author and his colleagues to explore a route to 'oxidation therapy' based on equation (27) as a source of peroxy radicals, where *Ind*- = indol-3-yl [73]:



It was expected that peroxy radical generation in cells (or extracellularly, at the interface with the cytoplasmic membrane) might stimulate lipid peroxidation and so be damaging. In the event, biological effects were observed, but lipid peroxidation seems not to be the most important.

## 6.2 Biological effects of oxidation of indole-3-acetic acid derivatives

Indole-3-acetic and derivatives with e.g. methyl or methoxy substituents (to vary the ease of oxidation) were oxidized by horseradish peroxidase in the presence of mammalian cells [73]. Substantial cell kill was observed, but treatment with either drug or enzyme alone was ineffective; however, similar cytotoxic effects were observed even if the indole was oxidized without cells present and the oxidation products then added to cells. This ruled out peroxy radicals themselves as the challenging species (the original hypothesis), even though lipid peroxidation and protection by antioxidants (ascorbate,  $\alpha$ -tocopherol) was observed in liposome models [23,158,159]. Further biological studies have been summarized [160].

## 6.3 Pulse radiolysis studies of indolyl radicals

Several groups have contributed to our understanding of the chemistry of indolyl radicals using radiolysis methods [20]. The rate-limiting step in the formation of peroxy radicals in equation (27) is the activation by peroxidase; rates of reaction of horseradish peroxidase Compound I with substituted indole-3-acetic acids were correlated with reduction potentials of the indolyl radicals measured by pulse radiolysis. The rate constants increased by three orders of magnitude for a change (decrease) in reduction potential of only  $\sim 0.05$  V [161]. The data were interpreted in terms of the Marcus equation [162]. The radical fragmentation (decarboxylation) was shown to have a pH-dependence consistent with elimination only occurring from the radical-cation, and deprotonation of the radical-cation was characterized by a  $pK_a$  with substituent shifts predictable from Hammett substituent parameters.

Correlation of the chemical properties of the indolyl radicals from derivatives of indole-3-acetic acid failed to demonstrate clear structure/activity relationships for the peroxidase-catalysed cytotoxicity [159], and further work is required [160].

#### 6.4 Strategy to exploit peroxidase-catalysed cytotoxicity

Redox properties are central to this potential application in cancer therapy since the plant peroxidase used in the models is a rather 'stronger' oxidant than endogenous peroxidases. One strategy being pursued is to 'target' the activating enzyme to the tumour using antibody conjugation, which can also be used to activate the nitroarene 'mustards' illustrated above [163,164].

### 7 CONCLUSIONS

Drugs activated by redox processes are of interest in cancer therapy not only because of activity shown by lead compounds, but also because they offer opportunities for rational drug design. High throughput screening and combinatorial chemistry have limited value in this area. Many drugs of this type are activated via free-radical intermediates, and the redox properties required for drug activation are easily matched by radiation-chemically produced radicals. It is a routine matter to produce selected radicals in a microsecond or so and monitor their reactivities; the quantitative basis for radical production by radiation is also very valuable.

Space limitations mean that this article can present only an incomplete picture of the contributions of radiation chemistry in anti-cancer drug research. Nevertheless, it is hoped that both introductory discussion and specific examples will serve to illustrate the potential that radiation chemistry has in this area.

### ACKNOWLEDGEMENTS

This work is supported by the Cancer Research Campaign and the Gray Laboratory Cancer Research Trust.

### REFERENCES

1. P. Wardman, Some applications of radiation chemistry to biochemistry and radiobiology, in *Radiation Chemistry. Principles and Applications*, Farhataziz and M.A.J. Rodgers (eds.), VCH Publishers, Deerfield Beach, 1987, p. 565.
2. J. Doroshov and P. Hochstein, Redox cycling and the mechanism of action of antibiotics in neoplastic diseases, in *Pathology of Oxygen*, A.P. Autor (ed.), Academic Press, New York, 1982, p. 245.
3. P. Kovacic, J.R. Ames, P. Lumme, H. Elo, O. Cox, H. Jackson, L.A. Rivera, L. Ramirez and M.D. Ryan, Charge transfer-oxy radical mechanism for anti-cancer agents, *Anti-Cancer Drug Des.*, 1 (1986) 197.



4. P. Kovacic, W.J. Popp, J.R. Ames and M.D. Ryan, Anti-cancer action of metal complexes: electron transfer and oxidative stress? *Anti-Cancer Drug Des.*, 3 (1988) 205.
5. D. Ross, Mechanistic toxicology: a radical perspective, *J. Pharmac. Pharmacol.*, 41 (1989) 505.
6. R.P. Mason, Free radical metabolites of toxic chemicals and drugs as sources of oxidative stress, in *Biological Consequences of Oxidative Stress. Implications for Cardiovascular Disease and Carcinogenesis*, L. Spatz and A.D. Bloom (eds.), Oxford University Press, New York, 1992, p. 23.
7. J. Butler and B.M. Hoey, Redox cycling drugs and DNA damage, in *DNA and Free Radicals*, B. Halliwell and O.I. Aruoma (eds.), Ellis Horwood, Chichester, 1993, p. 243.
8. J. Butler, Redox cycling antitumor drugs, in *DNA and Free Radicals: Techniques, Mechanisms & Applications*, O.I. Aruoma and B. Halliwell (eds.), OICA International, Saint Lucia, 1998, p. 131.
9. G.E. Adams, Redox, radiation, and reductive bioactivation, *Radiat. Res.*, 132 (1992) 129.
10. G.E. Adams, A. Breccia, E.M. Fielden and P. Wardman (eds.), *Selective Activation of Drugs by Redox Processes*, Plenum Press, New York, 1990.
11. P. Wardman, Reduction potentials of one-electron couples involving free radicals in aqueous solution, *J. Phys. Chem. Ref. Data*, 18 (1989) 1637.
12. D.M. Stanbury, Reduction potentials involving inorganic free radicals in aqueous solution, *Adv. Inorg. Chem.*, 33 (1989) 69.
13. S. Steenken, Electron transfer equilibria involving radicals and radical ions in aqueous solutions, in *Landolt-Börnstein. Zahlenwerte und Funktionen aus Naturwissenschaften und Technik. Neue Serie. Kinetische Konstanten von Radikalreaktionen in Flüssigkeiten. Protonen- und Elektronenaustauschreaktionen. Biradikale*, H. Fischer (ed.), Vol. 13e, Springer-Verlag, Berlin, 1985, p. 147.
14. W.M. Clark, *Oxidation-reduction Potentials of Organic Systems*, Williams and Wilkins, Baltimore (1960).
15. K.B. Patel and R.L. Willson, Semiquinone free radicals and oxygen. Pulse radiolysis study of one electron transfer equilibria, *J. Chem. Soc., Faraday Trans. 1*, 69 (1973) 814.
16. P. Wardman, Chemistry of nitroarene and aromatic *N*-oxide radicals, in *The Chemistry of N-Centered Radicals*, Z.B. Alfassi (ed.), Wiley, New York, 1998, p. 615.
17. P.M. Wood, The two redox potentials for oxygen reduction to superoxide, *Trends Biochem. Sci.*, 12 (1987) 250.
18. J. Butler, V.J. Spanswick and J. Cummings, The autoxidation of the reduced forms of EO9, *Free Radical Res.*, 25 (1996) 141.
19. K.I. Priyadarsini, M. Tracy and P. Wardman, The one-electron reduction potential of 3-amino-1,2,4-benzotriazine 1,4-dioxide (tirapazamine): a hypoxia-selective bioreductive drug, *Free Radical Res.*, 25 (1996) 393.
20. L.P. Candeias, Indolyl radicals, in *The Chemistry of N-Centered Radicals*, Z. Alfassi (ed.), Wiley, New York, 1998, p. 577.
21. P. Wardman, The reduction potential of benzyl viologen: an important reference compound for oxidant/radical redox couples, *Free Radical Res. Commun.*, 14 (1991) 57.
22. G.R. Buettner, The pecking order of free radicals and antioxidants: lipid peroxidation,  $\alpha$ -tocopherol, and ascorbate, *Arch. Biochem. Biophys.*, 300 (1993) 535.
23. L.P. Candeias, L.K. Folkes and P. Wardman, Enhancement of peroxidase-induced lipid

- peroxidation by indole-3-acetic acid: effect of antioxidants, *Redox Rep.*, 2 (1996) 141.
24. P. Wardman, Pulse radiolysis and drug design, in *Radiation Science – Of Molecules, Mice and Men* (BJR Supplement 24), J. Denekamp and D.G. Hirst (eds.), British Institute of Radiology, London, 1992, p. 6.
  25. P. Wardman, L.P. Candeias, S.A. Everett and M. Tracy, Radiation chemistry applied to drug design, *Int. J. Radiat. Biol.*, 65 (1994) 35.
  26. P. Wardman and A.B. Ross, 'Radiation chemistry' literature compilations: their wider value in free-radical research, *Free Radical Biol. Med.*, 10 (1991) 243.
  27. A.B. Ross, W.G. Mallard, W.P. Helman, G.V. Buxton, R.E. Huie and P. Neta, NDRL-NIST Solution Kinetics Database: Ver. 3, Notre Dame Radiation Laboratory and National Institute of Standards and Technology, Notre Dame, Indiana and Gaithersburg, Maryland (1998).
  28. M. Molls and P. Vaupel (eds.), *Blood Perfusion and Microenvironment of Human Tumors. Implications for Clinical Radiobiology*, Springer, Berlin, 1998.
  29. L.H. Gray, A.D. Conger, M. Ebert, R. Nat, S. Hornsey and O.C.A. Scott, The concentration of oxygen dissolved in tissues at the time of irradiation as a factor in radiotherapy, *Br. J. Radiol.*, 26 (1953) 638.
  30. R.J. Hodgkiss, Use of 2-nitroimidazoles as bioreductive markers for tumour hypoxia, *Anti-Cancer Drug Des.*, 13 (1998) 687.
  31. D.R. Collingridge, W.K. Young, B. Vojnovic, P. Wardman, E.M. Lynch, S.A. Hill and D.J. Chaplin, Measurement of tumour oxygenation: a comparison between polarographic needle electrodes and a time-resolved luminescence-based optical sensor, *Radiat. Res.*, 147 (1997) 329.
  32. E.J. Hall, *Radiobiology for the Radiologist*, 4th ed., Lippincott, Philadelphia (1994).
  33. R.P. Mason and P.D. Josephy, Free radical mechanism of nitroreductase, in *Toxicity of Nitroaromatic Compounds*, D.E. Rickert (ed.), Hemisphere Publishing Corp, Washington, 1984, p. 121.
  34. R.J. Riley and P. Workman, DT-diaphorase and cancer chemotherapy, *Biochem. Pharmacol.*, 43 (1992) 1657.
  35. A.V. Patterson, M.P. Saunders, E.C. Chinje, D.C. Talbot, A.L. Harris and I.J. Stratford, Overexpression of human NADPH: cytochrome c (P450) reductase confers enhanced sensitivity to both tirapazamine (SR 4233) and RSU 1069, *Br. J. Cancer*, 76 (1997) 1338.
  36. A.M. Rauth, Z. Goldberg and V. Misra, DT-Diaphorase: possible roles in cancer chemotherapy and carcinogenesis, *Oncol. Res.*, 9 (1997) 339.
  37. P. Workman, Keynote address: Bioreductive mechanisms, *Int. J. Radiat. Oncol. Biol. Phys.*, 22 (1992) 631.
  38. D. Roos, B.G.J.M. Bolscher and M. de Boer, Generation of reactive oxygen species by phagocytes, in *Mononuclear Phagocytes. Biology of Monocytes and Macrophages*, R. van Furth (ed.), Kluwer Academic Publishers, Dordrecht, 1992, p. 243.
  39. K. Isobe and I. Nakashima, Abundant production of nitric oxide from murine macrophages by direct stimulation of tumor cells, *Biochem. Biophys. Res. Commun.*, 192 (1993) 499.
  40. L.L. Thomsen, F.G. Lawton, R.G. Knowles, J.E. Beesley, V. Riveros-Moreno and S. Moncada, Nitric oxide synthase activity in human gynecological cancer, *Cancer Res.*, 54 (1994) 1352.
  41. L.L. Thomsen, D.W. Miles, L. Happerfield, L.G. Bobrow, R.G. Knowles and S.

- Moncada, Nitric oxide synthase activity in human breast cancer, *Br. J. Cancer*, 72 (1995) 41.
42. G.M. Tozer and S.A. Everett, Nitric oxide in tumour biology and cancer therapy. Part 1: Physiological aspects, *Clin. Oncol.*, 9 (1997) 282.
  43. G.M. Tozer and S.A. Everett, Nitric oxide in tumour biology and cancer therapy. Part 2: Therapeutic implications, *Clin. Oncol.*, 9 (1997) 357.
  44. Y. Xia and J.L. Zweier, Superoxide and peroxynitrite generation from inducible nitric oxide synthase in macrophages, *Proc. Natl. Acad. Sci. USA*, 94 (1997) 6954.
  45. A.J. Jesaitis and E.A. Dratz (eds.), *The Molecular Basis of Oxidative Damage by Leukocytes*, CRC Press, Boca Raton, 1992.
  46. L.K. Folkes, L.P. Candeias and P. Wardman, Kinetics and mechanisms of hypochlorous acid reactions, *Arch. Biochem. Biophys.*, 323 (1995) 120.
  47. L.P. Candeias, K.B. Patel, M.R.L. Stratford and P. Wardman, Free hydroxyl radicals are formed on reaction between the neutrophil-derived species superoxide anion and hypochlorous acid, *FEBS Lett.*, 333 (1993) 151.
  48. P. Wardman and L.P. Candeias, Fenton chemistry: an introduction, *Radiat. Res.*, 145 (1996) 523.
  49. R.E. Huie and S. Padmaja, The reaction of NO with superoxide, *Free Radical Res. Commun.*, 18 (1993) 195.
  50. J.S. Beckman, T.W. Beckman, J. Chen, P.A. Marshall and B.A. Freeman, Apparent hydroxyl radical production by peroxynitrite: implications for endothelial injury from nitric oxide and superoxide, *Proc. Natl. Acad. Sci. USA*, 87 (1990) 1620.
  51. R. Radi, J.S. Beckman, K.M. Bush and B.A. Freeman, Peroxynitrite-induced membrane lipid peroxidation: the cytotoxic potential of superoxide and nitric oxide, *Arch. Biochem. Biophys.*, 288 (1991) 481.
  52. S. Goldstein and G. Czapski, Direct and indirect oxidations by peroxynitrite, *Inorg. Chem.*, 34 (1995) 4041.
  53. W.A. Pryor and G.L. Squadrito, The chemistry of peroxynitrite: a product from the reaction of nitric oxide with superoxide, *Am. J. Physiol.*, 268 (1995) L699.
  54. S.V. Lymar and J.K. Hurst, Rapid reaction between peroxynitrite ion and carbon dioxide: implications for biological activity, *J. Am. Chem. Soc.*, 117 (1995) 8867.
  55. J.S. Beckman and W.H. Koppenol, Nitric oxide, superoxide, and peroxynitrite: the good, the bad, and the ugly, *Am. J. Physiol.*, 271 (1996) C1424.
  56. A. Denicola, B.A. Freeman, M. Trujillo and R. Radi, Peroxynitrite reaction with carbon dioxide/bicarbonate: kinetics and influence on peroxynitrite-mediated oxidations, *Arch. Biochem. Biophys.*, 333 (1996) 49.
  57. S.V. Lymar and J.K. Hurst, Carbon dioxide: physiological catalyst for peroxynitrite-mediated cellular damage or cellular protectant?, *Chem. Res. Toxicol.*, 9 (1996) 845.
  58. S. Goldstein and G. Czapski, Formation of peroxynitrate from the reaction of peroxynitrite with CO<sub>2</sub>: evidence for carbonate radical production, *J. Am. Chem. Soc.*, 120 (1998) 3458.
  59. W.H. Koppenol, The basic chemistry of nitrogen monoxide and peroxynitrite, *Free Radical Biol. Med.*, 25 (1998) 385.
  60. L.J. Marnett, Forum: reactive species of peroxynitrite, *Chem. Res. Toxicol.*, 11 (1998) 709.
  61. R. Radi, Peroxynitrite reactions and diffusion in biology, *Chem. Res. Toxicol.*, 11 (1998) 720.

62. M.G. Bonini, R. Radi, G. Ferrer-Sueta, A.M. Da C Ferreira and O. Augusto, Direct EPR detection of the carbonate radical anion produced from peroxyxynitrite and carbon dioxide, *J. Biol. Chem.*, 274 (1999) 10802.
63. W.A. Seddon and H.C. Sutton, Radiation chemistry of nitric oxide solutions, *Trans. Faraday Soc.*, 59 (1963) 2323.
64. R.J. Knight and H.C. Sutton, Radiolysis of aqueous solutions of nitric oxide, *Trans. Faraday Soc.*, 63 (1967) 2628.
65. M. Grätzel, A. Henglein, J. Lilie and G. Beck, Pulsradiolytische Untersuchung einiger Elementarprozesse der Oxydation und Reduktion des Nitritions, *Ber. Bunsenges. Phys. Chem.*, 73 (1969) 646.
66. W.A. Seddon and M.J. Young, Pulse radiolysis of nitric oxide in aqueous solution, *Can. J. Chem.*, 48 (1970) 393.
67. M. Grätzel, S. Taniguchi and A. Henglein, Pulsradiolytische Untersuchung kurzlebiger Zwischenprodukte der NO-Reduktion in wäßriger Lösung, *Ber. Bunsenges. Phys. Chem.*, 74 (1970) 1003.
68. M. Grätzel, S. Taniguchi and A. Henglein, Pulsradiolytische Untersuchung der NO-Oxydation und des Gleichgewichts  $\text{N}_2\text{O}_3 = \text{NO} + \text{NO}_2$  in wässriger Lösung, *Ber. Bunsenges. Phys. Chem.*, 74 (1970) 488.
69. W.A. Seddon, J.W. Fletcher and F.C. Sopchyshyn, Pulse radiolysis of nitric oxide in aqueous solution, *Can. J. Chem.*, 51 (1973) 1123.
70. J. Brightwell and M.T. Tseng, Peroxidase content in cell subpopulations of 7,12-dimethylbenz(a)anthracene-induced mammary tumors in rats, *Cancer Res.*, 42 (1982) 4562.
71. T.P. Szatrowski and C.F. Nathan, Production of large amounts of hydrogen peroxide by human tumour cells, *Cancer Res.*, 51 (1991) 794.
72. H.B. Dunford, *Heme Peroxidases*, Wiley-VCH, New York (1999).
73. L.K. Folkes, L.P. Candeias and P. Wardman, Toward targeted 'oxidation therapy' of cancer: peroxidase-catalysed cytotoxicity of indole-3-acetic acids, *Int. J. Radiat. Oncol. Biol. Phys.*, 42 (1998) 917.
74. G.E. Adams, B.D. Michael, J.C. Asquith, M.A. Shenoy, M.E. Watts and D.W. Williams, Rapid-mixing studies on the time-scale of radiation damage in cells, *Radiat. Res.*, (1975) 478.
75. B.D. Michael, M. Folkard and K.M. Prise, Meeting report: microbeam probes of cellular radiation response, 4th L.H. Gray Workshop, 8-10 July 1993, *Int. J. Radiat. Biol.*, 65 (1994)
76. P. Wardman, The use of nitroaromatic compounds as hypoxic cell radiosensitizers, *Curr. Top. Radiat. Res. Q.*, 11 (1977) 347.
77. P. Wardman, Radiation chemistry in the clinic: hypoxic cell radiosensitizers for radiotherapy, *Radiat. Phys. Chem.*, 24 (1984) 293.
78. P. Wardman, The mechanism of radiosensitization by electron-affinic compounds, *Radiat. Phys. Chem.*, 30 (1987) 423.
79. P. Wardman, Sensitization and protection of oxidative damage caused by high energy radiation, in *Atmospheric Oxidation and Antioxidants*, G. Scott (ed.), Vol. III, Elsevier, Amsterdam, 1993, p. 101.
80. D. Meisel and P. Neta, One-electron redox potentials of nitro compounds and radiosensitizers. Correlation with spin densities of their radical anions, *J. Am. Chem. Soc.*, 97 (1975) 5198.

81. D. Meisel and G. Czapski, One-electron transfer equilibria and redox potentials of radicals studies by pulse radiolysis, *J. Phys. Chem.*, 79 (1975) 1503.
82. P.M. Wood, The redox potential of the system oxygen-superoxide, *FEBS Lett.*, 44 (1974) 21.
83. P. Wardman and E.D. Clarke, One-electron reduction potentials of substituted nitroimidazoles measured by pulse radiolysis, *J. Chem. Soc., Faraday Trans. 1*, 72 (1976) 1377.
84. S.G. Mayhew and F. Muller, Dimerization of the radical cation of benzyl viologen in aqueous solution, *Biochem. Soc. Trans.*, (1982) 176.
85. C.L. Bird and A.T. Kuhn, The electrochemistry of the viologens, *Chem. Soc. Rev.*, 10 (1981) 49.
86. R.F. Anderson and K.B. Patel, Radical cations of some low-potential viologen compounds, *J. Chem. Soc., Faraday Trans. 1*, 80 (1984) 2693.
87. P.M.S. Monk, *The Viologens. Physicochemical Properties, Synthesis and Applications of the Salts of 4,4'-Bipyridine*, John Wiley & Sons, Chichester (1998).
88. G.E. Adams, E.D. Clarke, I.R. Flockhart, R.S. Jacobs, D.S. Sehmi, I.J. Stratford, P. Wardman, M.E. Watts, J. Parrick, R.G. Wallace and C.E. Smithen, Structure-activity relationships in the development of hypoxic cell radiosensitizers: I. Sensitization efficiency, *Int. J. Radiat. Biol.*, 35 (1979) 133.
89. M.F. Dennis, M.R.L. Stratford, P. Wardman and M.E. Watts, Cellular uptake of misonidazole and analogues with acidic or basic functions, *Int. J. Radiat. Biol.*, 47 (1985) 629.
90. M.E. Watts, M.F. Dennis and I.J. Roberts, Radiosensitization by misonidazole, pimonidazole and azomycin and intracellular uptake in human tumour cell lines, *Int. J. Radiat. Biol.*, 57 (1990) 361.
91. G.E. Adams, I. Ahmed, E.D. Clarke, P. O'Neill, J. Parrick, I.J. Stratford, R.G. Wallace, P. Wardman and M.E. Watts, Structure-activity relationships in the development of hypoxic cell radiosensitizers. III. Effects of basic substituents in nitroimidazole side-chains, *Int. J. Radiat. Biol.*, 38 (1980) 613.
92. P. Wardman, M.F. Dennis and J. White, A probe for intracellular concentrations of drugs: delayed fluorescence from acridine orange, *Int. J. Radiat. Oncol. Biol. Phys.*, 16 (1989) 935.
93. P. Wardman, Chemical properties of 'radiation modifiers' of DNA damage and their radiobiological effects, in *Early Effects of Radiation on DNA*, E.M. Fielden and P. O'Neill (eds.), Springer-Verlag, Berlin, 1991, p. 249.
94. M.E. Watts, M.F. Dennis and M. Woodcock, Uptake and additivity of the radiosensitizing effects of Ro 03-8799 and SR-2508 in mammalian cells in vitro, *Br. J. Radiol.*, 60 (1987) 1233.
95. J.M. Brown and P. Workman, Partition coefficient as a guide to the development of radiosensitizers which are less toxic than misonidazole, *Radiat. Res.*, 82 (1980) 171.
96. G.E. Adams, E.D. Clarke, P. Gray, R.S. Jacobs, I.J. Stratford, P. Wardman, M.E. Watts, J. Parrick, R.G. Wallace and C.E. Smithen, Structure-activity relationships in the development of hypoxic cell radiosensitizers: II. Cytotoxicity and therapeutic ratio, *Int. J. Radiat. Biol.*, 35 (1979) 151.
97. G.E. Adams, I.J. Stratford, R.G. Wallace, P. Wardman and M.E. Watts, The toxicity of nitro compounds towards hypoxic mammalian cells in vitro: dependence upon reduction potential, *J. Natl. Cancer Inst.*, 64 (1980) 555.

98. S. Steenken, Addition-elimination paths in electron-transfer reactions between radicals and molecules, *J. Chem. Soc., Faraday Trans. 1*, 83 (1987) 113.
99. W.E. Griffiths, G.F. Longster, J. Myatt and P.F. Todd, Electron spin resonance studies of electron-transfer reactions with aromatic nitro-compounds in aqueous media, *J. Chem. Soc. (B)*, (1966) 1130.
100. P. Wardman and E.D. Clarke, Electron transfer and radical-addition in the radiosensitization and chemotherapy of hypoxic cells, in *New Chemo and Radiosensitizing Drugs*, A. Breccia and J.F. Fowler (eds.), lo Scarabeo, Bologna, 1985, p. 21.
101. V. Jagannadham and S. Steenken, Reactivity of  $\alpha$ -heteroatom-substituted alkyl radicals with nitrobenzenes in aqueous solution: an entropy-controlled electron-transfer/addition mechanism, *J. Am. Chem. Soc.*, 110 (1988) 2188.
102. V. Jagannadham and S. Steenken, One-electron reduction of nitrobenzenes by  $\alpha$ -hydroxyalkyl radicals via addition/elimination. An example of an organic inner-sphere electron-transfer reaction, *J. Am. Chem. Soc.*, 106 (1984) 6542.
103. C. Nese, M.N. Schuchmann, S. Steenken and C. von Sonntag, Oxidation vs. fragmentation in radiosensitization. Reactions of  $\alpha$ -alkoxyalkyl radicals with 4-nitrobenzotrile and oxygen. A pulse radiolysis and product analysis study, *J. Chem. Soc., Perkin Trans. 2*, (1995) 1037.
104. R.J. Hodgkiss and M.R.L. Stratford, Competitive dose-modification between ascorbate and misonidazole in human and hamster cells: effects of glutathione depletion, *Int. J. Radiat. Biol.*, 54 (1988) 601.
105. R.J. Hodgkiss, M.R.L. Stratford and R.R. Watfa, The effect of  $\alpha$ -tocopherol and  $\alpha$ -tocopheroyl quinone on the radiosensitivity of thiol-depleted mammalian cells, *Int. J. Radiat. Oncol. Biol. Phys.*, 16 (1989) 1297.
106. E. Bothe, G. Behrens, E. Böhme, B. Sethuram and D. Schulte-Frohlinde, Hydroxyl radical-induced strand break formation of poly(U) in the presence of oxygen: comparison of the rates as determined by conductivity, e.s.r. and rapid-mix experiments with a thiol, *Int. J. Radiat. Biol.*, 49 (1986) 57.
107. M.M.M. Bamatraf, P. O'Neill and B.S.M. Rao, Redox dependence of the rate of interaction of hydroxyl radical adducts of DNA nucleobases with oxidants: consequences for DNA strand breakage, *J. Am. Chem. Soc.*, 120 (1998) 11852.
108. P. Wardman, L.P. Candeias, L.K. Folkes and K.B. Patel, Oxidative damage: oxidation by radiation and by chemically-generated free radicals, in *Radiation Research 1985-1995. Congress Proceedings. Vol. 2: Congress Lectures*, U. Hagen, D. Harder, H. Jung and C. Streffer (eds.), 10th ICRR Society, Würzburg, 1996, p. 187.
109. H.W. Moore, Bioactivation as a model for drug design bioreductive alkylation, *Science*, 197 (1977) 527.
110. I.J. Stratford and P. Workman, Bioreductive drugs into the next millenium, *Anti-Cancer Drug Des.*, 13 (1998) 519.
111. P. Wardman, M.F. Dennis, S.A. Everett, K.B. Patel, M.R.L. Stratford and M. Tracy, Radicals from one-electron reduction of nitro compounds, aromatic *N*-oxides, and quinones: the kinetic basis for hypoxia-selective, bioreductive drugs, in *Free Radicals and Oxidative Stress: Environment, Drugs and Food Additives (Biochemical Society Symposium No. 61)*, C. Rice-Evans, B. Halliwell and G.G. Lunt (eds.), Portland Press, London, 1995, p. 171.

112. W.A. Denny, W.R. Wilson and M.P. Hay, Recent developments in the design of bioreductive drugs, *Br. J. Cancer*, 74 (Suppl. XXVII) (1996) S32.
113. W.C.J. Ross, *Biological Alkylating Agents. Fundamental Chemistry and the Design of Compounds for Selective Toxicity*, Butterworths, London (1962).
114. D.E.V. Wilman and T.A. Connors, Molecular structure and antitumour activity of alkylating agents, in *Molecular Aspects of Anti-Cancer Drug Action*, S. Neidle and M.J. Waring (eds.), MacMillan Press, London, 1983, p. 233.
115. C.J. Moody and E. Swann, Novel bioreductive anticancer agents based on indolequinones, *Il Farmaco*, 82 (1997) 271.
116. C.J. Moody, C.L. Norton, A.M.Z. Slawin and S. Taylor, Cyclopropyl indolequinones: mechanistic probes for bioreductive anticancer drug action, *Anti-Cancer Drug Des.*, 13 (1998) 611.
117. M. Jaffar, M.A. Naylor, N. Robertson, S.D. Lockyer, R.M. Phillips, S.A. Everett, G.E. Adams and I.J. Stratford, 5-Substituted analogues of 3-hydroxymethyl-5-aziridinyl-1-methyl-2[1*H*-indole-4,7-dione]prop-2-en-ol (EO9, NSC382459) and their regioisomers as hypoxia-selective agents: structure-cytotoxicity *in vitro*, *Anti-Cancer Drug Des.*, 13 (1998) 105.
118. M. Jaffar, M.A. Naylor, N. Robertson and I.J. Stratford, Targeting hypoxia with a new generation of indolequinones, *Anti-Cancer Drug Des.*, 13 (1998) 593.
119. M.A. Naylor, E. Swann, S.A. Everett, M. Jaffar, J. Nolan, N. Robertson, S.D. Lockyer, K.B. Patel, M.F. Dennis, M.R.L. Stratford, P. Wardman, G.E. Adams, C.J. Moody and I.J. Stratford, Indolequinone anti-tumor agents: reductive activation and elimination from (5-methoxy-1-methyl-4,7-dioxoindol-3-yl)methyl derivatives and hypoxia-selective cytotoxicity *in vitro*, *J. Med. Chem.*, 41 (1998) 2720.
120. S.A. Everett, M.A. Naylor, J. Nolan, K.B. Patel and P. Wardman, Indolequinone bioreductive drugs: kinetic factors which influence selectivity for hypoxia, *Anti-Cancer Drug Des.*, 13 (1998) 635.
121. C.J. Moody, N. O'Sullivan, I.J. Stratford, M.A. Stephens, P. Workman, S.M. Bailey and A. Lewis, Cyclopropamitosenes: novel bioreductive anticancer agents – mechanism of action and enzymic reduction, *Anti-Cancer Drugs*, 5 (1994) 367.
122. S.K. Carter, S.T. Crooke and N.A. Alder (eds.), *Mitomycin C: Current Status and New Developments*, Academic Press, New York, 1979.
123. P.A. Andrews, S.-S. Pan and N.P. Bachur, Electrochemical reductive activation of Mitomycin C, *J. Am. Chem. Soc.*, 108 (1986) 4158.
124. S. Rockwell, A.C. Sartorelli, M. Tomasz and K.A. Kennedy, Cellular pharmacology of quinone bioreductive alkylating agents, *Cancer Metastasis Revs.*, 12 (1993) 165.
125. J. Cummings, V.J. Spanswick, M. Tomasz and J.F. Smyth, Enzymology of mitomycin C metabolic activation in tumour tissue, *Biochem. Pharmacol.*, 56 (1998) 405.
126. B.M. Hoey, J. Butler and A.J. Swallow, Reductive activation of mitomycin C, *Biochemistry*, 27 (1988) 2608.
127. M.A. Naylor, M. Jaffar, J. Nolan, M.A. Stevens, S. Butler, K.B. Patel, S.A. Everett, G.E. Adams and I.J. Stratford, 2-Cyclopropylindolequinones and their analogues as bioreductively activated antitumor agents: structure-activity *in vitro* and efficacy *in vivo*, *J. Med. Chem.*, 40 (1997) 2335.
128. L.Y. Dirix, F. Tonnesen, J. Cassidy, R. Epelbaum, W.W. ten Bokkel Huinink, N. Pavlidis, R. Sorio, T. Gamucci, I. Wolff, A. Te Velde, J. Lan and J. Verweij, EO9 Phase II study in advanced breast, gastric, pancreatic and colorectal carcinoma by the EORTC

- early clinical studies group, *Eur. J. Cancer*, 32A (1996) 2019.
129. T.A. Connors, Bioreductive agents, hypoxic cells and therapy, *Eur. J. Cancer*, 32A (1996) 1833.
  130. P. Eyer and D. Galleman, Reactions of nitrosoarenes with SH groups, in Supplement F2: The Chemistry of Amino, Nitroso, Nitro and Related Groups, S. Patai (ed.), John Wiley & Sons Ltd, Chichester, 1996, p. 999.
  131. D. Herreno-Saenz, F.E. Evans, F.A. Beland and P.P. Fu, Identification of two *N*<sup>2</sup>-deoxyguanosinyl DNA adducts upon nitroreduction of the environmental mutagen 1-nitropyrene, *Chem. Res. Toxicol.*, 8 (1995) 269.
  132. A.B. Kelson, J.P. McNamara, A. Pandey, K.J. Ryan, M.J. Dorie, P.A. McAfee, D.R. Menke, J.M. Brown and M. Tracy, 1,2,4-Benzotriazine 1,4-dioxides. An important class of hypoxic cytotoxins with antitumor activity, *Anti-Cancer Drug Des.*, 13 (1998) 575.
  133. R.V. Lloyd, D.R. Duling, G.V. Rummyantseva, R.P. Mason and P.K. Bridson, Microsomal reduction of 3-amino-1,2,4-benzotriazine 1,4-dioxide to a free radical, *Mol. Pharmacol.*, 40 (1991) 440.
  134. K. Laderoute, P. Wardman and A.M. Rauth, Molecular mechanisms for the hypoxia-dependent activation of 3-amino-1,2,4-benzo-triazine-1,4-dioxide (SR 4233), *Biochem. Pharmacol.*, 37 (1988) 1487.
  135. J.S. Daniels and K.S. Gates, DNA cleavage by the antitumor agent 3-amino-1,2,4-benzotriazine 1,4-dioxide (SR4233): Evidence for involvement of hydroxyl radical, *J. Am. Chem. Soc.*, 118 (1996) 3380.
  136. G.D.D. Jones and M. Weinfeld, Dual action of tirapazamine in the induction of DNA strand breaks, *Cancer Res.*, 56 (1996) 1584.
  137. J.S. Daniels, K.S. Gates, C. Tronche and M.M. Greenberg, Direct evidence for bimodal DNA damage induced by tirapazamine, *Chem. Res. Toxicol.*, 11 (1998) 1254.
  138. J.S. Daniels, T. Chatterji, L.R. MacGillivray and K.S. Gates, Photochemical DNA cleavage by the antitumor agent 3-amino-1,2,4-benzotriazine 1,4-dioxide (tirapazamine, WIN 59075, SR-4233), *J. Org. Chem.*, 63 (1998) 10027.
  139. P. Wardman, K.I. Priyadarsini, M.F. Dennis, S.A. Everett, M.A. Naylor, K.B. Patel, M.R.L. Stratford and M. Tracy, Chemical properties which control selectivity and efficacy of aromatic *N*-oxide bioreductive drugs, *Br. J. Cancer*, 74 (Suppl XXVII) (1996) S70.
  140. A. Firestone, R.T. Mulcahy and R.F. Borch, Nitroheterocyclic reduction as a paradigm for intramolecular catalysis of drug delivery to hypoxic cells, *J. Med. Chem.*, 34 (1991) 2933.
  141. M. Tercel, W.R. Wilson and W.A. Denny, Nitrobenzyl mustard quaternary salts: a new class of hypoxia-selective cytotoxins showing very high in vitro selectivity, *J. Med. Chem.*, 36 (1993) 2578.
  142. N. Kornblum, R.E. Michel and R.C. Kerber, Chain reactions in substitution processes which proceed via radical-anion intermediates, *J. Am. Chem. Soc.*, 88 (1966) 5662.
  143. P. Neta and D. Behar, Intramolecular electron transfer in the anion radicals of nitrobenzyl halides, *J. Am. Chem. Soc.*, 102 (1980) 4798.
  144. R.F. Anderson, W.A. Denny, W. Li, J.E. Packer, M. Tercel and W.R. Wilson, Pulse radiolysis studies on the fragmentation of arylmethyl quaternary nitrogen mustards by one-electron reduction in aqueous solution, *J. Phys. Chem. A*, 101 (1997) 9704.
  145. S.A. Everett, M.A. Naylor, K.B. Patel, M.R.L. Stratford and P. Wardman, Bioreductively-activated prodrugs for targeting hypoxic tissues: elimination of aspirin



- from 2-nitroimidazole derivatives, *Bioorg. Med. Chem. Lett.*, 9 (1999) 1267.
146. W.R. Wilson, M. Tercel, R.F. Anderson and W.A. Denny, Radiation-activated prodrugs as hypoxia-selective cytotoxins: model studies with nitroarylmethyl quaternary salts, *Anti-Cancer Drug Des.*, 13 (1998) 663.
  147. M.V. Orna and R.P. Mason, Correlation of kinetic parameters of nitroreductase enzymes with redox properties of nitroaromatic compounds, *J. Biol. Chem.*, 264 (1989) 12379.
  148. E.D. Clarke, P. Wardman and K.H. Goulding, Anaerobic reduction of nitroimidazoles by reduced flavin mononucleotide and by xanthine oxidase, *Biochem. Pharmacol.*, 29 (1980) 2684.
  149. E.D. Clarke, K.H. Goulding and P. Wardman, Nitroimidazoles as anaerobic electron-acceptors for xanthine oxidase, *Biochem. Pharmacol.*, 31 (1982) 3237.
  150. C.J. O'Connor, D.J. McLennan, B.M. Sutton, W.A. Denny and W.R. Wilson, Effect of reduction potential on the rate of nitroreduction of nitroacridines by xanthine oxidase and by dihydro-flavin mononucleotide, *J. Chem. Soc., Perkin Trans. 2*, (1991) 951.
  151. R.P. Mason, Physical chemical determinants of xenobiotic free radical generation – the Marcus theory of electron transfer, in *Free Radical Toxicology*, K.B. Wallace (ed.), Taylor & Francis, 1997, p. 15.
  152. P. Wardman, Bioreductive activation of quinones: redox properties and thiol reactivity, *Free Radical Res. Commun.*, 8 (1990) 219.
  153. P. Wardman and E.D. Clarke, Oxygen inhibition of nitroreductase: electron transfer from nitro radical-anions to oxygen, *Biochem. Biophys. Res. Commun.*, 69 (1976) 942.
  154. O. Ben-Yoseph and B.D. Ross, Oxidation therapy: the use of a reactive oxygen species-generating enzyme system for tumour treatment, *Br. J. Cancer*, 70 (1994) 1131.
  155. T. Yoshikawa, S. Kokura, K. Tainaka, Y. Naito and M. Kondo, A novel cancer therapy based on oxygen radicals, *Cancer Res.*, 55 (1995) 1617.
  156. T. Yoshikawa, S. Kokura, H. Oyamada, S. Inuma, S. Nishimura, T. Kaneko, Y. Naito and M. Kondo, Antitumor effect of ischemia-reperfusion injury induced by transient embolization, *Cancer Res.*, 54 (1994) 5033.
  157. C.S. Parkins, S.A. Hill, M.R.L. Stratford, M.F. Dennis and D. Chaplin, Metabolic and clonogenic consequences of ischaemia-reperfusion insult in solid tumours, *Exp. Physiol.*, 82 (1997) 361.
  158. L.P. Candeias, L.K. Folkes, M. Porssa, J. Parrick and P. Wardman, Enhancement of lipid peroxidation by indole-3-acetic acid and derivatives: substituent effects, *Free Radical Res.*, 23 (1995) 403.
  159. L.K. Folkes, M.F. Dennis, M.R.L. Stratford, L.P. Candeias and P. Wardman, Peroxidase-catalyzed effects of indole-3-acetic acid and analogues on lipid membranes, DNA and mammalian cells *in vitro*, *Biochem. Pharmacol.*, 57 (1999) 375.
  160. L.K. Folkes and P. Wardman, Oxidative activation of indole-3-acetic acids to cytotoxic species – a potential new role for plant auxins in cancer therapy, *Biochem. Pharmacol.*, 61 (2001) 129.
  161. L.P. Candeias, L.K. Folkes, M. Porssa, J. Parrick and P. Wardman, Rates of reaction of indoleacetic acids with horseradish peroxidase compound I and their dependence on the redox potentials, *Biochemistry*, 35 (1996) 102.
  162. L.K. Folkes and L.P. Candeias, Interpretation of the reactivity of peroxidase compounds I and II with phenols by the Marcus equation, *FEBS Lett.*, 412 (1997) 305.
  163. K.D. Bagshawe, Antibody-directed enzyme/prodrug therapy (ADEPT), *Biochem. Soc.*

Trans., 18 (1990) 750.

164. R.J. Knox, F. Friedlos, M. Jarman, L.C. Davies, P. Goddard, G.M. Anlezark, R.G. Melton and R.F. Sherwood, Virtual cofactors for an *Escherichia coli* nitroreductase enzyme: relevance to reductively activated prodrugs in antibody directed enzyme prodrug therapy (ADEPT), *Biochem. Pharmacol.*, 49 (1995) 1641.

# The Chemistry Behind the Application of Ionizing Radiation in Water-Pollution Abatement

C. von Sonntag and H.-P. Schuchmann

Max-Planck-Institut für Strahlenchemie  
P.O. Box 101365, Stiftstrasse 34-36, D-45470 Mülheim an der Ruhr, Germany

## 1. INTRODUCTION

Ionizing radiation possesses several attractive features as a means to induce the destruction, *i.e.* in the limit, the mineralization, of aqueous organic pollutants. In particular, it operates at ambient temperatures and without the need to introduce further chemical reagents (except perhaps for the replenishment with oxygen, if the effluent is to be oxidatively degraded). Depending on the energy and the physical quality of the radiation, penetration depths can be achieved which are not affected by the concentration of the pollutant and the spectral properties of both the water and the pollutant and thus are usually much larger than those possible with UV radiation. However, consideration of the cost of investment, including shielding, and the cost of the energy required to generate the radiation necessary to eliminate a given concentration of pollutant must nowadays dampen the enthusiasm that may have greeted the prospects of the widespread use of this technology in the early days of the peaceful application of atomic energy when it was hoped that cheap  $\gamma$ -radiation, *e.g.* from spent atomic fuel, could be employed for this purpose. Since then, the appreciation of the dangers of radioactive pollution and of the radiation risk to life has become much keener. While some irradiation facilities employ  $\gamma$ -radiation sources, most large-scale applications of ionizing radiation involve electron-beam generators, the penetration depth of whose radiation is limited to a few centimeters at beam energies of around 10 MeV; larger beam energies are becoming increasingly impracticable as there is energy wastage because of the generation of an increasing proportion of bremsstrahlung [1] which at the same time necessitates increasingly heavy shielding of the irradiation chamber. Waste water has, however, also been irradiated as an aerosol [2]. The goal today usually is the *partial* oxidation of the water contaminants to enhance their

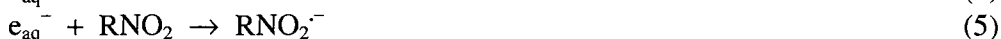
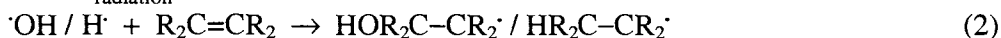
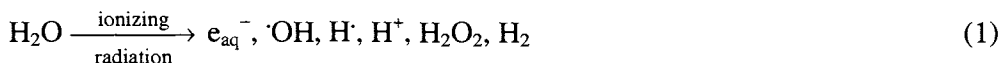
biodegradability, rather than their complete mineralization. Treatment procedures combining irradiation with ozonization [3-5] (e.g., oxidizing conditions beyond air saturation are essential in the radiolytic remediation of drinking-water in order to prevent the reduction of nitrate, a practically omnipresent constituent, by the hydrated electron to the poisonous nitrite), or with the precipitation of radiation-chemically modified contaminants and their separation upon aggregation [2, 6], e.g. by flocculation/filtration, have also been proposed. These latter procedures rest on the fact that oxidative functionalization often enhances the affinity of solutes, especially those of larger molecular size, to adhere to a suitable flocculant. Obviously, flocculation does not destroy the pollutant but is designed to improve its manageability while, however, at the same time adding to its mass. It has been observed that irradiation may lead to the precipitation of petroleum-derived contaminants which may then be filtered off [7]. In the case of municipal effluent, irradiation confers the additional benefit of thorough disinfection at high doses. In all of these cases, the ultimate stage of the treatment undergone by the filtered, irradiated effluent is its biological purification. For recent reviews of the environmental use of ionizing radiation in aqueous systems see [2, 4, 8-12]. See also *Radiation Physics and Chemistry*, Vol. 42 (1993), issue 4-6, section 5 where further examples of the environmental application of ionizing radiation are presented. An extreme situation is encountered in the radiolytic degradation of contaminants in soil which when moist may be considered an aqueous system.  $\gamma$ -Irradiation and electron-beam facilities have been set up on a pilot-plant scale [13, 14] for this purpose.

The present review emphasizes the chemical-mechanistic aspects of the radiolytic decomposition of certain classes of environmentally noxious chemicals in the aquosphere. The treatment of gaseous effluents (flue gases from combustion [15] and incineration [16], strip-gas from water-remediation [17]) will not be dwelt upon. In these processes, radical ions play a considerable role [18], while at the same time (here a *similarity* to aqueous media) the OH radical is a very important agent as well since these gases always contain water vapour. A mixed gas-liquid-phase situation is encountered in the use of the pulsed high-voltage (in the order of  $10^4$  V) corona discharge, a method recently developed to degrade organic pollutants in waste water [19].

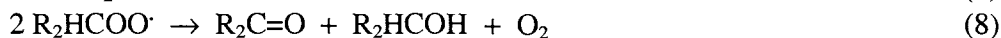
### 1.1. The chemistry of degradation

The chemistry at the basis of the technology consists in the reactions of the free radicals OH, H, and hydrated electron  $e_{aq}^-$ , created [reaction (1)] in the proportion of about 5/1/5 upon the radiolysis of the polluted water, with the pollutant solutes. These will react with a solute in various ways. The OH radical

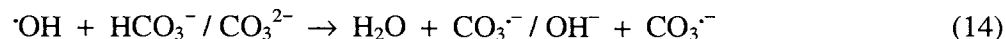
and the H atom undergo fast addition to the C=C double bond, but also abstract carbon-bound hydrogen [reactions (2) and (3)]; for a compilation of rate constants see [20]]. OH is not reactive toward saturated perhalogenated compounds. The hydrated electron may effect dehalogenation and other reduction processes [*cf.* reactions (4) and (5)] (for a compilation of rate constants see [20]); these are inhibited by oxygen where the electron is removed with the formation of superoxide [reaction (6)]; this inhibition is removed when the oxygen has been consumed at higher doses.



In practice, the ionizing radiation is often applied in the continuous presence of air. Thus, the initially formed radicals are largely transformed into peroxy radicals [reaction (7)] whose transformations [reactions (8)–(13)] [21–23] enhance the degradation process.



In the case of relatively small pollutant concentrations, the carbonate content may become a problem since carbonate competes for the OH radical, giving rise to the relatively unreactive [24] carbonate radical [reaction (14)], which inhibits the degradation of the pollutant. In the degradation of chlorinated hydrocarbons it also interferes by scavenging intermediate chlorine atoms which can carry a chain reaction and in this manner facilitate the degradation [25, 26].



The result of such reactions is a succession of products derived from a starting-pollutant molecule and the achievement of partial mineralization accompanied by biodegradability (one suspects that there have been cases where the criteria applied have been less stringent, *i.e.* in the treatment of dye-containing effluents where the removal of the discoloration of the effluent may already have been achieved upon reaching the first or second generation of products). Several examples of potential pollutants will be discussed, emphasizing halo- genated and aromatic solutes to which many of the more widespread and noxious pollutants belong.

## 2. SOME EXAMPLES

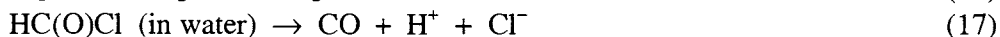
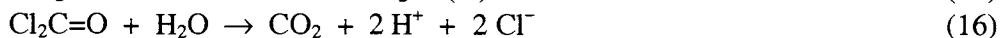
### 2.1. Non-aromatic halogenated compounds

The free-radical chemistry of this class of compound has been the subject of study by radiation chemists (*cf.* [11, 27-29]) ever since it was observed that they are reductively dehalogenated by electron attachment.

Examples where radiolysis has been presented as an industrially feasible means for pollutant removal [5, 30], and where the reaction mechanisms of degradation have recently been studied in great detail are provided for the cases of trichloroethane, trichloroethylene [17], and tetrachloroethylene [17, 25, 28]. The presence of dioxygen is decisive for the efficient degradation of these compounds. Highly-halogenated compounds (not *per*halogenated ones) degrade more easily, with the possibility of a chain process (pronounced in the gas phase but largely suppressed in aqueous solution [17]). Halogen-substituted OH-adduct radicals eliminate HCl (the *gem*-hydrines, reaction (15), a reaction which occurs within a few  $\mu$ s or less [27, 28]) or form peroxy radicals. These as well as the peroxy radicals formed from the *gem*-hydrine-derived radical are transformed into oxyl radicals in bimolecular reactions, which undergo fragmentation (these peroxy radicals are to be distinguished from, *e.g.*, chlorovinylperoxy radicals which require prior *reductive* chloride elimination from the chloroolefinic substrate [31]). Thus in a sequence of hydrolytic, peroxy-radical, and fragmentation reactions, the skeleton of the solute molecule is largely being broken up. A fraction of the original substrate may however be converted into halogenated-acyl chlorides (that hydrolyze into the acids) in pathways that are undesirable. A higher dose would then be required to effect their degradation to a sufficient degree. In fact, *per*halogenated acids such as trichloroacetic are practically impervious to further oxidative destruction.

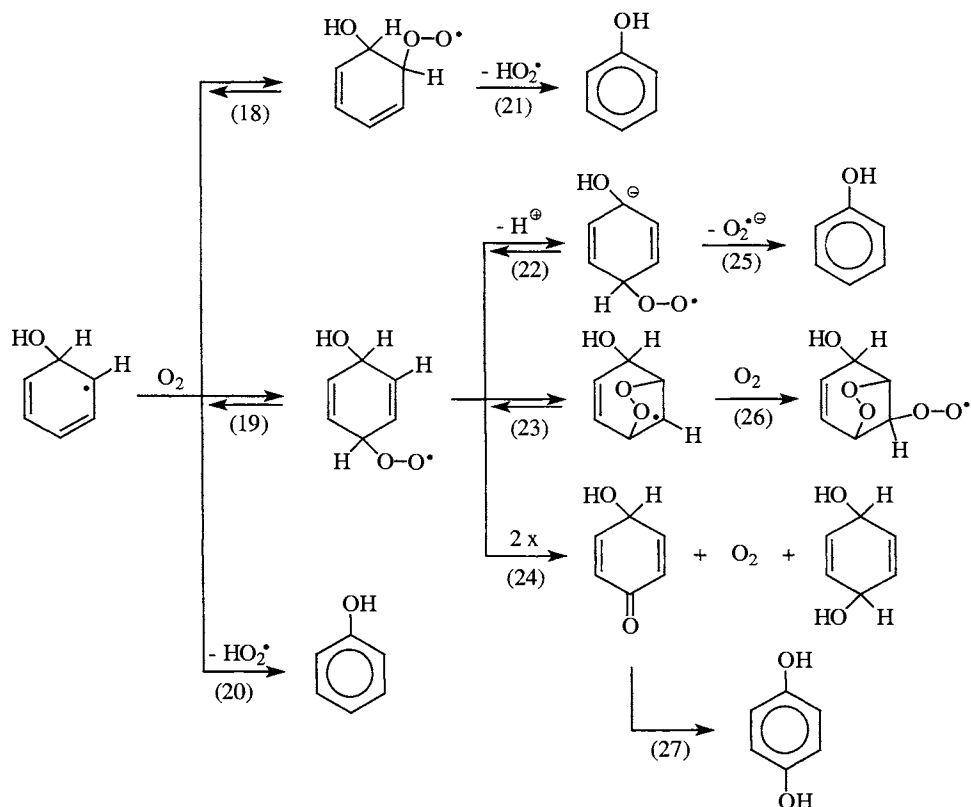
In the case of the above-mentioned solutes (especially of the tri- and tetrachloroethylenes where the annual industrial production runs into the

millions of metric tons), the resulting acid chlorides are mostly phosgene and formyl chloride. These undergo hydrolysis into carbon dioxide and hydrochloric acid (phosgene,  $k = 9 \text{ s}^{-1}$  [32]), or decompose into carbon monoxide and HCl in a water-catalyzed reaction (formyl chloride  $k = 10^4 \text{ s}^{-1}$  [33]).



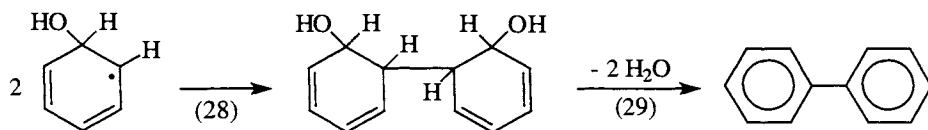
## 2.2. Aromatics

In the abatement of aromatic pollutants, the main initial transient species is the substrate-OH-radical adduct, hydroxycyclohexadienyl. Depending on the nature of the substituents in the ring, the addition of dioxygen to these radicals may be reversible [34]. The behaviour of the hydroxycyclohexadienylperoxyl



radical in the case of the prototype benzene has been studied in detail [35] [reactions (18)-(27)].

Phenol is the main product; there are a few further products with the six-membered ring intact. Together they account for roughly half of the starting material consumed, the rest being fragmentation products [36] which are not secondary but primary and owe their formation to repeated free-radical fragmentation, rearrangement, and peroxylation. The continued presence of dioxygen in these radiolyses is necessary in order to prevent the formation of biphenylic compounds by free-radical recombination and rearomatization reactions [reactions (28) and (29); the latter being proton-catalyzed (unpublished results)]. Because of their hydrophobicity, such products accumulate at the surface of the aqueous phase and tend to stick to its confinements where they are largely inaccessible to further degradation.



Treatment of aromatics with ionizing radiation in order to degrade them is not necessarily always entirely beneficial. Thus with an effluent that produces  $\text{NO}_2$  (which is especially the case in the treatment of aerosols), traces of nitro derivatives can be formed by free-radical recombination [cf. reactions (30)-(36), unpublished results]. These compounds are usually very resistant to biodegradation.

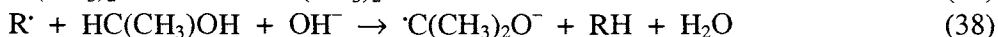
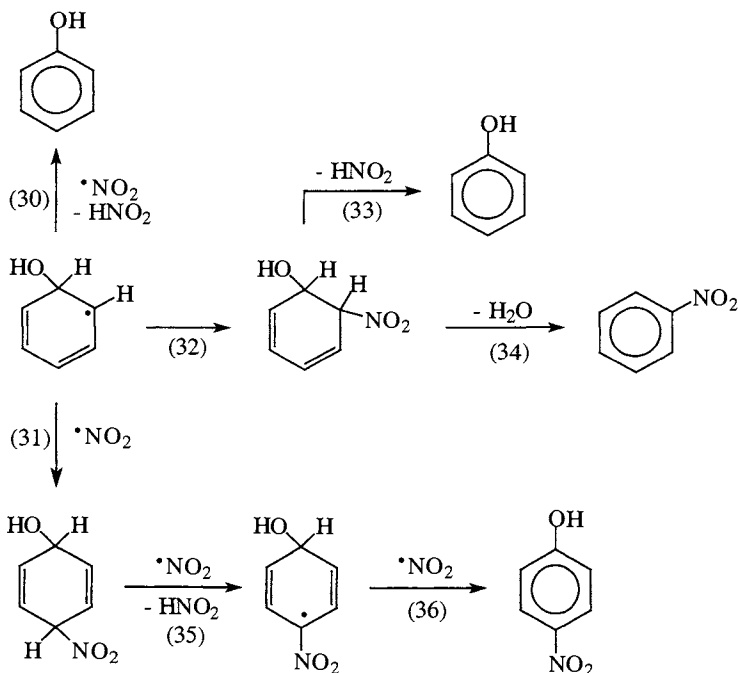
Hydroxylated aromatics are among the intermediates in the deep degradation of aromatic hydrocarbons. In addition, they form a class of pollutants of their own. Phenoxyl radicals are important intermediates in their oxidative oxidation. Some aspects of their degradation have been discussed from an environmental point of view [37-40].

Halogenated aromatics [11, 37, 41-45] are practically not dehalogenated directly by the OH radical since the addition at the *ipso* position is strongly avoided (cf. the prototype chlorobenzene [45]). Peroxyl radical reactions and the ensuing progressive fragmentation of the carbon skeleton eventually lead to acid chloride or gem-chlorohydrin functions which eliminate HCl, or to  $\alpha$ -chloroalkoxyl radicals which may eliminate the chlorine atom; this effects hydrogen abstraction giving rise to HCl.

Chlorinated biphenyls are sometimes encountered as hydrophobic soil contaminants. They have usually been extracted with organic solvents and reductively dehalogenated in such nonaqueous media [46, 47] [e.g. reaction (37)]



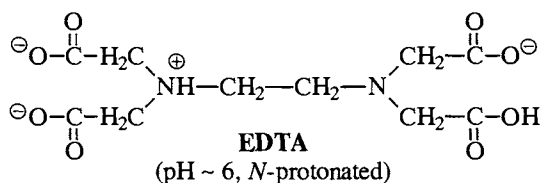
and (38)] but there has also been experimentation in mixed-aqueous systems [48-50].



The halogenated biphenyls represent a class of compounds where reductive conditions [51] (solvated electron, aromatic radical anions, ketyl radicals) answer the purpose much better than the OH radical. However, this is to be seen in the context that the toxicity of the *halogenated* biphenyls exceeds that of biphenyl itself by such a wide margin that the latter compound is considered as *relatively* harmless. Complete removal of the pollutant would still have to rely on the oxidative pathway. A similar situation exists with respect to nitroaromatics [52] which are also subject to reductive attack, indirectly by the OH radical *via*  $\alpha$ -hydroxyethyl radical generated from the additive ethanol [53].

### 2.3. EDTA

This compound is the most widely-used of the family of aminopolycarboxylic acids, which act as strong metal ion-complexing agents. Its near-ubiquity in surface waters has begun to cause concern. OH-induced degradation represents one way to cope with this problem. Radiolytic studies focusing on the action of OH have been undertaken recently [54, 55].



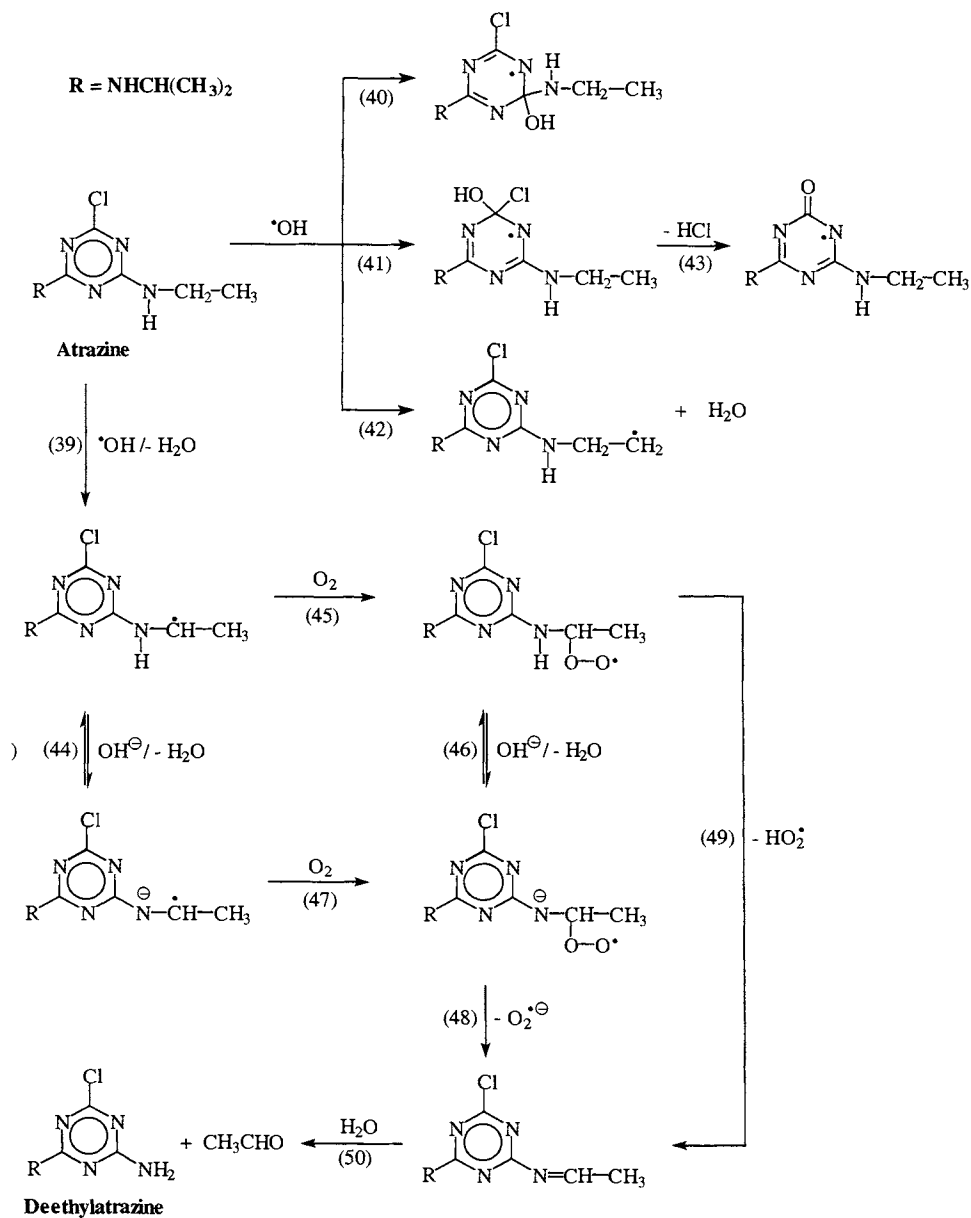
Two distinct primary transients have been observed by optical spectroscopy in its pulse radiolysis [54]. One of these is not affected by O<sub>2</sub> and has been attributed to an *N*-centered radical cation, "*N*<sup>+</sup>*N*-EDTA", directly bridged to the second EDTA nitrogen. Using strong reductants as probes, e.g. *N,N,N',N'*-tetramethylphenylenediamine,  $G(N^+N\text{-EDTA}) = 1.6 \times 10^{-7} \text{ mol J}^{-1}$  has been obtained. Besides generating *N*<sup>+</sup>*N*-EDTA, the OH radicals produce *C*-centered radicals by H-abstraction. These have reducing properties and are rapidly oxidized by tetranitromethane, giving rise to nitroform anion,  $G(\text{NF}^-) = 4.2 \times 10^{-7} \text{ mol J}^{-1}$ . The *C*-centered radicals react rapidly ( $k = 7.6 \times 10^8 \text{ dm}^3 \text{ mol}^{-1} \text{ s}^{-1}$ ) with O<sub>2</sub>, and subsequent fast O<sub>2</sub><sup>-</sup> elimination. The Schiff bases thus formed hydrolyze to the final products.

In the presence of oxygen, the following products ( $G$  values in units of  $10^{-7} \text{ mol J}^{-1}$  in parentheses) were observed after  $\gamma$ -radiolysis: formaldehyde (1.6), CO<sub>2</sub> (1.6), glyoxylic acid (4.2), iminodiacetic acid (2.1), ethylenediaminetriacetic acid (detected, not quantified).

### 2.4. Atrazine

Owing to its wide agricultural use in the past and its relative chemical stability, the persistent herbicide atrazine, a triazine derivative, has reached the ground-water table in many places, by seepage through the soil, and remains a concern even though its use has in the meantime been interdicted. A recent mechanistic radiolysis study [56] has shown that OH radicals give rise to equal amounts of deethylatrazine and acetaldehyde (the yield of each fragment 40% of OH radical yield) and deisopropylatrazine and acetone (16%), respectively. The precursors of deethylatrazine and acetaldehyde is a Schiff-base precursor which hydrolyzes slowly in a reaction that is OH<sup>-</sup>-catalyzed. The hydrolysis of the

Schiff base of deisopropylatrazine and acetone is too fast to be followed. Pulse radiolysis has shown that the intermediate formed upon OH-radical attack



decays in the presence of oxygen. The peroxy radicals thus formed eliminate superoxide. The prototype *s*-triazine reacts much more slowly with the OH radical. This may explain why in the case of atrazine in comparison to other aromatic compounds, *e.g.* toluene, the addition of the OH-radical to the ring (estimated at ~ 40%) is of relatively little importance as compared to an H-abstraction from (activated) positions of the side groups.

### 2.5. Transition metals

Their removal from aqueous media [57-59] is based on the reduction of the ions when they exist in higher-valence states to the lower-valent or zero-valent state where these elements can be precipitated and separated by filtration or flotation. This is effected under reducing conditions, *i.e.* the oxidizing OH radical is transformed into a reducing free radical by having it react with a suitable organic additive such as ethanol.

## 3. COST-BENEFIT CONSIDERATIONS

The technology today prefers electron-beam over  $\gamma$ -ray facilities because the former allow to deliver high dose rates such as appear at present not practicable with the latter. A drawback of the former is a moderate penetration depth of the electron beam; this requires sheet-flow or aerosol treatment which imposes narrower limits on throughput.

The generation of OH radical equivalent to 0.01 molar in 1 m<sup>3</sup> water (at  $G(\text{OH}) = 3 \times 10^{-7}$  mol J<sup>-1</sup> under air) ideally requires 9 kWh. For instance, 1 molecule of a simple haloaromatic may require at least 10 OH radicals for its advanced degradation in the presence of O<sub>2</sub>, to achieve easy biodegradability, *i.e.* 90 kWh per m<sup>3</sup> of a 0.01 molar solution of the pollutant. This corresponds to a dose of 3 kGy. The presence of carbonate can lead to wastage of OH radicals in water with pollutants present at higher dilutions. All of this suggests that irradiation as a means towards pollution abatement is relatively well suited economically to be employed in the melioration of drinking water [60], preferably with low carbonate content, as well as to the case of very noxious compounds in industrial effluents where the costs of the irradiation treatment assume secondary importance as other procedures may be even more expensive. As regards municipal effluent, it appears that the benefit of thorough disinfection is so considerable (especially in countries where infectious diseases are endemic) as to justify the setting up of the irradiation facility and carrying the charges for its operation and maintenance, while the additional energy cost

for providing radiation doses above those required for disinfection might be considered to be marginal.

In order to put the economics of electron-beam radiation treatment into perspective, it is necessary not only to know the energy cost, but also the operating costs in general, the capital requirements, and the rate of capital depreciation. Even for a plant of the same size, E-beam power, and effluent throughput these can vary widely from country to country. From the numbers given for a drinking-water purification plant (situated in an industrially advanced country) with a throughput of  $10^3 \text{ m}^3/\text{h}$ , *i.e.*  $8 \times 10^6 \text{ m}^3/\text{a}$ , imparting a dose of 50 Gy [60], a cost estimate per cubic meter treated indicates that the treatment cost should be about 7 cents per cubic meter (capital costs  $2.3 \times 10^6$  dollars, *i.e.* financing costs (at 7% interest) of  $1.6 \times 10^5$  dollar/a; depreciation at 5%, corresponding to a plant lifetime of about 20 a, of  $1.1 \times 10^5$  dollars/a; operating costs including energy  $2.7 \times 10^5$  dollar/a). The treatment cost per cubic meter at a predetermined throughput increases at higher dose requirements, in a stronger-than-linear fashion with respect to the dose, because plant with higher beam energies is progressively less energy-efficient, as well as because of progressively increasing shielding requirements; these complications will probably more than offset any potential economies of scale. A linear extrapolation of the above estimate to a dose of 3 kGy would then lead to a price of  $0.07 \text{ USD}/\text{m}^3 \times 3 \text{ kGy}/50 \text{ Gy} = 4.2 \text{ USD}/\text{m}^3$ .

#### **Note added in Proof**

Very recently, a three-part review [61-63] has appeared on the current status of the application of ionizing radiation to environmental protection.

**REFERENCES**

1. J.W.T. Spinks and R.J. Woods, *Introduction to Radiation Chemistry*, Wiley, New York, 1990.
2. A.K. Pikaev, in: *Radiation Technology for Conservation of the Environment*, ed. IAEA, Vienna, 1998 p. 243.
3. P. Gehringer, H. Eschweiler and H. Fiedler, *Radiat. Phys. Chem.*, 46 (1995) 1075.
4. Gehringer, P. Report OEFZS-4738, 1995.
5. Gehringer, P. Report IAEA-TECDOC-971, 1997.
6. A.V. Ponomarev, I.E. Makarov, A.V. Bludenko, V.N. Minin, D.K. Kim, B. Han and A.K. Pikaev, *High Energy Chem. (Engl.)*, 33 (1999) 177.
7. A.A. Pikaev and E.A. Podzorova, *High Energy Chem. (Engl.)*, 33 (1999) 233.
8. N. Getoff, *Radiat. Phys. Chem.*, 54 (1999) 377.
9. A.K. Pikaev, *High Energy Chem. (Engl.)*, 28 (1994) 1.
10. Waite, T. D., Kruger, P., Bryan, E., and Swinwood, J. F. *Appl. Isot. Radiat. Conserv. Environ., Proc. Int. Symp.* 1992, 143.
11. N. Getoff, *Radiat. Phys. Chem.*, 47 (1996) 581.
12. N. Getoff, *Proc. Indian Acad. Sci. (Chem. Sci.)*, 105 (1993) 373.
13. R.J. Hilarides, K.A. Gray, J. Guzzetta, N. Cortellucci and C. Sommer, *Water Environ. Res.*, 68 (1996) 178.
14. K.A. Gray and M.R. Cleland, *J. Adv. Oxid. Technol.*, 3 (1998) 22.
15. H.R. Paur, in: *The Modern Problems of Electrostatics with Application in Environment Protection*, ed. I.I. Inculet, Kluwer, Dordrecht, 1999 p. 111.
16. H.R. Paur, W. Baumann, H. Mätzing and K. Jay, *Radiat. Phys. Chem.*, 52 (1998) 355.
17. L. Prager, R. Mehnert, A. Sobottka, H. Langguth, W. Baumann, W. Mätzing, H.-R. Paur, J. Schubert, R. Rashid, K.M. Taba, H.-P. Schuchmann and C. von Sonntag, *J. Adv. Oxid. Technol.*, 3 (1998) 87.
18. H. Mätzing, *Adv. Chem. Phys.* 80 (1991) 315.
19. B. Sun, M. Sato and J.S. Clements, *J. Phys. D: Appl. Phys.*, 32 (1999) 1908.
20. G.V. Buxton, C.L. Greenstock, W.P. Helman and A.B. Ross, *J. Phys. Chem. Ref. Data*, 17 (1988) 513.
21. C. von Sonntag and H.-P. Schuchmann, *Angew. Chem. Int. Ed. Engl.*, 30 (1991) 1229.
22. C. von Sonntag and H.-P. Schuchmann, in: *Peroxy Radicals*, ed. Z.B. Alfassi, Wiley, Chichester, 1997 p. 173.

23. N. Getoff, in: Peroxyl Radicals, ed. Z.B. Alfassi, Wiley, Chichester, 1997 p. 483.
24. P. Neta, R.E. Huie and A.B. Ross, *J. Phys. Chem. Ref. Data*, 17 (1988) 1027.
25. R. Mertens and C. von Sonntag, *J. Photochem. Photobiol. A: Chem.*, 85 (1995) 1.
26. C. von Sonntag, P. Dowideit, X.W. Fang, R. Mertens, X.-M. Pan, M.N. Schuchmann and H.-P. Schuchmann, in: Radiation Research 1895-1995. Vol.2: Congress Lectures. Proceedings of Xth International Congress of Radiation Research, eds. U. Hagen, D. Harder, H. Jung and C. Streffer, 10th ICRR Society, Würzburg, 1996 p. 274.
27. R. Köster and K.-D. Asmus, *Z. Naturforsch.*, 26b (1971) 1108.
28. R. Mertens and C. von Sonntag, *J. Chem. Soc. Perkin Trans. 2*, (1994) 2181.
29. N. Getoff, *Appl. Radiat. Isot.*, 40 (1989) 585.
30. P. Gehringer, E. Proksch, H. Eschweiler and W. Szinovatz, *Int. J. Radiat. Appl. Instrum. Part A*, 43 (1992) 1107.
31. R. Mertens and C. von Sonntag, *Angew. Chem. Int. Ed. Engl.*, 33 (1994) 1262.
32. R. Mertens, C. von Sonntag, J. Lind and G. Merényi, *Angew. Chem. Int. Ed. Engl.*, 33 (1994) 1259.
33. P. Dowideit, R. Mertens and C. von Sonntag, *J. Am. Chem. Soc.*, 118 (1996) 11288.
34. X. Fang, X. Pan, A. Rahmann, H.-P. Schuchmann and C. von Sonntag, *Chem. Eur. J.*, 1 (1995) 423.
35. X.-M. Pan and C. von Sonntag, *Z. Naturforsch.*, 45b (1990) 1337.
36. X.-M. Pan, M.N. Schuchmann and C. von Sonntag, *J. Chem. Soc. Perkin Trans. 2*, (1993) 289.
37. Trojanowicz, M. Chudziak A. and Bryl-Sandelewska, T. *Radiat. Technol. Conserv. Environ., Proc. Symp.*, Vienna, IAEA 1998, p. 255.
38. F. Macasek, V. Mikulaj, P. Rajec, R. Cech, L. Matel, R. Kopunec, J. Kuruc and A. Svec, *J. Radioanal. Nucl. Chem.*, 191 (1995) 129.
39. J. Gierer, E. Yang and T. Reitberger, *Holzforschung*, 46 (1992) 495.
40. A. Kovacs, K. Gonter, G. Földiak, I. György and L. Wojnarovits, *Acta Chem. Hungarica* 134 (1997) 453.
41. W.D. Geppert and N. Getoff, *Radiat. Phys. Chem.*, 51 (1998) 281.
42. S. Schmid, P. Krajnik, R.M. Quint and S. Solar, *Radiat. Phys. Chem.*, 50 (1997) 493.
43. M. Ye and R.H. Schuler, *J. Liquid Chrom.*, 13 (1990) 3369.
44. R. Zona, S. Schmid and S. Solar, *Wat. Res.*, 33 (1999) 1314.

45. G. Merga, H.-P. Schuchmann, B.S.M. Rao and C. von Sonntag, *J. Chem. Soc. Perkin Trans. 2*, (1996) 1097.
46. R.D. Curry and B.J. Mincher, *Radiat. Phys. Chem.*, 56 (1999) 493.
47. M. Chaychian, J. Silverman, M. Al-Sheikhly, D.L. Poster and P. Neta, *Environ. Sci. Technol.*, 33 (1999) 2461.
48. R.J. Hilarides, K.A. Gray, J. Guzetta, N. Cortelucci and C. Sommer, *Environ. Sci. Technol.* 28 (1994) 2249.
49. M. Al-Sheikhly, J. Silverman, P. Neta and L. Karam, *Environ. Sci. Technol.*, 31 (1997) 2473.
50. D.C. Schmelling, D.L. Poster, M. Chaychian, P. Neta, J. Silverman and M. Al-Sheikhly, *Environ. Sci. Technol.*, 32 (1998) 270.
51. K.A. Gray and G.A. Zacheis, *CCS Newsletter*, 10 (1998) 3.
52. D.C. Schmelling, K.A. Gray and P.V. Kamat, *Environ. Sci. Technol.*, 32 (1998) 971.
53. G.R. Peyton, O.J. Bell, E. Girin and M.H. LeFaivre, *Environ. Sci. Technol.*, (1996)
54. B. Höbel and C. von Sonntag, *J. Chem. Soc. Perkin Trans. 2*, (1998) 509.
55. K. Krapfenbauer and N. Getoff, *Radiat. Phys. Chem.*, 55 (1999) 385.
56. A. Tauber and C. von Sonntag, *Acta Hydrochim. Hydrobiol.*, 28, (2000) 15.
57. D. Schmelling, D. Poster, M. Chaychian, P. Neta, W. McLaughlin, J. Silverman and M. Al-Sheikhly, *Radiat. Phys. Chem.*, 52 (1998) 371.
58. M. Chaychian, M. Al-Sheikhly, J. Silverman and W.L. McLaughlin, *Radiat. Phys. Chem.*, 53 (1998) 145.
59. M. Chaychian, M. Al-Sheikhly, J. Silverman and W.L. McLaughlin, in: *Environmental Applications of Ionizing Radiation*, eds. W.J. Cooper, R.D. Curry and K.E. O'Shea, Wiley, New York, 1998 p. 353.
60. P. Gehringer, E. Proksch, H. Eschweiler and W. Szinovatz, 10th Ozone World Congress, Monaco, (1991).
61. A. K Pikaev, *High Energy Chem. (Engl.)*, 34 (2000) 1.
62. A. K Pikaev, *High Energy Chem. (Engl.)*, 34 (2000) 55.
63. A. K Pikaev, *High Energy Chem. (Engl.)*, 34 (2000) 129.



## **High-performance polymeric materials for separation and reaction, prepared by radiation-induced graft polymerization**

**Kyoichi Saito<sup>a,b</sup> and Takanobu Sugo<sup>c</sup>**

<sup>a</sup>Department of Materials Technology, Chiba University,  
Inage, Chiba 263-8522, Japan

<sup>b</sup>"Form and Function", PRESTO,  
Japan Science and Technology Corporation, Japan

<sup>c</sup>Takasaki Radiation Chemistry Research Establishment,  
Japan Atomic Energy Research Institute,  
Takasaki, Gunma 370-1292, Japan

### **1. RADIATION-INDUCED GRAFT POLYMERIZATION HAS PROVIDED COMMERCIAL PRODUCTS**

#### **1.1. Advantages of radiation-induced grafting**

A radiation-induced grafting technique has been commercialized for the production of ion-exchange membranes as separators of batteries, hydrophilized hollow-fiber membranes for microfiltration of protein solutions, and ion-exchange nonwoven fabric for the removal of trace amounts of gases from ultraclean rooms [1, 2].

Radiation-induced graft polymerization is a powerful technique for modifying the existing polymeric materials. An analogy between grafting performed by a gardener and that by a radiation chemist is illustrated in Figure 1. A tree which is resistant to severe climate and poor soil has few fruits on its branches. The gardener creates a grafting site by cutting a branch. Then, he grafts another branch which is capable of producing succulent fruit. Similarly, chemists can produce radicals by irradiating a trunk polymer with electron beams and gamma rays. Then a polymer branch with functional capabilities is grafted onto the trunk polymer.

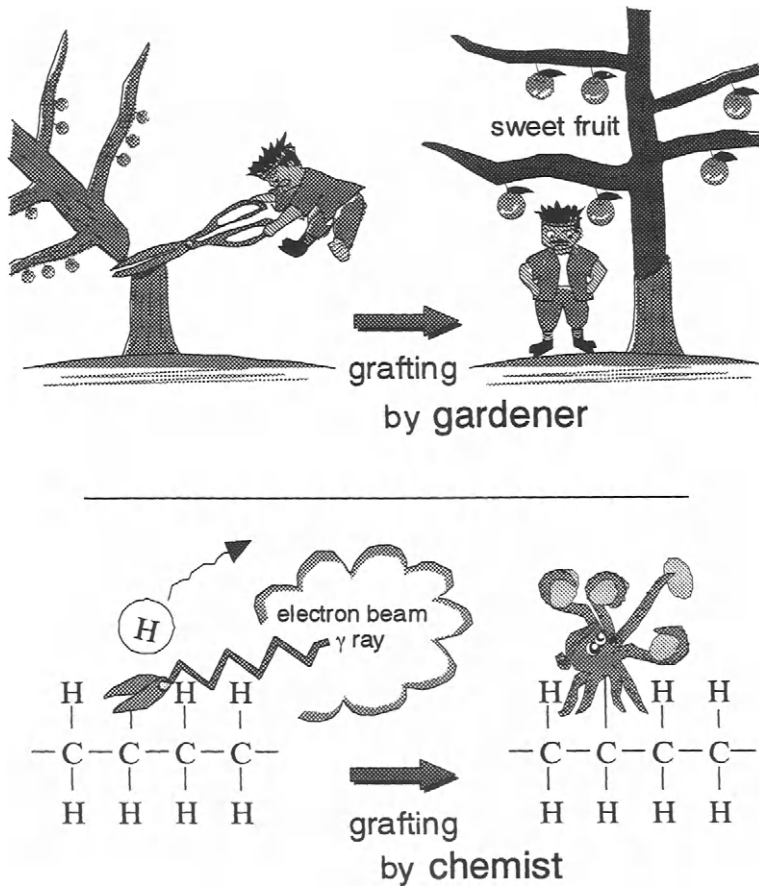


Figure 1 Radiation-induced graft polymerization.

Grafting enables role allotment in polymeric materials. The role of the trunk polymer is to provide an appropriate practical shape and to maintain chemical-resistant stability, while the branch polymer exhibits various functionalities such as separation and catalytic reaction.

Excitation sources for the production of radicals in grafting include chemicals, light, plasma, and radiation. Radiation-induced graft polymerization is superior to other grafting techniques because the high density of electron beams and gamma rays can create a large amount of radicals of arbitrary shapes of the polymer, such as a hollow fiber [2-41], nonwoven fabric [42] and film [43-54], and the quality of the polymer, such as polyethylene [2-41], polytetrafluoroethylene [42], and cellulose [55].

## 1.2. Classification of radiation-induced grafting

Radiation-induced graft polymerization can be classified into two techniques in terms of irradiation opportunity: (1) simultaneous grafting, i.e., the mixture of a trunk polymer and a monomer is irradiated, and (2) preirradiation grafting, i.e., a trunk polymer is previously irradiated and then brought into contact with the monomer [56]. From a practical viewpoint, the preirradiation technique is preferable because of the negligible formation of homopolymers and easier control of the degree of polymerization.

The use of a monomer mixture for grafting, i.e., cograftering, will be effective in appending functionalities onto the trunk polymer. Monomers containing a strongly acidic or basic ion-exchange group are difficult to graft directly onto hydrophobic polymers, because highly ionizable groups with a large hydration sphere are incompatible with the hydrophobic polymers. However, simple introduction of a sulfonic acid group onto variously shaped polymers made of polyethylene, polypropylene, or polytetrafluoroethylene was achieved by radiation-induced cograftering of sodium styrene sulfonate with hydrophilic monomers such as acrylic acid ( $\text{CH}_2=\text{CHCOOH}$ , AAc) and 2-hydroxyethyl methacrylate ( $\text{CH}_2=\text{C}(\text{CH}_3)\text{COOCH}_2\text{CH}_2\text{OH}$ , HEMA) [46]. Similarly, the trimethyl ammonium ( $-\text{N}(\text{CH}_3)_3$ ) group was appended by radiation-induced cograftering of vinyl benzyl trimethylammonium chloride with HEMA [46].

## 1.3. Storage of radicals

Specification of the radicals, formed on trunk polymers, such as species, locations, and lifetime, is required in order to tailor the functional polymer by radiation-induced graft polymerization. Radical species contributing to the preirradiation graft polymerization are governed by the reaction conditions. Electron beam irradiation on polyethylene forms three kinds of radicals, i.e., alkyl, allyl, and peroxy radicals. Identification and quantitative analysis of radicals are performed by means of electron spin resonance (ESR) [57]. The disappearance of the radicals on the trunk polymer with time was investigated to maintain the concentration of the radicals at a feasible level during storage in air between the steps of irradiation to graft polymerization in the preirradiation technique.

An electron beam was irradiated onto porous polyethylene to analyze the behavior of alkyl, allyl, and peroxy radicals at different atmospheres and temperatures. The decay of each radical was compared in air and nitrogen atmospheres [57]. The concentrations of the allyl and peroxy radicals were constant in either atmosphere. In contrast, a higher

concentration of alkyl radicals was found in the nitrogen atmosphere than in air at an identical contact time after irradiation. This difference can be explained by the accessibility of oxygen to the radical. Since the vinyl monomer also diffuses into the oxygen-accessible site, the radical contributing to graft polymerization is estimated to be the alkyl radical instead of the allyl radical. After being kept for 150 hours in air at 195 K at dry-ice temperature, almost no decrease in the alkyl radical concentration was observed. This suggests that the radical could be stored in dry ice, where the matrix polymers have no mobility below the glass transition temperature (203 K for polyethylene), whereas at 298 K in ambient temperature, about 90% of the initial concentration of alkyl radicals was lost during 10 hours of contact with air.

#### 1.4. Selection of monomers

Two reaction schemes for the modification of the trunk polymer by radiation-induced graft polymerization are shown in Figure 2. Scheme 1 consists of graft polymerization of a precursor monomer such as an epoxy-group-containing vinyl monomer, glycidyl methacrylate ( $\text{CH}_2=\text{C}(\text{CH}_3)\text{COOCH}_2\text{CHOCH}_2$ , GMA), and subsequent ring-opening of the epoxy group with various reagents such as amines, alcohols, and water to form functional groups [58-61]. In contrast, Scheme 2

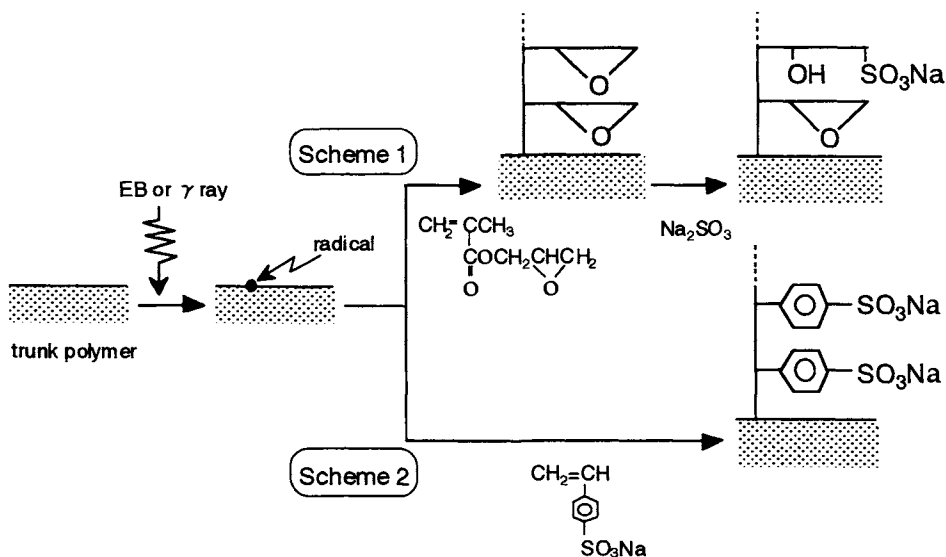


Figure 2 Two modification schemes of trunk polymer by radiation-induced graft polymerization.

involves direct grafting of a monomer already containing the functional group [62].

Scheme 1 is effective for the introduction of a ligand to the trunk polymer for protein collection. For example, some epoxy groups are coupled with a ligand for the enhancement of the specific adsorption of proteins, while others are converted into hydrophilic groups for the reduction of nonselective adsorption [40]. Although Scheme 2 is more convenient for the introduction of functional groups at a higher density compared to Scheme 1, the grafting rate of the functionalized monomer and the formation site of the graft chain will differ from those of the precursor monomer because the molecular size and hydrophilicity are altered.

GMA graft polymerization onto a porous membrane is a versatile technique for the production of other functional porous membranes bearing ion-exchange groups [6-19], chelate-forming groups [31-36], hydrophobic [20-23] ligands, and affinity [3-5] ligands. For example, a phenyl group can be easily introduced as a hydrophobic ligand onto polymer chains of GMA-grafted membranes by reaction with phenol in alkaline medium.

Svec et al. [63] and Iwakura et al. [64] performed extensive studies on the reactivity of the poly-GMA network with ammonia, amines, alcohol, acid and water. Their copolymers contained the epoxy group as a trunk polymer. On the other hand, Kim et al. [65] adopted a porous polyethylene membrane of a hollow-fiber form as the trunk polymer and the poly-GMA chain as a branch polymer. The produced epoxy group was converted into a diol group, ion-exchange (diethylamino and sulfonic acid) and chelate-forming (ethylenediamine and iminodiacetic acid) groups, and pseudoaffinity ligands (phenylalanine and tryptophan). The conversion of the epoxy group into the functional group was investigated as a function of the molecular mass of the reactants. A reagent with low molecular mass exhibited a high conversion. The high conversion of the ion-exchange group caused the extension of the polymer chain grafted onto the pore surface and decreased water permeability through the hollow-fiber membrane.

## **2. POROUS HOLLOW-FIBER MEMBRANES ENHANCE CONVECTIVE MASS TRANSPORT**

### **2.1. Purification of proteins**

The purification process of proteins in biological fluids governs the production cost of the proteins in pharmaceutical and food industries. Therefore, there is a constant demand for highly efficient recovery of

proteins. Of the various recovery techniques, chromatography is a powerful and versatile technique for protein purification in that various functional moieties such as ion-exchange groups, and hydrophobic and affinity ligands can be immobilized onto solid matrices.

Highly efficient recovery is defined as the fulfillment of the following three requirements: high rate, high capacity, and repeated use. These requirements are satisfied by a novel functional porous membrane that can be prepared by grafting of functional polymer chains onto a microfiltration membrane.

The key to attaining a high rate of protein purification is convective transport of protein. In the case of a conventional gel-bead-packed column, the proteins, driven by a concentration gradient, diffuse into the beads and reach the functional groups. In most cases, the rate of diffusion of the protein governs the overall adsorption rate. On the other hand, functional-group-containing polymer chains can be immobilized uniformly along the pores of a porous membrane. As a result, the proteins, driven by a pressure difference across the membrane, are transported by convection of the protein solution through the pores (Figure 3). Therefore, the diffusional mass-transfer resistance of the proteins to the functional groups can be neglected. This idea was

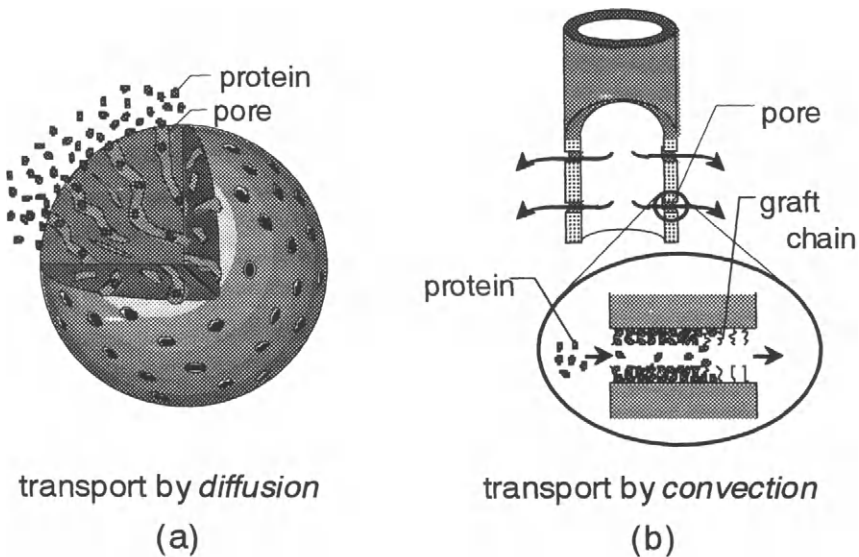


Figure 3 Transport modes of proteins. (a) by diffusion in conventional gel bead; (b) by convection in novel porous membrane.

suggested by Brandt et al. [66] for membrane chromatography.

The key to achieving high capacity is multilayer binding of proteins on the pore surface. Microfiltration membranes have a surface area of about  $10 \text{ m}^2$  per gram of the membrane. Ordinarily, monolayer adsorption of the protein onto the pore surface is observed. However, when polymer chains about 1 micrometer long extend from the pore surface towards the pore interior, it allows multilayer binding of a protein of about 10 nm diameter (Figure 4). This idea was first proposed by Muller [67]. He immobilized ion-exchange-group-containing polymer chains on the external surface of polymer beads, and referred to the multilayer binding of the protein as tentacle adsorption.

The key to repeated use is the coexistence of hydrophilic groups and functional groups. The surface of protein has hydrophobic patches. Therefore, proteins easily adsorb nonselectively onto the surface of a hydrophobic polymeric support. In order to realize repeated adsorption and elution of protein using functional porous membranes, alcoholic hydroxyl groups are appended along with the functional groups of the polymer chains grafted onto the pore surface. This idea is similar to that on which Svec's work [68] was based.

The polymer containing a diethylamino group as an anion-exchange group is capable of collecting proteins dissolved in biological fluids. The preparation scheme of the anion-exchange porous membrane by radiation-induced graft polymerization and subsequent chemical modifications consists of the following four steps (Figure 5): (1) the porous polyethylene membrane is irradiated with electron beams in order to produce radicals, (2) an epoxy-group-containing monomer,

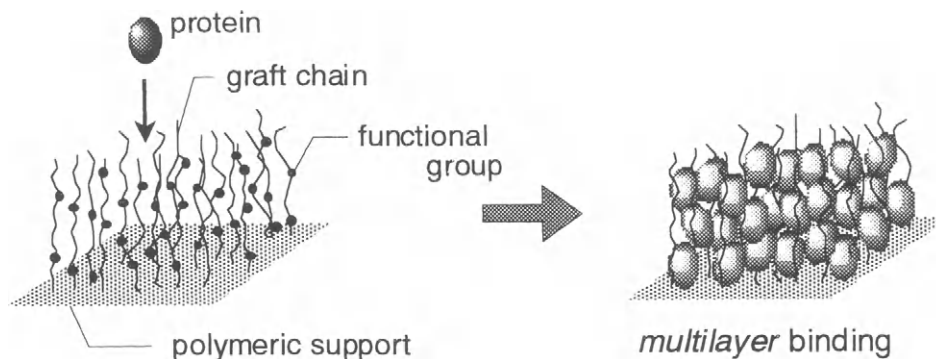


Figure 4 Multilayer binding of proteins in polymer chain grafted onto pore surface.

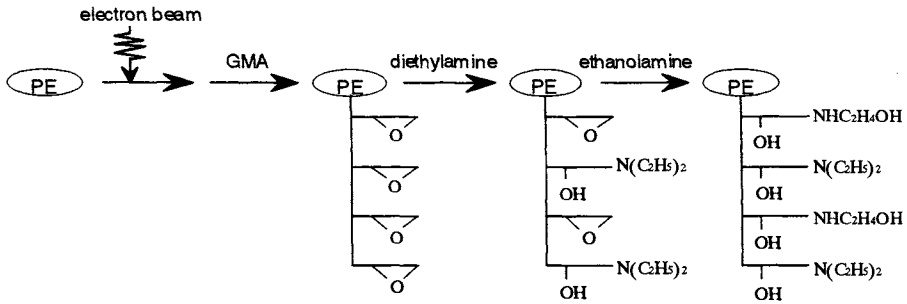


Figure 5 Preparation scheme of anion-exchange porous membrane of a hollow-fiber form.

GMA, is graft-polymerized onto the pore surface, (3) some of the epoxy groups produced are subjected to ring-opening with diethylamine for the introduction of anion-exchange groups, and (4) the remaining epoxy groups are hydrophilized with ethanolamine.

Polymer chains can be appended at a uniformly high density across the porous membrane of a hollow-fiber form. A phenomenon favorable for the permeation of the protein solution was observed after grafting of the polymer chains and introduction of the functional groups onto the membrane. Figure 6 depicts scanning electron microscopy images of the pore structure of the resultant membrane. The pore structure was

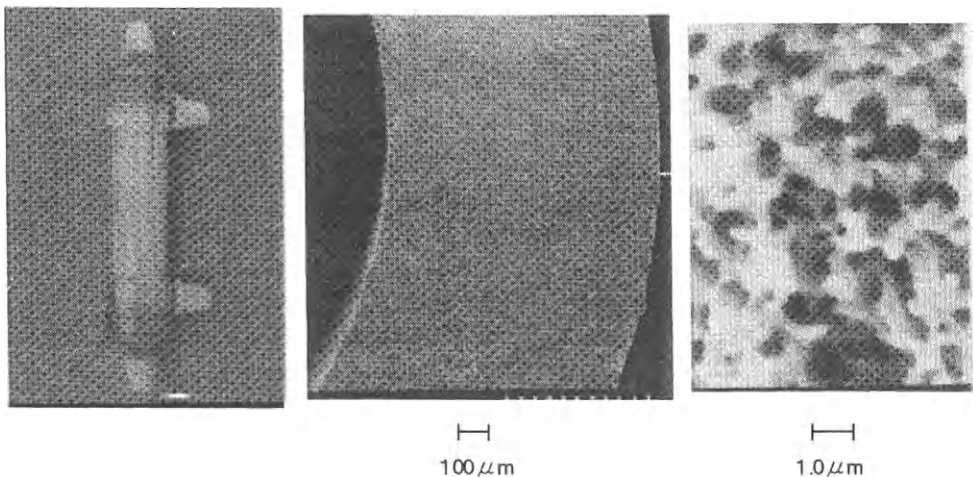


Figure 6 SEM images of cross-sectional area of porous membranes.



retained due to swelling of the entire membrane accompanied by invasion of the polymer chains into the polymer matrix. The inner and outer diameters of the anion-exchange porous membrane were 2.8 and 4.4 mm, respectively. Therefore, the thickness of the hollow-fiber membrane was 0.8 mm. The diethylamino (DEA) group density reached 2.9 mmol per gram of the membrane, which was comparable to that of the conventional anion-exchange bead.

The experimental apparatus used to determine the changes in the concentration of protein in the effluent with the effluent volume during the consecutive procedures of adsorption, washing, and elution, i.e., breakthrough and elution curves, is schematically shown in Figure 7. The abscissa gives the effluent volume  $V$ , and the ordinate the concentration of protein in the effluent  $C$ . The anion-exchange porous hollow-fiber membrane was attached to a syringe infusion pump in a dead-end mode. Bovine serum albumin (BSA;  $M_r$  67,500, pI 4.9) in a buffer (Tris-HCl buffer, pH 8.0) was forced to permeate through the pores from the inside of the hollow fiber to the outside at a constant flow rate. The effluent penetrating the outside of the hollow fiber was continuously sampled using a fraction collector and the protein concentration in each fraction was determined. After protein adsorption was saturated, the buffer, and subsequently a buffer containing 0.5 M sodium chloride, were forced

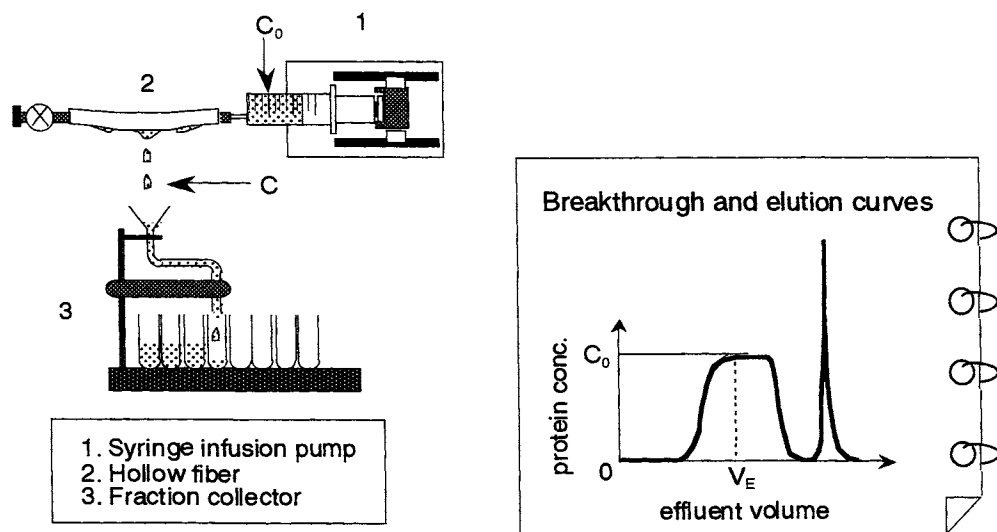


Figure 7 Experimental apparatus for determination of breakthrough curves.

to permeate through the pores from the inside to the outside for washing of the pores and elution of the adsorbed proteins.

The breakthrough and elution curves of the anion-exchange porous hollow-fiber membrane for BSA are shown in Figure 8 as a function of the flow rate of the protein solution. The flow rate of the protein solution in the range from 1 to 10 mL/min was converted to space velocity (SV) by dividing it by the membrane volume including the lumen volume. SV equals the reciprocal of the residence time of the protein solution in the membrane. The SV ranged from 52 to 560 h<sup>-1</sup>. These curves overlapped irrespective of the SV. This demonstrated that the diffusional mass-transfer resistance of BSA to the DEA group was negligible because the diffusional path was minimized by convective flow driven by the pressure difference across the membrane. Therefore, a higher flow rate resulted in a higher throughput in the case of this functional porous membrane.

Similar permeation experiments were performed using the hollow fiber with various DEA-group mole fractions of the graft chain. The DEA-group mole fraction is defined by

DEA-group mole fraction of the graft chain (-)

$$= (\text{DEA group}) / [(\text{DEA group}) + (2\text{-hydroxyethylamino group})] \quad (1)$$

where the parentheses designate mole number. First, for each run, the equilibrium binding capacity of BSA was calculated by integrating the breakthrough curve according to equation (2), where  $V_E$  is the effluent volume when the concentration  $C$  reaches the feed concentration  $C_0$  and  $W$  is the dry weight of the membrane.

$$Q_E (\text{g/g}) = \int_0^{V_E} (C_0 - C) dV/W \quad (2)$$

Second, the degree of multilayer binding of protein onto the pore surface, as defined by equation (3), can be determined by dividing  $Q_E$  by the theoretical monolayer binding capacity,  $Q_t$ .

$$\text{Degree of multilayer binding (-)} = Q_E / Q_t \quad (3)$$

The degree of multilayer binding increased with increasing DEA-group mole fraction, and protein binding to a maximum of 11 layers was observed (Figure 9).

We can visualize that when our hair is rubbed with a plastic plate, strands of hair stand up from the scalp due to electrostatic repulsion among them. Similarly, when charged functional groups, such as diethylamino groups, are introduced onto the graft chains, the polymer chains extend from the pore surface due to their mutual repulsion. This extended polymer brush conformation provides the protein with three-dimensional binding sites. The multilayer binding of various proteins onto the ion-

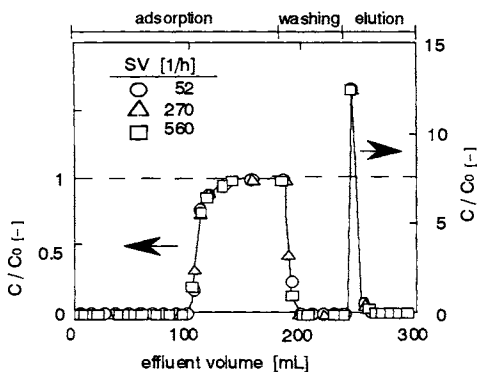


Figure 8 Breakthrough curves of BSA for anion-exchange porous membrane as a function of space velocity.

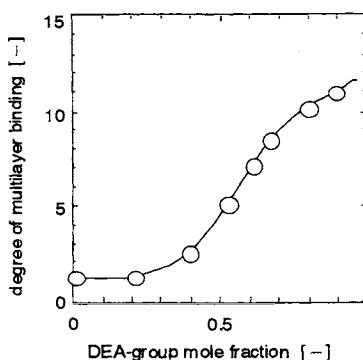


Figure 9 Degree of multilayer binding of BSA vs DEA-group mole fraction.

-exchange porous membranes was observed [8]. The multilayer binding structure is not exceptional. The multilayer binding of protein onto the pore surface is favorable for practical uses because it enables high-capacity protein recovery.

High-rate and high-capacity performance does not make a material perfect. A constant capacity for repeated cycles of adsorption and elution is required. No deterioration of the protein binding capacity or elution percentage of the anion-exchange porous hollow-fiber membrane was observed after five cycles. This demonstrates that role allotment in the polymer chain grafted on the pore surface works well: the anion-exchange groups enhance the selective adsorption of target proteins, and the coexisting alcoholic hydroxyl groups retard the nonselective adsorption of undesired proteins.

In order to determine whether the prepared anion-exchange porous membrane is superior to a gel-bead-packed bed in terms of protein recovery efficiency, an experimental comparison was performed with the same porous membrane and bead-packed bed volumes [12]. BSA in a buffer was permeated across the porous membrane and was made to flow downwards through the bed at a constant operating pressure of up to 0.1 MPa. The effluent was sampled from the outside of the hollow-fiber membrane, and from the bottom end of the bed. The effects of the protein solution flow rate on the dynamic binding capacity of the protein were compared between the membrane and the bed. The dynamic binding capacity is defined as the amount of protein adsorbed until the effluent concentration reaches 10% of the feed concentration. The SV as

a function of operating pressure, i.e., transmembrane pressure, and the dynamic binding capacity of protein versus SV are shown in Figures 10 (a) and (b), respectively. A linear relationship between the operating pressure and the SV of the BSA solution was observed for both the porous membrane and the gel-bead-packed bed. The SV of the membrane was twofold that of the bed. For example, an operating pressure of 0.1 MPa gives an SV of 600 h<sup>-1</sup> for the membrane. In addition, the dynamic binding capacity was distinctly different between the porous membrane and the gel-bead-packed bed. The dynamic binding capacity of the porous membrane was constant irrespective of SV up to 600 h<sup>-1</sup>. In contrast, the dynamic binding capacity of the bed decreased with increasing SV. The functional porous membrane exhibited ideal protein recovery in that an increase in flow rate resulted in an increase in throughput of the protein solution.

Membrane modules are required for practical use. A small-scale module containing eight anion-exchange porous hollow-fiber membranes 10 cm long was fabricated. The dynamic binding amounts for BSA were compared between a single hollow fiber and the module. Figure 11 shows that linear scale-up was possible because the amount of protein adsorbed by the module divided by the number of hollow fibers agreed well with the amount of protein adsorbed by a single hollow fiber [14, 15]. Therefore, an additional advantage of the porous membrane

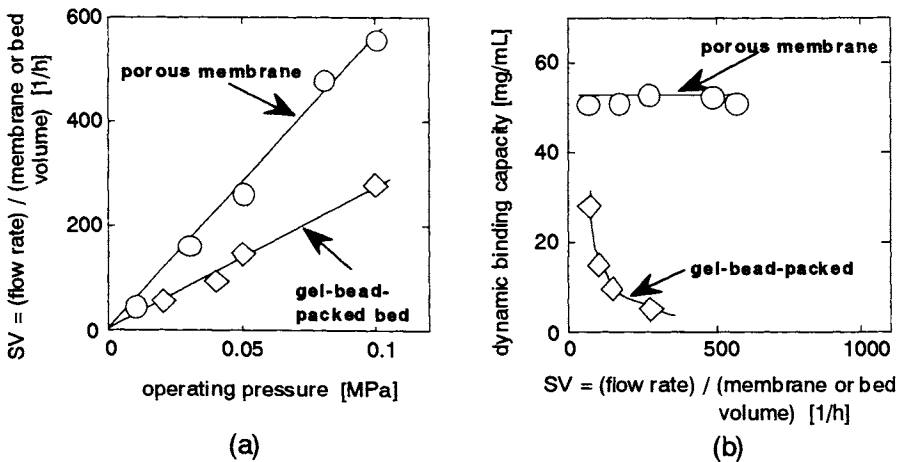


Figure 10 Comparison between porous membrane and gel-bead packed bed. (a) SV vs operating pressure; (b) dynamic binding capacity vs SV.

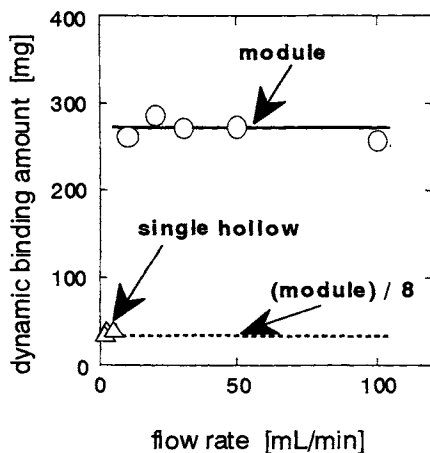


Figure 11 Comparison of dynamic binding amount between a single hollow fiber and the module.

over the bead-packed bed was demonstrated.

## 2.2. Chiral separation of chiral compounds

Racemic mixtures exhibit biological activity based on a small difference in conformation. In pharmaceuticals and the food industry, chiral separation of racemic mixtures has been demanded to raise their safety level and effectiveness. At present, selective crystallization and chiral chromatography are used to resolve various racemic chemicals; the latter is more versatile in that the chiral ligands can be immobilized on supporting matrices. The chiral ligands can be classified into three categories: cellulose derivatives [69], synthetic chiral ligands, e.g., the ligands synthesized by Pirkle et al. [70], and proteins such as bovine serum albumin [71] and ovoglycoprotein [72].

By permeating bovine serum albumin in a buffer solution through the pores, the membrane bound the BSA in the multilayers with a capacity as much as tenfold greater than the monolayer binding capacity [8]. This phenomenon can be explained by considering that the anion-exchange-group-containing polymer chains expand from the pore surface toward the pore interior due to mutual electrostatic repulsion and provide three-dimensional binding sites for proteins with negative charges. This BSA-multilayered structure on the surface of the pores is evaluated as a novel stationary phase for the chiral separation of DL-amino acid. The chiral separation of amino acids and their derivatives using the hollow-fiber membrane module based on liquid extraction has been

previously reported [73]; therefore, the membrane works as a support of the chiral selector-containing liquid, while the system suggested by Nakamura et al. [24-27] enables high-rate separation aided by permeation of the solution through the porous hollow-fiber membranes based on specific adsorption.

A BSA-multilayer-adsorbed porous membrane was prepared via three steps, as shown in Figure 12. (1) Radiation-induced graft polymerization of an epoxy-group-containing monomer onto a porous hollow-fiber membrane made of polyethylene: The hollow fiber had inner and outer diameters of 1.8 and 3.1 mm, respectively, with a pore size of 400 nm and a porosity of 70%. The hollow fiber, previously irradiated with an electron beam at a total dose of 200 kGy, was immersed in a 10 (v/v)% solution of glycidyl methacrylate (GMA) in methanol at 313 K. The amount of grafted GMA was set to 1.9 times the mass of the trunk polymer. (2) Introduction of an anion-exchange group: 60% of the epoxy groups of the poly-GMA chain were converted to diethylamino (DEA) groups ( $-\text{N}(\text{C}_2\text{H}_5)_2$ ) to selectively bind BSA, and the remaining epoxy groups were reacted with ethanolamine to reduce nonselective adsorption of BSA. The resultant anion-exchange porous hollow-fiber membrane is referred to as a DEA-EA fiber. (3) Multilayer binding of BSA onto the anion-exchange porous hollow-fiber membrane: The DEA-EA fiber was set in an I-configuration with one end connected to a syringe infusion pump and the other end sealed. A 2 mg-BSA/mL Tris-HCl buffer solution (pH 8) was forced to permeate radially outward through the pores, the surfaces of which were covered with the DEA-group-containing polymer chains, at a transmembrane pressure of 0.1 MPa. The amount of BSA bound,  $q$ , was calculated by integrating the concentration difference between the feed and the effluent.

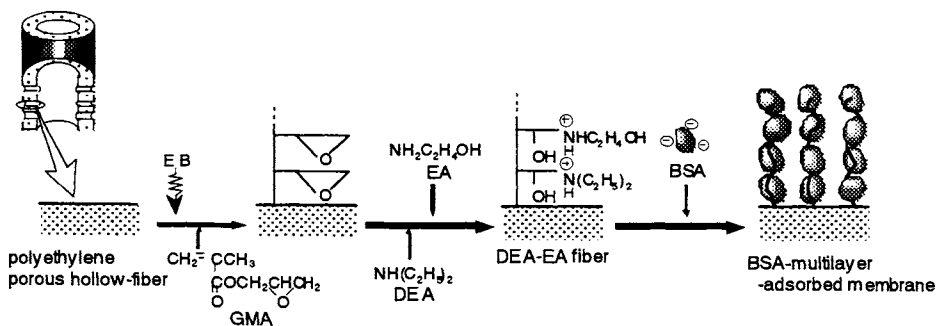


Figure 12 Preparation scheme of a BSA-multilayered porous hollow-fiber membrane.

A DEA group was appended onto a polyethylene porous hollow-fiber membrane with a density of 2.2 mmol per gram of the resultant DEA-EA fiber. The inner and outer diameters of the hollow fiber were 2.4 and 4.4 mm, respectively. The liquid permeability, i.e., the permeation rate per unit of inside surface area, of the DEA-EA fiber for the buffer was maintained at 50% of that of the original hollow fiber. Volume swelling of the porous hollow fiber accompanied by graft polymerization prevented the graft chains from filling the pores.

During permeation of BSA in the Tris-HCl buffer, 190 mg of BSA per gram of the membrane was bound to the DEA-EA fiber due to the anion-exchange interaction of BSA with the graft chains. This protein-binding capacity was equivalent to four times the theoretical monolayer-binding capacity (48 mg/g). A uniform distribution of the DEA groups introduced and the BSA adsorbed across the membrane was ascertained by observing the uniform distribution of chloride and sulfur, respectively, by X-ray microanalysis. The BSA-multilayer-adsorbed porous hollow-fiber membrane exhibited 50% of the flux of the DEA-EA fiber for the buffer. This decrease in the liquid permeability reflects the multilayer adsorption of BSA into the graft chains extending from the pore surface toward the pore interior.

The BSA-multilayer-adsorbed porous hollow-fiber membrane was mounted on a single hollow-fiber module, as shown in Figure 13. The module size was 5 mm in inner diameter and 40 mm in effective length. The module was incorporated into a liquid chromatography system. A sample of 20  $\mu$ L of 0.6 mM DL-tryptophan solution was loaded into the BSA-four-layer-adsorbed porous hollow-fiber module at a flow rate of 0.5 mL/min of a Tris-HCl buffer as the mobile phase. The separation

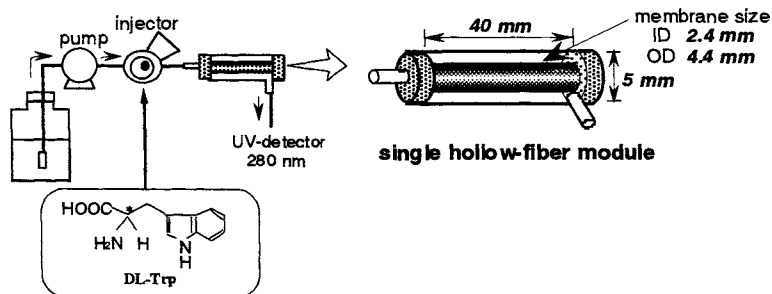


Figure 13 Experimental apparatus for chromatography using a single hollow-fiber module.

factor is defined as

$$\text{Separation factor} = (t_L - t_0) / (t_D - t_0) \quad (4)$$

where  $t_D$  and  $t_L$  are the retention times of D- and L-tryptophan in the chromatogram, respectively.  $t_0$  is the void time of the membrane module. DL-tryptophan was resolved with a separation factor of 6.6, as shown in Figure 14. In contrast, a BSA-monolayer-adsorbed porous hollow-fiber module exhibited a lower separation factor of 2.9. BSA adsorbed in the multilayers by the polymer chains grafted onto the pore surface worked well to prolong the retention time of L-tryptophan. The separation factor of DL-tryptophan for BSA immobilized on various supports under different mobile-phase conditions reported previously ranged from 1.2 to 14. The separation factor obtained with the BSA-multilayer-adsorbed porous hollow-fiber membrane ensures a satisfactory resolution.

The separation factor was determined at various flow rates of the mobile phase ranging from 0.3 to 3 mL/min, i.e., the residence times ranged from 4.6 to 46 s in the BSA-multilayer-adsorbed porous hollow-fiber membrane. As a result, the separation factor was constant

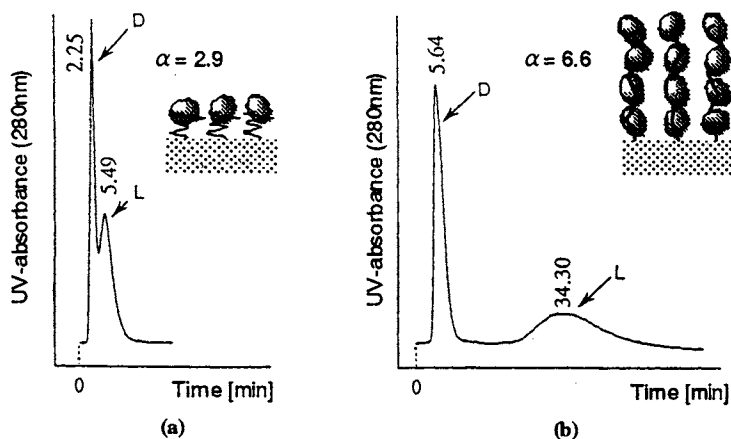


Figure 14 Chiral separation of DL-tryptophan during the permeation of a racemic solution through a BSA-multilayered porous hollow-fiber membrane.

- (a) membrane containing 2-hydroxyethylamino group  
(degree of multilayer binding: monolayer)
- (b) membrane containing both diethylamino and 2-hydroxyethylamino groups  
(degree of multilayer binding: four layers)



irrespective of the flow rate because diffusional mass-transfer resistance of the target molecule (tryptophan) to the recognition site of the chiral ligand (BSA) was negligible. This is a favorable attribute for scaling up for the chiral separation of racemic chemicals. Therefore, a separation at high resolution and high flow rate was realized by injecting racemic tryptophan to the BSA-multilayer-adsorbed porous hollow-fiber membrane. No leakage of BSA was detected after twenty injections. Multilayer binding of the proteins by the graft chain was observed for various proteins such as lactoglobulin [8], bovine gamma globulin [8], and urease [11]; immobilization of other proteins will enable chiral separations of other chiral molecules at a high resolution and a high flow rate.

### 2.3. Immobilization of enzymes

Extensive studies on bioreactors that use immobilized enzymes have been reported [74]. When immobilized onto solid supports, most enzymes are arranged in the interior of the supports; in place of the merit of requiring no recovery of the enzymes from the products, immobilization can cause diffusional mass-transfer resistance. To overcome this dilemma, the immobilization of enzymes on porous membranes is effective in that the enzyme can be transported to the site of immobilization by convective flow of the substrate solution through the pores. A method of appending various functionalities such as ion-exchange groups, hydrophobic and affinity ligands onto the porous membranes of flat-sheet and hollow-fiber membranes by radiation-induced graft polymerization and subsequent chemical modifications has been developed; this method is applicable to the immobilization of the enzymes.

Abed packed with Sephadex beads immobilizing aminoacylase capable of hydrolyzing L-amino acid derivatives has been commercialized to produce L-amino acids [75]. A method of producing an L-amino acid at a high throughput using an aminoacylase-multilayered porous hollow-fiber membrane was proposed [28]. The principle of the method is illustrated in Figure 15. Aminoacylase was immobilized onto anion-exchange porous hollow-fiber membranes, the pores of which were surrounded by the anion-exchange-group-containing graft chains, via ion-exchange adsorption and subsequent cross-linking.

First, a commercially available porous hollow-fiber membrane was used as a trunk polymer for grafting. This hollow fiber had inner and outer diameters of 1.2 and 2.2 mm, respectively, with an average pore diameter of 240 nm and a porosity of 70%. The trunk polymer was irradiated with an electron beam at a dose of 200 kGy and immersed in

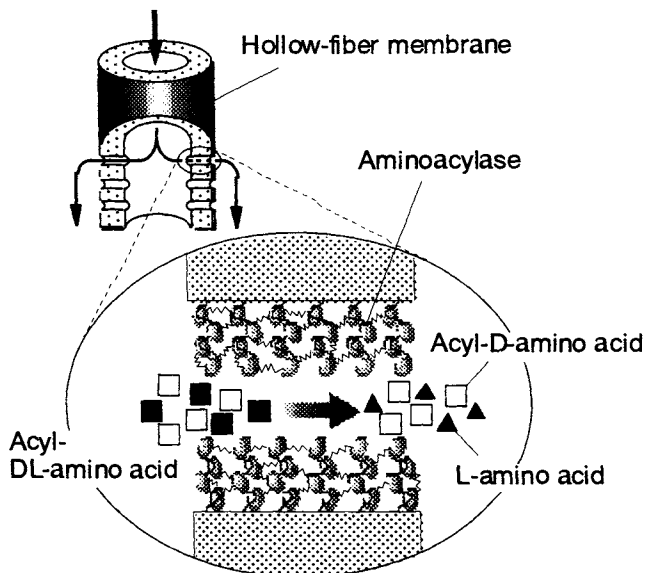


Figure 15 Enzymatic hydrolysis using porous enzyme-multilayered hollow-fiber membrane.

10 (v/v)% glycidyl methacrylate(GMA)/methanol solution at 313 K for 12 minutes. Graft chains were appended uniformly onto a pore surface across the membrane thickness. After graft polymerization, the weight of the poly-GMA chains as graft chains was two times that of the trunk polymer.

Second, the GMA-grafted hollow fiber was immersed in 50 (v/v)% aqueous solution of diethylamine at 303 K for 1 h and subsequently in ethanolamine at 303 K for 6 h. Sixty mole% of the epoxy groups was converted to diethylamino groups to enhance the anion-exchange adsorption of the enzyme, and subsequently, ethanolamine was added to the remaining epoxy groups to reduce the nonselective adsorption of proteins. The resultant hollow fiber was referred to as a DEA-EA fiber.

Third, aminoacylase was adsorbed in multilayers based on an ion-exchange interaction with the graft chains extending from the pore surface due to their electrostatic repulsion. A solution of aminoacylase dissolved in Tris-HCl buffer (pH 8.0) was fed to the inside surface of the DEA-EA fiber. The solution was allowed to permeate through the pores across the membrane thickness at a constant flow rate of 60 mL/h. From the determination of the change in enzyme concentration of the effluent with effluent volume penetrating the hollow fiber, the amount of enzyme adsorbed was calculated as 190 mg per gram

of the DEA-EA fiber. This value was converted to the degree of multilayer binding of 15, by dividing the amount of adsorbed enzyme by the theoretical monolayer binding capacity.

Finally, aminoacylase adsorbed in multilayers after ion-exchange interaction with the graft chains was cross-linked with glutaraldehyde to prevent the leakage of the enzyme induced by a change in pH of the external liquid. The aminoacylase-adsorbed hollow fiber was immersed in 0.05 wt% glutaraldehyde solution to cross-link the enzymes captured by the graft chains. The adsorbed aminoacylase had a degree of cross-linking of 94%. In other words, 6% of the adsorbed aminoacylase, i.e., 10 mg per gram of the hollow fiber, was eluted with 0.5 M NaCl. As a result, the aminoacylase-multilayered porous hollow fiber was prepared at an immobilization density of 180 mg per gram of hollow fiber.

The permeability of the resultant aminoacylase-immobilized hollow fiber was 80% that of the trunk polymer. This is favorable for a high rate of permeation of the substrate solution at a low permeation pressure across the enzyme-immobilized porous hollow fiber; for example, a permeation pressure of 0.01 MPa provided a space velocity of  $50 \text{ h}^{-1}$ , which was about tenfold that of a bed packed with enzyme-immobilized beads.

The acetyl-DL-methionine (Ac-DL-Met) solution was allowed to permeate through the pores of the aminoacylase-immobilized hollow fiber at a flow rate ranging from 30 to 180 mL/h; the space velocity (SV), defined below, varied from 40 to  $200 \text{ h}^{-1}$ .

$$\text{SV (h}^{-1}\text{)} = (\text{flow rate}) / (\text{fiber volume including the lumen side}) \quad (5)$$

The conversion of Ac-DL-Met into L-methionine (L-Met) and the activity of the fiber were defined as

$$\text{Conversion (\%)} = 100 \frac{(\text{moles of L-Met produced})}{(\text{moles of DL-Met fed})} \quad (6)$$

$$\text{Activity (mol/L/h)} = [(\text{conversion})/100] (\text{feed conc.}) (\text{SV}) \quad (7)$$

The substrate was allowed to permeate through the pores of the hollow fiber. With these fibers, a higher productivity of L-amino acid at a lower operating pressure than achieved by other methods was demonstrated. Conversions of Ac-DL-Met to L-Met are shown in Figure 16 as a function of the SV of the Ac-DL-Met solution during permeation through the pores of the aminoacylase-immobilized porous hollow fiber. At an Ac-DL-Met concentration of 10 mM, 100% conversion was achieved by asymmetrical hydrolysis. At higher concentrations of the substrate, a higher SV resulted in a lower conversion. This can be explained by considering that at a higher SV, i.e., a shorter residence time across the hollow fiber of the Ac-DL-Met solution, the overall reaction is governed

by the intrinsic enzyme reaction of the aminoacylase captured by the graft chain and not by convective mass transport of the substrate to the graft chain. In Figure 16, the conversion reported under an identical Ac-DL-Met concentration with the enzyme immobilized onto the glass beads [76] is included; the conversion by the fiber was about threefold higher than that by the bead-packed bed.

The conversions were calculated as activities according to equation (6), and are shown in Figure 17. A much higher activity of 4.1 mol/L/h was realized using the aminoacylase-immobilized porous hollow-fiber membrane at SV of up to 200 h<sup>-1</sup> because Ac-DL-Met as a substrate was transported by convective flow through the pores to a neighboring enzyme captured by the graft chain in multilayers. In addition, a membrane thickness of about 1 mm enabled a lower flow resistance of the substrate solution than in the bead-packed bed.

The membrane of a hollow-fiber form is a convenient polymeric material in that expansion from a laboratory to a plant scale can be carried out simply by bundling the hollow fibers into a hollow-fiber membrane module [14,15]. The phenomenon of multilayer binding of the enzymes into the polymer chains grafted onto the porous hollow-fiber membrane is applicable to other enzymatic reactions at a high throughput.

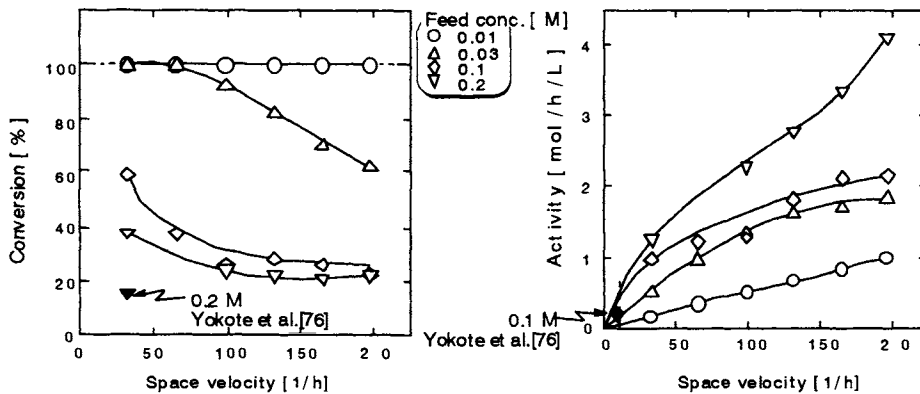


Figure 16 Conversion from acetyl-DL-methionine to L-methionine by aminoacylase-multilayered porous fiber as a function of the space velocity.

Figure 17 Effect of feed concentration and space velocity on the activity of immobilized aminoacylase.

### 3. NONWOVEN FABRICS ENABLE LARGE-SCALE URANIUM RECOVERY FROM SEAWATER

The concentration of uranium in seawater is remarkably constant at  $3.3 \text{ mg U/m}^3$ . The predominant dissolved form of uranium in seawater is the stable uranyl tricarbonate complex  $\text{UO}_2(\text{CO}_3)_3^{4-}$  [77]. The total uranium content of  $4.5 \times 10^9$  tons, dissolved in the world's oceans, is almost 1000-fold larger than terrestrial resources of reasonable concentrations. Atomic power plants continuously require uranium resources; therefore, the 4.5 billion tons of uranium in seawater will be essential for atomic power utilization.

A recovery program was begun in England in the early 1960's [78]. Extensive research on the recovery of uranium in seawater has been conducted to replace uranium locally deposited as terrestrial ore with uranium uniformly dissolved in seawater. Many methods of recovery have been suggested: coprecipitation, adsorption, ion floatation, and solvent extraction. Adsorption using solid adsorbents is promising with regard to economic and environmental impacts.

The molar concentration of uranium,  $1.4 \times 10^{-5} \text{ mol/m}^3$ , is about 1 part in  $4 \times 10^6$  of that of magnesium, which is a representative bivalent cation in seawater. Extensive efforts have been exerted to develop an adsorbent capable of separating uranium from the other elements [79-88]. At present, a resin containing an amidoxime group ( $-\text{C}(=\text{NOH})\text{NH}_2$ ), which can be prepared by reaction of cyano groups ( $-\text{CN}$ ) with hydroxylamine ( $\text{NH}_2\text{OH}$ ), is promising in view of adsorption rate, capacity, durability, and production cost.

The recovery process of uranium from seawater consists of three stages: (1) adsorption from seawater using an amidoxime resin, (2) purification of the eluate with another chelating resin, and (3) further concentration of uranium using an anion-exchange resin. Since an adsorbent is required to contact a tremendous volume of seawater in the first step, various effective contacting systems have been suggested and evaluated. The adsorption system in the recovery process of uranium from seawater can be classified with respect to three factors: (1) the shape of the adsorbent, i.e., spherical or fibrous; (2) the mode of the adsorption bed, i.e., fixed or fluidized; and (3) the method of moving the seawater, i.e., by pumping or ocean current [89-91]. The system consists of a combination of the three factors.

A recovery system for uranium in seawater using amidoxime (AO) fibers is promising in that the ocean current forces seawater to easily move through an adsorption bed charged with AO fibers. A research group at the Shikoku National Industrial Research Institute has

developed bundled AO fibers based on commercially available polyacrylonitrile fibers; the fibers exhibited a uranium adsorption rate of 2 mg U per g of fiber for 60 days of operation in a flow-through mode [92]. A research group at the Japan Atomic Energy Research Institute has proposed a method of preparing AO fibers based on polyethylene (PE) and polypropylene (PP) fibers by radiation-induced graft polymerization of acrylonitrile ( $\text{CH}_2=\text{CHCN}$ , AN) onto the fiber, followed by amidoximation [93-104].

Hydrophilization of AO adsorbents is effective in improving the uranium adsorption rate; the diffusion of uranyl tricarbonate ion, which is the predominant species of dissolved uranium in seawater, governs the overall adsorption rate of uranium. Cograftering of methacrylic acid ( $\text{CH}_2=\text{C}(\text{CH}_3)\text{COOH}$ , MAA) and 2-hydroxyethyl methacrylate ( $\text{CH}_2=\text{C}(\text{CH}_3)\text{COOCH}_2\text{CH}_2\text{OH}$ , HEMA) with AN onto PE and PP fibers was suggested as a method of enhancing the adsorption of uranium on AO adsorbents [105,106].

The preparation of hydrophilic AO fibers based on PE fibers by radiation-induced cograftering polymerization and subsequent chemical modifications is illustrated in Figure 18. PE fibers of about 30  $\mu\text{m}$  diameter were used as the trunk polymer for grafting. First, a combination of MAA with AN was cograftered onto the PE fiber using a preirradiation technique; irradiation by an electron beam was performed at a total dose of 200 kGy in nitrogen atmosphere at ambient temperature. The total concentration of the two monomers was set at 50 (w/w)% in DMSO solvent, where the weight ratio of AN to MAA in the monomer mixture ranged from 100/0 to 20/80. The degree of

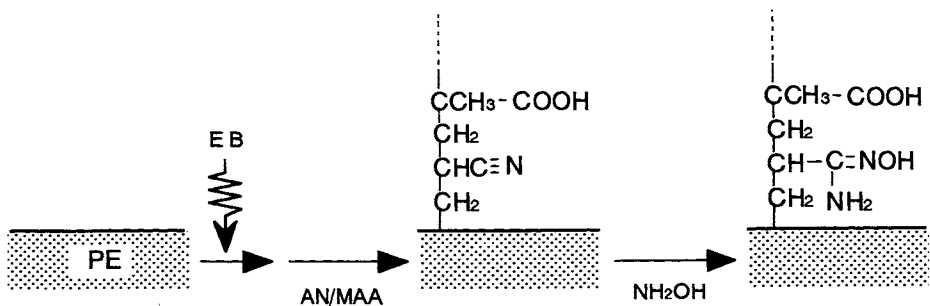


Figure 18 Preparation of hydrophilic amidoxime adsorbents by cograftering acrylonitrile and methacrylic acid.

cografting, defined below, was calculated from the weight gain due to cografting.

$$\text{Degree of cografting (\%)} = 100 (W_1 - W_0) / W_0 \quad (8)$$

Here,  $W_0$  and  $W_1$  are the weights of the trunk and the AN/MAA-cografted fiber, respectively. The resultant fibers were referred to as AN/MAA( $x/y$ , dg) fiber, where  $x/y$  and dg designate the weight ratio of AN to MAA in the monomer mixture and the degree of cografting, respectively. Time course studies of the degree of cografting are shown in Figure 19 for various weight ratios of AN to MAA in the monomer mixture for cografting, which was diluted with DMSO to a percentage of 50 (w/w)%. As the weight ratio of AN to MAA increased, the cografting rate also increased. However, the  $x/y$  weight ratios of 80/20 and 100/0 were almost identical with respect to the time course of the degree of cografting.

Second, the AN/MAA-cografted fibers were immersed in a 3 (w/v)% solution of hydroxylamine hydrochloride using 50/50 (v/v)% water/methanol as a solvent at 350 K for 45 minutes to convert the produced cyano groups to AO groups. The AO group density was evaluated from the weight gain. The fibers obtained through the amidoximation of AN/MAA( $x/y$ , dg) fibers were referred to as AO/MAA( $x/y$ , dg) fibers. The AN/MAA-cografted fibers prepared at various weight ratios of  $x/y$  were reacted with  $\text{NH}_2\text{OH}$  to convert the cyano groups into AO groups. The AO group density and water content of the resultant AO fibers are shown in Figure 20 as a function of the value of  $x/y$ . The water content of the resultant hydrophilic AO fibers was determined as

$$\text{Water content (\%)} = 100 (W_w - W_d) / W_d \quad (9)$$

where  $W_d$  and  $W_w$  are the weights of the hydrophilic AO fibers in the dry and wet states, respectively. For AO/MAA fiber, as the AN content in the monomer mixture increased, the AO group density in the fibers increased while their water content decreased.

Finally, the AO/MAA fiber was immersed in 2.5 (w/v)% KOH solution at 353 K for 1 h. Prior to the uranium adsorption experiments, the fibers were repeatedly washed with deionized water. The uranium adsorption rate of the hydrophilic AO fibers was evaluated in a submerged mode of operation in the ocean far from the coast of Japan; about 0.5 g of the AO/MAA fiber was charged in a container made of plastic mesh, which was attached to the outside of a frame (adsorption unit) made of stainless steel 30 cm in diameter and 10 cm in height, as illustrated in Figure 21. The adsorption units were submerged for 20 days 15 m below the surface of the sea located about six kilometers off the coast of Mutsu Sekine-Hama in Aomori Prefecture. The fibers

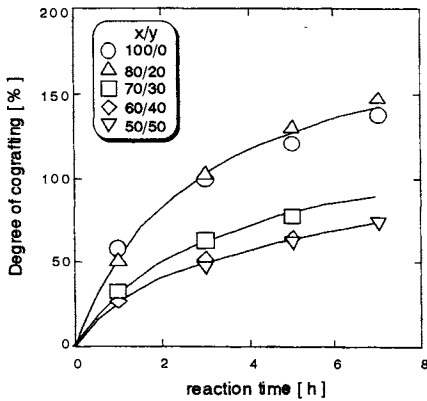


Figure 19 Cografting rate of AN/MAA for various weight ratios of AN to MAA in the monomer mixture.

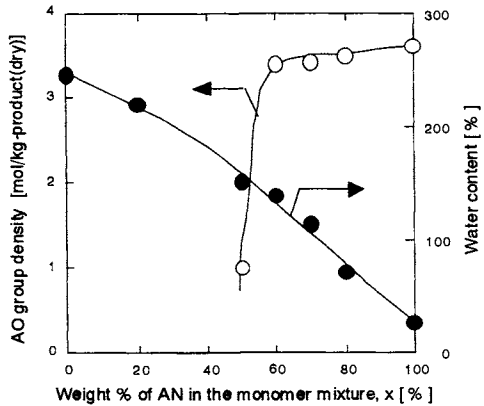


Figure 20 Amidoxime group density and water content as a function of weight % of AN in the monomer mixture.

removed from the container were immersed in 1M HCl to elute the adsorbed metals. The AO/MAA fiber adsorbed 0.75 g uranium per kg of the dry product after 40 days of contact, which was three times the amount adsorbed using the AO fiber. The MAA as a cograft monomer was found to be effective in improving the uranium adsorption rate.

Uranium adsorption onto the AO adsorbent in seawater proceeds via three steps. (1) Film diffusion: uranyl tricarbonate ion,  $\text{UO}_2(\text{CO}_3)_3^{4-}$ , as the predominant species in seawater, transfers to the external surface of the adsorbent. (2) Interior diffusion: the ion diffuses into the interior of the adsorbent through the pores formed by the polymer network. (3) Intrinsic adsorption: the uranyl species forms complexes specifically with the AO group. Overall adsorption of uranium onto the adsorbents continues until the concentration gradient induced by the complexation becomes zero. The cografting of MAA with AN is related to the second step; a higher water content of the adsorbent enhances the diffusion of  $\text{UO}_2(\text{CO}_3)_3^{4-}$  to the AO groups in the adsorbent. The AO group density for capturing uranium in seawater and the hydrophilic group density for ensuring the porosity of the AO adsorbent should be balanced to maximize the uranium adsorption rate.

The amount of uranium adsorbed in the submerged mode of operation at an ocean site for 20 days of contact is shown in Figure 22 as a function of the weight ratio of AN to MAA in the monomer mixture. The AO fibers prepared by cografting MAA with AN at a weight ratio of AN to MAA of 60/40 and subsequent amidoximation exhibited a maximum



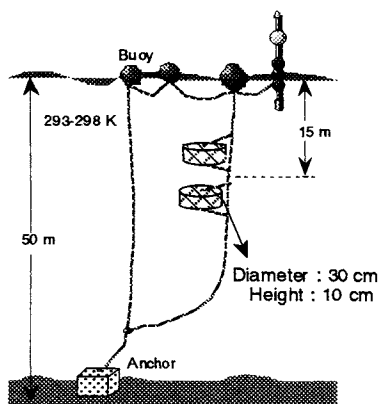


Figure 21 Experimental apparatus for uranium recovery from seawater in the submerged mode of operation at the ocean site.

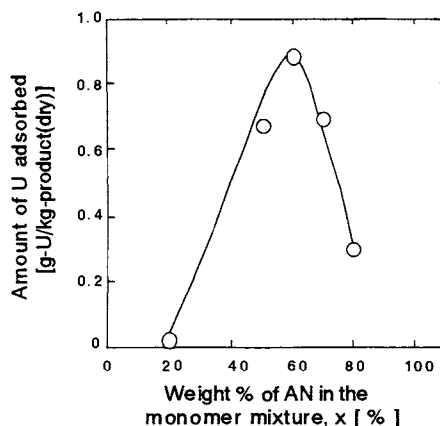


Figure 22 The amount of uranium adsorbed in the submerged mode as a function of weight % of AN in the monomer mixture.

value of 0.90 g U/kg. However, the submerged mode of operation includes some uncertainty because the temperature and velocity of the seawater vary according to weather and seawater conditions. The uranium adsorptivity of the fibrous adsorbents was ascertained in the flow-through mode in a laboratory, where the temperature and flow rate of seawater were maintained at prescribed values. A similar dependence of the amount of uranium adsorbed on  $x/y$  was observed.

#### 4. APPLICATIONS PROMOTE NEW CHARACTERIZATION OF GRAFT CHAINS

Processes of graft polymerization of vinyl monomers onto preirradiated films and nonwoven fabrics have been continuously operated on a commercial scale [1]. Radiation-induced grafting is still promising for the following reasons.

- (1) Various shapes of trunk polymers can be supplied in response to the demanded functionality; adsorbents based on porous hollow-fiber membranes and nonwoven fabrics enable high-speed recovery of target molecules and ions by utilizing convective flows through the pores of the membranes and among the fibers, respectively.
- (2) Convenient vinyl monomers are commercially available for grafting;

the use of vinyl monomers containing strongly acidic and basic groups, and reactive monomers containing epoxy groups simplifies the preparation scheme of functional polymeric materials.

(3) Many facilities for the irradiation of electron beams and gamma rays have been constructed; therefore, radicals can be produced on trunk polymers with economical feasibility.

New applications have been suggested to highlight the features of the grafted polymer branches.

(1) Sulfonic acid groups on the graft chains act as acidic catalysts for sucrose hydrolysis; their activity is identical to that of sulfuric acid [107,108]. This demonstrates the flexibility of the graft chains.

(2) Positively charged groups on the graft chains capture microbial cells (*Staphylococcus aureus*) at a reaction-rate constant of about 1000-fold that of the same group immobilized on a conventional polymer network [109-111].

(3) Silver ions immobilized on the graft chains form complexes with polyunsaturated fatty acid (PUFA) ethyl esters such as docosahexaenoic acid (DHA) ethyl ester [112-114].

At present, a definite characterization of the graft chains prepared by radiation-induced grafting is difficult because the graft chain could not be isolated from the chemically stable trunk polymer. Determinations of the molecular weight distribution (MWD) of the graft chains, and their location in the trunk polymer matrix help to tailor high-performance polymeric materials for separation and reaction. Direct characterization, i.e., determination of MWD of the graft chains, was possible only in a model combination of polymethyl methacrylate (MMA) and a cellulose triacetate membrane, where the poly-MMA chains, the grafted chains could be isolated by dissolving the cellulose triacetate, the trunk polymer, in concentrated sulfuric acid [115]. However, a satisfactory isolation of the graft chains for practical combinations has not been achieved. Using the fluorescence probe technique, an indirect characterization of the graft chains was suggested; an amino-group-containing graft chain was labeled with a dansyl group which served as a fluorescence probe, and the rotational diffusion coefficients of the dansyl probe were determined to evaluate the local mobility of the graft chain [116,117].

Insufficient characterization of the graft chains does not mean unsatisfactory materials with respect to specific functionality. The high performance of functional polymeric materials prepared by radiation-induced graft polymerization and subsequent chemical modifications has been verified experimentally. Moreover, phenomena such as multilayer binding of proteins to the graft chains [7-11,16-18] and

decrease in permeability of water through the pores immobilizing the graft chains [19,41] can provide a semiquantitative image of the grafted polymer branch. Both preparation and characterization of the graft chains should be clarified.

## ACKNOWLEDGEMENT

We thank Tomomi Kawai and Tsuyoshi Yoshida for preparing the schematic illustrations.

## REFERENCES

1. K. Saito and T. Sugo, *Cats and Graft Polymerization*, 1995, Maruzen, Tokyo, Japan.
2. T. Hori, M. Hashino, A. Omori, T. Matsuda, K. Takasa and K. Watanabe, *Synthesis of Novel Microfilters with Ion-Exchange Capacity and Its Application to Ultrapure Water Production System*, *J. Membrane Sci.*, 132 (1997) 203.
3. H. Iwata, K. Saito, S. Furusaki, T. Sugo and J. Okamoto, *Adsorption Characteristics of an Immobilized Metal Affinity Membrane*, *Biotechnol. Prog.*, 7 (1991) 412.
4. M. Kim, K. Saito, S. Furusaki, T. Sugo and I. Ishigaki, *Adsorption and Elution of Bovine Gamma-Globulin Using an Affinity Membrane Containing Hydrophobic Amino Acids as Ligands*, *J. Chromatogr.*, 585 (1991) 45.
5. M. Kim, K. Saito, S. Furusaki, T. Sugo and I. Ishigaki, *Protein Adsorption Capacity of a Porous Phenylalanine-Containing Membrane Based on a Polyethylene Matrix*, *J. Chromatogr.*, 586 (1991) 27.
6. H. Shinano, S. Tsuneda, K. Saito, S. Furusaki and T. Sugo, *Ion Exchange of Lysozyme during Permeation across a Microporous Sulfopropyl-Group-Containing Hollow Fiber*, *Biotechnol. Prog.*, 9 (1993) 193.
7. S. Tsuneda, H. Shinano, K. Saito, S. Furusaki and T. Sugo, *Binding of Lysozyme onto a Cation-Exchange Microporous Membrane Containing Tentacle-Type Grafted Polymer Branches*, *Biotechnol. Prog.*, 10 (1994) 76.
8. S. Tsuneda, K. Saito, S. Furusaki and T. Sugo, *High-Throughput Processing of Proteins Using a Porous and Tentacle Anion-Exchange Membrane*, *J. Chromatogr. A*, 689 (1995) 211.
9. S. Tsuneda, H. Kagawa, K. Saito and T. Sugo, *Hydrodynamic Evaluation of Three-Dimensional Adsorption of Protein to a Polymer Chain Grafted onto a Porous Substrate*, *J. Colloid Interface Sci.*, 176 (1995) 95.
10. S. Tsuneda, K. Saito, T. Sugo and K. Makuuchi, *Protein Adsorption Characteristics of Porous and Tentacle Anion-Exchange Membrane Prepared by Radiation-Induced Graft Polymerization*, *Radiat. Phys. Chem.*, 46 (1995) 239.
11. S. Matoba, S. Tsuneda, K. Saito and T. Sugo, *Highly Efficient Enzyme Recovery Using a Porous Membrane with Immobilized Tentacle Polymer Chains*, *Bio/Technology*, 13 (1995) 795.

12. N. Kubota, S. Miura, K. Saito, K. Sugita, K. Watanabe and T. Sugo, Comparison of Protein Adsorption by Anion-Exchange Interaction onto Porous Hollow-Fiber Membrane and Gel Bead-Packed Bed, *J. Membrane Sci.*, 117 (1996) 135.
13. N. Kubota, Y. Konno, S. Miura, K. Saito, K. Sugita, K. Watanabe and T. Sugo, Comparison of Two Convection-Aided Protein Adsorption Methods Using Porous Membranes and Perfusion Beads, *Biotechnol. Prog.*, 12 (1996) 869.
14. N. Kubota, Y. Konno, S., K. Saito, K. Sugita, K. Watanabe and T. Sugo, Module Performance of Anion-Exchange Porous Hollow-Fiber Membranes for High-Speed Protein Recovery, *J. Chromatogr. A*, 782 (1997) 159.
15. N. Kubota, Y. Konno, K. Saito, K. Sugita, K. Watanabe and T. Sugo, Protein Adsorption and Elution Performances of Modules Consisting of Porous Anion-Exchange Hollow-Fiber Membranes, *Maku*, 22 (1997) 105.
16. N. Sasagawa, K. Saito, K. Sugita, T. Ogasawara and T. Sugo, Adsorption Characteristics of Binary Proteins onto Anion-Exchange Porous Hollow-Fiber Membrane, *J. Ion Exchange*, 9 (1998) 74.
17. N. Sasagawa, K. Saito, K. Sugita, Kunori and T. Sugo, Ionic Crosslinking of SO<sub>3</sub>H-Group-Containing Graft Chains Helps to Capture Lysozyme in a Permeation Mode, *J. Chromatogr. A*, 848 (1999) 161.
18. K. Saito, S. Tsuneda, M. Kim, N. Kubota, K. Sugita and T. Sugo, Radiation-Induced Graft Polymerization is the Key to Develop High-Performance Functional Materials for Protein Purification, *Radiat. Phys. Chem.*, 54 (1999) 517.
19. T. Kawai, K. Saito, K. Sugita and T. Sugo, Extension and Shrinkage of Polymer Brush Grafted onto Porous Membrane Induced by Protein Binding, *Macromolecules*, 33 (2000) 1306.
20. N. Kubota, M. Kounosu, K. Saito, K. Sugita, K. Watanabe and T. Sugo, Preparation of a Hydrophobic Porous Membrane Containing Phenyl Groups and Its Protein Adsorption Performance, *J. Chromatogr. A*, 718 (1995) 27.
21. N. Kubota, M. Kounosu, K. Saito, K. Sugita, K. Watanabe and T. Sugo, Control of Phenyl-Group Site Introduced on the Graft Chain for Hydrophobic Interaction Chromatography, *Reactive Polym.*, 29 (1996) 115.
22. N. Kubota, M. Kounosu, K. Saito, K. Sugita, K. Watanabe and T. Sugo, Protein Adsorption and Elution Performances of Porous Hollow-Fiber Membranes Containing Various Hydrophobic Ligands, *Biotechnol. Prog.*, 13 (1997) 89.
23. N. Kubota, M. Kounosu, K. Saito, K. Sugita, K. Watanabe and T. Sugo, Repeated Use of a Hydrophobic Ligand-Containing Porous Membrane for Protein Recovery, *J. Membrane Sci.*, 134 (1997) 67.
24. M. Nakamura, S. Kiyohara, K. Saito, K. Sugita and T. Sugo, Chiral Separation of DL-Tryptophan Using Porous Membranes Containing Multilayered Bovine Serum Albumin Crosslinked with Glutaraldehyde, *J. Chromatogr. A*, 822 (1998) 53.
25. I. Koguma, M. Nakamura, K. Saito, K. Sugita, S. Kiyohara and T. Sugo, Chiral Separation of DL-Tryptophan Using Bovine-Serum-Albumin-Multilayered Porous Hollow-Fiber Membrane, *Kagaku Kogaku Ronbunshu*, 24 (1998) 458.

26. S. Kiyohara, M. Nakamura, K. Saito, K. Sugita and T. Sugo, Binding of DL-Tryptophan to BSA Adsorbed in Multilayers by Polymer Chains Grafted onto a Porous Hollow-Fiber Membrane in a Permeation Mode, *J. Membrane Sci.*, 152 (1999) 143.
27. M. Nakamura, S. Kiyohara, K. Saito, K. Sugita and T. Sugo, High Resolution of DL-Tryptophan at High Flow Rates Using a Bovine Serum Albumin-Multilayered Porous Hollow-Fiber Membrane, *Anal. Chem.*, 71 (1999) 1323.
28. M. Nakamura, K. Saito, K. Sugita and T. Sugo, Application of Crosslinked-Aminoacylase-Multilayered Membranes to Bioreactor, *Maku*, 23 (1998) 316.
29. K. Saito, T. Kaga, H. Yamagishi, S. Furusaki, T. Sugo and J. Okamoto, Phosphorylated Hollow Fibers Synthesized by Radiation Grafting and Cross-Linking, *J. Membrane Sci.*, 43 (1989) 131.
30. K. Saito, M. Ito, H. Yamagishi, S. Furusaki, T. Sugo and J. Okamoto, Novel Hollow-Fiber Membrane for the Removal of Metal Ion during Permeation: Preparation by Radiation-Induced Cograftering of a Cross-Linking Agent with Reactive Monomer, *Ind. Eng. Chem. Res.*, 28 (1989) 1808.
31. S. Tsuneda, K. Saito, S. Furusaki, T. Sugo and J. Okamoto, Metal Collection Using Chelating Hollow-Fiber Membrane, *J. Membrane Sci.*, 58 (1991) 221.
32. H. Yamagishi, K. Saito, S. Furusaki, T. Sugo and I. Ishigaki, Introduction of a High-Density Chelating Group into a Porous Membrane without Lowering the Flux, *Ind. Eng. Chem. Res.*, 30 (1991) 2234.
33. S. Konishi, K. Saito, S. Furusaki and T. Sugo, Sorption Kinetics of Cobalt in Chelating Porous Membrane, *Ind. Eng. Chem. Res.*, 31 (1992) 2722.
34. S. Konishi, K. Saito, S. Furusaki and T. Sugo, Binary Metal-Ion Sorption during Permeation through Chelating Porous Membranes, *J. Membrane Sci.*, 111 (1996) 1.
35. G.-Q. Li, S. Konishi, K. Saito and T. Sugo, High Collection Rate of Pd in Hydrochloric Acid Medium Using Chelating Microporous Membrane, *J. Membrane Sci.*, 95 (1994) 63.
36. G.-Q. Li, S. Konishi, K. Saito, S. Furusaki, T. Sugo and K. Makuuchi, Collection of Palladium Using an Ethylenediamine-Immobilized Chelating Microporous Membrane, *Maku*, 20 (1995) 224.
37. M. Kim, K. Saito, S. Furusaki, T. Sugo and J. Okamoto, Synthesis of New Polymers Containing Tannin, *J. Appl. Polym. Sci.*, 39 (1990) 855.
38. M. Kim, K. Saito, S. Furusaki and T. Sugo, Comparison of BSA Adsorption and Fe Sorption to the Diol Group and Tannin Immobilized onto a Microfiltration Membrane, *J. Membrane Sci.*, 85 (1993) 21.
39. M. Kim, K. Saito, S. Furusaki, T. Sugo and J. Okamoto, Water Flux and Protein Adsorption of a Hollow Fiber Modified with Hydroxyl Groups, *J. Membrane Sci.*, 56 (1991) 289.
40. M. Kim, J. Kojima, K. Saito, S. Furusaki and T. Sugo, Reduction of Nonselective Adsorption of Proteins by Hydrophilization of Microfiltration Membranes by Radiation-Induced Grafting, *Biotechnol. Prog.*, 10 (1994) 114.
41. S. Tsuneda, K. Saito, S. Furusaki, T. Sugo and I. Ishigaki, Water/ Acetone Permeability of Porous Hollow-Fiber Membrane Containing Diethylamino Groups on the Grafted Polymer Branches, *J. Membrane Sci.*, 71 (1992) 1.

42. Kim, M. Sasaki, K. Saito, K. Sugita and T. Sugo, Protein Adsorption Characteristics of a Sulfonic-Acid-Group-Containing Nonwoven Fabric, *Biotechnol. Prog.*, 14 (1998) 661.
43. S. Sugiyama, S. Tsuneda, K. Saito, S. Furusaki, T. Sugo and K. Makuuchi, Attachment of Sulfonic Acid Groups to Various Shapes of PE, PP and PTFE by Radiation-Induced Graft Polymerization, *Reactive Polym.*, 21 (1993) 187. M.
44. K. Saito, S. Yamada, S. Furusaki, T. Sugo and J. Okamoto, Characteristics of Uranium Adsorption by Amidoxime Membrane Synthesized by Radiation-Induced Graft Polymerization, *J. Membrane Sci.*, 34 (1987) 307.
45. K. Saito, T. Hori, S. Furusaki, T. Sugo and J. Okamoto, Porous Amidoxime-Group-Containing Membrane for the Recovery of Uranium from Seawater, *Ind. Eng. Chem. Res.*, 26 (1987) 1977.
46. S. Tsuneda, K. Saito, S. Furusaki, T. Sugo and K. Makuuchi, Simple Introduction of Sulfonic Acid Group onto Polyethylene by Radiation-Induced Cograftering of Sodium Styrenesulfonate with Hydrophilic Monomers, *Ind. Eng. Chem. Res.*, 32 (1993) 1464.
47. W. Lee, K. Saito, S. Furusaki, T. Sugo and K. Makuuchi, Design of Urea-Permeable Anion-Exchange Membrane by Radiation-Induced Graft Polymerization, *J. Membrane Sci.*, 81 (1993) 295.
48. S. Tsuneda, K. Saito, H. Mitsuhashi and T. Sugo, Novel Ion-Exchange Membranes for Electrodialysis Prepared by Radiation-Induced Graft Polymerization, *J. Electrochem. Soc.*, 142 (1995) 3659.
49. W. Lee, A. Shibasaki, K. Saito, K. Sugita, K. Okuyama and T. Sugo, Proton Transport through Polyethylene-Tetrafluoroethylene-Copolymer-Based Membrane Containing Sulfonic Acid Group Prepared by RIGP, *J. Electrochem. Soc.*, 143 (1996) 2795.
50. A. Katakai, T. Sugo and K. Makuuchi, Water Selective Separation of Ethanol-Water Mixture through Acrylic Acid Grafted Membrane Prepared by Radiation Grafting, *Nippon Kagaku Kaishi*, (1994) 68.
51. K. Sunaga, M. Kim, K. Saito and K. Sugita and T. Sugo, Characteristics of Porous Anion-Exchange Membranes Prepared by Cograftering of Glycidyl Methacrylate with Divinyl Benzene, *Chem. Mater.*, in press.
52. H. Yamagishi, K. Saito, S. Furusaki, T. Sugo and J. Okamoto, Permeability of Methyl Methacrylate Grafted Cellulose Triacetate Membrane, *Chem. Mater.*, 2 (1990) 705.
53. H. Yamagishi, K. Saito, S. Furusaki, T. Sugo and J. Okamoto, Comparison of Simultaneous and Preirradiation Grafting of Methyl Methacrylate onto a Porous Membrane, *Chem. Mater.*, 3 (1991) 987.
54. W. Lee, T. Oshikiri, K. Saito, K. Sugita and T. Sugo, Comparison of Formation Site of Graft Chain between Nonporous and Porous Films Prepared by RIGP, *Chem. Mater.*, 8 (1996) 2618.
55. T. Ohkawara and K. Saito, Evaluation of Performance of Pulp-Ball-Based Deodorants, *Kankyo Gijyutsu*, 22 (1993) 272.
56. H. Yamagishi, K. Saito, S. Furusaki, T. Sugo and J. Okamoto, Effect of Vapor- and Liquid-Phase Radiation Grafting on Water Permeability of Porous Membrane, *Nippon Kagaku Kaishi*, (1988) 212.

57. K. Uezu, K. Saito, S. Furusaki, T. Sugo and I. Ishigaki, Radicals Contributing to Preirradiation Graft Polymerization onto Porous Polyethylene, *Radiat. Phys. Chem.*, 40 (1992) 31.
58. K. Kobayashi, S. Tsuneda, K. Saito, H. Yamagishi, S. Furusaki and T. Sugo, Preparation of Microfiltration Membranes Containing Anion-Exchange Groups, *J. Membrane Sci.*, 76 (1993) 209.
59. S. Kiyohara, M. Sasaki, K. Saito, K. Sugita and T. Sugo, Amino Acid Addition to Epoxy-Group-Containing Polymer Chain Grafted onto a Porous Membrane, *J. Membrane Sci.*, 109 (1996) 87.
60. K. Uezu, K. Saito, T. Sugo and S. Aramaki, Reactor of Vapor-Phase Graft Polymerization of Reactive Monomer onto Porous Hollow Fiber, *AIChE J.*, 42 (1996) 1095.
61. S. Kiyohara, M. Kim, Y. Toida, K. Saito, K. Sugita and T. Sugo, Selection of a Precursor Monomer for the Introduction of Affinity Ligands onto a Porous Membrane by Radiation-Induced Graft Polymerization, *J. Chromatogr. A.*, 758 (1997) 209.
62. S. Kiyohara, M. Sasaki, K. Saito, K. Sugita and T. Sugo, Radiation-Induced Grafting of Phenylalanine-Containing Monomer onto a Porous Membrane, *Reactive Polym.*, 31 (1996) 103.
63. J. Kalal, F. Svec and V. Marousek, Reaction of Epoxide Groups of Glycidyl Methacrylate Copolymers, *J. Polym. Sci.*, 47 (1974) 155.
64. Y. Iwakura, T. Kurosaki, N. Ariga and T. Ito, Copolymerization of Methyl Methacrylate with Glycidyl Methacrylate and the Reaction of Copolymer with Amines, *Makromol. Chem.*, 97 (1966) 128.
65. M. Kim, S. Kiyohara, S. Konishi, S. Tsuneda, K. Saito and T. Sugo, Ring-Opening Reaction of Poly-GMA Chain Grafted onto a Porous Membrane, *J. Membrane Sci.*, 117 (1996) 33.
66. S. Brandt, R. A. Goffe, S. B. Kessler, J. L. O'Connor and S. E. Zale, Membrane-Based Affinity Technology for Commercial Scale Purification, *Bio/Technology*, 6 (1988) 779.
67. W. Muller, New Ion Exchangers for the Chromatography of Biopolymers, *J. Chromatogr.*, 510 (1990) 133.
68. T. B. Tennikova, M. Bleha, F. Svec, T. V. Almazova and B. G. Belenkii, High-Performance Membrane Chromatography of Proteins. A Novel Method of Protein Separation, *J. Chromatogr.*, 555 (1991) 97.
69. T. Shibata, I. Okamoto and K. Ishii, Chromatographic Optical Resolution on Polysaccharides and Their Derivatives, *J. Liq. Chromatogr.*, 9 (1986) 313.
70. W. H. Pirkle, J. M. Finn, J. L. Schreiner and B. C. Hamper, A Widely Useful Chiral Stationary Phase for the High-Performance Liquid Chromatography Separation of Enantiomers, *J. Am. Chem. Soc.*, 103 (1981) 3964.
71. S. Allenmark, Optical Resolution by Liquid Chromatography on Immobilized Bovine Serum Albumin, *J. Liq. Chromatogr.*, 9 (1986) 425.
72. J. Haginaka, C. Seyama and N. Kanasugi, The Absence of Chiral Recognition Ability in Ovomuroid: Ovoclycoprotein-Bonded HPLC Stationary Phases for Chiral Recognition, *Anal. Chem.*, 67 (1995) 2539.
73. H. B. Ding, P. W. Carr and E. L. Cussler, Racemic Leucine Separation by Hollow-Fiber Extraction, *AIChE J.*, 38 (1992) 1493.

74. E. Katchalski-Katzir, Immobilized Enzymes - Learning from Past Successes and Failures, *TIBTECH*, 11 (1993) 471.
75. T. Tosa, T. Mori, N. Fuse and I. Chibata, Studies on Continuous Enzyme Reactions. IV. Preparation of a DEAE-Sephadex-Aminoacylase Column and Continuous Optical Resolution of Acyl-DL-Amino Acids, *Biotechnol. Bioeng.*, 9 (1967) 603.
76. Y. Yokote, M. Fujima, G. Shimura, S. Noguchi, K. Kimura and H. Samejima, Immobilized Aminoacylase on Porous Glass Beads, *J. Solid-Phase Biochem.*, 1 (1976) 1.
77. K. Saito and T. Miyauchi, Diffusivities of Uranium in Artificial Seawater, *Kagaku Kogaku Ronbunshu*, 7 (1981) 545.
78. R. V. Davies, J. Kennedy, R. W. McIlroy, R. Spence and K. M. Hill, Extraction of Uranium from Seawater, *Nature*, 203 (1964) 1110.
79. H. Egawa, H. Harada and T. Nonaka, Preparation of Adsorption Resins for Uranium in Seawater, *Nippon Kagaku Kaishi*, (1980) 1767.
80. H. Egawa, H. Harada and T. Shoto, Recovery of Uranium from Sea Water by the Use of Chelating Resins Containing Amidoxime Groups, *Nippon Kagaku Kaishi*, (1980) 1773.
81. N. Ogata, Review on Recovery of Uranium from Seawater. III, *Nippon Kaisui Gakkaishi*, 34 (1980) 3.
82. M. Kanno, Present Status of Study on Extraction of Uranium from Seawater, *J. Atom. Energy Soc. Japan*, 23 (1981) 36.
83. H. J. Schenk, L. Astheimer, E. G. Witte and K. Schwochau, Development of Sorbents for the Recovery of Uranium from Seawater. 1: Assessment of Key Parameters and Screening Studies of Sorber Materials, *Sep. Sci. Technol.*, 17 (1982) 1293.
84. S. Katoh, K. Sugasaka, K. Sakane, N. Takai, H. Takahashi, Y. Umezawa and K. Itagaki, Preparation of Fibrous Adsorbent Containing Amidoxime Group and Adsorption Property for Uranium, *Nippon Kagaku Kaishi*, (1982) 1449.
85. S. Katoh, K. Sugasaka, K. Sakane, N. Takai, H. Takahashi, Y. Umezawa and K. Itagaki, Enhancement of the Adsorptive Property of Amidoxime-Group-Containing Fiber by Alkaline Treatment, *Nippon Kagaku Kaishi*, (1982) 1455.
86. L. Astheimer, H. J. Schenk, E. G. Witte and K. Schwochau, Development of Sorbents for the Recovery of Uranium from Seawater. 2: The Accumulation of Uranium from Seawater by Resins Containing Amidoxime and Imidoxime Functional Groups, *Sep. Sci. Technol.*, 18 (1983) 307.
87. Y. Kobuke, I. Tabushi, T. Aoki, T. Kamaishi and I. Hagiwara, Composite Fiber Adsorbent for Rapid Uptake of Uranyl from Seawater, *Ind. Eng. Chem. Res.*, 27 (1988) 1461.
88. T. Kato, T. Kago, K. Kusakabe, S. Morooka and H. Egawa, Preparation of Amidoxime Fibers for Recovery of Uranium from Seawater, *J. Chem. Eng. Japan*, 23 (1990) 744.
89. H. Nobukawa, M. Tamehiro, M. Kobayashi, H. Nakagawa, J. Sakakibara and N. Takagi, Development of Floating Type-Extraction System of Uranium from Sea Water Using Sea Water Current and Wave Power. 1, *J. Shipbuild. Soc. Jpn.*, 165 (1989) 281.



90. H. Nobukawa, J. Michimoto, M. Kobayashi, H. Nakagawa, J. Sakakibara, N. Takagi and M. Tamehiro, Development of Floating Type-Extraction System of Uranium from Sea Water Using Sea Water Current and Wave Power. 2, *J. Shipbuild. Soc. Jpn.*, 168 (1990) 321.
91. H. Nobukawa, M. Kitamura, M. Kobayashi, H. Nakagawa, N. Takagi and M. Tamehiro, Development of Floating Type-Extraction System of Uranium from Sea Water Using Sea Water Current and Wave Power. 3, *J. Shipbuild. Soc. Jpn.*, 172 (1992) 519.
92. T. Hirotsu, N. Takagi and S. Katoh, Recovery of Uranium from Seawater, *Nippon Kaisui Gakkaishi*, 49 (1995) 202.
93. T. Hori, K. Saito, S. Furusaki, T. Sugo and J. Okamoto, Synthesis of a Hollow-Fiber Type Porous Chelating Resin Containing the Amidoime Group by Radiation-Induced Graft Polymerization for the Uranium Recovery, *Nippon Kagaku Kaishi*, (1986) 1792.
94. T. Hori, K. Saito, S. Furusaki, T. Sugo and J. Okamoto, Adsorption Equilibrium of Uranium from Seawater on Chelating Resin Containing Amidoxime Group, *Kagaku Kogaku Ronbunshu*, 13 (1987) 795.
95. T. Hori, K. Saito, S. Furusaki, T. Sugo and J. Okamoto, The Effect of Alkaline and Acidic Treatment on the Properties of Amidoxime Resin Synthesized by Radiation-Induced Graft Polymerization, *Nippon Kagaku Kaishi*, (1988) 1607.
96. K. Uezu, K. Saito, T. Hori, S. Furusaki, T. Sugo and J. Okamoto, Performance of Fixed-Bed Charged with Chelating Resin of Capillary Fiber Form for Recovery of Uranium from Seawater, *J. Atom. Energy Soc. Jpn.*, 30 (1988) 359.
97. K. Saito, K. Uezu, T. Hori, S. Furusaki, T. Sugo and J. Okamoto, Recovery of Uranium from Seawater Using Amidoxime Hollow Fibers, *AIChE J.*, 34 (1988) 411.
98. K. Uezu, K. Saito, S. Furusaki, T. Sugo and J. Okamoto, Application of Adsorption Unit Charged with Amidoxime Capillary Fibers to Recovery of Uranium from Seawater Utilizing Flow of Ocean Current, *J. Atom. Energy Soc. Jpn.*, 32 (1990) 919.
99. K. Saito, T. Yamaguchi, K. Uezu, S. Furusaki, T. Sugo and J. Okamoto, Optimum Preparation Conditions of Amidoxime Hollow Fiber Synthesized by Radiation-Induced Grafting, *J. Appl. Polym. Sci.*, 39 (1990) 2153.
100. T. Takeda, K. Saito, K. Uezu, S. Furusaki, T. Sugo and J. Okamoto, Adsorption and Elution in Hollow-Fiber-Packed Bed for Recovery of Uranium from Seawater, *Ind. Eng. Chem. Res.*, 30 (1991) 185.
101. S. Konishi, H. Yamada, K. Saito, S. Furusaki, T. Sugo and J. Okamoto, Effect of Prefiltering on Adsorption Characteristics of Uranium from Seawater, *J. Atom. Energy Soc. Jpn.*, 33 (1991) 703.
102. N. Kabay, A. Katakai, T. Sugo and H. Egawa, Preparation of Fibrous Adsorbents Containing Amidoxime Groups by Radiation-Induced Grafting and Application to Uranium Recovery from Sea Water, *J. Appl. Polym. Sci.*, 49 (1993) 599.
103. K. Sekiguchi, K. Saito, S. Konishi, S. Furusaki, T. Sugo and H. Nobukawa, Effect of Seawater Temperature on Uranium Recovery from Seawater Using Amidoxime Adsorbents, *Ind. Eng. Chem. Res.*, 33 (1994) 662.

104. K. Sekiguchi, K. Serizawa, S. Konishi, K. Saito, S. Furusaki and T. Sugo, Uranium Uptake during Permeation of Seawater through Amidoxime-Group-Immobilized Micropores, *Reactive Polym.*, 23 (1994) 141.
105. A. Katakai, N. Seko, T. Kawakami, K. Saito and T. Sugo, Adsorption of Uranium in Sea Water Using Amidoxime Adsorbents Prepared by Radiation-Induced Cograftering, *J. Atom. Energy Soc. Jpn.*, 40 (1998) 878.
106. A. Katakai, N. Seko, T. Kawakami, K. Saito and T. Sugo, Adsorption Performance in Sea Water of Amidoxime Nonwoven Fabrics Prepared by Radiation-Induced Cograftering of Acrylonitrile and Methacrylic Acid, *Nippon Kaisui Gakkaishi*, 53 (1999) 180.
107. T. Mizota, S. Tsuneda, K. Saito and T. Sugo, Hydrolysis of Methyl Acetate and Sucrose in SO<sub>3</sub>H-Group-Containing Grafted Polymer Chains Prepared by Radiation-Induced Graft Polymerization, *Ind. Eng. Chem. Res.*, 33 (1994) 2215.
108. T. Mizota, S. Tsuneda, K. Saito and T. Sugo, Sulfonic Acid Catalysts Prepared by Radiation-Induced Graft Polymerization, *J. Catalysis*, 149 (1994) 243.
109. W. Lee, S. Furusaki, K. Saito, T. Sugo and K. Makuuchi, Adsorption Kinetics of Microbial Cells onto a Novel Brush-Type Polymeric Material Prepared by Radiation-Induced Graft Polymerization, *Biotechnol. Prog.*, 12 (1996) 178.
110. W. Lee, K. Saito, S. Furusaki and T. Sugo, Capture of Microbial Cells on Brush-Type Polymeric Materials Bearing Different Functional Groups, *Biotechnol. Bioeng.*, 53 (1997) 523.
111. W. Lee, S. Furusaki, K. Saito and T. Sugo, Tailoring a Brush-Type Interface Favorable for Capturing Microbial Cells, *J. Colloid Interface Sci.*, 200 (1998) 66.
112. A. Shibasaki, Y. Irimoto, M. Kim, K. Saito, K. Sugita, T. Baba, S. Moriyama and T. Sugo, Selective Binding of DHA Ethyl Ester to Ag-Ion-Loaded Porous Hollow-Fiber Membrane, *JAOCS*, 76 (1999) 771.
113. M. Kim and K. Saito, Radiation-Induced Graft Polymerization and Sulfonation of Glycidyl Methacrylate onto Porous Hollow-Fiber Membrane with Different Pore Sizes, *Radiat. Phys. Chem.*, 57 (2000) 167.
114. M. Kim and K. Saito, Preparation of Silver-Ion-Loaded Nonwoven Fabric by Radiation-Induced Graft Polymerization, *Reactive Polym.*, 40 (1999) 275.
115. H. Yamagishi, K. Saito, S. Furusaki, T. Sugo, F. Hosoi and J. Okamoto, Molecular Weight Distribution of Methyl Methacrylate Grafted onto a Microfiltration Membrane by Radiation-Induced Graft Polymerization, *J. Membrane Sci.*, 85 (1993) 71.
116. S. Tsuneda, T. Endo, K. Saito, K. Sugita, K. Horie, T. Yamashita and T. Sugo, Local Mobility of Polymer Chain Grafted onto Polyethylene Monitored by Fluorescence Depolarization, *Chem. Phys. Letters*, 275 (1997) 203.
117. S. Tsuneda, T. Endo, K. Saito, K. Sugita, K. Horie, T. Yamashita and T. Sugo, Fluorescence Study on the Conformational Change of an Amino Group-Containing Polymer Chain Grafted onto a Polyethylene Microfiltration Membrane, *Macromolecules*, 31 (1998) 366.

## Radiation pasteurization and sterilization of food

I. A. Taub

U.S. Army Soldier and Biological Chemical Command, Natick Soldier Center,  
Natick, Massachusetts 01760-5018, United States

### 1. INTRODUCTION

The effectiveness with which irradiation enhances the safety of foods and extends their storage lifetime relates directly to the chemistry that takes place in the contaminating microorganisms, in the food itself, and in any protective packaging. This chemistry can be understood by considering separately the nature of the reactive entities formed in each major food constituent and the influence of the medium and irradiation conditions on their subsequent reactions to form stable radiolysis products. Such an understanding can be exploited to optimize the irradiation treatment and to minimize any objectionable effects.

Irradiation can be used on various foods with different objectives in mind. Table 1 lists the uses of this treatment in the United States that are approved by the Food and Drug Administration (FDA). It can affect the food biochemically and prevent sprouting or delay ripening. It can disinfest foods of insects or parasites. It has even been used to degrade certain constituents so as to improve texture or shorten cooking time. Most often, the purpose is to reduce or completely eliminate pathogenic or spoilage microorganisms. Pathogenic *Escherichia coli* O157:H7 often contaminates raw beef, poultry, and other foods, causes hemorrhagic diarrhea, and can lead to fatalities. Other contaminating pathogens, such as *Listeria monocytogenes*, *Campylobacter jejuni*, *Salmonella*, and *Staphylococcus aureus* can cause fever, vomiting, and diarrhea. If chilled fresh foods are irradiated to doses up to 4.5 kGy to destroy these nonspore-forming pathogens, they are considered *pasteurized* and must be kept refrigerated to control the growth of residual spoilage and spore-forming microorganisms. If frozen, precooked foods are irradiated to doses greater than 44 kGy, they are considered *sterilized* and can be stored at ambient temperature, since pathogenic spores of *Clostridium botulinum* and essentially all spoilage microorganisms are eliminated. The International Consultative Group on Food Irradiation (ICGFI) maintains an updated list of worldwide approved uses of food irradiation.

**Table 1**  
**Food in the U.S. currently approved for irradiation treatment**

Food	Purpose	Dose (kGy)
White potatoes	Inhibit sprouting	0.05-0.15
Papaya, carambola, litchi	Eliminate insects	0.15-0.25
Pork (fresh)	Prevent trichinosis	0.3-1.0
Fruits and vegetables	Reduce contaminants	<1.0
Meat/poultry (fresh, chilled)	Reduce microbes	<4.5
Meat/poultry (fresh, frozen)	Reduce microbes	<7.0
Dry enzymes	Reduce microbes	<10.0
Spices, herbs, seasonings	Reduce microbes	<30.0
Meat (cooked, packed, frozen)	Eliminate microbes	>44.0

To put into perspective the chemistry associated with radiation pasteurization and sterilization, the basic chemical processes occurring in the constituents of irradiated meat and poultry are considered. Major constituents include the aqueous phase, the muscle and pigment proteins, the lipid (or fat) phase, and the carbohydrates. Minor constituents include salts, vitamins, and nucleic acids. The implications for assessing the wholesomeness of irradiated products, for gaining additional regulatory approvals, and for optimizing product quality and functionality are also considered.

## 2. FUNDAMENTAL ASPECTS

The complex phenomena associated with the interaction of ionizing radiation with diverse liquids and solids, addressed in detail elsewhere in this book, are relevant and applicable to irradiated chilled or frozen foods. Specific influences of the food composition and structure directly affect the nature and reaction of the resulting free radicals formed [1]. Irradiation parameters and conditions further affect the reaction pathways of the radicals and the yield of stable products derived from them [2, 3].

### 2.1. Free radicals

Although the primary radicals formed in the sarcoplasmic fluid of the muscle tissue, in the myofibrillar proteins of the muscles, and in the lipids of the intercellular and depot fats are expected to be similar to those formed in dilute aqueous solutions, in polypeptides, and in meat triglycerides, respectively, the radical yields and reactivities are affected by density and solute concentration

effects. Diffusion out of the spurs or migration from the site of formation can be significantly impeded. Primary radicals from each of the constituents in their separate phases, whether small enough to diffuse freely or of a size to move only in a structurally constrained way, could react with each other by combination or disproportionation as well with other components or dissolved solutes by abstraction, addition, or oxidation/reduction [4]. These radical-component reactions generate secondary radicals that in systems above their glass transition temperatures react by similarly diverse and competitive pathways, leading ultimately to stable radiolysis products.

## 2.2. Dose and dose-rate effects

As a consequence of competitive pathways for radical reactions, the yield of a particular radiolysis product depends on the accumulated dose and dose rate.

If the precursor of the product is the major constituent and the product does not react with other radicals, then its yield will be linear. In some instances, a product with high reactivity toward primary radicals is formed, resulting eventually in a steady-state level of that product and in a delayed linear increase in an associated secondary product. If the precursor is a minor constituent, then the yield of the product will increase initially with dose and then level off when the precursor is depleted. The different possible yield-dose relationships and their implications for extrapolating data are discussed in earlier work [5].

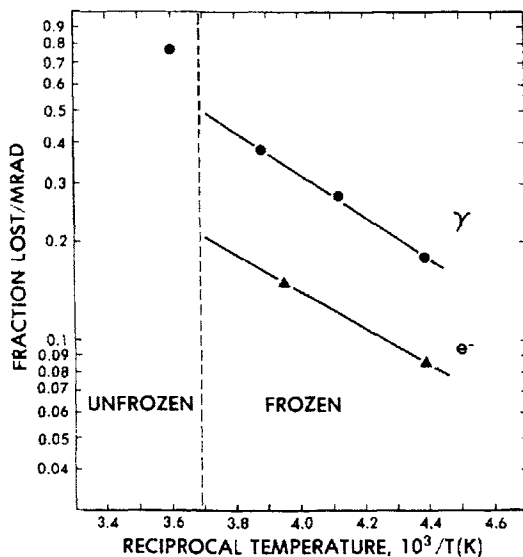


Figure 1. Fraction of thiamin lost per 10 kGy of dose as a function of reciprocal temperature. Symbols: ● - gamma ray irradiated; ▲ - electron beam irradiated. Reproduced from Thomas et al. [6] with permission.

The direction of radical reactions that involve competitive, mixed-order kinetics could be changed as dose rate is increased. Bimolecular reactions would be favored in competition with unimolecular (or pseudo-unimolecular) reactions, because of the higher instantaneous radical concentrations. This effect could be encountered in lipids and in polymers. It is responsible for the greater retention of vitamin B<sub>1</sub> (thiamin) in pork when irradiated with electron beams than when irradiated with gamma rays (Figure 1) [6].

### 2.3. Phase and temperature effects

The increase in viscosity associated with the formation of either an amorphous solid at the glass transition temperature or a crystalline lattice at the phase transition temperature will significantly reduce the mobility of most radicals. An increase in viscosity in rubbery liquids, due to decreases in temperature down towards the glass transition, will also reduce mobility. Consequently, recombination of primary radicals at the site of formation would be favored, lowering their yield. Other reaction pathways not involving diffusion and migration might also be favored. These effects are discernible and sometimes can be pronounced.

The changes in the yields of products associated primarily with the aqueous phase upon transitioning from the liquid to the frozen state are illustrative [7]. Figure 2 compares the formation or loss of several different analytes derived from reaction of primary radicals with solutes in solution either at 20°C or frozen to -40°C. For example, the formation of NH<sub>3</sub> results from reaction of e<sub>s</sub><sup>-</sup>

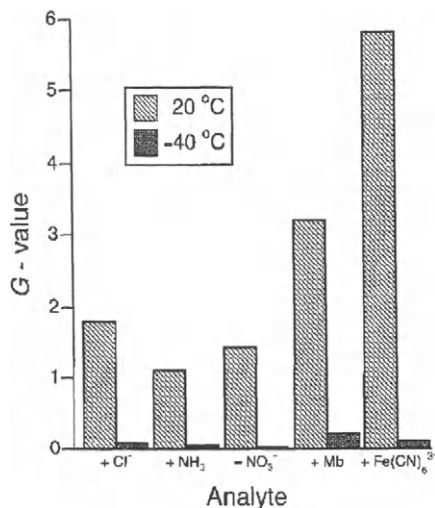


Figure 2. Comparison of *G*-values resulting from irradiation in liquid solutions at 20°C and in frozen solutions at -40°C; the abscissa indicates the formation (+) or loss (-) of the indicated analyte. Adapted from Taub [3] with permission.

with glycine, ferromyoglobin (Mb) from  $e_s^-$  reduction of the iron in ferromyoglobin, and ferricyanide ( $\text{Fe}(\text{CN})_6^{-3}$ ) from the oxidation of ferrocyanide ion by  $\text{OH}^\bullet$  in an  $\text{N}_2\text{O}$ -saturated solution.

That temperature and solute concentration can further influence reactions even in frozen solutions is illustrated by the reduction of nitrate by  $e_s^-$ . The yield of nitrite in a solution with a particularly high nitrate concentration decreases as the temperature is decreased from  $-10^\circ\text{C}$  to  $-100^\circ\text{C}$  [1, 2]. The decrease is especially pronounced below  $-30^\circ\text{C}$ .

#### 2.4. Expressing chemical changes

The concentration of a stable product in an irradiated food can be expressed using the  $G$ -value for either the product or its precursor radical and the absorbed dose. For example, the concentration of a product or products formed from the reaction of either  $e_s^-$  or  $\text{OH}^\bullet$  with a solute in the fluid aqueous phase of a food irradiated to 4.5 kGy would be 1.2 mmol/L. In contrast to other pasteurization and sterilization treatments, irradiation produces a small and generally predictable amount of chemical change.

Regulatory agencies and toxicologists, however, express chemical quantities not in molar units but in weight fractions, such as parts per million (ppm), which can be misleading with respect to product yields, as the following illustrates. The  $G$ -value for the formation of palmitic acid from tripalmitin, and presumably most fats, is 60% greater than the  $G$ -value for the formation of  $\text{H}_2$  from an aqueous phase containing organic solutes. Yet in a system containing both phases and irradiated to 3 kGy, the yield of palmitic acid (MW=256) expressed in ppm would be 123 ppm while the yield of  $\text{H}_2$  would 0.6 ppm, giving the impression that 200 times more of the former is produced than the latter.

### 3. MAJOR CONSTITUENTS

The radiolysis of a complex food matrix can be considered the sum of the radiolysis of its major constituents, which essentially represent distinct and immiscible phases. In muscle foods, the composition is primarily water (65%), protein (20%), and lipids (15%). The water phase (or sarcoplasmic fluid) contains minor constituents, including certain proteins (myoglobin and albumin), small peptides, vitamins, and salts. The proteinaceous myofibrils comprise primarily bundles of long chain myosin molecules with which are associated actin and other functional proteins, all of which are hydrated by and surrounded by the sarcoplasmic fluid. The proteins can bind certain compounds, including thiamin. The fat phase comprises distinct triglycerides, representing the esters of glycerol and different fatty acid moieties, along with small amounts of free fatty acids and soluble vitamins A and E. Carbohydrates

amount to only about 0.5% of the muscle food mass and include glycogen and glucose. They are considered here, because meat sandwiches and complete meals with meat and starch components have been irradiated. The overall chemistry of irradiated muscle foods is considered within this framework.

### 3.1. Aqueous phase

The same phenomena of primary radical formation, distribution, and reactivity, as described in other chapters, apply to the radiolysis of the aqueous phase in food, but certain distinctive factors affect their fate. One factor is that, in the case of high dose treatment for sterilization, this phase will be frozen. Another factor is the high concentration of reactive solutes. Accordingly, the yields and reactions of  $e_s^-$ ,  $H^\bullet$ , and  $OH^\bullet$  will be significantly modified, as already indicated in section 2.3. Their reactions with relevant salts, vitamins, and nucleic acids, either normally in foods or purposefully added to foods, are considered.

#### 3.1.1. Salts

Though reactions of primary radicals with sulfates and phosphates are unlikely, reactions of  $e_s^-$  with endogenous or added nitrates or nitrites, which are used in the curing of meats, could lead to their reduction. The extent would be limited by competition for  $e_s^-$  by other solutes. Reduction of nitrate, already mentioned, is illustrative. Stoichiometrically, for every two moles of  $e_s^-$  reacting with one mole of  $NO_3^-$ , one mole of  $NO_2^-$  would be formed. As explained, the extent of  $NO_2^-$  formation even in frozen systems would depend significantly on the concentration of  $NO_3^-$  and on temperature.

#### 3.1.2. Vitamins C and B<sub>1</sub>

The nutritional importance aside, the radiolysis of ascorbic acid [8] and thiamin is of interest, because it illustrates certain distinctive kinetic processes.

Ascorbic acid is highly reactive to all the primary water radicals, because of its carbonyl group and double bond. Reaction with  $e_s^-$  or  $H^\bullet$  reduces ascorbic acid to a ketyl radical, while reaction with  $OH^\bullet$  oxidizes it to the relatively unreactive tricarbonyl radical ion [9]. Aside from a possible reaction with cytochrome-c (or ferrimyoglobin), the radical ion is most likely to undergo a complex disproportionation reaction that regenerates the ascorbic acid and produces dehydroascorbic acid, which has essentially the same vitamin activity. These reactions need to be considered, because ascorbic acid is added to foods to fortify them, to facilitate curing meats, and to enhance antioxidants.

Thiamin is also reactive to the primary water radicals and, possibly to protein radicals, resulting in its conversion to product or products without vitamin activity. As Figure 1 shows, the loss of thiamin in pork decreases substantially



upon freezing and further decreases with decreasing temperature when irradiated either with electron beams or gamma rays. The loss, however, is greater with the latter than with the former. This difference is attributed to a dose-rate effect, mentioned before, that is related to a competition between radical-radical reaction and radical-thiamin reaction. The radicals could be either  $\text{OH}^\bullet$  or  $\text{P}^\bullet$ , which denotes a protein radical [6]. Similarly, more thiamin is lost in gamma ray-irradiated chicken than in electron beam-irradiated chicken [10].

### 3.1.3. *Nucleic acids*

Reactions of primary radicals with nucleic acids present in the food or in bacteria contaminating the food are relevant to the efficacy and safety of the irradiation treatment. The sequence of reactions following the formation of secondary radicals on the purine and pyrimidine bases is covered in detail in other chapters. Reactions of  $\text{OH}^\bullet$  formed in or near the DNA with either the base moieties or the sugar moiety in the backbone ultimately result in altering the bases and in breaking the two strands keeping the double helix together [11]. In the microorganism, the ability to replicate is then compromised and self-destruction takes place. In the food, the likelihood of the initial reaction with primary radicals is limited by competition with other solutes, but some base alteration might take place. With respect to implication for safety, it is unlikely that any altered bases could be incorporated into the human genome, since DNA synthesis involves enzymes acting on precursors of the bases and any incorrectly matched bases would be excised by DNA polymerases [12].

## 3.2. **Proteins**

### 3.2.1. *Myofibrillar proteins*

The radiolysis of the myofibrillar proteins in muscle leads to the formation of a generic peptide backbone radical, reflecting in effect the scission of the C-H bond in the peptide chain [13]. Figure 3 shows the ESR spectrum of the radicals formed upon irradiating a frozen suspension of myosin and actomyosin. Based on spectral analyses of spectra for diverse dipeptides, the asymmetric doublet represents contributions from many similar radicals having an unpaired electron on the carbon in the peptide chain that interacts primarily with the single proton on the neighboring carbon of the side chain amino acid moiety. The less intense bands on the wings of the spectrum represent contributions from radicals formed by the addition of  $\text{H}^\bullet$  to the benzene ring of aromatic amino acid moieties. Similar ESR spectra are obtained by irradiating a frozen suspension of myofibrils, indicating that the mechanism of peptide radical formation is not dependent on how the myosin molecules are macroscopically organized [14].

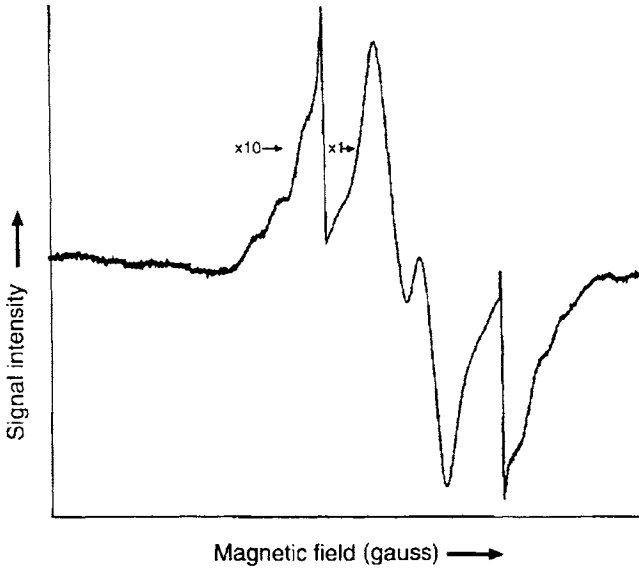


Figure 3. Electron spin resonance spectrum of suspended myosin/actomyosin irradiated to 60 kGy at  $-40^{\circ}\text{C}$  and scanned at 77 K. Reproduced from Taub et al. [13] with permission.

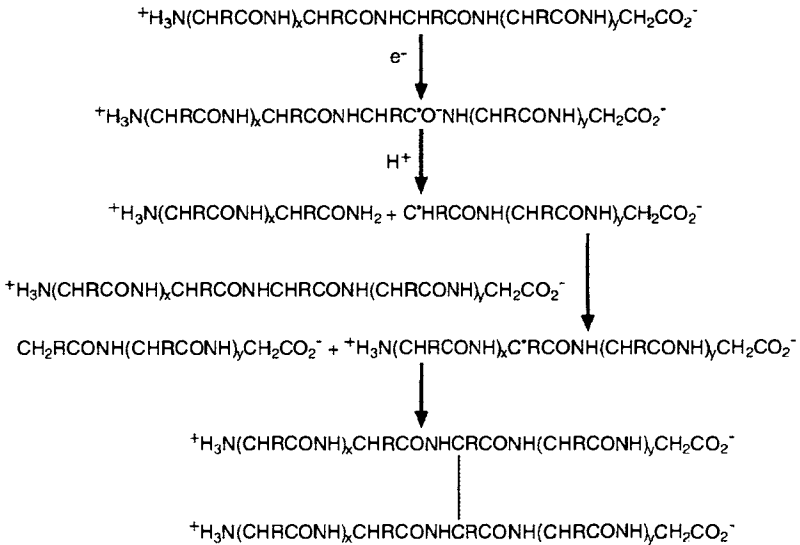


Figure 4. Mechanistic scheme for reactions in proteins initiated by solvated electron addition to the carbonyl group in the peptide backbone.

Although there are several mechanistic steps that could lead to the formation of the peptide radical following the ionization and excitation of the protein and the surrounding water, the sequence initiated by electron reaction is particularly instructive [13] and is shown in Figure 4. The first step involves the formation of an observable carbonyl anion radical that dissociates into a stable amide compound and an alkyl radical. A subsequent step involves abstraction by the alkyl radical of hydrogen from the C-H in the peptide backbone forming a stable compound and the large relatively immobile peptide backbone radical. Despite its size, this radical will react bimolecularly very slowly at  $-10^{\circ}\text{C}$  (Figure 5), but very rapidly upon thawing either to dimerize or to disproportionate. The dimerization produces a higher molecular weight, crosslinked myosin, while the disproportionation regenerates a stable myosin and produces an imine, which upon hydrolysis of the  $\text{N}=\text{C}$  linkage leads to chain scission.

Reactions initiated by  $\text{H}^{\bullet}$  and  $\text{OH}^{\bullet}$  would lead to these and other radicals.  $\text{H}^{\bullet}$  could react at the backbone C-H and at the carbonyl group, forming the peptide radical, but is more likely to add to aromatic or heterocyclic amino acid moieties, forming side chain radicals.  $\text{OH}^{\bullet}$  could also react by abstraction or, more likely, by addition. The formation of addition radicals facilitates crosslinking through the side chains. Studies with polyphenylalanine peptides confirm such crosslinking and show how crosslinked products with and without hydroxyl groups can be produced [15, 16].

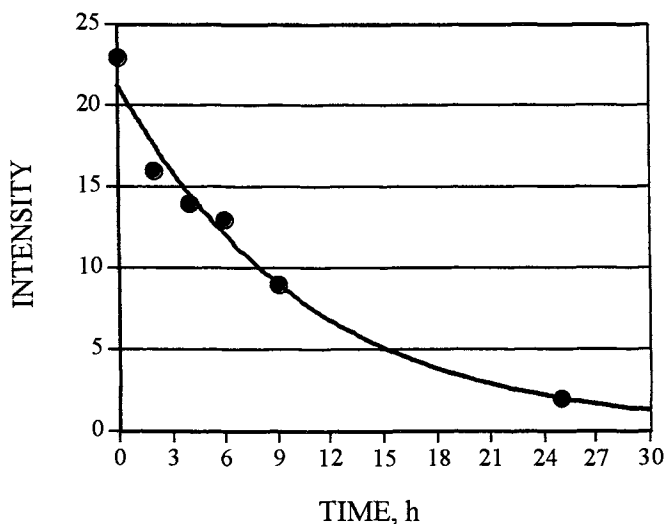


Figure 5. Decay of the ESR signal of the peptide radical in meat at  $-10^{\circ}\text{C}$ .

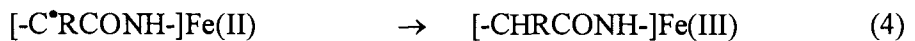
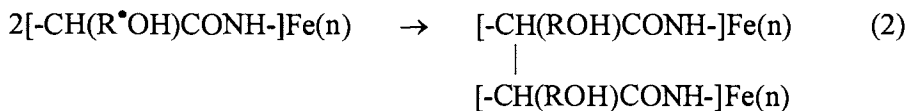
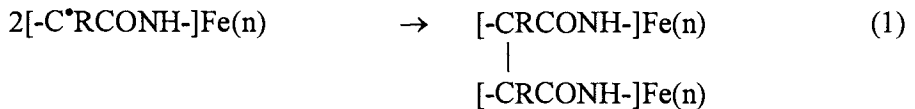
Other radiolytic processes can occur in such proteins that lead to side chain scission and the formation of volatiles from specific amino acid moieties [17].

### 3.2.2. Metalloproteins

Proteins with a metal ion that can be reduced or oxidized provide additional pathways for reaction of both primary and secondary radicals. The fixed location of the iron within the protein geometry strongly limits its accessibility to primary radicals, small secondary radicals, and radical sites on the host protein. These considerations are especially relevant to myoglobin, the globular protein responsible for meat pigmentation. Several distinctive reactions involving myoglobin have been studied in model and meat systems [18, 19].

Reactions of  $e_s^-$ ,  $H^\bullet$ , and  $OH^\bullet$  are expected generally to follow the pattern for proteins, leading to peptide radicals and addition radicals associated with aromatic and heterocyclic amino acid moieties. The iron ion, centered in the planar heme group and coordinated at one apical site with a histamine moiety from a proximal  $\alpha$ -helix and at the other to  $H_2O$ ,  $O_2$ , or  $NO$  (formed during curing), is also accessible. Reaction of  $e_s^-$  with brownish ferrimyoglobin ( $Fe^{3+}$ ) leads to reddish ferromyoglobin ( $Fe^{+2}$ ). Other complex reactions of  $e_s^-$  and  $OH^\bullet$  with these myoglobin species and with cherry red oxymyoglobin have been observed that are influenced by  $O_2$  and  $H_2O_2$  and that involve additional intermediate species [20-23]. Any overall mechanism for the radiolysis of myoglobin in meats should take into consideration the multiple pathways for reaction of the different radicals formed.

A particularly important consideration is the potential for competitive intermolecular and intramolecular reactions:



These reactions show that dimers can be formed (and have been observed) if either peptide radicals or side chain radicals on the globin surface react intermolecularly. They also show that if these radicals are close enough to the iron center, electron transfer can occur leading to either reduction or oxidation, depending on the valence state, and to an associated color change.

### 3.3. Lipids

The radiolysis of triglycerides in the lipid portions of meats and poultry leads to a generic radical on a fatty acid moiety, reflecting the predominant scission of a C-H bond alpha to the carbonyl group[24, 25]. Dimeric triglycerides resulting from the combination of two such radicals have been detected [26]. The ESR spectrum for tripalmitin powder irradiated at  $-125^{\circ}\text{C}$  and annealed to  $40^{\circ}\text{C}$ , shown in Figure 6, is characterized by an asymmetric quintet consistent with a radical having an unpaired electron that interacts with hydrogen atoms on both the same and neighboring carbon atoms. Figure 6 also shows that the broad singlet observed at  $-125^{\circ}\text{C}$  converts into a more complex spectrum upon annealing to  $-25^{\circ}\text{C}$ .

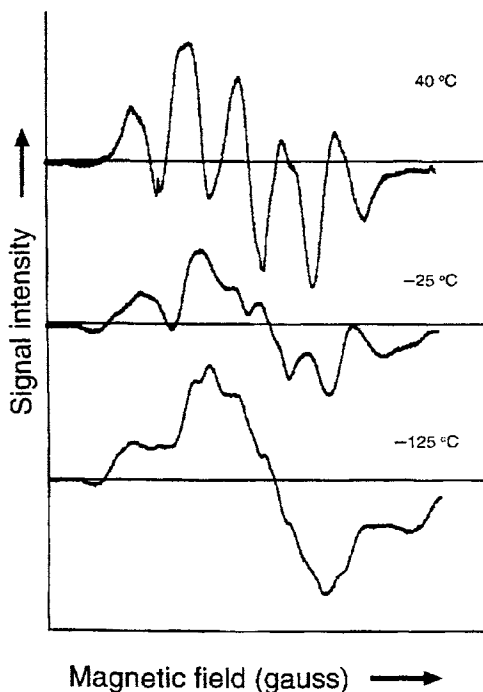


Figure 6. Sequential electron spin resonance spectra (recorded at 77 K) of powdered tripalmitin irradiated at  $-125^{\circ}\text{C}$  and annealed first at  $-25^{\circ}\text{C}$  and then  $40^{\circ}\text{C}$ . Reproduced from Taub [3] with permission.

These spectral results and those from product analyses, particularly from extensive studies by Nawar [27] on related triglycerides, fatty acid esters, and fatty acids, indicate that other radicals are formed and some participate in reactions leading to the more stable alpha carbon radical.

Because of the ester linkage and associated carbonyl group in the triglycerides, the sequence of reactions that leads to the alpha carbon radical is similar to the sequence in proteins [28]. As is shown in Figure 7 for the electron-initiated sequence, the electron adds to the C=O bond forming the carbonyl anion radical (responsible for the singlet ESR spectrum), which then dissociates into the free fatty acid and an alkyl radical on the residual propanedioldiester (responsible in part for the more complex spectrum at intermediate times or temperatures), which subsequently abstracts a hydrogen from a triglyceride, ultimately forming the carbon radical alpha to the carbonyl group. This large radical (responsible for the quintet spectrum) can react either by combination with other radicals or with an identical radical, so as to dimerize or to disproportionate, reforming a triglyceride or forming an analogous compound with a double bond alpha to the carbonyl group. Though the sequence is shown for the ester linkage in the 1-position, it could occur at the other two linkages, involving the fatty acid moieties at the 2- and 3-positions of the triglyceride.

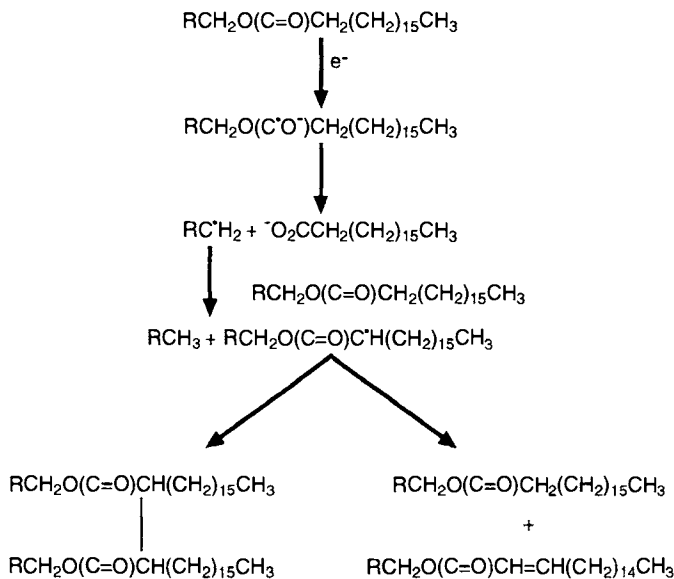


Figure 7. Mechanistic scheme for reactions in triglycerides initiated by electron addition to the carbonyl group near the ester linkage. R corresponds to the rest of the triglyceride molecule.

Some of the yields for various radiolysis products from tripalmitin as a model are 1.6 for palmitic acid and .04 for palmityl aldehyde. Other yields and those from the monoglyceride ethylpalmitate as a model are listed elsewhere [1].

The generality of the sequential formation and reaction of free radicals, initiated by either electrons or hydrogen atoms, is borne out by ESR spectral data on irradiated fats from beef, pork, and chicken [14]. Each fat contains a diverse combination of triglycerides with differing proportions of fatty acid moieties. Figure 8 shows the spectra for beef fat [1]. Though the same most stable radical is ultimately formed in all cases, Sevilla [29] has shown in low dose studies that this radical disappears more rapidly in chicken fat than in pork fat (Figure 9). The former has more of the unsaturated linoleic acid than the latter and presumably has a lower viscosity. All of these results imply a commonality in the radiolysis of the lipids.

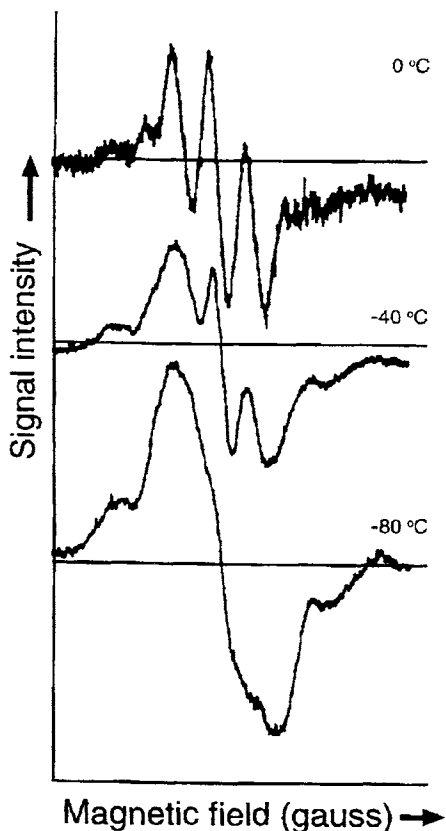


Figure 8. Sequential electron spin resonance spectra (recorded at 77 K) of beef fat irradiated at  $-80^{\circ}\text{C}$  and annealed first at  $-40^{\circ}\text{C}$  and then at  $0^{\circ}\text{C}$ . Reproduced from Taub [3] with permission.

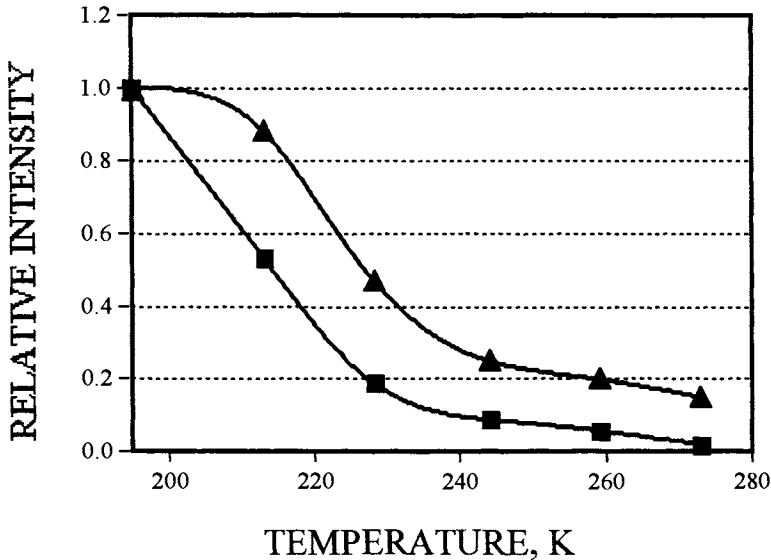


Figure 9. Relative residual concentration of the lipid radical in chicken fat (■) and pork fat (▲) irradiated at 77 K to 1 kGy and annealed to the indicated temperatures.

The overall yield of radiolysis products is relatively low and their distribution will depend on the fatty acid composition of the triglycerides. In meats irradiated in the absence of oxygen, low levels of the free fatty acid, the associated propanedioldiester, hydrogen, and products derived from the triglyceride radical are to be expected. Much lower yields of volatile hydrocarbons are produced that provide insight into other scission processes and reaction pathways [27, 30, 31].

### 3.4. Carbohydrates

The radiolysis of either a complex carbohydrate, such as starch, or solutions of simpler saccharides, such as glucose or sucrose, leads primarily to scission of C-H bonds and disruption of the ether linkages between glucose units [32-34].

In solid systems, similar radicals centered on the C-1 and C-6 positions are formed from starches of different origins, as evidenced by similar ESR spectra [35-38]. These radicals slowly disappear upon subsequent storage, the rates in different starches being similar and dependent upon moisture content [35, 36]. Qualitatively, the formation and disappearance of the radicals are similar in systems irradiated at either room temperature or at 77 K with or without oxygen present. The associated rupture of the glycosidic linkage results in some



depolymerization and in the formation of soluble dextrans [37-40]. Other radiolysis products include formic acid, malonaldehyde, dihydroxyacetone, and glyceraldehyde.

In aqueous solutions, the reactions of  $e_s^-$ ,  $H^\bullet$ , and  $OH^\bullet$  with simpler saccharides would be similar to those with alcohols and ethers. Accordingly,  $e_s^-$  would react with the ether linkage and carbonyl group, while  $H^\bullet$  would abstract hydrogen from accessible C-H bonds. These abstraction reactions would lead to radicals at all carbon atoms sites on the glucose ring, with some preference for the C-1 and C-6 positions. Subsequent reactions of these radicals lead to radiolysis products, as Figure 10 illustrates for the C-1 glucose radical. It can disproportionate to regenerate the intact ring and gluconic acid. It can also eliminate  $H_2O$  or rearrange, so that 2- and 5-deoxygluconic acids are formed. Their yields have been determined [33]. Glucose ring radicals in oligosaccharides can undergo other reactions, some leading to scission of the glycosidic linkage. Studies with the disaccharide cellobiose show that such scission occurs when the radicals are formed at the C-1, C-4, and C-5 positions and that glucose can be formed [41]. These results imply that carbohydrates can be degraded both by initial reaction at the C-O-C linkage as well as by abstraction of hydrogen at nearby sites.

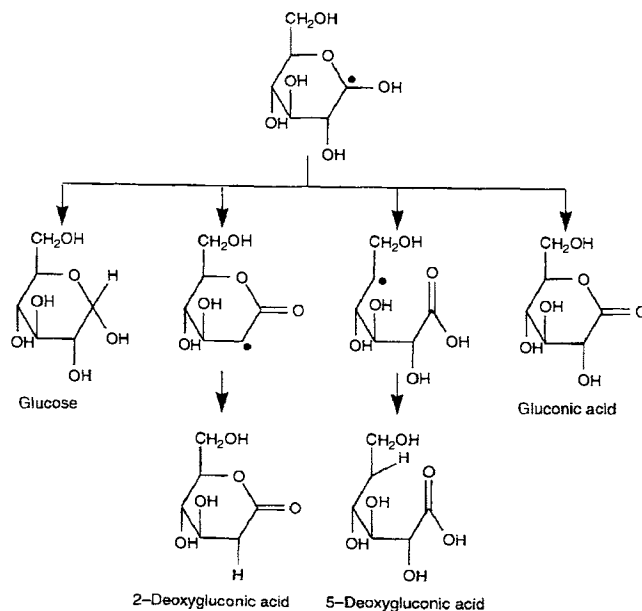


Figure 10. Illustrative mechanism for the reactions of the glucose radical formed by loss of hydrogen from the C-1 position; final products are indicated. Reproduced from von Sontag [33] and WHO Technical Report No. 890 [43] with permission.

#### 4. WHOLESOMENESS IMPLICATIONS

The radiation chemical considerations would imply that suitable foods properly irradiated should be wholesome, namely safe to consume and nutritionally adequate [42-45]. In determining wholesomeness and in clearing the use of the irradiation technology, regulatory agencies basically assess the process efficacy, the resulting nutritive value, and the toxicological potential. Efficacy refers to achieving the technical objective, which for pasteurized or sterilized meats corresponds to microbial destruction. Nutritive value refers to the retention of macronutrients and micronutrients. Most important, toxicological potential refers to the possible formation of a radiolysis product that, at the concentration level attained, could have a chronic or genotoxic effect. Such assessments are discussed briefly.

##### 4.1. Microbial destruction

Because irradiation causes double strand breaks in the DNA of microorganisms, it is highly effective in reducing or eliminating completely the population of microbial contaminants in the food. Their sensitivity to radiation, however, differs widely [43, 46], presumably reflecting differences in the DNA environment and the activity of base excision repair enzymes. The comparison in Table 2 of  $D_{10}$ -values (the dose required to reduce the population by 90%) shows that this sensitivity can be very high for the nonspore-forming *Vibrio* species in shellfish, moderate for such bacterial pathogens as *E. coli*, but relatively low for the spore-forming, essentially dry, *Clostridium botulinum* in uncured (non-nitrited) meats. For nonspore-forming bacteria, adequate oxygen availability can double this sensitivity, because it "fixes" the damage. Freezing, in contrast, can halve this sensitivity, presumably by reducing the yield or diffusion of  $\text{OH}^\cdot$ . For the spore-formers, there is a distinct decrease in sensitivity with decrease in temperature, as Figure 11 shows for *C. botulinum* [47]. Consistent with the chemistry in the DNA being initiated in the track of a low LET radiation, the  $D_{10}$ -value for spore-forming *B. subtilis* was shown to be independent of dose rate over 13 orders of magnitude [48]. It is on the basis of these considerations that the doses in Table 1 were approved: maxima in the case of pasteurization to allow at least a six log cycle reduction; and minima in the case of sterilization to ensure a twelve log cycle reduction of proteolytic spores of *C. botulinum*. As would be expected, the  $D_{10}$ -value for a specific pathogen is independent of the nature of the meat [49].

Table 2  
D<sub>10</sub>-values of representative contaminants

Contaminant	Medium	D <sub>10</sub> (kGy)
<i>Vibrio parahaemolyticus</i>	Fish	0.03
<i>Pseudomonas fluorescens</i>	Beef	0.12
<i>Aspergillus glaucus</i>	Aqueous	0.25
<i>Escherichia coli</i> O157:H7	Beef	0.30
<i>Staphylococcus aureus</i>	Chicken	0.36
<i>Saccharomyces cerevisiae</i>	Aqueous	0.36
<i>Salmonella</i> species	Chicken	0.38-0.77
<i>Clostridium perfringens</i>	Pork	0.83
<i>Clostridium botulinum</i>	Beef(-30°C)	3.43
Coxsackie virus B2	Aqueous	7.0

Adapted from WHO Technical Report No. 890 [43] with permission.

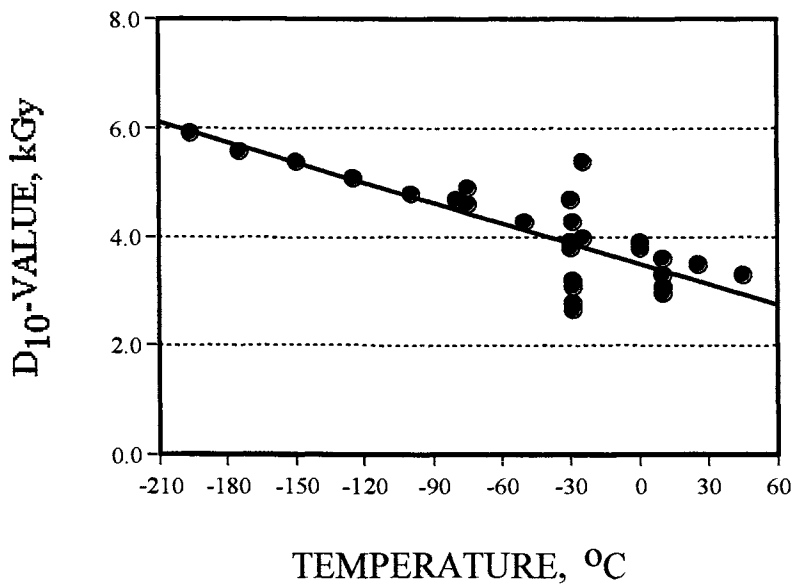


Figure 11. Dependence of the D<sub>10</sub>-value for *C. botulinum* on temperature.

#### 4.2. Nutritive value

Because the radiolysis of the meat constituents results in a limited amount of molecular change, there is essentially no loss of nutritive value. The macronutrients – proteins, lipids and carbohydrates – adequately remain sources of metabolic energy and tissue replenishment [42, 44, 50]. Protein digestibility, amino acid composition, and essential fatty composition are unaffected [50]. These determinations were made by chemical analysis and feeding studies (see below). The micronutrient vitamins differ in their susceptibility to radiolytic degradation, but with one exception are not compromised. Among the fat solubles, vitamin E ( $\alpha$ -tocopherol) is most sensitive, while vitamin K is least sensitive. Nevertheless, the loss of vitamin E is insignificant if irradiation is done either in the absence of oxygen or at subfreezing temperature [50]. Among the water solubles, vitamin B<sub>1</sub> (thiamin) is the most sensitive, so its degradation by both radiolysis and thermolysis has been extensively studied [6, 51, 52]. The extent of radiolytic degradation is essentially independent of the meat matrix (see Table 3) and is minimized by excluding oxygen, by irradiating at subfreezing temperatures, and by using high dose rates (Figure 1). The retention of thiamin in radiation sterilized meats, where the abovementioned minimizing conditions are for the most part met, is equal to or greater than in thermally sterilized counterparts [53]. The retention in radiation pasteurized meats is considered adequate, even for pork, which is an important dietary source of thiamin [54]. In general, a judicious choice of irradiation conditions ensures adequate overall nutritional value.

#### 4.3. Toxicological assessment

Any possible risk in consuming irradiated meats or other irradiated foods would have to be associated with a significant formation of a radiolysis product with a potent chronic toxicity or genotoxicity potential. Based on the radiolytic

Table 3  
Thiamin retention in different meats (2 kGy, 5°C)

Meat	% Retained
Chicken	81
Beef	70
Pork	81
Turkey thigh	81
Bison	76
Caiman (Alligator)	70
Ostrich thigh	40

Adapted from Fox et al. [52] with permission.

mechanisms outlined for the major constituents, the putative formation of a carcinogen, mutagen, or teratogen would represent a minor fraction of the chemistry. Nevertheless, extensive studies to discern any deleterious effects have been conducted over the last 40 years. These have included feeding irradiated foods to animals and humans for assessing growth, reproduction, gross pathology, and longevity and also testing with sensitive *in vivo* and *in vitro* systems to discern genotoxicity [43-45]. Studies were even done with milk powder irradiated to 45 kGy to form high concentrations of free radicals (which are expected to react when dissolved) and then fed to rats and mice to assess long-term effects [55]. The preponderance of the evidence indicates that properly irradiated foods are nutritionally adequate and pose no toxicological risks [42, 43, 54, 56].

Two major studies were conducted that are especially relevant to radiation sterilized meats: the Dutch National Institute of Public Health and Environmental Hygiene (NIPHEH) study on ham [57-59] and the U.S. Army-sponsored Raltech study on chicken [53, 60]. In an attempt to trace the communication of toxic potential from feed to food, the Dutch toxicologists fed pigs irradiated feed and then fed rats irradiated (37 and 74 kGy) ham produced from these pigs. No difference in any index of toxicity among the various control and test groups was found. In the Raltech study, one of the most comprehensive food safety study ever conducted, enzyme-inactivated chicken, irradiated at subfreezing temperatures to an average dose of 58 kGy with gamma rays and 10 Mev electrons was compared against frozen and thermally sterilized counterparts and against a control. These foods were fed to four generations of mice and three generations of dogs. Comparisons were made for chronic toxicity and for genotoxicity, which included teratogenicity testing in mice, rats, rabbits, and hamsters and mutagenicity testing using drosophila, Ames tests, and several chromosomal aberration measurements. In reviewing the data from this study, the FDA concluded that there were no radiation-related effects at the doses used [56]. In assessing both the Dutch and Raltech studies and all other relevant data on radiation sterilized products, an international panel of experts went further and concluded that foods irradiated according to established standards to any dose needed to achieve the intended technical objective are deemed wholesome [43].

#### **4.4. Chemiclearance**

The need to conduct such toxicological testing of each irradiated food is now obviated by the chemiclearance principle. Expounded in the early 1980s, it implies that similar foods that are similarly irradiated will respond radiolytically in the same way, so the chemical, microbiological and toxicological effects will be essentially equivalent [14, 61]. Consequently, if in a generic class of foods

one member is proven to be wholesome, then all other members are correspondingly safe and nutritionally adequate. A comparison of the chemical intermediates and stable products formed in the radiolysis of various meats against those formed in irradiated chicken, which was first cleared [56], provides a basis for granting generic clearances of irradiated meats and meat products [43, 54].

#### 4.4.1. Common intermediates

That the radiolysis of meats containing similar proteins and comparable fatty acids involves similar primary and secondary processes leading to a common set of radicals stable at  $-40^{\circ}\text{C}$  is shown by the ESR spectra in Figure 12 for irradiated, enzyme-inactivated chicken, beef, ham, and pork [3, 62]. These spectra reflect the commonality in radicals derived from the muscle proteins, myosin and actin, and from the constituent triglycerides, which have slightly different fatty acid compositions. The minor consequences of this compositional

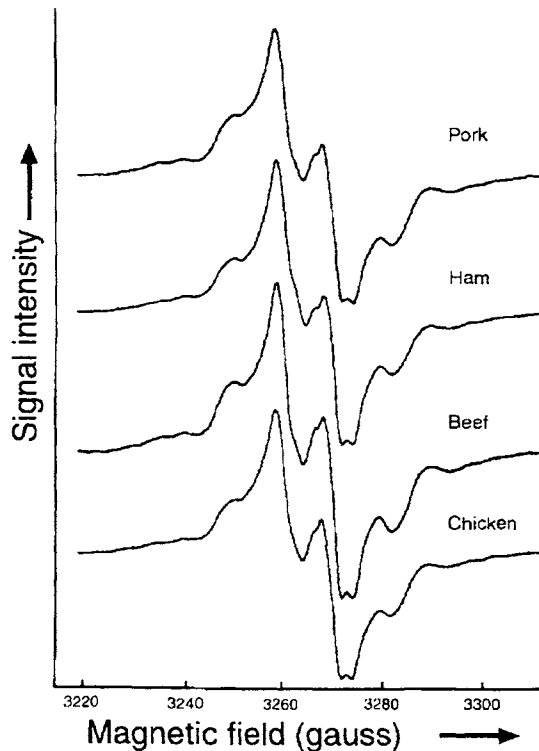


Figure 12. Comparison of the electron spin resonance spectra of four different enzyme-inactivated muscle foods irradiated to 50 kGy at  $-40^{\circ}\text{C}$ . Reproduced from Taub [3] with permission.

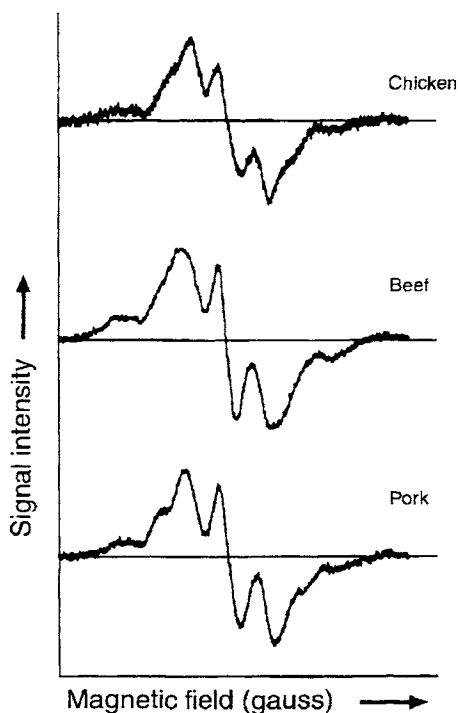


Figure 13. Comparison of the electron spin resonance spectra of fats from chicken, beef and pork irradiated to 50 kGy at  $-40^{\circ}\text{C}$ . Reproduced from Taub [14] with permission.

difference can be seen in the ESR spectra in Figure 13 for fats from chicken, beef, and pork irradiated at  $-40^{\circ}\text{C}$ . As previously explained, these spectra reflect a combination of radicals, including those that would eventually form the more stable triglyceride radical.

This commonality in the radiolysis was established not only for cooked meats irradiated to high doses at  $-40^{\circ}\text{C}$ , but also for raw meats irradiated to lower doses at 77 K [29]. The ESR spectra for raw pork, beef sirloin, and chicken breast (Figure 14) show the singlets associated with radicals formed by electron addition to the carbonyl groups, the yields of which linearly increased with dose. After annealing at  $-78^{\circ}\text{C}$ , the spectral features changed to the predominant asymmetric doublet associated with the peptide backbone radical. Moreover, a direct comparison of spectra at  $-78^{\circ}\text{C}$  for raw and roasted turkey breasts irradiated to 3.8 kGy showed no differences, indicating that native and denatured conformers of the protein respond radiolytically in similar ways [29].

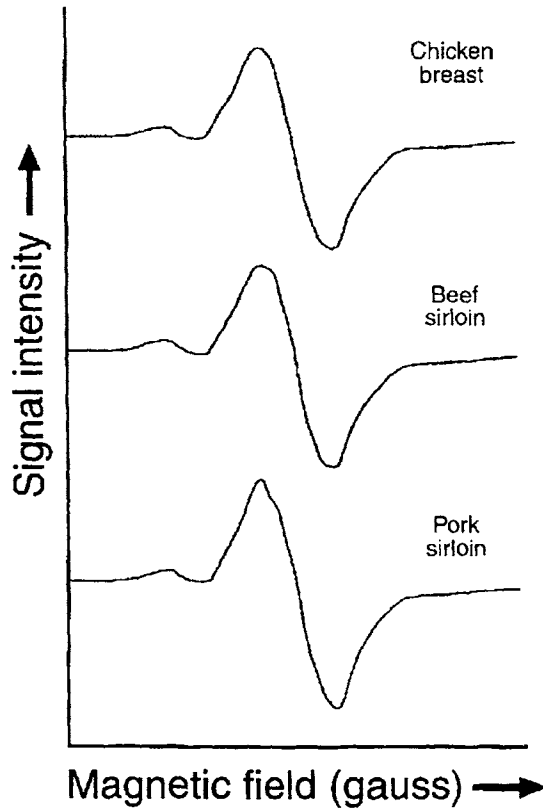
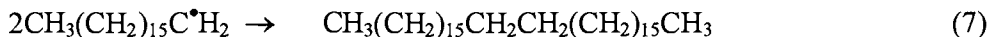
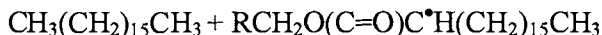


Figure 14. Comparison of the electron spin resonance spectra of three uncooked muscle foods irradiated to 1 kGy at 77 K.

#### 4.4.2. Common lipid-derived products

That the radiolysis of triglycerides in meats involves a common set of radicals reacting to form stable products corresponding to their precursor fatty acids is shown by chromatographically analyzing product yields in relation to fat composition [14, 62, 63]. Radicals other than those described and formed by C-O and C-C bond scission in the fatty acid chain lead to distinctive and predictable products. The acyl and acyloxy radicals can react by abstraction, combination, and even dissociation to produce corresponding alkyl radicals along with CO and CO<sub>2</sub>. The alkyl radical reaction possibilities, as shown in for the C<sub>17</sub> radical, include abstraction, dimerization, and disproportionation, which forms a double bond at the terminal carbon:





It is instructive to see how the products of these reactions reflect commonality and substantiate the chemiclearance principle.

*Dependence on total fat.* For scission of C-C bonds up to about six carbons from the aliphatic end of the chain, the stable hydrocarbon products formed will be the same for most of the fatty acids. Consequently, the yields of such hydrocarbons as pentane and hexane should be independent of the fatty acid composition but dependent solely on the total fat content of the meat sample. This dependence is seen for several low molecular weight hydrocarbons [14, 62] when their normalized yields in four different enzyme-inactivated meats irradiated at  $-30^\circ\text{C}$  are plotted against fat content, as Figure 15 illustrates for hexane.

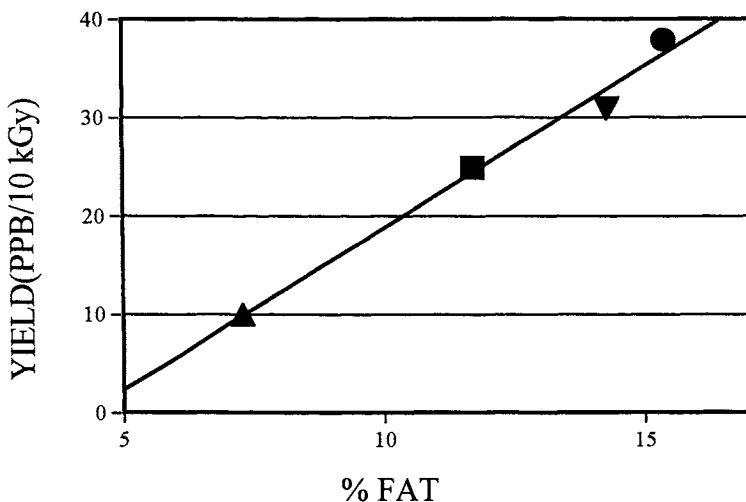


Figure 15. Normalized yield of hexane as a function of fat content in irradiated enzyme-inactivated muscle foods, expressed as nanograms per gram and normalized to 10 kGy of dose applied at  $-30^\circ\text{C}$ . Adapted from Taub et al. [14] with permission.

*Dependence on fatty acid composition.* For scission of the C-C bonds alpha and beta to the carbonyl group in the fatty acid,  $C_{n-1}$  and  $C_{n-2}$  alkyl radicals are formed, respectively, that will produce by abstraction the corresponding hydrocarbon and by disproportionation a corresponding hydrocarbon with an additional double bond at the original radical site. Accordingly, the normalized yields of  $C_{14}$  to  $C_{17}$  hydrocarbons produced in either raw or cooked meats irradiated over a wide dose range have been shown to depend directly on the level of the precursor fatty acid in the meat fat [14, 17, 64]. The linear dependence of heptadecadiene ( $C_{17:2}$ ) on linoleic acid is shown in Figure 16 for high dose irradiated, enzyme-inactivated chicken, pork, and beef. Since there is six times as much linoleic acid in the chicken as in the beef, the yield is six times as much. Similarly, the linear dependence of hexadecatriene ( $C_{16:3}$ ), derived from the  $C_{n-2}$  radical, on linoleic acid was shown for a variety of raw meats irradiated from 1-10 kGy at  $-5^{\circ}\text{C}$  and for several enzyme-inactivated meat products irradiated from 45-60 kGy at  $-30^{\circ}\text{C}$  [64]. A direct comparison of the yield of  $C_{16:3}$  normalized per mg of precursor linoleic acid as a function of dose for both raw and cooked chicken (Figure 17) shows that the slopes differ slightly. This difference suggests that the radical yield or its reactivity is slightly lower in the cooked meats, because of the higher viscosity at the lower irradiation temperature. The overall similarity in yields, however, indicates that the radicals formed and the reactions they undergo are independent of the molecular environment of the fatty acid moieties.

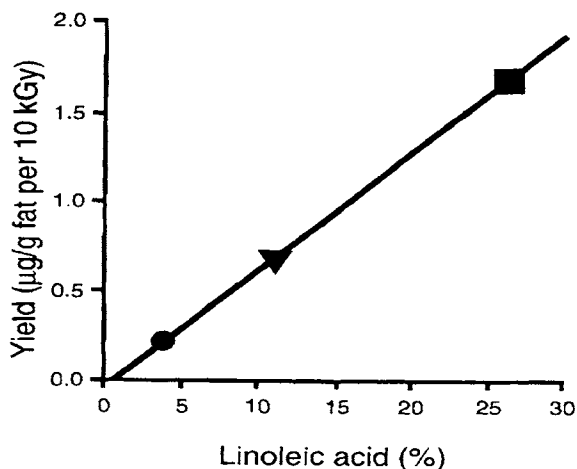


Figure 16. Normalized yield of heptadecadiene ( $C_{17:2}$ ) as a function of linoleic acid content in irradiated, enzyme-inactivated muscle foods, expressed as micrograms of the hydrocarbon per gram of fat and normalized to 10 kGy of dose applied at  $-30^{\circ}\text{C}$ . Reproduced from Merritt et al. [17] with permission.

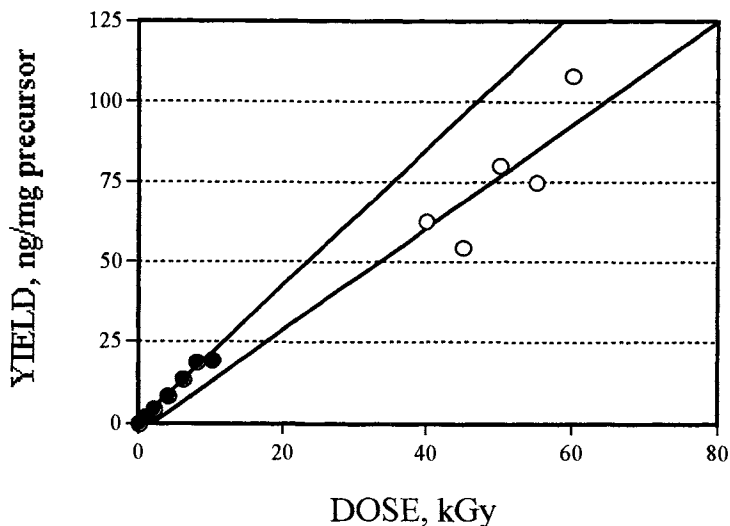


Figure 17. Yield of hexadecatriene normalized for the level of precursor linoleic acid in the fats of raw chicken (●) and cooked chicken (○) irradiated at  $-5^{\circ}\text{C}$  and  $-30^{\circ}\text{C}$ , respectively, to the indicated doses.

*Dependence on triglycerides.* For scission of the C-O bond between the glycerol and fatty acid moieties, which is primarily but not exclusively due to the dissociative electron attachment reaction, an alkyl radical is formed that, upon abstracting hydrogen, produces a stable propanedioldiester. This product indirectly reflects the composition of the original triglyceride, which can be designated as:  $\text{H}_2\text{C}(\text{O}_2\text{R}'')\text{CH}(\text{O}_2\text{R}')\text{CH}_2(\text{O}_2\text{R})$ , where the  $\text{O}_2\text{R}''$ ,  $\text{O}_2\text{R}'$ , and  $\text{O}_2\text{R}$  correspond to different fatty acid moieties in the 3, 2, and 1 positions (reading left to right) of the glycerol backbone. If scission occurs at the 1-position, the resulting radical is:  $\text{H}_2\text{C}(\text{O}_2\text{R}'')\text{CH}(\text{O}_2\text{R}')\text{C}^{\bullet}\text{H}_2$ . If both  $\text{O}_2\text{R}''$  and  $\text{O}_2\text{R}'$  are palmitic acid moieties, then the resulting product is 2,3 propanedioldipalmitate:  $\text{H}_2\text{C}(\text{O}_2\text{C}_{16}\text{H}_{31})\text{CH}(\text{O}_2\text{C}_{16}\text{H}_{31})\text{CH}_3$ . This product could also be formed from other triglycerides with at least two palmitate moieties, provided that scission occurs at such a position that the resulting radical retains two palmitates. A 1, 3 propanedioldipalmitate could be produced and would be analyzed along with its positional isomer. Consequently, the yield of propanedioldipalmitate from different irradiated meats should depend on the percent abundance of appropriate precursor triglycerides in each meat. This dependence is shown in Figure 18 in which the dose-normalized yield of propanedioldipalmitate from the irradiation of four different meats at  $-40^{\circ}\text{C}$  is plotted against the abundance

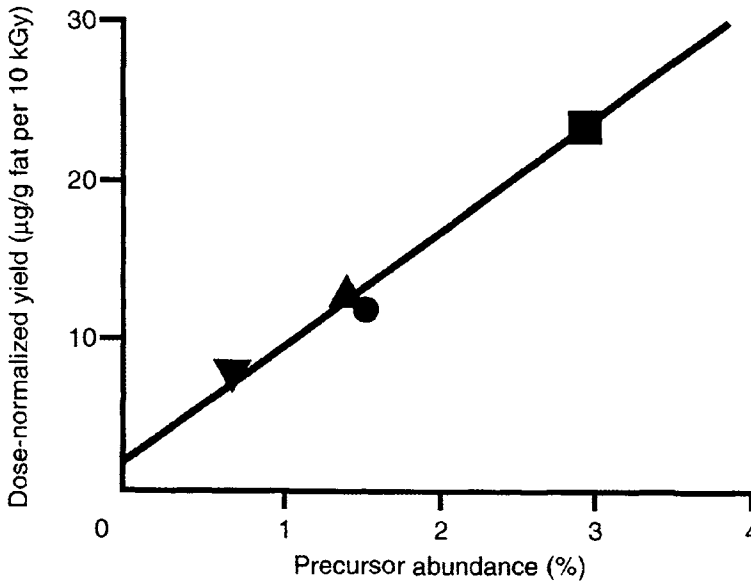


Figure 18. Relationship of the dose normalized yield of propanedioldipalmitate to its triglyceride precursors in four muscle foods irradiated to 10, 60, and 90 kGy at  $-40^{\circ}\text{C}$ . Adapted from Merritt et al. [17] with permission.

of precursor triglycerides, computed on the basis of the analyzed fatty acid composition and certain assumptions on biosynthetic combinations [17, 62]. These data are consistent with a commonality in the radiolysis and a predictability in the product distribution based on compositional differences.

## 5. QUALITY IMPLICATIONS

The radiolysis of food constituents leads to minor but sometimes perceptible changes in sensory qualities associated with the net formation or degradation of a specific constituent. Color, texture, and rancidity are qualities that can be affected either during irradiation or subsequent storage, depending on the food, the atmosphere, the packaging, and the irradiation dose and temperature. Often, there are implications in the radiation chemistry for ensuring optimal quality of irradiated meat products.

### 5.1. Color

Since the color of meat products depends on both the valence of the iron in the porphyrin ring and the ligand coordinated at the apical position, any oxidation or

reduction occurring during or after irradiation could produce some change [19, 65]. In raw beef, rich in the red-purple ferromyoglobin (Mb), the presence of oxygen produces oxyferromyoglobin (MbO<sub>2</sub>) with its familiar cherry red color. Irradiation of chilled, raw beef in oxygen permeable packaging could oxidize the pigment to ferrimyoglobin (metMb), producing a brownish coloration. If vacuum-packaged raw beef is irradiated, residual oxygen is depleted at about 0.6 kGy and a mixture of Mb and metMb results, the proportion depending on dose. Post-irradiation exposure to oxygen could regenerate MbO<sub>2</sub>, which eventually would convert to metMb. Consequently, brownish raw beef could be avoided by limiting the dose, by manipulating the oxygen, and by irradiating at subfreezing temperature. In cooked beef, the pigment is predominantly denatured metMb as a consequence of the heat-induced oxidation of MbO<sub>2</sub> and the color is distinctively brown. Irradiating enzyme-inactivated beef in evacuated, oxygen-impermeable packaging to high doses at -30 °C or lower will reduce the metMb to Mb, giving the beef a reddish appearance. Subsequent exposure to oxygen and warming to serving temperatures, as would normally be done when the product is to be consumed, restores the brownish color. In cured (nitrited) meats, such as corned beef and ham, the coordination of the iron with nitric oxide gives these products their pink coloration, which varies only slightly with change in valence, so irradiation has less of an effect on the color. Irradiation of frozen pork at low doses appears to change the color from pale gray to slightly reddish [66], suggesting a higher initial level of metMb. Implied in all these considerations is that the color can be optimized by a judicious choice of atmosphere, packaging, and irradiation parameters.

## 5.2. Texture

Since textural characteristics of meat muscle tissue, such as toughness and friability (pulling apart), are associated with the structure of the myofibrils, any radiolytically initiated reaction that degrades the proteins, compromises their water-holding capacity, or crosslinks them could affect texture. Depending on dose and temperature, the radiolysis of proteins does produce some peptide chain fragmentation and aggregation. However, the texture of enzyme-inactivated meats (containing salt and tripolyphosphates to improve water binding [65, 67]) that are vacuum-packed and irradiated to high doses at -30°C is acceptable to subjects consuming them, including astronauts [68] and outdoor sports enthusiasts [43, 69]. Objective measurements of the force needed to shear through precooked meats that were irradiated at -30°C to relatively precise doses from 40-60 kGy (Figure 19) indicate an increased softening with increasing dose. This softening could be associated with some fragmentation in the small proteins that bind the long chain myosin into myofibrils. If too high a dose is used, the product could become mushy and unacceptable to consumers.

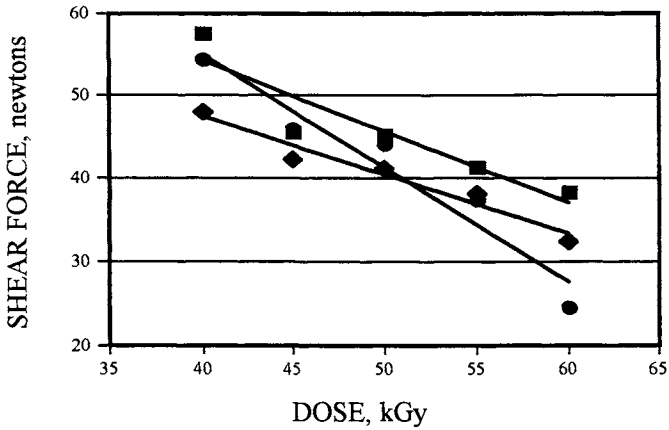


Figure 19. Dependence of shear force on the accumulated dose for various irradiated meats. Symbols: ● - corned beef; ■ - roast beef; and □ - smoked turkey.

### 5.3. Rancidity

Processed or stored meat products become unacceptably rancid when the constituent unsaturated fatty acids are extensively oxidized. This oxidation can be initiated in several ways and involves a chain reaction that consumes oxygen and produces several products, including hydroperoxides, methyl ketones, alkanals, and alkanes [70]. Irradiation processing could produce such oxidative changes, depending on oxygen availability, temperature, and dose. However, radiation sterilization of meats does not produce significant oxidation [65], because the oxygen is excluded and the irradiation temperature is low, which compensates for the high dose. Radiation pasteurization of meats at chilled temperatures could produce some oxidation, the extent being limited by the low doses used. Oxidation could be further minimized by using either oxygen-impermeable packaging or low oxygen permeable packaging in combination with high dose rates (to prevent replenishment of depleted oxygen). Storage of irradiation-processed meats could in principle produce rates of autoxidation higher than would be expected for the nonirradiated counterparts only if there were a significant increase in the level of unsaturated fatty acids or a significant decrease in natural antioxidants, such as  $\alpha$ -tocopherol. Based on the radiolysis of lipids and vitamins, such increases and decreases are not expected under normal irradiation conditions. If autoxidation upon storage (of irradiated or nonirradiated products) is unavoidably encountered, then the use of synergistic antioxidants would break the chain reaction and minimize oxidative changes [4].

#### 5.4. Packaging

Maintaining the quality of radiation-preserved meats requires that the polymeric packaging retain its ability to limit air and moisture permeation and to minimize extraction of polymer components into the meats [43]. The chain scission and crosslinking associated with polymer radiolysis could increase or decrease these functional properties, depending on the polymer structure and irradiation conditions. In the case of polyethylene, the level of heptane extractables, presumably corresponding to intentionally added antioxidants, decreases with increasing dose (Figure 20) [71]. These results suggest that crosslinking of the polymer or covalent binding of the antioxidants to the polymer prevents migration and extraction. In general, the use of radiation-durable polystyrene or polyethyleneterephthalate will minimize any significant change in package integrity or functionality.

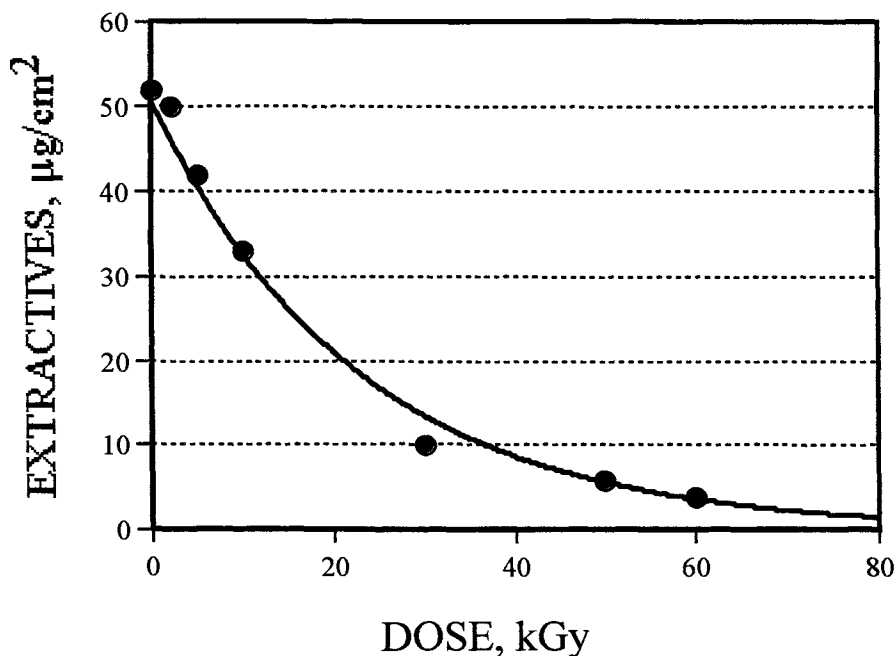


Figure 20. Level of components extracted with heptane from polyethylene film irradiated to the indicated doses.

## 6. CONCLUSION

Our understanding of the radiation chemical reactions occurring in irradiated foods is sufficiently advanced to assure the safety and high quality of such foods. The overall radiolytic effects on the food constituents are relatively minor, are similar in foods of similar composition, and can generally be predicted and quantified on the basis of composition and irradiation conditions. The effects on the contaminating pathogenic and spoilage bacteria, nevertheless, are sufficient to destroy them efficiently and quantitatively even at chilled or subfreezing temperatures. As a consequence, the risk of foodborne illness is reduced without adversely affecting the nutrients and without introducing any toxicological hazards. Moreover, a judicious choice of readily controllable irradiation conditions ensures that chemical changes affecting the major quality attributes of taste, color, and texture can be minimized. These desirable aspects of the irradiation processing contrast sharply with conventional thermoprocessing in which thermolytic reactions tend to be extensive and excessive. The commonality in the radiation chemistry of generic foods, in particular, has facilitated the process by which regulatory agencies grant approvals to broaden the application of irradiation processing.

## REFERENCES

1. I.A. Taub, Radiation chemistry and the radiation preservation of food, *J. Chem. Ed.*, 58 (1981) 162.
2. I.A. Taub et al., Factors affecting radiolytic effects in food, *Radiat. Phys. and Chem.*, 14 (1979) 639.
3. I.A. Taub, Reaction mechanisms, irradiation parameters, and product formation, in *Preservation of Food by Ionizing Radiation*, Vol. II, E.S. Josephson and M. Peterson (eds.), CRC Press, Boca Raton, 1983, pp. 125-166.
4. I.A. Taub, Free radical reactions in food, *J. Chem. Ed.*, 61 (1984) 313.
5. I.A. Taub, P. Angelini, and C. Merritt Jr., Irradiated food: Validity of extrapolating wholesomeness data, *J. Food Sci.*, 41 (1976) 942.
6. M.H. Thomas et al., Effect of radiation and conventional processing on the thiamin content of pork, *J. Food Sci.*, 46 (1981) 824.
7. I.A. Taub, R.A. Kaprielian, and J.W. Halliday, Radiation chemistry of high protein foods irradiated at low temperatures, in *Proceedings, International Symposium on Food Preservation by Irradiation*, International Atomic Energy Agency, Vienna, Vol. I, 1978, pp. 371-384.
8. B.H.J. Bielski, Chemistry of ascorbic acid radicals, in P.A. Sieb and B.M. Tolbert (eds.), *Advances in Chemistry Series*, No. 200, American Chemical Society, Washington, 1982, pp. 81-100.
9. G.P. Laroff, R.W. Fessenden, and R.H. Schuler, The electron spin resonance spectra of radical intermediates in the oxidation of ascorbic acid and related substances, *J. Am. Chem. Soc.*, 94 (1972) 9062.
10. D.W. Thayer, Food irradiation: Benefits and concerns, *J. Food Qual.*, 13 (1990) 147.



11. P. O'Neill and E.M. Fielden, Primary free radical processes in DNA, *Advances in Radiation Biology*, 17 (1993) 53.
12. J.F. Ward, Chemical consequences of irradiating nucleic acids, *J. Agric. Food Chem.*, 26 (1978) 25.
13. I.A. Taub, J.W. Halliday, and M.D. Sevilla, Chemical reactions in proteins irradiated at subfreezing temperatures, *Advances in Chemistry Series*, No. 180, American Chemical Society, Washington, 1979, pp. 109-140.
14. I.A. Taub et al., Chemiclearance: Principle and application to irradiated meats, in *Proceedings of the 26<sup>th</sup> European Meeting of Meat Research Workers*, American Meat Science Association, Colorado Springs, Vol. One, 1980, pp. 233-236.
15. H-J. Kim et al., Binding-site specificity of the radiolytically induced crosslinking of phenylalanine to glucagon, *Radiat. Res.*, 98 (1984) 26.
16. H-J. Kim et al., Binding-site specificity of the gamma radiation induced crosslinking between phenylalanine and phenylalanine-containing tetrapeptide, *Radiat. Res.*, 100 (1984) 30.
17. C. Merritt, Jr. et al., A quantitative comparison of the yields of radiolysis products in various meats and their relationship to precursors, *J. Am. Oil Chem. Soc.*, 62 (1985) 708.
18. J.J. Shieh et al., Radiation chemistry of myoglobin, its derivatives, and model compounds in aqueous solution, in *Radiation Biology and Chemistry: Recent Developments*, Proceedings of the Association for Radiation Research Meeting, Elsevier, Amsterdam, (1979) 179.
19. J.J. Shieh et al., Radiation chemistry of meat proteins: myoglobin irradiated in frozen aqueous solutions, in C.C. Tsen and C. Li (eds.), *Proceedings of International Symposium on Recent Advances in Food and Technology*, Hua Shiang Hwan, Taipei, 1981, p. 277.
20. K.D. Whitburn, M.Z. Hoffman, and I.A. Taub, Formation of a steady state in the radiolysis of ferrimyoglobin in aqueous solution, *Arch. Biochem. Biophys.*, 208 (1981) 319.
21. K.D. Whitburn et al., Globin-mediated redox processes in the interaction of hydroxyl radicals with ferrimyoglobin in aqueous solution, *Int. J. Radiat. Biol.*, 40 (1981) 297.
22. K.D. Whitburn, M.Z. Hoffman, and I.A. Taub, Simultaneous reaction of hydroxyl radical and aquated electrons with ferrimyoglobin in irradiated solutions, *J. Food Sci.*, 48 (1983) 1888.
23. K.D. Whitburn, M.Z. Hoffman, and I.A. Taub, Interaction of radiation-generated radicals with myoglobin in aqueous solutions, *Radiat. Phys. Chem.*, 23 (1984) 271.
24. C. Sevilla, S. Swarts, and M.D. Sevilla, An ESR study of radical intermediates formed by gamma radiolysis of tripalmitin and dipalmitoyl phosphatidylethanolamine, *J. Am. Oil Chem. Soc.*, 60 (1983) 950.
25. M.D. Sevilla, Mechanisms for radiation damage in lipids, Final report, 1982 (unpublished document, United States Army Contract No. DAAK-60-78-C-0060).
26. C. Merritt, Jr. and M. Vajdi, *J. Am. Oil Chem. Soc.*, 59 (1982) 172.
27. W.W. Nawar, Reaction mechanisms in the radiolysis of fats: A review, *J. Agric. Food Chem.*, 26 (1978) 21.
28. M.D. Sevilla, K.M. Morehouse, and S. Swarts, An ESR study of electron reactions with esters and triglycerides, *J. Phys. Chem.*, 85 (1981) 923.
29. M.D. Sevilla, Commonality of chemical entities in irradiated muscle foods, Final Report, 1994 (unpublished document, United States Contract No. DAAL03-91-0034).

30. A.P. Handel and W.W. Nawar, Radiolytic compounds from mono-, di-, and triacylglycerols, *Radiat. Res.*, 86 (1981) 428.
31. K.M. Morehouse and Y. Ku, Gas chromatographic and electron spin resonance investigations of  $\gamma$ -irradiated shrimp, *J. Agric. Food Chem.*, 40 (1992) 1963.
32. C. von Sonntag, *The chemical basis of radiation biology*, Taylor and Francis, London, 1987, pp. 375-393.
33. C. von Sonntag, Free radical reactions of carbohydrates as studied by radiation techniques, *Advances in Carbohydrates, Chemistry and Biochemistry*, 37 (1980) 7.
34. J.F. Dauphin and L.R. Saint-Lève, Radiation chemistry of carbohydrates, in A.J. Cohen and P.S. Elias (eds.), *Radiation Chemistry of Major Food Components*, Elsevier, Amsterdam, 1983, pp. 131-185.
35. J.J. Raffi and J-P. Agnel, Influence of the physical structure of irradiated starches on their ESR spectra kinetics, *J. Phys. Chem.*, 87 (1983) 2369.
36. J.J. Raffi et al., Glucose oligomers as models to elucidate the starch radiolysis mechanism, *Stärke*, 37 (1985) 228.
37. J.J. Raffi et al., Gamma radiolysis of starches derived from different foodstuffs, IV: Study of radiodepolymerization, *Stärke*, 33 (1981) 301.
38. J.J. Raffi et al., Study of  $\gamma$ -irradiated starches derived from different foodstuffs: A way for extrapolating wholesomeness data, *J. Agric. Food Chem.*, 29 (1981) 1227.
39. J.J. Raffi et al., Theoretical study of the radiodepolymerization of starch, *Stärke*, 32 (1980) 227.
40. J-P. Michael, J. Raffi, and L. Saint-Lève, Experimental study of the radiodepolymerization of starch, *Stärke*, 32 (1980) 295.
41. M. Dizdaroglu and C. von Sonntag,  $\alpha$ -Radiolysis of cellobiose in  $N_2O$ -saturated aqueous solution, *Z. für Naturforschung*, 28b (1973) 635.
42. Wholesomeness of Irradiated Food: Report of a Joint FAO/IAEA/WHO Expert Committee, World Health Organization (WHO Technical Report Series, No. 659), Geneva, 1981.
43. High-Dose Irradiation: Wholesomeness of Food Irradiated with Doses above 10 kGy, Report of a Joint FAO/IAEA/WHO Study Group, World Health Organization (WHO Technical Report Series No. 890), Geneva, 1999.
44. Safety and nutritional adequacy of irradiated food, World Health Organization Geneva, 1994.
45. J.F. Diehl, *Safety of Irradiated Foods*, 2<sup>nd</sup> Ed., Marcel Dekker, New York, 1995.
46. M. Ingram and J. Farkas, Microbiology of foods pasteurized by ionizing radiation, *Acta Alimentaria*, 6 (1977) 123.
47. R. Eden, Radiation sensitivity of bacterial spores: *Clostridium botulinum* and *Bacillus subtilis*, Interim Report, 1997 (unpublished document, United States Army Contract No. DAAK60-97-P-4326).
48. A. Brynjolfsson, Mathematical models for microbial kill by radiation, in *Proceedings, International Symposium on Food Preservation by Irradiation*, International Atomic Energy Agency, Vienna, Vol. I, 1978, pp. 227-239.
49. D. Thayer et al., Variations in radiation sensitivity of foodborne pathogens associated with the suspending meat, *J. Food Sci.*, 60 (1995) 63.
50. J.F. Diehl and E.S. Josephson, Assessment of wholesomeness of irradiated foods (A review), *Acta Alimentaria*, 23 (1994) 195.
51. J.B. Fox et al., Gamma irradiation effects on thiamin and riboflavin in beef, lamb, pork and turkey, *J. Food Sci.*, 60 (1995) 596.

52. L.L. Lakritz, J.B. Fox, and D.W. Thayer, Thiamin, riboflavin, and  $\alpha$ -tocopherol content of exotic meats and loss due to gamma radiation, *J. Food Prot.*, 61 (1998) 1681.
53. D.W. Thayer et al., Toxicology studies of irradiation-sterilized chicken, *J. Food Prot.*, 50 (1987) 278.
54. FDA, Irradiation in the production, processing, and handling of food: Final Rule, *Fed. Regist.* 62 (1997) 64107.
55. H.W. Renner and D. Reichelt, Safety of high concentrations of free radicals in irradiated foodstuffs, *Zentralblatt für Veterinärmedizin, B. Reihe* 20 (1973) 648.
56. FDA, Irradiation in the production, processing, and handling of food: Final Rule, *Fed. Regist.*, 55 (1990) 18538.
57. M.J. van Logten, J.M. Berkvens, R. Kroes, Investigation of the wholesomeness of autoclaved or irradiated feed in rats (Report 33/78 Alg. Tox), Netherlands National Institute of Public Health, Bilthoven, 1978.
58. M.J. van Logten et al., Long-term wholesomeness study of autoclaved or irradiated pork in rats (Report No. 61740 001), Netherlands National Institute of Public Health, Bilthoven, 1983.
59. J.J.T.W.A. Strik, Toxicological investigations on irradiated feed in pigs, *Tijdschrift voor Diergeneeskunde* 111 (1986) 240.
60. Raltech Scientific Services, A chronic toxicity, oncogenicity and multigeneration study using CD-1 mice to evaluate frozen, thermally sterilized, cobalt-60 irradiated, and 10 MeV electron irradiated chicken meat, Final Report, 1984 (unpublished document, United States Army Contract No. DAMD 17-76-C-6047).
61. R.A. Basson et al., Chemiclearance approach to evaluation of safety of irradiated fruits, in *Recent Advances in Food Irradiation*, P.S. Elias and A.J. Cohen (eds.), Elsevier, Amsterdam, 1983, pp. 59-77.
62. C. Merritt, Jr. and I.A. Taub, Commonality and predictability of radiolytic products in irradiated meats, in P.S. Elias and A.J. Cohen (eds.), *Recent Advances in Food Irradiation*, Elsevier, New York, 1983, pp. 25-57.
63. K.M. Morehouse, M. Kiesel and Y. Ku, Identification of meat treated with ionizing radiation by capillary gas chromatographic determination of radioytically produced hydrocarbons, *J. Agric. Food Chem.*, 41 (1993) 758.
64. K. M. Morehouse and I. A. Taub, Relationship of volatile hydrocarbons to lipids in irradiated meats, in *Proceedings of International Conference on Future Nuclear Systems*, American Nuclear Society, LaGrange, 1999, Paper No. 144.
65. I.A. Taub et al., Effect of irradiation on meat proteins, *Food Tech.* 38 (1979) 184.
66. S.E. Luchsinger et al., Color and oxidative rancidity of gamma and electron beam-irradiated boneless pork chops, *J. Food Sci.*, 61 (1996) 1000.
67. E. Wierbicki, Technological feasibility of preservation of meat, poultry and fish products using a combination of conventional additive, mild heat treatment and irradiation, in *Combination Processes in Food Irradiation*, International Atomic Energy Agency, Vienna, 1981, pp. 181-203.
68. C.T. Bourland, The development of food systems for space, *Trends Food Sci. Tech.*, 4 (1993) 271.
69. I. de Bruyn, Application of high dose irradiation, in *Proceedings of National Seminar on Food Irradiation*, Toluca, 1997, pp. 32-40.
70. W.W. Nawar, Chemical changes in lipids produced by thermal processing, *J. Chem. Ed.*, 61 (1984) 299.
71. J.J. Killoran and A. Brynjolfsson, 1977 (unpublished data, Report of Invention).

### Index terms

- 1,n-bromochloroalkanes, 230  
 1,n-bromiodoalkanes, 231  
 1,n-chloriodoalkanes, 230  
 1-bromo-2-chlorobenzene, 242  
 1-bromo-2-fluorobenzene, 245  
 1-chloro-2-fluorobenzene, 244  
 1-chloro-2-iodobenzene, 242  
 1-fluoro-2-iodobenzene, 244  
 1-methyl-5,6-dihydrouracil, 529  
 1-methylcytosine, 516  
 1,2 hydrogen atom shift, 336, 347, 499, 523  
 1,2-benzoquinone, 308  
 1,3-dimethyl-5,6-dihydrouracil, 529  
 1,3-dimethylthymine, 528  
 1,3-dimethyluracil, 517, 520, 528, 543, 544  
 1,3,6-trimethyluracil, 544  
 193 nm light, 601, 602, 614  
 2'-deoxy-5',8-cyclonucleosides, 536  
 2'-deoxyadenosine, 532, 536  
 2'-deoxycytidine, 545  
 2'-deoxyguanosine, 532, 538  
 2'-deoxyuridine, 545  
 2-alkoxyl-hydroxyalkyl radical, 483  
 2-Deoxy-D-ribose, 502  
 2-deoxy-D-ribose, 502  
 2-hydroxyethyl methacrylate, 692  
 2-methylcytosine, 516  
 2 $\sigma$ /1 $\sigma^*$  bond, 354  
 2 $\sigma$ /1 $\sigma^*$  concept limits, 386  
 2 $\sigma$ /1 $\sigma^*$  structure, 364  
 3-methyl-5,6-dihydrouracil, 529  
 5',8-cyclonucleotides, 536  
 5'-thymidylic acid, 543  
 5-Carboxycytosine, 516  
 5-electron bond, 373  
 5-methyl-5,6-dihydrouracil, 529  
 5-methylcytosine, 516  
 5,6-dihydrouracil, 529  
 6-methyl-5,6-dihydrouracil, 529  
 6-methyluracil, 528  
 6-methyluracil4, 516  
 8-oxo-7,8-dihydroguanine, 596, 597, 599, 602, 603  
 $\alpha$ -alkoxyalkyl radicals, 490  
 $\alpha$ -hydroxy- $\beta$ -phosphatoalkyl radical, 488  
 $\alpha$ -hydroxyalkyl radical, 470, 485  
 $\alpha$ -hydroxyalkylperoxyl radicals, 494  
 $\alpha$ -hydroxyl radicals, 262  
 $\alpha$ -Lactobiose H<sub>2</sub>O, 502, 503  
 $\alpha$ -methoxy- $\beta$ -phosphatoalkyl radical, 488  
 $\alpha$ -tocopherol, 637, 644, 722, 732  
 absorption spectra, 361, 417  
 absorption spectrophotometry, 254  
 abstraction, 707, 713, 719, 726, 728  
 ABTS, 546  
 acetone, 91  
 acetyl methionine, 689  
 acid-base dissociation constants, 294  
 acidic solutions, 230, 239  
 activation by 2 $\sigma$ /1 $\sigma^*$  bonds, 378  
 activation energy, 160  
 acyl radicals, 726  
 addition reactions, 94  
 adenine, 513, 515, 533, 546  
 adenosine, 533, 534  
 adriamycin, 288, 304, 626, 627  
 adsorption, 421  
 aggregation, 226, 266, 731  
 albumin, 709  
 alcohols, 413  
 aliphatic hydrocarbon, 55  
 alkaline solutions, 457  
 alkanals, 732  
 alkanes, 732  
 alkyl, 228  
 alkyl bromides, 233  
 alkyl radicals, 198, 207, 470, 471, 713, 716, 726, 728, 729  
 alkylating agents, 638  
 alloy, 438  
 alloyed clusters, 435  
 alpha-(alkylthio)alkyl radical, 362  
 alpha magnet, 27  
 alumino-silica gels, 433  
 Ames test, 723  
 amidoxime fibers, 691

- amine acylase, 687
- aminyl radicals, 345
- ammonia, 555
- amphiphilic structure, 275
- aniline radical cations, 348
- anilino radicals, 348
- anion exchange, 678
- anion exchange membrane, 681
- anthracycline, 302
- anthraquinone, 457
- anthraquinone-2-sulfonate, 457
- anthroquinone derivatives, 288
- anthrosemiquinone, 293
- antibody, 645
- antitumour drug, 287
- aqueous solution, 223
- arginine, 568
- Argonne National Laboratory, 22, 49, 75
- aromatic halides, 234
- aromatic hydrocarbon, 53
- aromatic pollutants, 661
- aromaticity, 60
- Arrhenius expression, 152
- Arrhenius - non-linear, 158
- Arrhenius plot, 95, 153, 155, 159, 160
- artificial bilayer membranes, 266
- aryl radical, 227
- As-As three electron bonds, 379
- ascorbate, 546, 627, 628, 637
- ascorbic acid, 710
- atomic dissociation of three-electron bonds, 381
- atrazine, 664
- autoionization, 196
- autoxidation, 732
- avoided-level -crossing, 99
- aziridine ring opening, 305
- B. subtilis*, 720
- $\beta$ -amino- $\alpha$ -hydroxyalkyl radicals, 485
- $\beta$ -cleavage, 336
- $\beta$ -fragmentation, 499
- $\beta$ -hydroxy elimination, 470
- $\beta$ -ketoalkyl radical, 485
- $B_{12r}$ , 470
- backbone linkage, 356
- bacteriochlorophyll, 460
- Barkas's formula, 41
- base damage, 593, 600, 614
- base radical, 596, 613
- base release, 526
- base-induced  $\beta$ -elimination, 307
- beef, 705, 717, 721, 722, 724, 725, 728, 731, 732
- benzene, 55
- benzyl glycosides, 493
- benzyl radical, 493
- beta scission, 347
- Bethe formula, 39
- bilayer, 438
- bilayered clusters, 435
- bimetallic clusters, 434
- biomarker, 597
- bioreductive drug selectivity, 643
- bisbenzimidazole derivatives, 546
- bisfunctionalized fullerene derivatives, 263
- blue cluster, 425
- Brookhaven National Laboratory, 49
- boiling water reactors, 145
- bond dissociation enthalpy, 322, 333
- bond energies, 370
- boron-boron one electron bond radical anion, 377
- bovine serum albumin, 683
- $Br_2^{\cdot\cdot}$ , 458, 466
- Bragg curve, 39
- branched alkanes, 175, 208
- bromobenzene, 240
- bubble state, 98
- $C_{60}$ , 457
- cage of ion pairs, 346
- calixarenes, 264
- campylobacter jejuni*, 705
- cancer, 623, 631, 632, 633
- cancer therapy, 586
- CANDU, 145
- carbene, 470
- carbenium ion, 404, 405, 406

- carbohydrates, 706, 709, 718, 719, 722  
 carbon tetrachloride, 90, 461  
 carbonate, 659  
 carbonate radical, 148, 632  
 carbonium ions, 186  
 carbonyl anion radical, 710, 713, 716  
 carcinogen, 723  
 carotene, 461  
 catalysis, 411  
 catalyst, 440  
 catalysts, 460, 464  
 catalytic processes, 101  
 catalyze, 465  
 cavity model, 420  
 $\text{CBr}_3\cdot$ , 469  
 $\text{CCl}_3\cdot$ , 469  
 $\text{CCl}_3\text{O}_2\cdot$ , 458, 461  
 cell death, 588  
 cell inactivation, 591  
 cellobiose, 492  
 cellulose, 496, 505  
 cellulose triacetate, 58  
 Cerenkov, 28  
 CERN, 60  
 $\text{CF}_3\cdot$ , 469  
 $\text{CF}_3\text{C}\cdot\text{CHCl}$ , 469  
 $\text{CH}_2\cdot\text{NH}_2$ , 346  
 $\text{CH}_2\cdot\text{CHO}$ , 458, 466  
 $\text{CH}_3\cdot$ , 469  
 $(\text{CH}_3)_2\cdot\text{COH}$ , 255  
 $(\text{CH}_3)_2\text{C}\cdot\text{OH}$ , 455  
 chain reaction, 485, 502, 503, 543, 544, 545, 659  
 chalcogenide, 335  
 charge migration, 472, 601  
 charge pools, 440  
 charge repulsion, 277  
 charge transfer, 119, 123, 132, 614  
 charge-separated radical pairs, 262  
 charged dimers, 417  
 chemical modifiers, 610  
 chemiclearance, 723, 727  
 chemotherapy, 304  
 chicane, 26  
 chicken, 711, 717, 718, 721, 722, 723, 724, 725, 728, 729  
 Chini clusters, 426  
 chiral separation, 683  
 chitin, 483, 496  
 chitosan, 483, 496, 497  
 chlorate solutions, 170  
 chlorin, 456  
 chlorinated biphenyls, 662  
 chlorinated hydrocarbons, 659  
 chlorobenzene, 240  
 chlorophyll, 458, 460, 462  
 chloropropane, 229  
 chromatography, 676  
 chromium porphyrins, 470  
 cis-decalin, 178  
 cis-trans isomerization, 352  
 $\text{Cl}_2^{\cdot\cdot}$ , 246, 458, 466  
 clearances, 724  
 clostridium botulinum, 705, 720, 721  
 cluster, 275  
 cluster formation, 255  
 cluster stabilization, 415  
 clustered DNA damage, 589, 591, 592, 610, 616, 617  
 clusters, 411  
 CNDO/S calculations, 255, 257  
 Co-B<sub>12</sub>, 468  
 Co-phthalocyanine, 468  
 $\text{CO}_2^{\cdot\cdot}$ , 455  
 coalescence, 414  
 cografting, 692  
 collagen, 563  
 collisional momentum transfer, 111  
 colloidal Pt, 458  
 commonality, 717, 724, 725, 727, 730, 734  
 competition kinetics, 296  
 complexed silver atom, 418  
 composite materials, 447  
 concentrated solutions, 163  
 conductivity, 114, 118, 136  
 confined nanoclusters, 433  
 conformation-dependent antigenic structure, 575

- continuous slowing down
  - approximation (CSDA), 112
- convective transport, 675
- copper, 431
- copper oligomers, 426
- core, 41
- core-shell clusters, 434
- corona discharge, 658
- corrected absorption spectra, 293
- corrosion, 422
- corrphycenes, 471
- coulombic repulsion, 298
- counter-ion release, 498
- coupled cluster theories, 3
- Cr<sup>III</sup>-porphyrin, 463, 467
- critical cluster, 421
- cross recombination of ions, 195
- cross-interaction constant, 327, 330
- crosslinking, 713, 733
- CTTS (charge transfer to solvent, 418
- cyclic sulfonium salts, 358
- cyclic voltammetry, 324
- cyclization, 560
- cycloalkane, 175, 178
- cycloalkane holes, 178
- cyclodextrin, 262, 471
- cycloheptane, 179
- cyclohexadienyl, 92
- cyclohexane, 55, 178
- cyclooctane, 55, 57, 179
- cyclopentane, 55, 179
- cystamine, 355
- cytidine, 545
- cytochrome P<sub>450</sub>, 469
- cytochrome-c complexes, 573
- cytosine, 513, 515, 516, 517, 518, 530
- cytosine glycol, 518
- D-fructose, 501, 503
- D-glucose, 482, 487, 496, 500
- D<sub>10</sub>-value, 720, 721
- damage amplification, 536
- daunomycin, 288, 304
- dc conductivity, 178
- decarboxylation, 557, 560
- decarboxylation of amino acids, 345
- decay of alkane holes, 71
- decay of squalane holes, 78
- deglycosylation, 306
- degradation, 446
- dehydroascorbate radical, 567
- delocalization, 254
- demetallation, 461
- density functional theory, 3
- depletion, 291
- deprotonation, 178, 337
- deprotonation of sulfide and disulfide radical cations, 362
- detection techniques, 342
- deuteroporphyrin, 454
- developer, 429
- development, 432, 440
- dianion, 456
- dibromobenzene, 243
- dichlorethane, 461
- dichlorobenzene, 243
- dielectric continuum, 4, 271
- diethyl amino groups, 684
- diffusion, 96
- diffusion coefficients, 97
- diffusion controlled, 130, 131, 134
- diffusion-controlled reactions, 268
- dihydroxyacetone, 719
- dihydroxyanthraquinone, 310
- dimer fluorescence, 131, 132
- dimer radical cation, 232
- dimer rare-gas fluorescence, 127, 129, 136
- dimeric triglycerides, 715
- dimerization, 309, 713, 726
- dipolarity/polarizability, 331
- diquinone, 309, 310
- direct action, 163
- direct effects, 514, 541, 600, 602, 603, 604, 607
- disaccharides, 491
- dismutation reaction, 305
- disproportionation, 298, 418, 456, 707, 710, 719, 726, 728
- disproportionation of sulfide and radical cations, 362

- dissociation energy of three-electron SS bonds, 370
- dissociative electron capture(attachment), 257, 729
- disulfide bonds, 555
- disulfide free radicals, 566
- disulfide radical anions, 354, 355
- disulfide radical cations, 373
- disulfide radicals, 569
- disulfide reduction, 568
- dithia compounds electrochemical oxidation, 375
- dithia cyclic compounds, 367
- dithia open-chain compounds, 367
- dithia-4-methyl heptane (3,5), 369
- dithiacyclooctane (1,5), 367
- dithiacyclopentane (2-substituted-1,3), 369
- dithiacyclopentane (1,3), 368
- dithiahexane 2,5, 369
- dithiane (1,4), 369
- dithiothreitol, 355, 567
- DNA, 481, 484, 492, 585, 633, 637, 639, 640, 711, 720
- DNA damage, 585, 589, 591, 598, 611
- DNA free radicals, 593
- DNA hydration, 588
- DNA lesions, 591
- DNA radicals, 593
- DNA strand breakage, 603
- DNA structure, 587, 593
- DNA-binding proteins, 575
- donor-acceptor distances, 573
- donor-bridge-acceptor dyads, 284
- dose rate, 414, 432, 439
- dose-rate effect, 435, 707, 708, 711
- double strand break, 606
- doxorubicin, 626, 627
- drugs, 623, 629, 632, 637, 639, 643
- dry electrons, 554
- duroquinone, 634
- dynamic light scattering, 275
- dynamics of three-electron bond formation, 375
- EDTA, 429, 663
- electric field, 90
- electrical breakdown, 119
- electrical property, 59
- electrochemical oxidation of dithia compounds, 375
- electrodes, 441
- electron acceptor, 269, 423
- electron addition, 716, 725
- electron capture, 110, 114, 115, 118, 119
- electron degradation spectra, 108
- electron donor, 269, 421
- electron energy spectrum, 108
- electron exchange, 71
- electron fraction, 164
- electron gun, 23
- electron migration, 597
- electron mobility, 91, 113, 118
- electron slowing down, 108
- electron thermalization distance distribution, 193
- electron transfer, 232, 268, 420, 457, 624, 633, 636, 639, 640, 642
- electron transfer by tunnelling, 616
- electron transfer process, 596
- electron transfer rate, 272
- electron tunnelling, 615
- electron-beam nano-lithography, 14
- electron-donating substituents, 243
- electron-hole pairs, 176
- electron-ion recombination, 125
- electron-transfer reactions, 189
- electron-withdrawing substituents, 243
- electronegativity, 233
- electronic configuration, 258
- electronic interactions, 268
- electronic structure computation, 2
- elimination of ammonia, 485
- elimination of water, 485
- ELOSS, 41
- elution curves, 678
- ELYSE, 26
- emission spectroscopy, 108, 116
- emission yields, 132, 136, 138
- end group termini, 613



- end termini, 606, 607
- end-of-track probe, 85
- end-of-track process, 86
- endonuclease II, 596
- endonuclease III, 597, 598, 599
- energy deposition, 38, 107
- energy gap, 253
- energy transfer, 119, 312
- energy-loss calculations, 199
- enzyme immobilization, 687
- enzyme-inactivated meats, 723, 724, 727, 728, 731
- EO9, 626, 627
- equilibrium, 263, 299
- equilibrium between C- and S-centered radicals, 349
- equilibrium concentration, 303
- equilibrium constant, 269
- $e_s^-$ , 413, 708, 709, 710, 714, 719
- escherichia coli, 705, 720, 721
- ESR, 185, 254, 294, 296, 303, 332, 395, 396, 401, 600, 601, 602, 607, 673, 711, 713, 715, 716, 717, 718, 724, 725
- ester linkages, 716
- ethyl bromide, 229
- ethylene glycol, 485
- exciplex, 127, 128, 131, 132, 133, 134, 135, 136, 138
- excited iodine atoms, 139
- excited krypton atoms, 140
- excited rare gas, 126
- excited state, 107, 108, 110, 112, 116, 127, 133, 134, 138, 289
- excited state - nonfluorescing, 203
- excited states-lower, 202
- excited xenon atoms, 131
- FAPY, 535
- fatty acid moieties, 709, 715, 716
- $Fe(CN)_6^{3-}$ , 238
- $Fe(II)EDTA$ , 522
- $Fe^0$ -porphyrins, 464
- $Fe^I$ -porphyrins, 464
- $Fe^{II}$ -porphyrins, 464
- femtosecond pulse radiolysis, 214
- Fermi potential, 424
- Ferredoxins, 572
- ferrimyoglobin, 709, 710, 714, 717, 728, 729
- ferromagnetic, 428
- ferromyoglobin, 709, 714, 731
- final products, 561
- flavin mononucleotide, 627, 641
- flavins, 566
- flavoproteins, 556, 631, 641
- flue gases, 658
- fluorescence, 70
- fluorescent additive, 110, 111
- fluorescent probes, 111, 112
- fluoride, 227
- fluorobenzene, 246
- food, 705, 706, 709, 710, 711, 720, 722, 723, 730, 734
- Food and Drug Administration, 705
- formamidopyrimidine-DNA glycosylase, 596
- formate radicals, 413
- formation rate constants, 294
- formic acid, 52, 719
- formyl chloride, 661
- formylmethyl radical, 486
- Fpg proteins, 597, 598, 599
- fraction of singlet-correlated pairs, 74
- fragment radical cation, 181
- fragmentation, 208, 553, 731
- fragmentation sites, 554
- free radical processes, 585, 586, 591
- free radicals, 85, 107, 115, 116, 140
- frequency of quantum oscillations, 73
- Fricke solution, 51
- fullerene, 253, 457
- fullerene homologues, 258
- G-value, 107, 136, 147, 157, 291, 709
- G-values of destruction, 562
- GANIL, 50
- gas basicity, 334
- gases, 90
- gem-dialkyl effect, 370
- geminate dynamics, 193

- geminate recombination, 72, 311  
 genotoxicity, 720, 722, 723  
 geometry constraints, 405  
 glass fiber reinforced epoxy, 60  
 glass transition temperature, 707, 708  
 glucose radical, 719  
 glucoseamin, 483  
 glutathione, 566, 567  
 glyceraldehyde, 719  
 glycidyl methacrylate, 674, 688  
 glycosides, 494  
 glycyglycine, 52  
 gold, 430  
 graft chains, 695  
 graft polymerization, 675  
 grafting, 672  
 growing centers, 422  
 growth, 416  
 guanine, 490, 513, 545  
 guanine radical cation, 602  
 guanosine, 515, 533, 534, 540  
 guest host structures, 260  
 H abstraction, 94  
 H atoms, 413  
 H radical, 710, 711, 713, 719  
 H-atom abstraction, 606, 607  
 H/D exchange, 406, 407  
 H<sub>2</sub>, 148  
 H<sub>2</sub> formation, 458  
 H<sub>2</sub>N<sup>+</sup>-CR<sub>2</sub>-CO<sub>2</sub><sup>-</sup> zwitterion, 346  
 (H<sub>2</sub>SSH<sub>2</sub>)<sup>+</sup>, 368  
 haemeproteins, 575  
 half-wave potential, 624  
 halogen, 329  
 halogen-halogen three electron bonds, 380  
 halogenated aromatics, 662  
 halogenated benzene, 329  
 halogenated biphenyls, 663  
 halogenated compounds, 225  
 Hammett constant, 237  
 Hammett equation, 325  
 Hammett plot, 326  
 Hammett  $\sigma$ , 633  
 heat-labile ssb, 599  
 hemoglobin, 563  
 Hendersen's equation, 294  
 heparin, 496  
 heptadecadiene, 728  
 heteroaromatic-N-oxides, 626, 640, 643  
 heteroatom, 328  
 heteroatom-centered free radicals, 341  
 heterogeneous catalysis, 395  
 heterolysis, 636, 637  
 hexacyanateferrate, 148  
 hexafluorobenzene, 237  
 hexane, 727  
 hfi constants, 79  
 high LET, 145  
 high LET pulse radiolysis facility, 7  
 high-mobility cations, 178  
 high-mobility holes, 184  
 highly excited hydrocarbon states, 194  
 highly excited solvent states, 196  
 Hildebrand solubility parameter, 331  
 HIMAC, 44, 75  
 histidine, 555  
 HIT, 44  
 HN<sup>-</sup>-CR<sub>2</sub>-CO<sub>2</sub><sup>-</sup>, 346  
 HO<sub>2</sub>-elimination, 494  
 hole capture, 76  
 homodisperse, 437  
 homodispersity, 427  
 hopping mechanism, 616  
 hot processes, 92  
 hot tritium, 92  
 hyaluronan, 496  
 hyaluronic acid, 481, 483, 496, 498  
 hydrated electron, 2, 147, 158, 226, 455, 555  
 hydrated electron precursors (see also dry electrons), 9  
 hydrocarbon solutions, 68  
 hydrocarbons, 718, 727, 728  
 hydrodynamic radius, 98  
 hydrogen abstraction, 637, 640  
 hydrogen abstraction by thiyl radicals, 350

- hydrogen atom abstraction -
  - intramolecular RS<sup>-</sup>- induced, 351
- hydrogen atoms, 715, 717
- hydrogen diffusion, 98
- hydrogen isotope effects, 103
- hydrogen peroxide, 149, 631, 632, 643
- hydroperoxides, 732
- hydrophilic addends, 274
- hydrophilic groups, 677
- hydrophilic substructures, 267
- hydrophobic groups, 687
- hydrophobic substructures, 267
- hydroquinone, 290, 298, 307, 624, 628, 631, 639
- hydroxy sulfuranyl radical, 559
- hydroxycyclohexadienyl radical, 319
- hydroxycyclohexadienylperoxyl radical, 661
- hylan, 499
- hyperfine coupling, 99
- hyperfine coupling constants, 2, 3
- hyperfine interaction, 69, 195
- hypochlorous acid, 632
- hypoxia, 630, 641
- hypoxic cells, 631, 637, 643
- HZSM5, 400
- icosahedral nucleus, 427
- ICRU report, 39, 40
- imaging, 411
- immunoassay, 514
- incineration, 658
- indirect action, 163
- indirect effect, 588
- indole-3-acetic acid, 628, 643
- indolequinones, 626, 639, 641
- indolyl radical, 627, 628, 644
- induction time, 412, 430
- inelastic collisions, 107
- inflection point, 232
- inhomogeneity, 37
- inter-metal electron transfer, 439
- intermolecular electron transfer, 267, 270
- intermolecular reactions, 714, 715
- intersystem crossing, 260
- intramolecular cation, 233
- intramolecular electron transfer, 560
- intramolecular H-bonding, 295
- intramolecular hydrogen bonding, 293
- intramolecular reactions, 714
- intramolecular SS ( $2\sigma/\sigma^*$ ) radical cations, 367
- iodobenzene, 240, 243
- iodochloromethane, 229
- iodopentafluorobenzene, 237
- ion, 118
- ion exchange groups, 687
- ion mobilities, 136
- ion recombination, 110, 118, 126, 129, 130, 131, 132, 133, 134, 135, 136, 138
- ion-electron recombination, 116, 118, 119, 120, 121, 122, 123, 124
- ion-exchange membranes, 671
- ion-ion recombination, 125, 127
- ion-molecule reactions, 188
- ionic dissociation of three-electron bonds, 381
- ionic mobilities, 131
- ionising radiation, 585, 588, 592
- ionization, 399
- ionization potential, 320, 321, 329, 412, 545
- ionization potentials, 270
- ions, 107, 108, 116, 135
- IRaP, 57
- iridium, 431
- iron deuteroporphyrin, 469
- IrO<sub>x</sub>, 460
- irradiated foods, 722, 723, 734
- irradiated meats, 722, 724, 729, 732
- isolated ion pairs, 177
- isooctane, 179
- isoorotic acid, 516
- isopyrimidine, 526
- isopyrimidines, 517, 524
- isotope label, 407
- JAERI, 44, 60
- Kamlet-Taft, 331
- ketone, 57

- kinetic isotope effects, 93
- kinetic stability of  $2\sigma/\sigma^*$  species, 371
- Langevin-Harper, 129, 134, 135
- laser flash photolysis, 324
- laser-coupled linacs, 214
- Laser-Electron Accelerator Facility, 23
- leaving group properties, 641
- LET, 586, 588, 589, 590, 591, 592, 599, 601, 603, 608, 610, 617
- LET effects, 37
- lifetime, 239
- ligands, 416
- light scattering, 265
- linac, 224
- linear accelerator, 6, 22, 22
- linear free energy relationships, 320
- linoleic acid, 717, 728, 729
- lipid radicals, 718
- lipids, 706, 708, 709, 715, 717, 722, 732
- lipoamide, 567
- lipoate, 566
- lipoic acid, 355
- lipophilicity, 635
- Listeria monocytogenes*, 705
- $\lambda_{\max}$ , 292
- localization dynamics, 194
- long-lived clusters, 428
- lost fraction of polarization, 86
- low energy secondary electrons, 592
- low LET, 145
- LSS, 40
- luminescence, 112, 125
- lysine, 563
- lysozyme, 553
- macronutrients, 720, 722
- macroscopic phase, 424
- magnetic field dependence, 88
- magnetic field effect, 67, 195
- magnetic level crossing, 179, 195
- magnetic probe, 84, 103
- magnetic resonance, 84
- malonaldehyde, 719
- Marcus inverted region, 271, 283
- Marcus theory, 11, 569
- Mary spectra, 68, 80
- matrix isolation technique, 225
- mechanical property, 59
- medium effects, 4
- methyl viologen, 457
- menadione, 541, 627
- mercury halide, 442
- mesoscopic phase, 424
- (MeSSMe)<sup>+</sup>, 374
- metal atoms, 417
- metal cluster reactivity, 419
- metal displacement, 436
- metal ions, 412
- metal oxides, 445
- metal sulfide, 444
- metal-carbon bonds, 468
- metalloporphyrins, 267, 453
- metalloproteins, 472, 563, 714
- metastable complex, 191
- methacrylic acid, 692
- methionine, 559, 566, 570
- methionine decarboxylation, 384
- methyl iodide, 231
- methyl ketones, 732
- methylcyclohexane, 178
- methylviologen, 539
- metronidazole, 626, 627, 634
- MFI zeolite, 397
- micelles, 460, 461
- microbial contaminants, 722
- microdosimetry, 42
- microelectrode, 12
- microelectrode potential, 425
- microfiltration, 677
- micronutrients, 720
- microwave conductivity, 121, 123, 124, 178
- Mie theory, 419
- misonidazole, 626, 627, 634, 637
- mitomycin C, 304
- mixed solvent, 301
- Mn<sup>III</sup>-porphyrins, 466
- Mn<sup>IV</sup>-porphyrins, 466
- mobile holes, 78
- mobility, 118, 122

- model quinones, 302
- molar absorptivity, 236
- molar extinction coefficient, 291
- molecular metal clusters, 426
- molecular sulfide radical cation, 360
- momentum transfer cross section, 112, 115
- monoamine oxidase, 575
- monofunctionalized fullerene derivatives, 273
- monomer radical cation, 234
- monomer selection, 674, 675
- monosubstituted benzene radical cation, 327
- Monte Carlo simulations, 199
- Mordenite, 403
- multicenter radical cations, 373
- multilayer binding, 677, 681, 684
- multiphoton ionization, 187, 193
- multiple-pair spur, 177, 186, 192
- multiply functionalized fullerenes, 279
- multisubstituted benzene radical cation, 327
- muon, 84
- muonium, 85, 92
- muonium formation, 91
- muonium reactions, 93
- mutagen, 723
- myofibrils, 709, 711, 731
- myoglobin, 709, 710
- myosin, 709, 711, 712, 713, 724, 731
- mytomicin c, 639
- N,N,N',N'-tetramethyl-p-phenylenediamine, 516, 546, 664
- N'-formylkynurenine, 571
- N-Acetylglucos-amine, 502
- N-acetylglucosamine, 483
- N-Acetylglucosamine, 503
- n-dodecane, 57
- N-oxides, 626
- $N_3^{--}$ , 458
- Nafion membrane, 422
- nanocolloids, 411
- nanoparticle synthesis, 13
- naphthazarin, 294, 299, 302
- nascent atoms, 416
- NaZSM5, 402
- Near Infrared, 265
- NERL, 26
- Nernst's equation, 323
- neutral solution, 52
- neutron, 60, 145
- nickel, 431
- nickel oligomers, 426
- Ni<sup>II</sup>-porphyrin, 463, 467
- nimorazole, 626
- nitrate radical, 166
- nitrate solutions, 165
- nitrates, 710
- nitric acid, 165
- nitric oxide synthase, 631
- nitrites, 710, 720, 731
- nitro compounds as radiosensitisers and chemotherapeutics, 345
- nitro-aromatics, 612, 613
- nitroarene radiosensitizers, 634, 636
- nitroarenes, 626, 639
- nitrobenzenes, 633, 636
- nitrobenzyl halide radical-anions, 640
- nitrofurantoin, 626, 627, 634
- nitrogen-centered radical anions, 344
- nitrogen-nitrogen three-electron bonds, 377
- non-homogeneity, 38
- non-polar media, 175
- nonwoven fabrics, 691
- nuclear probe techniques, 83
- nuclearity, 411
- nucleation, 416
- nuclei, 422, 437
- nucleobases, 513
- nucleophilic attack on sulfide and disulfide radical cations, 362
- nucleosides, 490
- nutritive value, 720
- $O_2^{\cdot-}$  dismutation, 465
- octaethylporphyrin, 454
- OD ESR, 78, 80
- odd-electron bonds, 343, 363

- OER (oxygen enhancement ratio), 590, 611
- OH adduct, 235, 238
- OH interactions, 599
- OH radical, 148, 158, 413, 588, 592, 593, 595, 596, 599, 600, 603, 604, 606, 608, 612, 613, 617, 709, 710, 711, 713, 714, 719, 720
- oligomeric structure dissociation, 554
- oligomers, 414
- one-electron oxidation, 308, 311, 596, 601
- one-electron redox potentials, 12
- one-electron reduced nitroso compounds, 343
- one-electron reduced organic nitro compounds, 343
- one-electron reduction, 288
- one-electron reduction potential, 299, 300, 320, 321, 323, 326
- one-electron reduction (second), 303
- optical absorption of  $2\sigma/1\sigma^*$  three-electron-bonded species, 365
- optical absorption, 116, 290
- optical properties, 417
- optical property, 59
- optically forbidden states, 110
- organic halides, 223
- organic liquids, 175
- organized assemblies, 12
- organometallic chemistry, 468
- ortho substituent, 328
- ORNL, 44
- orotic acid, 516
- ortho scale, 328
- orthoquinone, 308
- Osaka University Radiation Laboratory, 22
- osmium porphyrins, 467
- oxazolone, 538
- oxidants, 224
- oxidation potential, 246, 460, 600
- oxidised radical, 311
- oxidizing radicals, 458
- oxyferromyoglobin, 731
- oxygen, 626, 642
- oxygen addition to thiyl radicals, 352
- oxygen effect, 633
- oxygen reactivity, 307
- oxygen-mimetic drugs, 632
- oxygen-oxygen three electron bonds, 379
- oxyl radicals, 499, 523
- ozone dosimetry, 128, 132, 136
- p-nitroacetophenone, 539
- $\pi$ - $\pi$  association forces, 266
- P-P three electron bonds, 379
- $\pi$ - $\pi^*$  transitions, 293
- $\pi$ -radical anion, 256, 455
- $\pi$ -radical cation, 256, 458
- packaging, 705, 730, 731, 732, 733
- palladium, 431
- palmitic acid, 709, 717, 729
- palmityl aldehyde, 717
- parabolic dependence, 283
- parabolic dependency, 271
- paraffins, 175, 208
- pathogens, 705, 720
- peak oxidation potential, 324
- penicillamine thiyl radicals, 350
- Penning ionisation, 116, 118, 119
- pentafluorophenol, 227
- pentane, 727
- peptide backbone, 575
- peptide backbone radical, 711, 713, 725
- peptide bond, 555, 557
- peptide radical, 711, 713, 714, 715
- perchloric acid, 241
- perfluorobenzene, 228
- permeation, 680
- peroxidase, 632, 643
- peroxodisulfate, 545
- peroxyl radical, 228, 466, 494, 522, 538, 557, 559, 605, 658
- peroxynitrite, 632
- perthiyl radical, 356
- perthiyl reactivity, 357
- pH gradients, 635

- phase shift of quantum oscillations, 77  
 phenoxyl radical, 236  
 phenyl radicals, 228  
 phenylalanine, 559  
 pheophytin, 460  
 phlorin anion, 456  
 phonon-assisted hopping, 183  
 phosgene, 661  
 phosphate radicals, 169  
 phosphate release, 488  
 phosphate solutions, 169  
 phosphoester, 484  
 phosphoric acid, 169  
 photo-oxidised DNA, 615  
 photocathode, 24  
 photochemical reduction of CO<sub>2</sub>, 464  
 photodynamic therapy, 313  
 photoemission spectroscopy, 194  
 photographic development, 429  
 photographic emulsions, 441  
 photographic processes, 15  
 photoionization, 239, 412, 541  
 phthalocyanines, 472  
 picosecond Laser-Electron Accelerator Facility, 6  
 picosecond pulse radiolysis, 110  
 pK, 292, 302  
 pK<sub>a</sub>, 322, 332, 333, 334, 337  
 plasma, 107, 112, 115, 116, 120, 140  
 plasmid DNA, 599, 604, 617  
 platinum oligomers, 426  
 polar head group, 278  
 polar interface, 278  
 polarization transfer, 86  
 poly(acrylic acid), 499  
 poly(methacrylic acid), 499  
 poly(U), 497  
 poly-GMA reactivity, 675  
 polycyclic aromatic hydrocarbons, 112  
 polyethylene, 733  
 polyethyleneterephthalate, 733  
 polyhdric alcohol, 482  
 polyhydroxylation, 282  
 polymer, 431  
 polymeric membrane, 433  
 polypeptide chain breakage, 554  
 polypeptidic backbone modifications, 574  
 polyphenylalanine, 713  
 polysaccharides, 490  
 polystyrene, 733  
 pork, 706, 708, 710, 717, 718, 721, 722, 724, 725, 728, 731  
 porous hollow-fiber membranes, 674  
 porphycenes, 471  
 porphyrin triplet state, 458  
 porphyrins, 453  
 positively charged groups, 696  
 positron, 83  
 positronium, 92  
 poultry, 705, 706, 715  
 pre-exponential factor, 94  
 pre-thermalized charges, 176, 194  
 preexisting sulfur-sulfur interaction, 376  
 preirradiation grafting, 673  
 pressurised water reactors, 145  
 prodrugs, 638  
 product analysis, 206  
 product selectivity, 400  
 proline, 570  
 propanedioldiester, 716, 718, 729  
 propanedipalmitate, 729, 730  
 prosthetic group, 556  
 protein active site, 574  
 protein purification, 676  
 protein radicals, 710  
 proteins, 706, 709, 711, 712, 714, 716, 722, 724, 731  
 proton, 87  
 proton affinity, 334  
 proton-transfer reactions, 189, 190  
 protonation, 263, 456, 457  
 protonation of HN<sup>-</sup>-CR<sub>2</sub>-CO<sub>2</sub><sup>-</sup>, 347  
 pulse compression, 26  
 pulse radiolysis, 5, 108, 111, 114, 115, 116, 120, 124, 126, 134, 140, 224, 288, 323, 342, 586, 633, 639, 640

- pulse-probe detection, 30  
 pulsed conductance, 296, 303  
 pump-probe conductivity, 188  
 purine, 513, 532, 545  
 purine bases, 711  
 pyrimidine bases, 711  
 pyrimidines, 513, 515, 541  
 pyrrolidinium salt, 277  
 quantitative structure-activity relationships, 634  
 quantum beat spectroscopy, 179, 195  
 quantum beats, 68  
 quantum effects, 93  
 quantum nature, 84  
 quantum size effects, 12  
 quinizarin, 294  
 quinizarin sulphonate, 307  
 quinone, 287, 307, 457, 624  
 $(R_2S)_2^{\cdot+}$  dimer radical cation, 364  
 $R_2S^+(OH)$ , 359, 385  
 $(R_2S \cdot OH_2)^+$ , 385  
 radiation chemical techniques, 283, 341  
 radiation chemistry, 223, 586  
 radiation pasteurization, 705, 706, 720, 732  
 radiation sterilization, 705, 706, 710, 720, 732  
 radiation track, 75  
 radiation-induced carcinogenesis, 585  
 radiation-induced DNA damage, 589  
 radiation-induced graft polymerization, 671  
 radiation-induced processes in nuclear waste, 14  
 radiation-induced reduction, 259  
 radical addition, 257, 636  
 radical adduct, 256  
 radical anion, 457, 458, 517  
 radical anion decay, 456  
 radical anion lifetime, 456  
 radical anion of 1,2,3,4-tetraphenylcyclopentadiene, 79  
 radical anion of hexafluorobenzene, 70  
 radical anion of p-terphenyl, 75  
 radical anion stability, 457  
 radical cation, 319, 326, 395, 396, 401, 460, 461, 462, 505, 541, 664  
 radical cation of alkanes, 71  
 radical cation of cis-decaline, 71  
 radical cation of diphenylsulphide, 75  
 radical cation of p-terphenyl, 70  
 radical cation reactions, 402  
 radical cation stability, 459  
 radical centers, 302  
 radical ion pairs, 67  
 radical kinetics, 101  
 radical solutions, 231  
 radioluminescence, 69  
 radiolysis, 107, 111, 225  
 radiolysis/EPR method, 399, 400  
 radiolytic spin labeling, 396  
 radiolytically-oxidized arenes, 269  
 radioprotection, 514  
 radiosensitisers, 586, 591, 611, 611, 633  
 radiosterilization, 553  
 radiotherapy, 630  
 Raltech, 723  
 rancidity, 730, 732  
 rare gas, 110, 113, 114, 115, 123, 124, 136  
 rare gas-monohalide, 126  
 rate combination, 131  
 rate constant, 111, 118, 119, 120, 121, 122, 123, 126, 129, 130, 132, 133, 134, 135, 140, 141, 149, 259, 296, 565  
 rate constants, 236  
 rate constants-semiquinones, 297  
 reaction selectivity, 403  
 reactive oxygen species, 592  
 reactivity, 319  
 reactor coolant chemistry, 146  
 reactors, 145  
 recoil tritium, 83  
 redox, 623, 629  
 redox characteristics, 299  
 redox equilibrium, 300



- redox potential, 241, 412  
redox properties, 595  
redox reactions, 455  
reductases, 631  
reduction, 254  
reduction of sulfoxides, 361  
reduction potential, 624  
reduction potentials, 361, 460, 562  
reduction potentials for (RSSR)<sup>•+</sup>-  
RSSR, 375  
reduction rate constants, 276, 281  
reorientation dynamics, 102  
repair, 596  
resonant charge transfer, 181  
reversed micelles, 433  
rhodium porphyrins, 470  
riboflavin, 541  
Ribose-5-phosphate, 489  
ring cleavage, 490  
RNA, 484  
rotator-phase solids, 102  
RS<sup>••</sup> addition to double bonds, 352  
(RS<sup>••</sup>:Br<sup>-</sup>), 382  
RSS<sup>•</sup> absorption, 357  
(RSSR)<sup>•+</sup> radical cation optical  
absorption, 374  
Ru<sup>II</sup>-porphyrin, 467  
RuO<sub>2</sub>, 460  
S<sub>1</sub> state dynamics, 193  
salmonella, 705, 721  
salt effect, 296  
satellite ions, 181  
saturated hydrocarbons, 175  
scavenger molecules, 88  
scavenging systems, 629  
Scission of the glycosidic linkage,  
490  
Se-Se three electron bonds, 379  
secondary electrons, 107, 111, 113,  
116, 119, 127  
selenium-centered radicals, 363  
semi-oxidised quinones, 309  
semiconductor cluster, 415, 442  
semiquinone, 288, 289, 290, 298,  
302  
semiquinone -charge on, 295  
semiquinone structure, 296  
sensitizers, 514  
signal transduction, 553  
silica, 445  
silver cluster, 425, 429  
silver halide, 443  
silver ions, 696  
simultaneous grafting, 673  
single strand breaks (ssb), 602, 604,  
607, 608, 613, 613, 617  
single-pair spur, 192  
single-photon ionization, 193  
singlet excited state, 209  
singlet recombination probability,  
211  
singlet state, 196  
singlet state formation, 195  
singlet-correlated ion pairs, 195  
singlet-triplet evolution, 68  
site of attack, 242  
small polaron, 183  
SO<sub>4</sub><sup>••</sup>, 246  
solar energy, 455, 459  
solid state, 499  
solid/liquid interface, 13  
solute fluorescence, 209  
solvation, 96, 330, 333  
solvent effect, 321, 330, 332  
solvent friction, Kramers, 96  
solvent hole migration, 182  
solvent radical cation, 257  
space velocity, 679  
spectral parameters, 235  
spectroscopic characteristics, 292  
Spencer and Fano, 108  
spin coherence, 67, 80  
spin effects, 195, 196  
spin label, 85, 99  
spin polarization, 84  
spin relaxation, 197  
spin trap, 89  
spontaneous oxidation method, 403  
spur, 87, 176  
spur, last, 88  
spur model, 156  
spur radii, 157

- spur reactions, 149
- S $\cdot$ :N radical cation, 384
- S $\cdot$ :P coupled radical cation, 383
- squalane, 178
- (S $\cdot$ :X)<sup>+</sup> radical cation, 382
- S $\cdot$ :X three electron bonds, 380
- (>SS<)<sup>+</sup> as a reductant, 372
- (>SS<)<sup>+</sup> ionization energy, 372
- (>SS<)<sup>+</sup> redox potential, 371
- stability, 299
- stabilization, 335
- stabilizing polymers, 416
- stacked porphyrins, 472
- staphylococcus aureus, 705, 721
- steric effects on SS radical cations, 367
- stochastic simulations, 199
- stochastic techniques, 5
- Stokes-Einstein equation, 97
- stopping power, 87, 108, 128
- storage of radicals, 673
- strand breakage, 589
- strand breaks, 588, 590
- structural assignments, 303
- subcritical clusters, 423
- subexcitation, 112, 114
- subexcitation electron, 110, 111, 113
- submitochondrial particle, 575
- substituent constant, 325
- substituent effect, 325
- substituent effects on lambda max, 366
- sugar radical, 601, 610, 611
- sulfanato-propyl viologen, 422
- sulfate radical, 168, 483, 541
- sulfate solutions, 168
- sulfonic acid groups, 696
- sulfonyl radical, 353
- sulfur-centered radical cations, 361
- sulfur-oxygen interaction, 385
- sulfur-sulfur interactions in polypeptides, 377
- sulfuranyl radical, 358, 359
- sulfuric acid, 168, 241
- sulfuric-acid glasses, 522
- sulphonate loss, 307
- super acids, 404, 406
- superconductivity, 253
- supercritical clusters, 423, 424
- supercritical fluids, 10
- superoxide, 564, 631
- superoxide dismutase, 563
- superoxide dismutation, 465
- superoxide elimination, 495
- superoxide radical, 308, 465
- supported clusters, 441
- supported nanoclusters, 433
- surface curvature, 257
- surface magnetism, 103
- surface plasmon band, 419
- surface-adsorbed species, 102
- surface-enhanced Raman scattering, 7
- surfactants, 264
- t-butyl alcohol, 234
- tabletop accelerators, 214
- Taft's constant, 238
- tandem lesions, 596
- tautomerisation, 307
- tellurium-centered radicals, 363
- temperature dependence, 123, 124
- temperature effect, 571
- teratogen, 723
- tertiary structure, 554
- tetrachloroethylene, 659
- tetrakis[4-(N,N,N-trimethylamino)phenyl]porphyrin, 454
- tetrakis(4-carboxylphenyl)porphyrin, 454
- tetrakis(4-sulfonato-phenyl)porphyrin, 454
- tetrakis(N-methyl-X-pyridyl)porphyrin, 454
- tetramethylthiourea radical cation, 545
- tetranitromethane, 516
- tetraphenylporphyrin, 454
- tetrasulfophthalocyanine, 470
- texaphyrins, 471
- texture, 705, 730, 731
- thermal distribution, 113
- thermal electron capture, 127

- thermalisation time, 114, 115
- thermalised electron, 111
- thermalization track, 89
- thermochemical cycle, 322
- thermodynamic stability of  $2\sigma/\sigma^*$  bonds, 370
- thiamin, 707, 708, 709, 710, 711, 722
- thiobenzoic acid, 335
- thiol, 486, 590, 591
- thiyl, 566
- thiyl displacement process, 359
- thiyl radical optical absorption, 356
- thiyl radical reaction with oxygen, 352
- thiyl radical reactions with polyunsaturated fatty acids, 351
- thiyl radicals, 349
- thiyl radicals as H-atom abstracting agent, 349
- thiyl radicals as oxidants, 353
- thiyl/disulfide radical anion conjugation, 354
- three body, 125, 127
- three electron bonds S-X, 380
- three-body, 121, 122, 123, 123, 124, 126, 128, 131
- three-body reaction, 120
- three-body recombination, 130
- through bond mechanism, 572
- through-space pathway, 570
- thymidine, 528, 543, 545
- thymine, 513, 515, 516, 517, 528, 529
- time-dependent Spencer Fano (TSF), 108
- time-resolved ESR, 344
- time-resolved microwave conductivity, 114, 116
- time-resolved resonance Raman spectroscopy, 348
- time-resolved techniques, 342
- tirapazamine, 626, 627, 640
- track electrons, 90
- track model, 156
- track structure, 586, 608
- trans-decalin, 178
- transient species, 226
- transition metal porphyrins, 462
- transition metals, 666
- transition radiation (TR), 28
- triazine, 665
- trichloroethane, 659
- trichloroethylene, 659
- triglycerides, 706, 709, 715, 716, 717, 718, 724, 726, 729, 730
- trilayer, 438
- tripalmitin, 709, 715, 717
- triplet characteristics, 312
- triplet energy transfer, 260
- triplet lifetimes, 266
- triplet state, 260, 289, 311
- triplet state formation, 195
- Triton X 100, 460
- tryptophan, 559, 565, 566, 570
- tryptophanyl radical, 566
- tumours, 630
- tunneling, 94
- two-body, 120, 121, 124, 125, 126, 127, 130, 131
- two-body neutralization, 131
- two-body rate constant, 111
- two-electron potential, 301
- two-electron reduction, 306
- tyrosine, 559, 565, 570
- ultrafast pulse-probe laser spectroscopy, 193
- ultrafast spin-lattice relaxation, 180
- University of Tokyo Nuclear Engineering Research Laboratory, 22
- uracil, 515, 516, 517, 522, 524, 528, 529
- uranium recovery, 691
- uridine, 526
- van der Waals radius of fullerenes, 260
- vesicular systems, 265, 278
- vibrational frequencies, 3
- vibrational stretching frequencies, 374
- viologens, 634

- vitamin E, 722
- W-value, 136, 138
- water elimination, 517
- water oxidation, 459
- water radicals, 586, 592, 593, 593, 608
- water radiolysis, 146
- water-pollution abatement, 657
- water-soluble functionalized fullerenes, 279, 282, 283
- water soluble host-guest structures, 261
- wavefunction structure, 196
- wholesome, 720, 723, 724
- wholesomeness, 706, 720
- xanthine oxidase, 574, 641
- xenon excited state, 132
- yield-dose relationships, 707
- Zeeman interaction, 195
- zeolite, 433
- zeolites, 101
- zero-point energy, 93
- ZSM5, 397
- zwitterion, 335, 337